RADIAL SWIRLERS
FOR
LOW EMISSIONS GAS TURBINE COMBUSTION

HISHAM SALMAN AL KABIE, B.Sc., M.Sc.

A thesis submitted for the degree of Doctor of Philosophy
at the University of Leeds, under the supervision of
Dr. G.E. Andrews.

Department of Fuel and Energy,
Houldsworth School of Applied Science,
The University of Leeds,
England.

1989

TO

MY FAMILY

HERE AND ABROAD

ABSTRACT

Radial swirler were investigated for gas turbine combustor applications, with low NOx emissions as the main aim of the project. The flow regime of the combustor which was imposed by the radial swirler flow was shown by flow visualisation to feature a conical shaped swirling shear layer boundary and a corner recirculation zone. The flow patterns was independent of the swirl-vane angle but was a function of the swirler passage depth.

A minimum swirler expansion ratio of 1.8 was required to achieve an adequate combustion efficiency. A high efficiency was not achieved in the weak region until there was a significant outer expansion and associated recirculation zone. However, there was a little influence of the expansion ratio on the weak extinction limit.

Various non-conventional fuel injection methods such as swirler vane passage, radial central and wall injection were used with gaseous propane and natural gas and liquid kerosene and gasoil. Passage injection was undertaken to exploit the twin benefits of peripheral fuel injection and partial fuel and air mixing upstream of the swirlers outlet. Generally, most of the mixing between fuel/air took place in the shear layer. However, there was a major influence of the method of fuel injection on the NOx emissions. Low NOx emissions were achieved with the radial central injection, but ultra-low NOx emissions, comparable with the premixed situation, were achieved for passage and wall injection. This was due to the dependency of the local shear layer mixing near the swirler exit on the fuel placement as shown by the radial gas analysis traverse results in the plane just downstream of the radial swirler.

Staged air and fuel combustion was investigated using lean-lean combustion concept. Low NOx emissions compatible with a high combustion efficiency was demonstrated with stable switching from pilot to main stage combustion. Finally, a double radial swirler with a high air flow was investigated using co and counter swirl and demonstrated ultra low NOx with a good stability with central injection

into counter rotating swirler.

These systems were shown to have the potential for dry solution to the industrial gas turbine NOx emissions regulations with a very high combustion efficiency.

ACKNOWLEGEMENTS

The author wishes to express his gratitude to the Fuel and Energy Department, Leeds University, for the provision of research facilities.

Sincere thanks must be expressed to my supervisor Dr. Gordon E. Andrews for his encouragement, guidance and advice throughout the project.
Special thanks must also be expressed to the members of the Houldworth school Workshop and to the members of the Departmental Workshop for their co-operation during the rig manufacturing, installation and during the experimental work.
Thanks must also be expressed to the kind and helpful secretaries in Fuel and Energy Department, especially to Mrs.Sheilagh J. Ogden.
Thanks must be expressed to the members of General Photography section for their help in preparing the photographs.

The author also wishes to thank the Iraqi Government for their three years scholarship.
The author also thanks all the friends and members of Leeds university staff who showed any kind of help.

Finally, the author wishes to thank his dearest wife for her kindness and encouragement throughout the course of this research and also to thank his sons the 3S for making just a little noise.

CONTENTS

NOMENCLATURE

A_1 Approach flow pipe cross sectional area.

A_2 Effective open flow area of the radial swirler.

A_3 Swirler outlet cross sectional area.

R_1 Inner radius of curvature of the passage.

R_2 Outer radius of curvature of the passage.

R_3 Radius of centre for R1 and R2.

L Vane depth (height).

h Minimum passage width.

n Number of swirl vanes.

d_o Vane inlet diameter.

d Swirler outlet diameter.

D Combustor diameter.

V_1 Mean inlet (approach) velocity.

V_2 Mean velocity inside the passages.

V_3 Mean outlet velocity.

V_r Radial velocity.

V_θ Tangential velocity.

C_c Contraction coefficient (free discharge coefficient).

C_d Discharge coefficient.

m_r Mass accelerated toward the centre.

m_θ Mass rotating tangentially.

m Total mass of the flow.

F_θ Axial flux of angular mometum.

F_x Axial flux of linear momentum.

I_e Intencity of rotation.

S Swirl number.

M Mach number.

D/d Expansion ratio.

R_e Reynolds number.

H Enthalpy.

H_f Enthalpy of formation.

p Inlet pressure.

P_a Atmospheric pressure.

P propane fuel.

NG Natural gas fuel.

$\Delta P/P$ Pressure loss.

R Gas constant for air (287.04 J/Kg. K)

T Flame temperature.

T_{in} Combustor inlet temperature.

r/R Dimensionless radial distance from the centre of combustor.

EQR Equivalence ratio.

A/F Air to fuel ratio by weight (AFR).

GREEK LETTER

θ Radial swirler vane angle

η Combustion efficiency.

μ Viscosity.

γ Ratio of specific heat.

ρ Density.

CHAPTER ONE

1.1 GENERAL INTRODUCTION

Swirl is used extensively in combustion systems as a means of increasing mixing rates, reducing the flame size,improving the completion of combustion, reducing pollutants and stabilizing the flame. Swirl is thus a powerful aerodynamic "tool" in the hands of the designer and need to be better understood if full advantage is to be taken of it. The swirler investigation in the present work have applications in lean burning primary zones of gas turbine combustion chambers and in furnace burners.

Conventional gas turbine combustion chambers essentially consist of three main sections. These are primary, intermediate and dilution zones. A typical schematic diagram of the three zones is shown in Fig.1.1. The most vital section for the combustion chamber designer is the primary zone since combustion of fuel is initiated in this section. Conventional primary zones involves complex aerodynamics with large spatial variation in air/fuel, temperature and turbulence(1-5), and it is these variation that result in many of the pollution problems of gas turbines. The achievement of complete combustion in the primary zone which was the aim of the present work reduces the need for other sections of the combustor especially that of the intermediate zone, fulfilling the requirements of small size and weight which are of importance area in gas turbines. For industrial gas turbines,NOx legislation exists in several countries that can only be met by using water or steam injections with an associated performance penalty. The present work is concerned with dry combustor design solutions. Using lean well mixed swirling flow primary zone. The level of reduction in NOx emission in lean primary zones is closely related to the quality of the improved fuel and air mixing and this will be decided using internal gas composition traverses.

The present work was carried out on a simulated lean primary zone gas turbine. Single and double co and counter rotating radial swirler were used to

stabilise the flame. Ahmad et al(85) investigated single axial vane swirlers for lean primary zone applications. They showed for both single and counter rotating swirlers that the radial flame propagation was very slow due to the large swirler size relative to the combustor diameter. It was concluded that a larger expansion ratio from the swirler was necessary to ensure rapid flame spread. In the present work this was much easier with the radial swirlers as the swirler diameter can be varied without changing the flow area or swirler pressure loss. This is due to the ability to change the radial passage depth as the swirler diameter is changed so as to maintain the same flow area.

In previous investigation of radial swirler system for low emission gas turbine combustors, the radial passages have been carried through a bend into annules around a central fuel injector, thus becoming a form of axial swirler but with the benefit of greater passages fuel and air mixing time(173). In the present work several fuel injection system were investigated to achieved different mixing by the turbulence generated at the shear layer of jet boundary. Good mixing between fuel and air will reduce the size of the zones of highest temperature and hence the NOx emissions. Thus NOx emission will be sensitive to the method of injection into the same turbulent swirling shear layer.

Staged combustion is used to modulate combustion stoichiometry so that NOx and CO emissions are both well controlled at high and low powers. The most common type of staged combustion is the rich-lean concept. However, staged combustion can be more complex and involve various fuel injection locations and types of injectors, various combustion regions, variable air flow geometry and sophisticated fuel scheduling. In the present work double swirler staged combustion was investigated with a lean-lean concept, which involved air and fuel staging to permit the completion of combustion efficiently and with low NOx emissions. Combustion aerodynamics were investigated using a full size perspex water study the flow pattern generated by the radial swirlers.

1.2 SWIRL REVIEW

1.2.1 INTRODUCTION

The generation of swirl in a flowing medium is simply the impartation of a tangential or azimuthal velocity component to the flow. Various modes of swirl generation have been used to accomplish this task(6): 1-Guide vanes, 2-Tangential entry swirler, 3-Rotating honey comb(7) or thick perforated disk, 4-High speed rotating of a pipe(5) and 5-Ijmuiden or moveable-block type swirler(6,9).

Obviously several structural or geometrical perturbations may exist for each mode of swirl generation with their accompanying disparities in swirl generation efficiencies and resultant velocity profiles. Since the velocity profiles existing from the swirler determines, in part, the downstream flowfield aerodynamics, it is important to examine the shape of such profiles. The tangential velocity profile is generally discused in terms of the forced vortex flow. Forced vortex flow is categorized as a subset of rotational flow. A float or marker following circular stream lines in rotational flow will rotate about its own axis (in Eulerian sense). Free vortex flow which describes the approximate motion in tornadoes and whirl--pools, is classified as an example of irrotational flow. A float in irrotational flow will flow a circular stream line without rotation about its own axis. Additional characteristics, such as the tangential velocity distribution, the angular velocity, the vorticity (at a point), and the circulation, which describe the forced and free vortices are given in ref(6,17). Tangential velocity profiles issuing from swirl generators generally assume a combination of the forced and free vortex distributions. The mean tangential velocity in the field must go to zero on the axis of symmetry, and hence, solid-body rotation necessarily exists in the centreline region. Since the tangtial velocity must go to zero either within the enveloping stagnant fluid (free jet) or at the reaction chamber wall (enclosed jet). A free vortex distribution, form a resultant profile denoted as the combined, Burgers or Rankine vortex. The terms forced and free vortex serve as rough guides for the

apparent behavior of the vortex. The location of the tangential velocity maximum and its interaction with the axial velocity profile constitute critical elements in the downstream aerodynamics, The central forced vortex region exhibits flowfield and turbulence characteristic which appear to be significantly different from those displayed by the surrounding irrotational vortex flowfield. This central region is often defined as the inner viscous or vortex core. The vortex core(6,10-14) is described as being "shear" or "strain" free, but not vorticity free. The core is generally limited to that region of flow with substantial rigid-body rotation, but the core boundary has also been extended to the radius of maximum tangential velocity.

1.2.2 VORTEX BREAKDOWN

Concentrated vortex cores as a function of swirl magnitude and Reynolds number, exihibit a number of remarkable features. As swirl and / or Reynolds number are slowly increased, a number of different flow states or disturbances emerge. Each disturbance forms in the evolutionary heirachy (numbered, by Faler and Leibovich(15)) in reverse order from six to zero, generally migrater to a new position somewhat upstream from its predecessor. They used a dye filament to study swirler aerodynamics. At the near zero degree vane-setting the central dye filament traced the inner vortex core without a noticeable change. As the swirl level was increased a slight oscillatory behavior was initiated at a particular downstream location. The oscillation increased in amplitude with axial distance downstream until the filament is broken up. For large swirl, the "bubble" or near-axisymmetric breakdown (disturbance type 0 and 1) evolve from the spiral breakdown.

It is this breakdown form which is most prevalent in axisymmetric swirling flow in tubes, and which has been extensively studied both experimentally and theoretically. The near-axisymmetric breakdown is identified by a slowly varying vortex core which undergoes an abrupt and rapid deceleration, forming a free stagnation point followed by a region of flow reversal. The dyed filament within

the core appears to spread symmetrically and smoothly from the stagnation point and to enclose the recirculation region. A pronounced divergence and swelling of the stream surfaces occurs near the axis, However, the aft or near portion of the recirculation bubble generally is not closed, due to a complex filling and emptying process which exchanges fluid between the recirculation zone and the exterior flow. Immediately downstream of the bubble, a new vortex core is established which is significantly larger than the vortex core upstream of the bubble. The axial velocity distribution within the core may resemble the velocity defect profile of a conventional wake behind a solid obstacle. The new core may deflect, often forming a second vortex breakdown form, before breaking into large scale turbulence. At large swirl only the bubble breakdown form is evident.Increasing the swirl will move the bubble upstream until it reaches a solid boundary. Further increases in swirl may eventually form a "Columnar" vortex with reverse flow a long the entire axis. This was seen in the water flow visualization studies in the present work.

Divergence of the stream tubes must occur at the stagnation point since the core cannot convectively penetrate the recirculation zone. Only fluid originating from the centre of the upstream vortex core may attain entrance to the nearly closed axisymmetric bubble, either by a circuitous route through an injection (filling) location at the rear of the bubble or by viscous diffusion (assuming a laminar approach flow). The amount of fluid actually recirculated from the upstream core is usually relatively small compared to the total inlet flow rate(16). Vortex breakdown also redistributes the azimuthal velocity in the vicinity of the bubble envelope (17,18,19,20). Fluid particles adjacent to the bubble boundary travel on trajectories which originate near the tube axis and thus carry little angular momentum As a fluid particle flows radially outward in its traverse around the bubble, angular momentum must be conserved (except for viscous effects), forcing the region of the exterior bubble surface to exhibit a very low tangential velocity.

In some turbulent approach flows, however, swirl velocity magnitudes are not diminished within the recirculation zone. This substantial radial transfer of circumferential velocity to the bubble is probably associated with turbulent diffusion mechanisms(19,21). The direction of the spin of the swirl component within the reverse flow zone is in the same direction as the exterior flowfield(15). An increase in the swirl level tends not only to move the bubble upstream, but also tends to increase the rotational frequency of the tail and to move the location of the emptying tail closer to the axis(15). Not only does vortex breakdown provide evidence of complex azimuthal asymmetry, but it also displays unsteadiness in the axial direction(16,21). These axial excursions are completely random and take place about same mean breakdown position. The axial drift may range from very small lengths to distances on the order of thew chamber radius, but it generally does not exceed the order of a few vortex core diameters. Vu and Gouldin(19) suggest that the strong diffusional effects in turbulent flowfields may dominate the inertial effect in the wake region preventing the second breakdown.

1.2.3 PRECESSING VORTEX CORE

Vortex breakdown is believed to be the phenomenon primarily responsible for centreline recirculation zone formation in many swirling combustion systems, and not simply a precursor to a higher Reynolds number mechanism(21,23). Although the Reynolds number for such systems are usually large and well into the turbulent regime, periodic oscillations and associated instabilities are still prevalent. The predominant nonaxisymmetric, 3-D time dependent coherent structure is often referred to as the precessing vortex core, or simply as the PVC. The PVC has been documented pictorially in a number of visualization experiments(17,24,25,26,27). Gouldin and his colleagues(19,21,28) believe the oscillations which their systems experienced were associated with the lower energy fluctuating and axial excursions, rather than large energy PVC. The PVC is defined as a central forced vortex core which becomes unstable and begins to precess about the axis of symmetry. The PVC is usually situated in the immediate vicinity of, but outside of, the reverse flow zone boundary(13,17,24,25,29,30,31).

The reverse flow zone may act as the feedback mechanism for the PVC(32).

The definition of the term PVC has also been extended to encompass precessional vortex behavior in the wake, in which the PVC appears to wind around in the axis in rotating spiral configuration(26,27). The PVC is responsible for high levels of fluctuating pressure and temperature(24,25,29) and for the associated high levels of turbulence mixing within (or near) the recirculation zone envelope(13,29). The apparent turbulence intensity levels, of times maximising near the centreline, may be raised above their true base values by the precession or unsteadiness of the core (11,21).

Although the phenomenon of precessing vortex cores may be patentially beneficial in the sense that it promotes mixing and aids in extending the range of flame stability, it is usually not a desirable characterestic in industrial burners. The large PVC may couple resonantly with fundamental modes of oscillation in the furnace, thus creating violent flame pulsation and noise pollution at levels above the normal combustion roar(24). A survey of the conditions under which the PVC is damped or amplified has been conducted by Syred and co-workers (13,24,25,29,31). The classic reasoning for the disparity in PVC stability is borrowed from the Rayleigh criterion advocated for axisymmetric disturbances in inviscid flow with zero axial mean flow but it has served as a precursor for Richardson numbers and more complex stability analyses. The Rayleigh criterion proposes that a system is:

1- Stable if ρwr increases locally with r (e.g Isothermal forced vortex).

2- Neutrally stable if ρwr is constant with r (e.g Isothermal free vortex).

3- Unstable if ρwr decreases with r.

For isothermal system, the free vortex segment of an idealized Rankine profile dictates that disturbances are not suppressed. In fact, small deviations from the free vortex profile could easily amplify the disturbance. Accordingly, the precessional trajectory of PVC is situated outside of the reverse flow boundary near the radius of the maximum azimuthal velocity(24). The enhanced PVC

damping effect noted(24,31) for diffusion flames may be explained by the positive radial density gradient induced by the annular ring of air around the flame. The excited instability of the premixed flames seems to be associated with small negative radial density or pressure gradients(31).

Despite the detailed observational studies of vortex breakdown an acceptable theoretical understanding of the phenomenon has proven elusive. However, the existence of a centreline reverse flow zone may be parially understood from a simplified analysis of the role of pressure and centrifugal forces. If it is assumed that the flow field upstream of a breakdown varies little in the axial direction (axial gradients much less than radial gradients) and that the streamtube surrounding the vortex core is essentially cylindrical, the corresponding simplification to the equations of motion is termed the "quasi-cylindrical" approximation(11,18,19,33). Application of the quasi-cylindrical approximation to the radial component of momentum, with the added assumption of axisymmetric, steady-state laminar flow yields:

$$\frac{dP}{dr} = \rho\frac{w^2}{r} \qquad \text{....(1.1)}$$

The above equation represents a balance between the centrifugal forces accelerating a fluid volume and the restraining pressure force which is transmitted to the walls of the tube enclosure. If the fluid particles were released from the constrains of the enclosure the particles would tend to trace a straight line of flight tangent to their original circular trajectory(6). Integrating equ.1.1 with respect to r from the axis to the reactor wall and then differentiating with respect to x, the resultant expression is equ.1.2:

$$\left(\frac{\partial P}{\partial x}\right)_{r=0} = \left(\frac{\partial P}{\partial x}\right)_{r=R} - \frac{\partial}{\partial x}\left(\rho\frac{w^2}{r}\right)dr \qquad \text{....(1.2)}$$

The first term on the right hand side is relatively small, although it may apparently be negative(21), positive(33), or identically zero (if the upper integration limit is radial infinity). The integrated angular momentum term on the right hand side generally decays continuously with axial distance down the

reactor inducing a significant adverse (positive) axial pressure gradient along the symmetry axis. This type of adverse axial pressure gradiant was found in the present work. when the centreline adverse pressure gradient is sufficiently steep to completely decelerate the axial flow, vortex breakdown ensues. It should be noted that eq.(1.1) and (1.2) apply only to upstream "cylindrical" flow; when the recirculation zone begins to form and axial gradient become appreciable, the quasi-cylindrical equations must fail, just as boundary layer equations must fail at the point of incipient separation(22,33,34)

The decay rate of the integrated angular momentum term in eq.(1.2) in the laminar case, is subject to the convective or inertial terms in the momentum equations, as well as viscous dissipation or transport. However, the abruptness or rapidity of the onset of the breakdown transition as well as an order of magnitude analysis of the terms in the Navier-stokes equations, suggests that the dominant underlying mechanism for vortex breakdown is inertially controlled, viscous diffusion forces being secondary(20,22,35). For that reason, inviscid wave and stability theories, which rely particularly on the quasicylindrical equations (without the viscous terms), have been used extensively for the study of disturbance mechanisms in vortices (22,34,36,37).

Ribeiro and Whitelaw(38,39) claim that the upstream swirling flowfield is initially dictated by inertial forces, but gradually becomes more dependent on turbulent diffusion as the centrifugal effects decay. Gouldin et al(21) argues very strongly that turbulent momentum transport is significant only in the regions of large mean velocity gradients and turbulence intensities, such as in the mixing shear layer between concentric jet or in the vicinity of the reverse flow zone. The approach flow, in which the formation breakdown mechanism operates is only weakly influenced by dissipative or turbulent diffusional processes.

1.2.4 REVERSE FLOW ZONE

In an isothermal or inert jet, swirl acts to enhance the rate of jet growth, entrainment, and mean velocity decay relative to a nonswirling jet(30,40,41). In a

reacting system, the swirl induced, toroidal recirculation zone primarily aids in flame stabilization. Flame retention requires that there an adequate flame velocity and that sufficient heat is conveyed for stable ignition(6). In a non swirling flow field, the flame stabilisation mechanism (fluid mechanical) is controlled either by a wall boundary layer velocity gradient or a recirculation zone / eddy induced by a reaction chamber expansion or a mechanical flame holder. In swirling flow systems the recirculation zone, engendered by vortex breakdown, provides the aerodynamic blockage and reduced velocities necessary to stabilize the flame(30,42). The recirculation zone has traditionally been regarded as a reservoir or store of heat and active chemical species(6,17,31,42,43). The reverse flow zone cyclically transports hot combustion products from downstream region into the flame. The high temperature products , despite the dilution effect, serve as an energy source for preheating(44), fuel preparation such as evaporation and devolatilization (45) and ignition assistance(30).

While the heat source effect does play a role in flame stability, the predominant mechanism is thought to occur via turbulent transport(28,45,46). Between the forward flow and the reverse flow zone boundary is a region of steep velocity gradients and high intensity turbulence, which promotes high intensity turbulence, which promotes high entrainment rates and rapid mixing between the fuel and air (in diffusion flame systems). Hence, the recirculation zone is regarded as a well mixed region, in which large turbulent diffusion prohibits complete recirculation, and in which flame stabilization is provided by intimate mixing of hot active species and fresh reactants. As a results of the high entrainment and increased mixedness of the jets, swirl reduces both flame lengths and flame attachment length and consequently shortens the combustion chamber length necessary for complete combustion(17,30,42). Swirl also promotes high combustion efficiency, easy ignition, reactant residence time, pollutant optimization, potential and widened stability and blow-off limits(30,47,48). The blow-off velocity is the mean axial velocity of air and fuel at which flame extinction occurs For non-swirling systems, the optimum fuel/air ratio for

maximum fuel through put lies well into the fuel lean regime; consequently, the fuel through put load at the stoichiometric ratio, near which it is often desirable to operate industrial burners, is relatively small. One of the major benefits of swirl is that it displaces the optimum fuel/air ratio towards the fuel rich regimes that occur during normal process operations and also enlarging the blow-off limits(17,45,49,50).

1.2.5 EFFECT OF SWIRL LEVEL

1.2.5.1-In Isothermal System

A large number of experimental research facilities where swirling flow studies have been conducted, have yielded a wide variation in parametric effects and observations. Differing swirl generators, swirler outlet geometries, chamber geometries, flow rates and fuels, all produce details and differences which may not be easily resolved. With an increase in swirl level, the breakdown recirculation zone bubble has generally been observed to migrate upstream toward and oftimes into the inlet pipe not only in experimental studies(15,19,51) but also in theoretical predictions(52,53). This latest effect can not occur in practicle axial and radial vane swirlers. An increase in swirl with large expansion from the swirler expands the width of recirculation zone somewhat but particularly increases the length(6,25,31,41,54,55). Theoretical prediction also display the same qualitative effect(26,44,53,56). The extent of the expansion tends to approach an asymptotic limit dicated by the chamber or inlet confinement(25,31,41,57).

After the initial expansion, well established recirculation zones may either remain essentially unaltered in size with an increase in swirl level(57,58) or begin to decrease in length with significant increase in width (31,59,60,61,62,63). Other perturbations may also exist at high swirl such as reverse flow extending over the entire length of the furnace(54) approaching columnar back flow, or a forward velocity region, surrounded by an annular reverse flow region developing in the aft section of the bubble(64). Recirculated mass flow rates increase with swirl magnitude (25,31,57,64) and vary greatly. Quoted values, expressed as a percent

of the inlet flow rate range from 10% or less(17,19,46,57) to 25% (25,42,55) to 50%(31), and even to 82%(43). In accordance with the recirculated mass flow rate, both forward and reverse mean velocities have been observed to increase with an increase in swirl strength(19,31,55,57). The same trend is also followed by the turbulent kinetic energy(19,25,41,57,61). Increased swirl consequently promotes greater jet spreading angles mixedness, reduction of the potential core and transport variable decay(6,30,41,59,65).

1.2.5.2-In Combustion Systems

Flame interaction with a bubble recirculation zone displays an evolutionary history as the swirl strength is systematically varied. Leukel and Fricker(58) describe two separate flame characterizations drived from their IFRF trials. The natural gas diffusion flame, with relatively low secondary swirl or high primary flow rate, produced a "bubblous" combustion zone near the inlet with a long luminous flame "tail" i.e type 1 flame. Here, the fuel jet had completely penetrated the recirculation zone forming an annular "doughnut" reverse flow region. Similar results were found by Syred et al(31). The long flame tail appeared to be a consequence of delayed mixing within the oxygendepleted core. A second flame structure, at high swirl or low primary flow rate, displayed a short and intense blue flame (i.e type 2 flame) In this case the recirculation zone had sufficient strength relative to the primary fuel jet to force the fuel through an abrupt radial arc a way from the centreline, circumventing the bubble. thus, it can be seen that increased swirl, as result of intensified mixing generally produces a decrease in flame length(41,48), as well as moving the flame upstream(46,66). Claypole(25) , Beltagui and MacCallum(57) provides detailed description of four flame type, lettered "a" through "d". Under weak swirl or type 'a' conditions, no recirculation zone is formed and a long, yellow turbulent diffusion flame stabilizes at a detached location remote from the inlet nozzle. At a slightly incremented swirl strength, a small recirculation zone forms with the flame stabilized in low velocity highly turbulent wake region. This type 'b' flame retain characteristics very similar in nature to the IFRF type 1 flame. Larger swirl levels

significantly increase the strength of the reverse flow zone. The flame type 'c' moves upstream into reverse flow region and stabilizes on the envelope of the recirculation zone as a pure blue flame, which is very reminiscent of the IFRF type 2 structure. The 'tulip-shaped' type 'd' flame, which exists at even larger swirl levels, retains the basic type 'c' appearance with added detail that the recirculation zone has grown in length and row extends downstream of the main flame region A high level of radial turbulent diffusion is apparent at the recirculation zone boundary. Both entrainment of fresh reactants into the unreacted forward flow occur, with subsequent quenching. The reverse flow zone is characterized as a well uniform mixed region with a uniform temperature distribution. However, the maximum temperature generally appear to lie immediately within the bubble envelope in an area reasonably coincident with the location of the PVC and maximum turbulent kinetic energy(17,24,43,44,57).

1.2.6 COMPARISON BETWEEN ISOTHERMAL AND REACTING FLOW

A combusting system affects the flowfield by accelerating the axial mean velocity, expanding the gas, and decreasing the density(67). The interaction of such an effect upon a given inlet swirl level may, in part be intuitively deduced by examining the swirl number. The swirl is useful as a relative measure of the azimuthal momentum imparted to the flow and is approximately defined as the axial flux of angular momentum divided by the product of the appropriate limiting radius and the axial flux of axial momentum. Both the numerator and denominator are idealistically conserved in a free, isothermal system. The temperature increase and gas acceleration accompanying reaction serves to increase the jet momentum quantity in the denominator relative to the angular momentum term in the numerator, thus decreasing the apparent swirl number at a given axial location. Therefore the evolutionary and transitionary recirculation patterns observed in isothermal systems may necessitate a somewhat larger inlet swirl number in combusting systems to generate a recirculation bubble of comparable magnitude, strength and location.

Comparisons between the isothermal and reacting counter parts generally confirm the above expectations(19,54). Both predictions and observations demonstrate that combustion usually causes the recirculation bubble to slightly increase in width and reduce in length(25,30,43,44,57,68). Although the width or size of the recirculation zone may have increased with combustion, the recirculation mass flow rate is lower because of the appreciable decrease in density(17,25,30,44,57). The reverse velocities in combustion systems appear to be higher than the isothermal equivalents(44,47,57,68) due to the lower density, but the turbulent kinetic energy or rms velocities may be either lower in combusting systems(25,41) or higher(30,47,68,69). Burning jets with swirl may expand more rapidaly with an increased rate of jet spread than the corresponding isothermal jets(48,57). However, downstream mean velocity decay in combusting systems tends to be less than the decay observed in isothermal systems (41,44).

1.2.7 COMBUSTOR GEOMETRY EFFECT ON RECIRCULATION ZONE

The location and the shape of the recirculation zone are a function of the various inlet and swirl generator configurations, enclosure size extent of reaction and any other factor which manipulates the imposed pressure gradient. Confinement has been observed to noticeably affect the central recirculation zone dimensions(54,70). In particular, the maximum width and length of a bubble are observed both experimentally (31,57) and theoretically(44) to increase with the chamber diameter. The initial spreading rate of enclosed jets appears to be noticeably more rapid than the corresponding unconfined jet, although opinion differs as to which offers the stronger or more pronounced reverse flow(57,59). Syred et al(31) suggested that smaller chamber diameters reduce the interference between the flowfield and the furnace enclosure, thus providing a recirculation zone which is longer and more advantageous for flame stabilization. An inlet quarl encourage the swirling jet to follow the slope of the wall, thus promoting stream tube divergence and intensifying the centreline adverse pressure gradient. Such divergent nozzles aid in swirling flow deceleration and augment the

existing reverse flow, or reduce the swirl number necessary to achieve a particular level of recirculation(6,17,21,25,30,42,43,60). Numerical predictions also support this conclusion(26,53). Chamber exits with a convergent angle or with contraction blocks positioned at downstream location may have an opposite effect(60-62,71). The contraction nozzle accelerates the flow producing a favorable pressure gradient which is superimposed on the adverse pressure gradient promoted by swirl. Hence, in certain cases where the contraction is strong enough to influence the upstream flowfield, the size of the bubble is diminished. Any means of changing the pressure field, such as hub or bluff body along the inlet centreline or a mass flux imbalance between the primary and secondary jets, may have pronounced effects on the wave reinforced vortex breakdown. Experimentation dealing with influence of various inlet configurations swirl generators, fuel injectors, quarl lengths and angles,confinement ratio, etc. has been performed by several investigators(17,25,30,31,45, 57,58,59,70,72).

1.3 SWIRL FLOW CHARACTERISTICS

1.3.1 Swirl number

Experimental studies have shown that the flame size, shape, stability and combustion intensity are affected by the degree of swirl imposed on the flow. This degree of swirl is denoted by the swirl number S, which is a non-dimensional number characterizing the amount of rotation imposed to the flow. In general the swirl number defined by Beer and Chigier(6,9) as the normalized ratio of the fluxes of angular and linear momentum is now widely used for characterizing the intensity of swirl in enclosed and fully separated flows. The parameter can be given as:

$$S = \frac{G_\phi}{G_\chi \, . \, D/2} \qquad \ldots.(1.3)$$

Where

G_ϕ = axial flux of angular momentum

G_χ = axial flux of axial momentum

$\frac{d}{2}$ = equivalent nozzle radius

These can be written as:

$$G_\phi = \int_0^R 2\pi\rho w r^2 u \, . \, dr \qquad ....(1.4)$$

$$G_\chi = \int_0^R 2\pi\rho (u^2 - \frac{w^2}{2}) r \, dr \qquad ....(1.5)$$

or alternatively a static pressure distribution instead of $\rho \frac{w^2}{2}$ may be used in the expression for G_χ For cases where mixing at the boundary of the recirculation zone is dominated by the action of a precessing vortex core another parameter is required for characterization of rotating flow. Claypole and Syred(114) proposed a geometrical swirl no. S_g which was taken as non-dimensional measure of the tangential momentum supplied to the flow and if the perfect mixing on conservation of momentum is assumed, then the swirl no. can be defined in terms of the geometry of the combustor, where:

$$S_g = \frac{r_0 \pi r_e}{A_t} (\frac{\text{tangential flow}}{\text{total flow}})^2 \qquad ....(1.6)$$

where

A_t = Area of tangential inlets.

r_e = Radius of the exit of the combustor.

r_0 = Radius of the tangential inlets from the centre of the combustor.

Beltagui et al (1) have correlated their results for flow conditions under which the CRZ appeared in their furnace, by a swirl number S_* which was based on the furnace and not the swirler diameter. The critical value for establishment of the CRZ was found to be 0.11.

Various investigations on the effects of swirl on the flame stability have shown an increasing fuel/air mixing as the degree of swirl was increased (45,90,91). The size and strength of the central recirculation zone also increases by an increase in swirl intensity (55). At low flow rates or swirl number a long, yellow and highly

luminous flame is produced (90) indicating a poor mixing. However, when the swirl number is increased, the CRZ increases in size, initially in width until restricted by the diameter of the combustor and then begins to increase in length (90). Measurements of flame length and stabilisation distance carried out in a series of Butane-propane-air flames with swirl (91) have shown that both decrease markedly with increasing degree of swirl. In the present work swirl number has been suggested based on the mean swirler outlet axial velocity (based on the outlet area) for axial momentum and the tangential vane passage outlet velocity (based on minimum flow area) for the tangential momentum. As will be discused in the following chapter.

1.3.2 CENTRIFUGAL EFFECTS

An advantage of swirling flow combustion is the fact that a centrifugal force field, present in swirling or vortex flow, tends to accelerate the mixing of two flows having different densities and thus increase the reaction rate in the combustion processes (90). The importance of the centrifugal forces have been neglected until recently (90,92-94). The centrifugal forces act on pockets of burnt gas having lighter densities, to move them inwards relative to heavier unburnt gas. This can greatly increase the rate of mixing if the combustion is initiated at the periphery rather than the central region. In the latter case the rate of mixing can be retarded by the movement of light burnt gases inwards to the rich centre core (95) and forcing the air to the outer region. It can be shown that the diameter of a liquid droplet at equilibrium in a swirling field is proportional to the distance from the centre of the rotation. Thus the heavier fuel droplets will be in the outer region of the swirling flow relative to the lighter or smaller diameter droplets.

The centrifugal force acting on the droplet must be equal and opposite to the drag force.

$$\text{centrifugal force} = \text{drag force}$$

$$\rho_d \cdot \frac{d^3}{6} \cdot \frac{V^2_{tan}}{R} = C_d \cdot 1/2 \cdot \rho_a \cdot V^2_{rad} \cdot \frac{\pi d^2}{4} \qquad \text{....(1.7)}$$

where

ρ_d = Droplet density

ρ = Air density

V_{tan} = Tangential velocity of fuel droplet and air

V_{rad} = Radial inward velocity of air

d = Droplet diameter

R = Radius of swirl flow

C_d = Drag coefficient

Assuming small Reynolds number at the vicinity of the droplet, the stokesian flow exists. Thus

$$C_d = \frac{24}{R_e}$$

and

$$R_e = \rho_a \cdot V_{rad} \frac{d}{\eta}$$

where R_e is Reynolds number of flow and η is air viscosity. Also assuming a free vortex flow

$$\frac{V_{tan}}{V_{rad}} = \text{constant}$$

Therefore equation (1.7) becomes

$$d \cdot \frac{V_{tan}}{R} = \text{constant}$$

In free vortex flow

$$V_{tan} \cdot R = \text{constant}$$

Therefore $d \sim \text{constant} \cdot R$

This shows that larger droplets will be sent to larger radius from the centre of rotation and hence close to the wall relative to the smaller droplets which stay close to the centre. Swirl in variable density flows may suppress or enhance turbulence (96). For swirl combustion, this interaction is significant and may not be neglected in turbulence model development.

be neglected in turbulence model development.

Investigations on the effects of centrifugal force in swirling flows are rare (97-101). Lewis (102) investigated the effect of centrifugal forces on a stoichiometric mixture of propane and air in a rotating pipe combustor. His results showed that appling a centrifugal field to a burning fuel-air mixture can substantially increase the rate of combustion.

The need for proper aerodynamic design to most effectively use centrifugal effects to increase fuel evaporation and subsequent mixing was outlined by Shekleton (103). He showed that substantial benefits can be achieved by the use of centrifugal force to control combustion (93). He concluded that fine and accurately located fuel droplets dominate the design of the typical small vortex combustors.

1.3.3 SWIRLER PRESSURE DROP

Fuel/air mixing in gas turbine combustors are important both in terms of emissions (104,105) and for future poorer fuel quality (106,107). The problem of coal derived gaseous fuels with low calorific values and high combustion exit temperatures (108,109) and heavy residual fuels (110,111) all involve improved mixing within the combustor as a key element in the solution of these problems.

To achieve rapid fuel and air mixing downstream of a swirl stabiliser, turbulence must be generated to promote the mixing. Turbulent energy is created from pressure energy dissipated downstream of the stabiliser. In swirlers, turbulence can be generated by increasing the blockage or pressure drop of the swirler. This can be done by a number of ways with the axial swirler(85):

a) increasing the degree of swirl, b) decreasing the swirler outer diameter (d/D) or increasing the swirler hub diameter, c) increasing the number of vanes. All these factors also increase the size of the recirculation zone. An increase in the size of the recirculation together with the turbulence generated in the shear layer region can increase fuel/air mixing significantly. In the present work the

swirler diameter can be varied without changing the flow area or pressure loss. This is due to the ability to change the radial passage depth as the swirler diameter is changed so as to maintain the same flow area.

Values of pressure loss in a typical gas turbine combustor lie between 2 to 7% (59) at reference Mach number of 0.047 (155). The pressure loss can be calculated by using the following equation:

$$\frac{\Delta P}{P} = \frac{\gamma}{2}\left(\frac{M}{C_D} \cdot \frac{A_1}{A_2}\right)^2 \qquad \text{...(1.8)}$$

where

$\frac{\Delta P}{P}$ = swirler pressure loss

γ = ratio of specific heat

M = air flow Mach number

C_D = swirler discharge coefficient

A_1 , A_2 = combustor and swirler open area

The calculation of swirler pressure drop and discharge coefficient are detailed in Appendix (A1) together with the correction of the pressure drop to a reference Mach number and the calculation of Reynolds number.

1.3.4 Combustor wall static pressure

The flow aerodynamics downstream swirlers of various pressure losses are different due to the change in the recirculation zone size, flow expansion, wall impingement, etc. These variations have a direct effect on the wall static pressure (5), the profiles of which can be a good indication of the flow aerodynamics inside the combustor. i.e. flow impingement, recirculation zone size, etc (31).

Syred et al (31) showed that the centrifugal forces present in the swirling flow affect the radial static pressure distribution at any given section in the combustor. The radial pressure profiles were obtained by integration of $\rho W^2 / r$ (centrifugal force) across a given radial section

$$\int_0^R dp = \int_0^R \rho \frac{w^2}{r} dr \qquad .....(1.9)$$

where

p = static pressure

ρ = density

w = tangential velocity m/sec

r = radius

1.3.5 SWIRL STABILISED FLAMES

The primary zone air flow pattern of gas turbine combustors is of major importance to flame stability. Various types of air flow pattern are employed, but one feature common to all is the creation of a toroidal flow reversal. This toroidal vortex system plays an important role in flame stabilisation since it entrains and recirculates a portion of the hot combustion products to mix with the incoming air and fuel. The high intensity turbulence that prevails in the vortex region continously transports heat and mass from combustion products to the fresh combustible mixture.

One of the most effective ways to induce flow recirculation in the primary zone is by fitting a swirler around the fuel injector. A toroidal vortex type recirculation zone is set up in the central region in the wake of the swirler if the angular to linear momentum ratio exceeds a critical value. This type of recirculation zone may provide better mixing than that obtained by other means such as bluff bodies. This is because of the strong shear regions, high turbulence and rapid mixing rates produced by the swirling action. Swirlers have other advantages in that the presence of a solid surface exposed to high temperatures is reduced and the deposition of coke such as occurs on bluff bodies in heterogeneous combustion is also reduced.

These advantages have le d to air swirlers being widely employed in furnaces and gas turbine combustors (1,6,17,28,31,59,66,72). Swirlers can be of various types, single (20) or double with co or counter rotating air flows (21,22), or radial

swirlers (23). The swirl vanes are often flat for ease of manufacturing, but curved vanes may sometimes be preferred for their potentially better aerodynamic properties (24).

The recirculation zone in swirl flows is rather similar to a well-stirred reactor since the temperature and gas composition within the reverse flow zone are almost uniform (25). The levels of temperature and gas composition can be controlled by the nature of the fuel injection and the amount of fuel injected into the zone.

The dimensions of the recirculation zone can be varied by the degree of swirl imposed on the flow. The degree of swirl is usually denoted by "swirl number" S, which is a non-dimensional number. The recirculation zone size is also dependent on the ratio of the combustor diameter to that of the swirler outer diameter (D/d). The existence and size of the corner recirculation zone is also influenced by the D/d ratio. The blockage ratio of the swirler causes a pressure drop in the air flow which generates the turbulence necessary for fuel/air mixing. All swirling flows produce a centrifugal field in the flow which can increase the burning rate of the combustible mixture depending on the nature of the fuel injection employed.

All the above mentioned factors and their influence on the recirculation size and mixing will be discussed in the subsequent sections.

1.4 EMISSIONS IN SWIRL STABILISED COMBUSTION

1.4.1 GAS TURBINE AND FURNACE EMISSIONS

Emission performance has become of overriding concern for both the designer and user of combustion devices in recent years. Exhaust emissions that are normally considered pollutants are produced in the combustion system, either during the thermochemical reactions or in the post-flame zones. It is in the reaction zone of the combustor where most of the emission abatement work has been most effective. Emission reduction has become the most important combustion design objective, which must be optimized during the development and engineering of a combustion system for any new machine size or application.

The emissions from gas turbines which give rise to concern are generally recognised to be those of oxides of nitrogen (NOx), smoke, carbon monoxide (CO) and unburned hydrocarbon (UHC). The two former emissions occur largely at high power conditions, whereas the latter two pollutants are only problems at low power. The larger part of a typical gas turbine's operating cycle is covered at high power conditions. Therefore, concern has been centred on NOx and smoke emissions (76,77) at high power. However, the CO and UHC emissions occur largely in the vicinity of airports and for industrial gas turbines at ground level and are therefore of interest. Also many low NOx and smoke designs have a CO and UHC emissions problem at some conditions.

The engine emissions threat to the stratosphere at high power condition are mainly water vapor and carbon dioxide which could produce a green house effect on the earth's atmosphere and NOx emissions which could deplete the ozone layer. Sulfur compounds in the fuel also cause a problem for industrial gas turbines as these could lead to acid rain and particulate formation which could divert solar radiation away from the earth. This problem can be dealt with by removal of sulfur at the refinery. The pollutant of main interest for both aero and industrial gas turbines is oxides of nitrogen which could deplete the ozone layer and allow increased penetration of solar ultraviolet radiation. The reation

mechanism could be shown as:

$$NO + O_3 \text{ ----- } NO_2 + O_2$$

$$NO_2 + O \text{ ----- } NO + O_2$$

As shown above, ozone is destroyed by the first reaction and the reformation of nitric oxide NO is shown in the second reaction. The uncertainty of the importance of this reaction mechanism to the stratospheric ozone concentration has led to more intense research in the reduction of NOx emission levels.

1.4.2 POLLUTION FROM GAS TURBINES

The main atmospheric pollutants emitted from gas turbine combustors are carbon monoxide (CO), unburned hydrocarbon (UHC), oxides of nitrogen (NOx) and smoke together with combustion noise. Species concentration measurements have been performed by many investigators using gas analysers(1,5,96,112,115) and recently by new techniques (114). various investigators have examined the effects of different parameters such as inlet air swirl, pressure, fuel and air velocity, etc on exhaust emissions (28,110-113). The parameters governing the formation of the above mentioned pollutants and the techniques employed to reduce these emissions will be discused below.

1.4.3 NOx EMISSIONS

The two major sources for NOx production in vehicular and stationary combustion sources are thermal and organic NOx. NOx is the term given for the combination of NO which is mostly emitted from combustors, and NO2 which is the dominant form of NOx in lean burning gas turbines (96,119) in the exhaust of the combustors. conditions favorable to NO formation are those of high temperature, long residence time, high pressure and high oxygen availability. Nitric oxide can be produced by three different mechanisms; thermal, prompt and fuel nitrogen.

1.4.3.1 Thermal NO

Thermal NO is produced by oxidation of atmospheric nitrogen in the postflame gases (119,120). It is now well established that NO formation in combustion processes proceeds by the Zeldovich chain mechanism (121,122).

$$O_2 \longrightarrow 2O \qquad \text{....(1.10)}$$

$$O + N_2 \longrightarrow NO + N \qquad \text{....(1.11)}$$

$$N + O_2 \longrightarrow NO + O \qquad \text{....(1.12)}$$

The main reaction governing the formation of NO in fuel lean mixtures is the breakup of the strong triple bond holding N molecule together. This is done by the free oxygen from the equilibrium dissociation of unburned oxygen molecules which initiate the chain.

In their experiments on lean CO-air mixtures in a jet stirred reactor, Molte and Pratt (123) showed that the formation of NO in a low temperature fuel lean, well stirred combustion may be produced via N_2 O. They proposed a set of reaction mechanism through which N_2 O is formed and destroyed to produce NO.

$$N_2 + O + M \longrightarrow N_2O + M \qquad \text{....(1.13)}$$

$$N_2O + O \longrightarrow NO + NO \qquad \text{....(1.14)}$$

$$N_2O + O \longrightarrow N_2 + O_2 \qquad \text{....(1.15)}$$

$$N_2O + H \longrightarrow N_2 + OH \qquad \text{....(1.16)}$$

1.4.3.2 Prompt NO

Prompt NO is produced by high speed reactions at the flame front in hydrocarbon fuels (124-126,159). Fenimore (127) showed that NO is formed by the enhanced reaction rates as a result of interactions among the many intermediate species produced during the main hydrocarbon air reactions. He estimated that prompt NOx account for 30% of the total NOx emitted from gas turbines under normal operating conditions. It will be shown in the present work

that prompt NOx is a major source of NOx emissions in lean burning swirl stabilised flame.

Claypole and Syred (115) investigated the influence of levels of swirl on aerodynamics and NOx emissions. They found that the major area of NOx formation was the reaction zone in the flame front. The moderate flame temperatures and the rapid formation of NO indicated that NO was formed via the prompt mechanism. Similar results for the NO formation zone was found in the present work. Radial gas concentration profiles will be presented in the present work. These show that the prompt NO mechanism is the major source of NOx emissions from swirl stabilised combustors with central injection of fuel. The major part of NO is formed in the flame front close to the stabiliser with little burnt gas thermal NOx.

1.4.3.3 Fuel NO

Fuel NO is produced by oxidation of nitrogen contained in the fuel. The fuel nitrogen is converted to HCN in the flame zone (128) and depending on the degree of nitrogen conversion, the fuel NO can represent a considerable portion of the total NO (129).

Fuel NO does not form any part of the NO in the present work for gaseous flames. For liquid fuels, kerosene does not contain any fuel bound nitrogen (130,131), but gasoil contains a significant amount of nitrogen (in order of 50-100 ppm). The higher levels of NOx for gasoil tests in the present work may be due to this fuel nitrogen content. The work of Appleton et al(132) on vane swirled combustor at atmospheric pressure showed that the degree of fuel/air mixing was a major factor covening the degree of conversion of fuel nitrogen to NO. Unfortunately, analytical technique was not available in the present work to quentify the fuel nitrogen at 100 ppm level. Associated work on nitro-PAH(130,131) has shown the gasoil used contain NPAH.

1.4.3.4 NO_2 emissions

NO_2 which is the major source of atmospheric pollutant is formed by the oxidation of NO in the atmosphere This is because at low temperatures NO_2 is more stable than NO. Normally, NOx emissions from combustion are dominated by NO. However, evidence has shown that NO_2 can be formed in the combustor where large amounts of excess air is present (133-135). Hori(52) in his measurement of NO_2/NOx ratio in a laboratory swirl combustor, reported that it is likely that NO_2 can be formed and survive in the mixing region between the hot combustion gas and the cool air stream near the combustor wall under very fuel-lean conditions.

The sampling devices used for measuring emissions usually do so by freezing the reactions. This could create regions within the sampling probes suitable for the formation of NO_2(135,157). The extent of the conversion of NO to NO_2 in the probes varies considerably according to the probe parameters and the sample gas parameters. The measurements of NO_2 with a probe having a high cooling rate of the sample and high sample pressure, greatly overestimates the proportion of NO_2 in high temperature regions (96,112)

Sano(166)has shown by numerical simulation that NO_2 formation is to be expected in the mixing region of cool air and combustion gases. Sano(167) has also shown by simulation that NO_2 formation in mixing region should be enhanced by the presence of unburned hydrocarbons. This conclusion is supported by the experimental findings of Jaasma and Borman(168). Recent results obtained by Bromly et al(169) showed that the presence of the combustible agent UHC strongly facilitated the oxidation of the NO to NO_2. It was found that the hydrocarbons had a greater effect than either hydrogen or carbon monoxide.

1.4.4 NOx reductions

The study of emissions regulations especially that of NOx has been (136) and still is under investigation (137-139). Many ways have been adopted to decrease

NOx emissions such as water or steam injection (140), dry controls (141,142), or selective catalytic reduction (143,144). Water injection has some major drawbacks such as A) requirement of large source of water, B) reduction of thermal efficiency, C) increased CO emissions and D) increased pressure oscillations within the combustor (145). The main problem with regard to developing a catalytic combustor is the durability of catalysts. The catalysts deteriorate during high temperature operation. However, this problem can be improved (146). Premixing is an effective way to reduce NOx emissions (116,147,148). Beyler and Gouldin (28) showed that premixing/prevaporising combustors operating either on lean mixtures or on rich mixtures as the first stage of a rich-lean combustor are attractive candidates for low NOx combustors, especially in gas turbines.

Mikus and Heywood (117) in their work on automotive gas turbines concluded that leaning out the primary zone or reducing the residence time of conventional combustor designs using conventional fuel injection techniques was unlikely to reduce NO emissions enough to meet the 1976 emission standards. This was due to the presence of stoichiometric fuel/ air ratio in parts of the flow within the primary zone even if excess air was present. To achieve a significant reduction in NO emissions, combustors need to be developed with both a leaner and much more homogeneous fuel/air ratio distribution in the primary zone than is attainable in conventional designs. The present work focuses on injecting fuel in the passages between the vanes of the radial swirler and at the periphery of the wall as well as the conventional method of central fuel injection to produce such a homogeneous fuel/air ratio distribution in the primary zone and thus to reduce NOx emissions significantly. Conclusion can be made that the dry low NOx schemes seek to lower the NOx emissions through the reduction of stoichiometric regions in the combustor. This can take a variety of forms(175), (each with specific problems) including (1) premixing prior to combustion to prevent local stoichiometric region (stability and CO emission problems), (2) very lean combustion to minimize stoichiometric region (potential CO emission problems),

(3) catalytic combustion to permit very lean combustion (potential catalyst durability and transient problems), and (4) staged combustion to modulate combustion stoichiometry so that NOx and CO emissions are both well controlled (more complex combustion system and operation).

1.4.5 CO AND UHC EMISSIONS

These pollutants are sometimes, extremely low, except during start-up and very low-load conditions. Unburned hydrocarbon emissions are due to vaporized unburned fuel or partially burned products which exit the combustion reaction zone and are emitted in the exhaust. Carbon monoxide is an intermediate species of the combustion process which, after it has been formed, is one of the slowest of all the combustion reactions to reach completion. It is a well known fact that carbon monoxide is a poisonous gas and can be very harmful at high concentrations. Carbon monoxide is an inevitable intermediate in hydrocarbon combustion. Emission levels of CO can therefore only be minimized by completing, as far as equilibrium allows, its oxidation to carbon dioxide. Conditions favourable to its oxidation are high temperatures, oxygen availability, high pressure and long residence time. The predominant mechanism for CO oxidation is (149,150)

$$CO + OH \text{ ------ } CO_2 + H \qquad ....(1.17)$$

Investigations in both experimental and theoretical techniques have shown that CO formation and destruction are kinetically controlled (154,155).

Unburned hydrocarbons are the main source of the odors at the vicinity of the airports. On its own, it does not posses any major threat to the environment. However, together with nitrogen oxides and the presence of sunlight, it can produce a 'photochemical smog' which is usually prevailing in large cities.

Conditions favourable to CO oxidation such as those mentioned above are also beneficial for hydrocarbon combustion. The trends for UHC emissions, therefore, follow those for CO emissions (153). In practice, it is found that

engines capable of meeting CO emission standards are generally capable of meeting the UHC standards too (154). However, an additional factor in UHC emissions could be due to quenching of hydrocarbon oxidation near the combustor wall at idling conditions, or poor fuel/air mixture resulting in locally rich zones in the combustor (153,155). The present work also shown that in general CO emissions dommenat the inefficiency except very close to the weak extinction when UHC becomes more important.

1.5 FLAMMABILITY LIMITS IN SWIRLING FLOW

Not all fuel-air mixtures will burn, flames can propagate through fuel-air mixture only within certain limits of composition if small a mounts of combustible fuel gas or vapor are added gradually to air, a point will be reached at which the mixture just becomes flammable. The percentage of fuel gas at this point is called the lower flammable limit, or weak limit or lean limit. If more fuel is added another point will eventually be reached at which the mixture will no longer is called the upper flammable limit or rich limit. Analysis of experimental data suggests that the weak limits for aparticular fuel correspond to minimum flame temperature for methane this is about 1400 K, as compared to stoichiometric flame temperature of about 2200 K(160).

1.5.1 Flame Stability

In swirling flames there are many factors that could cause blowoff, i.e cause the contours of zero axial velocity, fuel concentration, and air concentration not overlap properly. Rawe and Kremer(50) found that excessive swirl can impart centrifugal forces that force the fuel-air contours to move too far radially outward and thus eliminate the critical region of overlap Fig.1.2.

Claypole and Syred(25,46,115) have shown that for swirl flows with recirculation, the flame stabilises on the recirculation zone boundary with majority of the chemical reaction downstream of the recirculation zone(115). The

mechanism of flame stabilisation in this region is similar to the mechanism of flame stabilisation behind a bluff body in that the flame stability in well stirred shear layer regions in the wake of the reverse flow zone in which the low temperature fresh reactants become intimately mixed with hot active species(25). They have also shown that there was a little reaction in the reverse flow zone which contains burnt gases inside the recirculation zone by the centrifugal force action. Claypole and Syred(25) shown that the maximum root mean square(R.S.M) velocity contours in the combustion lie on the boundary of the high temperature reverse flow zone and they are of similar levels to those in the isothermal case. Furthermore, they found(176) that the location of the flame was a function of turbulent flame speed and not the equivalence ratio, assuming that the flame front was in the mean temperature range of 1200 to 1400 K and was formed when the coherent eddy structures grew in size until a point was reached where the increase in the turbulent Reynolds number produced a turbulent flame speed equal to the local non-isotropic turbulence intensities(L.T.I) which were based on the total root mean square(R.M.S) turbulent velocity component and the vector sum of local mean velocities. They also shown(25) that increasing the swirl number would move the flame front upstream. Tangirala et al(165) identified three blowoff limits, they were correspond to maximum fuel velocity, a maximum swirl velocity, and a minimum swirl number. By using anon-intrusive LDV and Rayleigh scattering diagnostics, they shown that blowoff due to excess fuel velocity occurred after the fuel jet penetrated and reduced the recirculation bubble. Excessive swirl caused visible stretching and fragmentation of the flame and caused local acceleration near the recirculation zone edge Fig.(1.2).

Margolin and Karpov(162) and somewhat later followed by Babkin et al(170)used rotating cylinderical combustion chamber to initiate laminar swirling flow. They found out that, for swirling flow the rate of decrease in the flame propagation velocity depended on the speed of rotation, the greater the rotational speed, the more rapid the decrease in the propagation velocity of the flame. Babkin et al(170)considered the rotational speed gradient of the gas dw/dr, as one

of the possible factors influencing the flame quenching process. They noted that this gradientcould cause considerable stretch of the flame along the flame front. They considered that flame quenching as a result of this stretch was less probable than quenching as a result of heat loss from the hot gases to the wall. On the other hand from the work of Zawadzki(163)in which the temperature of the swirling gas was measured, it follows that under conditions of much more intense swirl and turbulent flow the combustion gases were not cooled during the passage of flame from the centre of the cylindrical combustion chamber towards its periphery, and the flame was not extinguished, despite the fact that the propagation velocity of the flame was not much higher than the laminar burning velocity. It follows that the heat loss from the hot gases to the walls was not important during the extinction process . It should be noted that as the heat loss increased from the flame to the wall. The thickness of the cooled flame increases and the burning velocity decreases(161). In the limit case the flame was quenched at the wall in the same manner as it is in a quenching channel. The flame quenching initiated at the wall, spreads over the entire surface of the flame. Under conditions of intense turbulent swirling flow no flame quenching action was observed(161,163).The flame propagated over the entire volume. The burning velocities were independent of the parameters of turbulence and were contained within the same range of values as found by Andrews and Bradley(164) for laminar flames.

1.5.2 The influence of the initial temperature on flammability

The data obtained by White and quoted in the book by Bone and Townend(171)indicate that an increase in the initial temperature of a mixture results in an apparently linear rise in the flammability limits. An analysis made by Egerston and Powling(172) showed that the reduction in the heat of chemical reaction per unit volume of the mixture due to the lowering of the lower limit was approximately compensated for by increase initial enthalpy of the mixture. In the present work the influence of inlet temperature on stability was important as preheat up to 600 K was needed.

CHAPTER ONE

REFERENCES

1-1 Beltagui,S.A. and MacCallum,N.R.L: Aerodynamics of vaneswirled flames in furnaces. J. Inst. Fuel 49, 1976.

1-2 Goulard,R., Meller,A.M. and Bilger,R.W.: Combustion measurements in air breathing propulsion engines: Survey and research needs. Combustion Science and Technology,14,p.195,1976.

1-3 Jones W.P., McGuirk J.J.: Mathematical modelling of gas-turbine chambers. AGARD-CP-275,1979.

1-4 Jones W.P., Whitelaw J.H.: Calculation methods for reacting turbulent flow:-a review. Combustion and Flame ,48,pp.1-26,1982.

1-5 Heitor M.V. and Whitelaw J.H.: Velocity, Temperature and Species characteristics of the flow in a gas-turbine combustor. Combustion and Flame,64,pp.1-32,1986.

1-6 Beer, J.M. and Chigier, N.A. : Combustion Aerodynamics. Applied Science Publishers ltd, 1972.

1-7 Scott C.J. and Bartelt K.W.: Decaying annular swirl flow with inlet solid body rotating. Trans. Am. Soc. Mech. Eng. J. Fluids Eng.,98, pp.33-40,1976.

1-8 Rose W.G.: A swirling round turbulent jet:1-mean flow measurement Trans Am. Soc. Mech. Eng. J. Appl. Mech.,29;pp. 615-625, 1962.

1-9 Harding N.S.: Effects of secondary swirl and other burner parameters on nitrogen pollution formation in a pulverized coal combustor Ph.D. Dissertation, Brigham Young University, Provo,UT,1980.

1-10 So K.L.: Vortex phenomena in a conical diffuser,AIAA,5,pp. 1072-1078,1967.

1-11 Bradshow P.: Effects of streamline curvature on turbulent flow. AGARD-AG-169. Aug. 1973.

1-12 Kopecky R.M. and Torrance K.E.: Initiation and structure of axisymmetric eddies in a rotating stream. Comp. fluids,1,pp.289-300, 1973.

1-13 Syred N. and Beer J.M.: Effect of combustion upon processing vortex cores generated by swirl combustors.14th Symposium (Int.) on combustion ,The combustion institute,Pittsburgh PA, pp.537-550,1973.

1-14 Garg A.K. and Leibovich S.: Spectral characteristics of vortex breakdown flowfields, Physics, Fluids 22,pp.2053-2064,1979.

1-15 Faler J.H. and Leibovich S.: Disrupted states of vortex flow and vortex breakdown. Physics Fluids,20,pp.1385-1400,1977.

1-16 Bornstein J. and Escudier M.P.: LDA measurements within a vortex breakdown bubble. International Symposium on application of laser-doppler anemometry to fluid mechanics, Lisbon, Portugal paper 10.3, July 5-7,1982.

1-17 Syred N. and Bee'r J.M.: Combustion in swirling flows:a review.

Combustion and Flame ,23,pp.143-201, 1974.

1-18 Grabowski W.J. and Berger S.A.: Solutions of the Navier-Stokes equations for vortex breakdown. J. Fluid Mech.,75,pp.525-544,1976.

1-19 Vu B.T. and Gouldin F.C.: Flow measurements in a model swirl combustor. AIAA J1,20,642-651,1982.

1-20 Leibovich S.: Vortex stability and breakdown; survey and extension, AIAA J1,22,1192-1206,1984.

1-21 Gouldin F.C., Depsky J.S. and Lee S.L.: Velocity field characteristics of a swirling flow combustor. AIAA-83-0314,AIAA 21st Aerospace sciences meeting,Reno, NV Jan. 10-13,1983.

1-22 Leibovich S.: The structure of vortex breakdown; a review. Fluid Mech.,10,221-246, 1978.

1-23 Escudier M.P. and Keller J.I.: Recirculation in swirling flows: a manifestation of vortex breakdown. AIAA J1,23,111-116,1985.

1-24 Syred N., Gupta A.K. and Bee'r J.M.: Temperature and density gradient changes arising with the precessing vortex core and vortex breakdown in swirl burners. 15th Symposium (Int.) on combustion. The combustion institute, Pittsburgh, PA,587-597, 1975.

1-25 Claypole T.C.: Pollutant formation in swirling jets. Ph.D. Dissertation, Mech. Eng. Dept. and Energy Studies, University of Wales, 1980.

1-26 Rhode D.L., Lilley D.G. and Mclaughlin D.K.: On prediction of swirling flowfields found in axisymmetric combustor geometries. Trans. Am. Soc. Mech. Eng. J. Fluids Eng. 104,378-384, 1982.

1-27 Rhode D.L., Lilley D.G. and Mclarghlin D.K.: Mean flowfield in axisymmetric combustor geometries with swirl,AIAA J1,21,593-600, 1983.

1-28 Beyler C.L. and Gouldin F.C.: Flame structure in a swirling stabilized combustor inferred by radiant emission measurements. 18th Symposium (Int.)on combustion, The combustion Institute, Pittsburgh,PA, 1011-1019,1981.

1-29 Claypole T.C. and Syred N.: Coherent structures in swirl generators and combustors, vortex flows. W.L. Swift ,P.S. Barna and C. Dalton(Eds.). The Am. Soc. Mech. Eng., New York, 1980.

1-30 Lilley D.G.: Swirl flows in combustion: A review, AIAA J1,15, 1063-1078, 1977.

1-31 Syred N. and Dahman K.R.: Effect of high confinement upon the aerodynamics of swirl burners. J. Energy, 2,8-15, 1978.

1-32 Chanaud R.C.: Observations of oscillatory motion in certain swirling flows. J. Fluid Mech.,21,111-127,1965.

1-33 Hall M.G.: Vortex breakdown, A review. Fluid Mech.,4,195-217, 1972.

1-34 Leibovich S.: Wave propagation, instability and breakdown of vortices, vortex motion, H. G. Hornung and E-A Muller(Eds.) Friedr. Vieweg and Sohn.Braunschwerg,1982.

1-35 Bossel H.H.: Swirling flows in streamlines of variable cross-section,AIAA J1,11,1161-1165,1973.

1-36 Maslowe S.A. and Stewartson K.: On the linear inviscid stability of rotating pipe flow, Physics Fluids,25,1517-1523,1982.

1-37 Leibovich S. and Stewartson K.: A sufficient condition for the instability of columnar vortices. J. Fluid Mech.,126,335-356,1983.

1-38 Ribeiro M.M. and Whitelaw J.H.: Coaxial jets with and without swirl. J. Fluid Mech.,96,769-795, 1980.

1-39 Ribeiro M.M. and Whitelaw J.H.: The structure of turbulent jets. Proc. R. Soc. London,ser. A.370,281-301,1980.

1-40 Lilley D.G.: Nonisotropic turbulence in swirling flows. Acta. astr.,3,919-933,1976.

1-41 Lilley D.G.: Primitive pressure-velocity code for the computation of strongly swirling flows. AIAA J1,14,749-756, 1976.

1-42 Chigier N.A.: Gas dynamics of swirling flow in combustion systems. Astronautica Acta,17,387-395, 1972.

1-43 Syred N., Chigier N.A. and Bee'r J.M.: Flame stabilization in recirculation zone of jets with swirl. 13th symposium (Int.) on combustion, The combustion institute, Pittsburgh,PA,617-624, 1971.

1-44 Novick A.S. ,Miles G.A. and Lilley D.G.: Numerical simulation of combustor flowfields:a primitive variable design capability, J. Energy, 3,95-105, 1979.

1-45 Fricker N. and Leukel W.: The characteristics of swirlstabilized natural gas flames, Part3: The effect of swirl and burner mouth geometry on flame stability, J. Inst. Fuel,49,152-158, 1976.

1-46 Claypole T.C. and Syred N.: The stabilization of flames in swirl combustors, J. Inst. Energy, 55,14-19, 1982.

1-47 Chigier N.A. and Dvorak K.: Laser anemometer measurements in flames with swirl, 15th symposium (Int.) on combustion, The combustion institute, Pittsburgh,PA,573-585, 1975.

1-48 Lilley D.G.: Modeling of combustor swirl flows, Acta Astr. ,1,1129-1147, 1974.

1-49 Rao G.V.S.N. and Sriramulu V.: Investigation of a coaxial swirl burner, combustion flame, 34,203-207,1979.

1-50 Rawe R. and Kremier H.: Stability limits of natural gas diffusion flames with swirl. 18th symposium (Int.) on combustion. The combustion institute,Pittsburgh,PA, 667-677, 1981.

1-51 Owen F.K. ,Spadaccini L.J. ,Kennedy J.B. and Bowman C.T.: Effects of inlet air swirl and fuel volatility on structure of confined spray flames. 17th Symposium (Int.) on combustion. The combustion institute, Pittsburgh,PA,467-473, 1979.

1-52 Uchida S., Nakamura Y. and Suehiro F.: Numerical calculation of swirling flows in a circular pipe. Trans. Japan Soc. Aeronaut. Space Sci.,24,17-25, 1981.

1-53 Narain J.P.: numerical prediction of confined swirling jets. Comp. Fluids,5,115-125, 1977.

1-54 Wu H.L. and Fricker N.: The characteristics of swirlstabilized natural gas flames Part2: The behavior of swirling jet flames in a narrow cylindrical furnace, J. Inst. Fuel,49,144-151, 1976.

1-55 Khalil K.H., El-Mehallawy F.M. and Moneib H.A.: Effect of combustion air swirl on the flow pattern in a cylindrical oil fired furnace. 16th symposium (Int.) on combustion, The combustion institute, Pittsburgh,PA,135-143, 1977.

1-56 Ramos J.I.: A numerical study of turbulent confined swirling jets: Numerical methods in laminar and turbulent flow, C. Taylor and B.A. Schrefler(Eds.) Pineridge press, Swansea, United Kingdom, 1981.

1-57 Beltagui S.A. and MacCallum N.R.L.: Aerodynamics of vaneswirled flames in furnaces. J. Inst. Fuel,49,183-193, 1976.

1-58 Leukel W. and Fricker N.: The characteristics of swirlstabilized natural gas flames,Part1: Different flame types and their relation to flow and mixing patterns, J. Inst. Fuel,49,103-112, 1976.

1-59 Mathur M.L. and MacCallum N.R.L.: Swirling air jets issuing from vane swirlers.Part1: Free jets, J. Inst. Fuel,40,214-225, 1967.

1-60 Yoon H.K.: Five hole pitot probe time-mean velocity measurement in confined swirling flows, M.S. Thesis Mech. Eng. Dept., Oklahoma state University, Stillwater,OK, 1982.

1-61 Jackson T.W. and Lilley D.G.: Single-wire swirl flow turbulence measurements, AIAA-83-1202, 19th joint propulsion conference, seattle, WA, June 27-29, 1983.

1-62 Yoon H.K. and Lilley D.G.: Five-hole pitot probe time-mean velocity measurements in confined swirling flows. AIAA-83-0315, AIAA 21st Aerospace Sci. meeting, Reno, NV. Jan. 10-13, 1983.

1-63 Yoon H.K. and Lilley D.G.: Further time mean measurements in confined swirling flows, AIAA J1,22,514-515, 1984.

1-64 Lockwood F.C., El-Mahallawy F.M. and Spalding D.B.: An experimental and theoretical investigation of turbulent mixing in the cylindrical furnace. Combustion Flame,23,283-293, 1974.

1-65 Kerr N.M. and Fraser D.: Swirl. Part1: Effect on axisymmetrical turbulent jets, J. Inst. Fuel,38,519-538, 1965.

1-66 Sloan D.G., Smith P.J. and Smoot L.D.: Modeling of swirl in turbulent flow systems. Prog. Energy Comb. Sci.,12,1-24, 1986.

1-67 Brum R.D. and Samuelsen G.S.: Two-component laser anemometry measurements in non-reacting and reacting complex flow model combustor. Western States Section/ The combustion institute,Sandia National Laboratories, Livermore, CA, 1982.

1-68 Gupta A.K. Bee'r J.M. and Swithenbank J.: On the operational characteristics of multi-annular swirl burner, Combustion Science Technology,17,197-214, 1978.

1-69 Beltagui S.A. and MacCallum N.R.L.: The modeling of vaneswirled

flame in furnaces. J. Inst. Fuel,49,193-200, 1976.

1-70 Abujelala M.T. and Lilley D.G.: Confined swirling flow predictions. AIAA-83-0316, AIAA 21st Aerospace Sciences meeting ,Reno,NV Jan. 10-13, 1983.

1-71 Kerr N.M.: Swirl, PartII: Effect on flame performance and the modeling of swirling flames. J. Inst. Fuel,38,527-538, 1965.

1-72 Al-Dabbagh, N.A. : Emissions and Stability of Gas Turbine Combustors with Rapid Fuel and Air Mixing. Ph.D. Thesis, Department of Fuel and Energy, University of Leeds, 1982.

1-73 Ali, A.F. and Andrews, G.E. : Conical Grid Plate Flame Stabili sers for Combustor Primary Zones. ASME paper, 85-GT-53, 1985.

1-74 Kowkabi M. : Swirl combustors for low emission gas turbine. Ph.D. Thesis, Department of Fuel and Energy, University of Leeds, 1988.

1-75 Abdul-Aziz, M.M., Abdul-Hussain, U.S., Al-Dabbagh, N.A. and Andrews, G.E. : The Influence of Flame stabiliser Pressure Loss on Fuel Atomization, Mixing and Combustion Performance. 8th International Symposium on Air Breathing Engines (ISABE). June 1987.

1-76 Lefebvre, A.H. and Durrent, T. : Design Characteristics Affect ing the Turbine Combustion Performance. Paper 240C, SAE National Aeronautic Meeting, Los Angeles, 1960.

1-77 Smith, D.S., Sawyer, R.F. and Starkman, E.S. : Oxides of Nitrogen from Gas Turbines. Air Pollution Control Association, 60th Annual Meeting, Cleveland, Ohio, Paper No. 67-125, 1967.

1-80 Chigier, N.A. and Chervinsky, A. : Aerodynamic Study of Turbulent Burning Free Jets with Swirl. 11th Symposium (International) on Combustion. The Combustion Institute, pp.489-499, 1967.

1-81 Chigier, N.A. and Beer, J.M. : Velocity and Static Pressure Distributions in Swirling Air Jets Issuing from Annular and Divergent Nozzles. J. Basic Eng., Vol.36, No. 4, pp.788-796, 1964.

1-82 Syred, N., Chigier, N.A. and Beer, J.M. : Flame Stabilisation in Recirculation Zones of Jets with Swirl. 13th Symposium (International) on Combustion. The Combustion Institute. pp.563-570, 1971.

1-83 Gupta, A.K. and Lilley, D.G. : Flowfield Modelling and Diagnostics. Abacus Press, Tunbridge Wells, England, 1985.

1-84 Khalil, E.E. : Modelling of Furnaces and Combustors. Abacus Press. Tunbridge Wells, England, 1982.

1-85 Ahmad, N.T. : Swirl stabilised Gas Turbine Combustion. Ph.D. Thesis, Department of Fuel and Energy, University of Leeds, 1986.

1-86 Bahr, D.W. and Gleason, L.L. : Experimental Clean Combustor Program, Phase 1. Final report, NASA CR134737, 1975.

1-87 Mularz, E.J., Wear, J.D. and Verbulecz, P.W. : Pollution Emissions from Single Swirl-Can Combustor Modules at Parametric Test Conditions. NASA TM X-3167, 1975.

1-88 Mcewan, M.W. : Hot and Cold Studies on an Oil-Fired Burner with

Swirler Fitted in a Refinery Oil Heater. Journal of the Institute of Fuel, pp.107-112, 1972.

1-89 Kilik, E. : The Influence of Swirler Design Parameters on The Aerodynamics of the Downstream Recirculation Region. Ph.D. Thesis, School of Mechanical Engineering, Cranfield Institute of Technology, England, 1976.

1-90 Mestre, A. and Benoit, A. : Combustion in Swirling Flow. 14th Symposium (International) on Combustion. The Combustion Institute. pp.719, 1973.

1-91 Chervinsky, A. and Mankeimer-Timnat, Y. : Effect of Swirl on Flame Stabilisation. Israel Journal of Technology. Vol. 6, No. 1-2. pp.25-31, 1968.

1-92 Mestre, A. : Efficiency and Pollutant Formation Studies in a Swirling Flow Combustor. Proc. of ASME Fluid Mech of Combustion Conf. Montreal, 1974.

1-93 Shekleton, J.R. : The Civic: A Concept in Vortex Induced Combustion for The Solar Gemini 10KW Gas Turbine. Transaction of the ASME. Vol. 103, pp.34-42, 1981.

1-94 Vranos, A., Knight, B.A. and Zubielski, M.F. : Centrifugal Mixing: A Comparison of Temperature Profiles in Nonrecirculating Swirling and Nonswirling Flames. Combustion and Flame 48, 109-119, 1982.

1-95 Takagi, T., Okamoto, T., Taji, M. and Nakasuji, Y. : Twentieth Symposium (International) on Combustion. The Combustion Institute. pp.251. 1984.

1-96 Oven, M.J., Gouldin, F.G. and Mclean, W.J. : Temperature and Concentration Measurements in a Swirl-Stabilised Combustor. 17th Symposium (International) on Combustion. The Combustion Institute. pp.363-374, 1979.

1-97 Lewis, G.D. : Centrifugal Force Effects on Combustion. 14th Symposium (International) on Combustion. The Combustion Institute. Pittsburgh. pp.413, 1973.

1-98 Lewis, G.D. : AIAA paper No. 73-1250, Las Vegas, Nevada, 5-7 November, 1973.

1-99 Lewis, G.D. and Smith, C.E. : Investigation of Centrifugal Force and Reynolds Number Effects on Combustion Processes. AFOSR-TR-75-1167, 1975.

1-100 Clements, T.R. : Effects of Swirling Flow on Augmentor Performance. Phase I and II, NASA-CR-134639, 1974 and NASA-CR-135024, 1976.

1-101 Mestre, A. : Proc. of ASME Fluid Mech of Combustion Conference. Montreal, p.89, 1974.

1-102 Lewis, G.D. : Combustion in a Centrifugal Force Field. 13th Symposium (International) on Combustion. The Combustion Institute. Pittsburgh, pp.625-629, 1971.

1-103 Shekleton, J.R. : The Civic: A concept in Vortex Induced Combustion. Part II. Transactions of the ASME, Vol 103, pp.708-717, 1981.

1-104 Mellor, A.M. : Gas Turbine Engine Pollution. Prog. Energy Combust. Sci. Vol. 1, pp.111-133, 1976.

1-105 Jones, R.E. : Gas Turbine Engine Emissions Problems and Progress. Prog. Energy Combust. Sci. Vol.4, pp.73-113, 1978.

1-106 Blazowski, W.S. : Future Jet Fuel Combustion Problems and Requirements. Prog. Energy. Comb. Sci. Vol.4, pp.177-199, 1978.

1-107 Bahr, D.W. : Impacts of Broadened-Specification Fuels on Aircraft Turbine Engine Combustors. ASME paper 81-GT-2, 1981.

1-108 Otsuka, T. and Hattori, H. : Experimental Investigations of Rapid Combustion of Low Grade Gaseous Fuel. 6th Symposium (International) on Combustion. The Combustion Institute. pp.843-849, 1956.

1-109 Grant, J.R. et al : Design and Operation of Low NOx Combustors With Medium Heating Value, Coal-Derived Gas. ASME Paper 80-GT-14, 1980.

1-110 White, D.J. et al : Low Nox Combustion Systems For Burning Heavy Residual Fuels and High-Fuel-Bound Nitrogen Fuels. ASME Paper 81-GT-109, 1981.

1-111 Novick, A.S., Troth, D.L. and Yacobucci, H.G. : Design and Preliminary Results of a Fuel Flexible Industrial Gas Turbine Combustor. ASME Paper 81-GT-108, 1981.

1-112 Hori, M. : Measurements of NO2/NOx Ratio in a Laboratory Swirl Combustor. International Gas Turbine Congress. 83-Tokyo-ITGC-33, 1983.

1-113 Diehl, L.A. and Biaglow, J.A. : Swirl-Can Combustor Performance to Near-Stoichiometric Fuel-Air Ratio. ASME Paper. 76-GT-10. 1976.

1-114 Peterson, R., Ikegawa, M. and Lucas, D. : Direct Sampling Electron Impact Fluorimetry. A technique for Measuring Combustion Species. Combustion and Flame 64, 219-228, 1986.

1-115 Claypole, T.C. and Syred, N. : The Effect of Swirl Burner Aerodynamics on NOx Formation. 18th Symposium (International) on Combustion. The Combustion Institute. pp.81-89, 1981.

1-116 Anderson, D. : Effects of Equivalence Ratio and Dwell Time on Exhaust Emissions From an Experimental Premixing Prevaporizing Burner. ASME 75-GT-69. 1975.

1-117 Owen, F.R., Spadaccini, L.J. and Bowman, C.T. : Pollution Formation and Energy Release in Confined Turbulent Diffusion Flames. 16th Symposium on Combustion. The Combustion Institute. pp.105-117, 1977.

1-118 Mikus, T. and Heywood, J.B. : The Automotive Gas Turbine and Nitric Oxide Emissions. Combustion Science and Technology. Vol.4, pp.149-158, 1971.

1-119 Bowman, C.T. : Kinetics of of Pollutant Formation and Destruction in Combustion. Prog. Energy Combust. Sci. Vol.1, pp.33-35, 1975.

1-120 Mellor, A.M., Plee, S.L. and Leonard, R.A. : Nitric Oxide Formation From Fuel and Atmospheric nitrogen, Comb. Sci. and Tech. Vol.14,

pp.183-193, 1976.

1-121 Zeldovich, Y.B. : The Oxidation of Nitrogen in Combustion Explosions. ACTA Physicohimica. Vol. XXI, No.6, U.SS.R. 1946.

1-122 Heywood, J.B., Fay, J.A. and Linden, L.H. : Jet Aircraft Air Pollutant Production and Dispersion. AIAA paper, 70-115, 1970.

1-123 Molte, P.C. and Pratt, D.T. : The Role of Energy-Releasing Kinetics in NOx Formation. Fuel-Lean, Jet Stirred CO-Air Combustion. Comb.Sci. and Tech. Vol.9, pp.221-231, 1974.

1-124 Molte, P.C., Schmidt, S.C. and Pratt, D.T. : Measurement of Atomic Oxygen and Nitrogen Oxides in Jet Stirred Combustion. Proc. 15th Symposium (International) on Combustion. The Combustion Institute. p.1061, 1975.

1-125 Burdet, N.A. and Hayhurst, A.M. : Some Observations of NOx ion and Neutral NO in Atmospheric Pressure Flames of Acetylene and Hydrogen, Proc. 16th Symposium (International) on Combustion. The Combustion Institute. p.903, 1977.

1-126 Iverach, D., Kirov, N.Y. and Haynes, B.S. : The Formation of Nitric Oxide in Fuel-Rich Flames. Comb. Sci. Tech. Vol. 8, p159, 1973.

1-127 Fenimore, C.P. : Formation of Nitric Oxide in Premixed Hydrocarbon Flames. 13th Symposium (International) on Combustion. The Combustion Institute. Pittsburgh. pp.373-380, 1971.

1-128 Moreley, C. : Formation and Destruction of Hydrogen Cyanide From Atmospheric and Fuel Nitrogen in Rich Atmospheric Pressure Flames. Combustion and Flame. Vol.27, p.189, 1976.

1-129 Merryman, E.L. and Levy, A. : Nitrogen Oxide Formation in Flames: The Role of NO2 and Fuel Nitrogen. 15th Symposium (International) on Combustion. The Combustion Institute. Pittsburgh. pp.1073-1083, 1975.

1-130 Williams, P.T., Bartle, K.D., Andrews, G.E., and Mills, D.G. 6th Int, Symp. on Capillary Chromatography, Riva del Garda, Italy, May 1985.

1-131 Williams, P.T., Bartle, K.D. and Andrews, G.E. : 9th Int. Symp. on Polynuclear Aromatic Hydrocarbons, Columbus, Ohio, Oct. 30th-Nov. 1st 1984.

1-132 Appleton, J.P. and Heywood, J.B. : The effects of Imperfect Fuel-Air Mixing in a Burner on NO Formation From Nitrogen in The Air and The Fuel. 14th Symposium (International) on Combustion. The Combustion Institute. pp.777-786, 1973.

1-133 Mclean, W.J., Chen, S.Y., Gouldin, F.C. and Oven, M.J. : Direct Formation of NO2 in Combustion Products, Proc. 14th International Colloquium on Atmospheric Pollution, Benarie, M.M. (Ed.), Studies in Environmental Science, Vol. 8, pp.173-180, 1980.

1-134 Cernansky, N.P. and Sawyer, R.F. : NO and NO2 Formation in a Turbulent Hydrocarbon/ Air Diffusion Flame. 15th Symposium (International) on Combustion. The Combustion Institute. Pittsburgh, pp.133-136, 1975.

1-135 Johnson, G.M., Smith, M.Y. and Malcahy, M.F.M. : The Presence of NO2 in Premixed Flames. 17th Symposium (International) on

Combustion. The Combustion Institute, Pittsburgh, pp.647-680, 1979.

1-136 Mori, K., Kimura, T., Kitajima, J. and Kato, K. : Study of Emission Controls on Gas Turbine Combustors. (Report 1), KAWASAKI Technical Review. No 69, 1979.

1-137 Solt, J.C. : Coping With Gas Turbine Emissions Regulations. ASME Paper 87-GT-239, 1987.

1-138 King, J.L. and Clements, M.A. : Development and Application of a Second Generation Low NOx Burner. First European Dry Fine Coal Conference. Institute of Energy. pp.V/1/-1-13, 1987.

1-139 Cooke, M.J. and Pragnell, R.J. : Technology To Meet Proposal Environmental Standards. First European Dry Fine Coal Conference. Institute of Energy. pp.V/3/-1-17, 1987.

1-140 Touchton, G.L. : Influence of Gas Turbine Combustor Design and Operating Parameters on Effectiveness of NOx Suppression by Injected Steam or Water. ASME Paper No. 84-JPGC-GT-3, 1984.

1-141 Aoyama, K. and Mandai, S. : Development of a Dry Low NOx Combustor for a 120-MW Gas Turbine. ASME J. Engineering For Gas Turbines and Power. Vol. 106, pp.795-800, 1984.

1-142 Washam, R.M. : Dry Low NOx Combustion System For Utility Gas Turbines. ASME Paper No. 83-JPGC-GT-13, 1983.

1-143 Mori, K., Kitajima, J. Kajita, S. and Ichihara, S. : Development of a Catalytic Combustor For Small Gas Turbines. ASME Paper, 87-GT-62, 1987.

1-144 Hoshino, A., Kajita, S., Hagiwara, Y., Fujimoto, K. and Kitajima, J. : Preliminary Tests of Catalytic Combustion in a Small Gas Turbine. ASME Paper, 87-GT-100, 1987.

1-145 Touchton, G.L., Savelli, J.F. and Hilt, M.B. : Emission Performance and Control Techniques for Industrial Gas Turbines. General Electric Co. GER-2486H, 1982.

1-146 Furuya, T., Hayata, T., Yamanaka, S., Koyuka, J., Yoshine, T. and Ohkoshi, A. : Hybrid Catalytic Combustion for Stationary Gas Turbine Concept and Small Scale Test Results. ASME Paper 87-GT-99, 1987.

1-147 Becker, B., Berenbrink, P. and Brandner, H. : Premixing Gas and Air to Reduce NOx Emissions With Existing Proven Gas Turbine Combustion Chambers. ASME Paper, 86-GT-157, 1986.

1-148 Sood, V.M. and Shekleton, J.R. : Ongoing Development of a Low Emission Industrial Gas Turbine Combustion Chamber. ASME Paper, 79-GT-203, 1979.

1-149 Westenburg, A.A. : Kinetics of NO and CO in Lean, Premixed Hydrocarbon-Air Flames. Combustion Science and Technology, 4. pp.59-64, 1971.

1-150 Howard, J.B., Williams, G.C. and Fine, D.H. : Kinetics of Carbon Monoxide in Post Flame Gases. 14th Symposium (International) on Combustion. The Combustion Institute. pp.975-986, 1973.

1-151 Lefebvre, A.H. : Pollution Control in Continues Combustion Engine.

15th Symposium (International) on Combustion. The Combustion Institute. Pennsylvania, pp.1169-1179, 1974.

1-152 Fenimore, C.D. : Chemistry in Premixed Flames. The Macmillan Company, New York, 1964.

1-153 Lefebvre, A.H. : Pollution Control in Continuous Combustion Engines. 15th Symposium (International) on Combustion. The Combustion Institute. Pennsylvania, pp.1169-1179, 1974.

1-154 Verkamp, F.J. et al : Impact of Emission Regulations on Future Gas Turbine Combustors. AIAA Paper, No. 73-1277, 1973.

1-155 Vranos, A. and Taback, E.D. : Combustion Products Distribution in the Primary Zone of a Gas Turbine Combustor, Combustion and Flame. Vol. 26. No.1, p.129, 1976.

1-156 Odgers, J. : Current Theories of Combustion Within Gas Turbine Chambers. 15th Symposium (International) on Combustion. The Combustion Institute. pp.1321-38, 1974.

1-157 Dutergne, J., Arezard, N. and Borghi, R. : Further Results in Nitrogen Oxides Production in Combustion Zones. Combustion Science and Technology. Vol.25, pp.85-95, 1981.

1-158 Watson, J.T.R. : Thermal Conductivity of Gases in Metric Units. Dep. of Trade and Industry. National Engineering Laboratory. 1973.

1-159 Hayhurst A.N. and Vince I.M.: Nitric oxide formation from N2 in flames: The importance of "prompt" NO. Prog. Energy Combustion Sci ,6,pp.35-51, 1980.

1-160 Lefebvre A.H: Gas Turbine Combustion. Hemisphere Publishing Corporation, 1983.

1-161 Jarosinski J.: Asurvey of recent studies on flame extinction. Prog. Energy Combust. Sci.,12,81-116, 1986.

1-162 Margolin A.D. and Karpov V.P.: Combustion and Explosion. p.372 Nauka, Moscou, 1977.

1-163 Zawadzki A and Jarosinski J.: Laminarization of flames in rotating flow. Combustion Science and Technology,35,1-13, 1983.

1-164 Andrews G.E. and Bradley D.: Determination of burning velocities: A critical review. Combust. Flame,18,133-153, 1972.

1-165 Tangirala V., Chen R.H. and Driscoll J.F.: LDV/ Rayleigh scattering measurements to study the blow off of swirling flames. AIAA 24th Aerospace Sciences meeting, Jan. 6-9 Reno, Nevada, 1986.

1-166 Sano T.: NO2 formation in the mixing region of hot burned gas with cool air. Combust. Sci. Tech.,38,129-144, 1984.

1-167 Sano T.: NO2 formation in the mixing region of hot burned gas with cool air-effect of surrounding air. Combust. Sci. Tech.,43, 259-269, 1985.

1-168 Jaasma D. and Borman G.: Peculiarities associated with the measurement of oxides of nitrogen produced by diffusion flames. Combust. Sci. Tech.,23,83-88, 1980.

1-169 Bromly J.H., Barnes F.J. and Little L.H.: The effect of low levels of CO, H2 and hydrocarbons on NO2/NO ratios in heated gases. J. Inst. Energy,89-97, June 1988.

1-170 Babkin V.S., Badalyan A.M., Borisenko A.V. and Zamashchikov, V. V. Fizika Goren, Vzryva,18, 17-20, 1982.

1-171 Bone W.A. and Townend D.T.A.: Flame and Combustion in Gases, p100, Longmans, Green and Co. Ltd., London, 1927.

1-172 Egerton A. and Powling J. Proc. R. Soc. A193, 172, 1948.

1-173 Smith K.O., Kurzynke F.R. and Angello L.C.: Experimental evaluation of fuel injection configurations for a lean premixed low NOx gas turbine combustor,ASME paper 87-GT-141, 1987.

1-174 Beltagui S.A. and MacCallum N.R.L : Characteristics of enclosed swirl flames with peripheral fuel injection, J. Inst. of Energy ,Vol. LXI,446,pp.3-16, March 1988.

1-175 Deters J.E. : Current gas turbine combustion and fuels researc h and development, ASME paper 87-GT-107, 1987.

1-176 Claypole T.C. and Syred N.: Turbulent flame propagation in swirl stabilised flames. AIAA paper, Air Breathing Engine Conference, 83-7022, pp 182-185, 1983.

FIGURES

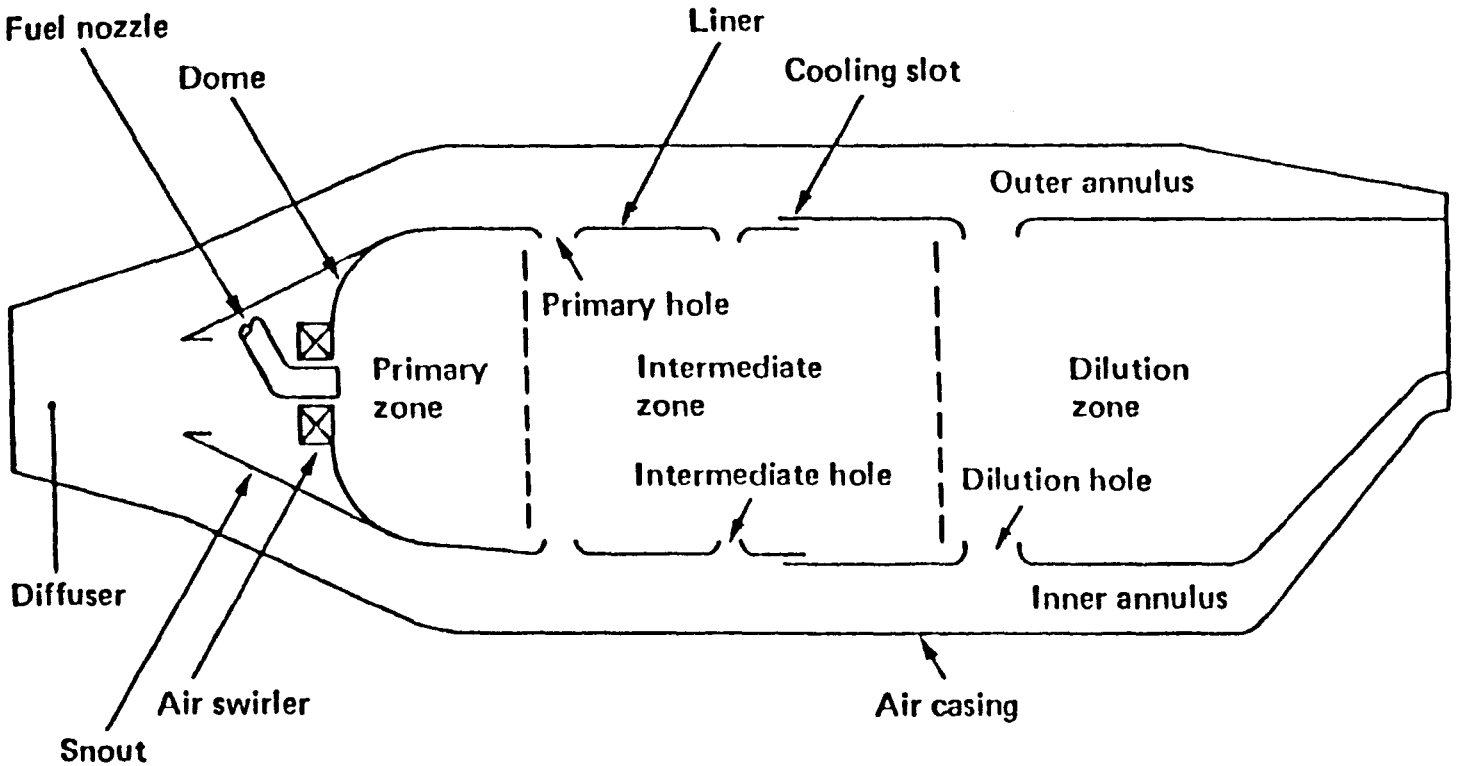

Fig.1.1 Main components of a Gas Turbine combustor ref.(160).

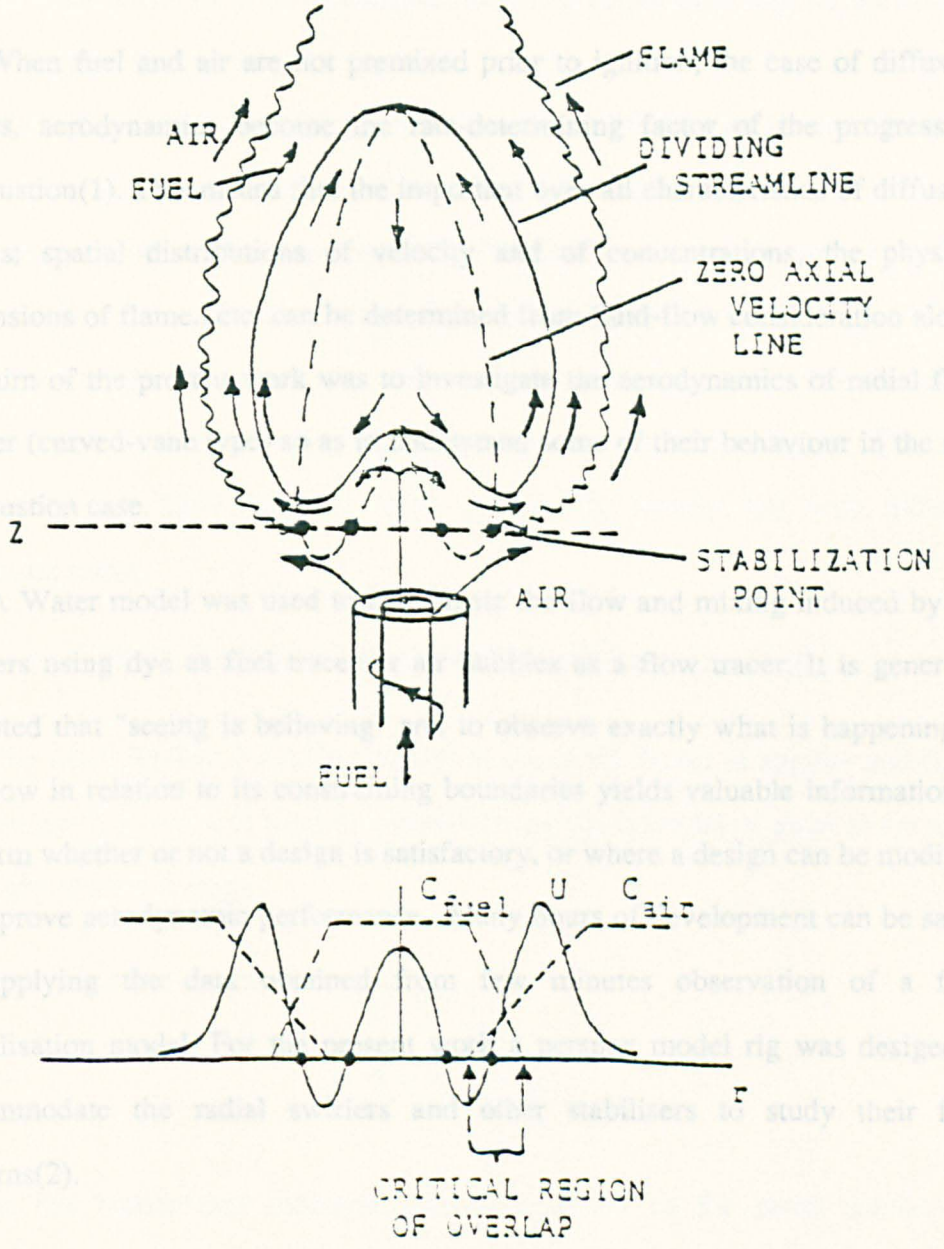

Figure1.2 Schematic of Flame Stabilization Region ref.(165).

CHAPTER TWO

RADIAL SWIRLERS COLD FLOW CHARACTERISTICS AND MODELLING

2.1 INTRODUCTION

When fuel and air are not premixed prior to ignition, the case of diffusion flames, aerodynamics become the rate-determining factor of the progress of combustion(1). This means that the important over-all characteristics of diffusion flames; spatial distributions of velocity and of concentrations, the physical dimensions of flame...etc. can be determined from fluid-flow consideration alone. The aim of the present work was to investigate the aerodynamics of radial flow swirler (curved-vane type) so as to understand some of their behaviour in the real combustion case.

A Water model was used to investigate the flow and mixing induced by the swirlers using dye as fuel tracer or air bubbles as a flow tracer. It is generally accepted that "seeing is believing" and to observe exactly what is happening to the flow in relation to its constraining boundaries yields valuable information to confirm whether or not a design is satisfactory, or where a design can be modified to improve aerodynamic performance. Many hours of development can be saved by applying the data obtained from few minutes observation of a flow visualisation model. For the present work a perspex model rig was desiged to accommodate the radial swirlers and other stabilisers to study their flow patterns(2).

2.2 RADIAL SWIRLER DESIGN

The radial swirlers used a curved blade passage design in an attempt to avoid flow separation in the channels. The design features are shown in Fig.2.1 and plate 2.1 which details the vane angle Θ. The vane angle Θ was the effective radial vane passage jet outlet angle. As will be discussed shortly, water flow visualization showed that the outlet flow attached to this blade surface.

Table 2.1 shows the various dimensions of the radial flow swirlers used in the present work, with a vane angle range between 0 - 70 degrees. The 45 degrees angle swirler were made in two peripheral diameters, 76mm and 127mm with outlet diameters of 40mm and 76mm respectively. They were manufactured in various vane depth so as to investigate the effect of pressure loss on the overall performance of the swirler.

Generally, the swirlers can be grouped into three different categories, one with approximately equal effective open area but with various vane angle. The vane depth and passage widths were made of different dimensions to keep more or less the same flow area with the same swirler outlet diameter. Secondly, large swirlers with various effective open area but constant vane angle and Thirdly, small swirlers with various effective open area but constant vane angle. The later effectively they have the same open area as the former, but with different expansion ratios.

2.3 GEOMETRICAL CHARACTERIZATION OF SWIRL NUMBER

The swirl number is usually defined as the of the fluxes of angular and linear momentum(3,4) and it is used for characterizing the intensity of swirl in enclosed and fully separated flows.

The parameter can be given as:

$$S = 2 \frac{G_\phi}{G_\chi . D}$$

In the combustion literature, two formulation of the swirl number are commonly used those which included the static pressure term in the axial momentum equation and those which used only the dynamic term. For cases where mixing at the boundary of the recirculation zone is dominated by the action of a precessing vortex core another parameter is required for characterization of rotating flow. A nondimensional frequency parameter similar to that suggested by Cassidy and Falvey(5). The derivation of such parameter was demonstrated by Syred and Beer(6).

The swirl number can be computed from geometric and parameters of swirl generators(1,7), when the swirl number is calculated from the input velocity distribution in the swirl generator rather than the velocity distribution in the jet, the static-pressure term can be omitted and the swirl number be given with good approximation(1) For a guide-vane cascade in a radial flow, the angular momentum can be expressed as:

$$G_\phi = \sigma \cdot \frac{M^2}{\rho\, 2\pi B}$$

If the Reynolds number influence is assumed to be negligible, the swirl number depends only upon the geometrical dimensions of the guide-vanes in the axis perpendicular cross-section.

2.3.1 SWIRL NUMBER

The determination of the swirl number for radial swirlers from swirler geometry is difficult and no simple formulae exists that is equivalent to that of Kerr and Fraser(21) for axial swirler. In the present work a swirl number based on the mean axial outlet area velocity of the swirler and the mean blade passage throat velocity as the basis of the tangential velocity is suggested. The intensity of rotation can be defined as follows:-

$$\frac{\text{Tangential velocity}}{\text{Axial velocity}} = \frac{V_\theta}{V_x}$$

Now , from Fig.2.2, we have:

By conservation of mass:-

$$\rho_1 A_1 V_1 = \rho_2 C_c A_2 V_2 = m$$

Where C_c is the contraction coefficient of the radial vane passage jets which is equivalent to the free discharge coefficient.

$$V_2 = \frac{A_1}{C_c A_2} \cdot V_1 \qquad \text{....(1)}$$

Since $\rho_1 = \rho_2 = \rho_3$

The velocity of flow inside the vane passages will have two components after leaving the passages.

$$V_\theta = V_2 \sin\theta \qquad ....(2)$$

from equation(1), we have:

$$v_\theta = \frac{A_1}{C_c A_2} . \sin\theta \qquad (3)$$

and,

$$V_R = V_2 \cos\theta \qquad ....(4)$$

or

$$V_R = \frac{A_1}{C_c A_2} . \cos\theta \qquad ....(5)$$

from the continuity equation, we have;

$$V_1 A_1 = V_3 A_3 \qquad ....(6)$$

hence,

$$V_3 = \frac{A_1}{A_3} V_1 \qquad ....(7)$$

Hence,

Intensity of rotation,[22]

$$I_e = \frac{A_3}{C_c A_2} . \sin\theta \qquad ....(8)$$

or

$$I_e = \frac{1}{C_c} . \frac{\pi R_3^2}{8 . l . h} . \sin\theta$$

i.e the intensity of rotation:

$$I_e = \frac{\pi}{n . C_c} . \frac{R_3^2}{l . h} . \sin\theta \qquad ....(9)$$

Swirl number can be defined as:

$$S = \frac{\text{Angular momentum flux}}{R . \text{Axial momentum flux}}$$

$$S = \frac{F_\theta}{R_3 . F_x} \qquad ....(10)$$

The flux of angular momentum will be generated by the moment of momentum of the mass of the flow which is rotating tangentially around the centre of the radial flow swirler i.e m_θ

Where the total mass ,

$$m = m_\theta + m_R \qquad ....(11)$$

The ratio of

$$\frac{m_\theta}{m_R} = \frac{V_2 \sin \theta}{V_2 \cos\theta}$$

i.e

$$\frac{m_\theta}{m_R} = \tan\theta \qquad ....(12)$$

by subs. equation(12) in (11), we have,

$$m_\theta = \left(\frac{m}{1+\frac{1}{\tan}\theta}\right) \qquad ....(13)$$

$$F_\theta = m_\theta . V_\theta . R_3 \qquad ....(14)$$

Hence,

$$F_\theta = \left(\frac{m}{1+\frac{1}{\tan\theta}}\right) . V_2 \sin \theta . R_3$$

and

$$F_x = m . V_x \qquad ....(15)$$

Since

$$F_x = m . V_3 = m . \frac{A_1}{A_3 . V_1}$$

Hence

$$\text{Swirl number ,} S = \frac{m}{1+\frac{1}{\tan}\theta} . \frac{V_2 . \sin\theta . R_3}{R_3 . m . \frac{A_1}{A_3} . V_1}$$

$$S = \frac{\sin\theta}{1 + \frac{1}{\tan\theta}} \cdot \frac{A_3}{C_c \cdot A_2} \qquad \text{....(16)}$$

or

re-arranging the above equation, we have :

$$S = \frac{\tan\theta}{\tan\theta + 1} \cdot \frac{A_3}{C_c A_2} \cdot \sin\theta$$

But

$$I_e = \frac{A_3}{C_c A_2} \cdot \sin\theta$$

Therefore,

$$S = \frac{\tan\theta}{\tan\theta + 1} \cdot I_e \qquad \text{....(17)}$$

$$S = \frac{\sin\theta}{1 + \tan^{-1}\theta} \cdot \frac{A_3}{C_c \cdot A_2} \qquad \text{....(18)}$$

2.4 COMPARISON WITH PREVIOUS FORMULA

Previous workers(1,6) suggested the following expression as a measure for the swirl for guide - vane cascade in a radial flow:-

$$\sigma = \frac{1}{1 - \psi} \cdot \frac{\tan\alpha}{1 + \tan\alpha \cdot \tan\frac{\pi}{2}}$$

Where

$\psi = \frac{z \cdot S}{2\pi R_1 \cdot \cos\alpha}$ is a blockage factor

S = thickness of the vanes.

z = number of vanes

α = Angle of the swirler outlet

The above expression does not hold for all radial flow swirlers, infact some of the results obtained from the above equation are misleading.

Claypole and Syred(23) reported a geometric swirl number, based on the combustor geometry, where the air was supplied tangentially:

$$S_g = \frac{r_0 \pi r_e}{A_t}\left(\frac{\text{Tangential flow}}{\text{Total flow}}\right)^2$$

Where

A_t = Area of tangential inlets

r_e = Radius of the exit of the combustor

r_0 = Radius of the tangential inlets the combustor.

For the present work , we have :-

$$S_g = \frac{r_0 \pi r_e}{A_t}\left[\frac{\tan\theta}{\tan\theta+1}\right]^2$$

The results for S_g obtained by the above expression were in reasonable agreement with the present work results as shown in Table 2.1a.

2.5 DISCHARGE COEFFICIENTS AND WALL STATIC PRESSURE PROFILES

The test rig shown in Fig.2.3 was used to measure the discharge coefficients of the radial swirlers. This was done by passing a metered air flow through the radial swirler and combustor tube and monitoring the static pressure loss upstream of the swirlers relative to the atmospheric pressure discharge. Two can combustors 330mm long were used. The first was of 76mm I.D which gave the swirler expansion ratios of 1.9 and 1.0 for the 40mm and 76mm outlet swirlers respectively. The second 330mm long can combustor was 140mm I.D. The two outlet swirlers gave expansion ratio of 3.5 and 1.8 respectively in this combustor. The 140mm combustor was a similar size to many gas turbine can combustor such as the Rolls Royce 'Spey and Tay' and Ruston 'Tornado' combustor.

The C_D was calculated according to the general appendix-A.

Table 2.2 summerised the measured discharge coefficient for the various radial swirlers ,for both combustors compared with that of free discharge coefficient or the contraction coefficients. Figs.2.4 - 2.12 illustrates the variation of discharge and contraction coefficients(C_D, C_C)with Reynold number Re and shown that both C_D and C_C were only slightly dependent on Re for the range of Reynolds

number used in the present work. The radial swirlers discharge coefficients were low, approximately 0.6 compared with that of zero swirl, approximately 0.9 (ie.swirler K), shown in Table 2.2. This indicates that it is the vane angle that given poor CD and not just the 90 inlet and outlet blade. This led to a major consideration of the flow field inside the radial swirler passages as the low CD implied that flow separation occured inthe passages inspite of the curved vanes.

Table(2.2) shows that the measured (CD) associated with the large swirler outlet used in the 76mm combustor was lower than the corresponding values of (CC). This was due perhaps, to the presence of the 76mm combustor, and the additional wall friction and velocity profiles. place.

Figs.2.5 and 2.6, and Table 2.2 show that when the passage width and vane angle were kept constant the discharge coefficient was inversely proportional to the passage depth. Similarly, this has been noticable in Figs.2.8 - 2.9 and for contraction coefficients in Figs.2.11a -2.11b.

The reason behind this was probably due to the reduction of separation inside the passages due to the reduction of the depth, because as the passage depth was reduced the separation on the vertical back plate of the radial swirler seems to be reduced. Furthermore, flow visualisation showed that the contraction at the outlet of the swirler was reduced with an impingement point for the lower passage depth swirler was near to the swirler outlet than the others. The variation of discharge and contraction coefficient with passage vane depth for the 40 and 76mm outlet 45 degrees swirlers is shown in Fig.2.12. The combination of B&C double swirlers, discussed in chapter six, resulted in a further data point at higher area ratio. These calibration lines should be used in future designs of this type of swirler.

2.7 ZERO-VANE ANGLE SWIRLER

With zero vane angle the radial inlet jets showed the classic behaviour of a straight confined jet with a flow system containing large outer recirculation zone in the corner between the jet boundaries and the confining walls. Exchange of

mass then takes place between the expanding jet and the recirculation flows all along the jet boundary between the two flows(8).

Figs.2.15 and Fig.2.18, show that the recovery by the flow from the stabiliser in the 76mm combustor was much earlier than when the same stabiliser was used in the 140mm combustor. With the later case, the sudden enlargement adds more loss in energy for the fluid in flow(9 ,10).Moreover, the flow in the later case exhibits larger corner recirculation zone than the former case. However, the jets issues from stabiliser(K) in both combustor size 76mm and 140mm were impinged on the walls at more than one combustor diameter which is in agreement with Wu at el(11) and Rhode at el(10). The impingement points can be estimated from Fig.2.15 and 2.18 to be approximately at twice the combustor diameter.

2.8 WALL STATIC PRESSURE PROFILES

Figs.2.13 - 2.18 show the measured wall static pressure profiles at ambient temperature for the radial swirlers with different vane angles and area ratios for the two sizes can combustors 76mm and 140mm diameter. The wall static pressure profiles exhibited some major features, these are the presence of zones with high wall static pressure regions which increase as the swirler flow area A2 is decreased. These features are associated with recirculation zones and are influenced by the swirler design(12-16) The radial static pressure distribution at any given section in the combustor occurs mainly due to the centrifugal force w/r of the swirling flow. Furthermore, due to the sudden expansion and mixing effect, the tangential velocity shows a rapid decay downstream of the swirler. This tangential velocity decay was proportional to x/D(27). However, the radial distribution of the static pressure inside the combustor can explain some of the complex flow pattern that occurs with highly confined flow(27). In the present work, as will be demonstrated later by a flow visualisation, the flow expands due to the radial pressure gradient with an outer corner recirculation zone and an internal recirculation zone established downstream of the swirler outlet.

For a swirler with a vane angle of (45) and a range of area ratios the wall static pressure profiles are shown in Figs.2.13a, 2.14 and 2.17. Figs.2.13a and 2.17 show that for the same swirler expansion ratio in the two combustor sizes the corner recirculation zone size was similar. The minimum in the static pressure profile represent the maximum width of a recirculation zone, when the swirler flow dynamic pressure is high. Typical wall static pressure profiles and the associated flow patterns are shown in Fig.2.18a. The minimum in Fig.2.18a is the shear layer impingement point with maximum tangential wall velocities. This occured at the same axial position for both combustors. Upstream of this point was the low velocity corner recirculation with a high wall static pressure and downstream was the central recirculation zone of maximum width at the minimum in the minimum in the static pressure profile. Downstream of this region was a free vortex flow region with a reverse core region of reduced width with axial distance, gving a high static pressure at the wall.

These flow profiles are clearly shown by the dye injection flow visualisation results discussed later. The CFD prediction of the flow also support this in representation of the wall static pressure profiles. As the passage depth decreased and hence the effective open area decreases, the swirl number increased and the wall static pressure increased accordingly. Furthermore, as the swirl number increased the corner recirculation zone size decreased as was shown using flow visualisation. Similarities in the profiles between the 40mm outlet swirler used in the 76mm combustor with that of the 76mm outlet swirler (45) used in the 140mm combustor. Thus the aerodynamics of the two combustors was similar and scaling between the two size combustors could be investigated, as discussed in chapter four. The effect of no swirler expansion on the wall static profiles is demonstrated in Figs.2.14 and 2.15 for the 76mm outlet swirlers in 76mm combustor. Due to the high tangential velocity the static pressure remained at a high level. These highly potential level of tangential velocity depended on the swirler geometry, especially the passage depth and the angle of rotation.

There was no effect for the combustor inlet temperatures on the wall static pressure profiles as demonstrated by Fig.2.13b.

2.9 SEPARATION IN THE VANE CURVED PASSAGES

2.9.1 Behaviour of separated flows

A separated flow is usually divided into two regions:

1- Flow between the separation limiting-stream line skeleton and the wall (ie. the stalled, stagnant or back flow region).

2- Shear flow, containing the former boundary-layer vorticity, between the free stream and the limiting streamline skeleton.

The common boundary of these regions is a zone of a certain and unsteady shape and character. However, separation occurs because too much diffusion of the boundary layer is demanded.

2.9.2 Flow visualization of passages

A simple perspex model was assembled for flow observation through the curved passages of the radial swirler, as shown in Fig.2.19a. This comprised a 152mm I.D perspex tube as the approach water supply pipe which was covered on its two ends by square perspex sheets of 200x200 mm . The whole structure connected to four bolted bars and in between the sheets and the approach pipe rubber gaskets were placed to prevent any water leakages. The water outlet was through the middle part of the swirler using the fuel pipe hole. This created a flow restriction which limited the maximum flow to 50 l/min. However, that was quite sufficient to give turbulent flow in the vane passages and to observe the flow inside the passage with help of beam of light projected through the passage inlet.

Plate 2.2 ,demonstrates the results of the present observation. Flow separation occured at the radial passage inlet at the outer radius of curvature of the passage. Flow reattachement occured within the passage, but the flow was controlled by the direction of the passage wall with no flow separation. However, the existance of a separation inside the curved passages was not surprising, since a rather abrupt reduction of the geometrical blockage creates a strong radial decelaration. The separation creates a blockage in addition to the geometrical

blockage. This was the main reason to the low CD values discussed above and the curved blades may be concluded to be of no advantage in avoiding flow separation.

The flow separation in the blade passage was three dimensional There was separation at the blade inlet tip and separation off the curved vane surface as discussed above. Separation has also been observed by others in two dimensional cases without swirl(17). The recent work by Hassa et al(30) reported a separation of the flow at the downstream side of the blade when testing a radial swirl generator with profiled radial vanes in a fuel nozzle model.

2.10 COMBUSTOR FLOW PATTERNS

2.10.1 Rig Description

The water model rig which was used in the present work to study the flow field imposed by the radial swirler is shown in plate 2.3. The perspex rig was designed to accommodate different sizes of can combustors mainly, 76mm, 140mm and 250mm I.D perspex combustors. This can be mounted in a larger rectangular perspex tank. This was connected to the main water model circuit shown in Fig.2.19. Water was the main working fluid with air bubbles or dye as tracer. A slit light was arranged such that either a longitudinal or radial section could be illuminated.

For the present work the water flow rate was in the range of 90 l/min - 120 l/min with dye injection at the rate of 3.5 l/min - 4.5 l/min. A conventional 35mm Camera with a 35-20mm macro zoom lens was used to photograph the combustor flow patterns.

2.10.2 FLOW REGIME DISCRIPTION ISSUED BY RADIAL SWIRLERS

Radial vane swirlers are commonly used for industrial burners, and create a Rankine type vortex which has a solid body rotation core surrounded by a free vortex region. Analytical demonstration for this type of vortex was described by Benjamin(18). Some of the visualization results of the present work are illustrated by plates 2.4 - 2.7. The flow regime can be categorised into six different regions as follows:

a-Region 1: Swirler outlet contraction

In this region the motion of the water is implying a fully solid body rotation flow with vortex radius much less than the swirlers outlet diameter which was ranging between 0.4-0.5 d. This type of swirl flow contraction continued for some distance, x=15-20mm, away from the swirler outlet before it was deflected towards the combustor walls where at approximately 45mm (ie. at 0.32 x/D) the impingement point was observed and recorded for the large swirler(B) and at

70mm (0.5 x/D) for the smaller swirler(A) in 140mm combustor model as shown in plate 2.4. In general, the radial swirler outlet gave Rankine vortex type that can separated into two regions, a rotational core where the recirculation increases with increasing radius and irrotational region which is which is surrounding the core region. Both these regions plays an an important part in stabilising and destabilising the swirl flame due to their immediate interaction with fuel jet.

b- Region 2: Corner recirculation zone

Corner recirculation zone was predominant in this region which was a function of swirler outlet and the degree of confinement or the expansion ratio D/d as can be shown in plate in plate 2.4 for the two swirlers with 40mm and for 76mm outlet or swirler(A) and (B) respectively. However, in this region the expectation for the axial and tangential velocities can be very low and turbulent level high. The corner recirculation zone will then experience the circular motion which is counter clock-wise upon its center plus the circulation in the direction of the main swirling flow. This is encountered just upstream of the impingement point on the combustor wall as shown in plate 2.7. Plate 2.6 shows the cross-sectional view of the region 30mm downstream. of the swirler, the central swirling core flow is sharply separated from the corner recirculation flow.

c-Region 3: Outer recirculation zone

Another peripheral recirculation zone was created due to the flow impingement on the combustor walls as shown in plate 2.7. The rotational motion in this case counter rotating the one in region(2). Furthermore, the viscous force perhaps is the main dominant in this part of the flow. However, it was certainly a very good function of the main velocity of the flow.

d-Region 4: Central recirculation zone

The main feature of this region was its strong participation in feeding the central vortex core with air bubbles all the way, along the combustor length after the impingement point had occur, this can be shown after careful examination of

the flow pattern which is shown in plate 2.4 ,2.5 and plate 2.7. However, visualization has shown that some of the air bubbles loses its rotational speed to take a different rotational path, near the centre of the rotation or vortex core. This depends on thier initial speed after the vortex breakdown to form a reverse recirculation zones. All the air bubbles near to the combustor wall region escape through the combustor outlet and the one which is at radius of between 0.0-0.7d can join in the formation of the vortex core region.

The size of region-4- always depends on the main flow inlet velocity and the other physical properties of the flow. In fact, region-3- and region-4- can be considered as a double cell structure region where the first cell always have forward velocity in the centre and the second cell is reverse in the centre.

e-Region 5: Vortex core or fluctuating central-spiral reverse zone

This is clearly shown in plate 2.4 and 2.5. This vortex core region exhibited a precessing vortex of the type discussed by Syred et al(5). The existance of the precessing vortex core has been ascribed to the inertial wave perturbations by Lilley and coworkers(36-38) for their experimental results using an axial swirler.

f-Region 6: Shear layer between 2&3

This region is the conical shaped shear-layer which is between the counter rotating swirling recirculation zones of region 2 and 3. This shear-layer plays very vital part in the mixing processes as will be discussed later.

h-Region 7: Shear layer between 4&5

The existance of this region is due to the interaction between the precessing vortex core and the central recirculation region.

2.10.3 Effect of expansion ratio(D/d)

With swirling flows, the swirler expansion ratio(D/d) has a dominant effect of the flow in the corner reverse flow region as shown in plate 2.4 by comparing swirler (B) with expansion ratio of 1.8 and swirler (A) with expansion ratio of 3.5.

Both swirlers have the same effective open flow area but different outlets. However, swirler A promoted a much larger corner recirculation zone than swirler(B) which is indicated by the two impingement points at x=45mm and at x=70mm for swirler (B) and swirler(A) respectively.

Solid-body rotation is imposed on the swirler(B) flow field (not shown), when used with an expansion ratio of D/d=1, ie. the swirler outlet and combustor internal diameter are the same dimensions, which means that there is no space for the flow to expand.

One of the major differences between swirler(A) and (B) was that of the vortex core in the swirlers outlet. The swirler(B) had a bigger core diameter of (40mm) than that of the small swirler(A) of (20mm), ie. approximately half the swirlers outlet diameter. However, visualization observation showed that the swirling jet issued from swirler(A) with expansion ratio of (3.5) seems to have a more rapid forward rotation jet on axis than the jet with a smaller expansion ratio of (1.9) issued by the same swirler which is similar, to the observation reported by Syred and Dahman(27).

2.10.4 Influence of vane angle passage depth on flow pattern

Flow visualization results showed no effect of the radial-vane angle on the main flow features for the vane angle range between 20-60 degrees which have more or less the same effective open area. The only noticable effect was when changing the depth of the swirler passages. This was done with the 45 degrees angle swirler when it was placed in 140mm I.D combustor. The observed points of impingement are illustrated in Table 2.3.

By comparing the above results with those for the swirl number and for the same radial swirlers, one can detect that the jet spread increased with the increase of the swirl number, caused by the decrease of the passages depth. The vane passage depth is the dominant factor in controlling the magnitude of the tangential velocity issued to the combustor which was due perhapes to the decrease of the

separation effects in the passages.

2.10.5 Mixing Process

For the present work dye was injected through central radial fuel injection system at rate of 4.5 l/min, in flow field of water rated at 90 l/min. The flow visualisation results are shown in plates 2.8 and 2.9 for swirlers (B) and (A) respectively.

The six flow region discussed above a clearly visible from the flow path taken by the dye. A key feature is that the centrally injected dye (radial holes) directly feed the shear layer and not the corner recirculation zone or the central vortex core. The dye mainly follow the second inner recirculation zone and is well mixed in this. It is clear, that the direction of the column of the vortex core region was in the opposite direction to that of the main flow which is evident from the presence of fresh water in the centre that is coming from the combustor outlet region.

2.11 MATHEMATICAL MODELLING

2.11.1 Introduction

Over the last few years, the use of the computer as an engineering tool has increased which was due to better computational software and facilities in terms of computer access, storage, speed and relative cost.

There has been also a substantial increase in the use of computational fluid dynamics(CFD) in gas turbine combustor applications(31). Sturgess et al(31) suggested that it is important to note the CFD applications for gas turbine combustors are driven not only by the potential cost and times saving but also to provide additional insight into complex problems that do not lend themselves to analytical solutions and may be too costly and time consuming to pursue experimently.

A generic description for most type of computer codes is schematically outlined in Fig.2.20. Time averaging is applied to the basic. The Reynolds stress terms that appear are modeled using an eddy viscocity concept where the turbulence model used for closure is the K-E model. This provides two additional transport equations, one for the turbulent kinetic energy and one for eddy dissipation rate(32). In the present work, the computer code FLUENT (33-35) was used to predict the present isothermal flow which is imposed by the radial swirler. The FLUENT computational code was successfully demonstrated by the recent work done by Hand et al(41), on the interaction calculation of turbulence/chemistry where their results shows good quantative agreement between local experimental data and overall model prediction. Two turbulence models were investigated , the widely used K-E and algebriac stress(ASM) or Reynolds stress models. The method of so called "stair-step" was adapted to handle the complex geometric shapes of the radial swirler. Through this method the discretizes curved surfaces into a series of steps.

The present work was considered to be the first attempt to compute fluid flow through this type of radial swirler with curved passages. The geometrical shape

of the radial swirler was considered to be too complicated to do a reasonable time computational work on it. However, there have been various attempt to compute similar domain to the present work. Computational afforts was done by Blumcke et al(28) and Harvay and Leuckel(29) on straight vane radial swirler. Furthermore, work was done by Hassa et al(30) on complex swirl generator which used a radial curve vanes to predict the profiles at the swirler outlet.

2.11.2 PRESENT APPROACH

The numerical prediction of a combustor flows depends on the correct prescription of inlet conditions(31). Blumcke et al(28) reported the necessity of starting the computation in the fuel nozzel at the outlet of the swirl generators, because the reverse flow region of the combustor reaches into the nozzle. Since, the development of the flow patterns in the combustor is known to be sensitive to the amount of swirl issued at that inlet, there was a need to determine the velocity profiles there.

Two computational approaches were made to solve the present problem; first, to predict the flow field at the swirlers outlet using 3-D calculation in a polar-coordinates. The flow field issued by the radial swirler was assumed to be symmetrical and each 45 sector identical to that of the opposite side. Only a 45 sector of the whole domain was considered to be sufficient and it was computed using the conventional method of turbulent model (K-E) and Algebraic Stress Model (ASM).

Fig.2.21 Shows the polar coordinates computational grid using the well known method of "stair-step" for the curved passage and inclinde surfaces(33-35,40) The main inlet boundary condition for the radial swirler calculation were obtained from similar measured cold run on the main rig such as inlet pressure, mean inlet velocity, Reynold no....etc.). Swirler(B) was taken as the modelling example for the present case.

Second, was to predict the combustor flow field in a 2-D calculation applying polar-coordinates as well for the main domain. Furthermore, the three profiles of

the velocities U, V, W obtained from the first computational calculation were used as an inlet profiles to start the calculation in the main combustor. This was done by applying polynomial relation between the variables(U, V, W) and the outlet radius intervals which proved to be inaccurate especially for polynomial to the 3rd degree which is what "Fluent" is limited to use, or by using the Patch option available to insert the true values from the previous solution. Alternatively, the available swirler outlet computation were used on the inlet cells to provide the true inlet profiles. In the present work the later was applied in both models together with one polynomial relation applied to K-E case for comparison using the proper constants for each velocity profile as shown in Table 2.4 where the general form equation-19 was used to estimate each individual velocity profile of (U,V,W) with respect to Y-axis at swirler outlet and neglect their variation with respect to Z-axis since it is used for 2-D case.

For the present work the number of grid point that have been used was as follows:

For 3-D case, number of grid $= X \cdot Y \cdot Z$

$= 11 * 52 * 17$

$= 9724$

For 2-D case, number of grid $= X \cdot Y$

$= 66 * 44$

$= 2904$

2.11.3 PREDICTION RESULTS

Using the K-E method, forthe 3-D and 2-d case, the time for each iteration was 85 and 25 seconds respectively. Using (ASM) method, the time for each iteration for both cases was 95 and 25 seconds respectively. So, the time consumption in 3-D cases was quite high to get an accurate and reliable solution. In three dimensional cases both methods predicted small separation in the curved passages in the Z-direction but a noticable separation in X-direction. This was due to the flow being deflected sharply at the entry point to the swirlers passages. From Figs.2.22 and 2.23 the profiles at the outlet was the combined vortex or known as "Rankine Vortex" profile. This can start close to the centre of the outlet indicating that the solid body rotation was followed by a sharp fall in the indicating the free vortex region.

The tangential velocity profiles assuming from swirl generators generally assume a combination of the forced and free vortex distributions. Figs.2.22 and 2.23 show that the mean tangential velocity in the flow field goes down to zero at the axis of symmetry and hence solid body rotation exists in the centerline region. Moreover, a free vortex is a characteristics of the outer jet skirt and the two vortex distributions patched together to form a resultant profile denoted as the combined Burgers or Rankine vortex. The location of the maximum tangential velocity and its interaction with the axial velocity profile constitutes the critical element in the downstream aerodynamics development. Some of the results which were predicted by K-E model for the 3-D case are shown in Figs.2.24a - 2.31. Both K-E and ASM models predicted a small separation starting in the leading edge of the inlet to the passage which is due perhaps to the sharp gradient near to the sharp edge at that end. However, the similarities between the predicted flow field in the passage and that of plate 2.2 can be noticed in the general pattern. Numerical results also, show that there was another separation in the vertical plane of the back plate of the swirler which is caused by the flow being deflected at the sharp turning angle as can be demonstrated by Fig.2.25.

Fig.2.26 illustrates the spatial axial velocity distribution of the radial swirler where constant contour lines in the centre indicates the solid body rotation in that region and also it is a sign of flow contraction. The outer diameter of the contracted jet is at 0.65 swirler diameters which approximately corresponds to the measured value. Figs.2.27 and 2.28 shows the tangential velocity distribution at two planes 14 and 8 which were oriented on the Z and X-direction respectively. Again the centre of the swirler shows the constant velocity line, indicating the flow contraction in that region. This can be seen also in Fig.2.29. The large K.E of turbulence can be located in the centre core region of the radial swirler as shown in Fig.2.30 where the large eddy dissipation occurs in that region as shown in Fig.2.31. Figs.2.32 - 2.41 and Figs.2.42 - 2.54 illustrated some of the 2-D combustor flow-field results as predicted by the K-E and ASM models respectively.

Using the estimated velocity profiles by the polynomial equation(19) with the K-E model gives unexpected results. This method was denoted by K-E2 and the others by K-E1 where the true velocity profile obtained from the 3-D was used. K-E2 model results predicted the correct flow regime at the first section of the 140mm combustor which is approximately 1/3 of the combustor length. Furthermore, it predicted the correct size of the corner recirculation zone and the exact location of the impingement pointof the flow on the combustor wall. This is demonstrated by Figs.2.32a- 2.36a. However, K-E2 model failed to predict the correct length of the central reverse flow or the vortex core. On the contrary, the K-E1 and algebraic stress model(ASM) predicted a large reverse flow in the centre core region of the combustor but failed to predict the correct size of the corner recirculation zone. Furthermore, they predicted much earlier impingement on the combustor wall. This can be shown in Figs.2.42 - 2.46.

Fig.2.55 illustrates the wall static pressure as a function of the combustor length for the experimental and predicted results using both prediction models. It is a good demonstration of the differences between K-E and algebraic stress (ASM) or Reynolds stress models. It is obvious, that K-E1 and ASM over predicting the

wall static pressure in the first section of the combustor near the swirler outlet due to the inadquancy in predicting the size of the corner recirculation zone. However, the model predicted the wall static pressure with reasonably good agreement with measured values at the section beyond X=75mm while the K-E2 model under estimating the central region and hence gave lower static wall pressure than the measured values. Fig.2.56 shows a comparison between the flow pattern imposed by the radial swirler in 2-D combustor flow regime for the present work using K-E2 results with that of references(20,39). Although, each flow regime being predicted by different models (CFM) and different inlet boundary conditions. There are similarities in the flow field between the three patterns. This is probably accounted by the shape and distribution of all the three mean velocity components. The profiles provided upstream of the confluence or expansion plane rather than immediately downstream. At that location the jets are rapidly evolving and interacting and are more easily influenced by wakes, mixing layers, reverse flow boundaries ..etc.

2.12 Predicted Swirl Number

The following equation was used with the average velocity U and W to calculate the predicted swirl number by the two models. Equation-20 was used to avoid complexities due to the non-uniform velocity profiles and the pressure thrust term was not included in the axial momentum flux, unlike the conventional definition(42).

$$S_o = \frac{\int_{R_1}^{R_2} W\,U^2\,r^2\,dr}{R_2\int_{R_1}^{R_2} U^2\,r\,dr} \qquad \text{.....(20)}$$

From Fig.2.22 and Fig.2.23 the average axial and tangential velocities were 26.23 m/s ; 71.17 m/s and 27.11 m/s ; 68.94 m/s for both ASM and K-E models respectively. Thus, the calculated swirl number from equ.20 were as follows:

For K-E , S = 1.82

For ASM , S = 1.67

Compared to 1.41, which was calculated by equ.18.

2.13 CONCLUSIONS

1- Visualization is a useful and necessary augmentation of the measurements and prediction work described above, because first, "still" photographs complement some of the experimental schematic by providing a characterization of the physical hardware. Second, still photograph of the flow pattern provide a time-averaged view that is desirable for direct comparison to the spatial distribution of the time-averaged mean traverse measurements.

2- Visualization is a documentation of the flame dynamics and scale of the turbulent mixing. Although not quantitative, successive frames from a high-speed photographic sequence provides a visual indication of the dynamics underlying the time-averaged flow field and the scales of turbulent mixing, both of which are critical to the interpretation of a modeling data base.

3- The precessing vortex core was present.

4- The reason for the low discharge coefficients was due to the combination of two flow separations in the vane passages. They occured in the leading edge of the outer curvature of the passage and the vertical back plate of the swirler. With profiled radial flow swirler, the discharged coefficients can be increased with minimum losses. This will include a smooth nozzle type entrance to the vane passages to minimise the inlet flow separation.

5- The combustor flow regime can be catergorised into seven different zones according to its participation in forming the main flow patterns.

6- Mixing of the radially injected fuel simulated by the dye injection starts immediately after it incountered the forced vortex of the flow inside the swirlers inlet core and when the vortex breakdown, it will follow the same path-lines as the combustor flow-field pattern which is imposed by the radial swirler flow regime.

7- Using the computer code "FLUENT" proved to be reasonably adequate to simulate the isothermal flow-field of the present geometry.

8- The structure of the predicted recirculation zone is a function of the accuracy of the inlet conditions and the finite difference scheme used. However, the widely used K-E and algebriac stress (ASM) models under estimated the size of the corner recirculation zone and the impingement point on the combustor wall. The direct comparison of the predicted flow patterns led to conclude that in the analysed cases the Reynolds stress model was not far superior to the widely used K-E model.

CHAPTER TWO

REFERENCES

2-1 Beer J. M. and Leuckel W.: Turbulent flow in rotating flow systems. North American Fuels Conference, Ottawa, Canada, Canadian Comb. Inst. ASME- Inst. of Fuel(Energy), 1970

2-2 Abdul-Hussain U.S., Andrews G.E. and Shahabadi A.R.: Jet mixing shear layer combustion: An ultra low NOx system for natural gas fired gas turbines. I. Mech. E. combustion in engines conference, May 1988.

2-3 Beer J. M. and Chigier N. A.: 5th Journee d'Etudes sur les Flammes. Int. Flame Res. Found. Paris, 1963.

2-4 Chigier N. A. and Beer J. M.: Velocity and static pressure distribution in swirling air jets issuing from annular and divergent nozzle. J. Basic Eng. 4. 788-796, 1964.

2-5 Cassidy J. J. and Falvey H. T. :Observation of unsteady flow a rising after vortex breakdown. J. Fluid Mech. 41,727-736, 1970.

2-6 Syred N. and Beer J. M.: The damping of precessing vortex cores by combustion in swirl generators. Astronautica Acta. vol. 17,pp.783-801, 1972.

2-7 Leuckel W. : Swirl intensities swirl types and energy losses of different swirl generating devices. IFRF Doc. no. GO2/a/16, Nov. 1967.

2-8 Rao S.T.R. and Essenhigh R.H.: Experimental determination of stirring factors generated by straight and swirling jets in isothermal combustion-chamber models. 13th Symposium (Int.) on Combustion Pittsburgh, Pensylvania, 1971.

2-9 Rhode D.L. , Lilley D.G. and McLaughlin D.K: Mean flow fields in axisymmetric combustor geometries with swirl. AIAA 20th aerospace sciences meeting, Jan. 11-14, 1982.

2-10 Srinivasan R. and Mongia H.C: Numerical computations of swirling recirculating flows. NASA-CR-165196, Sept. 1980.

2-11 Wu H.L and Fricker N.:The characteristics of swirlstabilized natural-gas flames in a narrow cylinderical furnace. J. Inst. of Fuel, pp.144-151, Sept. 1976.

2-12 Ahmad N.T. and Andrews G.E.: Emissions from enclosed swirl stabilised premixed flames. ASME paper 83-GT-192, 1983.

2-13 Ahmad N.t. and Andrews G.E.: Gas and Liquid fuel injection into an enclosed swirling flow. ASME paper 84-GT-98, 1984.

2-14 Ahmad N. T.,Andrews G. E. and Kowkabi, M.: Centrifugal Mixing forces in Enclosed Swirl Flames. 20th.,Symposium(International) on Combustion/The Combustion Institute,pp.259-267, 1984.

2-15 Ahmad N.T., Andrews G.E., Kowkabi M. and Sharif S.F.: Centrifugal mixing in gas and liquid fuelled lean swirled stabilised primary zones. ASME paper 85-GT-103, 1985.

2-16 Ahmad N.T., Andrews G.E. and Kowkabi M.: Counter rotating double swirl stabilised flames. The 1987 Tokyo Inter. gas turbine conference

Oct. 1987.

2-17 Streeter V.L.: Handbook of fluid dynamics, MacGraw-Hill company Inc.,1961.

2-18 Benjamin B.: Theory of vortex breakdown phenomenon. J. Fluid Mech.,Vol. 14, 1962.

2-19 Greenspan H.: The Theory of rotating fluids. Cambridge University press, 1968.

2-20 Smith K.O., Kurzyncke F.R. and Angello L.C.: Experimental evaluation of fuel injection configurations for a lean premixed low NOx gas turbine combustor. ASME paper 87-GT-141, 1987.

2-21 Kerr N.M. and Fraser D.: Swirl part 1: Effect on axisymmetrical turbulent jets. J. Inst. Fuel(Energy), vol.38, pp.519-526, 1965.

2-22 McNeil N. and Curtet R.M.,,"Structure of rotating flow in a vortex chamber." Proc. of ASME , Fluid Mech.of combustion conference, Montreal, 1974.

2-22 Beer, J.M and Chigier: Combustion Aerodynamics, Applied Science publications Ltd. , (1972).

2-23 Claypole T.C. and Syred N.: The effect of combustion on the aerodynamics of swirling jets. ASME conference on fluid Mech.of combustion. 1981.

2-24 Beltagui S.A. and MacCallum N.R.L.: Aerodynamics of vane swirled flames in furnaces. J. Inst. Fuel(Energy), vol.49,pp.183-193, 1976.

2-25 Beltagui S.A. and MacCallum N.R.L.: Characteristics of enclosed swirl flames with peripheral fuel injection. J. Inst. Energy, vol.LXI,446, March 1988.

2-26 Gupta A.K., Lilley D.G. and Syred N.: Swirl Flows. Abacus press, 1984.

2-27 Syred N. and Dahman K. R.: Effect of High Level of Confinement upon the Aerodynamics of Swirl Burners. J. of Energy,vol.2,No.1, 1978.

2-28 Blumcke E., Eickhoff H., Hassa C. and Koopman J.: Analysis of the flow through double swirl airblast atomizers combustion and fuels in gas turbine Engines, AGARD-CP-422, 1987.

2-29 Harvay M. and Leuckel W.: LDA-Measurements of liquid swirl flow in coverging swirl chambers with tangential inlets. Laser Anemometer in fluid Mechanics-II, Lisbon, Potugal, 1984.

2-30 Hassa C., Blumcke E., Rachner M. and Eickoff H.: The influence of a radial swirl generator on flow field from a fuel nozzel model. 4th International Symposium on application of Laser-Anemometry to fluid Mechanics, Lisbon, Portugal, 1988.

2-31 Sturgess G.J and Syed S.A.: Importance of inlet conditions for numerical simulation of combustor flows. AIAA paper 83-1263 , 1983.

2-32 Khalil E.E.: Modeling of furnaces and combustors. Abacus press, 1982.

2-33 FLUENT Manual version 2.83, Creare Inc., Flow Simulation Ltd., 1985.

2-34 FLUENT Manual version 2.9 Update, Flow Simulation Ltd.,1987.

2-35 FLUENT Seminar Notes, Creare Inc., Oct. 1987.

2-36 Rhode D.L, Lilley D.G and McLaughlin D.K.: On the prediction of swirling flowfields found in axisymmetric combustor geometries. Trans. Am. Soc. Mech. Eng. J. Fluids Eng., 104,378 - 384, 1982.

2-37 Jackson T.W and Lilley D.G.: Single-wire flow turbulence measurements pap. no. AIAA-83-1202, 1983.

2-38 Yoon H.K and Lilley D.G.: Five-Hole pitot probe time-mean velocity measurements in confined swirling flows. AIAA-83-0315, 1983.

2-39 Rolls Royce, PACE visualisation program, private comunications, July 1989.

2-40 Weber R., Boyson F., Swithenbank J. and Roberts P.A.: Computations of near field aerodynamics of swirling expanding flow. 21st Symposium (International) on Combustion, The Combustion Institute, pp. 1435-1443, 1986.

2-41 Hand G., Missaghi M., Pourkashanian M. and Williams A.: Experimental studies and computer modelling of nitrogen oxides in a cylindrical furnace. Proceeding of IFRF 9th member conference, Holland, May 1989.

2-42 Hagiwara A., Bortz S and Weber R.: IFRF doc.nr F 259/a/3, 1986.

2-43 Peters J.E : ASME paper 87-GT-107, 1987.

TABLES

Table (2.1)
Radial swirlers design details

Swirler	A	A_1	A_2	A_3	B	C	D	E	F	G	H	I	J	K
R_1	46.0	46.0	46.0	46.0	78.0	78.0	78.0	78.0	61.2	70.0	84.7	88.7	92.3	*
R_2	54.0	54.0	54.0	54.0	94.3	94.3	94.3	94.3	84.8	90.0	97.0	97.9	98.8	*
R_3	35.0	33.0	33.0	33.0	59.2	59.2	59.2	59.2	35.0	44.0	54.0	61.0	66.0	*
L	30.5	21.5	15.0	12.2	15.0	11.5	8.0	6.2	8.0	9.0	14.5	19.5	32.0	11.0
h	8.0	8.0	8.0	8.0	16.3	16.3	16.3	16.3	23.6	20.0	12.3	9.2	6.5	17.0
n	<						8							>
Θ	<			45.0				>	20.0	30.0	50.0	60.0	70.0	0.0
S	0.54	0.63	0.77	0.86	1.41	1.84	2.18	2.59	0.41	0.98	2.15	2.91	3.25	0.0
d_0	<		76		> <					127				>
d	<		40		> <					76				>

* Straight radial vanes; zero vane angle

Table (2.1*a*)

Comparison between present work swirl number and reference(23)		
Radial Swirler	Claypole and Syred Eq.(23)	Present Work Eq-18
A	0.56	0.54
A1	0.80	0.63
A2	1.14	0.77
A3	1.41	0.86
B	1.07	1.41
C	1.39	1.84
D	2.00	2.18
E	2.58	2.59
F	0.40	0.41
G	0.82	0.98
H	1.70	2.15
I	2.27	2.91
J	2.93	3.25

Table (2.2)
Measured Discharge & Contraction Coefficients

Radial Swirler Type	With 76mm Combustor			With 140mm combustor			Free Discharge
	(A_2/A_1)	D/d	C_{D1}	(A_2/A_1)	D/d	C_{D2}	C_C
A	0.4280	1.9	0.45	0.1273	3.5	0.42	0.42
A_1	0.3017	=	0.53	0.0898	=	0.52	0.51
A_2	0.2105	=	0.62	0.0626	=	0.59	0.60
A_3	0.1710	=	0.68	0.0509	=	0.65	0.66
B	0.4289	1.0	0.54	0.1276	1.8	0.59	0.58
C	0.3288	=	0.55	0.0978	=	0.61	0.58
D	0.2288	=	0.64	0.0681	=	0.64	0.71
E	0.1773	=	0.71	0.0528	=	0.68	0.77
F	0.3298	=	0.62	0.0981	=	0.67	0.67
G	0.3000	=	0.58	0.0893	=	0.65	0.62
H	0.3180	=	0.56	0.0946	=	0.60	0.61
I	0.3250	=	0.54	0.0967	=	0.58	0.58
J	0.3368	=	0.57	0.1002	=	0.63	0.63
K	0.3280	=	0.96	0.0976	=	0.92	0.87

Table (2.3)
Influence of passage depth on impingement point for large and small radial swirler.

Large Swirler	Impingement point(mm)	Small Swirler	Impingement point(mm)
B	45	A	70
C	36	A_1	55
D	32	A_2	40
E	25	A_3	35

Table (2.4)

Regression Output for U-velocity profile

Constant			16.7
Std Err of Est.			4.6
R Squared			0.8
No. of Observations			24.0
Degrees of Freedom			20.0
Y coefficients	3.7	-0.2	0.0
Std. Err of Coef.	0.8	0.0	0.0

Regression Output for V-velocity profile

Constant			0.717
Std Err of Est.			1.855
R Squared			0.427
No. of Observations			24.000
Degrees of Freedom			20.000
Y coefficients	-1.155	0.074	-0.001
Std. Err of Coef.	0.308	0.019	0.000

Regression Output for W-velocity profile

Constant			-1.3
Std Err of Est.			8.8
R Squared			0.9
No. of Observations			24.0
Degrees of Freedom			20.0
Y coefficients	22.9	-1.3	0.0
Std. Err of Coef.	1.5	0.1	0.0

$$\text{Velocity (U, V, W)} = a + by + cy^2 \quad \text{.....(19)}$$

FIGURES

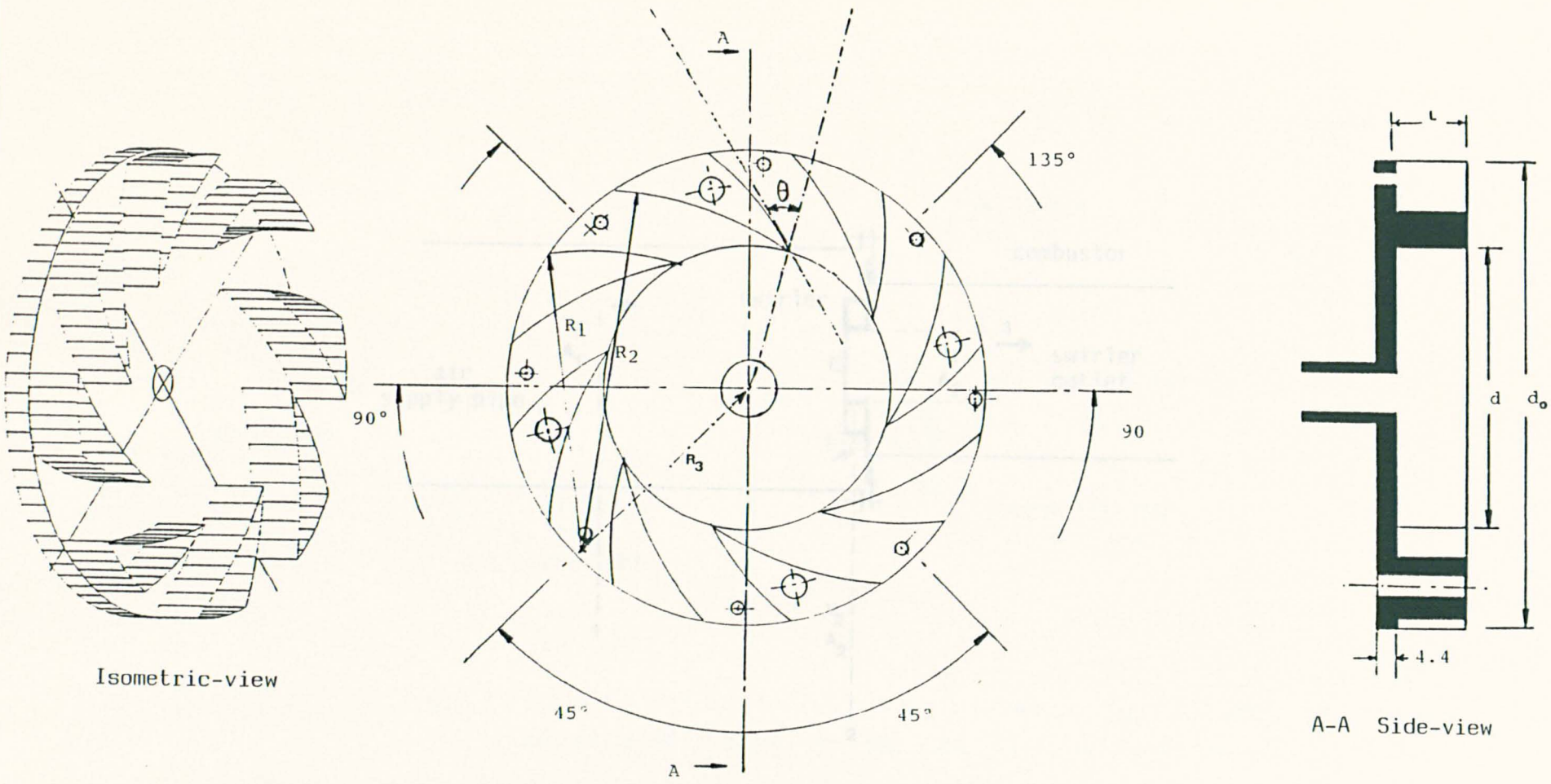

Isometric-view

Front-view

A-A Side-view

Fig.2.1 Radial swirler (Curved-passages) design features.

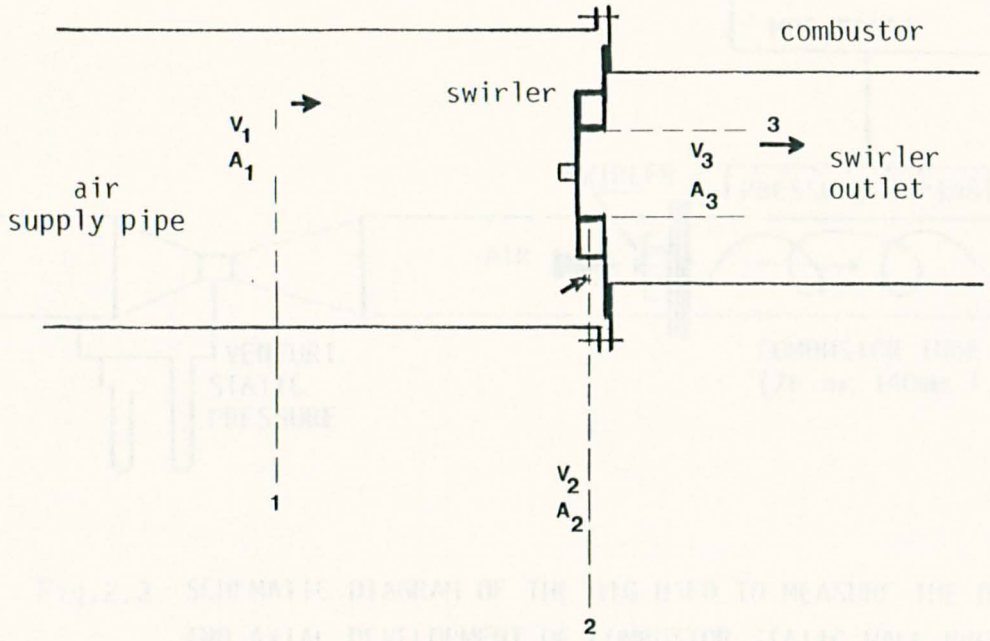

Fig.2.2 Schematic of the regions considered to calculate the Swirl number.

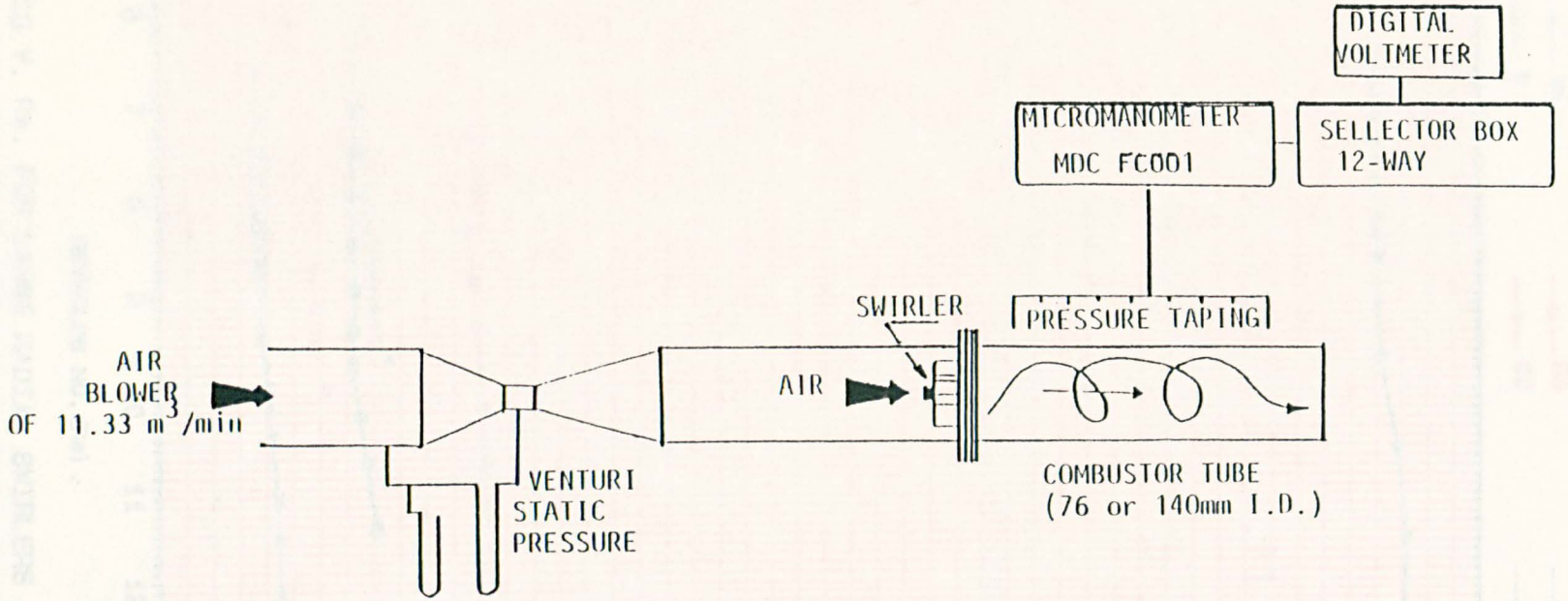

Fig.2.3 SCHEMATIC DIAGRAM OF THE RIG USED TO MEASURE THE DISCHARGE COEFFICIENTS AND AXIAL DEVELOPMENT OF COMBUSTOR STATIC WALL PRESSURE.

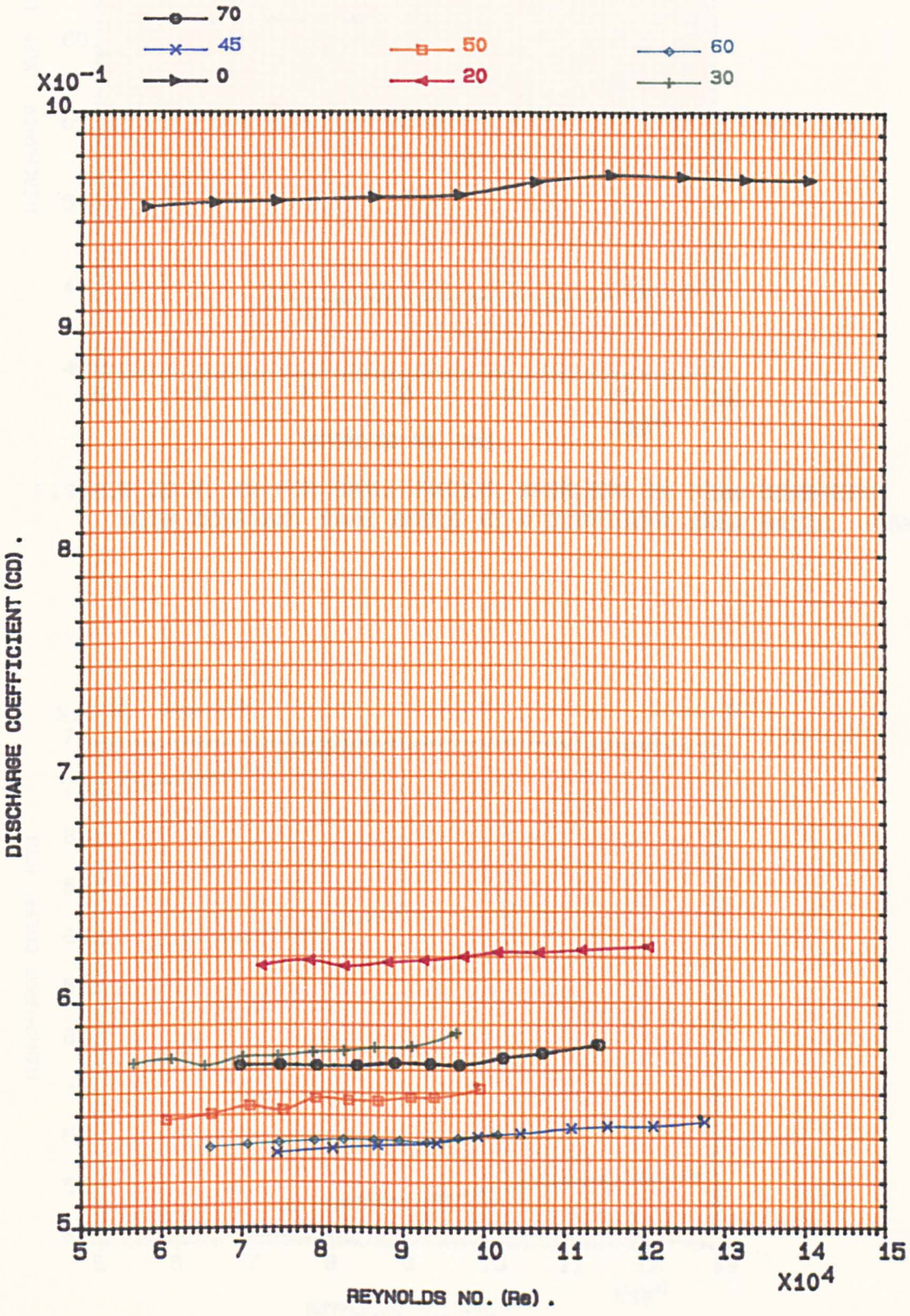

FIG.2.4 CD V. Re. FOR LARGE RADIAL SWIRLERS IN 76mm COMBUSTOR, WITH VARIOUS VANE ANGLE (DEGREES); WITH EQUAL OPEN AREA, 305 K.

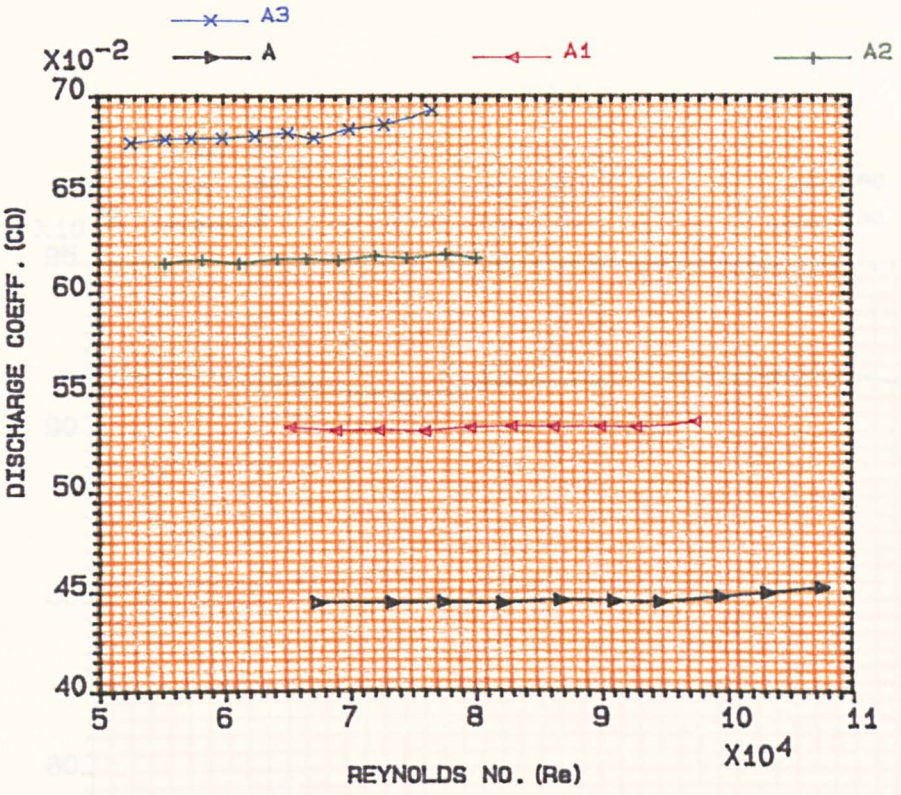

FIG.2.5 CD V. Re FOR SMALL RADIAL SWIRLERS IN 76mm COMBUSTOR, WITH CONSTANT VANE ANGLE 45 & DIFFERENT AREA RATIO, 305K.

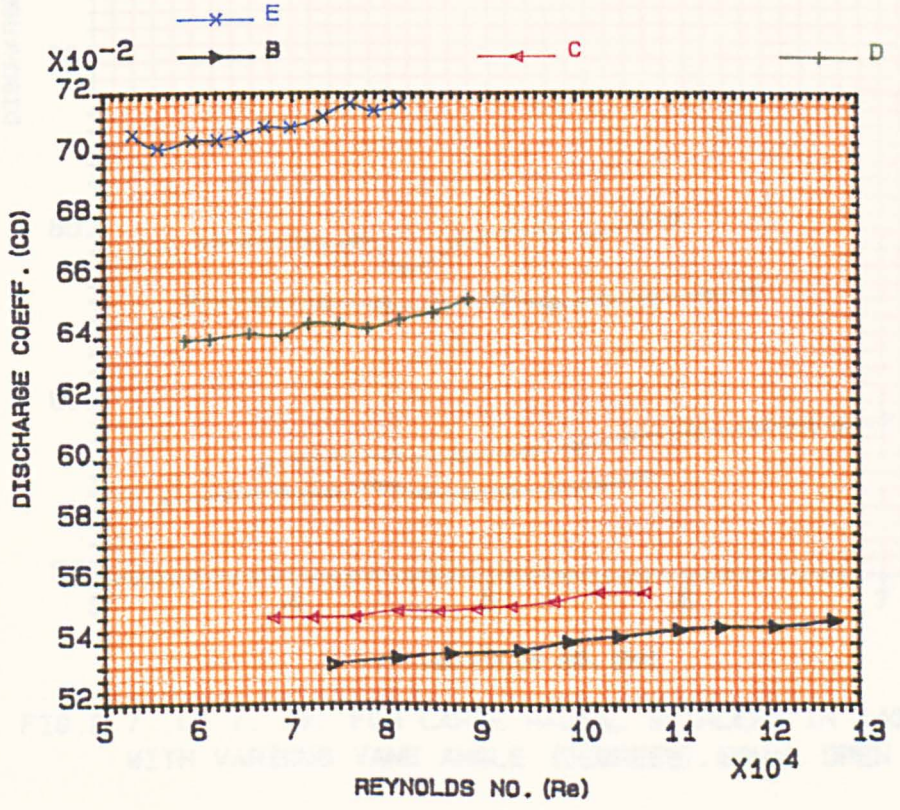

FIG.2.6 CD V. Re FOR LARGE RADIAL SWIRLERS IN 76mm COMBUSTOR, WITH CONSTANT VANE ANGLE 45 & DIFFERENT AREA RATIO, 305K.

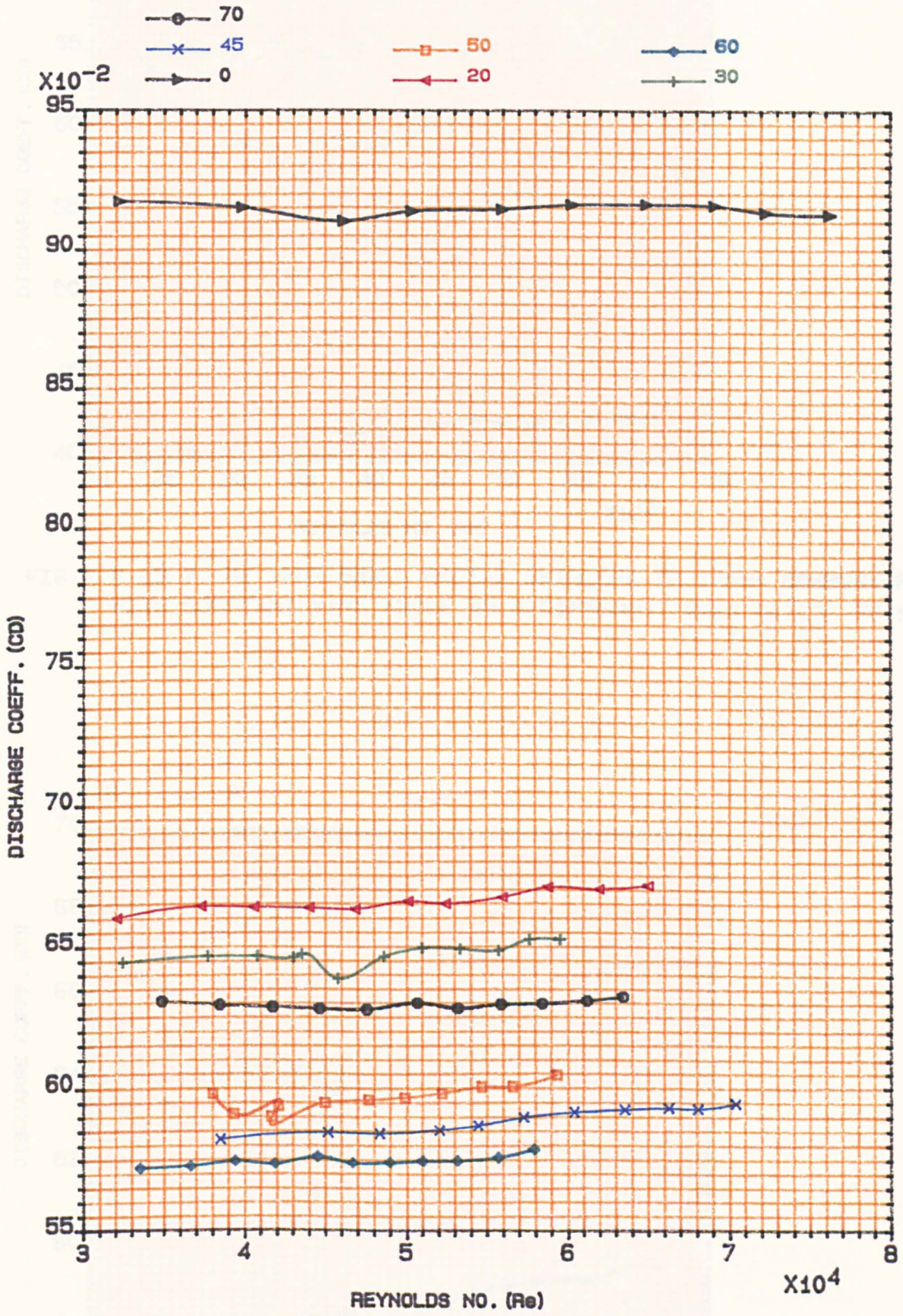

FIG.2.7 CD V. Re FOR LARGE RADIAL SWIRLERS IN 140mm COMBUSTOR, WITH VARIOUS VANE ANGLE (DEGREES), EQUAL OPEN FLOW AREA, 305 K.

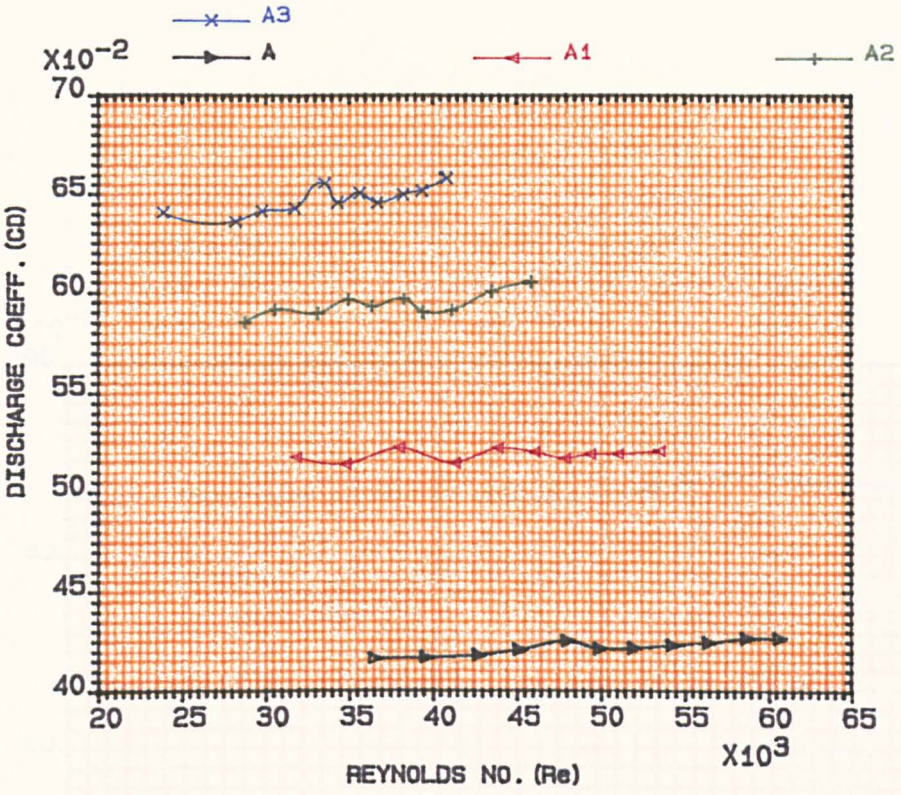

FIG.2.8 CD V. Re FOR SMALL RADIAL SWIRLERS IN 140mm COMBUSTOR, WITH CONSTANT VANE ANGLE 45 & DIFFERENT AREA RATIO, 305K.

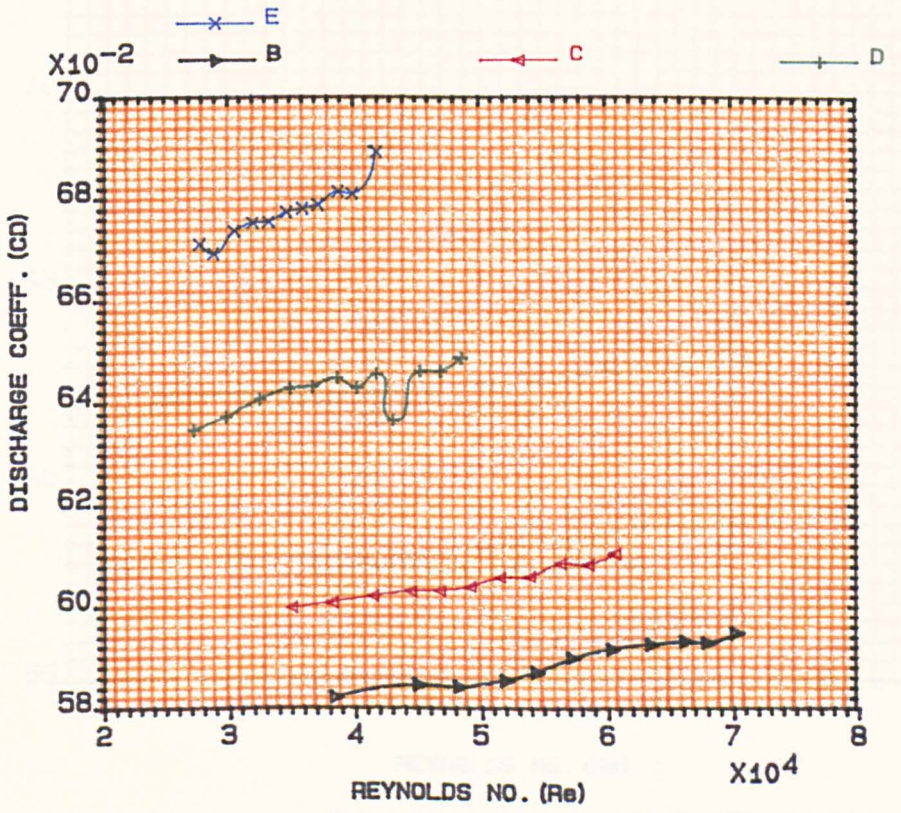

FIG.2.9 CD V. Re FOR LARGE RADIAL SWIRLERS IN 140mm COMBUSTOR, WITH CONSTANT VANE ANGLE 45 & DIFFERENT AREA RATIO, 305K.

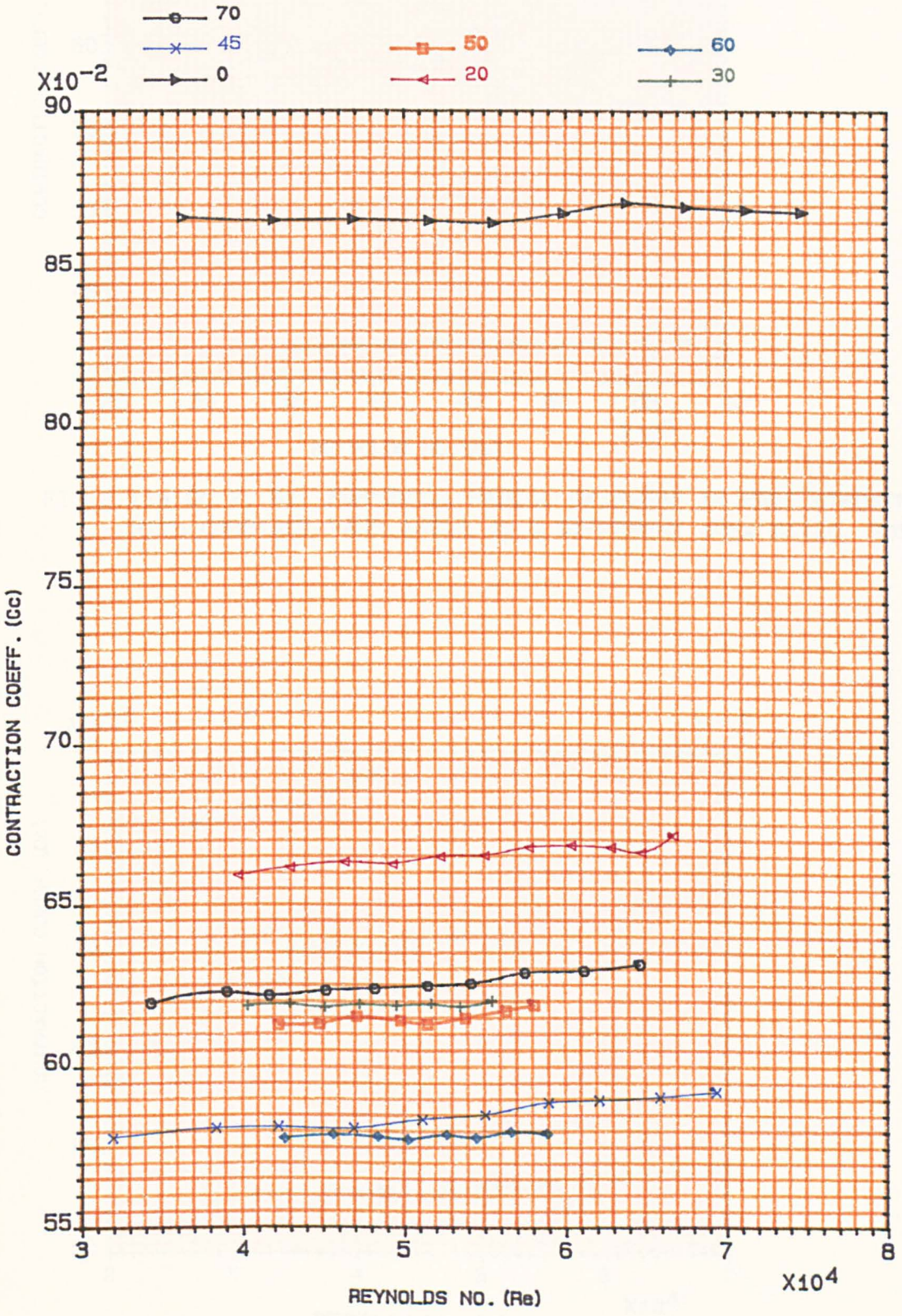

FIG.2.10 CC V. Re FOR LARGE RADIAL SWIRLERS IN FREE ATMOSPHERE, WITH VARIOUS VANE ANGLE (DEGREES), EQUAL OPEN FLOW AREA, 305 K.

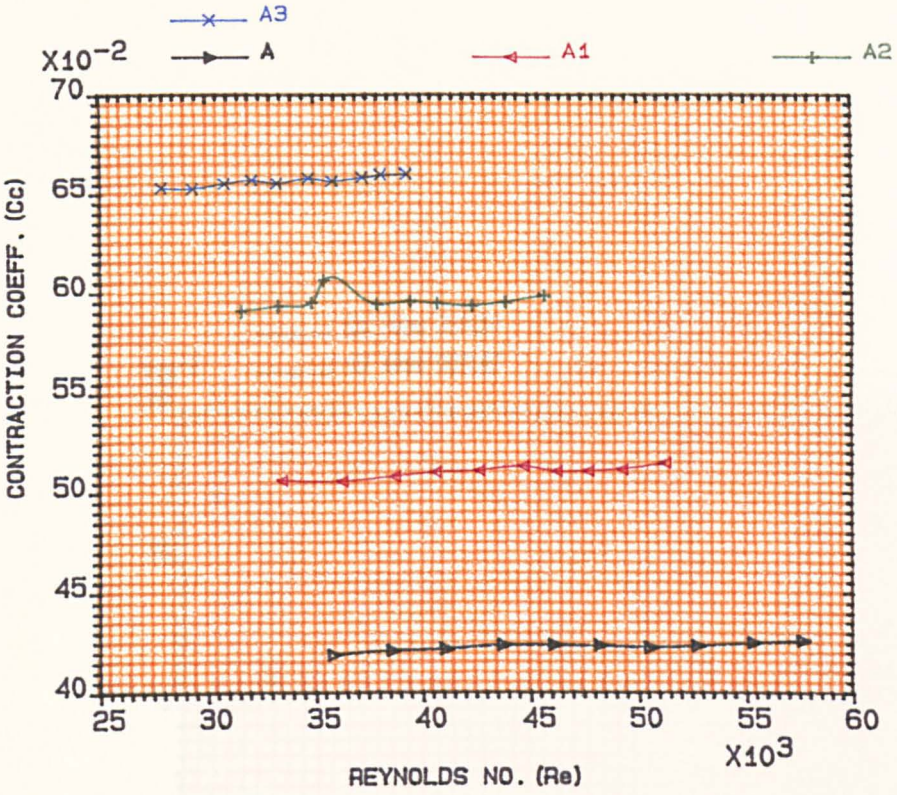

FIG.2.11a Cc V. Re FOR SMALL RADIAL SWIRLERS IN FREE ATMOSPHERE, WITH CONSTANT VANE ANGLE 45 & DIFFERENT AREA RATIO, 305K.

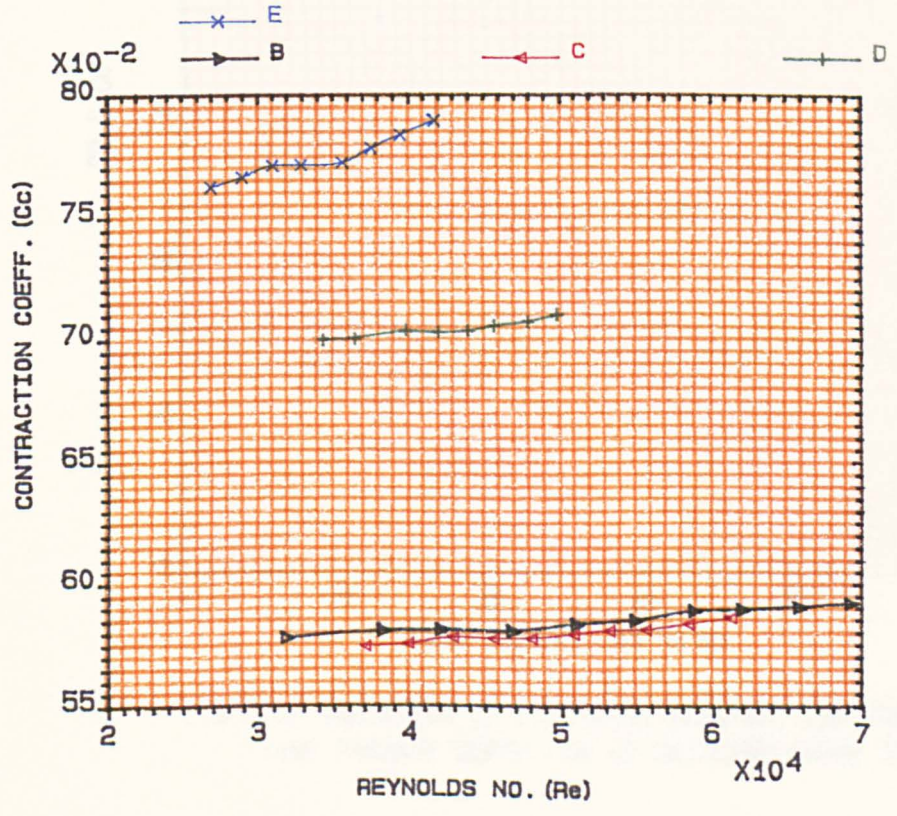

FIG.2.11b Cc V. Re FOR LARGE RADIAL SWIRLERS IN FREE ATMOSPHERE, WITH CONSTANT VANE ANGLE 45 & DIFFERENT AREA RATIO, 305K.

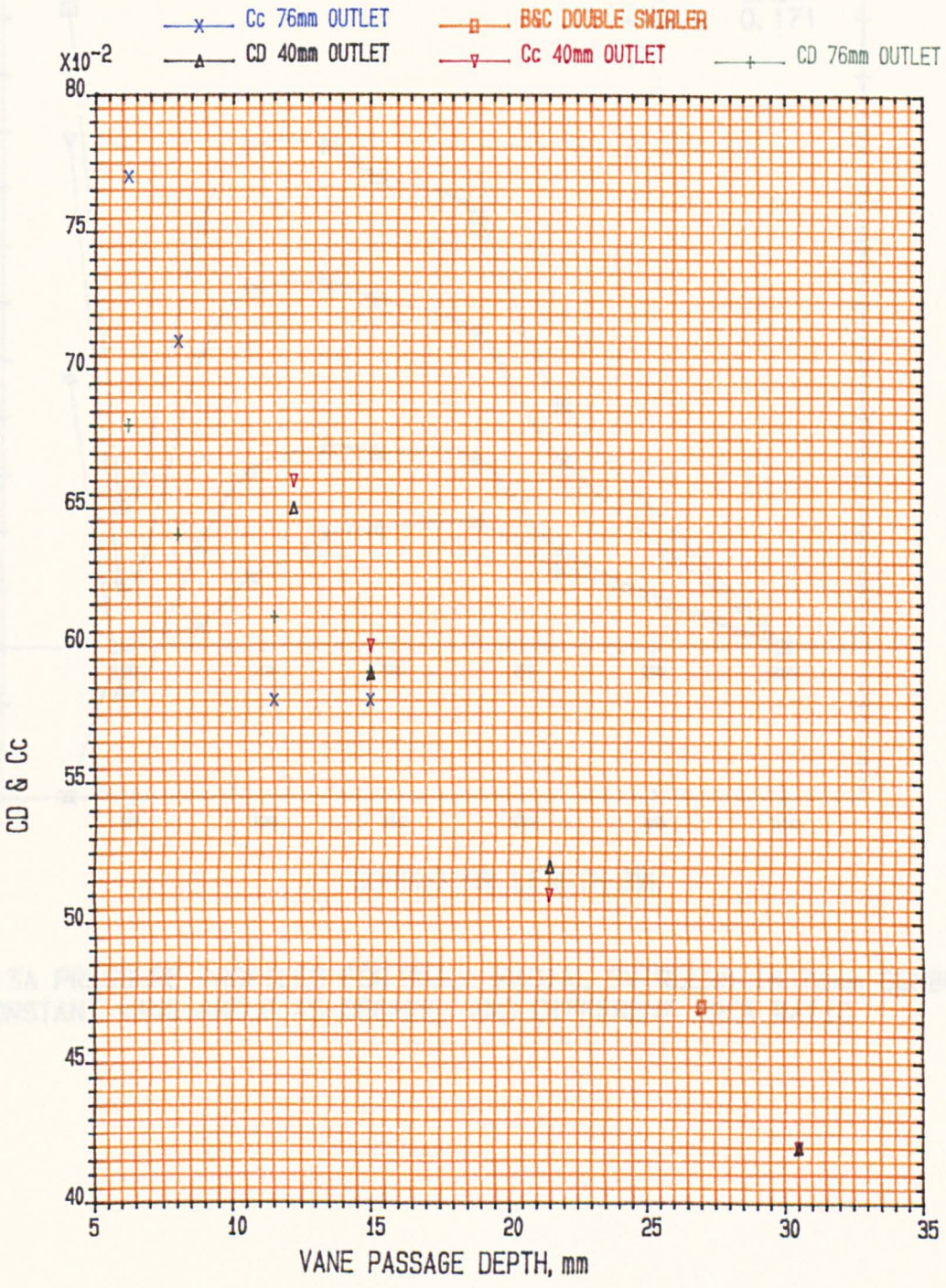

FIG.2.12 VARIATION OF DISCHARGE &CONTRACTION COEFFICIENT WIT VANE PASSAGE DEPTH FOR 45 SWIRLERS; 140mm COMBUSTOR; 305K.

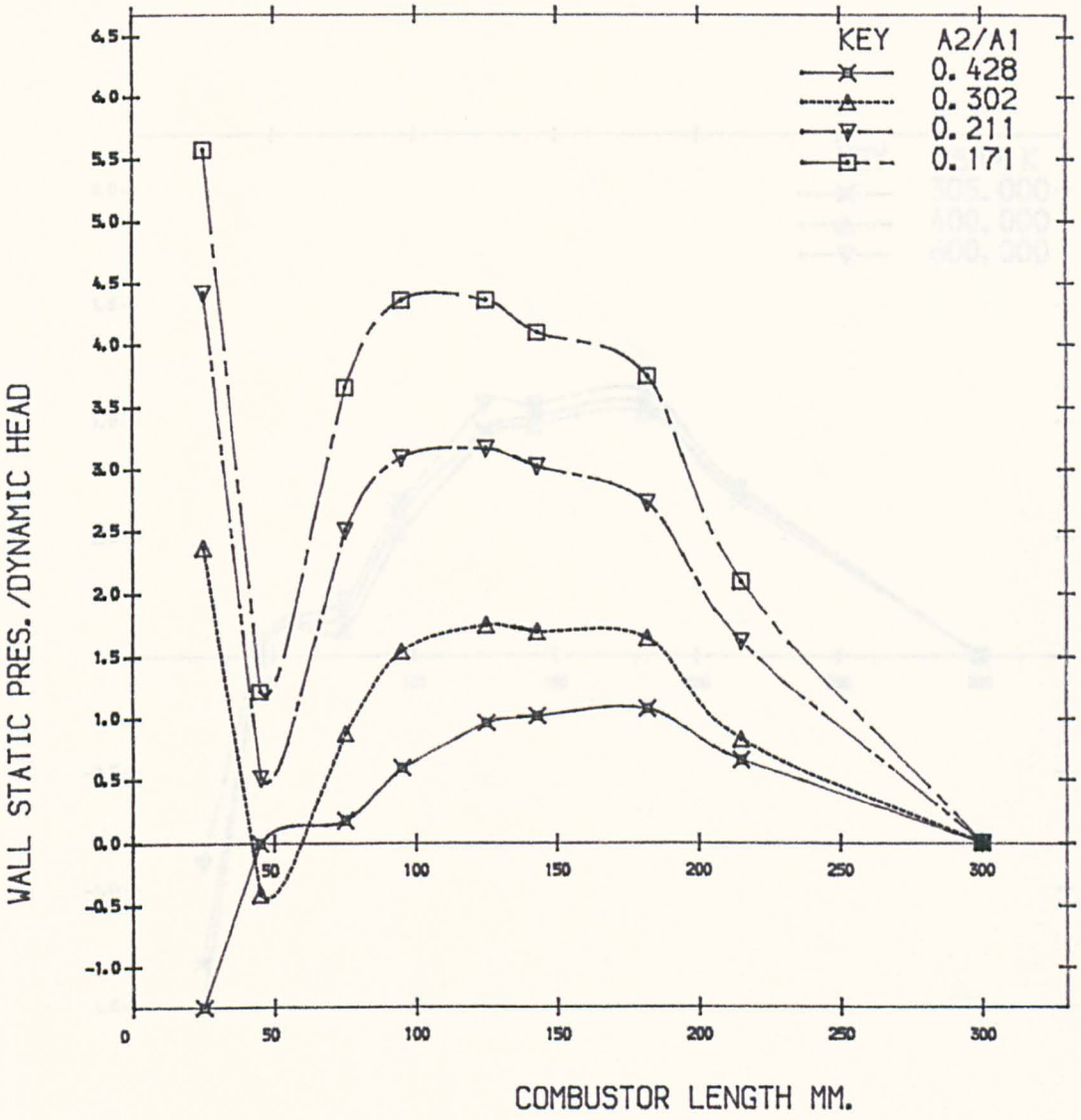

FIG. 2. 13A PRESSURE PROFILES FOR SMALL RADIAL SWIRLERS IN 76mm COMBUSTOR WITH CONSTANT VANE ANGLE 45 DEGREE, AND DIFFERENT AREA RATIO

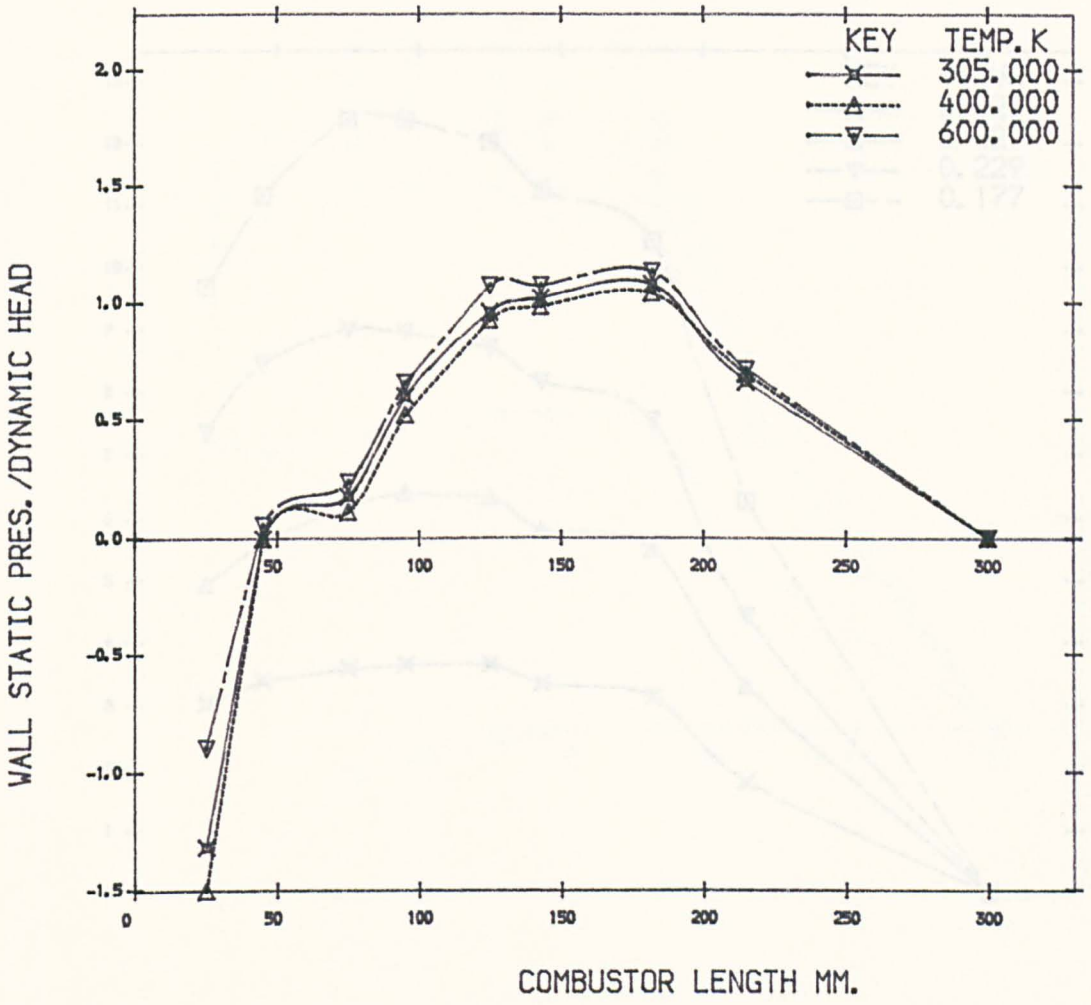

FIG. 2.13B PRESSURE PROFILES FOR SMALL RADIAL SWIRLER (A), 76mm COMBUSTOR FOR DIFFERENT INLET TEMPERATURE & MNO. = 0.047

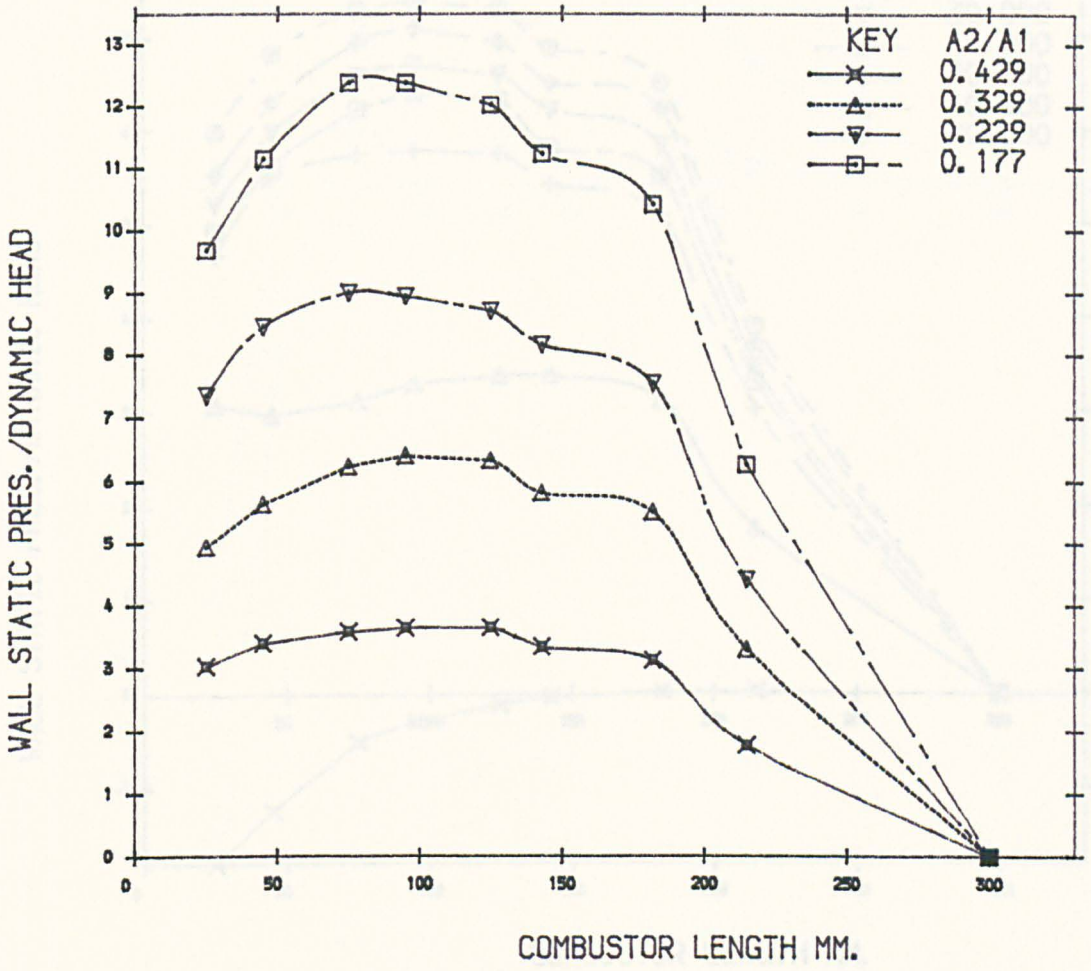

FIG. 2.14 PRESSURE PROFILES FOR LARGE RADIAL SWIRLERS IN 76mm COMBUSTOR WITH CONSTANT VANE ANGLE 45 DEGREE, AND DIFFERENT AREA RATIO

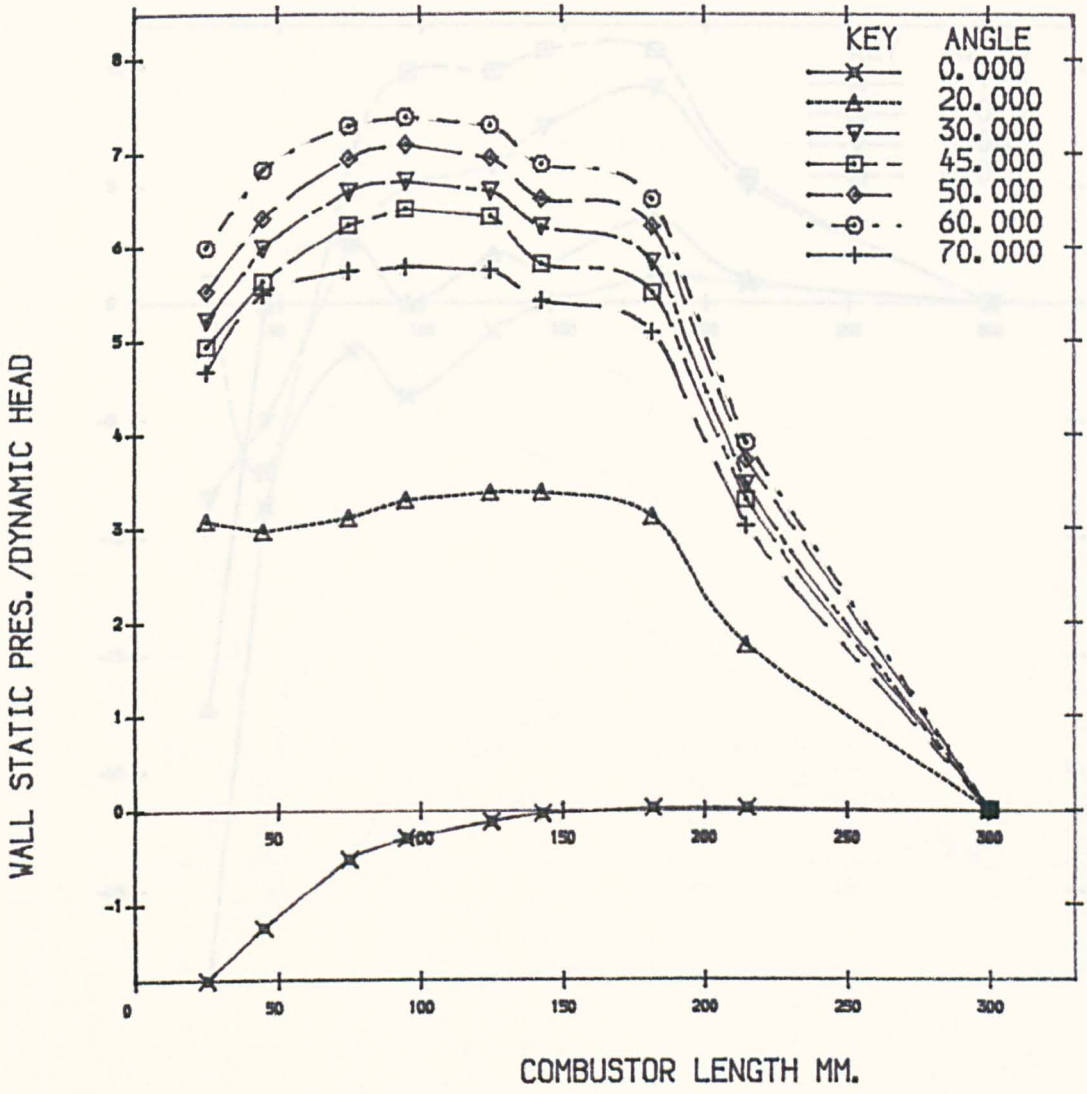

FIG. 2.15 PRESSURE PROFILES FOR RADIAL SWIRLERS IN 76mm COMBUSTOR WITH VARIOUS VANE ANGLE

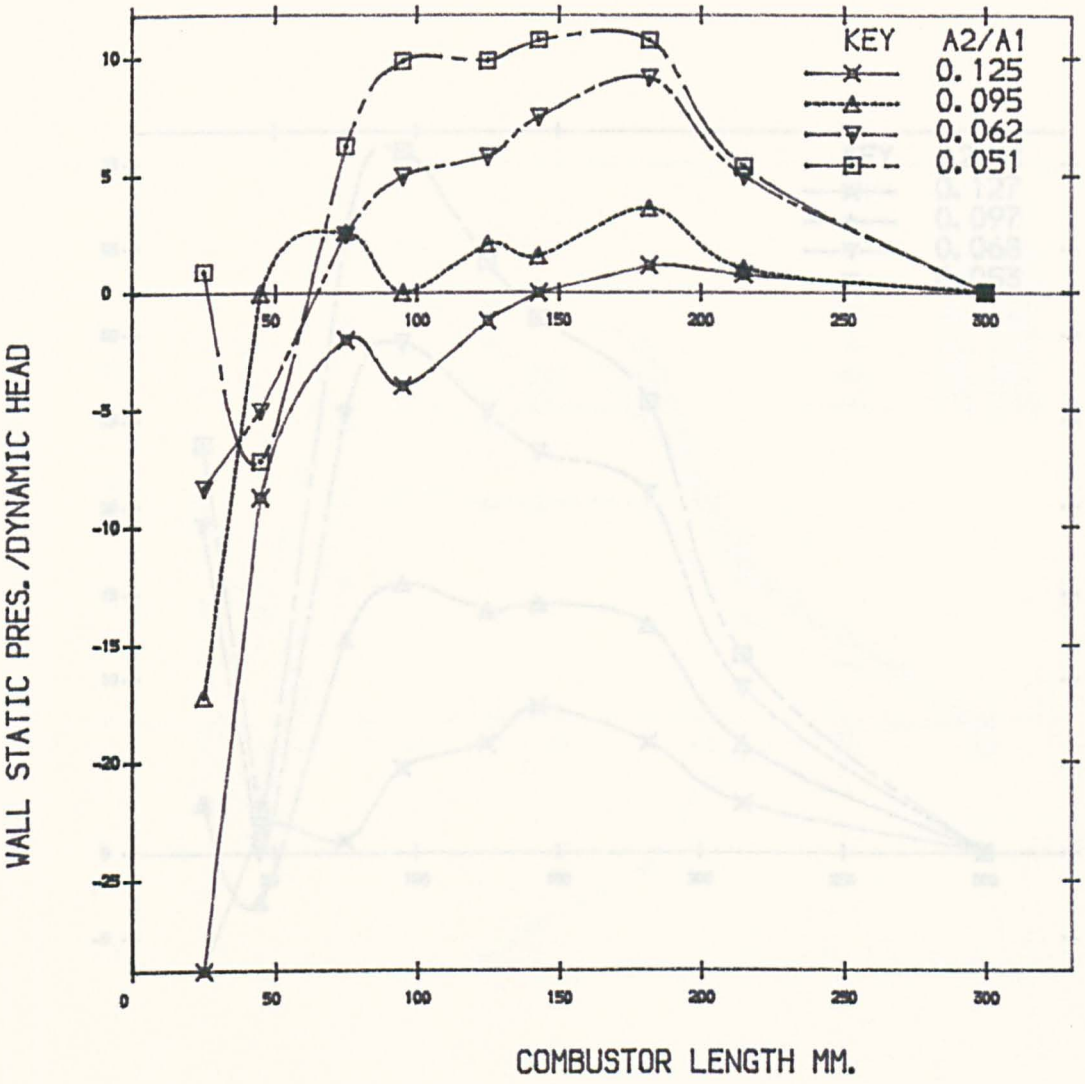

FIG. 2.16 PRESSURE PROFILES, FOR SMALL RADIAL SWIRLER, 140mm COMBUSTOR WITH CONSTANT VANE ANGLE 45 DEGREE AND VARIOUS AREA RATIO

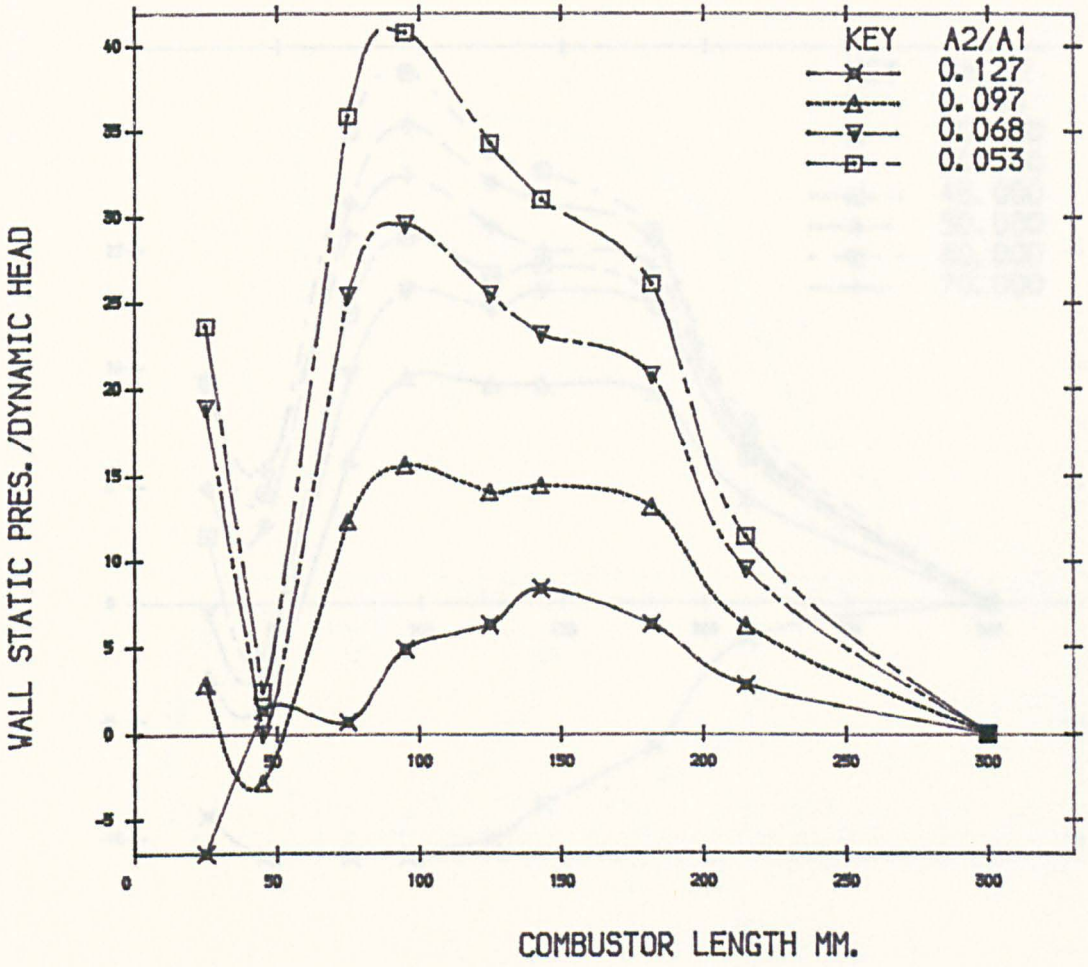

FIG. 2.17 PRESSURE PROFILES, FOR LARGE RADIAL SWIRLER IN 140mm COMBUSTOR WITH CONSTANT VANE ANGLE 45 DEGREE AND VARIOUS AREA RATIO

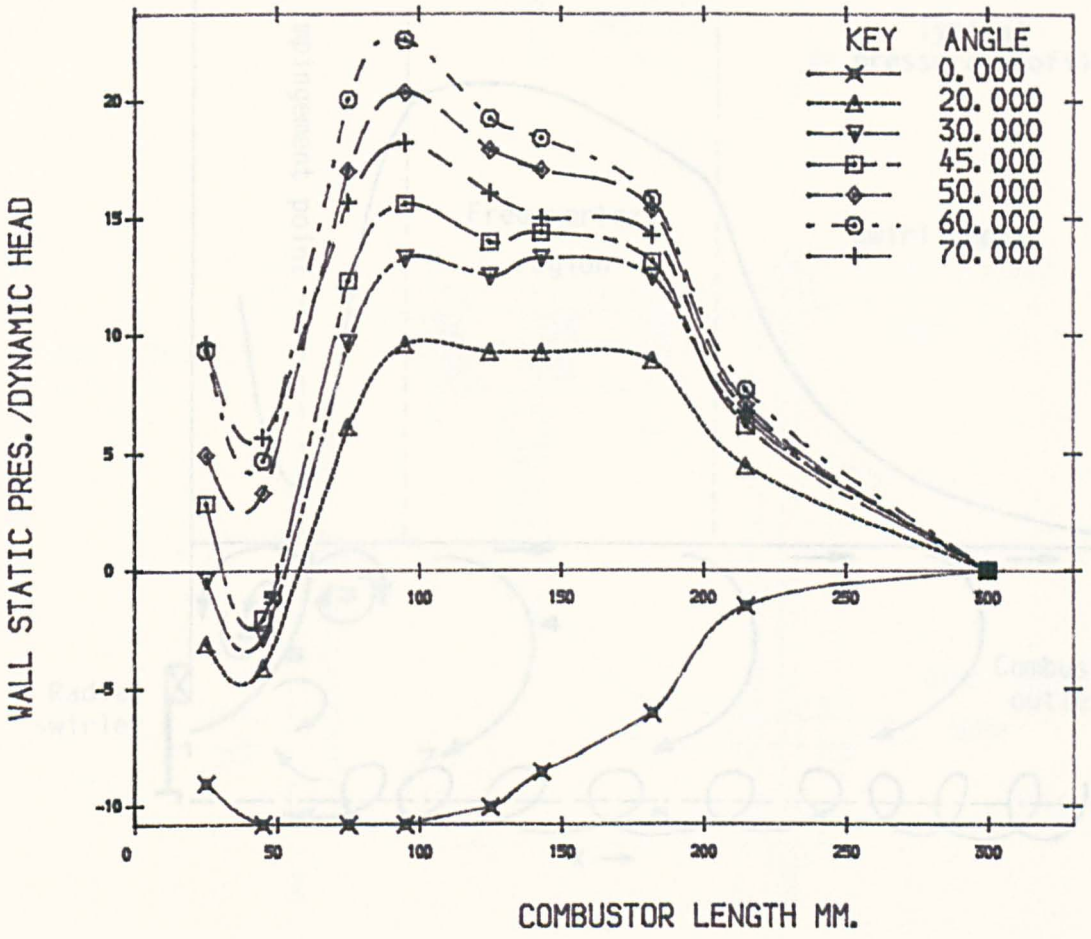

FIG. 2.18 PRESSURE PROFILES, FOR LARGE RADIAL SWIRLER, 140mm COMBUSTOR WITH VARIOUS VANE ANGLE.

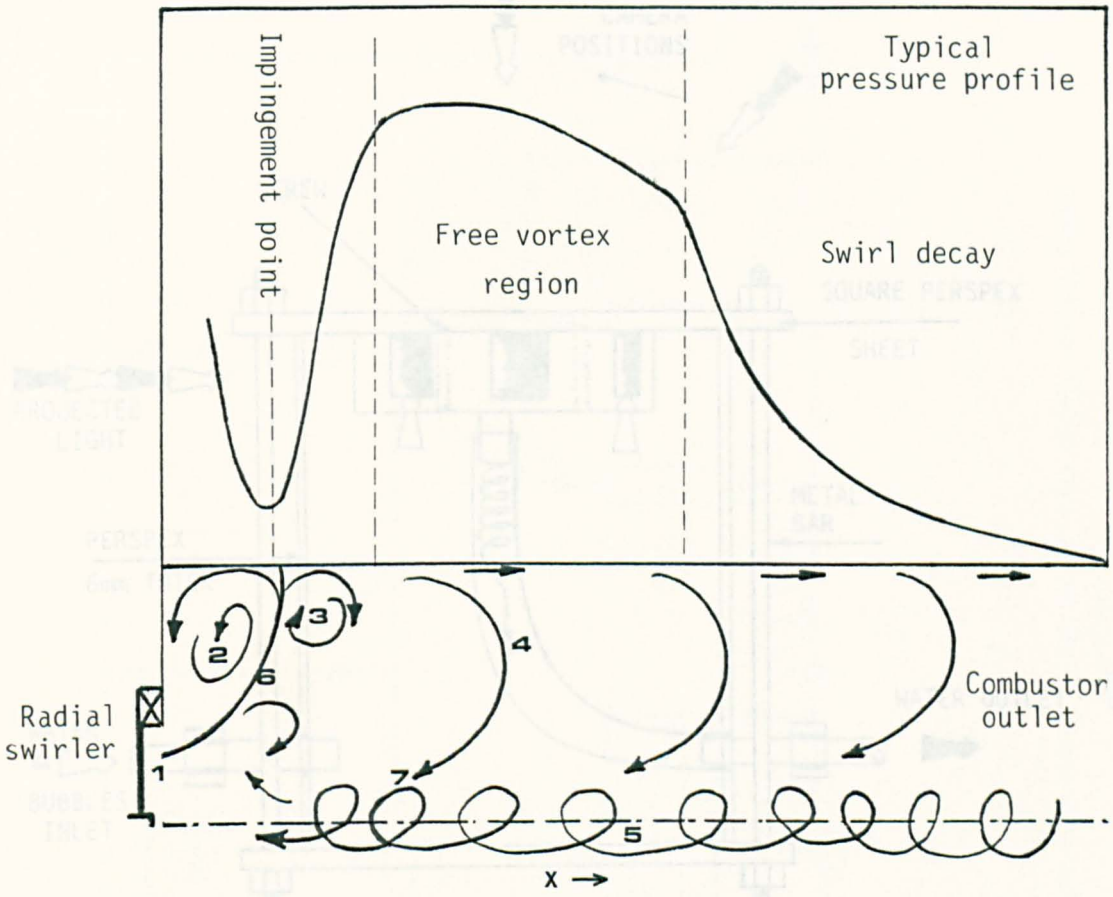

Fig.2.18a Correlation between wall static pressure and the flow pattern issued by the radial swirler

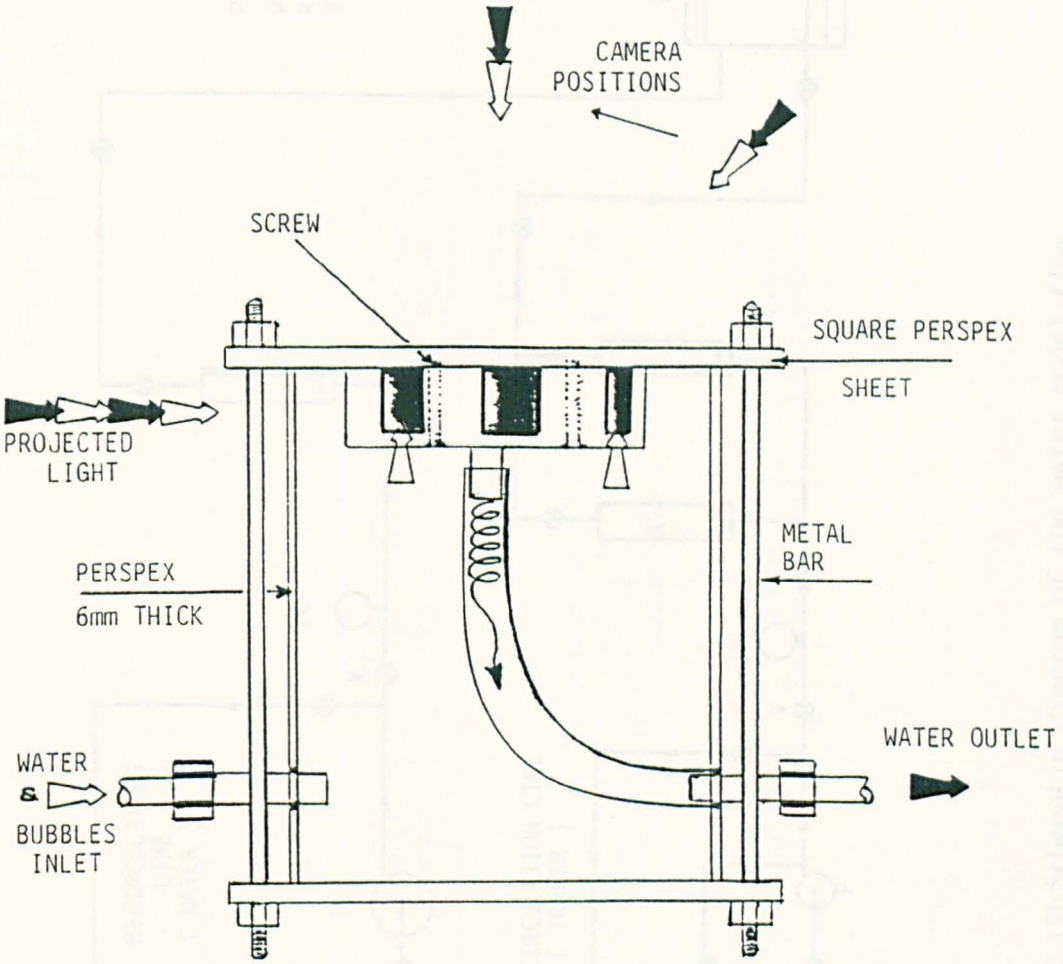

Fig.2.19a SCHEMATIC DIAGRAM OF THE PERSPEX WATER MODEL TO INVESTIGATE THE SEPARATION THROUGH RADIAL SWIRLERS CURVED PASSAGES.

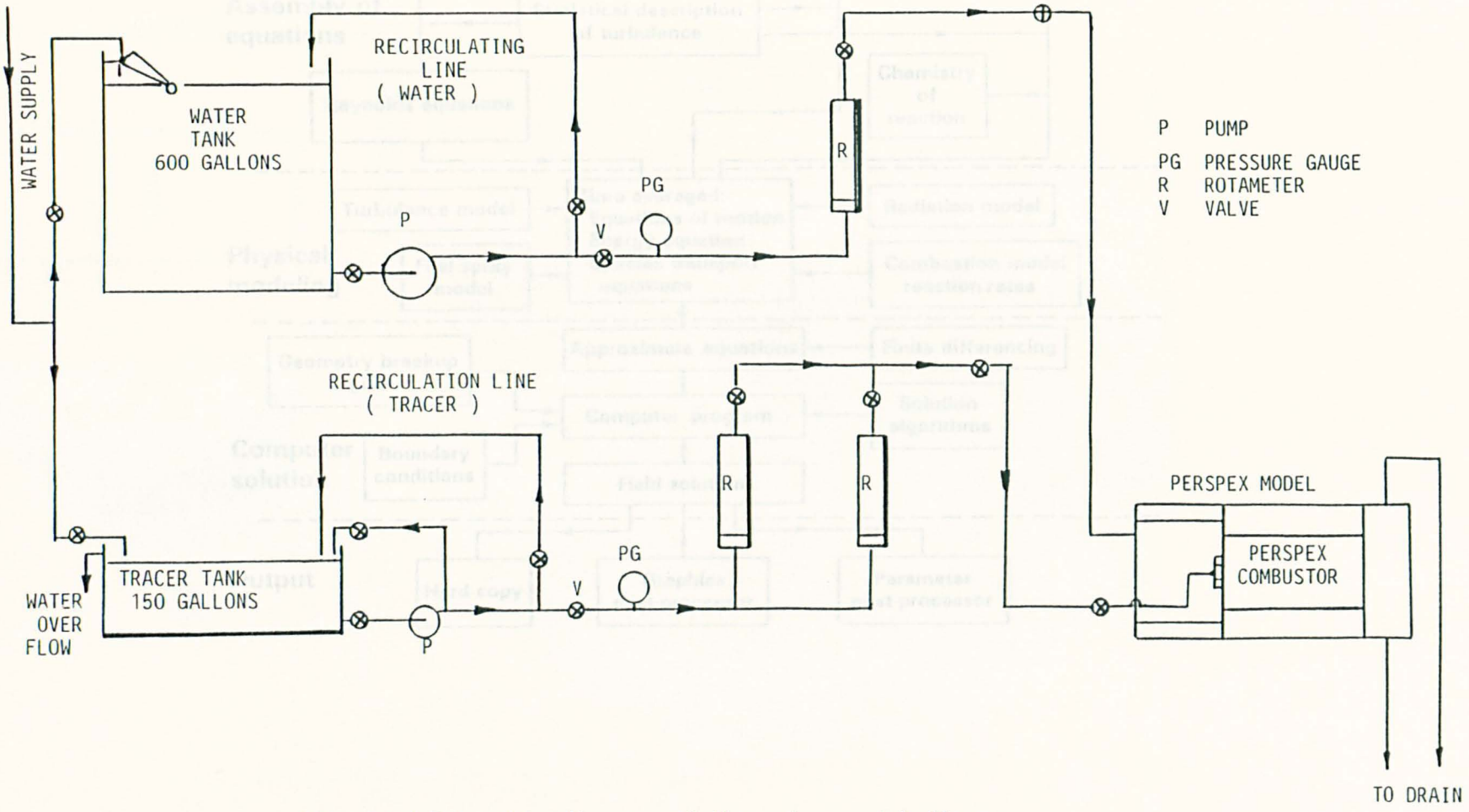

Fig.2.19b Schematic diagram of the water model flow system.

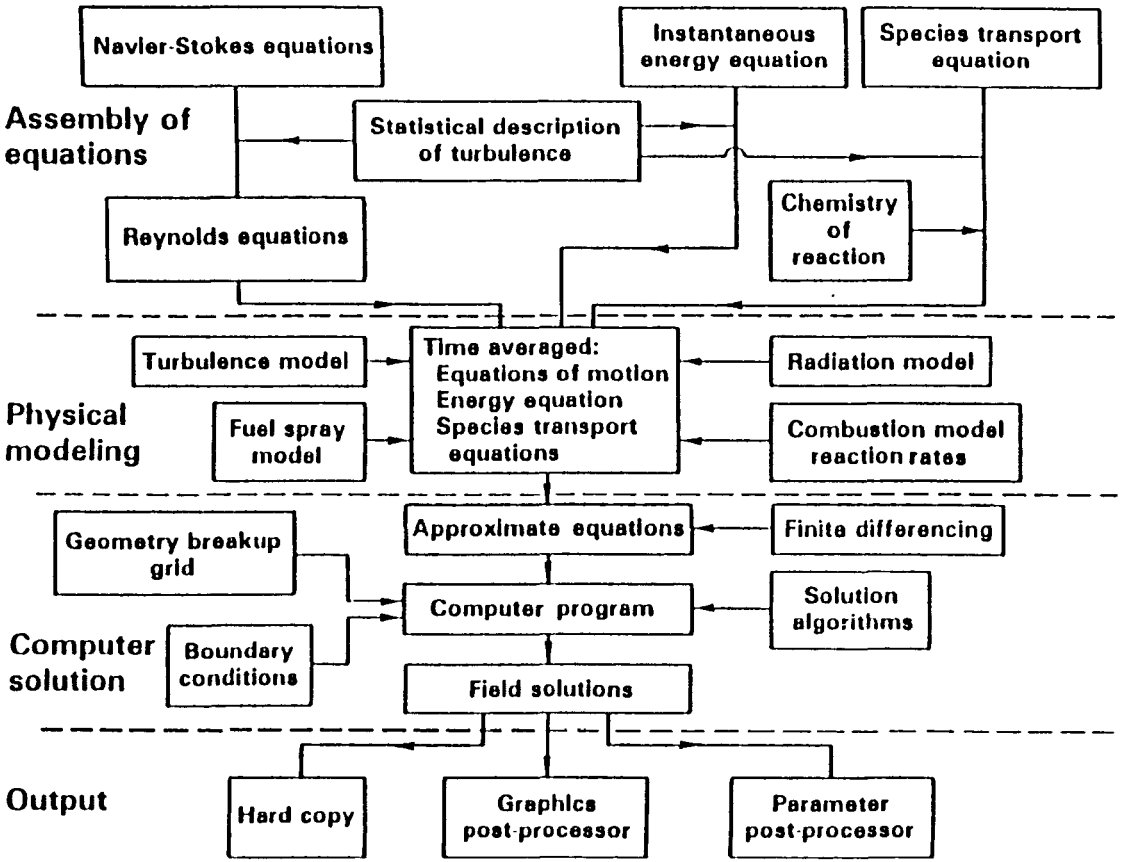

Fig.2.20 Flow diagram of the generic approach of combustors computational calculation process(43).

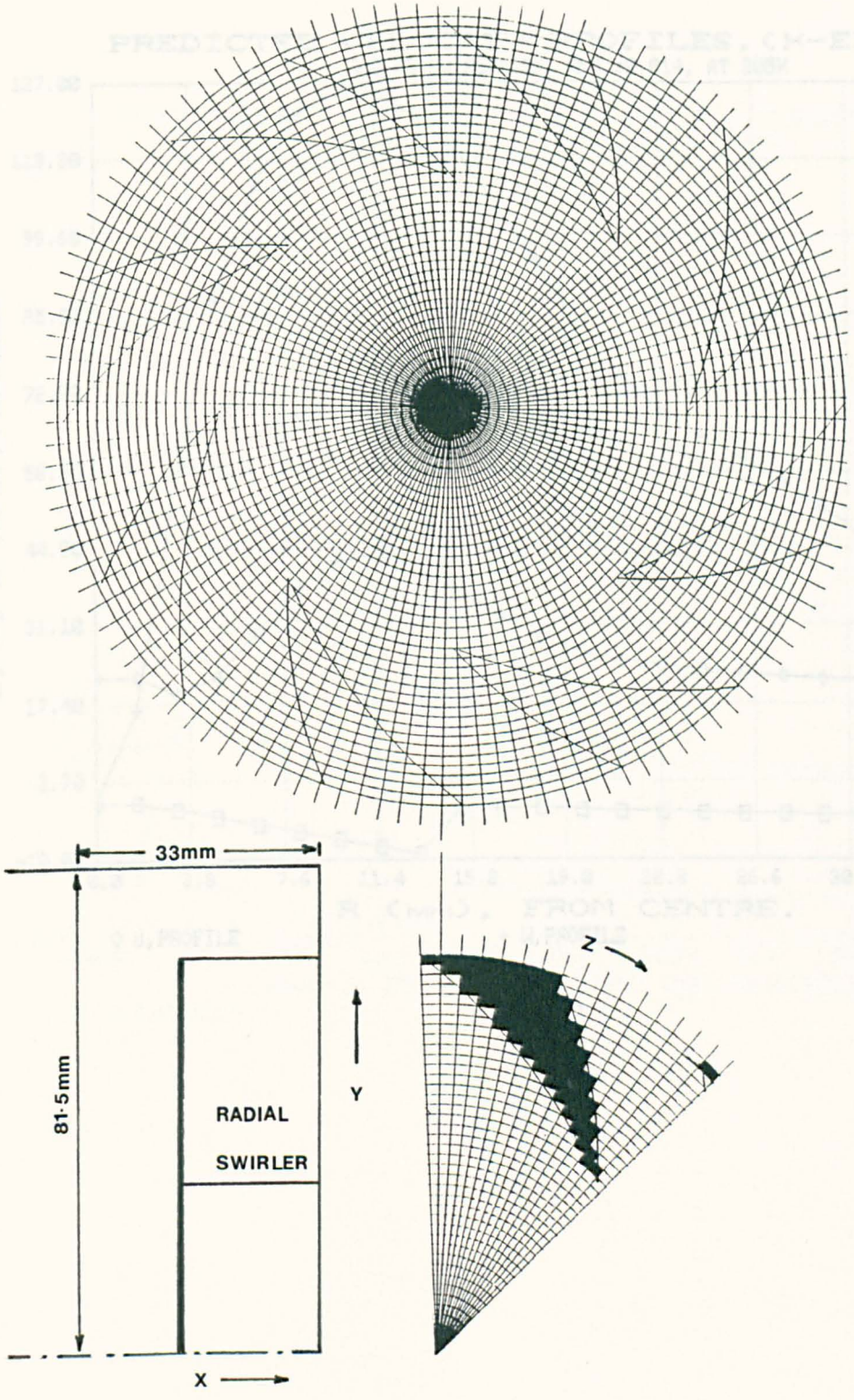

Fig.2.21 Front-view and the 45^{o} sector of the main grid representing radial swirler (B) in polar coordinates using stair-step approach for the curved-passages.

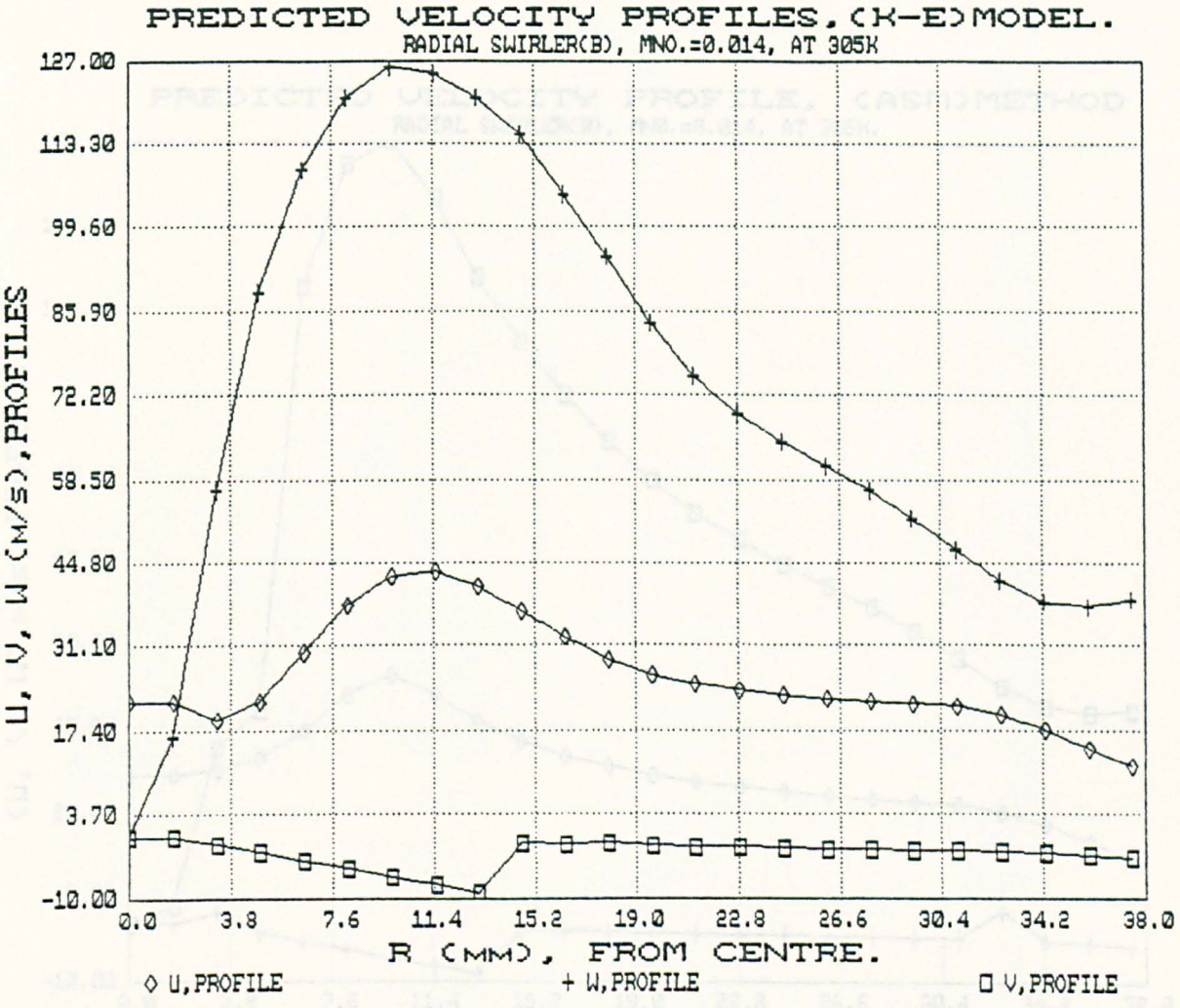
PREDICTED VELOCITY PROFILES,(K-E)MODEL.
RADIAL SWIRLER(B), MNO.=0.014, AT 305K
U, V, W (M/S),PROFILES
127.00
113.30
99.60
85.90
72.20
58.50
44.80
31.10
17.40
3.70
-10.00
0.0
3.8
7.6
11.4
15.2
19.0
22.8
26.6
30.4
34.2
38.0
R (MM), FROM CENTRE.
◇ U,PROFILE
+ W,PROFILE
□ V,PROFILE

Fig.2.22

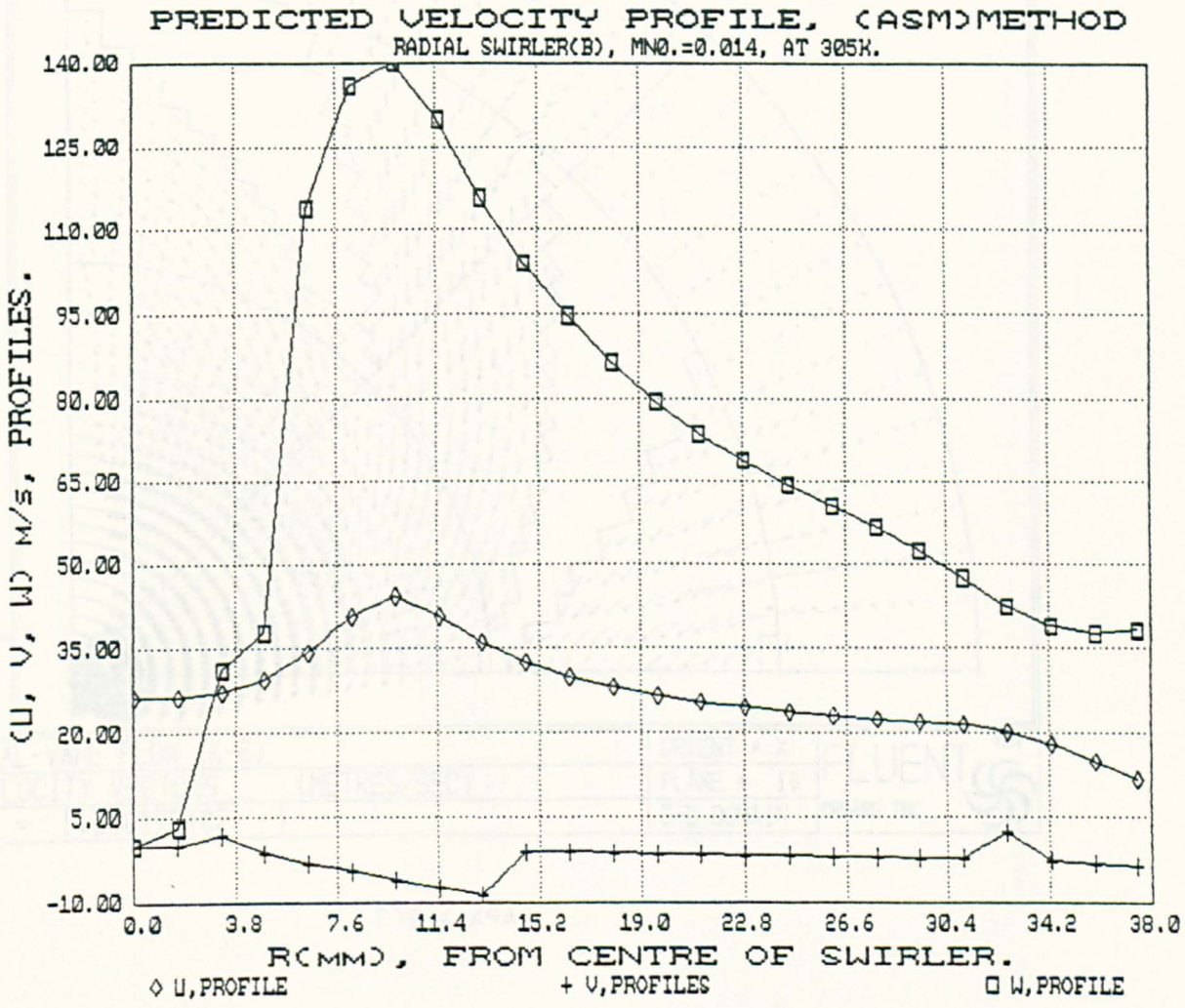
PREDICTED VELOCITY PROFILE, (ASM) METHOD
RADIAL SWIRLER(B), MN0.=0.014, AT 305K.
140.00
125.00
110.00
95.00
80.00
65.00
50.00
35.00
20.00
5.00
-10.00
(U, V, W) M/S, PROFILES.
0.0
3.8
7.6
11.4
15.2
19.0
22.8
26.6
30.4
34.2
38.0
R(MM), FROM CENTRE OF SWIRLER.
◊ U,PROFILE
+ V,PROFILES
□ W,PROFILE

Fig.2.23

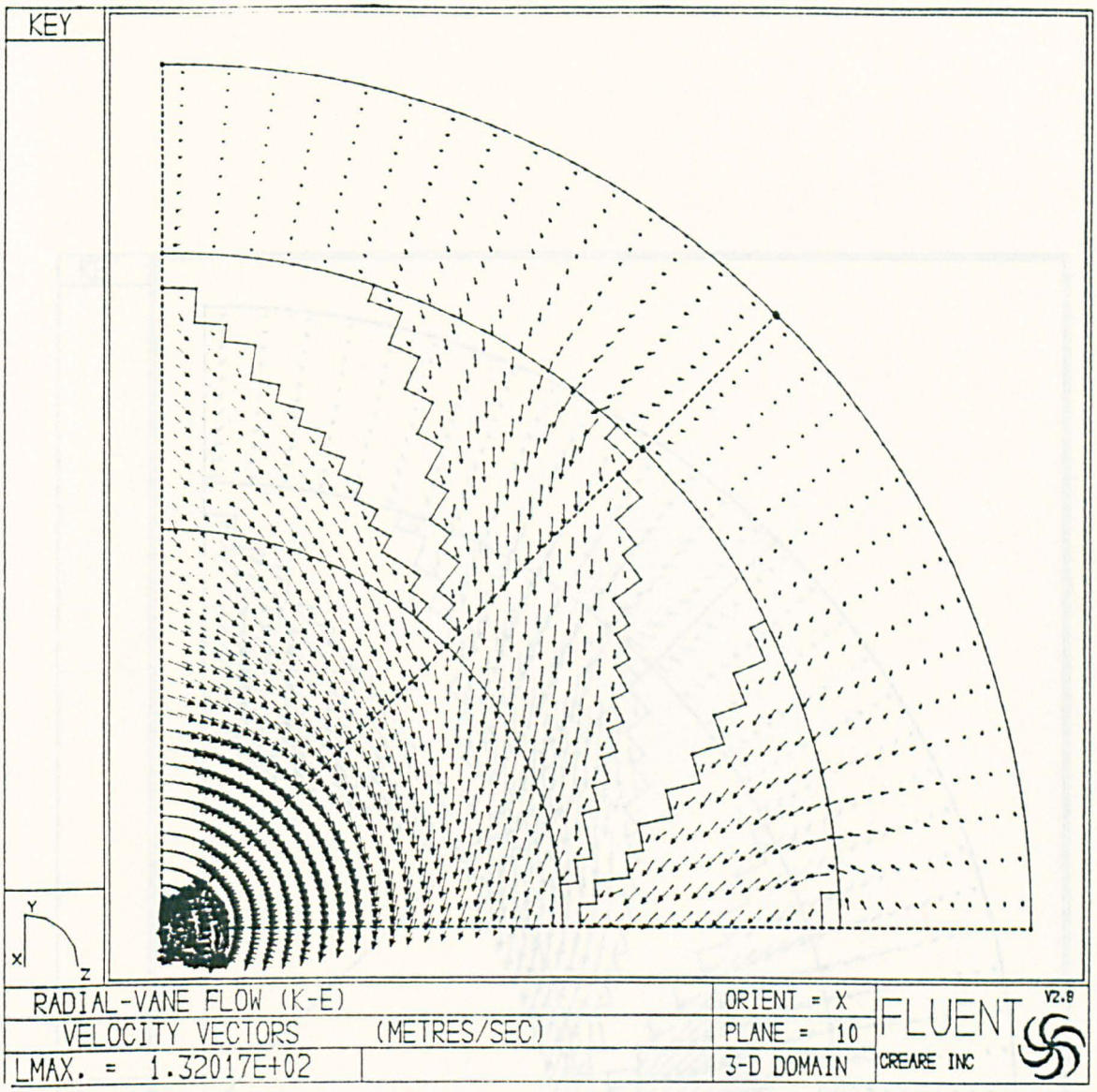
KEY
Y
X
Z
RADIAL-VANE FLOW (K-E)
VELOCITY VECTORS (METRES/SEC)
LMAX. = 1.32017E+02
ORIENT = X
PLANE = 10
3-D DOMAIN
FLUENT V2.8
CREARE INC

Fig.2.24a

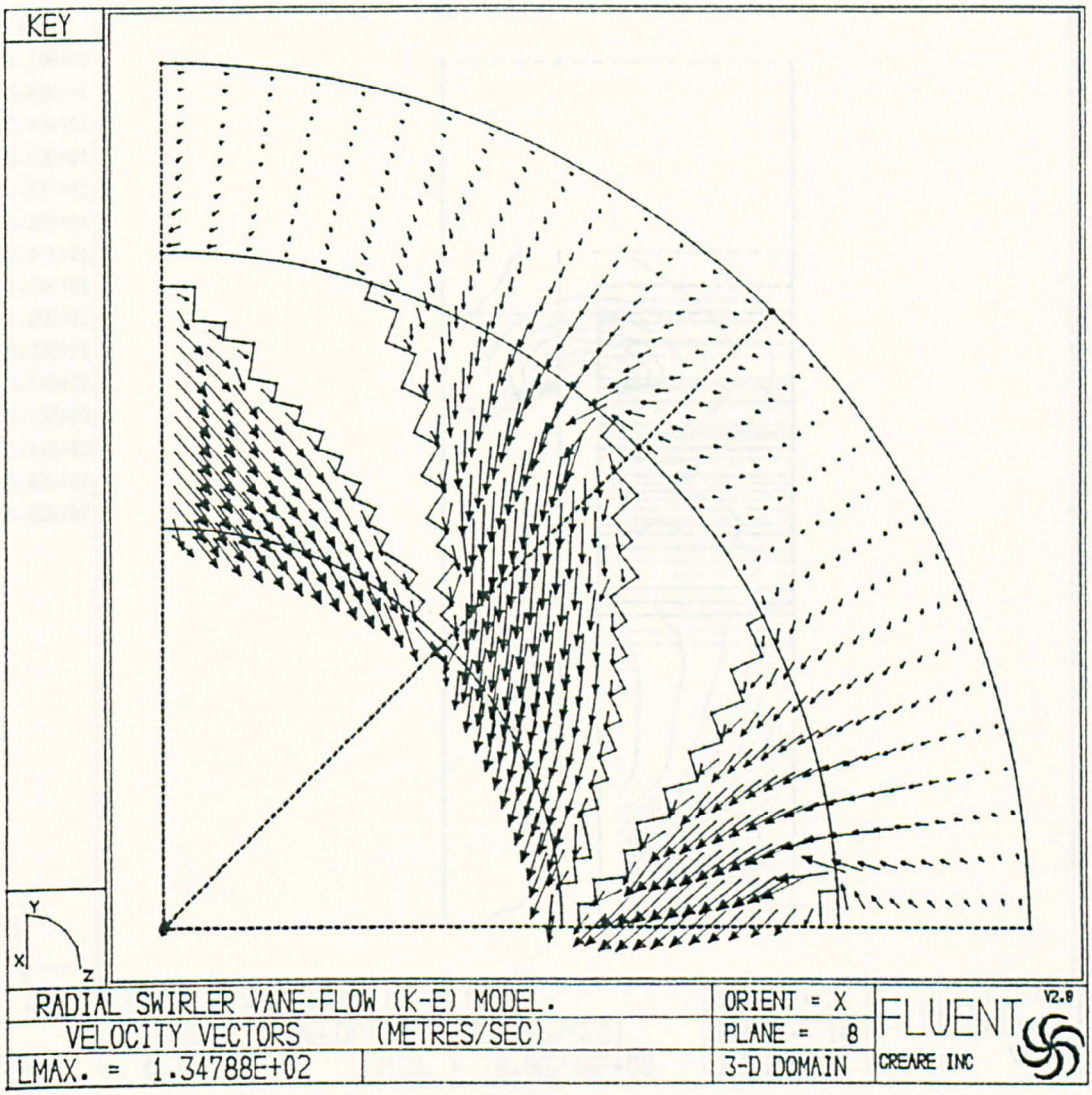
KEY
Y
X
Z
RADIAL SWIRLER VANE-FLOW (K-E) MODEL.
VELOCITY VECTORS (METRES/SEC)
LMAX. = 1.34788E+02
ORIENT = X
PLANE = 8
3-D DOMAIN
FLUENT V2.0
CREARE INC

Fig.2.24b

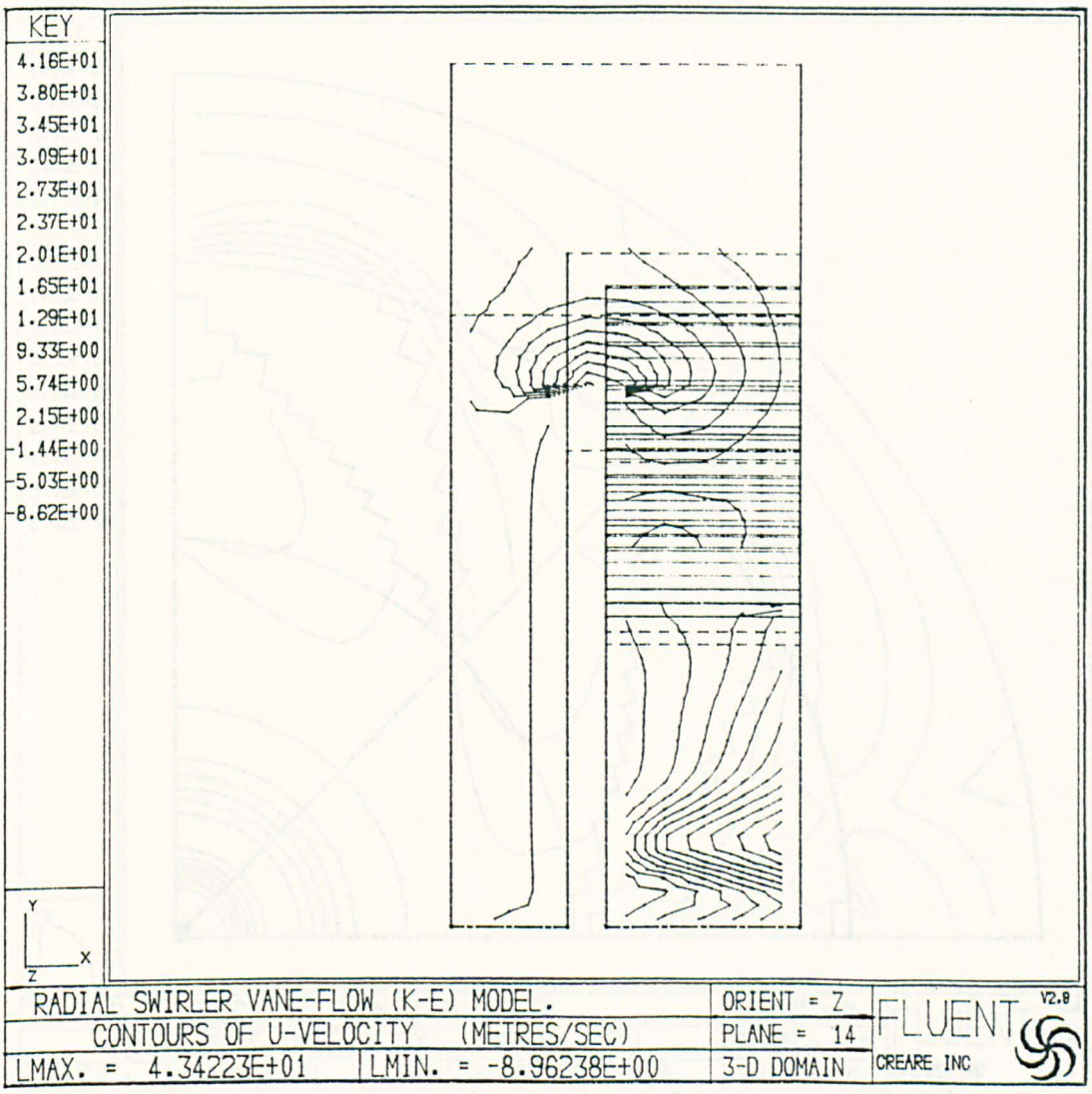
KEY
4.16E+01
3.80E+01
3.45E+01
3.09E+01
2.73E+01
2.37E+01
2.01E+01
1.65E+01
1.29E+01
9.33E+00
5.74E+00
2.15E+00
-1.44E+00
-5.03E+00
-8.62E+00
Y
X
Z
RADIAL SWIRLER VANE-FLOW (K-E) MODEL.
CONTOURS OF U-VELOCITY (METRES/SEC)
LMAX. = 4.34223E+01
LMIN. = -8.96238E+00
ORIENT = Z
PLANE = 14
3-D DOMAIN
FLUENT V2.8
CREARE INC

Fig.2.25

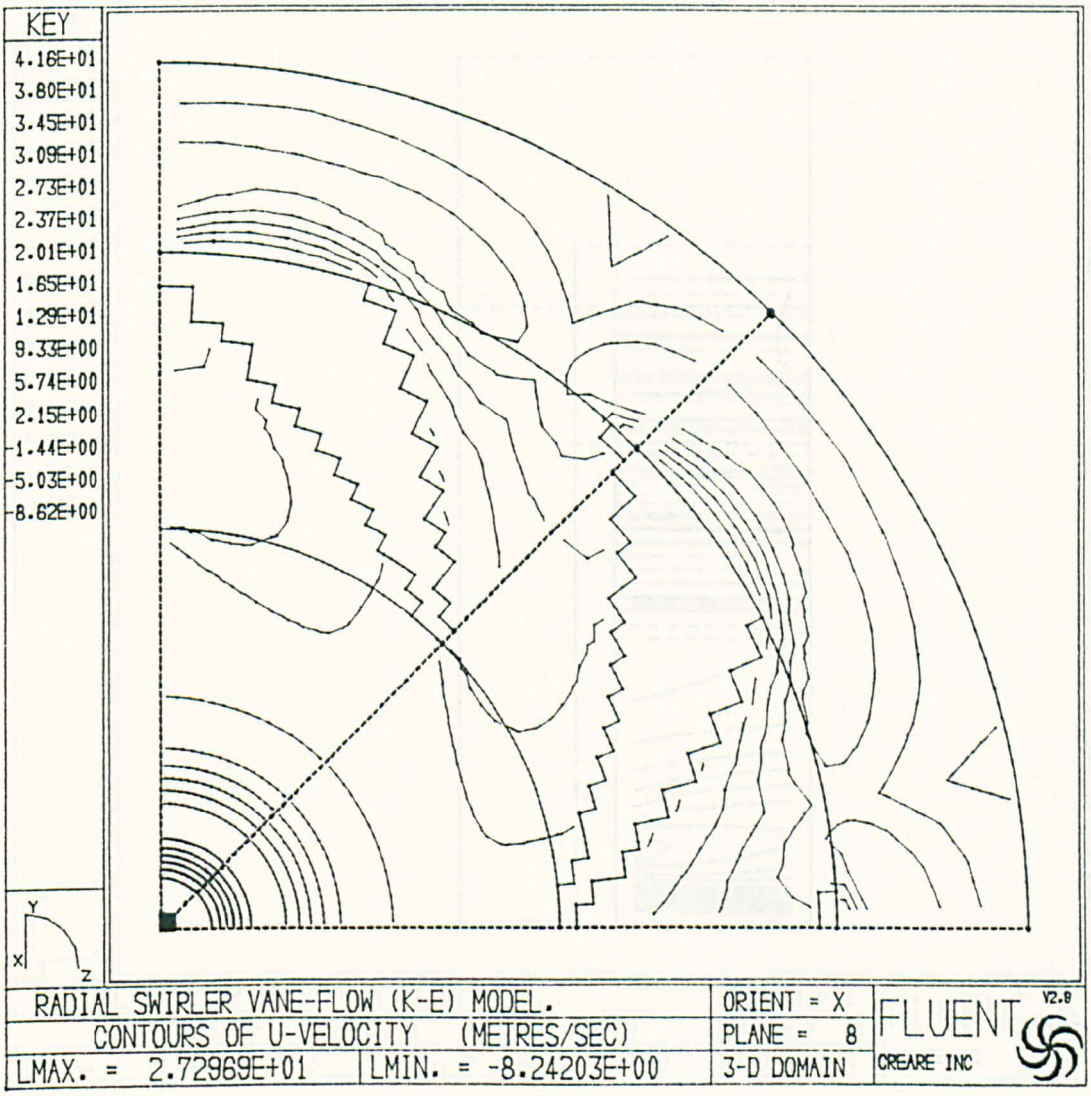
KEY
4.16E+01
3.80E+01
3.45E+01
3.09E+01
2.73E+01
2.37E+01
2.01E+01
1.65E+01
1.29E+01
9.33E+00
5.74E+00
2.15E+00
-1.44E+00
-5.03E+00
-8.62E+00
Y
X
Z
RADIAL SWIRLER VANE-FLOW (K-E) MODEL.
CONTOURS OF U-VELOCITY (METRES/SEC)
LMAX. = 2.72969E+01
LMIN. = -8.24203E+00
ORIENT = X
PLANE = 8
3-D DOMAIN
FLUENT V2.8
CREARE INC

Fig.2.26

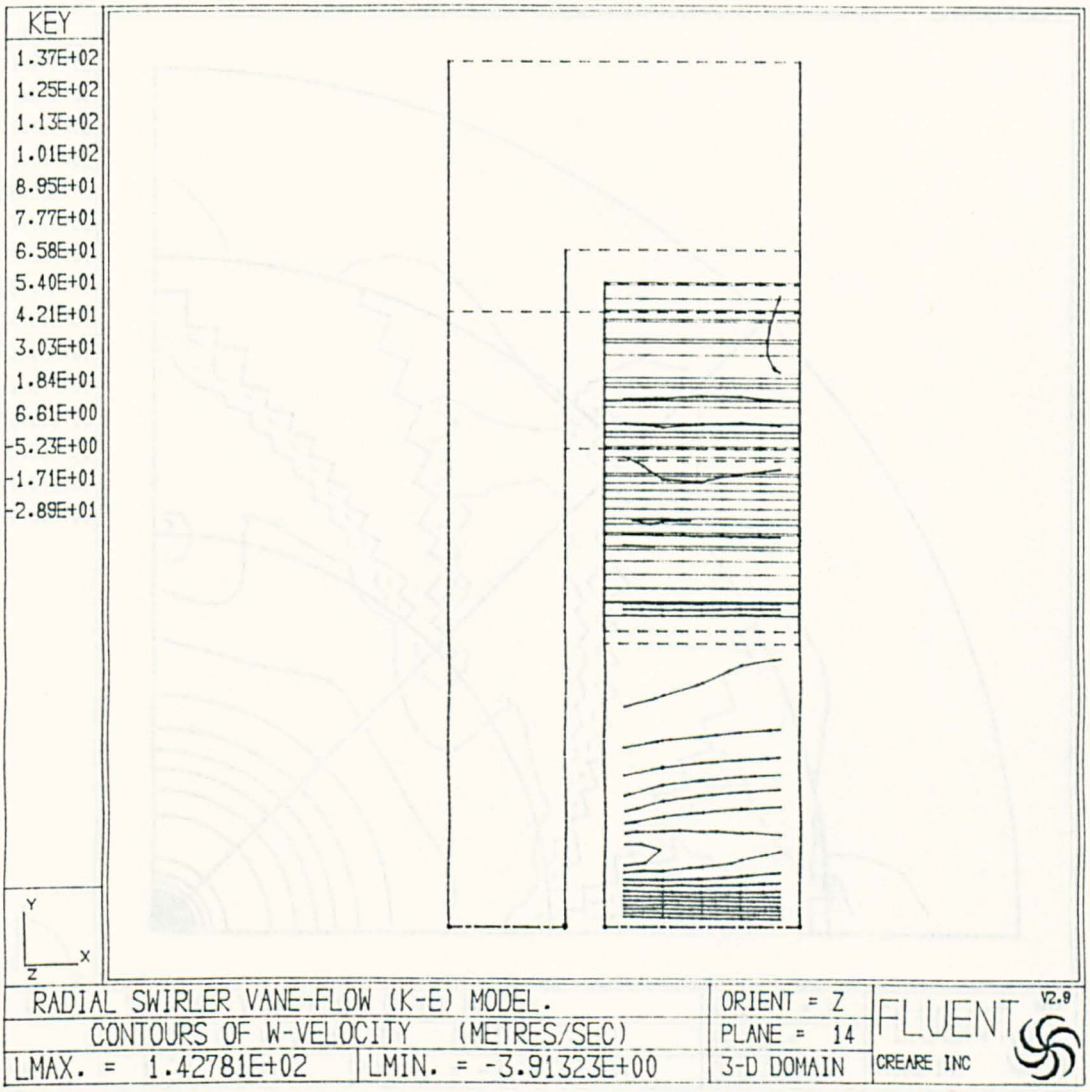
KEY
1.37E+02
1.25E+02
1.13E+02
1.01E+02
8.95E+01
7.77E+01
6.58E+01
5.40E+01
4.21E+01
3.03E+01
1.84E+01
6.61E+00
-5.23E+00
-1.71E+01
-2.89E+01
Y
X
Z
RADIAL SWIRLER VANE-FLOW (K-E) MODEL.
CONTOURS OF W-VELOCITY (METRES/SEC)
LMAX. = 1.42781E+02
LMIN. = -3.91323E+00
ORIENT = Z
PLANE = 14
3-D DOMAIN
FLUENT V2.9
CREARE INC

Fig.2.27

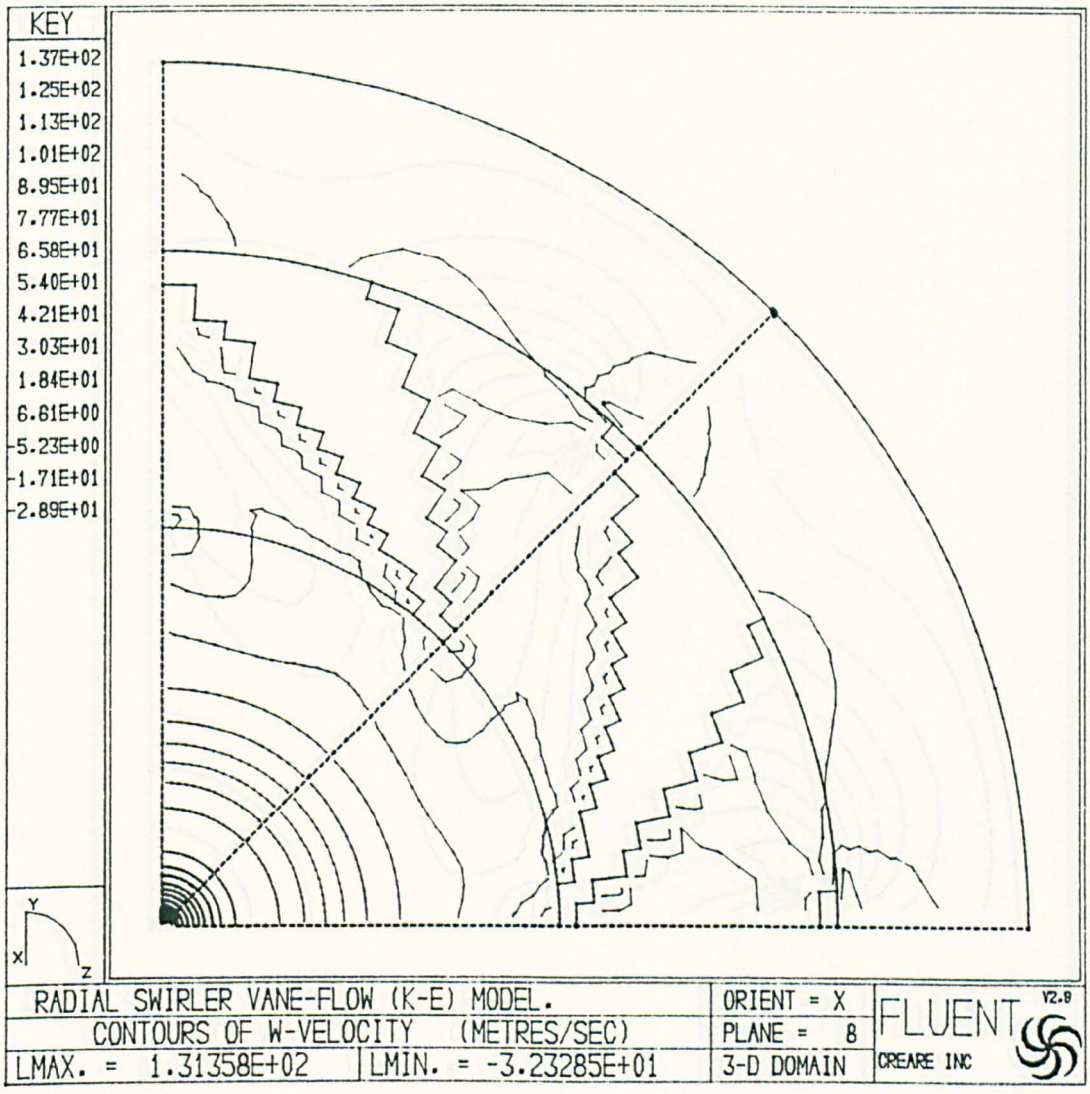
KEY
1.37E+02
1.25E+02
1.13E+02
1.01E+02
8.95E+01
7.77E+01
6.58E+01
5.40E+01
4.21E+01
3.03E+01
1.84E+01
6.61E+00
-5.23E+00
-1.71E+01
-2.89E+01
Y
X
Z
RADIAL SWIRLER VANE-FLOW (K-E) MODEL.
CONTOURS OF W-VELOCITY (METRES/SEC)
LMAX. = 1.31358E+02
LMIN. = -3.23285E+01
ORIENT = X
PLANE = 8
3-D DOMAIN
FLUENT
V2.8
CREARE INC

Fig.2.28

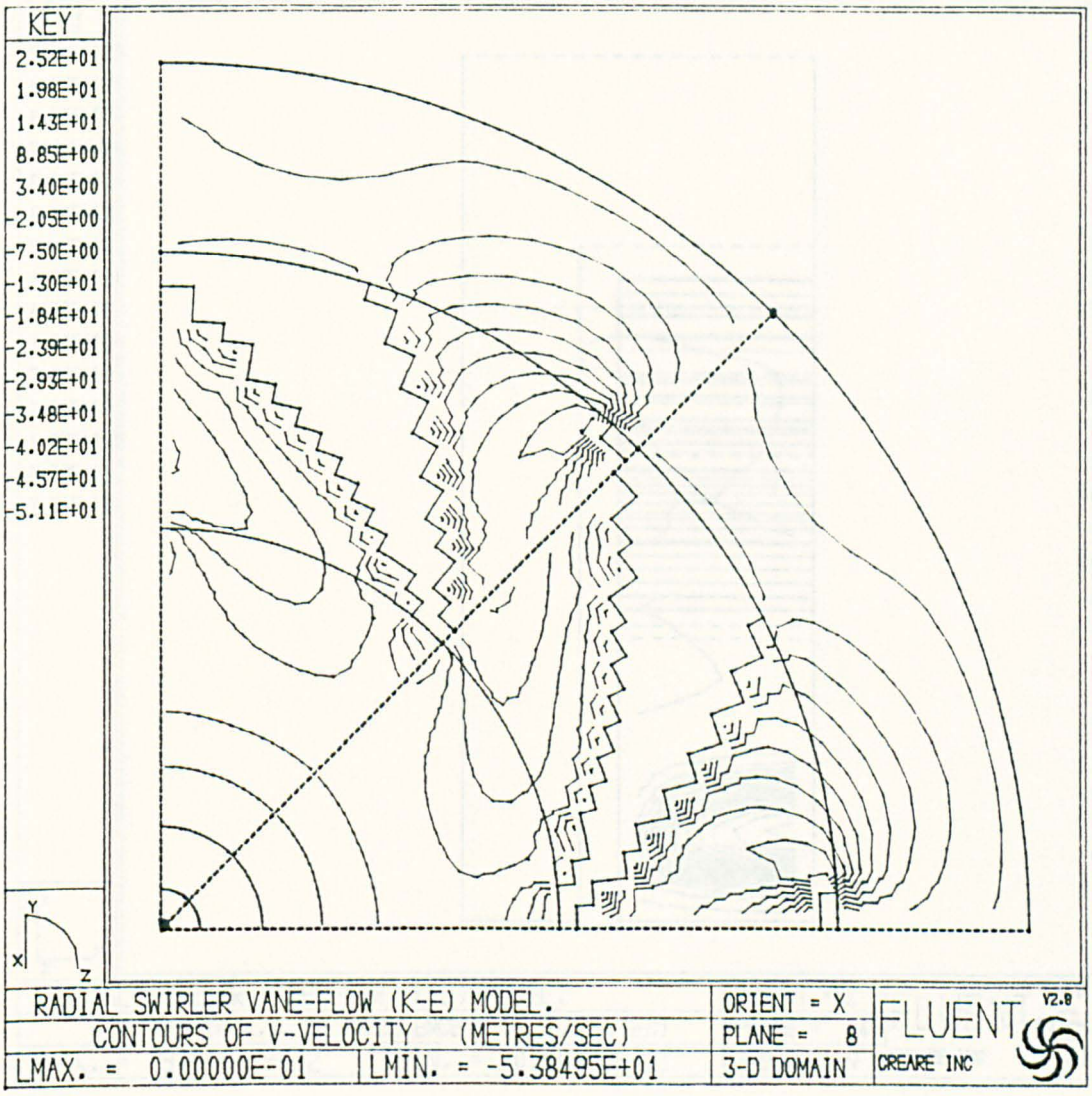
KEY
2.52E+01
1.98E+01
1.43E+01
8.85E+00
3.40E+00
-2.05E+00
-7.50E+00
-1.30E+01
-1.84E+01
-2.39E+01
-2.93E+01
-3.48E+01
-4.02E+01
-4.57E+01
-5.11E+01
Y
X
Z
RADIAL SWIRLER VANE-FLOW (K-E) MODEL.
CONTOURS OF V-VELOCITY (METRES/SEC)
LMAX. = 0.00000E-01
LMIN. = -5.38495E+01
ORIENT = X
PLANE = 8
3-D DOMAIN
FLUENT
V2.0
CREARE INC

Fig.2.29

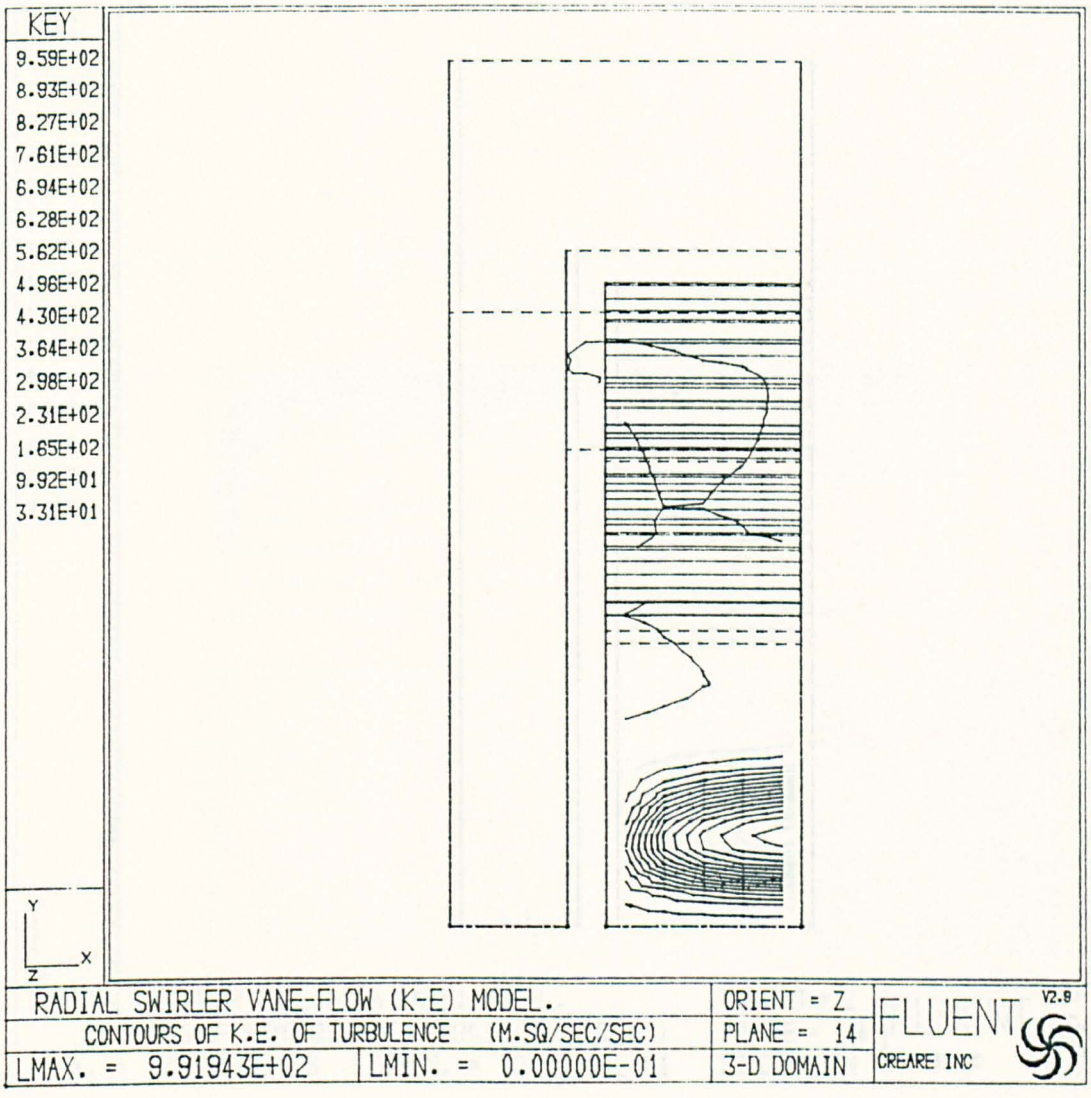
KEY
9.59E+02
8.93E+02
8.27E+02
7.61E+02
6.94E+02
6.28E+02
5.62E+02
4.96E+02
4.30E+02
3.64E+02
2.98E+02
2.31E+02
1.65E+02
9.92E+01
3.31E+01
Y
X
Z
RADIAL SWIRLER VANE-FLOW (K-E) MODEL.
CONTOURS OF K.E. OF TURBULENCE (M.SQ/SEC/SEC)
LMAX. = 9.91943E+02
LMIN. = 0.00000E-01
ORIENT = Z
PLANE = 14
3-D DOMAIN
FLUENT
V2.9
CREARE INC

Fig.2.30

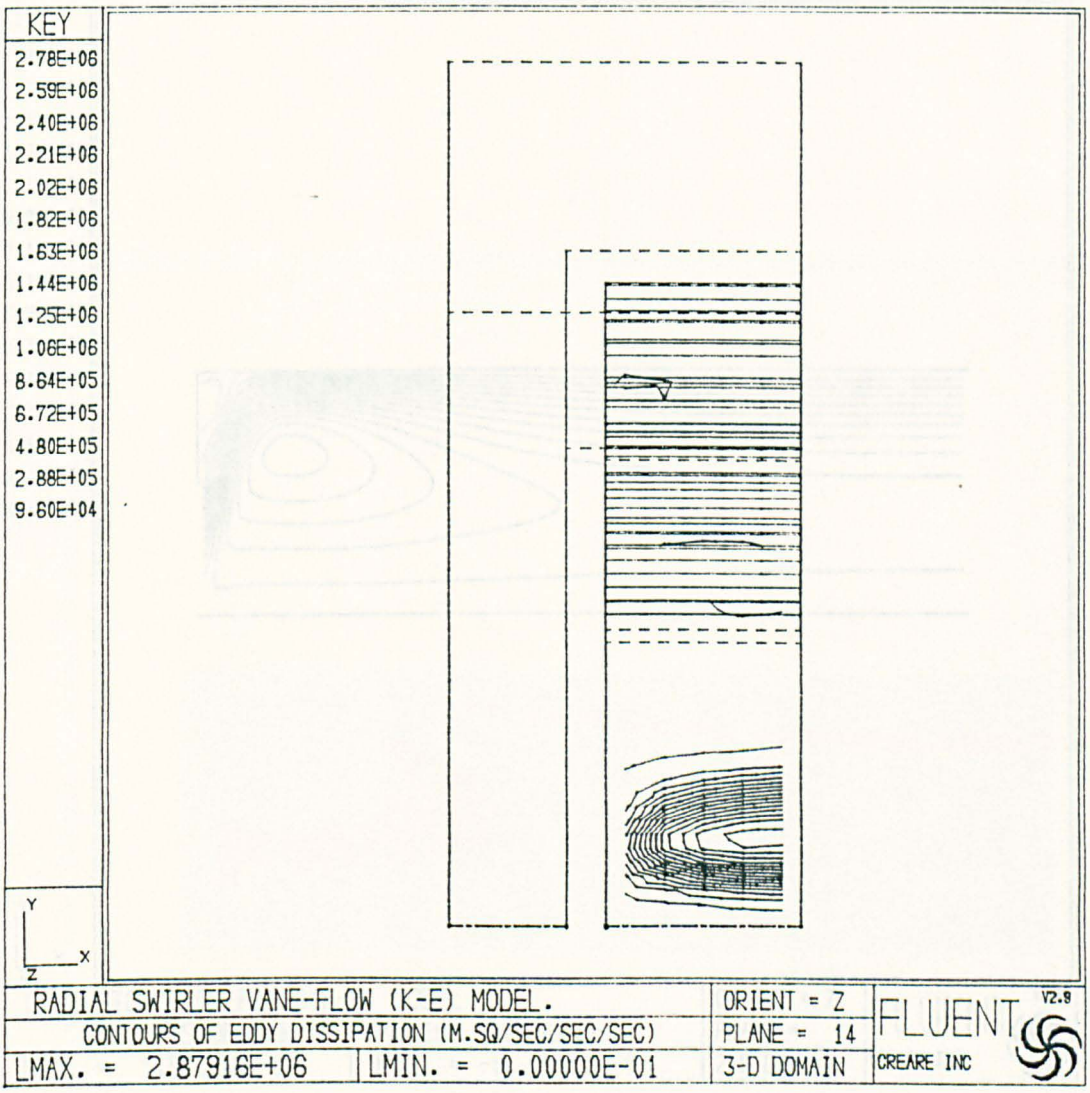
KEY
2.78E+06
2.59E+06
2.40E+06
2.21E+06
2.02E+06
1.82E+06
1.63E+06
1.44E+06
1.25E+06
1.06E+06
8.64E+05
6.72E+05
4.80E+05
2.88E+05
9.60E+04
Y
X
Z
RADIAL SWIRLER VANE-FLOW (K-E) MODEL.
CONTOURS OF EDDY DISSIPATION (M.SQ/SEC/SEC/SEC)
LMAX. = 2.87916E+06
LMIN. = 0.00000E-01
ORIENT = Z
PLANE = 14
3-D DOMAIN
FLUENT
V2.8
CREARE INC

Fig.2.31

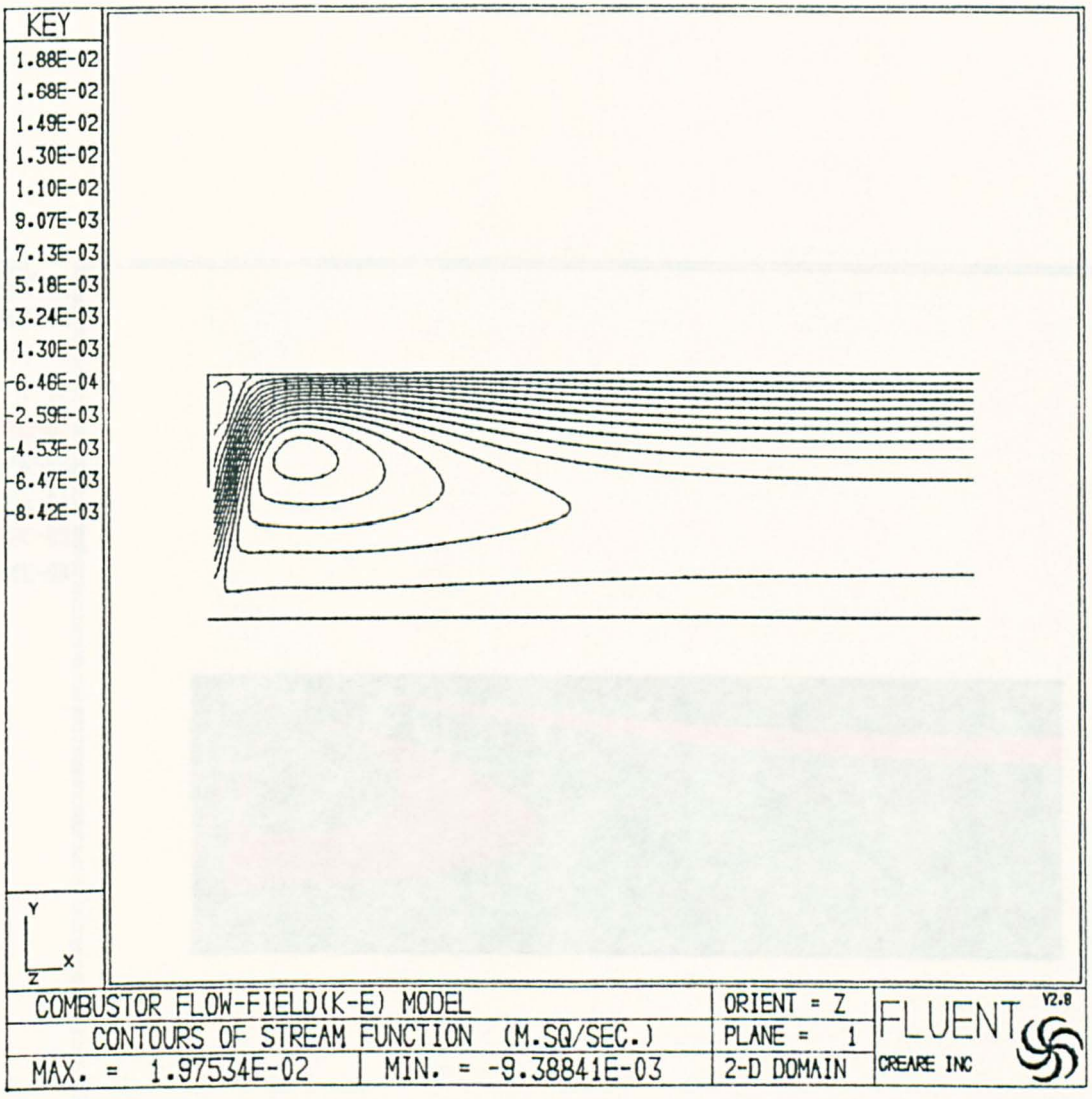
KEY
1.88E-02
1.68E-02
1.49E-02
1.30E-02
1.10E-02
9.07E-03
7.13E-03
5.18E-03
3.24E-03
1.30E-03
-6.46E-04
-2.59E-03
-4.53E-03
-6.47E-03
-8.42E-03
Y
X
Z
COMBUSTOR FLOW-FIELD(K-E) MODEL
CONTOURS OF STREAM FUNCTION (M.SQ/SEC.)
MAX. = 1.97534E-02
MIN. = -9.38841E-03
ORIENT = Z
PLANE = 1
2-D DOMAIN
FLUENT V2.8
CREARE INC

Fig.2.32

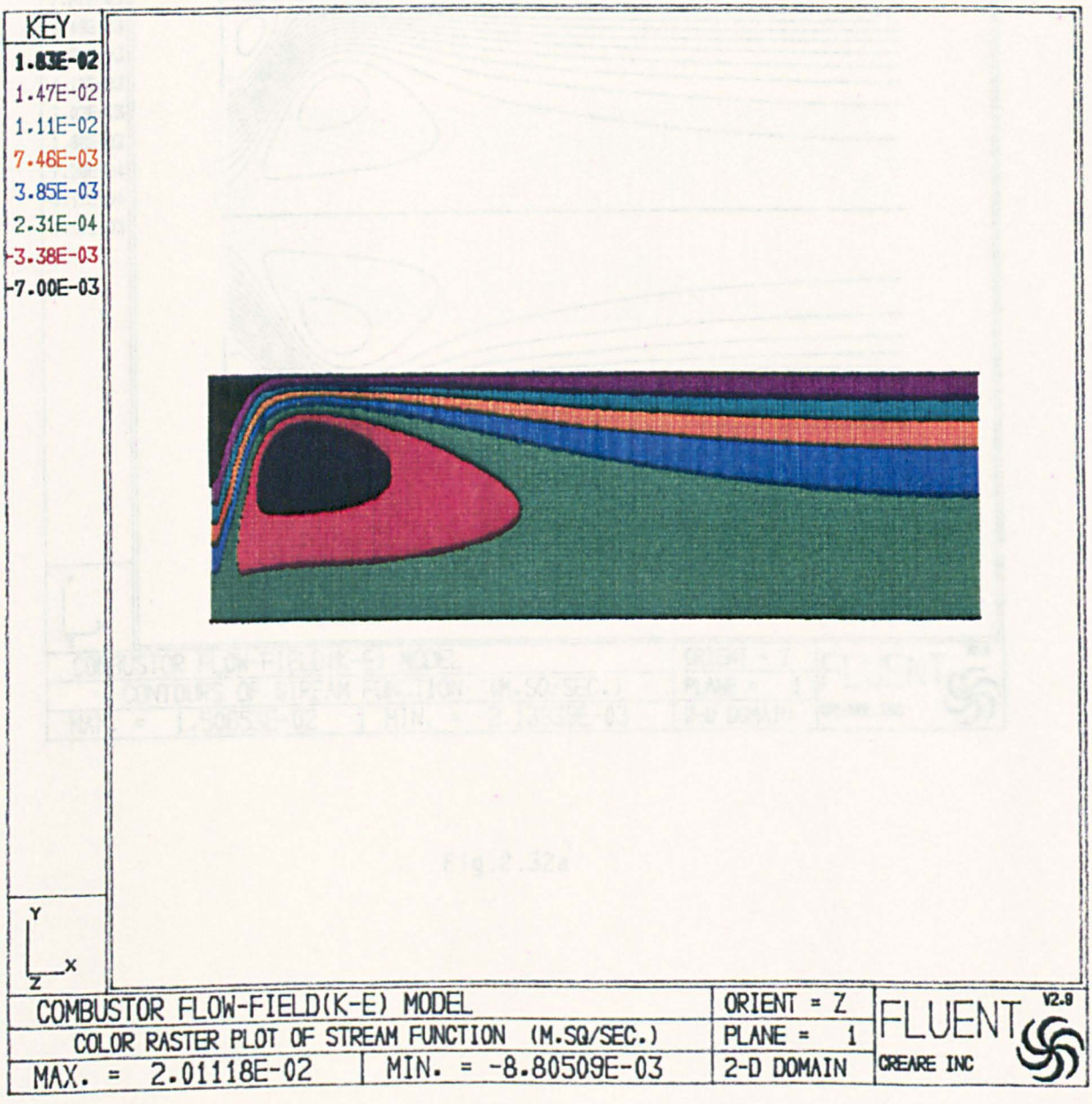
KEY
1.83E-02
1.47E-02
1.11E-02
7.46E-03
3.85E-03
2.31E-04
-3.38E-03
-7.00E-03
Y
X
Z
COMBUSTOR FLOW-FIELD(K-E) MODEL
COLOR RASTER PLOT OF STREAM FUNCTION (M.SQ/SEC.)
MAX. = 2.01118E-02
MIN. = -8.80509E-03
ORIENT = Z
PLANE = 1
2-D DOMAIN
FLUENT V2.8
CREARE INC

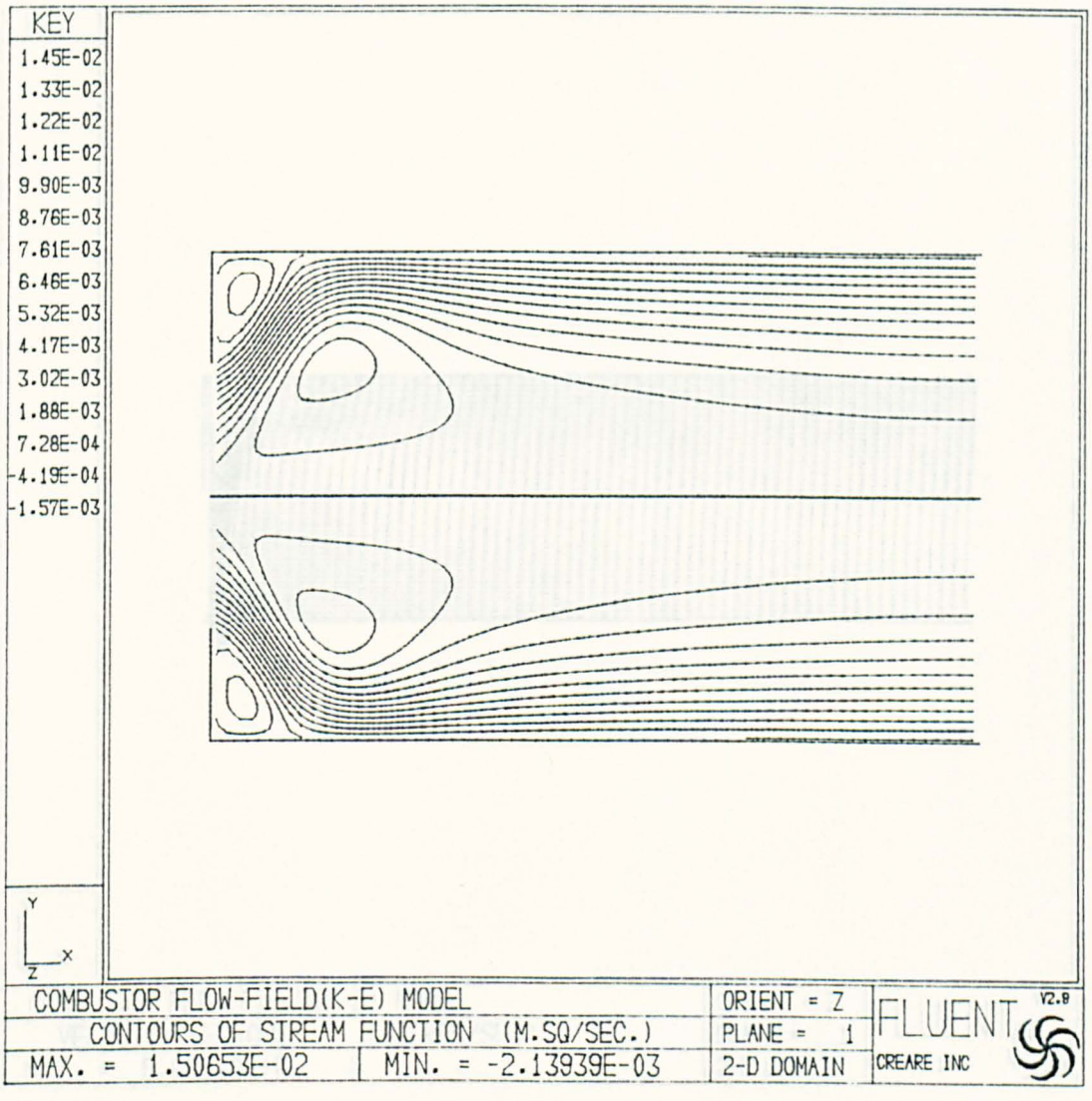
KEY
1.45E-02
1.33E-02
1.22E-02
1.11E-02
9.90E-03
8.76E-03
7.61E-03
6.46E-03
5.32E-03
4.17E-03
3.02E-03
1.88E-03
7.28E-04
-4.19E-04
-1.57E-03
Y
X
Z
COMBUSTOR FLOW-FIELD(K-E) MODEL
CONTOURS OF STREAM FUNCTION (M.SQ/SEC.)
MAX. = 1.50653E-02
MIN. = -2.13939E-03
ORIENT = Z
PLANE = 1
2-D DOMAIN
FLUENT
V2.8
CREARE INC

Fig.2.32a

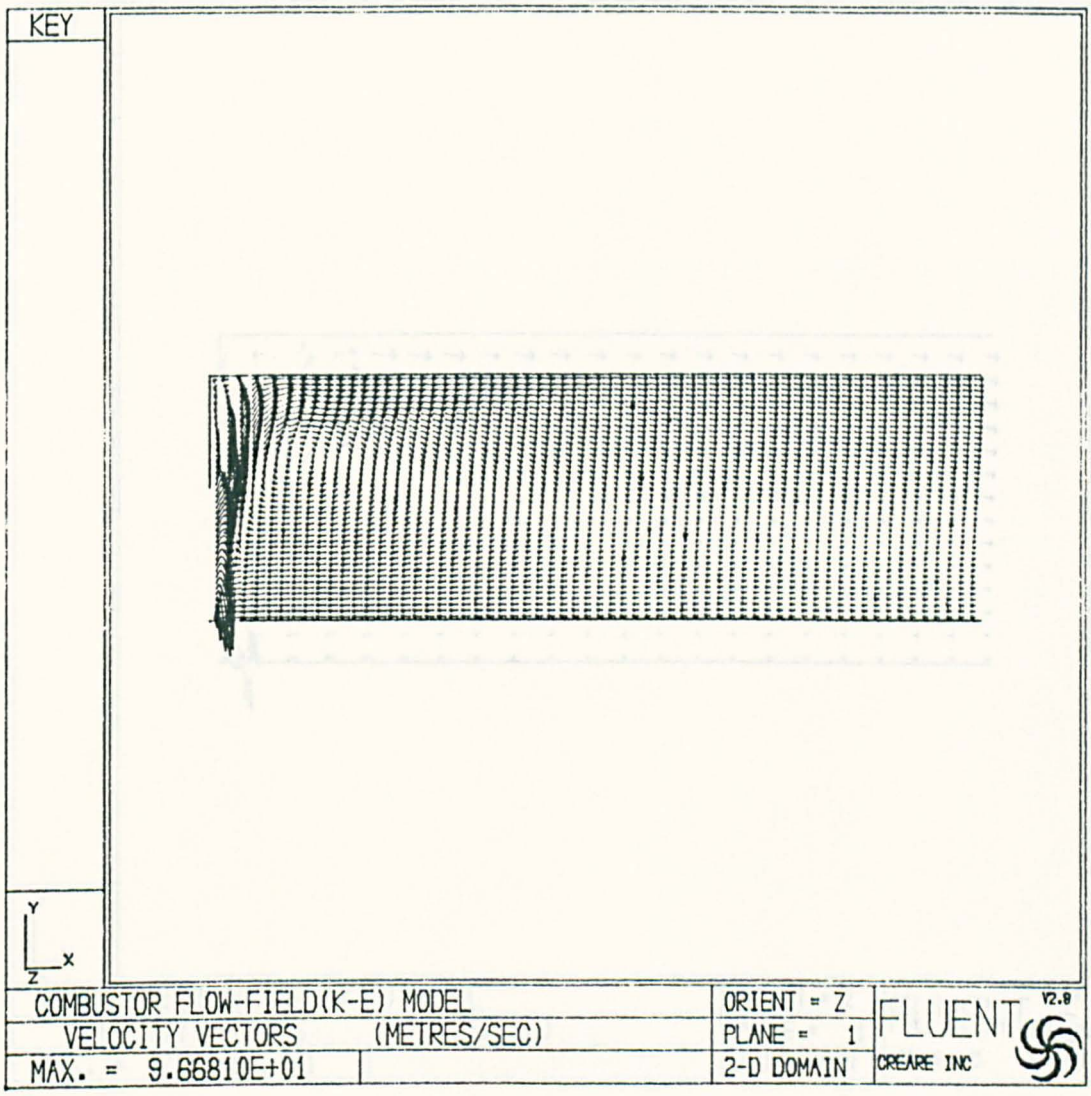
KEY
Y
X
Z
COMBUSTOR FLOW-FIELD(K-E) MODEL
VELOCITY VECTORS (METRES/SEC)
MAX. = 9.66810E+01
ORIENT = Z
PLANE = 1
2-D DOMAIN
FLUENT
V2.0
CREARE INC

Fig.2.33

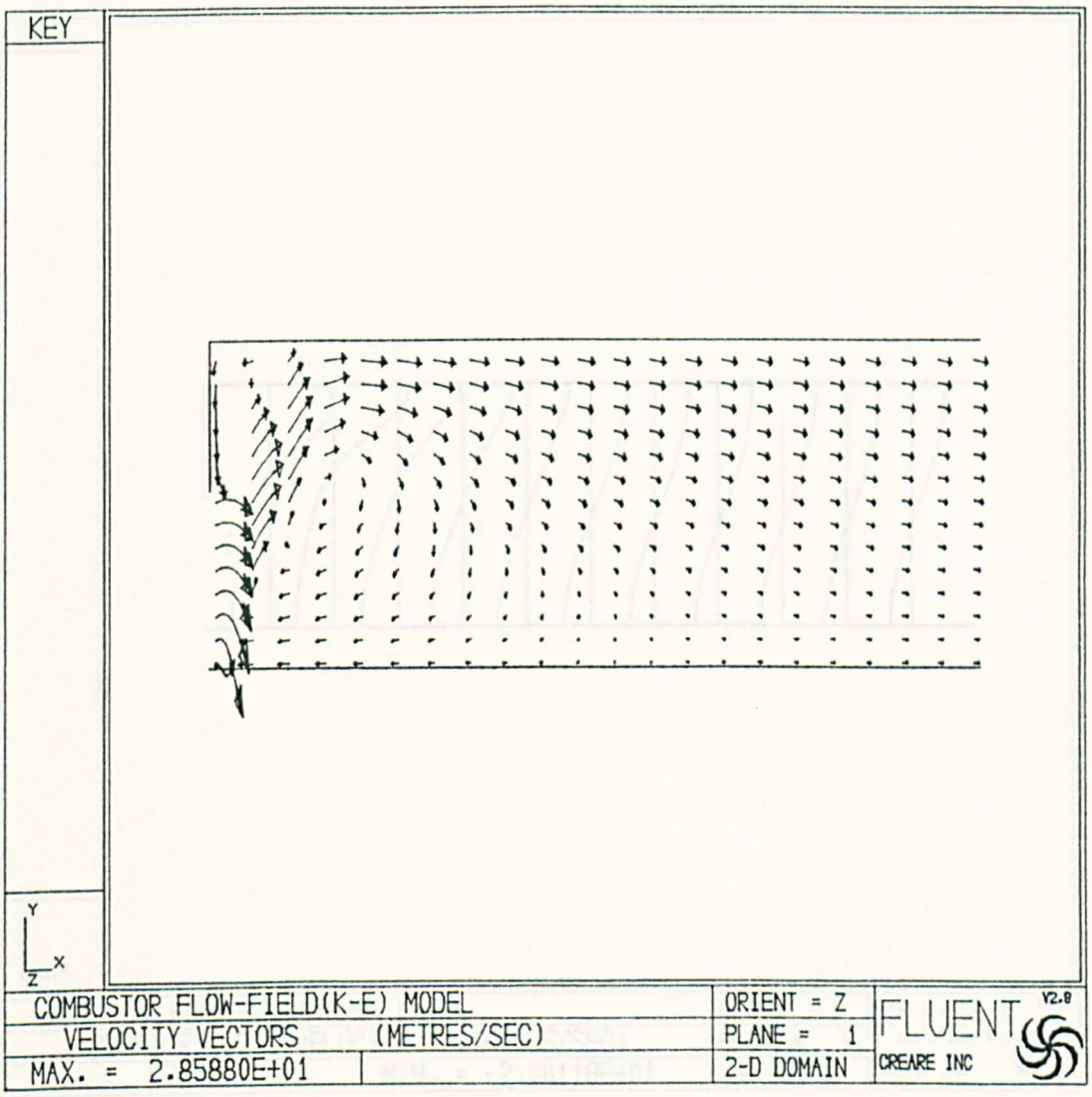
KEY
Y
X
Z
COMBUSTOR FLOW-FIELD(K-E) MODEL
VELOCITY VECTORS (METRES/SEC)
MAX. = 2.85880E+01
ORIENT = Z
PLANE = 1
2-D DOMAIN
FLUENT
V2.0
CREARE INC

Fig.2.33a

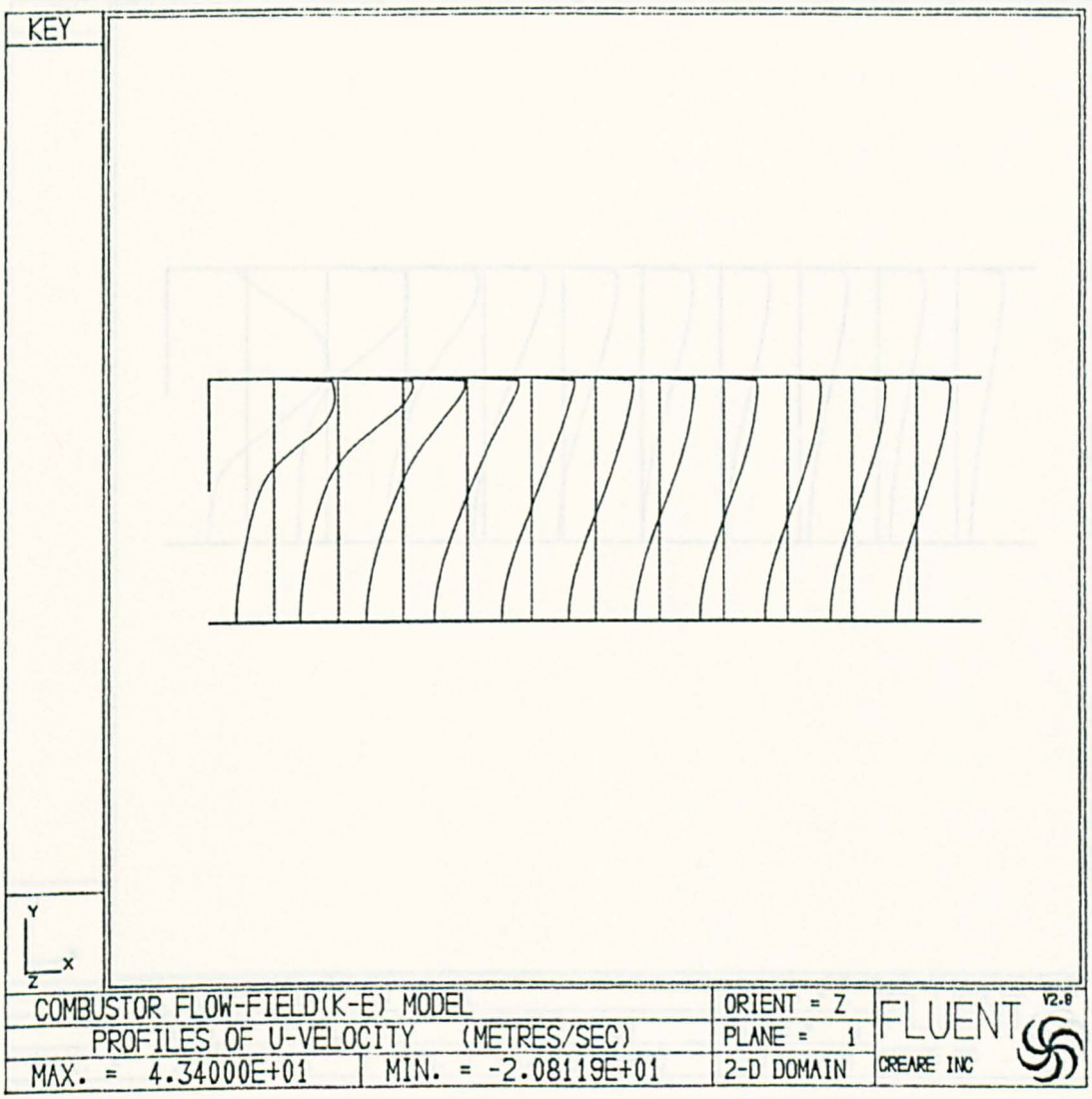
KEY
Y
X
Z
COMBUSTOR FLOW-FIELD(K-E) MODEL
PROFILES OF U-VELOCITY (METRES/SEC)
MAX. = 4.34000E+01
MIN. = -2.08119E+01
ORIENT = Z
PLANE = 1
2-D DOMAIN
FLUENT V2.0
CREARE INC

Fig.2.34

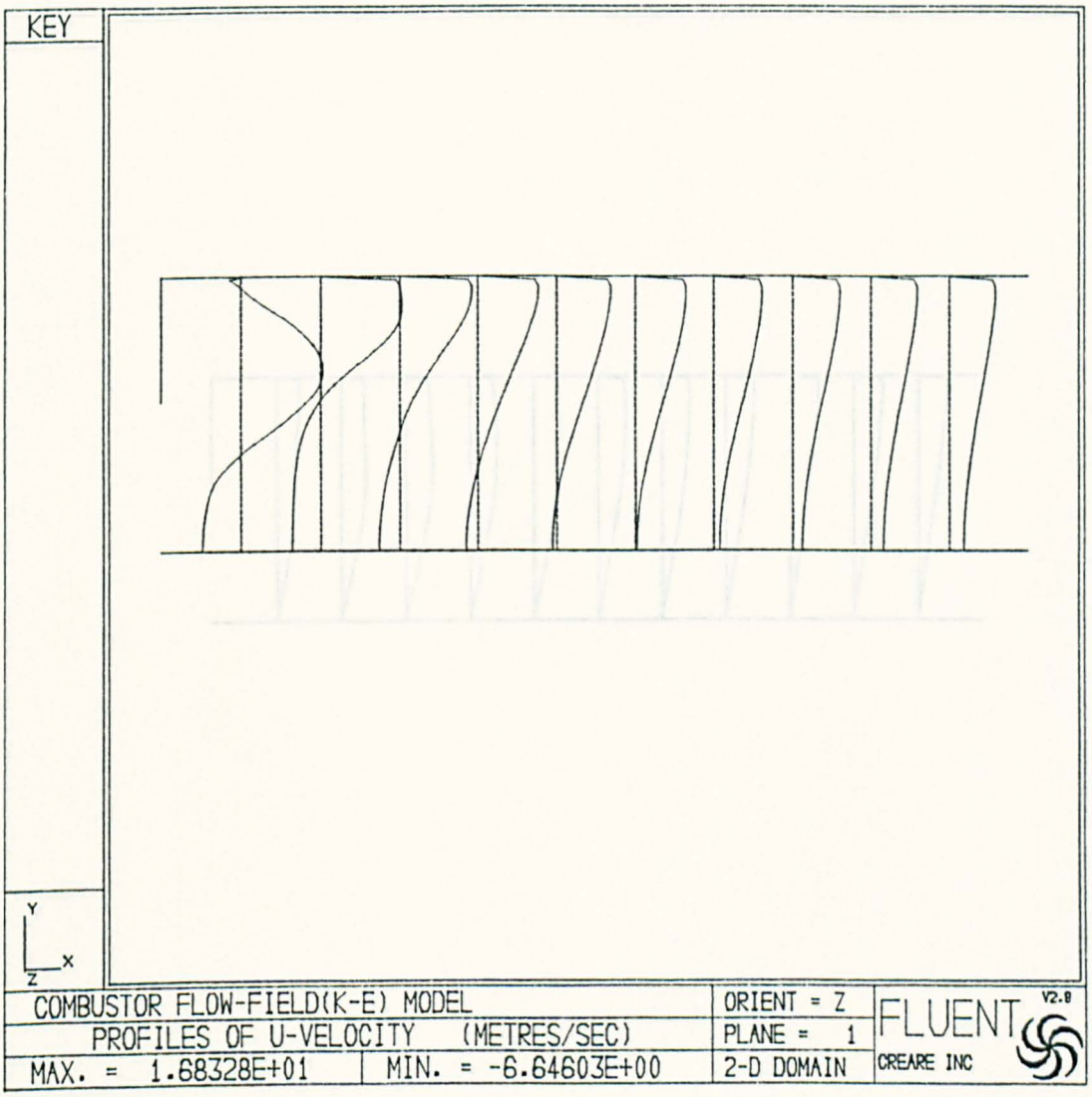
KEY
Y
X
Z
COMBUSTOR FLOW-FIELD(K-E) MODEL
PROFILES OF U-VELOCITY (METRES/SEC)
MAX. = 1.68328E+01
MIN. = -6.64603E+00
ORIENT = Z
PLANE = 1
2-D DOMAIN
FLUENT V2.8
CREARE INC

Fig.2.34a

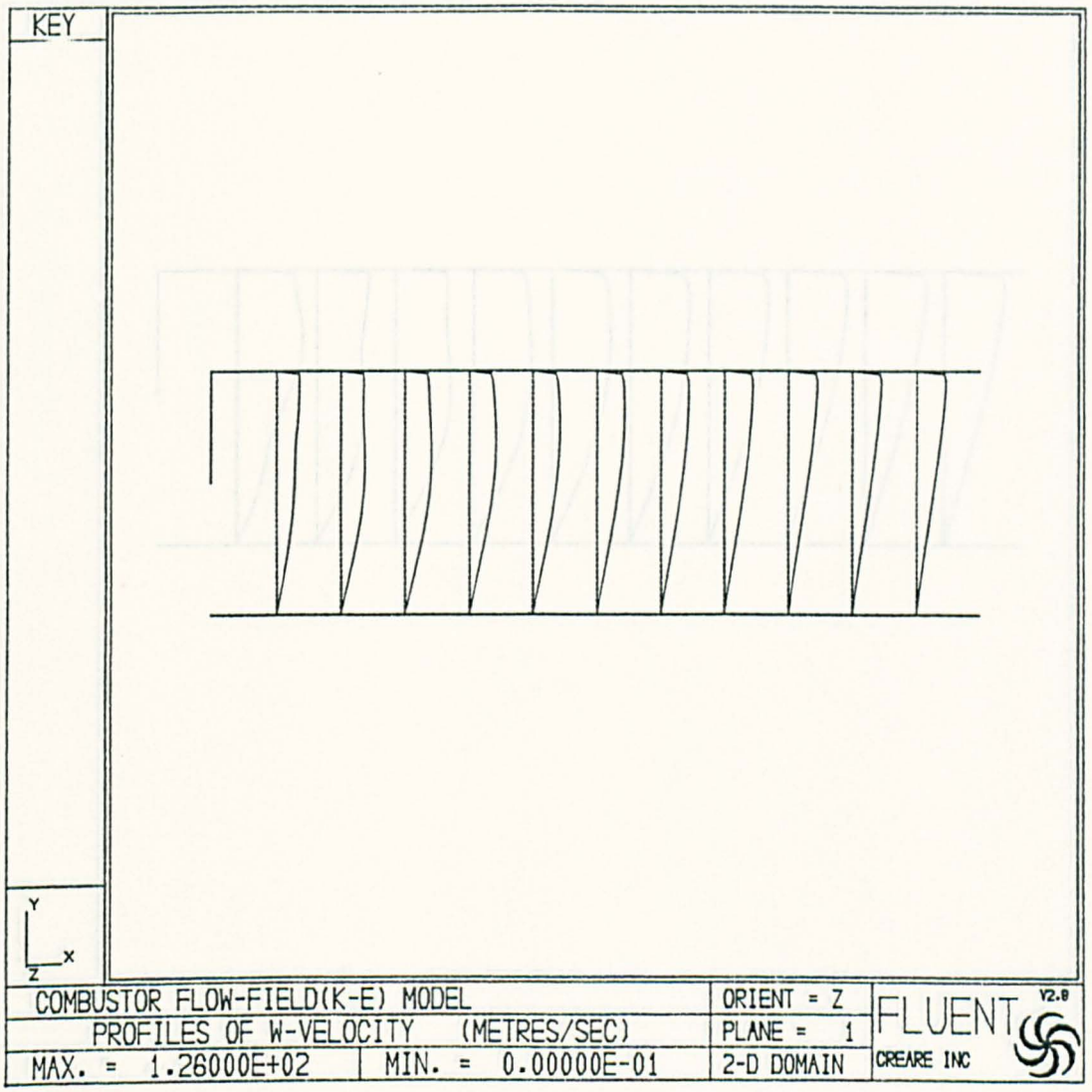
KEY
Y
X
Z
COMBUSTOR FLOW-FIELD(K-E) MODEL
PROFILES OF W-VELOCITY (METRES/SEC)
MAX. = 1.26000E+02
MIN. = 0.00000E-01
ORIENT = Z
PLANE = 1
2-D DOMAIN
FLUENT V2.0
CREARE INC

Fig.2.35

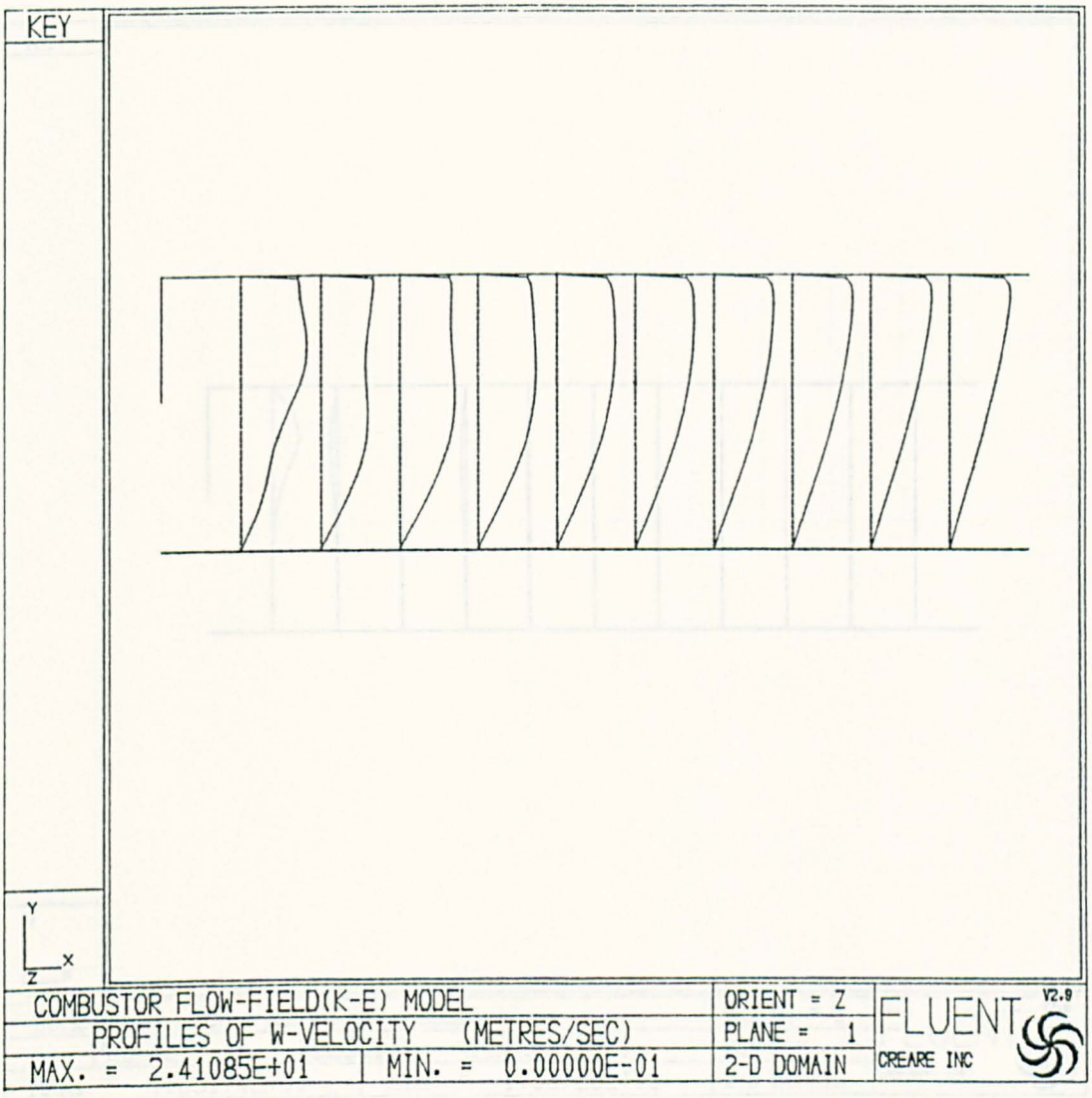
KEY
Y
X
Z
COMBUSTOR FLOW-FIELD(K-E) MODEL
PROFILES OF W-VELOCITY (METRES/SEC)
MAX. = 2.41085E+01
MIN. = 0.00000E-01
ORIENT = Z
PLANE = 1
2-D DOMAIN
FLUENT V2.9
CREARE INC

Fig.2.35a

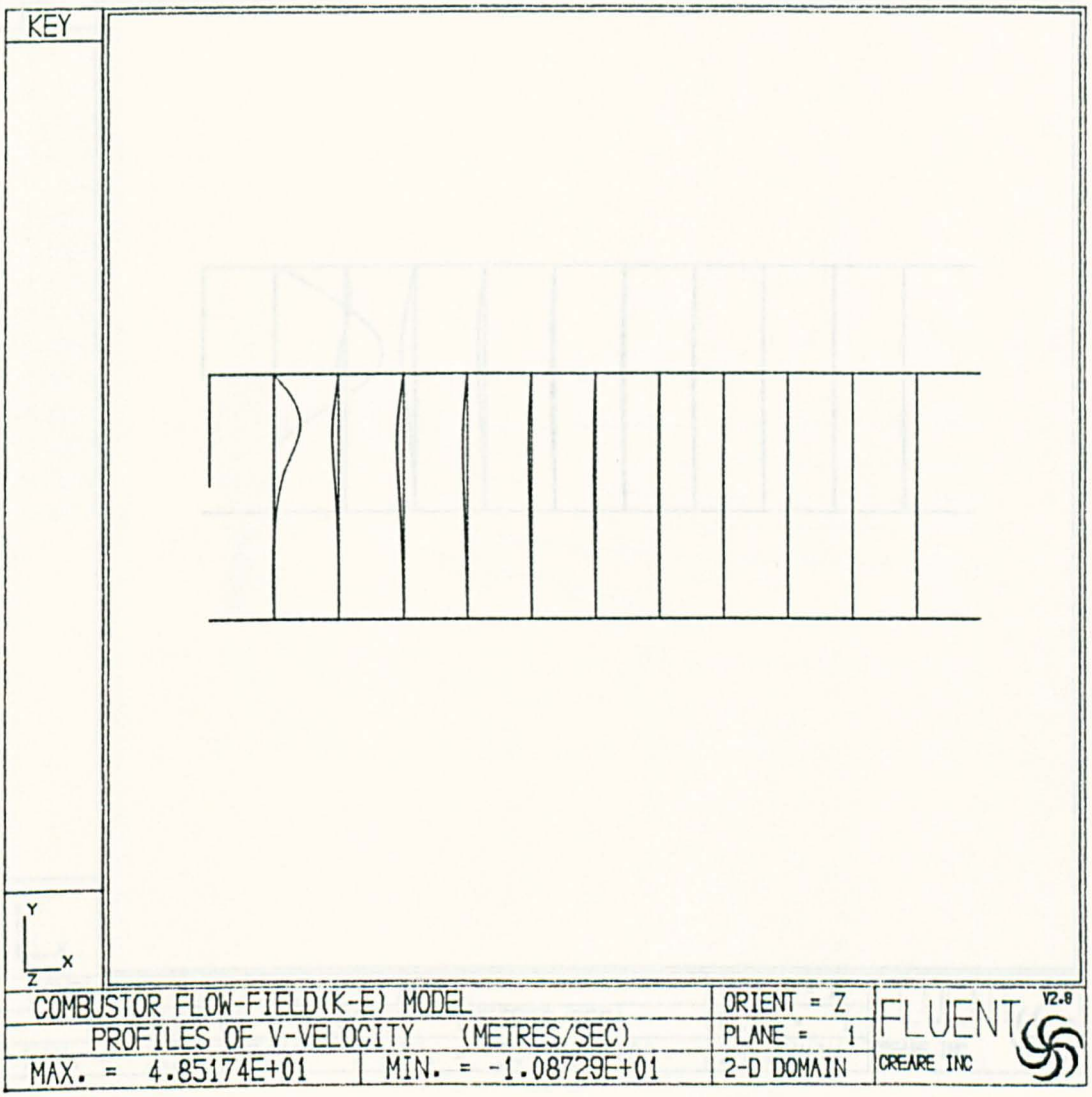
KEY
Y
X
Z
COMBUSTOR FLOW-FIELD(K-E) MODEL
PROFILES OF V-VELOCITY (METRES/SEC)
MAX. = 4.85174E+01
MIN. = -1.08729E+01
ORIENT = Z
PLANE = 1
2-D DOMAIN
FLUENT V2.8
CREARE INC

Fig.2.36

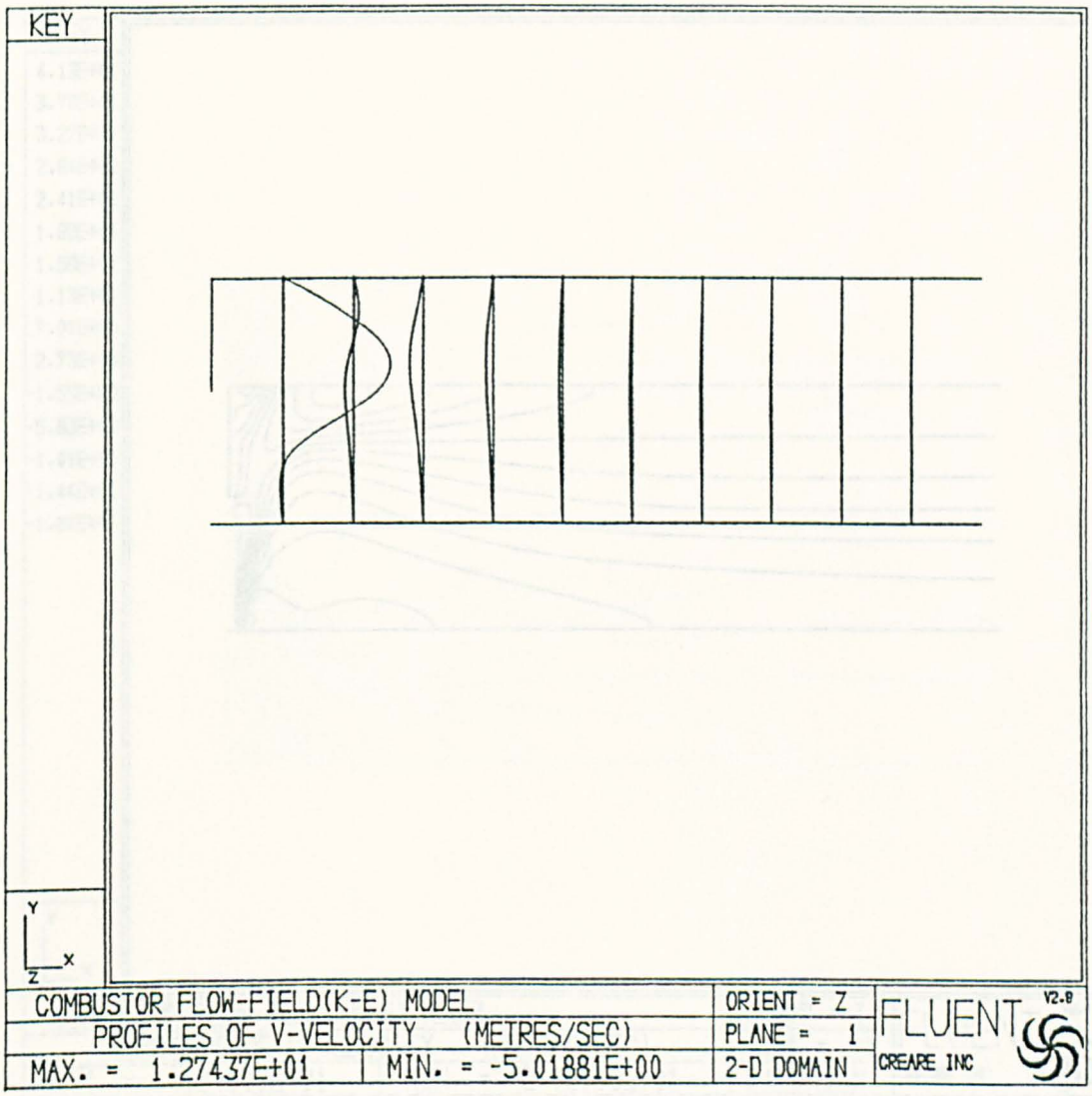
KEY
Y
X
Z
COMBUSTOR FLOW-FIELD(K-E) MODEL
PROFILES OF V-VELOCITY (METRES/SEC)
MAX. = 1.27437E+01
MIN. = -5.01881E+00
ORIENT = Z
PLANE = 1
2-D DOMAIN
FLUENT V2.8
CREARE INC

Fig.2.36a

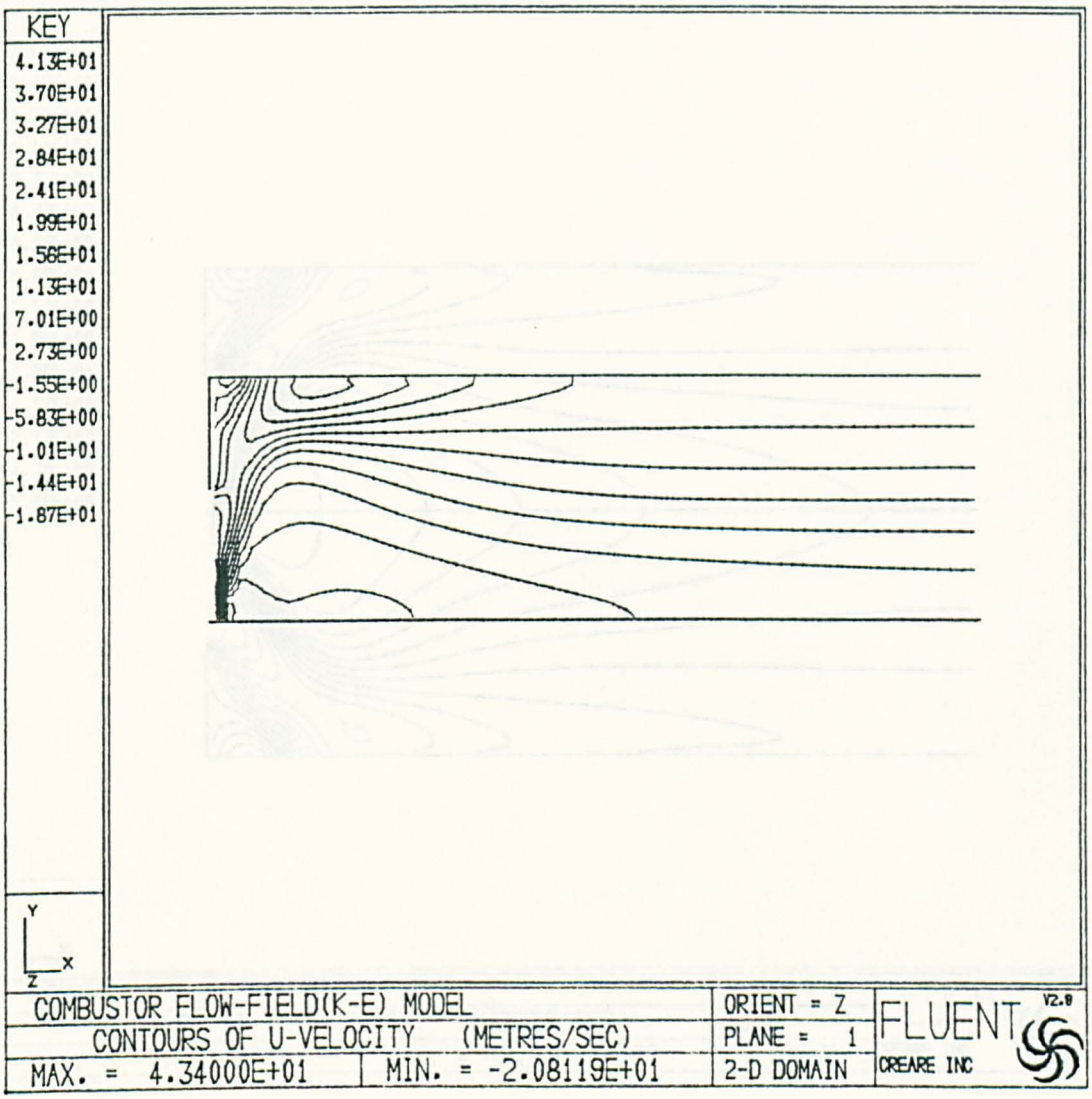
KEY
4.13E+01
3.70E+01
3.27E+01
2.84E+01
2.41E+01
1.99E+01
1.56E+01
1.13E+01
7.01E+00
2.73E+00
-1.55E+00
-5.83E+00
-1.01E+01
-1.44E+01
-1.87E+01
Y
X
Z
COMBUSTOR FLOW-FIELD(K-E) MODEL
CONTOURS OF U-VELOCITY (METRES/SEC)
MAX. = 4.34000E+01
MIN. = -2.08119E+01
ORIENT = Z
PLANE = 1
2-D DOMAIN
FLUENT V2.8
CREARE INC

Fig.2.37

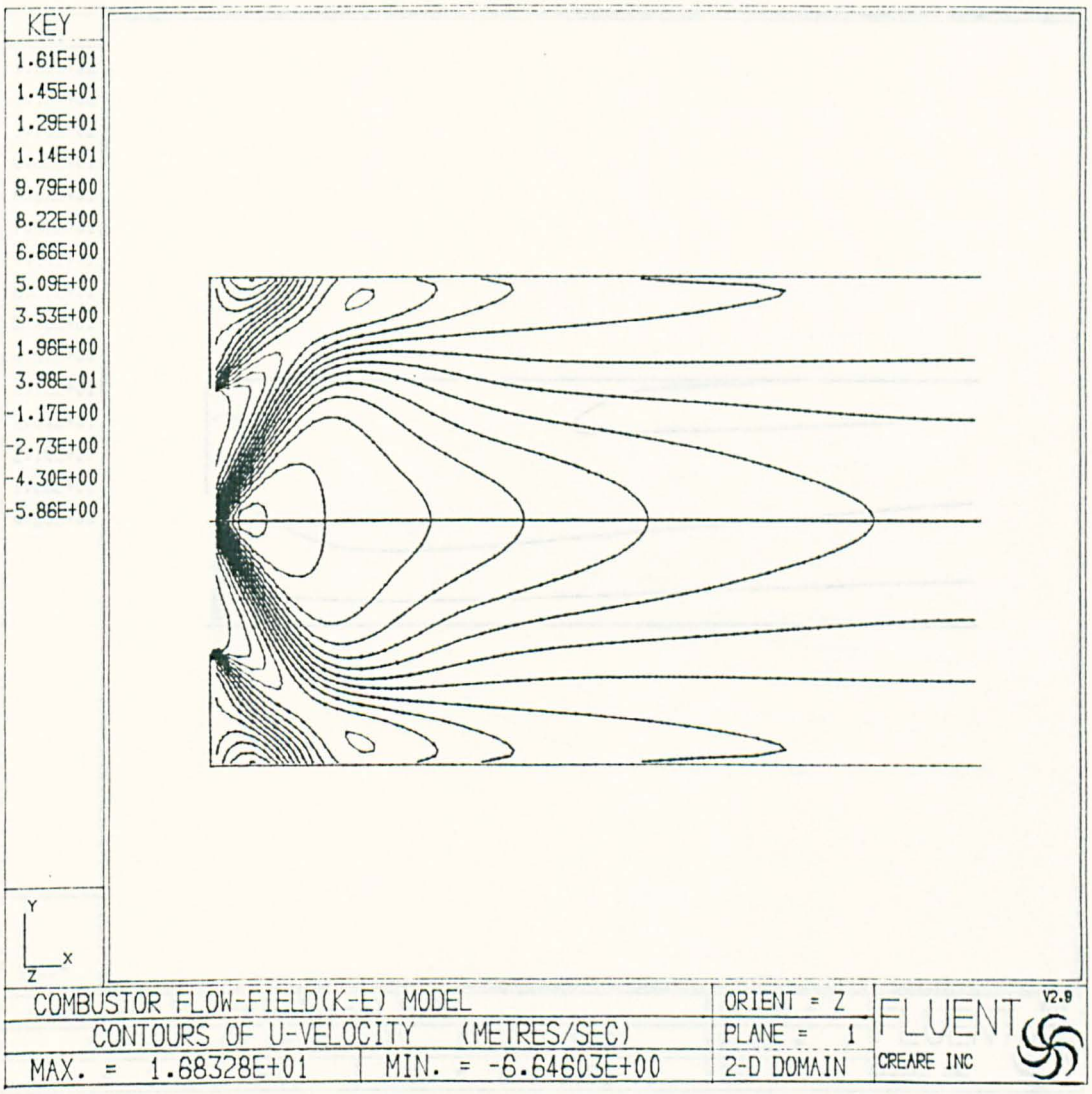
KEY
1.61E+01
1.45E+01
1.29E+01
1.14E+01
9.79E+00
8.22E+00
6.66E+00
5.09E+00
3.53E+00
1.96E+00
3.98E-01
-1.17E+00
-2.73E+00
-4.30E+00
-5.86E+00
Y
X
Z
COMBUSTOR FLOW-FIELD(K-E) MODEL
CONTOURS OF U-VELOCITY (METRES/SEC)
MAX. = 1.68328E+01
MIN. = -6.64603E+00
ORIENT = Z
PLANE = 1
2-D DOMAIN
FLUENT V2.9
CREARE INC

Fig.2.37a

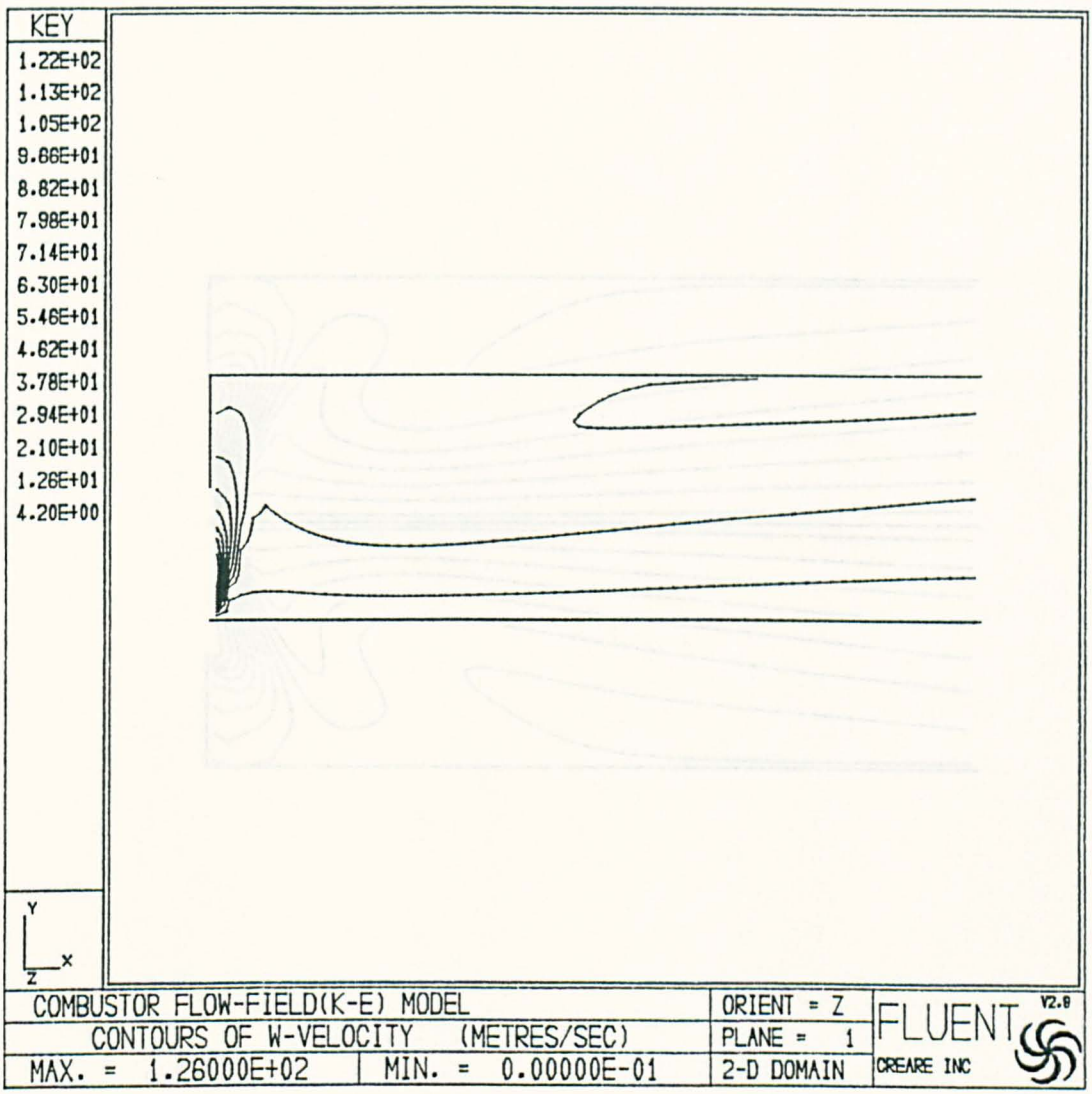
KEY
1.22E+02
1.13E+02
1.05E+02
9.66E+01
8.82E+01
7.98E+01
7.14E+01
6.30E+01
5.46E+01
4.62E+01
3.78E+01
2.94E+01
2.10E+01
1.26E+01
4.20E+00
Y
X
Z
COMBUSTOR FLOW-FIELD(K-E) MODEL
CONTOURS OF W-VELOCITY (METRES/SEC)
MAX. = 1.26000E+02
MIN. = 0.00000E-01
ORIENT = Z
PLANE = 1
2-D DOMAIN
FLUENT V2.0
CREARE INC

Fig.2.38

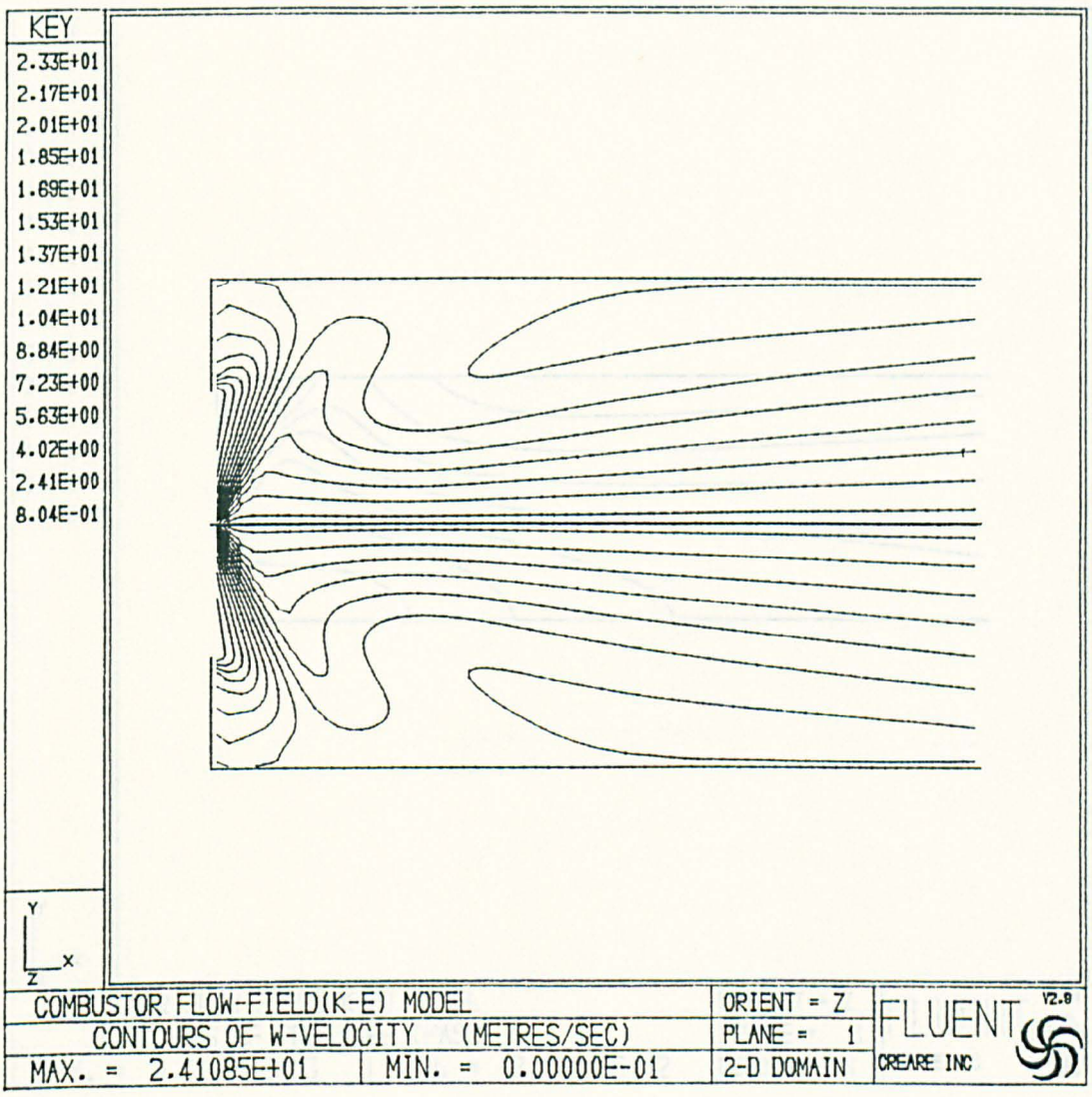
KEY
2.33E+01
2.17E+01
2.01E+01
1.85E+01
1.69E+01
1.53E+01
1.37E+01
1.21E+01
1.04E+01
8.84E+00
7.23E+00
5.63E+00
4.02E+00
2.41E+00
8.04E-01
Y
X
Z
COMBUSTOR FLOW-FIELD(K-E) MODEL
CONTOURS OF W-VELOCITY (METRES/SEC)
MAX. = 2.41085E+01
MIN. = 0.00000E-01
ORIENT = Z
PLANE = 1
2-D DOMAIN
FLUENT V2.0
CREARE INC

Fig.2.38a

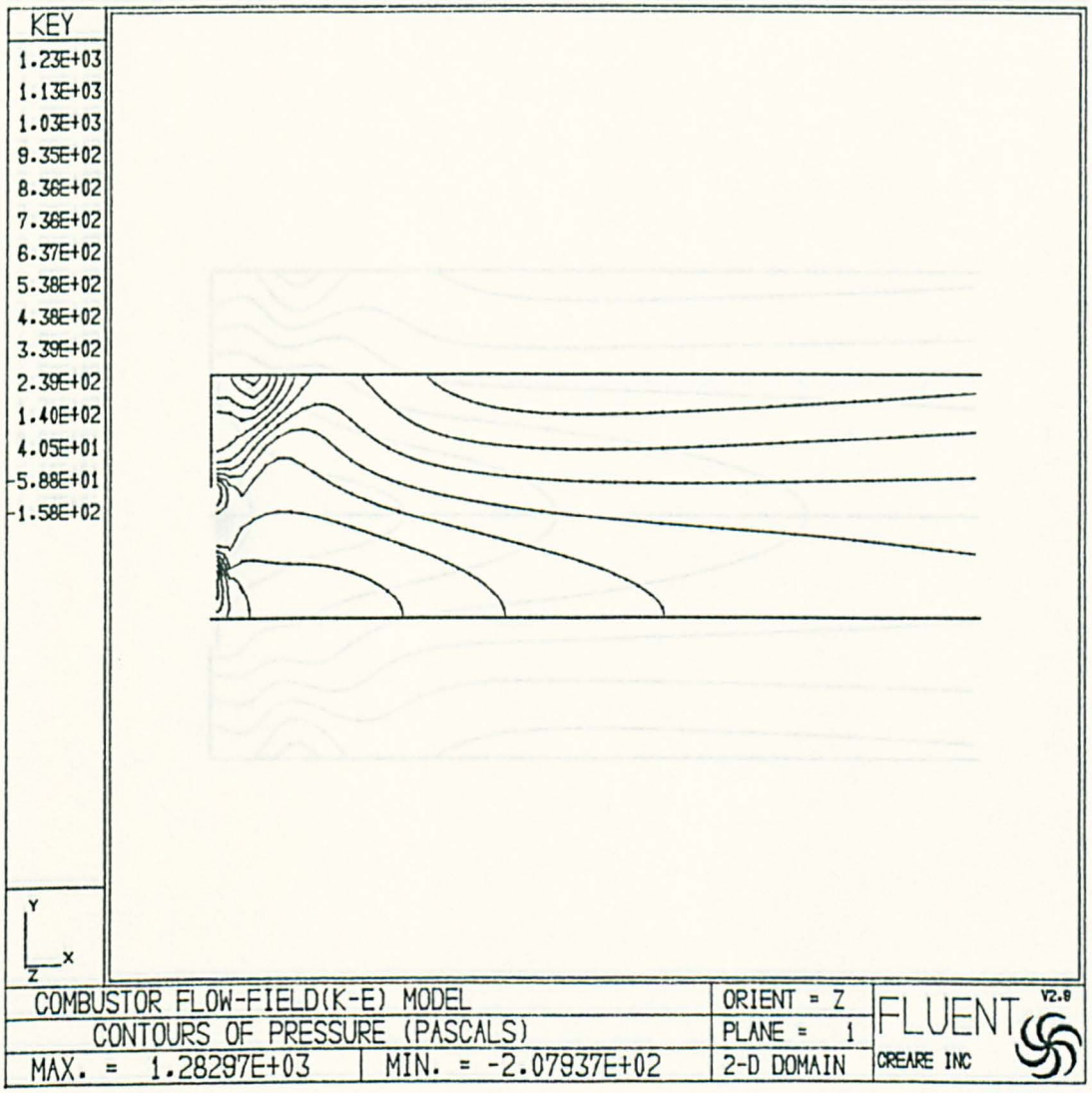
KEY
1.23E+03
1.13E+03
1.03E+03
9.35E+02
8.36E+02
7.36E+02
6.37E+02
5.38E+02
4.38E+02
3.39E+02
2.39E+02
1.40E+02
4.05E+01
-5.88E+01
-1.58E+02
Y
X
Z
COMBUSTOR FLOW-FIELD(K-E) MODEL
CONTOURS OF PRESSURE (PASCALS)
MAX. = 1.28297E+03
MIN. = -2.07937E+02
ORIENT = Z
PLANE = 1
2-D DOMAIN
FLUENT V2.0
CREARE INC

Fig.2.39

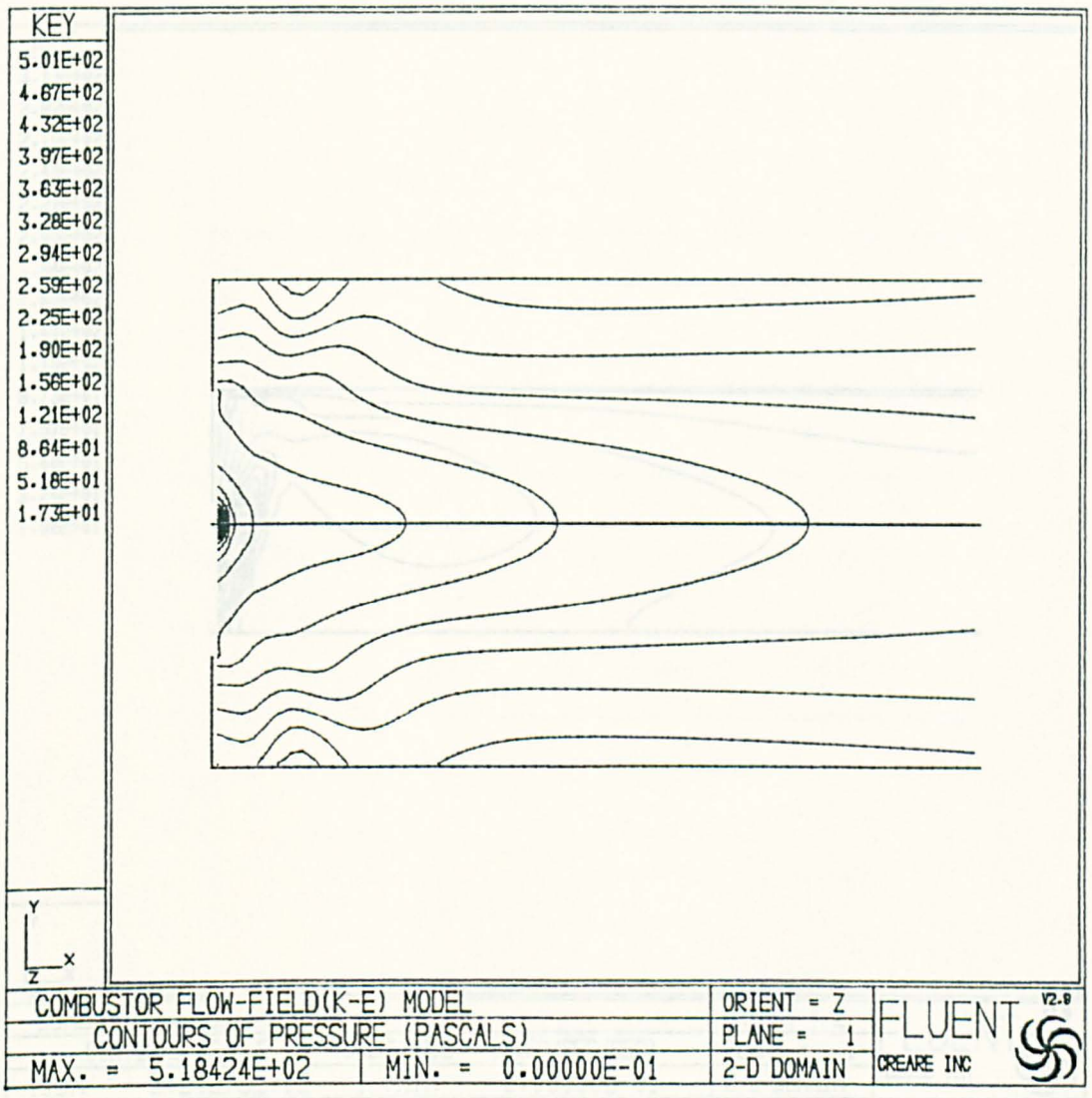
KEY
5.01E+02
4.67E+02
4.32E+02
3.97E+02
3.63E+02
3.28E+02
2.94E+02
2.59E+02
2.25E+02
1.90E+02
1.56E+02
1.21E+02
8.64E+01
5.18E+01
1.73E+01
Y
X
Z
COMBUSTOR FLOW-FIELD(K-E) MODEL
CONTOURS OF PRESSURE (PASCALS)
MAX. = 5.18424E+02
MIN. = 0.00000E-01
ORIENT = Z
PLANE = 1
2-D DOMAIN
FLUENT V2.0
CREARE INC

Fig.2.39a

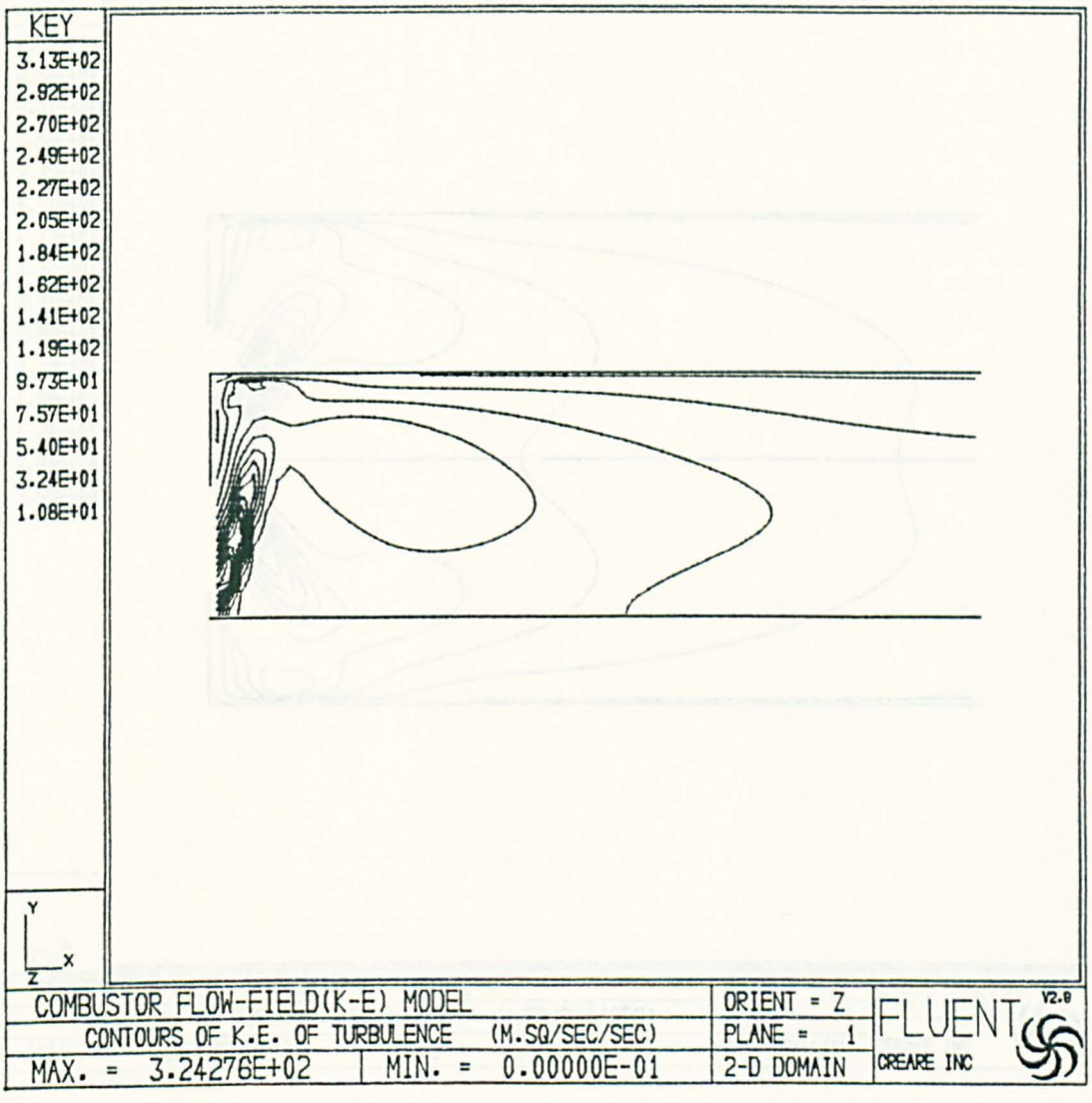
KEY
3.13E+02
2.92E+02
2.70E+02
2.49E+02
2.27E+02
2.05E+02
1.84E+02
1.62E+02
1.41E+02
1.19E+02
9.73E+01
7.57E+01
5.40E+01
3.24E+01
1.08E+01
Y
X
Z
COMBUSTOR FLOW-FIELD(K-E) MODEL
CONTOURS OF K.E. OF TURBULENCE (M.SQ/SEC/SEC)
MAX. = 3.24276E+02
MIN. = 0.00000E-01
ORIENT = Z
PLANE = 1
2-D DOMAIN
FLUENT V2.0
CREARE INC

Fig.2.40

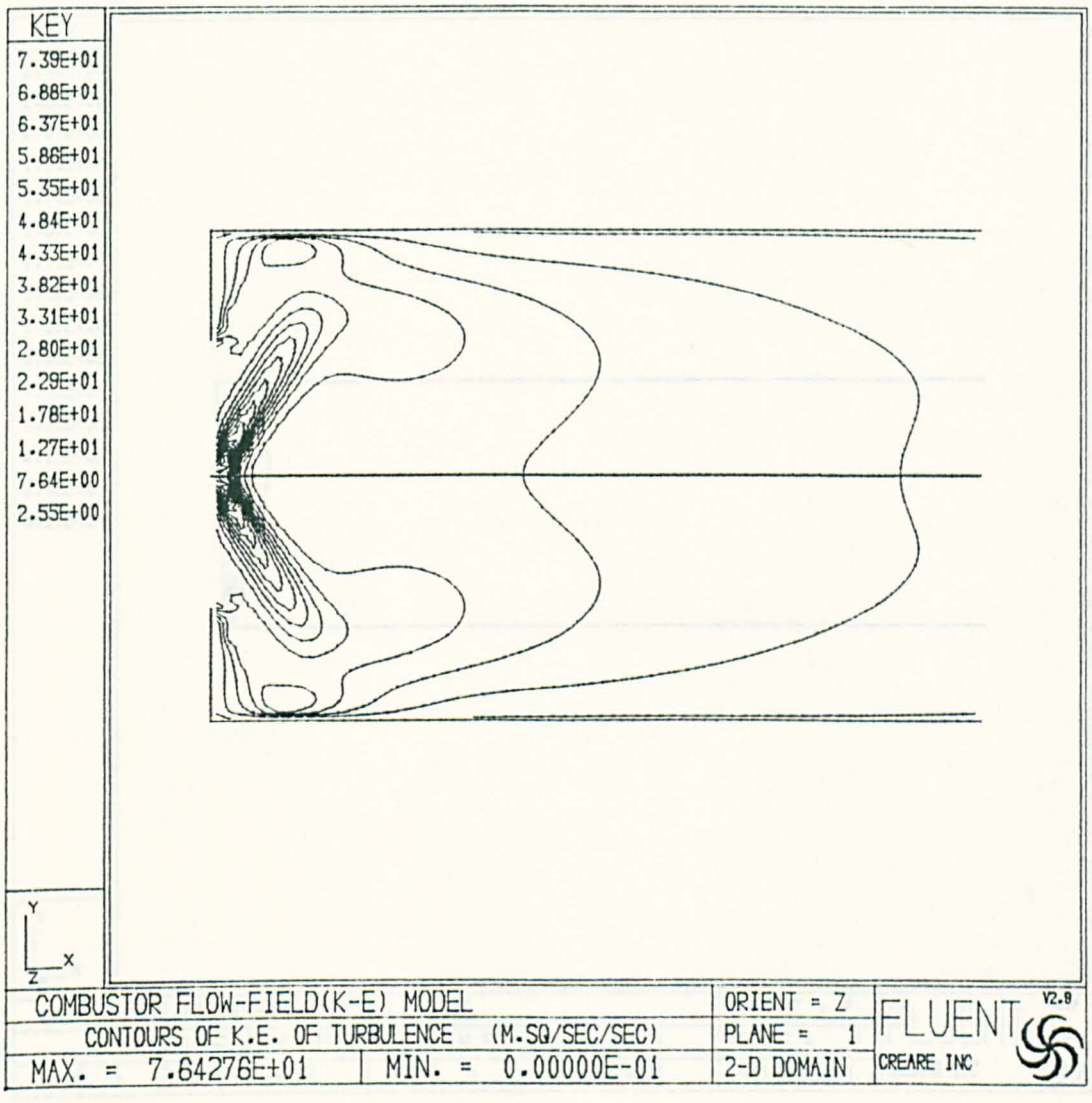
KEY
7.39E+01
6.88E+01
6.37E+01
5.86E+01
5.35E+01
4.84E+01
4.33E+01
3.82E+01
3.31E+01
2.80E+01
2.29E+01
1.78E+01
1.27E+01
7.64E+00
2.55E+00
Y
X
Z
COMBUSTOR FLOW-FIELD(K-E) MODEL
CONTOURS OF K.E. OF TURBULENCE (M.SQ/SEC/SEC)
MAX. = 7.64276E+01
MIN. = 0.00000E-01
ORIENT = Z
PLANE = 1
2-D DOMAIN
FLUENT
V2.0
CREARE INC

Fig.2.40a

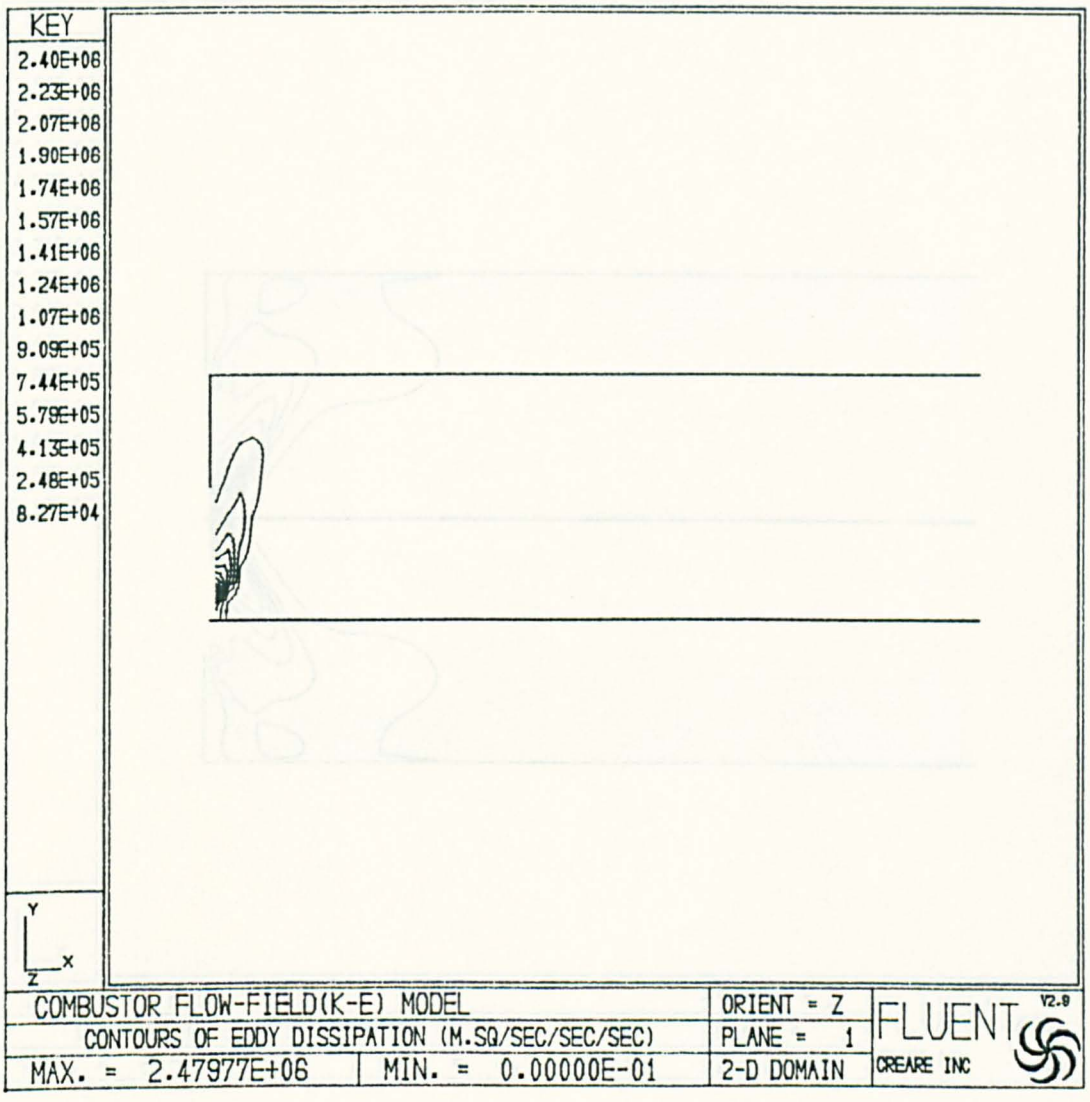
KEY
2.40E+06
2.23E+06
2.07E+06
1.90E+06
1.74E+06
1.57E+06
1.41E+06
1.24E+06
1.07E+06
9.09E+05
7.44E+05
5.79E+05
4.13E+05
2.48E+05
8.27E+04
Y
X
Z
COMBUSTOR FLOW-FIELD(K-E) MODEL
CONTOURS OF EDDY DISSIPATION (M.SQ/SEC/SEC/SEC)
MAX. = 2.47977E+06
MIN. = 0.00000E-01
ORIENT = Z
PLANE = 1
2-D DOMAIN
FLUENT V2.8
CREARE INC

Fig.2.41

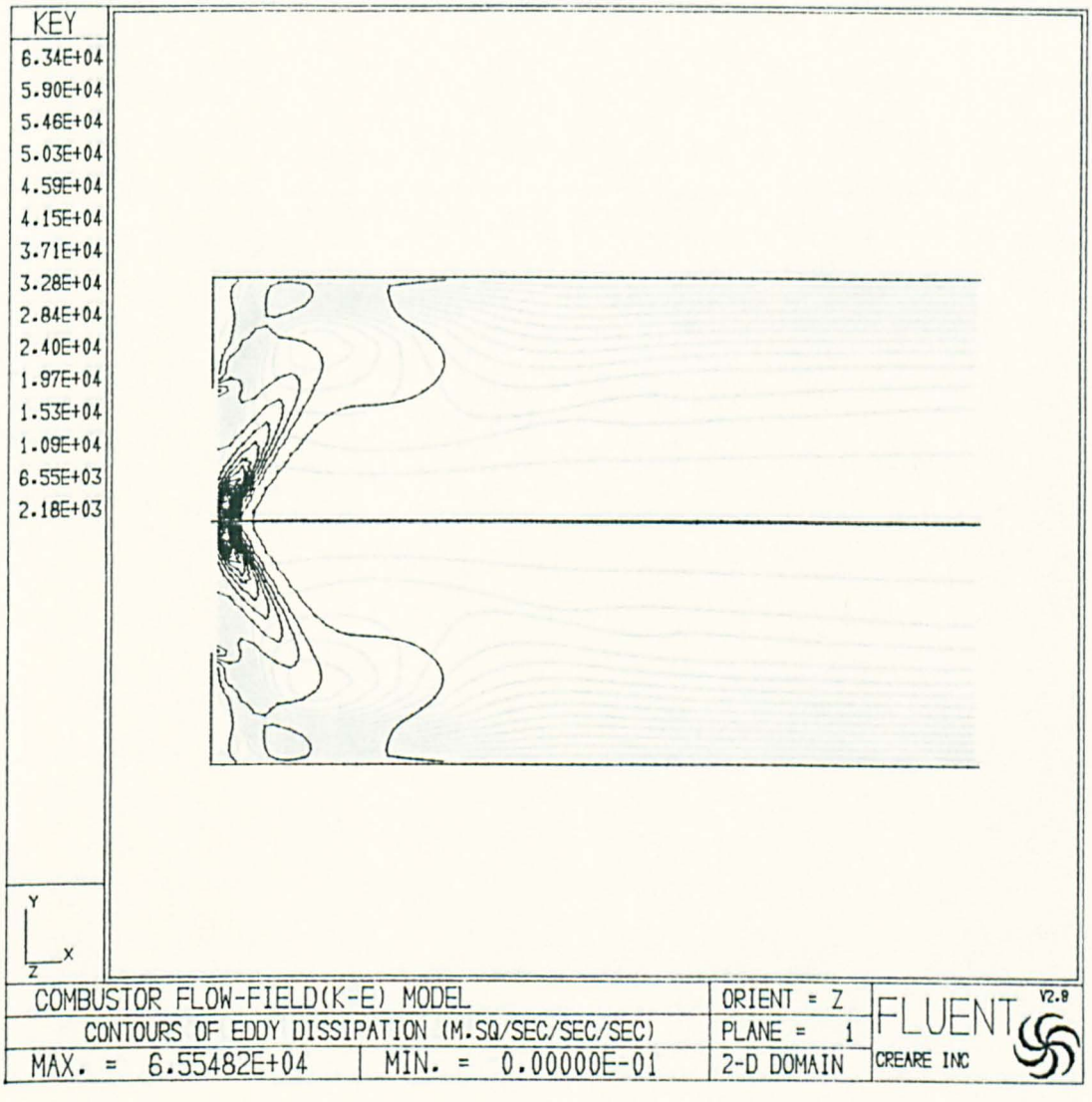
KEY
6.34E+04
5.90E+04
5.46E+04
5.03E+04
4.59E+04
4.15E+04
3.71E+04
3.28E+04
2.84E+04
2.40E+04
1.97E+04
1.53E+04
1.09E+04
6.55E+03
2.18E+03
Y
X
Z
COMBUSTOR FLOW-FIELD(K-E) MODEL
CONTOURS OF EDDY DISSIPATION (M.SQ/SEC/SEC/SEC)
MAX. = 6.55482E+04
MIN. = 0.00000E-01
ORIENT = Z
PLANE = 1
2-D DOMAIN
FLUENT V2.8
CREARE INC

Fig.2.41a

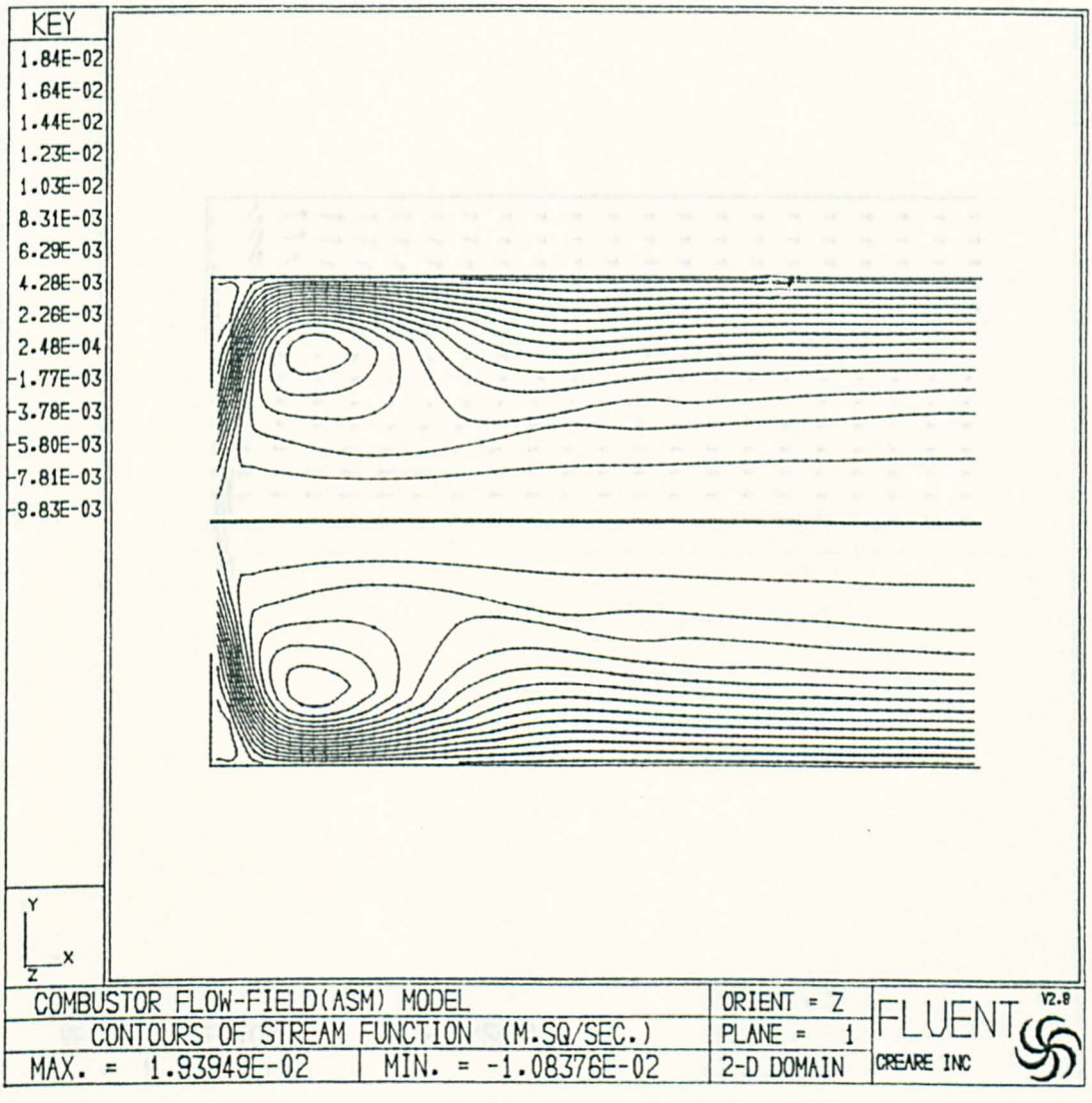
KEY
1.84E-02
1.64E-02
1.44E-02
1.23E-02
1.03E-02
8.31E-03
6.29E-03
4.28E-03
2.26E-03
2.48E-04
-1.77E-03
-3.78E-03
-5.80E-03
-7.81E-03
-9.83E-03
Y
X
Z
COMBUSTOR FLOW-FIELD(ASM) MODEL
CONTOURS OF STREAM FUNCTION (M.SQ/SEC.)
MAX. = 1.93949E-02
MIN. = -1.08376E-02
ORIENT = Z
PLANE = 1
2-D DOMAIN
FLUENT V2.8
CREARE INC

Fig.2.42

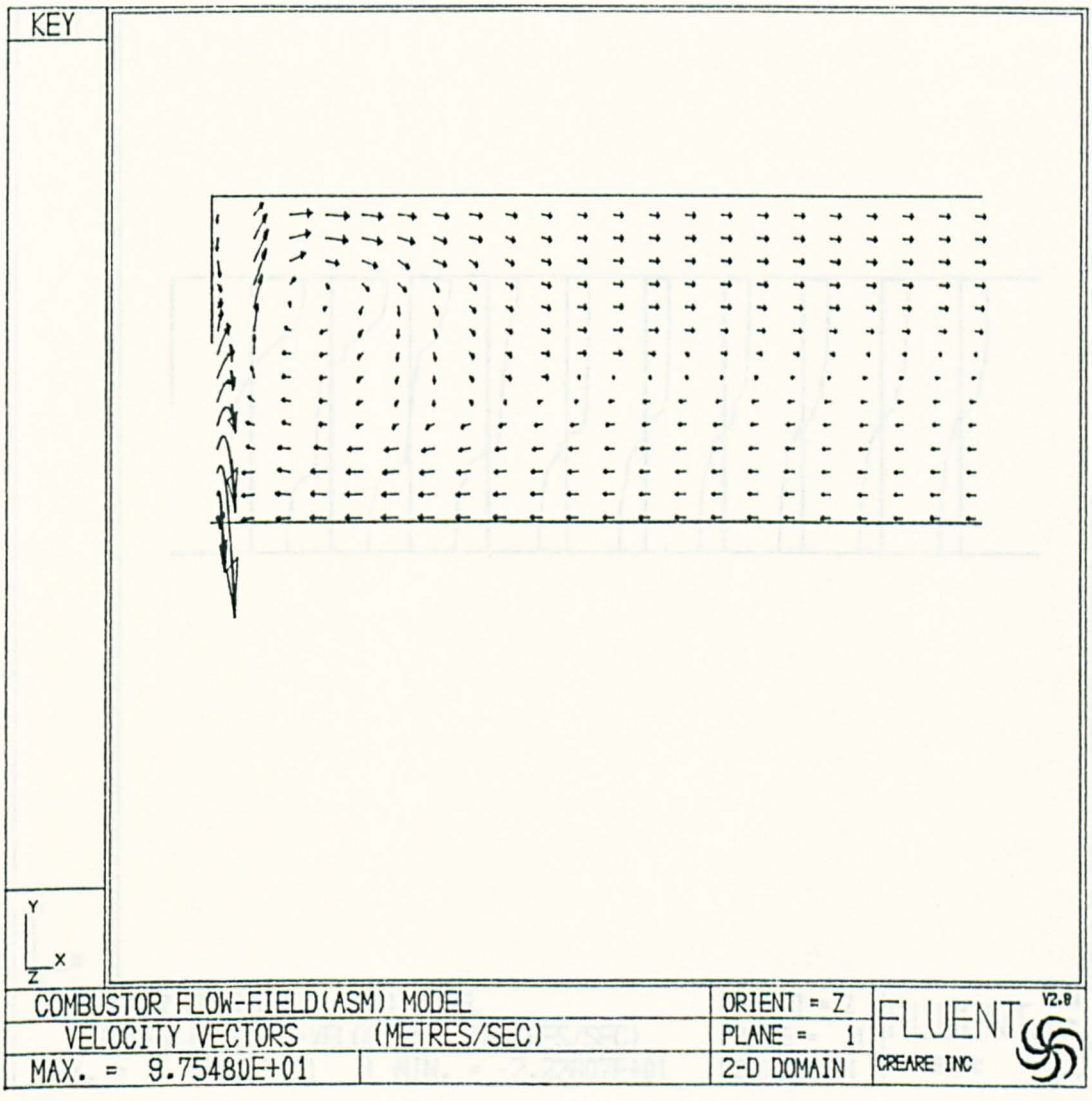
KEY
Y
X
Z
COMBUSTOR FLOW-FIELD(ASM) MODEL
VELOCITY VECTORS (METRES/SEC)
MAX. = 9.75480E+01
ORIENT = Z
PLANE = 1
2-D DOMAIN
FLUENT V2.0
CREARE INC

Fig.2.43

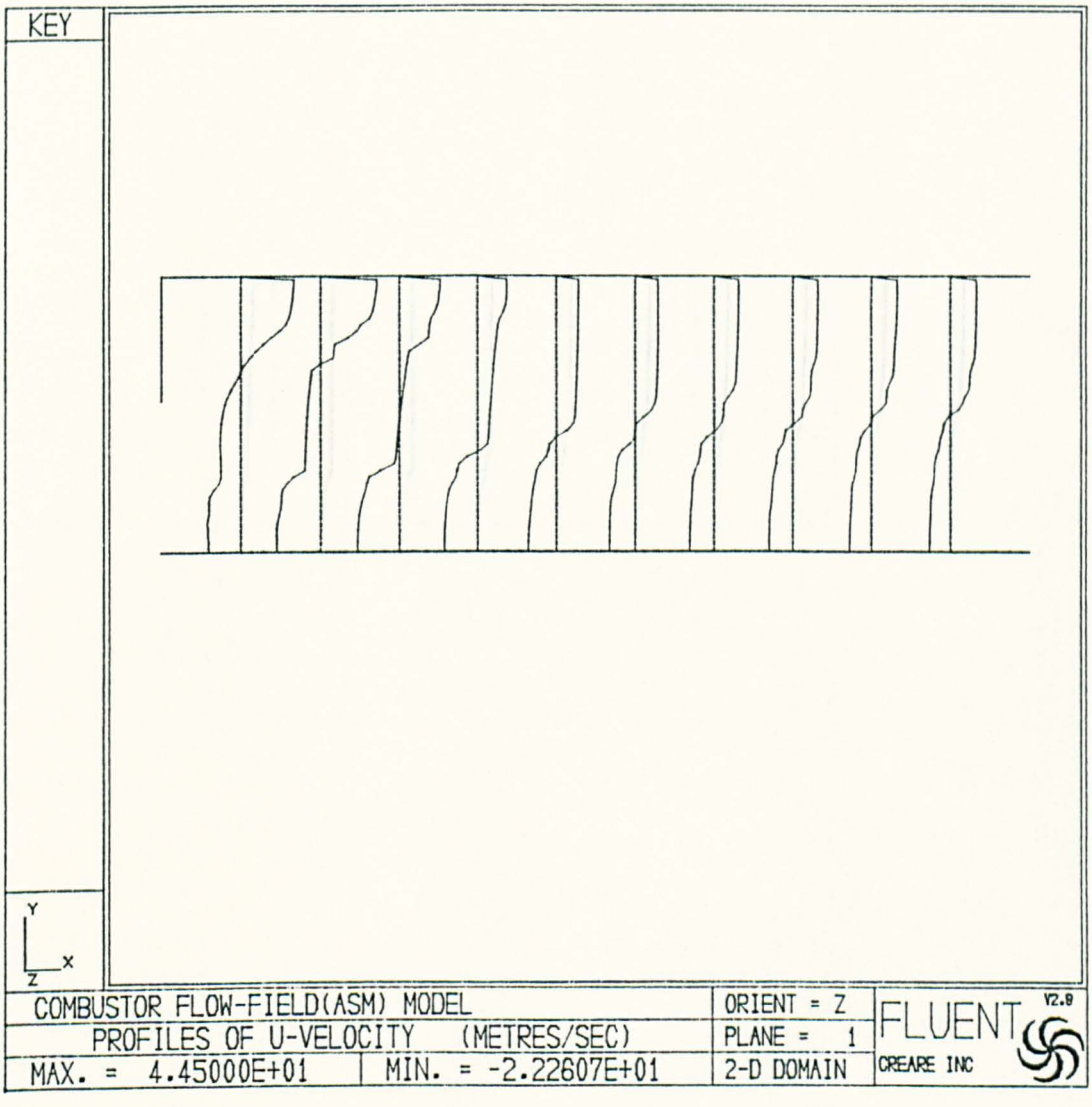
KEY
Y
X
Z
COMBUSTOR FLOW-FIELD(ASM) MODEL
PROFILES OF U-VELOCITY (METRES/SEC)
MAX. = 4.45000E+01
MIN. = -2.22607E+01
ORIENT = Z
PLANE = 1
2-D DOMAIN
FLUENT V2.9
CREARE INC

Fig.2.44

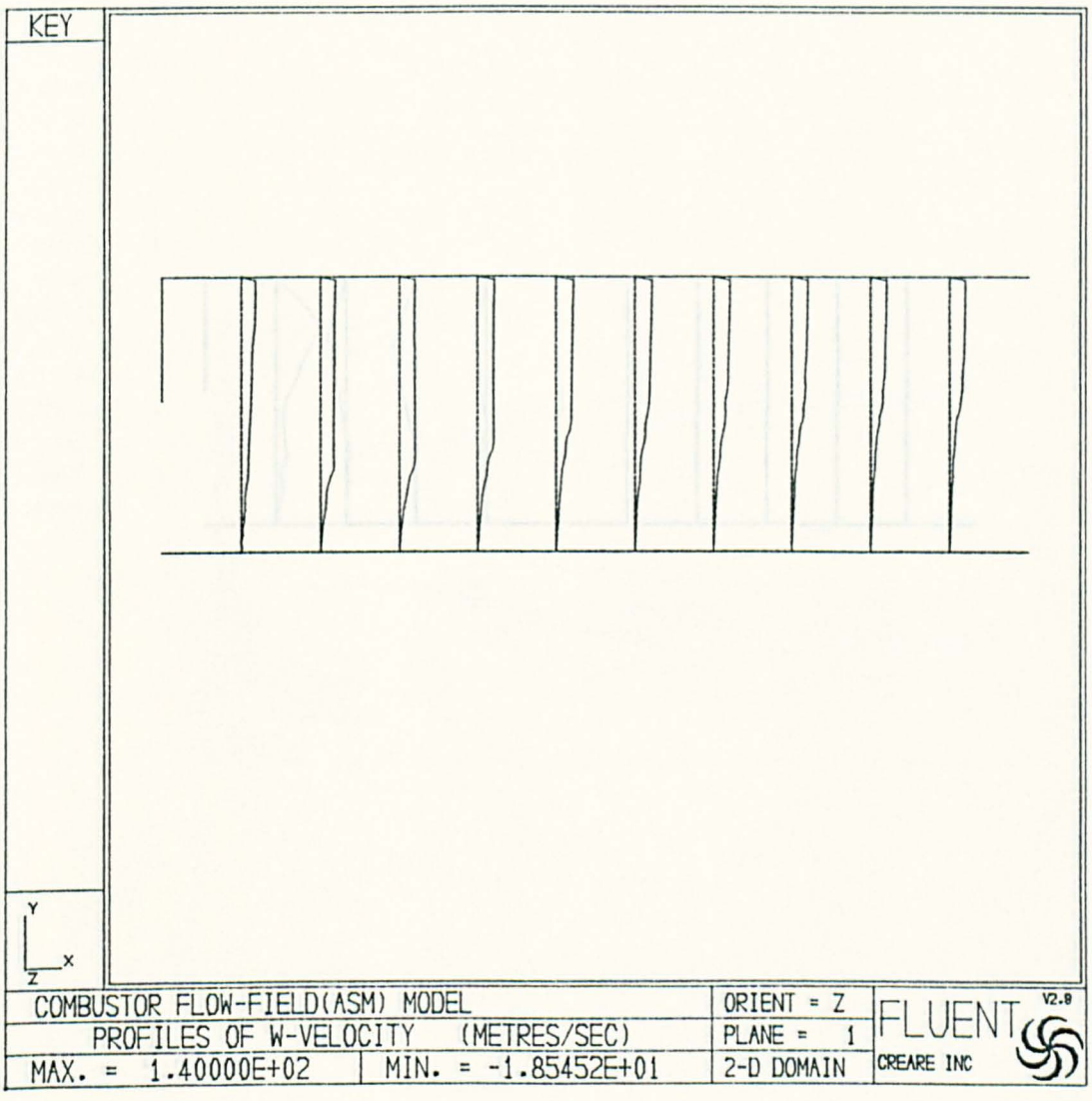
KEY
Y
X
Z
COMBUSTOR FLOW-FIELD(ASM) MODEL
PROFILES OF W-VELOCITY (METRES/SEC)
MAX. = 1.40000E+02
MIN. = -1.85452E+01
ORIENT = Z
PLANE = 1
2-D DOMAIN
FLUENT
V2.0
CREARE INC

Fig.2.45

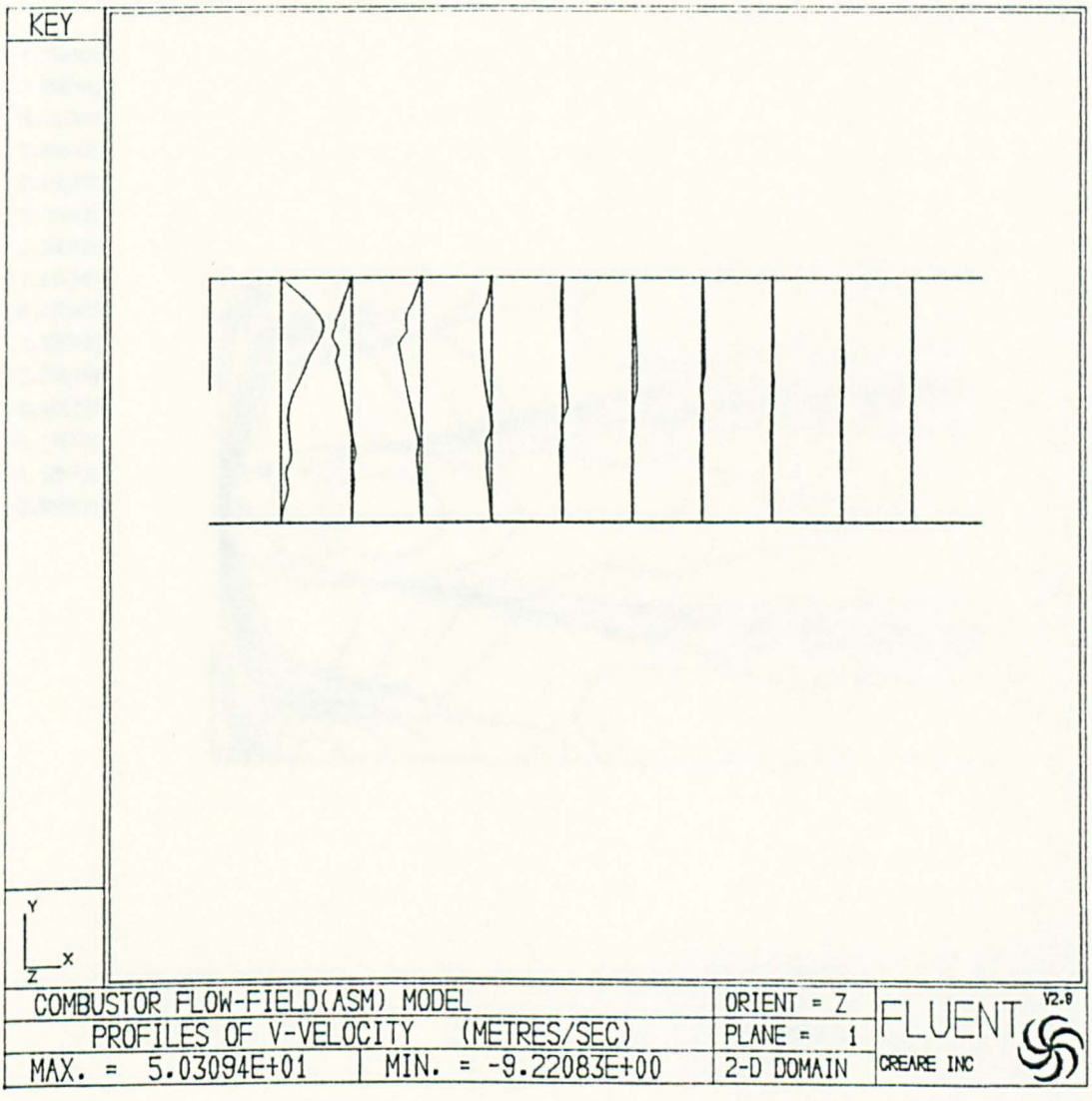
KEY
Y
X
Z
COMBUSTOR FLOW-FIELD(ASM) MODEL
PROFILES OF V-VELOCITY (METRES/SEC)
MAX. = 5.03094E+01
MIN. = -9.22083E+00
ORIENT = Z
PLANE = 1
2-D DOMAIN
FLUENT V2.0
CREARE INC

Fig.2.46

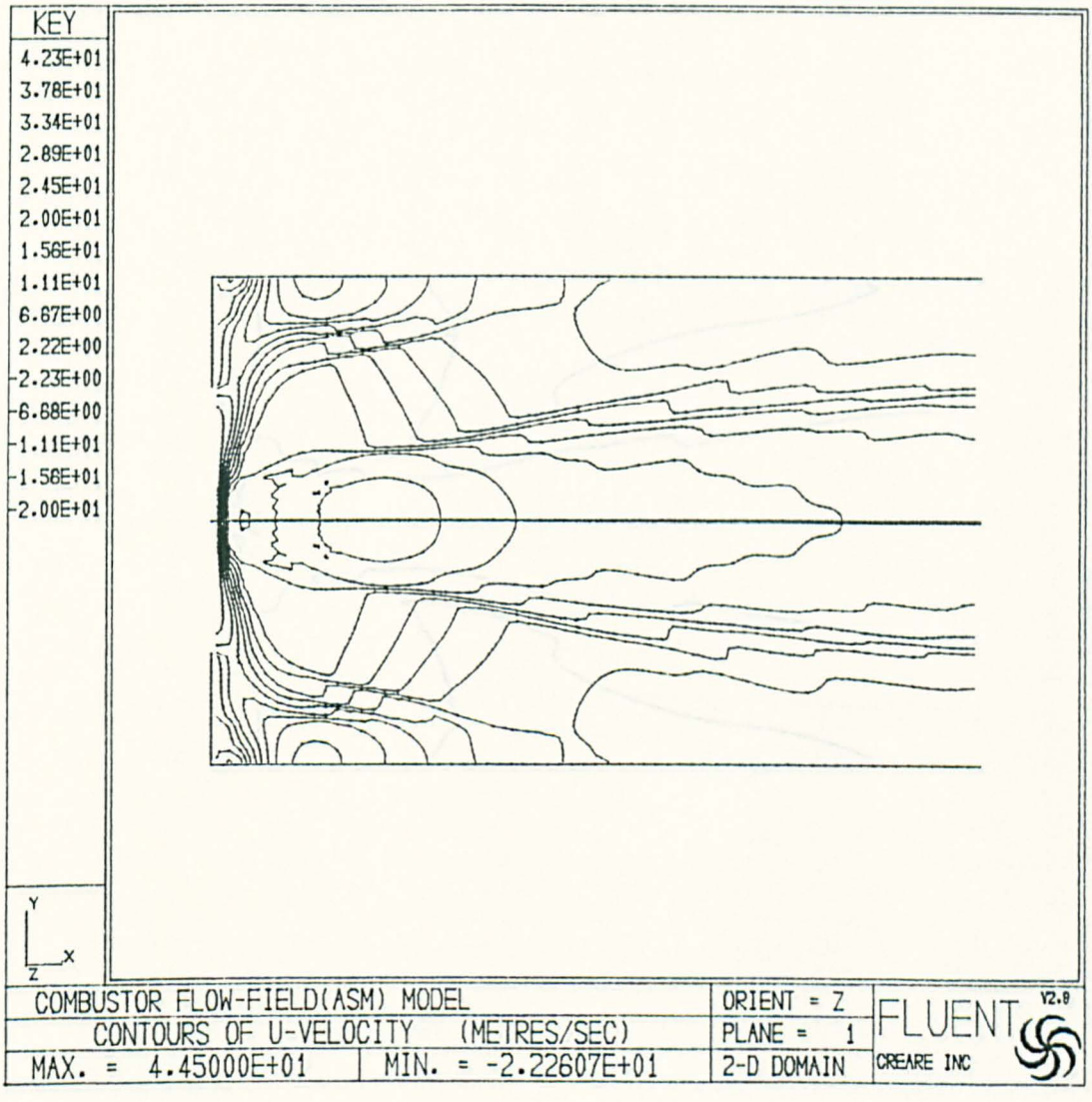
KEY
4.23E+01
3.78E+01
3.34E+01
2.89E+01
2.45E+01
2.00E+01
1.56E+01
1.11E+01
6.67E+00
2.22E+00
-2.23E+00
-6.68E+00
-1.11E+01
-1.56E+01
-2.00E+01
Y
X
Z
COMBUSTOR FLOW-FIELD(ASM) MODEL
CONTOURS OF U-VELOCITY (METRES/SEC)
MAX. = 4.45000E+01
MIN. = -2.22607E+01
ORIENT = Z
PLANE = 1
2-D DOMAIN
FLUENT V2.0
CREARE INC

Fig.2.47

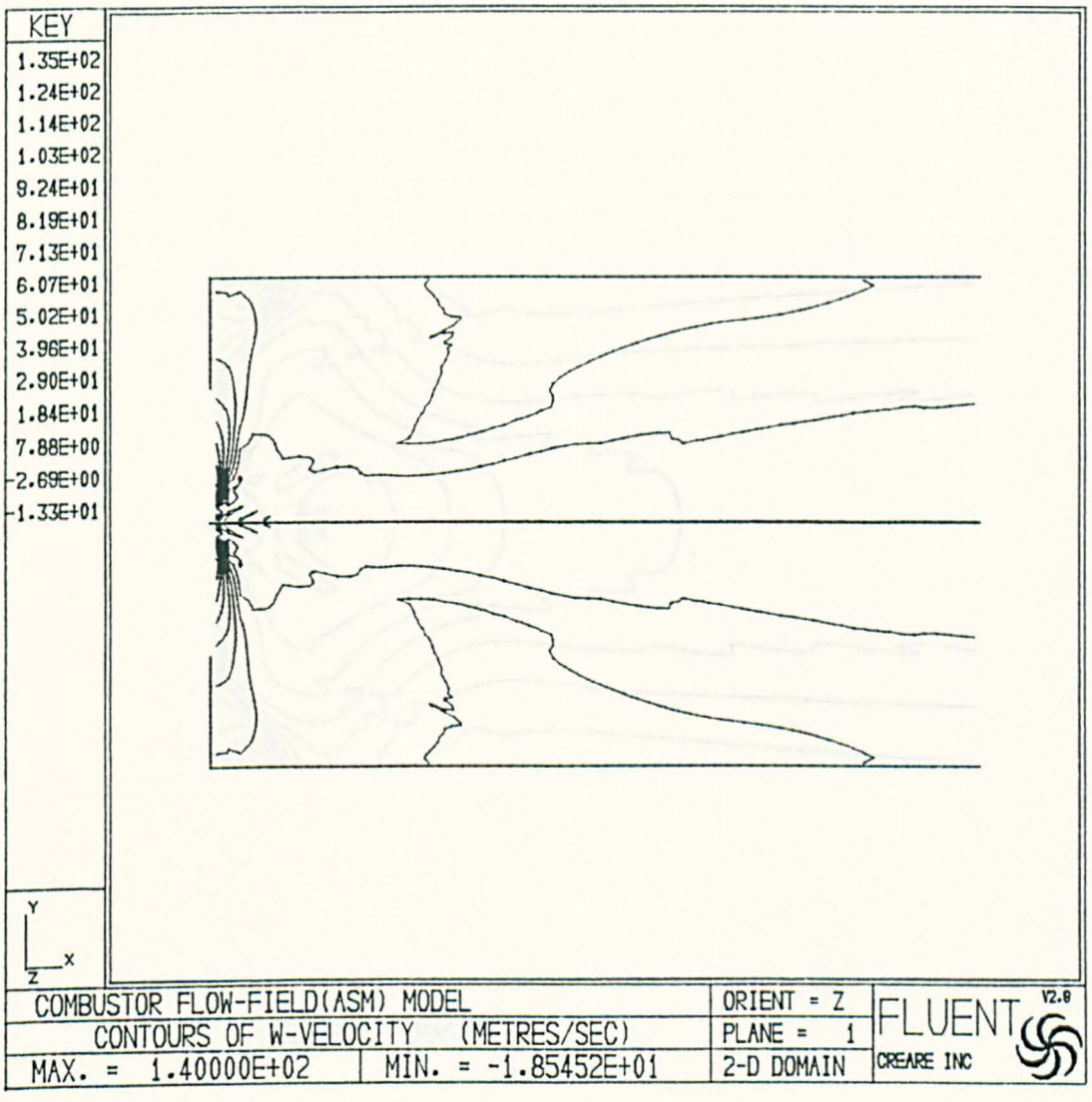
KEY
1.35E+02
1.24E+02
1.14E+02
1.03E+02
9.24E+01
8.19E+01
7.13E+01
6.07E+01
5.02E+01
3.96E+01
2.90E+01
1.84E+01
7.88E+00
-2.69E+00
-1.33E+01
Y
X
Z
COMBUSTOR FLOW-FIELD(ASM) MODEL
CONTOURS OF W-VELOCITY (METRES/SEC)
MAX. = 1.40000E+02
MIN. = -1.85452E+01
ORIENT = Z
PLANE = 1
2-D DOMAIN
FLUENT
V2.0
CREARE INC

Fig.2.48

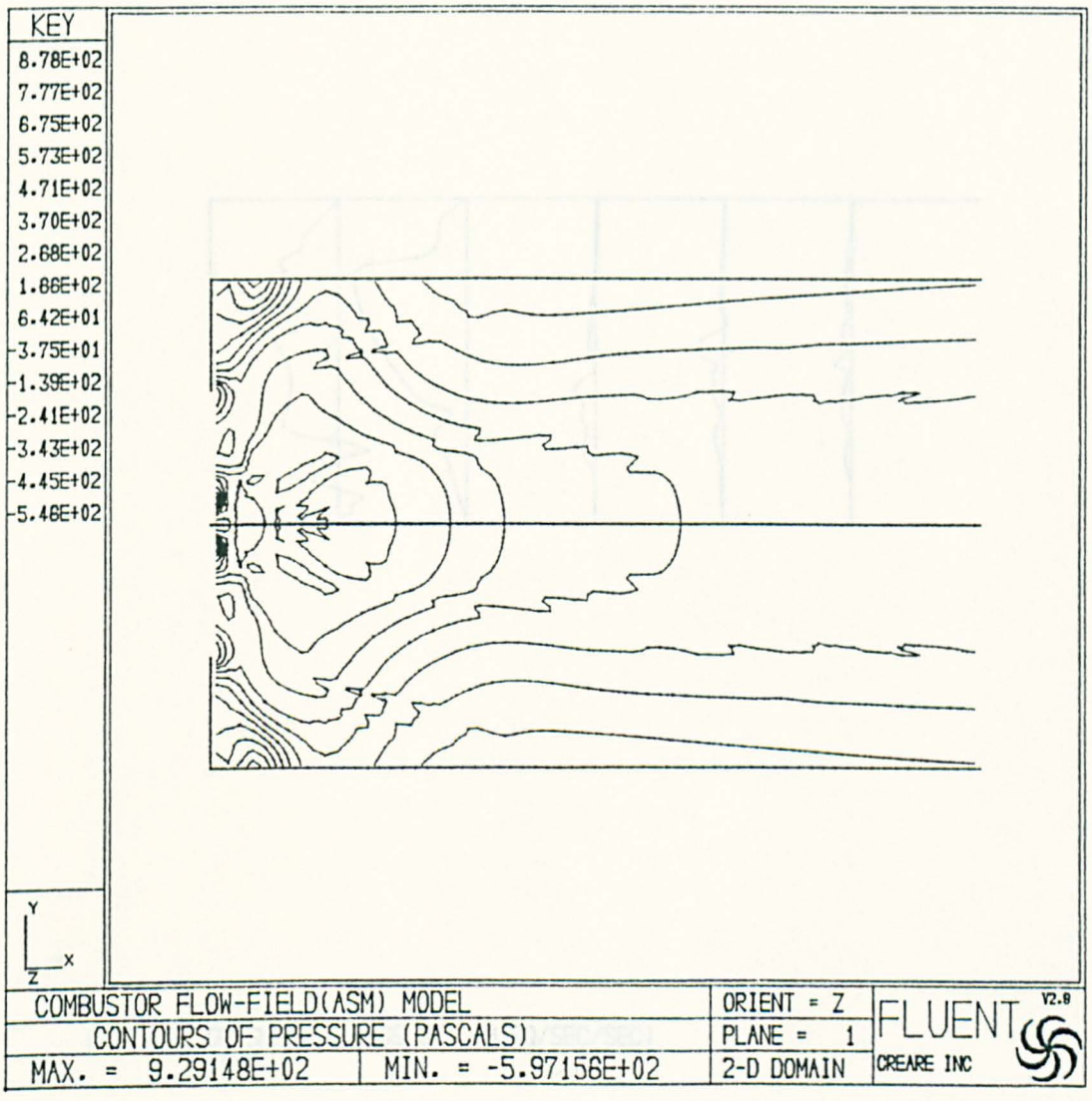
KEY
8.78E+02
7.77E+02
6.75E+02
5.73E+02
4.71E+02
3.70E+02
2.68E+02
1.66E+02
6.42E+01
-3.75E+01
-1.39E+02
-2.41E+02
-3.43E+02
-4.45E+02
-5.48E+02
Y
X
Z
COMBUSTOR FLOW-FIELD(ASM) MODEL
CONTOURS OF PRESSURE (PASCALS)
MAX. = 9.29148E+02
MIN. = -5.97156E+02
ORIENT = Z
PLANE = 1
2-D DOMAIN
FLUENT
V2.0
CREARE INC

Fig.2.49

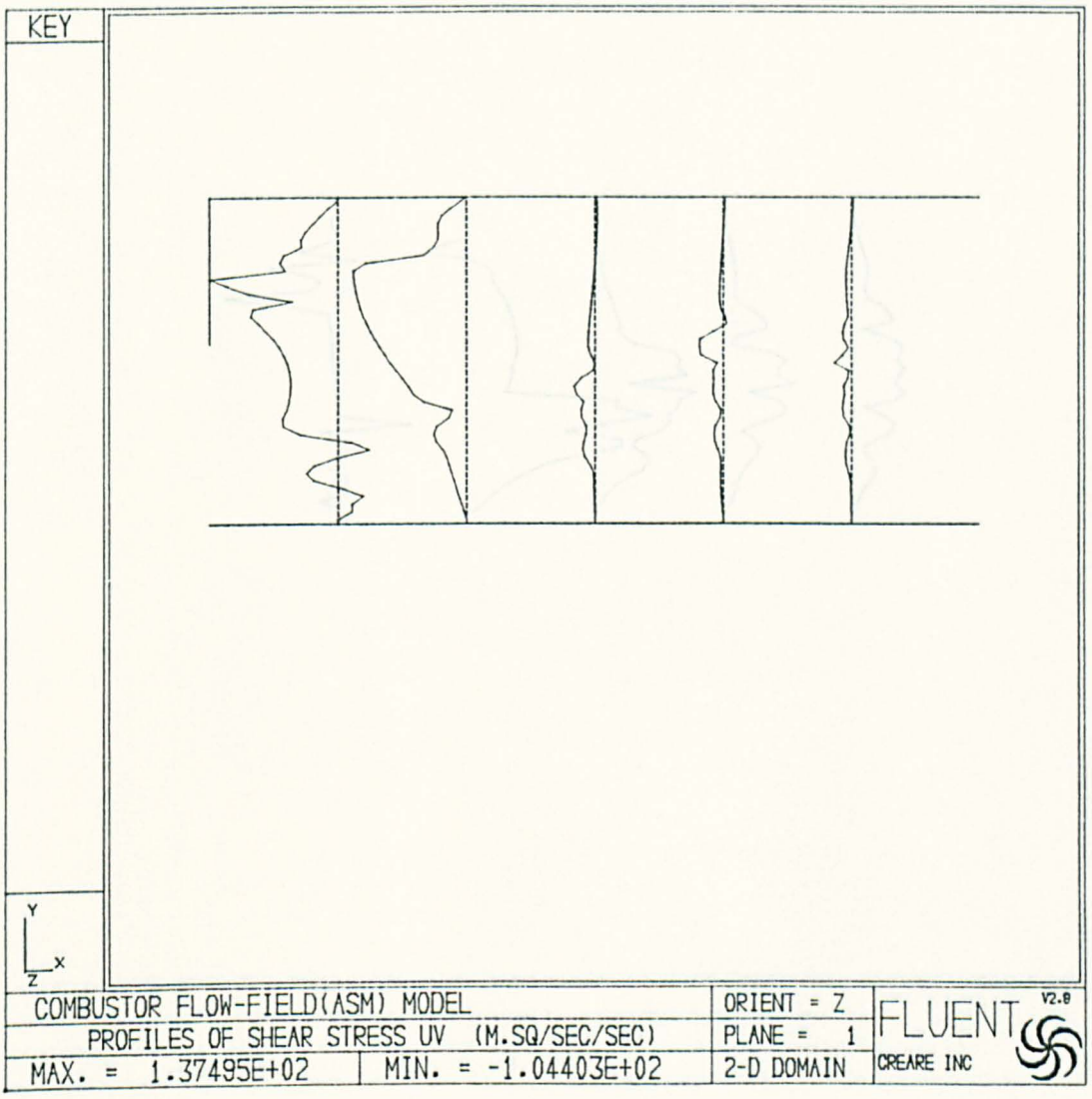
KEY
Y
X
Z
COMBUSTOR FLOW-FIELD(ASM) MODEL
PROFILES OF SHEAR STRESS UV (M.SQ/SEC/SEC)
MAX. = 1.37495E+02
MIN. = -1.04403E+02
ORIENT = Z
PLANE = 1
2-D DOMAIN
FLUENT
V2.0
CREARE INC

Fig.2.50

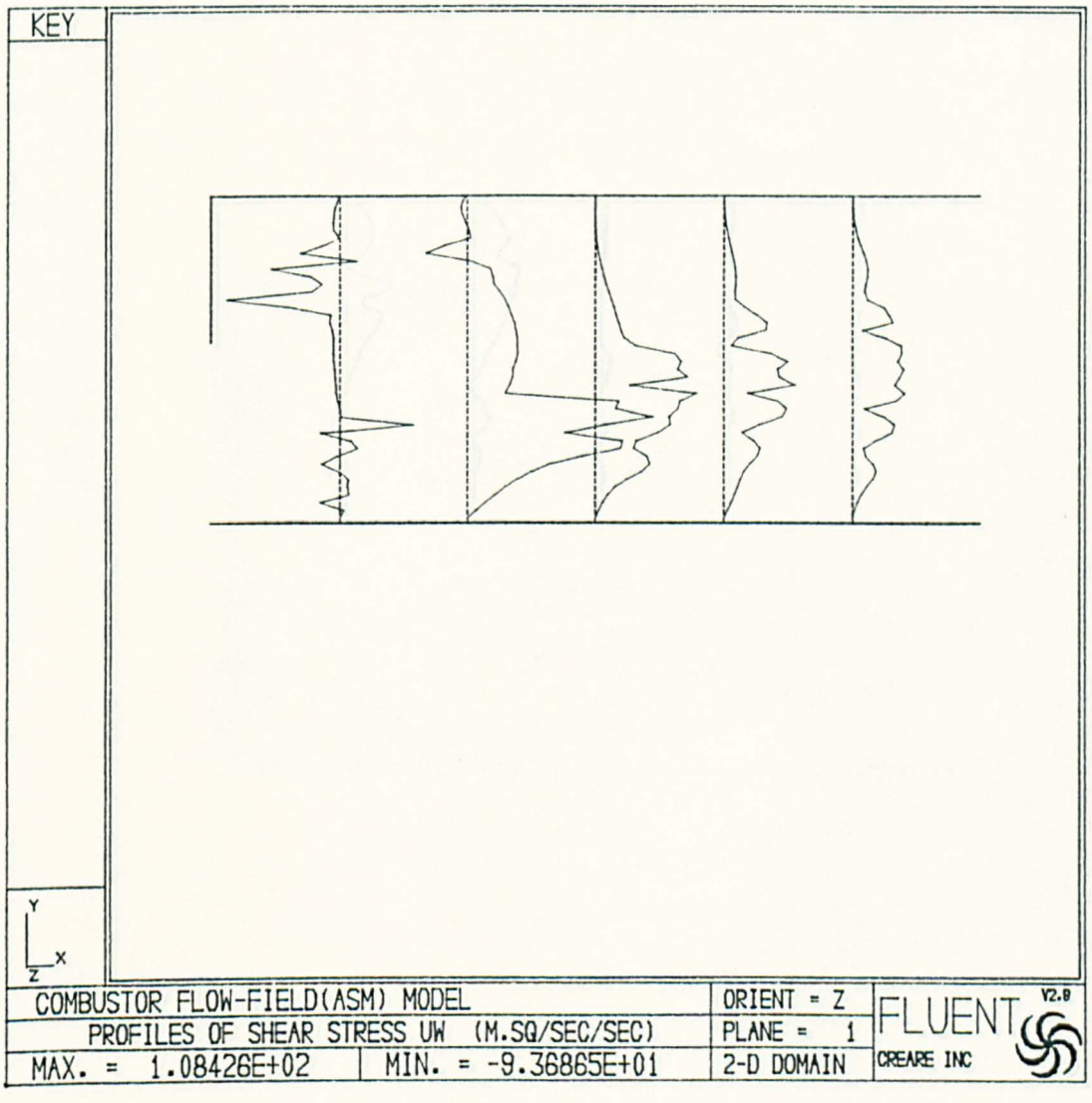
KEY
Y
X
Z
COMBUSTOR FLOW-FIELD(ASM) MODEL
PROFILES OF SHEAR STRESS UW (M.SQ/SEC/SEC)
MAX. = 1.08426E+02
MIN. = -9.36865E+01
ORIENT = Z
PLANE = 1
2-D DOMAIN
FLUENT
V2.0
CREARE INC

Fig.2.51

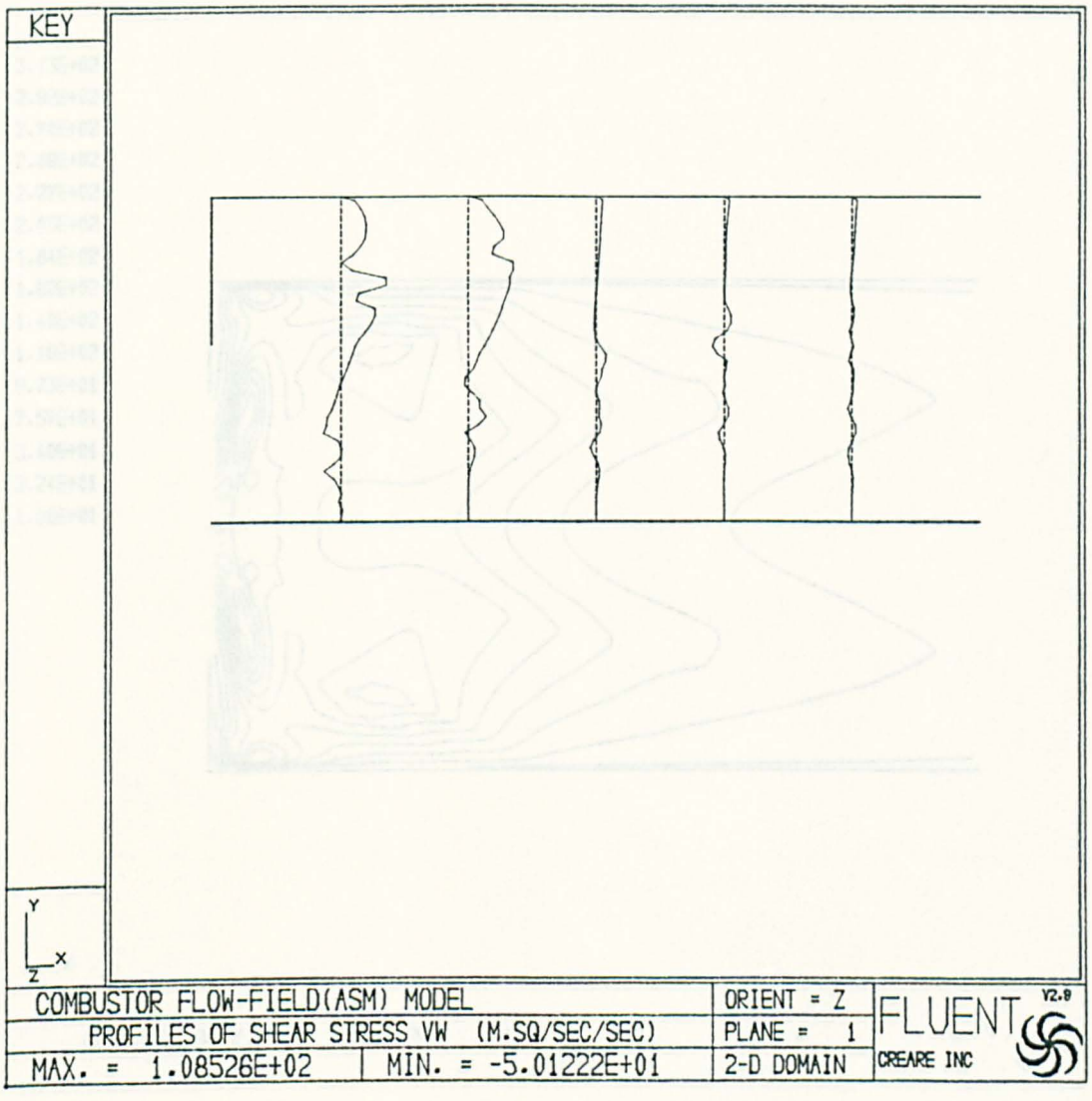
KEY
Y
X
Z
COMBUSTOR FLOW-FIELD(ASM) MODEL
PROFILES OF SHEAR STRESS VW (M.SQ/SEC/SEC)
MAX. = 1.08526E+02
MIN. = -5.01222E+01
ORIENT = Z
PLANE = 1
2-D DOMAIN
FLUENT V2.0
CREARE INC

Fig.2.52

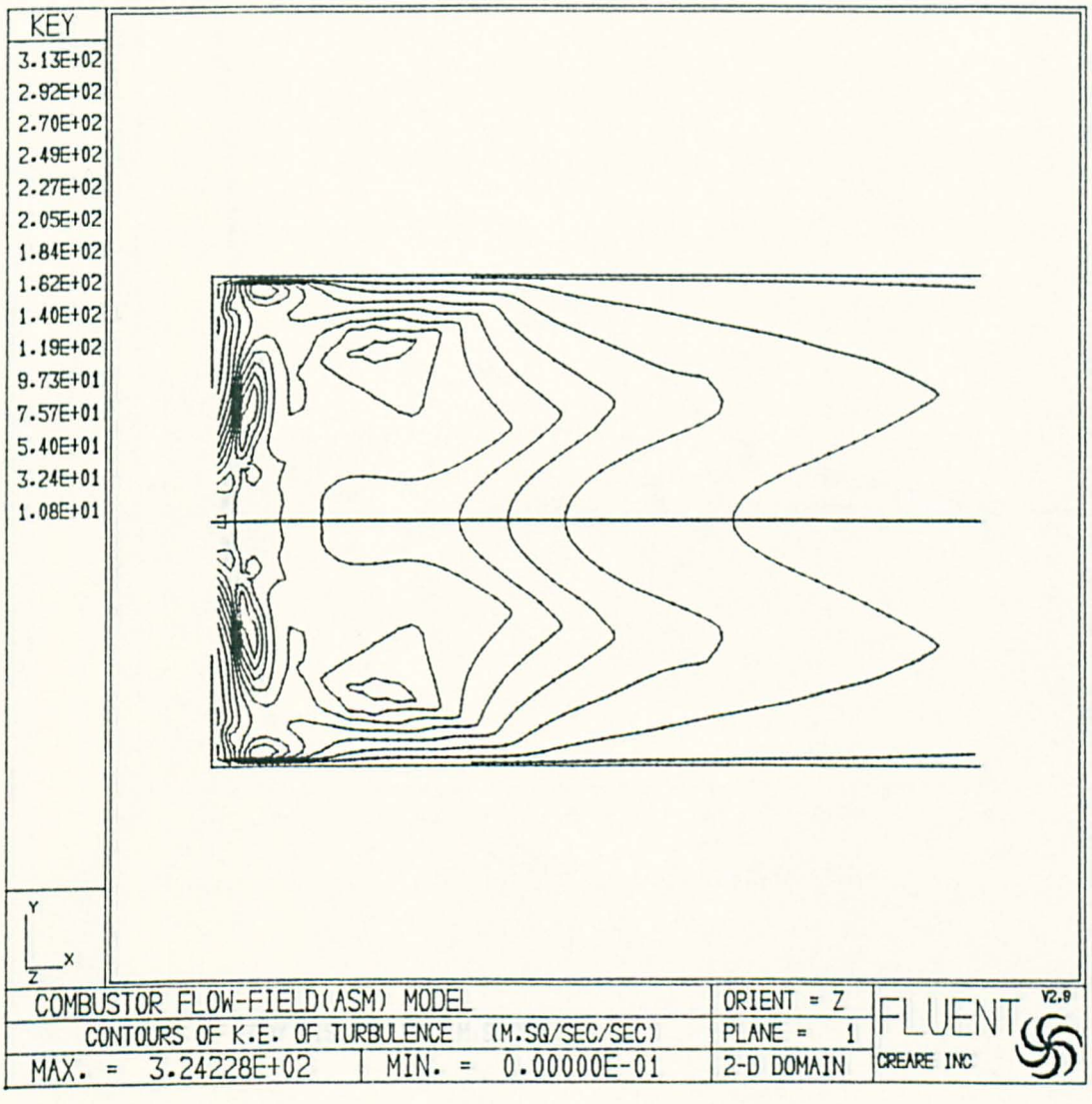
KEY
3.13E+02
2.92E+02
2.70E+02
2.49E+02
2.27E+02
2.05E+02
1.84E+02
1.62E+02
1.40E+02
1.19E+02
9.73E+01
7.57E+01
5.40E+01
3.24E+01
1.08E+01
Y
X
Z
COMBUSTOR FLOW-FIELD(ASM) MODEL
CONTOURS OF K.E. OF TURBULENCE (M.SQ/SEC/SEC)
MAX. = 3.24228E+02
MIN. = 0.00000E-01
ORIENT = Z
PLANE = 1
2-D DOMAIN
FLUENT V2.9
CREARE INC

Fig.2.53

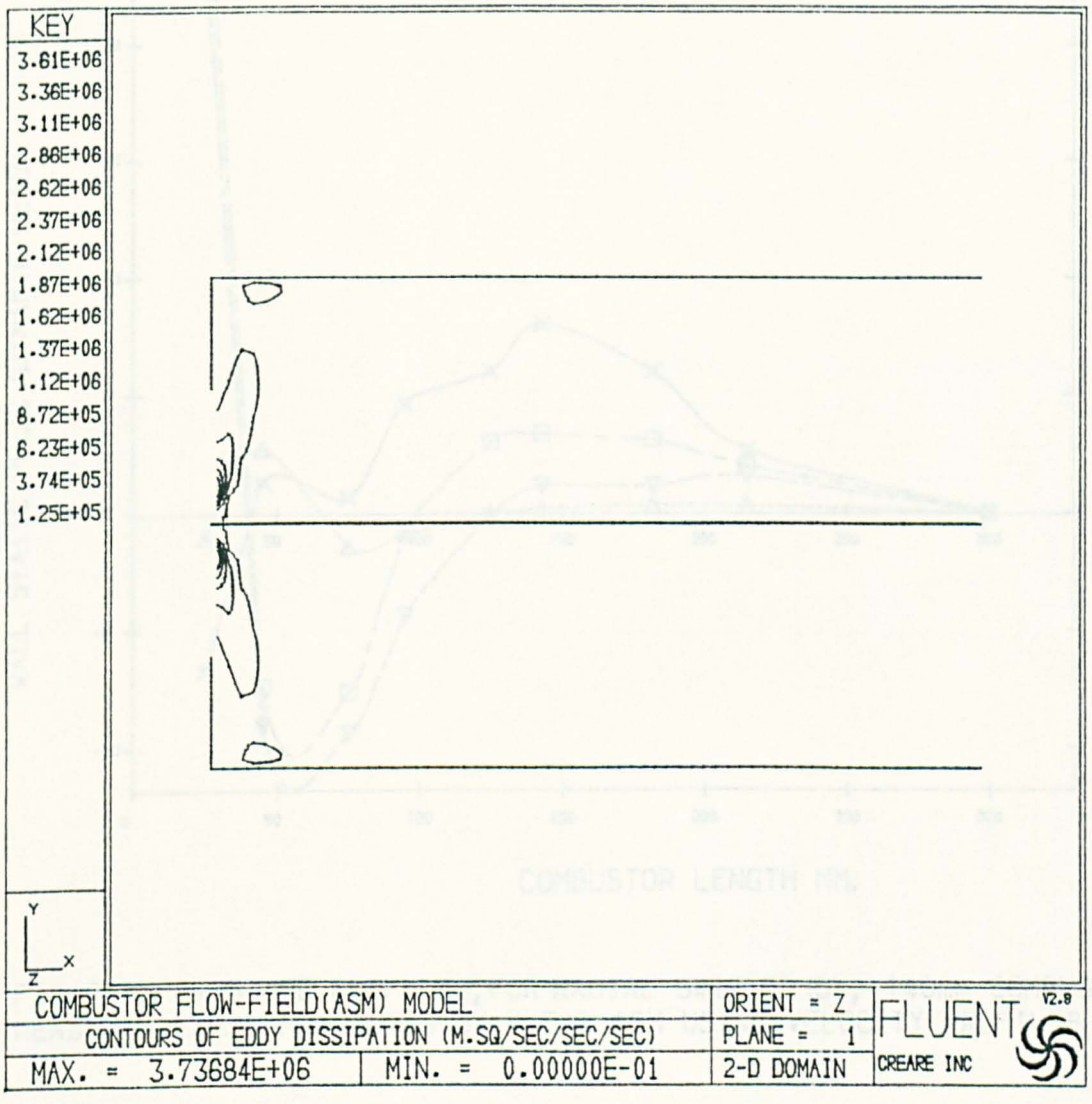
KEY
3.61E+06
3.36E+06
3.11E+06
2.86E+06
2.62E+06
2.37E+06
2.12E+06
1.87E+06
1.62E+06
1.37E+06
1.12E+06
8.72E+05
6.23E+05
3.74E+05
1.25E+05
Y
X
Z
COMBUSTOR FLOW-FIELD(ASM) MODEL
CONTOURS OF EDDY DISSIPATION (M.SQ/SEC/SEC/SEC)
MAX. = 3.73684E+06
MIN. = 0.00000E-01
ORIENT = Z
PLANE = 1
2-D DOMAIN
FLUENT
V2.8
CREARE INC

Fig.2.54

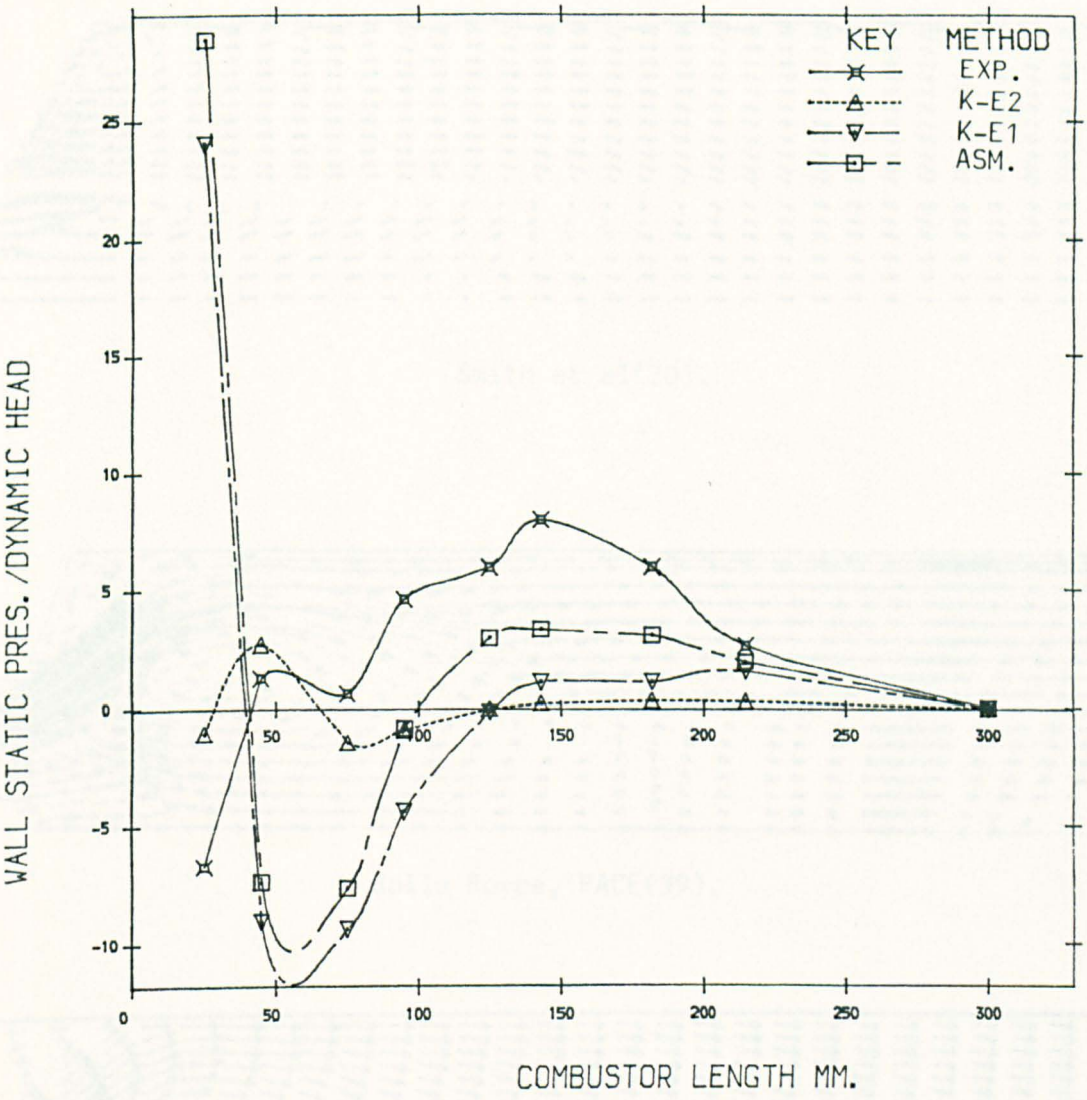

FIG. 2.55 PRESSURE PROFILES, FOR RADIAL SWIRLER (B), 140mm COMBUSTOR, AS MEASURED EXP. & PREDICTED BY K-E & ASM USING VELOCITY PROFILES AT INLET

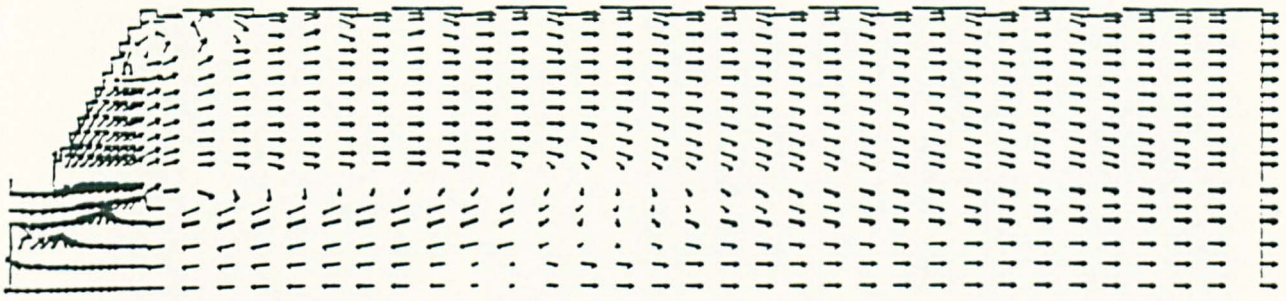

Smith et al(20).

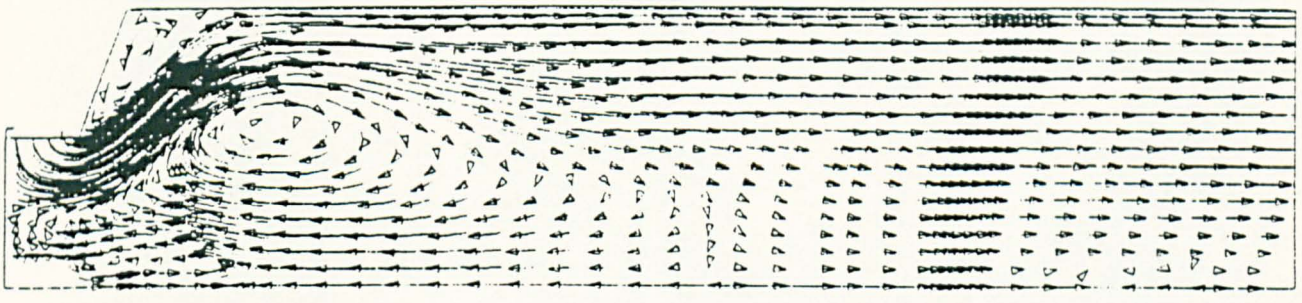

Rolls Royce, PACE(39).

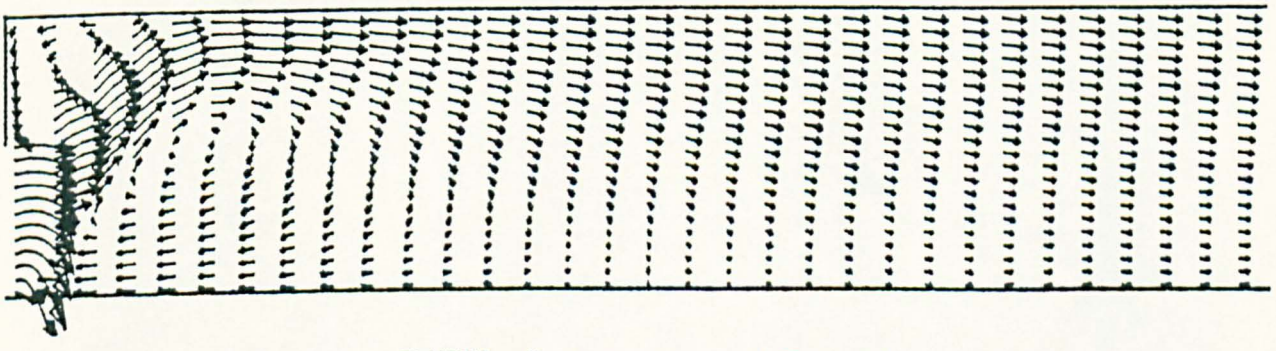

FLUENT, Present Work, K-E model.

Fig.2.56 Velocity-Vector representations as predicted by different Computer codes.

PLATES

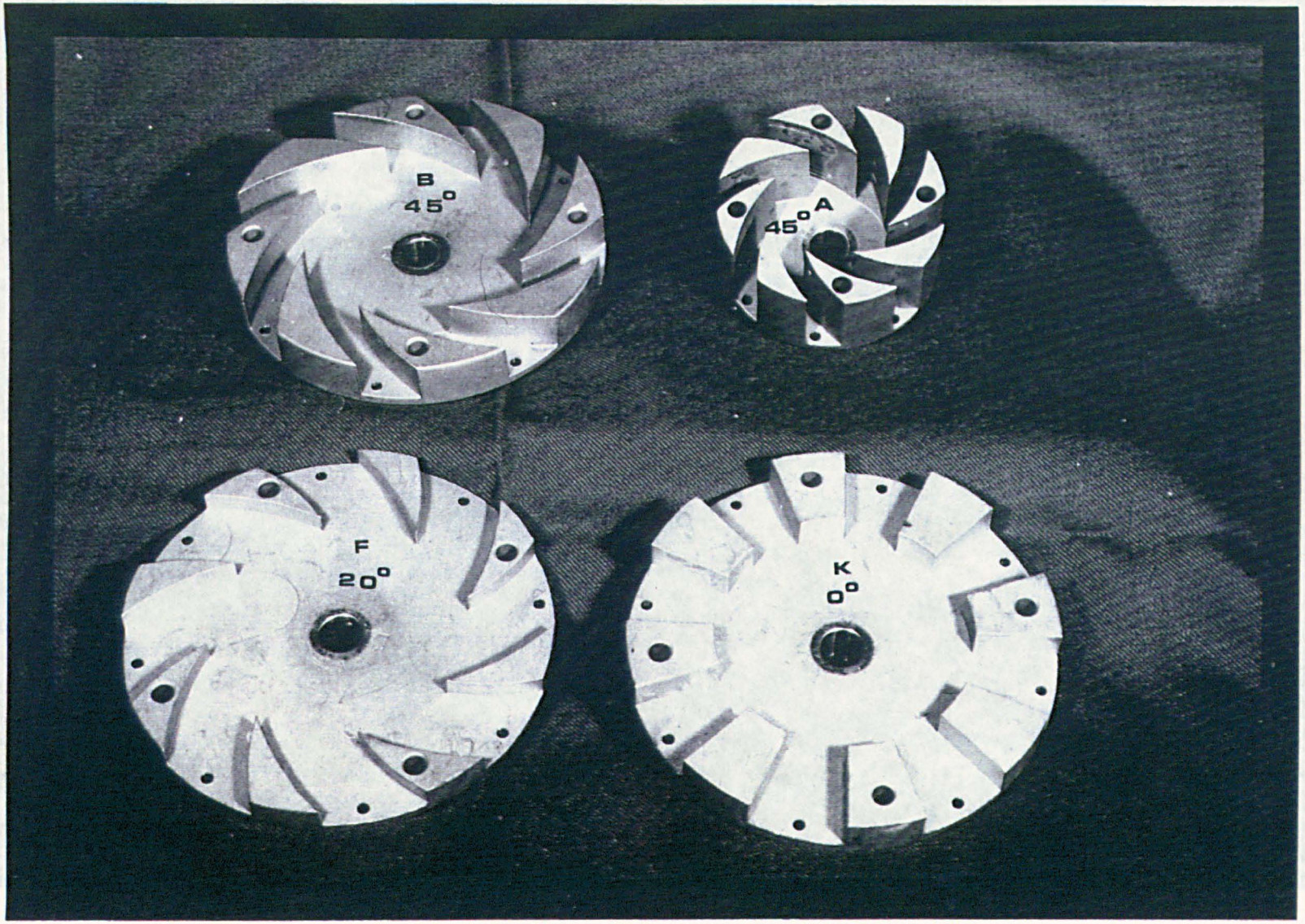

Plate 2.1 Radial swirlers (Curved-passages type) A,B,F and the zero-angle radial jets stabiliser (K).

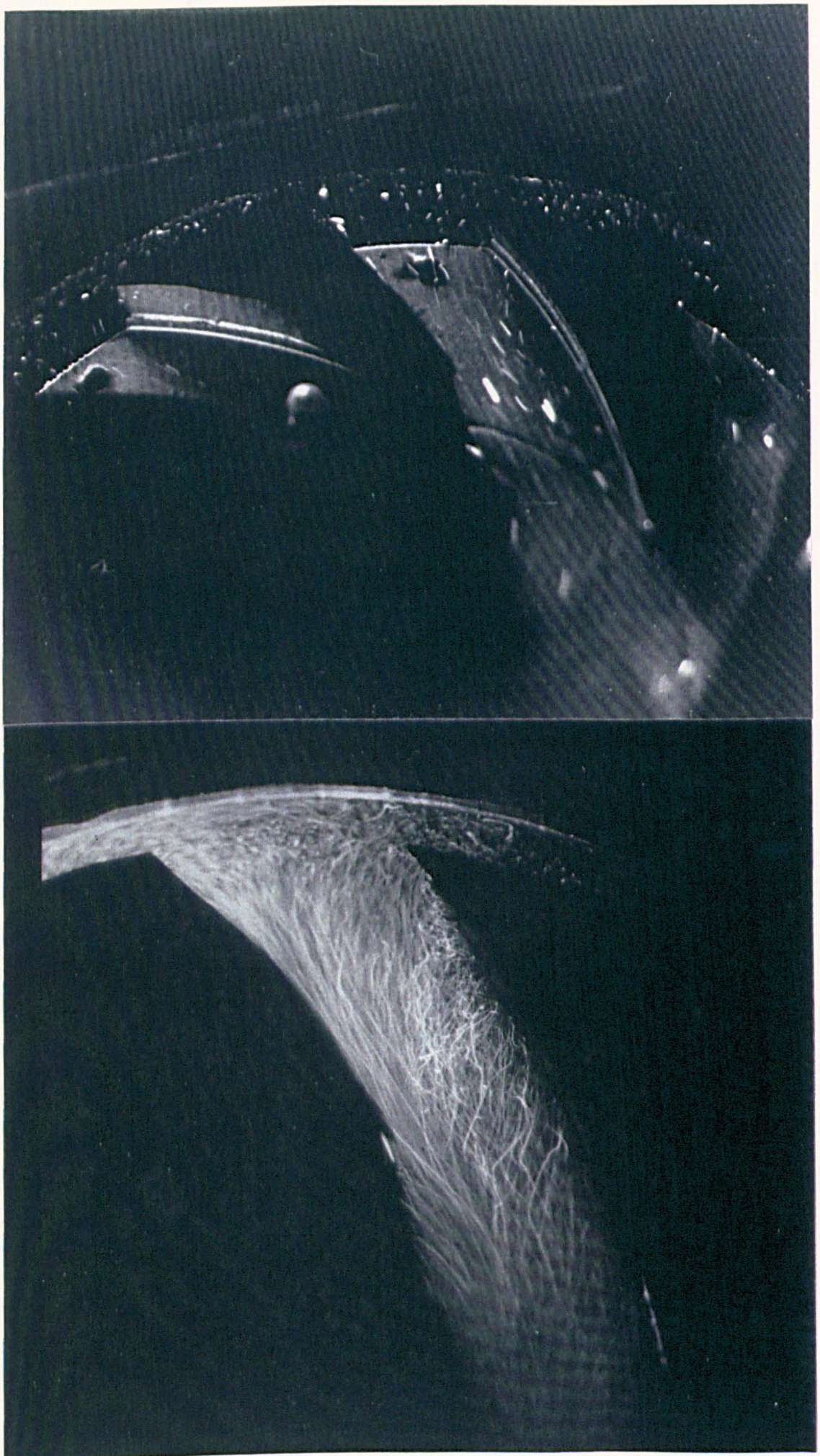

Plate 2.2 Separation in the curved-passage of radial swirler (B).

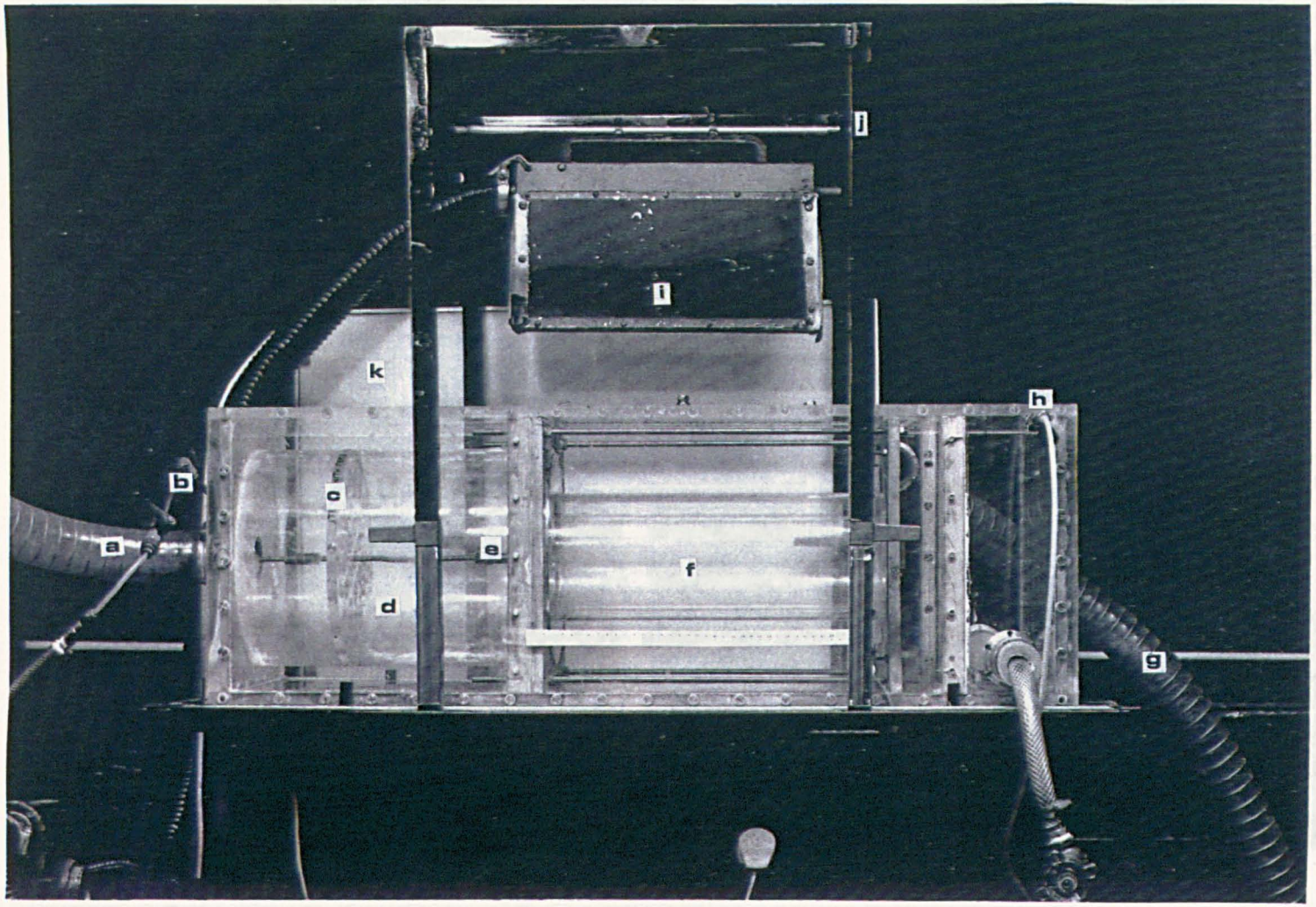

a-Water inlet
b-Dye inlet
c-Straightener
d-Approach pipe
e-Injector
f-140mm combustor
g-Outlet
h-Air-bubbles releif valve
i-Illumination light
j-Holder
k-Opal-light

Plate 2.3 Assembled perspex water-model rig used for visualization studies.

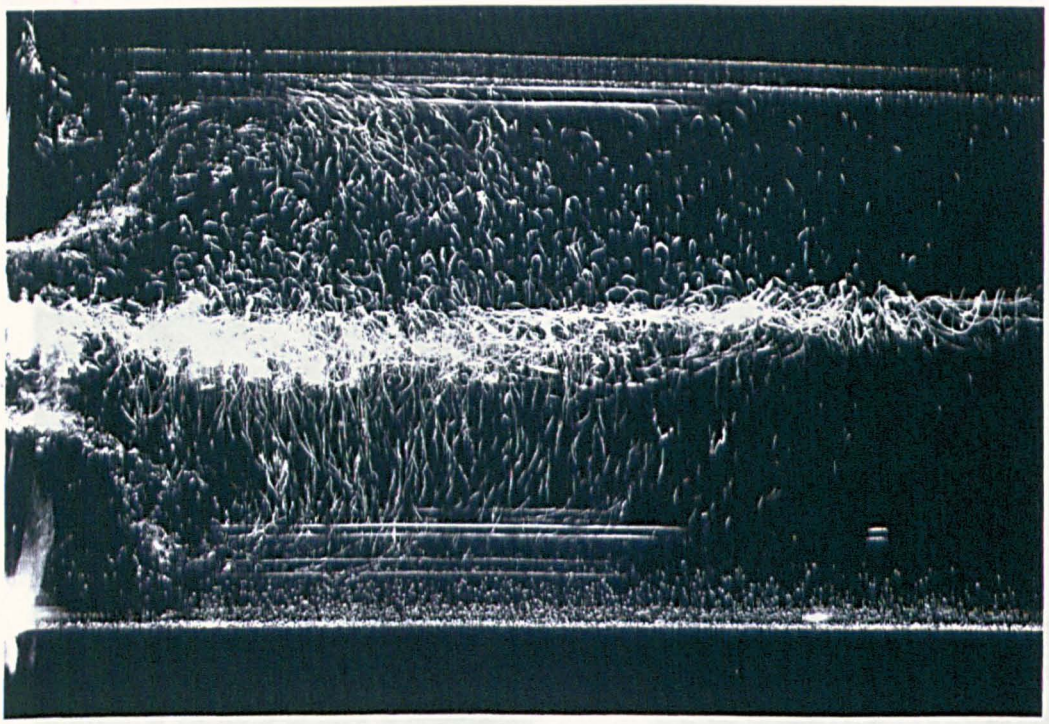

SWIRLER (B)

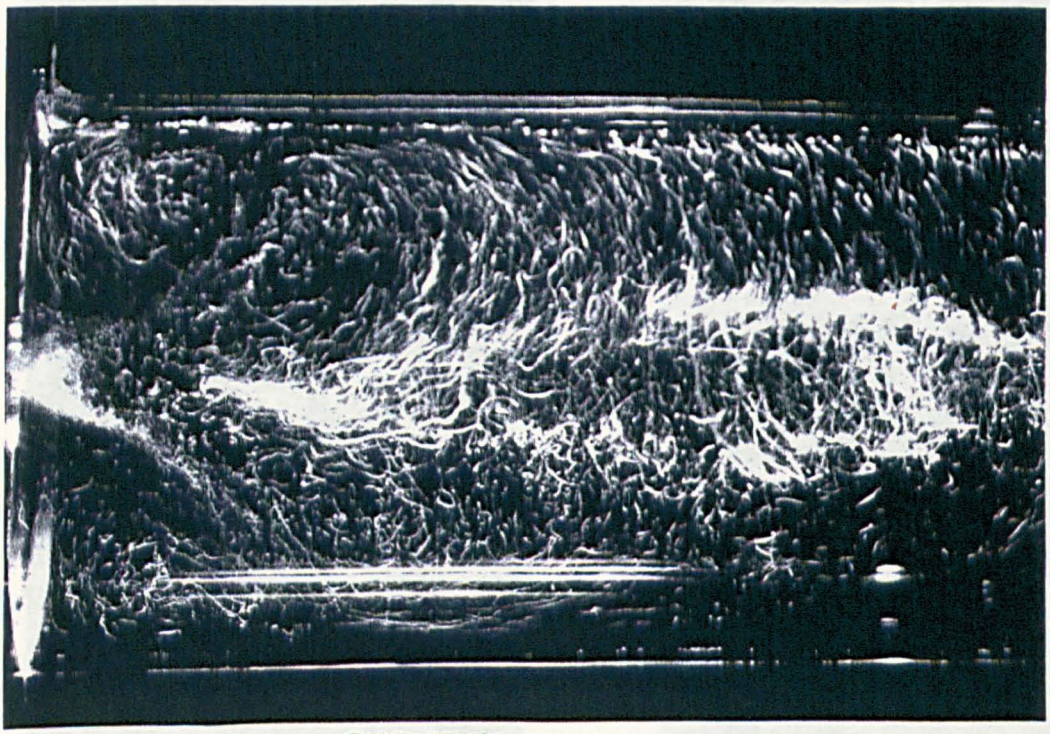

SWIRLER (A)

Plate 2.4 Comparison between flow field issued by radial swirler (B) and (A) in 140mm combustor , scale= 1.56/1

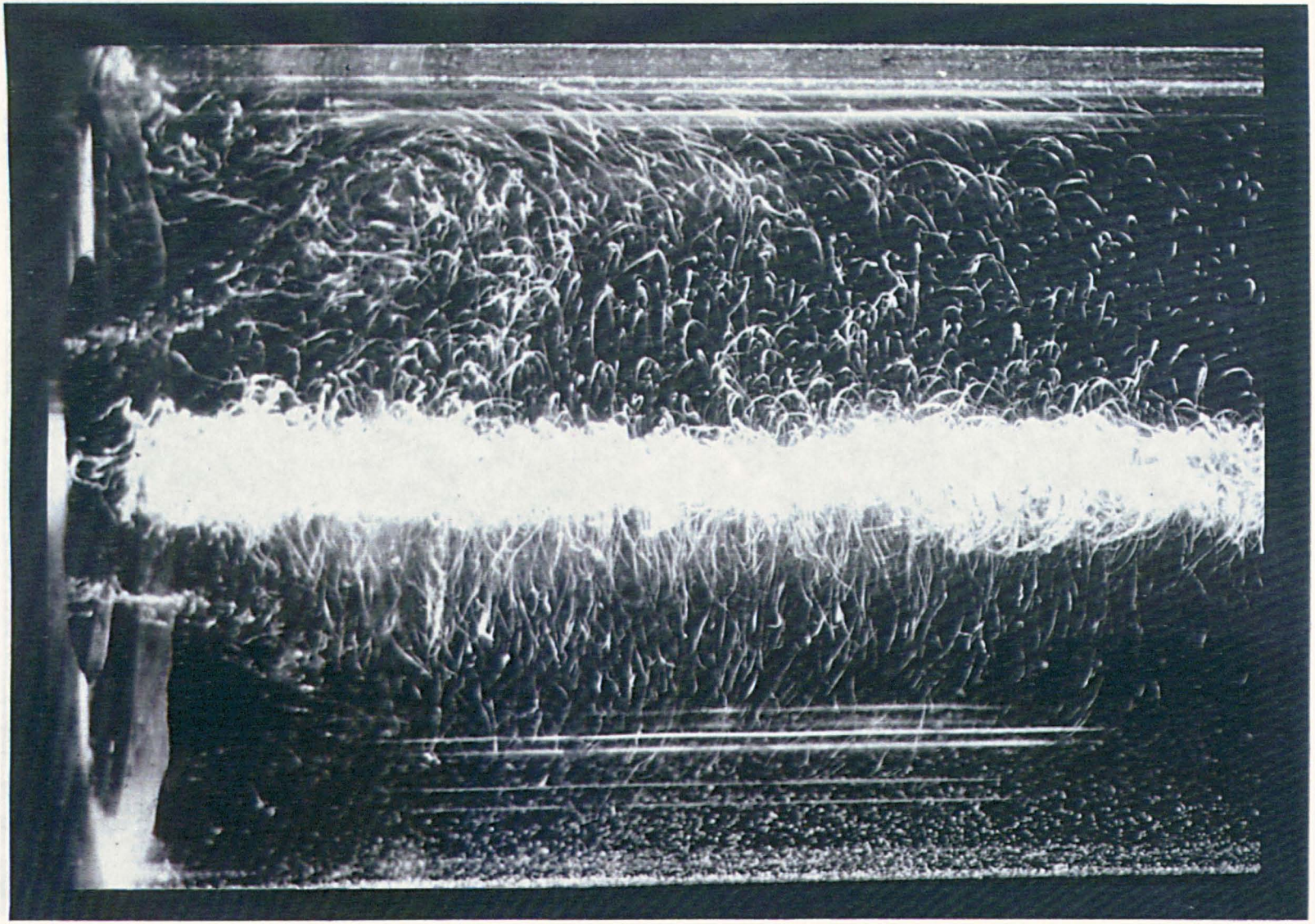

Plate 2.5 Flow pattern issued from swirler (B) in 140mm combustor, scale= 1.1/1

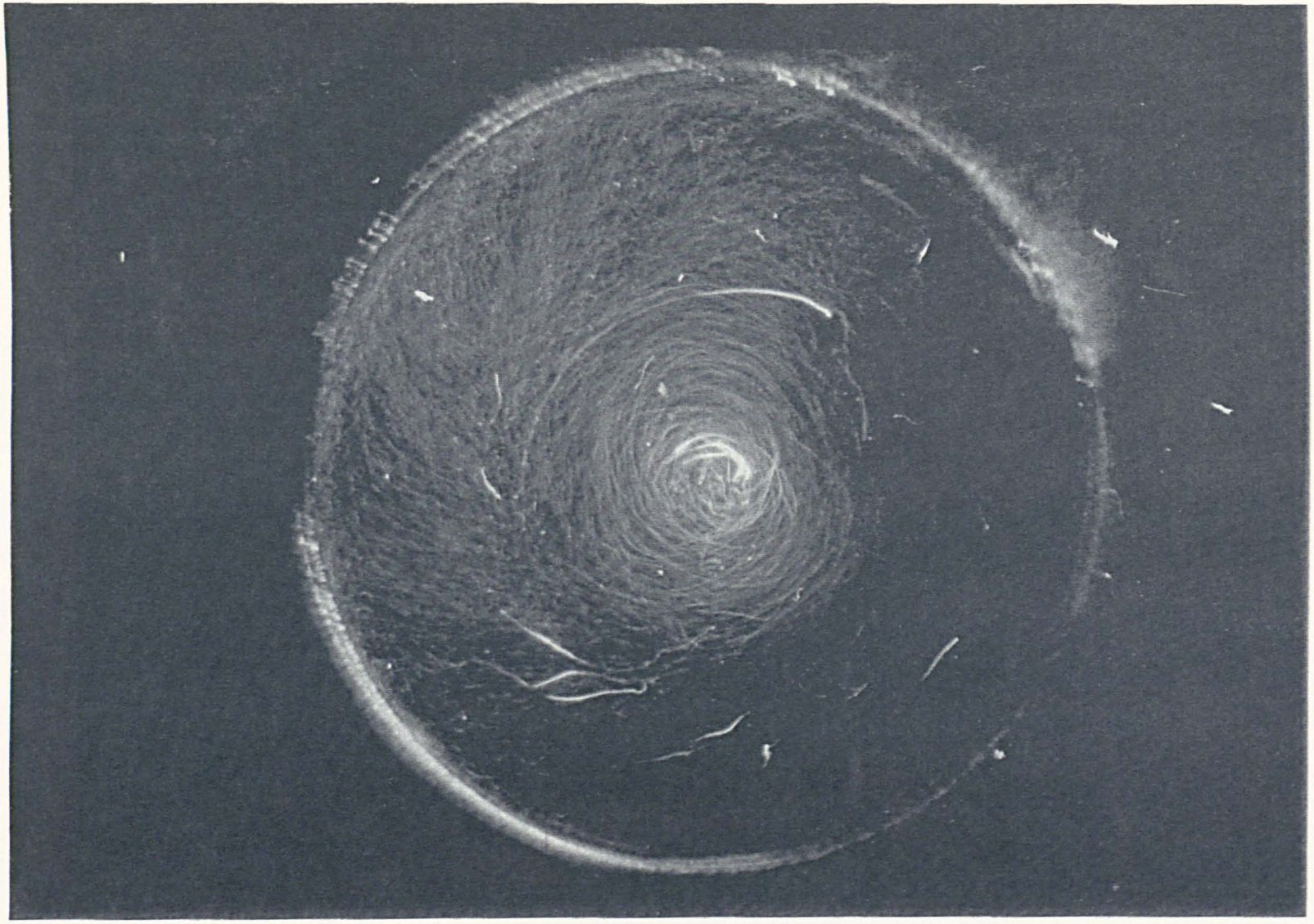

Plate 2.6 Cross-sectional view of the flow pattern issued by radial swirler(B) at X= 30mm , scale= 1.08/1

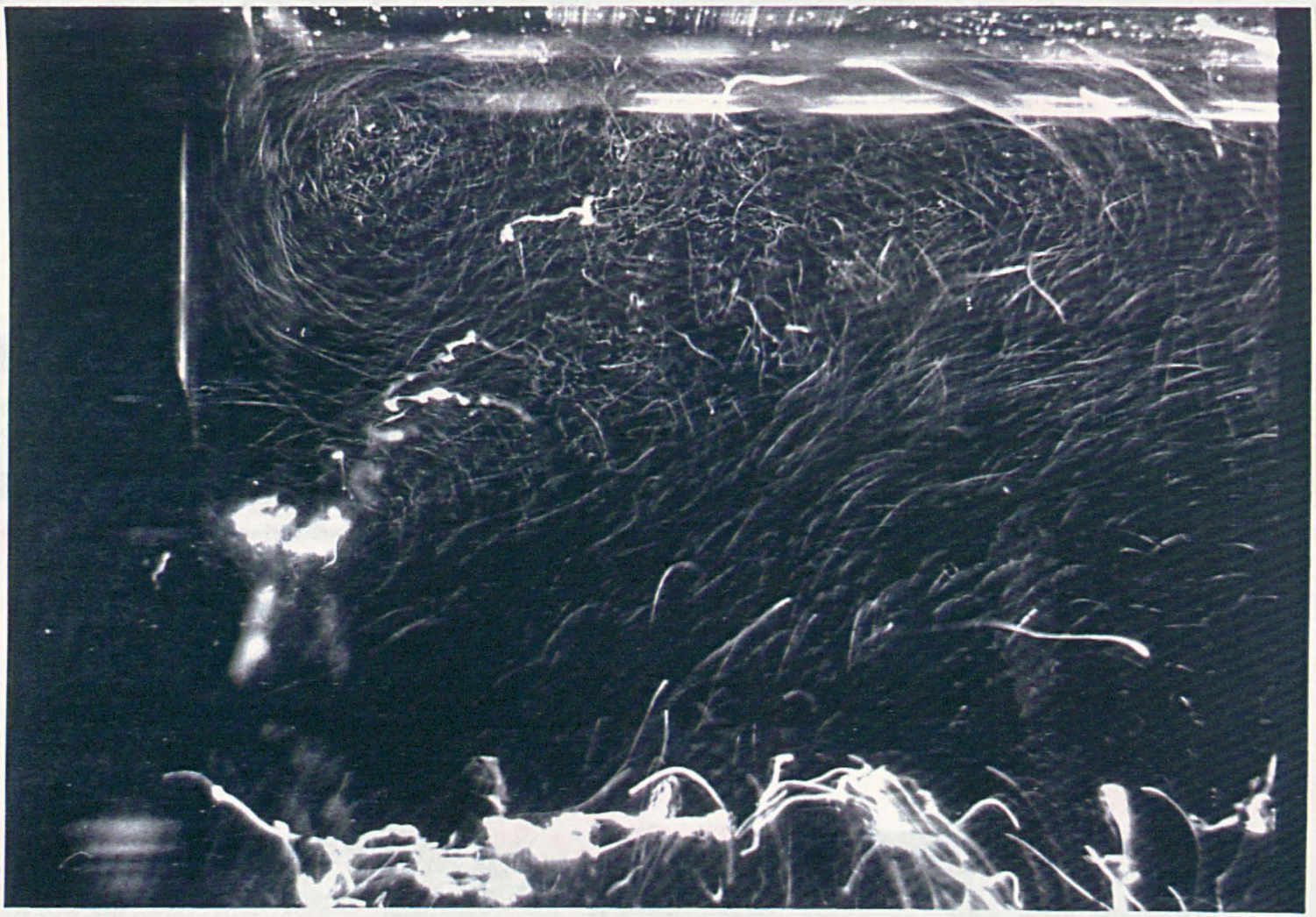

Plate 2.7 Longitudinal view demonstrating the corner-recirculation zone and the jet boundaries imposed by radial swirler (B) flow regime in 140mm combustor, scal= 0.77/1

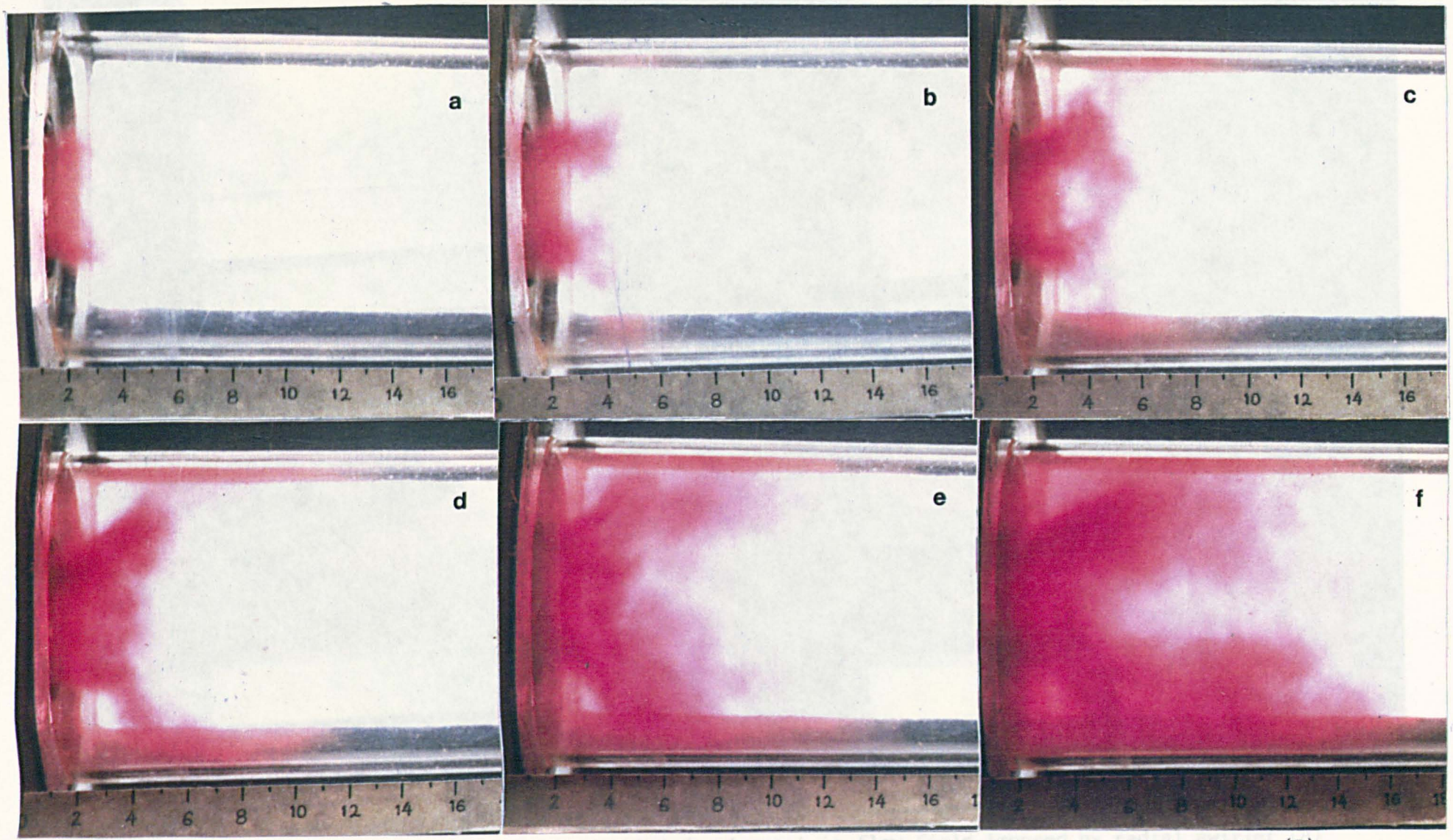

Plate 2.8 Radial central dye-injection development in flow regime issued by radial swirler (B) in 140mm combustor, scale= 2.8/1

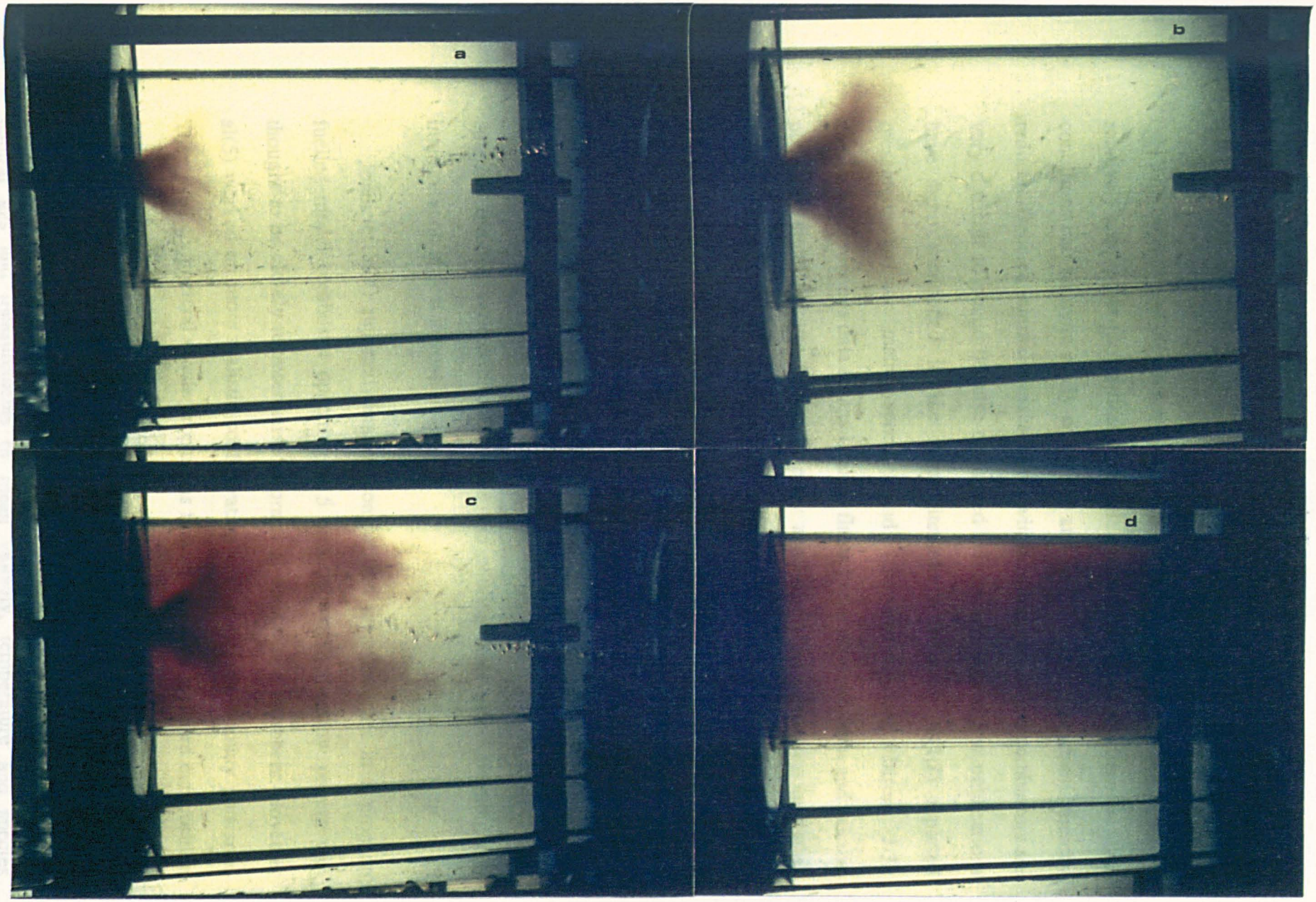

Plate 2.9 Radial central dye-injection development in flow field imposed by radial swirler (A) in 140mm combustor, scale= 3.6/1

CHAPTER THREE

INTERNAL FLAME STRUCTURE

3.1 INTRODUCTION

The objective of this work is to obtain detailed internal measurements on relatively simple but geometrically realistic combustion systems where the flow conditions can be more easily controlled and some of the uncertainties thereby reduced. Detailed internal measurements within actual gas turbine combustors are very difficult to obtain because of limited access; and only a few publications have been mentioned in the open literature. Tuttle et al(1,2) reported measurements of main species and temperature in Allison J-33 combustor.Emissions data for the internal flame in the axial direction and exhaust plane for simulated gas turbine primary zone at typical combustor operating conditions are reported. Their results indicated that with a well atomised fuel spray the large scale turbulent mixing controls the flame stoichiometry and hence the emissions characteristics. Vranos and Taback(3) also measured species concentrations and temperature. However, actual combustion chambers are usually not ideal for testing and development of model (e.g. turbulence, combustion model etc.). Uncertainties associated with the inlet air portions entering through various dilution holes and cooling slots make unambiguous interpretation almost impossible.

Jones et al(4) reported detailed composition measurements in a propane fuelled model combustor operating at 5 bars. However, the flow pattern was thought to be closely representative of practical combustion chambers. Noyce et al(5) worked on more realistic configuration with a variable primary port area. They used commercial -grade propane as fuel and the data included composition and temperature measurements for two different fuel injectors at atmospheric pressure. Toral and Whitelaw(6) reported a studies in a sector of an annular combustion chamber comprising two fuel holes. The combustor fuelled with natural gas and measurements of mean velocity, temperature and species

concentration were obtained at atmospheric pressure. The data was completed with isothermal velocity profiles and a passive scalar map for which helium was injected into the air flow through the fuel injectors.

The influence of dilution air onthe primary zone combustion was studied by Nakamura et al(7). They operated propane (97% purity) fuelled can type combustion chamber with swirl introduced somewhat upstream and reported concentration, temperature and residence time measurements in the hot flow as well as the penetration of the dilution jets measured with an argon trace method in the cold state. These experiments were restricted to atmospheric pressure. Jones and Toral(8) have obtained concentration and temperature measurements in a can type propane fuelled combustion chamber. Their investigations were made at atmospheric pressure for two different inlet air temperature (313 K and 523 K). Their results show that chemical equilibrium conditions prevail only for locally fuel-lean conditions and there is strong evidence that both fuel breakdown and CO to CO2 oxidation rate, are partly controlled by finite rate chemical kinetic mechanisms. Velocity and concentration profiles in a kerosene fuelled flow were reported by El Banhawy and Whitelaw(9). Their study included the influence of the mean droplet diameter on the combustion process for three different swirler vane angles.

Hori(10) reported species concentration measurements mainly NO and NO2, under a fuel-lean overall equivalence ratio of 0.37, using propane as fuel in laboratory swirl combustor. He concluded that No2 can be formed in the region of the combustor were the strong mixing occurs between the hot combustion gas and the cold air stream.

Heiter and Whitelaw(11) reported isothermal and combustion flow characteristics of a model can-type gas turbine combustor; their conclusion was that in primary zone, combustion controlled more by physical than chemical kinetic processes and the formation of pollutants was well described by a partial equilibrium model. Recently, Bicen et al(12) reported temperatures and species

concentration measurements in a model combustor operating at an inlet temperature of 515 K and atmospheric pressure. The combustor was fuelled with natural gas with purity of 94% CH4, which was delivered by T-vaporisor injector. Their results showed that the combustion efficiency was raised from 69% to 94.2% with an air/fuel ratio of 29; when raising the inlet temperature by 200 K.

Detailed measurements were reported by Takagi et al(13) of gas species concentration mainly NOX, CO, and hydrocarbons together with the temperature in a flame formed around a fuel propane jet surrounded by a swirling air flow. They noted that mixing and combustion of the fuel layer flowing around the recirculation zone in the swirling flame structure controlled the formation and emission of NOX, CO and UHC. Theoretical and experimental investigations into the aspects of axisymmetric confined swirling flows were reported by Wilhelmi(33). Experimental data for flows representing the primary zone of gas turbine combustion chambers were obtained, the data included LDA measurements of the mean velocities in three directions. For the reacting flow, probe measurements of the major species and temperature were also reported.

Various techniques are available to study the behaviour of turbulent flames in combustors. These may be non-intrusive techniques such as the laser doppler anemometer techniques for velocity measurements or intrusive methods such as thermocouples for temperature measurements, five hole probe for velocity and sampling probes for species concentration measurements. In the present work the latter technique has been adopted for emissions measurements. This was carried out both at the exhaust and internal sections of the combustor by means of a multi hole and single hole water cooled sampling probe respectively. Fig.3.1 shows schematic diagram of the sampling probes which have been used in the present work.

3.2 EXPERIMENTAL EQUIPMENT

A (6.4mm) thick stainless steel cylindrical combustor of 140mm internal diameter and 330mm long, built for pollution measurements on various stabilisers

such as swirlers, jetmix, gridcones, etc. The 330mm combustor length was a typical minimum size for aero gas turbines and was much shorter than most industrial gas turbines. Consequently, combustor residence times were representative of the minimum practical value.

The air was heated to the required inlet combustor temperature by a 108 KW electric heater. The gases were exhausted into a 140mm diameter water cooled tube and then to the exhaust stack. A schematic layout of the test rig can be seen in Fig.3.2 and plate 3.1. The flame tube and swirlers were only cooled by natural convection. Ignition was achieved by means of a 12 Joule surface discharge igniter mounted 25mm downstream of the stabiliser. This was mounted flush with the combustor wall so that no flow interference could be caused by the igniter. Air was supplied to the combustors by an air blower via a venture meter with a throat diameter of 34.9mm designed to BS1042(14). The combustor was receiving air from an approach pipe which is connected to the air supply pipe downstream of an electric heaters.

The inlet temperature to the combustor was measured 100mm upstream of the swirler using a chrome-alumel type K thermocouple and the inlet pressure was monitored using a ring of four static pressure tappings 150mm upstream of the flame stabilister linked to an electronic micromonometer. To obtain a mean gas sample, an 'X' configuration stainless steel water cooled probe was used at the exhaust with twenty holes at centres of equal area. A single point water cooled stainless steel tube was traversed across the horizontal combustor plane in order to obtain local gas samples radially at different axial positions.

The gas samples were transported to the gas analysis equipment along a 7.6m long heated teflon sample line. Sample gases were analysed for oxygen (O2), hydrogen (H2) and carbon monoxide and dioxide (CO, CO2), oxides of nitrogen (NO, NOx) and unburnt hydrocarbon (UHC) using on line rapid response analysers. Plate 3.2 show view and schematic illustration of the gas analysis technique used in the present work. The mean gas sample probe was designed to

be similar to that used by Lister and Wedlock(15) and the gas analysis technique followed the EPA standards(16,17).

3.3 GAS ANALYSIS SYSTEM

3.3.1 MEAN EXIT SAMPLING

An 'X' configuration gas sampling probe was used for mean exit sampling. It consisted of two stainless steel tubes welded eccentrically with water circulating in between the tubes to cool the gases and the probes. Sample gases were withdrawn through 20 holes of 1mm diameter, drilled at centres of equal areas in the inner tube. The sampling probe was designed to be similar to the oil cooled probe used by Lister(15). The gas analysis probe is shown in Fig.3.1.A

In order to check the accuracy of the mean gas sampling processes, the derived gas analysis equivalence ratios were compared with the rig metered equivalence ratios. This was carried out for all the tests performed. Fig.3.3-3.4 shows sample of results for each method of fuel injection. This indicates that a reasonable mean gas sample was obtained and the deviations were less than those reported in other similar studies (18,19). may be caused by a number of effects. The following were thought to be the main:

Calibration of gas analysis: This should be random as different calibration gas bottles were used over the period in which the tests were performed. Thus they may contribute to the data scatter, but not to the consistency of richer mixtures in gas analysis. Later on in the tests, High purity calibration bottles of high accuracy were purchased and used. This could significantly reduce the errors.

Air or Fuel Metering Errors: Any error in air or fuel metering could result in some consistent differences but every effort had been made to minimize the accurance of this type of error.

Mean Exhaust Gas Sampling Error: This is probably the main cause in the

sampling errors. Large radial composition gradients are present in swirl flows which make it difficult to obtain a reliable mean sample using the multi hole probe.

3.3.2 INTERNAL TRAVERSE SAMPLING

The radial traverse sampling probe was a single-point, water-cooled stainless steel tube, traversed across the horizontal combustor plane, was used to obtain internal gas samples. A remotely operated motorized traverse system was used to traverse the probe through the combustor side ports and the system was accurate to better than + 1mm. The probe shown in Fig.3.1B had an external diameter was 10mm, and the 1mm diameter gas sample hole was located on the side of the tube, 1mm from the end, and was positioned so as to face the swirler. The axial shown in Fig.3.1C traverse sampling probe was used to traverse along the combustor centre line. The probe outer diameter was 17mm, and the 1mm diameter sampling hole was located at front tip of the probe. The total length of the probe which can be inserted inside the combustor is 380mm. The sampling probe was positioned so as to face the incoming flow. It is acknowledged that the use of a stainless steel probe in the present work is likely to give to some undesirable catalysis effects (mainly NO to NO2 conversion) as reported by Allen(24) and Kyukuo et al(25). These problems could have been overcome by the use of a quartz micro probe. However, this was not possible due the high temperatures promoted by the combustion processes and the difficulty of getting over the problem of avoiding reheating of the sample.

The internal traverse sampling probe is shown in Fig.3.1.B and 3.1.C and plate 3.1. The flow blockage caused by the probe increased as it was traversed across the combustion plane. In the initial wall region, where the probe was only inserted a short distance, the flow disturbances were less than at the end of the traverse at combustor centre-line where the blockage was about 10%. Visual observation of the flame showed no major flame disturbances due to the fully inserted probe, as Oven et al (20) had also noted in a similar situation. However,

there are a number of factors can influence the accuracy of a local gas sampling probe, some of which has been pointed out in various studies concerning the probe effects (21-23).

Clark and Mellor (21) investigated the effects of probes in gas turbine combustor emission measurements. Four types of stainless steel probes were designed to assess the effects of tip shape, tip to body proximity, and probe entry point into the flow field on measured pollutant concentrations. The probe entry point and tip to body proximity were shown to imperceptibly affect the pollutant concentrations, but the probe tip geometry was shown to have a significant impact on the measured pollutant levels. The tapered-tip probe was shown to yield depressed CO and UHC and elevated NO concentrations compared with blunt tip probes. In the present work in order to check the accuracy of the traverse gas sampling processes, the equivalence ratio based on CO2 measurements were compared with the equivalence ratio based on O2 measurements as can be illustrated by Fig.3.5 - Fig.3.10.

The radial gas sampling traverses were carried out at six axial position of 10, 30, 50, 110, 200, and 300mm, although in general the radial profiles are approximately symmetrical about the centre line, there are deviations from symmetry as reported by Andrews et al(26) their results showed that these deviations may be associated with differences in the fuel supply to the different type of injectors which they have been using or due to the improper alignment. Oven et al(20) in a similar situation, concluded that sample probe effects are most significant in the swirl recirculation downstream of the swirler. However, beyond 0.3 pipe diameter the probe disturbances are small, except in regions of rapid property variations.

At the present, there are no non-intrusive devices that can make these measurements. The laser CARS system has yet to be demonstrated for low level pollution gas concentration.

3.5 CENTRAL FUEL INJECTION TRAVERSE

3.5.1 Radial gas composition profiles

3.5.1.1 Comparison of internal flame structure of propane and natural gas

Two fuel were investigated, propane and natural gas, propane is gaseous fuel representative of vaporized kerosene fuel, and natural gas is the dominant current fuel for industrial gas turbines. The radial traverse were carried in five axial planes. They were at 10, 30, 50, 110, 210mm away from the vertical plane of the radial swirler. The radial gas composition traverse were carried out at 600K inlet air temperature at an equivalence ratio of approximately 0.42. This was the equivalence ratio at which the mean exhaust gas analysis showed the lowest NOx emissions with at least a 0.01% combustion inefficiency as can be seen for central fuel injection from Fig.3.11 and Fig.3.12.

The results of various combustor traverses are illustrated throughout Fig.3.13 - Fig.3.21. These show the radial variation for various axial directions equivalence ratio, air/fuel ratio, total NOx, combustion inefficiency,carbon monoxide, unburned hydrocarbons, ,oxygen, and flame temperatures respectively. Fig.3.13 shows the distribution of both fuels was more or less uniform in the core region after the 30mm axial position. At the near swirler 10mm position, the central fuel injector created a rich near stoichiometric zone in the shear layer region. This rich zone acted to stabilise the flame. However, the rich shear layer was rapidly mixing with the peak equivalence ratio reduced from 1.2 to 0.8 between 10 and 30mm and to 0.7 at 50mm, with complete near uniform mixing by 110mm. It is this rapid mixing that gives rise to the lower NOx emissions.

Since the same central radial fuel injector holes were used, the different fuel densities resulted in different fuel jet velocities for the same fuel mass flow. This may influence the local fuel and air mixing, although the fuel jet momentum was not a major part of the mixing process. In addition the low molecular weight and hence high diffusivity of natural gas mean that the fuel quickly disperses in the turbulent regions of the jet boundary where there is an active shear layer. The

initial fuel-air mixing processes affected the details of the flame structure at axial plane 10 and 30mm. However, in spite of these fuel injection momentum difference, the fuels behaived in a similar way.

The most significant feature of plane the 10mm was the peak in the equivalence ratio for the natural gas and propane which is exceeded the stoichiometric limit at radial position approximately equal to 0.3R by 30% and for the propane at approximately 0.2R radial position by 20%. At axial planes of 50 - 210mm the burnt-gas eddies downstream of reaction zone would be more uniform in composition which is due to how the fuel have been distributed throughout the reaction zone. As the flow moves through the combustor, the action of turbulence and molecular diffusion will change the distribution. At the 50mm axial plane, the equivalence ratio of the natural gas had a richer shear layer zone, but by 110mm axial position both distributions were almost completely uniform.

The CO and UHC emissions were low in the central core region, Fig.3.15 and Fig.3.16, this was the result of the increase in air fuel ratio, Fig.3.14 which resulted in the entrainment of larger concentrations of O2, Fig.3.21 . However, this consisted of fully burnt combustion products. The inefficiency near the swirler vertical plane, Fig.3.17 showed better combustion efficiency was exhibited by propane. both fuel promoted low combustion inefficiency of less than 0.1% at axial position 30mm. The main flame development was from the inner jet boundary shear layer into the outer recirculation region. Natural gas exhibited a higher combustion inefficiency near the wall region at axial planes of 110 and 210mm, which were due to the higher rate of emissions of CO and UHC. The highest temperatures promoted by the two fuels were in the core region.

Gas analysis based temperature profiles were the similar for both gaseous fuel. The main difference was the hotter core temperature for propane at the 10mm axial position where the temperature profile rose to above 1800K in the vicinity of swirler plane and showed values in excess of 1700K almost to the 210mm plane. The temperature at the centre line and near 0.2R were in excess of

2050K. This together with the flow and mixing visualization results in the previous chapter show that the influence of the radial swirler were stronger in the centre of the combustor due to the existance of the vortex core. Fig3.18 shows that by the 110mm position the temperature profiles were close to uniform steady profiles for both fuel types and the flame propagation was mainly complete.

The difference in temperature profiles were due to small variations in the mean equivalence ratio. The NOx levels at all axial planes position were relatively high for propane as shown in Fig.3.19. The higher NOx emissions for propane were well established at all radial positions and this difference was maintained through to the 210mm axial plane except for the 50mm axial position at 0.5R where natural gas exhibited higher NOx level than propane. The dominant mechanism for NOx generation thus appears to be by a prompt NOx mechanism, with only small thermal NOx contribution. A strong thermal contribution should have resulted in a strong axial variation of NOx emissions.

Good fuel and air mixing minimised the thermal NOx production, However, there are few location where the flame temperatures were sufficient to generate thermal NOx rapidly. The higher level of CO2 concentration in Fig.3.20 indicated that the reaction rate of formation of CO2 from CO for propane was faster than for natural gas and was completed at 210mm plane. It seems that the low molecular weight and hence high diffusivity of natural gas means that the fuel quickly dispersed in the turbulent region of the shear layer and hence resulted in low NOx formation. However, for both fuels the combustion was mixing controlled. NOx was only formed in the early part of the combustor which contained the radical rich turbulent flame reaction zone. The NOx was mainly NO , as reported by Appeleton et al(28). Further mixing over the remainder of the combustor did not increase the NOx level.

3.5.1.2 Effect of small equivalence ratio variation on species concentration

Changing the equivalence may put the whole system into a region where high NOx emission or other pollutants are emitted beyond the exited regulation limits. Myers and Lefebvre(36) noted that the flame speeds increase with the fuel/air ratio and attain their maximum value at a mixture strength close to stoichiometric. Fig.3.22 - Fig.3.31 illustrate the effects on species profiles concentration for a central injection propane system fuelled at two equivalence ratios of 0.37 and 0.42. They show radial traverse profiles at three different axial planes 50, 110, 210mm positions. The higher equivalence ratio seems to enhance the flame spread towards the wall region, Fig.3.22. That was due to the more effective penetration of the fuel jet to the jet boundary of the incoming flow from swirler that will give rise to the higher UHC, Fig.3.25 and lower CO emissions, Fig.3.24 near the centre core for the higher equivalence ratio mixture. This was accompanied by lower UHC with higher CO concentrations in the wall region and corresponding changes in the combustion inefficiency , Fig.3.26. A higher combustion inefficiency promoted by the lower equivalence ratio mixture occured in the near wall region. The gas analysis based temperature profiles Fig.3.27 were similar due to the small difference in local equivalence ratio. Major differences were only found at the 110mm axial position, and were an order of 300K. The NOx levels were influenced by the two equivalence ratio Fig.3.28, due to the differences in flame temperature. For 0.4 the core temperature at 110mm was above the high NOx generation temperature of 1800K, whereas at 0.37 the core was below this temperature. The differences in the NOx were quite large inspite of the small difference in the equivalence ratios.

3.5.1.3 Influence of large variation in equivalence ratio on species concentration

Figs.3.32 - Fig.3.33 demonstrate the effect of large variation on various species concentrations profiles for a system fuelled with natural gas at

equivalence ratios of 0.42 and 0.80 using central injection method. At the 0.8 equivalence ratio combustion excessive heat and radiation from the 140mm combustor which was beyond the limitation of the experimental rig, the radial traverse was limited to one plane only which was the 210mm axial plane. A 0.014 Mach number condition was used with a 600K air inlet temperature. A large effect on emissions was exhibited by the higher equivalence ratio especially at the centre core of the combustor where the CO level was 0.5% compared to the lower equivalence ratio flow of 25 ppm. The reason was the higher levels of equilibrium CO for the 0.8 mixture. The equivalence ratio profiles show that at both equivalence ratios fairly uniform mixing had occured by the 210mm position. The flame temperature was also fairly uniform but the NOx profile at 0.8 was strongly bi reach to the centre, where at the weak mixture it was uniform. This may be due to the greater residence time of the centre core at high temperature. A strong thermal NOx and hence residence time dependence would be expected at the 0.8 condition.

3.5.1.4 Influence of primary zone Mach number on species concentrations

The investigation were carried out on two Mach number 0.014 and 0.02 using central natural gas injection with an air inlet temperature of 600K. The traverse procedures were carried out at a fixed overall equivalence ratio of 0.42, and the results are shown in Fig.3.34 - Fig.3.42. Similar equivalence ratio profiles were exhibited by both Mach numbers Fig.3.34. However, difference were found at the 210mm axial position where higher equivalence ratio was found in the core. This produced a higher flame temperatures, Fig.3.39 in the centre which exceeded the temperature for the higher Mach number flow by approximately 100K. The reason for this temperature difference at 210mm may be a result of the lower pressure loss at the lower Mach number which gives slower mixing of the lean lower temperature outer flow with the core.

The NOx results in Fig.3.40 do not follow the flame temperature trends. There was a large difference in NOx between the two Mach number at all these

axial traverses and no dependency of the NOx level on these axial distance or residence time, as should occur for Zeldovich thermal NOx. In the core region there is a large decrease in NOx with axial distance at both Mach numbers. Only in the wall region did the NOX increase with distance. However, the temperatures here were below 1800K at all axial distances and thermal NOx is negligible in this temperature region. the increase in NOx in the wall region was due to turbulent mixing with the higher NOx core region. It is considered that the prompt NOx mechanism close to the swirler was the main contributer to the results. Thermal NOx will contribute in the initial shear layer combustion upstream of 50mm position, where rich zone greater than those in Fig.3.34 will exist; it is this thermal NOx which will be sensetive to the Mach number as the shear layer residence time will vary in proportion to the Mach number. Fig.3.40 shows that this initial difference in NOx is maintained throughout the combustor with thermal NOx generation in the burnt gases negligible.

3.5.1.5 Internal axial gas composition

The axial centre line gas composition traverse were carried out at 600K inlet air temperature at a constant equivalence ratio of 0.37 for propane using central fuel injection with a Mach number of 0.02. Also axial traverse were carried out for a central injection of natural gas at two different Mach numbers, 0.014 and 0.02, at constant equivalence ratio of 0.42. These were the equivalence ratio at which the mean exhaust gas analysis showed the lowest NOx emission with at least 0.01% combustion inefficiency, Fig.3.11 and Fig.3.12. Figures 3.43 - 3.51 illustrates the axial gas composition profiles at the centre of the 140mm combustor. By sampling gases only at the combustor centreline, it should be possible to assume that the sample is the same as would result from an adiabatic burner(29). In general the equivalence ratio Fig.3.43 and the gas analysis based temperature profiles Fig.3.48 were similar in in shapes. Figure 3.43 shown that the near swirler region was richer than the mean equivalence ratio, but not excessively rich even though central fuel injection was used.

Figures 3.45 - 3.47 shown that the core region was rapidly fully burnt by 10% of the axial distance(30mm). This was because it was a region of recirculated burnt gases. The main combustion was in the shear layer and the outer swirling flow. The decrease in equivalence ratio, temperature and NOx with distance was mainly due to turbulent mixing with this outer region. Fig.3.49 illustrates clearly that there was little burnt gas thermal NOx generation, even for the low Mach number natural gas results when the temperature was above 1800K for the first half of the combustor.4.

Some of the NOx emissions in Fig.3.49 was generated near the swirler outlet and were due to a contribution of thermal NOx as well as prompt NOx mechanism as discussed above. The 1800K flame temperature for rapid thermal NOx generation was exceeded at the swirler outlet. Good fuel and air mixing minimised the thermal NOx contribution. The NOx emission level promoted at a Mach number of 0.02 by burning propane were approximately double that by burning natural gas. The lower Mach number natural gas flame produces higher NOx emissions and that was due to the longer shear layer residence time as discussed a bove. The highest NOx level emitted by propane and natural gas flame at 0.02 and 0.014 Mach number were 32.5, 25.7 and 33ppm respectively Fig.3.49 and the lowest being at the combustor exit plane 21, 13 and 19.5ppm respectively. These are corresponding to 13.8, 7.6 and 10.6ppm NOx corrected to 15% oxygen and standard day humidity Fig.3.2B.

3.6 PASSAGES FUEL INJECTION

3.6.1 Introduction

Passage fuel injection gave partial fuel and air mixing in the short curved passages in between the radial swirler vanes as shown in Fig.3.52. The objective was to quantify the expected reduction in stability and NOx emissions that this improved mixing would entail. A Mach number of 0.02 was used as the higher pressure loss would give greater turbulent mixing and lower NOx emissions as well as better liquid fuel atomisation in the radial vane passages. The ratio of the primary zone Mach number, 0.02 to the reference Mach number ,0.047, gave the simulated proportion of the total combustor air that was passed through the swirler as 43%. The radial swirler used had a pressure loss of 4.2% at the 0.02 test Mach number, which is a typical conventional combustor pressure loss.

3.6.2 Internal radial traverse composition profiles

The radial gas composition traverses were carried out at a 600K inlet temperature at an equivalence ratio of 0.43. This was the equivalence ratio at which the mean exhaust gas analysis showed the lowest NOx emissions with at least a 0.1% combustion inefficiency as shown in Fig.3.53 and Fig.3.54. Detailed gas composition data was obtained at six axial position as shown in Fig.3.55 - 3.63. Data for Gasoil was not obtained in the near burner region but was determine for propane and Kerosene. Fig.3.55 shows that at the 10mm position the propane fuel distribution was much more uniform than for Kerosene, which had a richer core region probably due to the transport of larger droplets into the core due the radial swirler passage air momentum. Propane was better mixed inside the passages giving the more uniform distribution. However, by the 30mm axial position the Kerosene was more uniformly distributed in the core region with only the outer recirculation zone being relatively weak. At the 110mm plane the Kerosene distribution was almost complete. The equivalence ratio profile for Gasoil at the 50mm axial position had a richer shear layer zone but it was uniformly distributed by 110mm axial plane. At the 200 and 300mm axial planes

the equivalence ratio profiles were very uniform for all three fuels.

The CO and UHC emissions shown in Figs.3.53 and 3.58, were low in the central core region even at the near swirler 10mm axial position. The core region is thus fully burnt recirculation gases, as also found with central fuel injection. The combustion inefficiency in this region for Kerosene was less than 10% at the 10mm position and less than 2% at the 30mm position, and better results were found for propane. The main flame development was from the shear layer to outer recirculation region.This outer recirculation zone was high in UHC, as shown in Fig.3.58 at the 10mm position and hence there was a high combustion inefficiency Fig.3.59, for both propane and Kerosene. Propane combustion inefficiencies were higher than for Kerosene in the wall region. This was also the case at the 30mm plane with inefficiencies in the wall region of 60% and 30% for propane and Kerosene respectively. This lower combustion inefficiency for Kerosene gave slightly higher temperatures in the wall region than for Propane, in spite of the much leaner local composition as shown in Fig.3.60. The combustion inefficiency at the 200 and 300mm positions were below 0.3% at all radial position for all three fuels. However, there was still evidence of the radial propagation of the flame with the outer regions with the worst inefficiency.

The gas analysis based temperature profiles in Fig.3.60 show that the central core region was at high temperature due to the high combustion efficiency. The wall region was at a relatively low temperature for both fuels up to the 30mm position. Kerosene and propane had very similar temperature profiles with the main difference being the hotter core temperature for kerosene at the 10mm position, due to locally richer mixtures, Fig.3.60. Also at the 110mm position the temperature profiles was close to uniform for all three fuels and flame propagation was predominantly complete. The differences in temperature were due to small differences in the mean equivalence ratio. At 200 and 300mm axial plane the temperature was very uniform for all three fuels.

The NOx levels at the near swirler position was relatively high as shown in

Fig.3.61 . At the 30mm axial plane position the higher NOx emissions of kerosene were well established at all radial positions and this differences was maintained through to the 300mm axial plane. The origin of the higher NOx emissions for kerosene can clearly be seen to be the higher temperature richer core region at 10mm position. The NOx level for kerosene was approximately 15ppm compared with 9ppm in the centre at the 300mm position. Even in the wall region the 3ppm NOx level at the 10mm position only increase to 8ppm at the 300mm position.. The dominant mechanism for NOx generation thus appears to be by a prompt NOx mechanism with only a small thermal NOx contribution. A strong thermal NOx contribution should have resulted in a strong axial variation of NOx. The good mixing of fuel and air minimised the thermal NOx production as there were few locations where the flame temperatures were sufficient to generate thermal NOx rapidly. Fig.3.60 shows that 1800K was not exceeded for propane at any radial positions. This is the temperature beyond which thermal NOx generation becomes rapid. Figure 3.61 shows that at the 50mm position the gasoil NOx emissions were considerably higher than for kerosene, but with a similar radial profile shape. However, the NOx level for gasoil at the 300mm axial plane was less than at the 50mm position in the central region and less than at most radial positions at the 110mm position. Thus thermal NOx was not the cause of the higher NOx emissions for gasoil. The cause of the higher NOx was likely to be due to the prompt NOx mechanism, but in the absence of data upstream of 50mm axial plane the presence of locally richer zones than for kerosene cannot be excluded. At the 50mm axial plane, there was a 35ppm peak in the gasoil NOx profile in the shear layer region, which was the richest zone. This shear layer zone may have had higher NOx levels due to richer local mixtures upstream of 50mm, as indicated by the leaner weak extinction results for gasoil at 600K which will discussed later. There may have been a fuel NOx contribution for gasoil and this would also give rise to early production of NOx. William et al(35) have shown that gasoil contains lower level fuel nitrogen (40 ppm.).

AT axial plane 200 and 300mm, the NOx emissions were very uniform

reflecting the uniformity of the equivalence ratio and flame temperature profiles. These uniform NOx emissions were identical to the mean NOx emissions at 0.43 equivalence ratio for all three fuels, Fig.3.53. The origin of the relatively large differences in NOx emissions between the three fuels was shown by these traverse results to be in the near burner swirling shear layer region and was not due to differences in thermal NOx generation.

3.7 INFLUENCE OF SWIRL GENERATION METHOD ON SPECIES CONCENTRATION

The primary goal of the present comparison is to assess how the fuel-air mixing effected by generating swirl with two different means of swirl generation. Radial and axial swirlers were compared at the present work. Both swirler had central fuel injection fuelled with propane of the same purity and approximatly the same expansion ratio (D/d) of about 2.0 and the same swirl angle 45 degrees, this would allow a relatively direct comparison of internal flame structure for both swirlers. Fig.3.64 and 3.65 show the mean gas analysis results for the NOx corrected to 15% oxygen variations with combustion inefficiency and mean equivalence ratio for both swirlers. This is an illustration of the general characteristics the radial swirler is slightly better than the axial swirler.

The effects of the differences in swirler design on the radial profiles are shown in Figs.3.66 - 3.75. These show the radial gas analysis profiles for the SW6 axial swirler compared with those for the type B radial swirler, both with central fuel injection at a Mach number of approximately 0.02 in the 140mm combustor. The traverses were carried out at an equivalence ratio of approximately 0.42. The equivalence ratio at three axial planes are shown in Fig.3.66, which shows that both swirler had lean equivalence ratios in the wall region. This indicated that the fuel had not yet fully mixed into the wall region. These was a peak equivalence ratio at 0.8R for both swirlers. The axial swirler had a richer peak than the radial swirler indicating that better mixing had taken place in later flow field than for the former at the 50mm position. At the 110 and 210mm axial plane position the fuel

distribution was also more uniform for the radial than the axial swirler.

Both concentrations for both swirlers the CO and UHC profiles were similar at all axial position, were low at the centre and high at the wall region. A low combustion inefficiency existed all the way through the combustor centre line due the existence of the same recirculation vortex core features for both swirlers. The Flame temperature profiles in Fig.3.71 were similar to the equivalence ratio profiles. The highest temperature was exhibited by the axial swirler at plane 50mm away from the swirler due to the richer mixture at this position. The temperature profiles were more uniform for the radial swirler at axial planes 110 and 210mm indicated better mixing. The temperature profile for the radial swirler at the 210mm position was uniform indicating that the flame propagation was predominantly complete. as shown in Fig.3.20 by an inefficiency less than 0.2% at all axial positions. However, the flame downstream of the axial swirler spread more slowly than for the radial swirler. This is consistent with experimental observation Smith et al(34) who reported lower wall temperatures with axial swirlers in the near burner region.

The NOx levels in Fig.3.72 for the axial swirler were relatively higher than that for the radial swirler especially at the centre line of the combustor for the three axial planes. In the wall region the NOx emission exhibited by both swirler were similar except at the 210mm plane, where the NOx level differ by an order of 7ppm. The difference in NOx emission between the two swirlers at 50, 110, 210mm axial planes where 37, 13, 17ppm respectively. These correspond to 15, 6, 9ppm NOx corrected to 15% oxygen and standard day humidity, as can be seen from Fig.3.73. The good mixing exhibited by the radial flow swirler in the near swirler region and at the 50mm axial plane was for the lower NOx than for axial swirler flow promoted. However, chemical kinetic mechanisms can not be rulled out in axial swirler case especially at 210mm plane, perhaps that is why the UHC had two peaks Fig.3.69 and the level of CO increased Fig.3.68. This is supported by the work reported by Bromly et al(30) The results obtained showed that the presence of the combustible agent strongly facilitated the oxidation of NO

to NO2. It was found that the hydrocarbons had a greater effect than hydrogen or carbon monoxide. It was also observed that the presence of NOx sensitised the hydrocarbon oxidation. Sano(31) has shown by simulation that NO2 formation in a mixing region would be enhanced by the presence of unburned hydrocarbons. This conclusion is supported by the experimental findings of Jaasma and Borman(32).

3.8 CONCLUSIONS

1- Most of the mixing between fuel and air takes place in the shear layer between the jet boundary of the swirling flow and the reverse flow zone. It is also here where ignition occurs and the flame is stabilized. Therefore, fuel injection should always take place into this region.

2- The only significant difference between propane and natural gas operation was in the NOx emissions, where natural gas had approximately half the NOx emissions of propane for the same test condition.

3- Radial vane swirlers with fuel injection in the vane passages improved the fuel and air mixing compared to central fuel injection. There was sufficient unmixedness in the stabilising swirling shear layer to give a considerable extension of the premixed stability limits, although inferior to those for central injection as will be discussed in chapter five.

4- Most of the differences of the influence of fuel type originated in the near swirler region. Thermal NOx was not a major contributor to the overall NOx emissions or to the differences between the fuel type used for central and passage injection.

5- Noticable improvement in performance and NOx emission of the radial over that of the axial swirler were due to the immediate contact of fuel with the turbulent swirled air as it leaves the central fuel injector. In the case of the axial swirler the fuel traveled some distance before coming into contact with the turbulent airstream.

6- The internal gas composition measurements showed that for the central and passages injection fuel injection method, the fuel and air mixing was good quite close to the swirler and this was the key to the low NOx emissions. The maximum local equivalence ratio for passage injection was 0.75 for mean of 0.43 and for central injection was approximately 1.2 for a mean of 0.42 and this occured in the swirler shear layer and was responsible for the enhanced stability.

CHAPTER THREE

REFERENCES

3-1 Tuttle J. H.,Altenkirch R. A. and Mellor A. M.: Emissions from and within an Allison J-33 combustor II:the effect of inlet temperature. Combustion science and technology, vol.7, p.125, 1973.

3-2 Tuttle J. H., Shisler R. A., Bilger R. W. and Mellor A. M.: Emissions from Aircraft fuel nozzle flames. Report No.PURDU-CL-75-04, PURDU university, July 1975.

3-3 Vranos A. and Taback E. F.: Combustion product distributions in the primary zone of a gas turbine combustor, combustion and flame, vol.26,p.129,1976.

3-4 Jones W. P., Clifford W. C., Priddin C.H and De Chair R.: A comparison between predicted and measured species concentrations and velocities in a research combustor. AGARD-CP-229, 1977.

3-5 Noyce J. R., Sheppard C. G. W. and Yamba F. D.: Measurements of mixing and species concentration within a gas turbine type combustor. Combustion science and technology,vol.25,pp.209-217, 1981.

3-6 Toral H. and Whitelaw J. H.: Velocity and scalar characteristics of the isothermal and combusting flows in a combustor sector rig. Combustion and flame, vol45, pp.251-271, 1982.

3-7 Nakamura S., Kawaguchi O., Sato G. T.: Study on the combustion in the primary region of a gas turbine-type continuous combustion chamber (the effect of secondary air on primary combustion), 1983.

3-8 Jones W. P. and Toral H.: Temperature and composition measurements in a research gas turbine combustion chamber, combustion science and technology, vol.31, pp.249-275, 1983.

3-9 El Banhawy Y. H. and Whitelaw J. H.: Experimental study of the interaction between a fuel spray and surrounding combustion air. Combustion and flame, vol.42, p.253, 1981.

3-10 Hori M.: Experimental study of Nitrogen Dioxide formation in combustion systems. 21st symposium (international) on combustion, the combustion institute, pp.1181-1188, 1986.

3-11 Heitor M.V. and Whitelaw J. H.: Velocity, temperature and species characteristics of the flow in gas-turbine combustor. Combustion and flame, vol.64, pp.1-32, 1986.

3-12 Bicen A.F., Senda M. and Whitelaw J.H.: Scalar characteristics of combustion flow in a model annular combustor. ASME paper No. 88-GT-14, 1988.

3-13 Takagi T. and Okamoto T.: Characteristics of combustion and pollutant formation in swirling flames. Combustion and flame, vol.43, pp.69-79, 1981.

3-14 BS1042: Methods for the measurement of fluid flow in pipes. British standard 1042, part1, 1964.

3-15 Lister D.H. and Wedlock M.I.: Measurements of emissions variability of a large turbofan Aero-engine. ASME paper No.78-GT-75, 1978.

3-16 EPA: Control of air pollution from Aircraft and Aircraft engine Environmental Protection Agency, Emission standards and test procedures for Aircraft, federal register, vol.38, No.136, partII, 1979.

3-17 EPA: Standard of performance for new stationary sources; gas turbines. Environmental Protection Agency, partII, 1979.

3-18 Mularz E.J., Wear J.D. and Verbulecz P.W.: Pollutant emissions from single swirl can combustor models at parametric test conditions. NASA TMX-3167, 1976.

3-19 Johnson G.M. and Smith M.Y.: Emissions of NO2 from a large gas turbine, power station, combustion science and technology, vol.19, pp.67-70, 1978.

3-20 Oven M.J.,Gouldin F.C. and MacClean W.J.: Temperature and species measurements in a swirl stabilized combustor. 17th Symposium (international) on combustion, p.363, The combustion institute, 1979.

3-21 Clark J.A. and Mellor A.M.: Probe effects in gas turbine combustor emission measurements. ASME paper 80-GT-71, 1981.

3-22 Kramlieh J.C. and Malte P.C.: Modeling and measurements of sample probe effects pollutant gases drawn from flame zones. Combustion science and technology, vol.18,pp91-104, 1978.

3-23 Malte P.C. and Kramlich J.C.: Further observations of the effect or sample probes on pollutant gases drawn from flame zones. Combustion science and technology, vol.22, pp.263-269, 1980.

3-24 Allen J.D.: Probe sampling of oxides of nitrogen from flames Combustion and flame, vol.24, p.133, 1975.

3-25 Kyukuo D., Sawada T. and Nistu A.: pollutant emission levels during transient operations of a small gas turbine. Combustion science and technology, vol.24, p.43, 1980.

3-26 Andrews G. E. and Kowkabi M.: Gas sampling probe influence on composition traverses through a swirling flow simulated gas turbine primary zone. NATO, advanced study institute on instrumentation for combustion and flow in engines,paper9,16pp, Ed. D.F.G. Durao, Institute of superior technico, Vimeiro,Portugal, 1987.

3-27 Joslin C. L.: The potential of methane as a fuel for advanced Aircraft. Aviation and Space: Progress and Prospects. ASME, pp.351-355, 1968.

3-28 Appleton J. P. and Heywood J. B.: The effects of imperfect fuel-air mixing in a burner on NO formation from nitrogen in the air and the fuel. 14th Symposium (International),The combustion institute, pp.777-786, 1975.

3-29 Anderson D.: Effects of equivalence ratio and dwell time on exhaust emissions from an experimental premixing prevaporizing burner. ASME paper 75-GT-69, 1975.

3-30 Bromly J.H., Barnes F.J. and Little L.H.: The effect of low levels of CO, H2 and hydrocarbons on NO2/NO ratios in heated gases. Journal of the institute of energy,pp.89-97, June 1988.

3-31 Sano T.: NO2 formation in the mixing region of hot burned gas with cool air-effect of surrounding air. Combustion science and technology,

43,pp.259-269, 1985.

3-32 Jaasma D. and Borman G.: Peculiarities associated with the measurement of oxides of nitrogen produced by diffusion flames. Combustion science and technology, 23,pp.83-88, 1980.

3-33 Wilhelmi J.: Axisymmetric swirl stabilized combustion. Ph.D. Thesis, Chemical eng. and chemical tech. dept., University of London, July 1984.

3-34 Smith K.O., Kurzynske F.R. and Angello L.C.: Experimental evaluation of fuel injection configurations for a lean-premixed low NOx gas turbine combustor. ASME paper 87-GT-141, 1987.

3-35 Williams P.T., Bratle K.D. and Andrews G.E.: The relation between polycyclic aromatic compounds in diesel fuels and exhaust particulates. Fuel,vol.65, pp.1150-1158, 1986.

3-36 Myers G.D. and Lefebvre A.H.: Flame propagation in heterogeneous mixtures of fuel drops and air. Combustion and Flame, vol.66, pp.193-210, 1986.

FIGURES

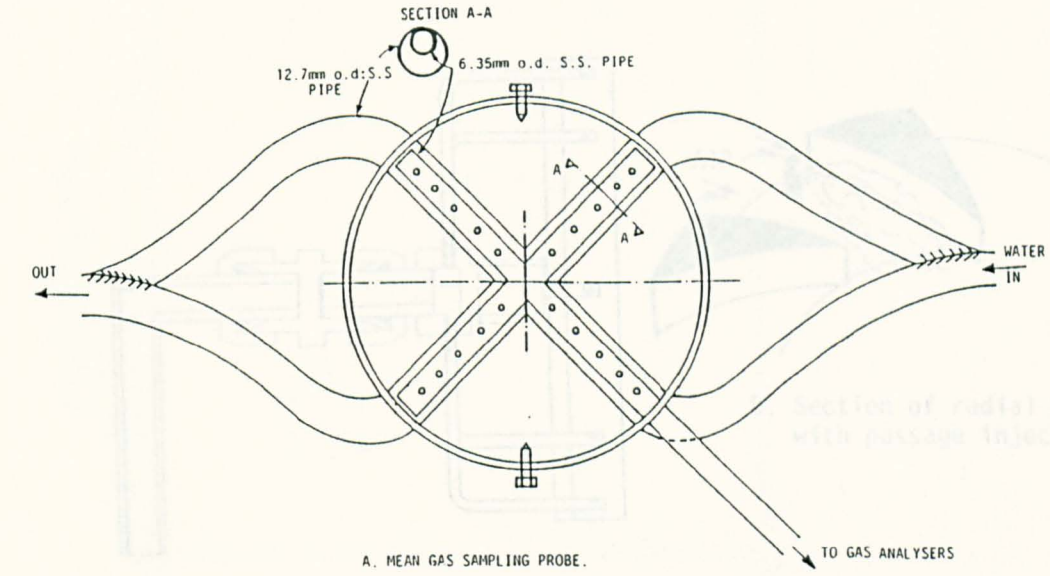

A. MEAN GAS SAMPLING PROBE.

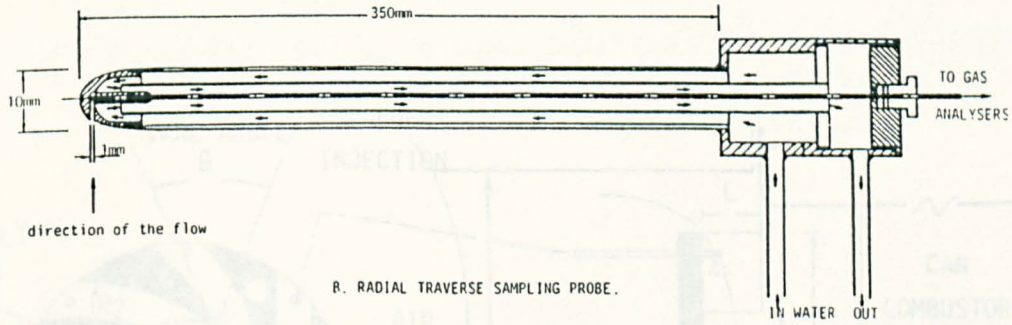

B. RADIAL TRAVERSE SAMPLING PROBE.

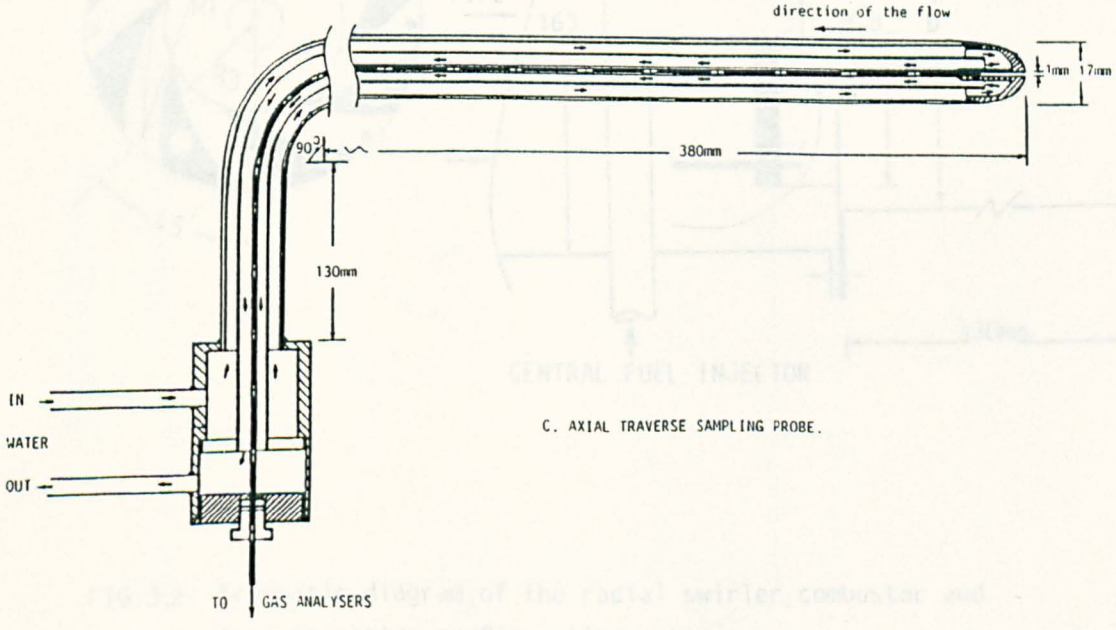

C. AXIAL TRAVERSE SAMPLING PROBE.

FIG. 3.1 Schematic diagram of the sampling probe used in the present work.

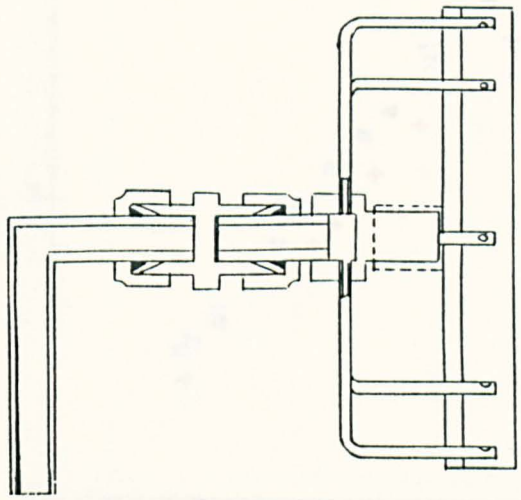

A. Passages fuel injector

B. Section of radial swirler with passage injection.

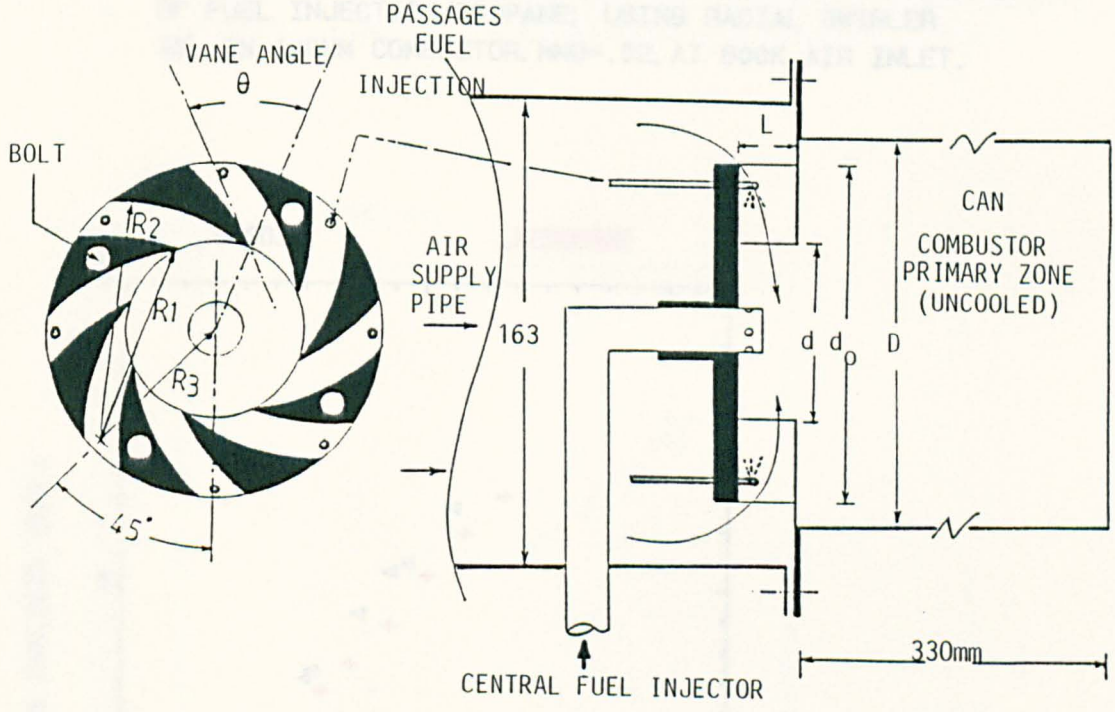

FIG.3.2 Schematic diagram of the radial swirler combustor and fuel injection configuration.

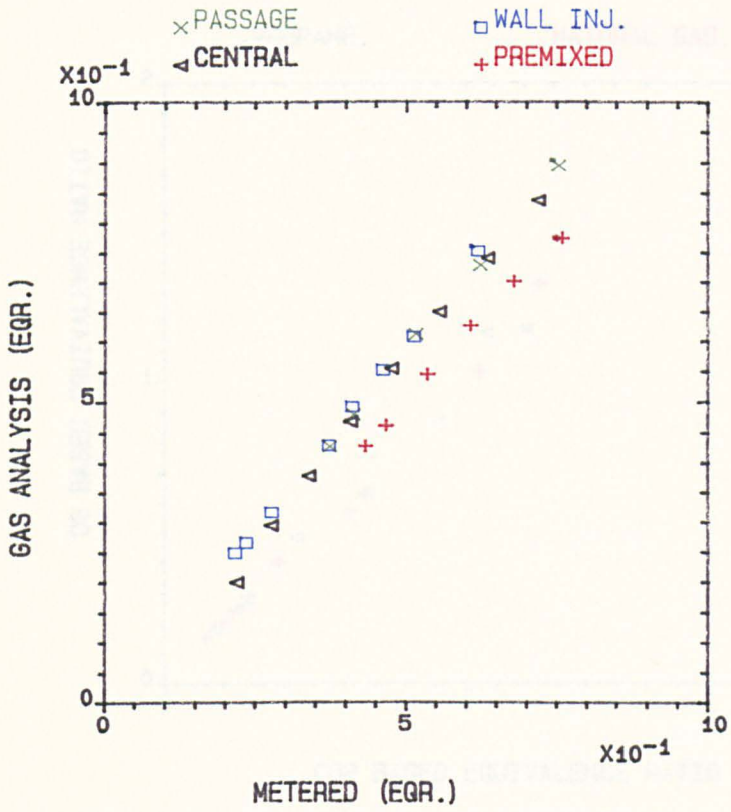

FIG.3.3 METERED EQR. V. GAS ANALYSIS EQR. FOR DIFFERENT METHOD OF FUEL INJECTION/PROPANE; USING RADIAL SWIRLER (B) IN 140MM COMBUSTOR, MNO=.02, AT 600K AIR INLET.

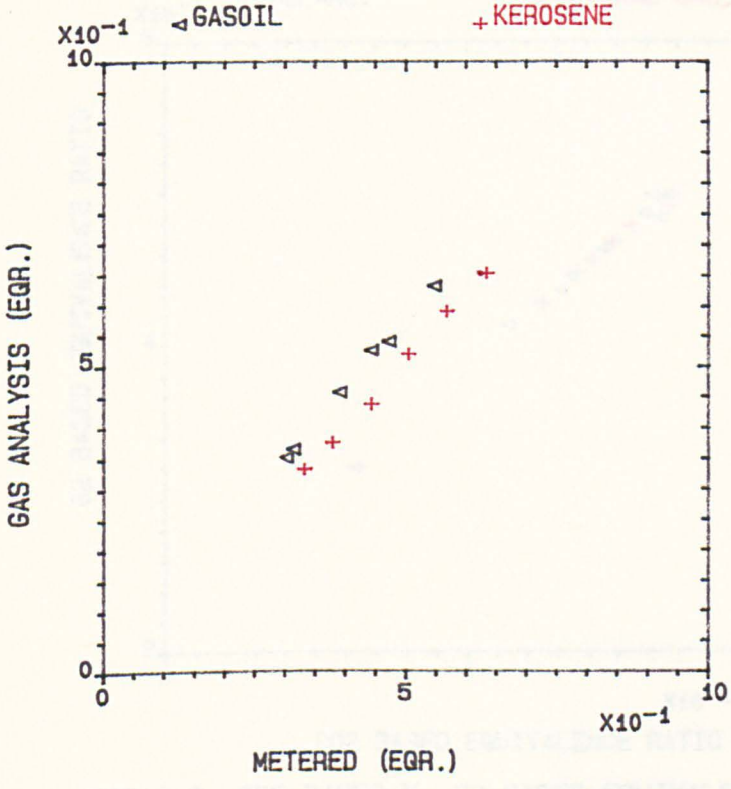

FIG.3.4 METERED EQR. V. GAS ANALYSIS EQR. FOR PASSAGES INJECTION GASOIL & KEROSENE USING RADIAL SWIRLER (B) IN 140MM COMBUSTOR, MNO=.02, AT 600K AIR INLET.

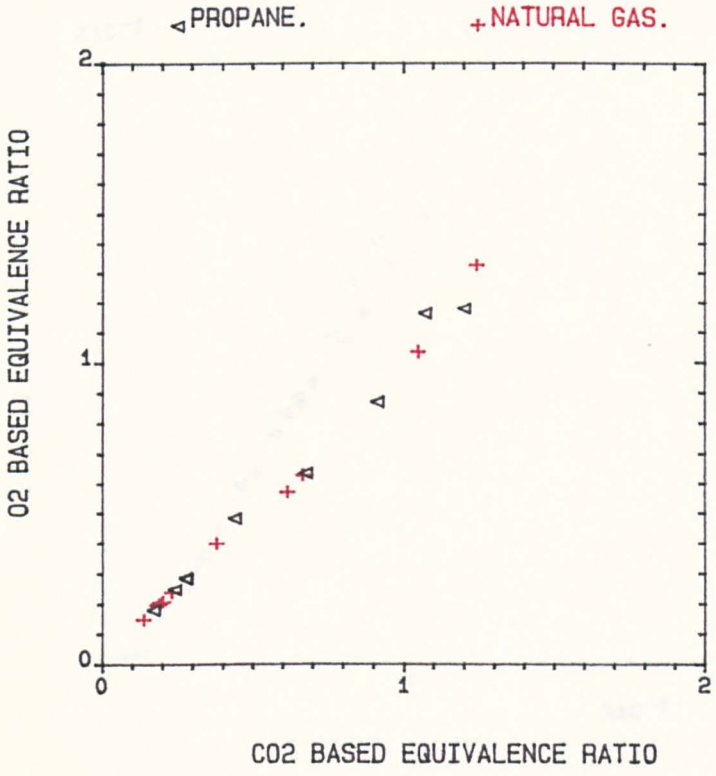

FIG.3.5 CO2 BASED V. O2 BASED EQUIVALENCE RATIO FOR PROPANE & NATURAL GAS CENTRAL INJECTION AT (X=10mm) AXIAL PLANE , MNO=.02, AT 600K AIR INLET.

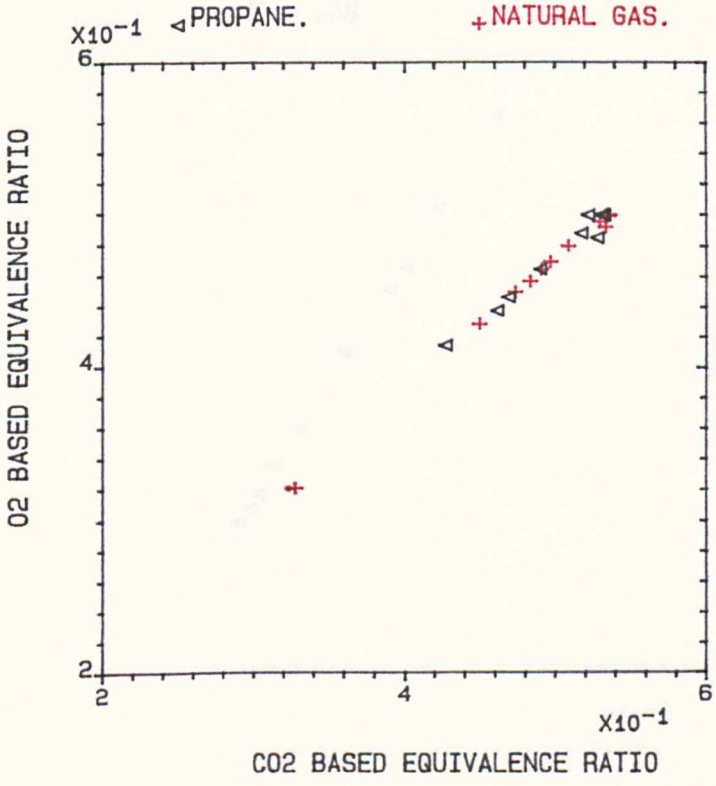

FIG.3.6 CO2 BASED V. O2 BASED EQUIVALENCE RATIO FOR PROPANE & NATURAL GAS CENTRAL INJECTION AT (X=110mm) AXIAL PLANE, MNO=.02, AT 600K AIR INLET.

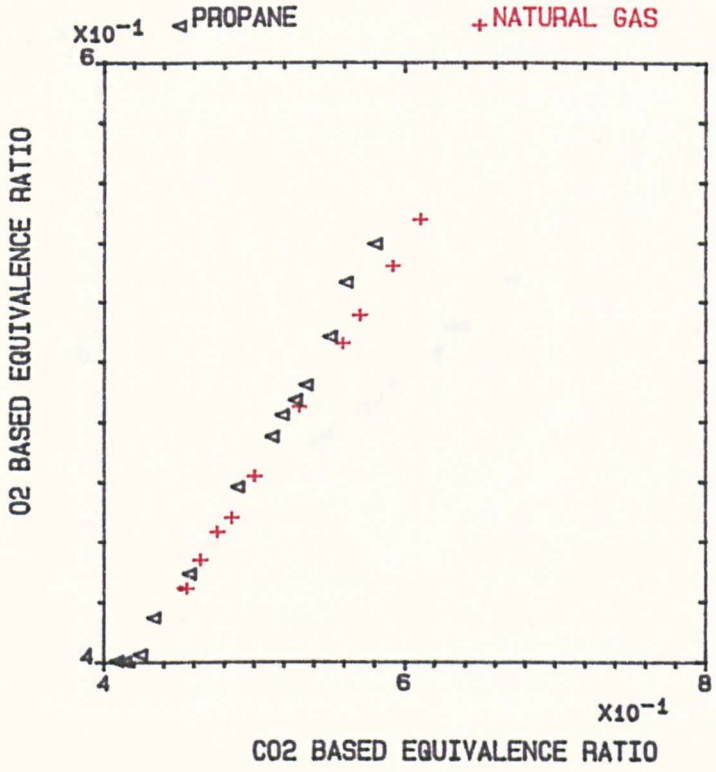

FIG.3.7 CO2 BASED V. O2 BASED EQUIVALENCE RATIO FOR PROPANE (EQR. 0.37) & NATURAL GAS (EQR. 0.42) AT (R=0.0) CENTRAL INJECTION, MNO=0.02, AT 600K INLET.

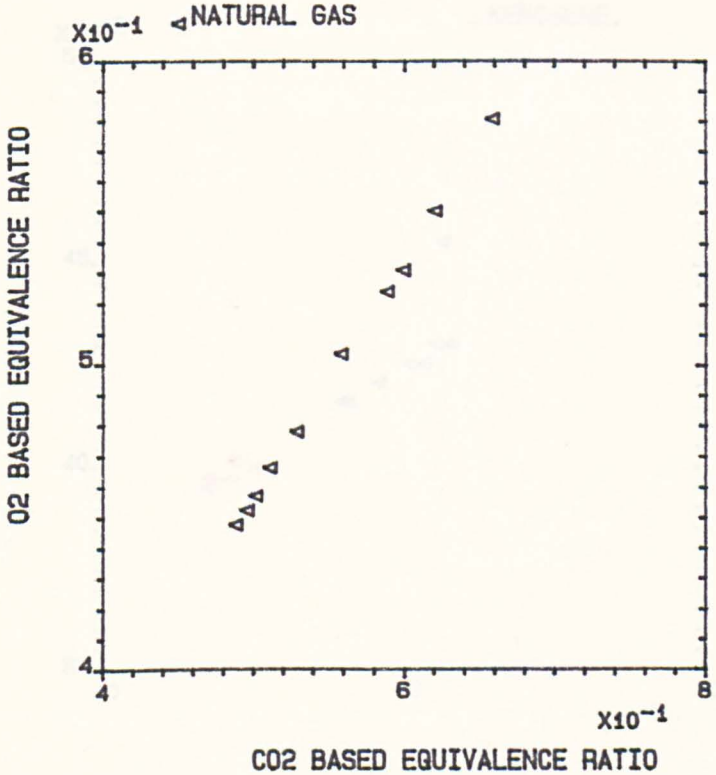

FIG.3.8 CO2 BASED V. O2 BASED EQUIVALENCE RATIO FOR NATURAL GAS (EQR. 0.42) CENTRAL INJECTION AT (R=0.0) MNO=0.014, AT 600 INLET.

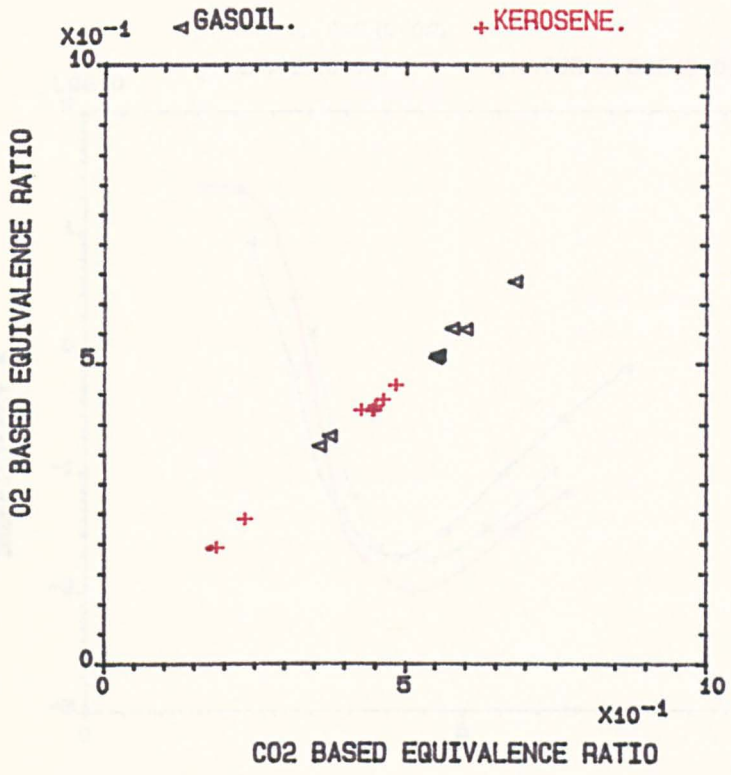

FIG.3.9 CO2 BASED V. O2 BASED EQUIVALENCE RATIO FOR GASOIL & KEROSENE PASSAGES INJECTION AT (X=50mm) AXIAL PLANE , MNO=.02, AT 600K AIR INLET.

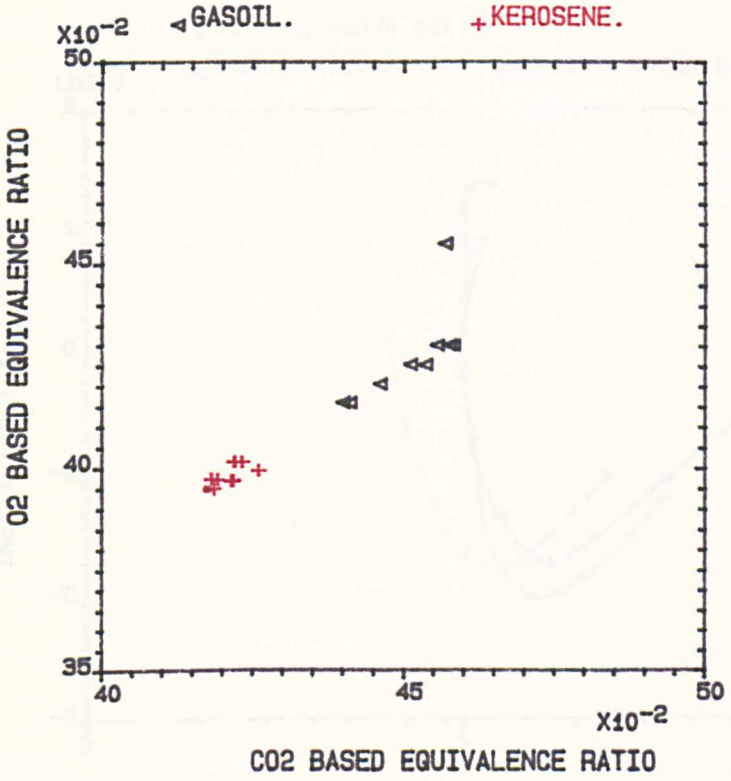

FIG.3.10 CO2 BASED V. O2 BASED EQUIVALENCE RATIO FOR GASOIL & KEROSENE PASSAGES INJECTION AT (X=300mm) AXIAL PLANE, MNO=.02, AT 600K AIR INLET.

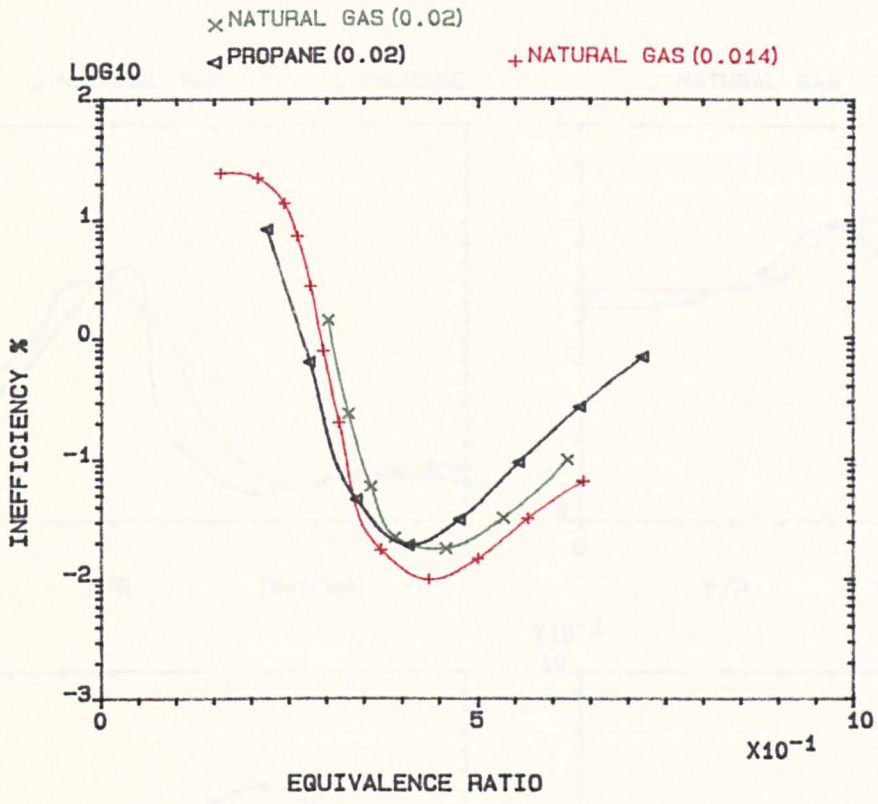

FIG.3.11 COMBUSTION INEFFICIENCY AS A FUNCTION OF EQUIVALENCE RATIO, FOR RADIAL SWIRLER (B) IN 140mm COMBUSTOR USING CENTRAL FUEL INJECTION NG & P FOR TIN=600K.

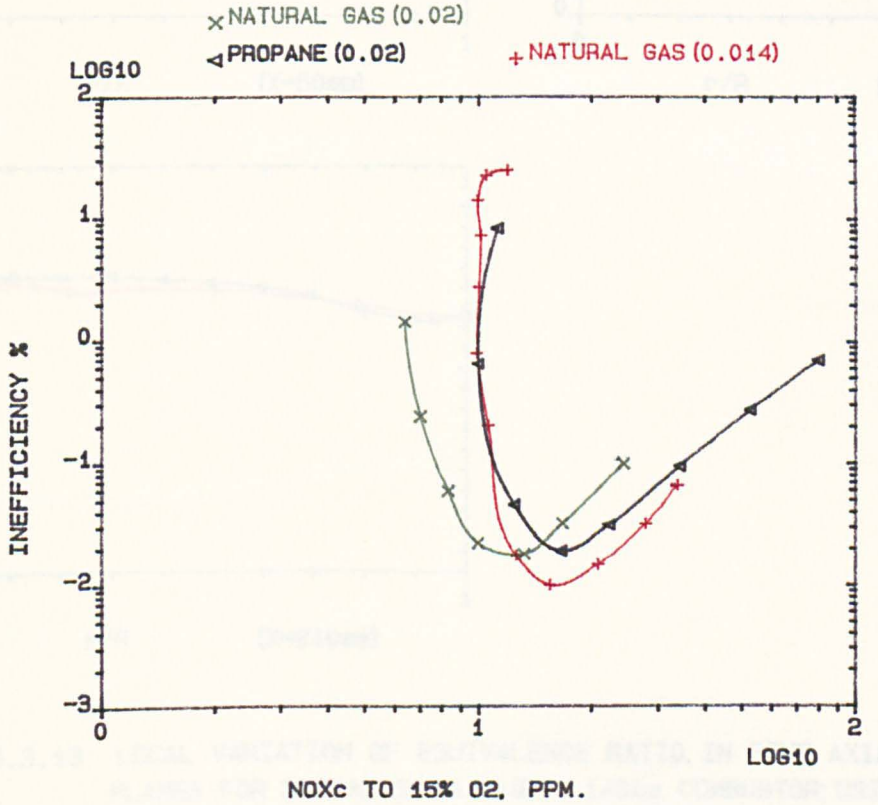

FIG.3.12 VARIATION OF COMBUSTION INEFFICIENCY WITH NOX CORRECTED TO 15% OXYGEN, RADIAL SWIRLER (B) IN 140mm COMBUSTOR USING CENTRAL FUEL INJECTION; NG & P FOR TIN=600 K.

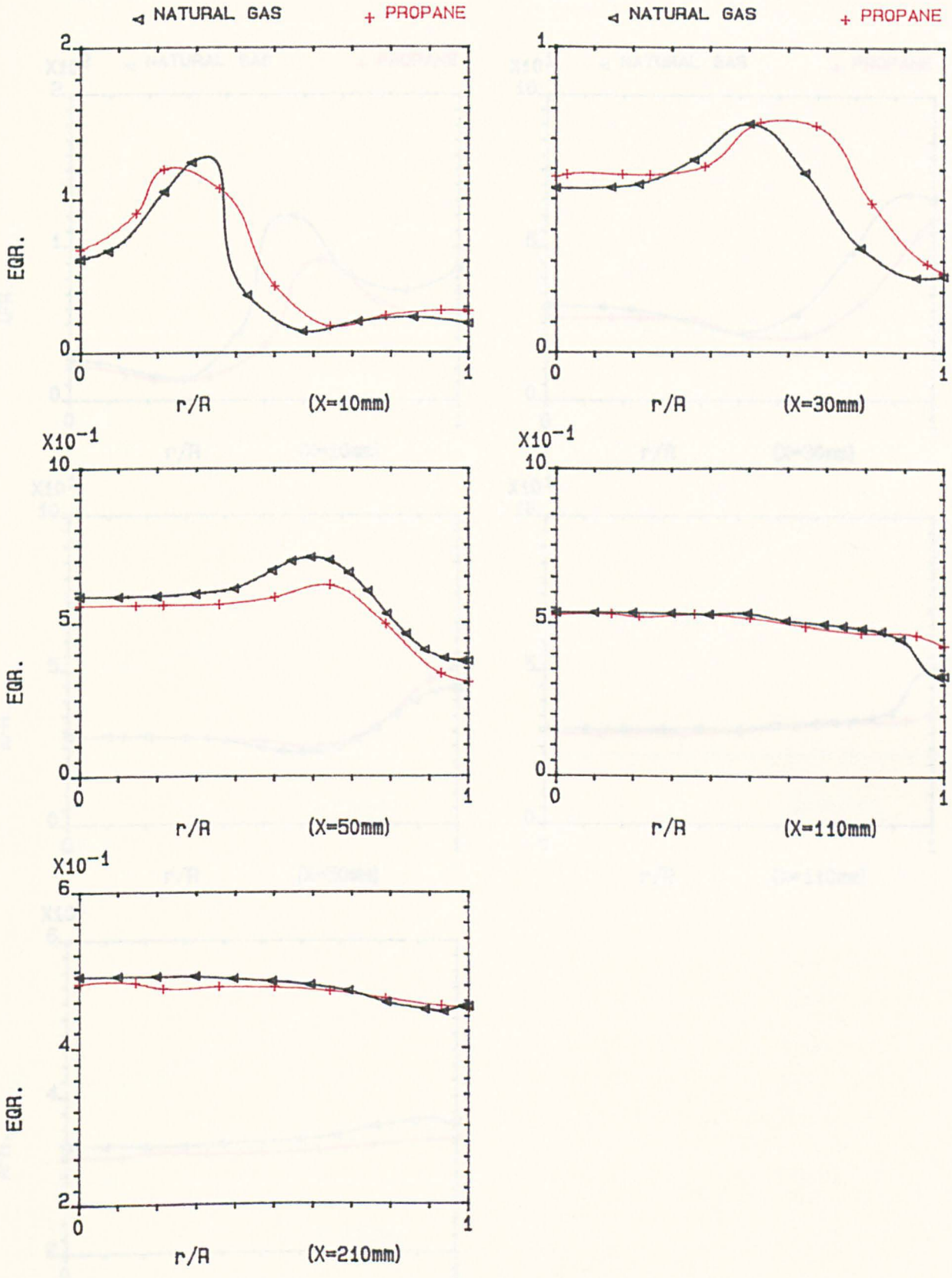

FIG.3.13 LOCAL VARIATION OF EQUIVALENCE RATIO, IN FIVE AXIAL PLANES FOR RADIAL SWIRLER (B); 140mm COMBUSTOR; USING CENTRAL INJECTION. NATURAL GAS & PROPANE. TIN=600K.

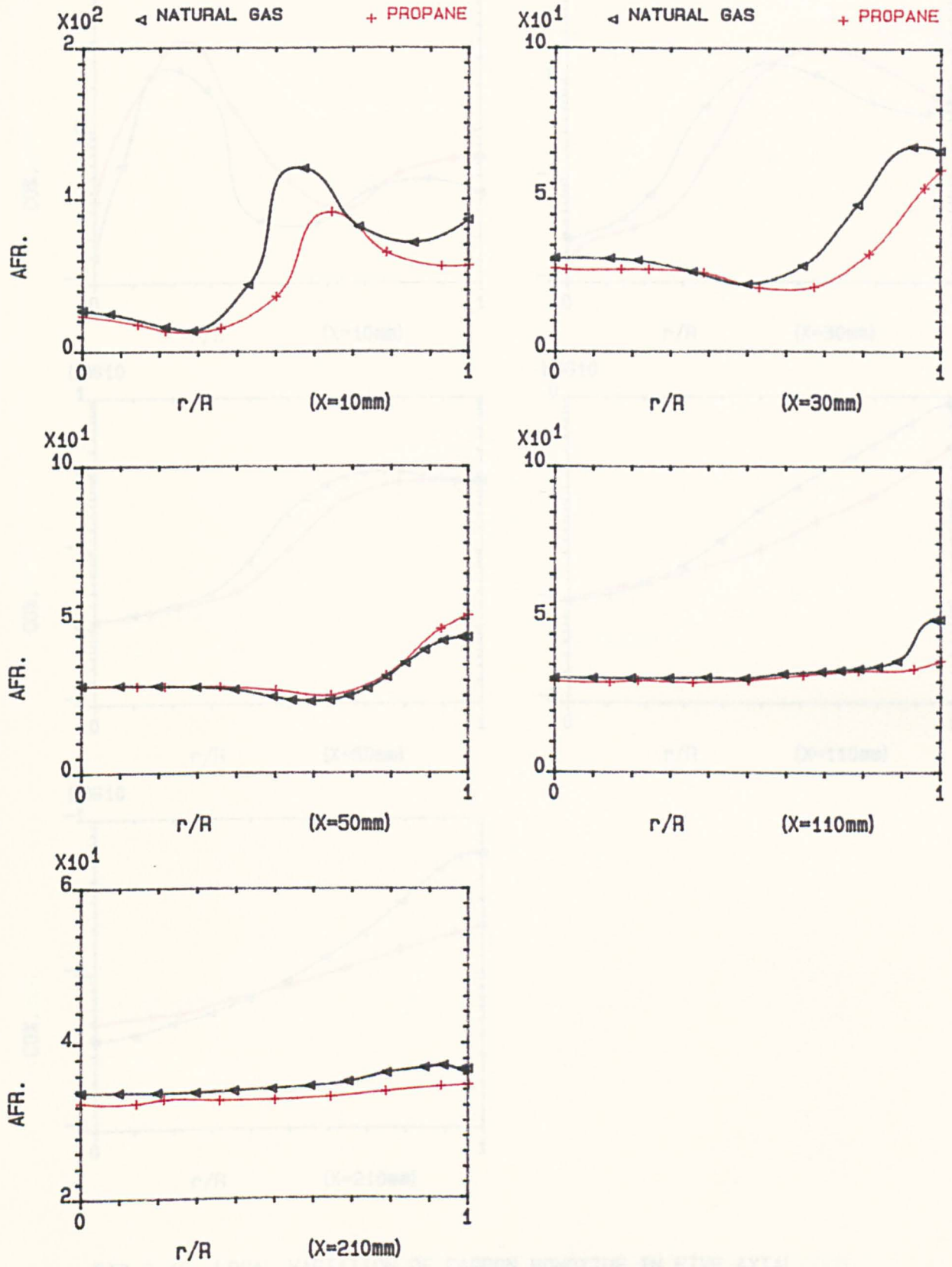

FIG.3.14 LOCAL VARIATION OF AIR/FUAL RATIO, IN FIVE AXIAL PLANES FOR RADIAL SWIRLER (B); 140mm COMBUSTOR; USING CENTRAL INJECTION, NATURAL GAS & PROPANE, TIN=600K.

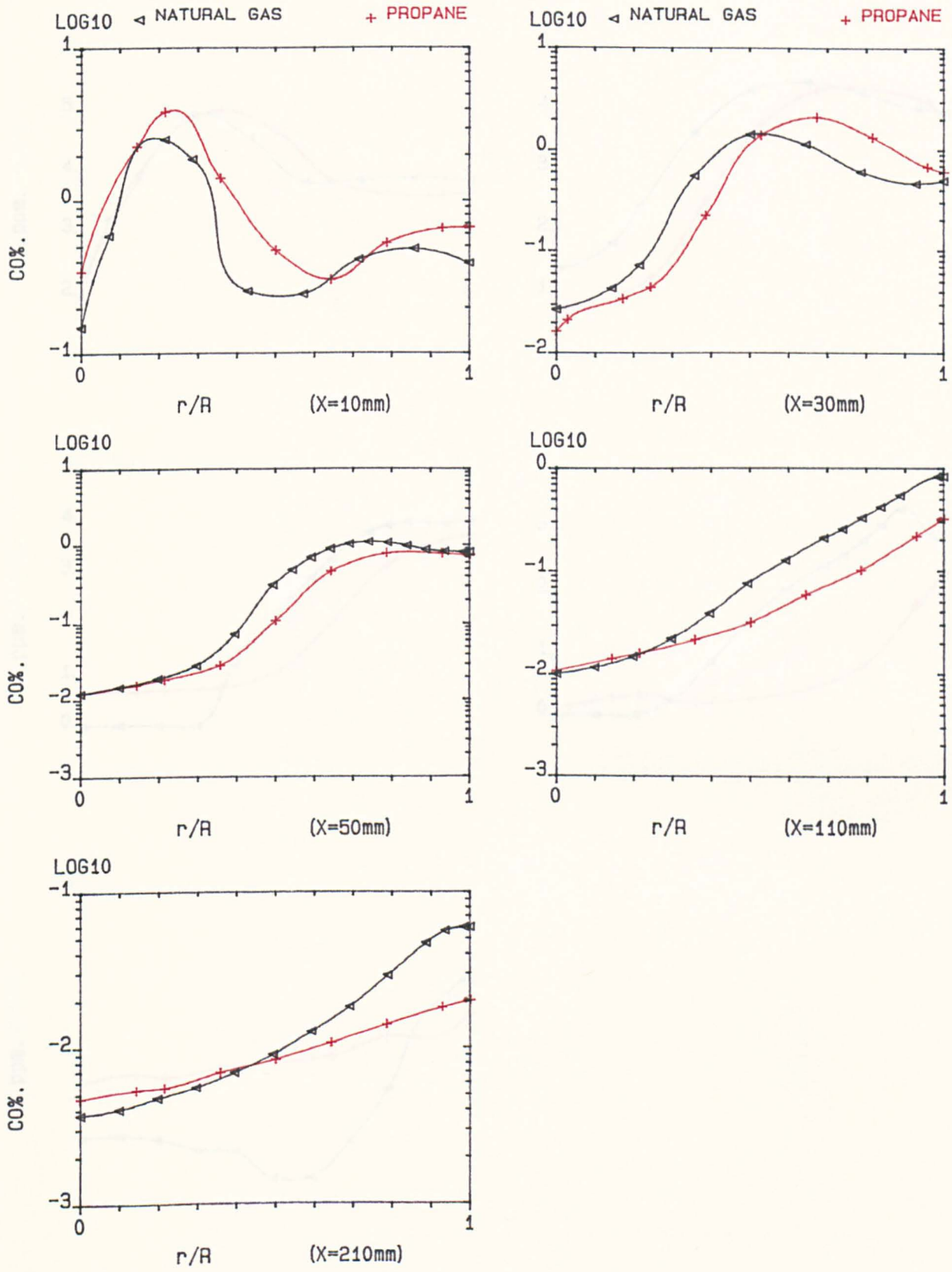

FIG.3.15 LOCAL VARIATION OF CARBON MONOXIDE, IN FIVE AXIAL PLANES FOR RADIAL SWIRLER (B); 140mm COMBUSTOR; USING CENTRAL INJECTION, NATURAL GAS & PROPANE, TIN=600K.

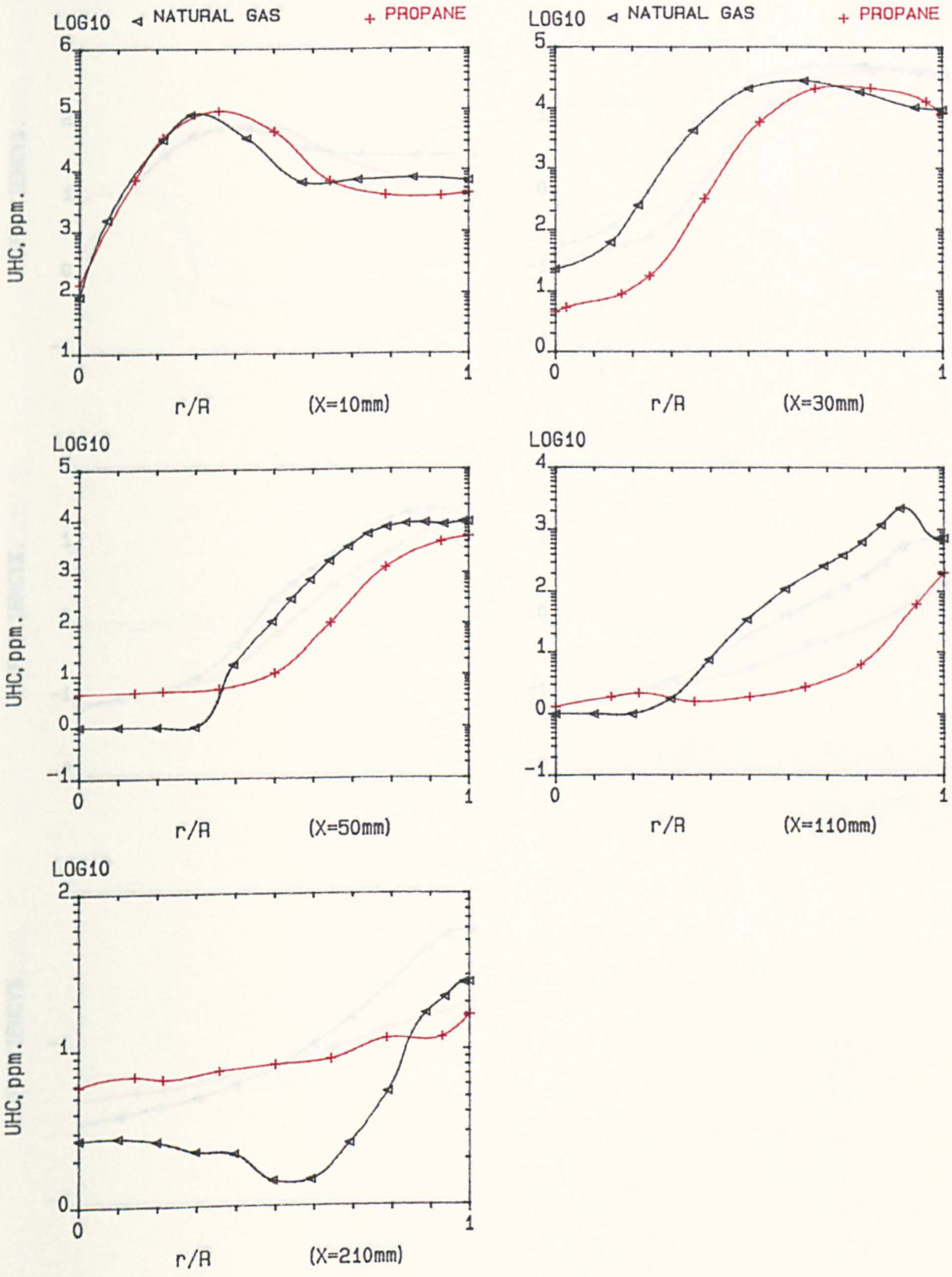

FIG.3.16 LOCAL VARIATION OF UNBURNED HYDROCARBONS, IN FIVE AXIAL PLANES FOR RADIAL SWIRLER (B): 140mm COMBUSTOR; USING CENTRAL INJECTION, NATURAL GAS & PROPANE, TIN=600K.

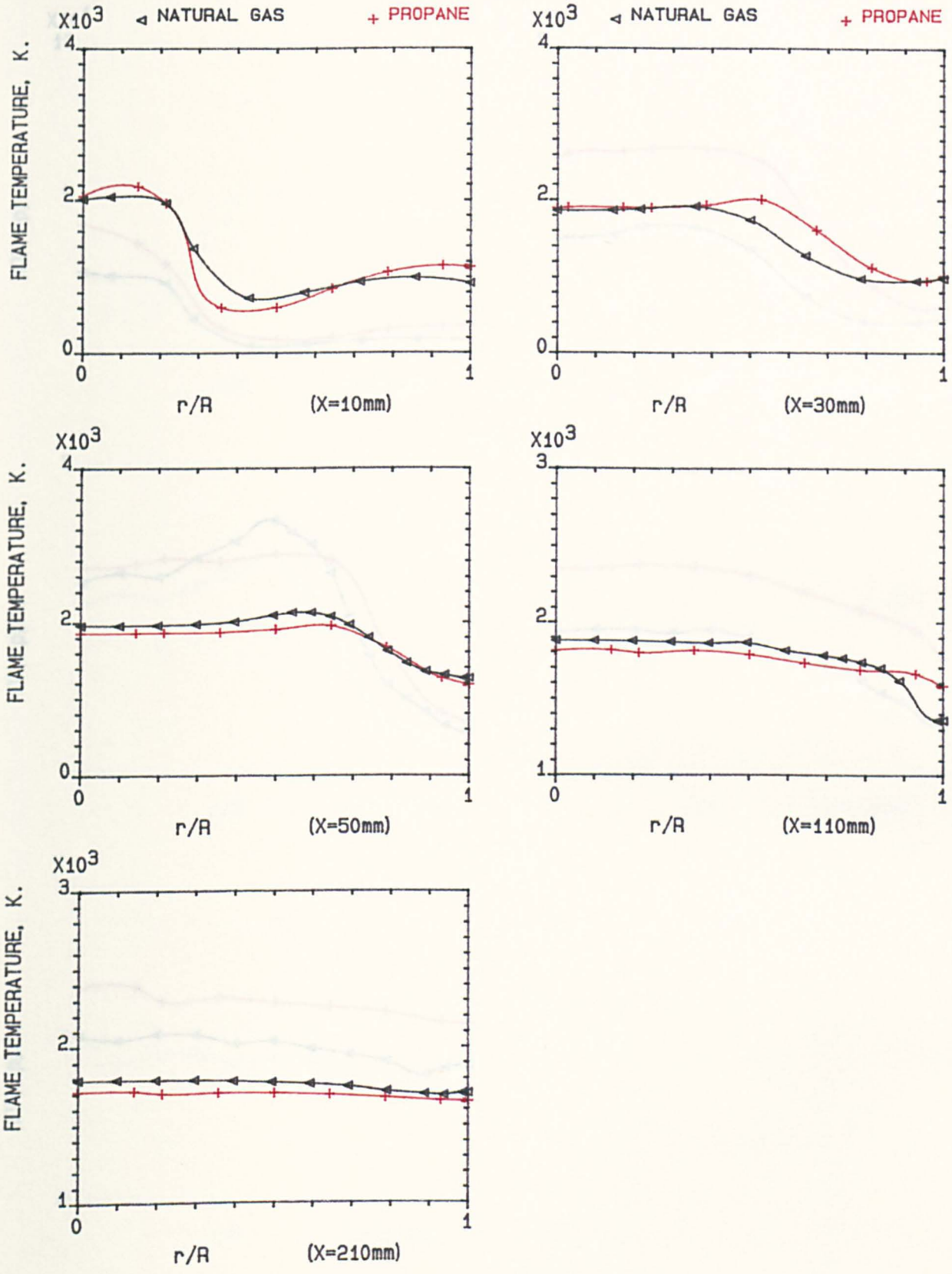

FIG.3.18 LOCAL VARIATION OF FLAME TEMPERATURE , IN FIVE AXIAL PLANES FOR RADIAL SWIRLER (B); 140mm COMBUSTOR; USING CENTRAL INJECTION, NATURAL GAS & PROPANE, TIN=600K.

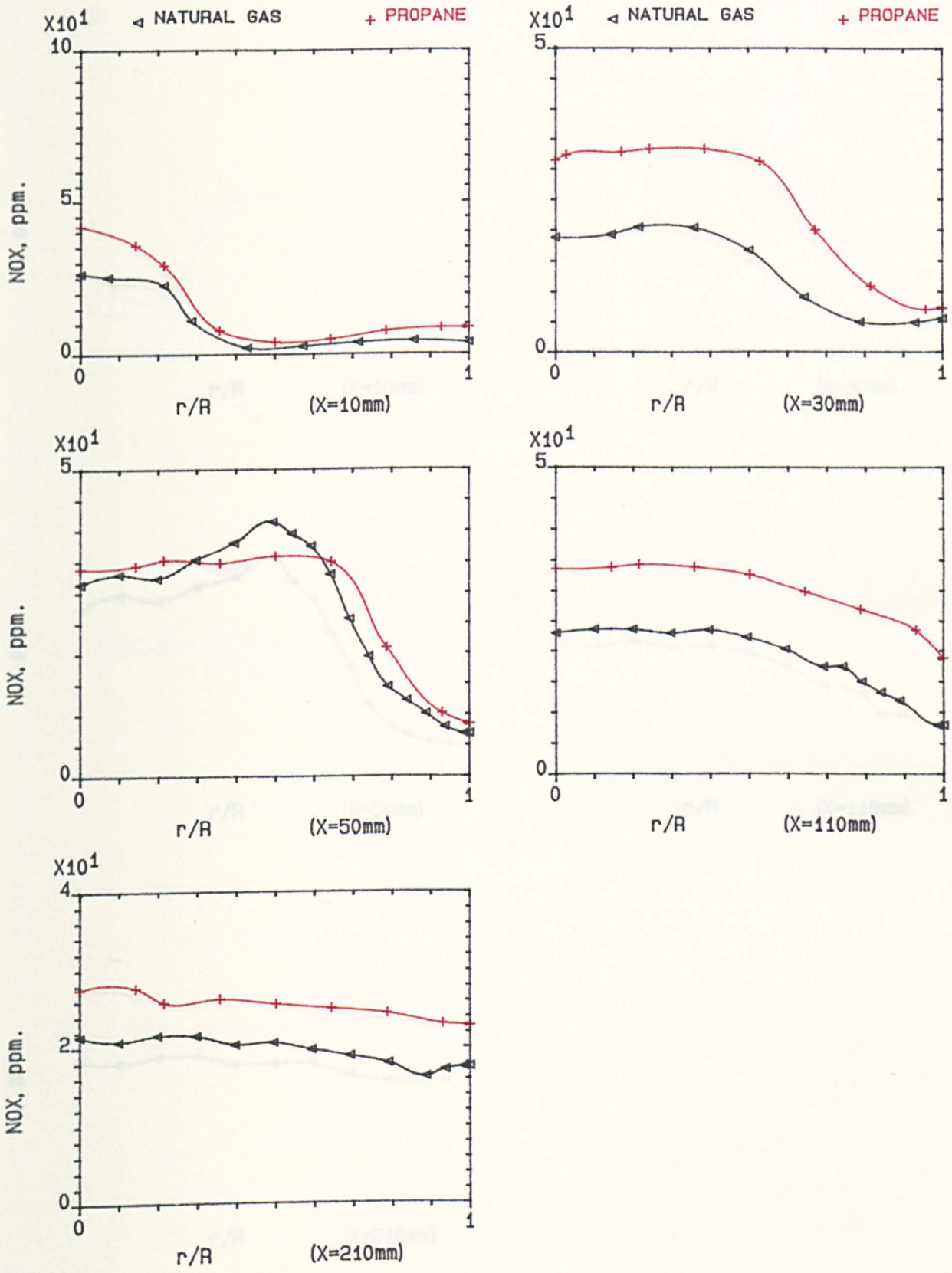

FIG.3.19 LOCAL VARIATION OF TOTAL NOX , IN FIVE AXIAL PLANES FOR RADIAL SWIRLER (B); 140mm COMBUSTOR; USING CENTRAL INJECTION, NATURAL GAS & PROPANE, TIN=600K.

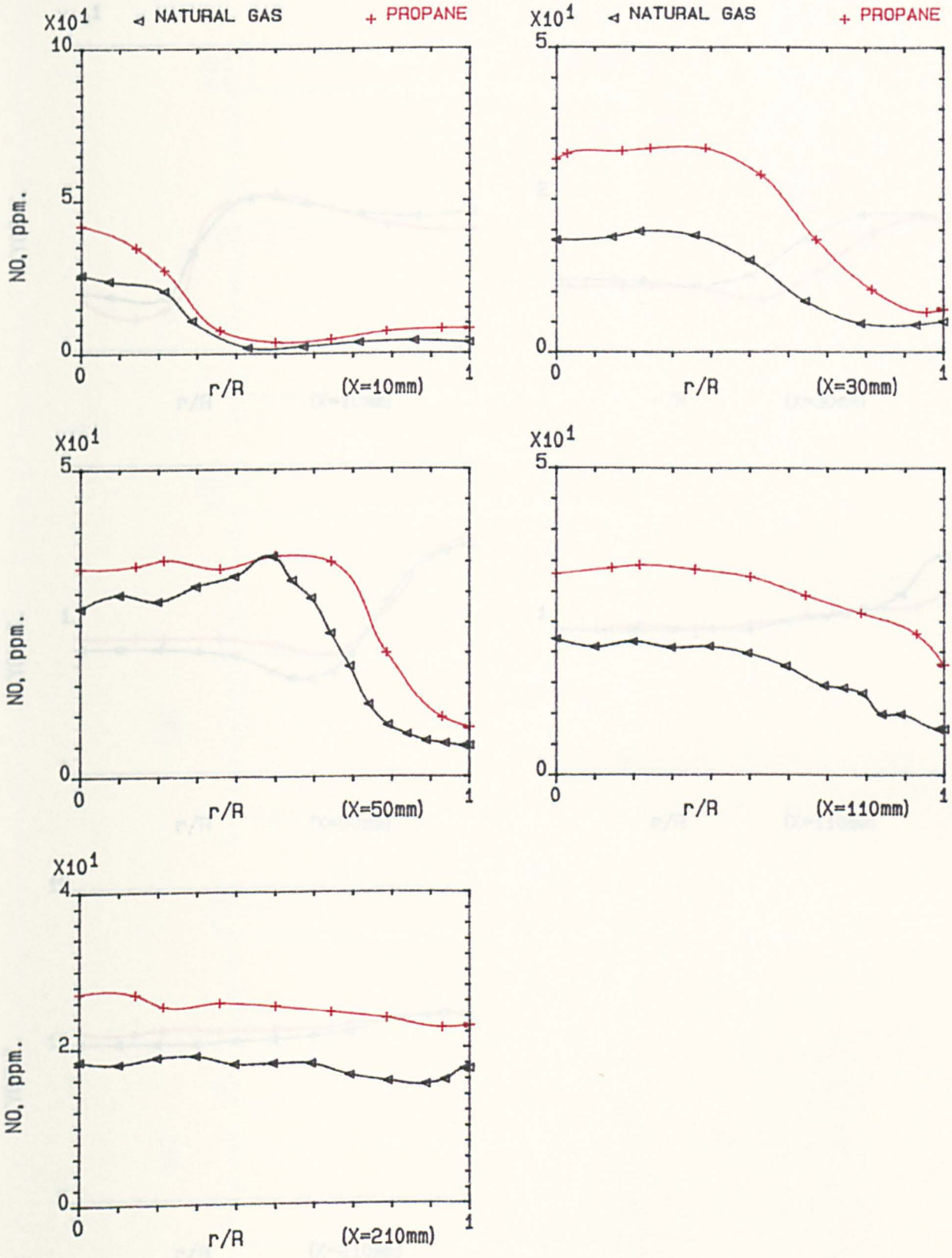

FIG.3.20 LOCAL VARIATION OF NITRIC OXIDE (NO), IN FIVE AXIAL PLANES FOR RADIAL SWIRLER (B); 140mm COMBUSTOR; USING CENTRAL INJECTION, NATURAL GAS & PROPANE, TIN=600K.

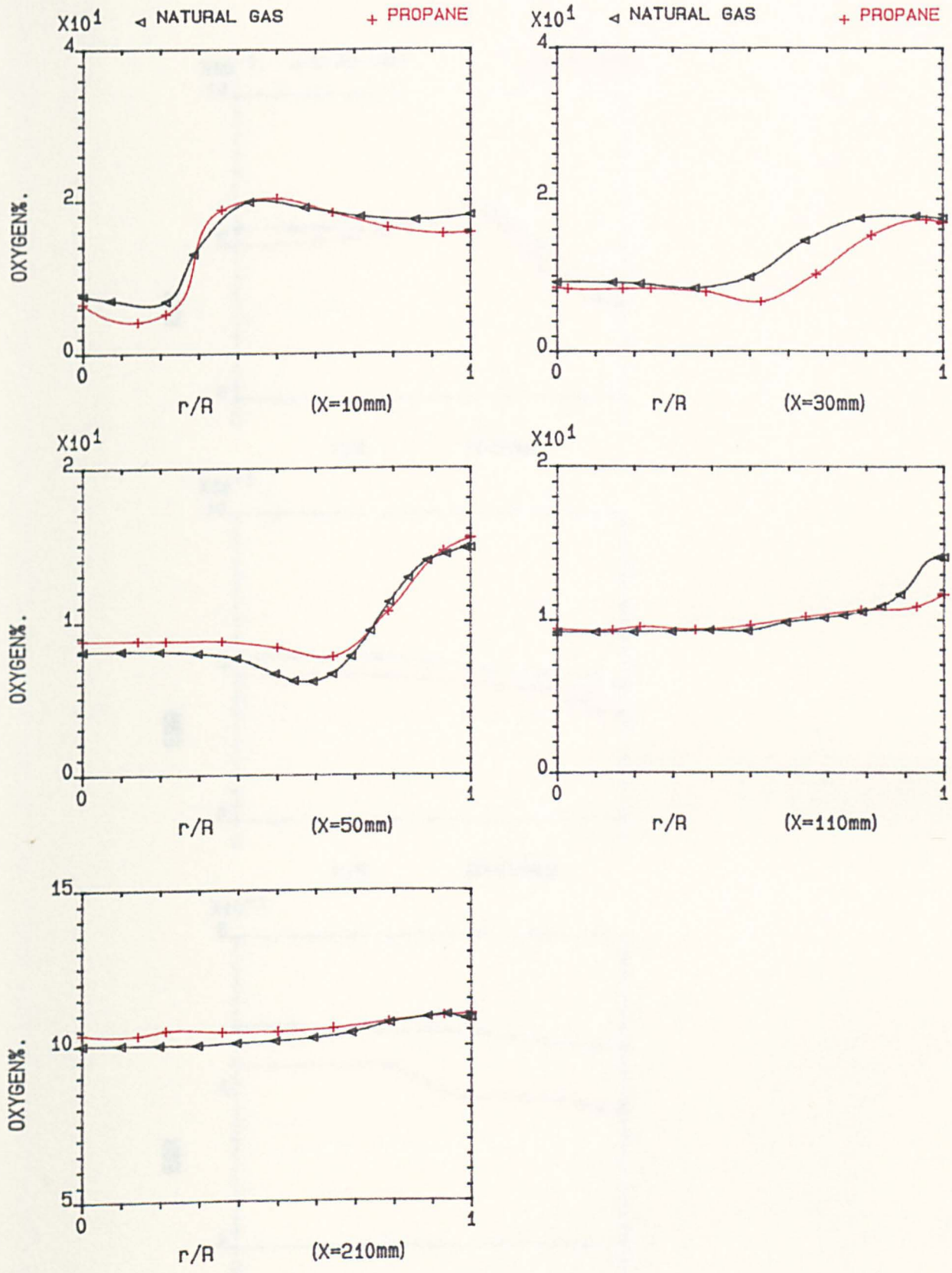

FIG.3.21 LOCAL VARIATION OF OXYGEN CONCENTRATION, IN FIVE AXIAL PLANES FOR RADIAL SWIRLER (B): 140mm COMBUSTOR; USING CENTRAL INJECTION, NATURAL GAS & PROPANE, TIN=600K.

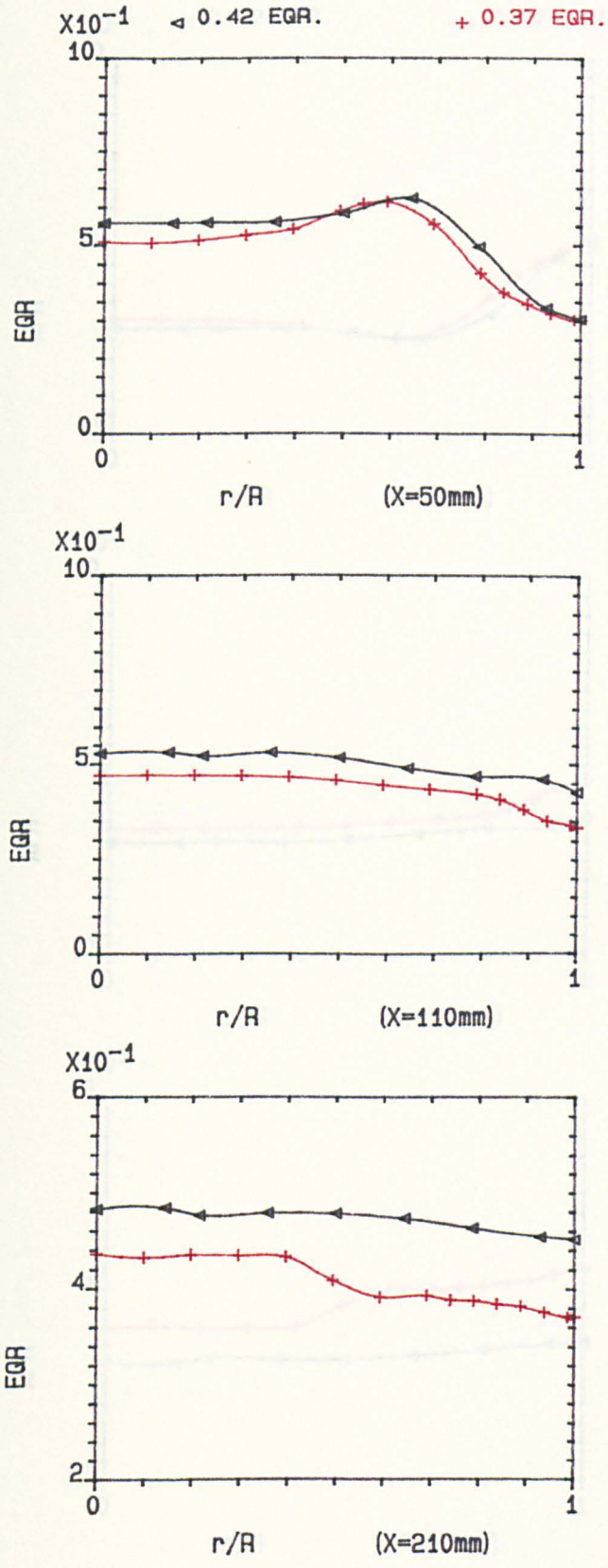

FIG.3.22 INFLUENCE OF DIFFERENT EQUIVALENCE RATIO ON LOCAL VARIATION OF EQUIVALENCE RATIO, USING SWIRLER(B) IN 140mm COMBUSTOR WITH CENTRAL INJECTION PROPANE, 600K.

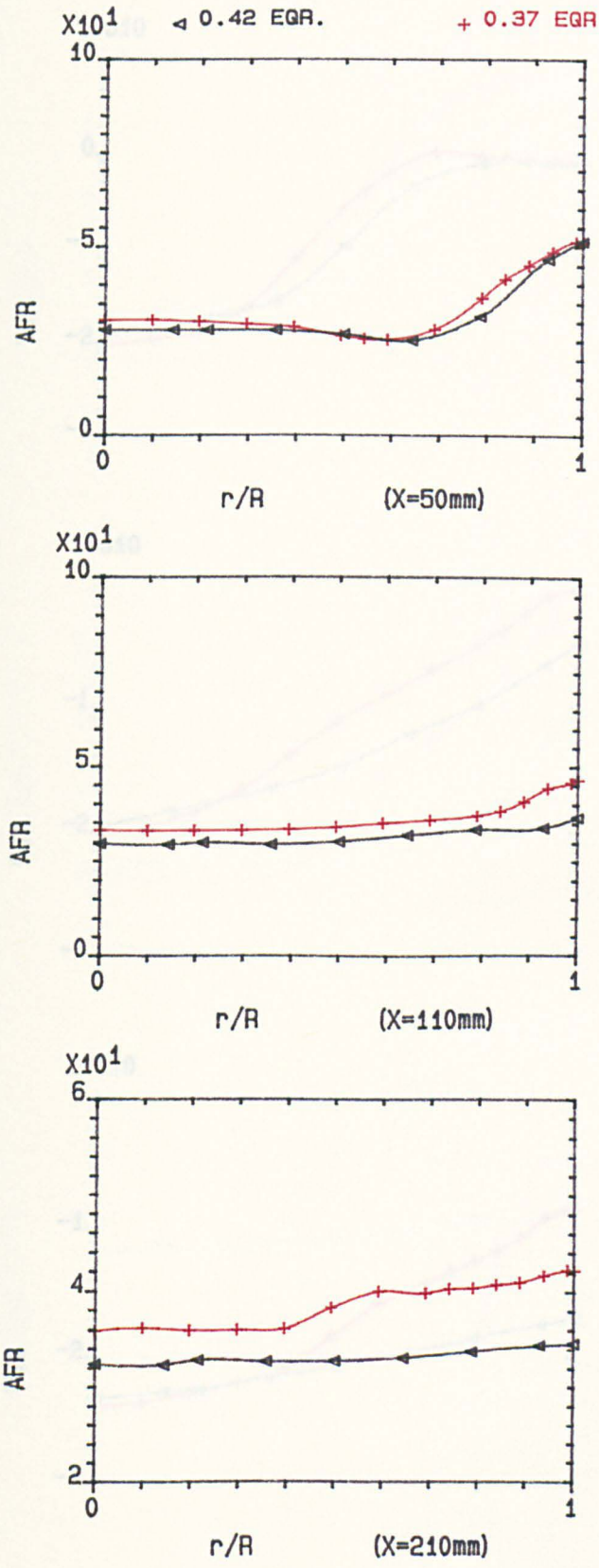

FIG.3.23 INFLUENCE OF DIFFERENT EQUIVALENCE RATIO ON LOCAL VARIATION OF (AIR/FUEL) RATIO, USING SWIRLER(B) IN 140mm COMBUSTOR WITH CENTRAL INJECTION PROPANE, 600K.

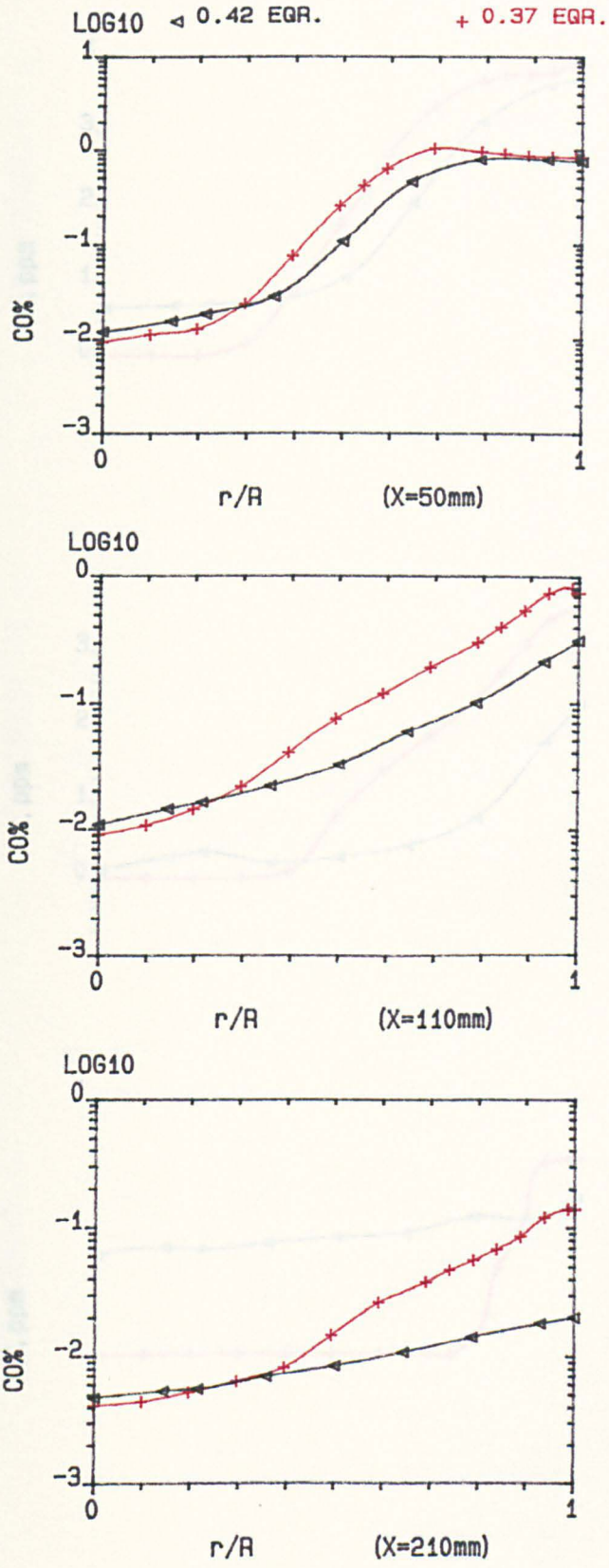

FIG.3.24 INFLUENCE OF DIFFERENT EQUIVALENCE RATIO ON LOCAL VARIATION OF CARBON MONOXIDE, USING SWIRLER(B) IN 140mm COMBUSTOR WITH CENTRAL INJECTION PROPANE, 600K.

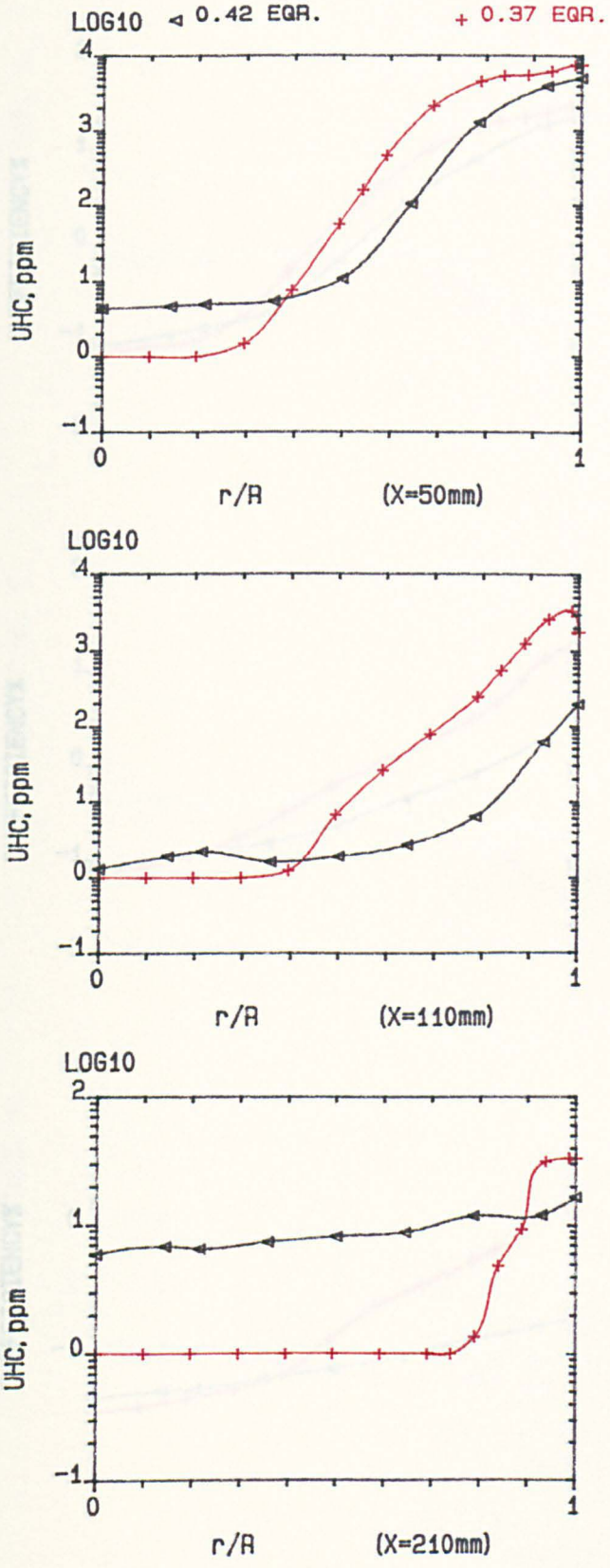

FIG.3.25 INFLUENCE OF DIFFERENT EQUIVALENCE RATIO ON LOCAL VARIATION OF UNBURNED HYDROCARBONS, USING SWIRLER (B) IN 140mm COMBUSTOR WITH CENTRAL INJECTION PROPANE, 600K.

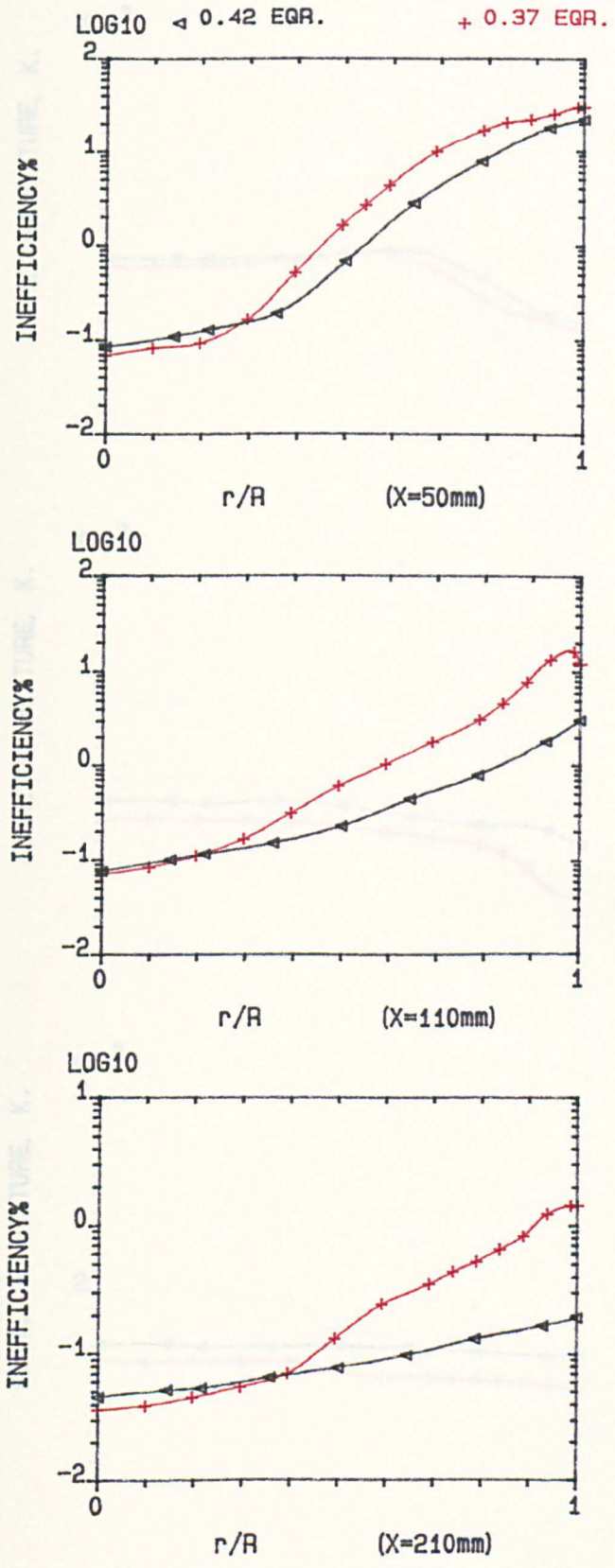

FIG.3.26 INFLUENCE OF DIFFERENT EQUIVALENCE RATIO ON LOCAL VARIATION OF COMBUSTION INEFFICIENCY, USING SWIRLER (B) IN 140mm COMBUSTOR WITH CENTRAL INJECTION PROPANE, 600K.

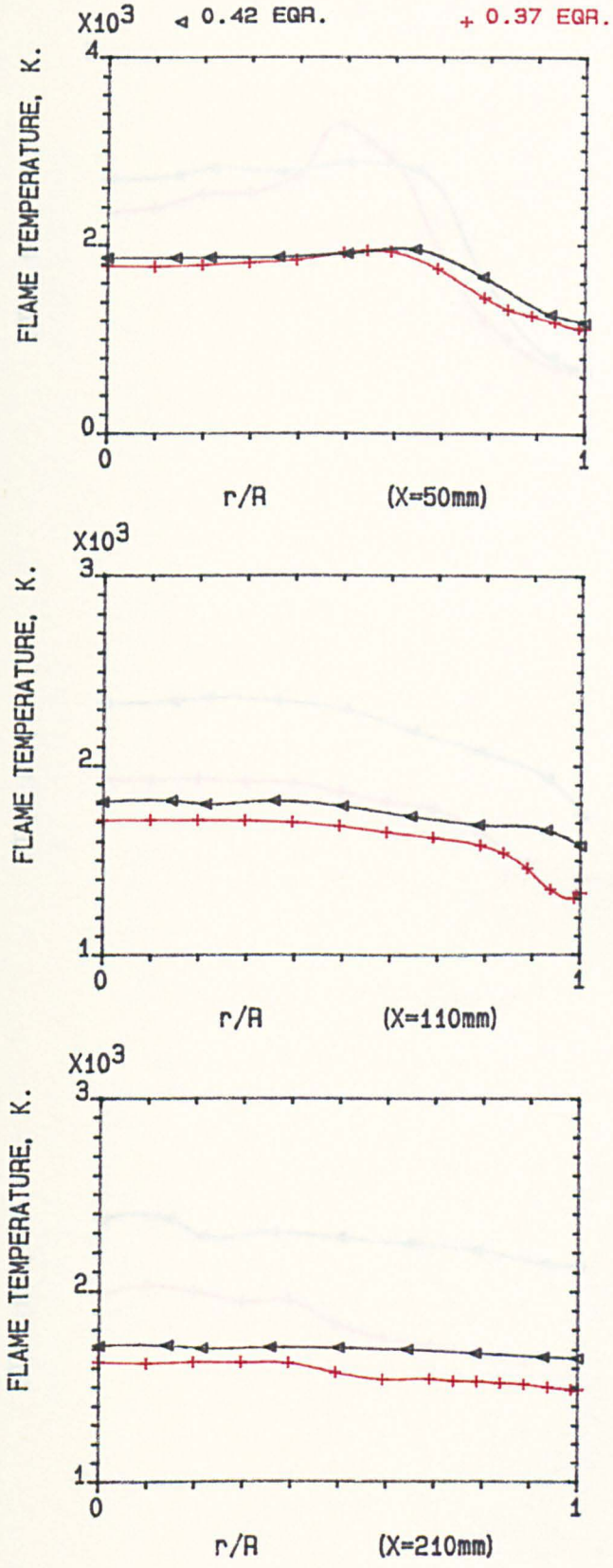

FIG.3.27 INFLUENCE OF DIFFERENT EQUIVALENCE RATIO ON LOCAL VARIATION OF FLAME TEMPERATURE, USING SWIRLER (B) IN 140mm COMBUSTOR WITH CENTRAL INJECTION PROPANE, 600K.

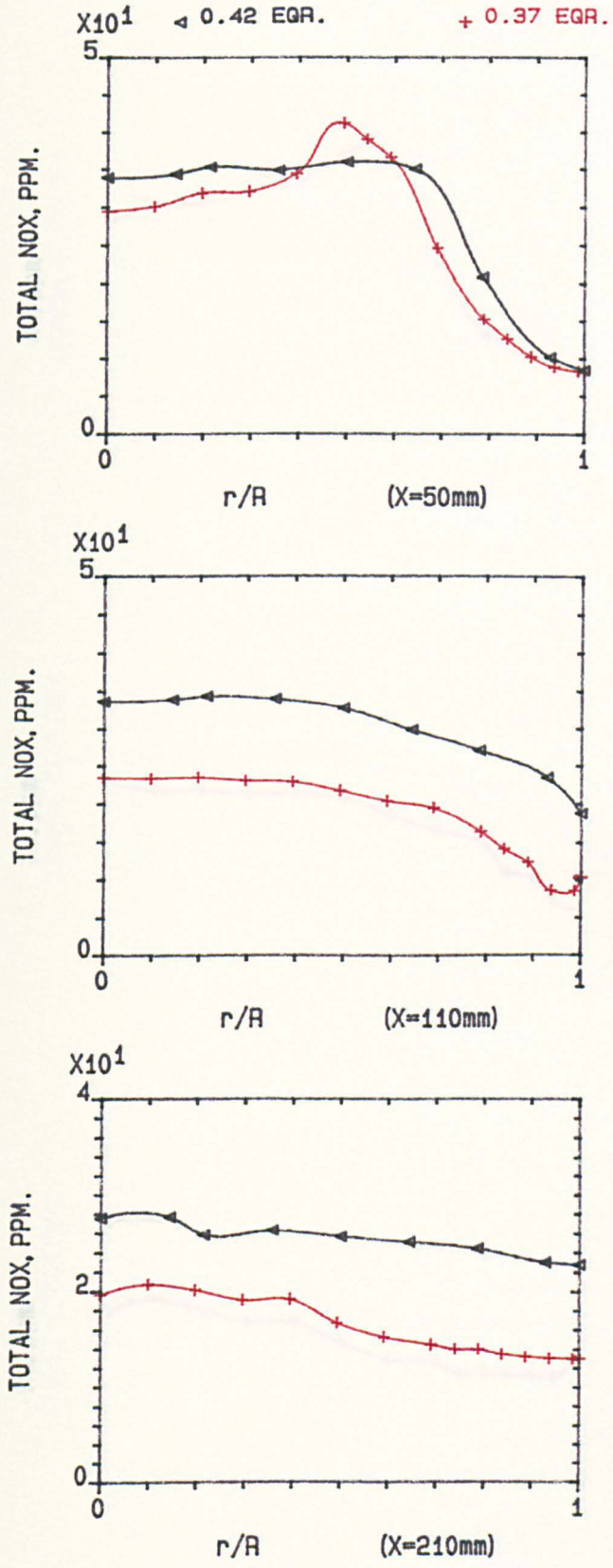

FIG.3.28 INFLUENCE OF DIFFERENT EQUIVALENCE RATIO ON LOCAL VARIATION OF TOTAL (NOX). USING SWIRLER (B) IN 140mm COMBUSTOR WITH CENTRAL INJECTION PROPANE, 600K.

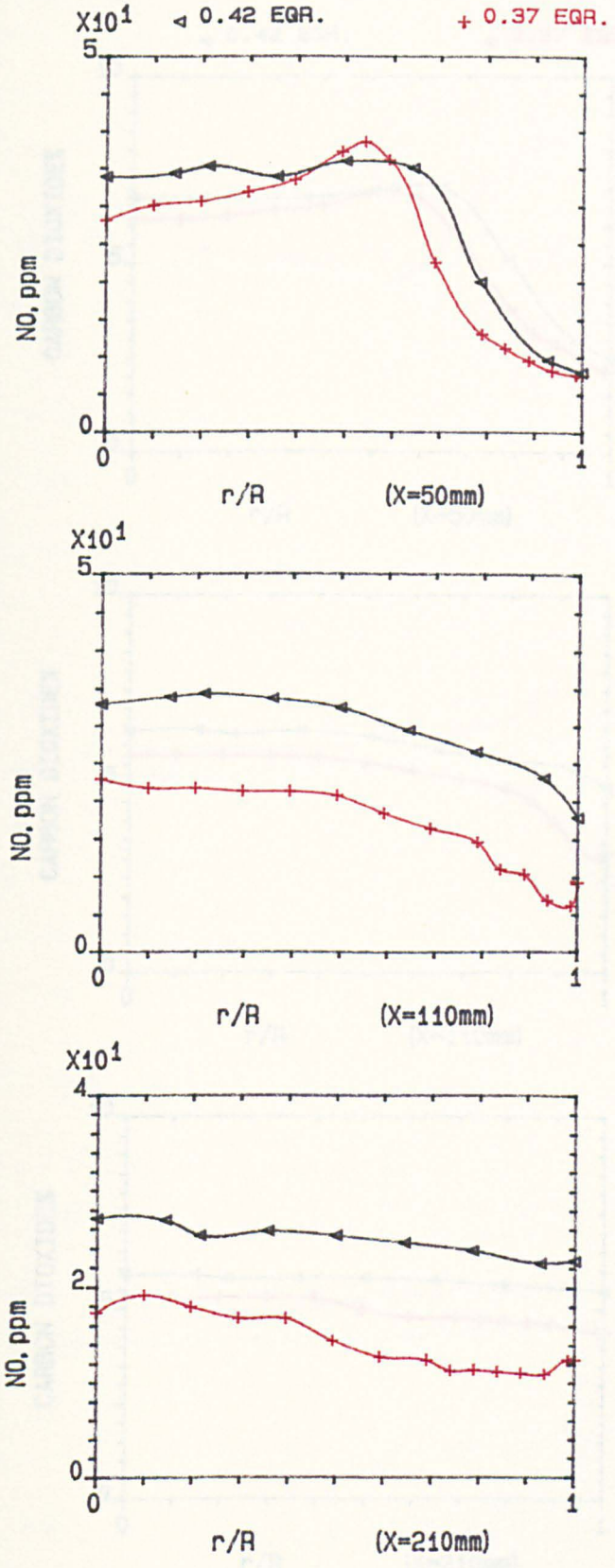

FIG.3.29 INFLUENCE OF DIFFERENT EQUIVALENCE RATIO ON LOCAL VARIATION OF NITRIC OXIDE (NO). USING SWIRLER (B) IN 140mm COMBUSTOR WITH CENTRAL INJECTION PROPANE, 600K.

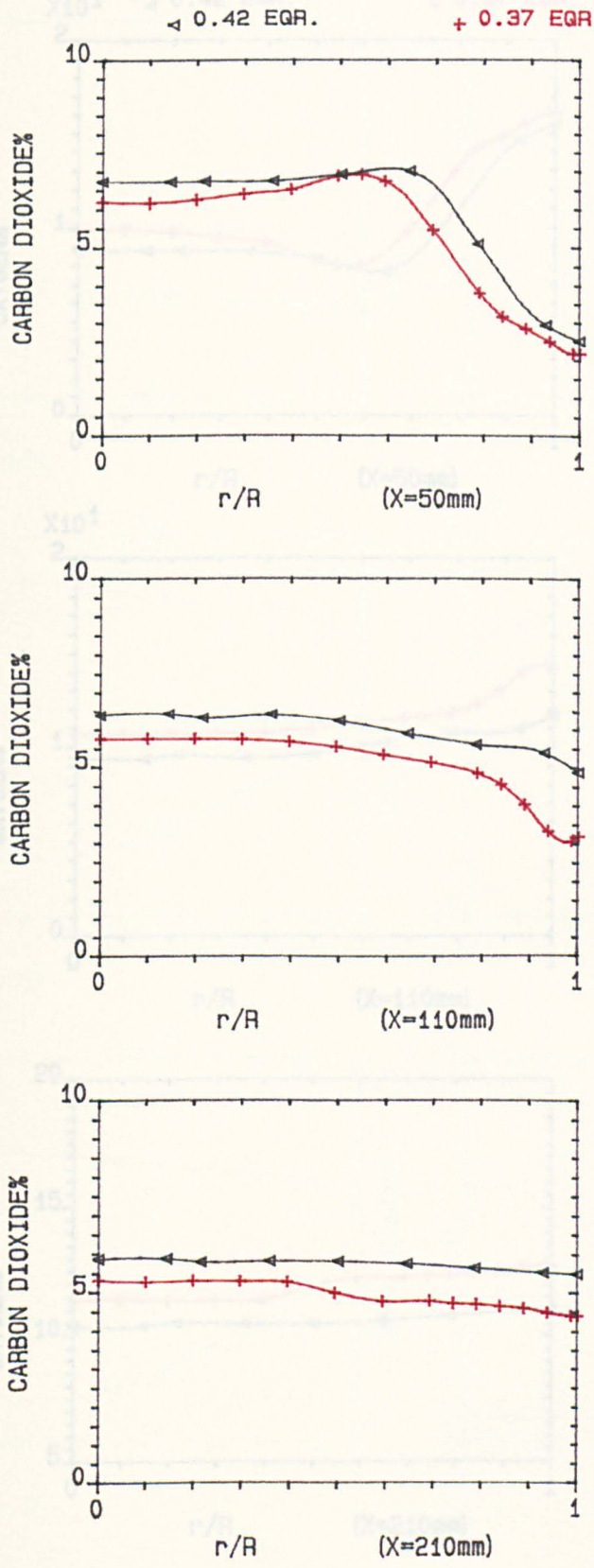

FIG.3.30 INFLUENCE OF DIFFERENT EQUIVALENCE RATIO ON LOCAL VARIATION OF CARBON DIOXIDE CONCENTRATION, USING SWIRLER (B) IN 140mm COMBUSTOR WITH CENTRAL INJECTION PROPANE, 600K.

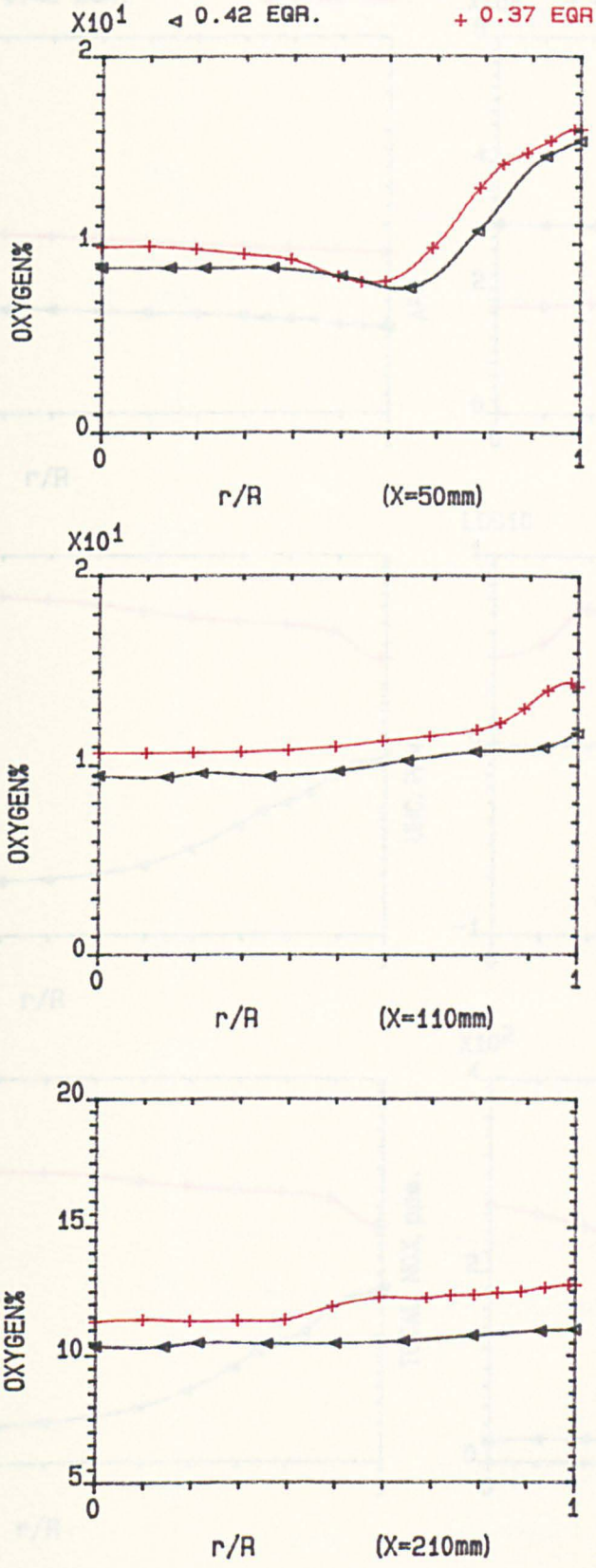

FIG.3.31 INFLUENCE OF DIFFERENT EQUIVALENCE RATIO ON LOCAL VARIATION OF OXYGEN CONCENTRATION, USING SWIRLER (B) IN 140mm COMBUSTOR WITH CENTRAL INJECTION PROPANE, 600K.

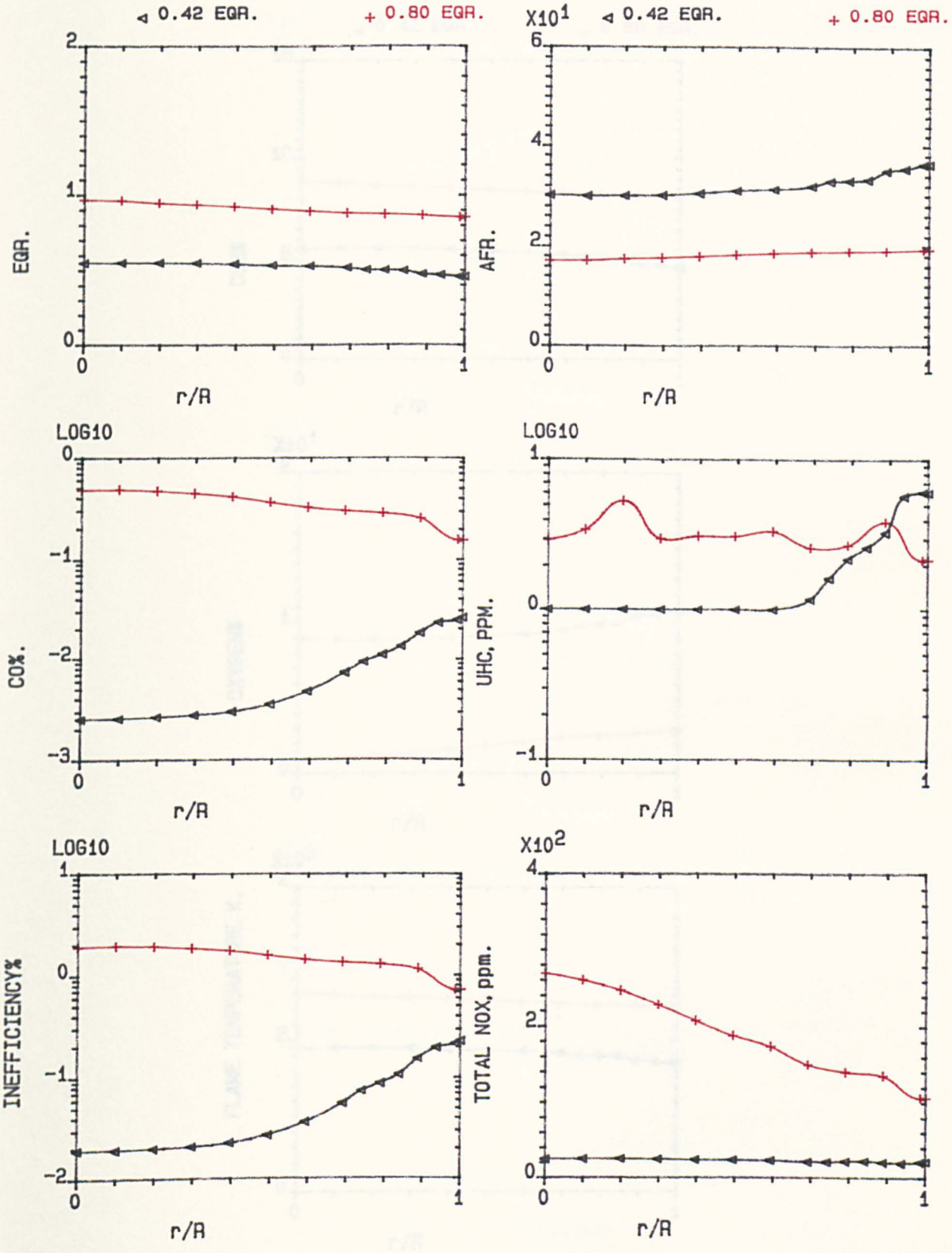

FIG.3.32 INFLUENCE OF EQUIVALENCE RATIO ON LOCAL SPECIES CONCENTRATION PLANE (X=210). USING SWIRLER (B) WITH CENTRAL NATURAL GAS INJECTION IN 140mm COMBUSTOR. MN=0.014, 600K.

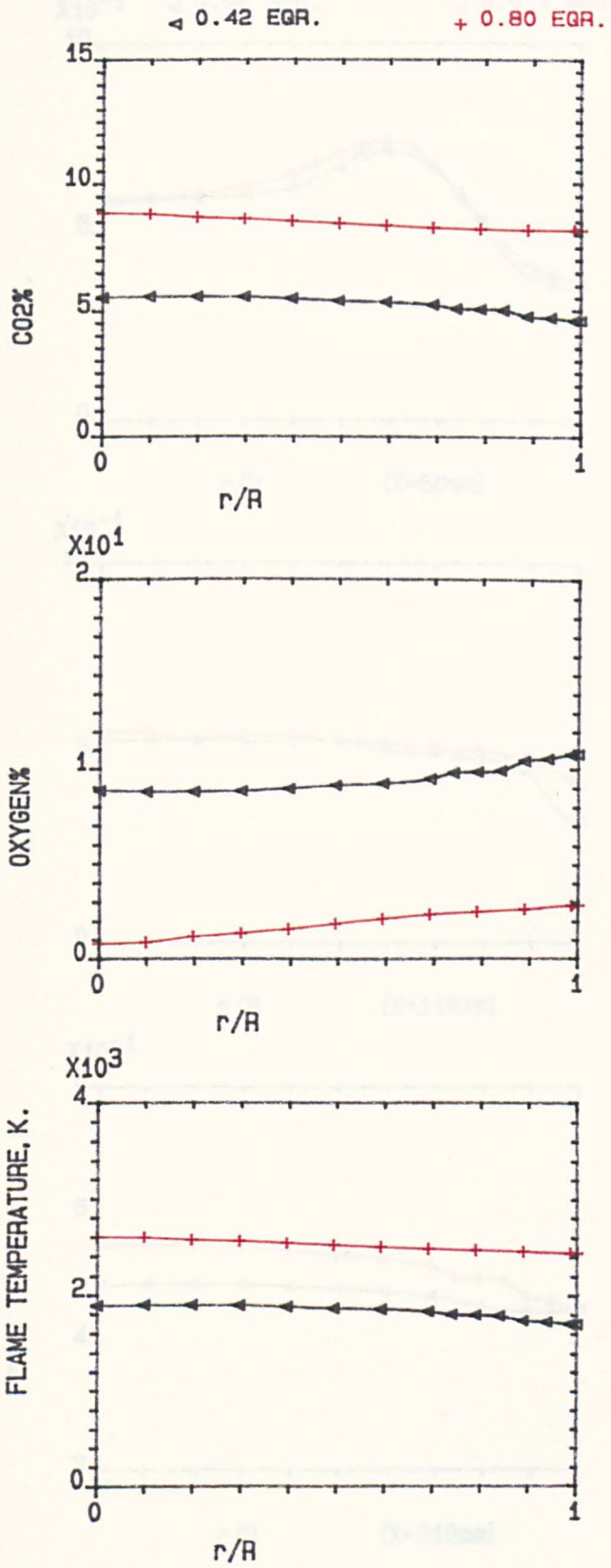

FIG.3.33 INFLUENCE OF EQUIVALENCE RATIO ON LOCAL SPECIES CONCENTRATION PLANE (X=210). USING SWIRLER (B) WITH CENTRAL NATURAL GAS INJECTION IN 140mm COMBUSTOR. MN=0.014. 600K.

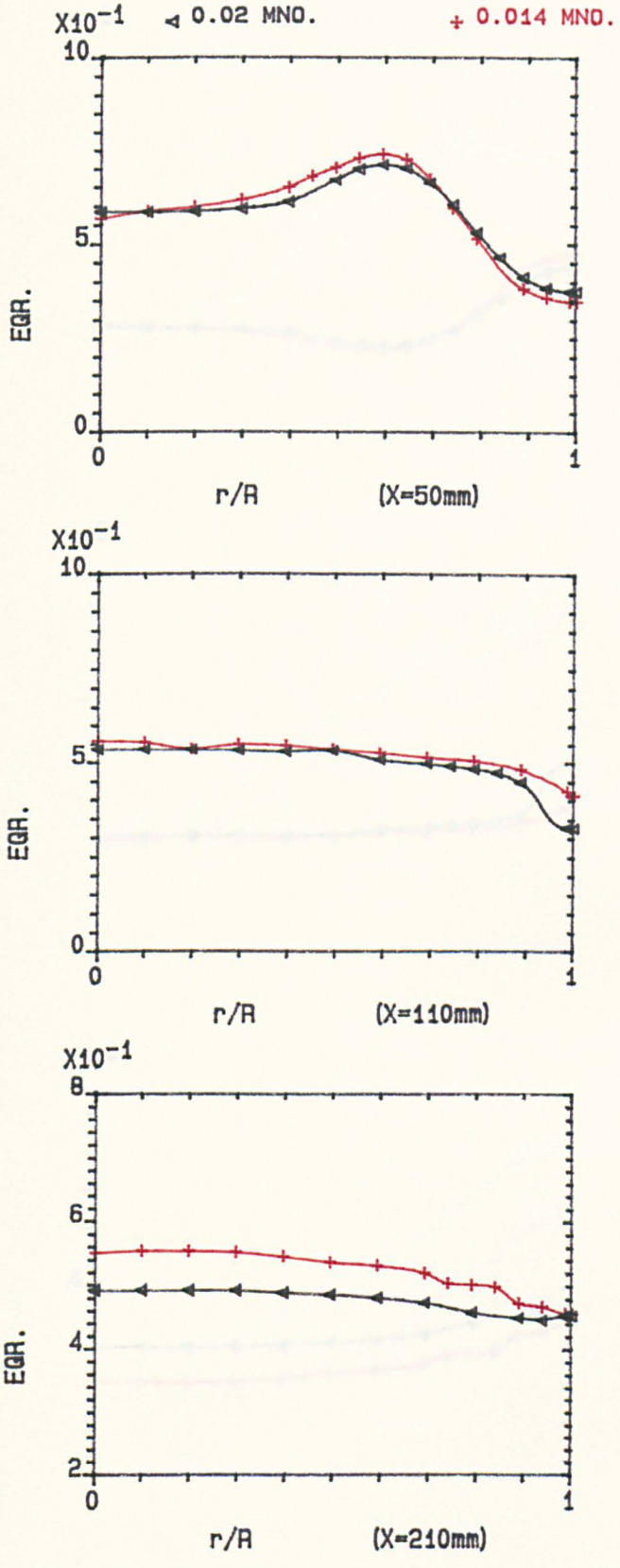

FIG.3.34 INFLUENCE OF RESIDENCE TIME ON LOCAL VARIATION OF EQR. OF CENTRAL INJECTION NATURAL GAS USING RADIAL SWIRLER(B), IN 140mm COMBUSTOR; 600K.

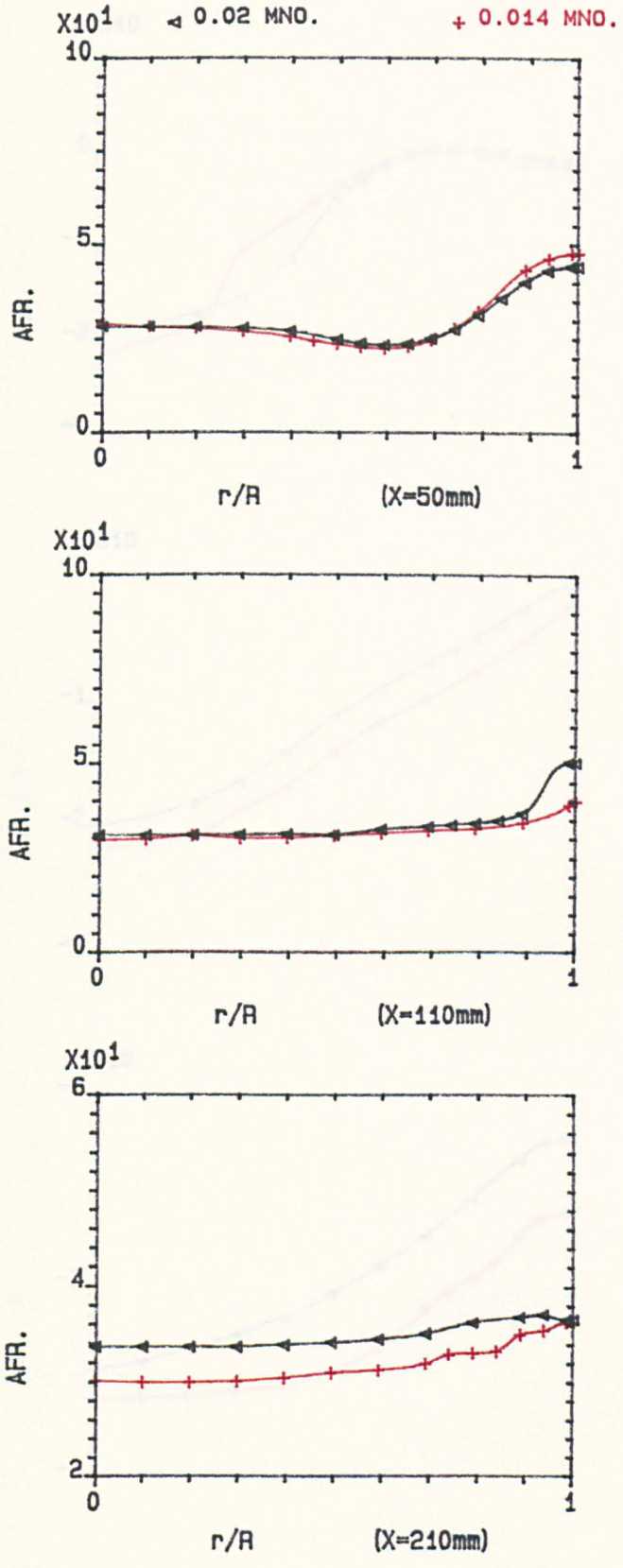

FIG.3.35 INFLUENCE OF RESIDENCE TIME ON LOCAL VARIATION OF AFR. OF CENTRAL INJECTION NATURAL GAS USING RADIAL SWIRLER(B), IN 140mm COMBUSTOR; 600K.

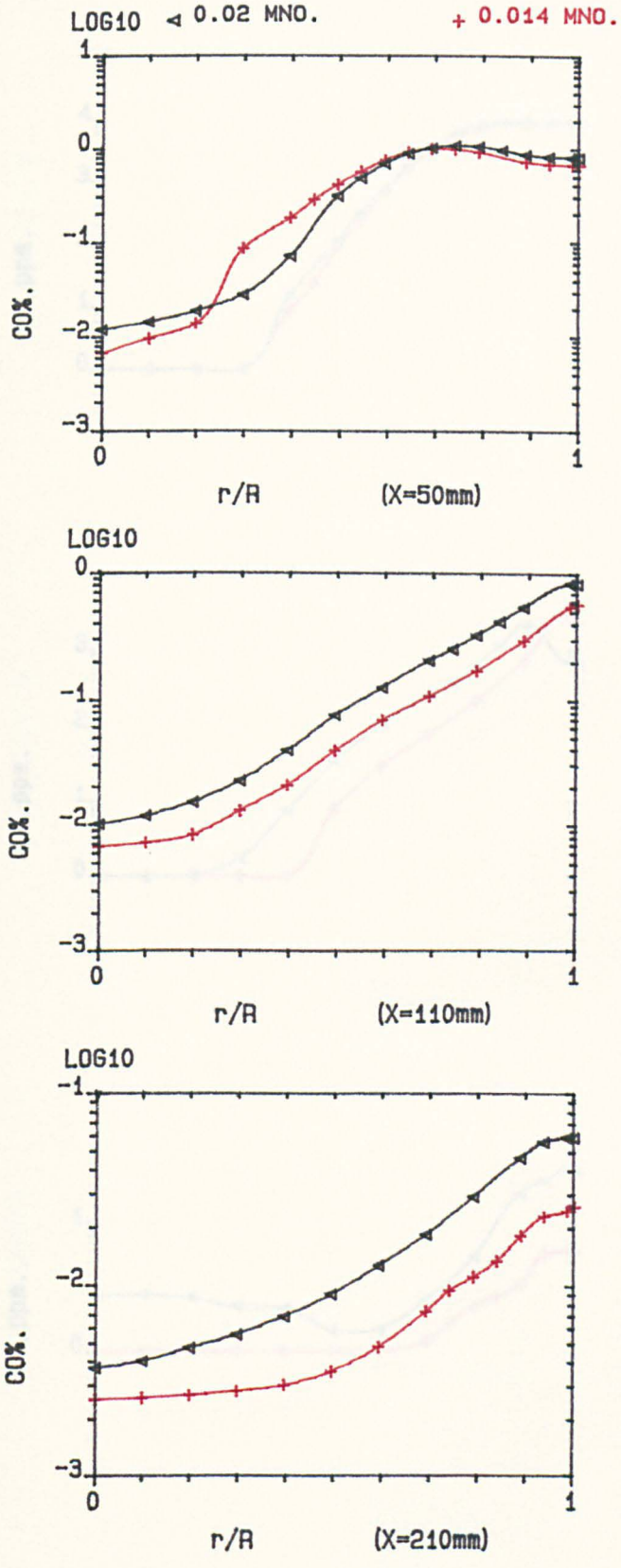

FIG.3.36 INFLUENCE OF RESIDENCE TIME ON LOCAL VARIATION OF CO%. OF CENTRAL INJECTION NATURAL GAS USING RADIAL SWIRLER (B). IN 140mm COMBUSTOR; 600K.

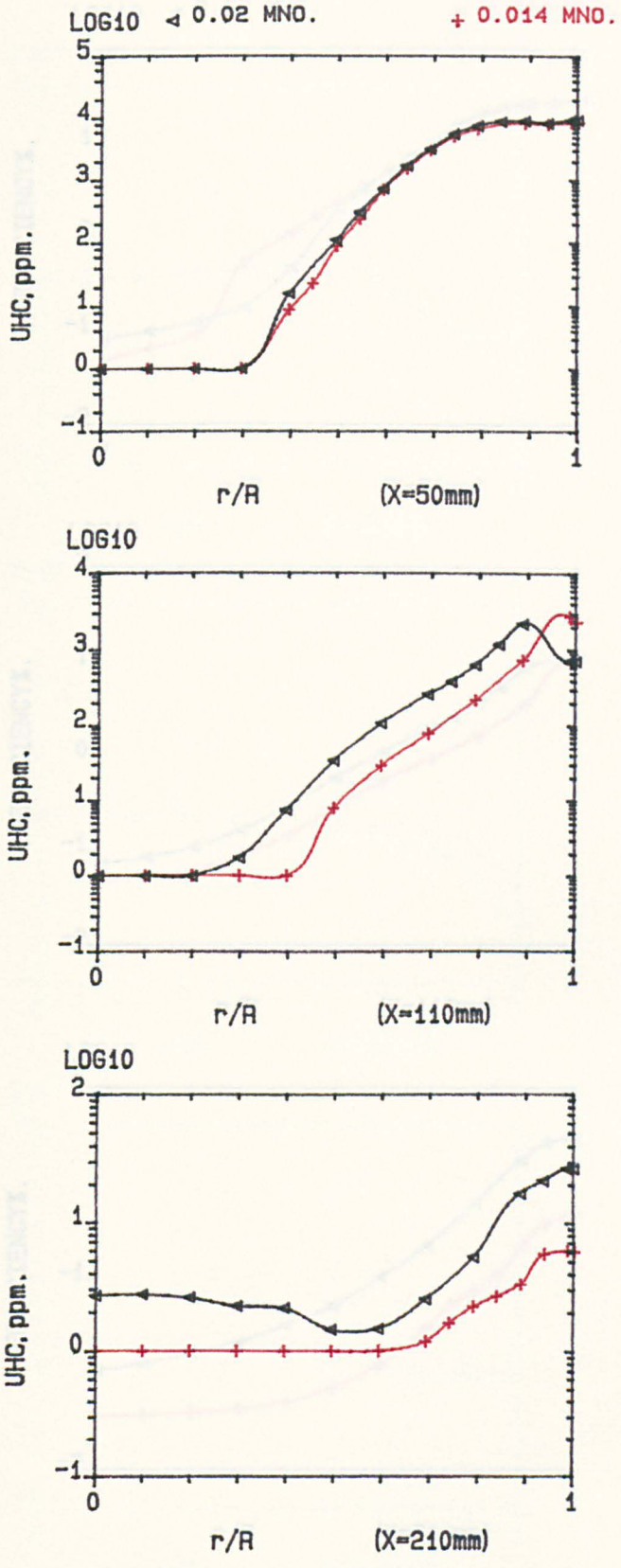

FIG.3.37 INFLUENCE OF RESIDENCE TIME ON LOCAL VARIATION OF UHC. OF CENTRAL INJECTION NATURAL GAS USING RADIAL SWIRLER(B). IN 140mm COMBUSTOR; 600K.

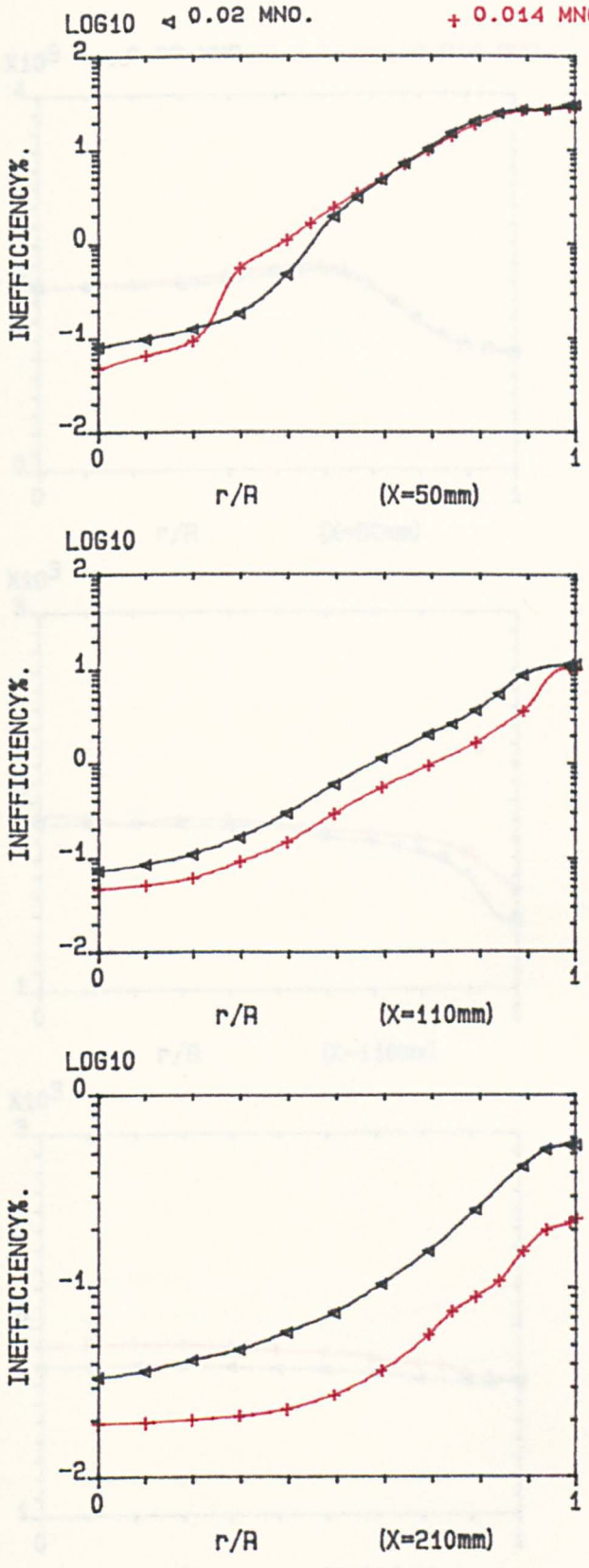

FIG.3.38 INFLUENCE OF RESIDENCE TIME ON LOCAL VARIATION OF INEFFICIENCY OF CENTRAL INJECTION NATURAL GAS USING RADIAL SWIRLER(B). IN 140mm COMBUSTOR; 600K.

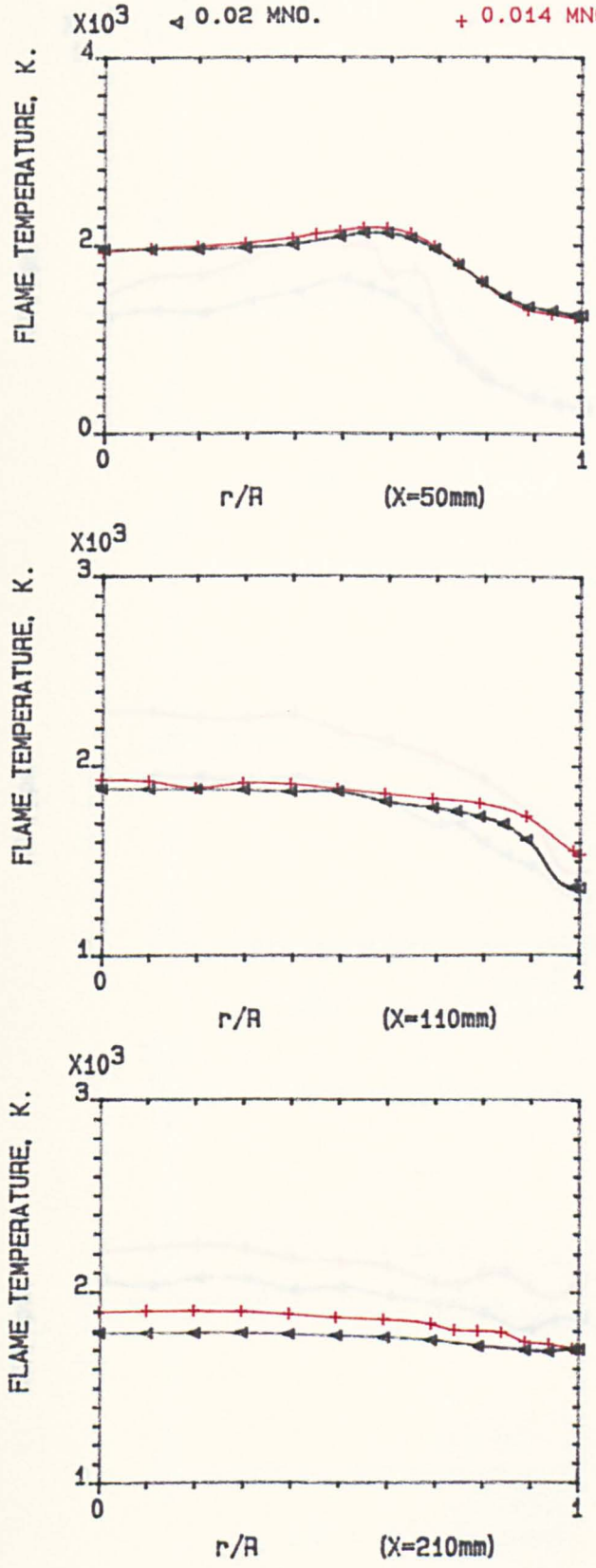

FIG.3.39 INFLUENCE OF RESIDENCE TIME ON LOCAL VARIATION OF FLAME TEMPERATURE OF CENTRAL INJECTION NATURAL GAS USING RADIAL SWIRLER (B), IN 140mm COMBUSTOR; 600K.

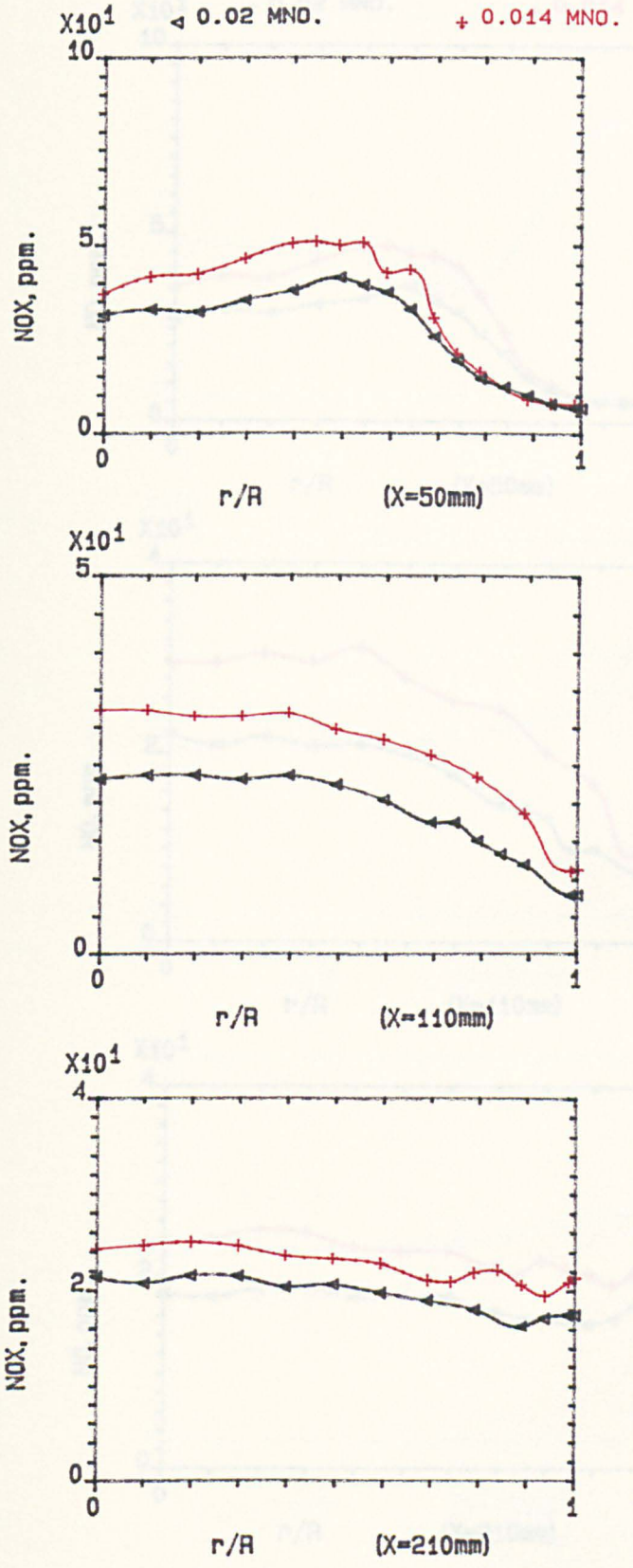

FIG.3.40 INFLUENCE OF RESIDENCE TIME ON LOCAL VARIATION OF TOTAL (NOX) OF CENTRAL INJECTION NATURAL GAS USING USING RADIAL SWIRLER (B). IN 140mm COMBUSTOR; 600K.

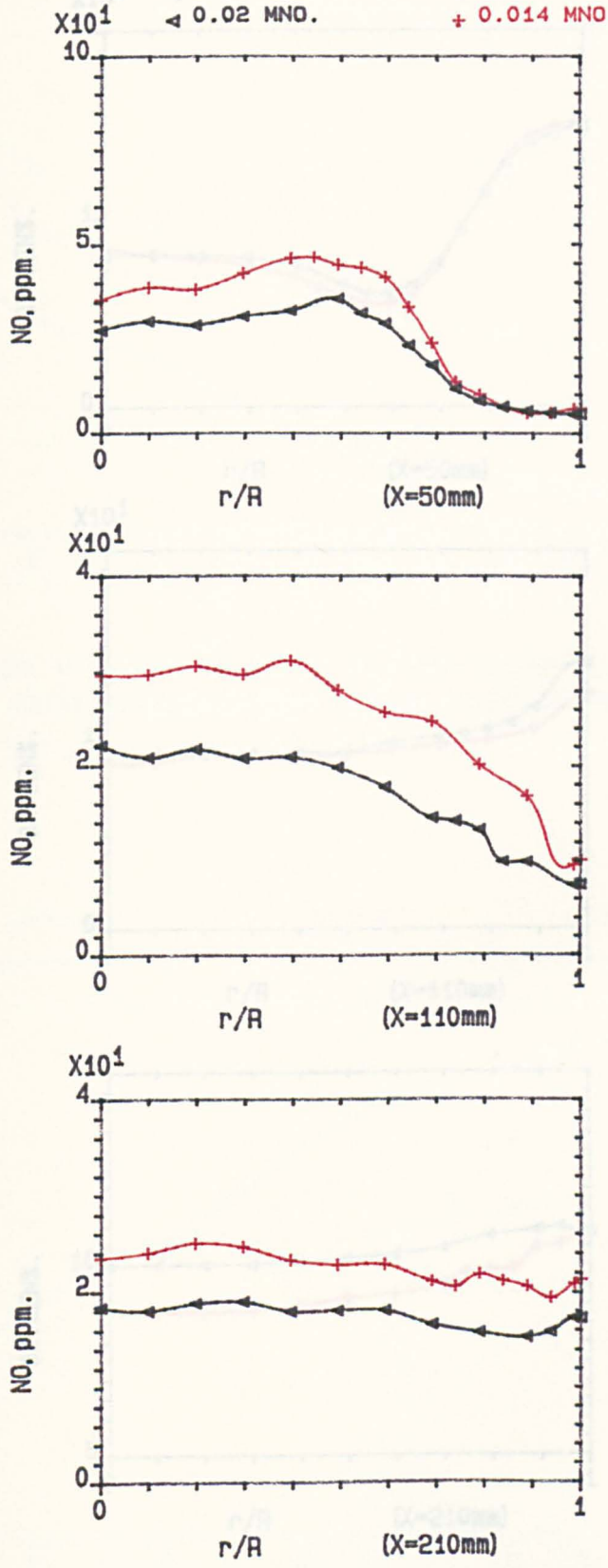

FIG.3.41 INFLUENCE OF RESIDENCE TIME ON LOCAL VARIATION OF TOTAL (NO) OF CENTRAL INJECTION NATURAL GAS USING USING RADIAL SWIRLER (B). IN 140mm COMBUSTOR; 600K.

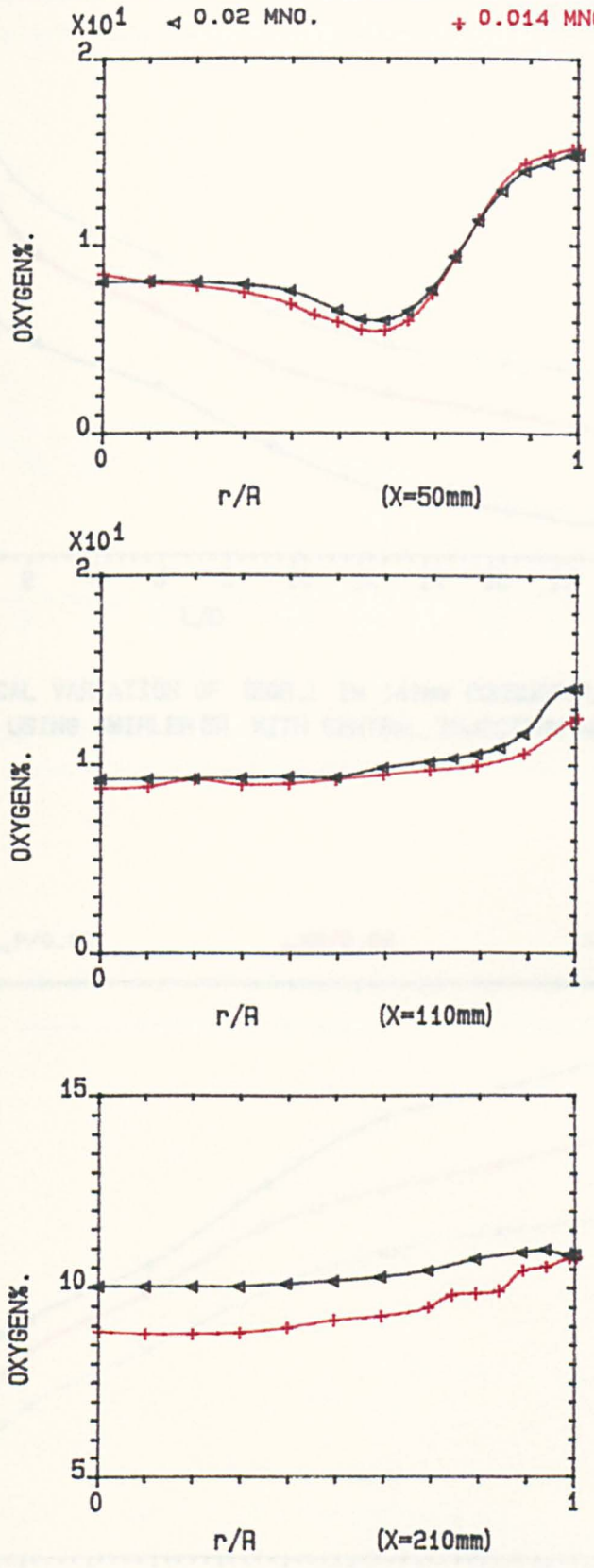

FIG.3.42 INFLUENCE OF RESIDENCE TIME ON LOCAL VARIATION OF OXYGEN OF CENTRAL INJECTION NATURAL GAS USING USING RADIAL SWIRLER (B). IN 140mm COMBUSTOR; 600K.

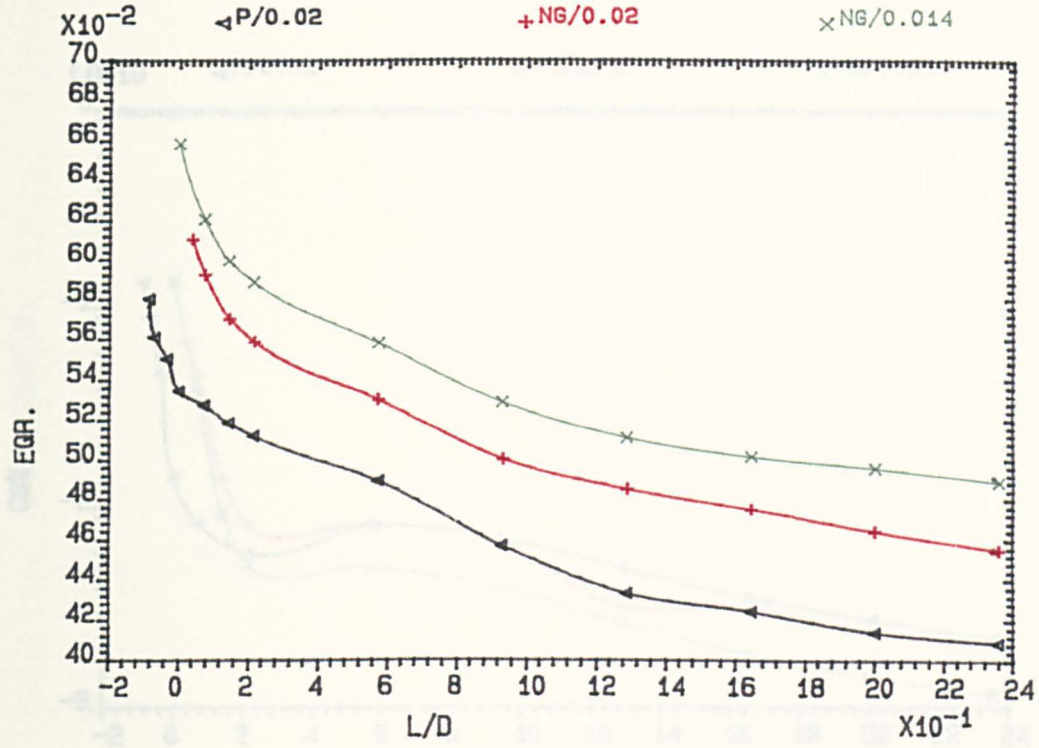

FIG.3.43 LOCAL VARIATION OF (EQR.) IN 140mm COMBUSTOR, CENTRE LINE, USING SWIRLER (B) WITH CENTRAL INJECTION NG & P, 600K.

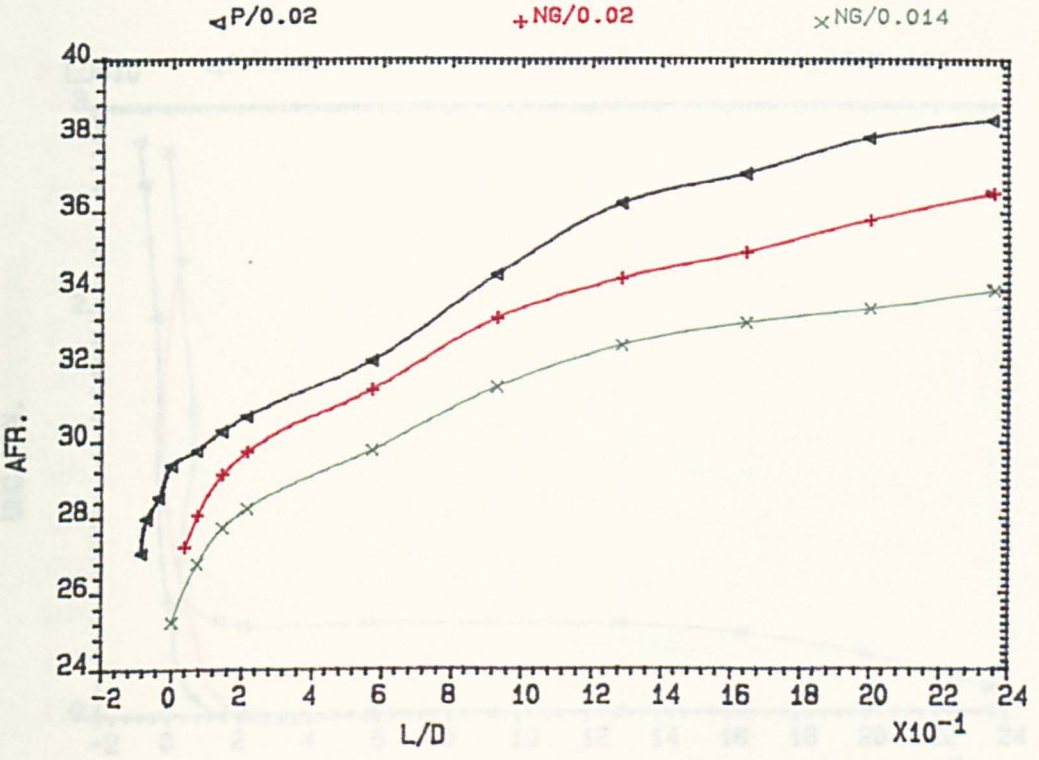

FIG.3.44 LOCAL VARIATION OF (AIR/FUEL) IN 140mm COMBUSTOR, CENTRE LINE, USING SWIRLER (B) WITH CENTRAL INJECTION NG & P, 600K.

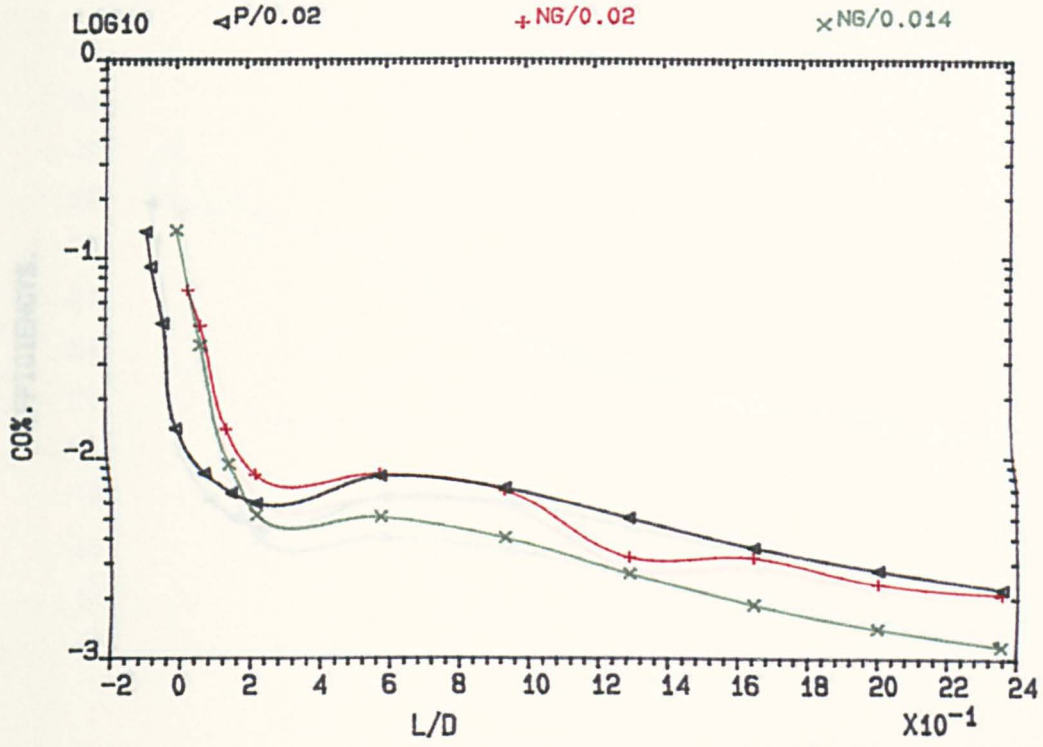

FIG.3.45 LOCAL VARIATION OF (CO%.) IN 140mm COMBUSTOR, CENTRE LINE, USING SWIRLER(B) WITH CENTRAL INJECTION NG & P, 600K.

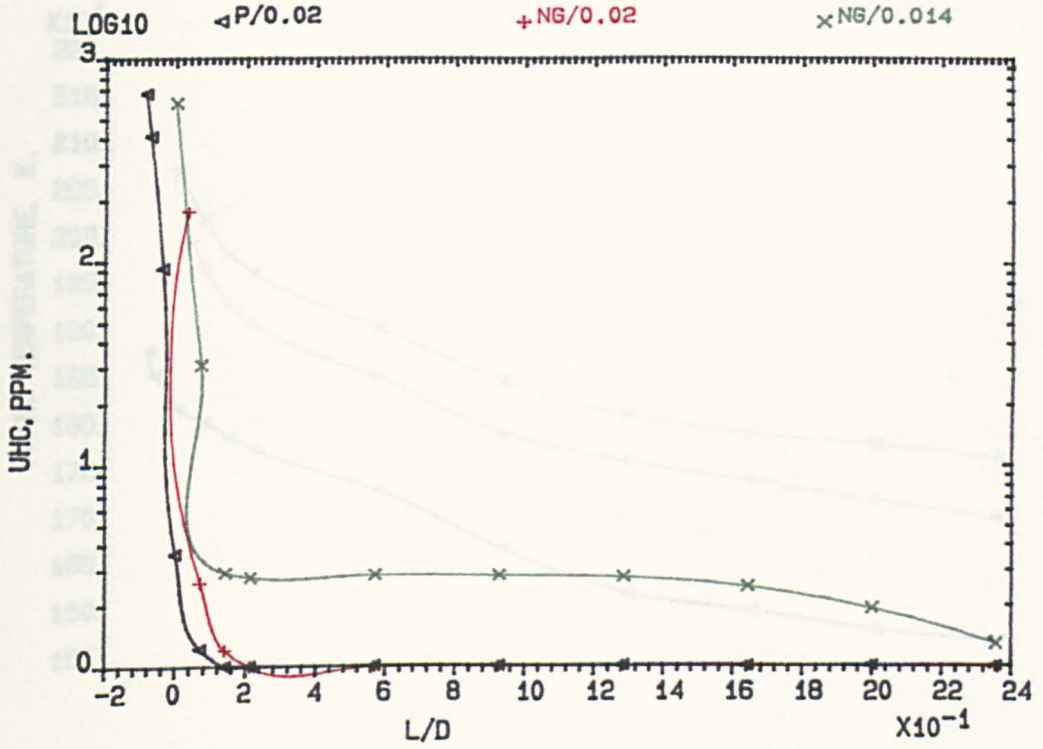

FIG.3.46 LOCAL VARIATION OF (UHC.) IN 140mm COMBUSTOR, CENTRE LINE, USING SWIRLER(B) WITH CENTRAL INJECTION NG & P, 600K.

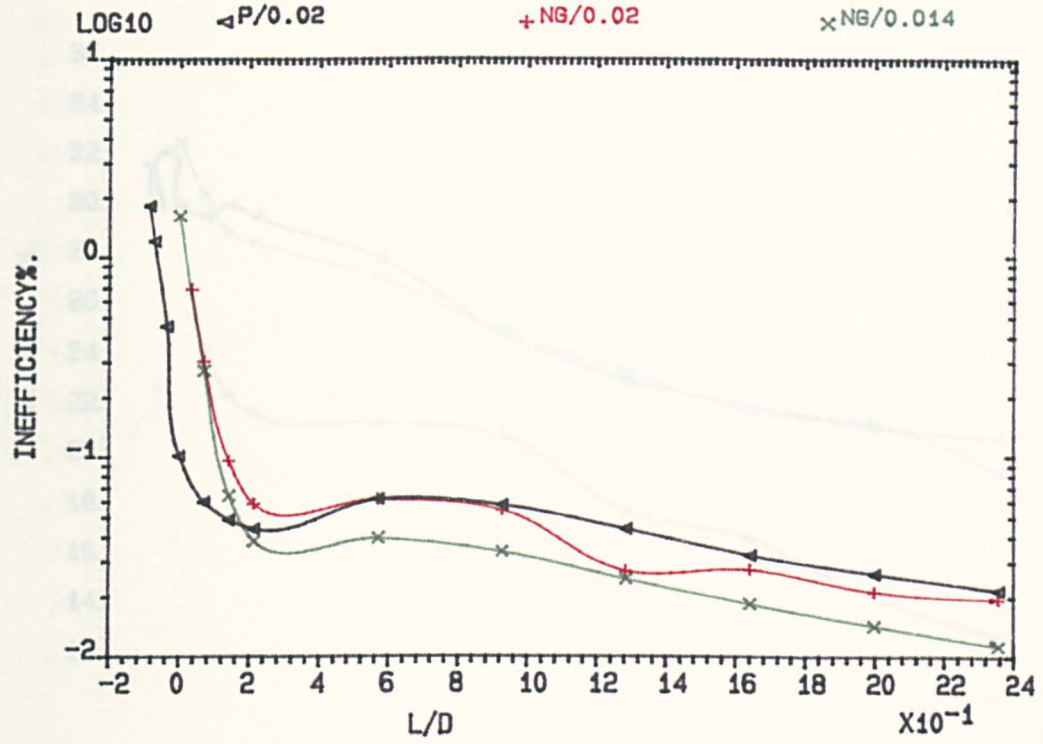

FIG.3.47 LOCAL VARIATION OF INEFFICIENCY% IN 140mm COMBUSTOR, CENTRE LINE, USING SWIRLER (B) WITH CENTRAL INJECTION NG & P, 600K.

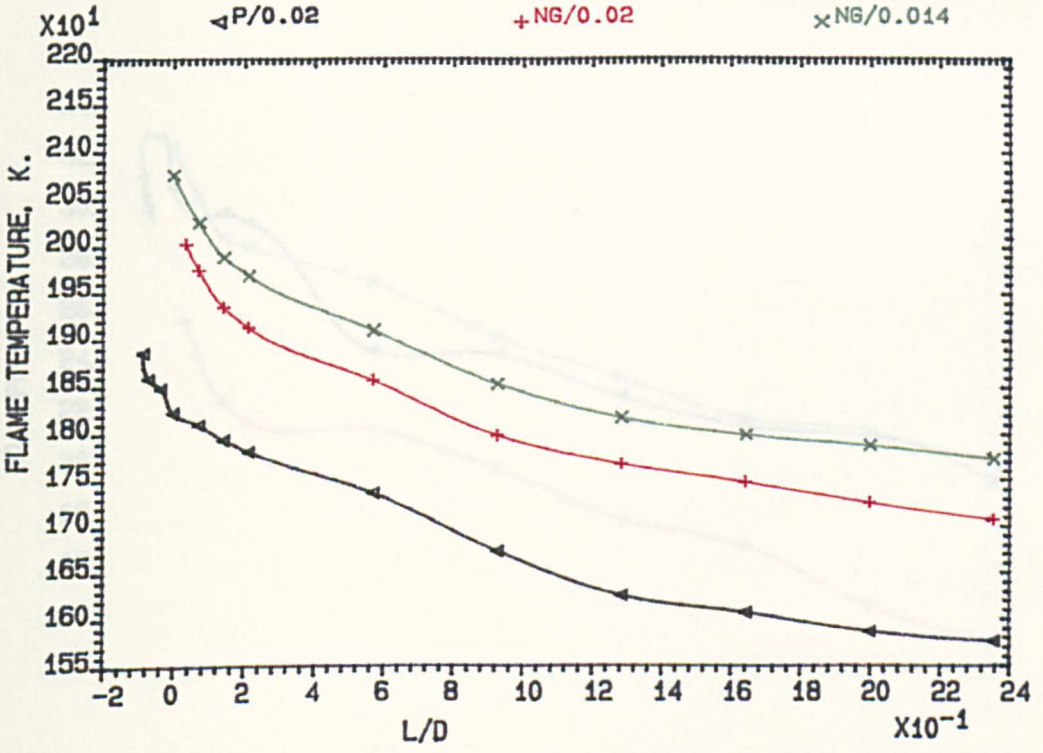

FIG.3.48 LOCAL VARIATION OF FLAME TEMPERATURE IN 140mm COMBUSTOR, CENTRE LINE, USING SWIRLER (B) WITH CENTRAL INJECTION NG & P, 600K.

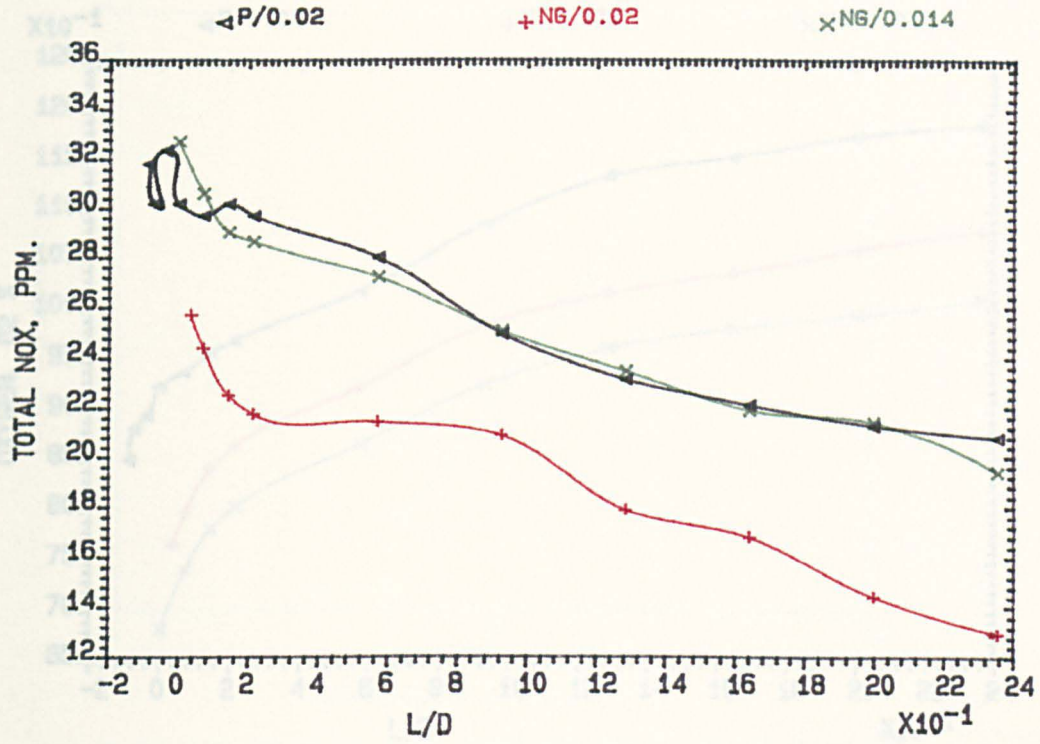

FIG.3.49 LOCAL VARIATION OF TOTAL (NOX) IN 140mm COMBUSTOR, CENTRE LINE, USING SWIRLER (B) WITH CENTRAL INJECTION NG & P, 600K.

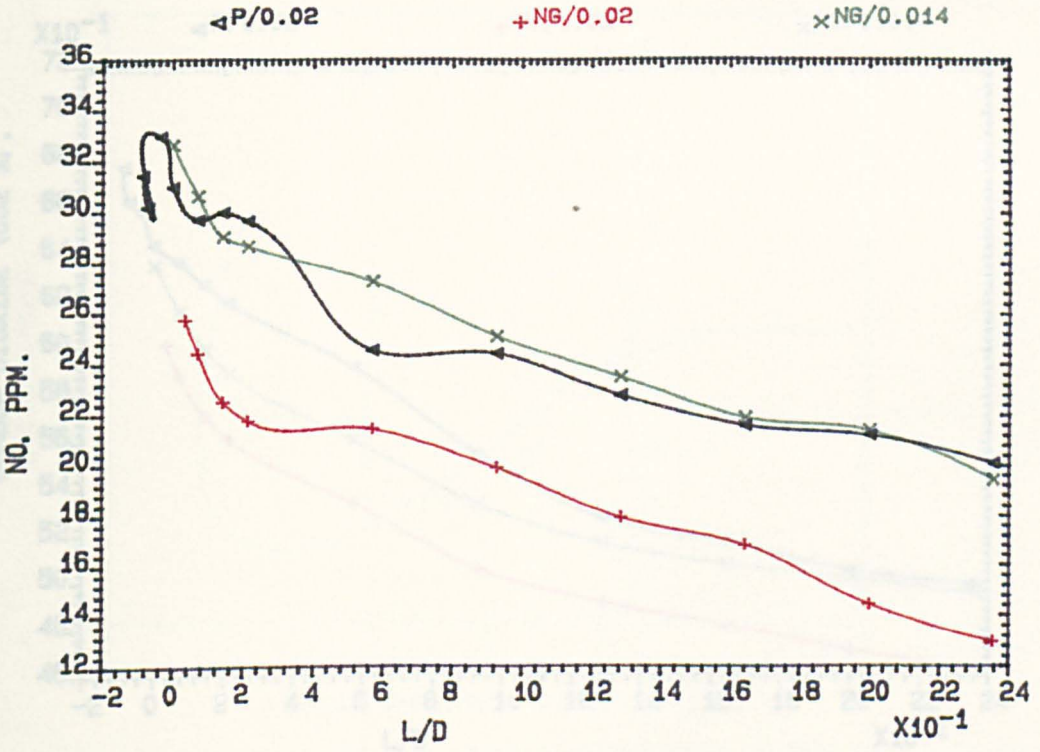

FIG.3.50 LOCAL VARIATION OF NITRIC OXIDE (NO) IN 140mm COMBUSTOR, CENTRE LINE, USING SWIRLER (B) WITH CENTRAL INJECTION NG & P, 600K.

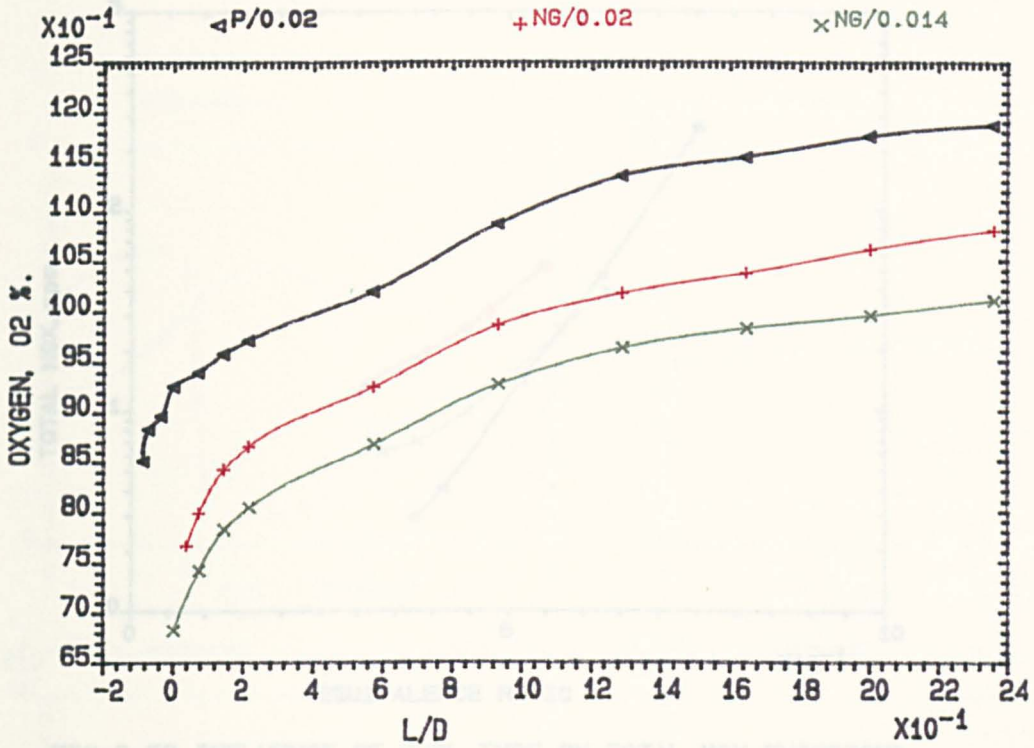

FIG.3.51 LOCAL VARIATION OF OXYGEN LEVEL IN 140mm COMBUSTOR, CENTRE LINE, USING SWIRLER (B) WITH CENTRAL INJECTION NG & P, 600K.

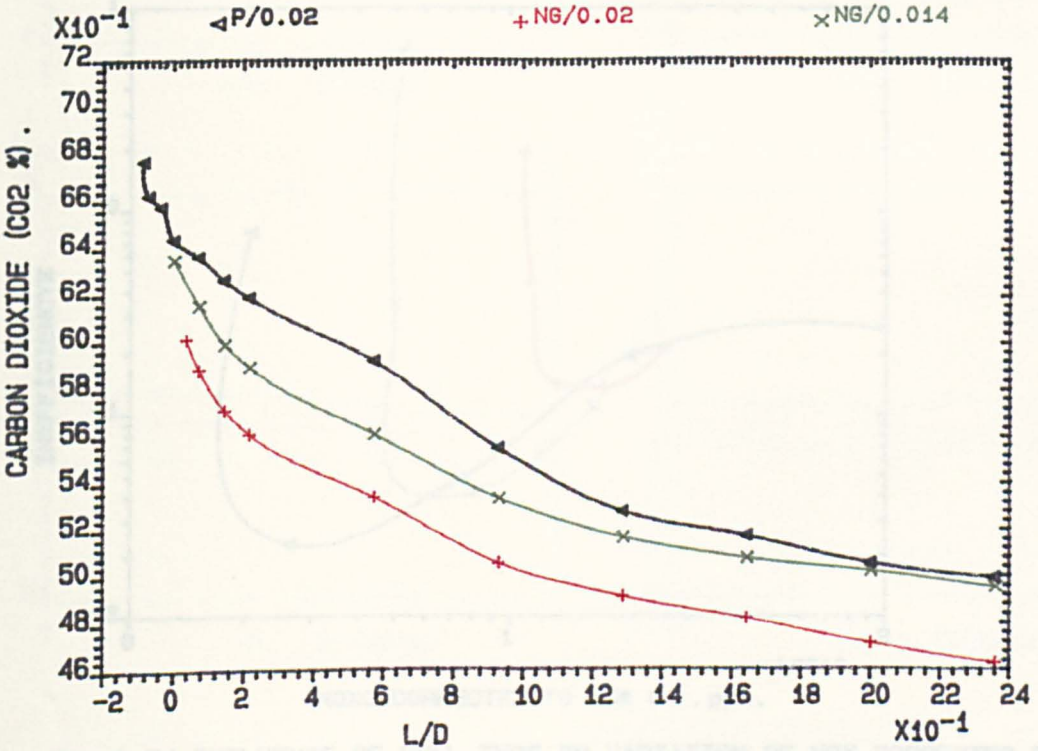

FIG.3.52 LOCAL VARIATION OF CARBON DIOXIDE IN 140mm COMBUSTOR, CENTRE LINE, USING SWIRLER (B) WITH CENTRAL INJECTION NG & P, 600K.

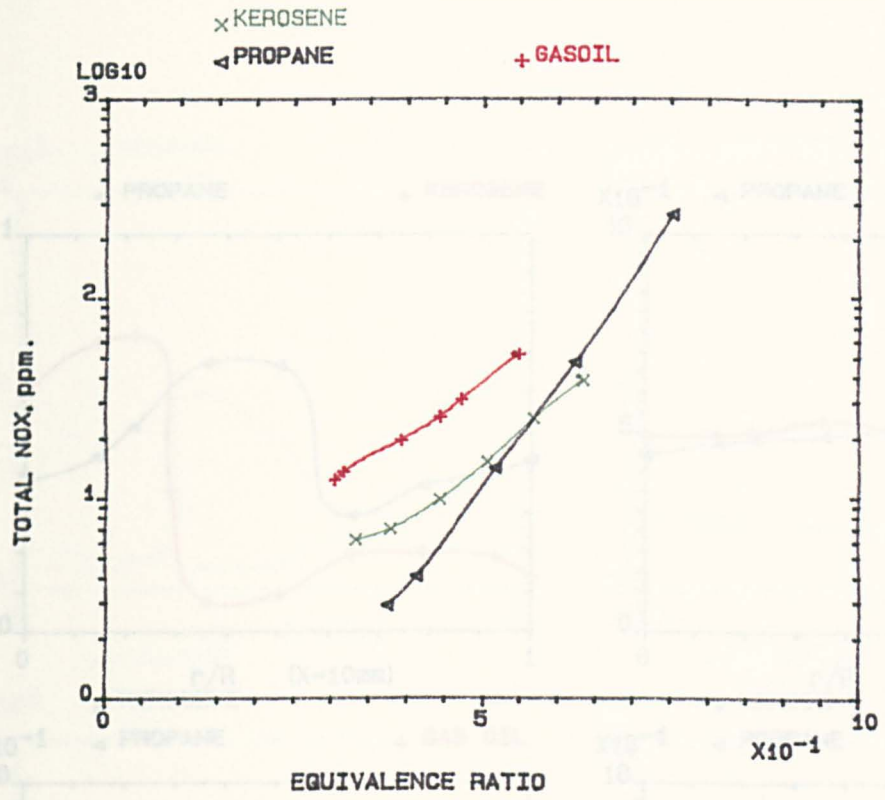

FIG.3.53 INFLUENCE OF FUEL TYPE ON TOTAL NOX EMISSIONS, RADIAL SWIRLER (B) WITH PASSAGES INJECTION IN 140mm COMBUSTOR, FOR MN=0.02 AND TIN=600 K.

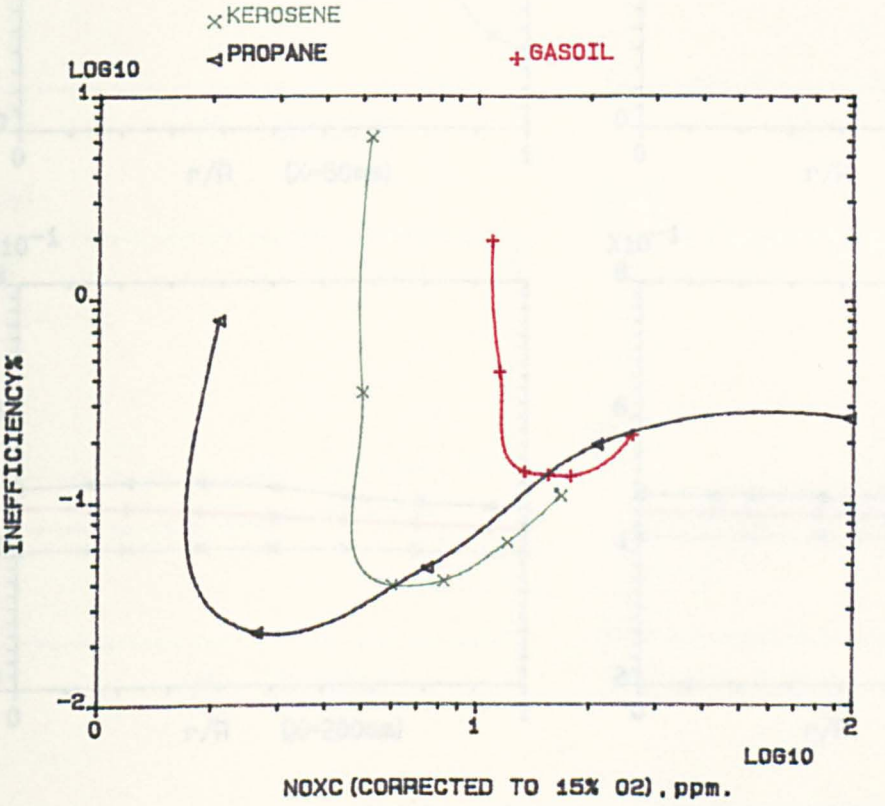

FIG.3.54 INFLUENCE OF FUEL TYPE ON VARIATION OF NOX CORRECTED TO 15% OXYGEN WITH COMBUSTION INEFFICIENCY FOR RADIAL SWIRLER (B) IN 140mm COMBUSTOR, PASSAGES INJECTION, MN=0.02, TIN=600 K.

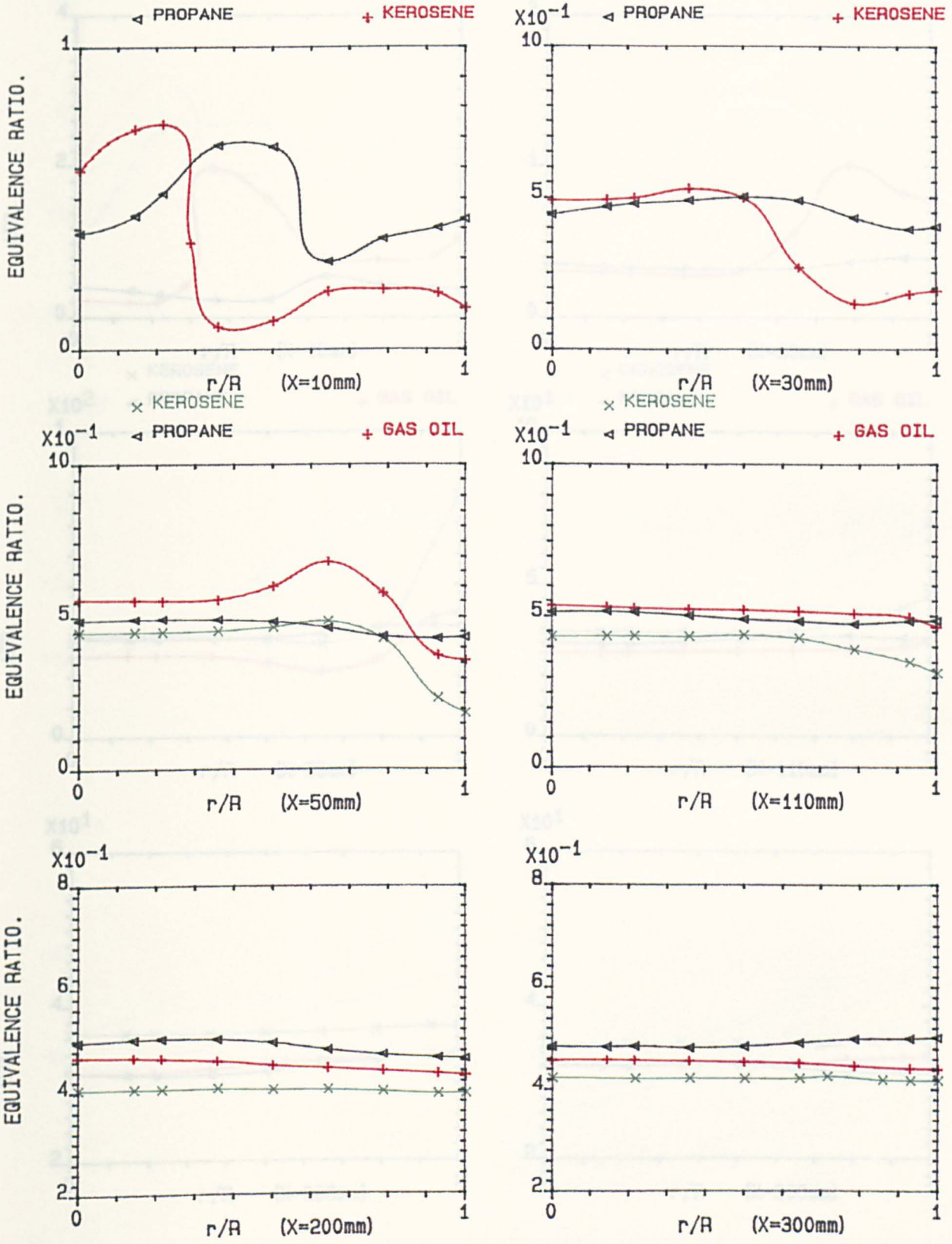

FIG.3.55 LOCAL VARIATION OF EQUIVALENCE RATIO IN SIX AXIAL PLANES, USING PASSAGES INJECTION FOR DIFFERENT FUELS USING SWIRLER(B). IN 140mm COMBUSTOR, MN=0.02, 600 K.

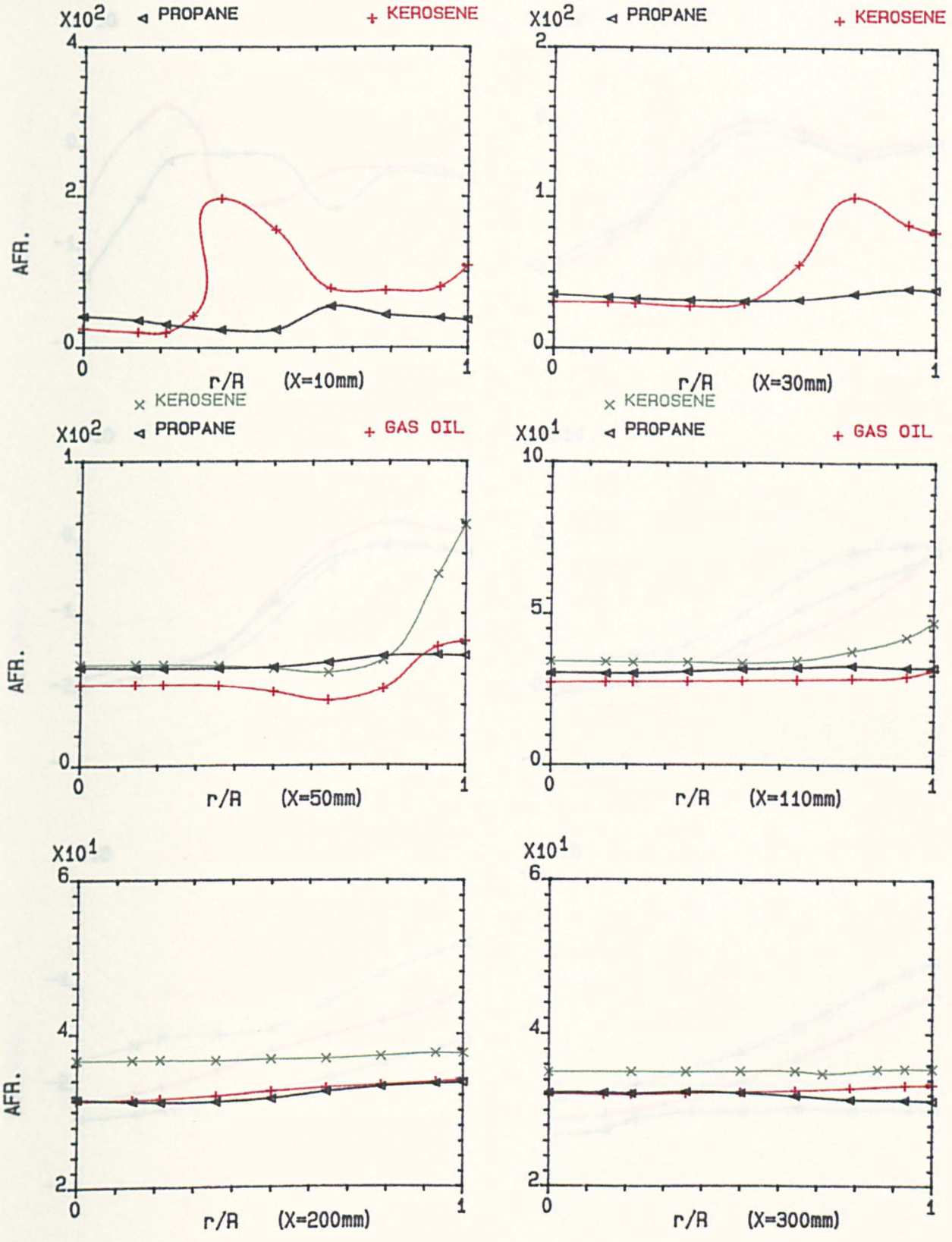

FIG.3.56 LOCAL VARIATION OF (AIR/FUEL) RATIO IN SIX AXIAL PLANES, USING PASSAGES INJECTION FOR DIFFERENT FUELS WITH SWIRLER(B). IN 140mm COMBUSTOR, MN=0.02, 600 K.

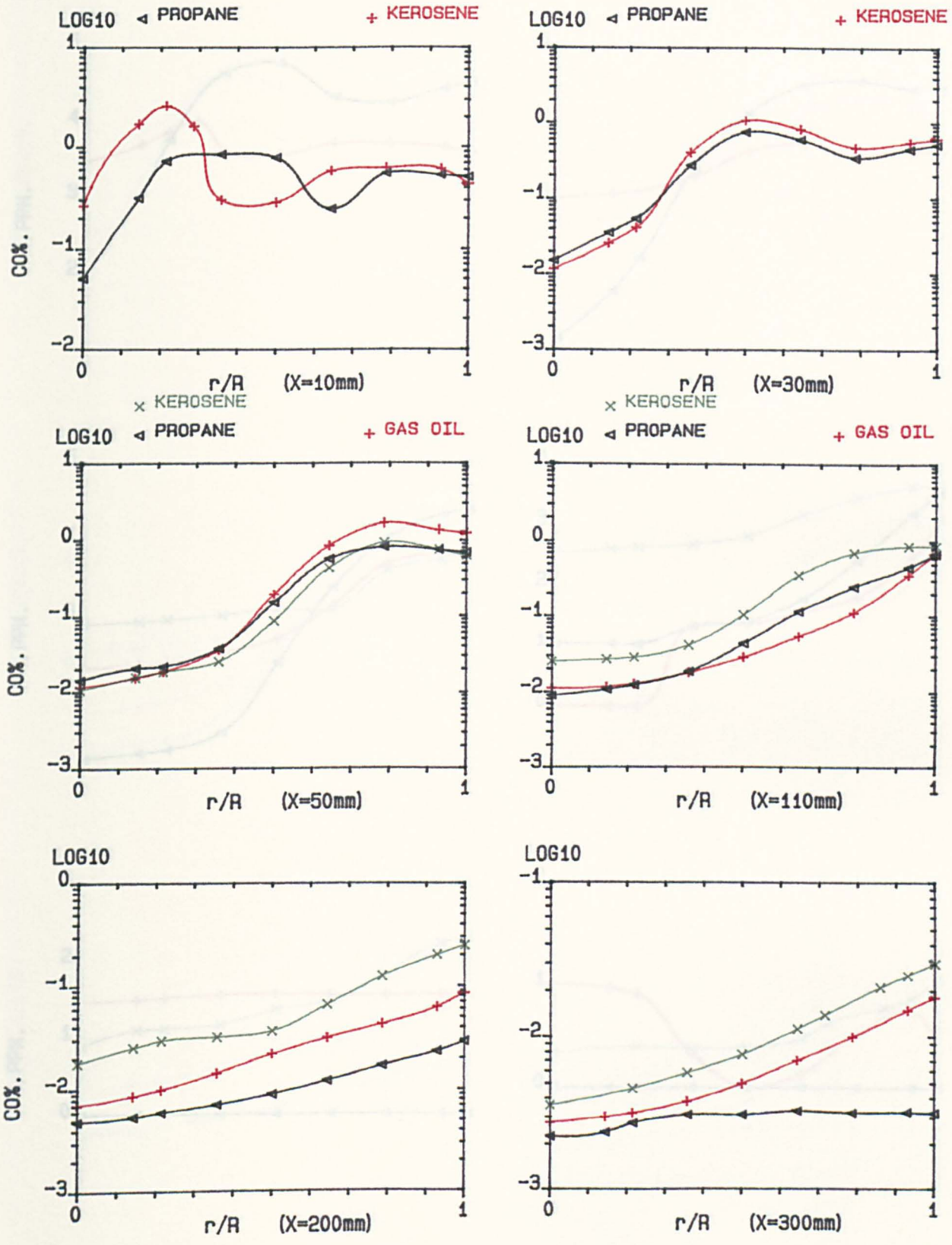

FIG.3.57 LOCAL VARIATION OF CARBON MONOXIDE IN SIX AXIAL PLANES, USING PASSAGES INJECTION FOR DIFFERENT FUELS WITH SWIRLER(B). IN 140mm COMBUSTOR, MN=0.02, 600 K.

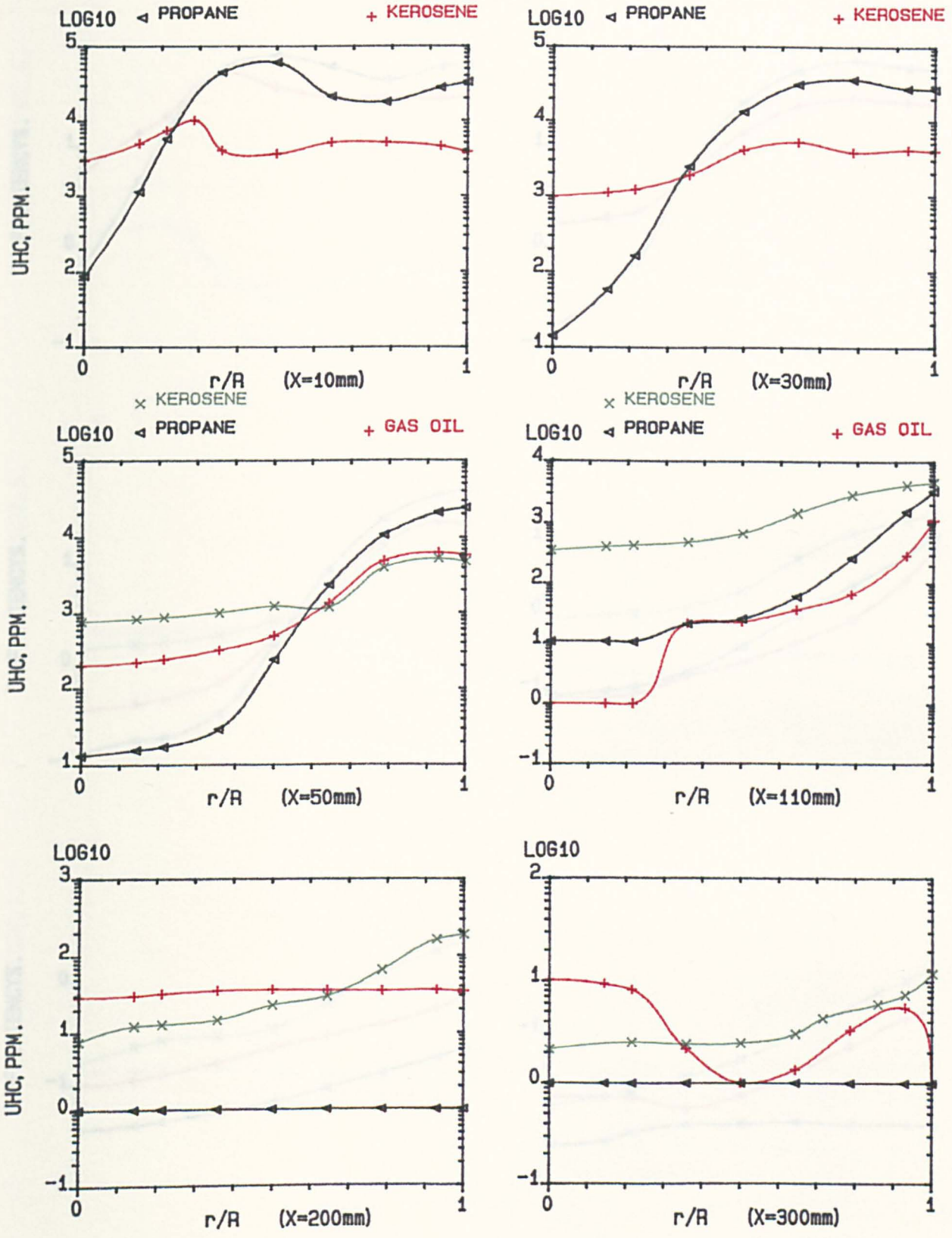

FIG.3.58 LOCAL VARIATION OF UNBURNED HYDROCARBONS IN SIX AXIAL PLANES, USING PASSAGES INJECTION FOR DIFFERENT FUELS WITH SWIRLER(B). IN 140mm COMBUSTOR, MN=0.02, 600 K.

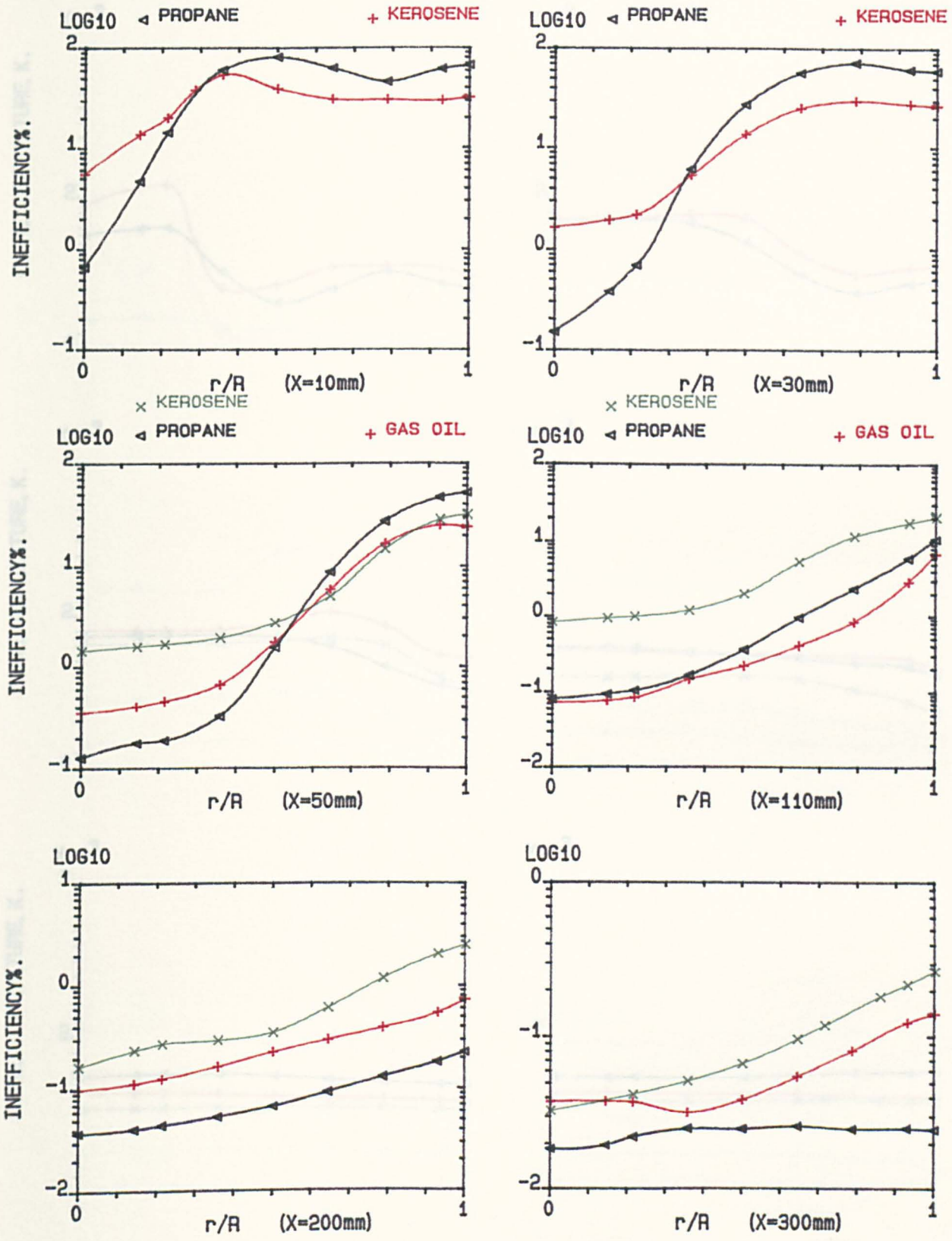

FIG.3.59 LOCAL VARIATION OF COMBUSTION INEFFICIENCY IN SIX AXIAL PLANES, USING PASSAGES INJECTION FOR DIFFERENT FUELS WITH SWIRLER(B), IN 140mm COMBUSTOR, MN=0.02, 600 K.

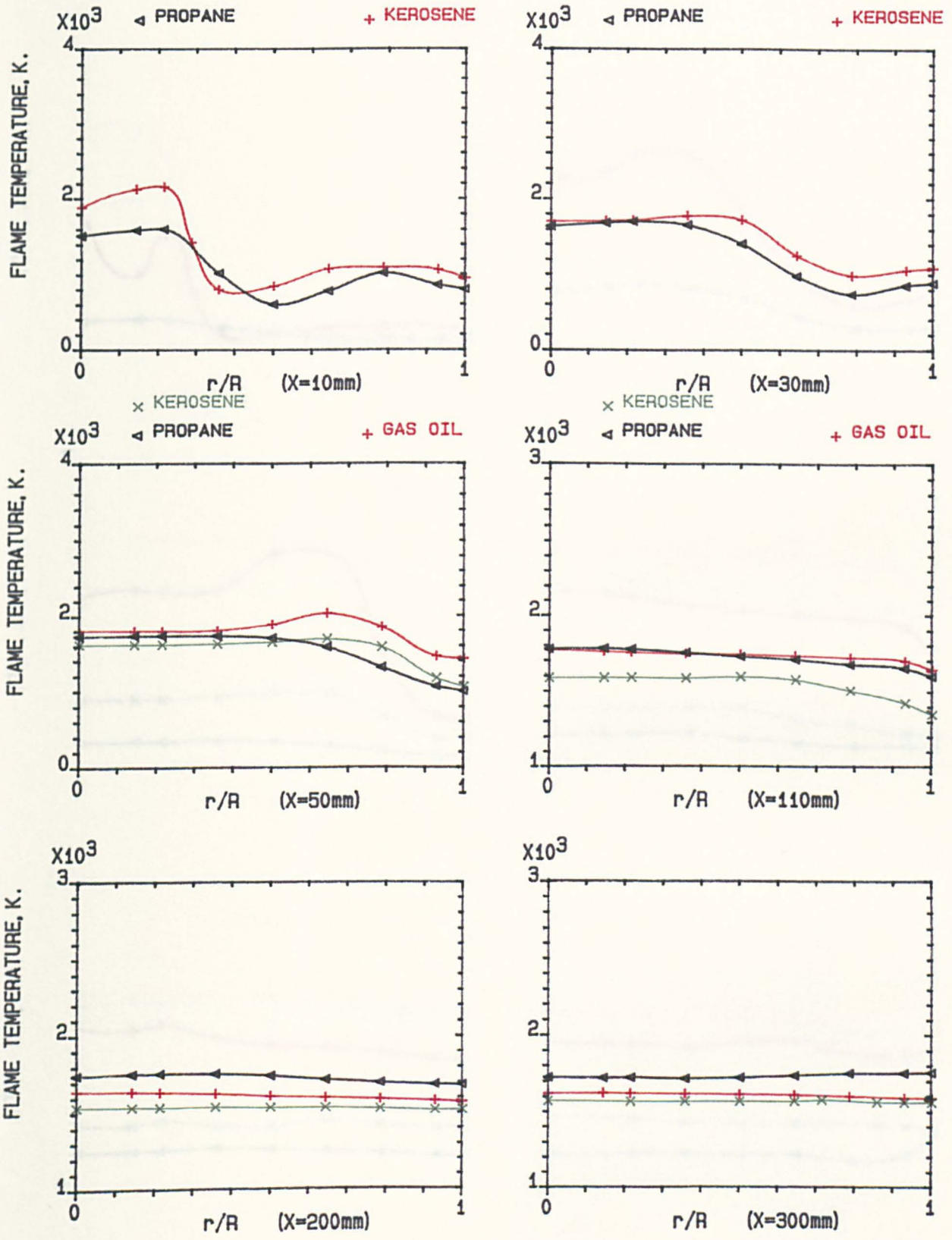

FIG.3.60 LOCAL VARIATION OF FLAME TEMPERATURE IN SIX AXIAL PLANES, USING PASSAGES INJECTION FOR DIFFERENT FUELS WITH SWIRLER (B). IN 140mm COMBUSTOR. MN=0.02. 600 K.

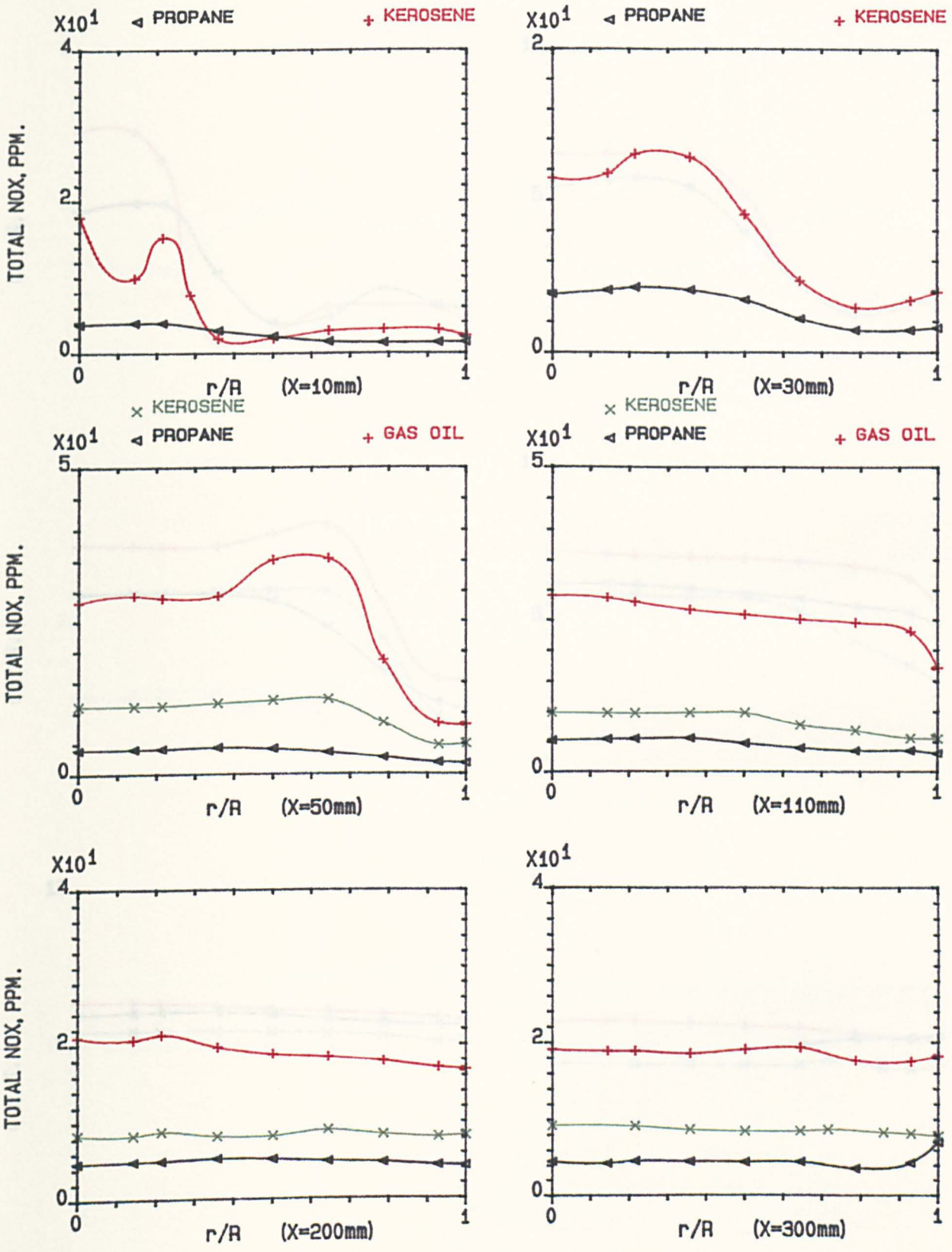

FIG.3.61 LOCAL VARIATION OF TOTAL (NOX) IN SIX AXIAL PLANES, USING PASSAGES INJECTION FOR DIFFERENT FUELS WITH SWIRLER(B). IN 140mm COMBUSTOR. MN=0.02, 600 K.

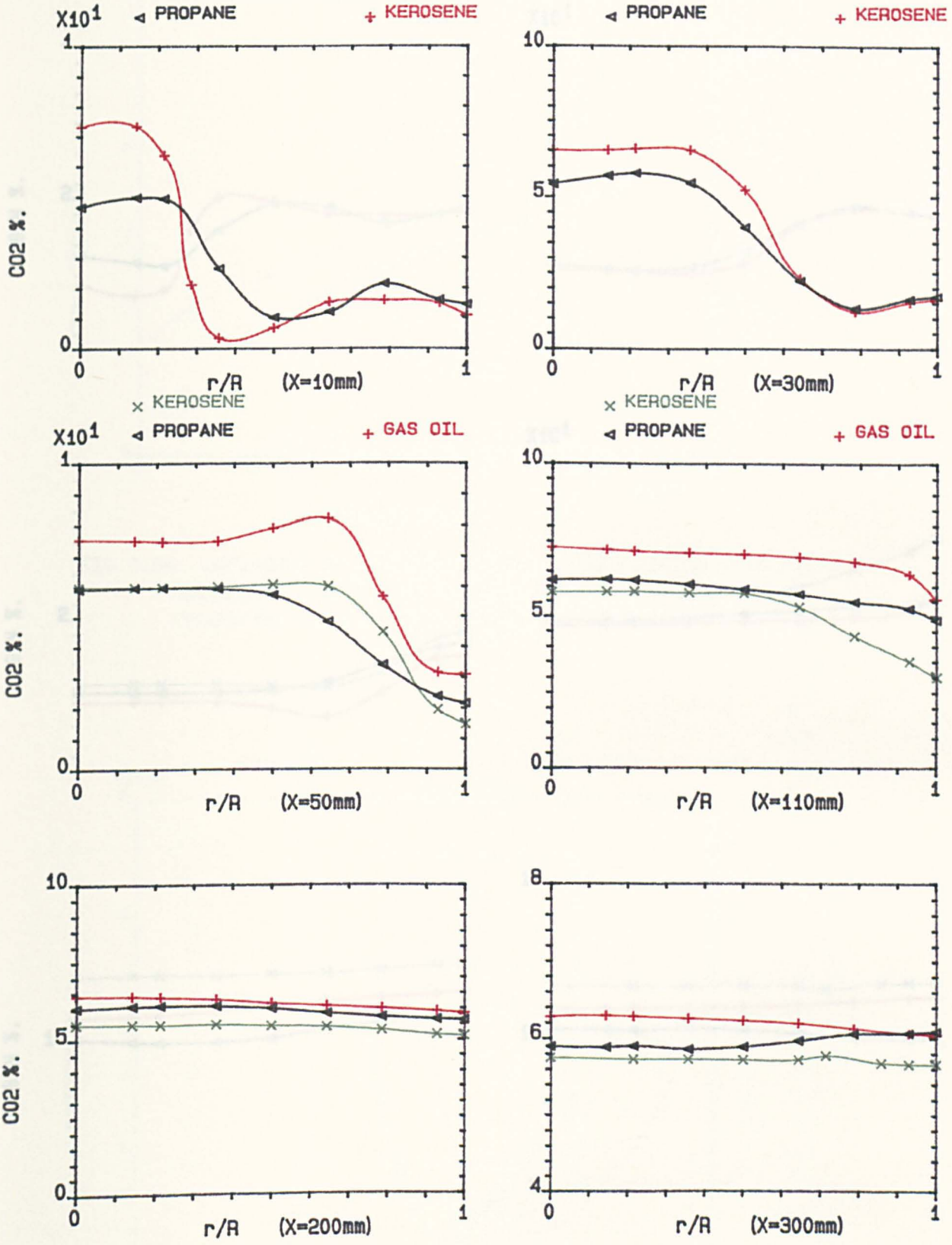

FIG.3.62 LOCAL VARIATION OF CARBON MONOXIDE IN SIX AXIAL PLANES, USING PASSAGES INJECTION FOR DIFFERENT FUELS WITH SWIRLER(B). IN 140mm COMBUSTOR. MN=0.02, 600 K.

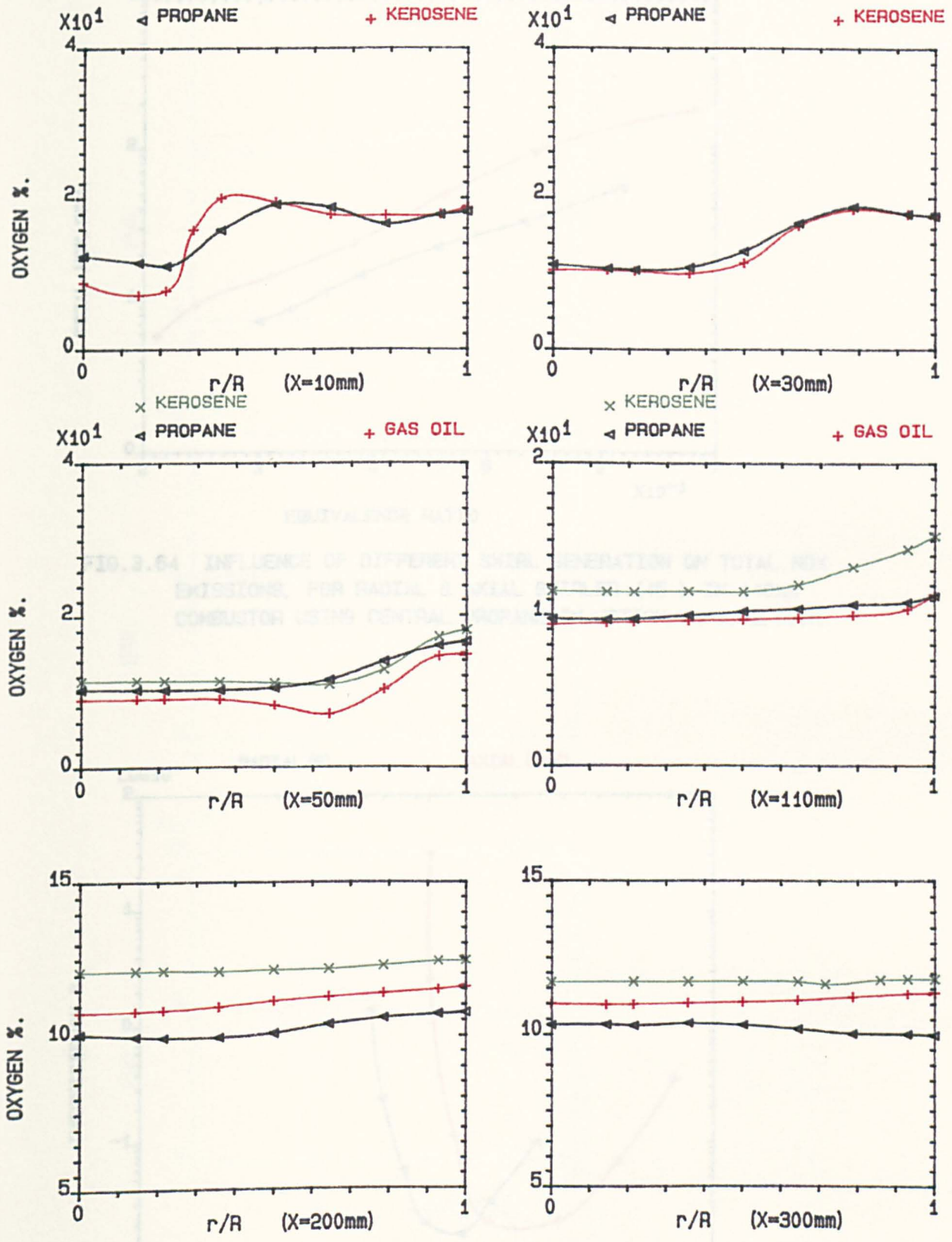

FIG.3.63 LOCAL VARIATION OF OXYGEN CONCENTRATION IN SIX AXIAL PLANES, USING PASSAGES INJECTION FOR DIFFERENT FUELS USING SWIRLER(B). IN 140mm COMBUSTOR, MN=0.02, 600 K.

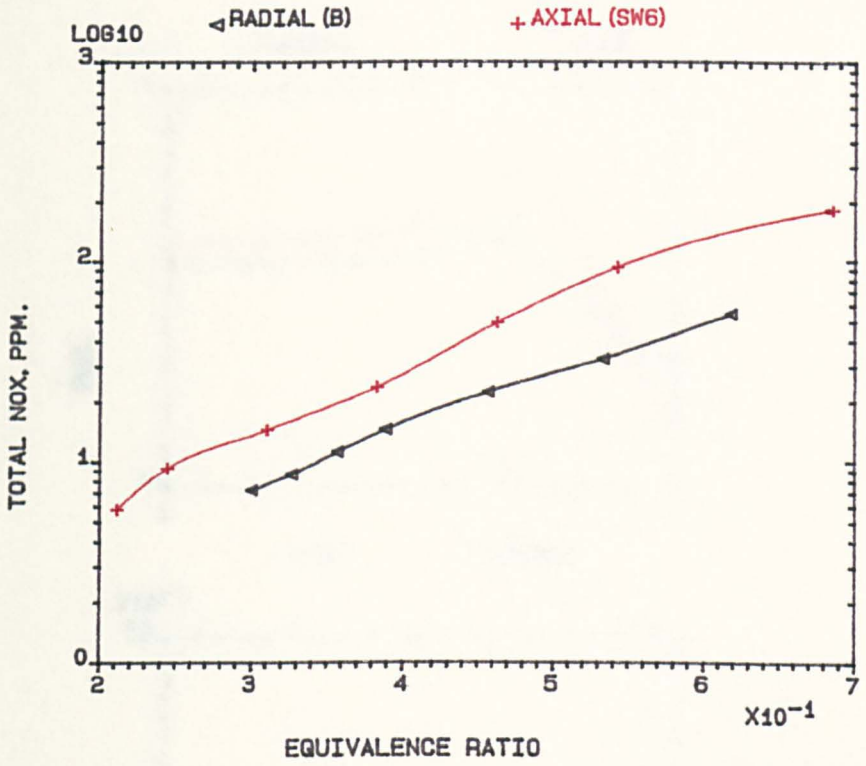

FIG.3.64 INFLUENCE OF DIFFERENT SWIRL GENERATION ON TOTAL NOX EMISSIONS, FOR RADIAL & AXIAL SWIRLER (45) IN 140mm COMBUSTOR USING CENTRAL PROPANE INJECTION, MN=0.02, 600K.

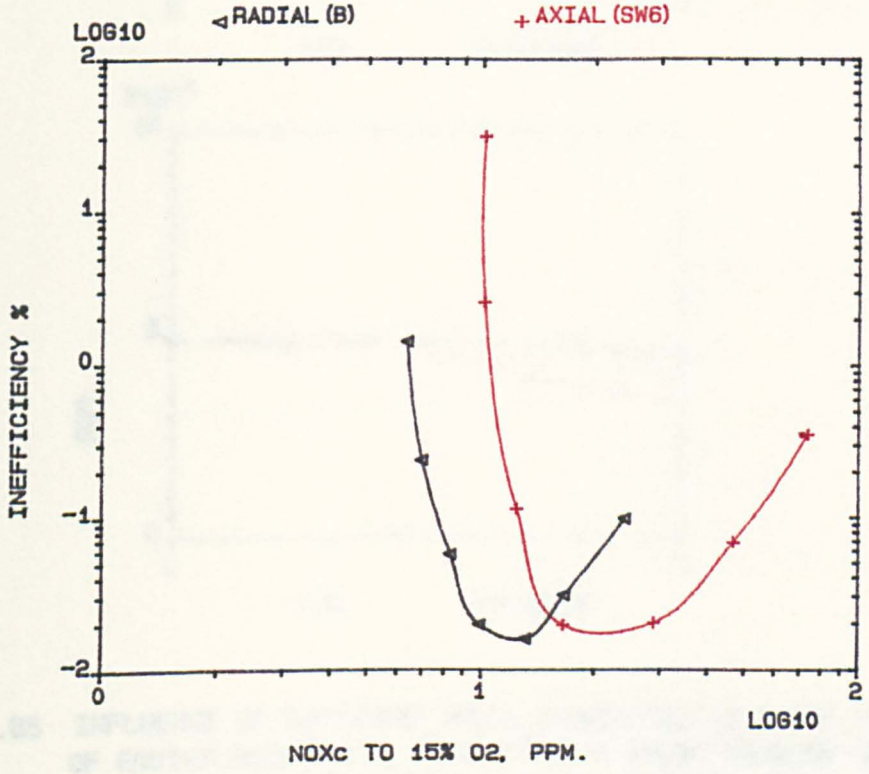

FIG.3.65 INFLUENCE OF SWIRL GENERATION ON VARIATION OF NOX CORRECTED TO 15% (02) WITH INEFFICIENCY FOR RADIAL & AXIAL SWIRLERS IN 140mm COMBUSTOR USING CENTRAL PROPANE INJECTION, MN=0.02, 600K.

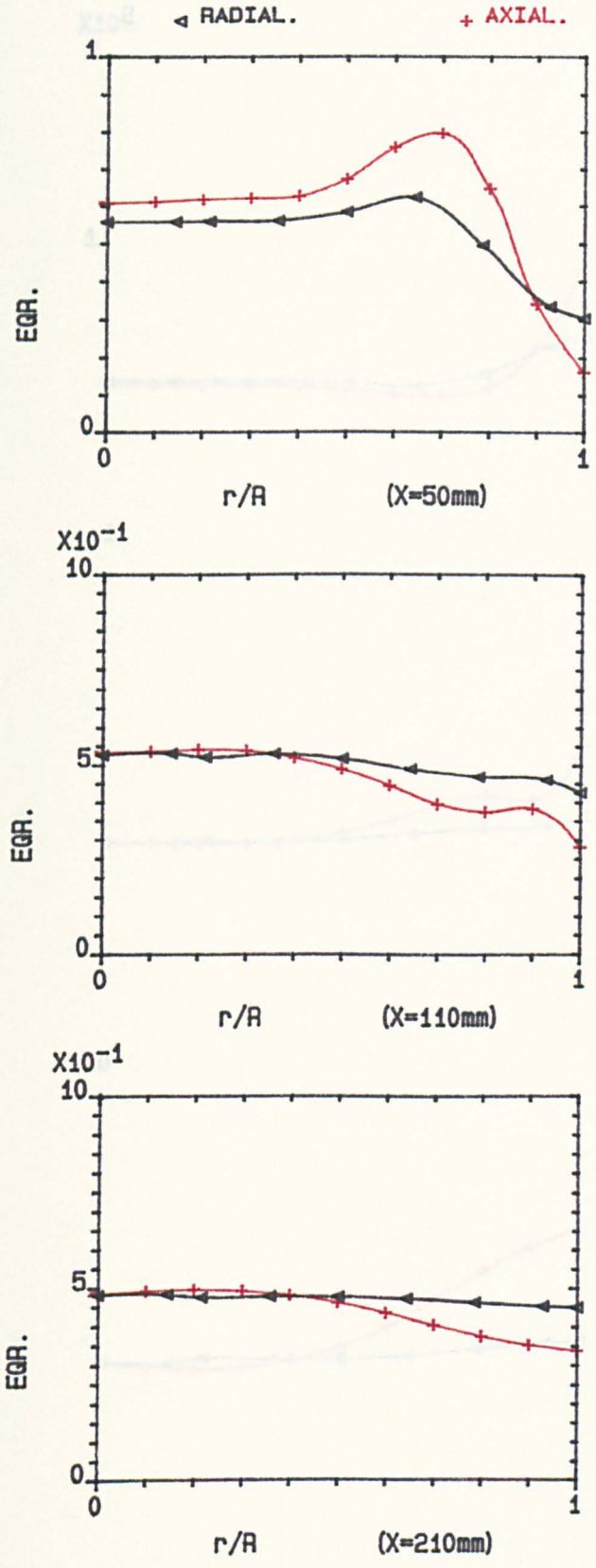

FIG.3.66 INFLUENCE OF DIFFERENT SWIRL GENERATION ON LOCAL VARIATION OF EQUIVALENCE RATIO, FOR RADIAL & AXIAL SWIRLER (45) IN 140mm COMBUSTOR, USING CENTRAL PROPANE INJECTION, MN=0.02, 600K.

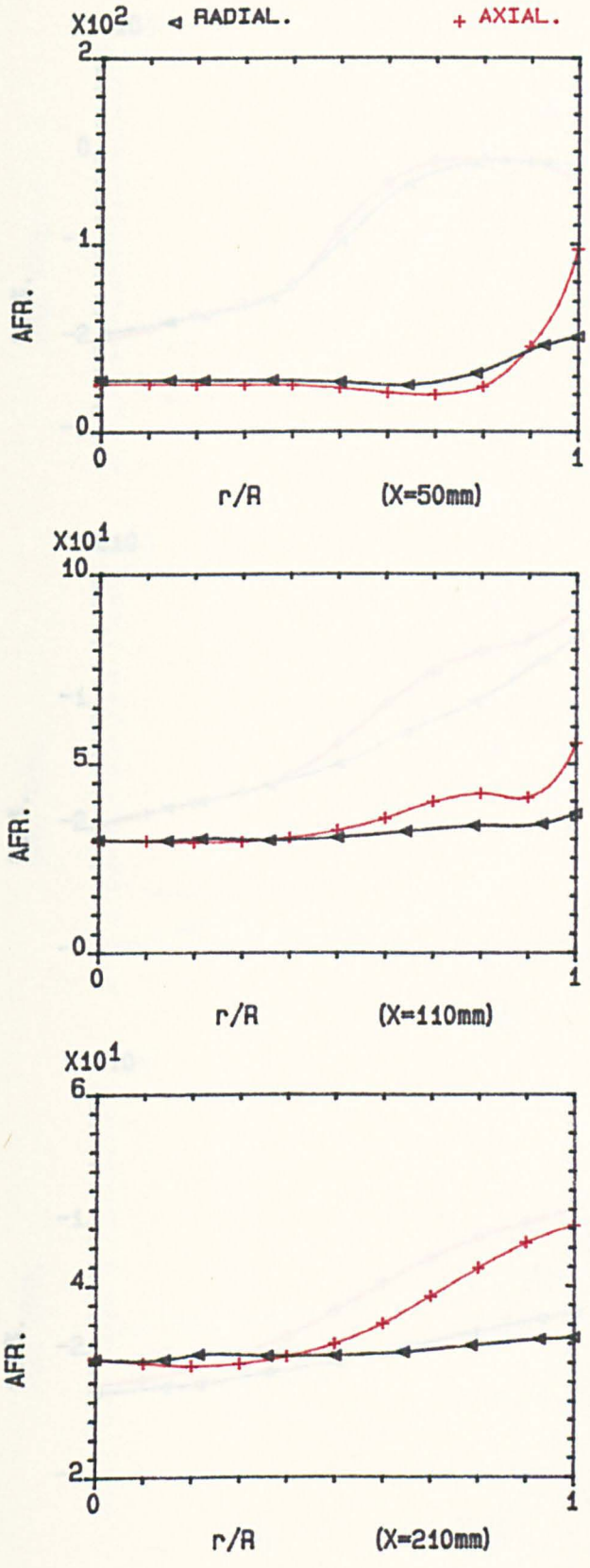

FIG.3.67 INFLUENCE OF DIFFERENT SWIRL GENERATION ON LOCAL VARIATION OF (AIR/FUEL) RATIO. FOR RADIAL & AXIAL SWIRLER (45) IN 140mm COMBUSTOR, USING CENTRAL PROPANE INJECTION. MN=0.02. 600K.

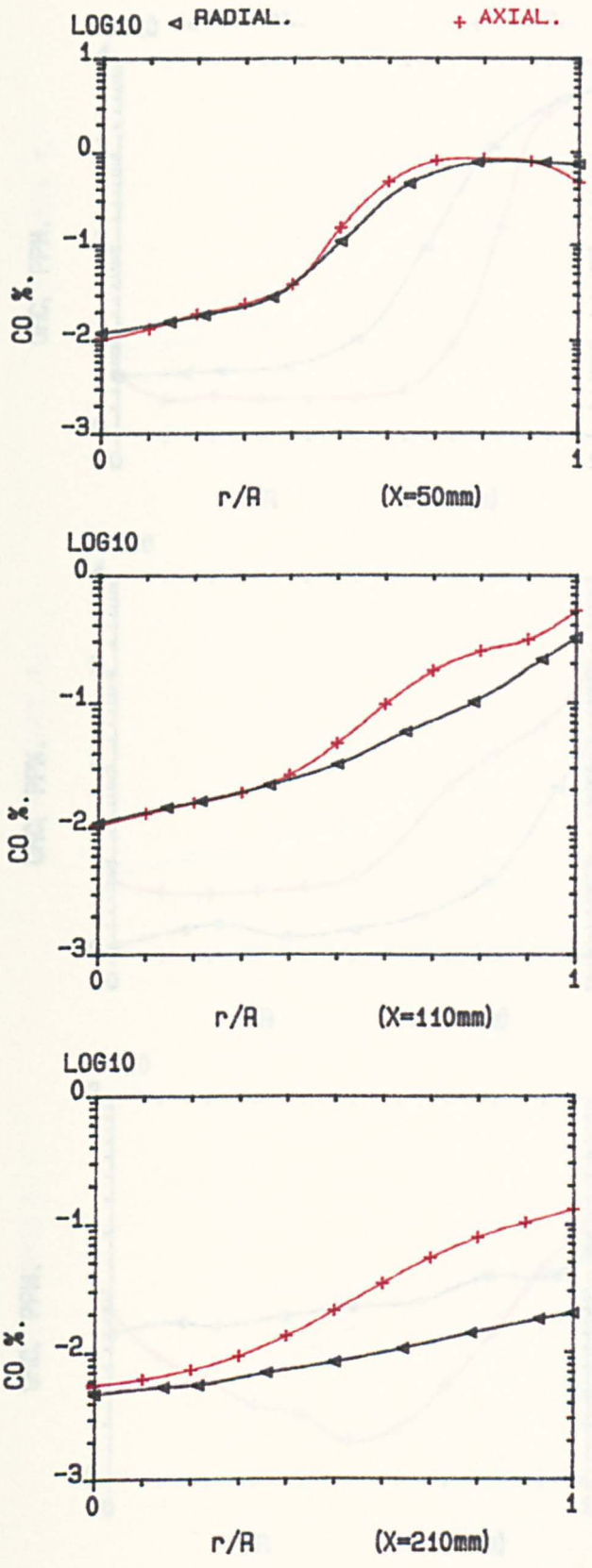

FIG.3.68 INFLUENCE OF DIFFERENT SWIRL GENERATION ON LOCAL VARIATION OF CARBON MONOXIDE, FOR RADIAL & AXIAL SWIRLER (45) IN 140mm COMBUSTOR, USING CENTRAL PROPANE INJECTION, MN=0.02, 600K.

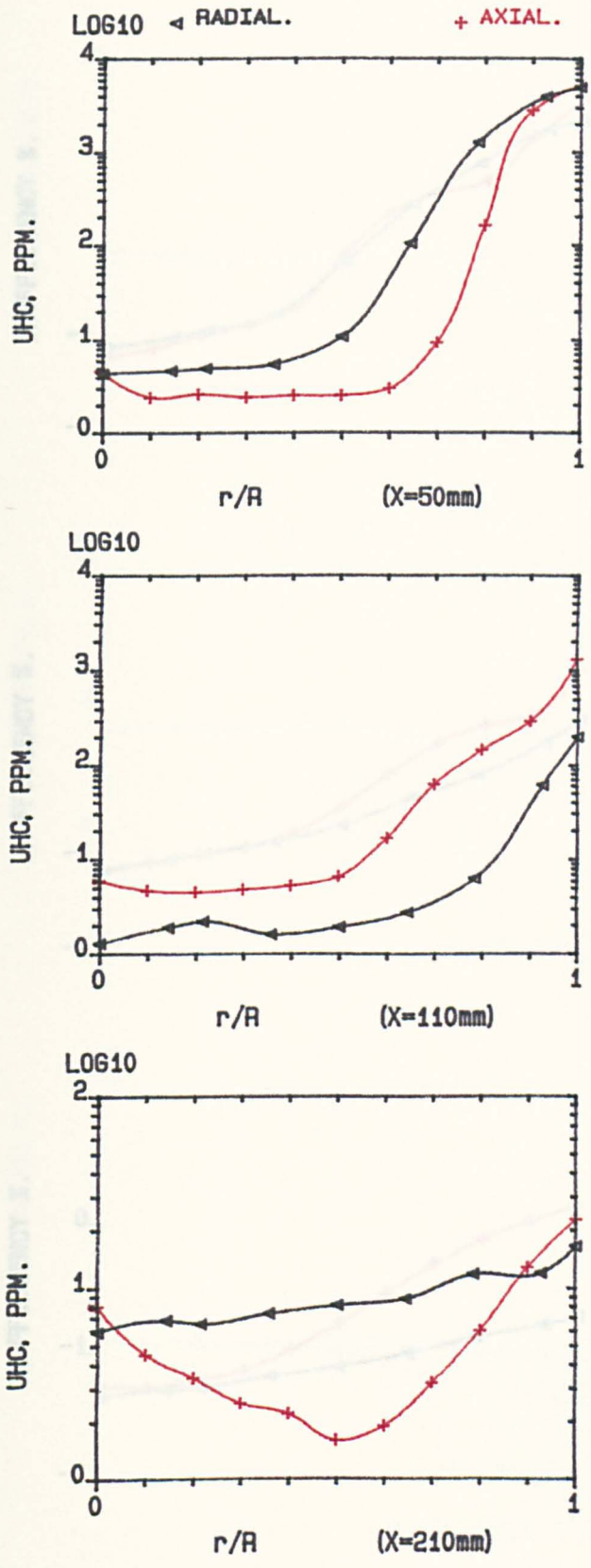

FIG.3.69 INFLUENCE OF DIFFERENT SWIRL GENERATION ON LOCAL VARIATION OF UNBURNED HYDROCARBONS, FOR RADIAL & AXIAL SWIRLER (45) IN 140mm COMBUSTOR, USING CENTRAL PROPANE INJECTION, MN=0.02, 600K.

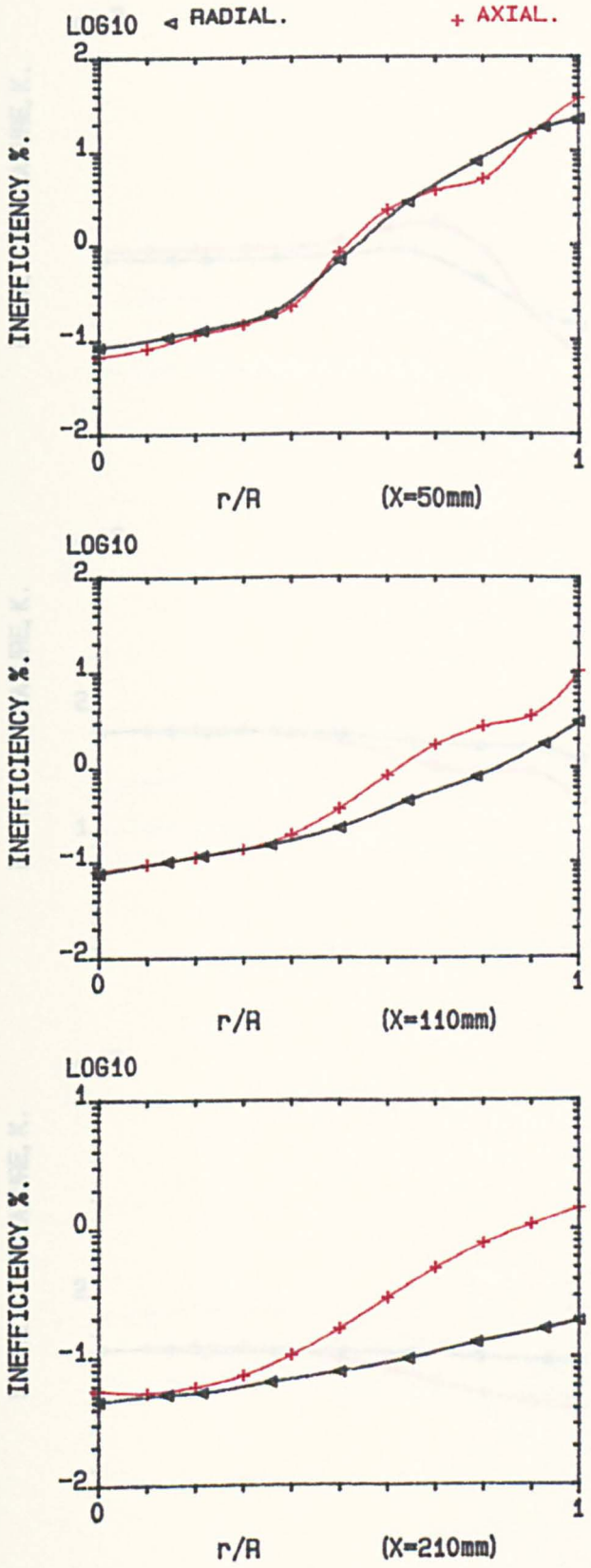

FIG.3.70 INFLUENCE OF DIFFERENT SWIRL GENERATION ON LOCAL VARIATION OF COMBUSTION INEFFICIENCY, FOR RADIAL & AXIAL SWIRLER (45) IN 140mm COMBUSTOR, USING CENTRAL PROPANE INJECTION, MN=0.02, 600K.

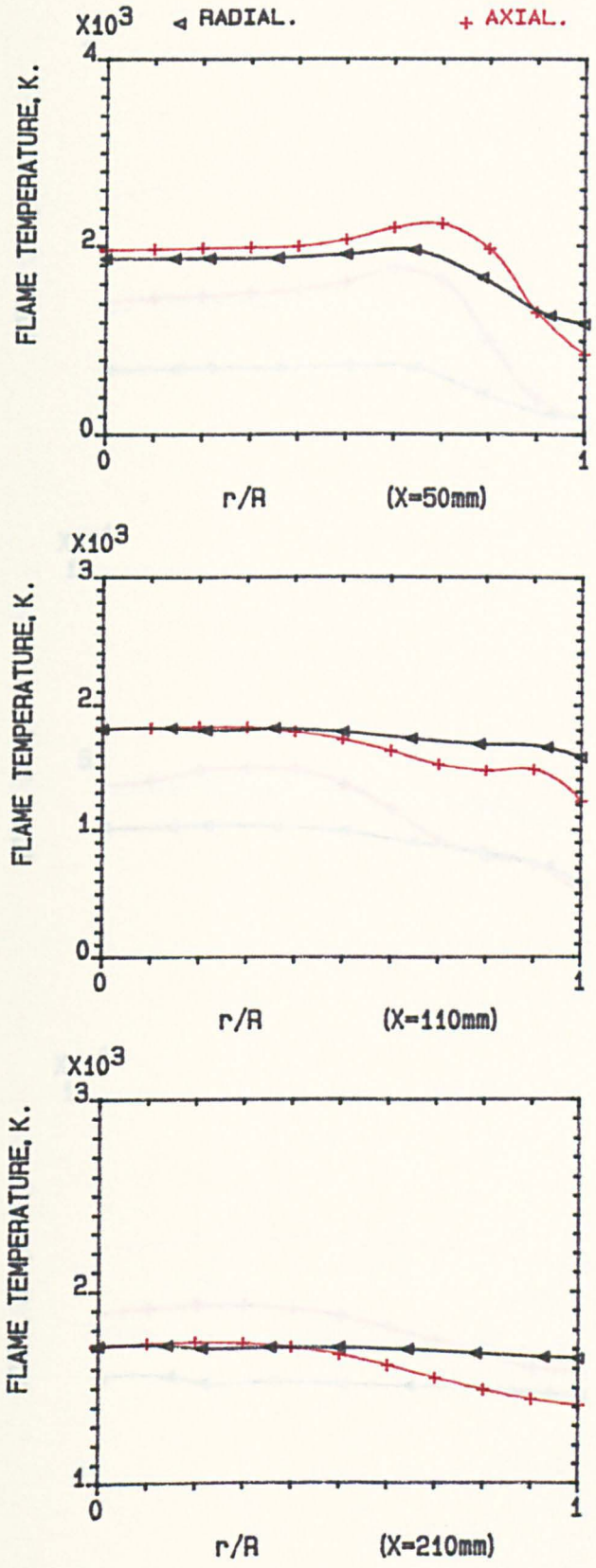

FIG.3.71 INFLUENCE OF DIFFERENT SWIRL GENERATION ON LOCAL VARIATION OF FLAME TEMPERATURE, FOR RADIAL & AXIAL SWIRLER (45) IN 140mm COMBUSTOR, USING CENTRAL PROPANE INJECTION, MN=0.02, 600K.

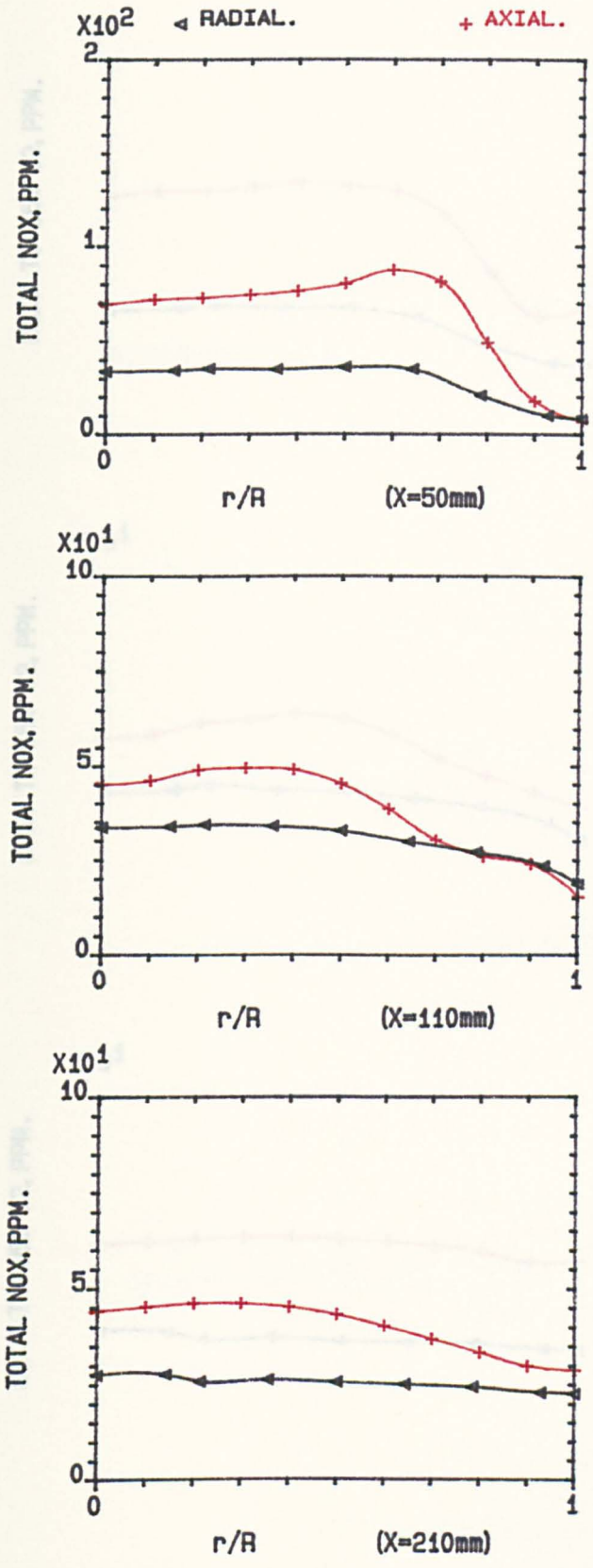

FIG.3.72 INFLUENCE OF DIFFERENT SWIRL GENERATION ON LOCAL VARIATION OF TOTAL (NOX), FOR RADIAL & AXIAL SWIRLER (45) IN 140mm COMBUSTOR, USING CENTRAL PROPANE INJECTION, MN=0.02, 600K.

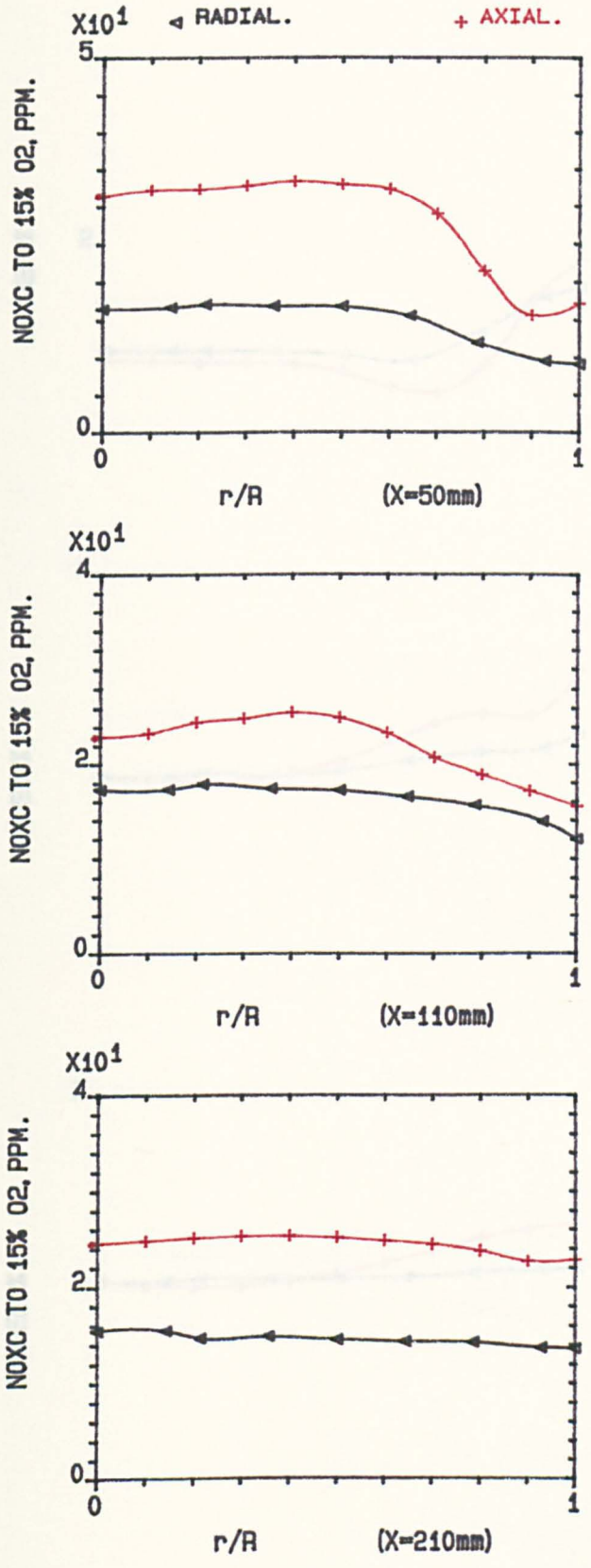

FIG.3.73 INFLUENCE OF DIFFERENT SWIRL GENERATION ON LOCAL VARIATION OF NOX (CORRECTED TO 15% OXYGEN). FOR RADIAL & AXIAL SWIRLER (45) IN 140mm COMBUSTOR. USING CENTRAL PROPANE INJECTION. MN=0.02, 600K.

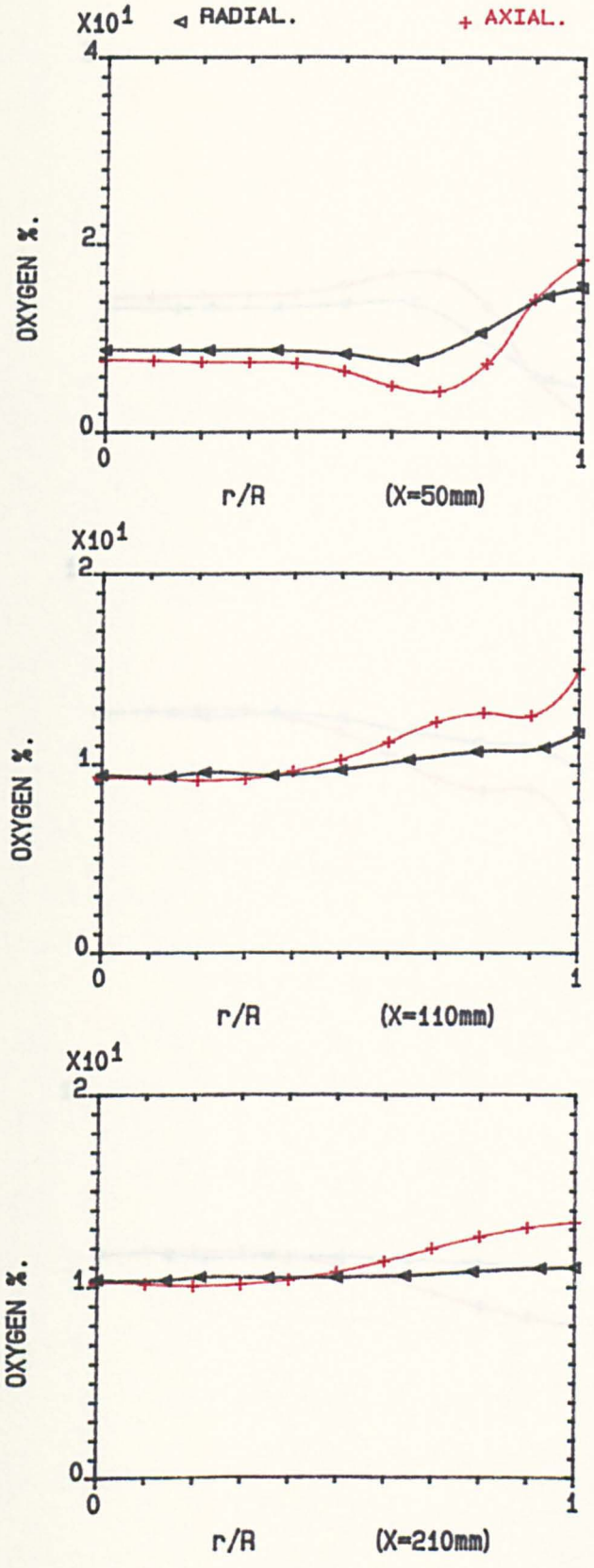

FIG.3.74 INFLUENCE OF DIFFERENT SWIRL GENERATION ON LOCAL VARIATION OF OXYGEN CONCENTRATION, FOR RADIAL & AXIAL SWIRLER (45) IN 140mm COMBUSTOR, USING CENTRAL PROPANE INJECTION, MN=0.02, 600K.

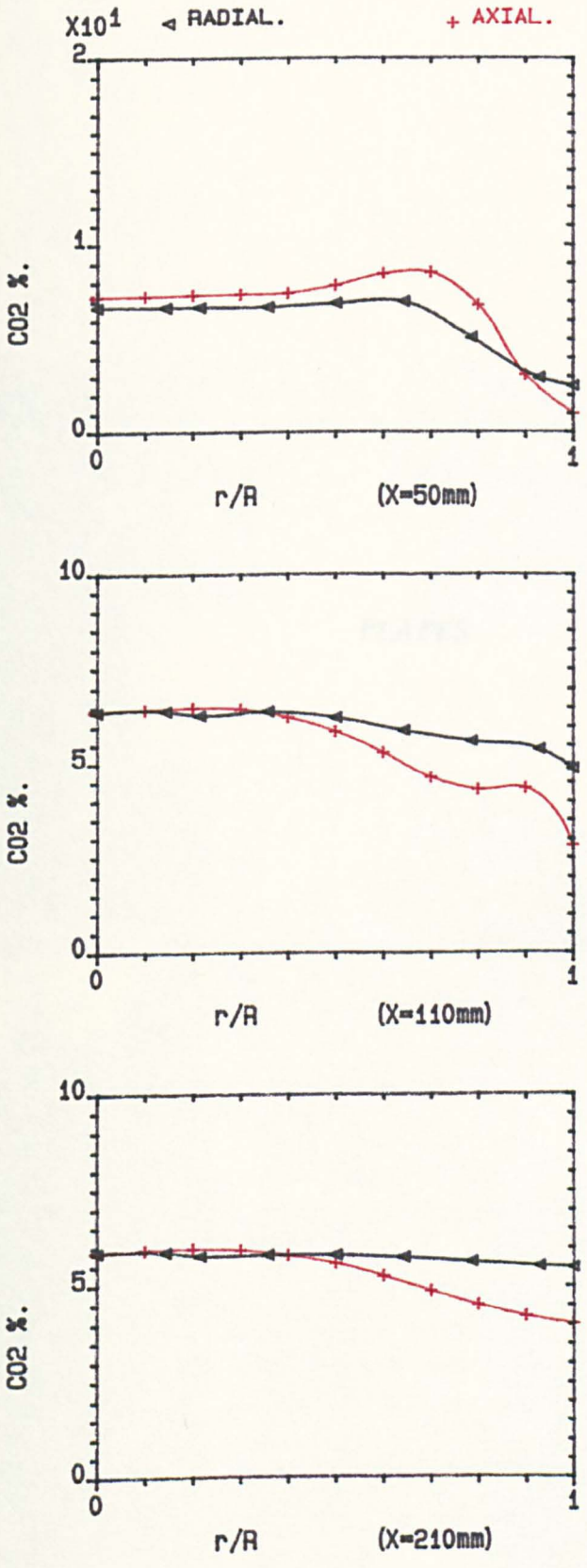

FIG.3.75 INFLUENCE OF DIFFERENT SWIRL GENERATION ON LOCAL VARIATION OF CARBON DIOXIDE, FOR RADIAL & AXIAL SWIRLER (45) IN 140mm COMBUSTOR, USING CENTRAL PROPANE INJECTION, MN=0.02, 600K.

PLATES

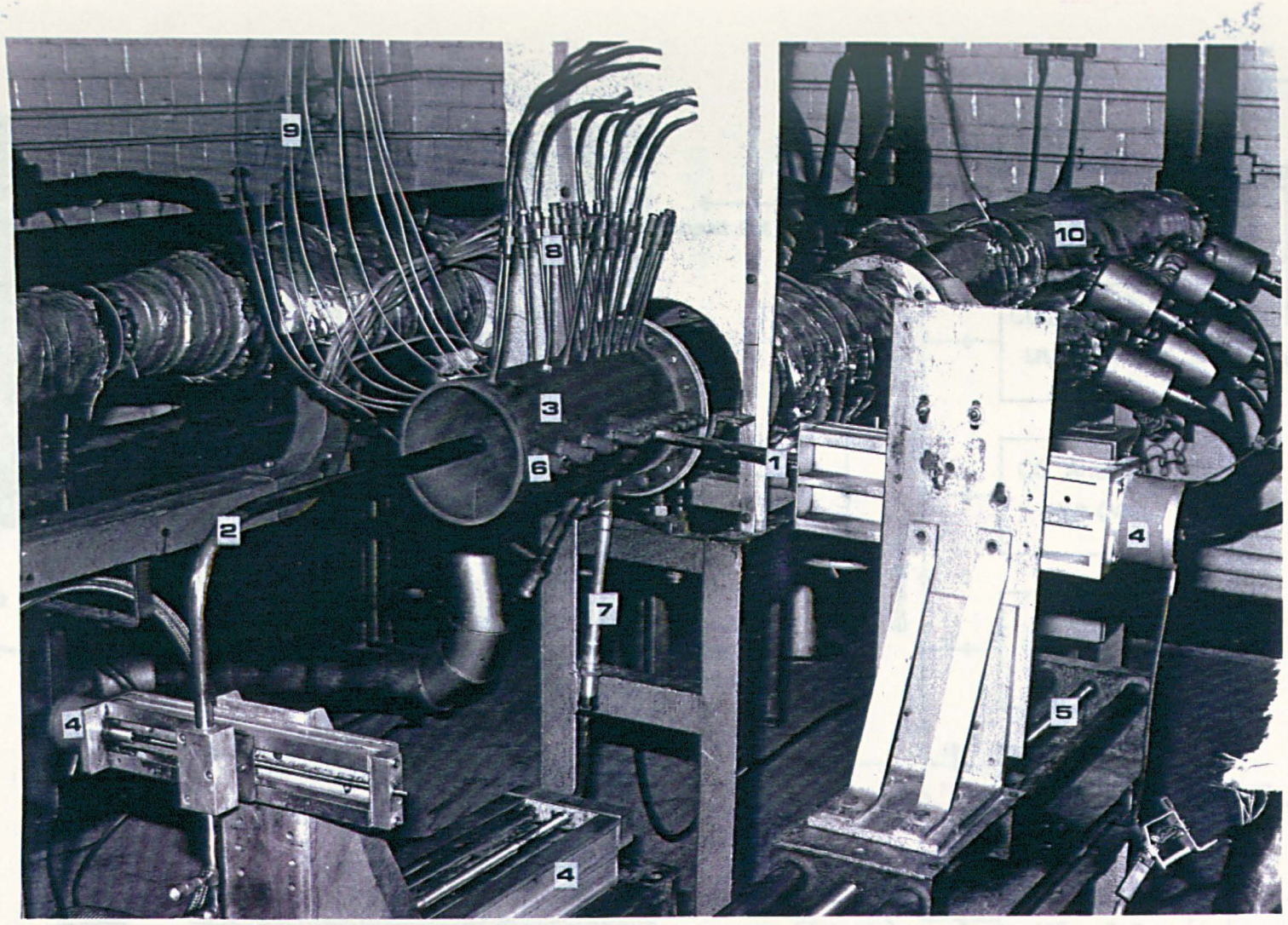

1- Radial traverse probe.
2- Axial traverse probe.
3- 140mm combustor.
4- Automated feed motors.
5- Manual feed traverse.
6- Radial ports.
7- Igniters.
8- Static pressure taps.
9- Thermocouples.
10- Electric air preheater.

Plate 3.1 Internal Traverse Probes With The Test Rig.

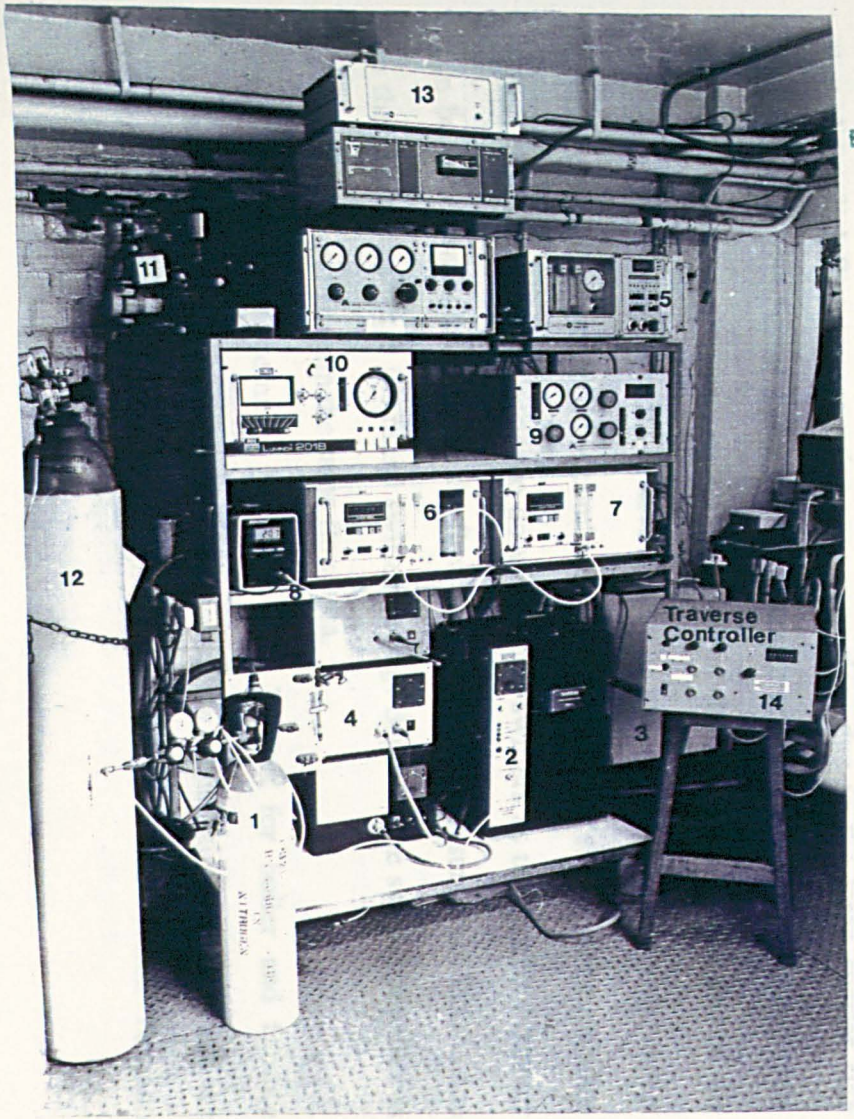

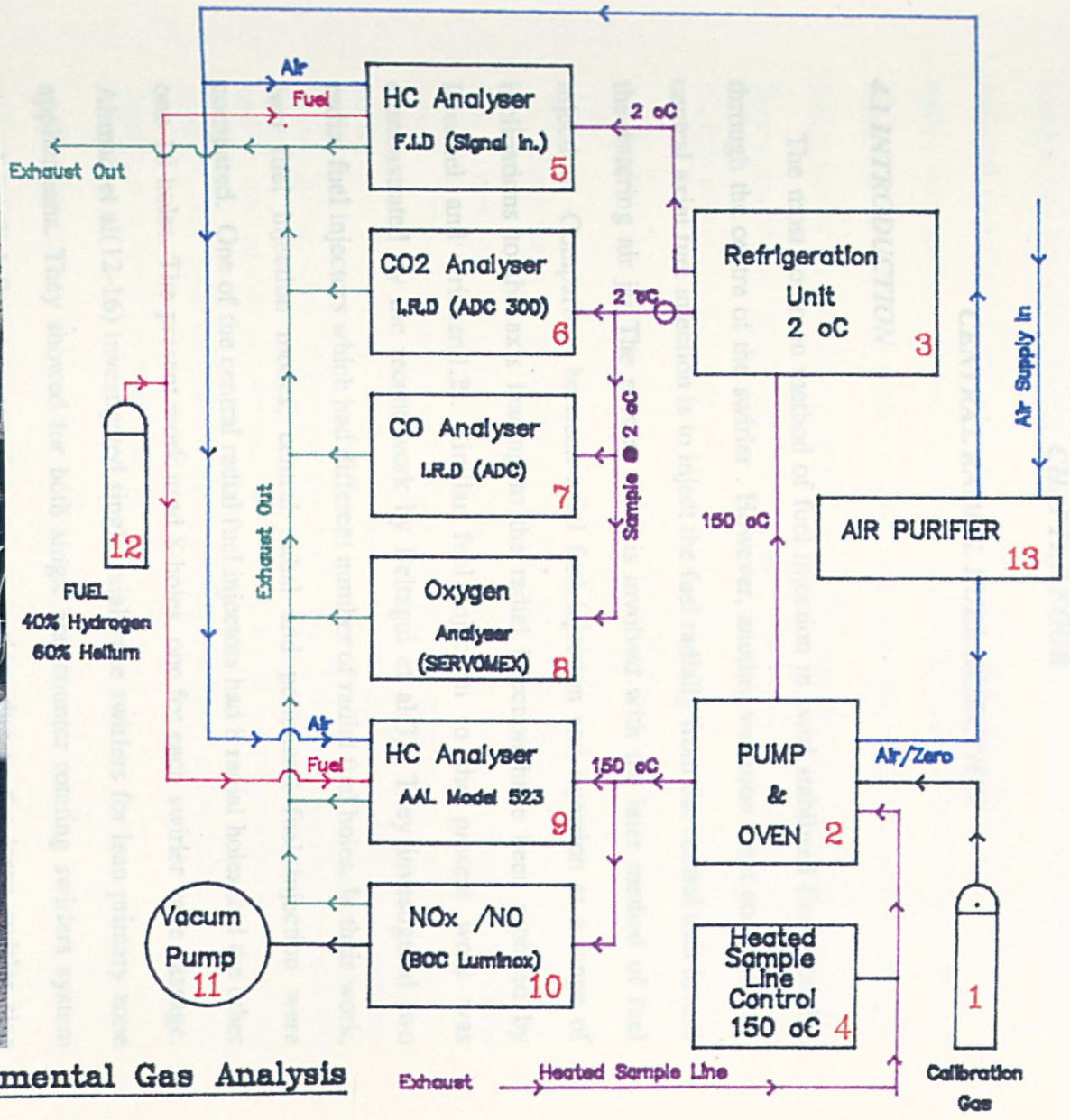

Plate 3.2 & Schematic Of Experimental Gas Analysis

CHAPTER FOUR

CENTRAL RADIAL FUEL INJECTION

4.1 INTRODUCTION

The most common method of fuel injection in swirl stabilised flows axially through the centre of the swirler . However, another variation from conventional central axial fuel injection is to inject the fuel radially from the central axis across the entering air jet The present work is involved with the later method of fuel injection. Comparison between axial fuel injection and injection at a range of inclinations to the axis leading to the radial injection have been reported by Leuckel and Fricker(1,2). Similar fuel injection to the present work was demonstrated by the recent work by Beltagui et al(3). They investigated two radial fuel injectors which had different number of radial fuel holes. In their work, two fuel injection modes, central radial and peripheral fuel injection were compared. One of the central radial fuel injectors had 8 radial holes and the other one 16 holes. The present work used 8-holes, one for each swirler vane passage. Ahmad et al(12-16) investigated single axial vane swirlers for lean primary zone applications. They showed for both single and counter rotating swirlers system that the radial flame propagation was very slow due to the large swirler size relative to the combustor diameter. It was concluded that a larger expansion ratio from the swirler was necessary to ensure rapid flame spread. It was one of the objective of the present work to investigate the influence of radial swirler outlet diameter or the influence of the combustion performance of the swirler expansion ratio(D/d). This is much easier to do with radial swirlers as the swirler diameter can be varied without changing the flow area or swirler pressure loss. This is due to the ability to change the radial swirler passage depth as the swirler diameter is changed so as to maintain the same flow area.

Radial swirlers are common in large scale burners for boiler and furnace applications. They are also common in reverse flow industrial gas turbines and the present swirlers are similar in design to those used in the Ruston Tornado

combustor, but with increase flow capacity. Radial swirlers have also been featured in some previous low emission gas turbine investigations(14-16) using radial vane passage as fuel injection and partial premixing channels. For the present chapter all the work was using the modified conventional central radial fuel injection system. In the present work the vane angle was varied at constant flow area, so that vane passage depth increased with vane angle, as discussed in chapter two.

4.2 FUEL INJECTORS

The swirlers were tested with central radial fuel injection using both propane and natural gas fuels at 3mm downstream of the upstream face of the radial swirlers. The same eight holes 12.7mm diameter injector was used for each fuel with a hole diameter of 2.2mm. The different fuel densities resulted in differences in fuel jet velocities for the same fuel mass flow. This may influence the local fuel and air mixing although the fuel jet momentum was not a major part of the mixing process. The geometry of the fuel jet system is more important in controlling mixing than fuel jet momentum(3).

4.3 COMBUSTION AND ANALYSIS SYSTEMS

4.3.1 COMBUSTION SYSTEMS

Figs.4.1 and 4.2 show schematic diagram of the combustion systems used for the present investigation, these mainly comprised two simple uncooled can combustors 330mm long. The first was of 76mm I.D. and was used in the previous investigations with axial swirlers(9-13). This combustor gave the 40mm and 76mm outlet swirlers an expansion ratio,D/d of 1.9 and 1.0 respectively. The second combustor was 140mm I.D. This had an upstream plenum chamber air feed and was connected to the exhaust system with a water cooled pipes. The two swirlers outlet diameters of 40mm and 76mm gave expansion ratios, D/d, of 3.5 and 1.8 respectively. Both combustors had similar expansion ratios of 1.8-1.9 when the 76mm and 40mm outlet swirlers were fitted respectively. This allowed the influence of combustor scalling at the same D/d to be investigated.

It was decided to operate two swirler sizes in both combustors at approximately the same pressure loss of 2.5% and to accept the difference in the Mach number for the two combustor tests. It was previously shown for non-swirling jet mixing system that Mach number effects on stability, combustion efficiency and NOx emissions were relatively small provided that the pressure loss was maintained constant(4,20). Mach number,M effects were important, particularly for NOx, if the same combustor, had tested at different M there would be a pressure loss and hence turbulent mixing variation with Mach number. It will be demonstrated in the present work that the same conclusion applies for radial swirlers, thus permitting the comparison of the results from the two combustors at different Mach number but the same pressure loss.

Both combustors used the same electrically heated air supply. Two inlet temperatures were used, 400 and 600K, to simulate low and high power operation respectively. Both combustors were instrumented with a line of wall static pressure tappings and Type K mineral insulated thermocouples. For both combustors mean gas samples were obtained

from a water cooled 'X' configuration probe mounted at the combustor exit plane. These were used to determine the overall combustor performance and emissions as a function of equivalence ratio.

4.3.2 GAS SAMPLING SYSTEM

To obtain a mean gas sample ,an 'X' configuration stainless steel water cooled probe was mounted in the exhaust plane at either 330mm or 1160mm from the swirler as shown in fig.4.3. This had twenty 1mm diameter holes on the centers of equal area.The probe only gave a true mean gas sample if the velocity and temperature distributions were uniform.The extent to which the probe deviated from this ideal may be assessed by comparing the computed air to fuel ratio of the mean gas sample and that determined from the measured flow rates.

The sample gas outlet temperature from the probes was monitored and kept above(150C) by regulating the coolant flow rate.The sample was transported

along an electrically heated (150C) Teflon line to aheated sample pump and filter system housted in an oven.Electrically heated pump furnance to the heated 150C chemiluminescence NOX analyser and and the analysis automation heated flame ionisation detector for unburned hydrocarbon(UHC) measurements. CO and CO2 were analysed using analytical developement corporation non-dispersive infra-red analysers, with samples cooled and dried prior to analysis.

The gas analysis were used to calculate 'wet' concentration of CO and CO2 the air to fuel ratio the combustion efficiency equilibrium NOX emissions corrected to 3% in the present work.

The flame temperature calculation was based on an energy balance, assuming no heat losses and no dissociation.A full equilibrium programme was used to check the range of equivalence ratios over which this latter assumption was valid.For the mean exhaust plane gas sample ,the flame temperature was computed based on the rig metered air to fuel ratio and the combustion efficiency based on the measured CO and UHC concentration.

4.4 INFLUENCE OF RADIAL VANE ANGLE ON COMBUSTION PERFORMANCE

4.4.1 Weak Extinction

The influence of the radial vane angle on the measured weak extinction are illustrated in Table 4.1. The weak extinction for all vane angles up to 50 degrees at an inlet temperature of 400K were around 0.3 equivalence ratio (A/F=55/1) for propane and around 0.4 equivalence ratio for the natural gas The 60 degrees vane angle had a slight improvement in the weak extinction. These results reflected the difference in the combustion properties for the two fuels at low power. However, for the 600K inlet condition ,similarities existed in the weak limits between the vane angle 20 and 30 degrees for both propane and natural gas which was due to perhaps the same mixing pattern at low rate fuel flow caused by the more or less the same contraction at the inlet of the two swirlers.

Similarly, in the case of the 45 and 60 degrees angles for the combustor fuelled with propane but not with natural gas. However, superior weak extinction limit was promoted by the 45 degrees angle swirler over the other swirlers using natural gas as fuel. The weak extinction equivalence ratio was 0.03 (A/F=553/1). However, as the vane angle was increased to 50 and 60 degrees the weak extinction limit deteriorated which was perhaps more due to the increase to the vane depth together with the local axial and the tangential velocity increase in the vicinity of the injecter tip, thus there was less chance to sustain the flame at very weak limits.

Generally, flame stabilisation and burning occured in the shear layer between the swirling jet and the main recirculating zone.

Most mixing takes place in the shear layer before the shear layer flow impinges on combustor wall. Furthermore, continued burning of the mixture takes place even after the impingement point in the conical shear layer where the recirculated hot combustion products meet the annular forward jet.

4.4.2 WALL STATIC PRESSURE AND TEMPERATURE PROFILES

Figs.4.4 and 4.7 shows the axial developement of the measured wall static pressure and temperature profiles for different vane angle radial swirlers at two inlet inlet temperatures of 400K and 600K respectively. The influence of inlet temperature on the profiles was very little. However, all vane angles exhibited the same static pressure and temperature profile shapes and the point of impingement evidently clear was not changed. Flame development was complete on the end of the outer recirculation zone, especially at 600K. Both at 400K and 600K flame development appeared to be more rapid for 30 degrees swirl vane angle. This vane angle also had the best NOx and combustion inefficiency characteristics, as discussed later.

4.4.3 MEAN COMBUSTOR EXIT EMISSIONS

The measured results of the mean exhaust plane emissions for the different vane angle radial swirlers at Mach Number of 0.014 and for the inlet temperature of 400K and 600K are shown in figs.4.8 - 4.31 for propane and natural gas.

4.4.3.1 Emissions at 400K

The CO and UHC emissions as function of the metered equivalence ratio are shown in figs.4.8 - 4.11 Only slight differences due to the vane angle variation can be noticed in the emission levels of these two major species, this is an indication that the rate of oxidation rate for all vane angles was similar with the exception of the 60 degrees radial swirler, which had slightly higher CO emissions. The combined effects of CO and UHC emissions can be seen as combustion inefficiency versus the metered equivalence ratio in figs.4.8 and 4.9 . The lowest combustion inefficiency for propane combustion was just below the 0.5 equivalence ratio and for the natural gas just above 0.5.

Figs.4.14 - 4.15 and figs.4.16 - 4.17 shows the NOx emissions as a function of equivalence ratio and the gas analysis calculated flame temperature respectively. The 60 degrees radial swirler exhibited more NOx emissions at all

associated equivalence ratio for both fuels which was due to , perhaps to more fuel and air mixing indicated by slightly the higher CO emissions and the better weak extinction. However, NOx emissions are strong function of the flame temperature as shown in figs.4.16 - 4.17.

For propane the NOx level increase rapidly beyond 1600K and for natural gas the rapid increase was encountered beyond 1800K. Low NOx emissions are only useful if they are achieved in combination with a high combustion efficiency. An optimum operating equivalence ratio can be determined by plotting the combustion inefficiency against the NOx emissions corrected to 15% oxygen and standard day humidity. The results in figs4.18 - 4.19 were plotted on this basis for propane and natural gas respectively. The measured results for the 60 degrees radial vane angle show significantly higher optimum NOx emissions than for the lower vane angles that ultra low NOx can be achieved with associated combustion efficiency of better than 99.9% for both fuels. The lowest NOx corrected were 5.5 and 4.5 (ppm) for propane and natural gas respectively and for the 20 and 30 degrees vane angle swirlers for a 0.1% combustion inefficiency

4.4.3.2 Emissions at 600K

The different radial vane angles swirlers exhibited the same CO emissions as shown in figs.4.20 - 4.21 for both propane and natural gas. The profile of UHC emissions as a function of equivalence ratio are shown in figs.4.22 - 4.23. The radial swirler with a vane angle of 20 degrees shows slightly more emissions than higher radial vane angles and that was for propane only. In general, all vane angles exhibited low CO and UHC emissions. These low emissions was reflected on the combustion inefficiency as shown in figs.4.24 - 4.25 where combustion efficiencies of better than 99.9% were achieved for almost all different vane angle swirlers.

The different vane angle swirlers gave more or less similar trends of NOx emissions as shown in figs.4.26 - 4.27 for both gaseous fuels.

The correlation between the NOx emissions corrected to 15% oxygen and

standard day humidity and combustion inefficiency are shown in figs4.30 - 4.31 All radial swirlers with different vane angles promoted low NOx compatible with very low combustion inefficiency. Significantly lower optimum NOx were generated at lower swirl, 6ppm for 20 and 30 degrees swirlers for natural gas compared with 8ppm to 45 and 50 degrees vane angles and 10ppm for 60 degrees swirler. For propane the NOx range was between 9 to 15ppm with increasing vane angle. High swirl may increase the residence time in the rich stabilising shear layer and thus increase the NOx emissions.

Investigation of the flow patterns using water flow visualisation reveals the similarity between all the vane angles, particularly the conical shape of the swirling jet shear layers and the corner recirculation zone size, which were almost identical as shown in chapter two. A slight variation in the contraction coefficients that give rise to different mixing patterns in the vicinity of the radial swirler outlets was observed. All the radial swirlers with different vane angle had the most important feature in common which was that the lean burning of the fuel/air mixture takes place on the inside of the conical shear layer where the recirculated hot combustion products meet the forward swirling jets. However, most of the mixing takes place in the shear layer between the fuel and air jets before they impinge on the combustor wall. It was demonstrated previously for the 45 degrees swirler using radial gas sample traverses that the unburned hydrocarbon level were reduced rapidly from a maximum to very low values near the wall reattachment point of the swirling jet shear layer.

4.5 INFLUENCE OF SWIRLERS OUTLET ON THE EMISSIONS

Four 45 degrees blade angle radial swirler configurations were investigated, consisting of the 40 and 76mm outlet swirlers tested in both of the 76 and 140mm combustors. The pressure loss was approximately the same with little variation. However, the 76mm combustor was tested at a Mach number of 0.03 and the the 140mm combustor at 0.014 as shown in Table(4.2). For the 140mm combustor, the pressure loss was kept constant by using different swirler blockages, as shown in Table(4.2), in the two combustors with the lower blockage in the 76mm combustor.

4.5.1 WEAK EXTINCTION

The weak extinction was determine at a constant air mass flow rate or Mach number and the fuel flow was gradually reduced until the flame was extinguished. The process was observed directly from the control room through a 100mm diameter air cooled window in the exhaust. Weak extinction was also easily identified by a sudden increase in the UHC emissions. Weak extinction data were reproducible to within +/- 0.02 of an equivalence ratio. The measured weak extinction results are listed in table(4.2) for both propane and natural gas fuels at the 400 and 600K inlet temperatures at atmospheric pressure. The results show that very similar weak extinction were obtained for different Mach numbers, this also showed little influence of Mach number on weak extinction for both combustors. This was also found by Al Dabbagh and Andrews(21) for premixed grid plate stabilised flames. The effect was attributed to the dependence of the stability on local turbulent burning velocity in the shear layer which varies directly with Mach number due to the dependence of pressure loss and hence turbulence on Mach number. Similar arguments apply to the present non-premixed work.

There are two important features of the weak extinction results; the similarity in the weak extinction results for the 76mm and 40mm outlet swirlers in both combustors and the very great difference in the weak extinction characteristics of

the two swirlers. The results show that the swirler expansion ratio had no influence on the weak extinction for the same swirler. This is in direct contrast with the strong effect the expansion ratio on the combustion efficiency which will be discussed later. The implication of the results is that the flame stability does not depend on the outer recirculation zone, neither on the presence of the zone nor on its temperature. It is considered that the stability is controlled by the local equivalence ratio within the conical swirling shear layer between the inner and the outer recirculation zones. Plate 4.1 shows cross-sectional view of the central propane injection flame near the weak extinction region at an equivalence ratio of 0.1 and 600K inlet temperature.

The weak extinction results show that the 76mm outlet swirler had an extremely wide stability, which is as good as most conventional gas turbine combustors. This occured in both combustors even though, as will be shown later the combustion efficiency was poor for no expansion situation. For axial swirlers, Ahmad et al(12) showed that at 600K the premixed weak extinction for propane in the 76mm combustor was 0.41 equivalence ratio, close to the present central radial fuel injection weak extinction of 0.38 in the 76mm combustor. The reason for this difference between the 40 and 76mm outlet swirlers was the local differences in the mixing at the swirlers outlet. Plate 4.2 shows cross-sectional view of the central propane injection flame for different expansion ratios. The flame stabilisation and burning clearly occured in the shear layer between the annular swirling jet and the main recirculation zone. However, swirler(A) or the 40mm outlet swirler had 30.5mm vane depth which was twice that for the larger swirler or swirler (B). Thus the fuel was injected 27mm upstream of the swirler outlet and considerable mixing with the swirler vane outlet flows was possible. The larger swirler with smaller depth (swirler B) and greater distance of the fuel jets from the vane passage outlets would not have this internal swirler mixing and would inject the fuel into the base of the conical rotating shear layer with the resultant of high stability.

These features of the local swirler mixing have been discussed in the previous chapter.

From plate 4.2 and plate 4.3, the thickness of the shear layer annular flame can be estimated to be approximately 5.0mm for propane and perhaps a little less than this value for natural gas. The difference in the colours is due to the physical properties of the two fuels which gives diffrent combustion characteristics(30).

4.5.2 WALL STATIC PRESSURE AND TEMPERATURE PROFILES

Figs.4.32 and 4.33 shows the axial development of the combustor wall static pressure/dynamic head as a function of the combustor walls axial distances for the different expansion ratios. The quite difference axial static pressure profiles indicate different aerodynamics. High static pressure was the feature of the swirler with no expansion (D/d=1) which is an indication that the highly swirling flow continued throughout the axial length of the combustor with little decay of the outer high velocity flow. It was these high velocity regionthat caused the slow development of the flame as indicated from the combustor wall temperature development in fig.4.33. For swirl flow with an outer expansion the outer recirculation zone caused a rapid decrease in the radial swirl flow. The wall temperature profiles shows that with the D/d of 1.8, the flame developed much earlier than with no expansion. This has confirmed previously and has been observed by others(25,26) in furnace situations with larger expansion ratios than the present work.

4.5.3 MEAN COMBUSTOR EXIT EMISSIONS

4.5.3.1 At 400K inlet temperature

The measured values of CO and UHC emissions as a function of equivalence ratio is shown in Figs.4.34 - 4.37 for both propane and natural gas. The results show that except for the zero expansion ratio situation, the UHC emissions were negligible at less than 10ppm for all equivalence ratios, except cllose the weak extinction. The inefficiency results in Figs.4.38 - 4.39 were similar to those for CO and were predominantly due to the CO emissions for the two fuels. Hence it may be concluded that the CO oxidation is the limiting factor controlling the combustion inefficiency. However, the large swirler with no expansion had a

very large inefficiency with propane and the level of unburned hydrocarbons was so high that it was not safe to continue testing or to repeat the same condition with natural gas as the fuel. All the other swirler configurations exhibited inefficiencies much less than 1% over a range of equivalence ratios. Hence it may be concluded that an expansion ratio D/d of approximately 1.8 is required to achieve an adequate combustion efficiency with an enclosed swirler.

An inefficiency of less than 1% is required at low power conditions and Figs.4.38 and 4.39 show that this was easily achieved for both combustor sizes provided the D/d was 1.8 or greater. The influence of a large D/d of 3.5 was somewhat greater than at 600K as will be discussed later, but still remained a small effect compared with the difference between a D/d of 1 and 1.8. For the 140mm combustor, the efficiencies were less than 0.1% over the equivalence ratios 0.45 - 0.65 for both propane and natural gas.
These are quite remarkable results and can be achieved by few conventional combustor designs.

Figs.4.40 - 4.43 show the NOx emissions as a function of the metered equivalence ratio and gas analysis calculated flame temperature for both propane and natural gas. Higher NOx emissions were exhibited by the swirler with no expansion due to the existance of the rich core region which is very clearly shown in plate(4.2). The nonuniformities in the distribution of the fuel in the shear layer caused differences in the NOx levels between the swirler configurations. However, the lowest NOx level was found for swirler(A) with an expansion ratio of 3.5 in a combustor fuelled with natural gas as shown in Fig.4.41, although it exhibited the same flame temperature as the large swirler with an expansion ratio of 1.8 as shown in Fig.4.43. The cause of lower NOx emissions was the better mixing promoted by swirler(A) before the impingement on the combustor wall.

The correlation between the combustion inefficiency and the NOx emissions corrected to 15% oxygen and standard day humidity are shown in Figs.4.44 and 4.45 for both propane and natural gas respectively. The small swirler exhibited

much lower corrected NOx than the other swirlers. The lowest corrected NOx were 10ppm and 5ppm compatible with better than 99.9% combustion efficiency for propane and natural gas respectively. The large expansion ratio did not help to improve the stability limits. Thus, it seems that the best choice is that of the swirler(B) for its wide stability limits and comparatively low NOx level which can meet the EPA standard of 20ppm for both fuels.

4.5.3.2 At 600K inlet temperature

Figs.4.46 - 4.49 show the CO and UHC emissions as a function of the metered equivalence ratios for propane and natural gas. Similar conclusion can be applied for the simulated high power condition as for the low power one. The UHC results show that except for the zero expansion ratio test, the UHC emissions were negligible at less than 10ppm for all equivalence ratios except close to the weak extinction. Therefore, the inefficiency was predominantly due to CO emissions as can be seen in Figs.4.46 and 4.47. These two figures have similar trends as the inefficiency profiles as a function of equivalence ratios in Figs.4.50 and 4.51.

The combustion inefficiency for a zero expansion ratio, for the 76mm outlet radial swirler in 76mm combustor, were relatively poor using propane, with a maximum efficiency at 600K of only 98% compared with better than 99.9% for the other configurations. This was considered to be an unacceptable performance and no tests were carried out on natural gas as there was no evidence from the other swirler tests that natural gas had a much better efficiency than propane at any test condition.

The 76mm outlet swirler in the 140mm combustor with a D/d of 1.8 had a minimum inefficiency of 0.01%, which is difficult to achieve even at very high combustor pressures using conventional combustors. Furthermore, an inefficiency better than 0.1% was mantained over a wide range of equivalence ratios from 0.3 - 0.6, with the apparent inefficiency at higher equivalence ratios being predominantly equilibrium CO. Fig.4.51 shows that the combustion inefficiency was similar using natural gas.

The main difference was in the lean burning region, weaker than an equivalence ratio of 0.4, where natural gas had an inferior combustion inefficiency than propane. For example at a 0.28 equivalence ratio, close to the overall equivalence ratio at high power, natural gas had an inefficiency of 1% compared with 0.1% for propane.

The large differences in the combustion inefficiency in the two combustors, for the same swirl number, shows that the poor combustion efficiency with no expansion ratio cannot be due to excessive swirl. The expansion ratio allows the swirl to decrease in the combustor, as well as creating the outer recirculation zone. It has been shown above that the D/d did not influence the weak extinction. The stability was extremely good for the 76mm outlet swirler in both combustor sizes with better stability achieved with a D/d of one. However, Fig.4.50 shows that there is a very significant difference in their combustion efficiences with a much superior performance with a D/d of 1.8. The expansion ratio creates an outer recirculation zone, which although it it does not effect the stability, clearly has an important influence on the combustion efficiency.

Ahmad et al(12-16) showed for axial swirlers that a low D/d also gave a poor combustion efficiency, even for the premixed situation. The reason was shown to be due to the difficulty of the flame spreading across the outer high velocity swirling flow. Most of this work was carriedout for a range of expansion ratios from 1.2 to 1.6. It was concluded that expansion ratio was a major parameter affecting the swirler performance. Large expansion ratios are difficult to achieve with high air flow axial swirlers, which was reason for using radial swirlers in the present work. It is likely that the present D/d of 1.8 is close to the minimum acceptable for the flame to spread rapidly downstream of swirler.

The very low combustion inefficiencies in Fig.4.50 and 4.51, demonstrate that large rich local zones are unlikely in the recirculation zones, as these would generate high CO which would be difficult to completely burn later. It is thus clear that the local rich zone in the rotating conical shear layer, which give the

extremely good stability characteristics, do not form the main heat release region which must occur in a better mixed zone.

The smaller swirler (A) results for both combustors in Fig.4.50 and 4.51, show a very similar low inefficiency compared with the larger swirler in the 140mm combustor. For the same D/d of 1.9, the inefficiency was slightly inferior in the 76mm combustor than for the D/d of 1.8 in the 140mm combustor. This was probably due to a residence time effect caused by the differences in Mach number as will be discussed later. This quite small difference between the combustors indicates that for the same D/d, swirlers will have a similar combustion performance, irrespective of the combustor size.. The poor stability of the 40mm outlet swirler, discussed above and attributed to better internal mixing upstream of the swirler exit phase, prevented any comparison of results in the very lean region.

The results for an expansion ratio of 3.5 with the 40mm swirler in the 140mm combustor show a small improvement in inefficiency compared with a D/d of 1.9 in the 140mm combustor. However, it is clear that expansion ratios as high as this are not necessary to achieve either a high combustion efficiency or good stability. The weak extinction results indicate that the 40mm swirler has considerable premixing upstream of the swirler exit plane. However, comparison with the 76mm outlet swirler results in the 140mm combustor shows no major advantage in terms of combustion efficiency in this premixing. The 76mm outlet swirler results conclusively show that it is possible to achieve a wide stability with good mixing in the main combustion zones.

The NOx are emissions presented as a function of equivalence ratio and gas analysis calculated flame temperature in Figs.4.52 - 4.55 for both propane and natural gas. The propane results in Fig.4.52 show that for the 76mm outlet swirler with no expansion or D/d of one, not only was the combustion efficiency poor, but also the NOx emissions were high. Ahmad et al(12-16) showed for axial swirlers that this was caused by the generation of rich zones in the central core

region with high NOx as a consequence. The expansion from the swirler was found to be necessary not only for a low combustion inefficiency but also for low NOx emissions and hence for good fuel and air mixing. Fig.4.52 shows similar conclusions may be made for the present radial swirlers. The 76mm outlet swirler with a 1.8 expansion ratio had NOx emissions of below 20ppm corrected to 15% oxygen and standard day humidity over a wide range of equivalence ratios (0.2 - 0.4).

The 40mm outlet swirler in both combustors had much lower NOx emission than for the larger swirler at the same equivalence ratio. This was due to the partial premixing upstream of the swirler exit plane, as discussed above in relation to the weak extinction results.

Unfortunately, the poor stability for the 40mm outlet swirlers in a very narrow range of equivalence ratio(0.4-0.5) close to the weak extinction over which corrected NOx emissions less than 20ppm were achieved. The natural gas results in Fig.4.53 were substantially lower than those for propane in Fig.4.52. The reduction was approximately a factor of 2 and this has also been found by Abdul Hussain and Andrews(7) for a non-swirling interacting jet shear layer system.

All three swirlers may thus be described as having ultra low NOx characteristics for natural gas. There is a 40K difference in the peak adiabatic flame temperatures between propane and natural gas and this often attributed to the cause of the lower NOx emissions with natural gas as shown in Figs.4.54 and 4.55. However, although this is a significant factor in the lower NOx emissions it is considered that the two fuels have diffrent 'prompt' NOx mechanisms with possibly lower prompt NOx for natural gas. The reason for this are the much larger number of hydrocarbon intermediate compounds for propane combustion. Internal flame gas sample traverses of these enclosed swirl flames have shown the importance of prompt NOx with an early formation of NOx close to the swirler.

Low NOx emissions are of little consequence unless they can be achieved with a low combustion inefficiency. Thus the combustion inefficiency and NOx

correlation is an important method for assessing the viability of low NOx systems. The present results for propane and natural gas are shown in Figs.4.56 and 4.57 respectively and the optimum low NOx conditions compatible with an acceptable inefficiency are summarised in Table(4.3). With the exception of the unity expansion ratio situation, all three swirler configurations exhibited corrected NOx emissions of less than 20ppm with a combustion inefficiency of below 0.2%. For natural gas Fig.4.57 and Table(4.3) show that all three swirlers can achieve 10ppm corrected NOx with an inefficiency of less than 0.1%. Table(4.3) also shows that approximately 50% lower optimum NOx emissions were achieved for natural gas compared with propane. It may be concluded that the low NOx emissions were achieved without any combustion efficiency penalty.

The poor stability of both 40mm outlet swirler system was a problem as the optimum equivalence ratio minimum NOx was too close to the stability limits in Table(4.2) for viable use in combustors. This is the same situation as most premixed/prevaporised designs, although they often have a combustion efficiency problem as well as a stability one. Table(4.2) shows the wider stability of the 76mm outlet swirler (B), allowed optimum NOx emissions to be achieved that were close to those for the 40mm outlet swirler (A) which had much lower NOx for the same equivalence ratio. Also the optimum equivalence ratio for swirler (B) gave a factor of 3 margin on the weak extinction equivalence ratio as shown in Table(4.2).

4.6 INFLUENCE OF PRIMARY ZONE MACH NUMBER ON COMBUSTION

The primary zone Mach number is based on the combustor cross sectional area A1, the total primary zone air mass flow and the upstream temperature (Appendix A). The ratio of the primary zone Mach number to the reference Mach number for the combustor gives the proportion of the air flow that is being simulated in the primary zone. It was necessary to test the two combustor sizes at different Mach numbers if the same swirlers were to be used in each combustor

with similar pressure loss.

One swirler (A) was investigated in the 76mm combustor at 0.03 and 0.0467 Mach number for two inlet temperatures of 400K and 600K. Three swirlers A, B and C were investigated in the 140mm combustor at 600K inlet temperature and for propane and natural gas. The 40mm outlet swirler was tested at two Mach numbers 0.008 and 0.014. The 76mm outlet swirler were tested at Mach number of 0.014 and 0.02.

4.6.1 WEAK EXTINCTION

The measured weak extinction of diffrent primary zone Mach number at two combustors are presented in Table(4.4). For swirler(A) in the 76mm combustor for both fuels propane and natural gas, the influence of the primary zone Mach number was small at both 400K and 600K inlet temperatures. A slight improvement was found at the reduced Mach number. The same swirler in the 140mm combustor had a similar stabilities as shown in Table(4.4), for the inlet temperature of 600K. The effect of operating different primary zone Mach number on the same geometry swirler was more for the swirlers (B) and (C) in the 140mm combustor fuelled with natural gas where the lower Mach number promoted wider stability limits. This may have been due to exceeding the minimum possible fuel concentration within the stabilisation region at higher Mach numbers. However, for the combustor operating at the same conditions but fuelled with propane the influence was small for both large swirlers at 600K inlet temperature.

4.6.2 MEAN COMBUSTOR EXIT PLANE EMISSIONS

The measured combustor exit plane emissions are presented as a function of the metered equivalence ratio in Figs.4.58 - 4.65. Little effect can be noticed due to the variation of the primary zone Mach number on the CO and UHC emissions as shown in Figs.4.58-4.61 for both propane and natural gas which is due to the combustion being completed at earlier stages. Furthermore, the similarity between

the flow regime probably gave the same mixing pattern along the initial combustor length before the combustio was completed which promoted more or less the same CO and UHC emissions. This is also shown by the combustion inefficiency as a function of equivalence ratio in Figs.4.62 and 4.63. However, the effect of the primary zone Mach number was significant for NOx emissions as shown in Figs.4.64 and 4.65 for both propane and natural gas respectively.

The variation of NOx emissions corrected to 15% oxygen and standard day humidity are shown as a function of combustion inefficiency in Figs.4.68 and 4.69 for propane and natural gas respectively. The influence of Mach number for the lower blockage 76mm swirler (B) had little influence on the inefficiency as both were less than 0.1% inefficient. However, there was a significant increase in the NOx emissions at lower Mach number which was not necessarily due to the increased residence time but may have due to the decrease in the fuel and air mixing at lower pressure loss and hence lower turbulence level at lower Mach number. That can be seen from the general performance of the 76mm outlet higher blockage swirler (C). The test of the higher blockage swirler (C) at 0.014 and 0.02 were carried out to assess this. The NOx level exhibited were found to be somewhat lower than the lower blockage swirler (B) at the 0.02 Mach number in spite of the higher residence time. Moreover, ultra low NOx emissions were demonstrated by swirler (C) with a pressure loss of more than 7% using natural gas as fuel. Thus, it may be concluded that it is valid to compare the swirlers at different Mach numbers, provided that the pressure loss is maintained at a similar level.

4.7 INFLUENCE OF CENTRAL RADIAL FUEL POSITION ON EMISSIONS

This work was carried out to investigate the effect of the distance of the central fuel placement from the swirler back-face on the emissions and stability limits of swirler (A) in the 76mm combustor using natural gas as fuel. A circular shaped baffle of 40mm diameter and 3mm in thickness was also used in conjuction with a long central radial fuel injectionas shown in Fig.4.1. The aim was to inject the fuel much further downstream of the swirler outlet to the base of the conical shear layer and to establish a central reverse flow zone where burned gases are recirculated to mix with and ignite the fresh fuel and air flow(27). This 76mm combustor with 40mm swirler was the pilot stage of the two stage combustion investigated in chapter7. An improved stability at low power was essential.

4.7.1 Weak Extinction

Table(4.5) illustrates the effect of the central fuel injection position without a baffle on the lean stability limit using radial swirler(A) for this perpose since as previously discussed was encountered with very narrow stability limits on the lean side. However, the combination of the flame observation with the measured weak extinction limits confirmed that the blow-out was determined by processes occuring in the region near to the injector tip in the vicinity of the fuel outlet holes and was uneffected by the injector position. It was considered that the centre vortex flow carried the fuel back to the swirler back plate whatever axial position was used. The baffle was used to stop this back flow of the fuel.

Using the baffle injecter promoted a situation where the flame stabilised in the low speed flow region approaching the forward stagnation point (or small recirculation zone) immediately after the baffle edge. The results showed a maximise extension of the stability with the baffle in place. This imply that a large recirculation zone, is not an essential flow feature for combustion stabilization. This conclusion supported by the work reported by Panton and

Sweat(28) and that of Oven et al(29).

4.7.2 MEAN EXIT PLANE EMISSIONS

The measured CO and UHC emissions as a function of equivalence ratio are shown in Figs.4.70-4.71. The lowest CO emissions was exhibited by the injecter at 3mm at an inlet temperature of 600K which is due to higher residence time and more chance of mixing prior to the outlet of the swirler which means higher oxidation rate than the formation rate. The placement of the injector at 70mm position away from the vertical back plane of the swirler increased the CO and UHC emissions relative to the standard 3mm results. However, the effect was small as found for the stability. This confirm that the predominant action in the reverse flow carrying the fuel to the swirler backplate and into the base of the shear layer with a very similar performance to that of injection close to the swirler backplate. The circular baffle was placed at the 70mm position with the injector approximately 3mm downstream of the baffle. The flow will generate a small central recirculation zone immediately after the baffle of encounting a low velocity rich core region close to injector which stabilises the flame. That was clear from the direct flame observations where flame luminosity was associated with use of the baffle, which is an indication of a rich core region. Poor mixing takes place at equivalence ratio of 0.45 which is indicated by the high emissions of CO and UHC at 400K. Reducing the fuel flow rate will tend to promote a reduction in the fuel spread radially towards the conical rotational flow with more fuel being continued in the rich core region downstream of the baffle with increment by high CO and UHC. The combined effects of CO and UHC emissions are presented in Fig.4.72 as combustion inefficiency and as a function of metered equivalence ratio. The highest combustion inefficiency was exhibited by the baffled injector at 400K inlet temperature and the lowest was associated with the injector holes at 3mm away.

The NOx emissions as a function of equivalence ratio and flame temperature are shown in Figs.4.73 and 4.74 respectively. Higher NOx was generated with

the 70mm fuel injector position with and without the baffle, This was unsurprising as there was little change in the stability which is commonly an indication of fuel and air mixing changes. However, NOx is sensitive to factor which influences the densities of uniform zones of around 0.8 equivalence ratio, where NOx , production is unmaximised, which are not the zones that govern stability.re. The correlation between the combustion inefficiency and the corrected NOx to 15% oxygen and a standard day humidity are shown in Fig.4.75 where the best results the injecter holes positioned at 3mm away from the vertical back plane of the swirler but with deterioration in the weak stability limits as discussed previously.

The injector holes positioned at 70mm exhibited the same combustion inefficiency but with higher NOx which was due to worse fuel and air mixing. Lower combustion inefficiency was promoted by the baffle injector at the 70mm position for both inlet temperatures. Placing the circular baffle on the position 70mm away from the back plane of the swirler will extend the weak stability limit but with a major sacrifice on the NOx emissions and combustion efficiency. Thus, this method of extinding the flame stability cannot be recommended.

4.8 RADIAL FLOW SWIRL BURNER FOR FURNACE APPLICATIONS

4.8.1 Introduction

Swirl burners have been designed and produced in different varieties for burning different types of fuel. Some typical industrial radial swirl flow burners have been reported in reference(32). However, typical industrial swirl burners employing a single swirl flame stabiliser present several problems from the viewpoint of stability and pollutant emissions. Recently, there is tendency towards the use of the two-stage rich-lean burners, due to better controlling of the flame temperature and NOx emissions. The specific requirements for NOx as revised by the Europian committions in February, 1985 (33), are indicated in Table(4.6).

4.8.2 SIMILARITY BETWEEN HIGH INTENSITY BURNERS AND LOW EMISSION GAS TURBINE COMBUSTORS

To minimise NOx emissions from gas turbine combustors it is necessary to increase the primary zone air flow and to improve the fuel and air mixing(34). Many low emission gas turbine combustor designs aim to pass as much air through the combustor head as possible with the remaining air added further downstream. The primary zone is thus a burner configuration of a flame stabiliser with a down stream tube burner. Although gas turbine combustors conventionally require some air to cool the combustor walls, the present work had no film cooling. The present work is thus identical to a high intensity burner configuration as shown in Figs.4.1 - 4.3.

Another similarity between gas turbine combustors and high intensity burners is the operating conditions of mean velocity, U1, and burner pressure loss, ΔP, or 'windbox pressure'. U1 is based on the burner approach pipe area A1, which is the downstream combustion area. In the present work, ΔP is often given directly as mbar or mm WG for burners but is usually referred to as a percentage of upstream absolute pressure in gas turbines $\Delta P/P$. Pressure loss is related to the velocity U1 and the burner stabiliser open area A2 by eq.1(34):

$$\frac{\Delta P}{P} = 1/2 \left(\frac{U_1}{C_D}\right)^2 \frac{1}{RT} \left(\frac{A_1}{A_2}\right)^2 = \frac{\gamma}{2} \left(\frac{M}{C_D} \cdot \frac{A_1}{A_2}\right)^2 \quad \text{....(1)}$$

Where C_D is the burner discharge coefficient defined by Eq.2:

$$m = C_D \cdot A_2 \cdot (2 \rho \Delta P)^{1/2} \quad \text{---(2)}$$

Where m is the burner mass flow and ρ is the upstream gas density $\rho = \frac{P}{RT}$

where R is the gas constant and T the upstream temperature).

Equation 1 shows that the pressure loss is simply expressed in terms of the burner approach Mach number, M, which includes both the velocity and temperature effects. For gas turbine combustors a typical Mach number is 0.05, which gives a mean approach velocity of 16 m/s at 300K and 24 m/s at 600K. These are typical of the maximum burner velocities used in some high intensity burners.

For the present work the burner velocities were used in the range of 2 - 10 m/s at 305K or to 24 m/s at 600K which covers a wide range of practical burner approach velocities.

Gas turbine combustor pressure losses are generally in the range of 2 - 5% which convert to burner windbox pressures of 200 - 500 mmWG, which is typical of many high intensity burners. Pressure losses of approximately between 100 - 300mm WG have been used for a range of Mach number between 0.0064 - 0.047. Use of Eq.2 with the stated Mach number ranges and pressure loss shows that the practical range of $\frac{A_1}{A_2}$ for both gas turbine primary zones and burners is approximately (2 - 12). This area ratio is more often expressed as burner blockage $(1 - \frac{A_2}{A_1})$ and the practical range is approximately 50 - 90%.

Gas turbine combustor must have a very wide stability range as there is a factor of 2 - 3 difference in the operating air/fuel ratio at high and low power output and a wide stability margin on the operating condition is required. This design condition is similar to the requirement of a wide turndown ratio in high intensity burners. The major difference is that burners are designed to give their

maximum output just on the weak side of stoichiometric (EQR=0.9), whereas material limitations in gas turbines limit the maximum power output to EQR<0.4. However, the primary zone with only a proportion of the combustion air will operate closer to the burner equivalence ratio situation.

4.8.3 BURNER CONFIGURATION

Figure(4.3) shows an outline of the equipment and test facility that was used in the present work. It consists of an air supply from a fan, venturi flow metering ,electrical preheater,1.5 m long 140mm diameter approach pipe,flange mounted swirler with integral central fuel injector, a 330mm long 140mm I.D. burner and an exhaust system with a flame observation window located a short distance from the burner exit.The stainless steel burner wall were ucooled except by natural convection. This was also coupled with a water cooled wall of the same internal diameter. The burner length was varied from 330mm to 1160mm by placing a water cooled pipe. A water cooled twenty holes 'X' configuration mean gas sampling probe was either at 330mm or at 1160mm from the swirler. The 330mm position was to demonstrate that combustion was completed close to the burner with good fuel and air mixing characteristics. The longer burner wall was required investigate residence time influence on NOx emissions. Ignition was achieved using a 12 Joules surface discharge igniter mounted 25mm down stream of the swirler.

The method of fuel injection used in the present work was direct central fuel injection using an eight hole nozzle with radial natural gas injection which give a radial jet velocity between 55m/s-180m/s depending on the fuel flow rate. There was no axial component of the gas momentum, which might penetrate the vortex core region as the burner throughput was increased. The fuel used was a natural gas analysed by gas chromatography (92.45% CH_4, 5.34% C_2H_6, 0.40%C_3H_8, 0.45% CO_2, 1.24% N_2, 0.12% O_2). This was taken from the 76mm diameter mains and heated to 1bar gauge pressure in a boost fan. This was then fed via a flow metering panel in the control room to the rig. Two different inlet air temperature were used (305K and 600K) simulating the ambient and the

preheated operating conditions at a flow velocity of 2.5m/s at 305K inlet temperature and 3.3m/s at 600K inlet temperature

4.8.4 WEAK EXTINCTION

The blowoff limits are of importance in the design of industrial burners as they determines the turndown ratio.

The flame stability or blowoff was determined by keeping the air flow rate fixed and decreasing the fuel flow. The process was observed directly from the control room through a 100mm diameter air cooled window in the exhaust. Weak extinction was also monitored through the gas analysis and was accompanied by a sudden increase in UHC emissions. The flame stability data were reproducible to within +0.02 of an equivalence ratio and are summerised in Table(4.7).

At conditions close to the weak extinction limit, the region of maximum peak wall temperature moved closer to the swirler and there was much less combustion in the forward stream adjacent to the CRZ. However, there was much more unburnt gas present within the CRZ (35), and the appearance of the flame becames less steady.

From Table(4.7) the weak extinction results show that at lower inlet air temperature, extinction occured at higher equivalence ratios and that was due to the wider flammability limits at higher inlet temperatures Table(4.7) also shows a close similarity between the flammability limits, and the flame stability limits, indicating that the fuel and air mixing was rapid and that the swirler(A) was behaving as through it was premixed. The reason for this was the relatively large swirler depth (30.5mm) with fuel injected at the base of the swirler.

The flame stability depends on the location of the reaction zone within the flow field near to the burner exit and the reason for flame extinction were(35):

-radial shift of the flame front in regions of excessive local fluid velocities.

-lifting of the flames by exceeding the maximum possible fuel concentration within the stabilisation region.

4.8.5 WALL STATIC PRESSURE PROFILES

The radial distribution of static pressure inside the burner can identify the complex flow patterns that occur with highly confined flows(36). The wall static pressure profiles in the present work are plotted as dimensionless quantity in terms of the burner inlet dynamic head Fig.4.76 shows that the wall static pressure profile exhibits three zones with high wall static pressure separated by lower wall static pressure regions. A low wall static presure followed by a high value is associated with a recirculation zone(RZ), the static pressure corresponding to the maximum width of the recirculation zone with high swirl velocities. The size and number of these recirculation zones are influenced by the swirler design.

It was previously shown using the water model technique, that the small swirler(A) swirling flow generated two peripheral recirculation zones counter directions each other and the impingement point was 0.5D from the swirler outlet vertical plane. The two peaks in the static pressure profiles in Fig.4.26 are the points where the flow axial velocity approaches the minimum at the the end of a recirculation zone. The first point where the values of static pressure is minimum indicates the potential flow going in the reverse direction of the flow to form the first outer corner recirculation zone. The second minimum value was inward recirculation zone that followed the shear layer wall interaction. The shear layer thus separates these two counter rotating recirculation zones.

4.8.6 AXIAL DEVELOPMENT OF BURNER WALL TEMPERATURE

From temperature surveys Beltagui et al(37) showed that at a condition sufficiently removed from the extinction limit, the central recirculation initiated combustion of the main forward flow and peak temperatures were observed in this forward flow within a distance of 0.5 to 1 swirlers diameters downstream from the swirler exit. their results were in agreement with the observations of Syred et al (38) and Claypole and Syred (39) using a tangential entry swirl burner.

For the present work, the axial temperature profile of the uncooled burner

tube was monitored using nine grounded junction, mineral insulated type K thermocouples. The wall temperature is related to the inner gas temperature and hence gives a good indication of the rate of flame development and location of the main heat release region. Fig.4.77 shows the variation of burner wall temperatures along the burner length for both conditions ie. with and without the water cooled pipe connected to the main burner.

The main feature of Fig.4.77 is the two peaks in the temperature, the first peak indicated the presence of high temperature regions adjacent to the wall. The two high temperature points coincide with the two recirculation zones discussed above. The wall temperatures were lower for the 305K inlet temperature as expected due to the lower flame temperatures. However, it is clear that the flame is stabilised close to the burner for both situations.

4.8.7 MEAN COMBUSTOR EXIT EMISSIONS

The carbon monoxide and unburnt hydrocarbons concentration variation with the equivalence ratio, are shown in Fig.4.78 and 4.79 respectively. Their combined effect as combustion inefficiency is shown in Fig.4.80, this was dominated by the CO emissions. Visual observation and photographs of the flame showed it to be predominantly blue with no luminous zones in the main flame reaction zone. The short uncooled burner gave the highest CO emissions and combustion inefficiency at both inlet temperatures.
The associated combustion inefficiency levels with water cooled pipe were much lower than for burner without water cooled pipe on, mainly due to the extra length for the CO and UHC burnout, which was not strogly effected by the cooling.

Fig.4.81 shows the NOx formation results as a function of equivalence ratio and the correlation of NOx formation with flame temperature is shown in Fig.4.82. The NOx level rises until it reaches the maximum at 0.8 equivalence ratio as predicted by the Zeldovich NOx kinetics. There was very little effect of burner length on NOx emissions at both inlet temperatures. It may be that the cooling action of the water cooled pipe cancelled the increase in NOx due to the

residence time effects. However, the residence time change was too large for this to be likely. Hence it may be concluded that NOx was generated in the early stages of the combustion and the internal traverse have confirmed this with the other swirler.

Fig.4.83 shows the correlation between NOx emissions and the combustion inefficiency.The NOx emissions have been corrected to a 3% oxygen condition to conform with industrial furnace NOx regulations. With the water cooled pipe section connected to the main burner rig ,it is evident that there was no appreciable change in NOx concentration but there was an improvement in the combustion inefficiency due to the extra residence time. However, the inefficiency after 330mm was generally quite low.

4.8.8 INFLUENCE OF APPROACH VELOCITY VARIATION ON EMISSIONS AT 305K

In order that the effect of higher flow on the combustion performance can be investigated, work was carried out to test the burner at a higher air mass flow rate and hence thermal output which gave a higher pressure loss of 3.3% at inlet temperature of 305 K.

Fig.4.84 and 4.85 shows the concentration of CO and UHC as a function of overall equivalence ratio respectively. In general the two conditions exhibits no major changes in the CO and UHC emissions for the higher air mass flow rate and lower residence time. The exhaust plane combustion efficiency results are presented on an inefficiency basis as a function of equivalence ratio in Fig.4.86. This shows clearly, that there was no influence of higher air mass flow rate or lower residence time on the combustion inefficiency.

Lower NOx emissions were measured at the lower approach velocity of 2.5m/s as shown in Fig.4.87 and Fig.4.88. This was partially due to the better turbulent mixing at higher pressure loss and partially to the lower residence time. Fig.4.89 shows the correlation between the burner combustion inefficiency and the NOx emissions corrected to 3% oxygen and standard day humidity. However, the the

burner at U1=3.3m/s exhibited lower corrected NOx compatible with a higher combustion efficiency which is mainly due to the higher turbulent mixing rate at higher pressure loss and the lower residence time.

The above discussion was also applicable with even higher air mass flow rates or approach velocity at the 305K inlet temperature. Figs.4.92 - 4.95 demonstrates this for two gaseous fuels propane and natural gas, with the small swirler(A) in the 76mm combustor with an associated approach velocity of 11.1m/s and the large swirler(B) in 140mm combustor with an associated approach velocity of 5.1m/s, both at ambient conditions.

4.8.9 BURNER THERMAL OUTPUT

Figs.4.96 and 4.97 shows the burner power output as a function of metered equivalence ratio. The influence of radial swirler vane angle was minimum for a fixed burner inlet approach velocity and preheated air temperature as shown in Fig.4.96. However, there was influence on burner thermal output which was due to the variation of the inlet temperature This effected the inlet velocity to the swirler and hence the power output as shown in Fig.4.97. The highest thermal output was exhibited at ambient temperature of 305K.

4.9 CONCLUSIONS

1- The radial vane angle did not influence the combustor exit plane emissions.

2- The swirler expansion ratio, D/d, and hence the size of recirculation zone, does not influence the flame stability. This is controlled by mixing in the conical shaped swirling shear layer.

3- The small swirler(A) with a large depth has considerable partial premixing of fuel and air upstream of the swirler exit plane. This achieves low NOx emissions, but with an inadequate stability margin.

4- A swirler expansion ratio of approximately 1.8 is required to achieve a high combustion efficiency. A larger D/d of 3.5 did not produce any major improvement in combustion efficiency , but there was a small NOx reduction.

5- The only significant difference between propane and natural gas operation was the NOx emissions where the natural gas had approximately half the NOx emissions of propane for the same test condition.

6- The radial swirler system for natural gas exhibits ultra low NOx emissions of 10ppm or less corrected to 15% oxygen at 1 bar, with a combustion efficiency better than 99.9%.

7- The upstream mixing inside the large swirler was not a crucial feature of the low NOx emissions.The large swirler achieved low NOx emissions without the flame stability problem of the small one.

8- The length of the radial swirl burner did not influence the NOx emissions due to higher residence time, but reduced the combustion inefficiency.

9- Radial swirl burners with natural gas can nearly meet the E.E.C standard regulation for the present and for the year 1995.

CHAPTER FOUR

REFERENCES

4-1 Leuckel W. and Fricker N.: The characteristics of swirlstabilized natural gas flames, part1: Different flame types and their relation to flow mixing patterns. J. Inst. Fuel(Energy),49,pp.103-112, June 1976.

4-2 Fricker N. and Leuckel W.: The characteristics of swirlstabilized natural gas flames, part3: The effect of swirl and burner mouth geometry on flame stability. J. Inst. Fuel(Energy),49,pp.152-158, June 1976.

4-3 Beltagui S.A., MacCallum N.R.L and Ralston T.: The effect of fuel injection modes on combustion of swirling flows. Session 1 paper5 British flame Days, British Flame Research Committees, Inst. of Energy, 1988.

4-4 Mellor A.M.: Gas turbine engine pollution. Prog. Energy Combust. Sci., vol.1,pp.111-133, 1976.

4-5 Aoyama K. and Mandai S.: Development of a dry low NOx combustor for a 120 MW gas turbine. ASME paper 84-GT-44, 1984.

4-6 Kuroda M. et al: Development of dry two-stage low NOx combustor for a gas turbine. ASME paper 87-GT-64, 1987.

4-7 Abdul-Hussain U.S., Andrews G.E. and Shahabadi A.R.: Jet mixing shear layer combustion: An ultra low NOx system for natural gas fired gas turbines. I. Mech. E. combustion in engines conference, May 1988.

4-8 Sotheran A., Pearce D.E and Overton D.L: Some practical aspects of staged premixed, low emissions combustion. ASME paper no. 84-GT-88, 1984.

4-9 Gleason G.C., Rogue D.W and Bahr D.W.: Experimental clean combustor program-phase II, NASA CR-134971, 1976.

4-10 Roberts R., Peduzzi A. and Vitti G.E.: Experimental clean combustor program-phase II, NASA 134969, 1976.

4-11 Neidzweicki R.W. and Jones R.E.: Parametric test results of swirl can combustor. AIAA J. vol.12, p.844, 1974.

4-12 Ahmad N.T. and Andrews G.E.: Emissions from enclosed swirl stabilised premixed flames. ASME paper 83-GT-192, 1983.

4-13 Ahmad N.t. and Andrews G.E.: Gas and Liquid fuel injection into an enclosed swirling flow. ASME paper 84-GT-98, 1984.

4-14 Ahmad N. T.,Andrews G. E. and Kowkabi, M.: Centrifugal Mixing forces in Enclosed Swirl Flames. 20th.,Symposium(International) on Combustion/The Combustion Institute,pp.259-267, 1984.

4-15 Ahmad N.T., Andrews G.E., Kowkabi M. and Sharif S.F.: Centrifugal mixing in gas and liquid fuelled lean swirled stabilised primary zones. ASME paper 85-GT-103, 1985.

4-16 Ahmad N.T., Andrews G.E. and Kowkabi M.: Counter rotating double swirl stabilised flames. The 1987 Tokyo Inter. gas turbine conference Oct. 1987.

4-17 Roberts P.B., Kubasco A.J. and Sekas N.J.: Development of a low Nox lean premixed annular combustor. ASME paper 81-GT-40, 1981.

4-18 Smith K.O.: Ultra-low NOX combustor concept for methanol firing. ASME paper 83-GT-29, 1983.

4-19 Smith K.O., Kurzyncke F.R. and Angello L.C.: Experimental evaluation of fuel injection configurations for a lean premixed low NOx gas turbine combustor. ASME paper 87-GT-141, 1987.

4-20 Kerr N.M. and Fraser D.: Swirl part 1: Effect on axisymmetrical turbulent jets. J. Inst. Fuel(Energy), vol.38, pp.519-526, 1965.

4-21 Beer J.M. and Chigier N.: Combustion Aerodynamics. 1973.

4-22 Ahmad N.T and Andrews G.E.: Enclosed swirl flames: Interaction between swirlers in lean primary zones. ASME paper 86-GT-278, 1986.

4-23 Abdul Aziz M.M., Abdul Hussain U.S., Al Dabbagh, Andrews G.E. and Shahabadi A.R.: Lean primary zones: Pressure loss and residence time influences on combustion performance and NOx emissions. 1987 Tokyo Inter. gas turbine conference, Oct. 1987.

4-24 Al Dabbagh N.A. and Andrews G.E.: Weak extinction and turbulent burning velocity for grid plate stabilised premixed flames. Combut. and Flame, vol.55, pp.31-42, 1984.

4-25 Khalil K.H, El-Mahallawy F.M. and Moneibi H.A: 16th Symposium (Inter.) on Combustion, The Combustion Institute,pp.135, 1976.

4-26 Beltagui S.A. and MacCallum N.R.L.: Aerodynamics of vane swirled flames in furnaces. J. Inst. Fuel(Energy), vol.49,pp.183-193, 1976.

4-27 Beltagui S.A. and MacCallum N.R.L.: Characteristics of enclosed swirl flames with peripheral fuel injection. J. Inst. Energy, vol.LXI,446, March 1988.

4-28 Oven M.J., Gouldin F.C. and McLean W.J.: Temperature and species concentration measurements in a swirl stabilized combustor. 17th Symposium(Int.) on Combustion, The Combustion Inst., pp.363-374, 1979.

4-29 Panton P.L. and Sweat R.H.: Comb. and Flame, 30, pp.133-142, 1977.

4-30 Wear J.D. and Jones R.E.: Comparison of combustion characteristics of ASTM A-1, propane, and natural gas fuels in a annular Turbojet combustor. NASA TN D-7135, Jan. 1973.

4-31 Appleton J.P. and Heywood J.B.: The effects of imperfect fuel-air mixing in a burner on NO formation from nitrogen in the air and fuel. 14th Symposium (Int.) on Combustion, The Combustion Inst., pp.777-786, 1974.

4-32 Gupta A.K., Lilley D.G. and Syred N.: Swirl Flows. Abacus press, 1984.

4-33 Clarke A.G. and Williams A.: NOx formation and Control in stationary combustion plant. I. Chem. Eng. Symposium series no.96, 1986.

4-34 Andrews G.E. et al: High intensity burners with low NOx emissins. British Flame Days 1988, Inst. Energy, 1988.

4-35 Rawe R., and Kremer H.: Stability limits of natural gas diffusion flame with Swirl." 18th.,Symposium(International) on Combustion, Combustion Institute,p.667, 1981.

4-36 Syred N., Chigier N. A. and Beer G. M.: Flame stabilisation in recirculation zone of flames with swirl. 13th Symposium (Int.) on combustion, Comb. Inst., pp.617-624, 1970.

4-37 Beltagui S.A. and MacCallum N.R.L.: Stability limits of free swirling premixed flames, part1: Experimental correlation. J. Inst. Energy, pp.160-164, 1986.

4-38 Syred N. and Dahman K. R.: Effect of High Level of Confinement upon the Aerodynamics of Swirl Burners. J. of Energy,vol.2,No.1, 1978.

4-39 Claypole T. C. and Syred N.: The stabilisation of flames in swirl burners. J. Inst. Energy, 55, 14-19, 1982.

TABLES

Table (4.1)
Measured weak extinction limits for various radial vane angles at Mach number = 0.014.

Vane angle (Degrees)	Fuel type	Inlet Temp.K	Weak Extinction EQR.	A/F	Pressure Loss%
20°	Propane	400	0.334	47	3.8
		600	0.092	171	3.5
	Natural Gas	400	0.418	40	3.8
		600	0.322	52	3.5
30°	Propane	400	0.362	43	4.0
		600	0.113	139	4.0
	Natural Gas	400	0.418	40	4.0
		600	0.322	52	4.0
45°	Propane	400	0.329	48	3.8
		600	0.038	413	3.8
	Natural Gas	400	0.422	39	3.8
		600	0.030	553	3.9
50°	Propane	400	0.325	48	3.8
		600	0.077	205	4.2
	Natural Gas	400	0.389	43	4.0
		600	0.076	219	4.0
60°	Propane	400	0.260	60	3.8
		600	0.038	412	3.9
	Natural Gas	400	0.354	47	3.8
		600	0.060	276	3.8

Table (4.2)
Measured weak extinction for different outlet radial swirlers in 76mm and 140mm combustor.

Radial Swirler	Mach No.	D/d	Fuel Type	Inlet Temp.K	Weak Extinction EQR.	(A/F)	(ΔP/P)%
A	0.03	1.9	P	400	0.473	33	2.0
				600	0.379	41	2.1
			NG	400	0.432	38	2.0
				600	0.376	44	2.0
	0.014	3.5	P	400	0.396	40	2.3
				600	0.363	43	2.3
				400	0.430	38	2.3
				600	0.360	46	2.3
B	0.014	1.8	P	400	0.063	247	2.5
				600	0.062	252	2.5
			NG	400	0.316	52	2.5
				600	0.077	215	2.5
C	0.03	1.0	P	400	0.031	508	2.0
				600	0.024	666	2.2

Table (4.3)
Optimum Primary Zone Conditions
at 600K.

Radial Swirler	Combustor I.D. (mm)	D/d	Mach No.	Fuel Type	NO_{xc} ppm.	Ineff.%	EQR.
A	76	1.9	0.03	P	21	0.06	0.45
				NG	9	0.06	0.47
	140	3.5	0.014	P	18	0.01	0.48
				NG	9	0.01	0.52
B	140	1.8	0.014	P	17	0.20	0.28
				NG	10	0.20	0.32

Table (4.4)
Influence of the primary zone Mach number
on the measured weak extinction.

Radial Swirler	Mach No.	Fuel Type	Inlet Temp.K	Weak Extinction EQR.	(A/F)	(ΔP/P)%
76mm Combustor						
A	0.047	P	400	0.486	32	4.7
			600	0.394	40	4.7
		NG	400	0.500	33	4.7
			600	0.399	41	4.7
	0.03	P	400	0.473	33	2.0
			600	0.379	41	2.0
		NG	400	0.432	38	2.0
			600	0.376	44	2.0
140mm Combustor						
A	0.014	P	600	0.363	43	2.3
		NG	600	0.360	46	2.3
	0.008	NG	600	0.365	45	1.8
B	0.014	P	600	0.062	252	2.5
		NG	600	0.077	215	2.5
	0.02	P	600	0.080	195	4.2
		NG	600	0.283	59	4.2
C	0.014	P	600	0.038	413	3.9
		NG	600	0.030	552	4.0
	0.02	P	600	0.078	201	7.7
		NG	600	0.343	48	7.7

Table (4.5)
Influence of central radial position on the weak exctinction
for radial swirler (A), 76mm combustor, Mach no. 0.03. natural gas.

Injector holes position	Inlet Temp.	Weak Extinction EQR.	(A/F)	(ΔP/P)%
3mm	400	0.432	38	1.9
	600	0.376	44	1.9
70mm	600	0.368	45	1.9
70mm & Baffle	400	0.016	1056	1.9
	600	0.018	900	1.8

Table (4.6)
Proposed Emission Limit Values for Oxides of Nitrogen in Waste Gases from Stationary Combustion Plant. (33)

Fuel	Plant Size Mw Th.	NO_x (expressed as NO_2, mg/m^3	
		from 1.1.1985	after 31.12.1995
Solid	> 300	< 650	< 200
	300-100	< 800	
	< 100	< 800 but < 1300 for pulverised hard coal firing with extraction of fused ash.	< 400 as a rule < 800 for pulverised hard coal firing with extraction of fused ash.
Liquid	All > 50	< 450	< 150
Gas	All > 50	< 350	< 100

i - Waste gas volume refered to 273 K and 1 atm; 3% O_2 for liquid and gaseous fuels, 6% O_2 from solid fuels, 200mg NO_2/m^3 = 97.5 ppmv.

ii - Continuous monitoring from which half-hour and daily average are to be calculated. Compliance requires that over a calender year.

- none of the daily mean values exceed the emission limit value.
- 97% of the half-hourly values do not exceed (6/5) x the limit value.
- none of the half-hourly values exceed 2 x the limit value.

Table (4.7)
Measured Weak Extinction limits for swirler (A) in 140 mm burner.

Approach Velocity (U1)	(ΔP/P) %	Weak Extinction EQR	(A/F)	Combustor inlet temperature, K
2.5	1.1%	0.59	28	305
3.6		0.37	45	600
2.5		0.53	31	305 with W.C.P.
3.6		0.41	40	600 with W.C.P.
3.3	2.1%	0.49	34	305 with W.C.P.

FIGURES

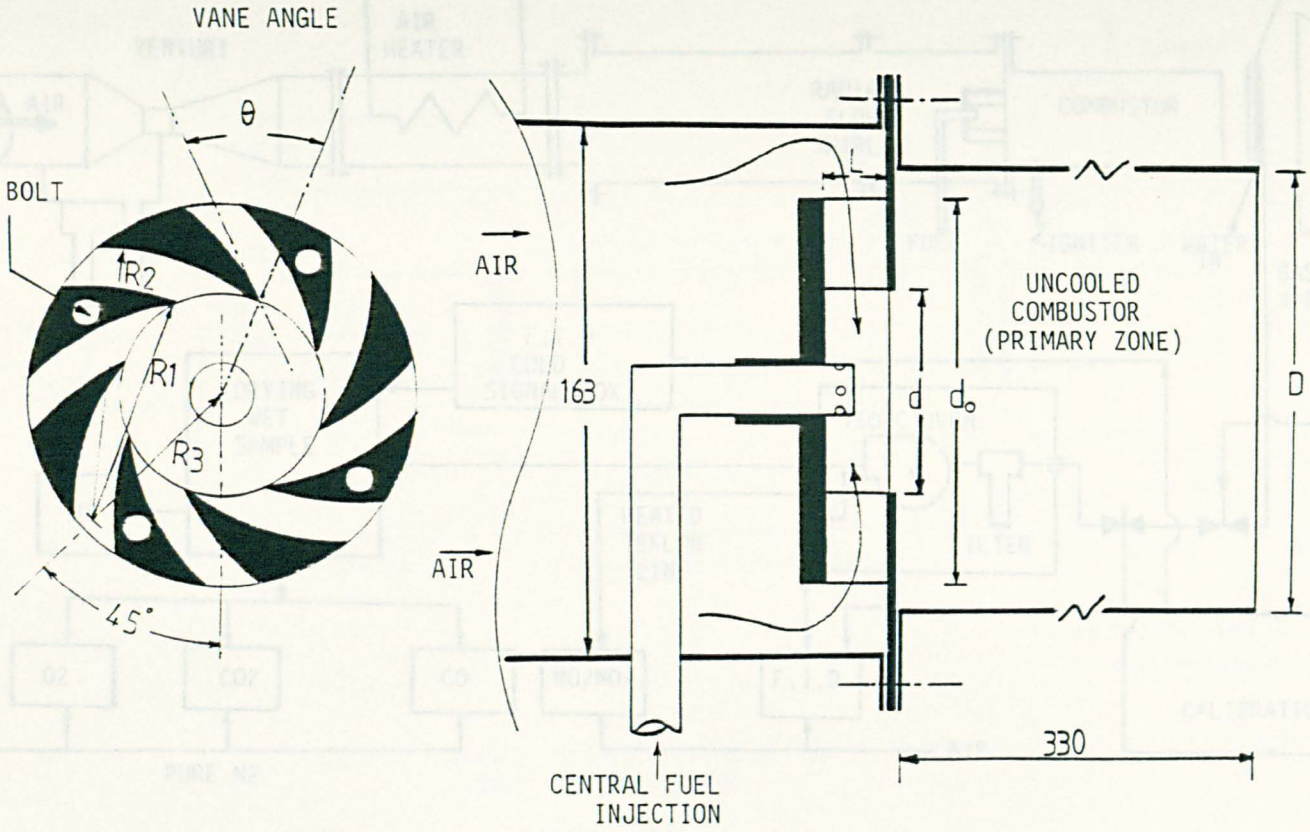

FIG.4.1 SCHEMATIC DIAGRAM OF THE RADIAL SWIRLERS COMBUSTOR WITH CENTRAL FUEL INJECTION CONFIGURATION.

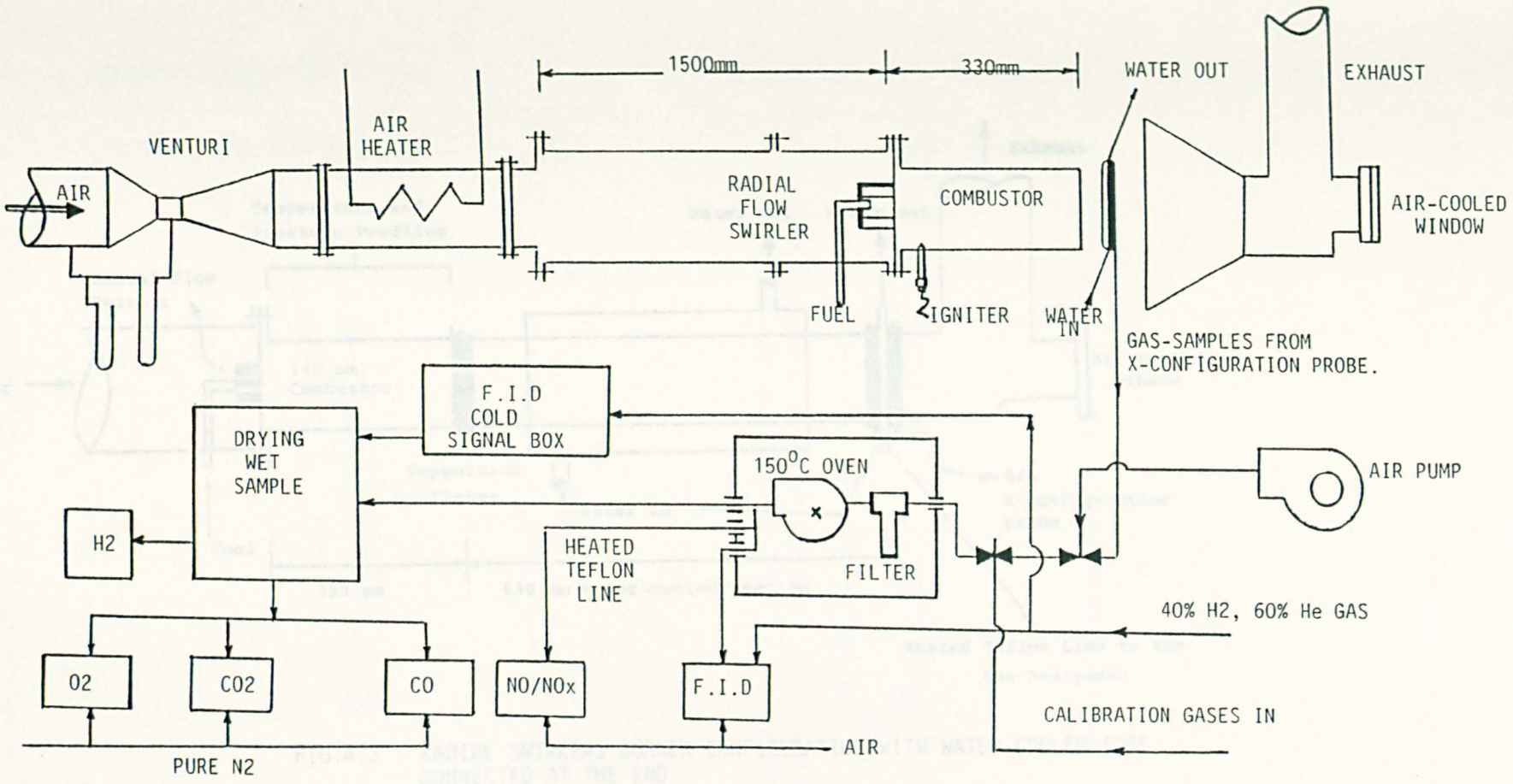

FIG.4.2. SCHEMATIC DIAGRAM OF THE RIG AND INSTRUMENTATIONS USED IN THE PRESENT WORK.

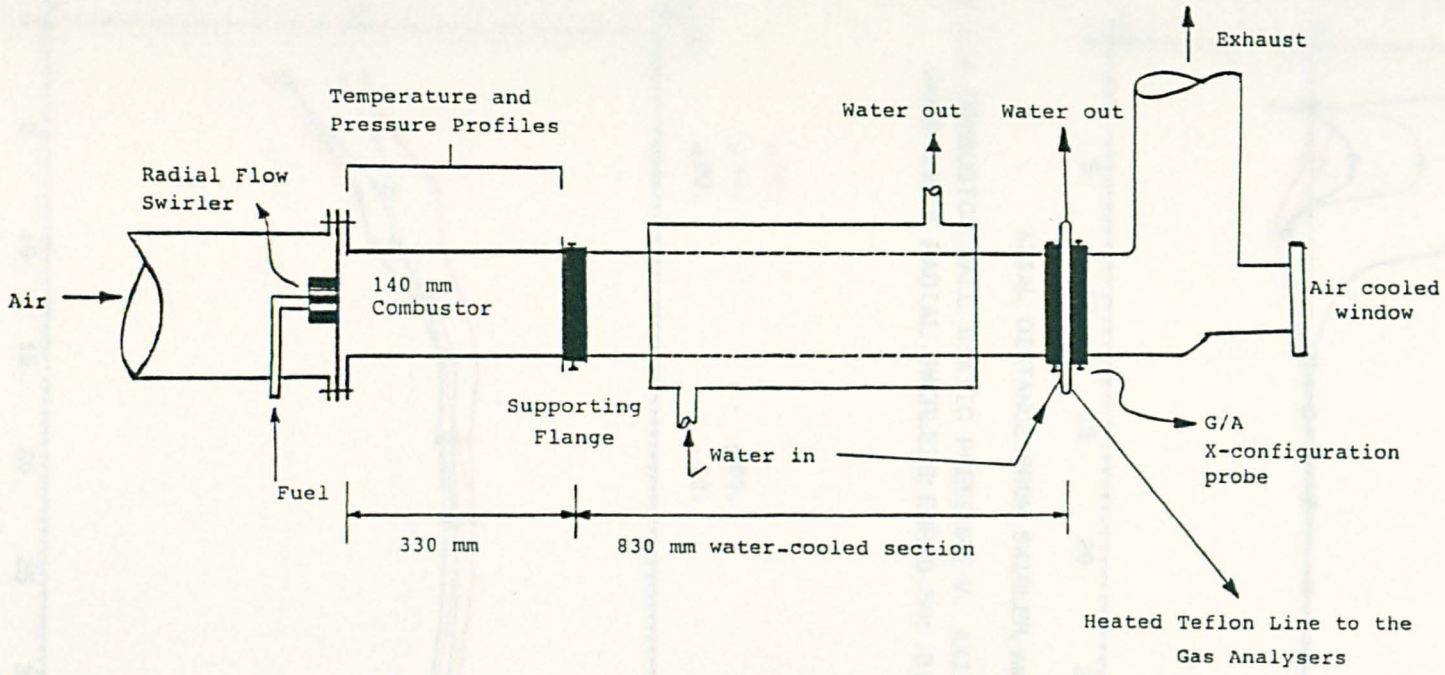

FIG.4.3 RADIAL SWIRLERS BURNER CONFIGURATION WITH WATER-COOLED TUBE CONNECTED AT THE END.

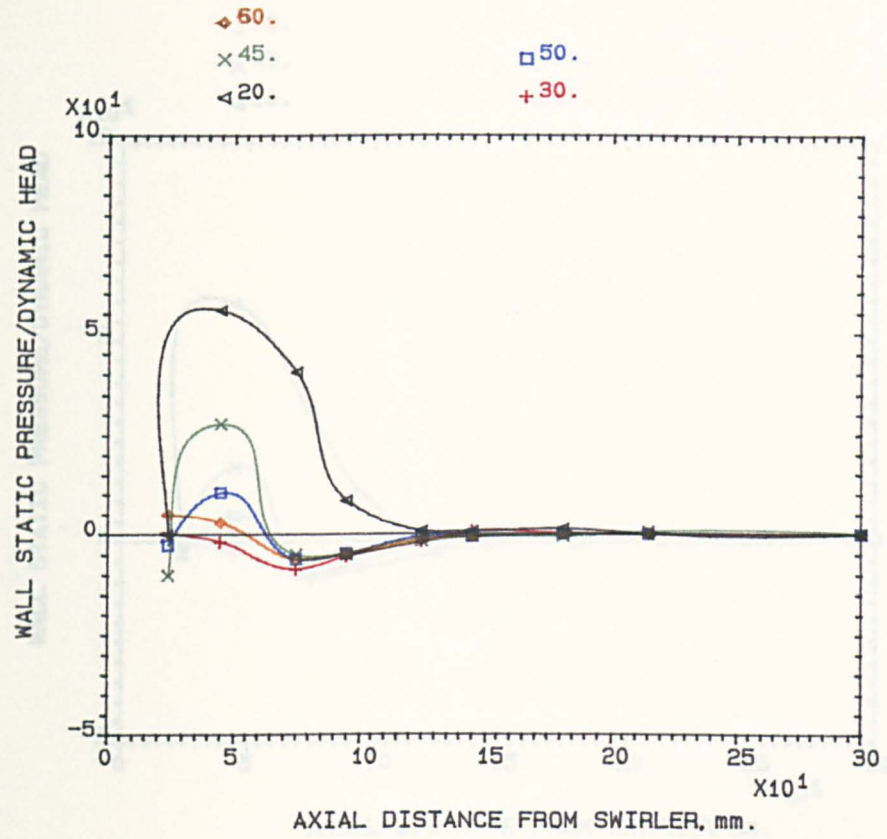

FIG.4.4 COMBUSTOR WALL STATIC PRESSURE V. AXIAL DISTANCE FOR VARIOUS VANE ANGLE RADIAL SWIRLERS; EQR=0.50; .014; PROPANE; 400K.

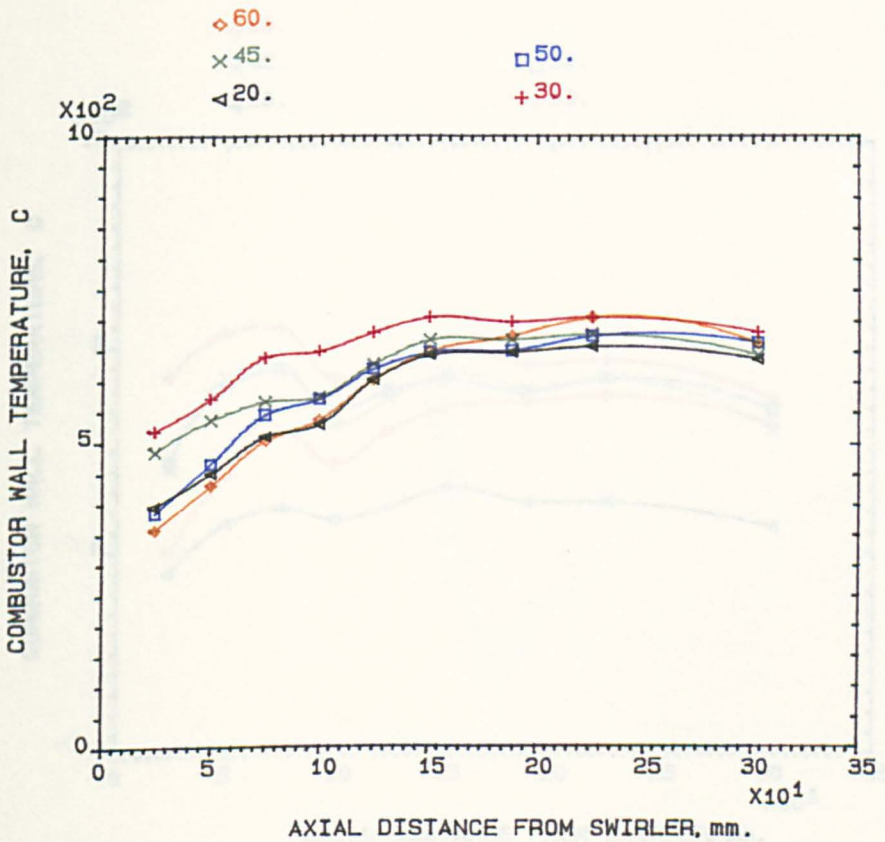

FIG.4.5 COMBUSTOR WALL TEMPERATURE V. AXIAL DISTANCE FOR VARIOUS VANE ANGLE RADIAL SWIRLERS; EQR=0.50; MN=0.014; PROPANE; 400K.

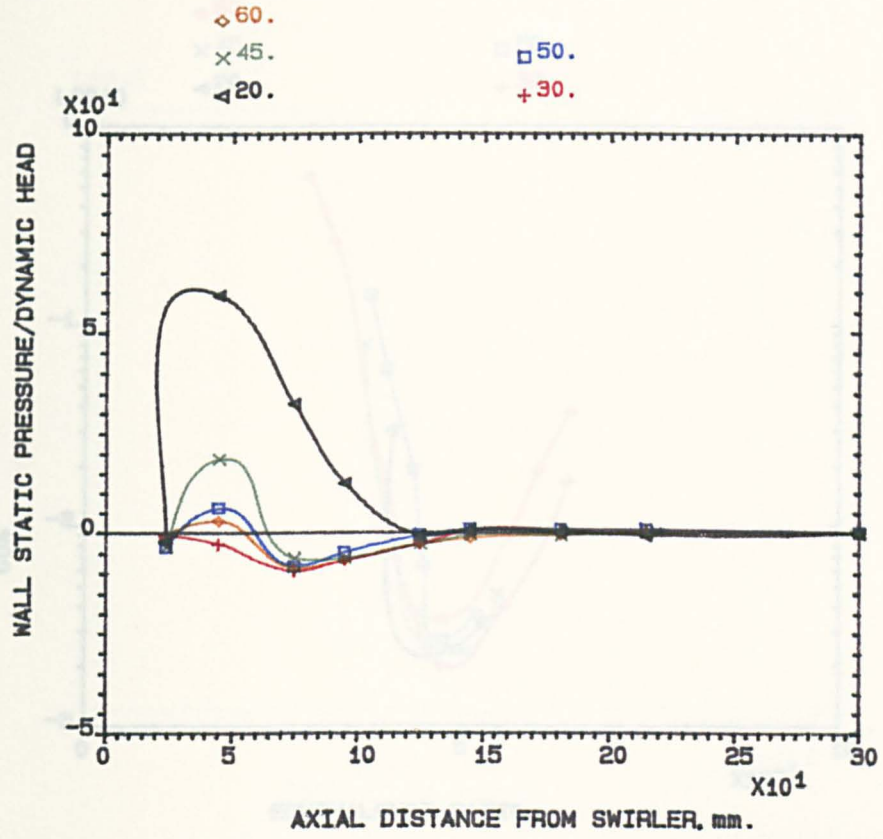

FIG.4.6 COMBUSTOR WALL STATIC PRESSURE V. AXIAL DISTANCE FOR VARIOUS VANE ANGLE RADIAL SWIRLERS; EQR=0.50; MN=.014; PROPANE; 600K.

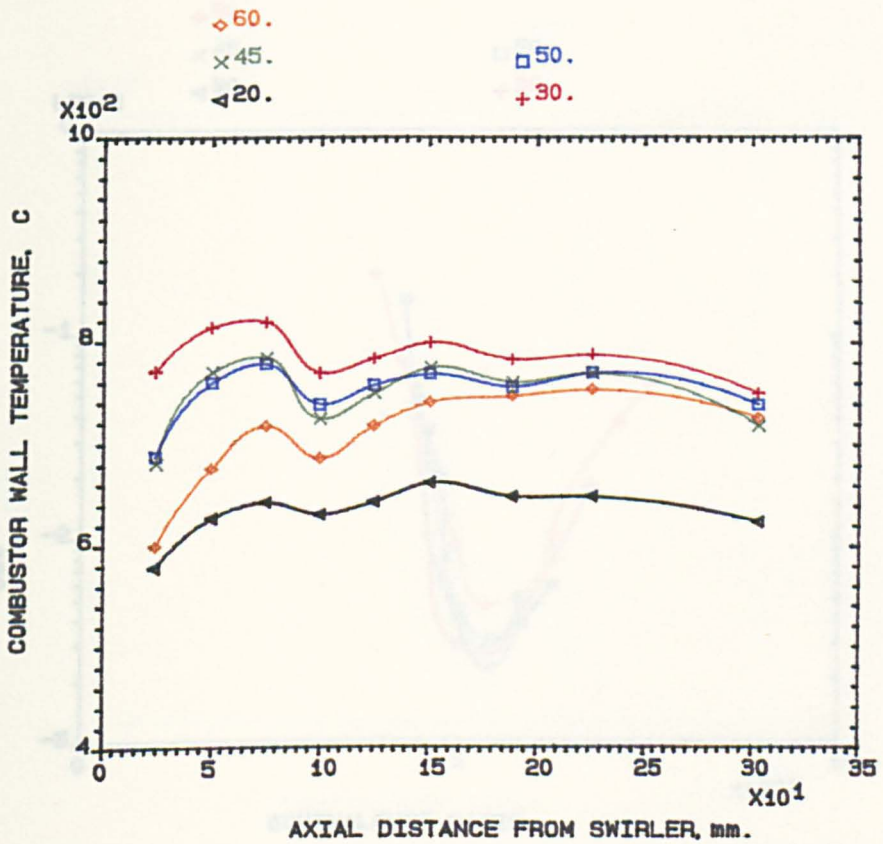

FIG.4.7 COMBUSTOR WALL TEMPERATURE V. AXIAL DISTANCE FOR VARIOUS VANE ANGLE RADIAL SWIRLERS; EQR=0.50; MN=0.014; PROPANE; 600K.

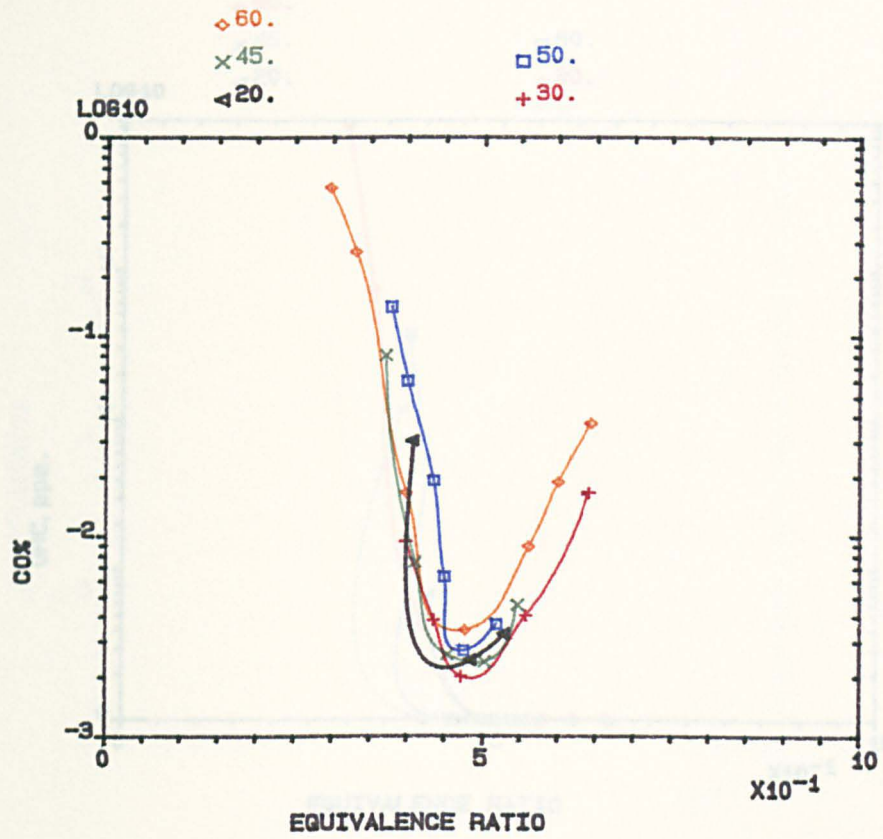

FIG.4.8 INFLUENCE OF RADIAL VANE ANGLE ON EMISSIONS. 140mm COMBUSTOR. MN=0.014; PROPANE; 400 K.

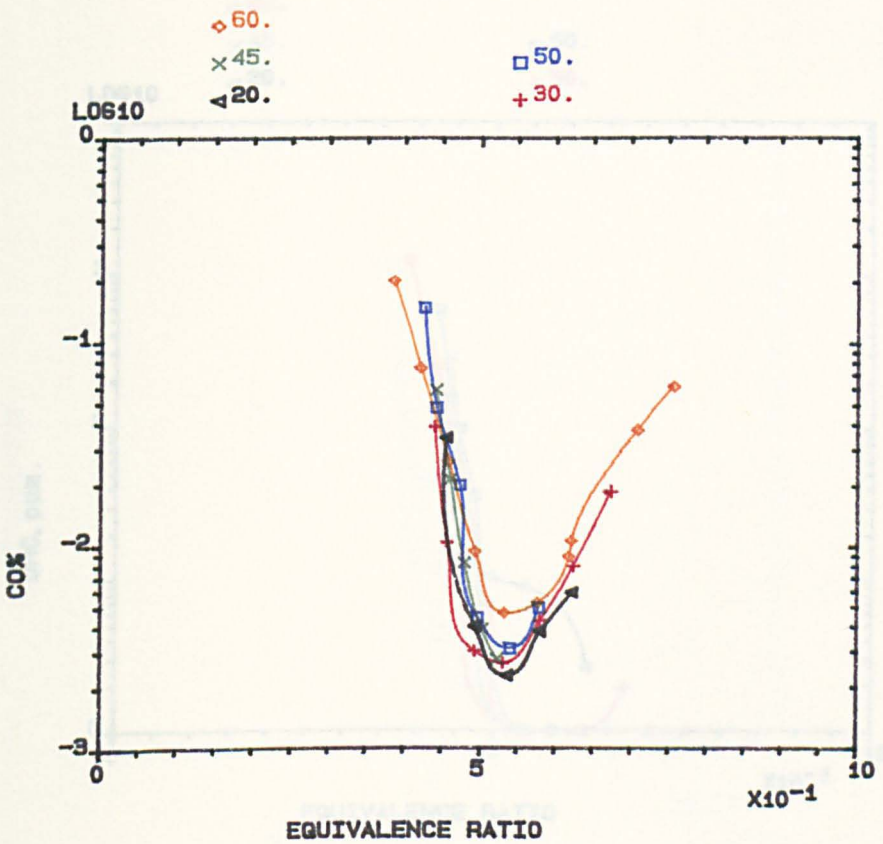

FIG.4.9 INFLUENCE OF RADIAL VANE ANGLE ON EMISSIONS. 140mm COMBUSTOR. MN=0.014; NATURAL GAS; 400 K.

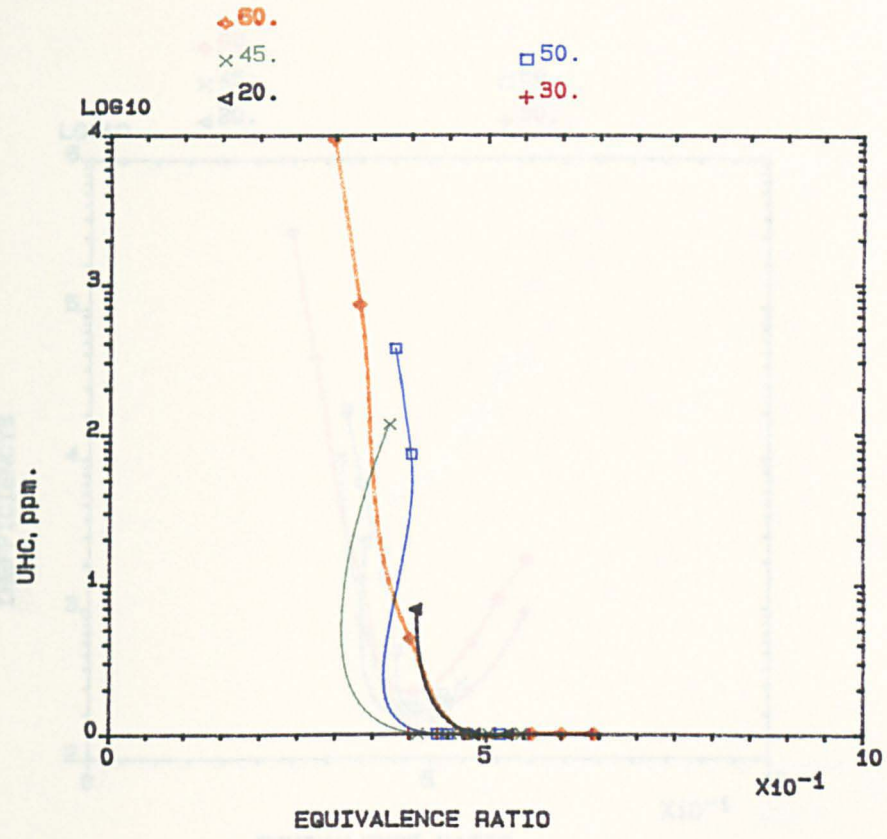

FIG.4.10 INFLUENCE OF RADIAL VANE ANGLE ON EMISSIONS. 140mm COMBUSTOR, MN=0.014; PROPANE; 400 K.

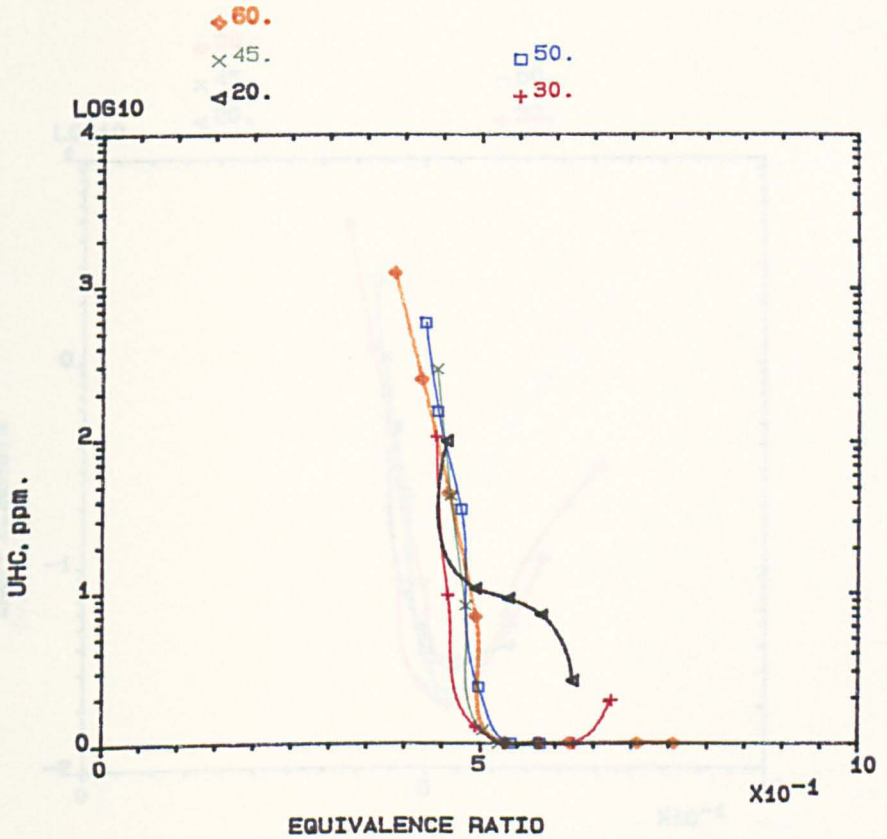

FIG.4.11 INFLUENCE OF RADIAL VANE ANGLE ON EMISSIONS. 140mm COMBUSTOR, MN=0.014; NATURAL GAS; 400 K.

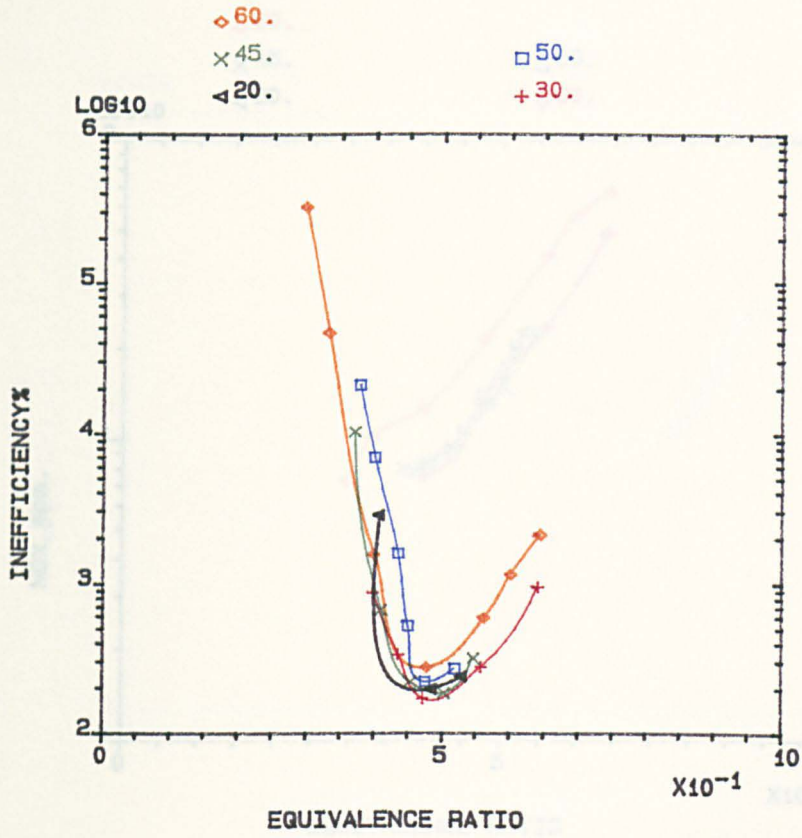

FIG.4.12 INFLUENCE OF RADIAL VANE ANGLE ON EMISSIONS, 140mm COMBUSTOR, MN=0.014; PROPANE; 400 K.

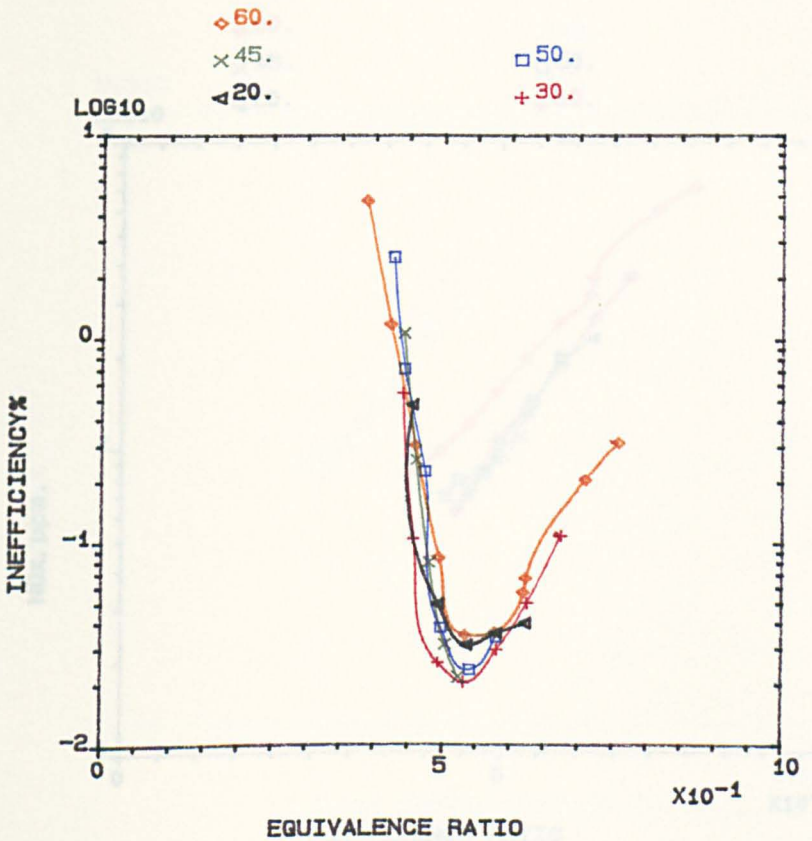

FIG.4.13 INFLUENCE OF RADIAL VANE ANGLE ON EMISSIONS, 140mm COMBUSTOR, MN=0.014; NATURAL GAS; 400 K.

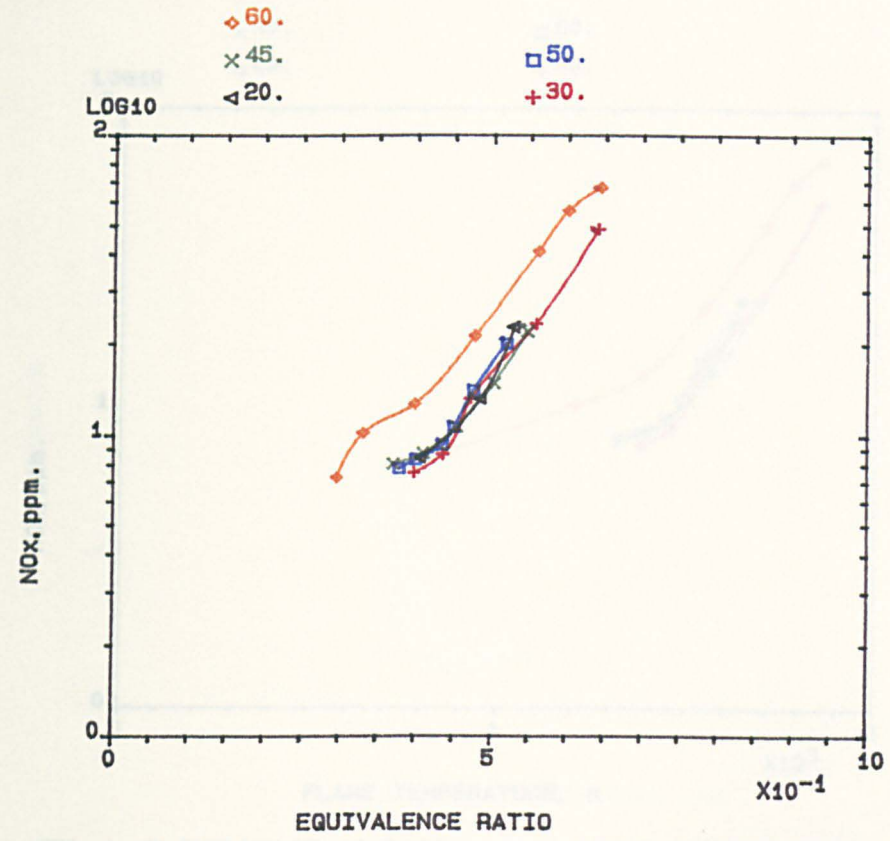

FIG.4.14 INFLUENCE OF RADIAL VANE ANGLE ON EMISSIONS, 140mm COMBUSTOR, MN=0.014; PROPANE; 400 K.

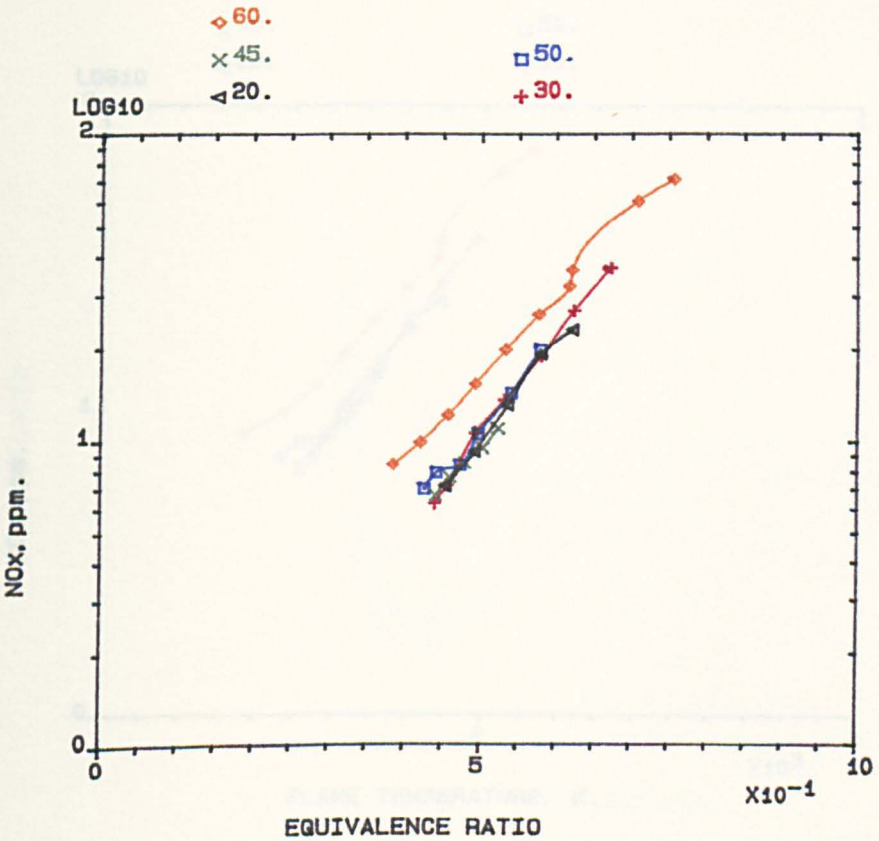

FIG.4.15 INFLUENCE OF RADIAL VANE ANGLE ON EMISSIONS, 140mm COMBUSTOR, MN=0.014; NATURAL GAS; 400 K.

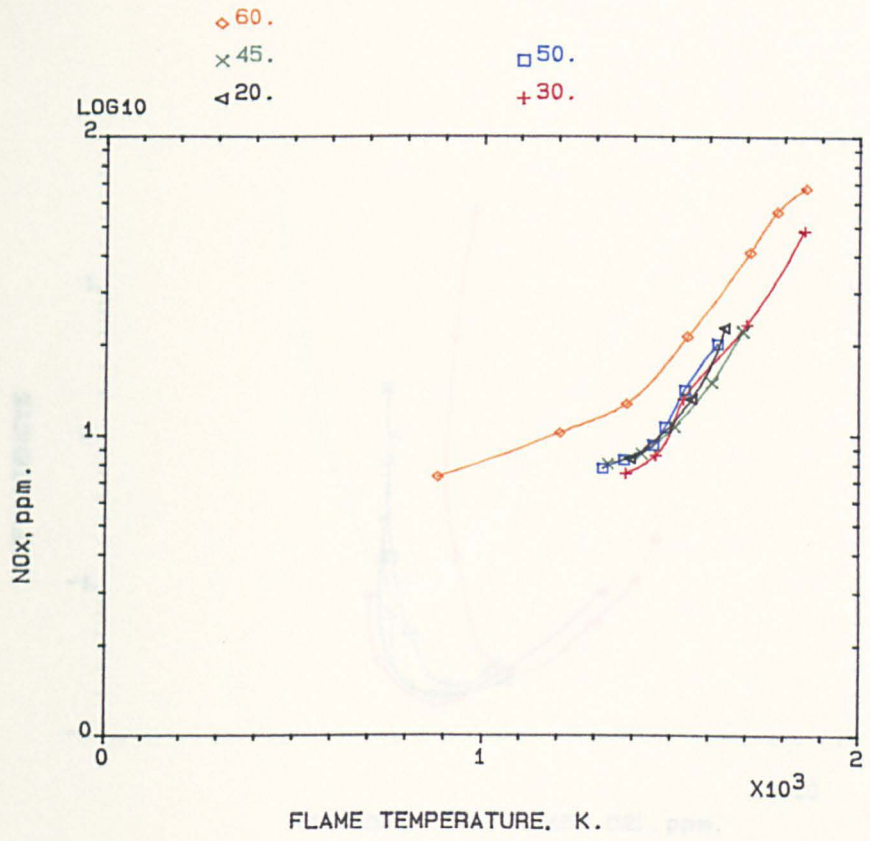

FIG.4.16 INFLUENCE OF RADIAL VANE ANGLE ON EMISSIONS.
140mm COMBUSTOR, MN=0.014; PROPANE; 400 K.

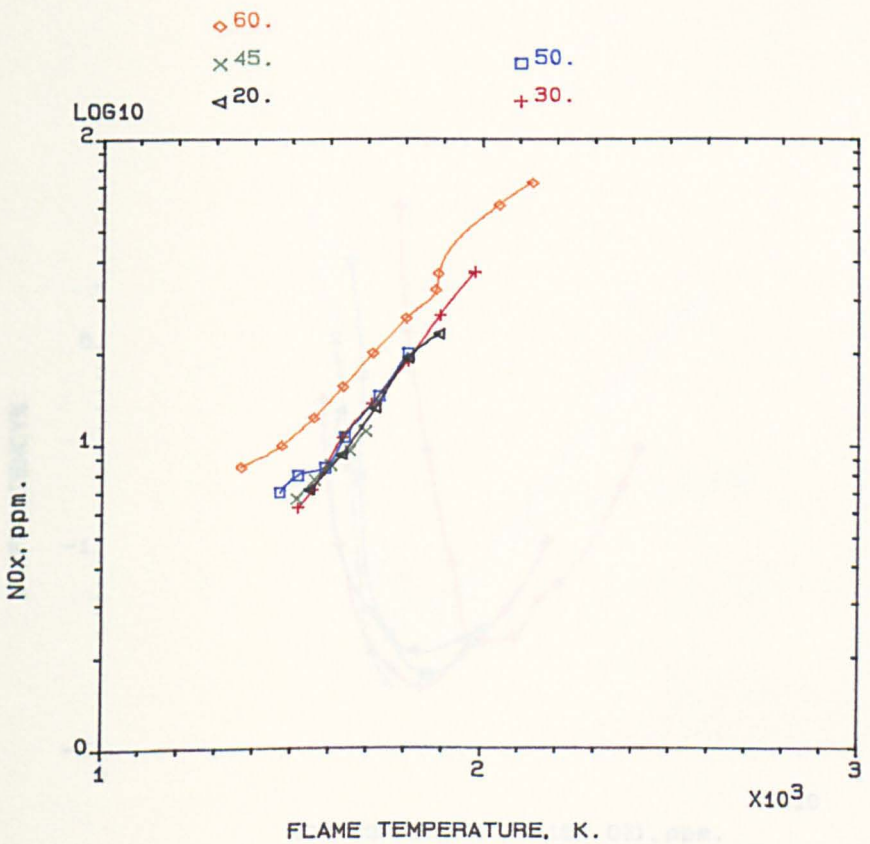

FIG.4.17 INFLUENCE OF RADIAL VANE ANGLE ON EMISSIONS.
140mm COMBUSTOR, MN=0.014; NATURAL GAS; 400 K.

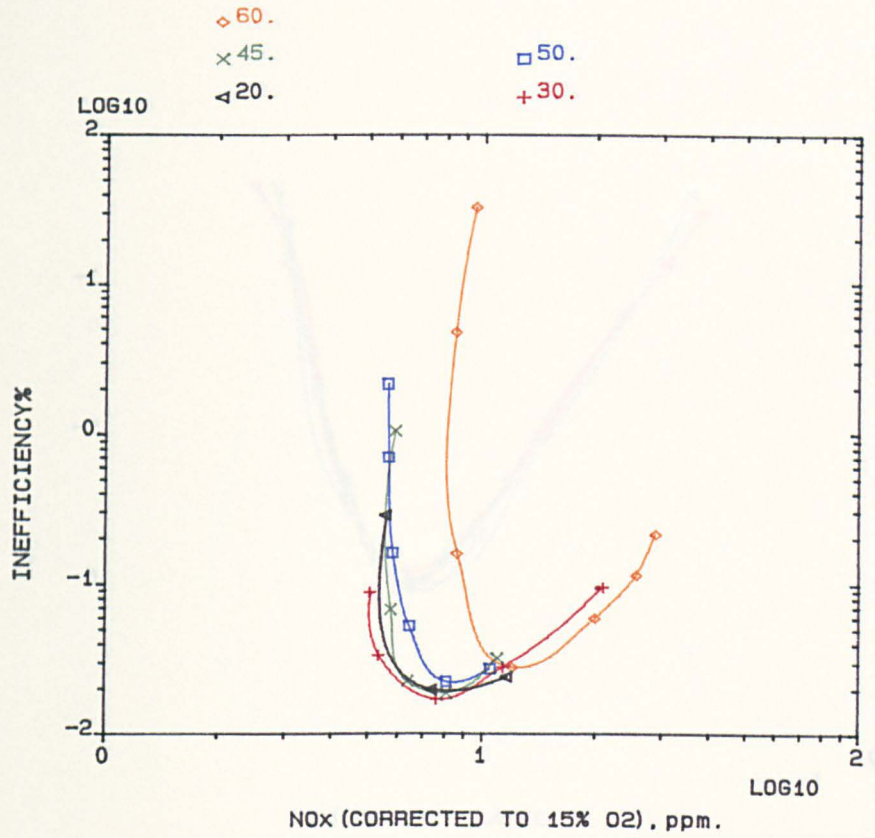

FIG.4.18 INFLUENCE OF RADIAL VANE ANGLE ON EMISSIONS.
140mm COMBUSTOR. MN=0.014; PROPANE; 400 K.

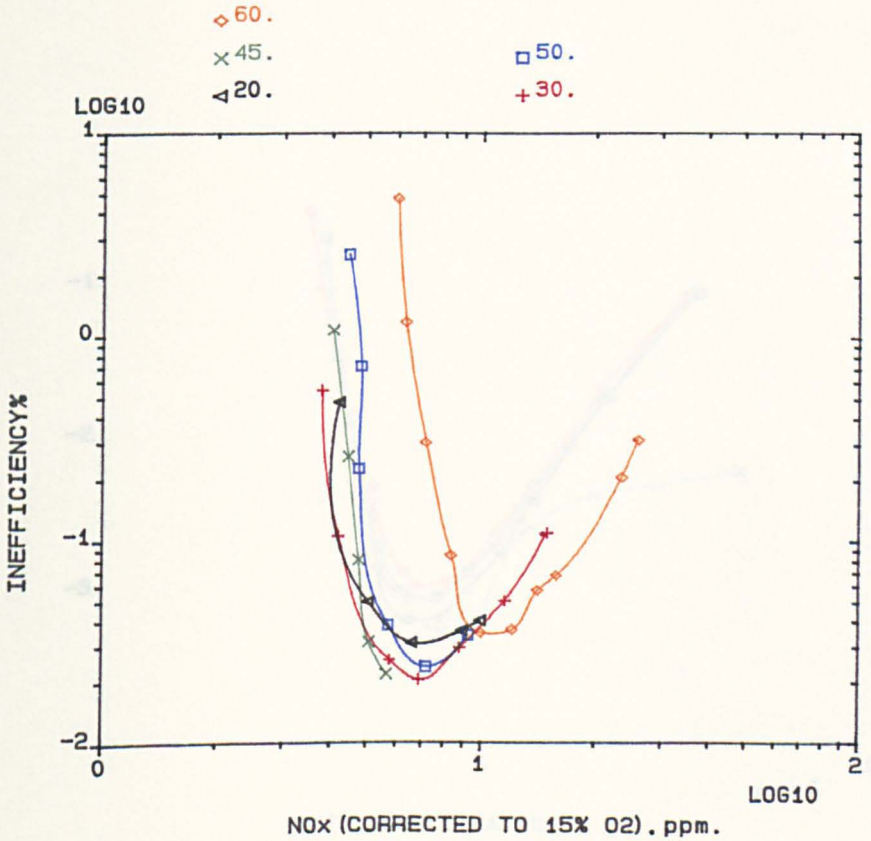

FIG.4.19 INFLUENCE OF RADIAL VANE ANGLE ON EMISSIONS.
140mm COMBUSTOR. MN=0.014; NATURAL GAS; 400 K.

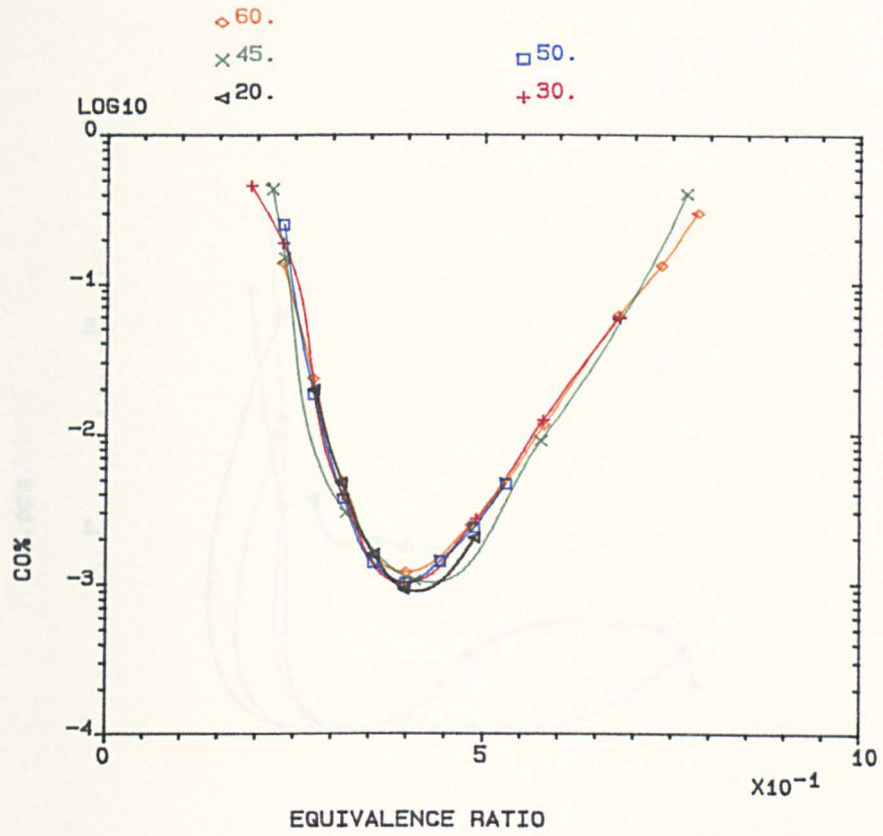

FIG.4.20 INFLUENCE OF RADIAL VANE ANGLE ON EMISSIONS. 140mm COMBUSTOR. MN=0.014; PROPANE; 600 K.

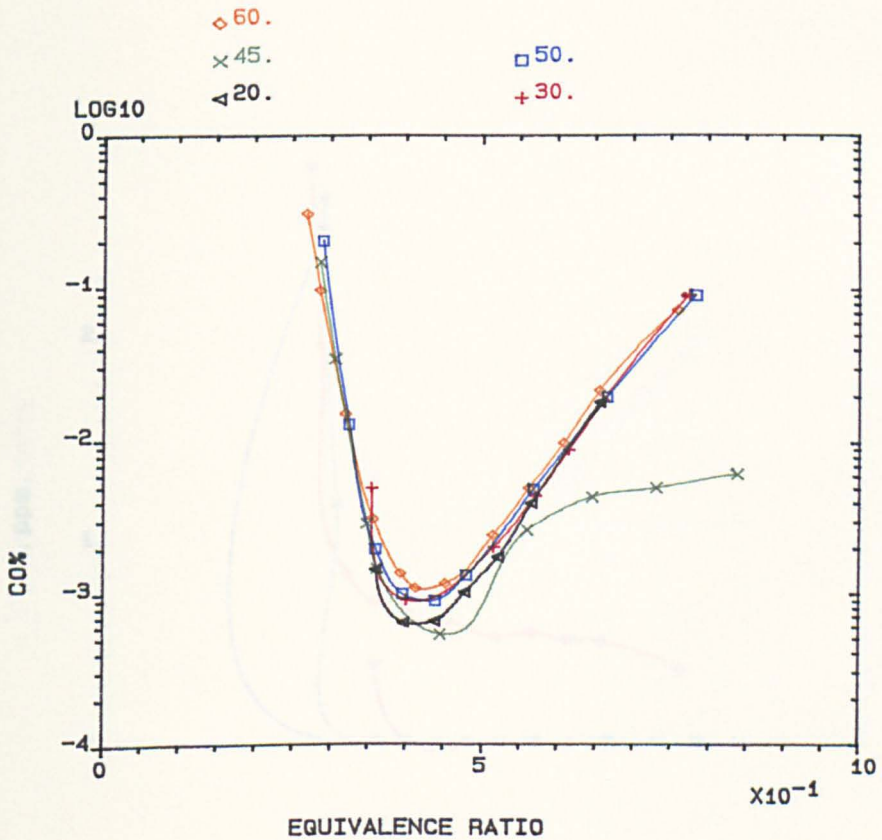

FIG.4.21 INFLUENCE OF RADIAL VANE ANGLE ON EMISSIONS. 140mm COMBUSTOR. MN=0.014; NATURAL GAS; 600 K.

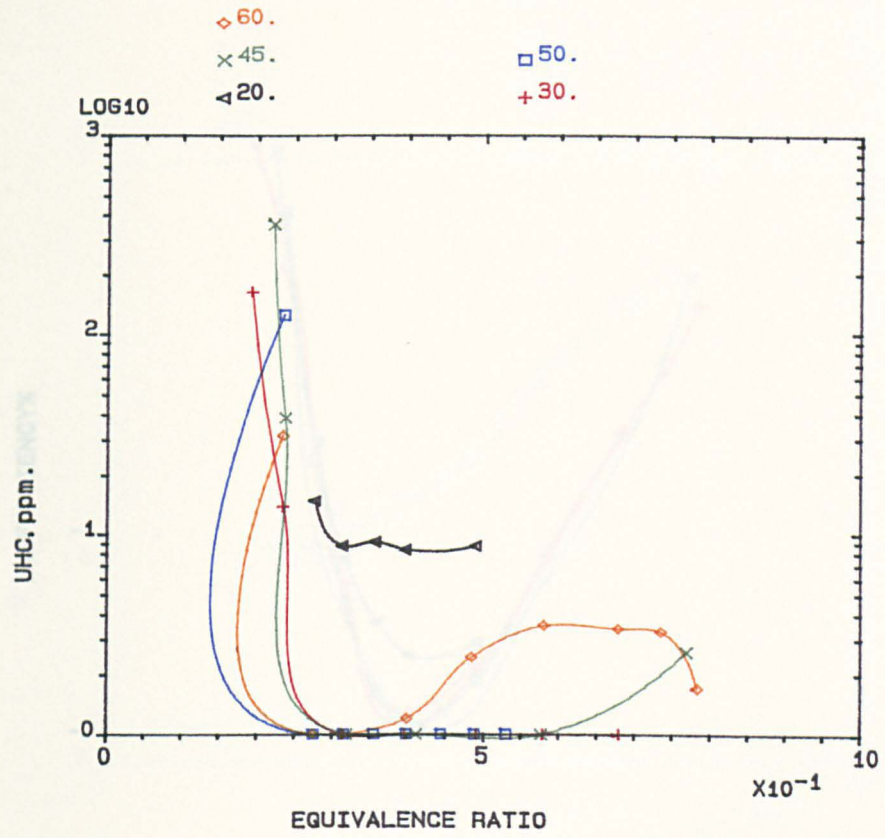

FIG.4.22 INFLUENCE OF RADIAL VANE ANGLE ON EMISSIONS, 140mm COMBUSTOR, MN=0.014; PROPANE; 600 K.

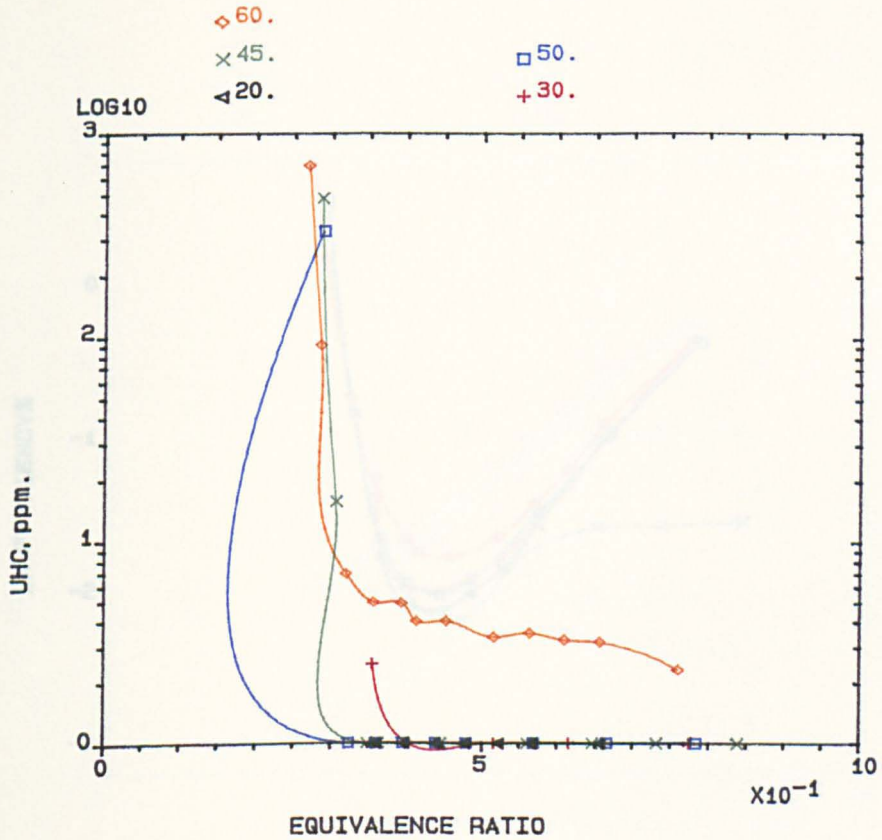

FIG.4.23 INFLUENCE OF RADIAL VANE ANGLE ON EMISSIONS, 140mm COMBUSTOR, MN=0.014; NATURAL GAS; 600 K.

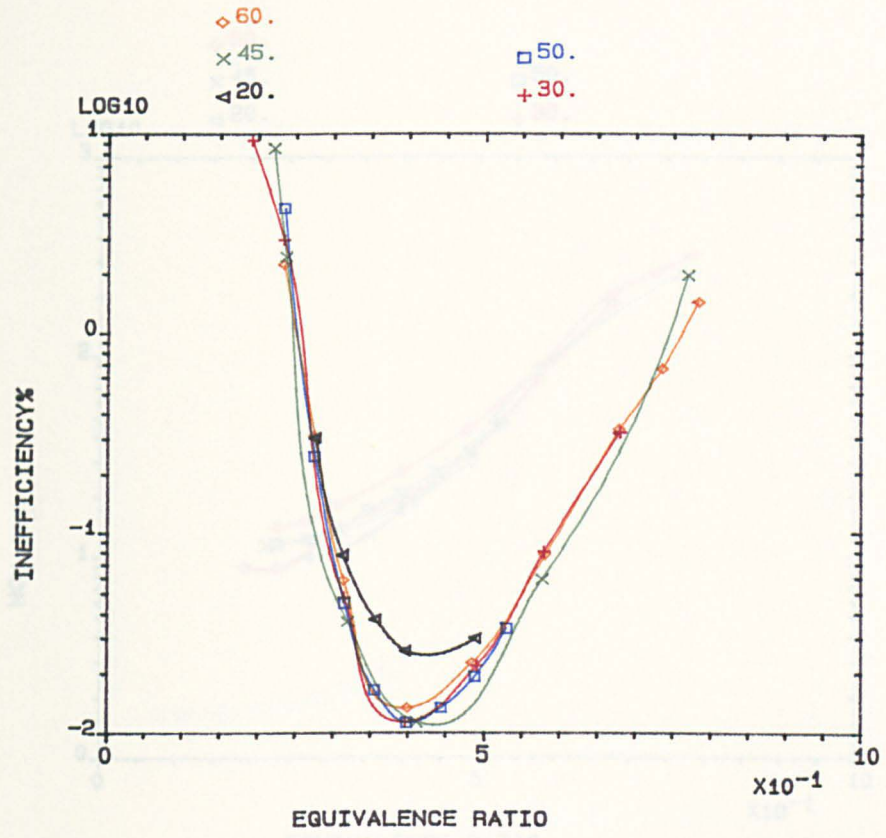

FIG.4.24 INFLUENCE OF RADIAL VANE ANGLE ON EMISSIONS, 140mm COMBUSTOR, MN=0.014; PROPANE; 600 K.

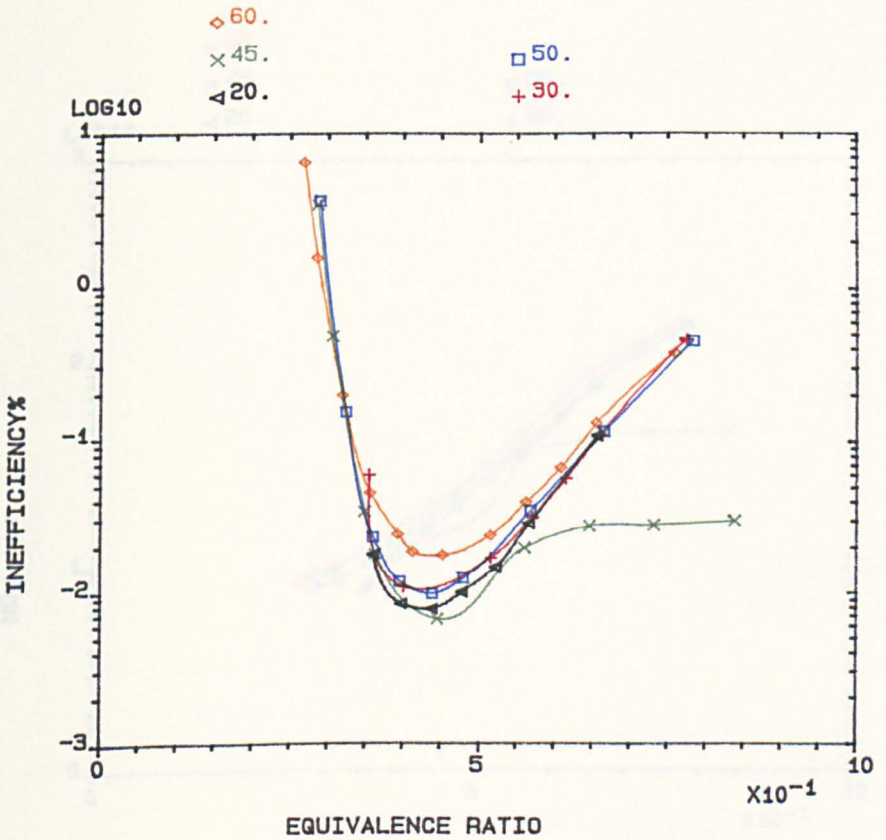

FIG.4.25 INFLUENCE OF RADIAL VANE ANGLE ON EMISSIONS, 140mm COMBUSTOR, MN=0.014; NATURAL GAS; 600 K.

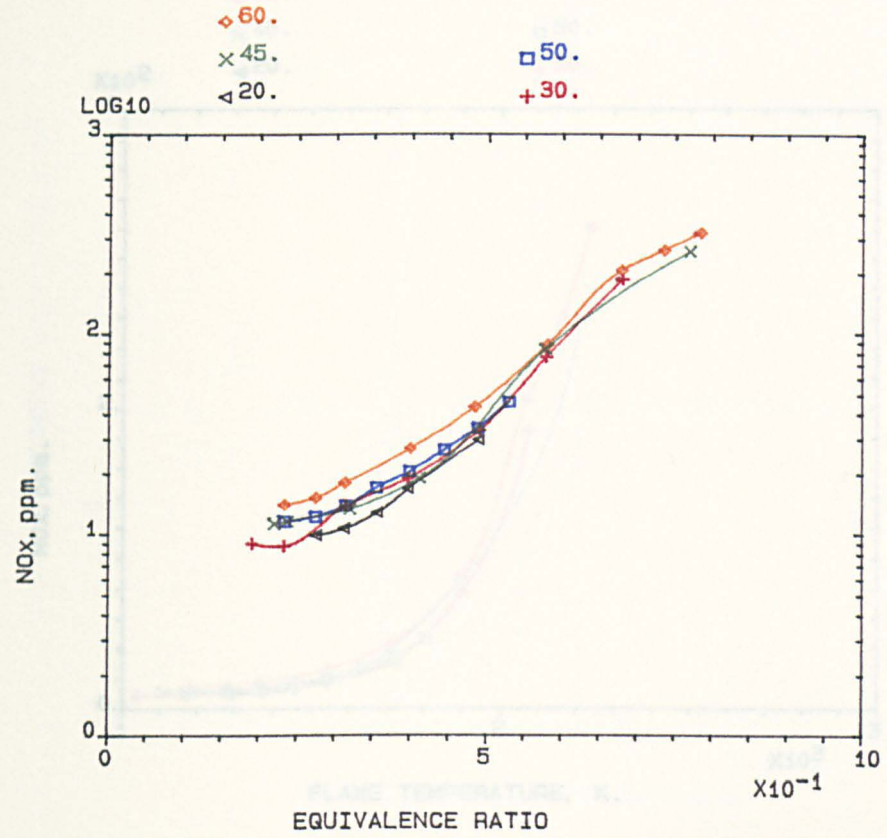

FIG.4.26 INFLUENCE OF RADIAL VANE ANGLE ON EMISSIONS, 140mm COMBUSTOR, MN=0.014; PROPANE; 600 K.

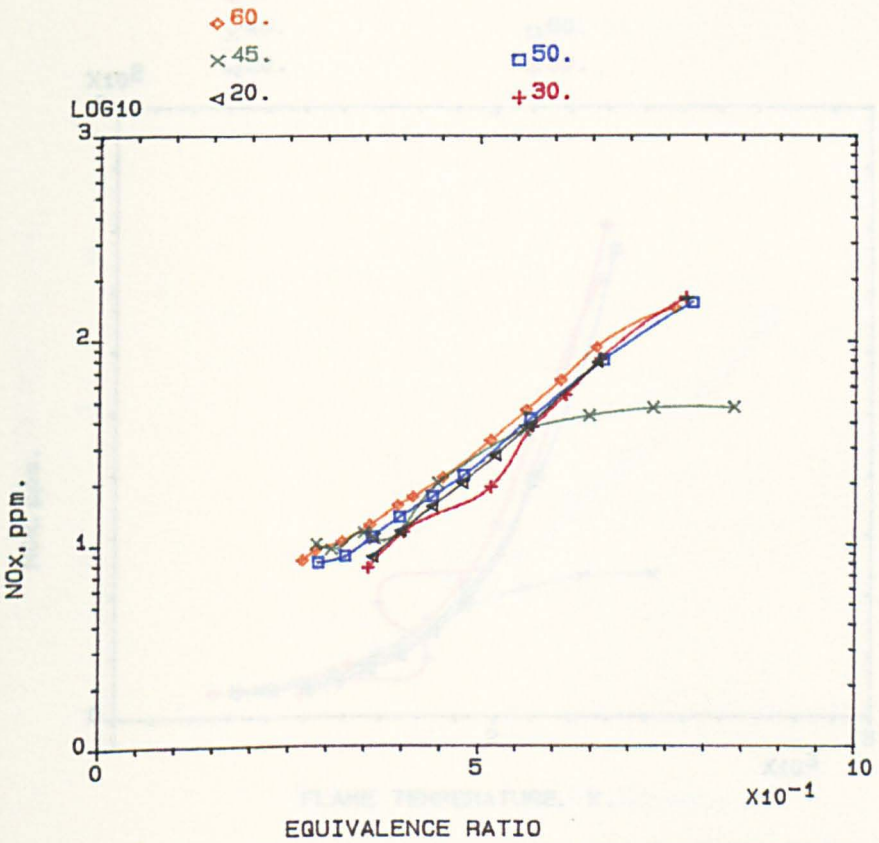

FIG.4.27 INFLUENCE OF RADIAL VANE ANGLE ON EMISSIONS, 140mm COMBUSTOR, MN=0.014; NATURAL GAS; 600 K.

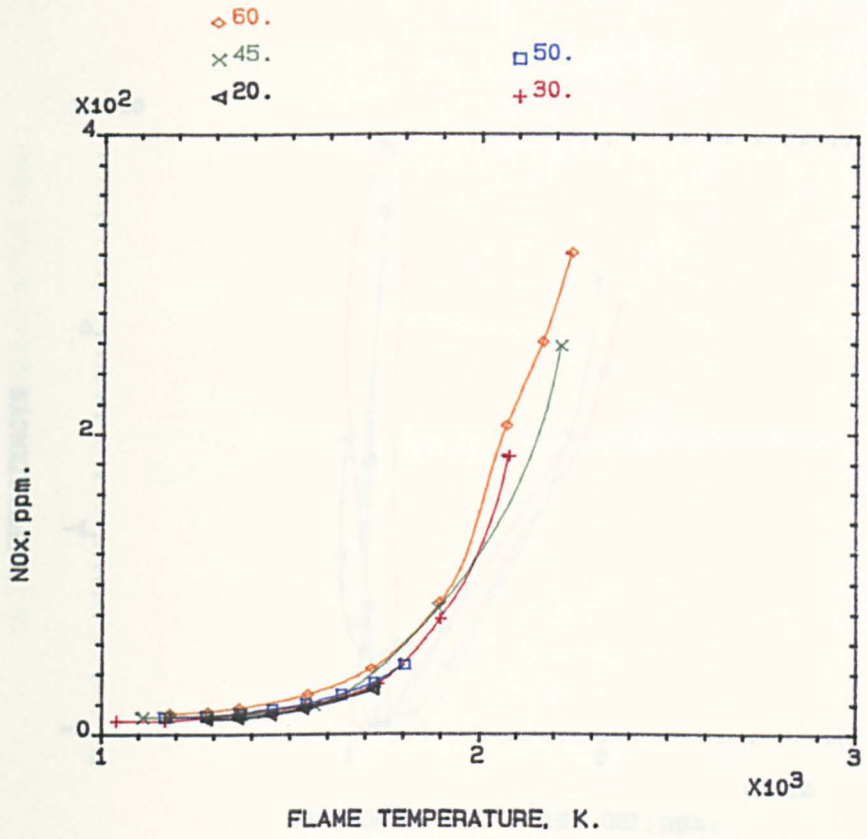

FIG.4.28 INFLUENCE OF RADIAL VANE ANGLE ON EMISSIONS, 140mm COMBUSTOR, MN=0.014; PROPANE; 600 K.

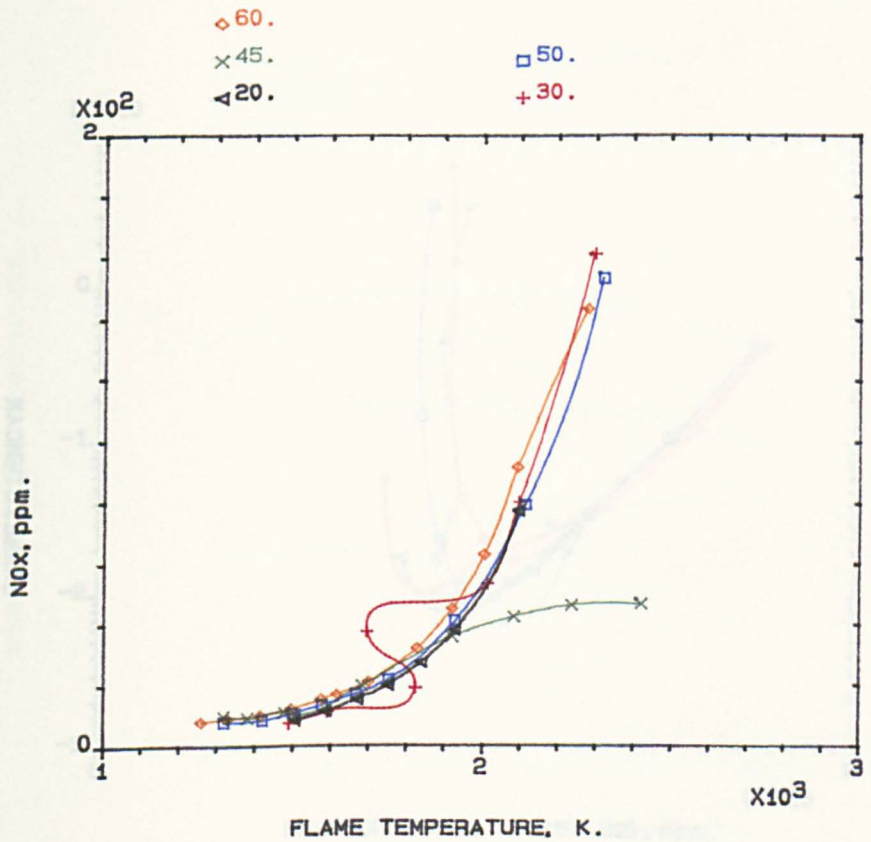

FIG.4.29 INFLUENCE OF RADIAL VANE ANGLE ON EMISSIONS, 140mm COMBUSTOR, MN=0.014; NATURAL GAS; 600 K.

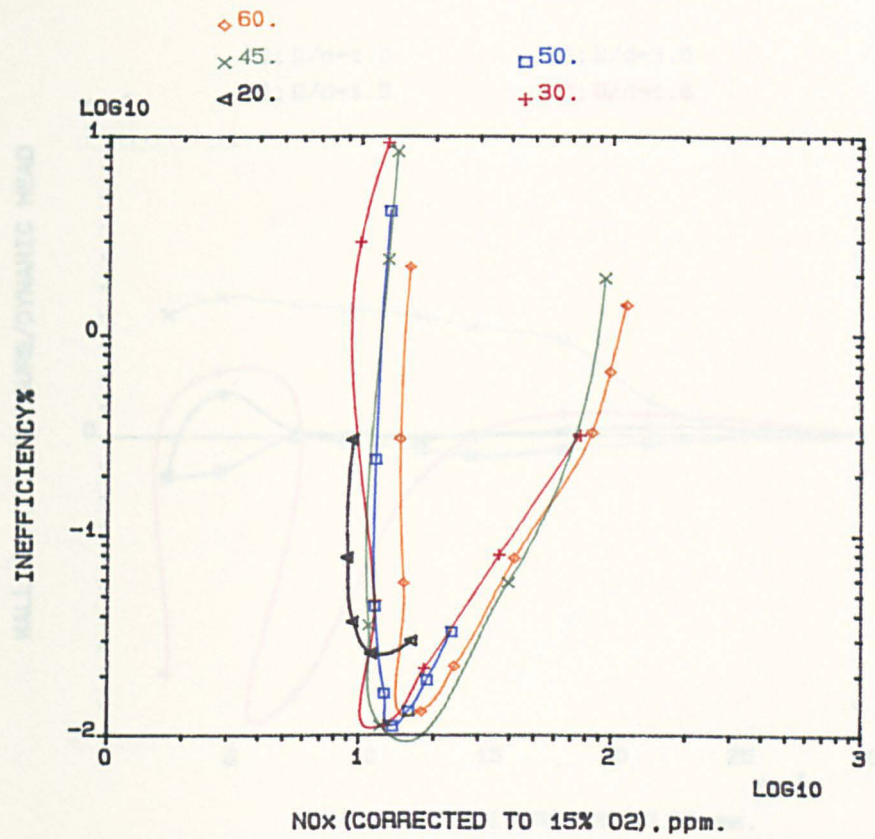

FIG.4.30 INFLUENCE OF RADIAL VANE ANGLE ON EMISSIONS.
140mm COMBUSTOR. MN=0.014; PROPANE; 600 K.

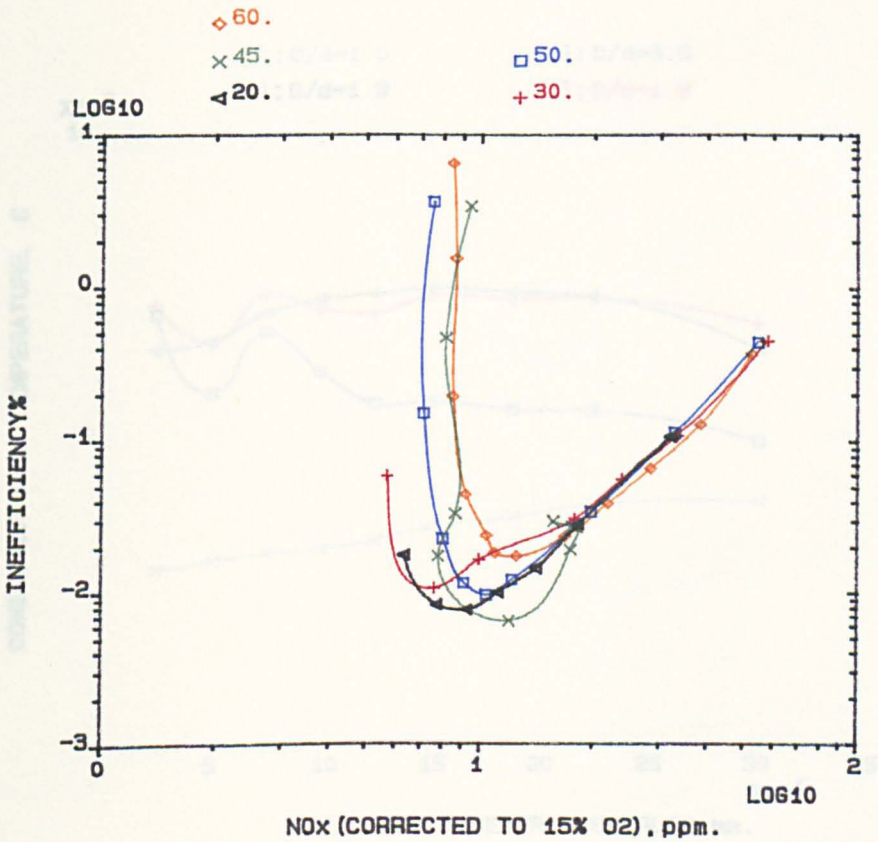

FIG.4.31 INFLUENCE OF RADIAL VANE ANGLE ON EMISSIONS.
140mm COMBUSTOR. MN=0.014; NATURAL GAS; 600 K.

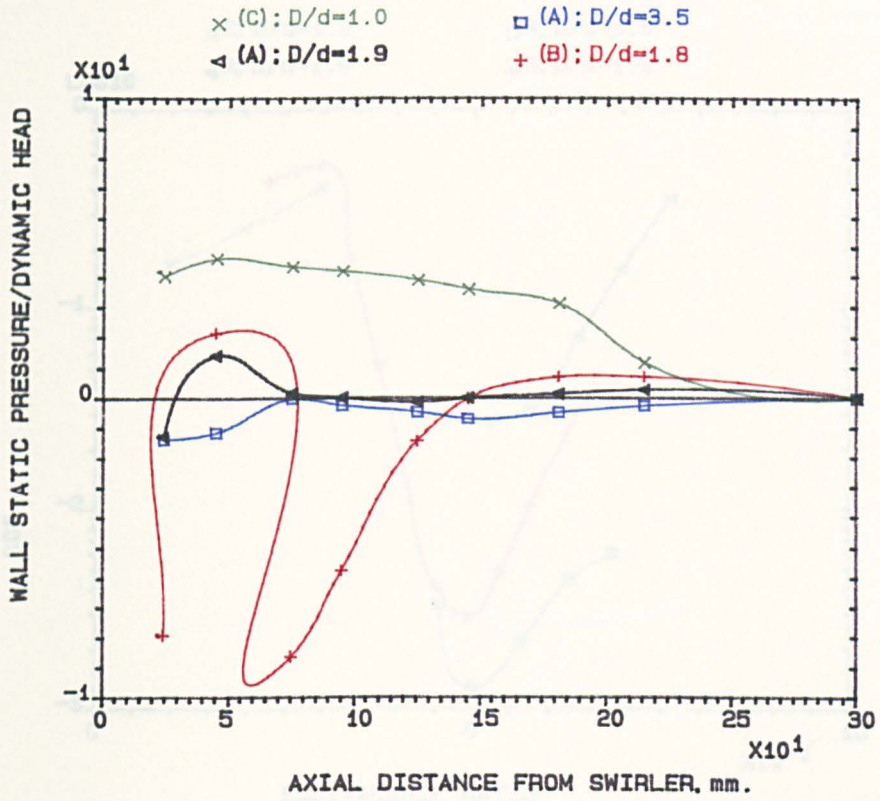

FIG.4.32 INFLUENCE OF SWIRLERS OUTLET DIAMETER ON WALL STATIC PRESSURE FOR 45 VANE ANGLE SWIRLERS; EQR=0.44; PROPANE; 600K.

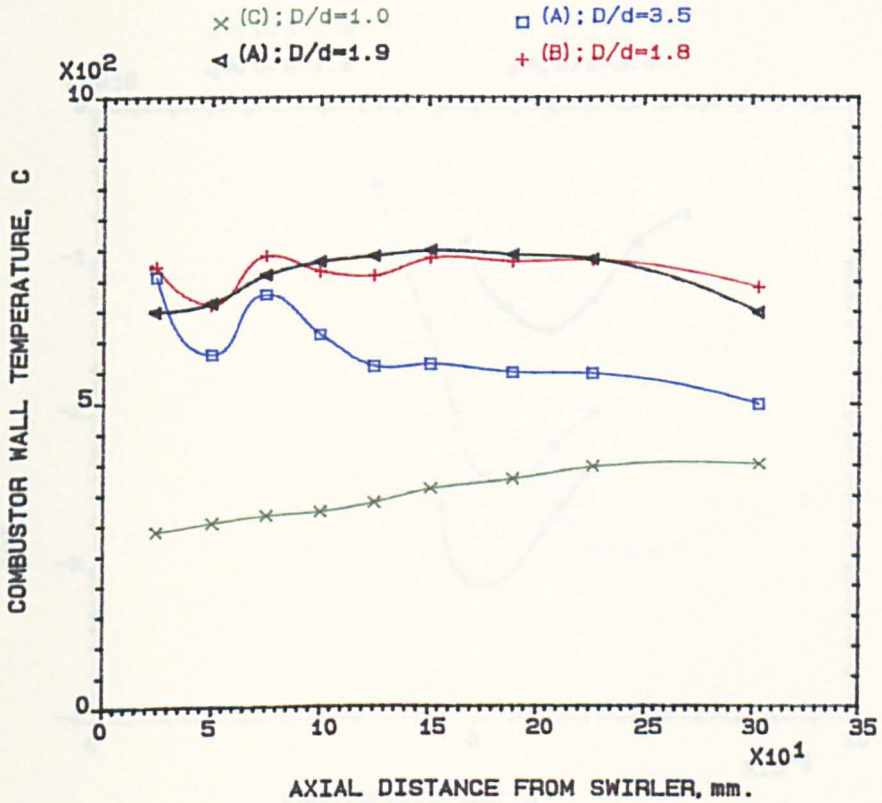

FIG.4.33 INFLUENCE OF SWIRLERS OUTLET DIAMETER ON AXIAL WALL TEMPERATURE PROFILES, 45 VANE ANGLE; EQR=0.44; PROPANE; 600K.

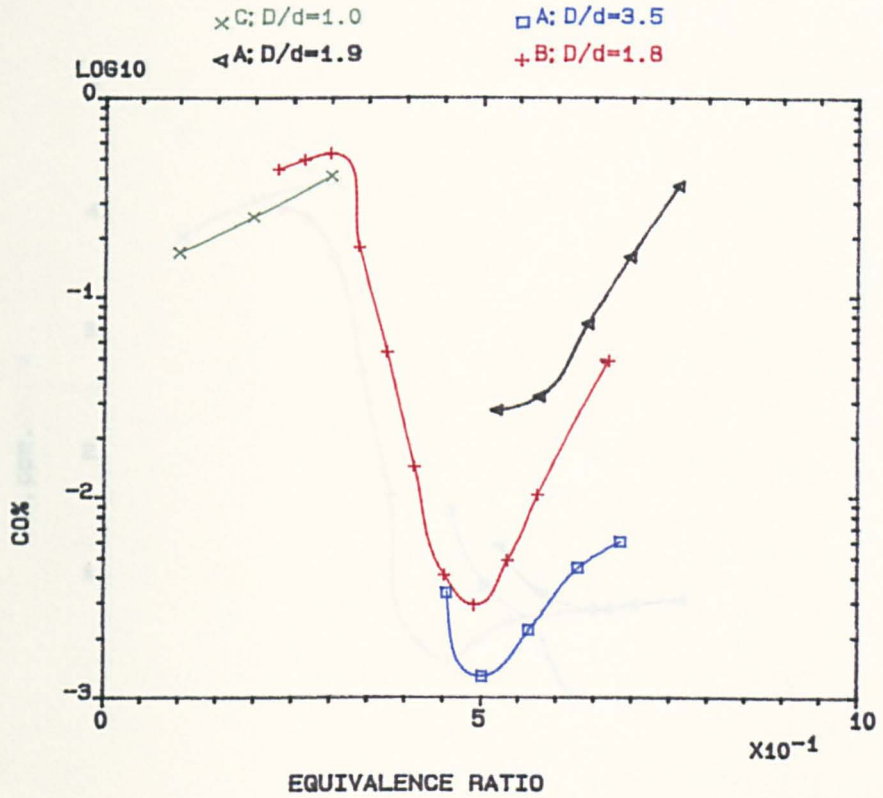

FIG.4.34 INFLUENCE OF RADIAL SWIRLER OUTLET ON EMISSIONS, FOR 76mm & 140mm COMBUSTOR; PROPANE; 400 K.

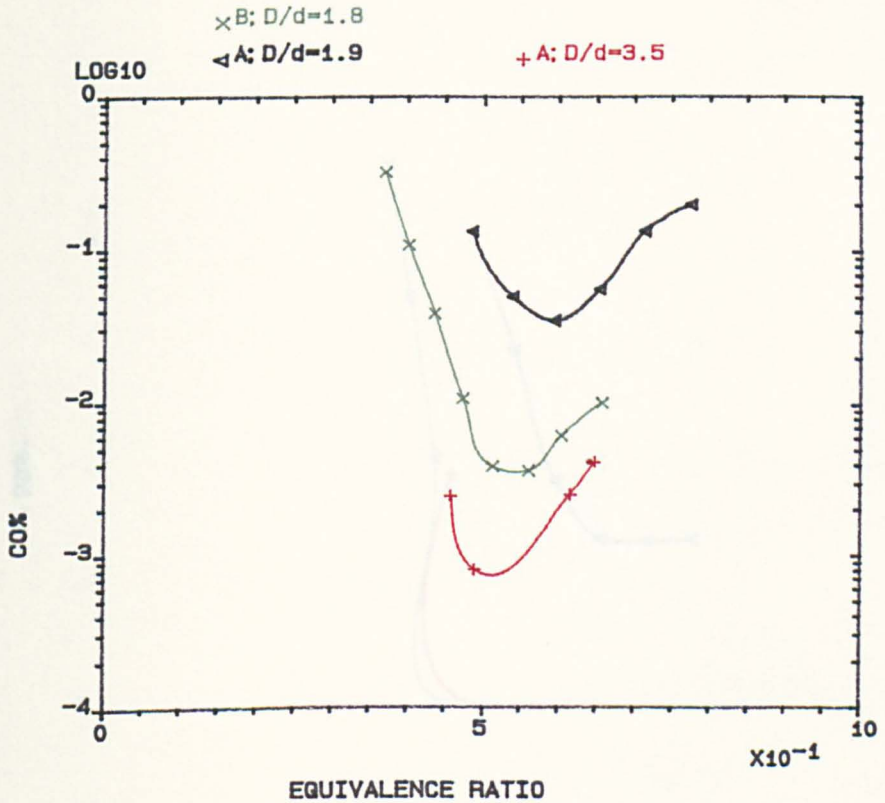

FIG.4.35 INFLUENCE OF RADIAL SWIRLER OUTLET ON EMISSIONS, FOR 76mm & 140mm COMBUSTOR; NATURAL GAS; 400 K.

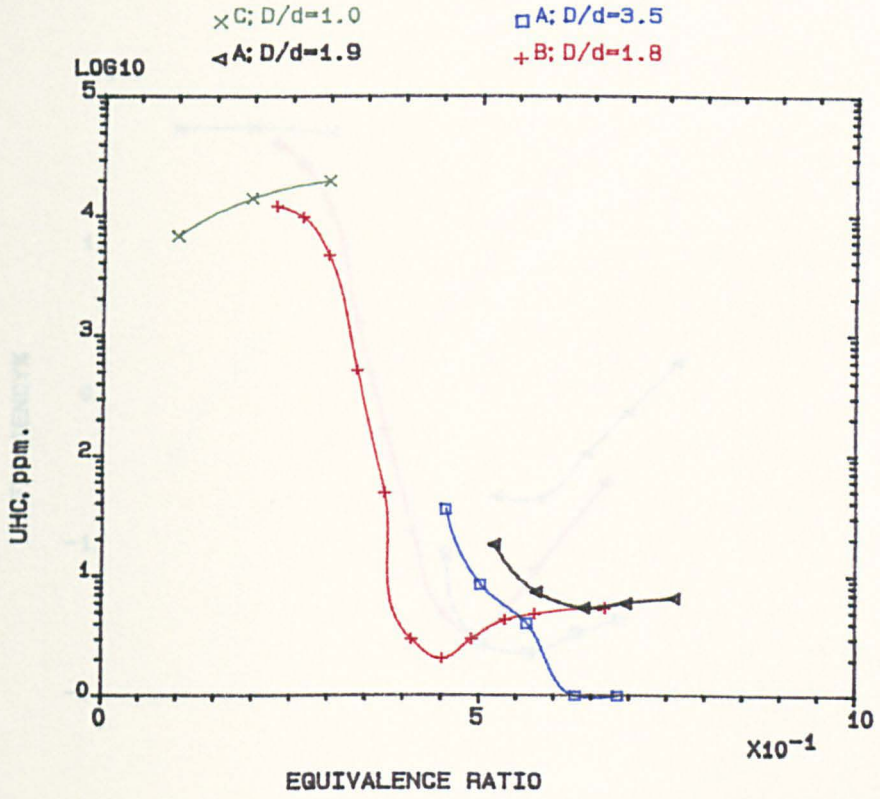

FIG.4.36 INFLUENCE OF RADIAL SWIRLER OUTLET ON EMISSIONS, FOR 76mm & 140mm COMBUSTOR; PROPANE; 400 K.

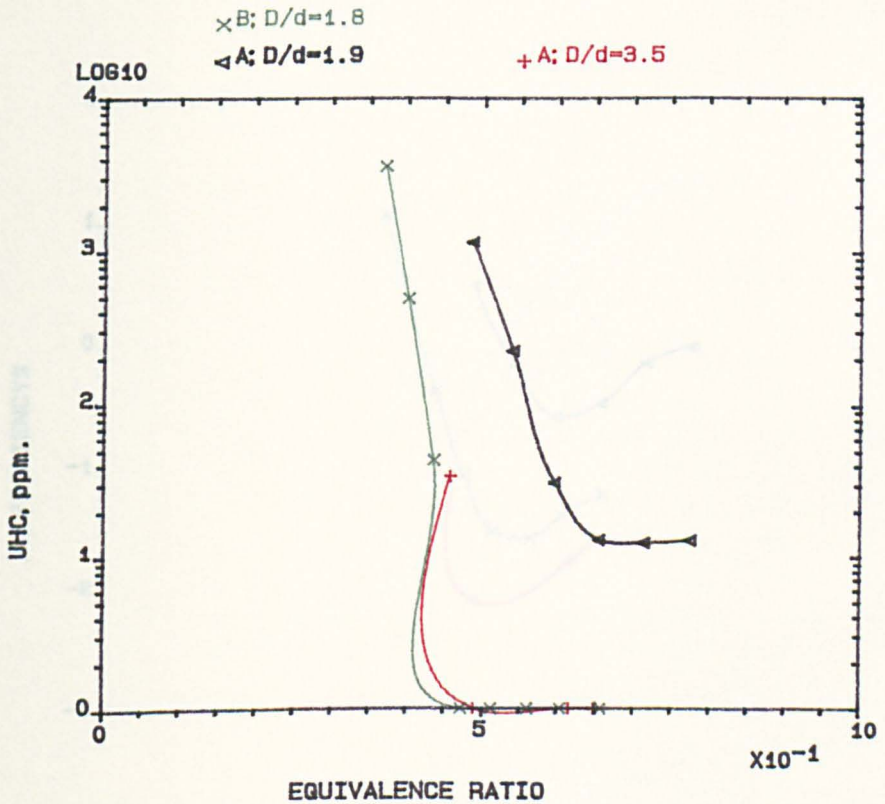

FIG.4.37 INFLUENCE OF RADIAL SWIRLER OUTLET ON EMISSIONS, FOR 76mm & 140mm COMBUSTOR; NATURAL GAS; 400 K.

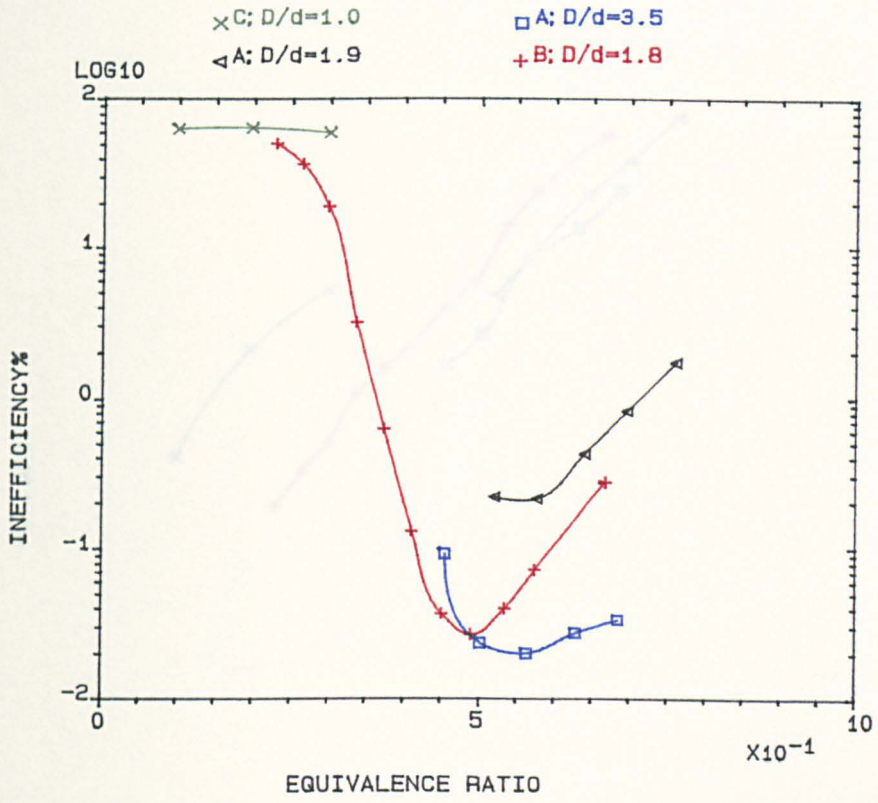

FIG.4.38 INFLUENCE OF RADIAL SWIRLER OUTLET ON EMISSIONS, FOR 76mm & 140mm COMBUSTOR; PROPANE; 400 K.

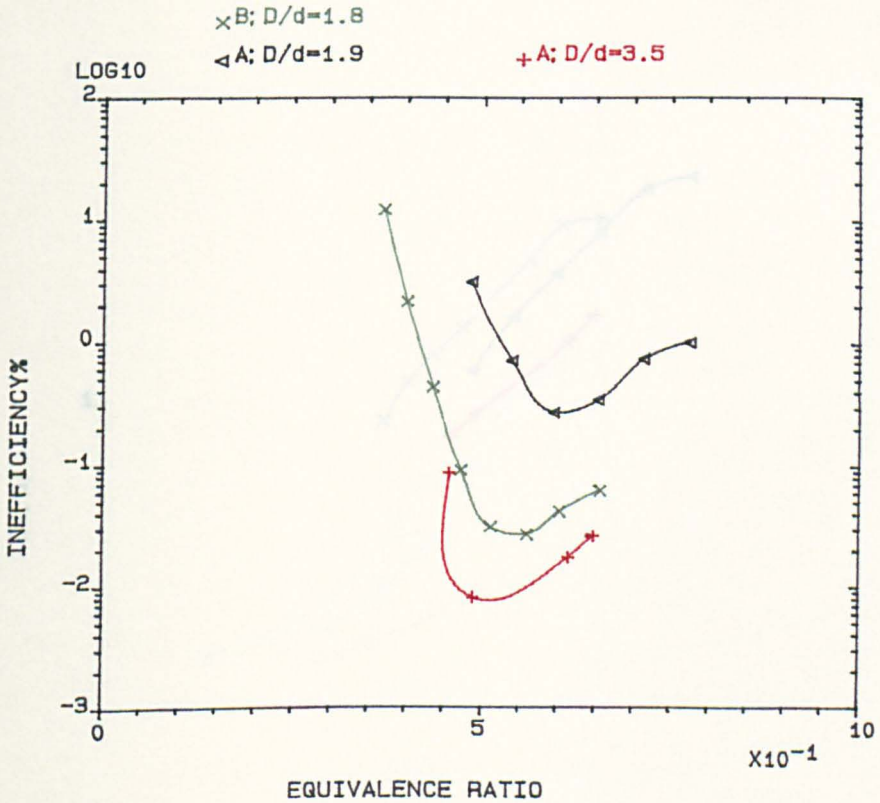

FIG.4.39 INFLUENCE OF RADIAL SWIRLER OUTLET ON EMISSIONS, FOR 76mm & 140mm COMBUSTOR; NATURAL GAS; 400 K.

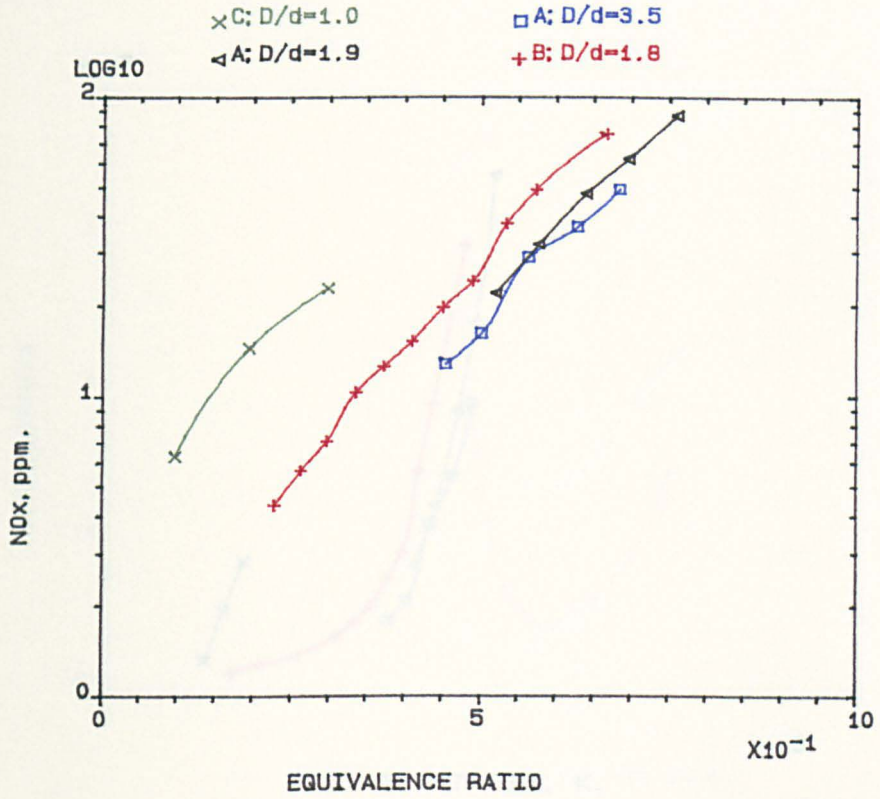

FIG.4.40 INFLUENCE OF RADIAL SWIRLER OUTLET ON EMISSIONS.
FOR 76mm & 140mm COMBUSTOR; PROPANE; 400 K.

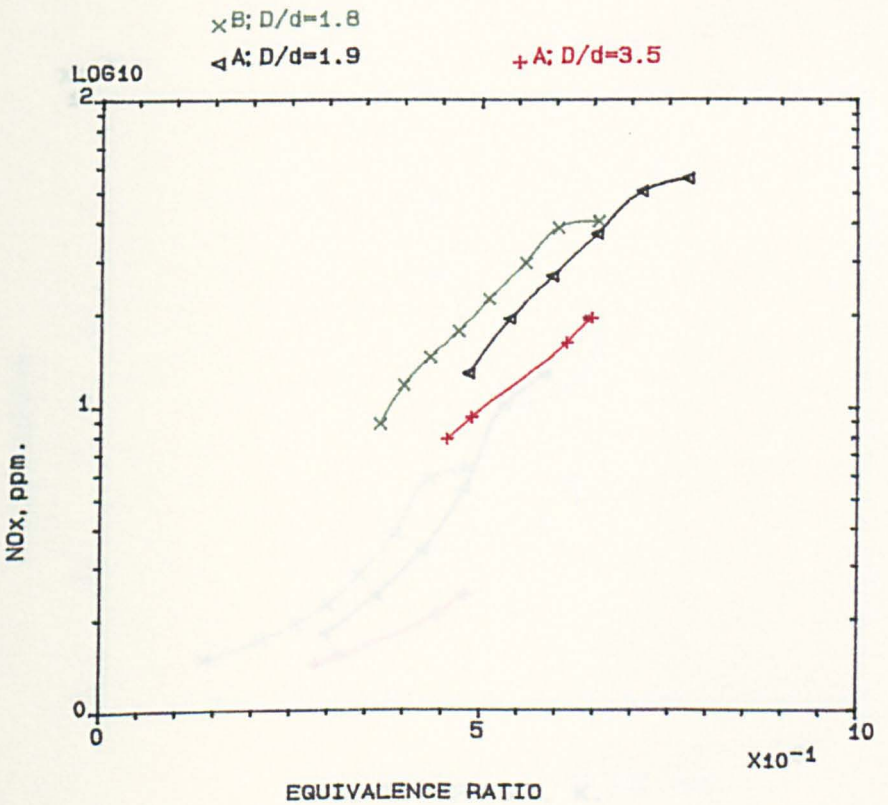

FIG.4.41 INFLUENCE OF RADIAL SWIRLER OUTLET ON EMISSIONS.
FOR 76mm & 140mm COMBUSTOR; NATURAL GAS; 400 K.

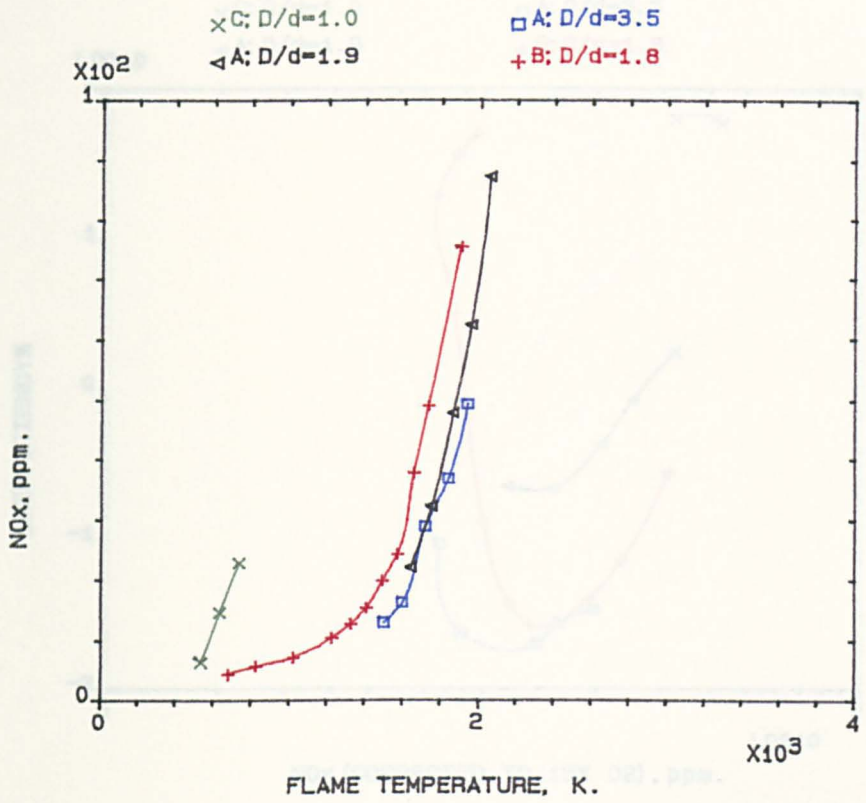

FIG.4.42 INFLUENCE OF RADIAL SWIRLER OUTLET ON EMISSIONS, FOR 76mm & 140mm COMBUSTOR; PROPANE; 400 K.

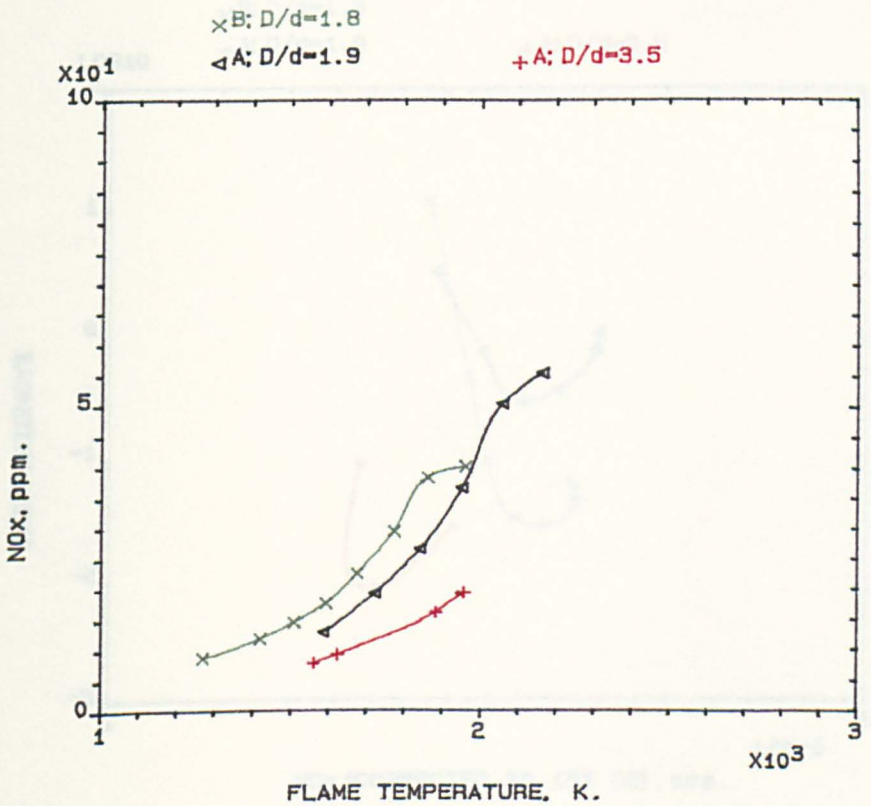

FIG.4.43 INFLUENCE OF RADIAL SWIRLER OUTLET ON EMISSIONS, FOR 76mm & 140mm COMBUSTOR; NATURAL GAS; 400 K.

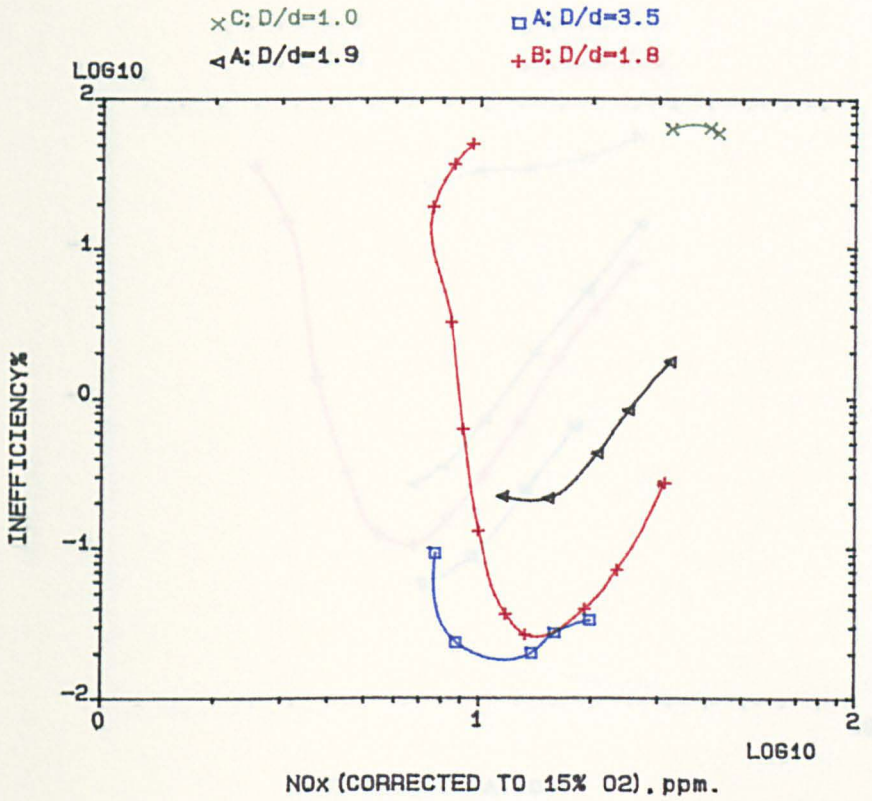

FIG.4.44 INFLUENCE OF RADIAL SWIRLER OUTLET ON EMISSIONS, FOR 76mm & 140mm COMBUSTOR; PROPANE; 400 K.

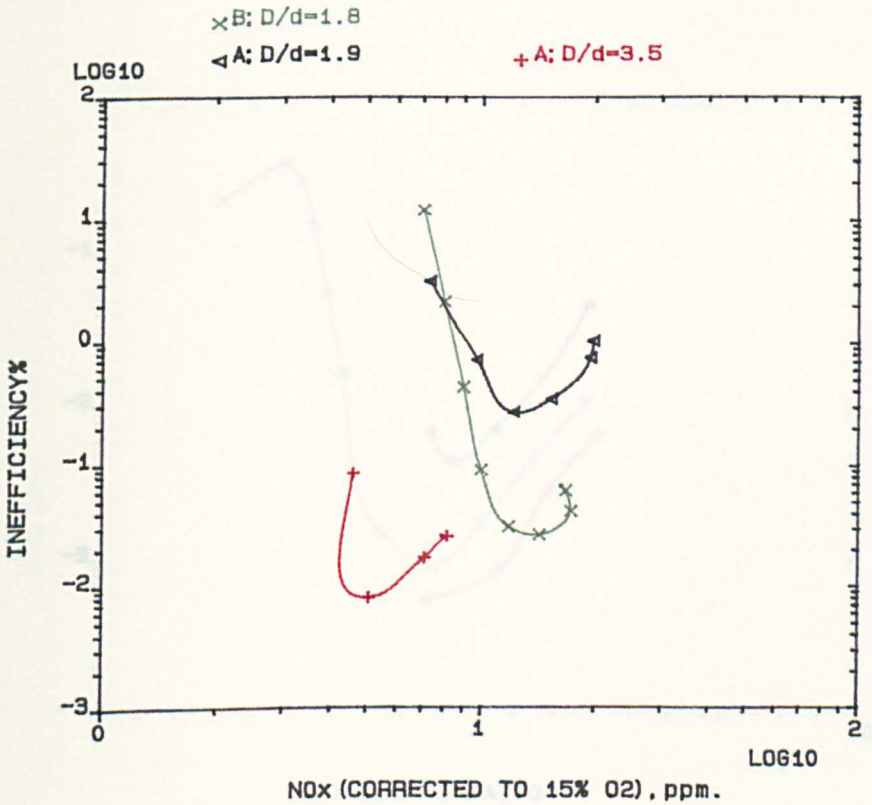

FIG.4.45 INFLUENCE OF RADIAL SWIRLER OUTLET ON EMISSIONS, FOR 76mm & 140mm COMBUSTOR; NATURAL GAS; 400 K.

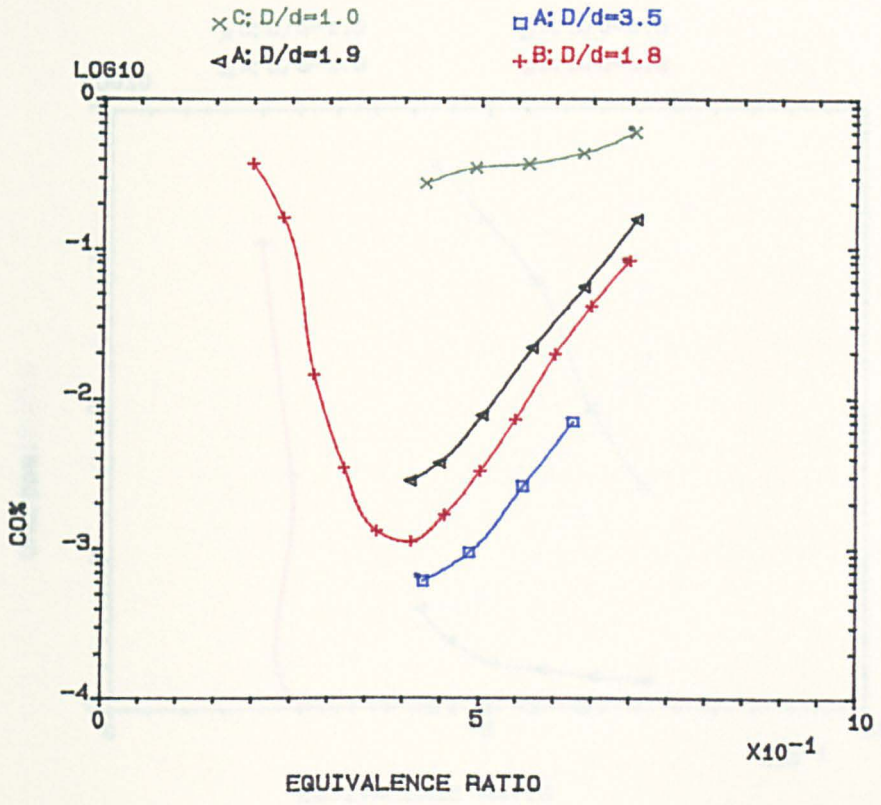

FIG.4.46 INFLUENCE OF RADIAL SWIRLER OUTLET ON EMISSIONS, FOR 76mm & 140mm COMBUSTOR; PROPANE; 600 K.

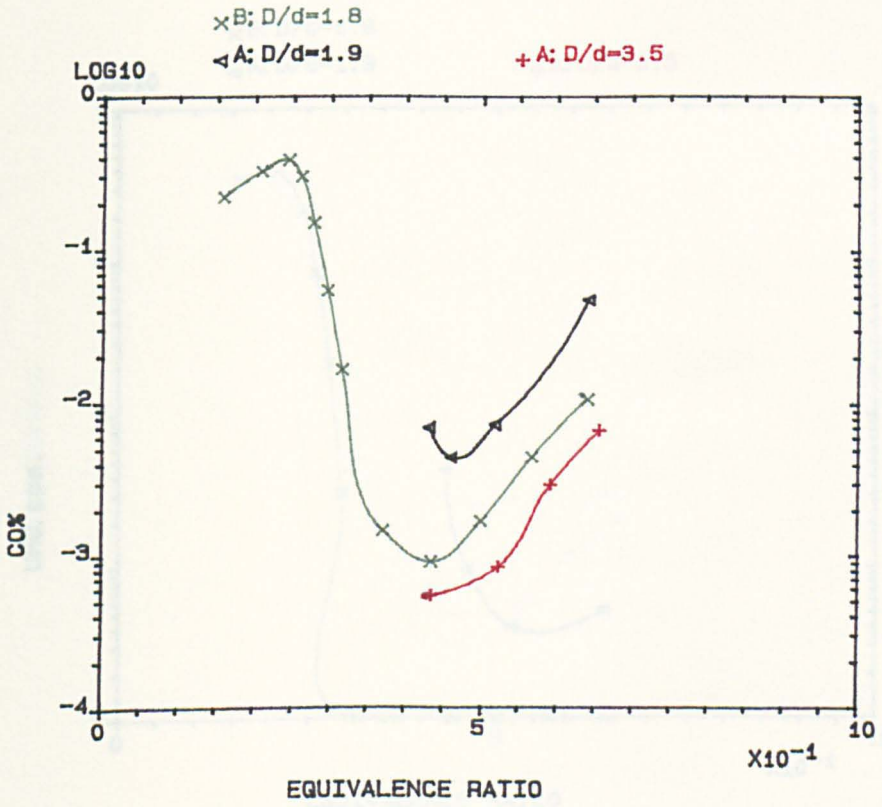

FIG.4.47 INFLUENCE OF RADIAL SWIRLER OUTLET ON EMISSIONS, FOR 76mm & 140mm COMBUSTOR; NATURAL GAS; 600 K.

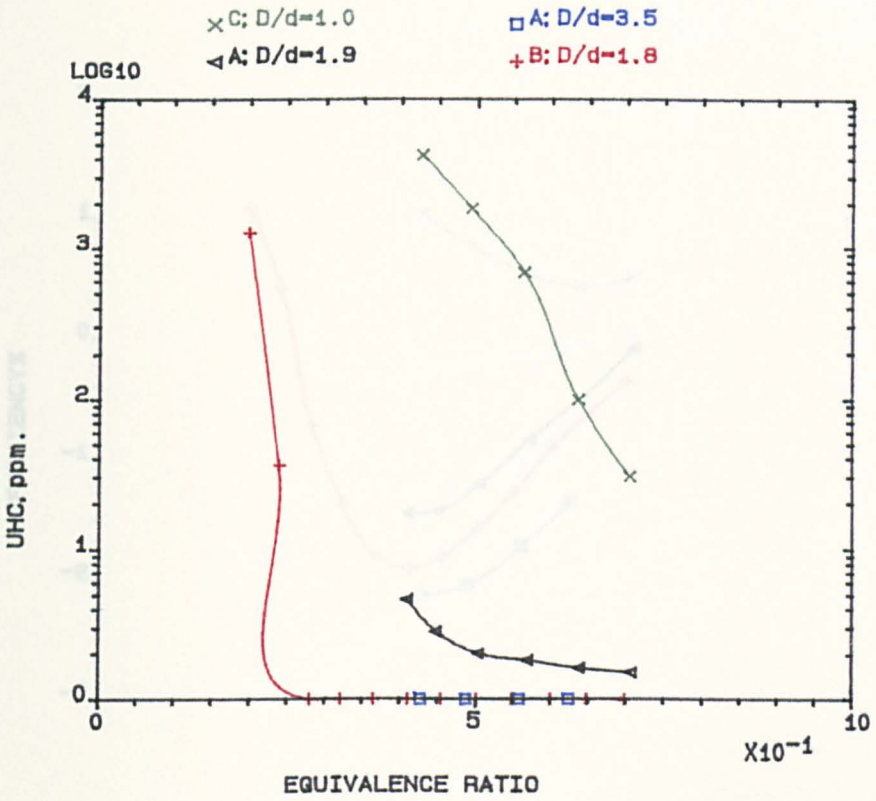

FIG.4.48 INFLUENCE OF RADIAL SWIRLER OUTLET ON EMISSIONS, FOR 76mm & 140mm COMBUSTOR; PROPANE; 600 K.

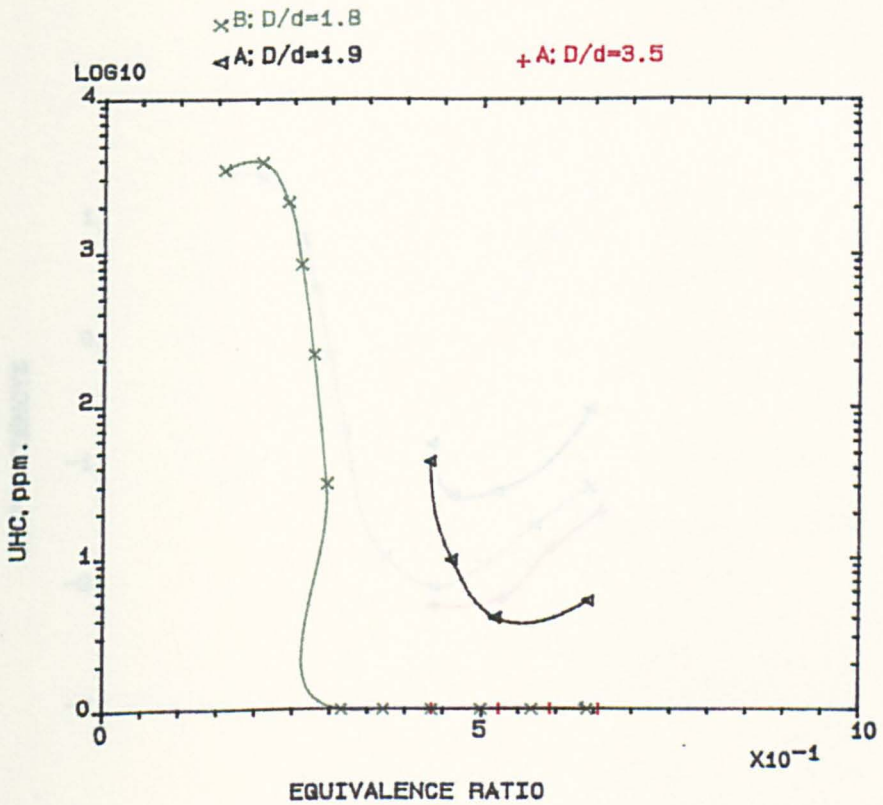

FIG.4.49 INFLUENCE OF RADIAL SWIRLER OUTLET ON EMISSIONS, FOR 76mm & 140mm COMBUSTOR; NATURAL GAS; 600 K.

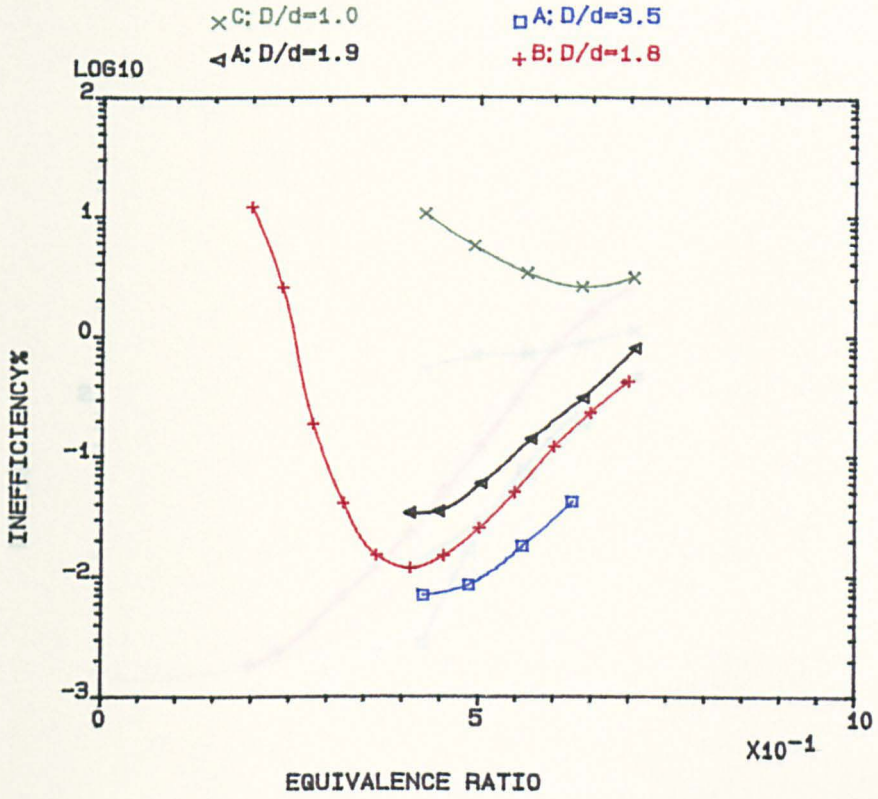

FIG.4.50 INFLUENCE OF RADIAL SWIRLER OUTLET ON EMISSIONS, FOR 76mm & 140mm COMBUSTOR; PROPANE; 600 K.

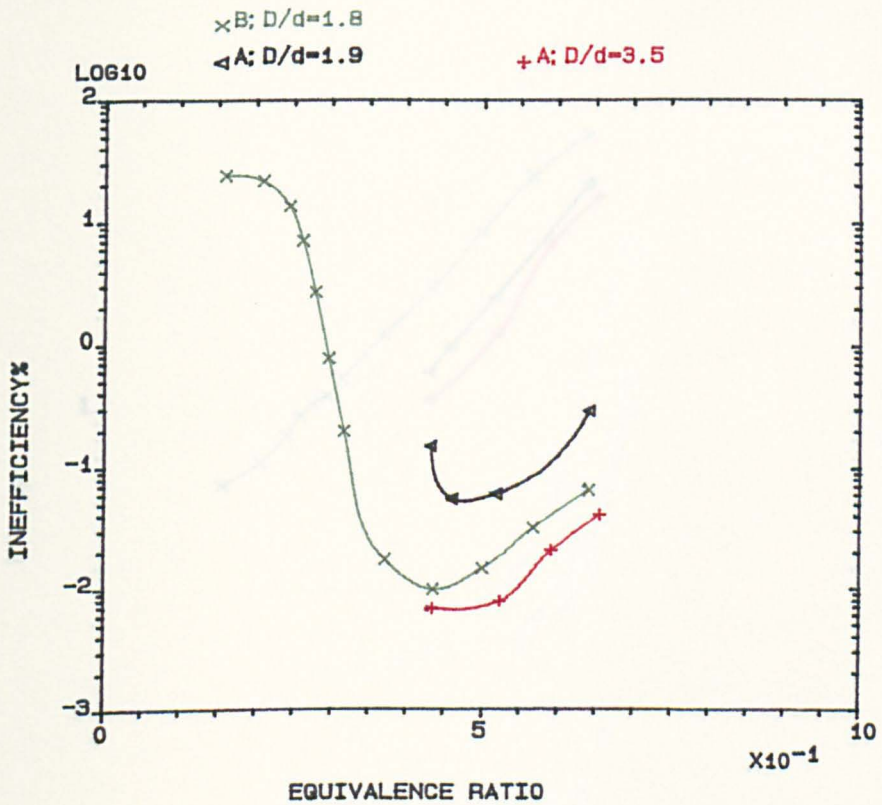

FIG.4.51 INFLUENCE OF RADIAL SWIRLER OUTLET ON EMISSIONS, FOR 76mm & 140mm COMBUSTOR; NATURAL GAS; 600 K.

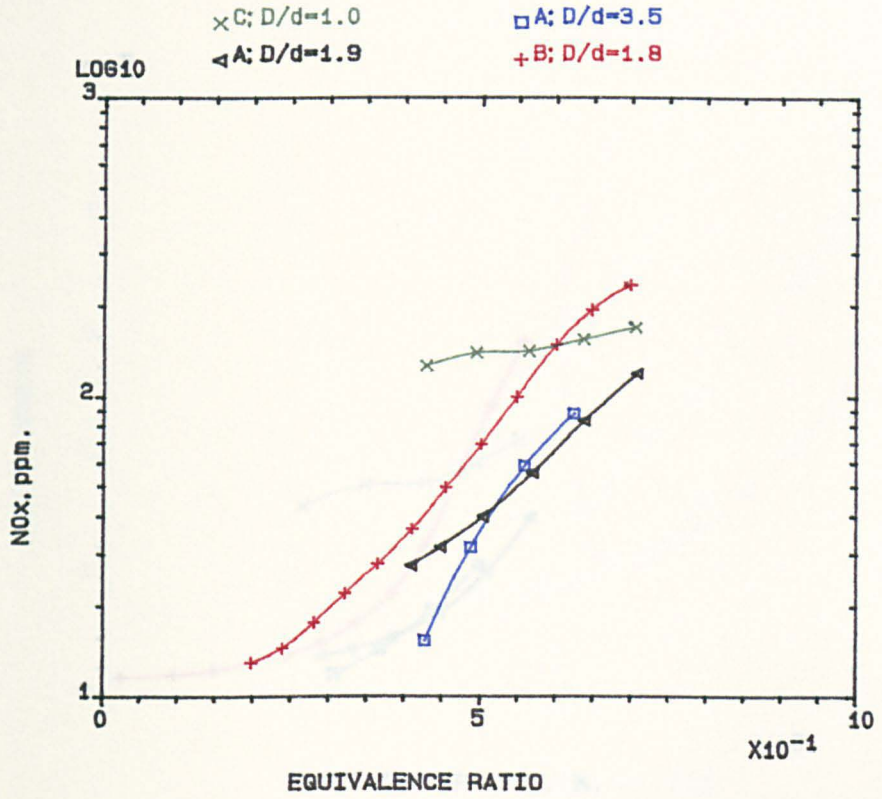

FIG.4.52 INFLUENCE OF RADIAL SWIRLER OUTLET ON EMISSIONS. FOR 76mm & 140mm COMBUSTOR; PROPANE; 600 K.

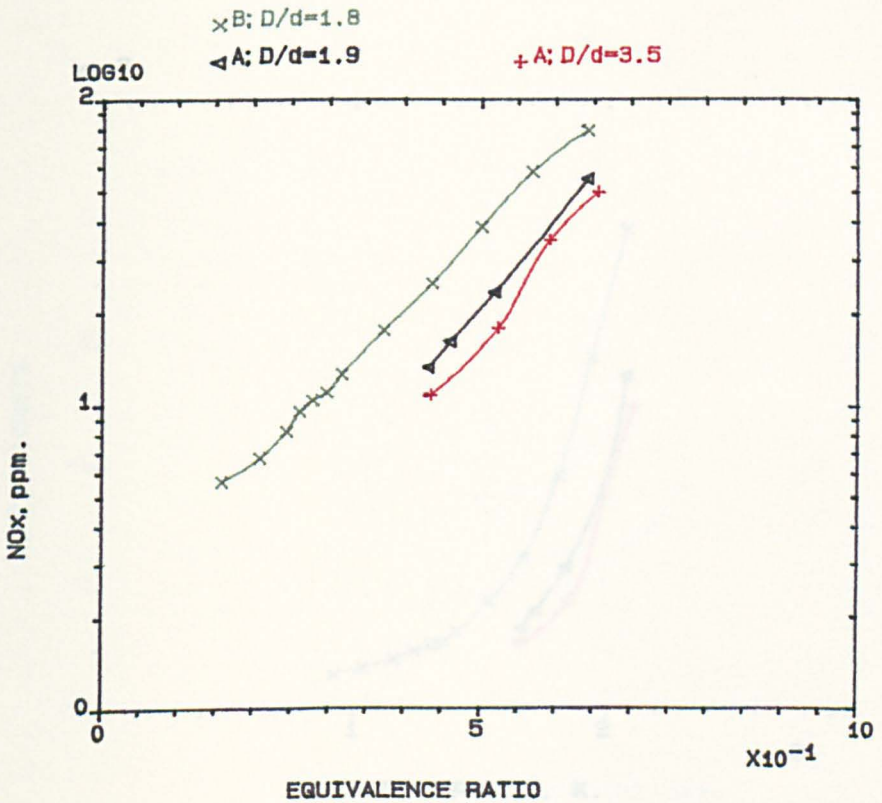

FIG.4.53 INFLUENCE OF RADIAL SWIRLER OUTLET ON EMISSIONS. FOR 76mm & 140mm COMBUSTOR; NATURAL GAS; 600 K.

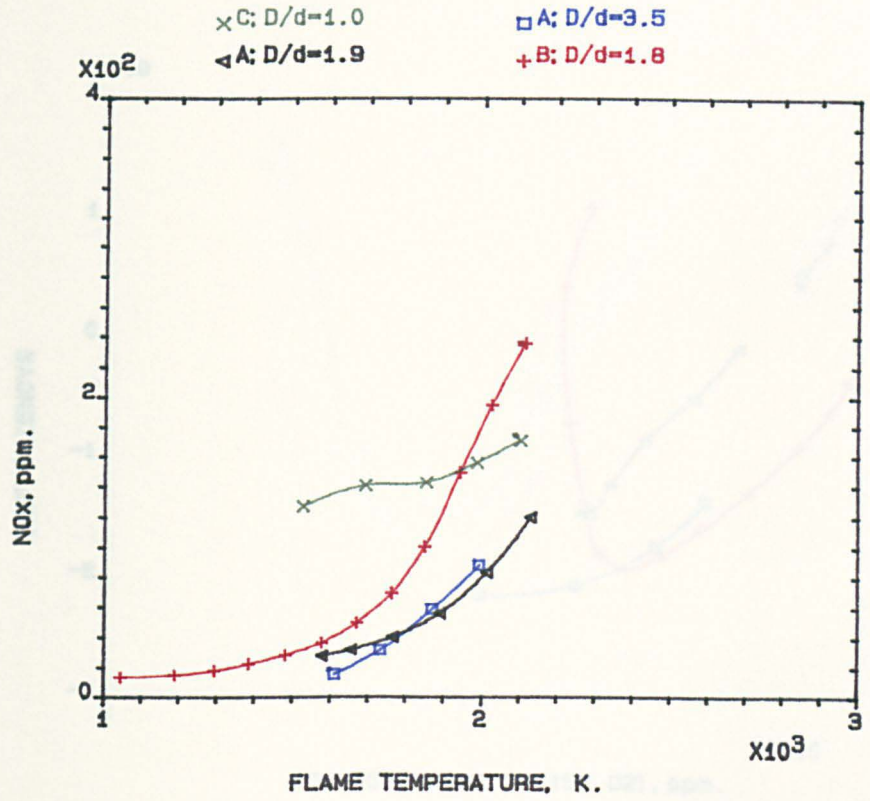

FIG.4.54 INFLUENCE OF RADIAL SWIRLER OUTLET ON EMISSIONS, FOR 76mm & 140mm COMBUSTOR; PROPANE; 600 K.

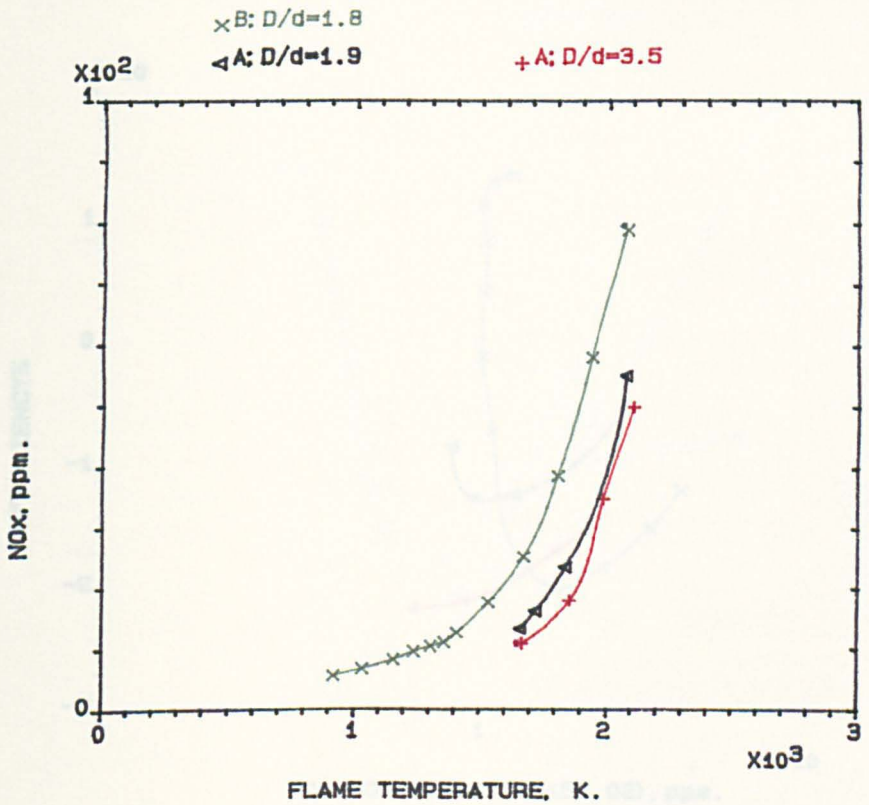

FIG.4.55 INFLUENCE OF RADIAL SWIRLER OUTLET ON EMISSIONS, FOR 76mm & 140mm COMBUSTOR; NATURAL GAS; 600 K.

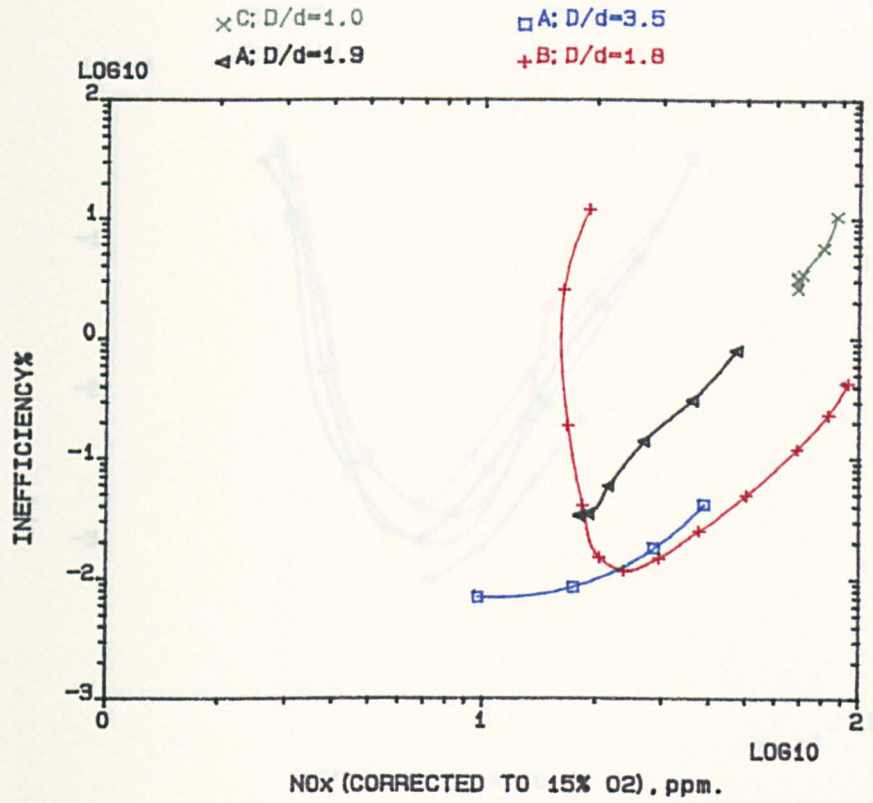

FIG.4.56 INFLUENCE OF RADIAL SWIRLER OUTLET ON EMISSIONS.
FOR 76mm & 140mm COMBUSTOR; PROPANE; 600 K.

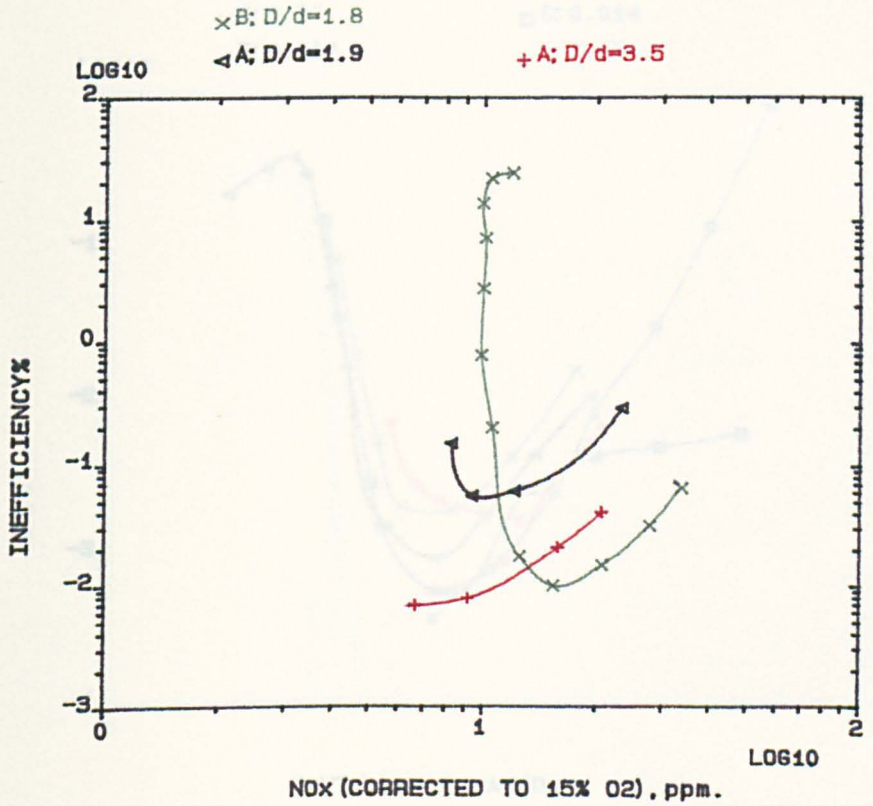

FIG.4.57 INFLUENCE OF RADIAL SWIRLER OUTLET ON EMISSIONS.
FOR 76mm & 140mm COMBUSTOR; NATURAL GAS; 600 K.

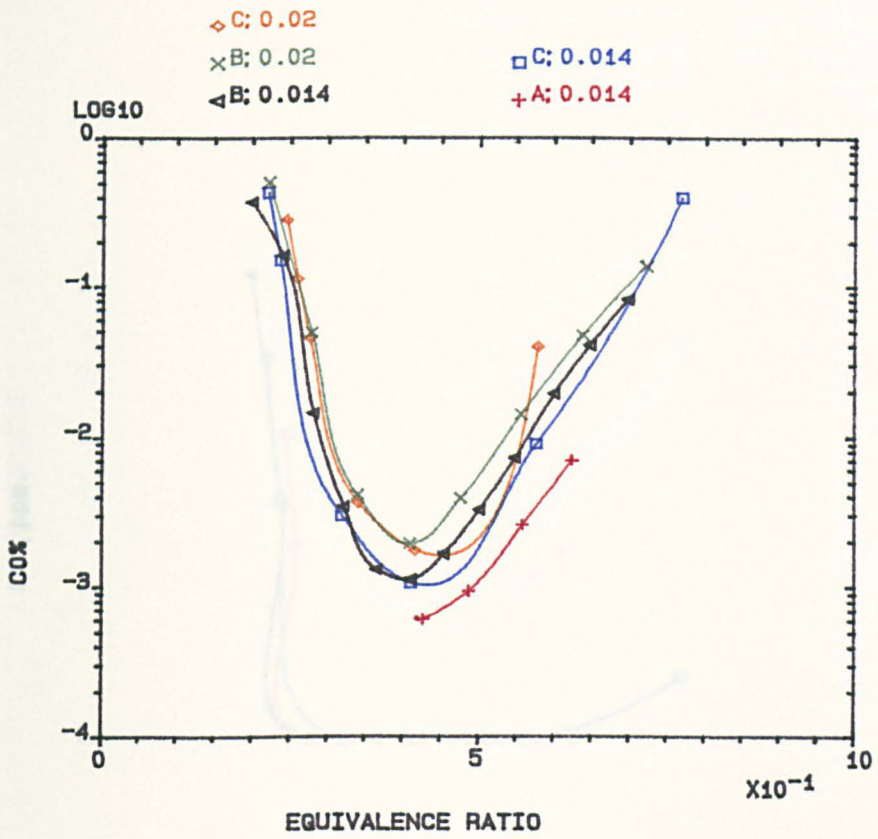

FIG.4.58 INFLUENCE OF PRIMARY ZONE MACH NO. ON EMISSIONS, FOR 140mm COMBUSTOR; PROPANE; 600 K.

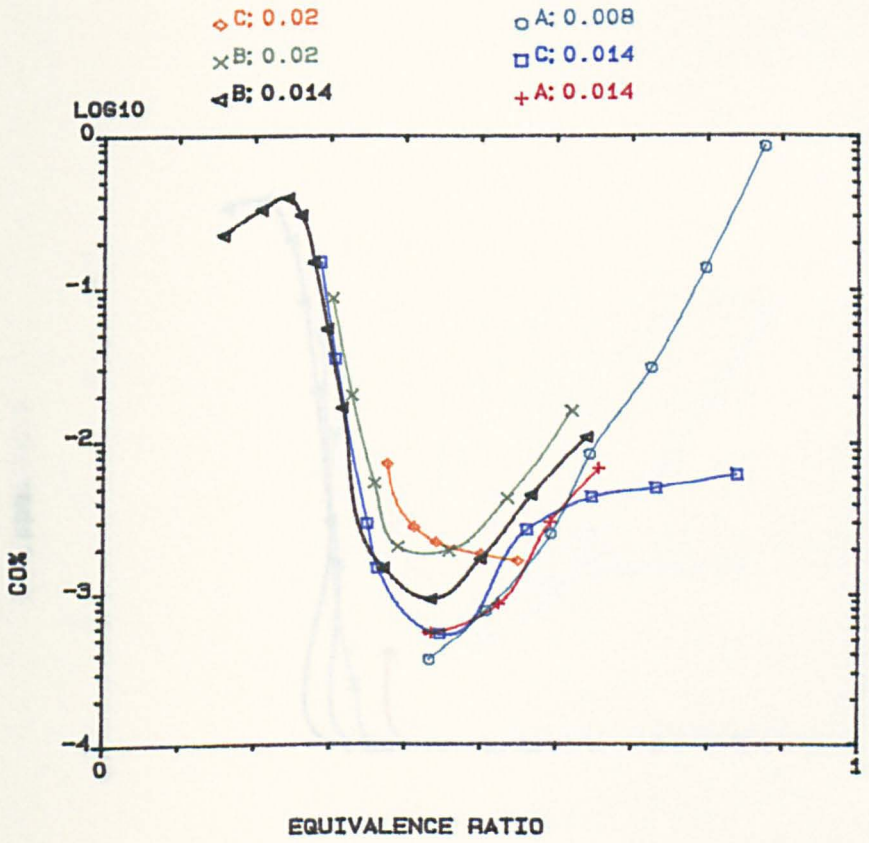

FIG.4.59 INFLUENCE OF PRIMARY ZONE MACH NO. ON EMISSIONS, FOR 140mm COMBUSTOR; NATURAL GAS; 600 K.

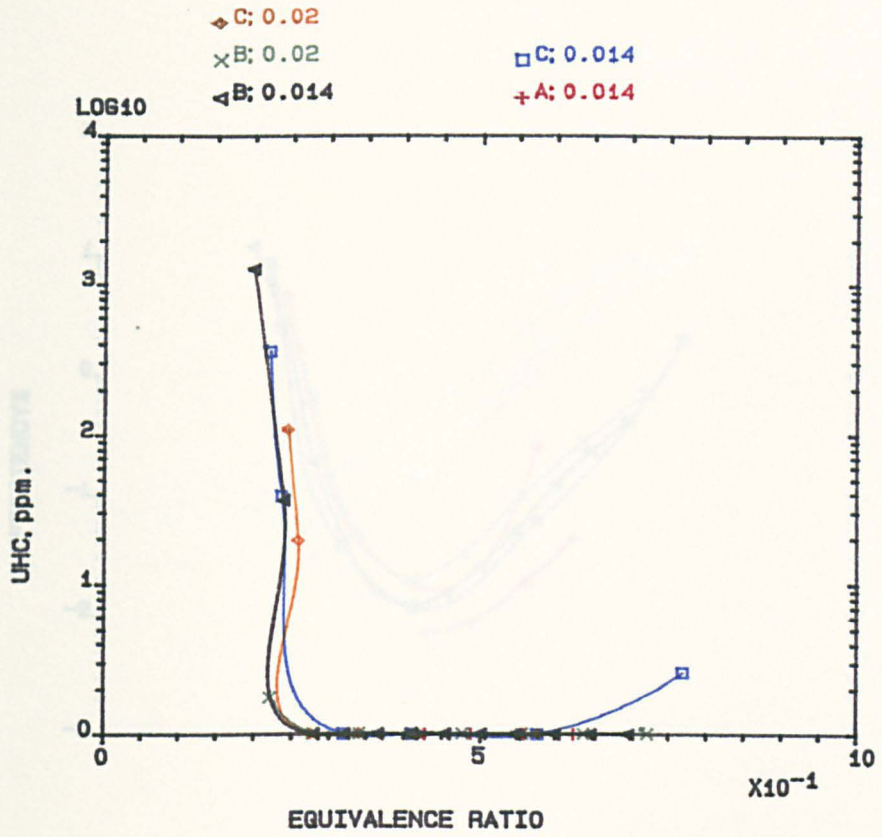

FIG.4.60 INFLUENCE OF PRIMARY ZONE MACH NO. ON EMISSIONS, FOR 140mm COMBUSTOR; PROPANE; 600 K.

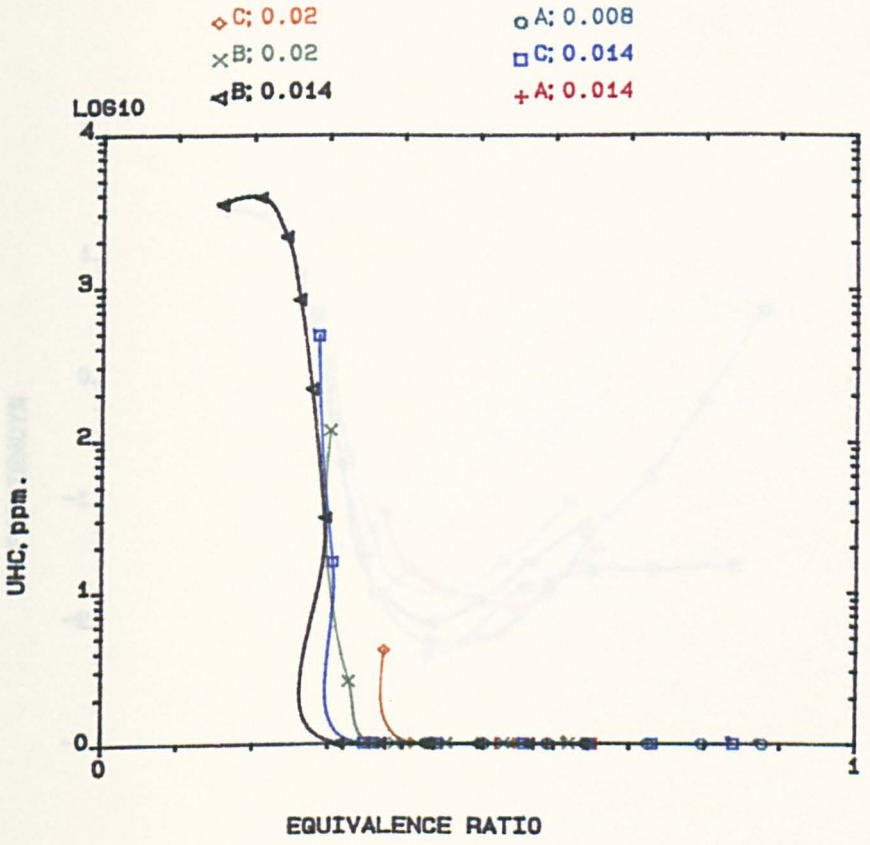

FIG.4.61 INFLUENCE OF PRIMARY ZONE MACH NO. ON EMISSIONS, FOR 140mm COMBUSTOR; NATURAL GAS; 600 K.

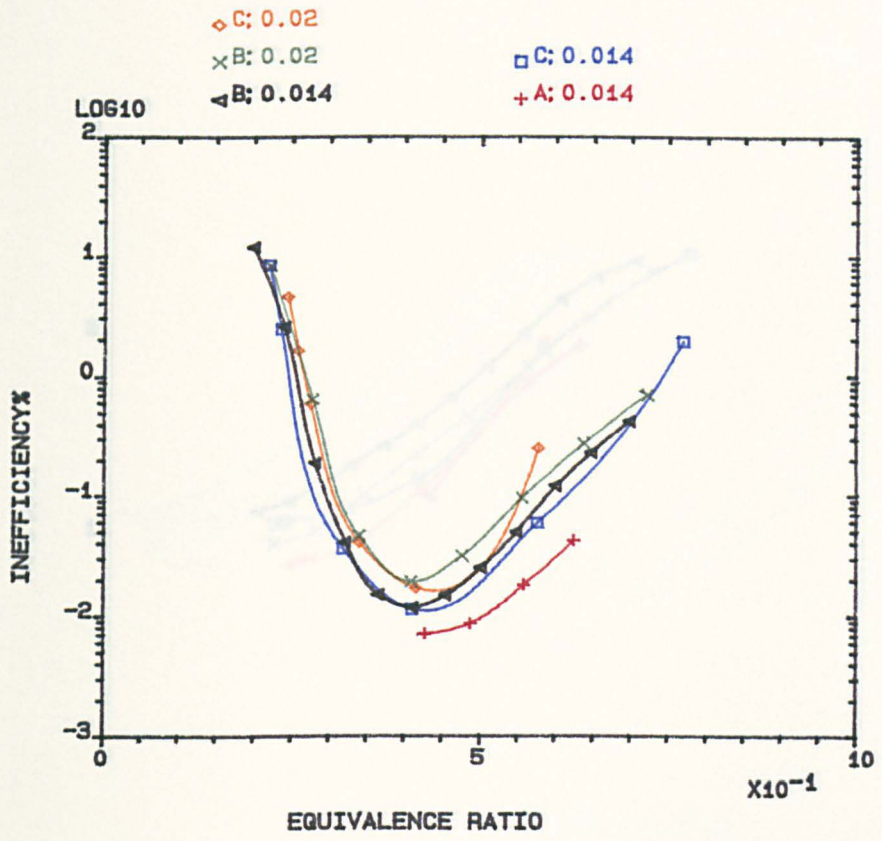

FIG.4.62 INFLUENCE OF PRIMARY ZONE MACH NO. ON EMISSIONS, FOR 140mm COMBUSTOR; PROPANE; 600 K.

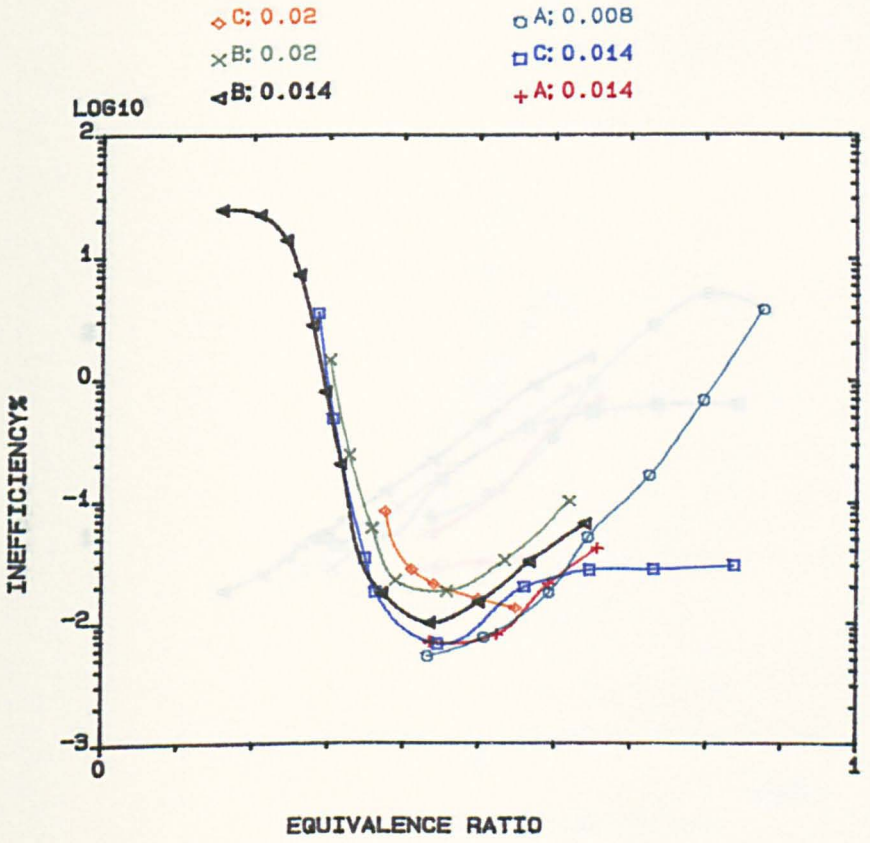

FIG.4.63 INFLUENCE OF PRIMARY ZONE MACH NO. ON EMISSIONS, FOR 140mm COMBUSTOR; NATURAL GAS; 600 K.

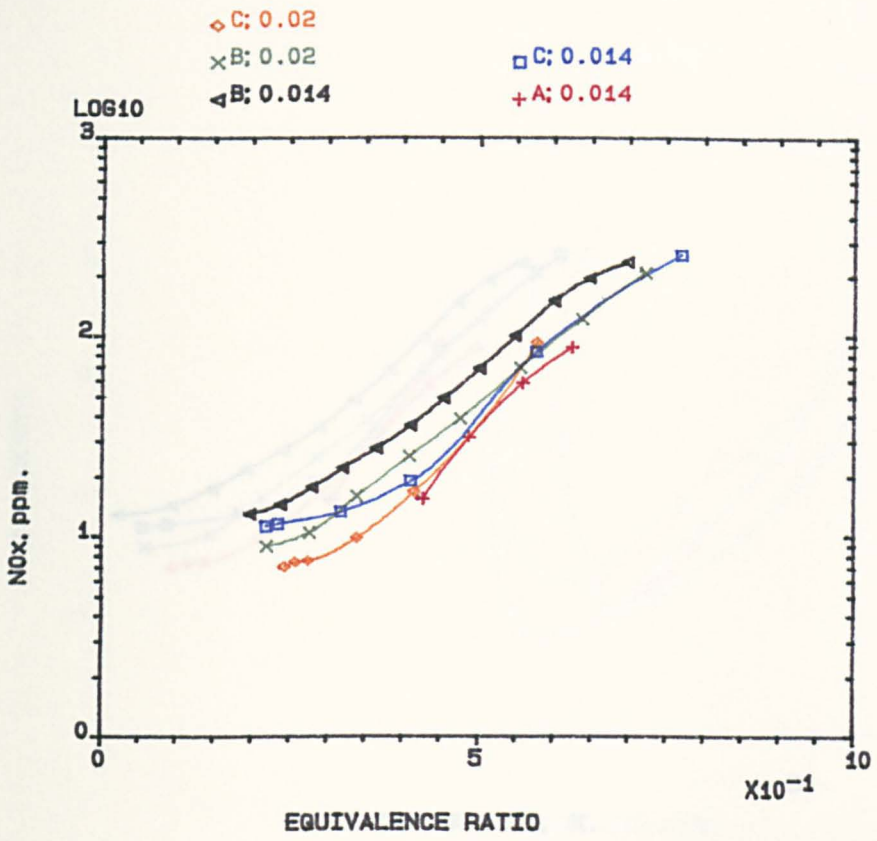

FIG.4.64 INFLUENCE OF PRIMARY ZONE MACH NO. ON EMISSIONS. FOR 140mm COMBUSTOR; PROPANE; 600 K.

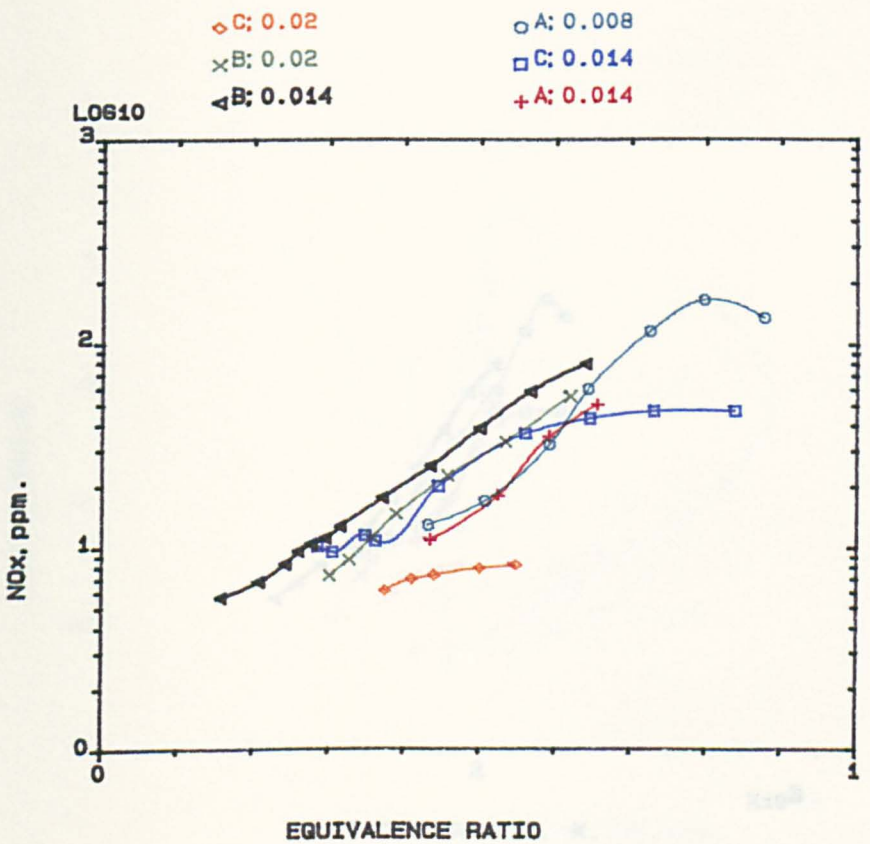

FIG.4.65 INFLUENCE OF PRIMARY ZONE MACH NO. ON EMISSIONS. FOR 140mm COMBUSTOR; NATURAL GAS; 600 K.

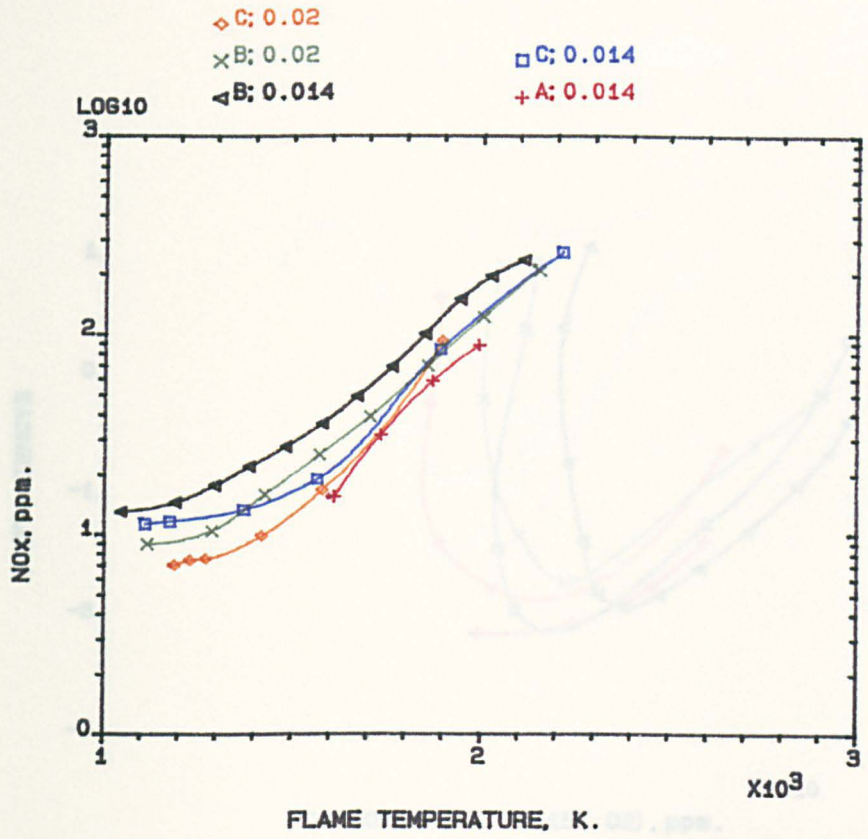

FIG.4.66 INFLUENCE OF PRIMARY ZONE MACH NO. ON EMISSIONS, FOR 140mm COMBUSTOR; PROPANE; 600 K.

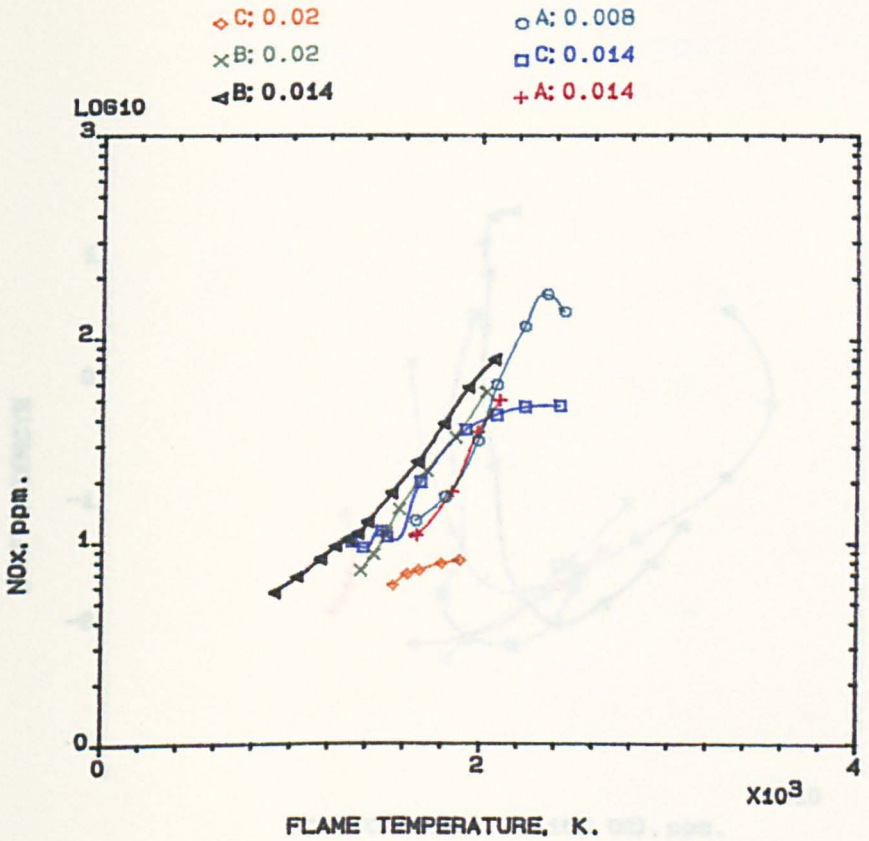

FIG.4.67 INFLUENCE OF PRIMARY ZONE MACH NO. ON EMISSIONS, FOR 140mm COMBUSTOR; NATURAL GAS; 600 K.

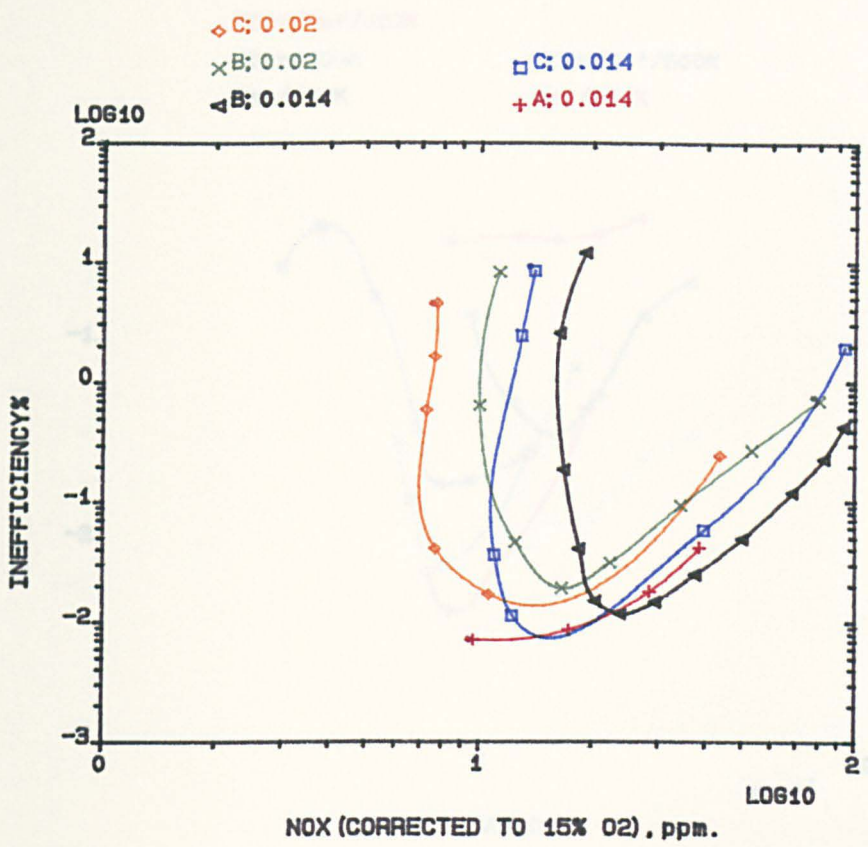

FIG.4.68 INFLUENCE OF PRIMARY ZONE MACH NO. ON EMISSIONS, FOR 140mm COMBUSTOR; PROPANE; 600 K.

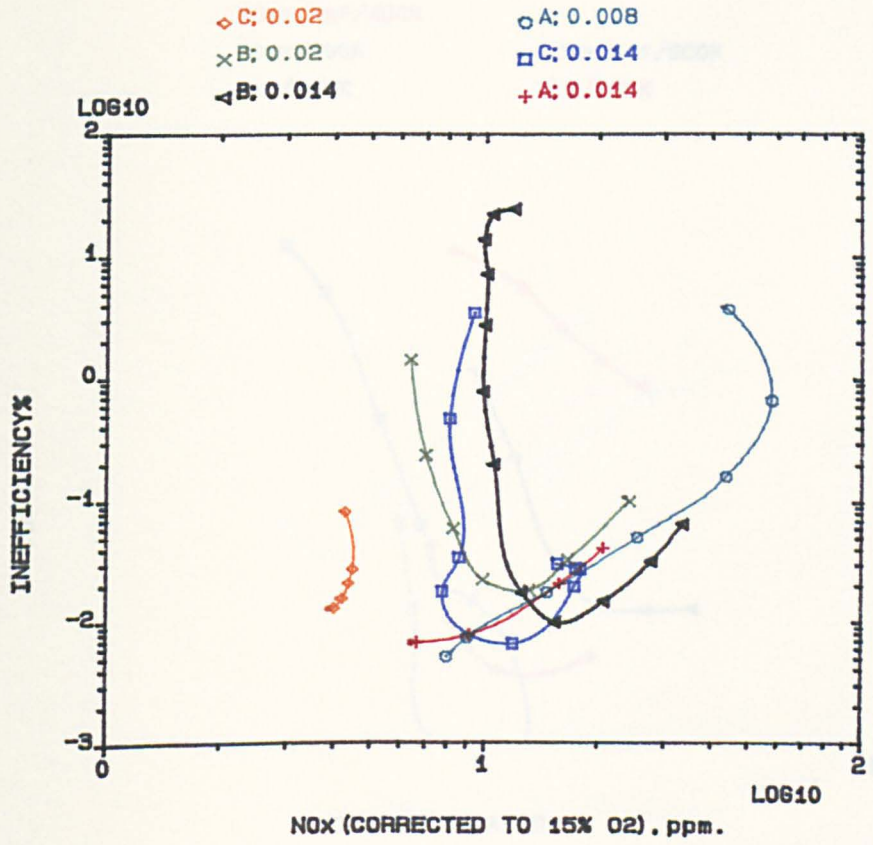

FIG.4.69 INFLUENCE OF PRIMARY ZONE MACH NO. ON EMISSIONS, FOR 140mm COMBUSTOR; NATURAL GAS; 600 K.

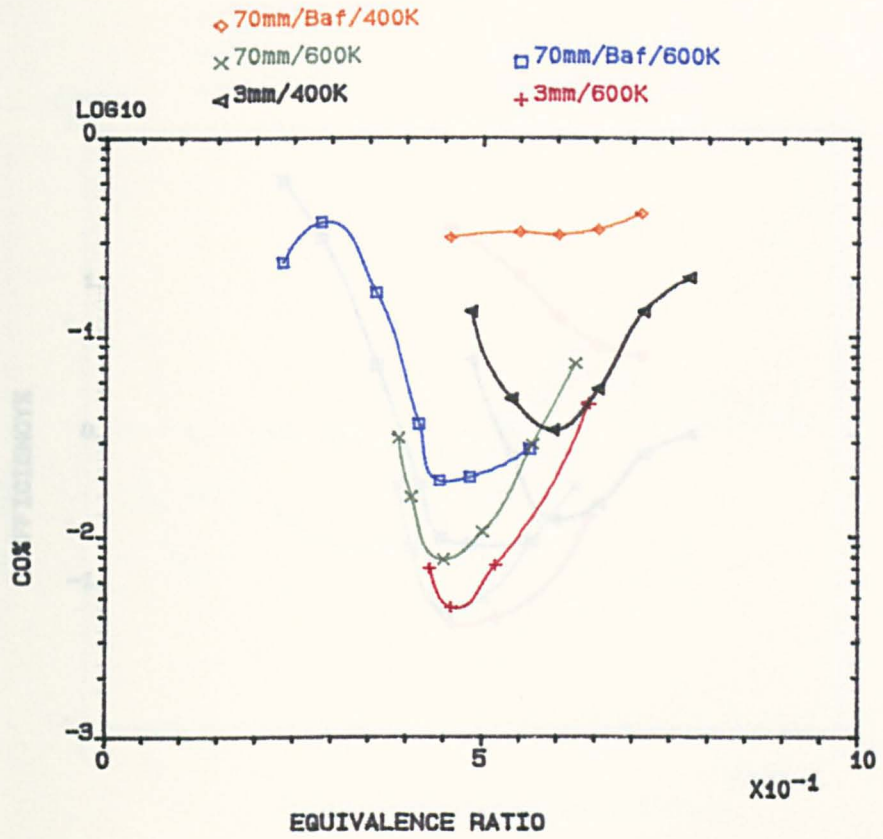

FIG.4.70 INFLUENCE OF CENTRAL FUEL INJECTOR POSITION ON EMISSIONS SWIRLER (A) IN 76mm COMBUSTOR; MN=.03; NATURAL GAS; 400 & 600K.

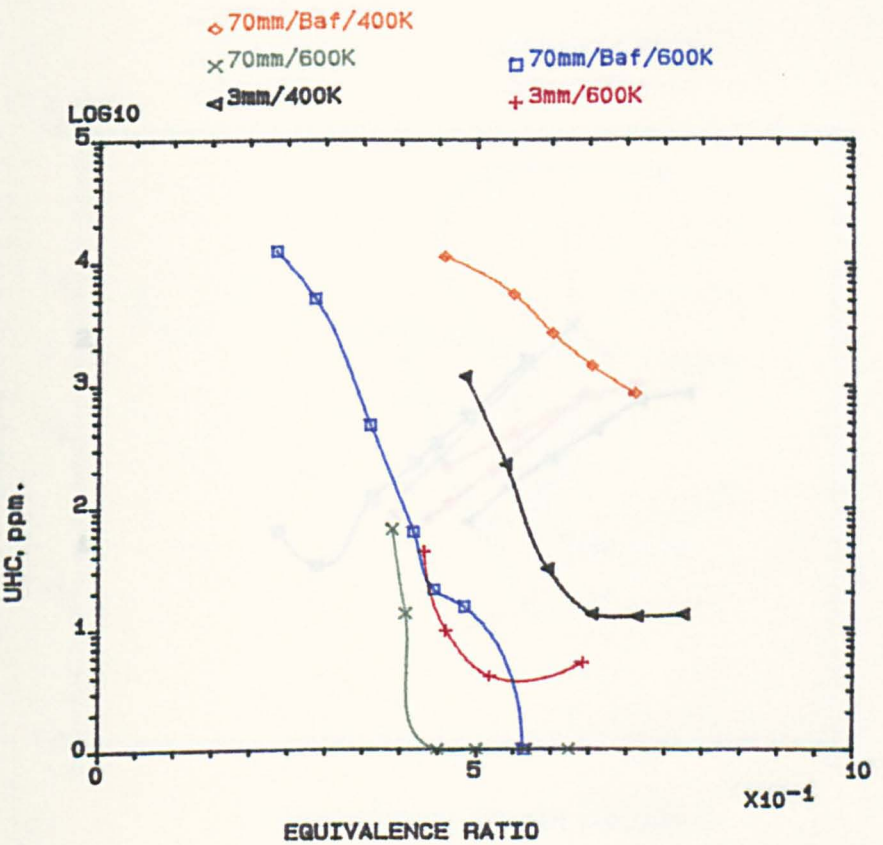

FIG.4.71 INFLUENCE OF CENTRAL FUEL INJECTOR POSITION ON EMISSIONS SWIRLER (A) IN 76mm COMBUSTOR; MN=.03; NATURAL GAS; 400 & 600K.

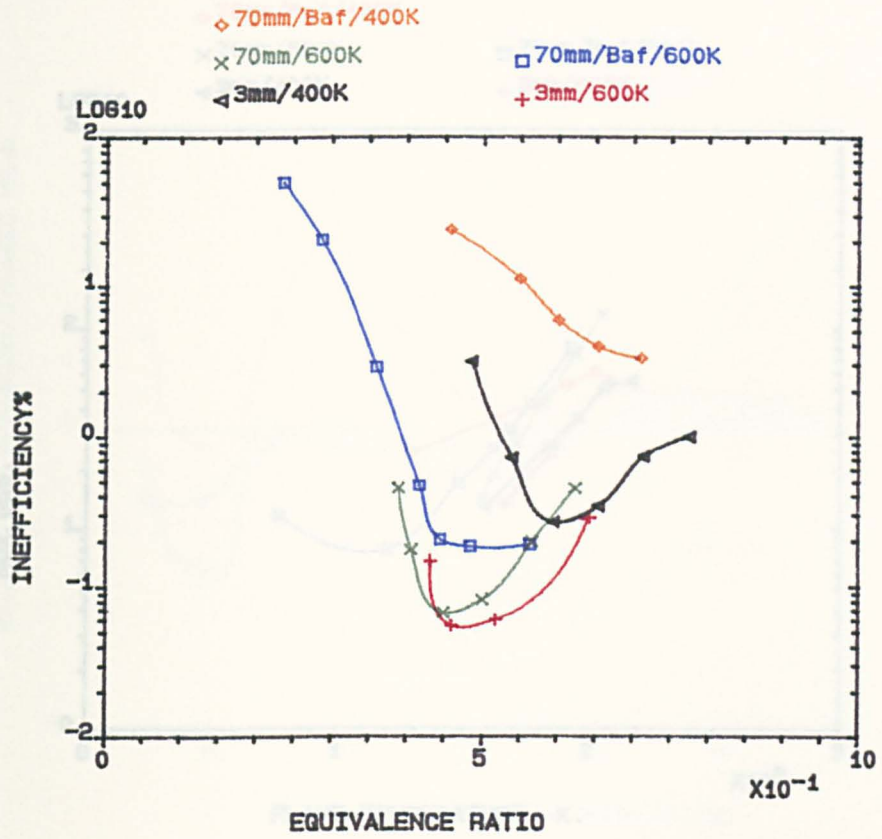

FIG.4.72 INFLUENCE OF CENTRAL FUEL INJECTOR POSITION ON EMISSIONS SWIRLER (A) IN 76mm COMBUSTOR; MN=.03; NATURAL GAS; 400 & 600K.

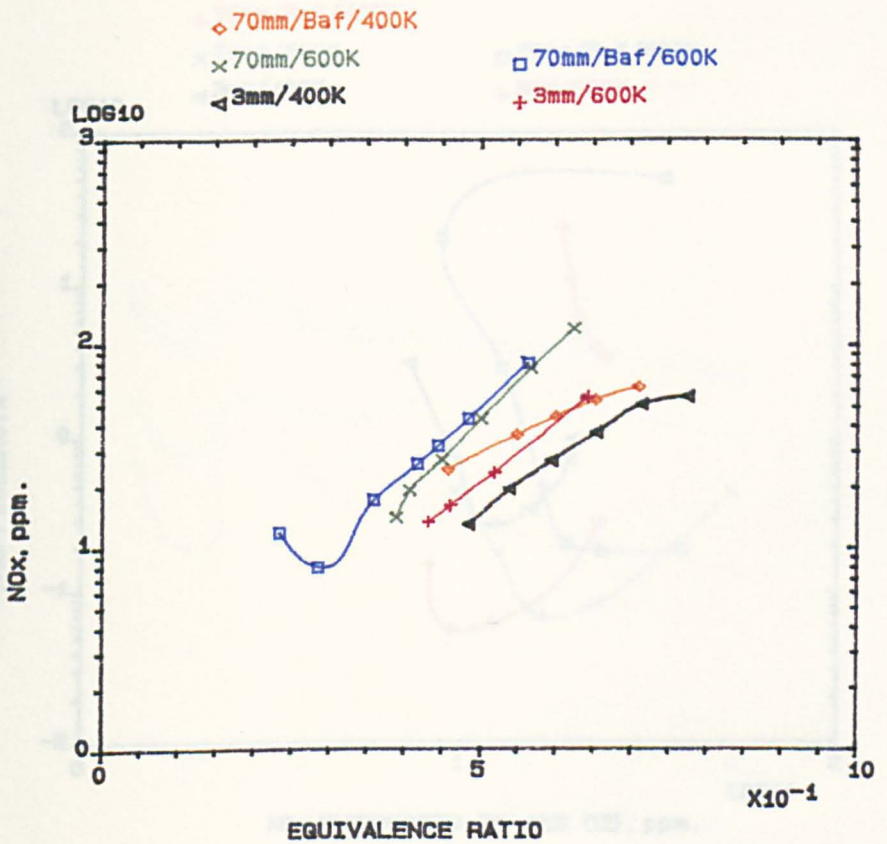

FIG.4.73 INFLUENCE OF CENTRAL FUEL INJECTOR POSITION ON EMISSIONS SWIRLER (A) IN 76mm COMBUSTOR; MN=.03; NATURAL GAS; 400 & 600K.

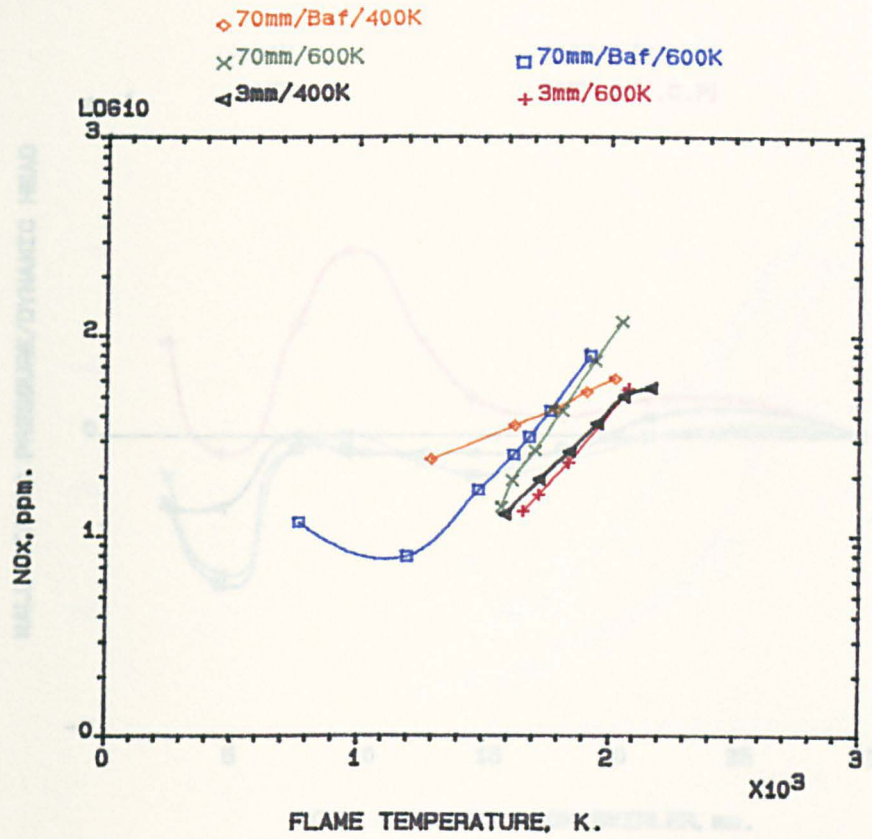

FIG.4.74 INFLUENCE OF CENTRAL FUEL INJECTOR POSITION ON EMISSIONS SWIRLER (A) IN 76mm COMBUSTOR; MN=.03; NATURAL GAS; 400 & 600K.

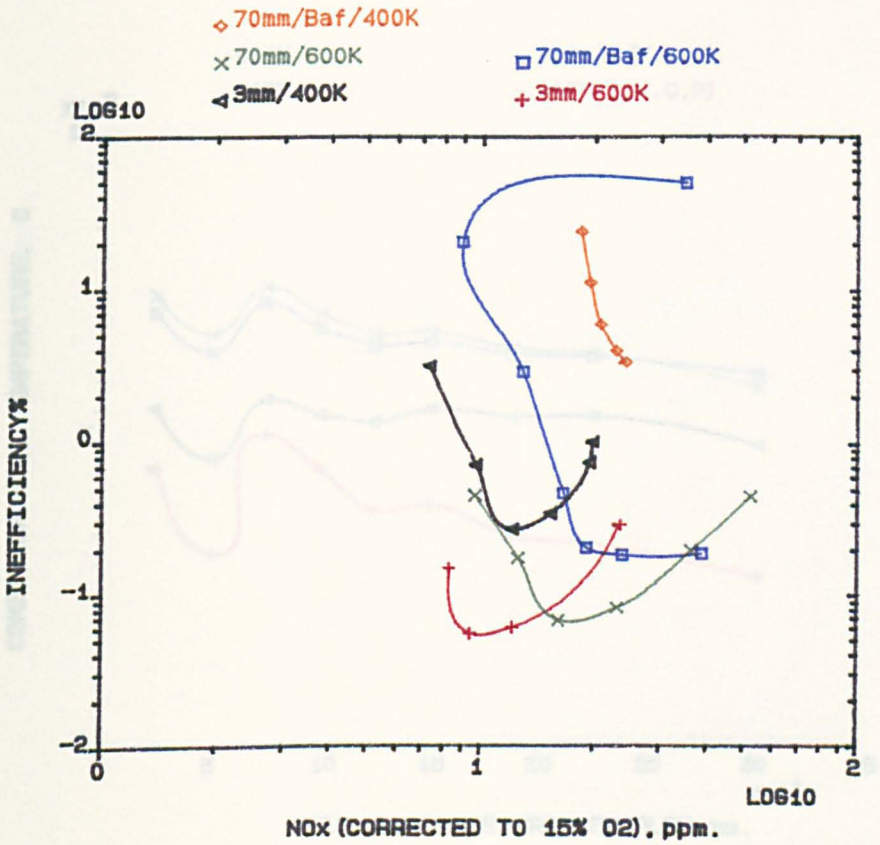

FIG.4.75 INFLUENCE OF CENTRAL FUEL INJECTOR POSITION ON EMISSIONS SWIRLER (A) IN 76mm COMBUSTOR; MN=.03; NATURAL GAS; 400 & 600K.

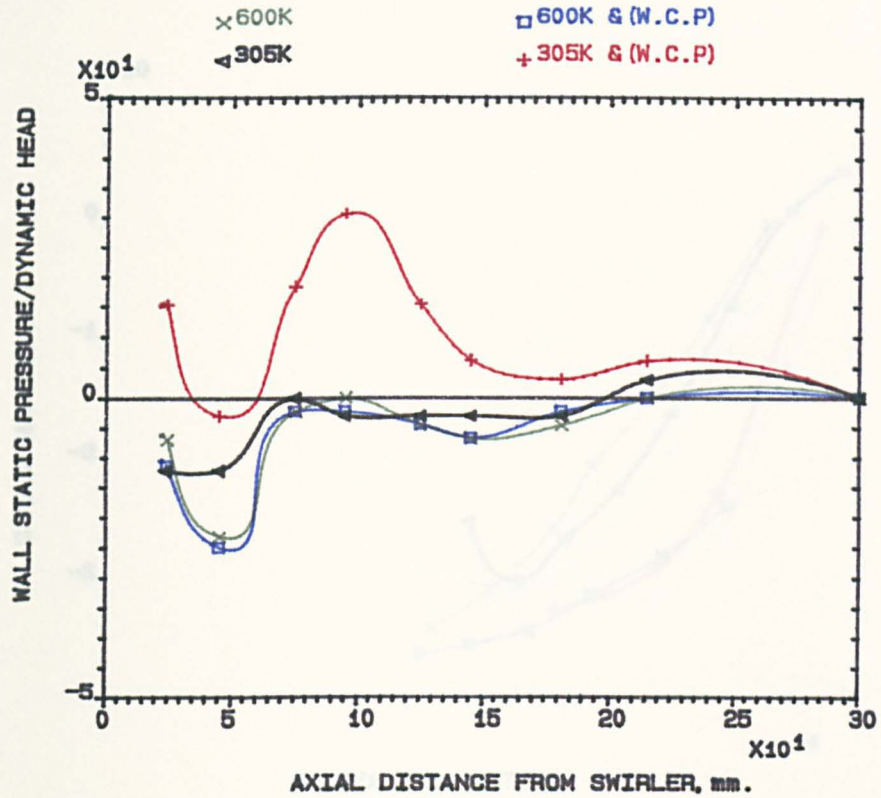

FIG.4.76 INFLUENCE OF BURNER LENGTH ON WALL STATIC PRESSURE PRESSURE FOR SWIRLER(A); EQR=0.44; D/d=3.5; NATURAL GAS.

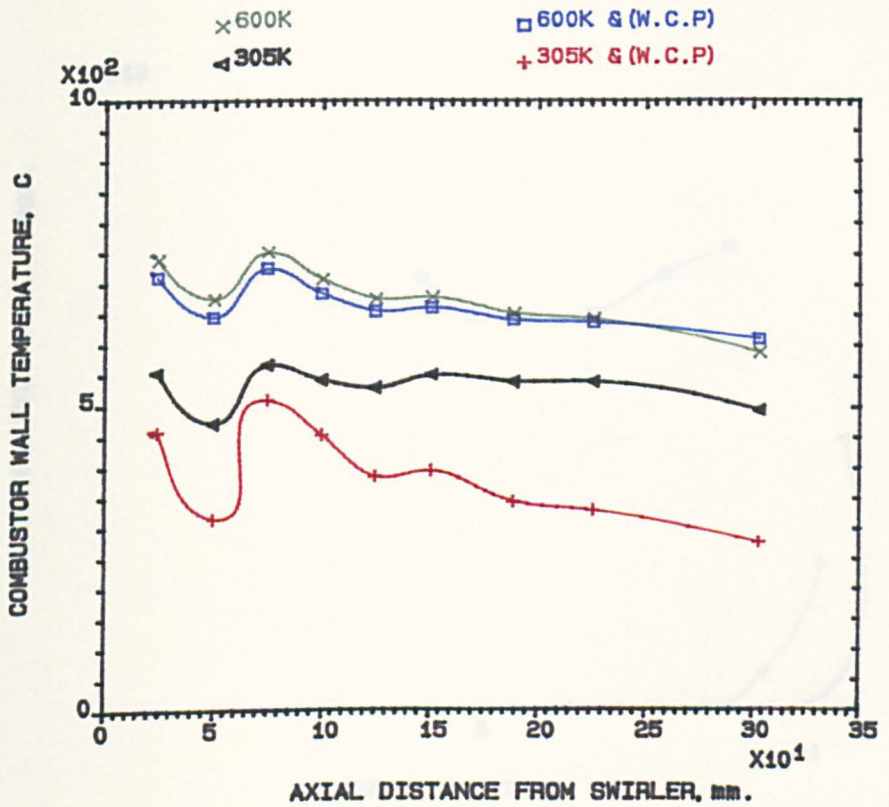

FIG.4.77 INFLUENCE OF BURNER LENGTH ON WALL TEMPERATURE PROFILES FOR SWIRLER(A); EQR=0.44; D/d=3.5; NATURAL GAS.

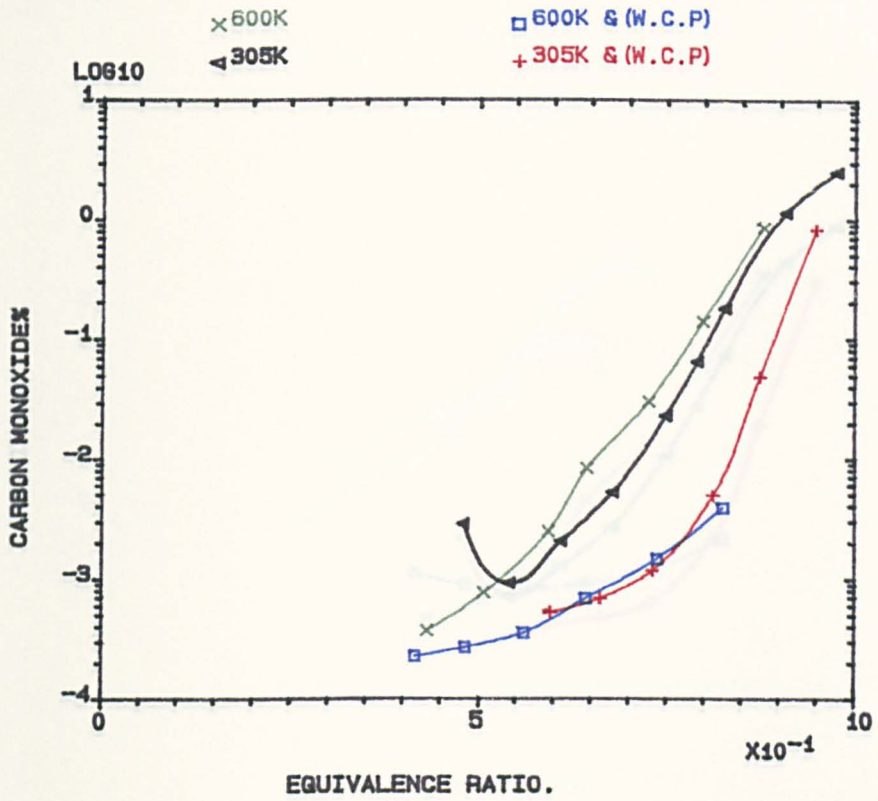

FIG.4.78 INFLUENCE OF BURNER LENGTH ON EMISSIONS FOR SWIRLER(A) D/d=3.5, AT 305K & 600K, WITH & WITHOUT (W.C.P), P.L=1.1%.

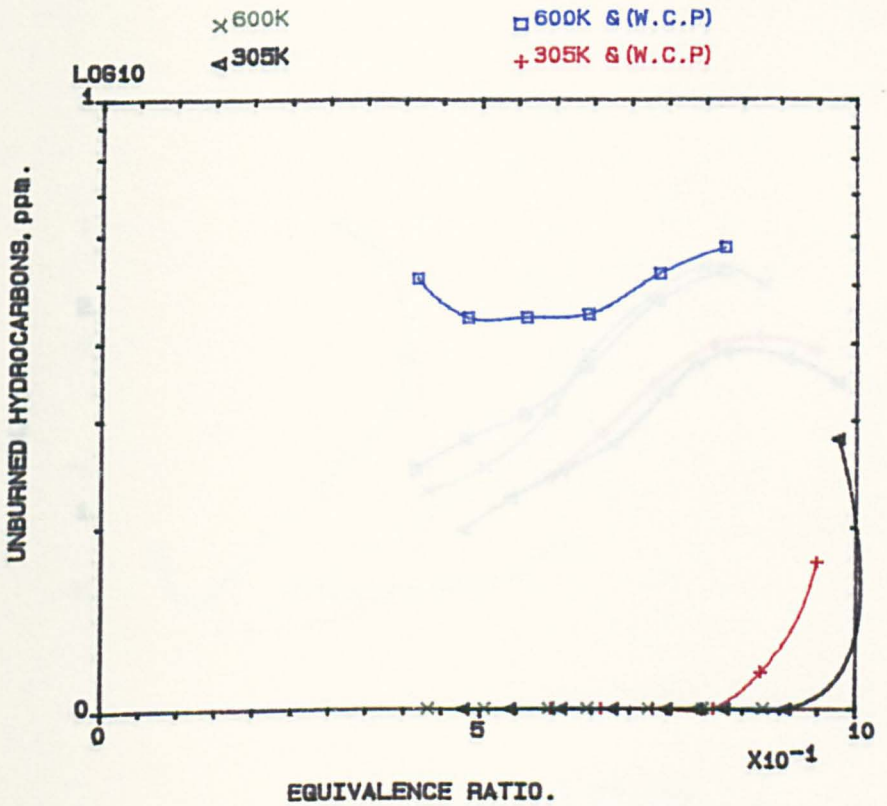

FIG.4.79 INFLUENCE OF BURNER LENGTH ON EMISSIONS FOR SWIRLER(A) D/d=3.5, AT 305K & 600K, WITH & WITHOUT (W.C.P), P.L=1.1%.

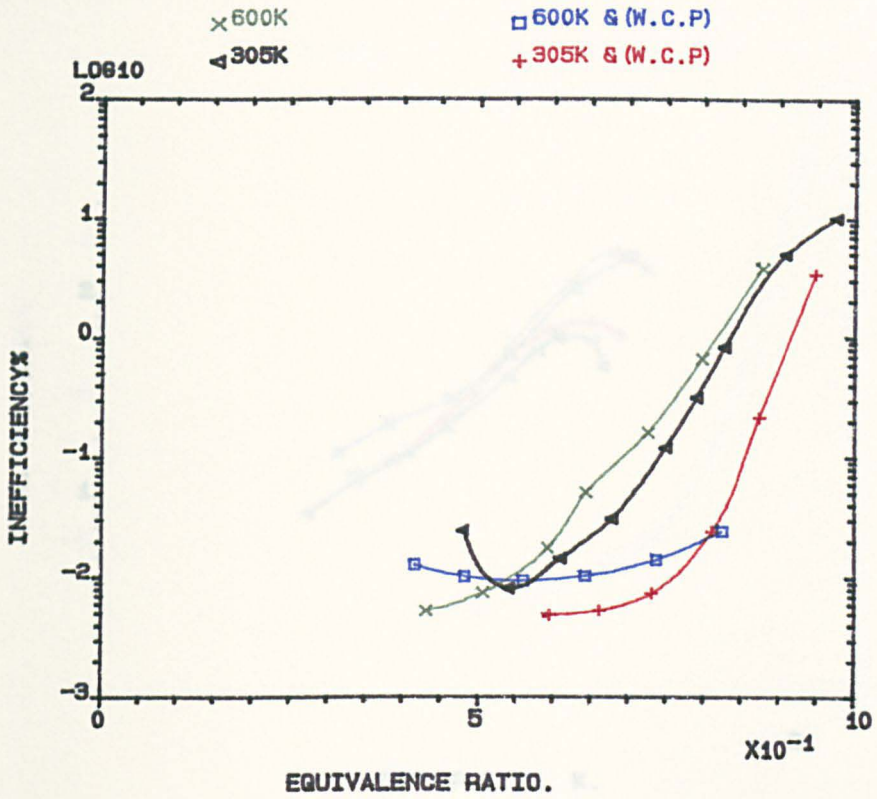

FIG.4.80 INFLUENCE OF BURNER LENGTH ON EMISSIONS FOR SWIRLER(A) D/d=3.5, AT 305K & 600K, WITH & WITHOUT (W.C.P), P.L=1.1%.

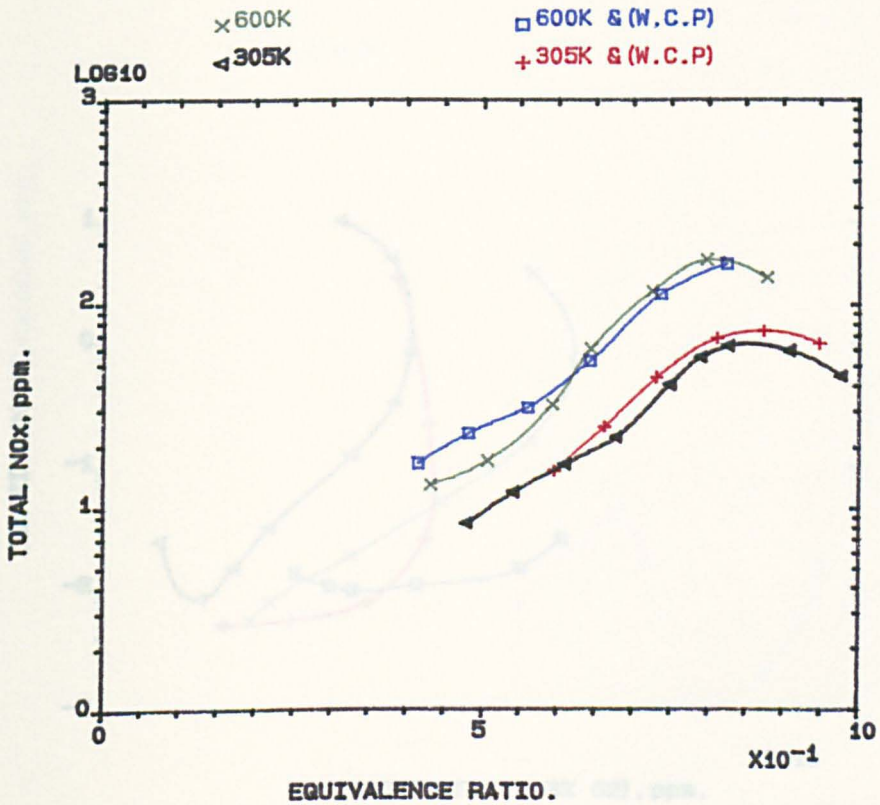

FIG.4.81 INFLUENCE OF BURNER LENGTH ON EMISSIONS FOR SWIRLER(A) D/d=3.5, AT 305K & 600K, WITH & WITHOUT (W.C.P), P.L=1.1%.

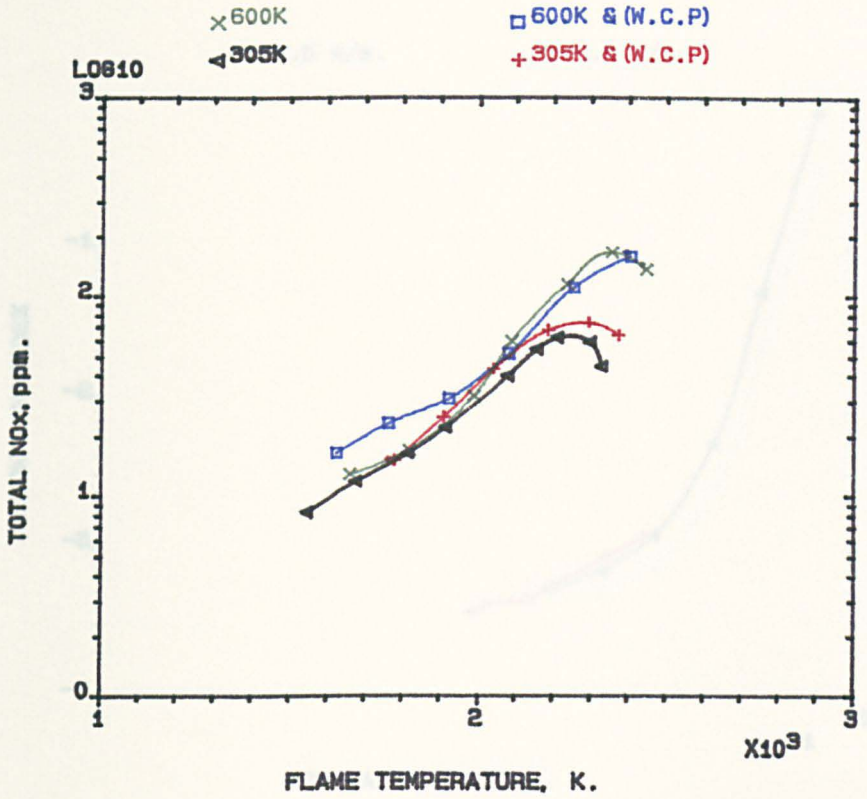

FIG.4.82 INFLUENCE OF BURNER LENGTH ON EMISSIONS FOR SWIRLER (A) D/d=3.5, AT 305K & 600K, WITH & WITHOUT (W.C.P), P.L=1.1%.

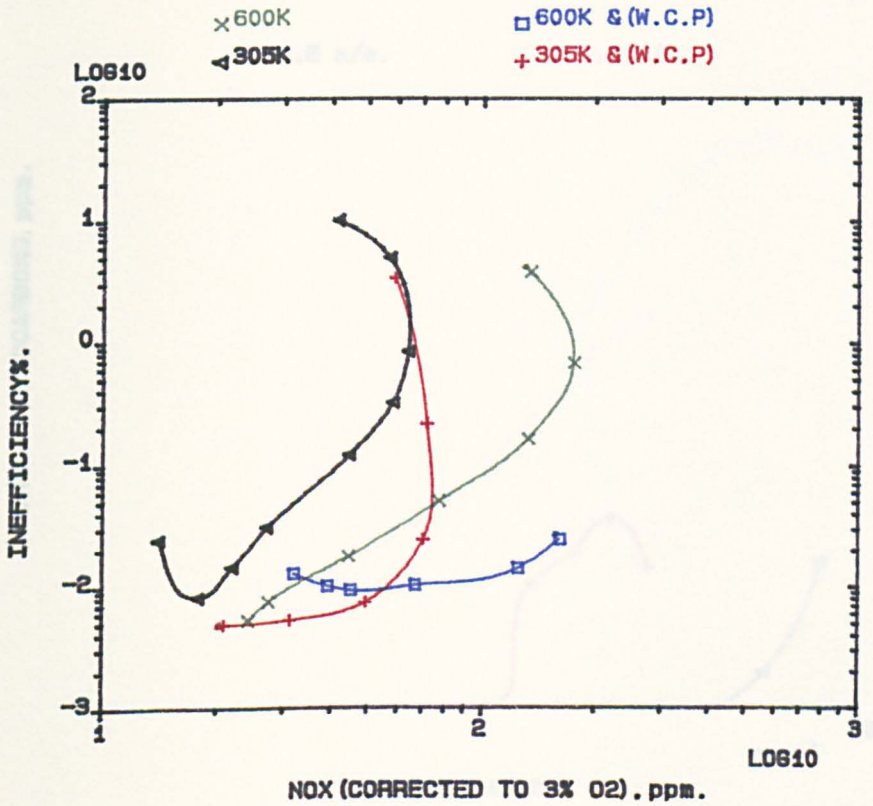

FIG.4.83 INFLUENCE OF BURNER LENGTH ON EMISSIONS FOR SWIRLER (A) D/d=3.5, AT 305K & 600K, WITH & WITHOUT (W.C.P), P.L=1.1%.

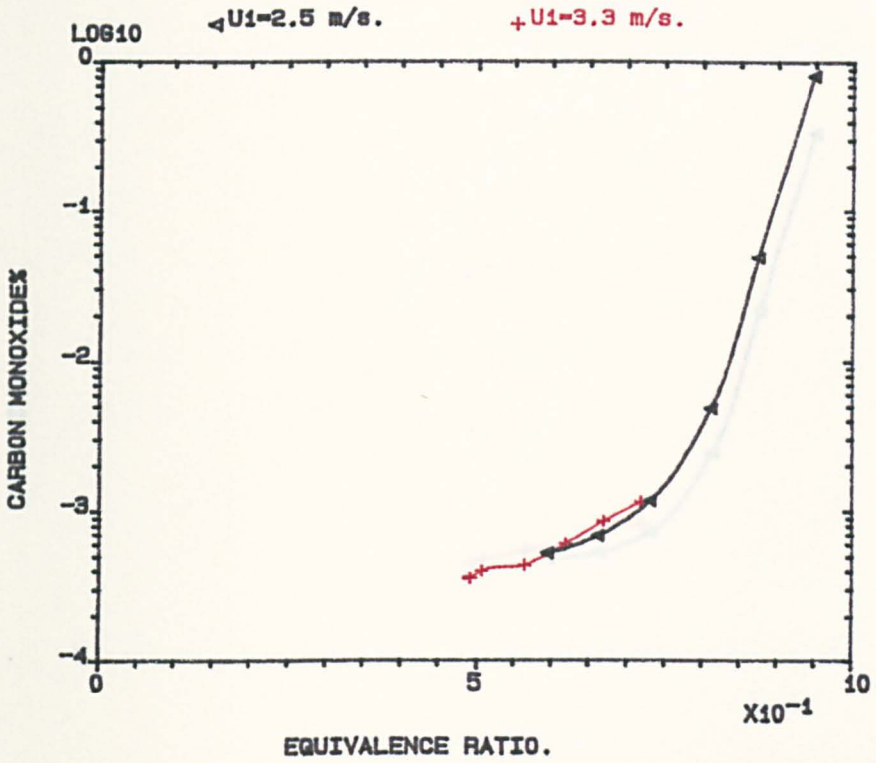

FIG.4.84 INFLUENCE OF HIGHER AIR MASS FLOW RATE ON BURNER EMISSIONS FOR SWIRLER(A), D/d=3.5, AT 305K WITH(W.C.P).

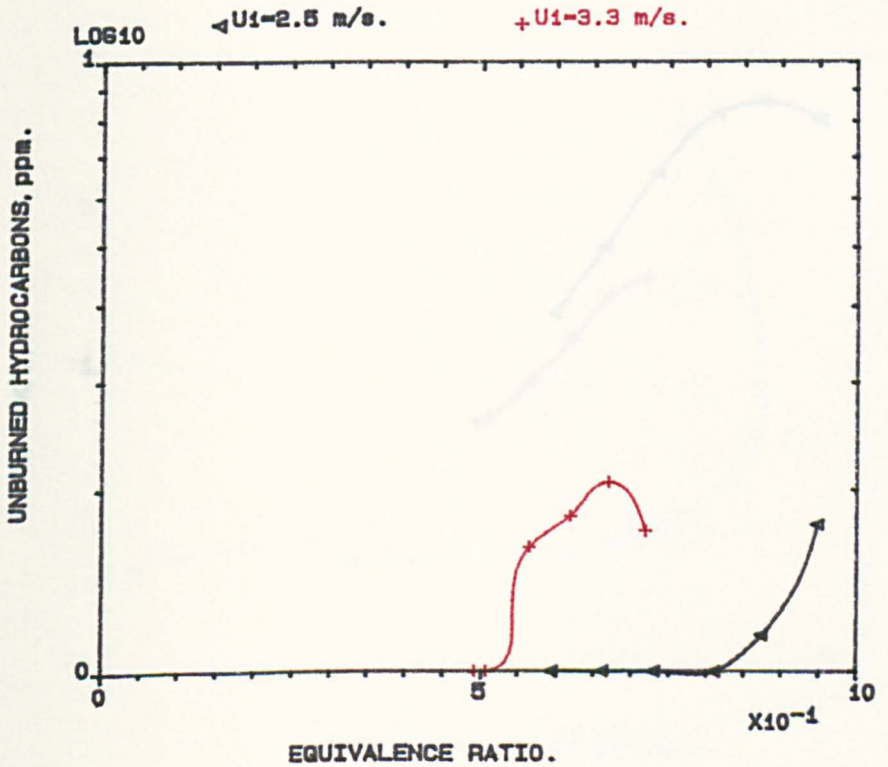

FIG.4.85 INFLUENCE OF HIGHER AIR MASS FLOW RATE ON BURNER EMISSIONS FOR SWIRLER(A).D/d=3.5, AT 305K WITH(W.C.P).

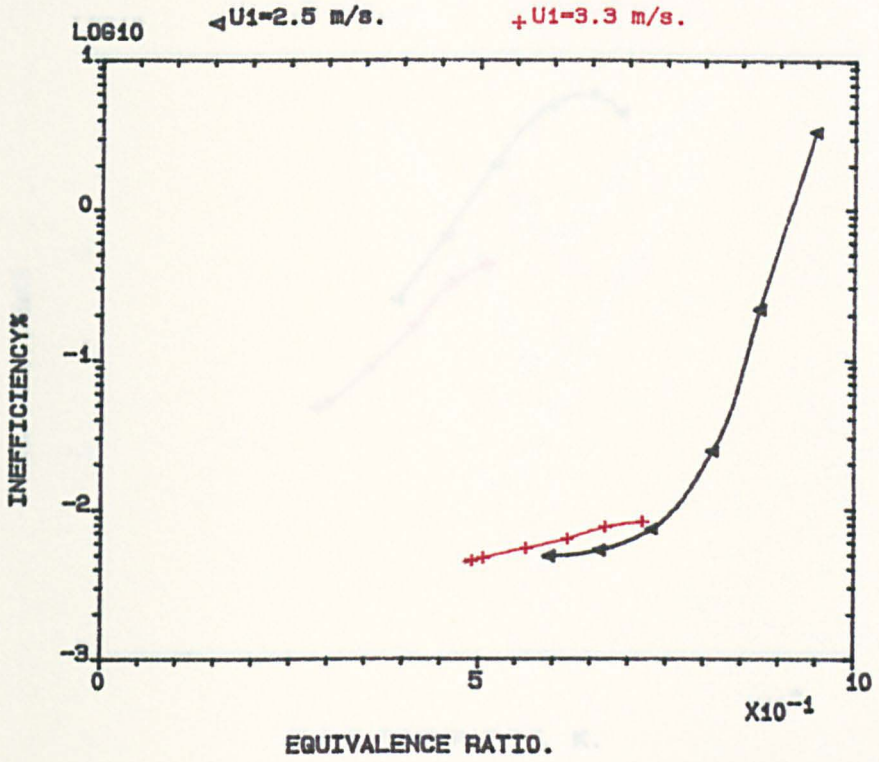

FIG.4.86 INFLUENCE OF HIGHER AIR MASS FLOW RATE ON BURNER EMISSIONS FOR SWIRLER(A). D/d=3.5. AT 305K WITH(W.C.P).

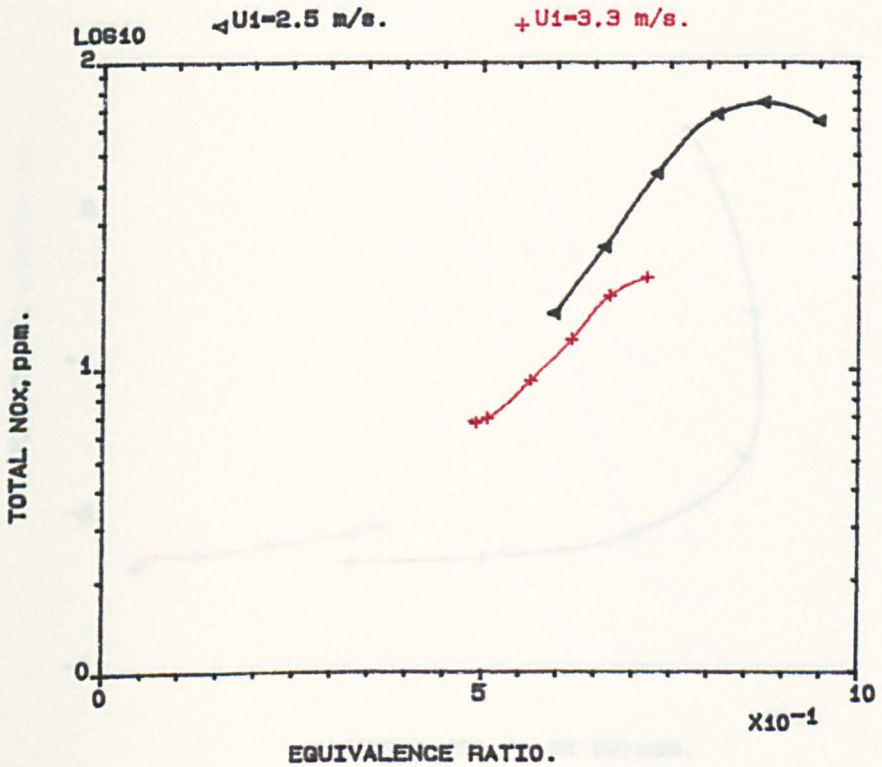

FIG.4.87 INFLUENCE OF HIGHER AIR MASS FLOW RATE ON BURNER EMISSIONS FOR SWIRLER(A). D/d=3.5. AT 305K WITH(W.C.P).

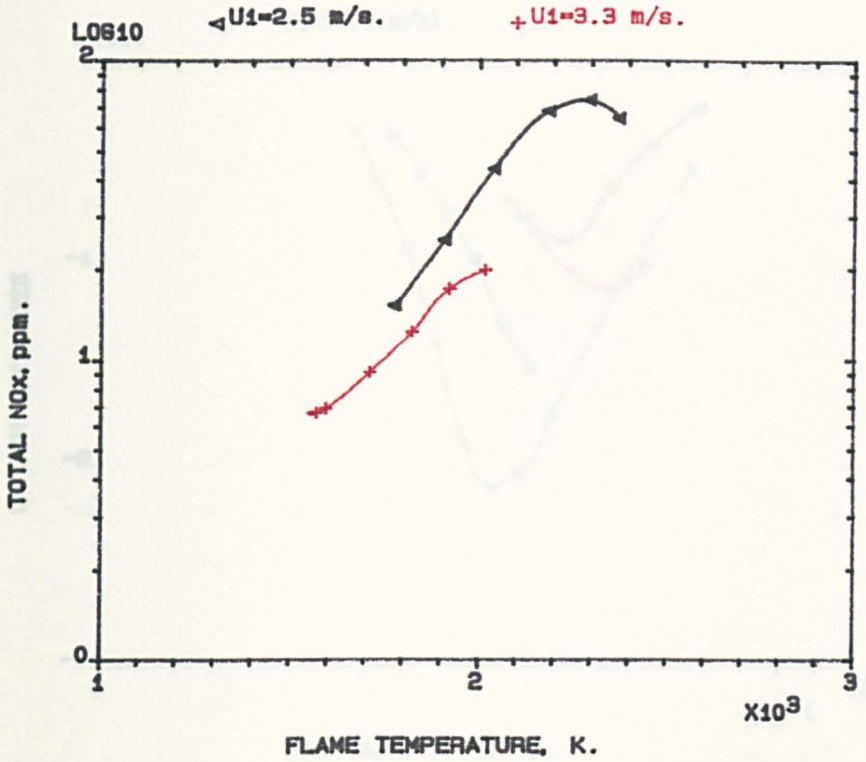

FIG.4.88 INFLUENCE OF HIGHER AIR MASS FLOW RATE ON BURNER EMISSIONS FOR SWIRLER(A), D/d=3.5, AT 305K WITH(W.C.P).

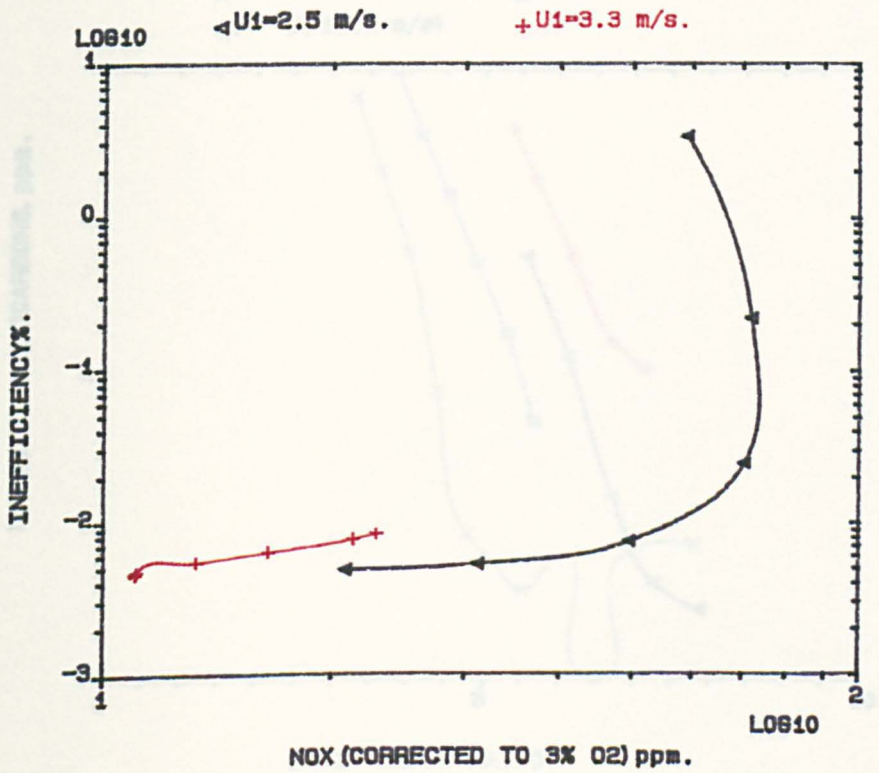

FIG.4.89 INFLUENCE OF HIGHER AIR MASS FLOW RATE ON BURNER EMISSIONS FOR SWIRLER(A), D/d=3.5, AT 305K WITH(W.C.P).

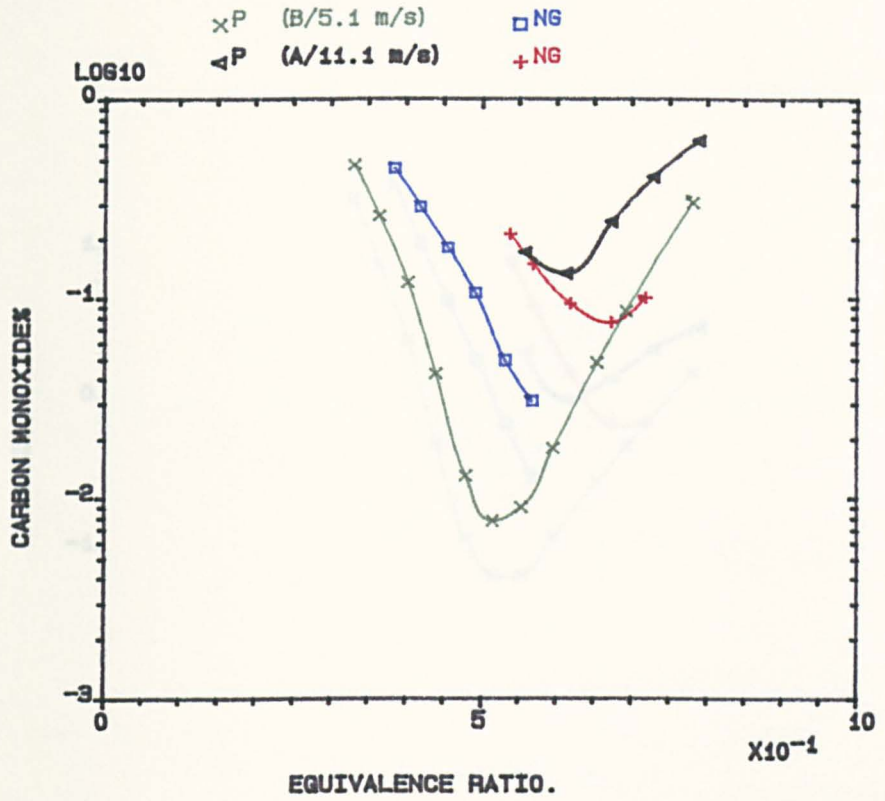

FIG.4.90 INFLUENCE OF FUEL TYPE ON BURNER EMISSIONS, AT HIGHER APPROACH VELOCITY FOR 76mm & 140mm BURNER, 305K.

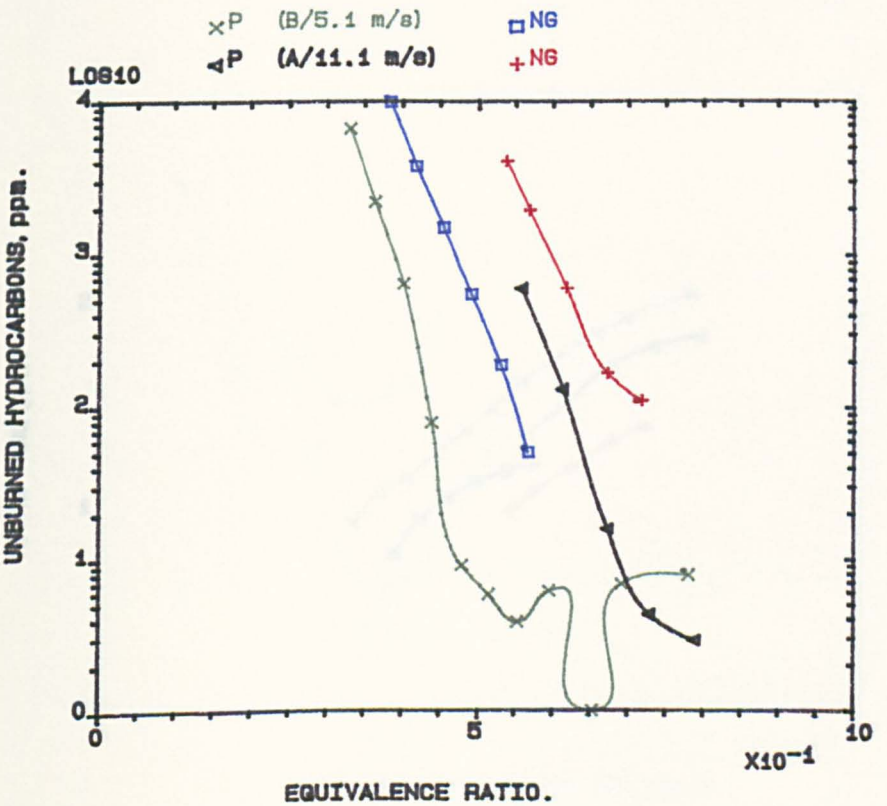

FIG.4.91 INFLUENCE OF FUEL TYPE ON BURNER EMISSIONS, AT HIGHER APPROACH VELOCITY FOR 76mm & 140mm BURNER, 305K.

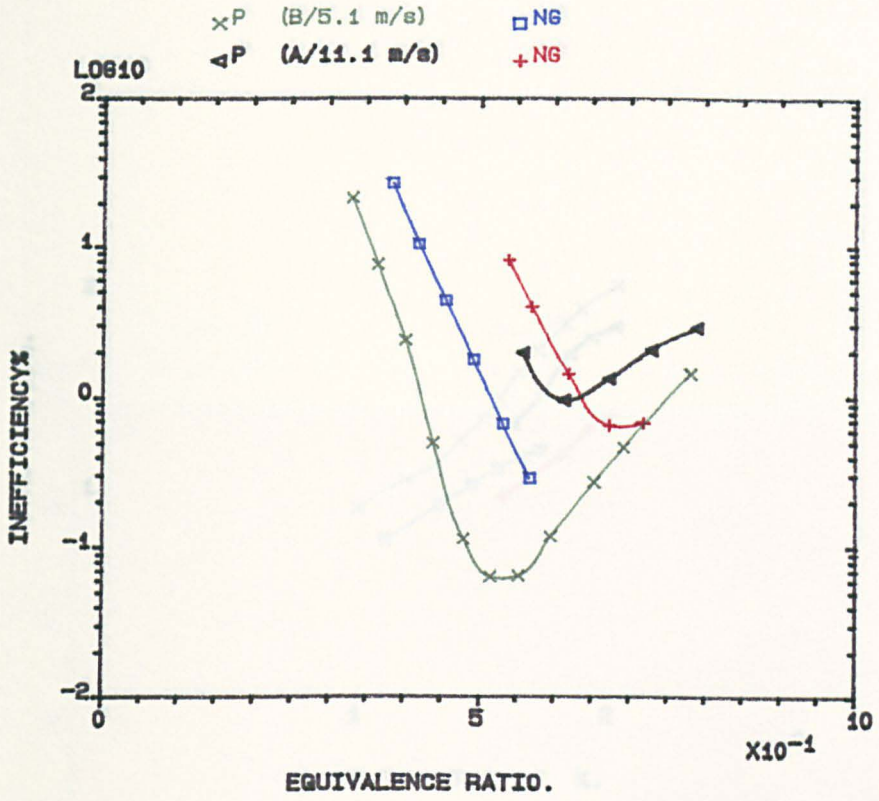

FIG.4.92 INFLUENCE OF FUEL TYPE ON BURNER EMISSIONS, AT HIGHER APPROACH VELOCITY FOR 76mm & 140mm BURNER, 305K.

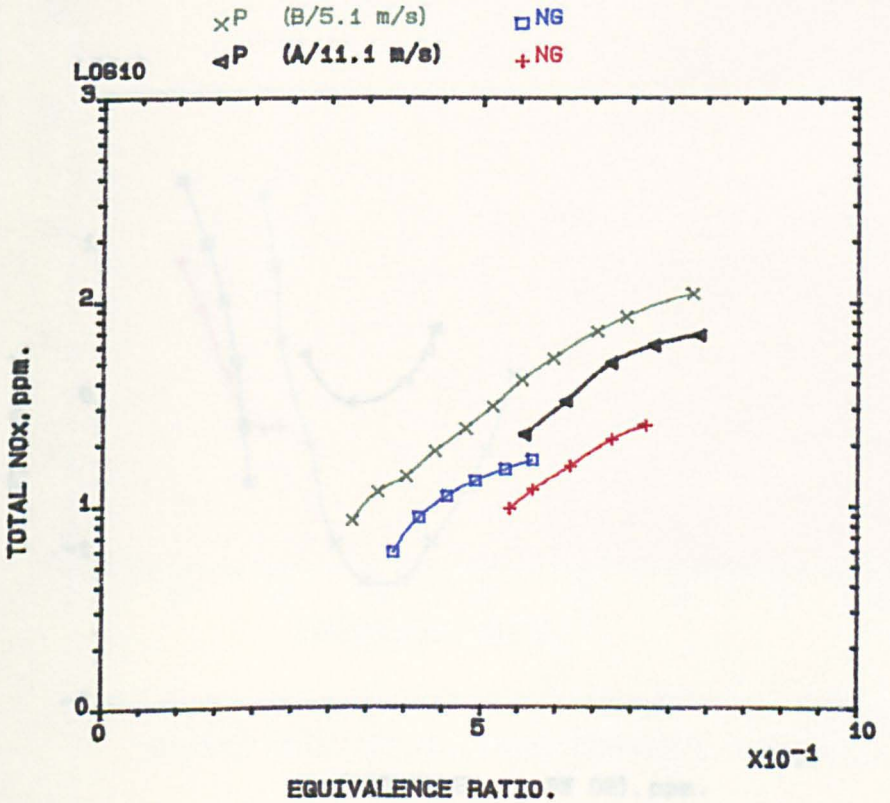

FIG.4.93 INFLUENCE OF FUEL TYPE ON BURNER EMISSIONS, AT HIGHER APPROACH VELOCITY FOR 76mm & 140mm BURNER, 305K.

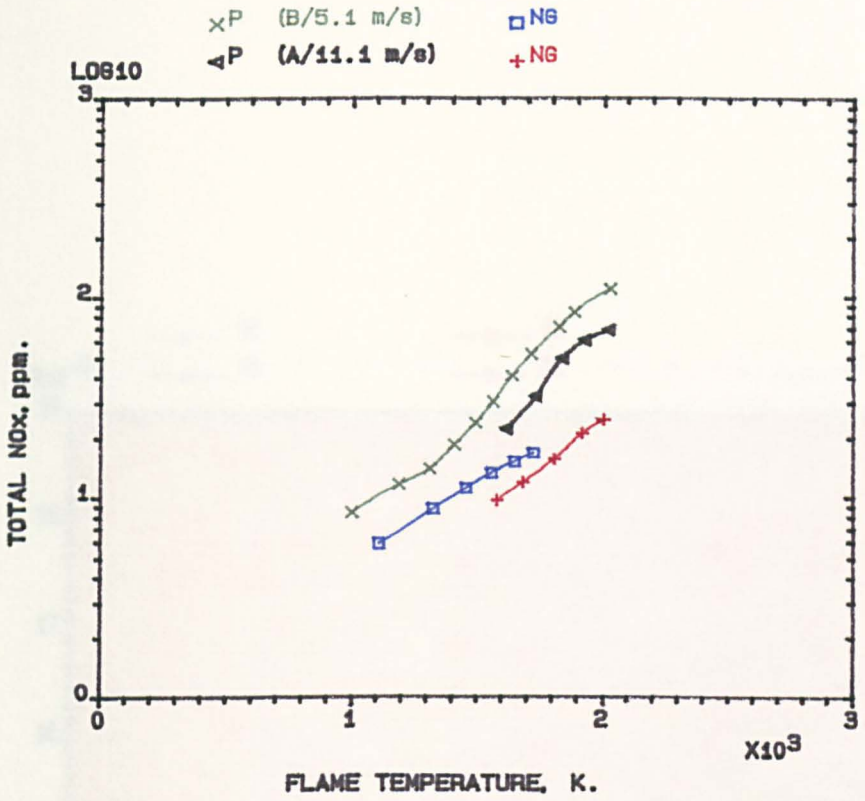

FIG.4.94 INFLUENCE OF FUEL TYPE ON BURNER EMISSIONS, AT HIGHER APPROACH VELOCITY FOR 76mm & 140mm BURNER, 305K.

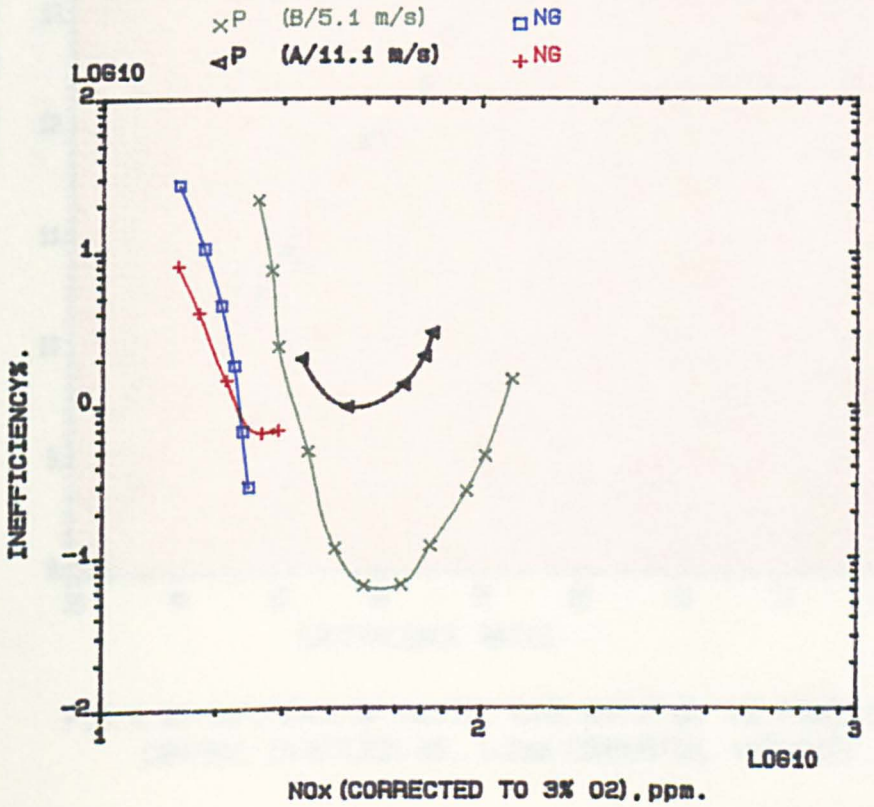

FIG.4.95 INFLUENCE OF FUEL TYPE ON BURNER EMISSIONS, AT HIGHER APPROACH VELOCITY FOR 76mm & 140mm BURNER, 305K.

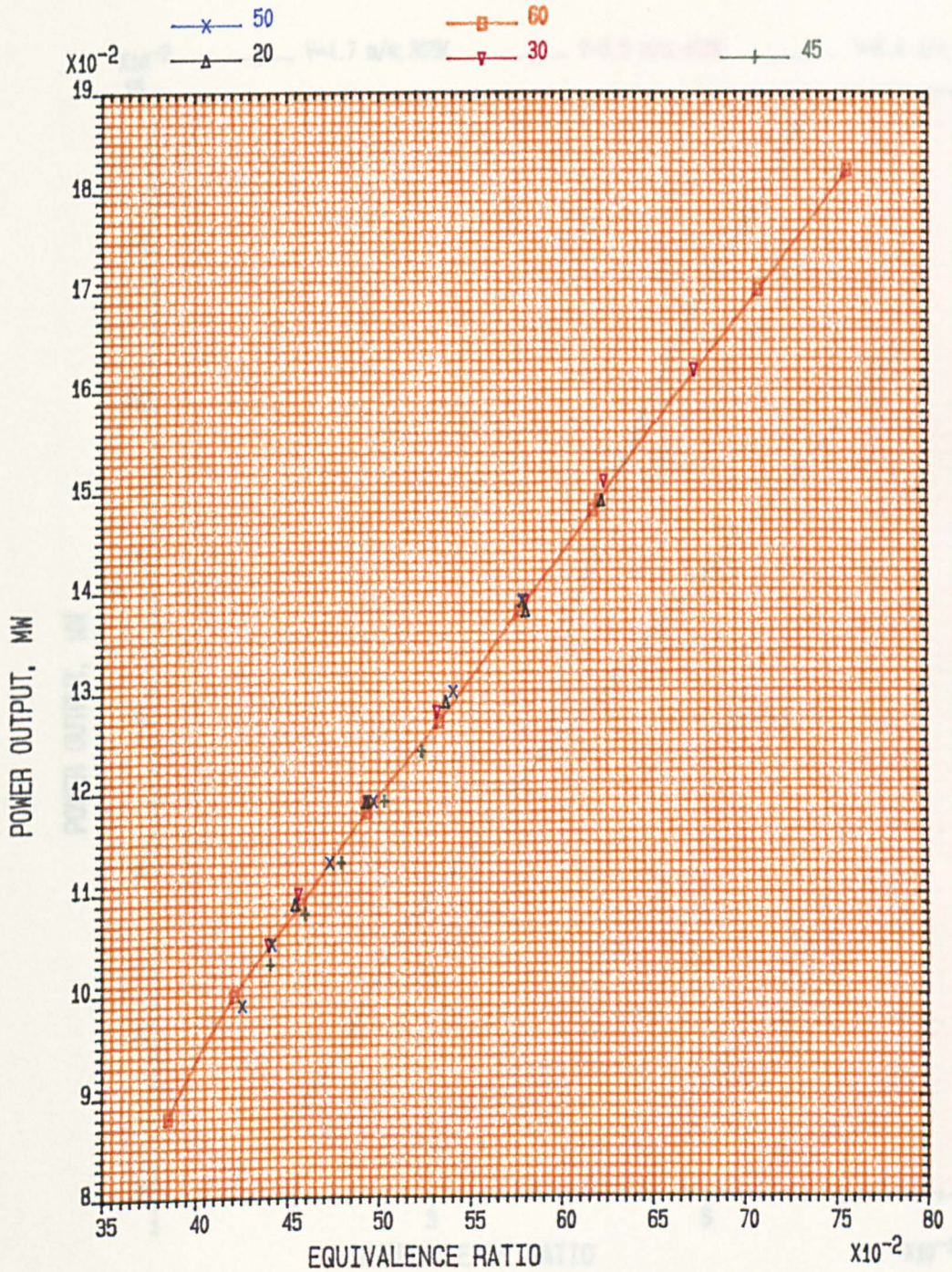

FIG.4.96 INFLUENCE OF RADIAL VANE ANGLE ON THE POWER OUPUT FOR CENTRAL INJECTION NG., 140mm COMBUSTOR, V=5.6m/s , 400K.

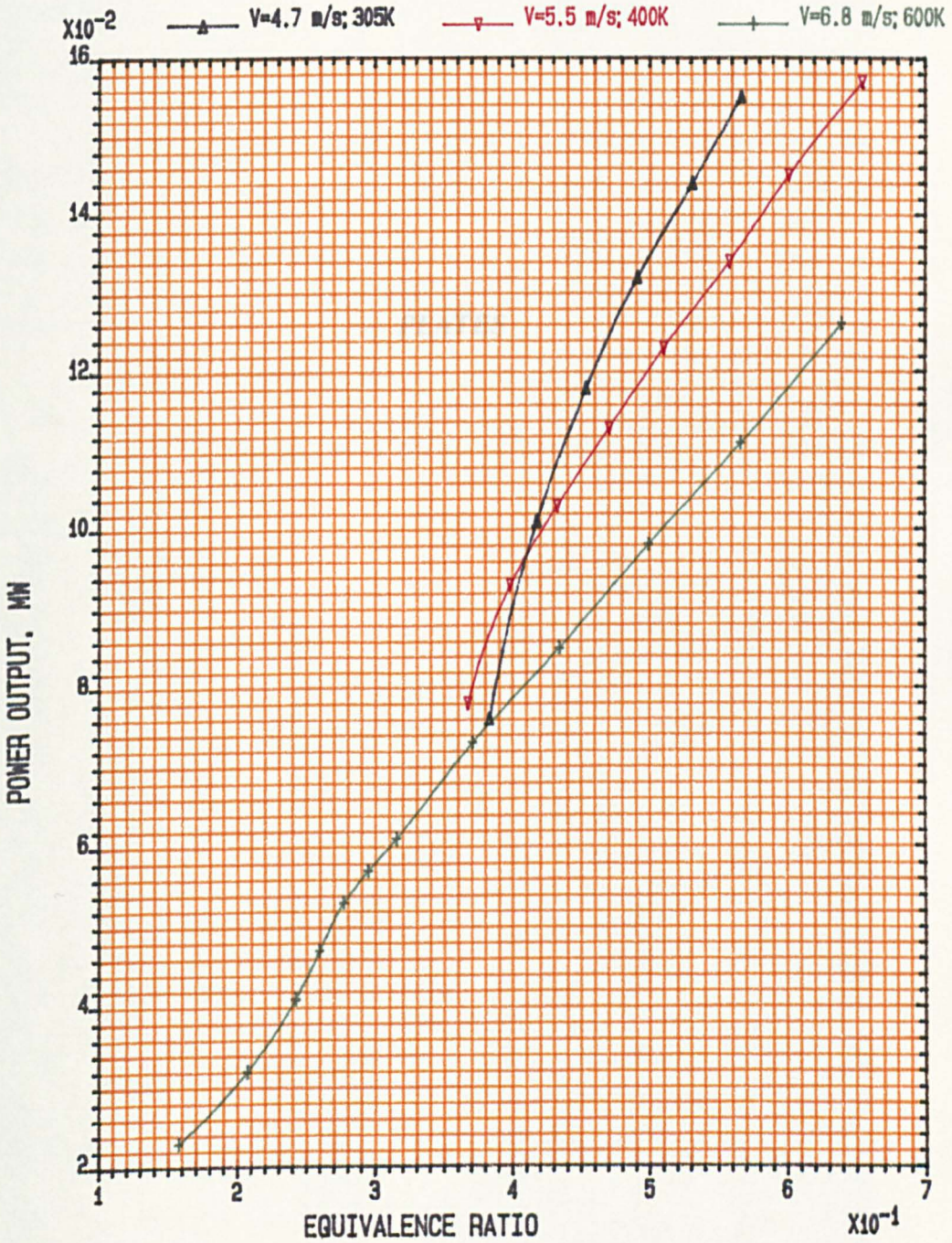

FIG.4.97 INFLUENCE OF INLET TEMPERATURE AND APPROACH VELOCITY ON POWER OUTPUT; CENTRAL INJECTION NG., SWIRLER (B); 140mm COMBUSTOR.

PLATES

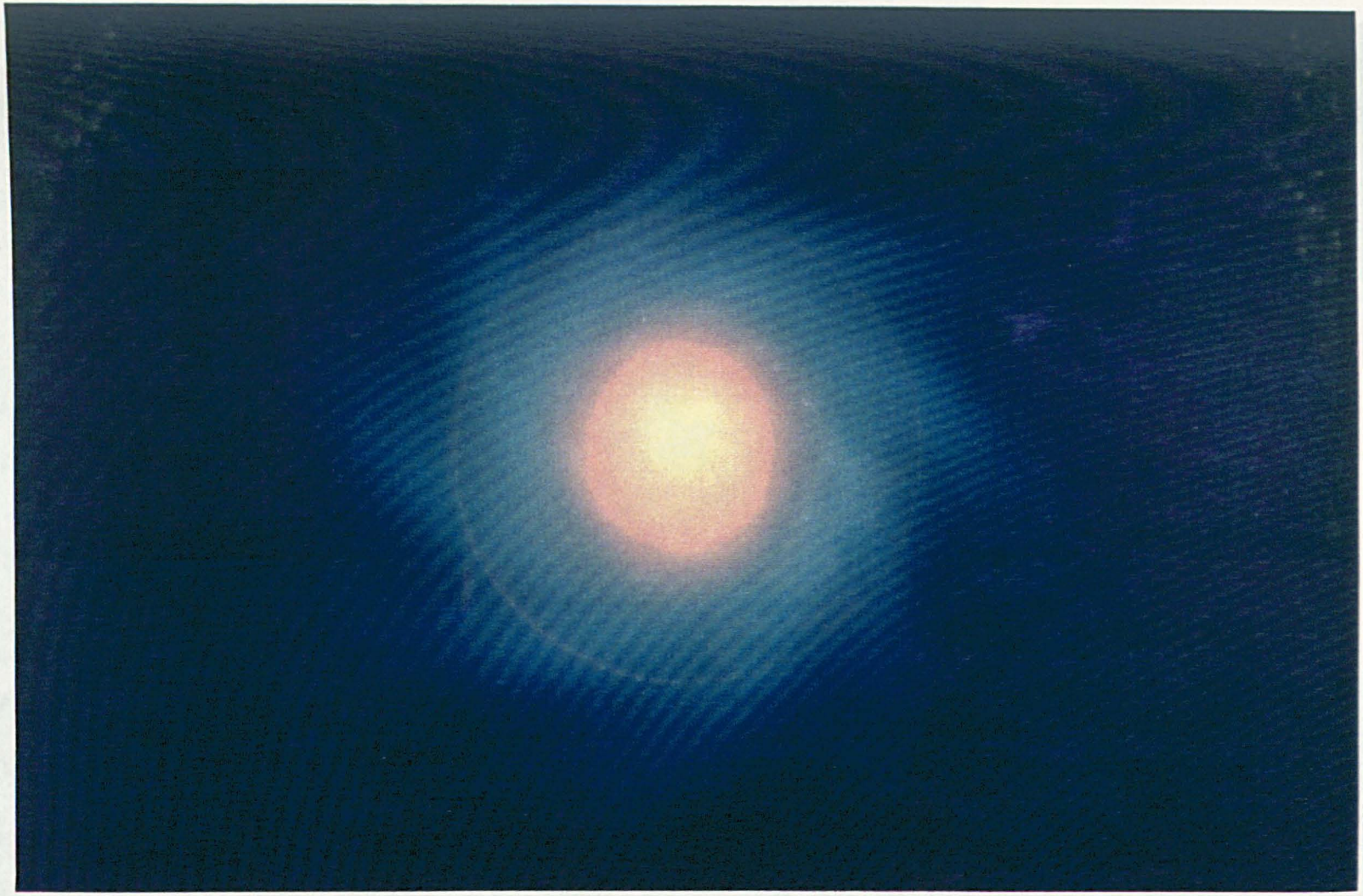

Plate 4.1 Near Weak Extinction for propane central injection using radial swirler(B) in 140mm combustor with pressure loss of 4.2% and inlet temperature= 600K, EQR.=0.1.

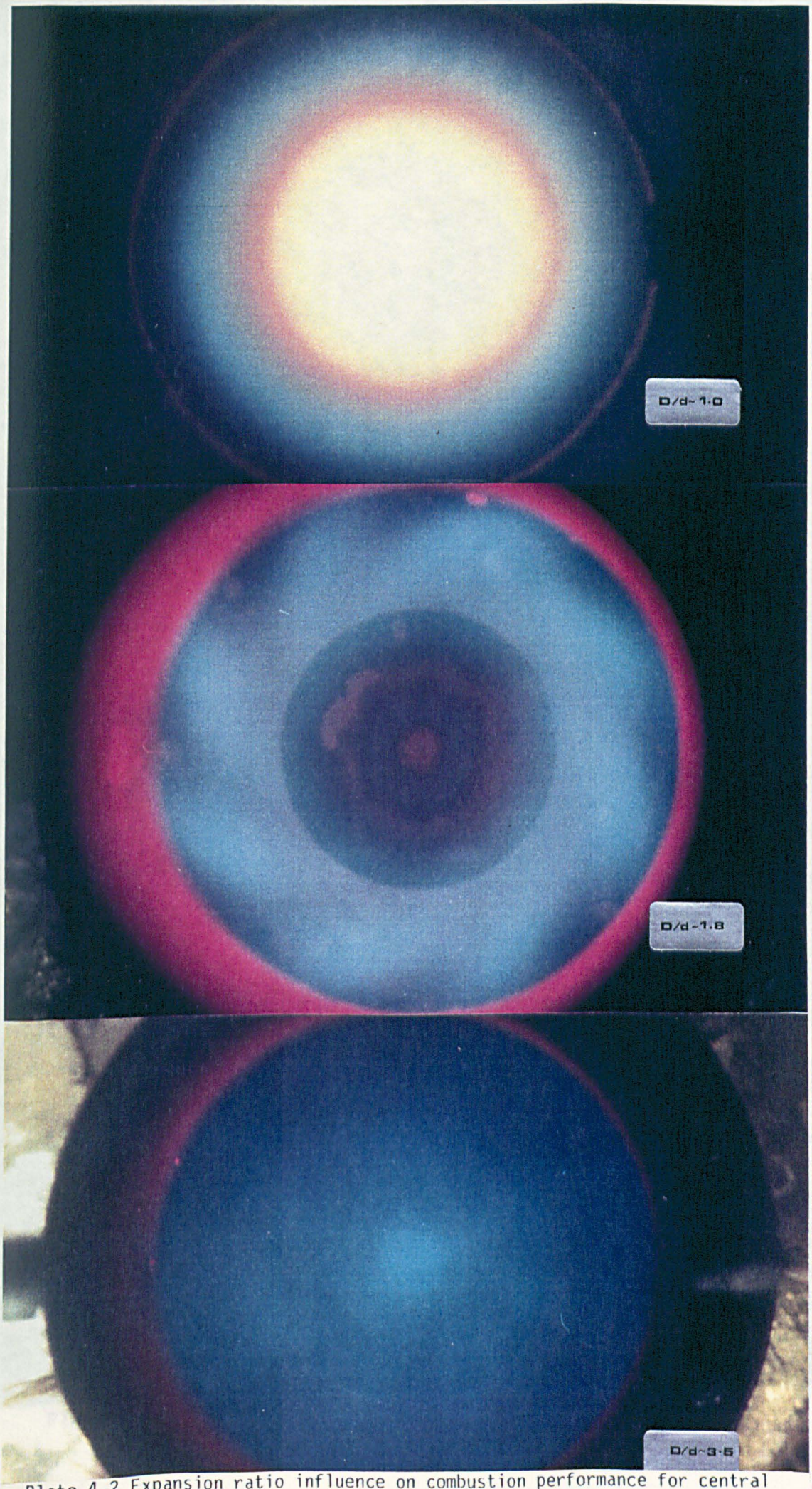

Plate.4.2 Expansion ratio influence on combustion performance for central propane injection with radial swirler in 140mm combustor, 600K, pressure loss=4.2%, EQR.=0.45.

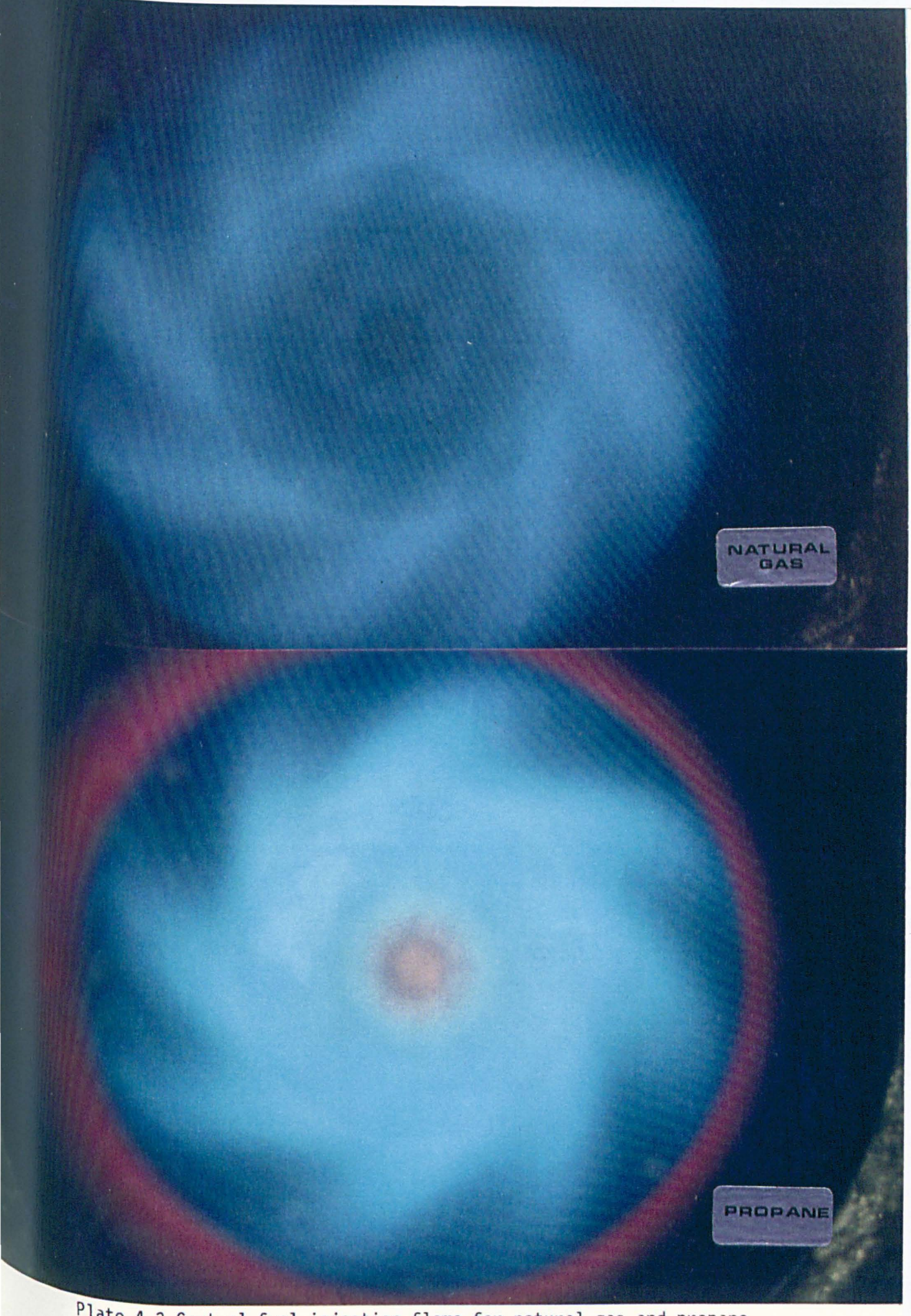

Plate 4.3 Central fuel injection flame for natural gas and propane using radial swirler(B) in 140mm combustor with pressure loss=4.2%, EQR.=0.43, Tin= 600K.

CHAPTER FIVE

COMBUSTION CHARACTERISTICS WITH PASSAGES AND WALL FUEL INJECTION

5.1 INTRODUCTION

The conventional mechanism for combustion in a non-premixed swirl burner system is by central fuel injection. Most of the experimental basis for the favorable properties of swirling flames comes from studies of furnace burners or free flames with central fuel injection (1,2,3,4).

The application of swirling flow to gas turbines involves enclosures whose dimensions are much closer to those of the swirler than for furnace applications and this can significantly alter the swirler aerodynamics. Also, it allows the fuel to be injected at the periphery of the swirler rather than at the centre. This was demonstrated by Ahmad et al(5,6) and more recently by Beltagui and MacCallum(7). In the present work similar technique have been used but by using two fixed wall injectors of diameters 76mm and 140mm with eight injector holes inclined upstream at 30 and 15 degrees to the vertical respectively. These were used in combination with the 76mm and 140mm combustors as shown in Fig.5.1. Fuel injection inside the vane passages of radial swirler have been used insome low NOx combustion designs, this a particular advantage of radial swirlers (8,9,10,11,12,13,14,15). In their investigations of radial swirl systems for low emission gas turbine combustors. Smith et al(11,12,13,14,15) used radial vane passages with a bend into an annulus around a centre body, thus becoming a form of axial swirler but with the benefit of greater passages fuel and air mixing. For the present work the fuel was injected through a shorter passages, using the benefit of the radial air flow for partial mixing with the injected fuel before being introduced to the primary zone. The sudden expansion from the radial swirler outlet gave a very rapid swirler expansion and strong shear layer which were advantageous to the swirler performance.

Although centrifugal forces are important, in swirl combustion, they have

been neglected until recently(16-19). The local density differences, due to combustion of pockets of gas surrounded by unburnt gas, cause the lower density hot gas to move inwards, relative to the high density unburnt gas. This relative movement promotes unburnt/burnt gas mixing and increases the flame propagation rate. this feature has not been included in numerical models of turbulent combustion(20), although the related problem of buoyancy induced burnt/unburnt gas mixing has been included in the theory of Bray and Moss(21).

The purpose of the present work was to investigate the significance of these centrifugal forces in enclosed swirling flames that simulate practical gas turbine primary zone conditions and to exploit the additional mixing forces on a low NOx combustor design. Many recent experimental combustors designed for low emissions and future fuels call for the use of swirl flame stabilisation with most of the combustion air flow passing through the swirler(8,9,16,19,22-24). It is well known that NOx emissions can be reduced by using lean well mixed primary zones, but the level of reduction is closely related to the quality of improved fuel and air mixing. Premixed fuel and air systems offer the lowest NOx emissions but involve major practical problems(25) . One of the major problems is that flame stability which may be overcome by fuel staging between a diffusion flame pilot and premixed main burner(26-28).

An alternative technique for overcoming the stability problem is that of variable air staging, with air switched from primary zone to dilution zone at low power and in reverse direction to give a lean primary zone at high power. This involves the complexity of moving parts in a high temperature environment and there have been few successful applications of this technique in small gas turbine combustor sizes, but it is more easily achieved in large industrial gas turbines(29).

Andrews et al(30) have developed a range of techniques for low NOX gas turbine primary zones with good flame stability, all of which use fuel injection into the base of jet shear layers. Low NOx emissions have been demonstrated for non-swirling jet shear layer for both gas and liquid fuels(31,32) and as

demonstrated in chapter four using just straight radial flow with central injection gaseous fuel. Thus the conclusion of Mestre(33) regarding non-swirling systems are not supported. However, the present work investigates techniques to produce further reductions in NOx emissions for radial swirlers, using the radial swirler passages as a partial fuel and air premixing zone.

5.2 REVIEW OF RELEVANT STUDIES

Perhaps one of the superior advantages of using radial flow swirler is the permittability of use of swirl vane passage fuel injection system to promote partial premixing of the fuel and air. The only previous work on passages injection which is close to the present work is that of Smith et al(11,12,13,14,15). They used filetest rig and the fuel injection modes which are shown in Figs.5.a - 5.b. In their work the radial passages were carried through a bend into an annulus around a central fuel injector, thus becoming a form of axial swirler but with the benefit of a greater passage fuel and air mixing time.

Ahmad et al(34) found problems in the achievement of an adequate combustion efficiency and stability with lean primary zones using large air flow axial swirlers with central fuel injection. By the use of radial swirler these problems could be overcome, with their quite different near swirler aerodynamics. Ahmad and Andrews(34) and Andrews and Kowkabi(35)showed that for a fixed axial swirler the position and direction of fuel injection had a major influence on the flame development and NOx emissions The objective of the present work was to investigate the potential for NOx reduction using better fuel placement in radial swirl stabilised combustor primary zones. One of the main advantages with swirling flow combustion is due to the fact that a centrifugal force field is generated which tends to accelerate the mixing of two flows having different densities and thus increase the reaction rate in combustion processes. This inherent property of swirling flow has frequently been utilised in premixed combustion to aid flame spread (10,34,36).

For central fuel injection in a swirling flow, the higher density fuel is centrifugally forced towards the wall of the combustor as soon as it passes the swirler vanes, thus promoting fuel/air mixing. For direct injection of fuel the two methods of forcing the fuel towards the wall is by injection at the wall or by central radial injection. The use of fuel injection at the wall has not been investigated previously for practical enclosed axial vane swirler stabilised flames. The technique is particularly suited to gas turbine combustor applications as the swirler expansion (D/d) is limited to less than two and hence the swirl velocities in the wall region remain sufficiently high for mixing and atomisation of the liquid fuel.

The CIVIC combustor design of Shekleton(9,37) was aimed at the exploitation of the centrifugal mixing effects. However, the fuel was injected closer to the centre than the wall. Vranos et al(17) have also recognised the possibilities of enhancing flame propagation rates by initiating combustion at the periphery of a swirl flow, but only a low swirl was investigated and no detailed gas composition measurements were taken. Previous investigation of swirling flames with liquid fuel injection at the wall was reported by Mestre(18,33) and Kowkabi(16). The former was aiming at the exploitation of the centrifugal mixing forces for a kerosene fuelled system. However, it was applied to an annular swirl flow with the inside cylinder water cooled and was a rather unrealistic situation for gas turbines. However, the results (33) included gas composition measurements for both swirling and non-swirling flows. These showed a significant improvement in the combustion efficiency and a reduction in the NOx levels with wall injected fuel and swirling flow compared with non-swirling flow. This was attributed to the beneficial influence of centrifugal mixing forces and better atomisation with the swirling flow(16).

Beltagui and Maccallum(7,48) demonstrated the better flame development for axial swirlers with peripheral fuel injection. Natural gas was introduced through an annular slit of 2mm width around the periphery of an air swirler. Comparing their results with central fuel injection systems they showed that the

peripheral injection systems with even weak swirl gave much more rapid mixing and combustion and uniform temperature in shorter furnace lengths. Axial central fuel injection, which is the most frequently used mode of fuel injection in swirl combustion, resulted for a confined swirl flame in a very rich core region for a weak overall mixture. Radial central fuel injection produced much better mixing, which was further improved by fuel injection at the swirler periphery.

Investigations of central radial injection of fuel are rare. Most of the central injection systems studied are multi hole divergent nozzles with divergent angles less than 90 degrees(38-40). Leuckel and Fricker(41) investigated flames produced when natural gas was injected directly into an internal reverse flow zone induced by strong rotation of the combustion air. They carried out a series of tests on central fuel injection systems with various nozzle divergent angles and an annular axial fuel gas jet. Their results indicated that with an angle of zero, i.e. a central axial fuel injection, a long slow mixing luminous flame was produced. The use of the annular axial gas jet with the same injection velocity, however, produced a short intense blue flame. the use of very large values of injection angles greater than 40 degrees also produced a well mixed intense flame depending on the velocity of the fuel.

Takagi et al(42) showed that the flame was elongated and concentrated in the centre of the tube. In their swirling flame, the main part of the burnt and unburnt gas species existed mostly in the central part of the flame with a radius of 10mm where the radial gradient of species were high. Charles and Samuelson(27) have shown a major improvement in the flame development of their air staged swirler flame when the direction of the central fuel injection was changed from predominantly axial to predominantly radial. The present investigation of passage fuel injection were undertaken to exploit the twin benefits of peripheral fuel injection and partial fuel mixing upstream of the swirler. For liquid fuels, passage injection also has the advantages of high airflow air blast atomisation.

5.3 PASSAGES FUEL INJECTION RESULTS

In the present work gaseous and liquid fuel injection into the radial swirler vane passages was investigated. Passage fuel injection was undertaken to exploit the twin benefits of peripheral fuel injection and partial fuel air mixing upstream of the swirler. For liquid fuels, passage injection also has the advantage of high velocity air blast atomisation. A Mach number of 0.02 was used with blockage suitable for the generation of a pressure loss 4%, similar to conventional combustors. This pressure loss was needed to create good turbulent fuel/air mixing with low NOx emissions, as well as good liquid fuel atomisation in the radial vane passages. The ratio of the primary zone mach number, 0.02, to the total mach number, 0.047 gave the primary zone proportion of the total combustor air that was simulated using the swirler above as 43%.

5.3.1 INFLUENCE OF FUEL TYPE ON MEAN EMISSIONS

5.3.1.1 Weak Extinction results

At a constant mean velocity and inlet temperature the fuel flow was gradually reduced until visual observation, through the 100mm window in the exhaust, showed the flame to go out. The extinction process was also detectable from the gas analysis by a sudden increase in UHC emissions. The weak extinction results were repeatable to +/- 0.02 equivalence ratio and are summarised in Table(5.1) for radial vane passage fuel injection of propane , kerosene and gas oil. The simulated overall weak extinction was determined by multiplying the measured weak extinction A/F by the ratio of the reference Mach number to test Mach number (0.047/0.02). This assumed that the addition of the remaining air would have no influence on the primary zone swirler weak extinction. This is valid for dilution air injected well downstream of the primary zone.

Comparative results are also included in Table(5.1) for central injection of propane using an eight hole radial fuel injector. Weak extinction data for central injection has also previously been obtained for a Mach number of 0.014 Alkabie

et al (43). This work also included data for natural gas which had a similar weak extinction to propane. However, the radial passage gas injector fuel feed system was complex and a third one was not available for the larger hole sizes needed for natural gas.

The weak extinction results showed that for propane the radial passage injection resulted in a marked deterioration in the weak extinction compared with central injection. However, it was still a 56% improvement on the premixed weak extinction and the simulated overall flame stability was well outside the operational requirements. This indicated that, as expected, there was better fuel and air mixing with fuel injection into the radial passages. Part of the improved mixing was due to the increase in pressure loss from 4.2 to 5.8% caused by the aerodynamic blockage of the fuel in the radial vane passages. This 1.6% increase in pressure loss was halved when using liquid fuel, indicating that full vaporisation did not occur in the radial vane passages.

The kerosene weak extinction were very similar to those for propane, but slightly wider. This indicated a substantially similar combustion performance to propane, which the gas analysis results support. The significantly wider stability limits for gas oil at 600K indicated less vaporisation in the radial vane passages than for kerosene, and richer regions at the base of the stabilising swirling jet shear layer, as shown by the radial traverses discussed later. Plate 5.1 shows cross-sectional view of the kerosene and gasoil flame for an equivalence ratio of 0.44 and 600K inlet temperature. At 400K gas oil had a worse stability than for kerosene and was no better than the premixed situation. The poor vaporisation at 400K would produce insufficient fuel vapor to create a rich zone at the base of the shear layer. The main burning was then downstream of the shear layer in the wall region where the fuel was more completely vaporised and mixed with the air. The combustion results support this with a Gas Oil combustion efficiency superior to that of kerosene and similar to that of premixed combustion at 400K.

5.3.1.2 Wall static pressure and temperature profiles

The axial wall temperature profiles at 400 and 600K inlet temperature are shown in Figs.5.2 and 5.13 at various equivalence ratio. The results show that the type of fuel had a significant influence on the axial temperature profiles. The internal gas composition results showed that passage injection carried fuel to the centre of the combustor creating a richer core than for central injection. This created a leaner wall region and a slower flame development, as shown by the wall temperature results.

Kerosene behaved in a similar way to propane, but the gas oil temperature profiles were substantially different to kerosene with a more rapid development of the flame. The internal traverses showed the propane and kerosene flames developed similar radial temperature profiles in the initial region near the wall, but gas oil burned hotter near the wall. This was because at 600K the delayed vaporisation of gas oil resulted in a richer shear layer and outer recirculation zone than for kerosene.

5.3.1.3 MEAN COMBUSTOR EXIT EMISSIONS

The measured mean combustor exit emissions are shown in Figs.5.14 - 5.21 The unburned hydrocarbon (UHC) emissions at 400 and 600K are shown as a function of the equivalence ratio in Figs.5.16 and 5.17 respectively. At 400K both propane and gas oil had very low UHC emissions for equivalence ratio as weak as 0.55. However, the kerosene emissions were much higher and were coupled with high CO emissions as shown in Figs.5.14 and 5.15. These results indicate that the kerosene flame had achieved sufficient vaporisation to stabilise the flame with a rich zone at the base of the shear layers. For gas oil the vaporisation was slower and flame stabilisation occured further downstream where more mixing had occured. The weak extinction results also indicated better mixing and worse stability for gas oil at 400K. At 600K all three fuels gave low UHC emissions, but gas oil gave the highest and these were higher than at 400K. The gas oil flame was stabilised in the shear layer, as shown by the wall temperature profiles and

the better stability. The slower vaporisation than kerosene would produce richer shear layer regions and hence higher UHC and CO emissions, as shown in Figs.5.17 and 5.15 for mixtures richer than 0.48.

The combustion inefficiencies are shown as a function of equivalence ratio in Figs.5.16.a and 5.17.a for 400 and 600K respectively. Apart from kerosene at 400K an inefficiency of approximately 0.1% was achieved by all the fuels in the weak region. The 98% efficiency for kerosene at 400K and one atmosphere pressure is a quite reasonable performance for a conventional combustor design. These results show that passage injection of liquid fuels did not produce any major problems of poor atomisation and vaporisation which would result in very high UHC emissions. The results also mean that there could be no major problem of radial passage wall wetting and fuel dribble from the passage exits because this would also cause high UHC emissions.

The NOx emissions at 600K are shown as a function of equivalence ratio in Fig.5.19. Kerosene and propane had similar low NOx emissions, except close to weak extinction where the kerosene NOx emissions were slightly higher. The internal traverse results in chapter three showed that these higher NOx levels were generated by local differences in mixing in the near burner shear layer region. The gas oil NOx emissions were higher at all equivalence ratios tested, but still relatively low. The higher emissions were caused by the richer burning in the shear layer, as discussed above. They may also have been increased by the significant levels of fuel nitrogen that occur in gas oil but not in kerosene Williams et al(44) The NOx emissions at 600K corrected to 15% oxygen and the standard day humidity are shown as a function of the inefficiency in Fig.5.21. The minimum NOx emissions compatible with a low inefficiency may be obtained from Fig.5.21. For an inefficiency of approximately 0.1% or lower the minimum corrected NOx emissions were 2.5, 6 and 13ppm for propane, kerosene and gas oil respectively. These are ultra low NOx emissions for both propane and kerosene. The gas oil results are the lowest attained by any combustor design for this fuel and are as low as for central injection with propane.

The EPA 75ppm NOx regulation converts, using the thermal NOx square root pressure relationship, to 20-24ppm at atmospheric pressure for the 15-20 bar operating pressure range of many industrial gas turbine combustor The present results indicate that for gas oil approximately half the EPA NOx limit may be achieved with a factor of ten reduction possible for propane and natural gas. Lean primary zones using radial swirlers with passage fuel injection thus offer one of the best potential solutions available for low NOx emissions, without the problems of a fully mixed system.

5.3.2 INFLUENCE OF INLET TEMPERATURE ON THE MEAN EMISSIONS FOR NATURAL GAS

5.3.2.1 Weak extinction

The measured weak extinction data for four air inlet temperature are summarised in Table(5.2). A slight improvement on the weak extinction was found when the inlet temperature risen was increased to 740K. There was reasonable agreement between the results for the mean adaibatic flame temperature at weak extinction. The effect of inlet temperature expected to be minor. Due to the low molecular weight of natural gas which permit it to disperse quite easily through incoming swirling air, With liquid fuels the situation may be different due to the dependency of vaporisation rate on the inlet temperature.

5.3.2.2 Wall static pressure and temperature profiles

Fig.5.22 - 5.29 demonstrates wall static pressure and temperature profile of the 140mm combustor for inlet temperature of 550, 600, 670 and 740K. The main feature of temperature profiles were that they showed the flame development was much faster as the inlet temperature increased The higher the equivalence ratio and the inlet temperature the faster the axial and radial flame flame development. However, for inlet temperatures of 600K and 550K the wall temperature profiles showed a cooler wall region adjacent to the swirler and a slower axial flame development. This is occured at nearly all equivalence ratios tested. For an inlet

temperature of 600K at equivalence ratio above 0.5 the wall temperature profile showed a faster flame development. The first drop in the wall temperature was associated with the impingement point where the swirler flow splits on wall region at a point approximately 0.32 combustor diameters downstream of the swirler Two flows recirculating in opposite directions were demonstrated in chapter two from the flow visualization studies.

5.3.2.3 MEAN COMBUSTOR EXIT EMISSIONS

The influence of the four inlet temperature upon the emission of carbon monoxide and unburned hydrocarbons are shown in Fig.5.30 and Fig.5.31 as function of metered equivalence ratio. The main feature of these two figures were the sudden increase of CO and UHC emissions as the equivalent ratio approach the weak extinction limits. Inside the weak extinction the CO and UHC emissions were very low at all high inlet temperatures as was the combustion inefficiency Fig.5.32. The equivalent mean flame temperature for the point of sudden increase in CO was 1650K and 1700K for UHC, for all inlet temperatures.

The major effect of inlet temperature was on NOx emissions as shown in Fig.5.33 and Fig.5.35. As the equivalence ratio was increased the NOx promoted by all inlet conditions were rapidly increased until it reach 0.4 equivalence ratio where the flame temperature about 1800K. This is the temperature beyond which thermal NOx generation become rapid, but as can be seen from Fig.5.35 the NOx formation increases slowly which means that thermal NOx was not the dominant mechanism for NOx generation. Thus prompt NOx appears to be the dominant NOx formation mechanism with small contribution from thermal NOx.

The NOx level at an equivalence ratio of 0.4 was less than 4.5, 4.5, 8 and 10ppm for 550, 600, 670 and 740K inlet air temperature respectively. These corresponded to 2 and 3ppm NOx corrected to 15% oxygen and standard day humidity as shown in Fig.5.34. Thus, radial passage fuel injection with natural gas has demonstrated ultra low NOx emissions at high inlet temperatures. The 760K inlet temperature is that of RB211 industrial gas turbine and hence this

design offers good prospects for a solution to the NOx emissions problem. This design is currently being assessed at high pressure condition by Rolls Royce.

5.4 WALL FUEL INJECTION RESULTS

Fuel injection at the periphery of the swirler or the wall overcomes a partial problem of radial swirl vane passage fuel injection namely that of spontanous ignition. It also exploit the centrifugal mixing forces inhance in swirling flows.
In the present work two configuration were investigated radially inward fuel injection at the swirler outlet (76mm wall injector) and radial inward fuel injection at 140mm combustor wall as shown in Fig.5.60.

5.4.1 Weak Extinction

Table(5.3) shows the measured weak extinction data for the wall injection system used in the present work. With liquid fuels there was a marked deterioration in the weak extinction. This effect was surprising as liquid fuel injection generally extend flame stability limits leanward, as reported by Mizutani and Nishimoto(45) and confirmed by Myers and Lefebvre(46). Their investigations concluded that the presence of droplets serve to wrinkle and lacerate the flame surface thereby increasing the flame speed(45). However, drops serve as high temperature ignition sources, extending the flammability limits and accelerating the burning velocity of adjacent flame elements. In the present situation, the deterioration in the weak extinction limit is considered to be associated with the action of the swirl flow on the fuel droplets. During the vaporisation process droplets will come under the action of centrifugal forces created by the swirl flow(37,47). These will force the droplets will be concentrations in the flame stabilising shear layer will be much lower than for gas injection.

5.4.2 INFLUENCE OF WALL INJECTION PLACEMENT ON EMISSIONS

5.4.2.1 Axial wall static pressure and temperature profiles

Fig.5.36 - 5.43 illustrates the combustor wall static pressure and temperature profiles for two gaseous fuels propane and natural gas using two different modes of wall injection. The first mode was to inject fuel immediately in the outer

(peripheral) recirculation zone using 140mm I.D wall injector and the second mode was to inject the fuel in the high potential rotational flow after leaving the radial swirler outlet before the flow being expanded to the combustion chamber. The time delay in expanding the flow to the main combustor would give more time for fuel to be mixed with the air.

The main feature with 140mm wall injector profiles were the high temperatures at 25mm axial distance. This associated with the fuel being injected into the peripheral (corner) recirculation zone creating a rich zone burning with a higher temperature. Downstream of the corner recirculation zone the flame development was more uniform as shown in Fig.5.37 and 5.41. For the 76mm wall injector Fig.5.38 - 5.43 show that the flame development was more or less uniform, this was due to the better mixing generated earlier in the extension length of the 76mm wall injector before being issued to the 140mm combustor. Plate 5.2 shows cross-sectional view of natural gas and propane flame using 76mm wall injection for an equivalence ratio of 0.46 and 600K inlet temperature.

5.4.2.2 MEAN COMBUSTOR EXIT EMISSIONS

Fig.5.48 - 5.53 demonstrate the effect of using the two modes of wall injection on the mean exhaust emissions. Carbon monoxide and unburned hydrocarbons emissions as a function of metered equivalence ratio are shown in Fig.5.48 and 5.49. Minimum CO emissions occured at a weaker equivalence ratio using 140mm wall injection as was found for the relative lean flammibility limit. For rich mixture the wall mixing of the 140mm wall injection produced higher CO emissions than for the 76mm wall injector. UHC emissions were found to be negligible except close to the weak extinction equivalence ratio. Fig.5.48 illustrate the combustion inefficiency variation with the metered equivalence ratio which more or less similer to Fig.5.50. Both modes of wall fuel injection were exhibited combustion efficiency more than 99.9% at approximately 0.4 equivalence ratio for the propane and at 0.54 for the natural gas where it exhibits the minimum CO level. CO emissions dominated the combustion inefficiency except at near weak

extinction equivalence ratio where UHC contribution to the combustion inefficiency was high.

NOx emissions are generally are correlated as a function of flame temperature as this is one of the major factor governing NOx formation. Flame temperature is preferable to equivalence ratio for correlating NOx as it takes into account any variation in the combustion efficiency. NOx emissions are shown as a function of both the metered equivalence ratio in Fig.5.51 and flame temperature in Fig.5.53. These show a marked increase in NOx emissions, especially with propane as the fuel, at a flame temperature of 1800K. The large gradient in NOx emission in reference to the flame temperature indicated that most of the NOx emissions beyond a flame temperature of 1800K were due to the thermal NOx mechanism. The much higher NOx emissions for the 140mm wall injection were due to the injection of fuel into the corner reciculation zone, making this a high residence time fuel rich region and hence prove to the generation of thermal NOx. However, the 76mm wall injection mode gave ultra low NOx emissions using natural gas as fuel. This was partly due to the good mixing between natural gas and air since the former has lower molecular weight than propane which means high diffusivity action and natural gas will be quickly dispersed into turbulent region of shear layer and hence low NOx formation. Fig.5.52 shows the NOx corrected to 15% oxygen and standard day humidity as a function of combustion inefficiency. Using the 76mm wall injection fuelled with natural gas would be generating less than 1ppm with the highest combustion efficiency but more than 10 times higher by using 140mm wall injector which is still a low NOx combustor design. These are the lowest NOx characteristic ever published for a gas turbine combustor design, including premixed and catalyst system and clearly wanting further development. Therefore, by injecting the fuel at the periphery of the jet boundary will enhances mixing between fuel and air rapidly much more than injecting the fuel in the corner recirculating zone using the 140mm wall injector. The 140mm injector did not extend the stability limits sufficiently to offset the disadvantage of the higher NOx emissions.

5.4.3 INFLUENCE OF FUEL TYPE ON MEAN EMISSIONS

The foregoing conclusion with 76mm wall injection system led to the present investigation whereby four different fuels were tested. Swirler(C) was used with the 76mm wall injector in the 140mm combustor Propane, natural gas, kerosene and gas oil fuels were used at combustor inlet temperature of 600K and at a Mach number of 0.014, the pressure loss of was 4% which is typical conventional combustor pressure loss.

5.4.3.1 Axial wall static pressure and temperature profiles

Previously, the axial wall static pressure and temperature profiles for propane and natural gas were discussed see Fig.5.38 - 5.39 and Fig.5.42 -5.43. Similarly Figs.5.44 - 5.47 show the combustor wall pressure and temperature profiles for kerosene and gas oil respectively. Fig.5.45 indicated that full vaporization was exhibited by kerosene and flame development was faster at equivalence ratios above 0.6 especially after the impingement point. However, a vaporization delay was indicated in Fig.5.47 for gas oil and hence slower flame development beyond 50mm away from the swirler. The flame was fully developed beyond 150mm due to the evaporation and combustion being completed.

5.4.3.2 MEAN COMBUSTOR EXIT EMISSIONS

Measured mean species emissions are shown in Figs.5.54 -5.59. Fig.5.54 shows that the emission of CO to decreased initially to a minimum level then to increase in the leanwards region. The kinetic behaviour of the combustion reaction is such that for lean mixtures both the rates of production and oxidation of CO increase with increasing in the metered equivalence ratio. Therefore, the results indicate that initially the rate of CO oxidation exceeds the rate of production due to oxygen availability, thereby decreasing CO emissions until an equivalence ratio was reached above which the rate of production of CO exceeded the oxidation rate due to locally rich mixture generating high CO. All fuels exhibited high combustion efficiency of better than 99.9% as can be seen in

Fig.5.56. For propane this optimum efficiencies corresponded to a 0.43 equivalence ratio, but for natural gas this was about 0.55. However, for liquid fuels the lowest combustion inefficiency occured at 0.5 and 0.4 equivalence ratio for kerosene and gas oil respectively.

NOx for gas oil combustion were the highest, as indicated by Fig.5.59 where the NOx is shown as a function of metered equivalence ratio. The greatest change of NOx with equivalence ratio was found for gas oil. The unmixedness which was promoted in the early stage (see wall temperature profile) was the reason behind the creation of the rich local zones which create the higher NOx also there may have been a fuel Nitrogen contribution(44) due to low level level fuel nitrogen. NOx was generated by natural gas fuel.

5.5 INFLUENCE OF FUEL PLACEMENT

Combustion performance is controlled by the mixing of fuel and air (oxidant). Mixing effectiveness controls emissions, heat release, stability and combustion intensity(49). Central axial injection is the most common method of fuel injection ,some dual fuel burners use spuds located away from the centre to inject the gas fuel while the centre pipe carries the other fuel. However, the fuel can be throughly mixed with the air before introducing the mixture to the combustor as in premixed combustion.

It is the intention of the present study to compare passages and wall fuel injection with premixed and central radial fuel injection. The central radial fuel injection is another variation from conventional central axial fuel injection which directed the fuel radially from the central axis across the rotational air as shown in chapter three and four. Some comparisons between axial fuel injection and injection at a range of inclinations to the axis leading to the radial have been reported by Leuckel and Fricker(50).

5.5.1 FUEL INJECTION MODES

Fig.5.60 shows the modes of fuel injection which have been investigated in the present work. They were numbered according to their positions relative to the jet boundary as follows:

1- Premixed fuel injection
2- Central radial fuel injection.
3- Passages fuel injection.
4- 76mm Wall fuel injection.
5- 140mm Wall fuel injection.

Each mode of fuel injection will contribute different mixing characteristic to the swirling jet shear layer and its surrounding recirculating flow. In the present work the use of passages injection will give partial fuel and air mixing in the short curved passage between each two radial vanes. However, each tangential vane

passage flow emerges from each single passage to be combined with neighbouring and opposing jets and this will enhance the mixing between air and fuel before introducing the mixture to the combustion chamber.

The 76mm wall injector injected the fuel around the outer periphery of the air jet which makes the use of high shear zones around the air jet and due to the centrifugal buoyancy forces which has been setup between air and fuel from one side and the hot combustion products from the other. These will tend to move the cold air outwards and the hot flame products inwards.

The 140mm wall injector inject the fuel in the high residence time outer(corner) recirculating zone. This created locally rich zone and high NOx, as discussed above.

5.5.2 Weak Extinction

The weak extinction results are shown in Table(5.4) Central radial fuel injection had the best stability, indicating the presence of the richest local mixture in the stabilising shear layer, which was confirmed by the internal traverses in chapter three. The 140mm wall injection had a leaner stability limit than the 76mm wall injection system. 76mm wall and vane passage injection was more or less the same indicating similar local mixing. Both were a significant improvement on the premixed weak extinction, indicating that local rich zones were still created in the shear layer.

5.5.3 MEAN COMBUSTOR EXIT EMISSIONS

The general influence of fuel injection method on the characteristics of the mean emissions is demonstrated by Figs.5.61 - 5.66. The mean combustion inefficiency results shown in Fig.5.63 were very similar for all method of fuel injection with a minimum of well below 0.1% at an equivalence ratio of 0.4 at 600K. However, there was a major influence of the method of fuel injection on the NOx emissions as shown in Fig.5.66. 76mm wall injection gave better results to the passage injection and was close to the premixed NOx emissions with a

reduced flame stability problem. The minimum NOx compatible with the lowest combustion inefficiency were shown in Table(5.5). This show that 76mm wall injection has lower optimum NOx than for premixed combustion, due to its better stability.

The radial traverse results just downstream of the swirler and near the exit place are shown in Fig.5.67. The strong influence of the method of fuel injection on local shear layer mixing near the burner is clearly shown with passage injection having half of the peak equivalence ratio of central injection. This was the main reason for the lower NOx emissions with passage injection. At the exhaust plane, there was no influence of the method of fuel injection on mixing or combustion temperature and inefficiency. However, there were large differences in the NOx emissions which originated in the near burner region and were due to a prompt NOx mechanism with little thermal NOx generation.

5.6 COMPARISON BETWEEN RADIAL AND AXIAL SWIRLERS

5.6.1 Weak Extinction

Table(5.6) shows the measured weak extinction for both type of swirlers and it is evidently clear that they have the same weak extinction limits.

5.6.2 Mean exit plane emissions

Comparison of the mean combustor exit emissions work that have been reported previously by Kowkabi(16) using 140mm Wall injection system in 140mm combustor are to be compared with the present 140mm wall injection results using propane as fuel. The two axial swirler were SW6 and SW5 compared with radial swirler(C), which gave approximately same pressure loss at a Mach Number of 0.014 for the same operational inlet air temperature which was 600K. The radial traverse results showed that the mixing for the radial swirler to be taking place earlier on than the axial swirler using the same fuel and central radial injector. Although, the mean combustor exit emissions were showing the same results, there was evidence to prove that mixing for the radial swirler was

completed by the third of combustor length while for the axial swirler mixing was completed in nearly twice that distance.

Figs.5.68 - 5.73 show the mean exhaust gas analysis results for both type of swirlers. Injecting fuel in the corner recirculation zone gave similar NOx emissions no matter what type of swirler was used. The radial swirler showed slightly better combustion efficiency than for the axial swirler Fig.5.70, which was due to lower CO emissions as shown in Fig.5.68. The NOx emissions were nearly the same at all equivalence ratios. the NOx level between 0.3 and 0.4 equivalence ratio which is due to perhaps experimental error. The difference in the NOx corrected to 15% oxygen are shown in Fig.5.72 . The radial swirler had a slightly higher optimum NOx than for the axial swirler, but both swirler had relatively high NOx compared with the other method of fuel injection for the radial swirler.

The general conclusion which can be drawn is that for the radial and axial swirlers with the same expansion ratio and approximately the same pressure loss, the mean combustor exit emissions characteristics approximately the same, provided that the same fuel and injector were used. This may be not true for other fuel systems which cannot be made identical, such as the passage injection technique. The work reported by Smith et al(12) which have been conducted on radial and axial swirler showed that the axial swirler gave higher NOx emissions than for radial swirler. By numerical analyses they showed that the combustor flow pattern downstream of the axial swirler was different from the flow pattern with the radial swirler. Their numerical analyses indicated a lack of a strong central recirculation zone in the burner with the axial swirler.

5.7 CONCLUSIONS

1- Radial vane swirlers with fuel injection in the vane passages improved the fuel and air mixing compared with central fuel injection There was a sufficient unmixedness in the stabilising swirling shear layer to give a considerable extension of the premixed stability limits, although inferior to those for central injection.

2- For propane at 600K inlet temperature the radial passage injection reduced the minimum corrected NOx emissions, compatible with a 0.1% inefficiency, from 13 to 2.5 ppm. NOx emissions very close to a fully premixed system were thus obtained.

3- For kerosene and gas oil the combustion development was very similar to propane. The minimum corrected NOx emissions were 6 and 13 ppm for kerosene and gas oil respectively. Thus the radial swirler passage fuel injection achieved low NOx emissions for liquid fuels.

4- The internal gas composition measurements showed that the fuel and air mixing was good quite close to the swirler and that this was the key to the low NOx emissions. The maximum local equivalence ratio was 0.75 for a mean of 0.43 and this occurred in the swirler shear layer and was responsible for the enhanced stability. The differences between the NOx emissions for the three fuels originated in the near swirler region. Thermal NOx was not a major contributor to the overall NOx emissions or to the differences between the three fuels.

5- There was a minor effect of inlet temperature on combustion efficiency using natural gas passage injection, but a major effect on the NOx emissions. Ultra low NOx emissions at a 740K inlet temperature were demonstrated.

6- Ultra low NOx was achieved by using 76mm wall injector fuelled with natural gas but with deterioration in the stability limits. The optimum NOx

was lower than for the passage and premixed injection.

7- With liquid fuel wall injection the favourable emissions characteristics for gaseous fuel wall injection were maintained but with a significant increase in NOx, although still at low level. and the flame was established in rich wall regions downstream of the recirculating flow.

8- The general combustion characteristics of the 76mm wall injection were superior to that of 140mm wall injection due to the injection of fuel into the corner recirculation zone with the later.

9- There was strong influence of the method of fuel injection on local shear layer mixing near the burner where most of the mixing occurs.

CHAPTER FIVE

REFERENCES

5-1 Beer,J.M. and Chigier,N.A.: Combustion Aerodynamics, Applied Science Publishers Ltd., London,1972.

5-2 Syred,N. and Beer,J.M. : Combustion in swirling flows: A review Combustion and Flame,23,pp.143-201, 1974.

5-3 Claypole,T.C. and Syred,N. : Eighteenth Symposium (International) on Combustion,P.81, The Combustion Institute, 1981.

5-4 Beltagui,S.A and Maccallum,N.R.L. : Aerodynamics of vaneswirled flames in furnaces. J. Inst. Fuel,49, 1976.

5-5 Ahmad,N.T., Andrews,G.E., Kowkabi,M. and Sharif,S.F.: Centrifugal Mixing Forces in Enclosed Swirl Flames. 20th Symposium (International) on Combustion, The Combustion Institute,Pittsburgh, pp.259-267,1984.

5-6 Ahmad,N.T., Andrews, G.E., Kowkabi M and Sharif, S.F.: Centrifugal Mixing in Gas and Liquid Fuelled Lean Swirl stabilised Primary Zones. ASME Paper 85-IGT-103, Int.J.Turbo Jet Engines, vol.3,pp.319-329.,1985.

5-7 Beltagui S.A. and MacCallum: Characteristics of enclosed swirl flames with peripheral fuel injection. Journal of Institute of Energy, vol.LXI,446,pp.3-16, March 1988.

5-8 Roberts,P.B., Kubasco,A.J. and Sekas,N.J. : ASME paper 81-GT-40.

5-9 Shekleton,J.R. : The CIVIC: A concept in vortex induced combustion for solar Gemini 10KW gas turbine. Trans. ASME,vol.103, pp.34-42, 1981.

5-10 Sood,V.M. and Shekleton,J.R. : Ongoing Development of a low emission industrial gas turbine combustion chamber. ASME paper 79-GT-203, 1979.

5-11 Smith K., Angello L. and Kurzynske F.: Design and testing of an ultra low NOx gas turbine. ASME paper 86-GT-263, 1986.

5-12 Smith, K.O., Kurzynke, F.R. and Angello, L.C.: Experimental Evolution of Fuel Injection Configurations for a Lean Premixed Low NOx Gas Turbine Combustor', ASME Paper 87-GT-141, 1987.

5-13 Smith K.O.: Ultra-low NOx combustor concept for methanol firing. ASME paper no. 83-GT-29, 1983.

5-14 Smith K.O., Wade G.W., Samii M.H. and Mak H.K.: Performance testing of a low emissions, natural-gas fired, small gas turbine combustor. ASME paper 89-GT-266, 1989.

5-15 Smith K.O. and Cowell L.H.: Experimental evaluation of a liquid-fueled lean-premixed gas turbine combustor. ASME paper 89-GT-264, 1989.

5-16 Kowkabi M.: Swirl combustors for low emission gas turbine. Ph.D. Thesis, Fuel and Energy Dept., University of Leeds, 1988.

5-17 Vranos,A., Knight,B.A. and Zabielski,M.F. : Centrifugal mixing A comparison of temperature profiles in nonrecirculating swirling and non-

swirling flames. Combustion and Flame,48,pp.109-119, 1982.

5-18 Mestre,J. and Benoit,A. : Combustion in swirling flow. 14th symposium (International) on combustion. The combustion Inst.,pp.719, 1973.

5-19 Markowski,S.J. Lohmann,R.P. and Reilly,R.G. : Trans.ASME, J.Eng. Power 98,123 (1976).

5-20 Jones,W.P. and Whitelaw,J.H. : Calculation methods for reacting. turbulent flow:- A review. Combustion and Flame,48,pp.1-26, 1982.

5-21 Bray,K.N.C. and Moss,J.B. : First Specialist Meeting (International) of the Combustion Institute ,Vol.1, 7 (1981).

5-22 Niedzwiecki,R.W. and Jones,R.E. : AIAA J. 12, 844 (1974).

5-23 Sood,V.M. and Shekleton,J.R. : ASME paper 80-GT-58 (1980).

5-24 Bahr,D.W. and Gleason,G.L. : Experimental Clean Combustion Program, Phase 1, Final Report,NASA CR134737, 1975.

5-25 Sotheran, A, Pearce, D.E. and Overton, D.L., 'Some Practical Aspects of Staged Premixed Low Emissions Combustors', ASME 84-GT-88, 1984.

5-26 Becker,B., Berenbrink,P. and Brandner,H., 'Premixing Gas and Air to Reduce NOx Emissions with Existing Proven Gas Turbine Combustion Chambers', ASME Paper, 86-GT-157, 1986.

5-27 Charles,R.E. and Samuelson,G.S., 'An Experimental Data Base for the Computational Fluid Dynamics of Combustion', ASME Paper 88-GT-25,1988.

5-28 Kuroda , 'Development of Dry Two-stage Low NOx Combustor for a Gas Turbine', ASME Paper 87-GT-64,1987.

5-29 Aoyama,K. and Mandai,S., 'Development of a Dry Low NOx Combustor for a 120MW Gas Turbine', ASME Paper 84-GT-44, 1984.

5-30 Andrews, G.E., Abdul Aziz, M.M., Abdul Hussain, U.S., Al-Dabbagh,N.A., Ahmad, N.A., Ali, A.F., Ali Al-Shaikly, A.F., Alkabie,H.S., Kowkabi, M. and Shahabadi, A.R., 'High Intensity Burners with Low NOx Emissions', British Flame Days 1988, Furnace Combustion Research and its Applications, The Institute of Energy, 1988.

5-31 Abdul Aziz, M.M., Abdul Hussain, U.S., Al Dabbagh, N.A., Andrews, G.E. and Shahabadi, A.R., 1987, 'Lean Primary Zones: Pressure Loss and Residence Time Influences on Combustion Performance and NOx Emissions', Tokyo International Gas Turbine Congress,vol.III, pp.89-96. ,1987.

5-32 Abdul Hussain, U.S., Andrews, G.E., Cheung, W.G. and Shahabadi,A.R. : Low NOx Primary Zones Using Jet Mixing Shear Layer Combustion , ASME Paper 88-GT-308.,1988.

5-33 Mestre,A. : Efficiency and pollutant formation studies in a swirling flow combustor. Proc. of ASME Fluid Mech. of combustion Conf. Montreal,pp.89-95, 1974.

5-34 Ahmad,N.T. and Andrews,G.E. : ASME paper 83-GT-192 (1983).

5-35 Andrews, G.E. and Kowkabi, M., 'Gas Sampling Probe Influences on Composition Traverses through a Swirling Flow Simulated Gas Turbine Primary Zone', NATO Advanced Study Institute, Instrumentation for Combustion and Flow in Engines, Paper 9, 16pp, Vimeiro, Portugal, Ed. D.F.G. Durao, Instituto Superior Tecnico, Lisbon.1987.

5-36 Ishizuka,S. Twentieth Symposium (International) on Combustion , The combustion Institute, 1984/PP. 287-294.

5-37 Shekleton J.R.: The CIVIC- A new concept in vortex induced combustion. Trans. ASME, J. Eng. Power,vol.103,pp.708-717, 1981.

5-38 Noyce,J.R., Sheppard,C.G.W. and Yamba,F.D. : Combustion Science and Technology, 1981, Vol.25, pp.209-217.

5-39 Katsuki,M.,Mizutani,Y. and Shibuya,K. : Combustion Science and Technology 1977,Vol. 17, pp.11-18.

5-40 Noyce,J.R. and Sheppard,C.G.W. : Combustion Science and Technology ,1982, Vol. 29,pp.37-52.

5-41 Fricker N. and Leuckel W.: The characteristics of swirl stabilized natural gas flames,Part3: The effect of swirl and burner mouth geometry on flame stability. J. Inst. Fuel(Energy),49,pp.152-158, 1976.

5-42 Takagi,T.,Okamoto,T., Taji,M. and Nakasuji,Y. : Twentieth Symposium(International) on Combustion, The Combustion Institute, 1984 / pp.251-258.

5-43 Alkabie, H.S., Andrews, G.E. and Ahmad, N.T.,'Lean Low NOx Primary Zones Using Radial Swirlers', ASME Paper 88-GT-245.,1988.

5-44 Williams, P.T., Bartle, K.D. and Andrews, G.E., 'The Relation between polycyclic aromatic compounds in diesel fuels and exhaust particulates', Fuel Vol.65, pp.1150-1158, 1986.

5-45 Mizutani Y. and Nishimoto T.: Comb. Sci. and Tech.,6,pp.1-10, 1972.

5-46 Myers G. D. and Lefebvre A.H.: Flame propagation in heterogeneous mixtures of fuel drops and air, comb. and flame,66, pp.193-210, 1986.

5-47 Ahmad N.T. and Andrews G.E.: Gas and liquid fuel injection into an enclosed swirling flow, International J. Turbo and Jet Engine, 3,pp.331-342, 1986.

5-48 Beltagui S.A. and MacCallum N.R.L.: The effect of fuel injection modes on combustion of swirling flows. British flame Days 1988, Furnace combustion research and its applications, the Inst. of Energy, 1988.

5-49 Gupta A.K., Lilley D.G. and Syred N.: Swirl flows, Abbcus press, 1984.

5-50 Leuckel W. and Fricker N.: The characteristics of swirlstabilized natural gas flames,Part1: Different flame types and their relation to flow and mixing patterns. J. Inst. Fuel(Energy),49, pp.103-112, 1976.

5-51 Alkabie, H.S. and Andrews, G.E., 'The Influence of Fuel Placement on NOx Emissions from Flames Stabilised by Radial Swirlers',Joint meeting of the British and French Sections of the Combustion Institute, Rouen,1989.

TABLES

Table (5.1)

Weak extension, for Passage injection as compared with central & premixed injection						
Fuel type	Inlet Temp. (K)	Measured W.E		(Δ P/P)%	Simulated overall W.E	
		EQR	A/F		EQR	A/F
Radial Passage fuel injection						
Propane	400	0.40	39	5.8	0.17	92
Propane	600	0.29	53	5.8	0.12	125
Kerosene	400	0.34	43	5.1	0.14	101
Kerosene	600	0.25	59	5.1	0.11	139
Gas Oil	400	0.43	34	5.1	0.18	80
Gas Oil	600	0.19	77	5.1	0.081	181
Central Radial fuel injection						
Propane	600	0.08	195	4.2	0.034	458
Premixed Propane & Air	600	0.47	34	4.4	0.20	80

Table (5.2)

Inlet temperature influence on emissions for N.G.,swirler(B),140mm combustor.				
Inlet temperature (K)	Measured	W.E	Simulated overall	W.E
	EQR	A/F	EQR	A/F
550	0.33	49	0.14	114
600	0.30	55	0.13	128
670	0.31	53	0.13	123
740	0.26	63	0.11	147

Table (5.3)

Weak Extinction for radial swirler(C) with wall injection,Mn=0.014,600K				
Fuel type	Wall injector I.D(mm)	EQR	A/F	Pressure loss%
Propane	140	0.18	87	3.8
Propane	76	0.31	51	4.2
Natural Gas	1 40	0.19	87	3.8
Natural Gas	76	0.39	43	4.4
Kerosene	76	0.38	39	4.2
Gas Oil	76	0.33	44	4.1

Table (5.4)

Influence of fuel injection method on Weak Extinction,propane,600K				
Fuel injection method	Measured W.E		Simulated Overall W.E	
	EQR	A/F	EQR	A/F
Direct Radial central	0.08	195	0.03	455
Premixed	0.47	34	0.20	79
Passage	0.29	53	0.12	124
76mm Wall	0.31	51	0.09	170
140mm Wall	0.18	87	0.05	290

Table (5.5)

Optimum NOx emissions for various injection modes,propane,600K.			
Fuel injection method	NOx(ppm)	NOx corrected to 15% O2(ppm)	EQR
Direct radial central	15.8	12.4	0.34
Premixed	5.7	2.9	0.53
Passage	4.0	2.6	0.41
76mm Wall	3.0	2.0	0.44
140mm Wall	38	25	0.41

Table (5.6)

Weak extinction for axial & radial swirler in 140mm combustor,propane,600K.			
Swirler type	EQR	A/F	Pressure loss%
Radial C	0.18	87	3.8
Axial1 (SW6)	0.18	87	3.5
Axial2 (SW5)	0.12	131	3.0

FIGURES

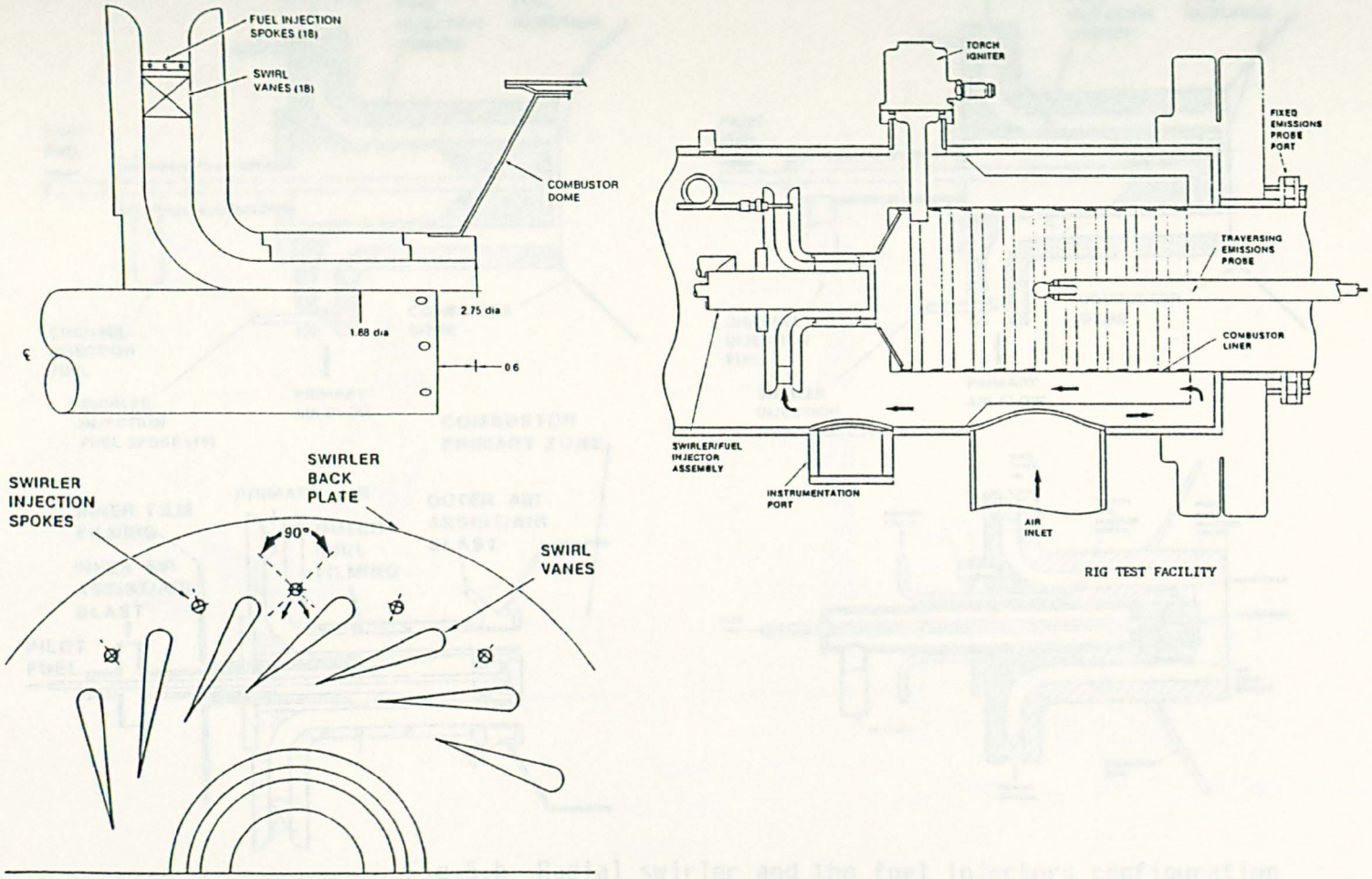

Fig.5.a Radial swirler/fuel injector assembly with the test Rig, used by Solar Turbines Incorporated(36).

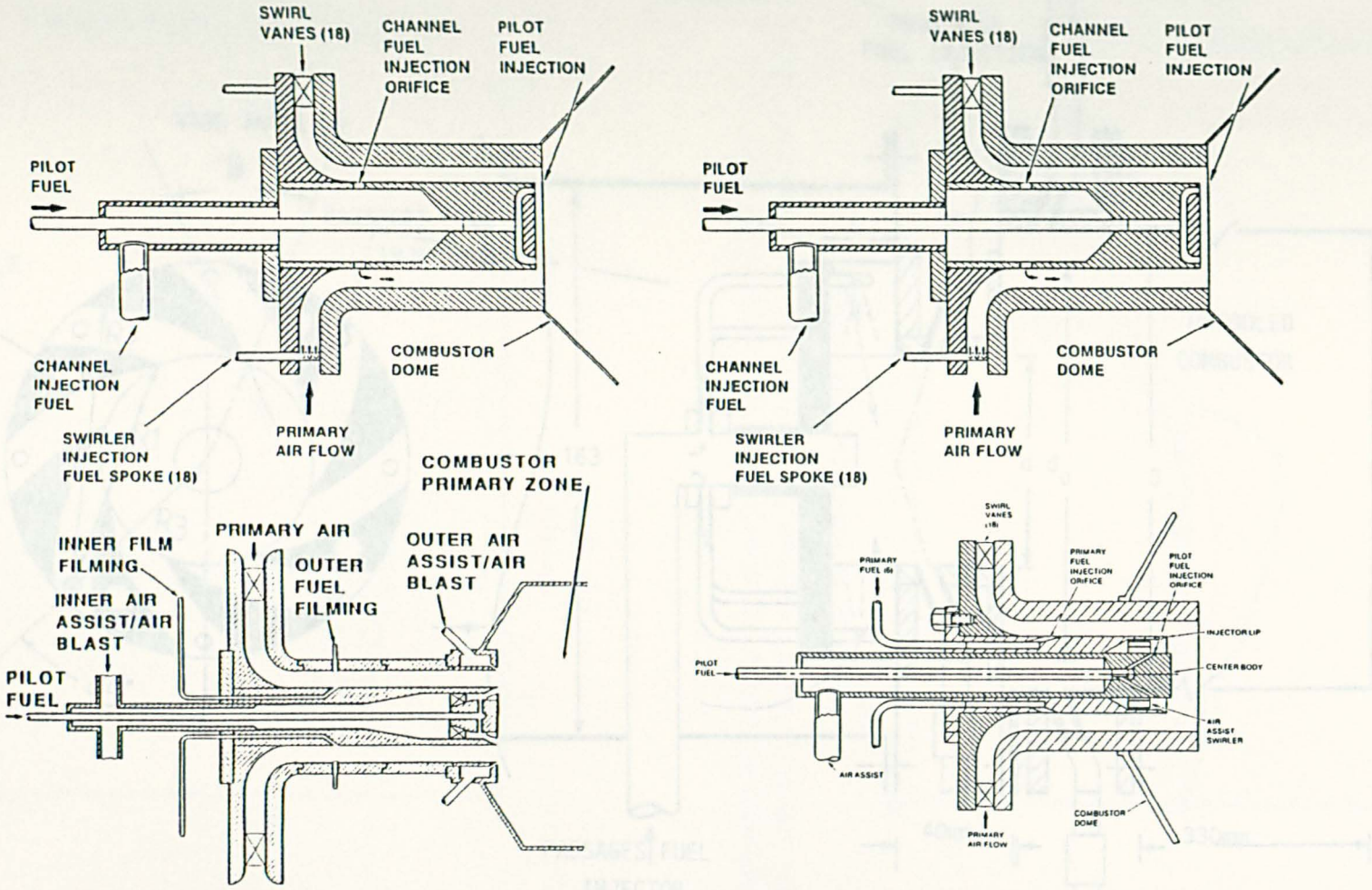

Fig.5.b Radial swirler and the fuel injectors configuration used by Smith et al.(36,52,56,57,58).

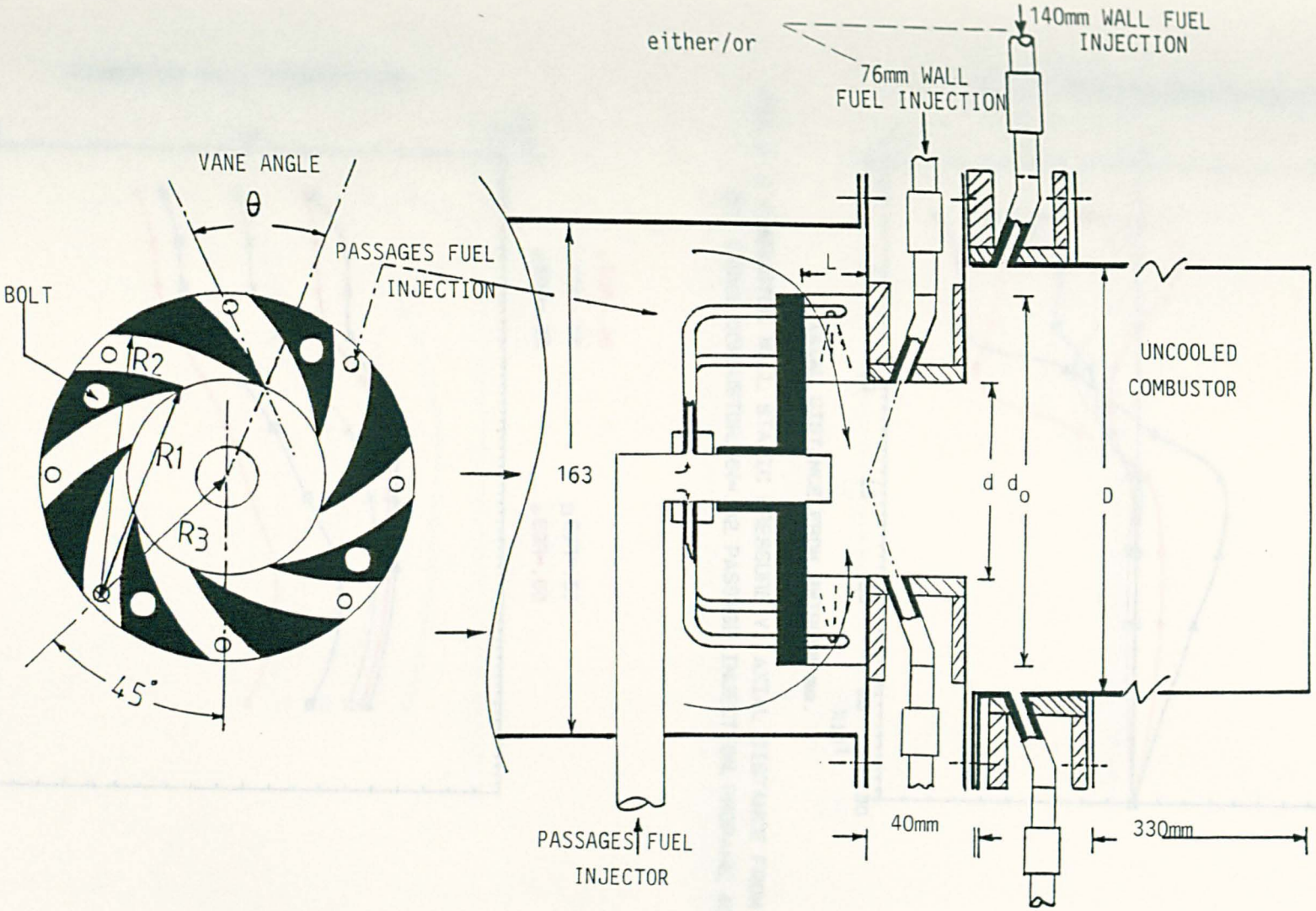

FIG.5.1 SCHEMATIC DIAGRAM OF THE RADIAL SWIRLER COMBUSTOR WITH EITHER PASSAGES FUEL OR 76mm WALL OR 140mm WALL INJECTION CONFIGURATION

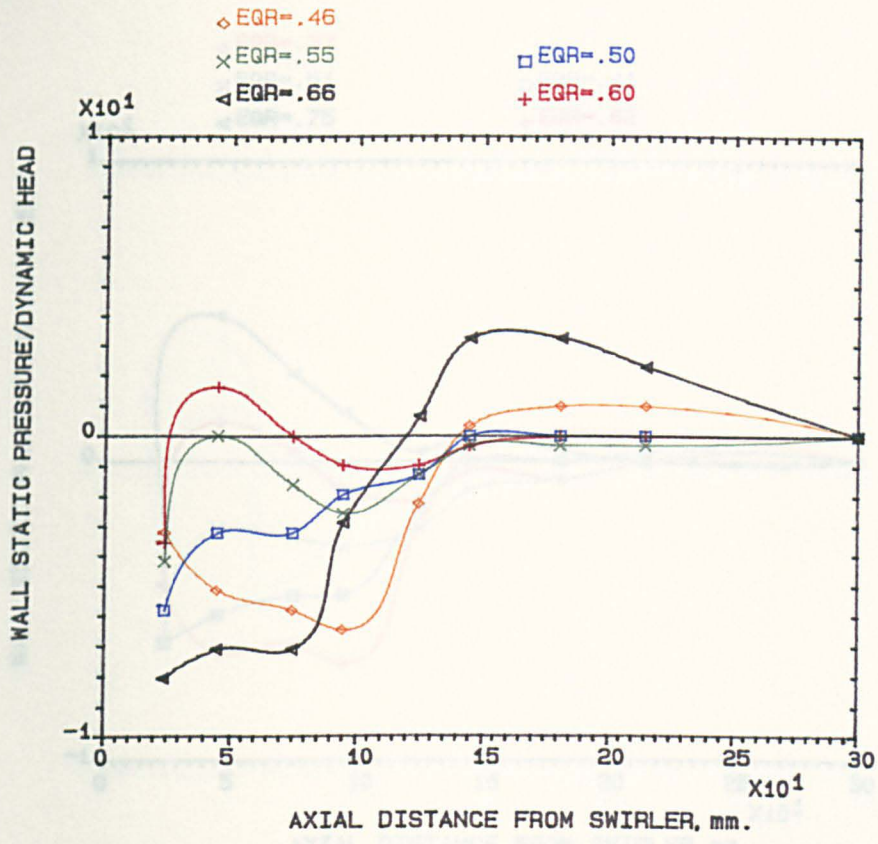

FIG.5.2 COMBUSTOR WALL STATIC PRESSURE V. AXIAL DISTANCE FROM SWIRLER (B), 140mm. COMBUSTOR, MN=.02, PASSAGE INJECTION, PROPANE, 400K.

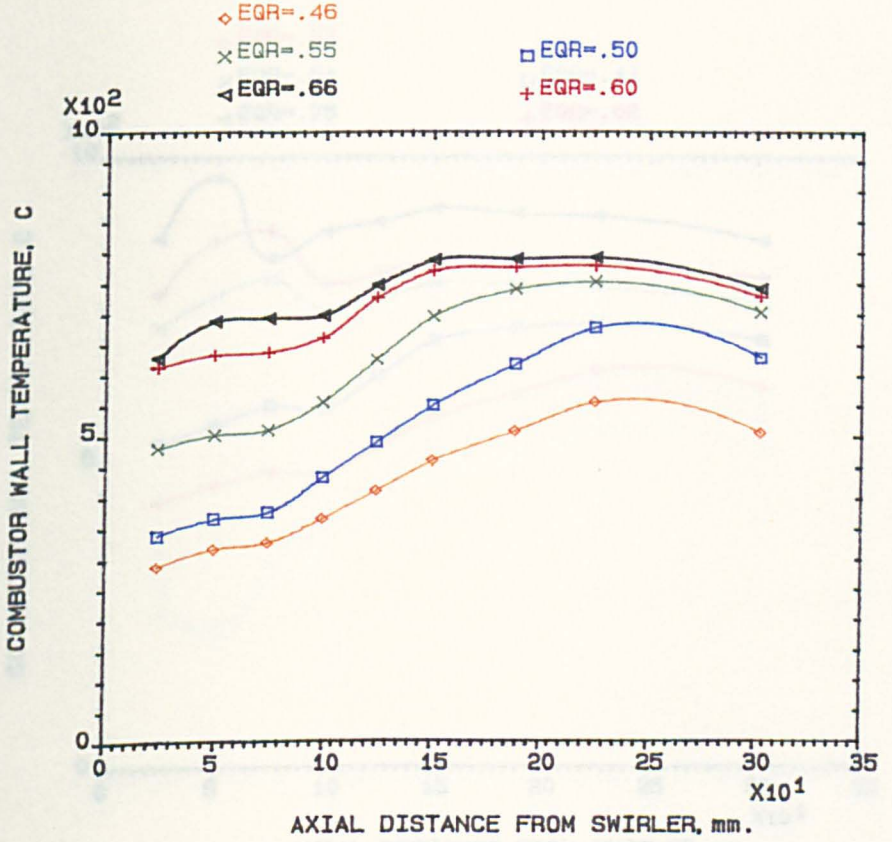

FIG.5.3 COMBUSTOR WALL TEMPERATURE V. THE AXIAL DISTANCE FROM SWIRLER (B), 140mm COMBUSTOR, MN=.02, PASSAGE INJECTION, PROPANE, 400K.

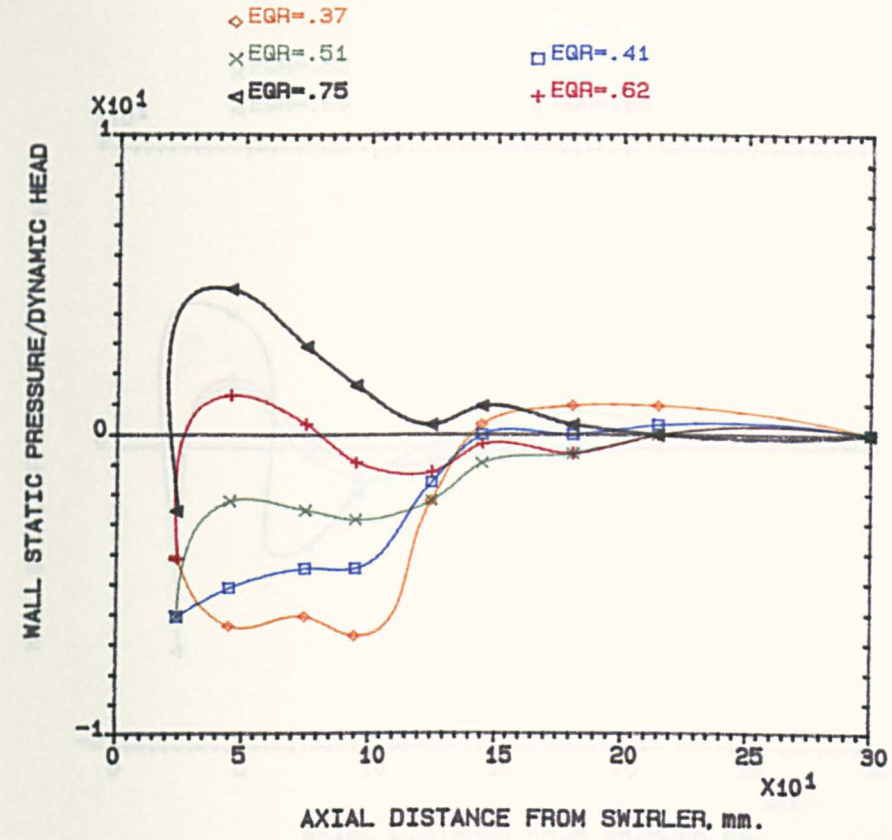

FIG.5.4 COMBUSTOR WALL STATIC PRESSURE V. AXIAL DISTANCE FROM SWIRLER (B). 140mm COMBUSTOR, MN=.02, PASSAGE INJECTION, PROPANE, 600K.

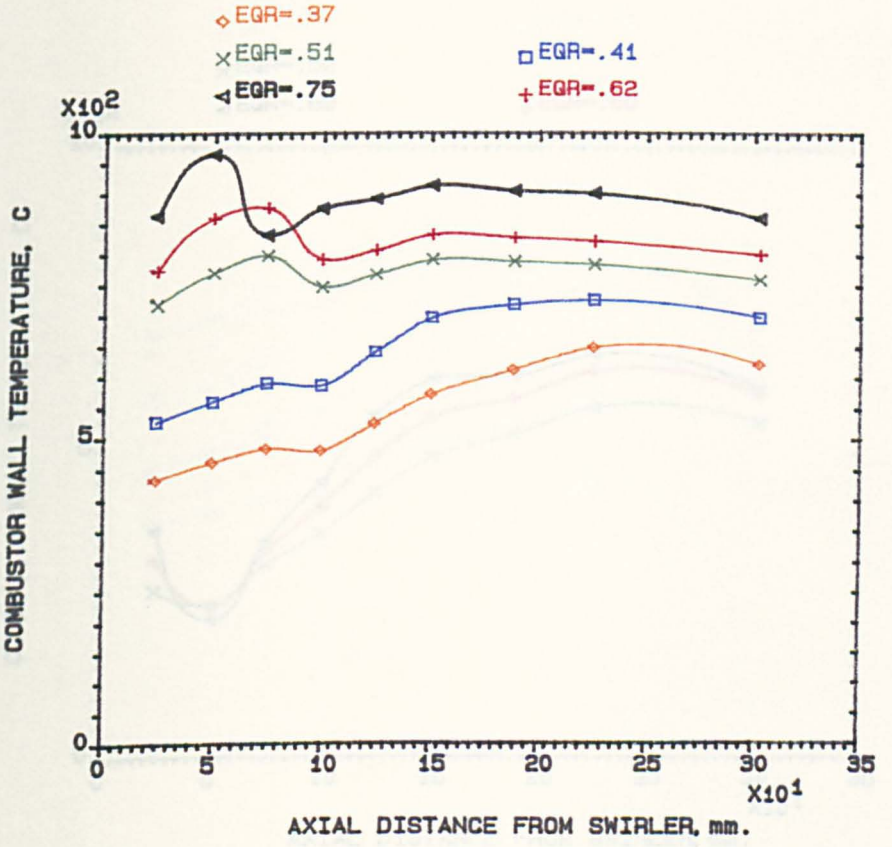

FIG.5.5 COMBUSTOR WALL TEMPERATURE V. THE AXIAL DISTANCE FROM SWIRLER (B). 140mm COMBUSTOR, MN=.02, PASSAGE INJECTION, PROPANE, 600K.

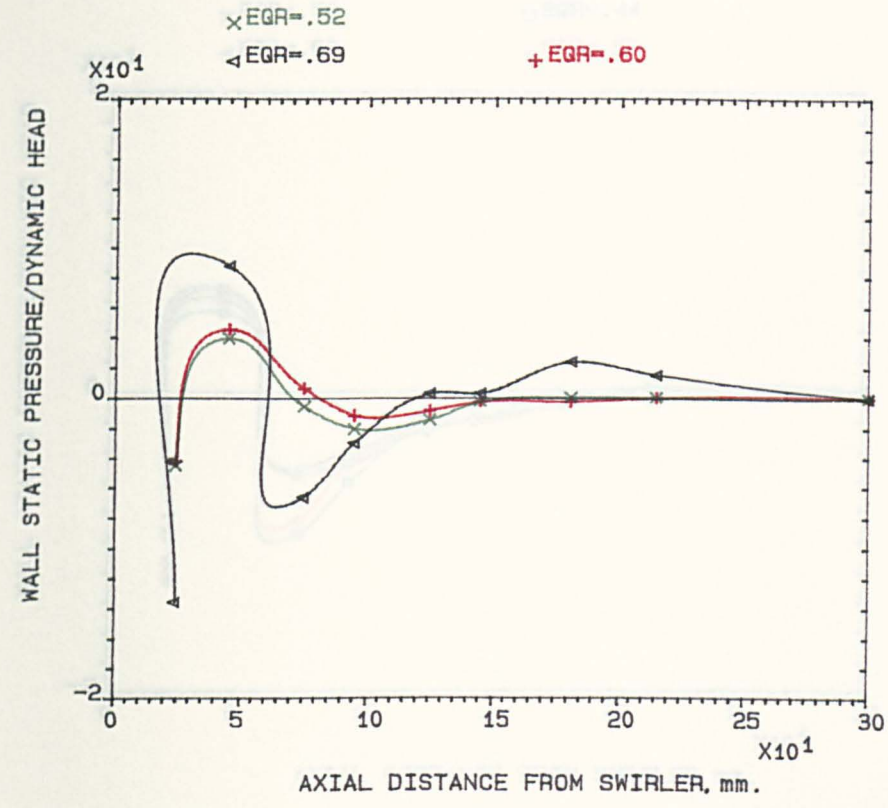

FIG.5.6 COMBUSTOR WALL STATIC PRESSURE V. AXIAL DISTANCE FROM SWIRLER (B), 140mm. COMBUSTOR. MN=.02. PASSAGE INJECTION. KEROSENE. 400K.

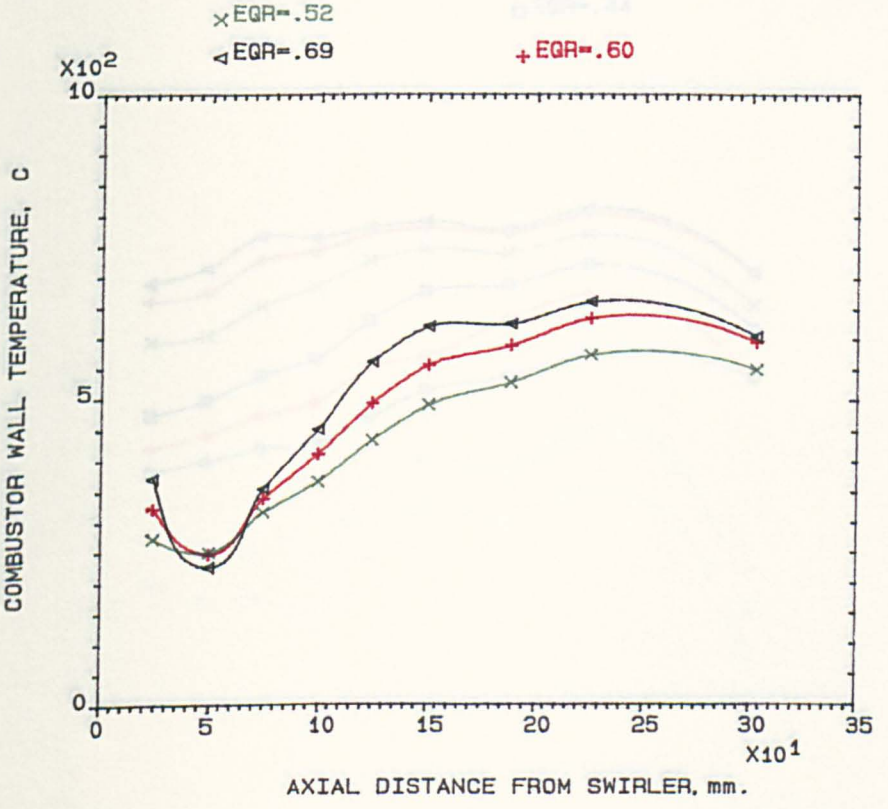

FIG.5.7 COMBUSTOR WALL TEMPERATURE V. THE AXIAL DISTANCE FROM SWIRLER (B), 140mm COMBUSTOR. MN=.02. PASSAGE INJECTION. KEROSENE. 400K.

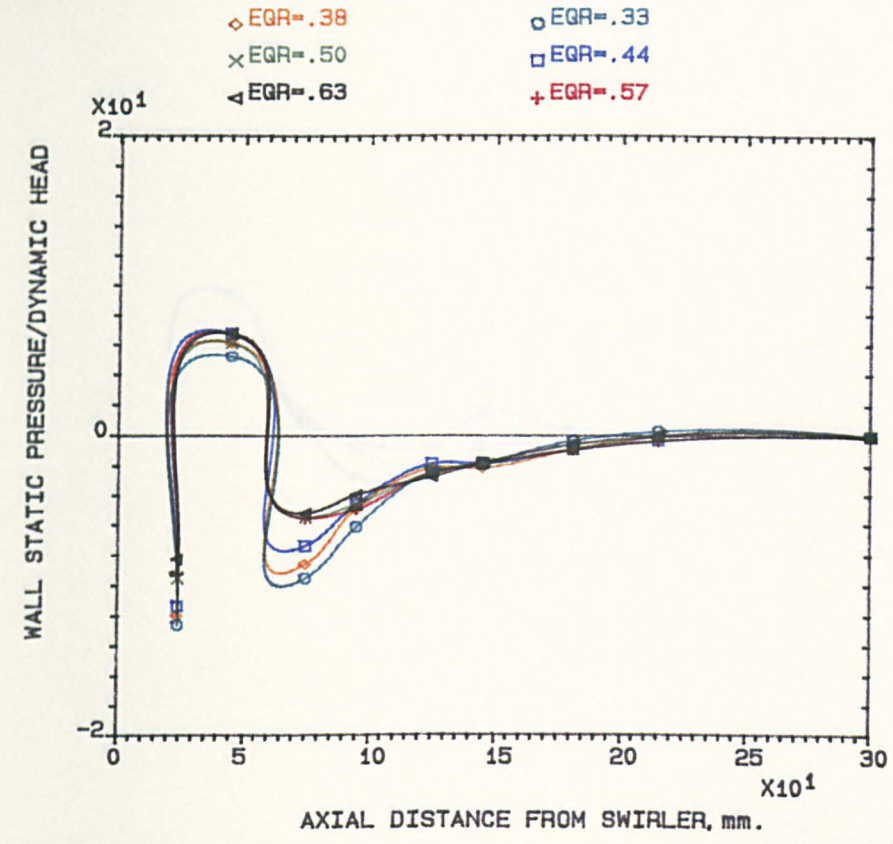

FIG.5.8 COMBUSTOR WALL STATIC PRESSURE V. AXIAL DISTANCE FROM SWIRLER (B), 140mm. COMBUSTOR, MN=.02, PASSAGE INJECTION, KEROSENE, 600K.

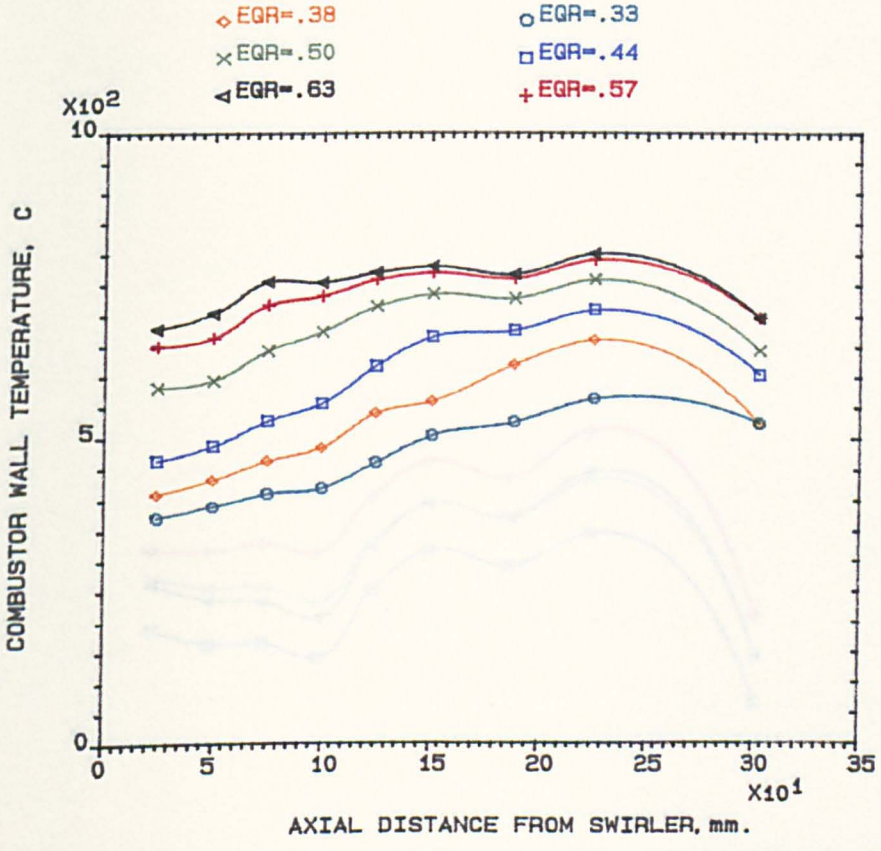

FIG.5.9 COMBUSTOR WALL TEMPERATURE V. THE AXIAL DISTANCE FROM SWIRLER (B), 140mm COMBUSTOR, MN=.02, PASSAGE INJECTION, KEROSENE, 600K.

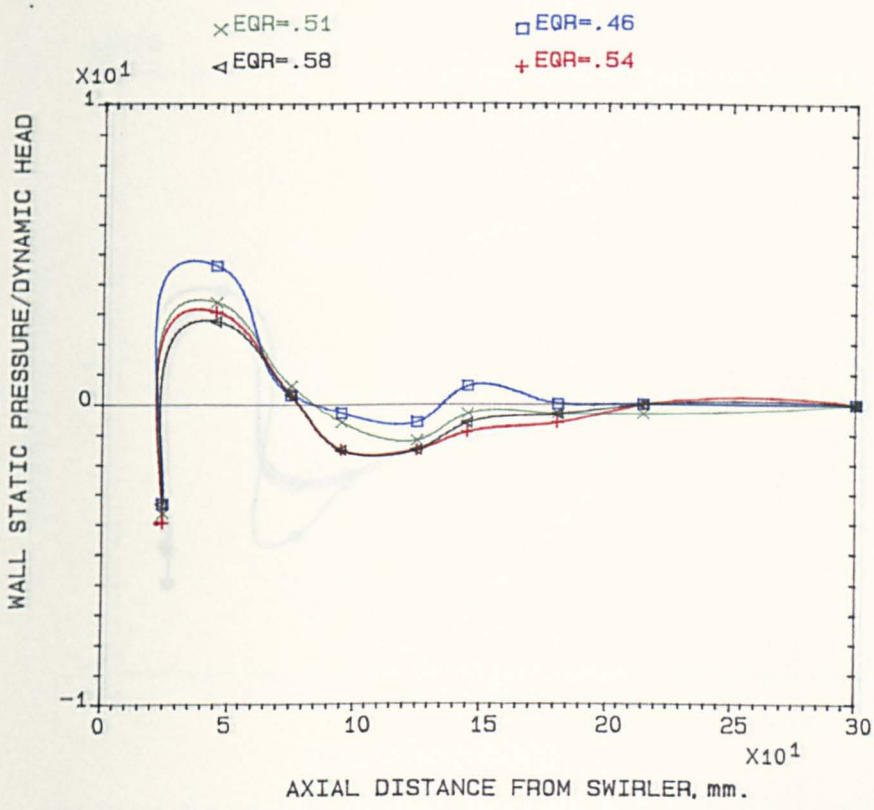

FIG.5.10 COMBUSTOR WALL STATIC PRESSURE V. AXIAL DISTANCE FROM SWIRLER (B), 140mm, COMBUSTOR, MN=.02, PASSAGE INJECTION, GAS OIL, 400K.

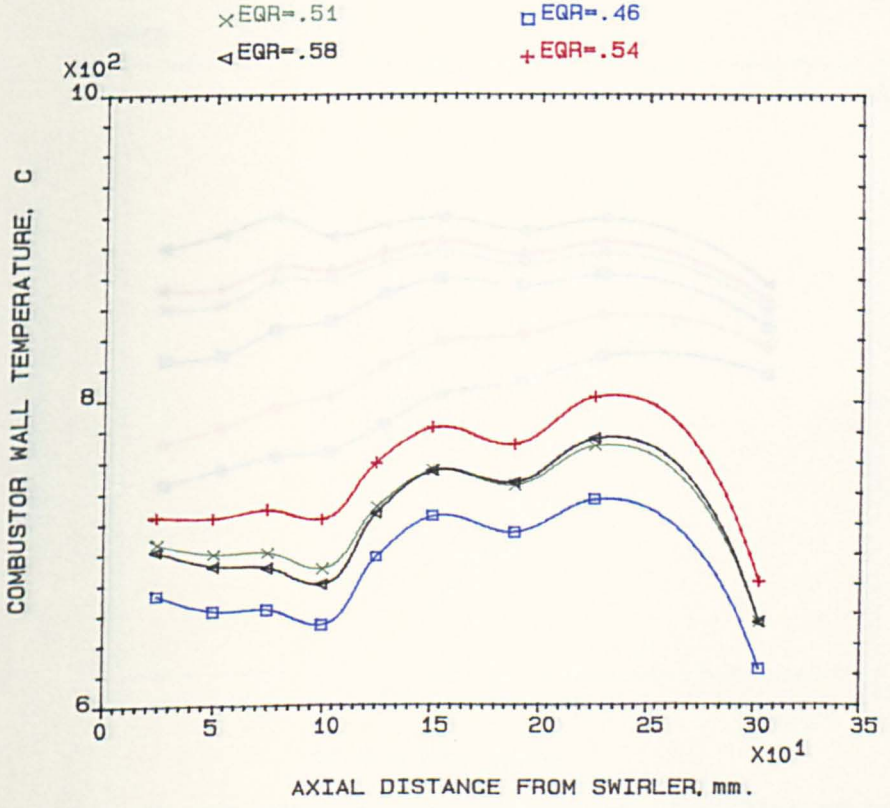

FIG.5.11 COMBUSTOR WALL TEMPERATURE V. THE AXIAL DISTANCE FROM SWIRLER (B), 140mm COMBUSTOR, MN=.02, PASSAGE INJECTION, GAS OIL, 400K.

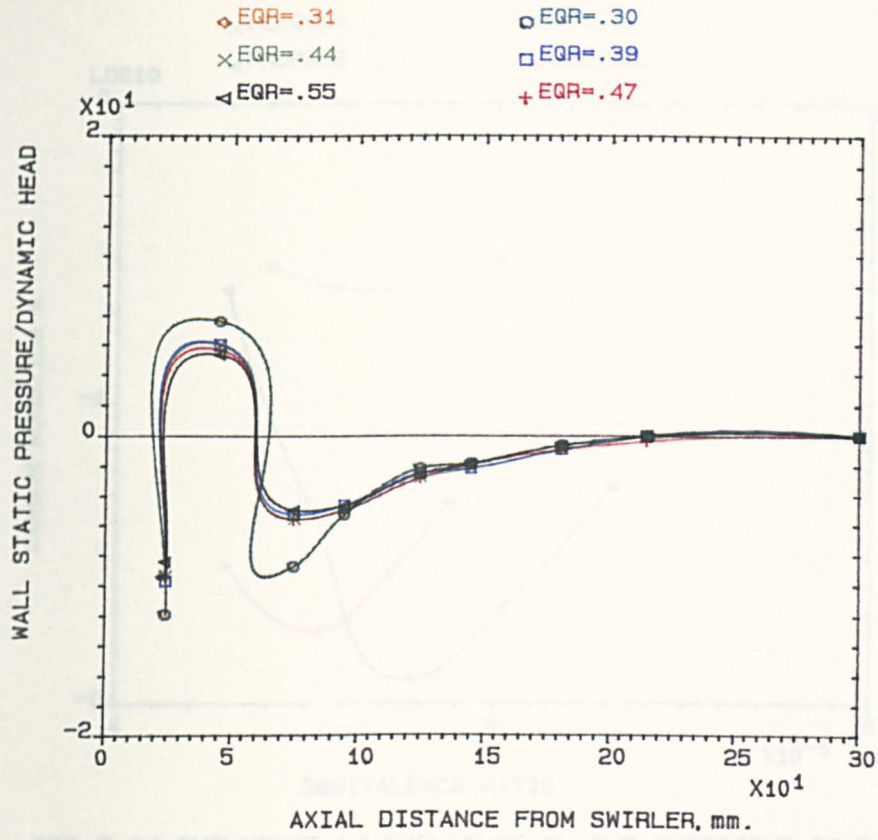

FIG.5.12 COMBUSTOR WALL STATIC PRESSURE V. AXIAL DISTANCE FROM SWIRLER (B), 140mm. COMBUSTOR, MN=.02, PASSAGE INJECTION, GAS OIL, 600K.

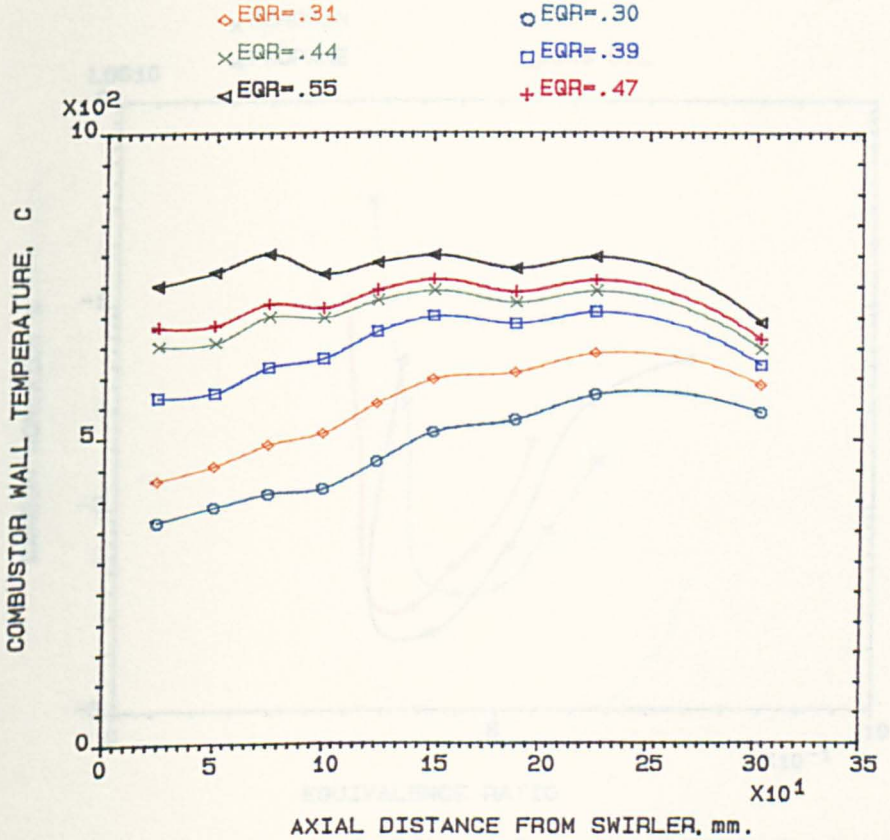

FIG.5.13 COMBUSTOR WALL TEMPERATURE V. THE AXIAL DISTANCE FROM SWIRLER (B), 140mm COMBUSTOR, MN=.02, PASSAGE INJECTION, GAS OIL, 600K.

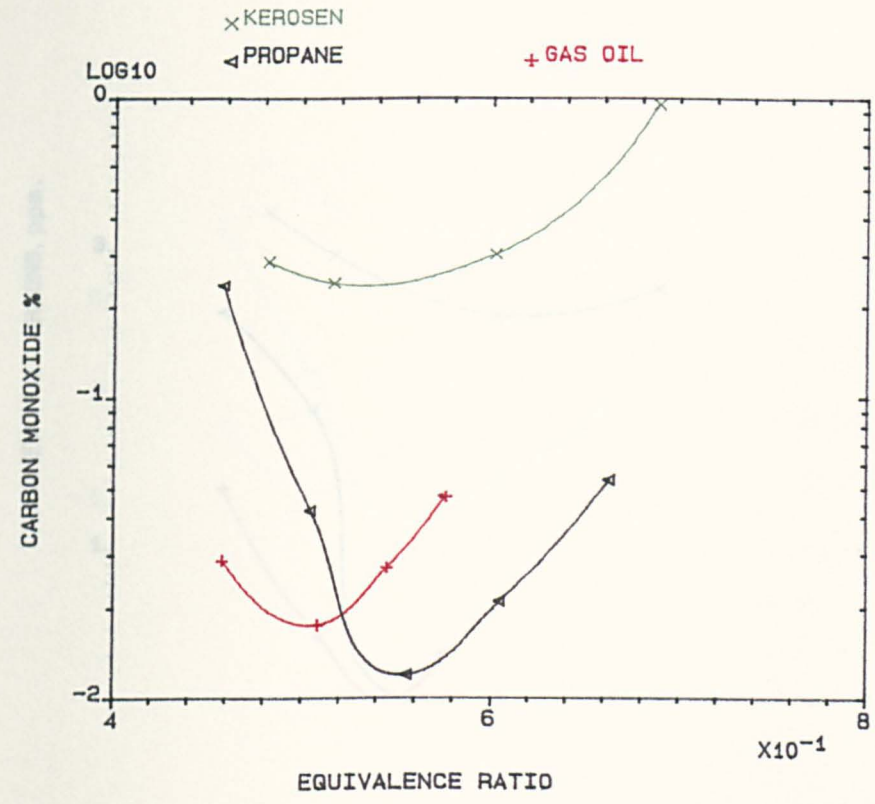

FIG.5.14 INFLUENCE OF FUEL TYPE ON THE EMISSIONS OF CARBON MONOXIDE FOR DIFFERENT FUELS USING PASSAGE INJECTION WITH SWIRLER (B) IN 140mm COMBUSTOR, MN=0.02, TIN=400K.

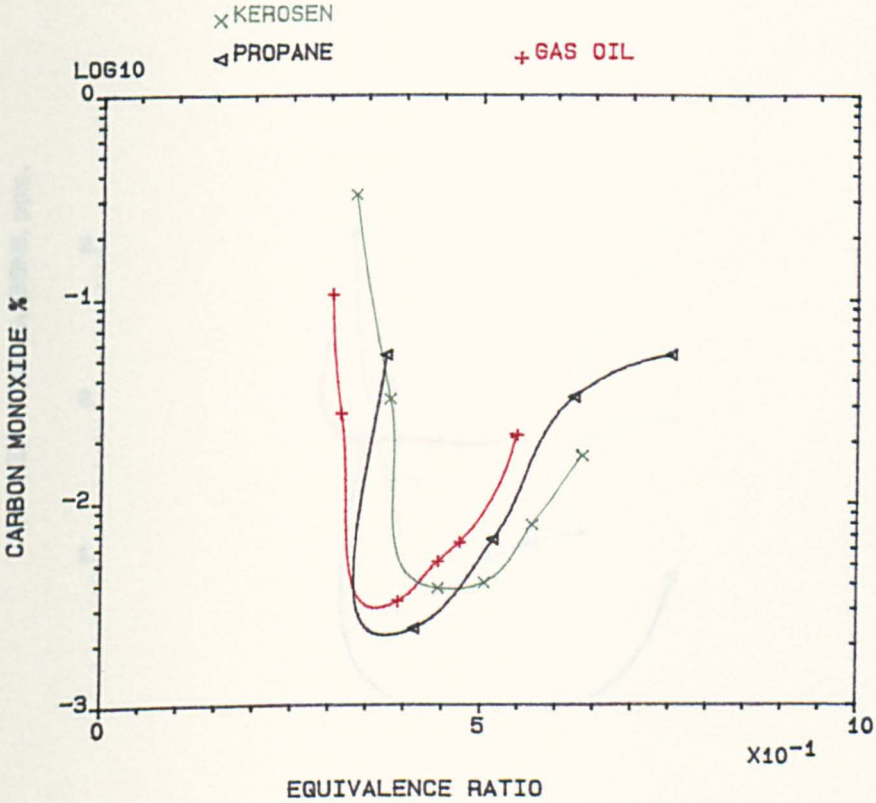

FIG.5.15 INFLUENCE OF FUEL TYPE ON THE EMISSIONS OF CARBON MONOXIDE FOR DIFFERENT FUELS USING PASSAGE INJECTION WITH SWIRLER (B) IN 140mm COMBUSTOR, MN=0.02, TIN=600K.

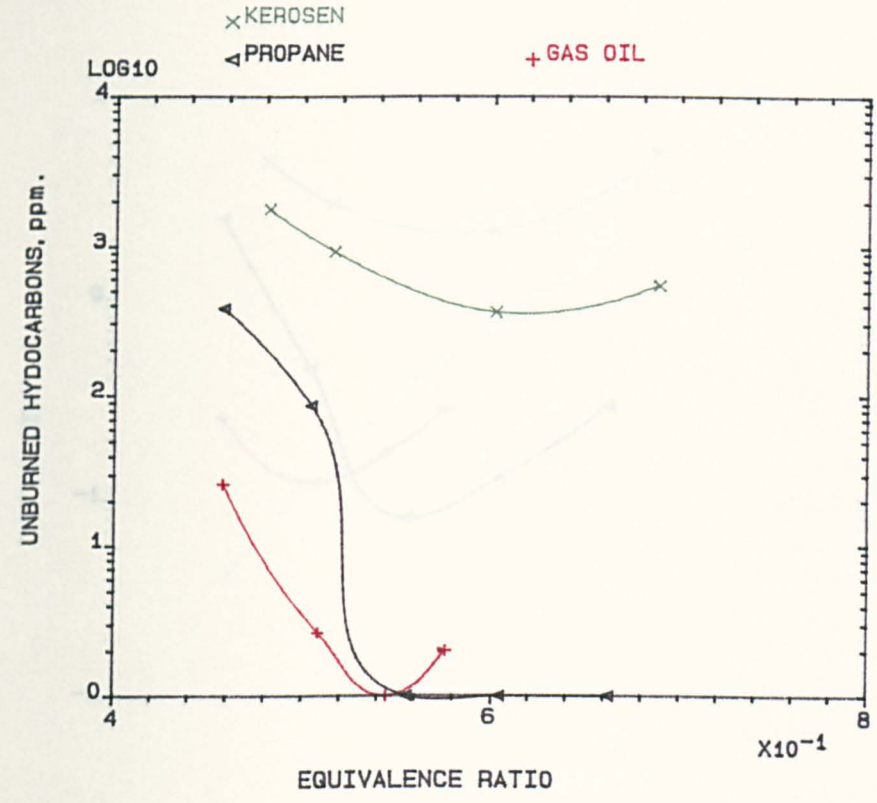

FIG.5.16 INFLUENCE OF FUEL TYPE ON THE EMISSIONS OF UNBURNED HYDROCARBONS FOR DIFFERENT FUELS USING PASSAGE INJECTION WITH SWIRLER (B) IN 140mm COMBUSTOR. MN=0.02. TIN=400 K.

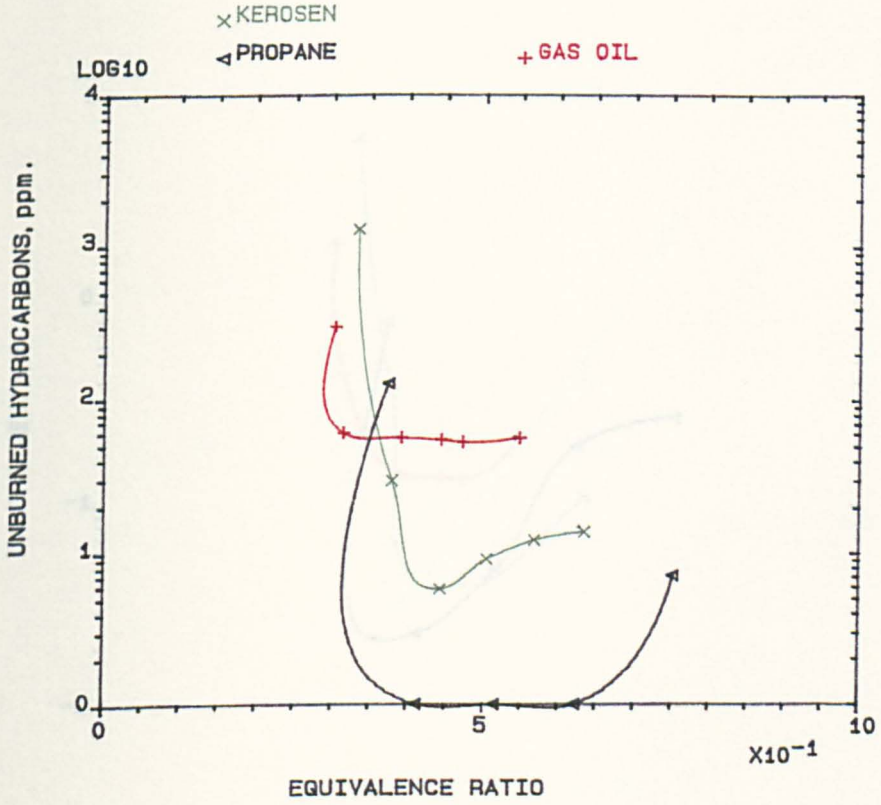

FIG.5.17 INFLUENCE OF FUEL TYPE ON THE EMISSIONS OF UNBURNED HYDROCARBONS FOR DIFFERENT FUELS USING PASSAGE INJECTION WITH SWIRLER (B) IN 140mm COMBUSTOR. MN=0.02. TIN=600 K.

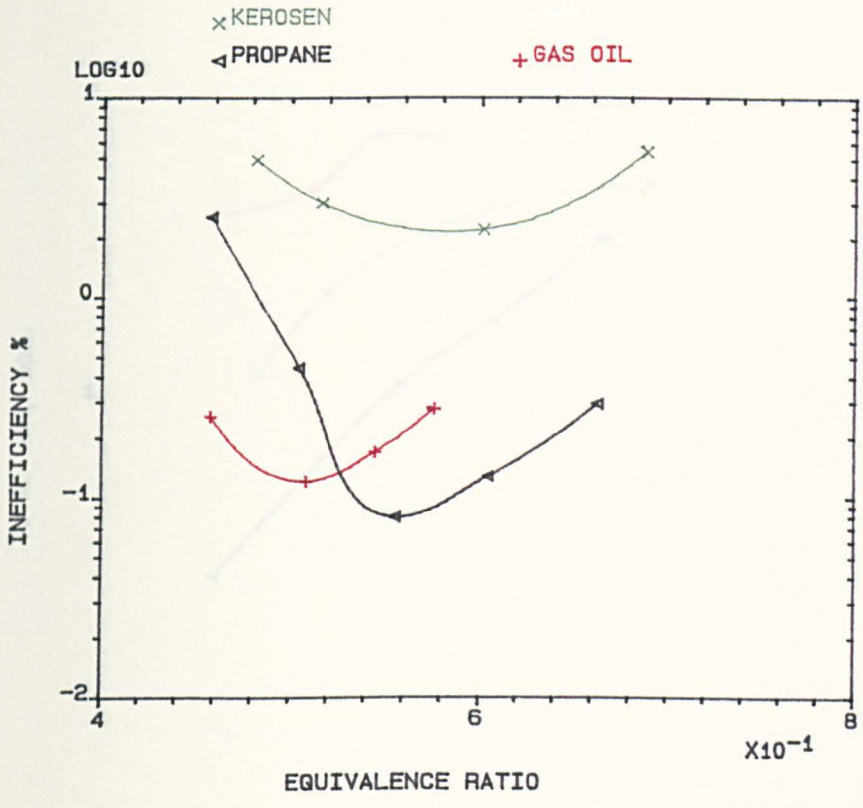

FIG.5.16a INFLUENCE OF FUEL TYPE ON COMBUSTION INEFFICIENCY FOR DIFFERENT FUELS USING PASSAGE INJECTION WITH SWIRLER (B) IN 140mm COMBUSTOR. MN=0.02, TIN=400K.

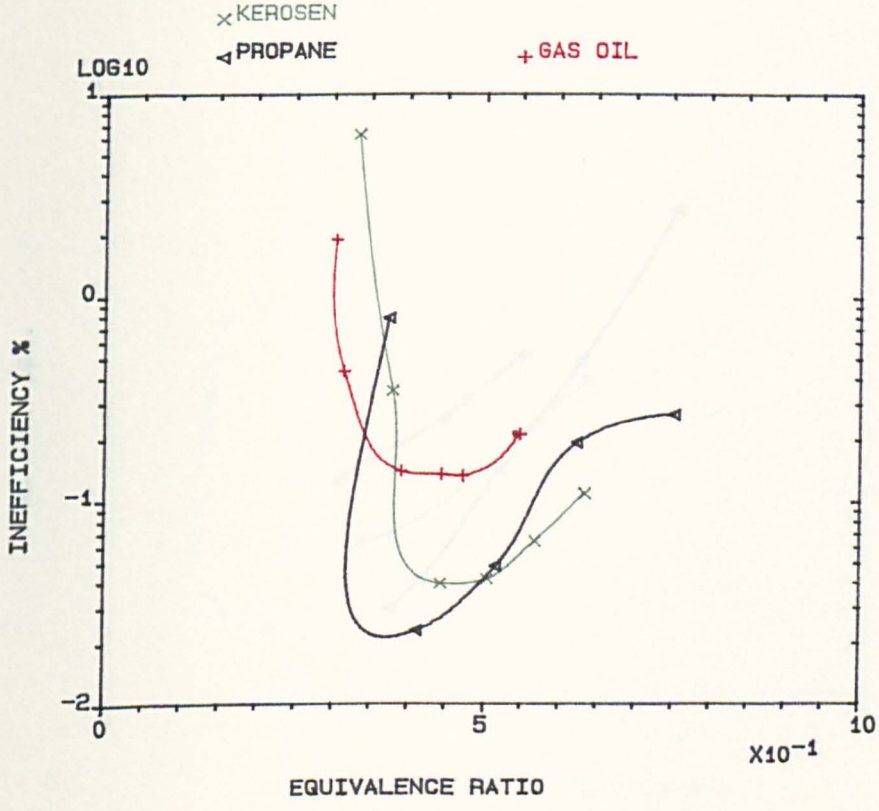

FIG.5.17a INFLUENCE OF FUEL TYPE ON COMBUSTION INEFFICIENCY FOR DIFFERENT FUELS USING PASSAGE INJECTION WITH SWIRLER (B) IN 140mm COMBUSTOR. MN=0.02, TIN=600K.

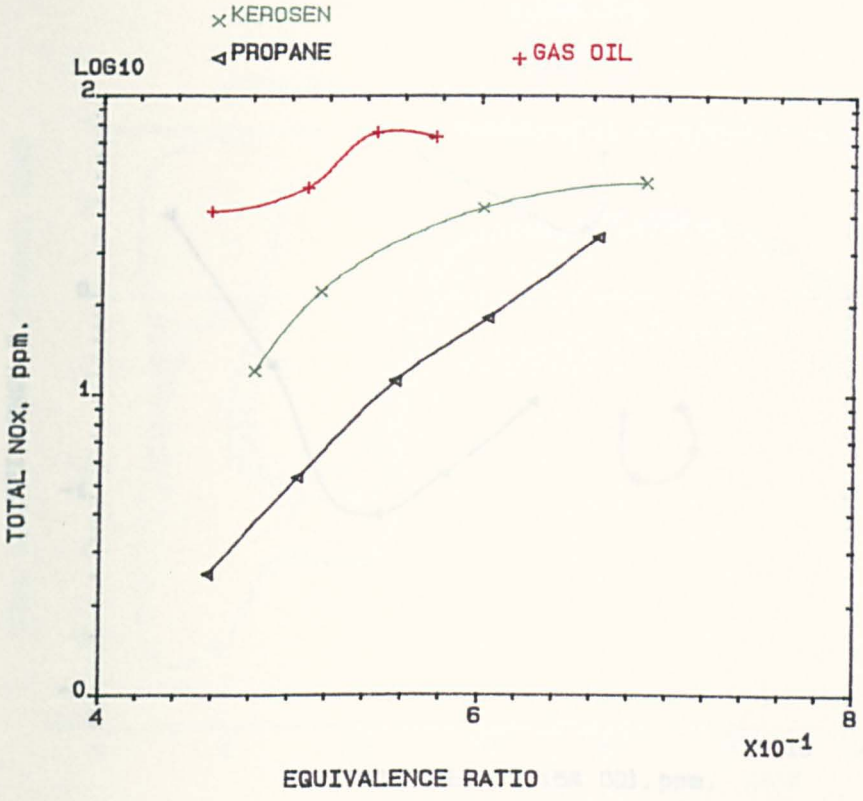

FIG.5.18 INFLUENCE OF FUEL TYPE ON THE EMISSIONS OF TOTAL NOx FOR DIFFERENT FUELS USING PASSAGE INJECTION WITH SWIRLER (B) IN 140mm COMBUSTOR. MN=0.02, TIN=400 K.

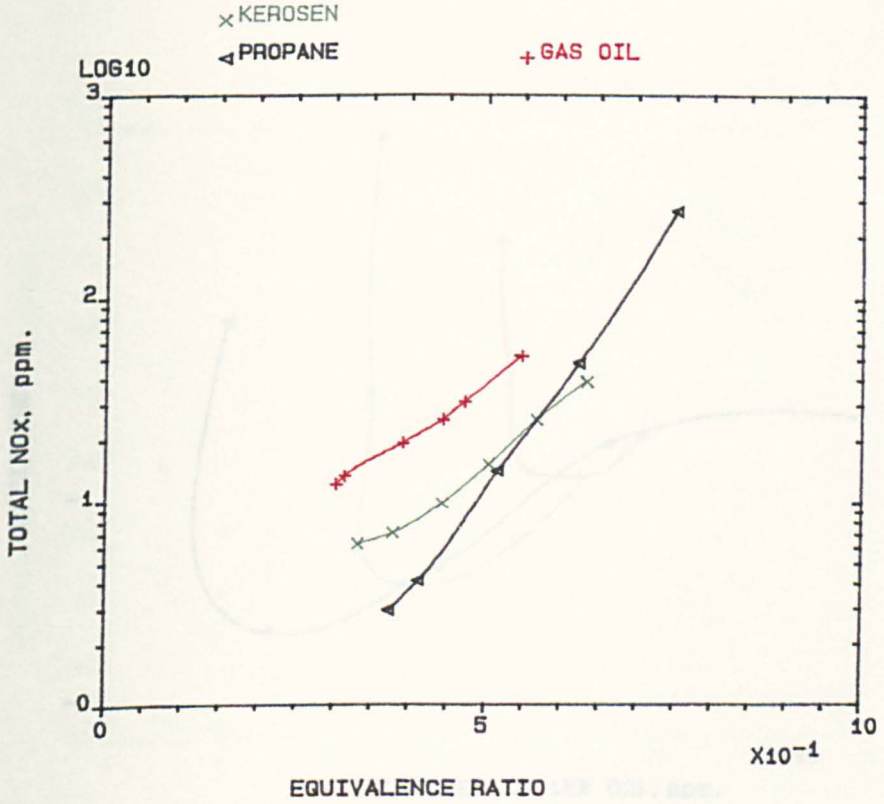

FIG.5.19 INFLUENCE OF FUEL TYPE ON THE EMISSIONS OF TOTAL NOx FOR DIFFERENT FUELS USING PASSAGE INJECTION WITH SWIRLER (B) IN 140mm COMBUSTOR. MN=0.02, TIN=600 K.

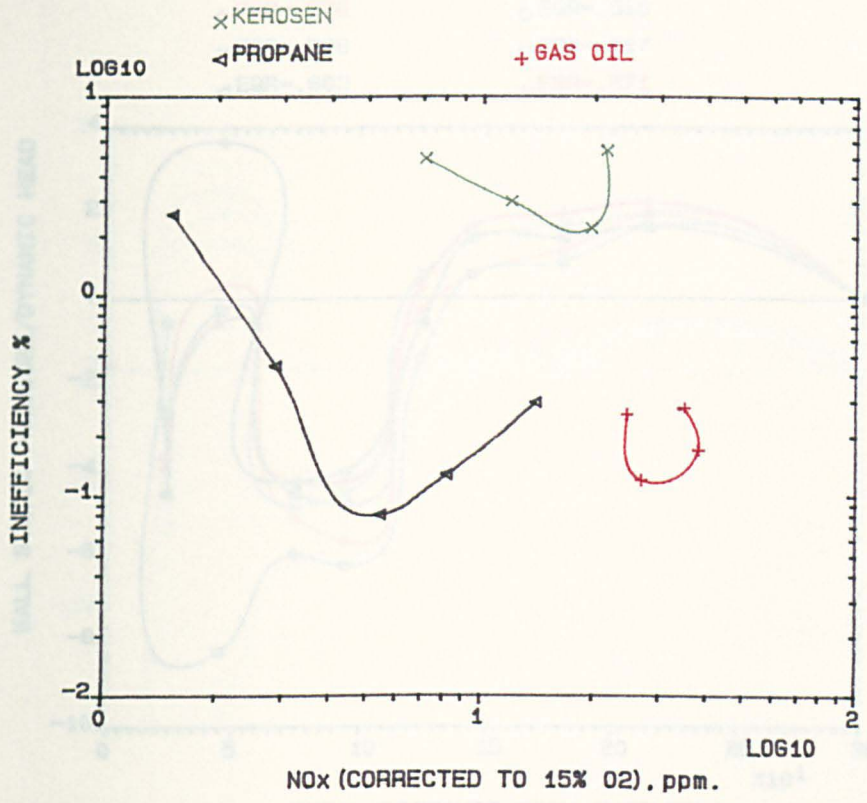

FIG.5.20 INFLUENCE OF FUEL TYPE ON VARIATION OF CORRECTED NOx WITH INEFFICIENCY FOR DIFFERENT FUELS USING PASSAGE INJ. WITH SWIRLER (B) IN 140mm COMBUSTOR. MN=0.02, TIN=400 K.

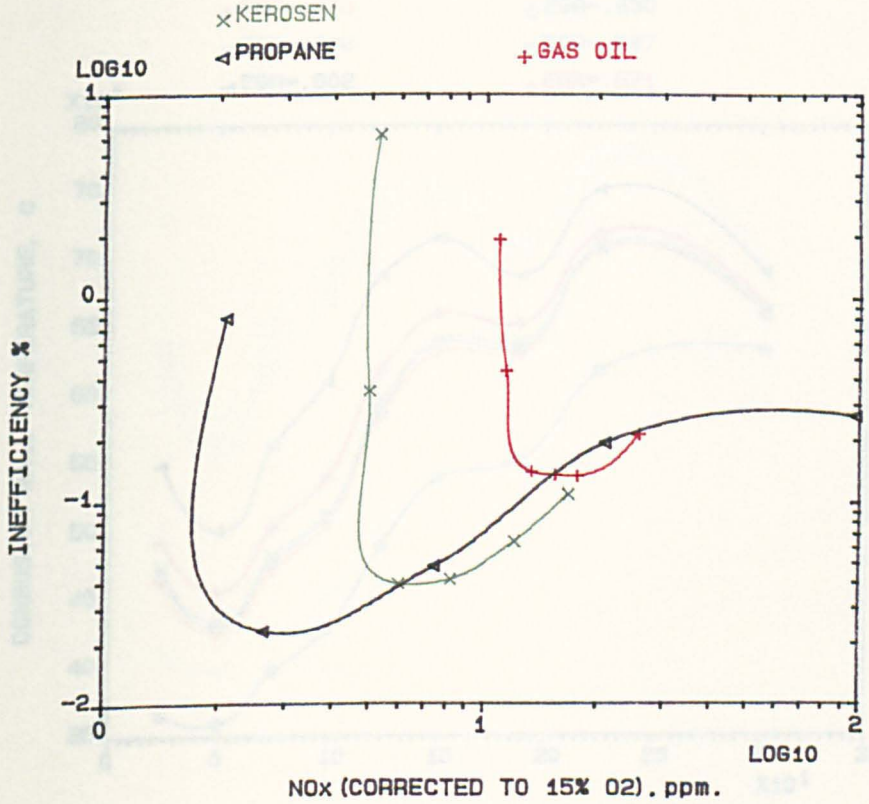

FIG.5.21 INFLUENCE OF FUEL TYPE ON VARIATION OF CORRECTED NOx WITH INEFFICIENCY FOR DIFFERENT FUELS USING PASSAGE INJ. WITH SWIRLER (B) IN 140mm COMBUSTOR. MN=0.02, TIN=600 K.

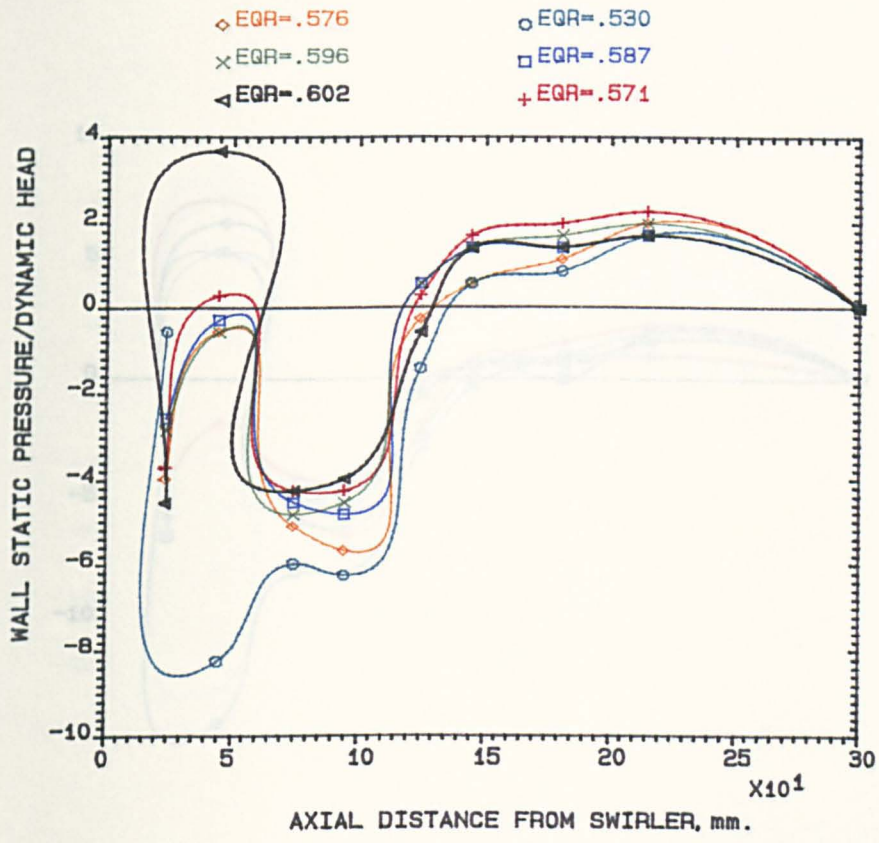

FIG.5.22 VARIATION OF COMBUSTOR WALL STATIC PRESSURE WITH AXIAL DISTANCE FROM SWIRLER (B). 140MM, MN=.02, PASS., N.G. 550 K.

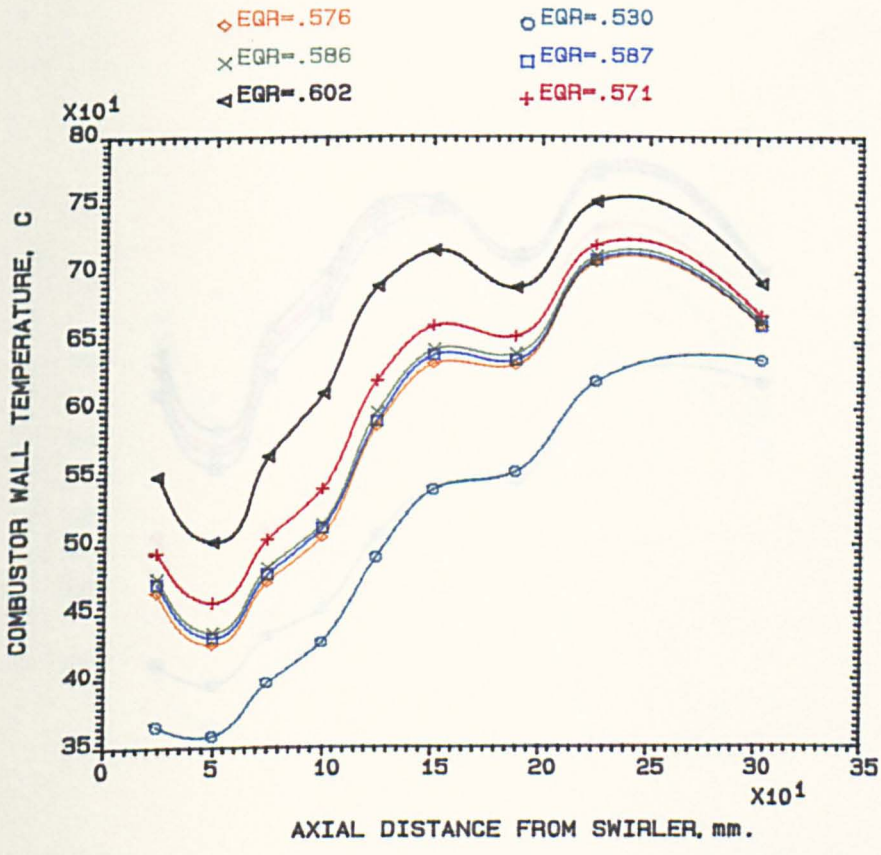

FIG.5.23 VARIATION OF COMBUSTOR WALL TEMPERATURE WITH THE AXIAL DISTANCE FROM SWIRLER (B). 140MM, MN=.02, PASS., N.G. 550K.

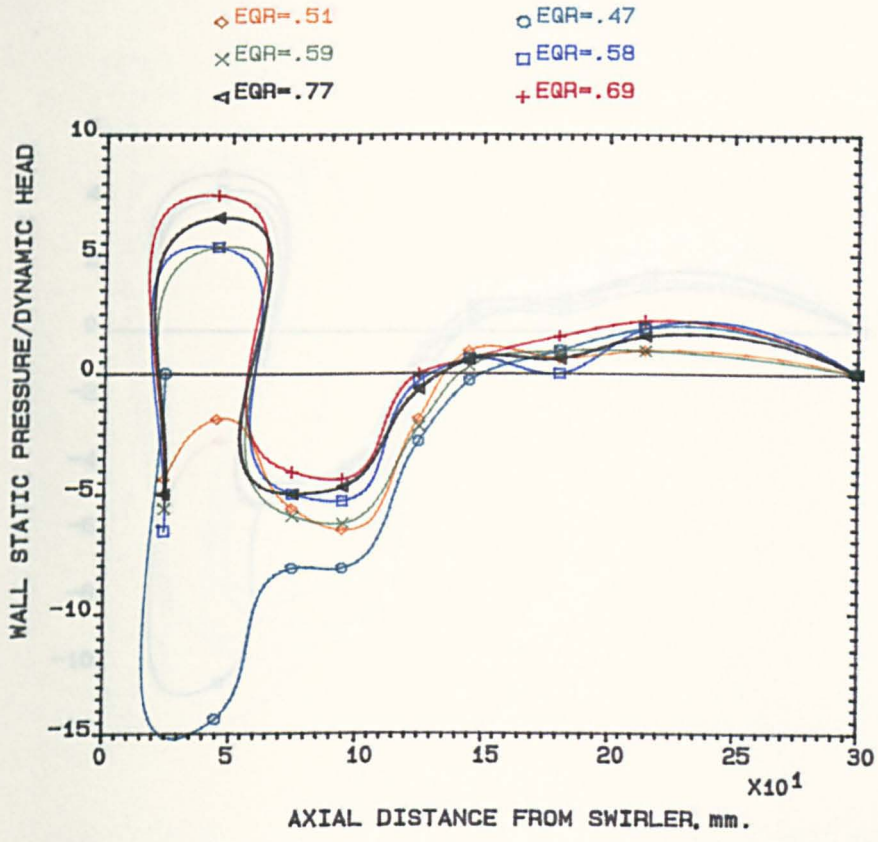

FIG.5.24 VARIATION OF COMBUSTOR WALL STATIC PRESSURE WITH AXIAL DISTANCE FROM SWIRLER (B). 140MM. MN=.02. PASS., N.G. 600 K.

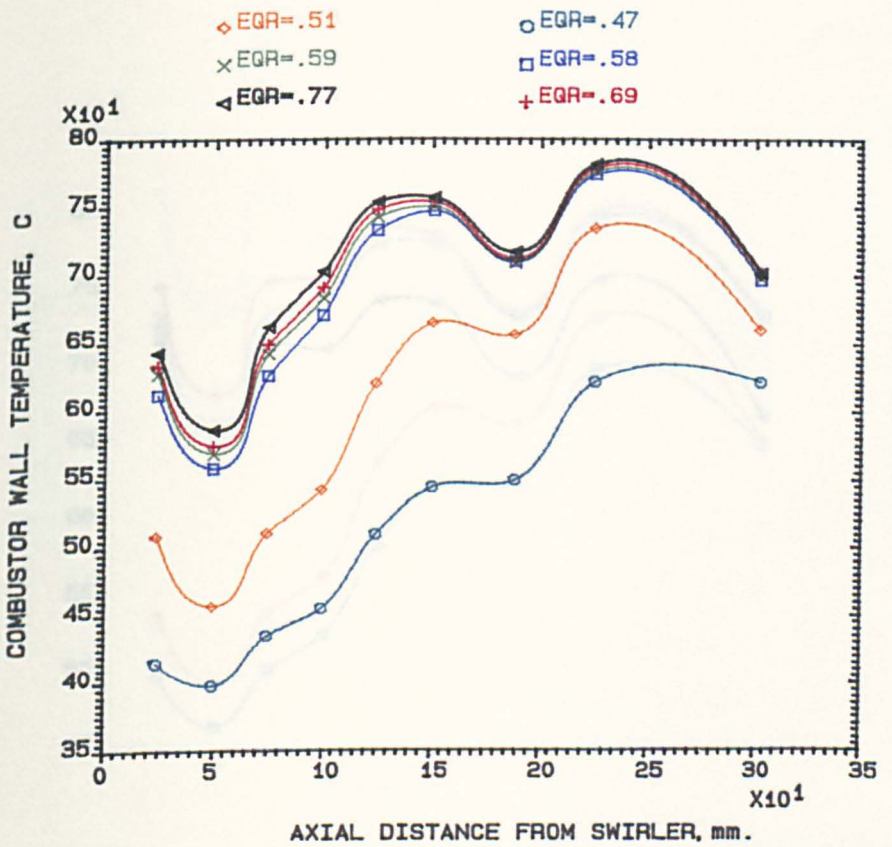

FIG.5.25 VARIATION OF COMBUSTOR WALL TEMPERATURE WITH THE AXIAL DISTANCE FROM SWIRLER (B). 140MM. MN=.02. PASS., N.G. 600K.

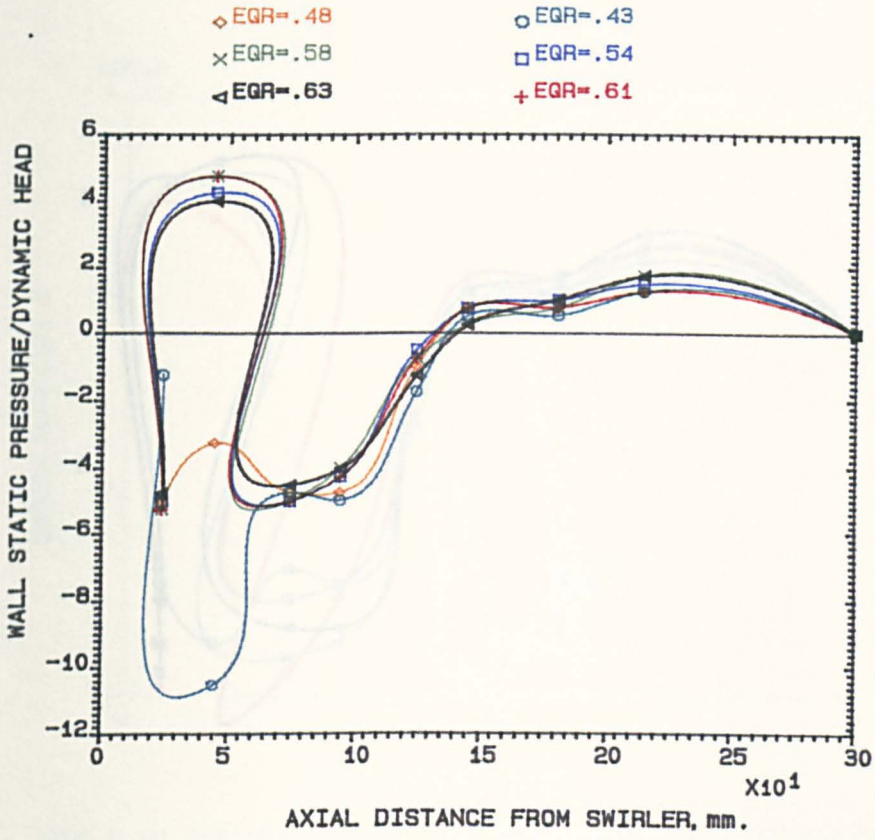

FIG.5.26 VARIATION OF COMBUSTOR WALL STATIC PRESSURE WITH AXIAL DISTANCE FROM SWIRLER (B). 140MM. MN=.02. PASS., N.G. 670 K.

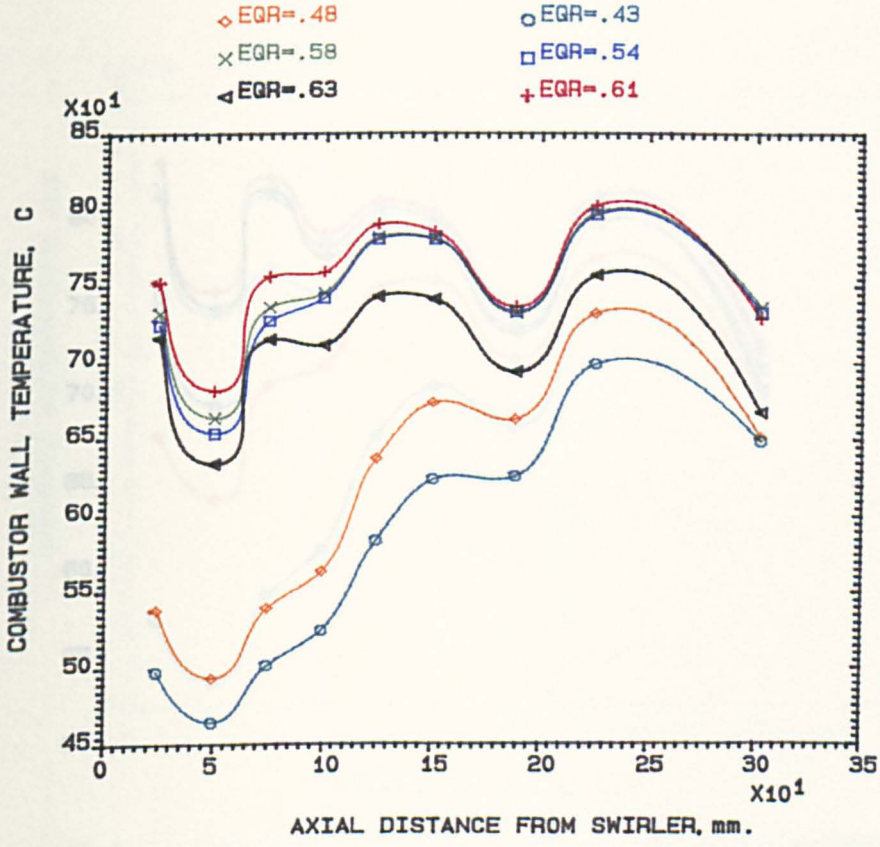

FIG.5.27 VARIATION OF COMBUSTOR WALL TEMPERATURE WITH THE AXIAL DISTANCE FROM SWIRLER (B). 140MM. MN=.02. PASS., N.G. 670K.

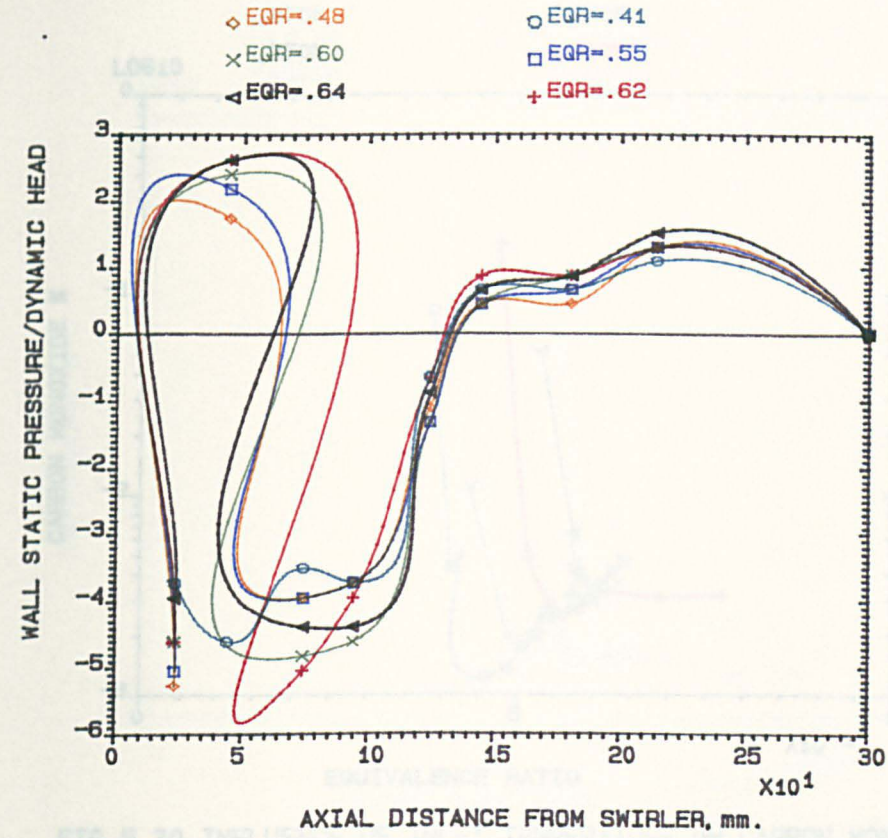

FIG.5.28 VARIATION OF COMBUSTOR WALL STATIC PRESSURE WITH AXIAL DISTANCE FROM SWIRLER (B), 140MM, MN=.02, PASS., N.G, 740 K.

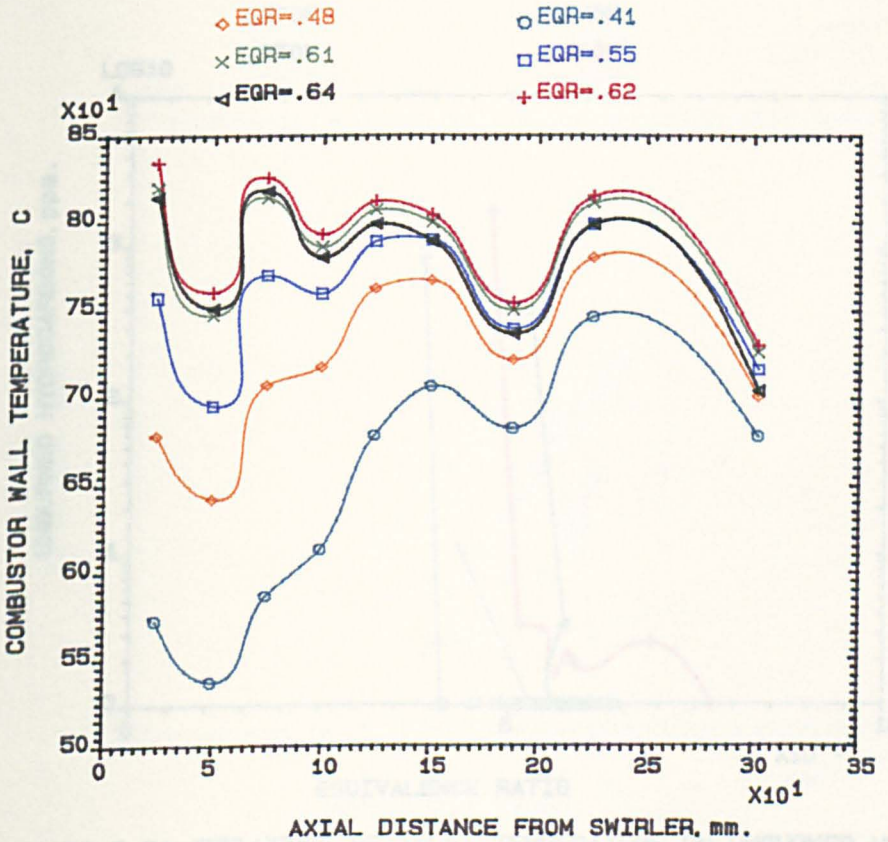

FIG.5.29 VARIATION OF COMBUSTOR WALL TEMPERATURE WITH THE AXIAL DISTANCE FROM SWIRLER (B), 140MM, MN=.02, PASS., N.G, 740K.

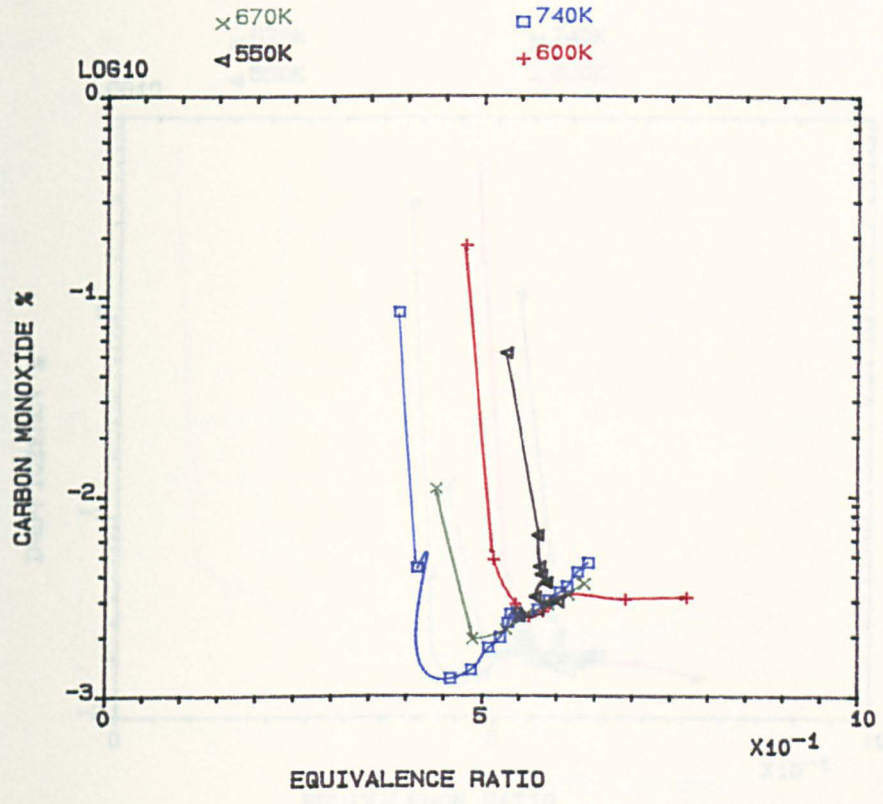

FIG.5.30 INFLUENCE OF INLET TEMPERATURE ON CARBON MONOXIDE EMISSIONS FOR RADIAL SWIRLER(B) IN 140mm COMBUSTOR USING NATURAL GAS WITH PASSAGE INJECTION. MN=0.02.

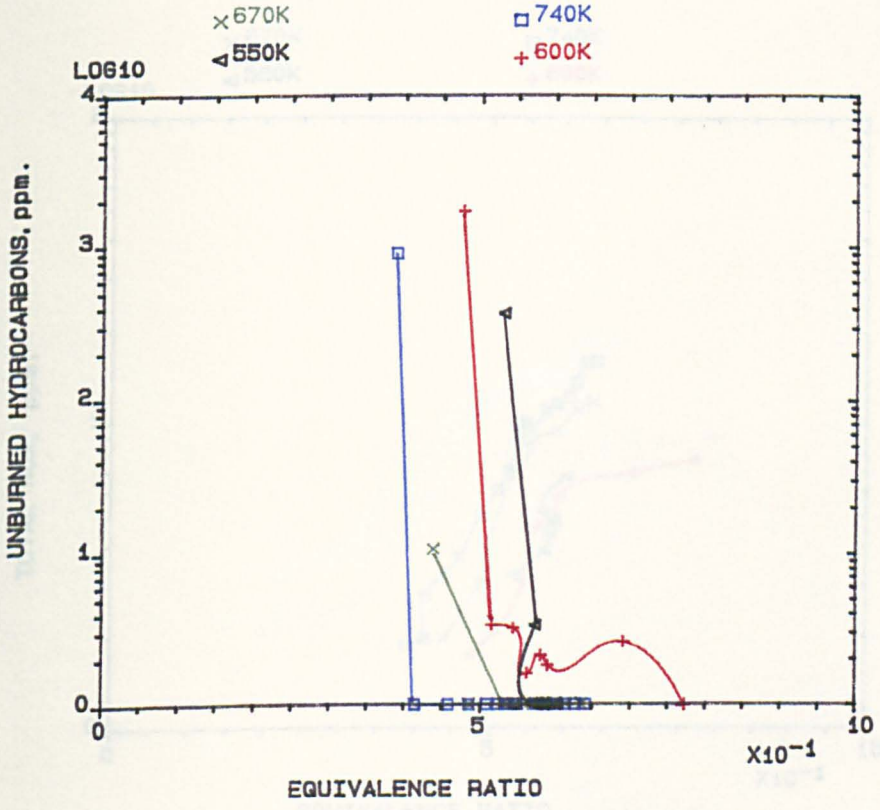

FIG.5.31 INFLUENCE OF INLET TEMPERATURE ON UNBURNED HYDROCARBONS EMISSIONS FOR RADIAL SWIRLER(B) IN 140mm COMBUSTOR USING NATURAL GAS WITH PASSAGE INJECTION. MN=0.02.

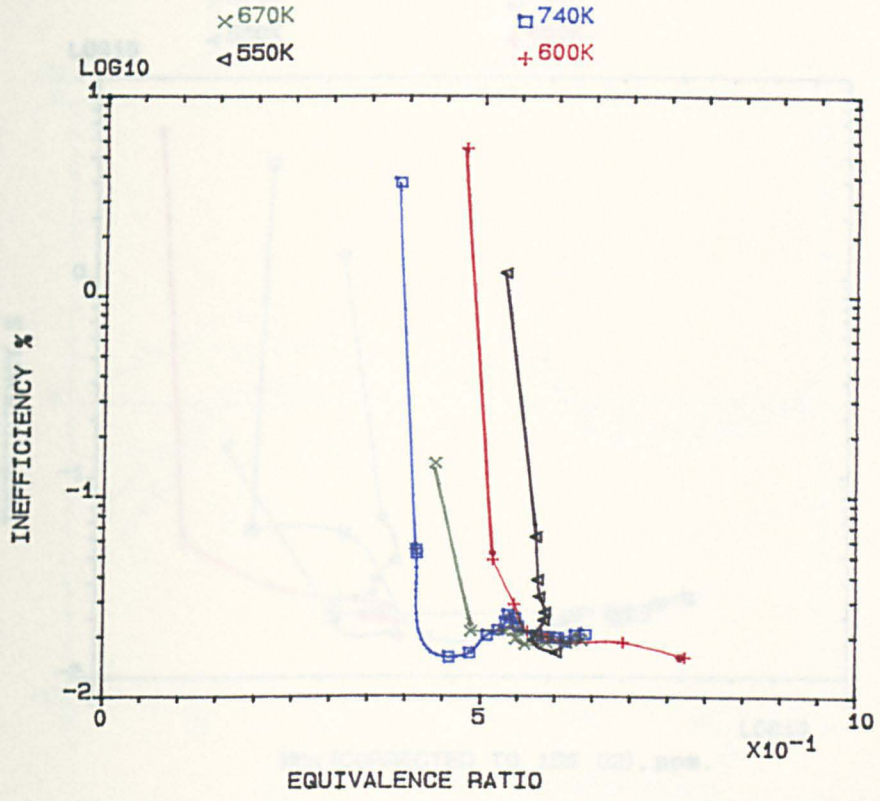

FIG.5.32 INFLUENCE OF INLET TEMPERATURE ON COMBUSTION INEFFICIENCY, RADIAL SWIRLER (B) IN 140mm COMBUSTOR USING NATURAL GAS WITH PASSAGE INJECTION, MN=0.02.

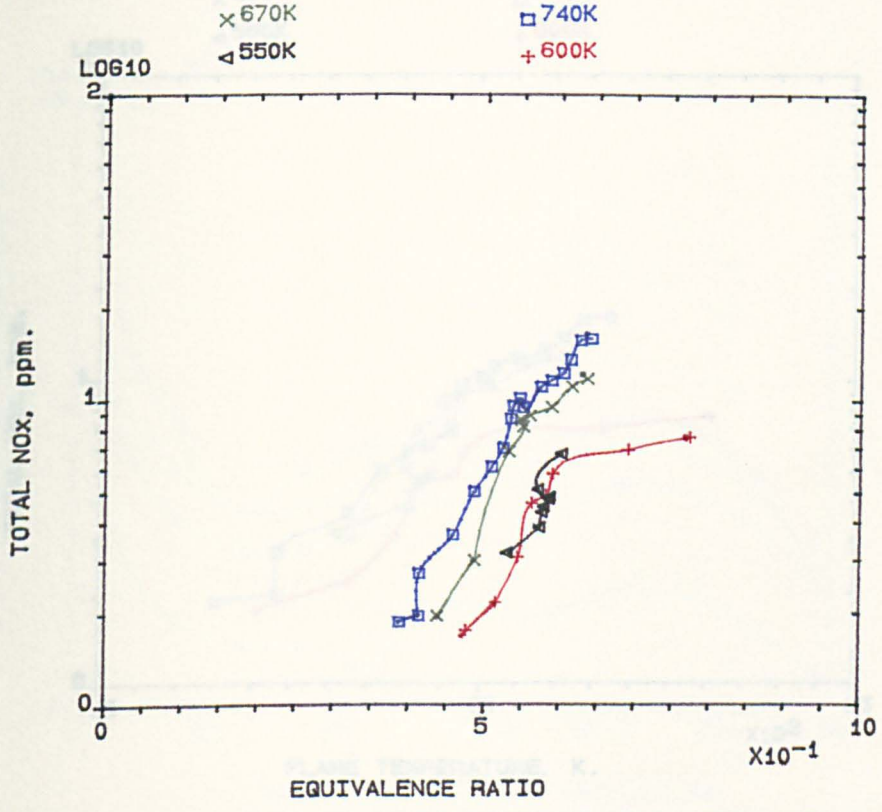

FIG.5.33 INFLUENCE OF INLET TEMPERATURE ON TOTAL (NOx) EMISSIONS, RADIAL SWIRLER (B) IN 140mm COMBUSTOR USING NATURAL GAS WITH PASSAGE INJECTION, MN=0.02.

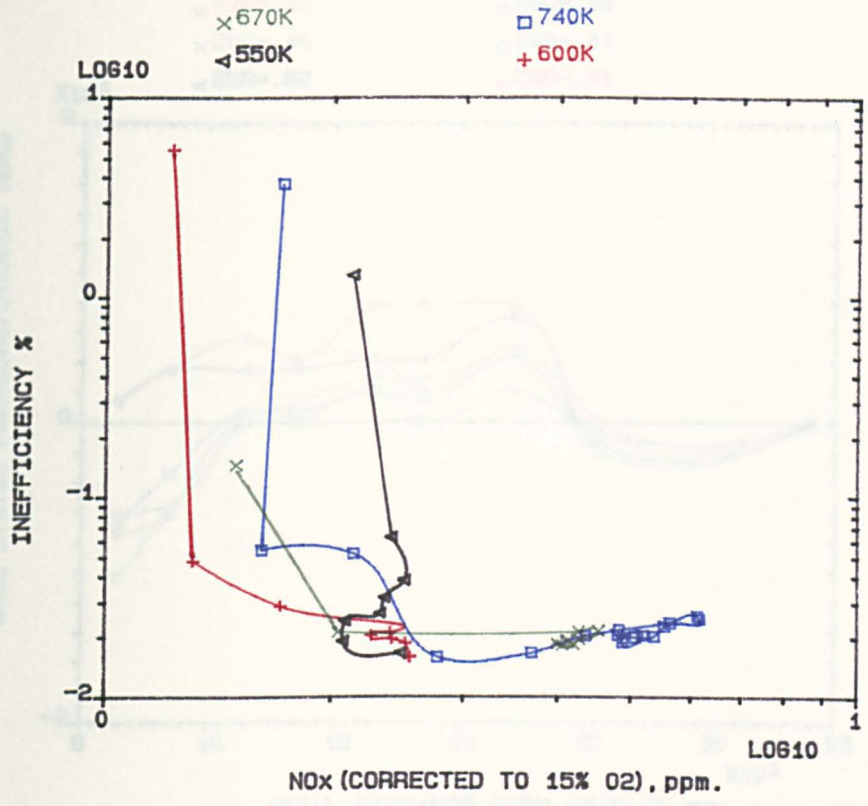

FIG.5.34 INFLUENCE OF INLET TEMPERATURE ON CORRECTED NOx VARIATION WITH COMBUSTION INEFFICIENCY, RADIAL SWIRLER (B) IN 140mm COMBUSTOR USING PASSAGE INJECTION NATURAL GAS MN=0.02.

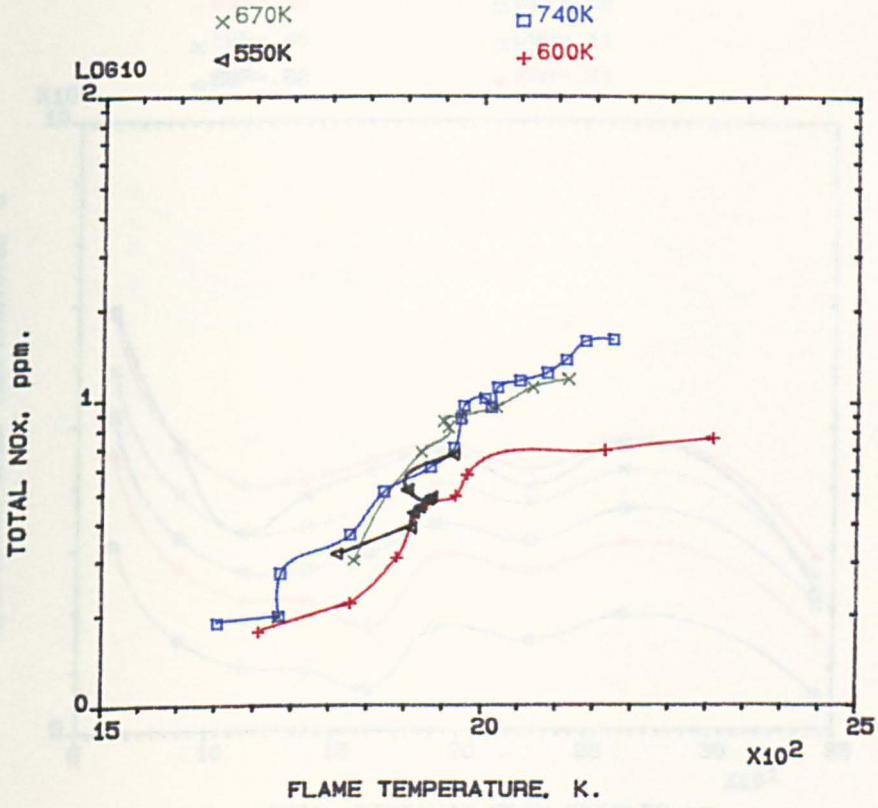

FIG.5.35 INFLUENCE OF INLET TEMPERATURE ON TOTAL (NOx) VARIATION WITH FLAME TEMPERATURE FOR RADIAL SWIRLER (B) IN 140mm COMBUSTOR USING NATURAL GAS PASSAGE INJECTION, MN=0.02.

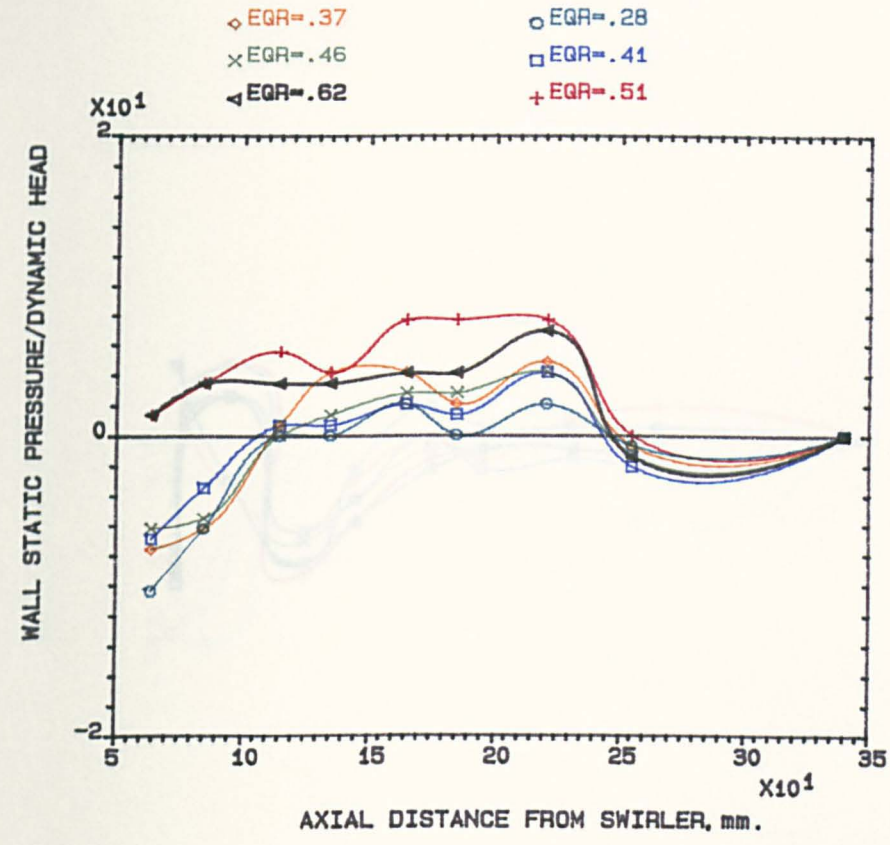

FIG.5.36 COMBUSTOR WALL STATIC PRESSURE V. AXIAL DISTANCE FROM SWIRLER (C), 140mm, COMBUSTOR, MN=.014, 140mm WALL INJ., PROPANE, 600K.

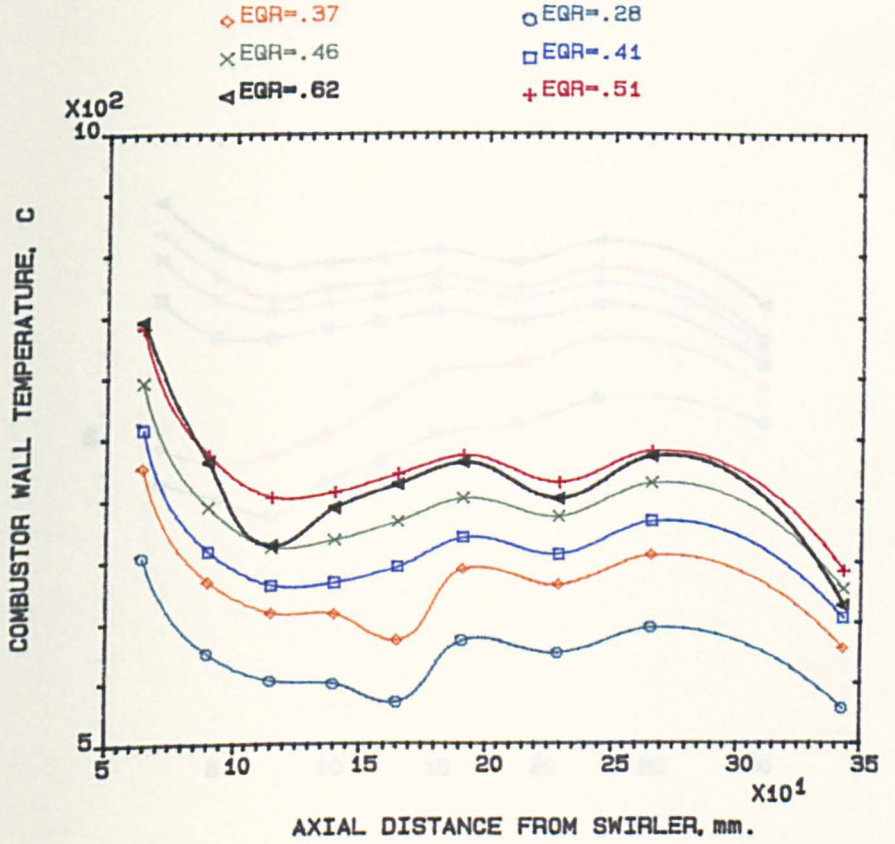

FIG.5.37 COMBUSTOR WALL TEMPERATURE V. THE AXIAL DISTANCE FROM SWIRLER (C), 140mm COMBUSTOR, MN=.014, 140mm WALL INJ., PROPANE, 600K.

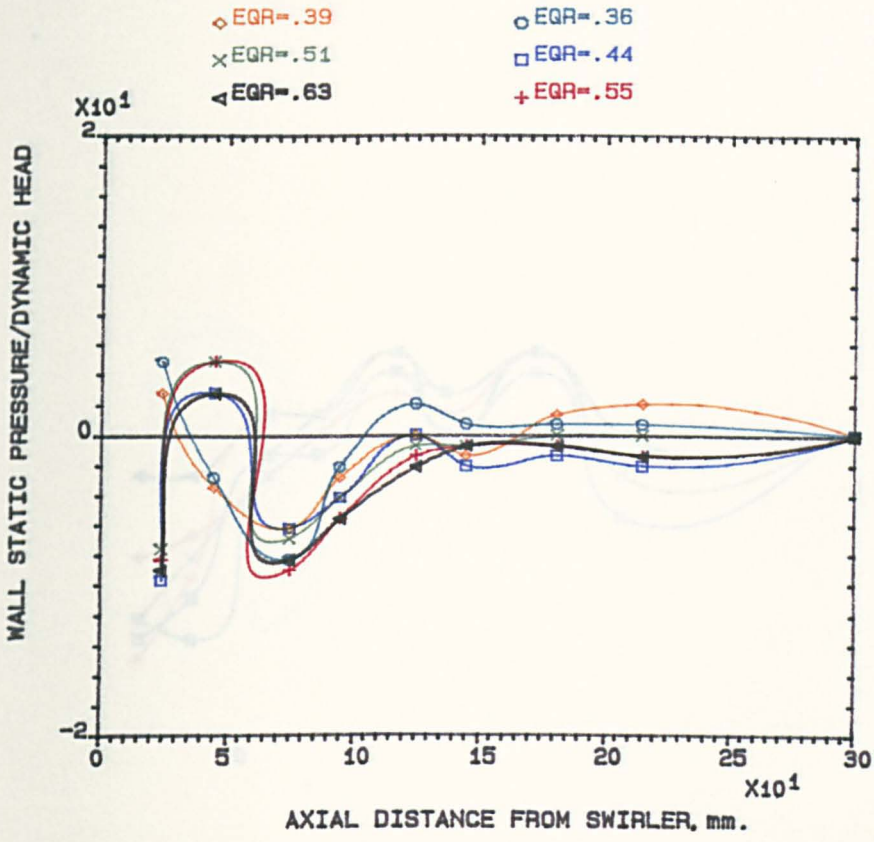

FIG.5.38 COMBUSTOR WALL STATIC PRESSURE V. AXIAL DISTANCE FROM SWIRLER (C), 140mm, COMBUSTOR, MN=.014/76mm WALL INJ., PROPANE, 600K.

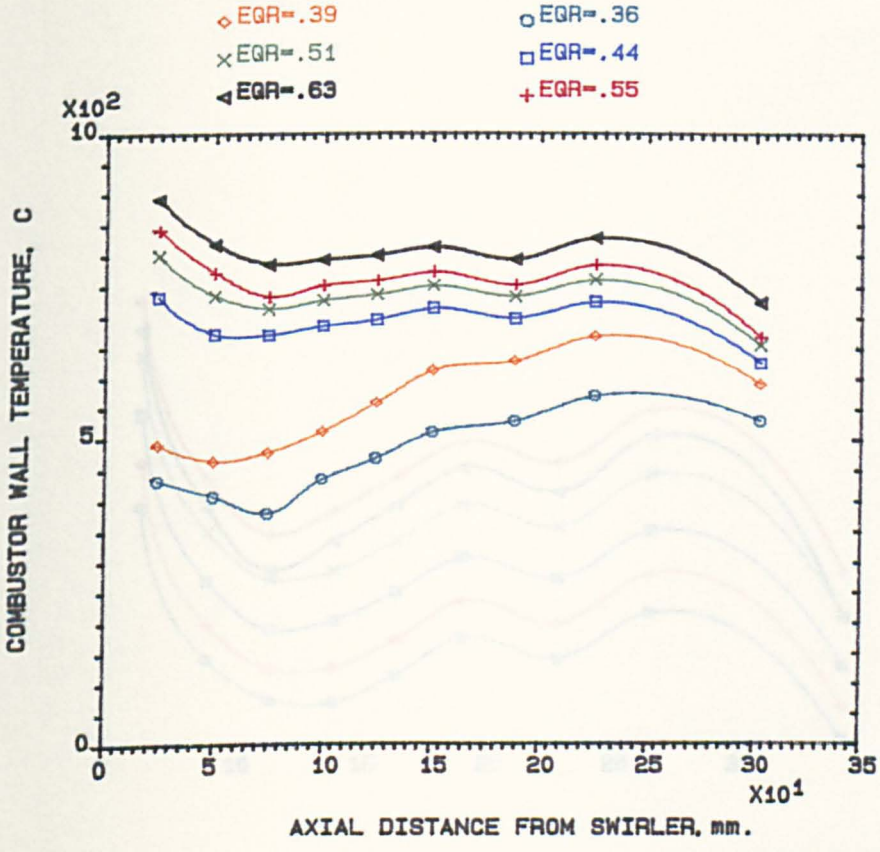

FIG.5.39 COMBUSTOR WALL TEMPERATURE V. THE AXIAL DISTANCE FROM SWIRLER (C), 140mm COMBUSTOR, MN=.014/76mm WALL INJ., PROPANE, 600K.

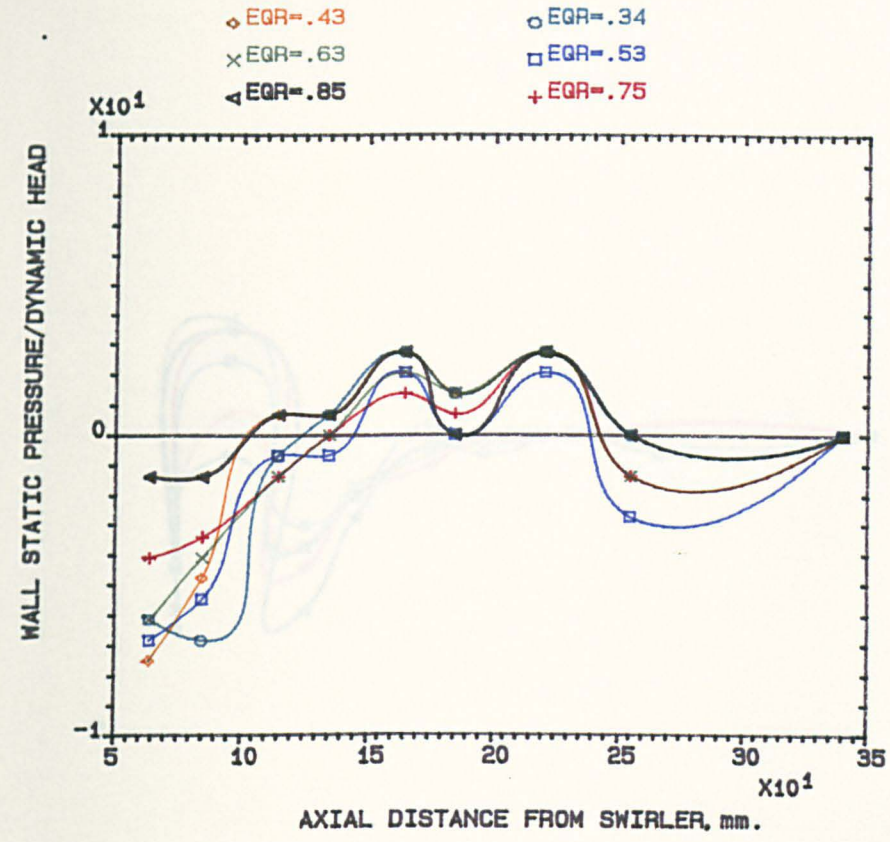

FIG.5.40 COMBUSTOR WALL STATIC PRESSURE V. AXIAL DISTANCE FROM SWIRLER (C), 140mm, COMBUSTOR, MN=.014, 140mm WALL INJ., N.G, 600K.

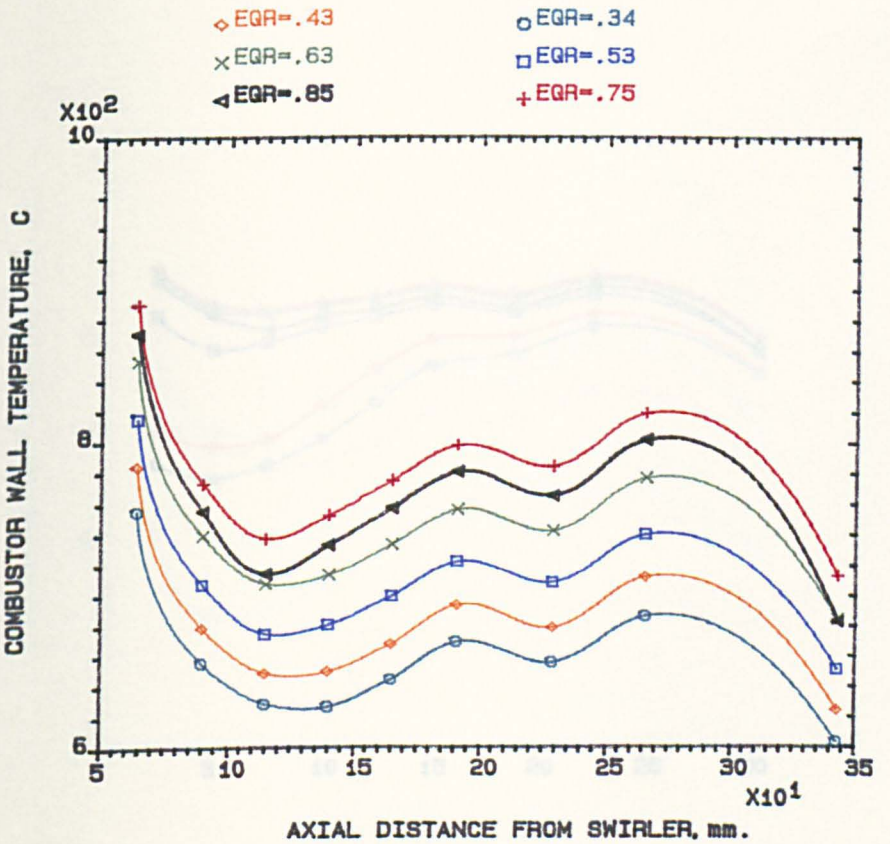

FIG.5.41 COMBUSTOR WALL TEMPERATURE V. THE AXIAL DISTANCE FROM SWIRLER (C), 140mm COMBUSTOR, MN=.014, 140mm WALL INJ., N.G, 600K.

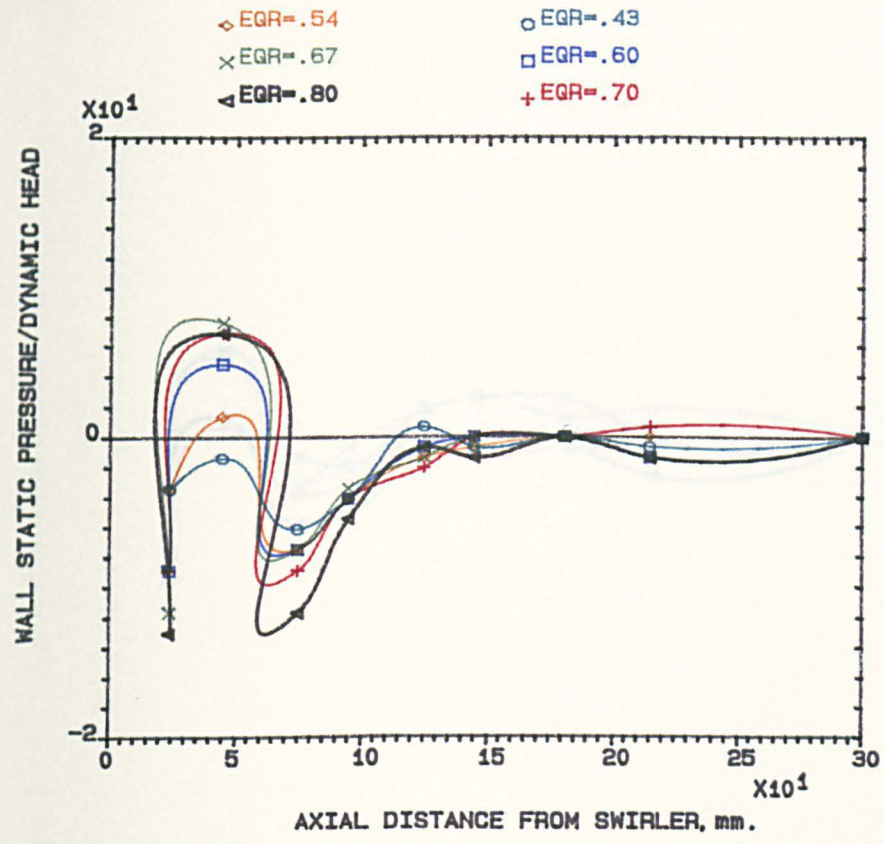

FIG.5.42 COMBUSTOR WALL STATIC PRESSURE V. AXIAL DISTANCE FROM SWIRLER (C), 140mm, COMBUSTOR, MN=.014/76mm WALL INJ., N.G., 600K.

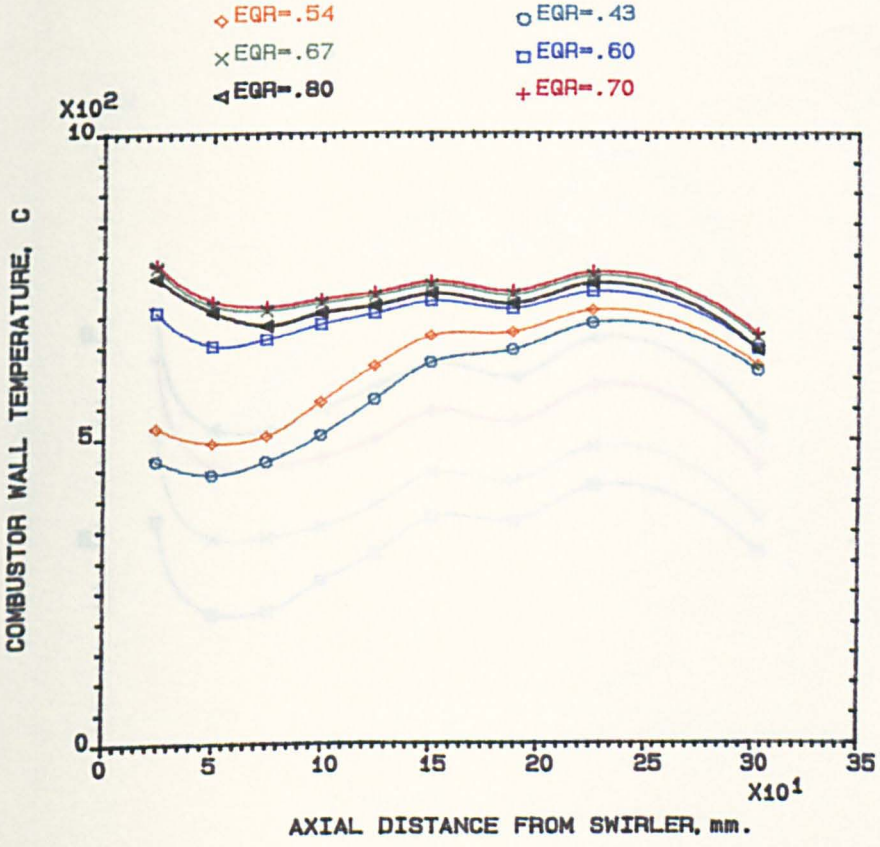

FIG.5.43 COMBUSTOR WALL TEMPERATURE V. THE AXIAL DISTANCE FROM SWIRLER (C). 140mm COMBUSTOR, MN=.014/76mm WALL INJ., N.G., 600K.

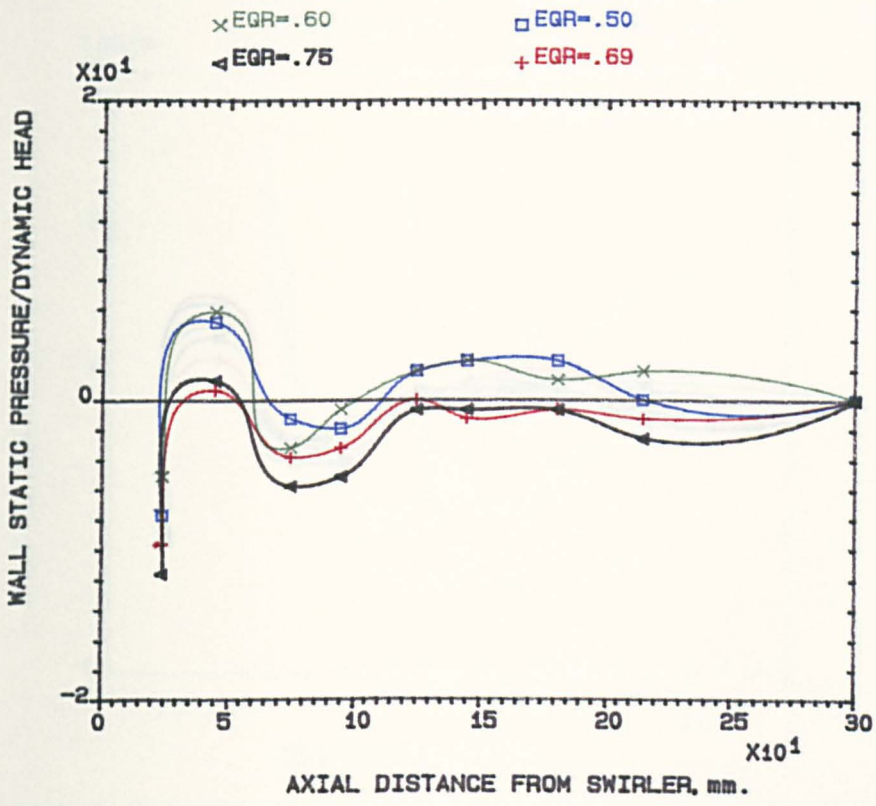

FIG.5.44 COMBUSTOR WALL STATIC PRESSURE V. AXIAL DISTANCE FROM SWIRLER (C). 140mm. COMBUSTOR. MN=.014/76mm WALL INJ., KEROSENE. 600K.

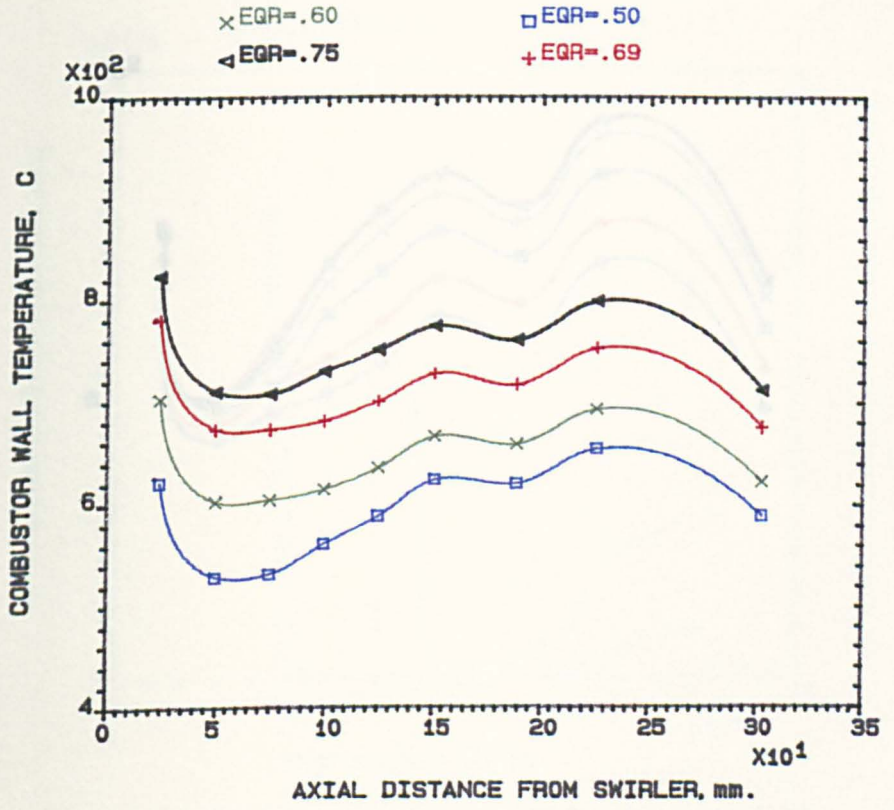

FIG.5.45 COMBUSTOR WALL TEMPERATURE V. THE AXIAL DISTANCE FROM SWIRLER (C). 140mm COMBUSTOR. MN=.014/76mm WALL INJ., KEROSENE. 600K.

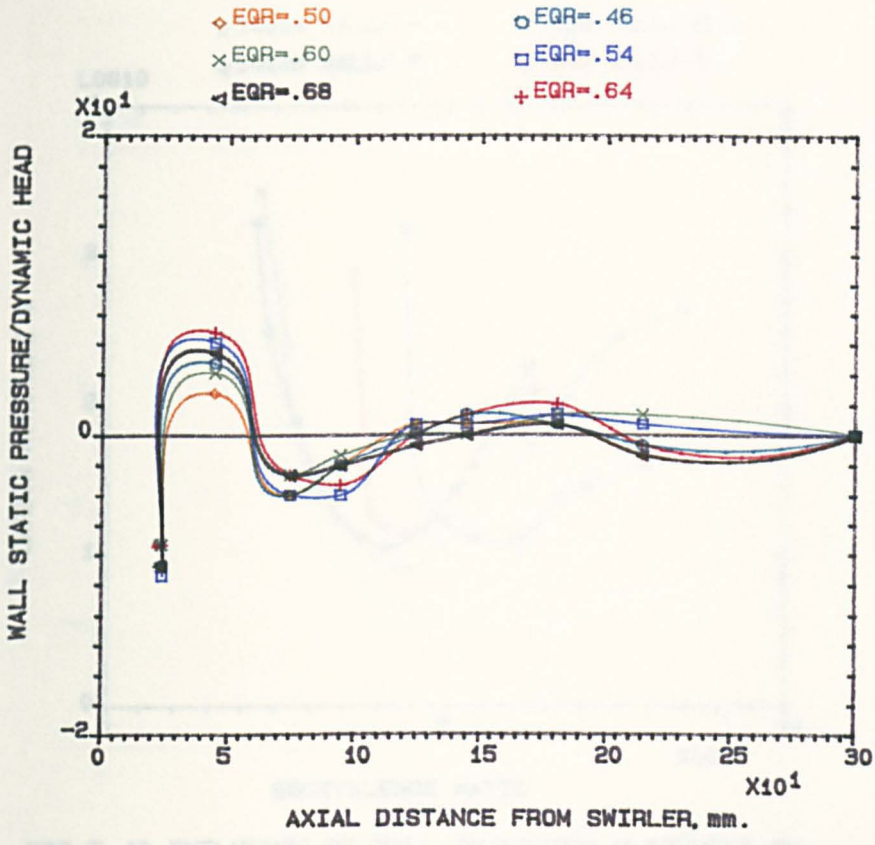

FIG.5.46 COMBUSTOR WALL STATIC PRESSURE V. AXIAL DISTANCE FROM SWIRLER (C), 140mm, COMBUSTOR, MN=.014/76mm WALL INJ., GAS OIL, 600K.

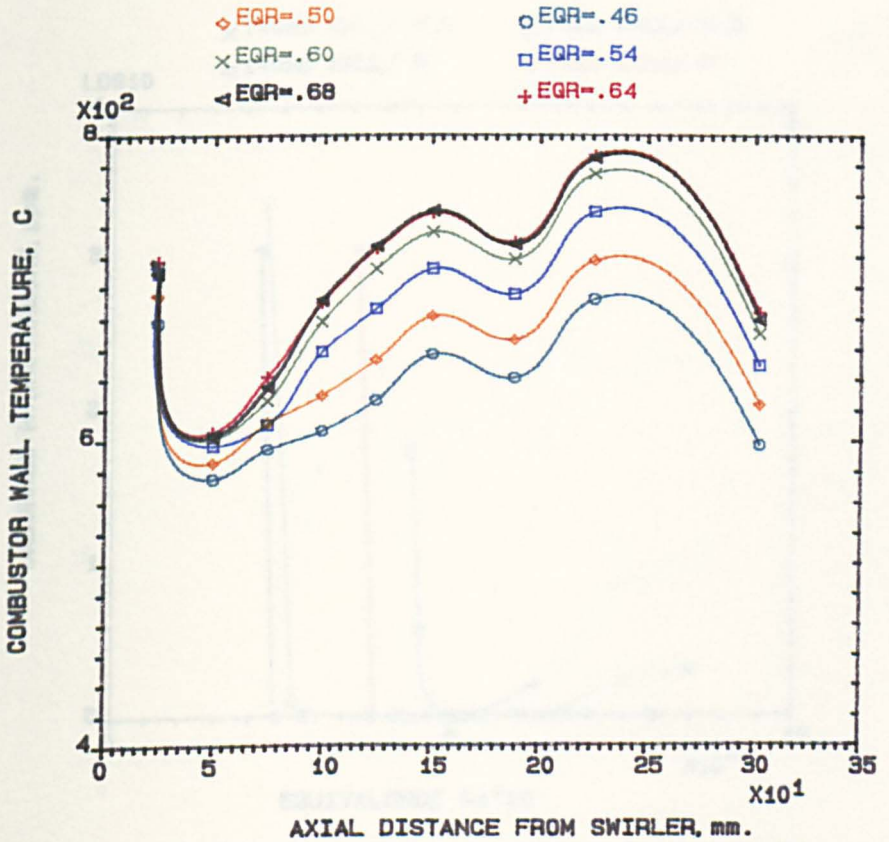

FIG.5.47 COMBUSTOR WALL TEMPERATURE V. THE AXIAL DISTANCE FROM SWIRLER (C), 140mm COMBUSTOR, MN=.014/76mm WALL INJ., GAS OIL, 600K.

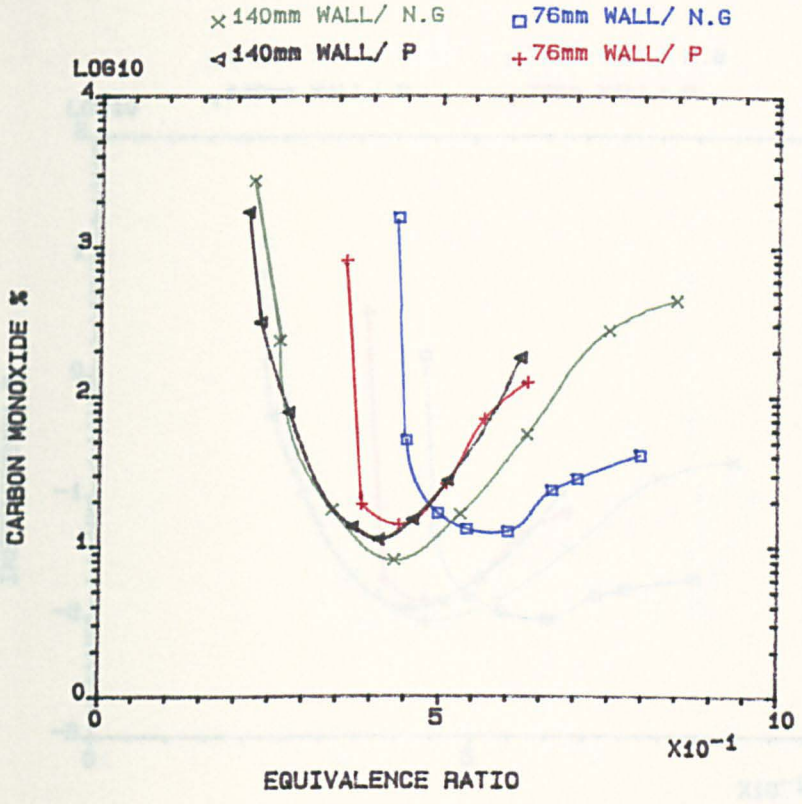

FIG.5.48 INFLUENCE OF WALL INJECTION PLACEMENT ON CARBON MONOXIDE EMISSIONS FOR RADIAL SWIRLER (C) IN 140mm COMBUSTOR. MN=0.014. TIN=600K.

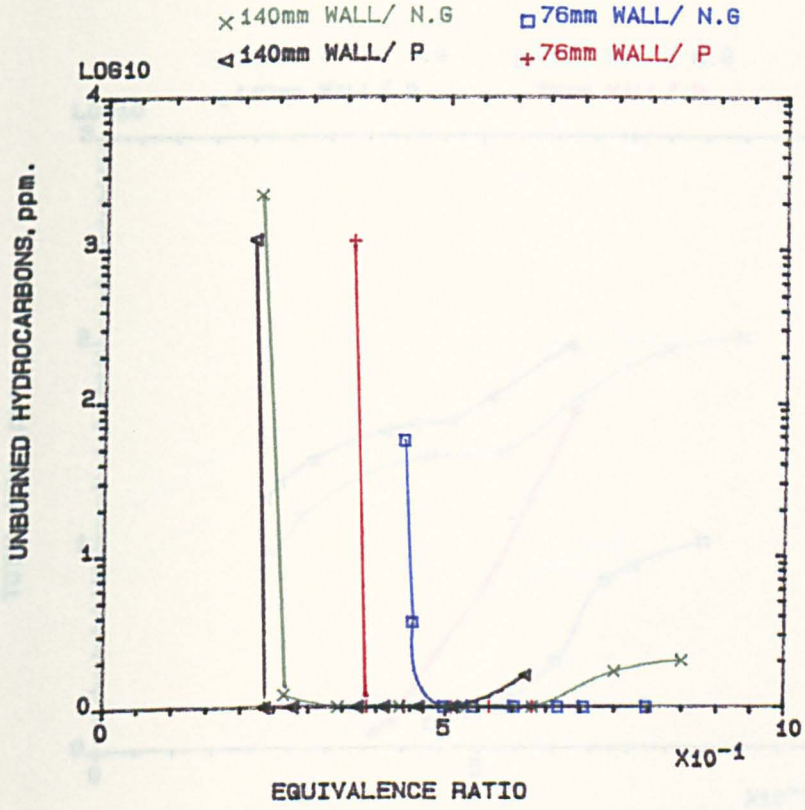

FIG.5.49 INFLUENCE OF WALL INJECTION PLACEMENT ON UNBURNED HYDROCARBONS EMISSIONS FOR RADIAL SWIRLER (C) IN 140mm COMBUSTOR, MN=0.014, 600K.

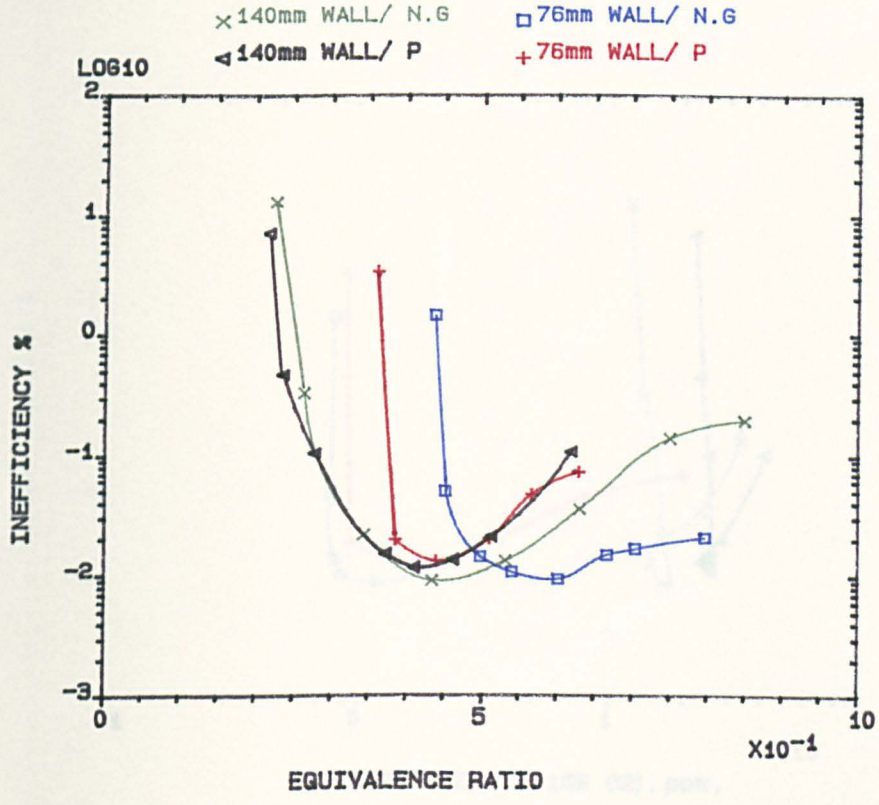

FIG.5.50 INFLUENCE OF WALL INJECTION PLACEMENT ON COMBUSTION INEFFICIENCY FOR RADIAL SWIRLER (C) IN 140mm COMBUSTOR, MN=0.014, TIN=600K.

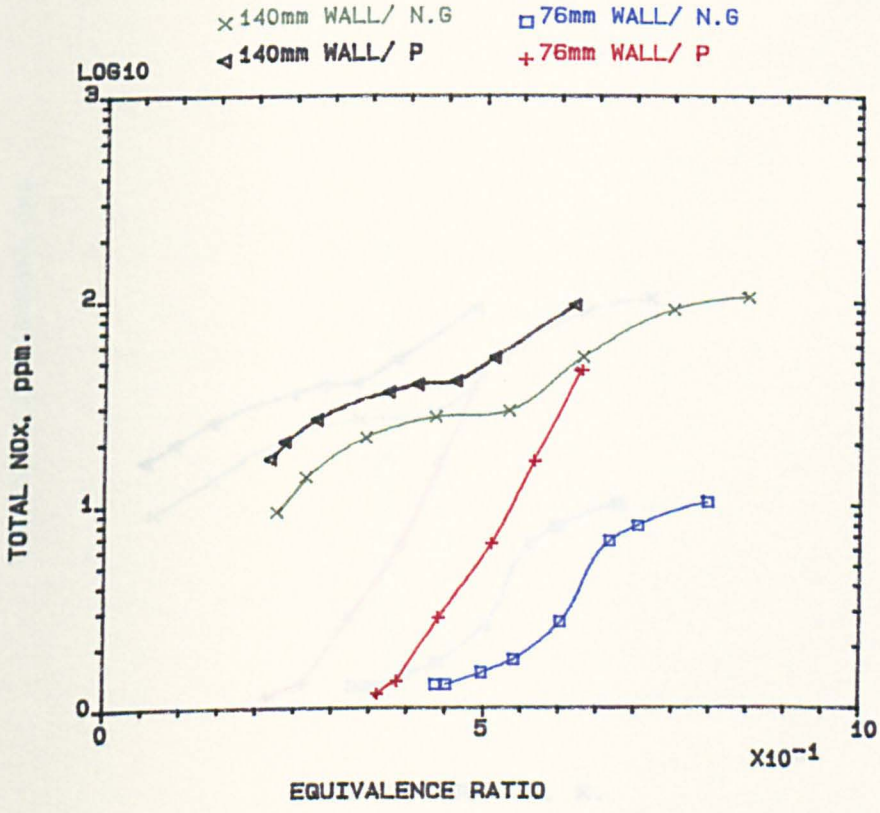

FIG.5.51 INFLUENCE OF WALL INJECTION PLACEMENT ON TOTAL NOX EMISSIONS FOR RADIAL SWIRLER (C) IN 140mm COMBUSTOR, MN=0.014, 600K.

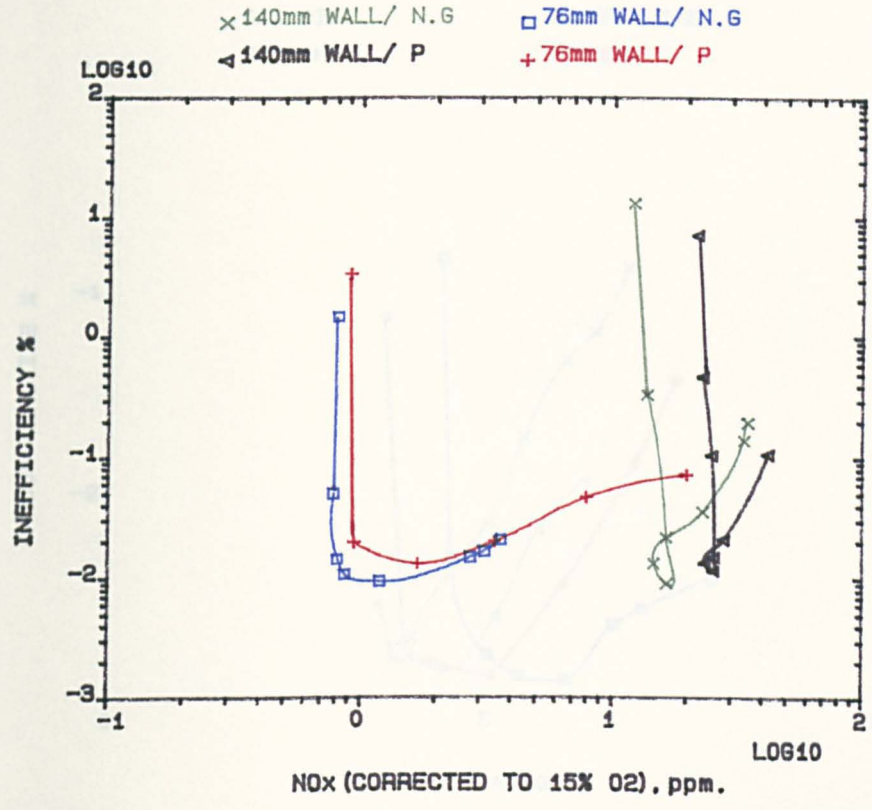

FIG.5.52 INFLUENCE OF WALL INJECTION PLACEMENT ON VARIATION OF CORRECTED NOx WITH COMBUSTION INEFFICIENCY FOR SWIRLER (C) IN 140mm COMBUSTOR, MN=0.014, TIN=600K.

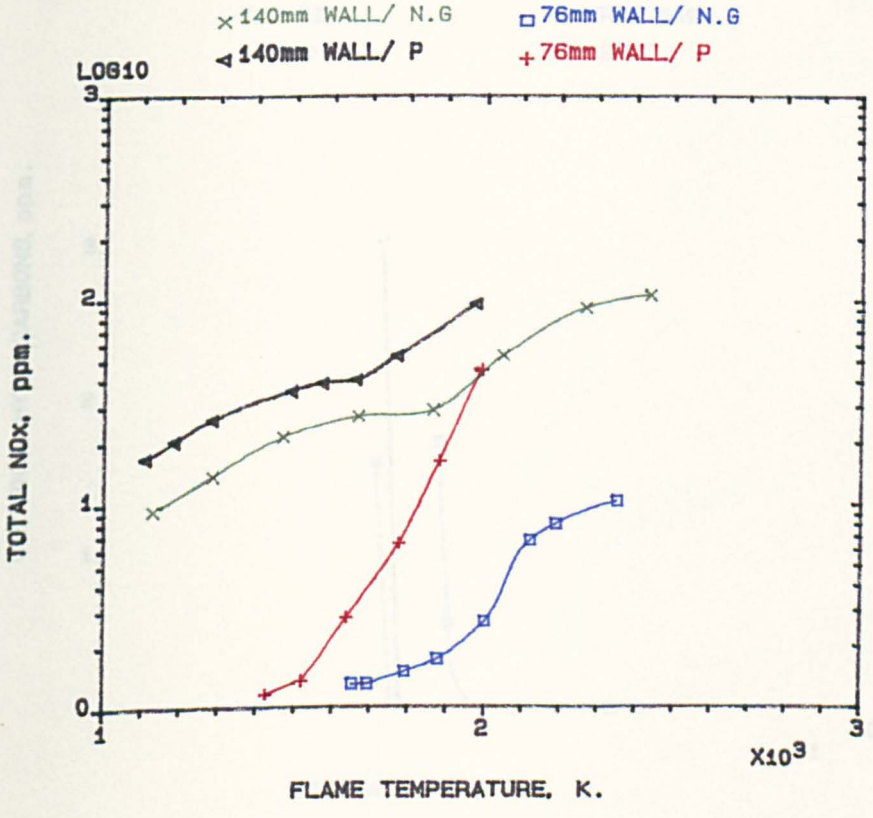

FIG.5.53 INFLUENCE OF WALL INJECTION PLACEMENT ON VARIATION OF NOX EMISSIONS WITH FLAME TEMPERATURE FOR SWIRLER (C) IN 140mm COMBUSTOR, MN=0.014, 600K.

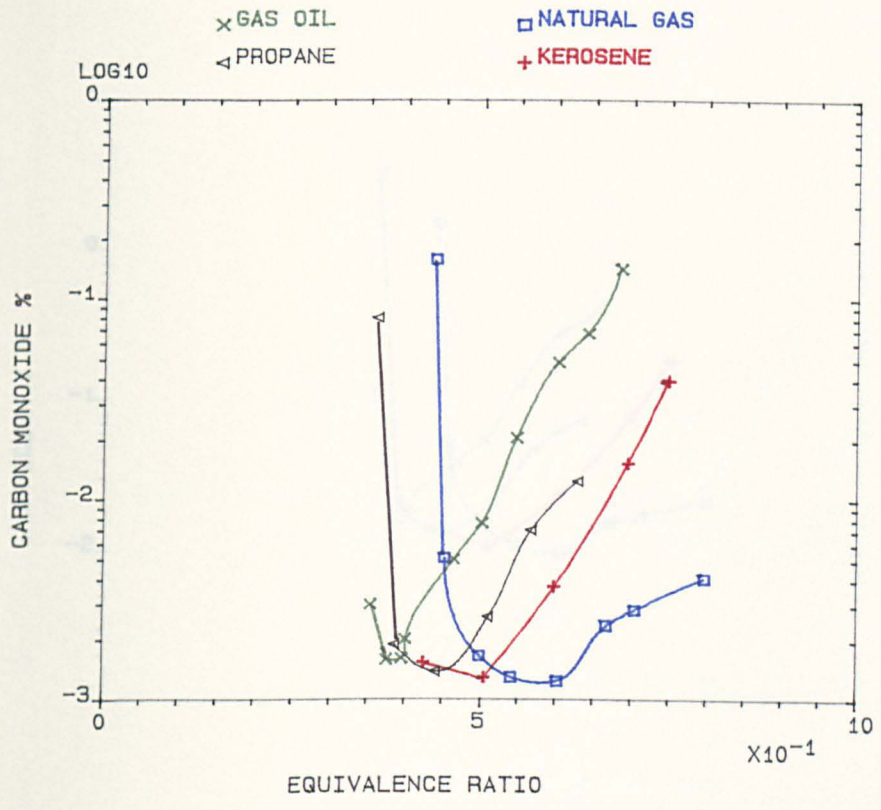

FIG.5.54 INFLUENCE OF FUEL TYPE USED WITH 76mm WALL INJECTION ON CARBON MONOXIDE EMISSIONS FOR RADIAL SWIRLER (C) IN 140mm COMBUSTOR, MN=0.014, TIN=600K.

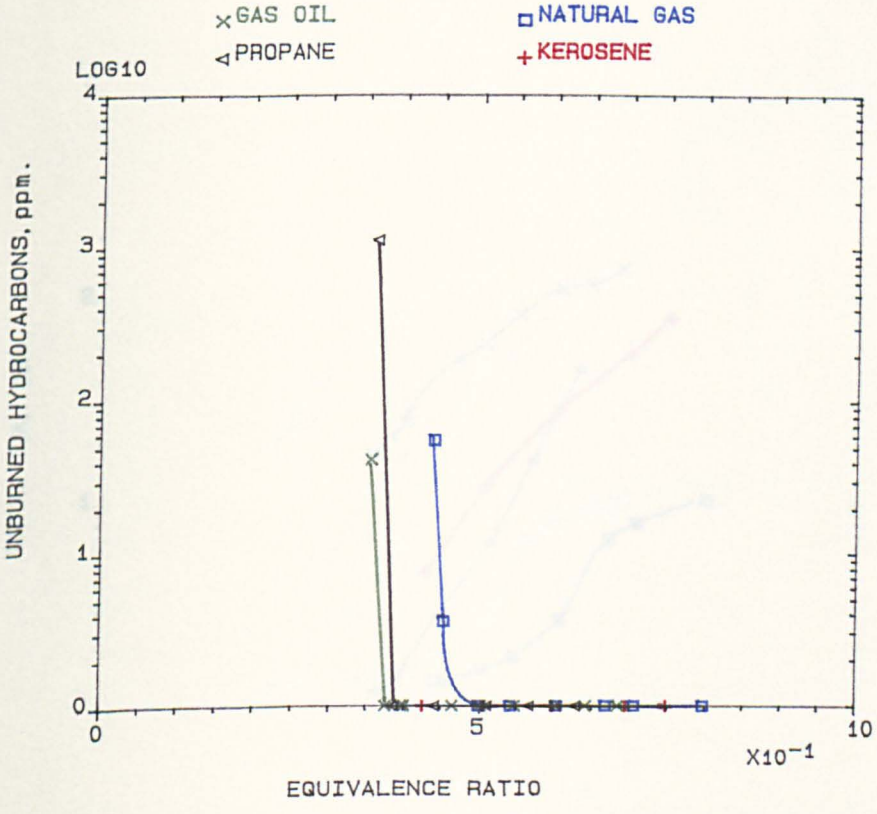

FIG.5.55 INFLUENCE OF FUEL TYPE USED WITH 76mm WALL INJECTION ON UNBURNED HYDROCARBONS EMISSIONS FOR RADIAL SWIRLER (C) IN 140mm COMBUSTOR, MN=0.014, 600K.

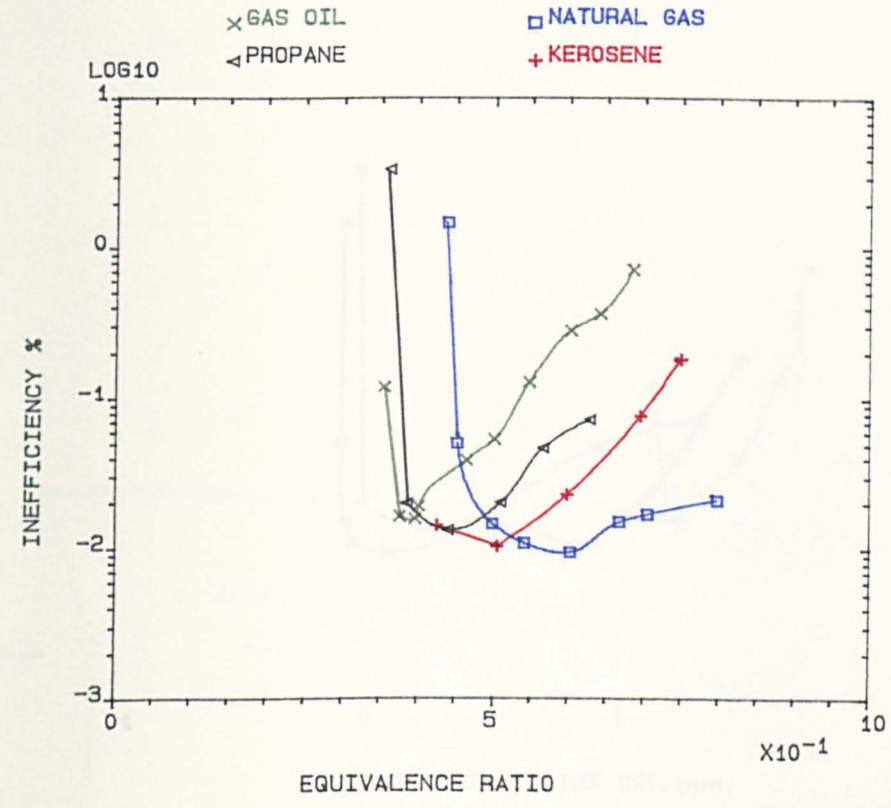

FIG.5.56 INFLUENCE OF FUEL TYPE USED WITH 76mm WALL INJECTION ON COMBUSTION INEFFICIENCY FOR RADIAL SWIRLER (C) IN 140mm COMBUSTOR, MN=0.014, TIN=600K.

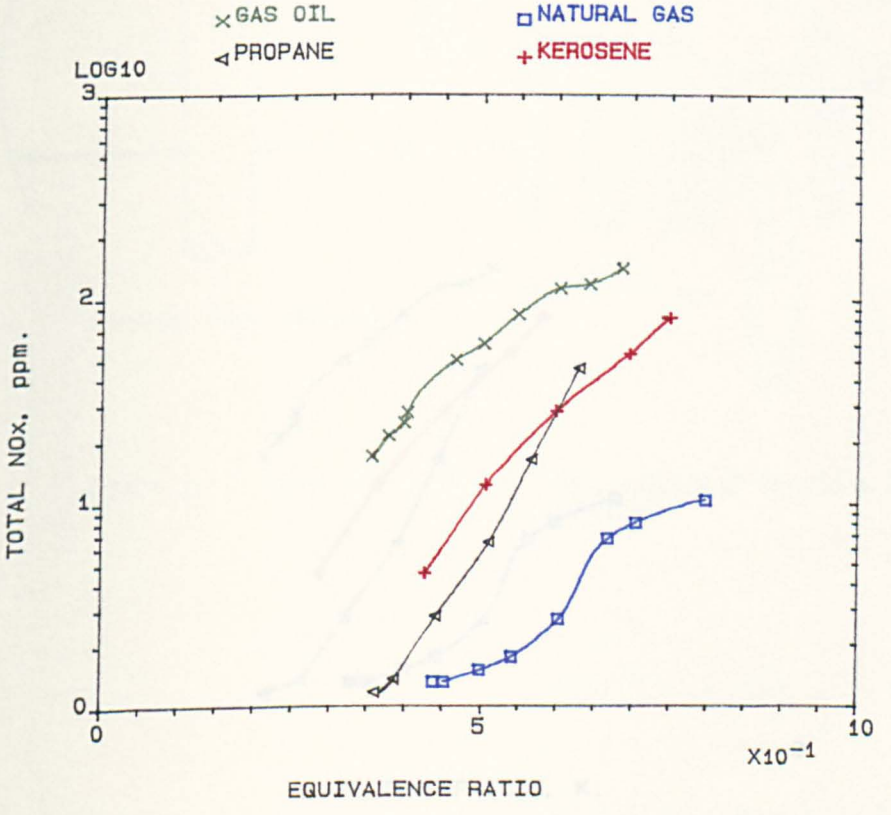

FIG.5.57 INFLUENCE OF FUEL TYPE USED WITH 76mm WALL INJECTION ON TOTAL NOx EMISSIONS FOR RADIAL SWIRLER (C) IN 140mm COMBUSTOR, MN=0.014, 600K.

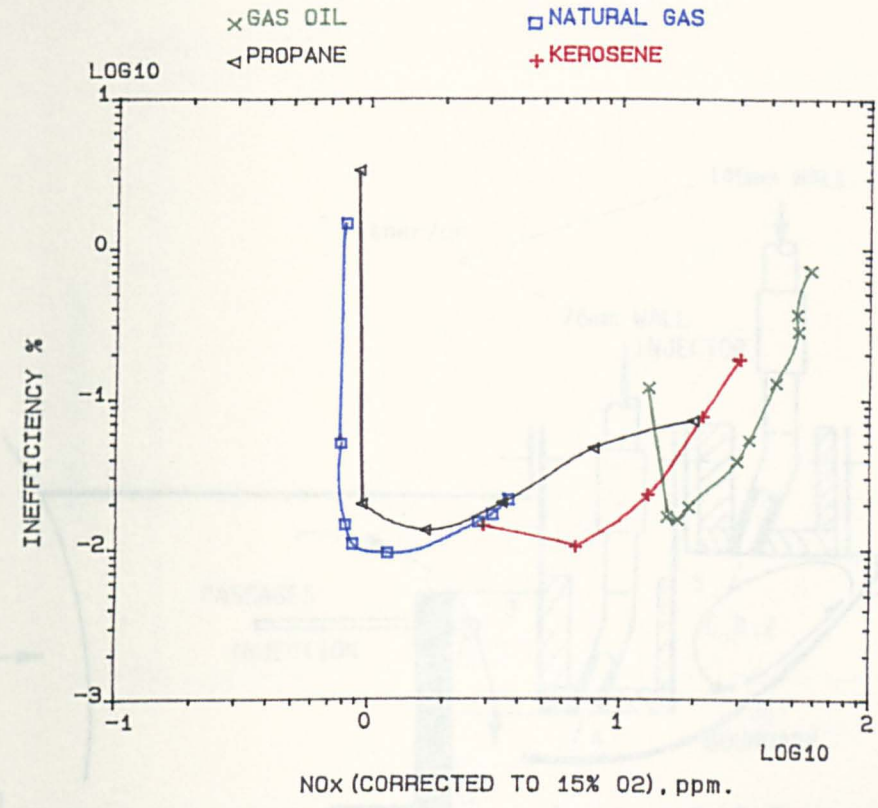

FIG.5.58 INFLUENCE OF FUEL TYPE USED WITH 76mm WALL INJECTION ON VARIATION OF CORRECTED NOx WITH COMBUSTION INEFFICIENCY RADIAL SWIRLER (C) IN 140mm COMBUSTOR. MN=0.014, TIN=600K.

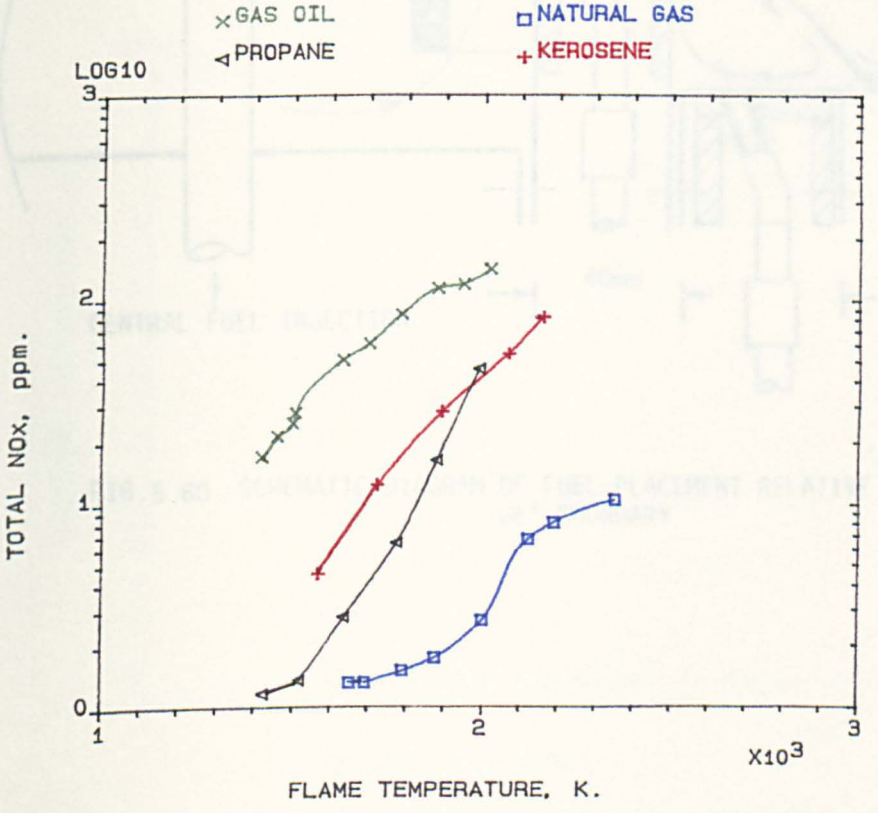

FIG.5.59 INFLUENCE OF FUEL TYPE USED WITH 76mm WALL INJECTION ON VARIATION OF NOx EMISSIONS WITH FLAME TEMPERATURE FOR RADIAL SWIRLER (C) IN 140mm COMBUSTOR. MN=0.014, TIN=600K.

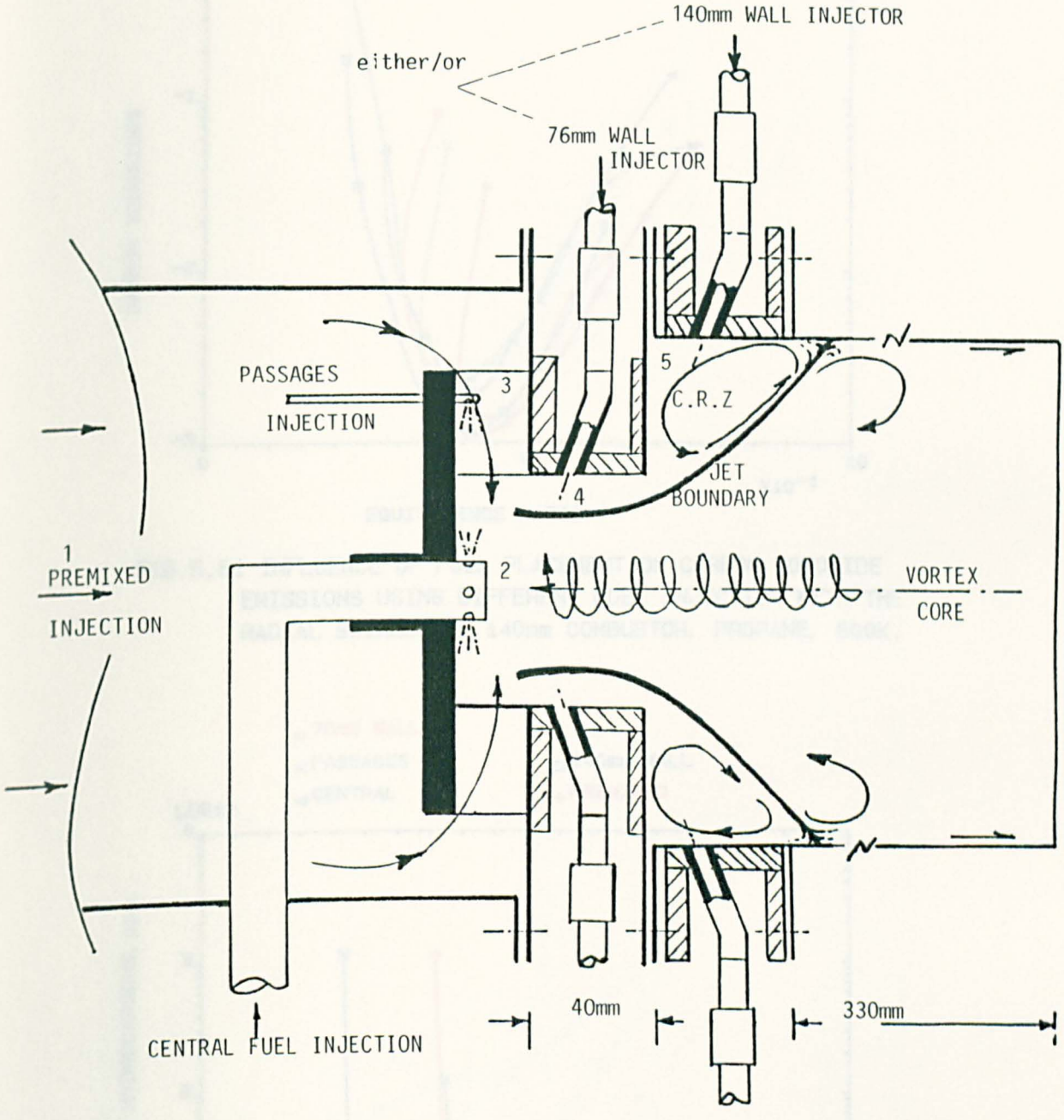

FIG.5.60 SCHEMATIC DIAGRAM OF FUEL PLACEMENT RELATIVE TO THE JET BOUNDARY

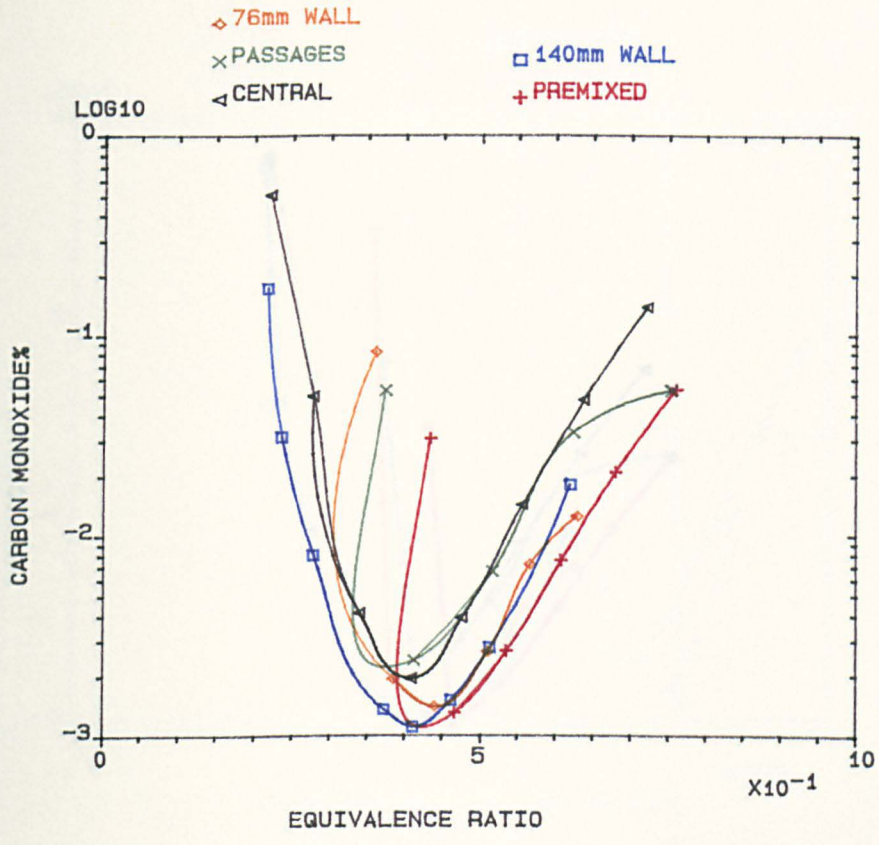

FIG.5.61 INFLUENCE OF FUEL PLACEMENT ON CARBON MONOXIDE EMISSIONS USING DIFFERENT FUEL INJECTION WITH THE RADIAL SWIRLER IN 140mm COMBUSTOR, PROPANE, 600K.

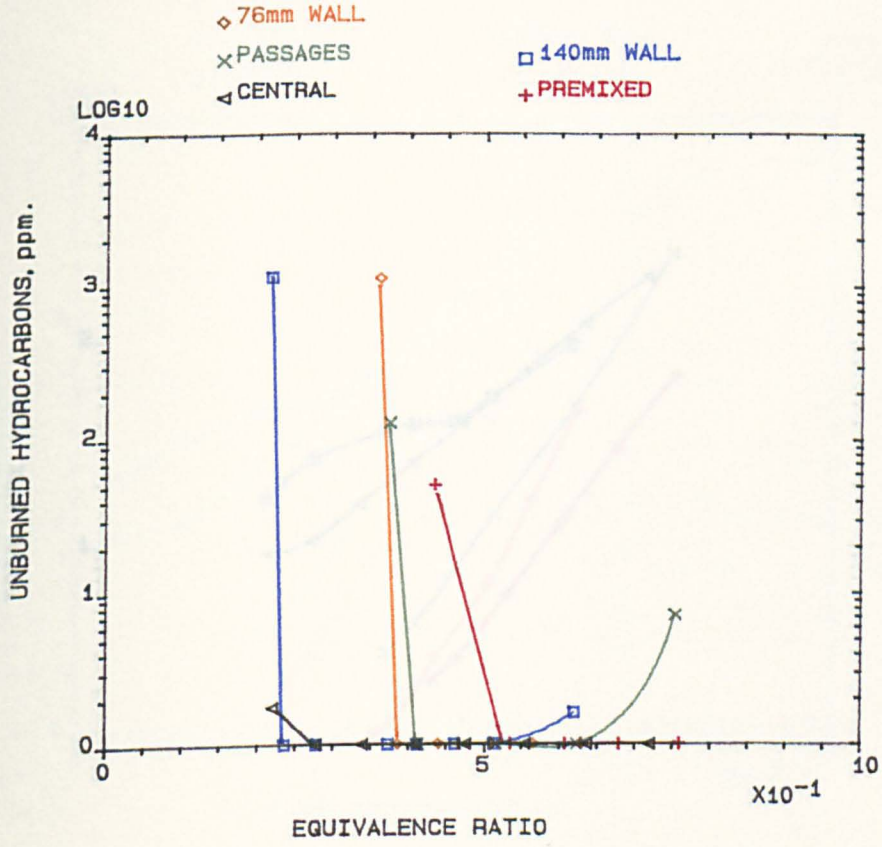

FIG.5.62 INFLUENCE OF FUEL PLACEMENT ON UNBURNED HYDROCARBONS EMISSIONS USING DIFFERENT FUEL INJECTION WITH THE RADIAL SWIRLER IN 140mm COMBUSTOR, PROPANE, 600K.

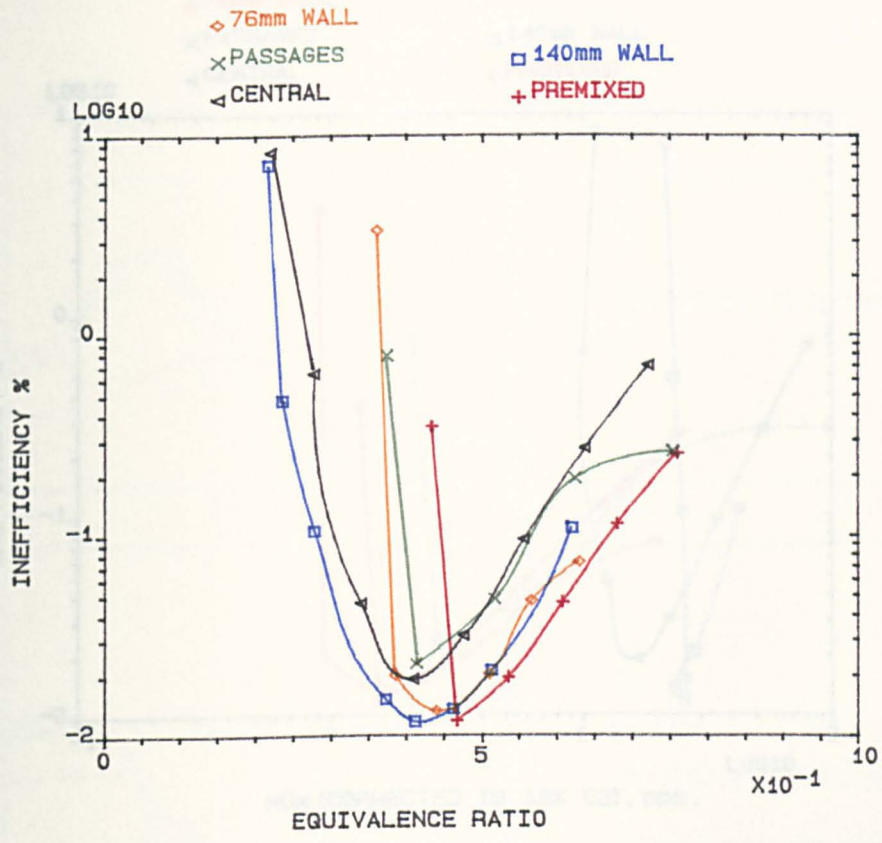

FIG.5.63 INFLUENCE OF FUEL PLACEMENT ON COMBUSTION INEFFICIENCY USING DIFFERENT FUEL INJECTION WITH RADIAL SWIRLER IN 140mm COMBUSTOR, PROPANE, 600K.

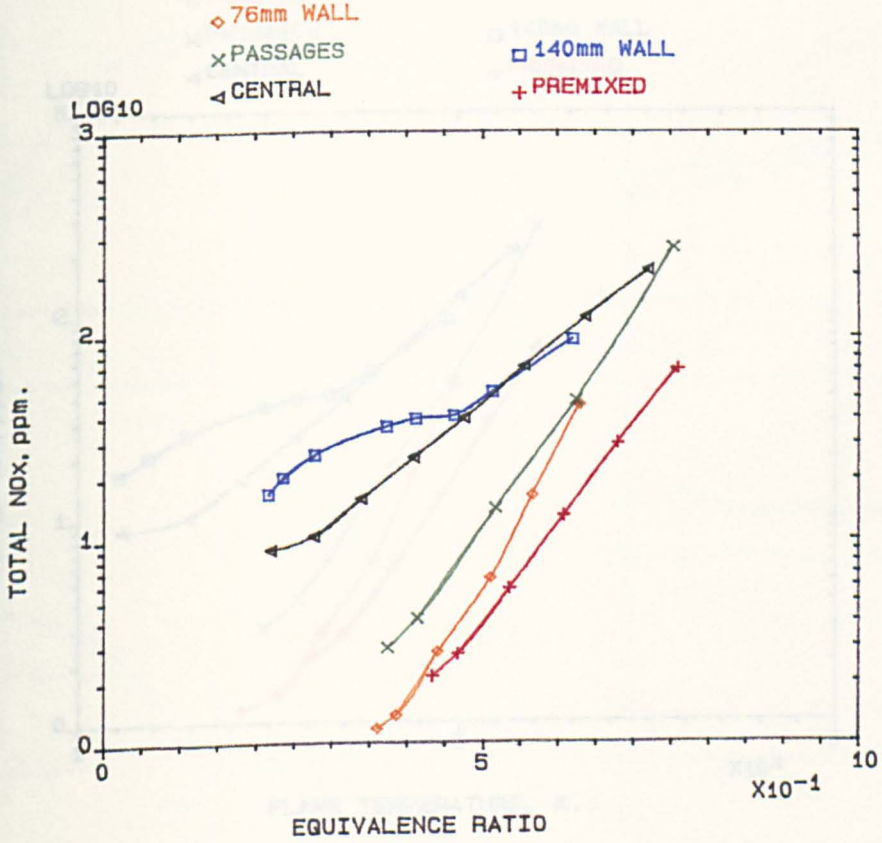

FIG.5.64 INFLUENCE OF FUEL PLACEMENT ON TOTAL NOx EMISSIONS USING DIFFERENT FUEL INJECTION WITH RADIAL SWIRLER IN 140mm COMBUSTOR, PROPANE, 600K.

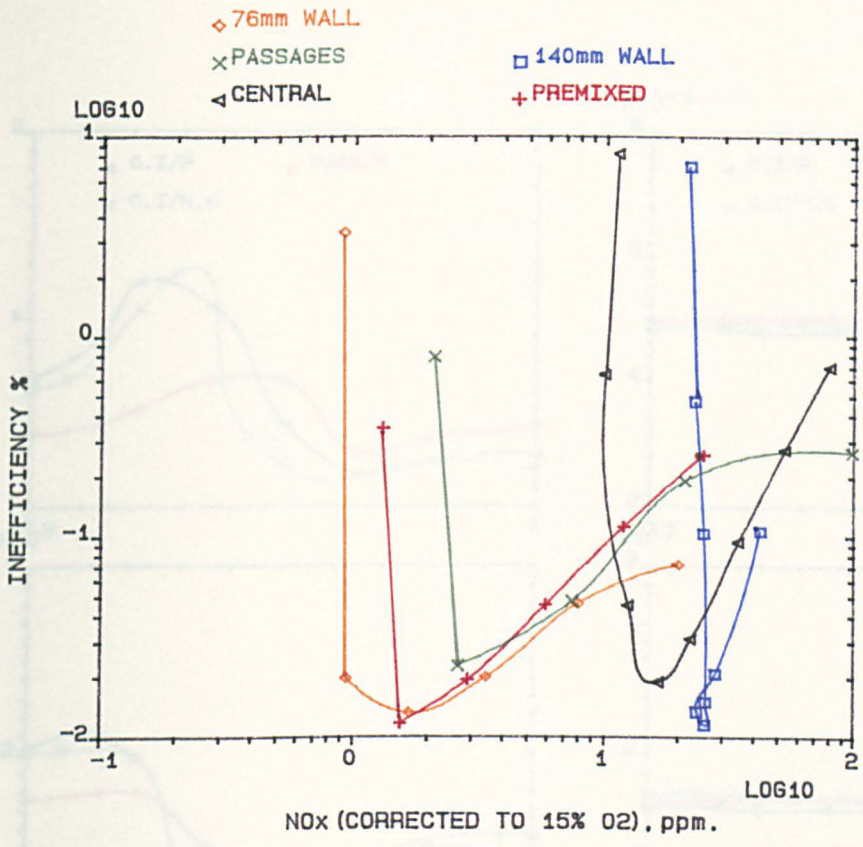

FIG.5.65 INFLUENCE OF FUEL PLACEMENT ON VARIATION OF CORRECTED NOX WITH INEFFICIENCY USING DIFFERENT FUEL INJECTION WITH RADIAL SWIRLER IN 140mm COMBUSTOR, PROPANE, 600K.

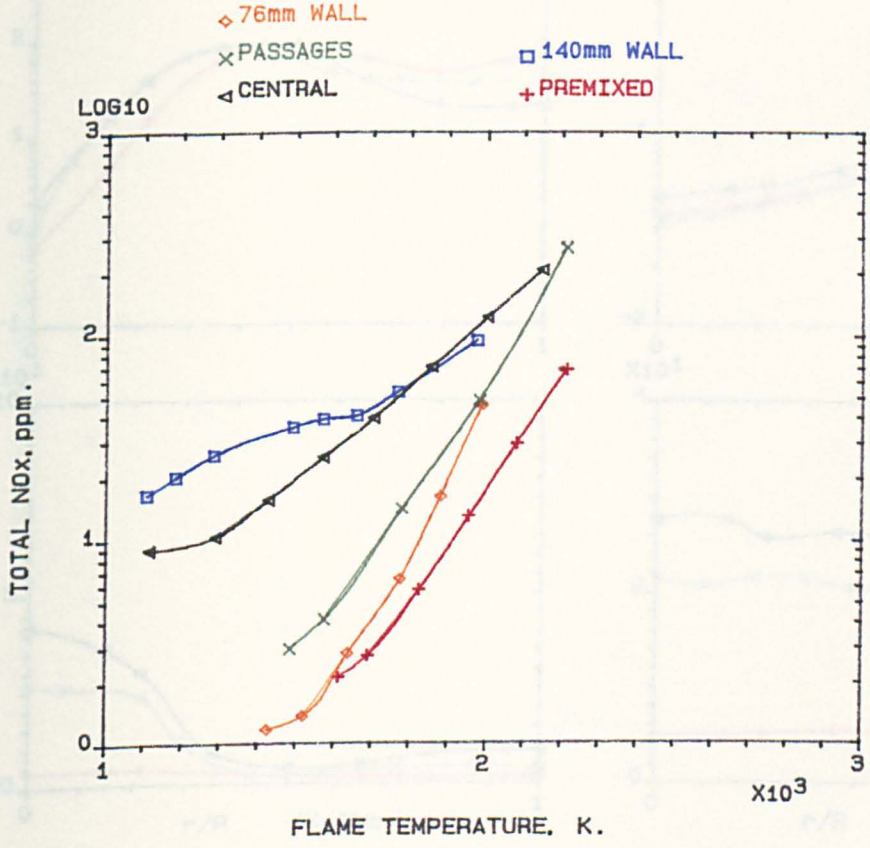

FIG.5.66 INFLUENCE OF FUEL PLACEMENT ON VARIATION OF TOTAL NOx WITH FLAME TEMPERATURE USING DIFFERENT FUEL INJECTION WITH RADIAL SWIRLER IN 140mm COMBUSTOR, PROPANE, 600K.

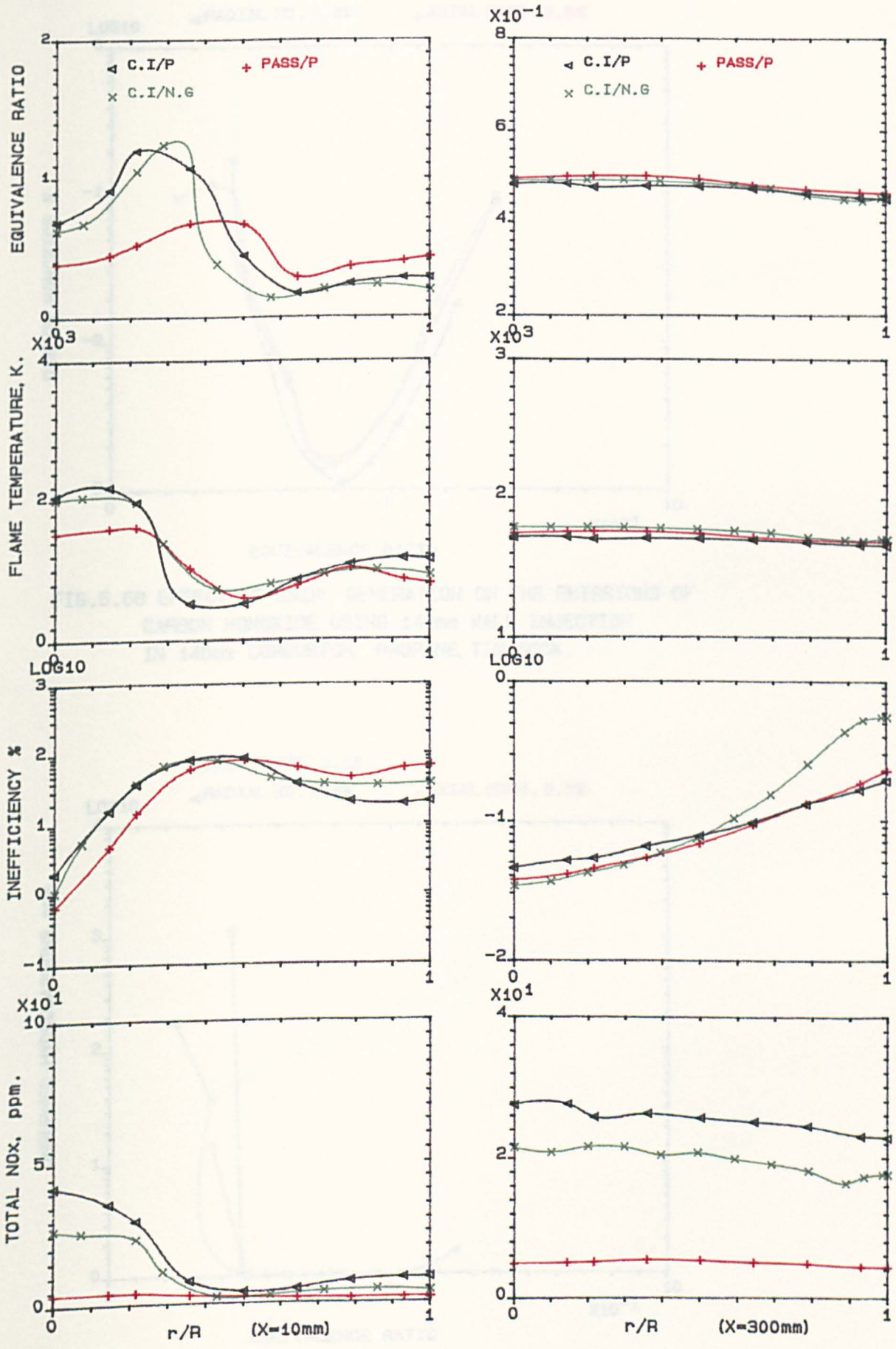

FIG.5.67 FUEL PLACEMENT INFLUENCE ON LOCAL SPECIES CONCENTRATION
MEAN EQR~0.42, RADIAL SWIRLER(B) IN 140mm COMBUSTOR, 600K.

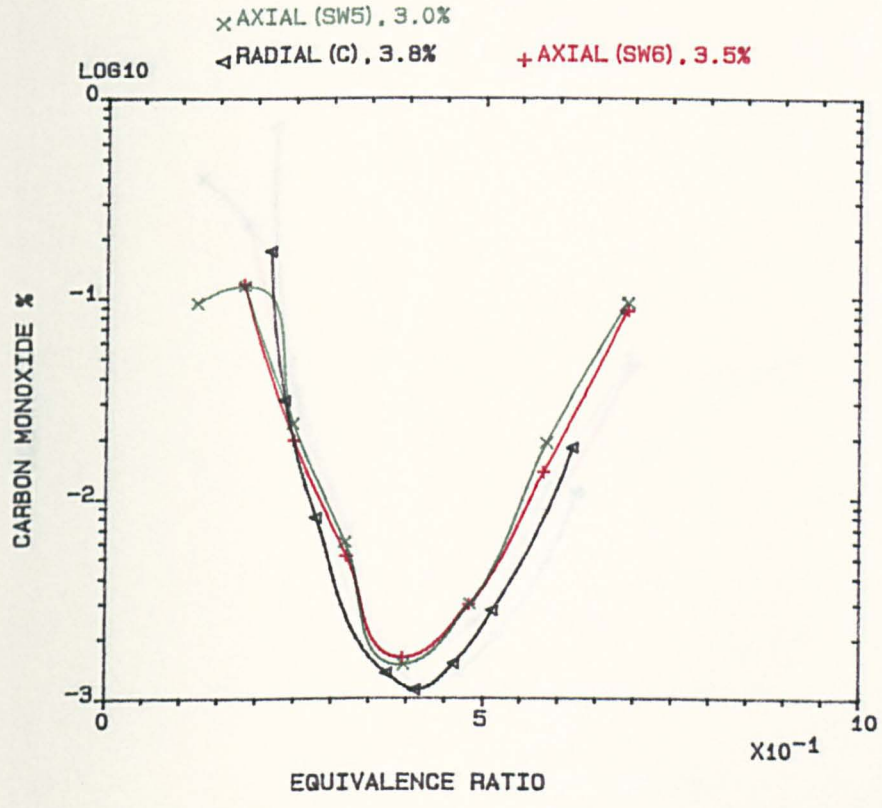

FIG.5.68 EFFECT OF SWIRL GENERATION ON THE EMISSIONS OF CARBON MONOXIDE USING 140mm WALL INJECTION IN 140mm COMBUSTOR, PROPANE, TIN=600K.

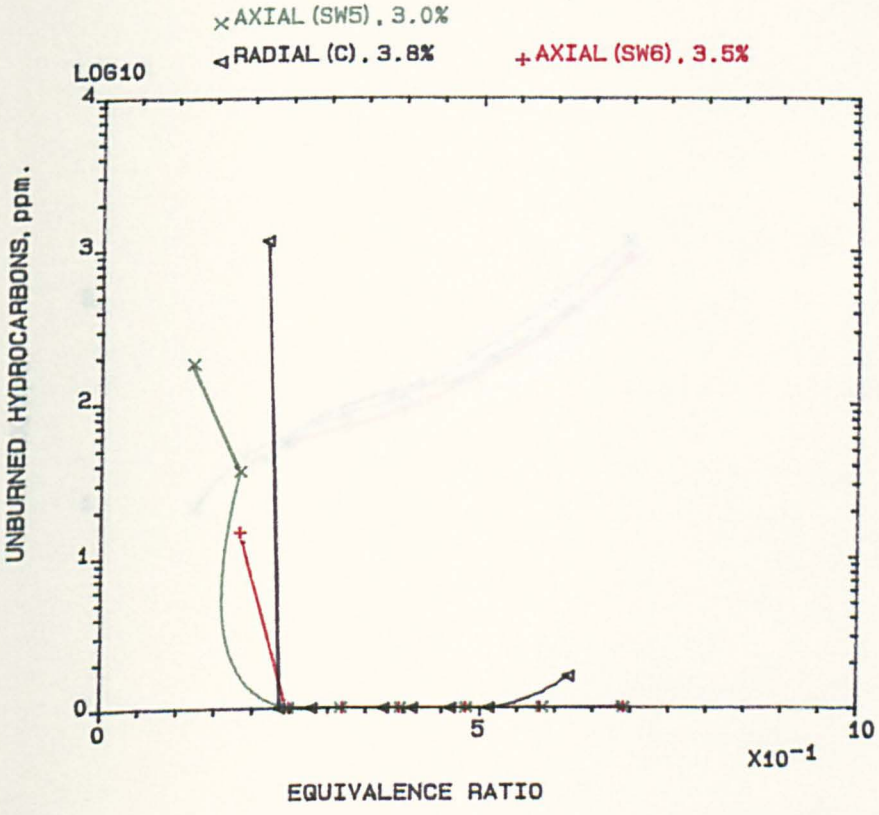

FIG.5.69 EFFECT OF SWIRL GENERATION ON THE EMISSIONS OF UNBURNED HYDROCARBONS EMISSIONS USING 140mm WALL INJECTION IN 140mm COMBUSTOR, PROPANE, TIN=600K.

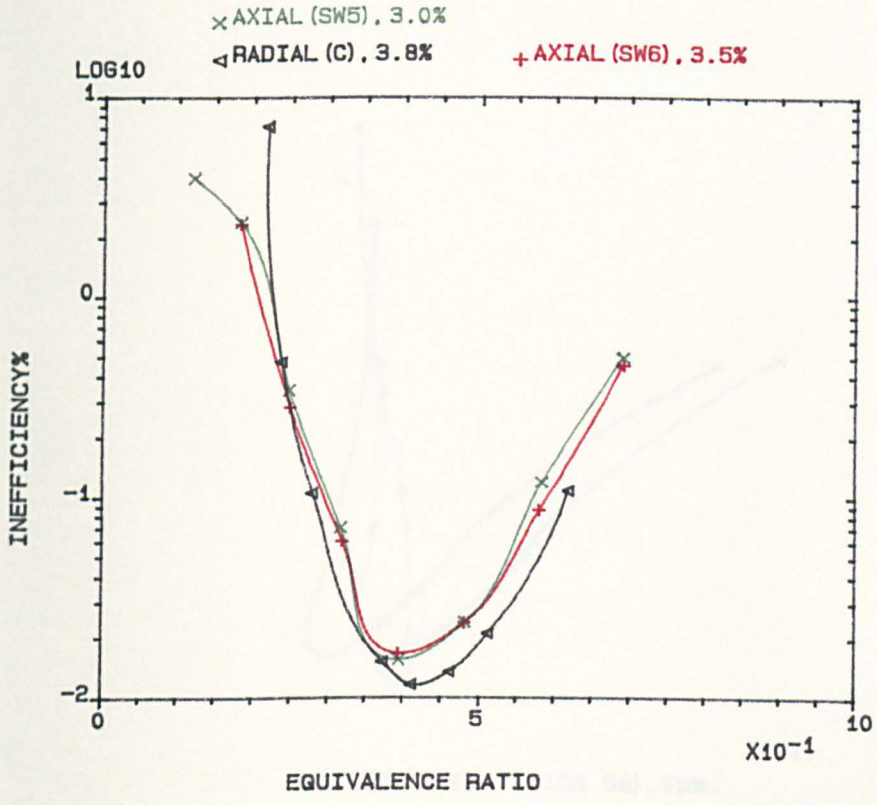

FIG.5.70 EFFECT OF SWIRL GENERATION ON THE COMBUSTION INEFFICIENCY USING 140mm WALL INJECTION IN 140mm COMBUSTOR, PROPANE, TIN=600K.

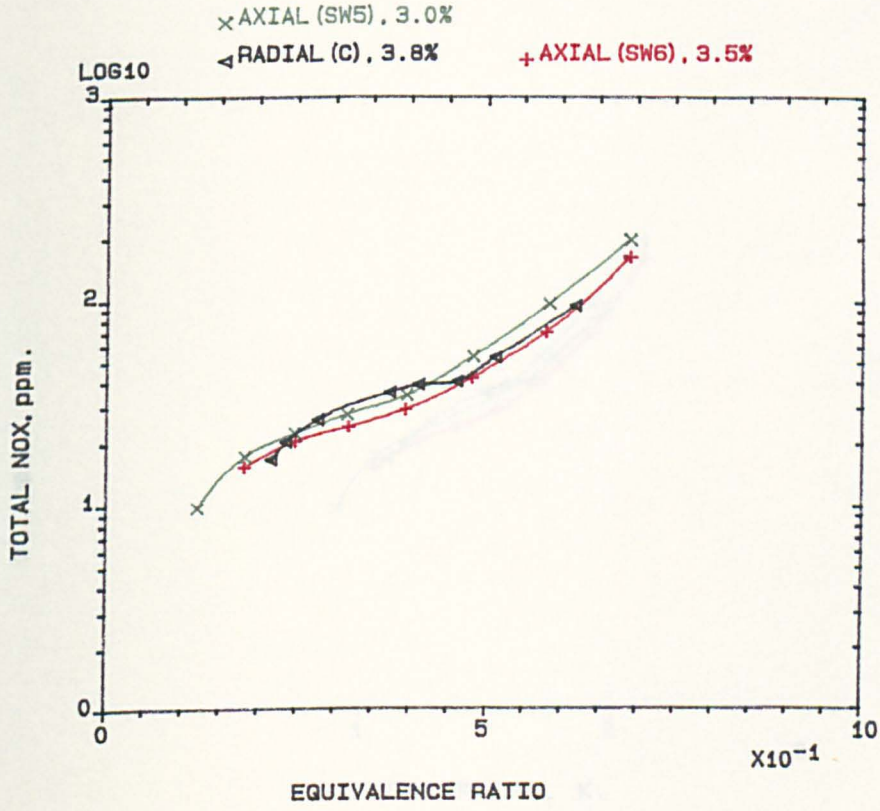

FIG.5.71 EFFECT OF SWIRL GENERATION ON THE EMISSIONS OF TOTAL NOx USING 140mm WALL INJECTION IN 140mm COMBUSTOR, PROPANE, TIN=600K.

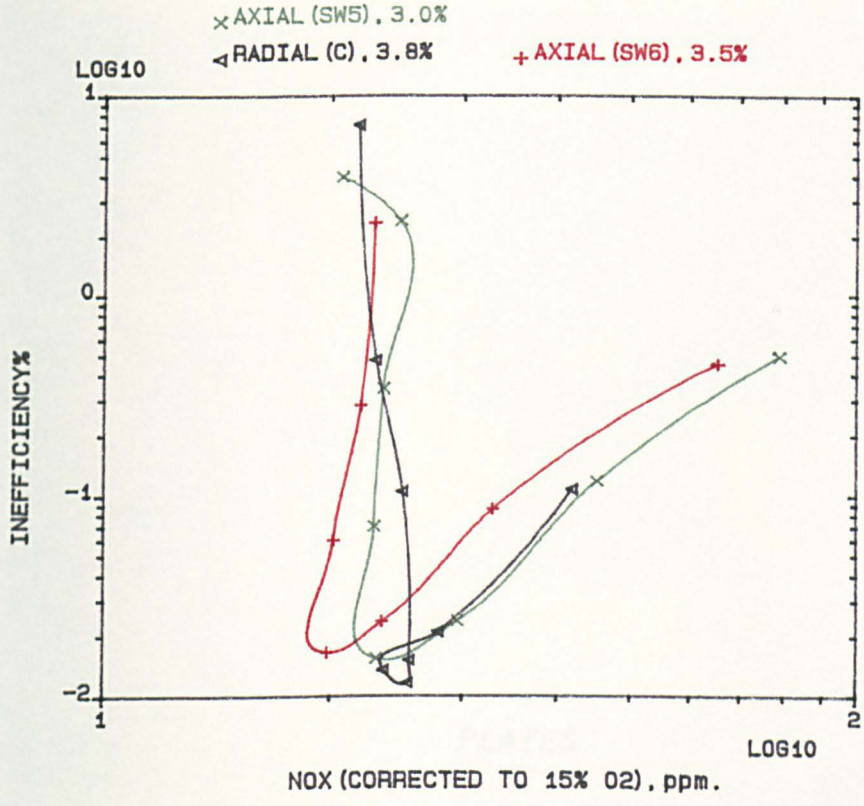

FIG.5.72 EFFECT OF SWIRL GENERATION ON THE VARIATION OF CORRECTED NOx WITH COMBUSTION INEFFICIENCY USING 140mm WALL INJ. IN 140mm COMBUSTOR, PROPANE, 600K.

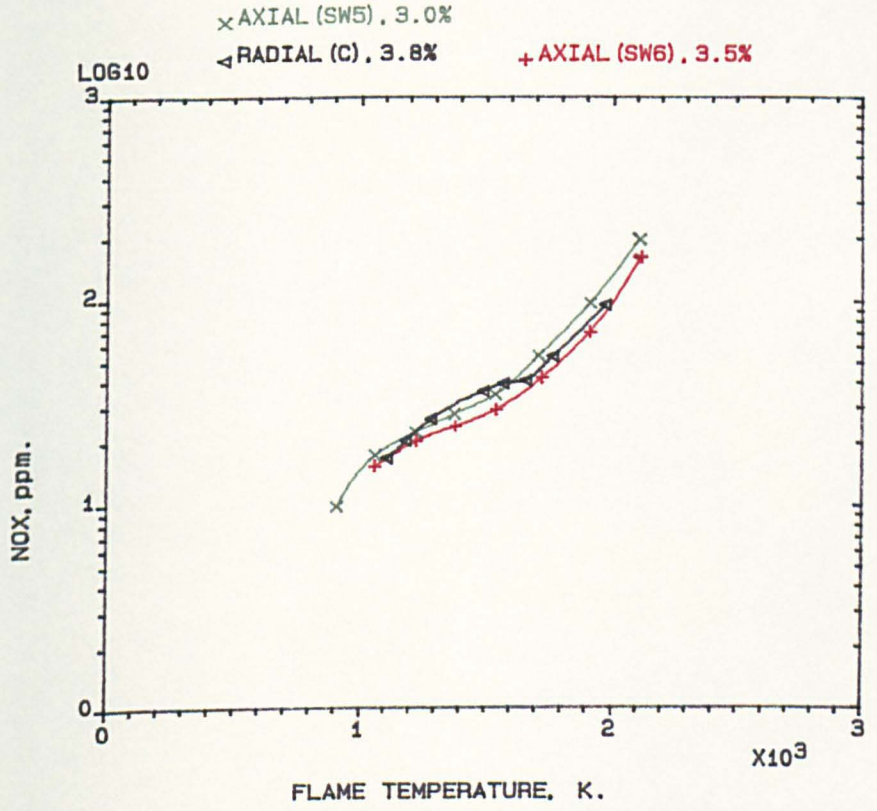

FIG.5.73 EFFECT OF SWIRL GENERATION ON THE VARIATION OF NOx WITH FLAME TEMPERATURE USING 140mm WALL INJECTION IN 140mm COMBUSTOR, PROPANE, 600K.

PLATES

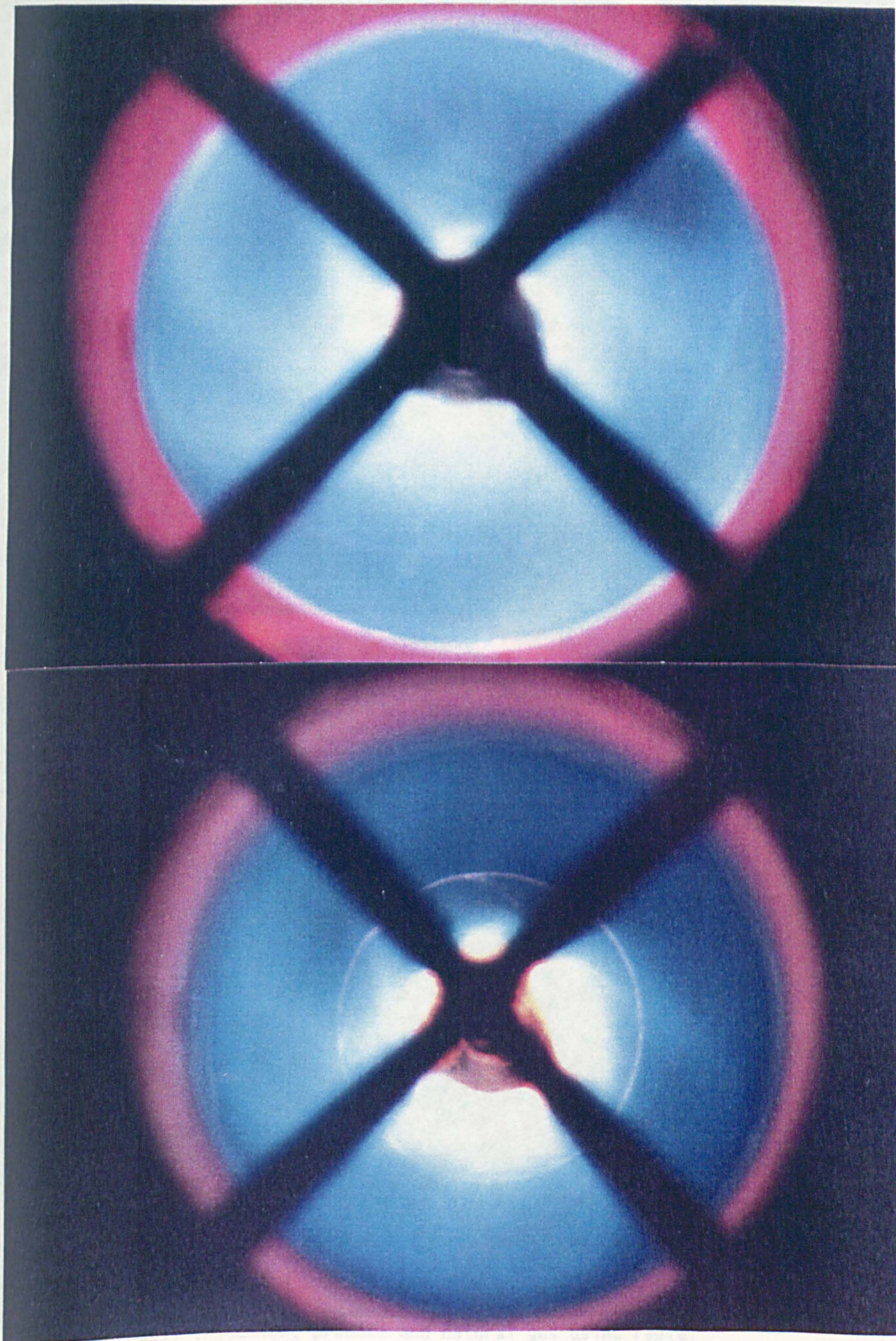

Plate 5.1 Kerosene and Gasoil passage injection using radial swirler(B) in 140mm combustor with pressure loss=5.1% and Tin= 600K EQR.=0.44.

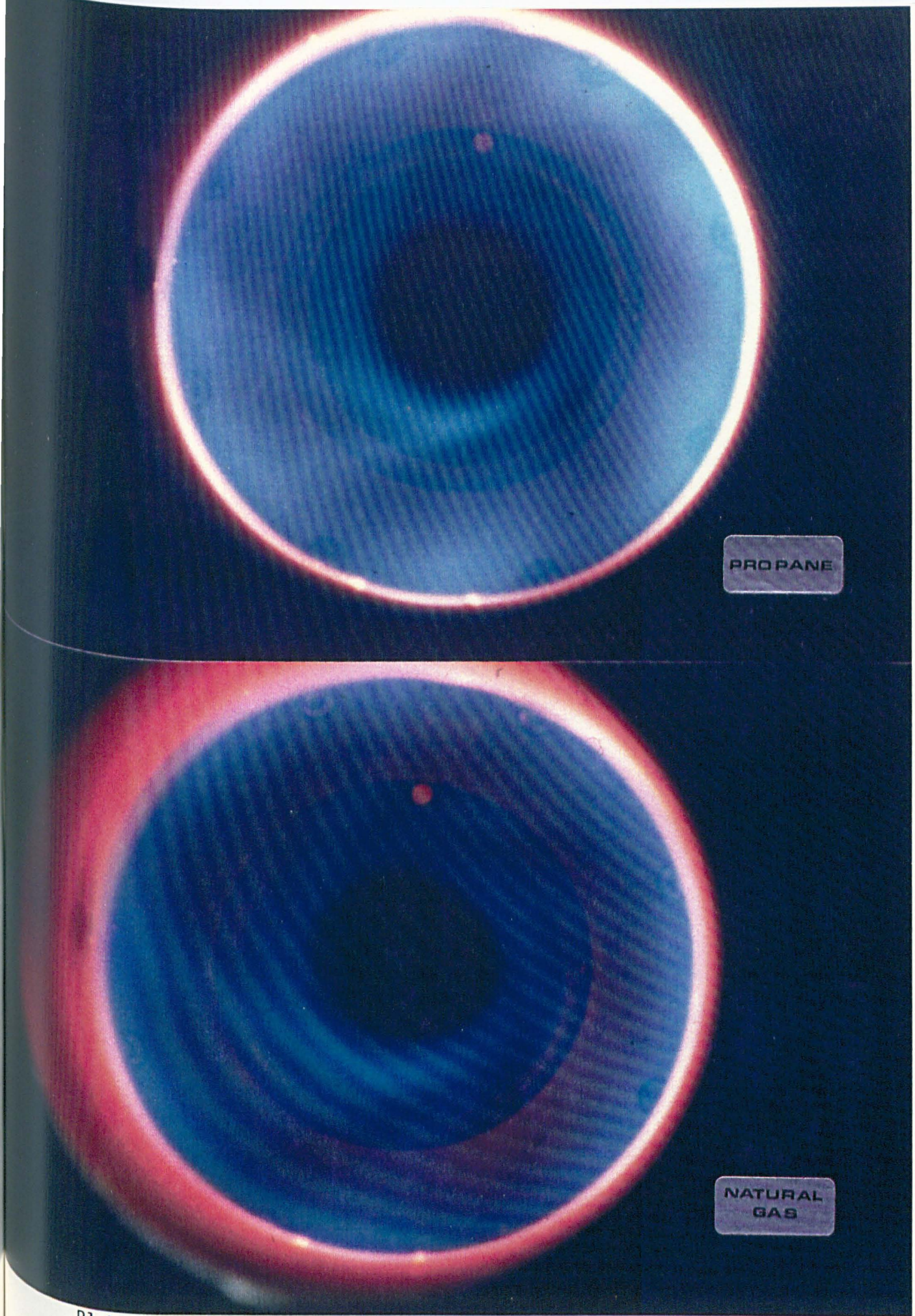

Plate 5.2 Wall injection, propane and natural gas using radial swirler(C) in 140mm combustor for EQR.=0.46 and pressure loss=4.2%, Tin= 600K.

CHAPTER SIX

CO-SWIRL AND COUNTER-SWIRL STABILISED FLAMES

6.1 INTRODUCTION

One of the common method of varing fuel-air mixing in industrial plant is to impart different amount of swirl to the combustion air. Changing the air swirl has the effect of altering the initial air direction ,velocity, turbulence and recirculation pattern in the combustion chambe. In gas turbine combustor, swirlers have been used to inject swirling air around the fuel injecter and coupled with the radial primary zone jets to establish a stable primary recirculation zone (1). For low emission gas turbines lean primary zones are required and for swirl systems this requires larger swirlers and a major increase on the 10% of the total air flow typically used for current primary zone swirlers. High air flow primary zone swirlers would operate with no radial primary zone jets, as this air would be incorporated into the swirler air. Various types of swirler designs have been investigated for this low emissions lean primary zone application (2-7). One design with the potential for good mixing was the counter rotating double axial swirlers(2,3).

In high velocity gas turbine flow systems fuel and air mixing requires high turbulence levels and these result from the combustor pressure loss. Whether this pressure loss is generated by a jet flow system or a swirl system, the air inlet aerodynamics generate shear layers which create the turbulence. For both swirlers and jet systems these shear layers are the zone of flame stability in lean burning systems (8-13). For swirlers the use of counter rotating systems may generate a larger shear region with more intense mixing characteristics than for a single swirler. The counter rotating action may also tend to dissipate the swirl so that in confined flows there is a more rapid decay of the high velocity outer swirl flow. Ahmad and Andrews(14,15) showed previously with axial swirlers that this high velocity outer region prevented the radial spread of the flame from the stabilising shear layer region and this was responsible for the poor performance of

single swirler systems. Hence, flames may spread radially more rapidly in a counter rotating swirler system.

For furnace applications, where there is a large expansion from the swirler, this problem does not arise as the outer swirl flow can expand rapidly and the decay of the swirl flow is more rapid. For gas turbine applications with large air flow swirlers the expansion from the swirler is limited by the combustor diameter, D, and decreases as the swirler diameter, d, increases to accommodate the higher air flow at the same pressure loss. However, this problem is not encountered with radial flow swirlers since the radial swirler outer diameter can be maintained constant and the vane depth increases to accomodate more air to achieve the pressure loss required. The expansion ratio for gas turbine applications should be more than 1.5, to create a corner recirculation zone and it is these regions which contribute to the rapid flame spread in furnace swirl burners (8-19).

6.2 REVIEW OF PREVIOUS WORK

There have been relatively few publications relating to the performance of double radial swirl flow systems, even though they are used in some combustion systems (41,43,44,46)

By comparing the co-swirl and counter-swirl systems Halthore and Gouldin(34) found that there was more dilution in counter-swirl system than co-swirl, which was consisted with the higher turbulence levels observed in the mixing layer between the jets for counter-swirl (35). In both cases ,they were using premixed natural gas and their radial flow configuration was similar to the second co-swirl assembly used in the present work. Bluncke et al(41) investigated a counter swirl airblast atomizer experimentally and numerically. The ratio of primary to secondary air swirlers was 1 to 2.25. They reported that the flow pattern shows the typical features of swirl flow with an inner recirculation zone and that the general features of the flow could be predicted with reasonable accuracy.

The work reported by Drake and Hubbard(43) invovled co-rotating swirlers with tangential air vanes. The expansion ratio was much higher than the present

work. However, their work showed that the position of maximum external recirculation moves towards the burner outlet as the swirl intensity was increased in the primary air swirler while maintaining the secondary air swirler at lower swirl intensity. This trend was reversed at higher secondary swirler vane angles. Further, they reported the magnitude and position of the recirculation zones were important in achieving the optimum combustion conditions.

Most of the previous investigation were done on the action of double co-rotating or counter-rotating axial swirler because they were more commonly used than the radial flow swirler. A series of combustor tests were conducted by Mularz et al (29) to evaluate three improved designs of swirl-can combustor modules, using axial swirlers and their objectives were to obtain low levels of exhaust pollutants while maintaining a high combustion efficiency at combustor operating conditions. The swirl can modules consisted of three components; a carburetor, an inner swirler and a flame stabiliser. The functions of the module were to mix fuel and air, swirl the mixture, stabilise combustion in its wake and provide large interfacial mixing areas between the bypass air around the module and combustion gases in its wake. One of the combustor models incorporated concentric swirlers for each module, with the air swirling in opposite directions from the two swirlers (counter swirl). The fuel was injected downstream of the swirlers by splashing against a 1.9 cm diameter disk attached to the inner swirler hub. They found that their swirl-can combustor model performed with high combustion efficiency at all conditions tested but the NOx emissions were still higher than the maximum allowable level of 20ppm which was needed to achieve the 1979 EPA emissions standards.

Thompson et al (30) examined the structure of unconfined propane flames stabilised on a NASA contra-swirl can, similar to that used by Mularz et al (29). In their investigations the diameter of the duct surrounding the can was selected so as to provide a bypass air flow rate of 82.2% with 7.1% and 10.7% air flow for the inner and outer swirler respectively. The fuel supply nozzle had been found to provide the best flame structure when placed close to the inner swirler hub, 1mm

upstream and accurately centralised. A non-axial location or a significantly larger distance between the fuel inlet and swirler hub caused significant changes to the flame structure. A highly compact flame was obtained over a narrow band of fuel-air ratio and was confirmed by chemical concentration profiles, temperature profiles and sodium chloride seeding experiments. Together with the axial recirculation core, they found that the flames also had a torroidal recirculation region over the bluff region between the inner and outer swirlers. However, at lower reference velocities, their laser doppler velocimetry measurements showed that a secondary recirculation region was not present.

One of the most intensive investigations of swirler designs was undertaken as part of the NASA swirl module combustion system development (3,4). This compared the performance of single and double swirler designs for swirl systems with a large proportion of baffle air bypass flow. The swirler air flow was varied from approximately 10-40% with the remainder passing around the swirler over a baffle. For this system it was found that the more complex counter rotating double swirler designs had little advantage compared with simple single swirlers(3).

6.3 PRESENT APPROACH

The radial swirlers combustor and fuel injector configurations used for the present work are shown in Fig.6.1 consisted of two concentric confined swirling jets. The first configuration comprised two large radial swirlers (B) and (C) and the second configuration comprised the small swirler (A) and large swirler (C), For both cases the radial swirler (A) and (B) was the primary swirler. The radial swirler (C) was either co-rotating or counter-rotating relative to the other swirlers. For the first combination (B&C) the expansion ratio for the flow were 1.0 and 1.84. However, for the second configuration the expansion ratio were 1.9 and 3.5 for the small swirler (A) and 1.0 and 1.84 for the large swirler (C). The second configuration was tested only with co-swirl condition.

For both assemblies the air split between the primary and secondary radial swirlers were 57% and 43% of the total flow respectively. This gave the ratio of

the primary to secondary air jet of 1.33/1. The motivation for conducting such work was to provide an improved understanding of combustion processes in swirling flow controlled by radial flow swirlers. Two method of fuel injection were used, they were direct central radial and 76mm wall (peripheral) fuel injection. Two air inlet condition with propane fuelled through a central injecter were tested which simulated the low and high power operation (ie. 400K and 600K inlet temperature). The air flow were simulated 60% of the total primary zone air with a Mach Number of 0.028 to give an approximately 4.4% pressure loss.

6.4 WEAK EXTINCTION

The measured weak extinction results are summarised in Table(6.1), together with the weak extinction of a single radial swirler for comparison. For central propane and natural gas injection with radial swirlers (B&C) at 600K the swirl direction had a little influence on the weak extinction but at 400K the co-swirl system was more stable than the counter-swirl system. Visual observation of the co-swirl case, at 600K showed the flame at very near weak extinction setback inside the swirler core. Thus, for direct central propane or natural gas injection the generation of local rich zones extended the flame stability limits. For wall injection the stability with liquid fuels was poor but similar to that for propane. With counter swirl the liquid fuel central injection weak extinction were much lower than for propane, but for wall injection were again similar. The weak extinction was much worse than for propane at 600K

For central liquid fuel injection Table(6.1) shows that for central injection with gasoil but similar for kerosene with co-swirl. The co-swirl system for kerosene was much superior to the counter-swirl at 600K. This was possibly due to the evaporisation rate with the counter-swirl system having a slower vaporasation rate and not achieving sufficient fuel recirculation into the core region.

Using the peripheral or the 76mm wall injector drastically reduced the flame stability with central propane and kerosene for co-swirl and for propane with counter swirl. The swirl direction had little influence on the stability for wall injection.

For small radial swirler configuration (A&C), the central injection system stability were deminated by the rotational field which was imposed by the small radial swirler (A) outlet flow field. This had a poor stability with central injection as discussed in chapter four, thus poor stability limits were found for the A/C swirler combination. However, for peripheral injection the results show that the weak extinction was demonited by the expansion immediatly after the 76mm injecter because the results show a similar trend to that of (B&C) essembly with wall injection. Comparing the weak extinction results to that of a single swirler one can deduce that for assembly (A&C) using peripheral injection the stability limits were controlled by the rotational action of the large radial swirler (C).

6.5 WALL STATIC PRESSURE AND TEMPERATURE PROFILES

Figs.6.2 - 6.35 show the measured combustor wall temperature and static pressure/dynamic head as a function of combustor length. For the co-swirl system with central fuel injection, the main features of the wall static pressure and temperature profiles were the initial low static pressure which indicated a high velocity corner recirculation zone upstream of the impingement on the wall about 50mm from the swirler outlet. The corner recirculation zone was relatively high in temperature which shows that the flame development was inside that 76mm section. The point of impingement on the combustor wall where the dynamic pressure was converted into static caused a peak in the wall static pressure profiles. This region had low wall temperatures especially at 400K. At wall impingement point the flow split into two counter recirculation zones, upstream and downstream of the impingement point. These create the two minimum values in the wall static pressure profiles.

The delay in flame development with liquid fuel was caused by the delay in the vaporisation process, during which the droplet was under the action of centrifugal forces created by the swirl flow. These forced the droplets radially outwards towards the wall region, thus most of the droplets will be concentrated in the high velocity outer swirl flow and the vapor concentrations in the flame stabilizing shear layer will be lower than for gas injection. For the gasoil case as shown in Fig.6.9, the flame was likely to be initiated in the wall region as indicated by the relatively high temperature at 75mm away from the outlet. However, for the kerosene the flame propagation started much earlier on as shown in Fig.6.11, but both profiles follow similar trends as the 400K case with propane Fig.6.5.

Using the 76mm wall injection system a hot outer recirculation zone was created. The fuel injected can be carried away by the outer jet boundary, more mixing will take place after the swirl jet impinges on the wall and splits. The main feature of this type of injection with the co-rotating double swirler system was the initial high wall temperature. This was due to the development of a hot region in the corner recirculation zone caused by an early flame development near to the swirler outlet region. However, the flame development was slow along the combustor length reaching its peak just by the point 200mm away from the outlet as shown in Figs.6.7 and 6.13.

For the counter-swirl system, the point of flow impingement moved further away from the swirler outlet. This was due to the reduction of the tangential velocity imposed by the counter rotating action by swirler (C), as can be shown in Figs.6.16 - 6.23 and Figs.6.32 - 6.33. The size of the corner recirculation zone was larger with the counter-swirl system but the reaction zone shape was the same as the co-swirl system as reported by Halthore and Gouldin(34). Their results confirm that the reaction zone began further upstream of the recirculation zone and for the most part lies outside it for counter-swirl compared with co-swirl the same reason Figs.6.15, 6.17 and 6.23 show that there was a more uniform axial flame development than the for co-swirl system.

Visual observation of the counter-swirl flames showed for central fuel injection with propane at 600K, that below an equivalence ratio of 0.3 the flame was stabilised in the 76mm section and for higher equivalence ratios the flame started to flash in and out of the 76mm section until the flame stabilised in the 140mm combustor. The reason was that local rich zones were generated close to the swirler. At weak mixture these stabilises the flame close to the swirler whereas at rich mixture the flame was too rich to burn and developed further downstream. In the case of the 76mm wall injection fuelled with propane at an inlet temperature of 600K, the flame tended to move inside the swirler outlet section at an equivalence ratio of 0.53. This is understandable from the work done by Myers and Lefebvre(38), they shown that the flame speed increased with the fuel/air ratios. In the present work the burning velocity exceeded the incoming flow velocity and the flame tended to go inside the extended section towards the points where the fuels meets the incoming flow. For central natural gas injection in the counter- rotating system, the flame tended to move inside the 76mm outlet towards swirler (B) for equivalence ratio below 0.29 where the flame started to flash-in and out of the 76mm section, then it sat back into the core of radial swirler (B).

The co-swirl jets generated by the combination of radial swirlers (A&C) had static pressure profiles as shown in Fig.6.24 which indicates the presence of three strong recirculation zones. With central injection the profiles were substantially different from the B and C swirler in Fig.6.2. The aerodynamics of this A&C swirler combination are complex and dependent on the method of fuelling. The central and wall injection static pressure profiles in Fig.6.24 and 6.26 are quite different. The wall temperature profiles showed that the flame development took place over the first two recirculation zones which occupied a greater axial distance from A&C than B&C. Both flow visualisation and internal gas composition traverses are required to understand these complex aerodynamics.

In general, the propane flame was stabilised for both mode of injections ie. central and wall injection by making use of the shear layer boundaries of the inner

and outer recirculation zone and the jet boundary imposed by the swirling flow. However, for kerosene the flame was stabilised by vaporised fuel recirculated into the core region, by which stage it will be well mixed with air. Hence, combustion was governed by the portion of kerosene which was recirculated into the core region. Slow vaporisation of kerosene and gasoil is thus a key to the poor flame stability. The action of centrifugal forces in this situation is two fold: firstly, in the initial outer swirl flow any vaporised fuel with density greater than that of air will be forced to remain in the wall region, secondly, when the combustion has been initiated in the outer swirl flow, downstream of the recirculation zone, centrifugal mixing of burnt and unburnt gases enhances the mixing and rates of flame spread which is in agreement with the work reported by Ahmad and Andrews(36,37) for axial swirlers.

6.6 CO-SWIRL STABILISED FLAME

6.6.1 MEAN COMBUSTOR EXIT EMISSIONS

6.6.1.1 Fuel type influence on combustion performance

The fuel type influence on metered mean emissions are illustrated in Figs.6.36 - 6.41. The carbon monoxide emissions are shown as a function of the metered equivalence ratio in Fig.6.36 at inlet temperature of 600K and for four different fuels. The similarity in profiles between CO and combustion inefficiency as a function of equivalence ratio in Fig.6.38 is an indication that the combustion inefficiency was mainly due to the carbon monoxide emissions and hence was caused by locally rich zones in the heat release region. The combustion inefficiency in Fig.6.38 summerises the net effect of CO and UHC in Figs.6.36 and 6.37 respectively. Thus it is useful way of presenting the combined emissions. However, the kinetic behaviour of the combustion reaction in such that for lean mixture both rates of production and oxidation of CO increase with increasing equivalence ratio. Therefore, Figs.6.36 - 6.38 indicate that initially the rate of CO oxidation exceeded the rate of production, thereby decreasing CO and UHC emissions. Hence combustion inefficiency decreased until the equivalence

ratio are reached above which the rate of production of CO exceeded the oxidation rate.

Fig.6.39 show that the natural gas contributed to the NOx emissions between 30% to 50% less than what propane generated.

Liquid fuels exhibited slightly larger combustion inefficiencies than gaseous fuels. That was due to the vaporisation delay which caused a slower flame development. This is shown by comparing the wall temperature profiles in Fig.6.3 for propane and 6.11 and 6.9 for kerosene and gas oil. The very low NOx emissions for kerosene and gas oil indicate that there was no deterioration in mixing with liquid fuels. The lower residence time at high flame temperature for liquid fuels probably produced the low NOx emissions. These liquid fuel NOx emissions are the lowest of any swirler configuration. The optimum NOx corrected to 15% oxygen in Fig.6.40 is 3.5ppm for kerosene and 8ppm for gas oil. There are lower NOx emissions than for passage injection in chapter five. However, it is possible that at pressure the vaporisation delay will be eliminated and flame will develope more quickly. The NOx level then increase to be closer to that of propane.

6.6.1.2 Central fuel injection combustion performance

In previous work, the small 40mm outlet diameter radial swirler A with a large blade depth had a considerable partial premixing of fuel and air upstream of the swirler exit plane. This achieved low NOx emissions, but with an inadequate stability margin. In the present work it was combined with the larger radial swirler C, with an improved stability However, the stability improvement has not of the order of the swirler flow split and hence considerable swirler air mixing must occur before the shear layer stabilising region.

The mean combustor exit emissions are illustrated in Figs.6.48 - 6.53 for central radial injection. Due to the fuel restriction in the 76mm wall injecter, the test for natural gas was terminated. The tests were not carried out with liquid fuels

for central injection due to the noise generation.

Figs.6.48 - 6.49 shows the CO and UHC emissions as a function of metered equivalence ratio for central radial injection with the co-swirl system for the combination of A&C as compared with B&C for the same inlet test conditions. The combination of A&C showed a slight improvement in CO and UHC emissions for central gaseous fuel injection and reduced the NOx emissions from 10 to 7ppm at 15% oxygen for natural gas, as shown in Figs.6.52.

6.6.1.3 Wall injection combustion performance

The A&C and B&C wall injection results are compared in Figs.6.54 - 6.59 for propane and kerosene. For propane the A&C results were very similar to B&C for both CO, UHC and NOx emissions. For each emission component A&C with wall injection was slightly worse than B&C. The low NOx characteristics of 76mm wall injection were maintained with the A&C co-swirl system, but there was no advantage of A&C compared with B&C. For kerosene A&C was much worse than B&C, both in terms of NOx and combustion efficiency. Visual observations of the propane flames shows that increasing the equivalence ratio with this system using central fuel injection will tend to let the flame goes out of the 76mm section to the expansion region of 140mm combustor and vice versa for lower equivalence ratios. However, the situation was different for the 76mm wall injection where the flame tended to go inside the 76mm section and by gradually decreasing the equivalence ratio the flame tend to leave the 76mm section to burn in the outer recirculation zone. This gives some indication of why the NOx emissions were high at large equivalence ratio for both modes of fuel injection. In general, the NOx emissions for A&C combination were lower than B&C combination using central fuel injection but the opposite was found using the 76mm wall injection as shown in Fig.6.59.

Low NOx emissions are of little consequence unless they can be achieved with a combustion inefficiency and NOx correlation in an important method for assessing the viability of low NOx systems. The present results for both co-swirl

systems and fuel injection modes are shown in Figs.6.52 and 6.58. The optimum low NOx conditions compatible with lowest combustion inefficiency are summarised in Table(6.2).

6.7 COUNTER-SWIRL STABILISED FLAME WITH CENTRAL FUEL INJECTION

6.7.1 Influence of fuel type on combustion performance

The B and C swirler combination was converted to counter swirl by reversing swirler C and inserting a splitter plate. The metered mean combustor exit emissions are shown in Figs.6.42 - 6.45. These figures demonstrate the major species emissions as a function of equivalence ratios for natural gas, propane and kerosene. For gasoil fuel there was unsuccessful attempts in igniting the fuel which was due perhaps to the rate of vaporisation or atomization characteristics that makes very hard to light-up. Propane and natural gas had similar CO and UHC emissions with a similar combustion inefficiency as shown in Figs.6.42 - 6.44. The equivalence ratio at which the UHC and CO increases was richer for natural gas, 0.45 compared with 0.35 for propane. Kerosene CO and UHC emissions were much higher than for propane or natural gas, indicating an atomisation problem with counter swirl which may be associated with the more rapid jet spread and velocity decay giving lower atomisation velocities.

The greater rate of swirling jet spread due to the two counter rotating resulted in earlier flame stabilisation as was shown by the wall temperature profiles. However, the most effective shear layer mixing did not increase the NOx emissions due to the earlier flame stabilisation, as shown in Fig.6.63. All these fuels with counter rotating jet and central injection gave very low NOx emissions as shown in Figs.6.45 - 6.47. The very low kerosene NOx results was due to the slow flame development and poor efficiency. The natural gas NOx emissions was substantialy below that of propane with optimum of 2.5ppm at 15% oxygen and 0.1% inefficiency close to that of passage injection into swirler B in chapter five. The lower NOx from natural gas , which was a factor of 4 at the same conditions, may have a contribution due to different near injector mixing due to the low molecular weight and hence high diffusivity of natural gas which means that the fuel quickly disperses in the turbulent regions of the primary zone.

These results show that central injection with counter rotating radial swirlers has ultra low NOx characteristics with a wide stability limit. It thus has a major stability benefit over the other ultra low NOx configuration discussed in this Thesis.

6.8 COMPARISON BETWEEN CO-SWIRL AND COUNTER SWIRL SYSTEM

6.8.1 Using central radial injection

The carbon monoxides and unburned hydrocarbons results at 600K and 400K as a function of metered equivalence ratio are shown in Figs.6.60 - 6.61 for propane central injection in co-swirl and counter-swirl system with the combination of (B&C) radial swirlers. Similarity, in the emissions of CO and UHC was exhibited by both systems at 600K inlet temperature. However, at 400K inlet condition the counterswirl had CO and UHC emissions and a deterioration in the stability limits. That effected the combustion inefficiency. However, co-swirl system premoted higher combustion efficiency than the counter-swirl as demonstrated in Fig.6.62. In general, the inefficiency difference were small and were predominantly due to CO emissions This is confirmed by the similarity in CO emissions profiles in Fig.6.60 and that of combustion inefficiency Fig.6.62.

Higher NOx emission levels was promoted by the co-swirl system as shown in Figs.6.63 - 6.65. The correlation between combustion inefficiency and NOx corrected to 15% oxygen and day humidity is shown in Fig.6.64. This shows that the counter-rotating swirlers system contributed less corrected NOx than the co-rotating system, the lowest being 3-5ppm compatible with minimum combustion inefficiency of 0.1% for 600K inlet temperature. The NOx corrected for the other conditions were below 20ppm which is within the EPA regulations.

6.8.2 Using 76mm wall injection(peripheral)

The overall performance and detailed flow field structure of a non-premixed swirl-stabilised distributed reaction are sensitive to modest changes in the inlet

conditions (e.g. fuel injection placement(27), inlet geometry, and swirl vane solidity(42). Injecting the fuel around the outer periphery of the air jet for co-swirl or counter-swirl system makes use of the high shear zones around the air jet(27,33). These major features were carried out in the present work to investigate their extended effects on the double rotating swirl systems.

The mean combustor exit emission of the major combustion species as a function of equivalence ratios are shown in Figs.6.66 - 6.69. Higher rates of oxidation were exhibited by the co-swirl system as shown in from Fig.6.66. The counter-swirl system had much higher CO emission with kerosene as the fuel. That was due to the evaporation rate and spray characteristics due the more rapid swirling jet spread and more atomisation as resultant of the lower velocities(41). The combined effect of CO and UHC emissions are represented in terms of combustion inefficiency as a function of metered equivalence ratio in Fig.6.68. For both systems achievement of 0.1% combustion inefficiency or even less seems to be within reach except for the counter-rotating swirlers fuelled with kerosene.

The NOx emissions as a function of equivalence ratio and flame temperature, computed from the mean gas composition are shown in Figs. 6.69 and 6.71 respectively. For the co-swirl system fuelled with propane low NOx emissions in the range of 0.4-0.5 equivalence ratio but higher NOx level were found for liquid fuels for both systems. However, propane with counter-rotating swirlers system offers lower NOx emissions for equivalence ratio of 0.5. The NOx emissions of the co-swirl system fuelled with gasoil were dramatically different to those for kerosene and are at high level at all equivalence ratios. This may have due to the slow vaporization rate which did not achieve sufficient fuel recirculation into the core region to achieve a flammable mixture. The resultant flame downstream of the recirculation zone has rich regions in the wall region which generate the high NOx emissions.

The combustion inefficiency as a function of NOx corrected to 15% oxygen

and day humidity are shown in Fig.6.70 for both systems. The co-swirl system fuelled with propane injected at the peripheral offers the lowest NOx corrected to 15% oxygen which equal to 3ppm, compatible with the minimum combustion inefficiency of 0.05%. The counter-swirl system exhibited ultra low NOx corrected of 6ppm but with 0.1% combustion inefficiency. The co-swirl system fuelled with wall fuel injection can contribute NOx emissions for kerosene which are within the EPA regulations of 20ppm.

6.9 COMPARISON WITH PREVIOUS WORK

In general there was no comparative work found to be similar to the present investigations of double-radial swirlers. There was some similarity in flow field of the present (A&C) co-swirlers combination with that reported by Gouldin and coworkers(25,34,35,45) or the work of Drake and Hubbard(43). Few aspects in the work reported by Blumcke et al(41) can be compared with the present work although, their primary to secondary air swirl ratio was 1/2.25 which is lower than in the present work.

For counter rotating double axial swirlers the most significant work has been that relating to the NASA swirl modules and sponsored work relevant to these (3,25,29,30). Mularz et al for both single swirl modules (3) and arrays of swirlers (29) have shown that there was no major performance improvement resulting from the extra complexity of double swirlers.

Thompson et al (30) investigated a single NASA double swirl module in an open flame configuration. Their temperature and gas composition profiles showed that there was a burnt gas high temperature central region and a rapid fall in temperature in the outer swirl flow. Oven et al (25) investigated a simplified test geometry of a double swirl system, without any practical vane swirler. The central swirler was operated premixed and the outer swirler was air. For an overall equivalence ratio of 0.2 and 30% of the air in the central swirler, they found that the overall combustion inefficiency was higher for counter swirl than for co swirl. Internal traverses by Oven et al (25) showed more rapid mixing for counter swirl

than for co swirl.

Ahmad and Andrews (31) have investigated the influence of counter rotating swirl in a three axial swirlers system and compared it with that for co swirl. The influence of the swirl direction was found to be small, especially for flame stability. The influence on the combustion efficiency was significant, but dependent on the inlet temperature. Comparison with the single swirler results in a cylindrical combustor showed considerable improvements for both swirl directions for the three swirler rectangular combustor. This was due to the greater outer expansion from the swirlers and the associated interswirler aerodynamics.

6.10 CONCLUSIONS

1- Central propane and natural gas with co and counter (B&C) radial swirlers had similar exellent flame stability characteristics, but the counter rotating swirler had much lower NOx emission than for co-swirl system.

2- Central kerosene injection showed a large extension of the flame stability limits due to the presence of a rich core and better vaporization with the co-swirl system. But in general, the liquid fuel showed some deterioration from the central gaseous injections due to the centrifugal forces action on the fuel droplets forcing them into the outer swirl flow where more vaporization takes place. Kerosene showed a better weak extinction than gasoil.

3- A slight improvement in the weak extinction with the combination of small swirler (A) with the large radial swirler (C) was found for the co-rotating swirl system. However, results showed that the weak extinction was still dominated by the flow field of the small radial swirler using the central radial fuel injection system.

4- Using central radial propane injection, the counter-swirl system contributed less corrected NOx than the co-swirl system which was 3.5ppm compatible with 0.1% combustion inefficiency for propane and 2.5ppm for natural gas.

5- Using 76mm wall injection(peripheral) with propane, the co-swirl system exhibited ultra low corrected NOx of 2.5ppm compatible with 0.05% combustion inefficiency.

6- The corner recirculation zone was considerably larger in the counterswirl condition than in co-swirl, as shown by the wall static pressure profiles.

CHAPTER SIX

REFERENCES

6-1 Clarke,A.E.: ASME/I.Mech.E. Conference on Combustion,354 (1955).

6-2 Bahr,D.W. and Gleason,L.L.: Experimental clean combustor program, Phase 1 final report, NASA CR 134737 (1975).

6-3 Mularz,E.J.,Wear,J.D. and Verbulecz,P.W.: Pollution emissions from single swirl-can combustor modules at parametric test conditions. NASA TM X-3167 (1975).

6-4 Niedzwiecki,R.W. and Jones,R.E.: AIAA J.,12,844 (1974).

6-5 Roberts,P.B.,Kubasco,A.J. and Sekas,N.J.: Development of a low NOx lean premixed annular combustor. ASME paper 81-GT-40 (1981).

6-6 Sood,V.M. and Shekelton,J.R.: Ongoing development of a low emissions axisymetric annular vortex combustor for an industrial gas turbine. ASME paper 80-GT-58 (1980).

6-7 Johnson,B.V.,Markowski,S.J. and Craig,H.M.: Cold flow and combustion experiments with a new burner air distribution concept. ASME paper 85-GT-40 (1985).

6-8 Claypole,T.C. and Syred,N.:Eighteenth Symposium (International) on Combustion, The Combustion Institute, pp.81 (1981).

6-9 Claypole,T.C. and Syred,N.: The Sixth International Symposium on Air Breathing Engines, pp.182 (1983).

6-10 Chervinsky,A. and Manheimer-Timnat,Y.: Isreal J.Tech. 6,25 (1968).

6-11 Al-Dabbagh,N.A. and Andrews,G.E.: Sixth International Symposium on Air Breathing Engines, pp.172 (1983).

6-12 Al-Dabbagh,N.A. and Andrews,G.E.: Combustion and Flame, 55,31 (1984).

6-13 Al-Dabbagh,N.A.,Andrews,G.E. and Manotharan,R.: Shear layer mixing for low emission gas turbine primary zones. ASME paper 84-GT-13 (1984).

6-14 Ahmad,N.T. and Andrews,G.E.: Emissions from enclosed swirl stabilised premixed flames. ASME paper 83-GT-192 (1983).

6-15 Ahmad,N.T. and Andrews,G.E.: Gas and liquid fuel injection into an enclosed swirling flow. ASME paper 84-GT-98 (1984).

6-16 Beltagui,S.A. and Maccallum,N.R.L: Second European Symposium on Combustion, The Combustion Institute, pp.672 (1975).

6-17 Beltagui,S.A. and Maccallum,N.R.L.: J.Inst.Fuel 49,193 (1976).

6-18 Khalil,K.H.,El-Mahallawy,F.M. and Moneib,H.A.: Sixteenth Symposium (International) on Combustion, The Combustion Institute, pp.135 (1976).

6-19 Wu,H.L. and Fricker,N.:J.Inst.Fuel 49,144 (1976).

6-20 Mathur,M.L. and Maccallum,N.R.L.:J.Inst.Fuel 40,238 (1967).

6-21 Kerr,N.M. and Fraser,D.: J.Inst.Fuel 38,519 (1965).

6-22 Ahmad,N.T.: Enclosed Swirl Stabilised Flames. Ph.D. Thesis, University of Leeds (1986).

6-23 Al-Dabbagh,N.A. and Andrews,G.E.: Trans. ASME, J. Eng. Power, 103, 749 (1981).

6-24 Bhangu,J.K.,Hawkins,H.L.,Pridden,C.H. and Walker,P.H.: Emissions variability and traversing on production RB211 engines, ASME paper 83-GT-141 (1983).

6-25 Oven,M.J.,Gouldin,F.C. and Mclean,W.:Seventeenth Symposium (International) on Combustion, The Combustion Institute, pp.363 (1979).

6-26 Takagi,T.,Okamoto,T.,Taji,M. and Nakasuji,Y.: Twentieth Symposium (International) on Combustion, The Combustion Institute, pp.251 (1984).

6-27 Beltagui S.A. MacCallum N.R.L. and Ralston T.: The effect of injection modes on combustion of swirling flows. British flame Days, 1988, Furnace Combustion research and its applications, The Inst. of Energy, 1988.

6-28 Larue,J.C.,Samuelson,G.S. and Steiler,E.T.: Twentieth Symposium (International) on Combustion, The Combustion Institute, pp.277 (1984).

6-29 Mularz,E.J.,Wear,J.D. and Verbulecz,P.W.: Exhaust pollutant emissions from swirl-can combustor module arrays at parametric test conditions. NASA TM X-3237 (1975).

6-30 Thompson,D.,Chigier,N.A. and Ungut,A.: Flame characteristics of a NASA contra swirler module. ASME paper 78-GT-163 (1978).

6-31 Ahmad,N.T. and Andrews,G.E., Enclosed swirl flames: interaction between swirlers in lean primary zones, ASME paper 86-GT-278, 1986.

6-32 Leuckel,W. and Fricker,N.:The characteristics of swirl-stabilised natural gas flames. part 1;different flame types and their relation to flow and mixing patterns. Journal of the institute of fuel, June 1976.

6-33 Beltagui,S.A. and Maccallum,N.R.L.: Characteristics of enclosed swirl flames with peripheral fuel injection. J. Istit. Energy, Vol.LXI, 446, pp.3-16, 1988.

6-34 Halthore R.N. and Gouldin F.C.: Laser scattering measurements for gas densities in a swirling flow combustor. AIAA Journal,vol.24,no.7, pp.1129-1136,Jully, 1986.

6-35 Gouldin F.C., Depsky J.S. and Lee S.L.: Velocity field chracteristics of a swirling flow combustor. AIAA Journal,Vol.23,pp.95 -102, 1985.

6-36 Ahmad N.T., Andrews G.E.,Kowkabi M. and Sharif S.F.: Centrifugal mixing forces in enclosed swirl flames. 20th symposium (Int.) on Combustion ,The combustion Institute, 1984.

6-37 Ahmad N.T., Andrews G.E., Kowkabi M. and Sharif S.F.: Centrifugal mixing in gas and liquid fuelled lean swirl stabilised primary zones. ASME paper 85-IGT_103, 1985.

6-38 Myers G.D. and Lefebvre A.H.: Flame propagation in heterogeneous mixtures of fuel drops and air. Combustion and Flame,66,pp.193-210, 1986.

6-39 Wear J.D. and Jones R.E.: Comparison of combustion characteristics of ASME A-1 propane, and natural gas fuels in an annular turbojet combustor. NASA TN D-7135, Jan. 1973.

6-40 Appletton J.P. and Heywood J.B.: The effects of imperfect fuel-air mixing in a burner on NO formation from nitrogen in the air and the fuel. 14th symposium (Int.) on Combustion, The Combustion Inst., pp.777-786, 1973.

6-41 Blumcke E., Eickhoff H., Hassa C. and Koopman J.: Analysis of the flow through double swirl airblast atomizers. Combustion and Fuels in Gas Turbine Engines, AGARD-CP-422,40,pp.1-13, 1987.

6-42 Charles R.E, Emdee J.L., Muzio L.J. and Samuelsen G.S.: The effect of inlet conditions on the performance and flow field structure of a non-premixed swirl-stabilised distributed reaction. 21st symposium (Int.) on Combustion, The combustion Inst.,pp.1455-1461, 1986.

6-43 Drake P.F. and Hubbard E.H.: Combustion system aerodynamics their effect on the burning of heavy fuel oil. Journal of the Inst. of Fuel,pp.98-109, March 1966.

6-44 Ivanov A.G.: A method of estimating the flow section of vortex burners. Thermal Eng.,Vol.15,part 5,pp.44-49, 1968.

6-45 Gouldin F.C., Halthore R.N. and Vu B.T.: Periodic oscillations observed in swirling flows with and without combustion. 20th symposium (Int.) on Combustion, The Combustion Inst.,pp.269-276, 1984.

6-46 Gupta A.K., Lilley D.G. and Syred N.: Swirl Flows. Abacus Press, p.253, 1984.

TABLES

Table (6.1)
Measured Weak Extinction for the Double-Rotating Radial Swirlers

Radial Swirlers Type	Type of Swirl	Fuel Type	Injection Method	Inlet Temp.K	Weak Extinction EQR.	Weak Extinction A/F	Pressure Loss %
(B&C)	Co	Propane	C.I	600	0.019	834	4.8
				400	0.143	109	5.0
			Wall	600	0.323	48	4.8
		Gas oil	C.I	600	0.329	45	5.0
			Wall	600	0.340	43	5.0
		Kerosene	C.I	600	0.046	323	5.1
			Wall	600	0.400	37	5.0
		Natural Gas	C.I	600	0.038	441	4.8
	Counter	Propane	C.I	600	0.019	828	4.4
				400	0.440	36	5.0
			Wall	600	0.361	43	4.4
		Kerosene	C.I	600	0.450	33	4.4
			Wall	600	0.296	50	4.3
		Natural Gas	C.I	600	0.010	1599	4.4
(A&C)	Co	Propane	C.I	600	0.274	57	4.5
			Wall	600	0.352	45	4.6
		Kerosene	Wall	600	0.383	39	4.7
		Natural Gas	C.I	600	0.313	53	4.7
			Single Swirler				
A		Propane	C.I	600	0.394	40	4.7
B		Propane	C.I	600	0.080	195	4.2
			Premix	600	0.466	34	4.4
C		Propane	Wall	600	0.307	51	4.2
		Kerosene	Wall	600	0.368	40	4.2
		Gas oil	Wall	600	0.381	39	4.2

Table (6.2)
NO_x corrected compatible with lowest combustion inefficiency.

Co-Swirlers Combination	Injecter Type	Fuel Type	NO_{xc} (ppm)	Lowest combustion Inefficiency %
(A&C)	C.I	Propane	15	< 0.1
	C.I	Natural Gas	9	< 0.1
	Wall	Propane	5	< 0.1
	Wall	Kerosene	25	> 0.1
(B&C)	C.I	Propane	15	< 0.1
	C.I	Natural Gas	10	0.1
	Wall	Propane	< 3	< 0.1
	Wall	Kerosene	15	< 0.1

FIGURES

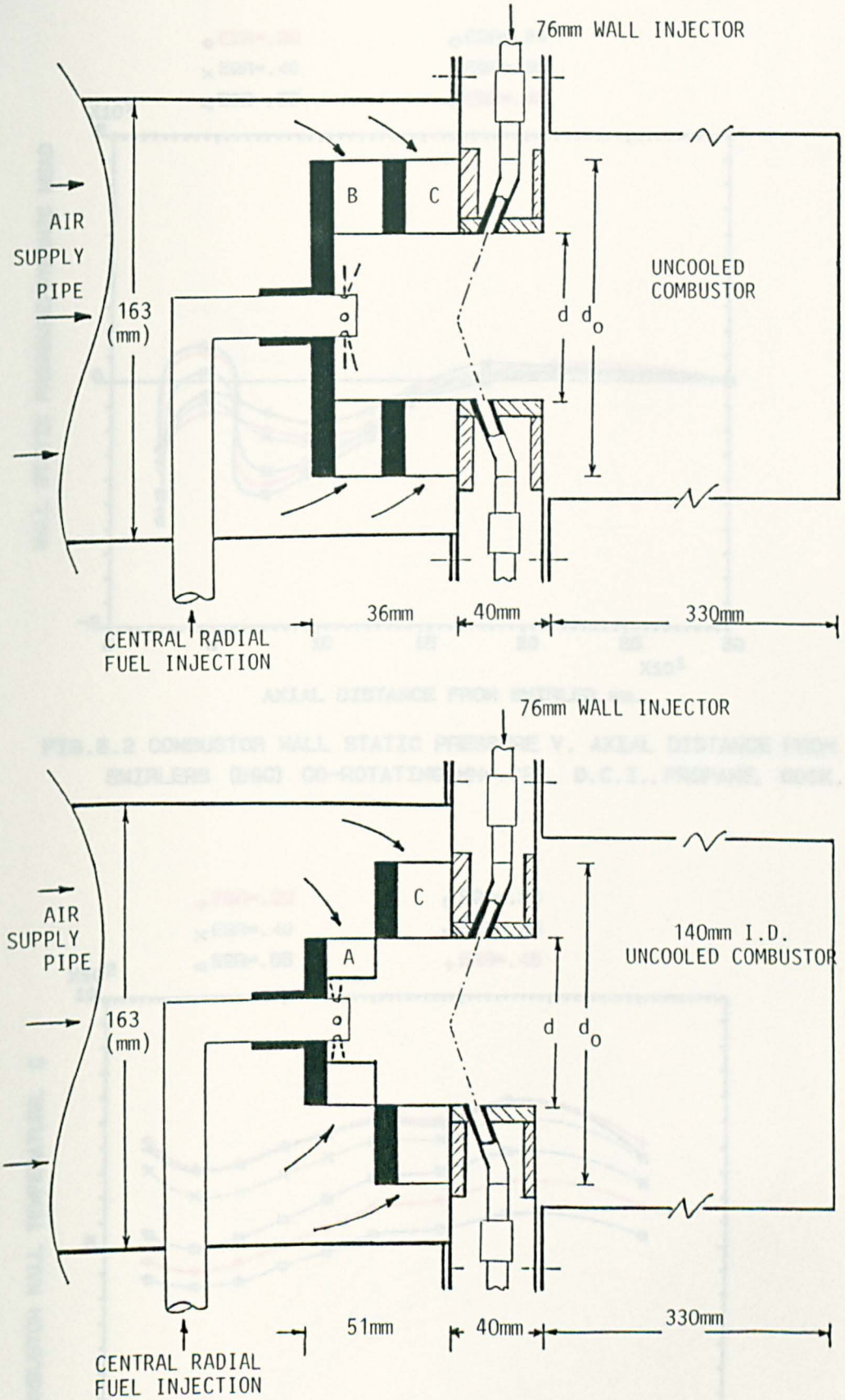

FIG.6.1 SHEMATIC DIAGRAM OF THE DOUBLE RADIAL SWIRLER WITH THE FUEL INJECTION CONFIGURATION.

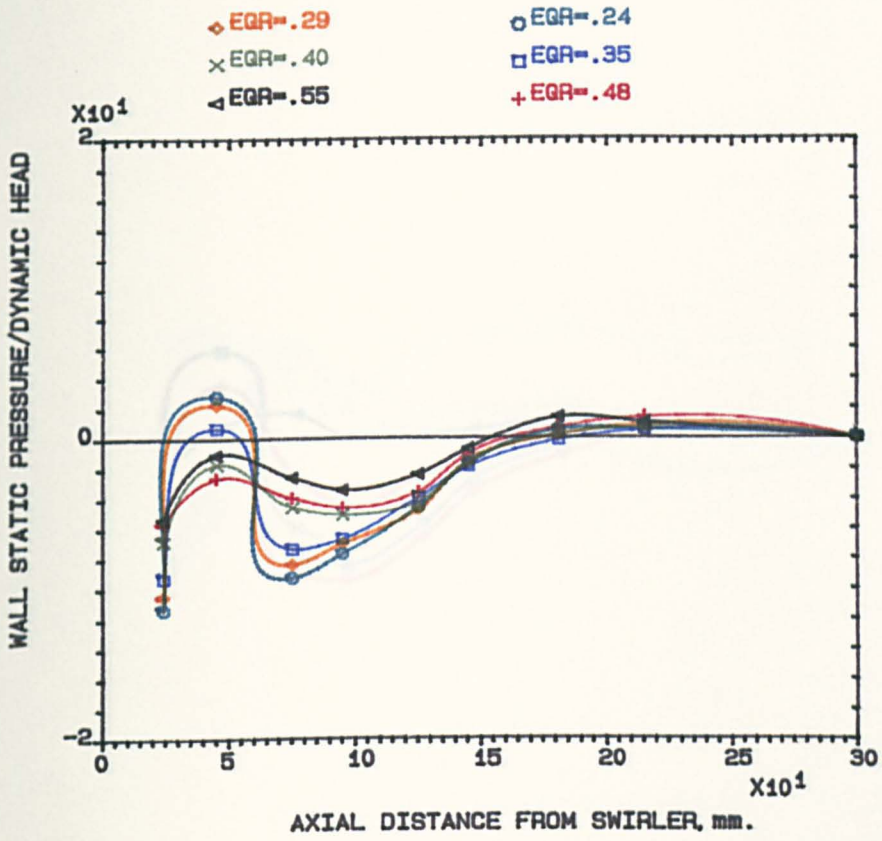

FIG.6.2 COMBUSTOR WALL STATIC PRESSURE V. AXIAL DISTANCE FROM SWIRLERS (B&C) CO-ROTATING, MN=.028, D.C.I., PROPANE, 600K.

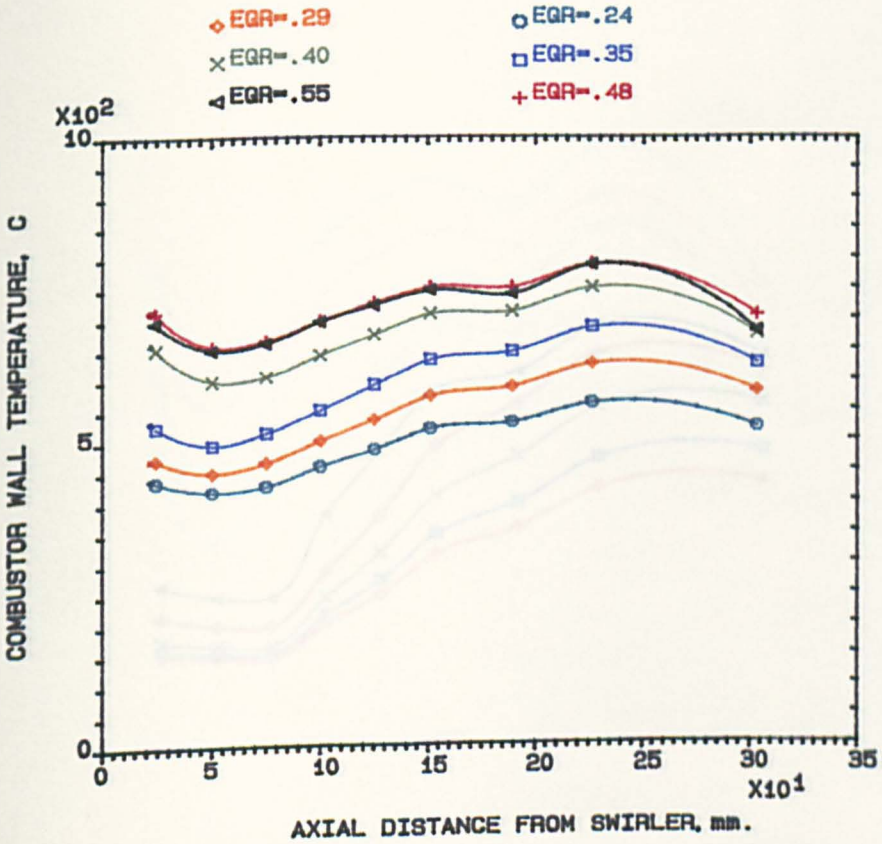

FIG.6.3 COMBUSTOR WALL TEMPERATURE V. AXIAL DISTANCE FROM SWIRLERS (B&C) CO-ROTATING, MN=.028, D.C.I., PROPANE, 600K.

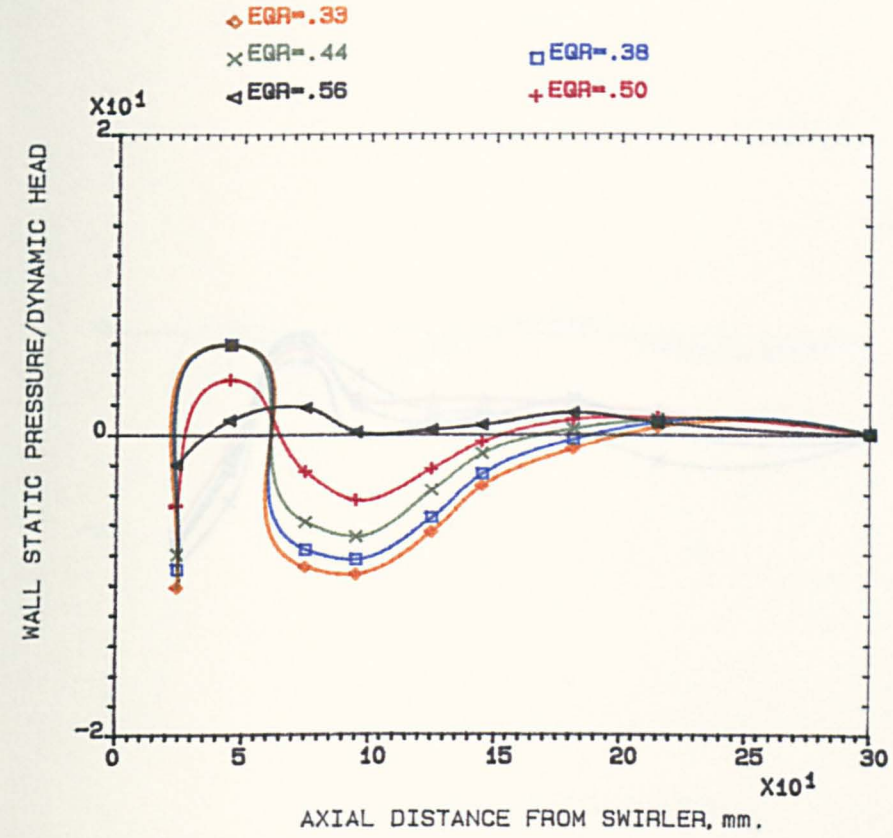

FIG.6.4 COMBUSTOR WALL STATIC PRESSURE V. AXIAL DISTANCE FROM SWIRLERS (B&C) CO-ROTATING, MN=.028, D.C.I., PROPANE, 400K.

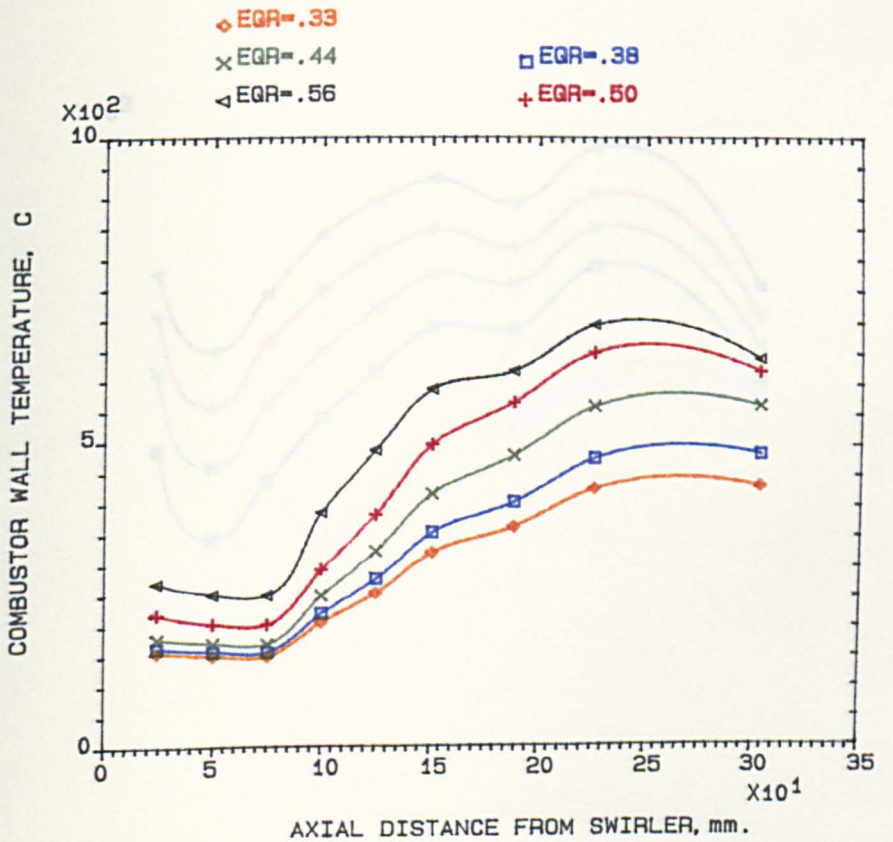

FIG.6.5 COMBUSTOR WALL TEMPERATURE V. AXIAL DISTANCE FROM SWIRLERS (B&C) CO-ROTATING, MN=.028, D.C.I., PROPANE, 400K.

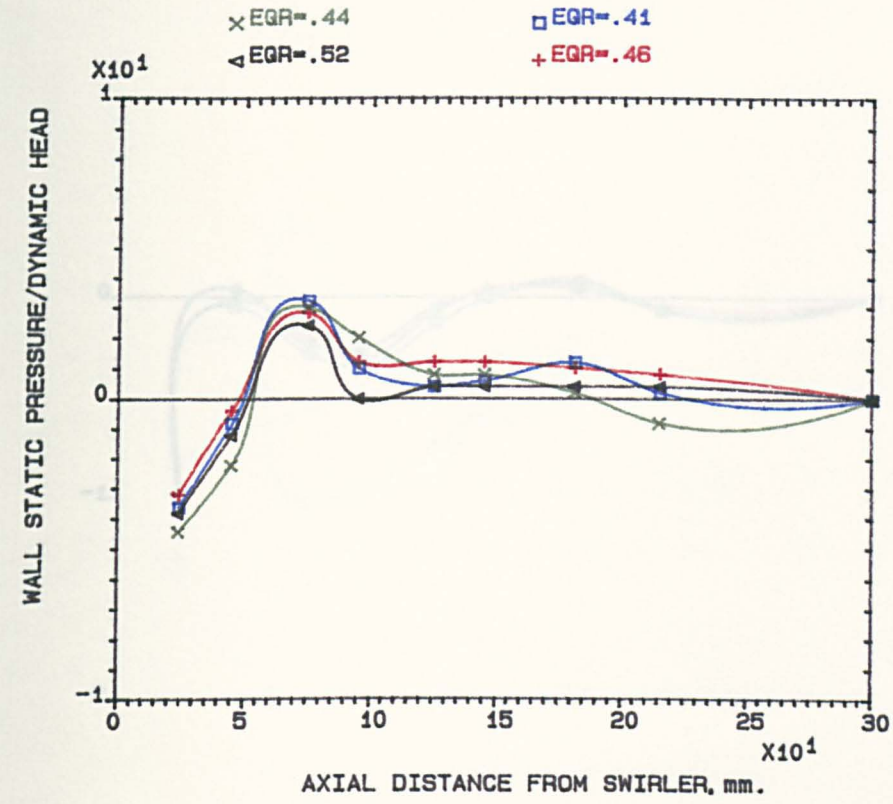

FIG.6.6 COMBUSTOR WALL STATIC PRESSURE V. AXIAL DISTANCE FROM SWIRLERS (B&C) CO-ROTATING, MN=.028, 76mm WALL INJ., PROPANE, 600K.

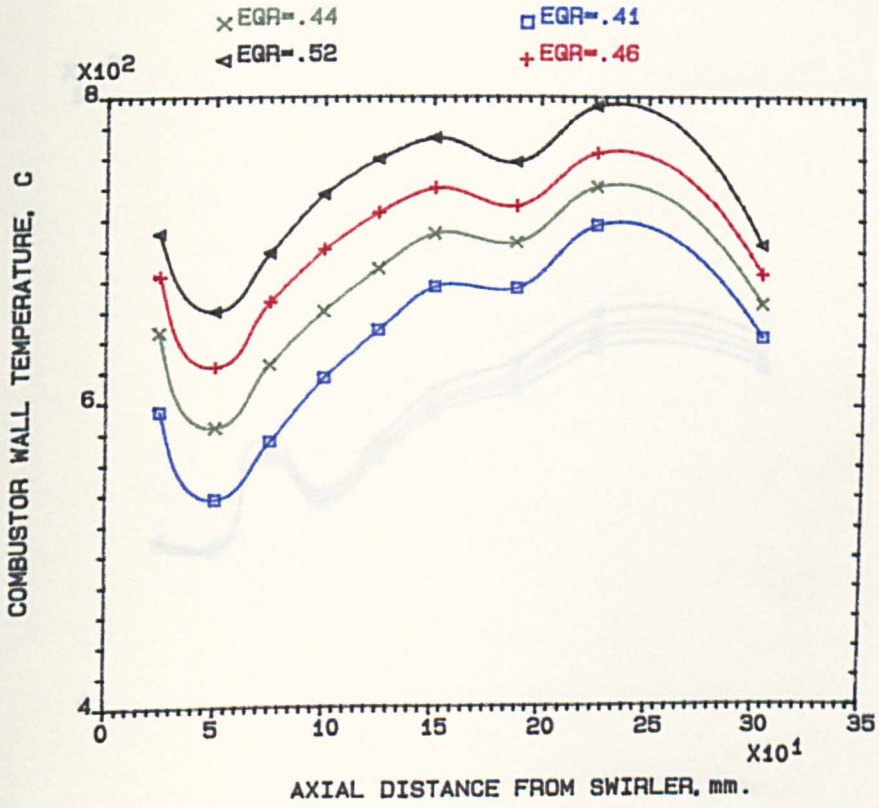

FIG.6.7 COMBUSTOR WALL TEMPERATURE V. AXIAL DISTANCE FROM SWIRLERS (B&C) CO-ROTATING, MN=.028, 76mm WALL INJ., PROPANE, 600K.

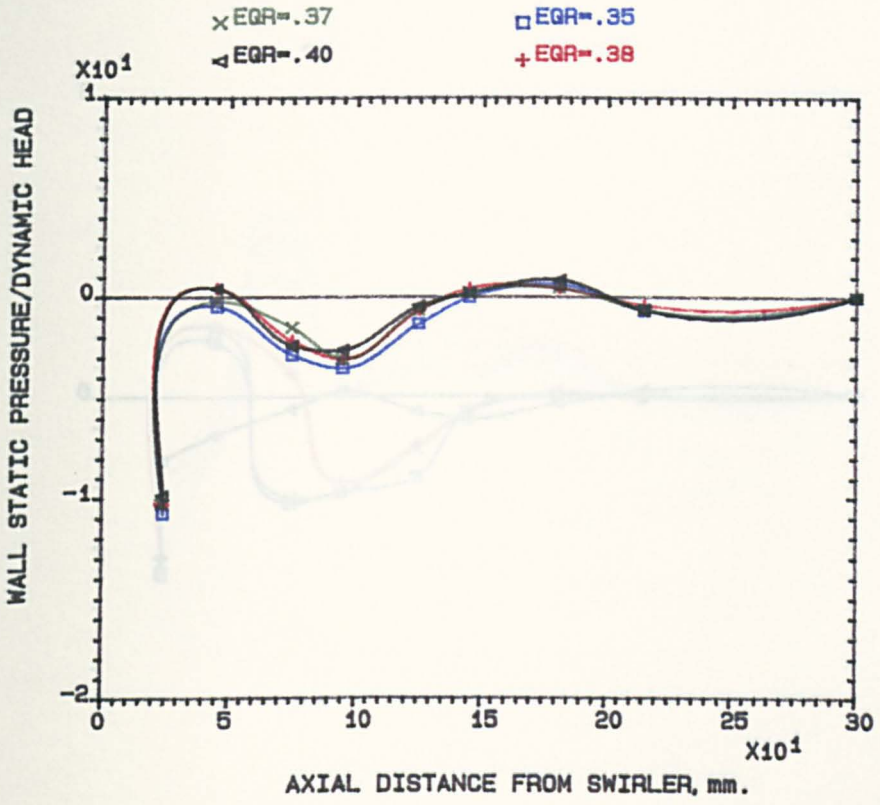

FIG.6.8 COMBUSTOR WALL STATIC PRESSURE V. AXIAL DISTANCE FROM SWIRLERS (B&C) CO-ROTATING, MN=.028, D.C.I., GAS OIL , 600K.

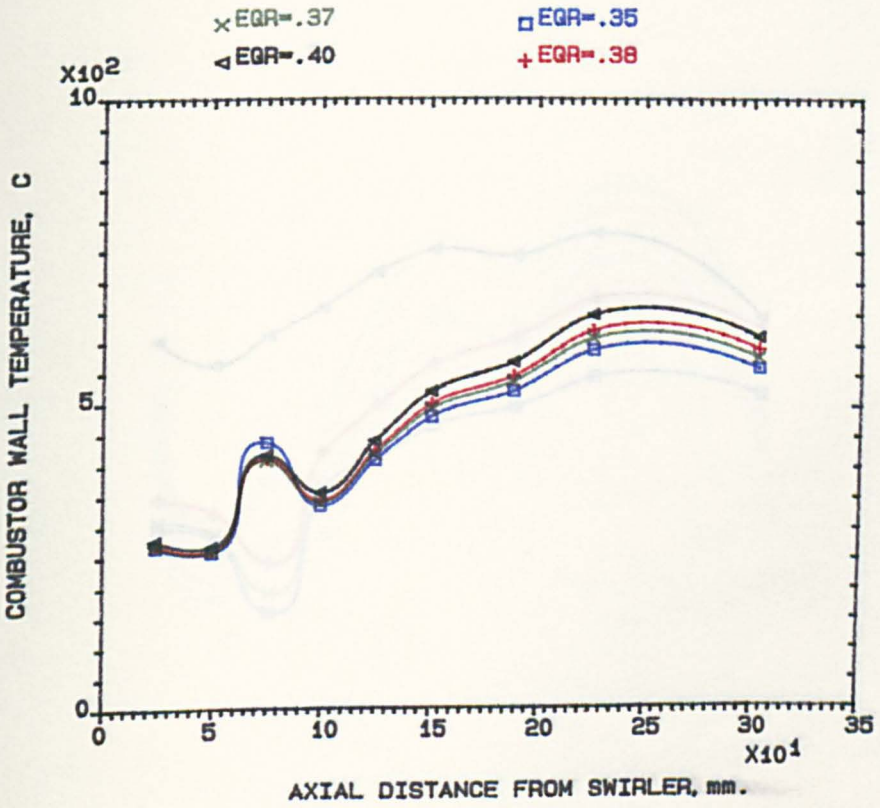

FIG.6.9 COMBUSTOR WALL TEMPERATURE V. AXIAL DISTANCE FROM SWIRLERS (B&C) CO-ROTATING, MN=.028, D.C.I., GAS OIL , 600K.

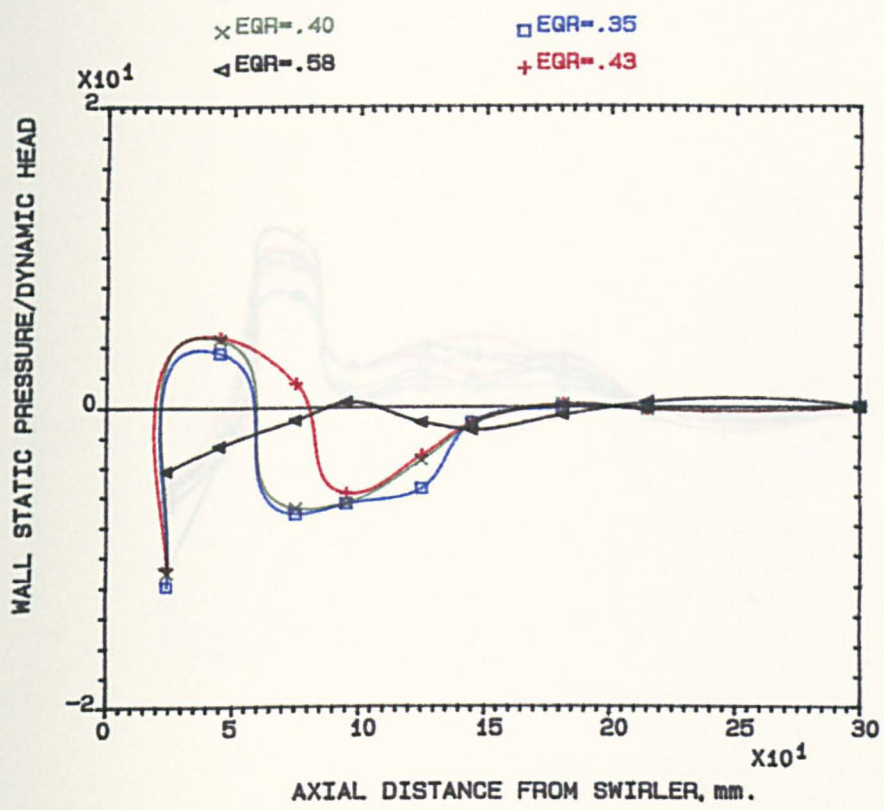

FIG.6.10 COMBUSTOR WALL STATIC PRESSURE V. AXIAL DISTANCE FROM SWIRLERS (B&C) CO-ROTATING, MN=.028, D.C.I., KEROSENE, 600K.

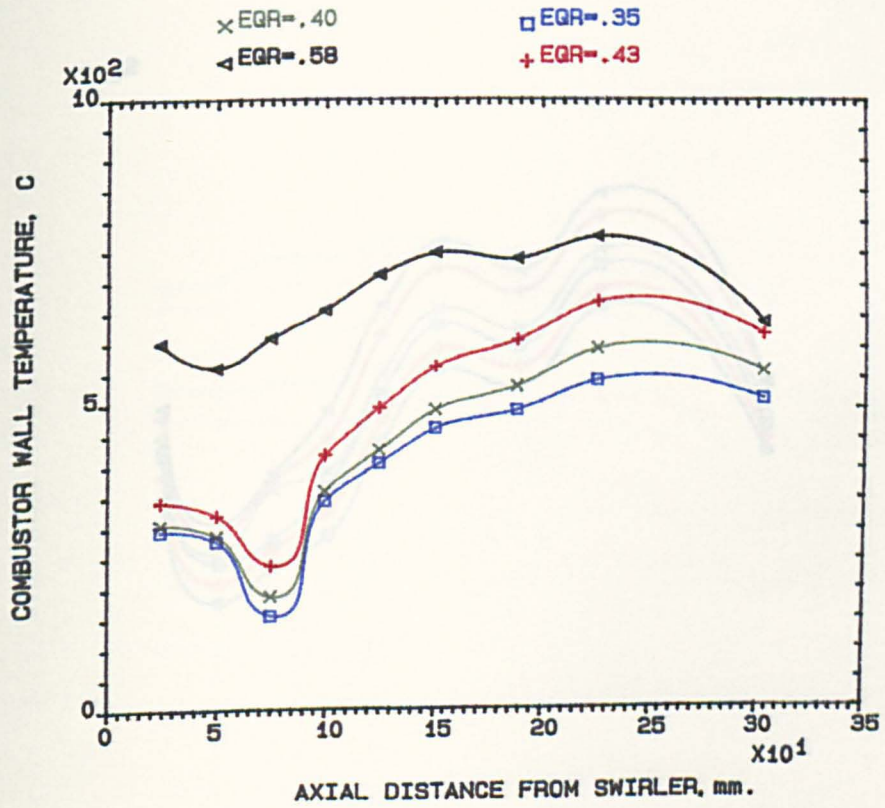

FIG.6.11 COMBUSTOR WALL TEMPERATURE V. AXIAL DISTANCE FROM SWIRLERS (B&C) CO-ROTATING, MN=.028, D.C.I., KEROSENE, 600K.

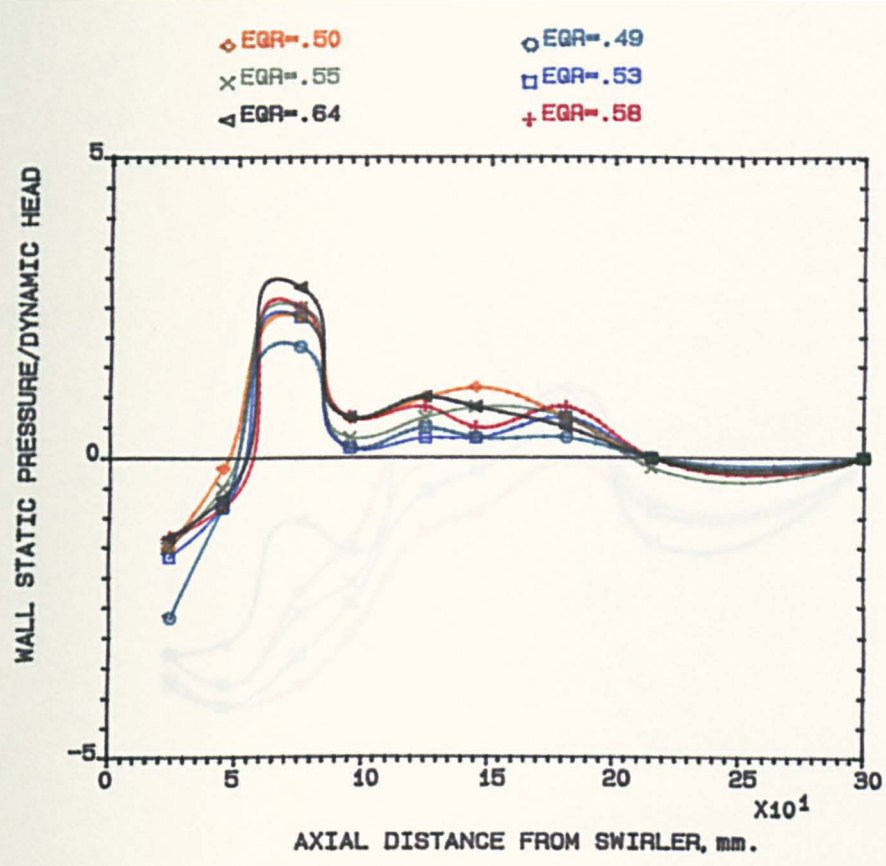

FIG.6.12 COMBUSTOR WALL STATIC PRESSURE V. AXIAL DISTANCE FROM SWIRLERS (B&C) CO-ROTATING, MN=.028, 76mm WALL INJ., KEROSENE, 600K.

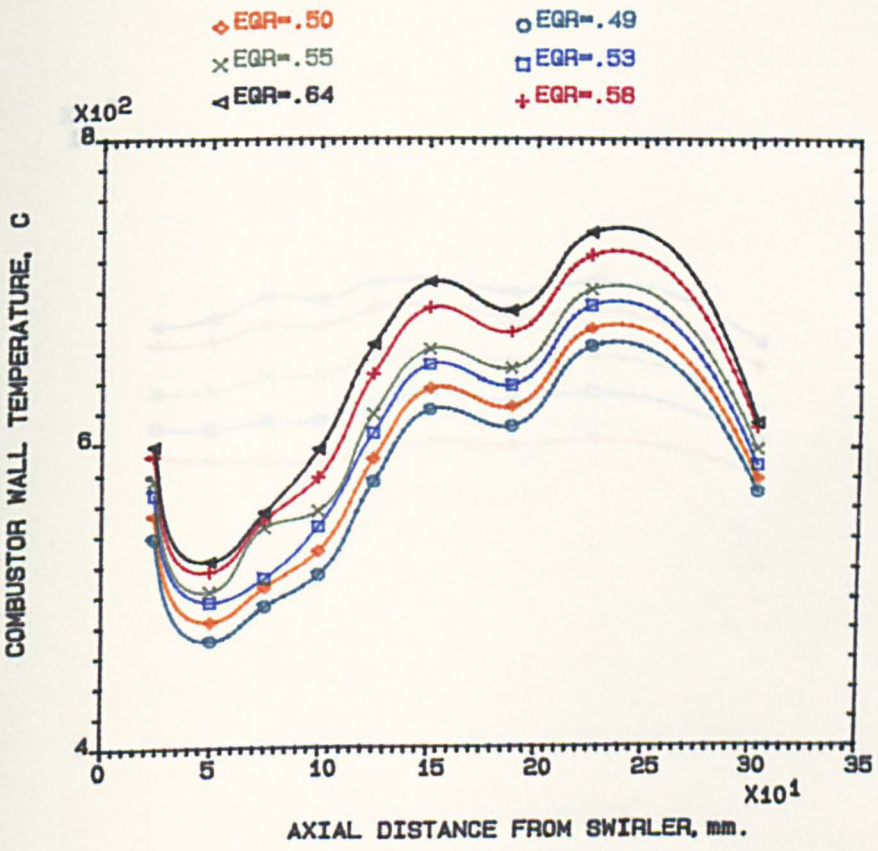

FIG.6.13 COMBUSTOR WALL TEMPERATURE V. AXIAL DISTANCE FROM SWIRLERS (B&C) CO-ROTATING, MN=.028, 76mm WALL INJ., KEROSENE, 600K.

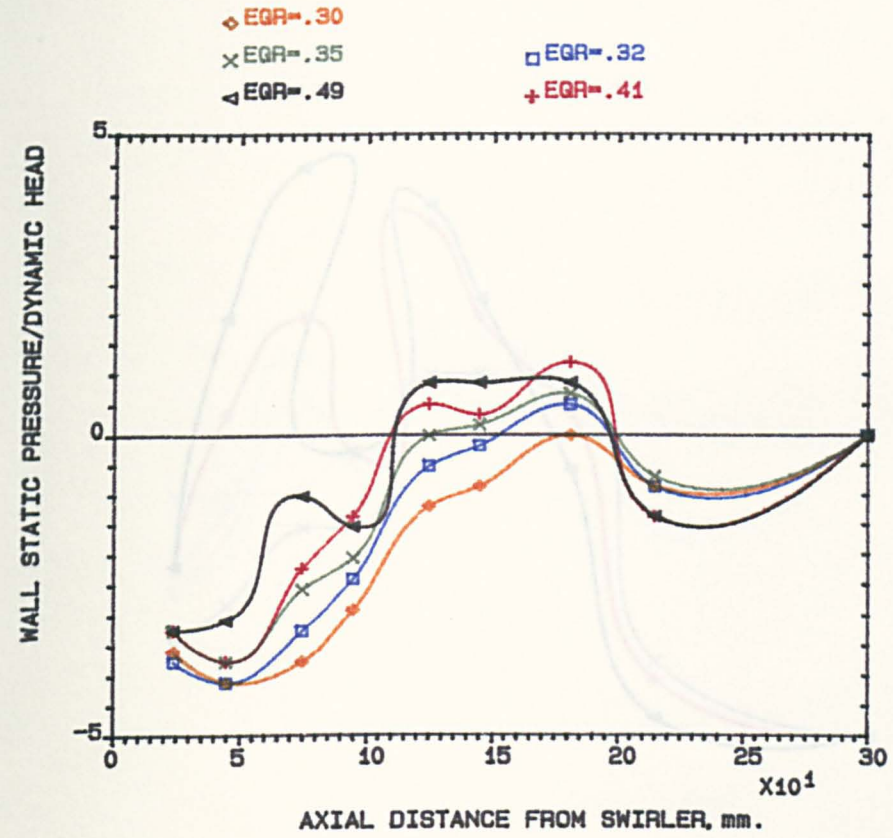

FIG.6.14 COMBUSTOR WALL STATIC PRESSURE V. AXIAL DISTANCE FROM SWIRLERS (B&C) COUNTER-ROTATING, MN=.028, D.C.I., PROPANE, 600K.

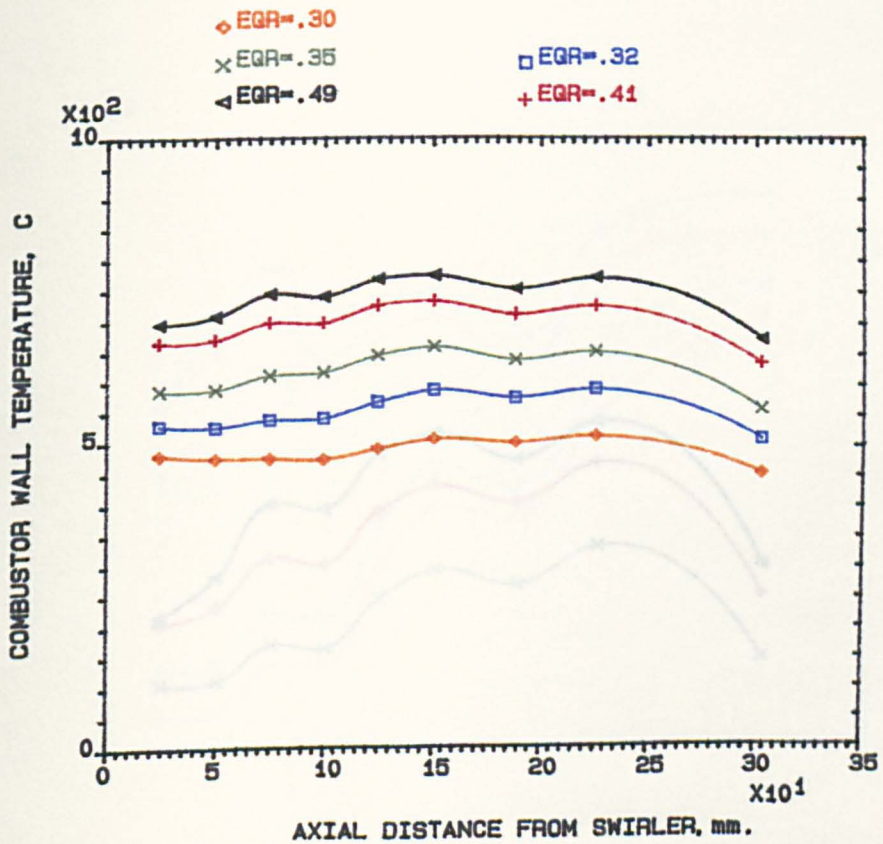

FIG.6.15 COMBUSTOR WALL TEMPERATURE V. AXIAL DISTANCE FROM SWIRLERS (B&C) COUNTER-ROTATING, MN=.028, D.C.I., PROPANE, 600K.

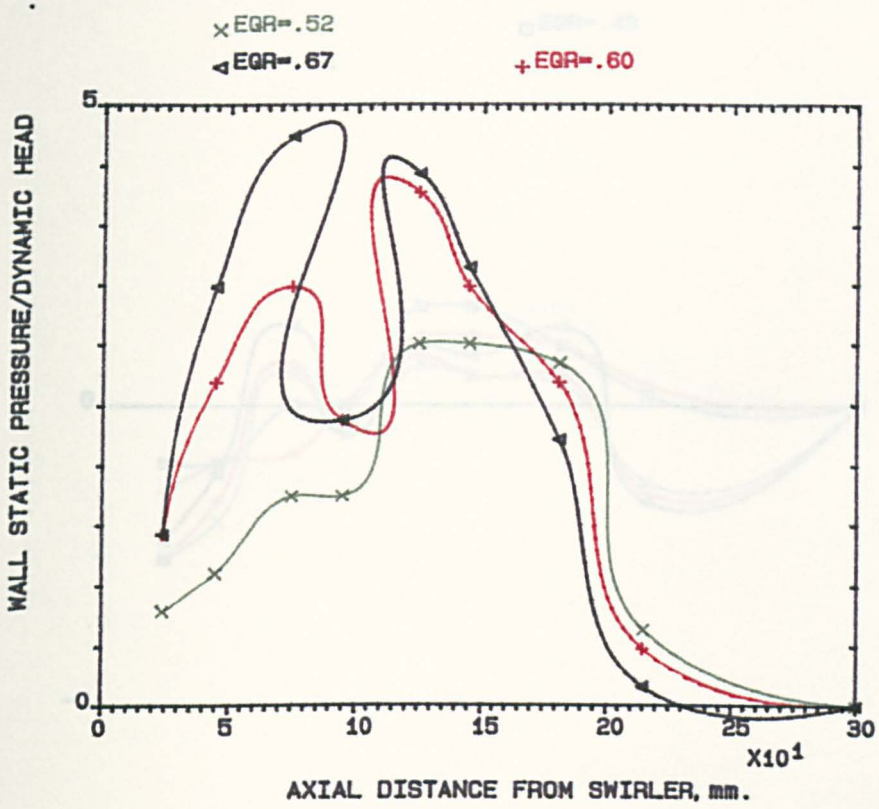

FIG.6.16 COMBUSTOR WALL STATIC PRESSURE V. AXIAL DISTANCE FROM SWIRLERS (B&C) COUNTER-ROTATING, MN=.028, D.C.I., PROPANE, 400K.

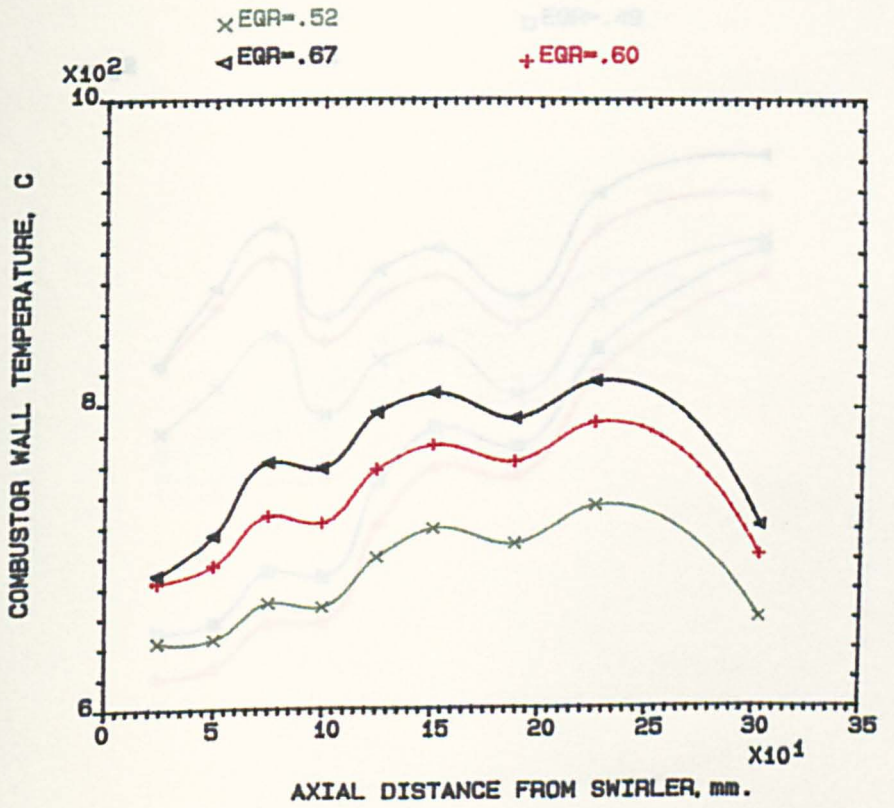

FIG.6.17 COMBUSTOR WALL TEMPERATURE V. AXIAL DISTANCE FROM SWIRLERS (B&C) COUNTER-ROTATING, MN=.028, D.C.I., PROPANE, 400K.

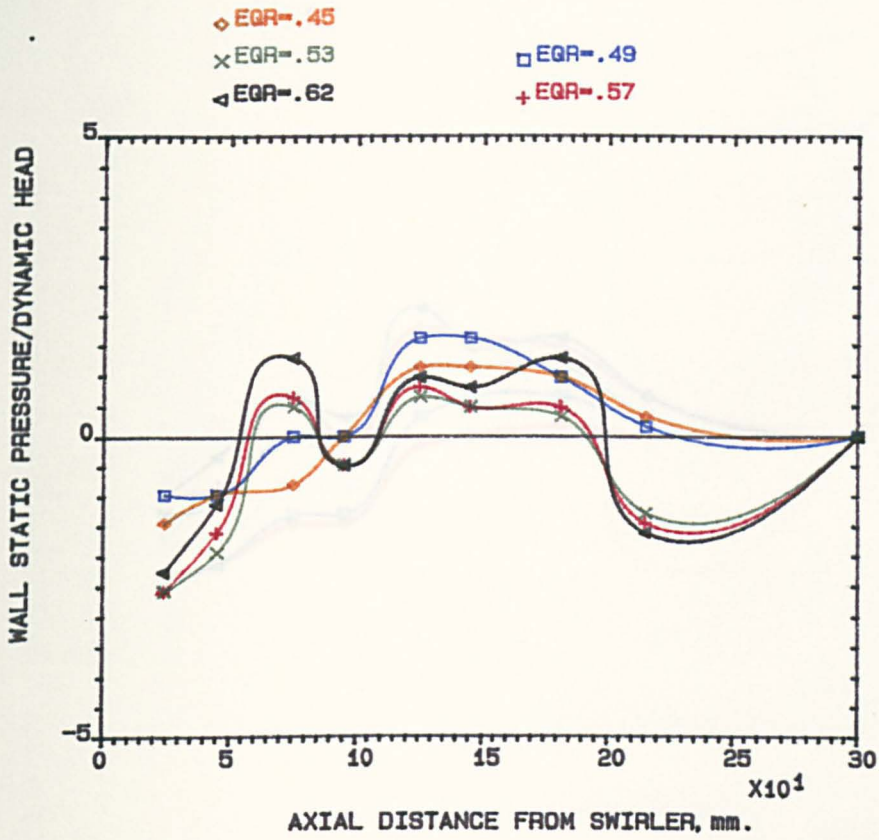

FIG.6.18 COMBUSTOR WALL STATIC PRESSURE V. AXIAL DISTANCE FROM SWIRLERS (B&C) COUNTER-ROTATING, MN=.028, 76mm WALL INJ., PROPANE, 600K.

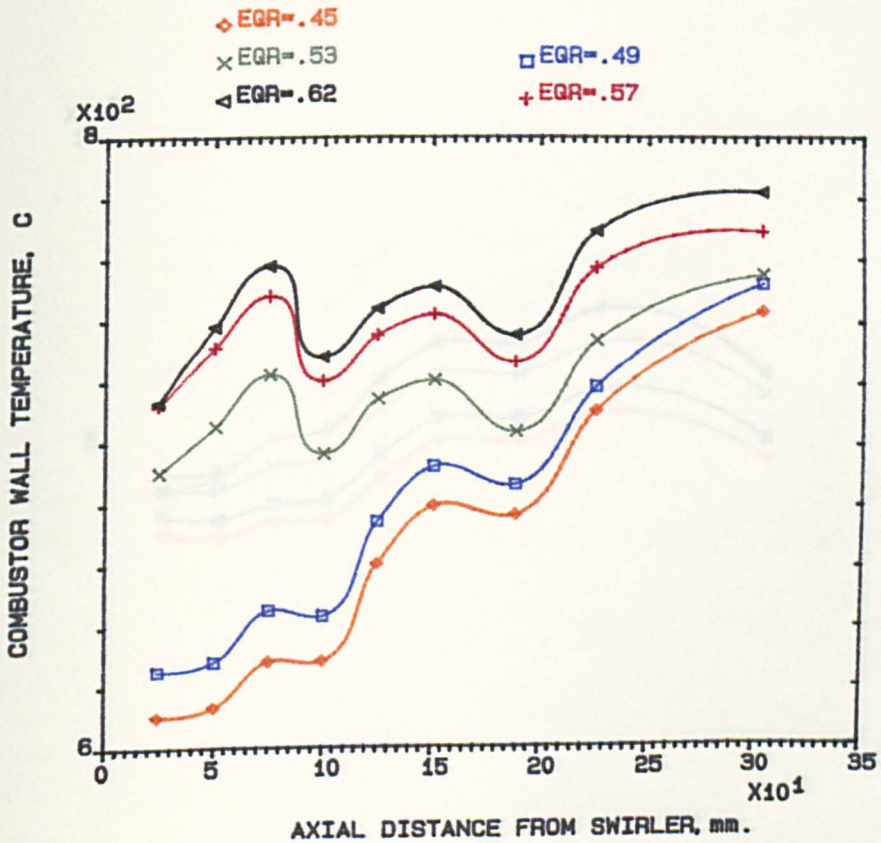

FIG.6.19 COMBUSTOR WALL TEMPERATURE V. AXIAL DISTANCE FROM SWIRLERS (B&C) COUNTER-ROTATING, MN=.028, 76mm WALL INJ., PROPANE, 600K.

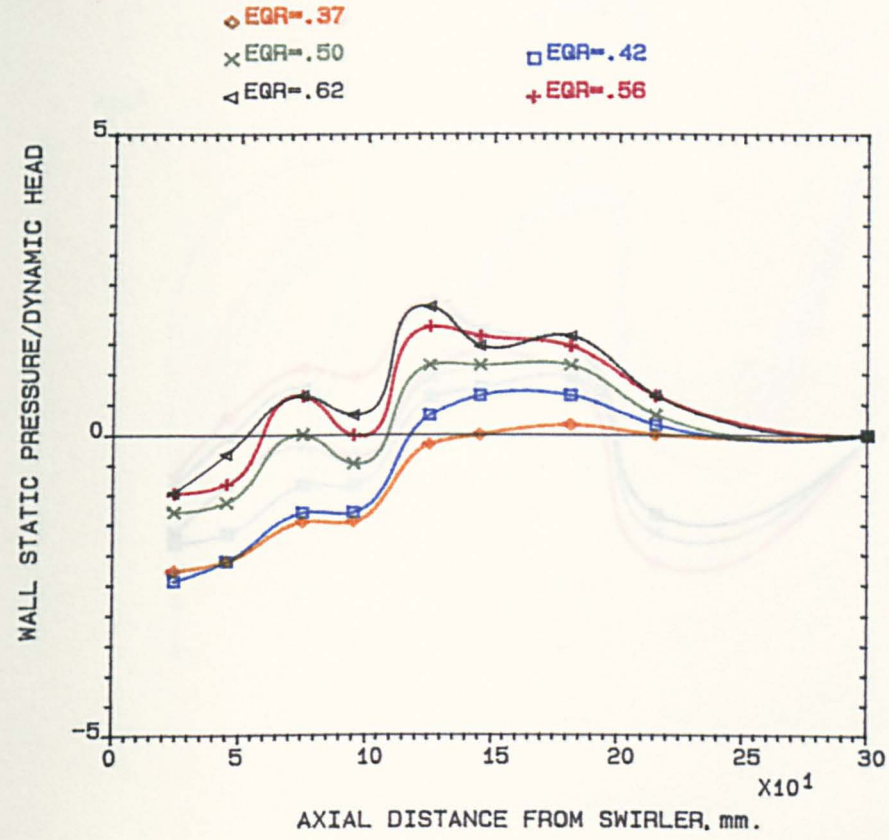

FIG.6.20 COMBUSTOR WALL STATIC PRESSURE V. AXIAL DISTANCE FROM SWIRLERS (B&C) COUNTER-ROTATING, MN=.028, 76mm WALL INJ., KEROSENE, 600K.

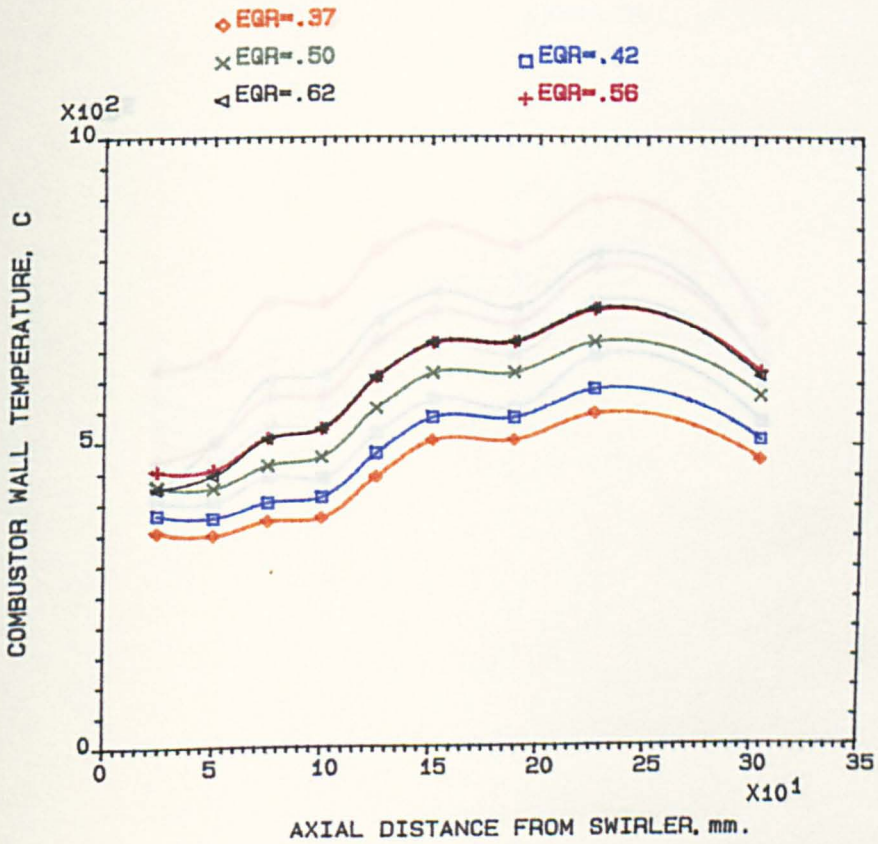

FIG.6.21 COMBUSTOR WALL TEMPERATURE V. AXIAL DISTANCE FROM SWIRLERS (B&C) COUNTER-ROTATING, MN=.028, 76mm WALL INJ., KEROSENE, 600K.

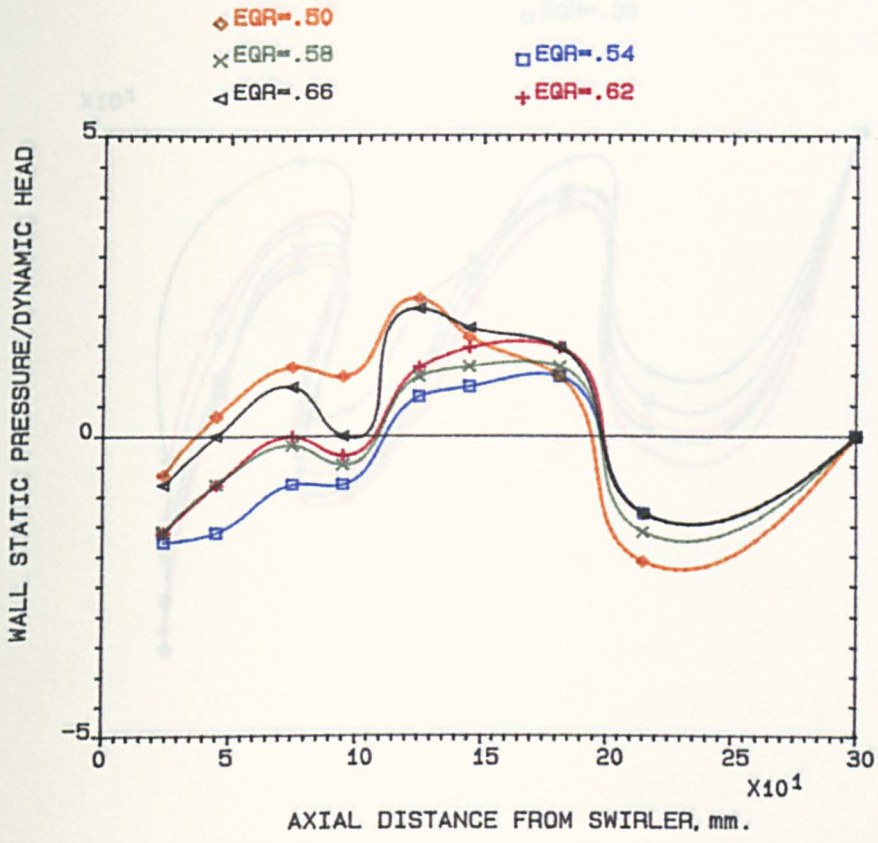

FIG.6.22 COMBUSTOR WALL STATIC PRESSURE V. AXIAL DISTANCE FROM SWIRLERS (B&C) COUNTER-ROTATING, MN=.028, D.C.I., KEROSENE, 600K.

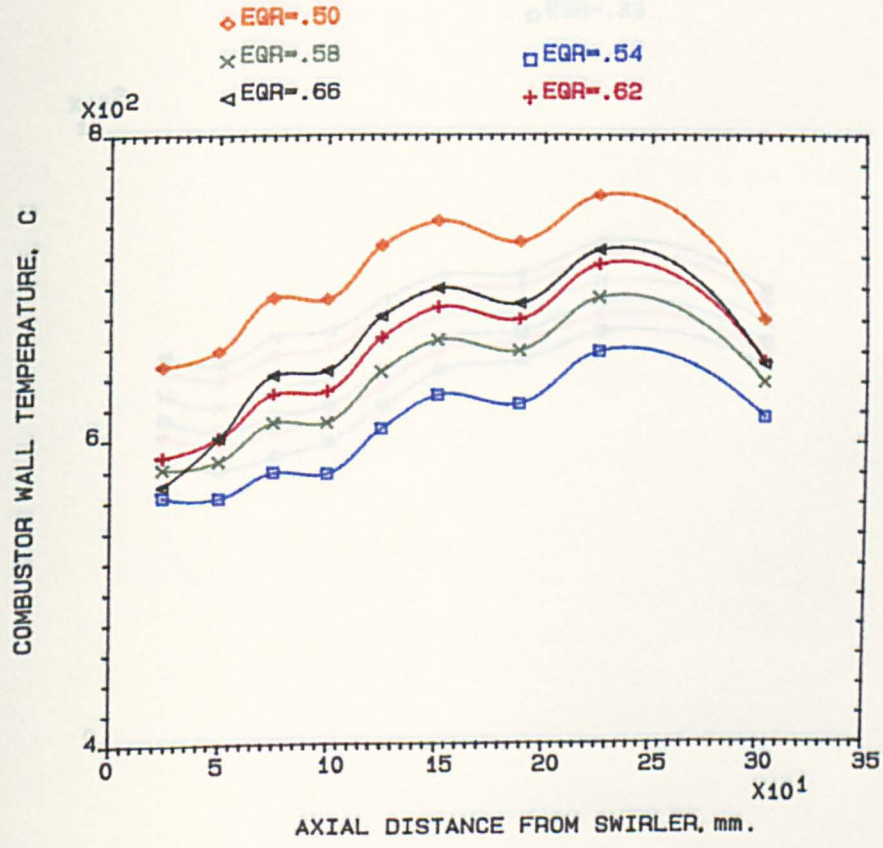

FIG.6.23 COMBUSTOR WALL TEMPERATURE V. AXIAL DISTANCE FROM SWIRLERS (B&C) COUNTER-ROTATING, MN=.028, D.C.I., KEROSENE, 600K.

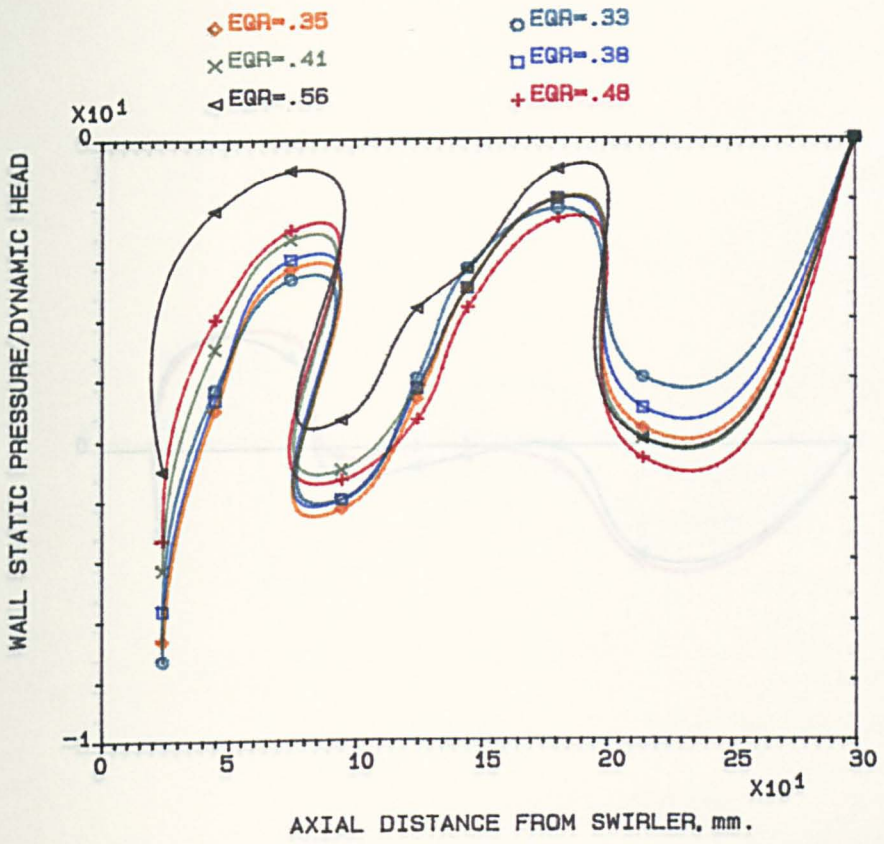

FIG.6.24 COMBUSTOR WALL STATIC PRESSURE V. AXIAL DISTANCE FROM SWIRLERS (A&C) CO-ROTATING, MN=.028, D.C.I., PROPANE, 600K.

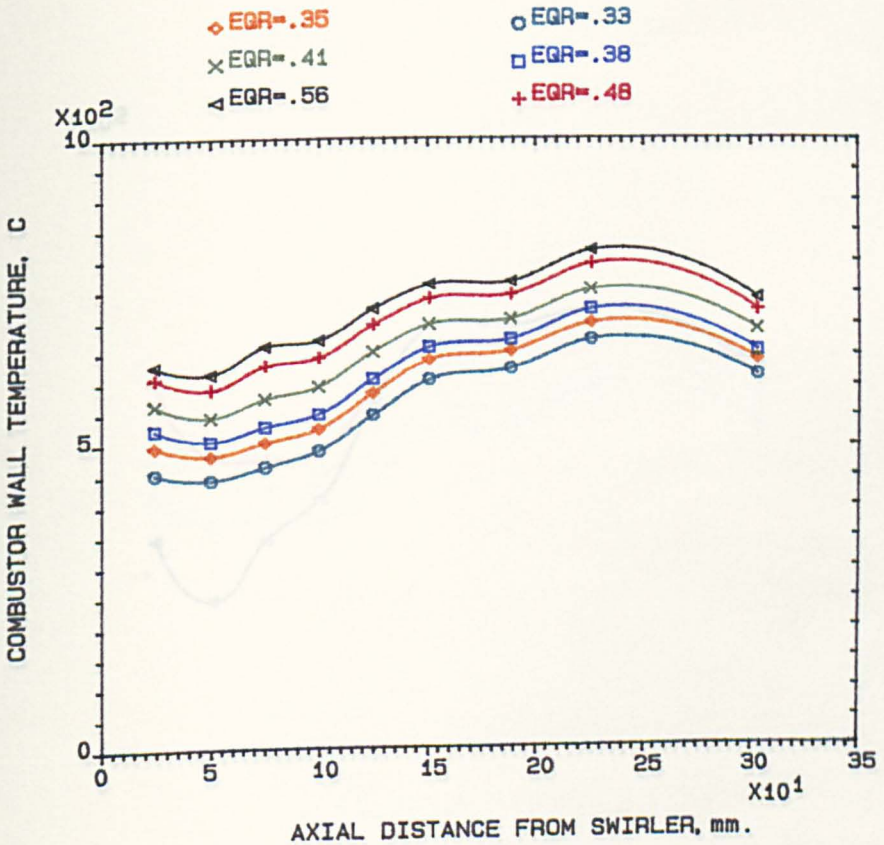

FIG.6.25 COMBUSTOR WALL TEMPERATURE V. AXIAL DISTANCE FROM SWIRLERS (A&C) CO-ROTATING, MN=.028, D.C.I., PROPANE, 600K.

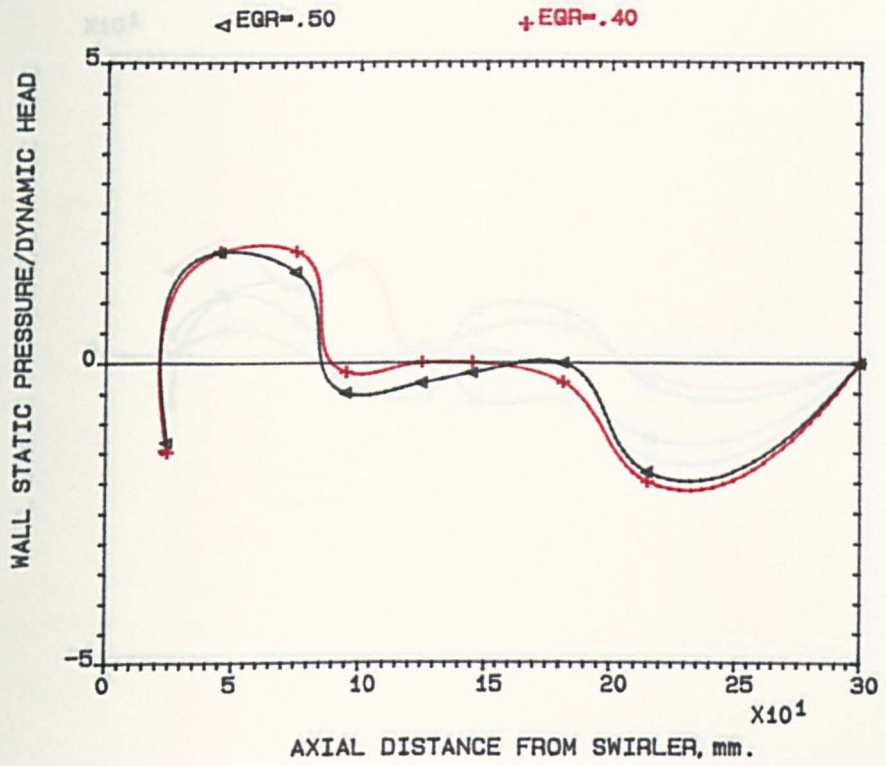

FIG.6.26 COMBUSTOR WALL STATIC PRESSURE V. AXIAL DISTANCE FROM SWIRLERS (A&C) CO-ROTATING, MN=.028, 76mm WALL INJ., PROPANE, 600K.

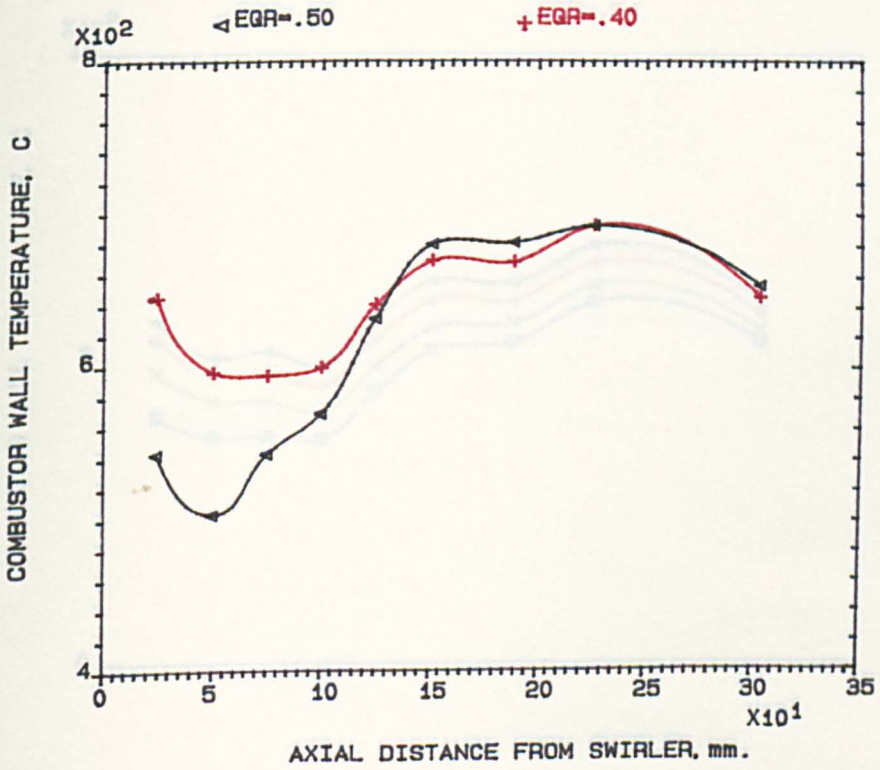

FIG.6.27 COMBUSTOR WALL TEMPERATURE V. AXIAL DISTANCE FROM SWIRLERS (A&C) CO-ROTATING, MN=.028, 76mm WALL INJ., PROPANE, 600K.

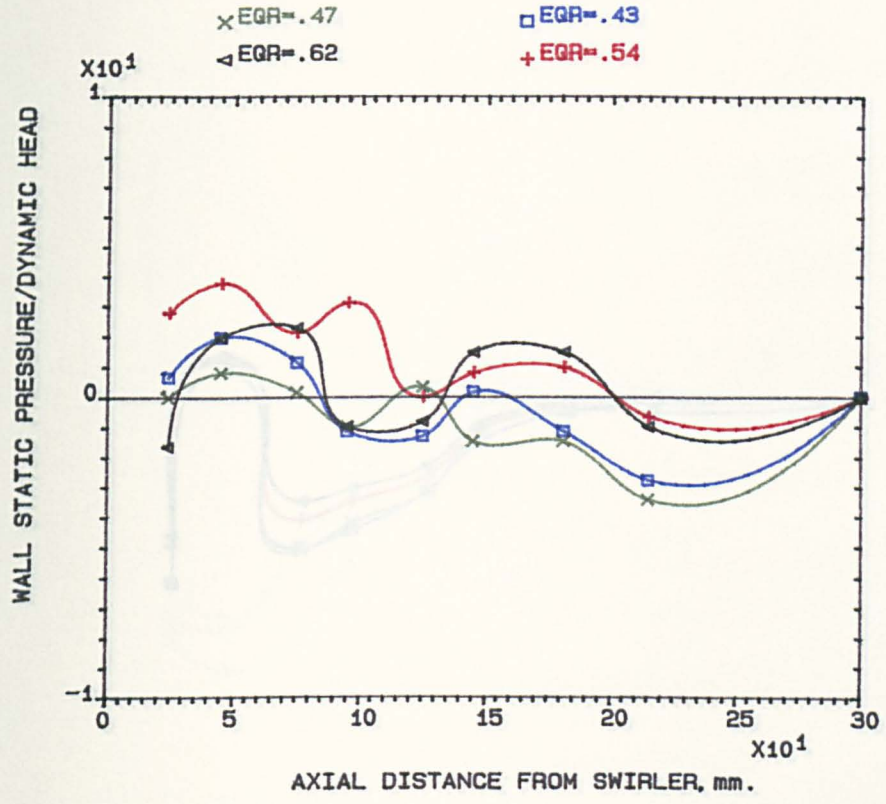

FIG.6.28 COMBUSTOR WALL STATIC PRESSURE V. AXIAL DISTANCE FROM SWIRLERS (A&C) CO-ROTATING, MN=.028, 76mm WALL INJ., KEROSENE, 600K.

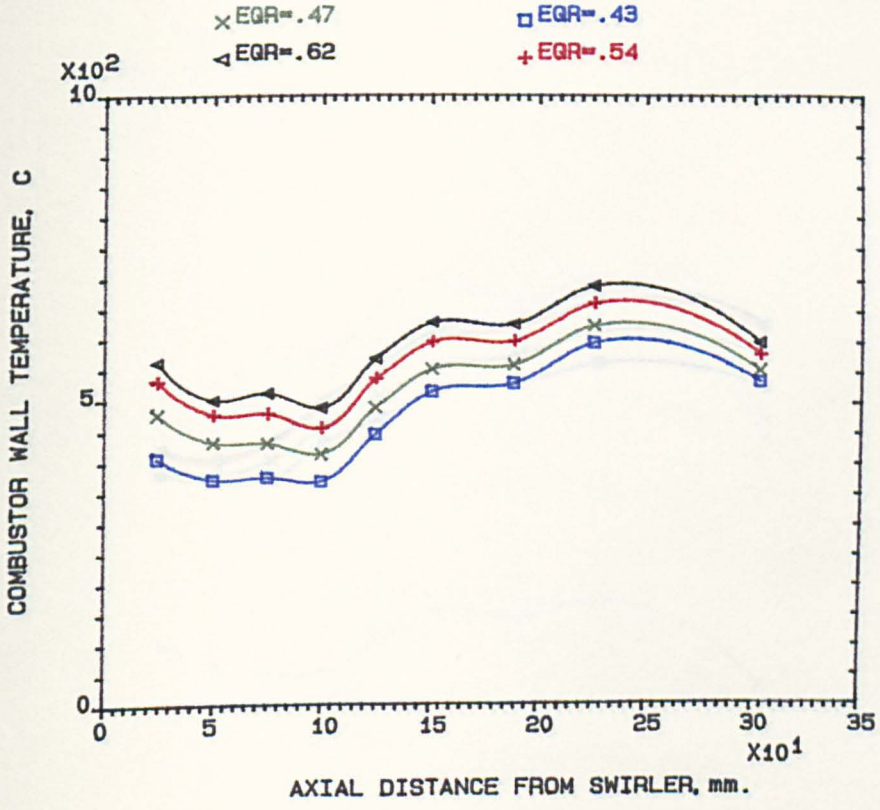

FIG.6.29 COMBUSTOR WALL TEMPERATURE V. AXIAL DISTANCE FROM SWIRLERS (A&C) CO-ROTATING, MN=.028, 76mm WALL INJ., KEROSENE, 600K.

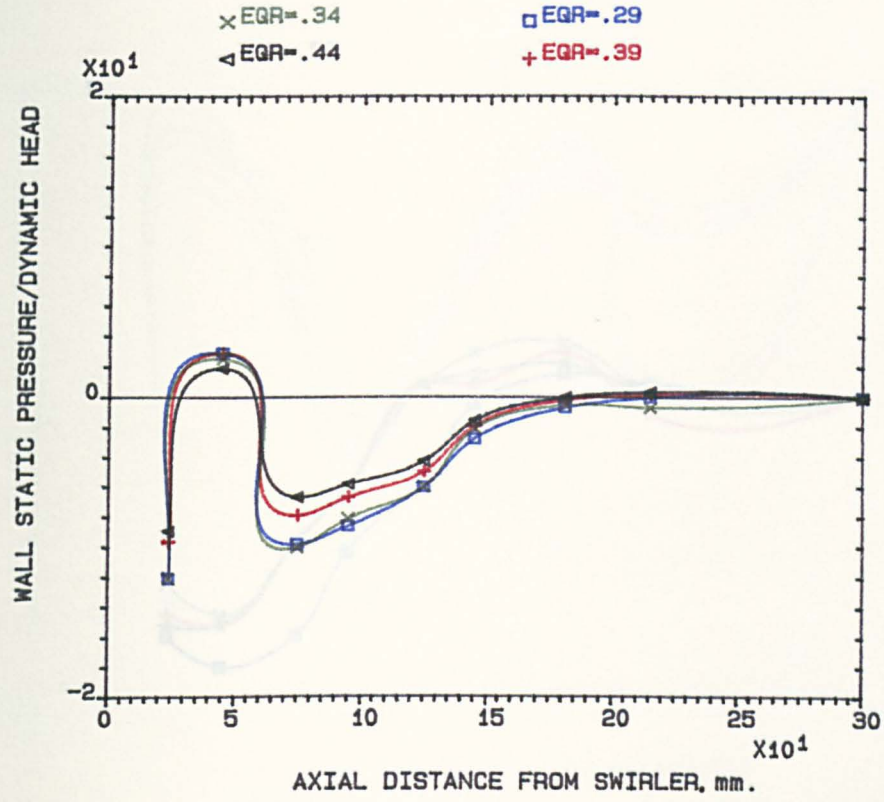

FIG.6.30 COMBUSTOR WALL STATIC PRESSURE V. AXIAL DISTANCE FROM SWIRLERS (B&C) CO-ROTATING, MN=.028, D.C.I., NATURAL GAS, 600K.

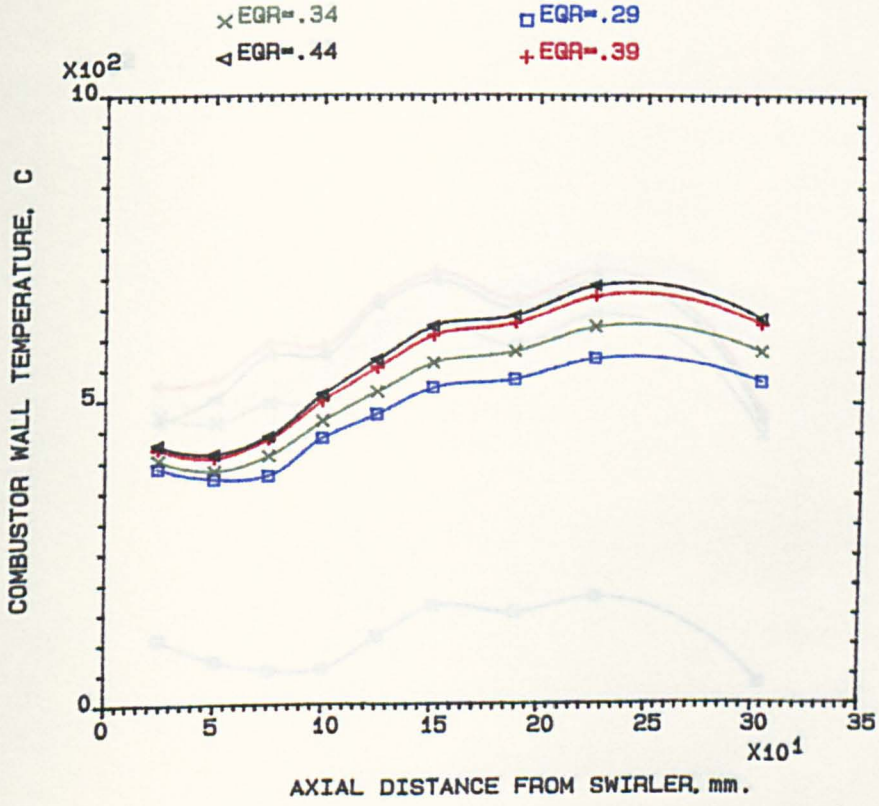

FIG.6.31 COMBUSTOR WALL TEMPERATURE V. AXIAL DISTANCE FROM SWIRLERS (B&C) CO-ROTATING, MN=.028, D.C.I., NATURAL GAS, 600K.

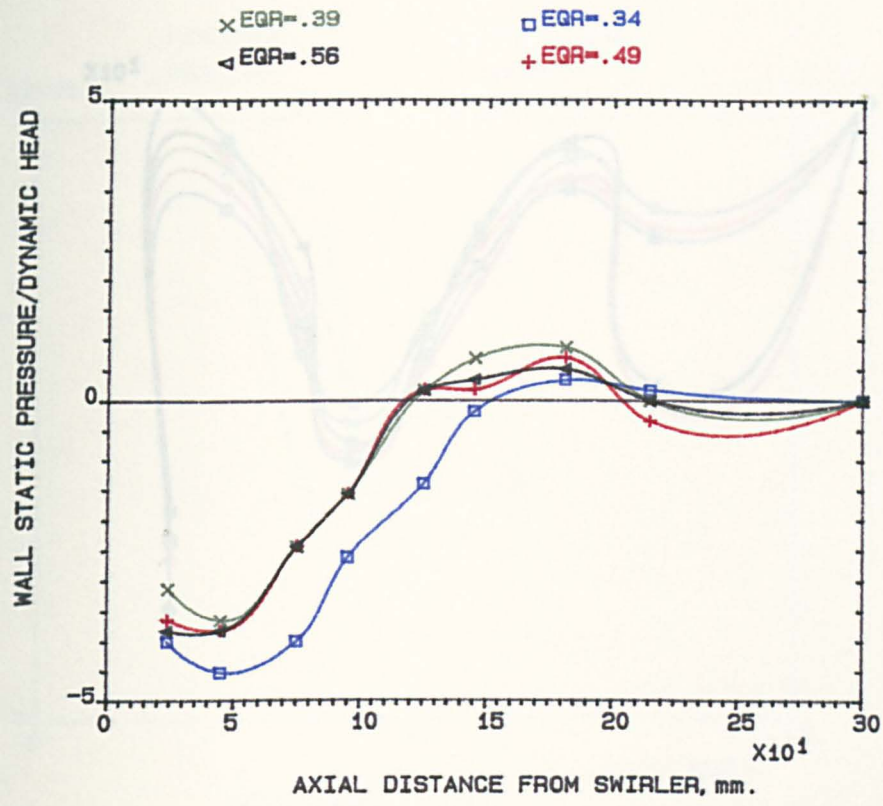

FIG.6.32 COMBUSTOR WALL STATIC PRESSURE V. AXIAL DISTANCE FROM SWIRLERS (B&C) COUNTER-ROTATING, MN=.028, D.C.I., NATURAL GAS, 600K.

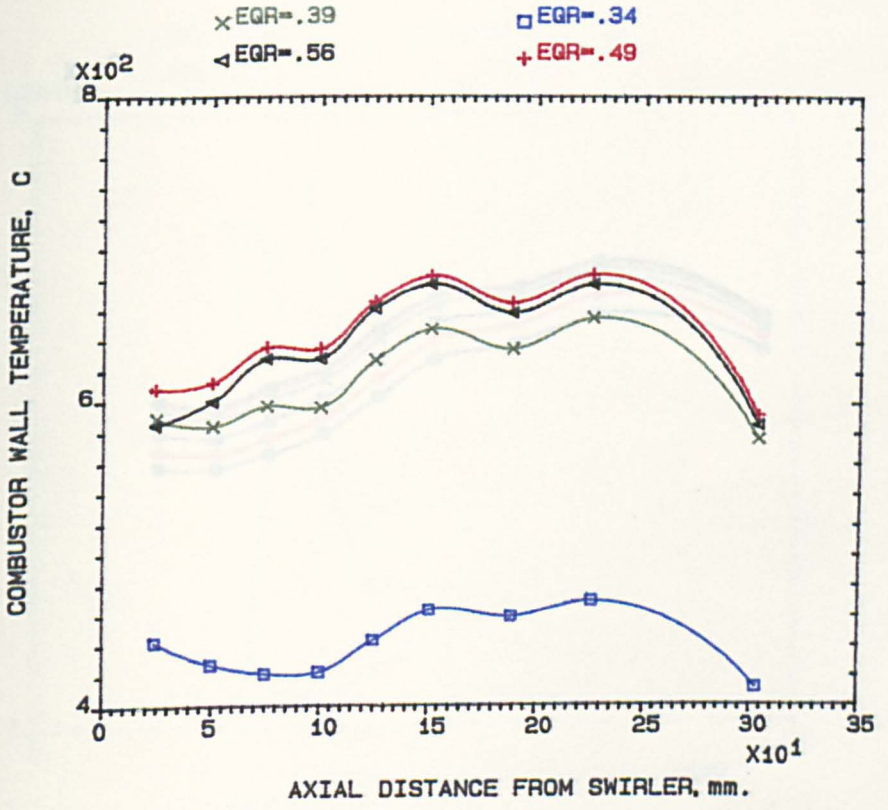

FIG.6.33 COMBUSTOR WALL TEMPERATURE V. AXIAL DISTANCE FROM SWIRLERS (B&C) COUNTER-ROTATING, MN=.028, D.C.I., NATURAL GAS, 600K.

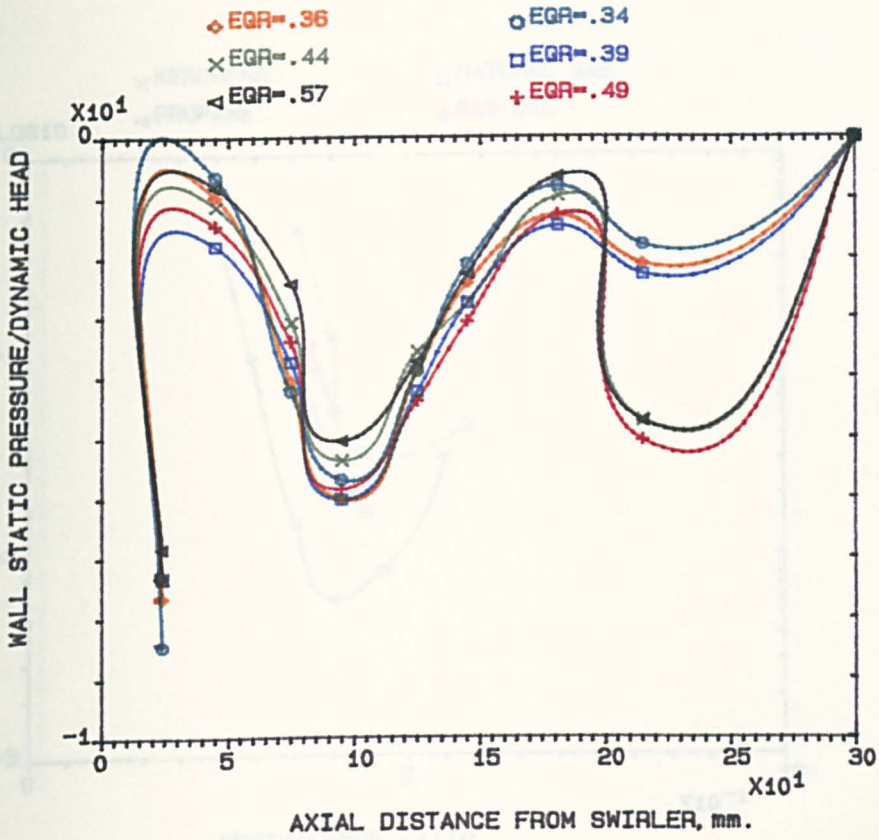

FIG.6.34 COMBUSTOR WALL STATIC PRESSURE V. AXIAL DISTANCE FROM SWIRLERS (A&C) CO-ROTATING, MN=.028, D.C.I., NATURAL GAS, 600K.

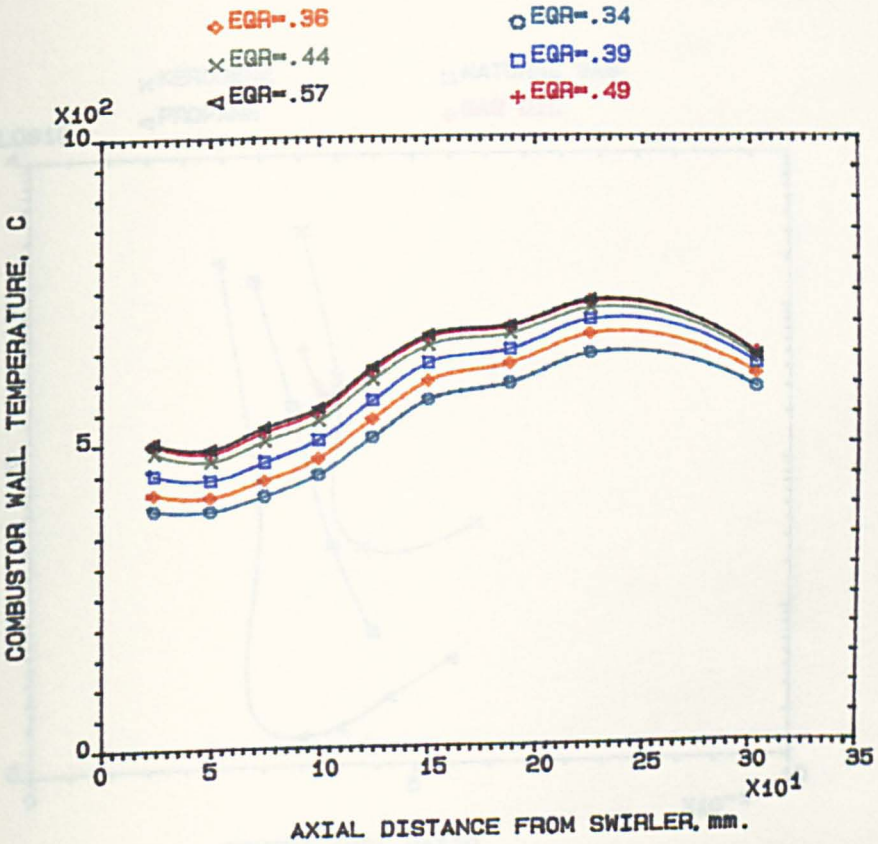

FIG.6.35 COMBUSTOR WALL TEMPERATURE V. AXIAL DISTANCE FROM SWIRLERS (A&C) CO-ROTATING, MN=.028, D.C.I., NATURAL GAS, 600K.

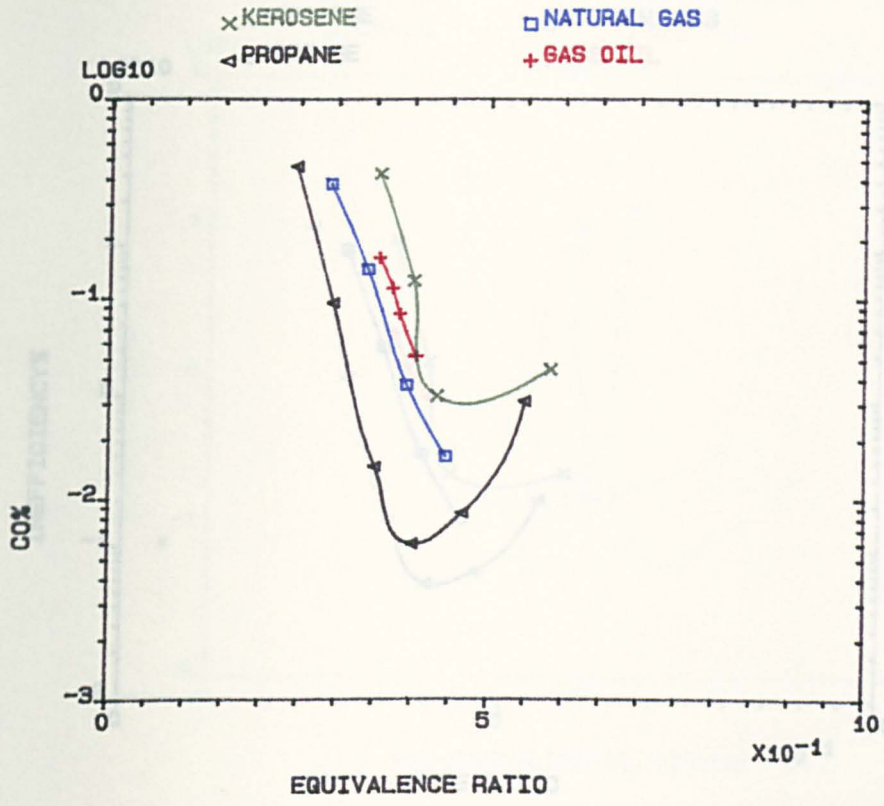

FIG.6.36 FUEL TYPE INFLUENCE ON CO-ROTATING RADIAL SWIRLER (B&C)
MEAN EMISSIONS OF CO% FOR CENTRAL RADIAL INJECTION, 600K.

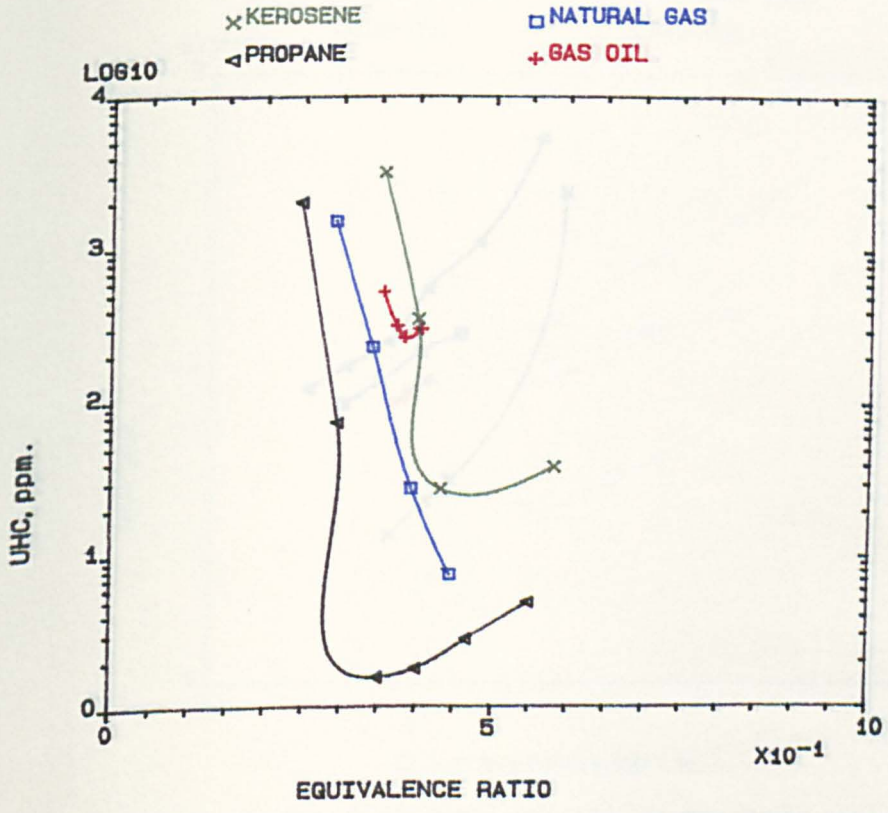

FIG.6.37 FUEL TYPE INFLUENCE ON CO-ROTATING RADIAL SWIRLER (B&C)
MEAN EMISSIONS OF UHC, FOR CENTRAL RADIAL INJECTION, 600K.

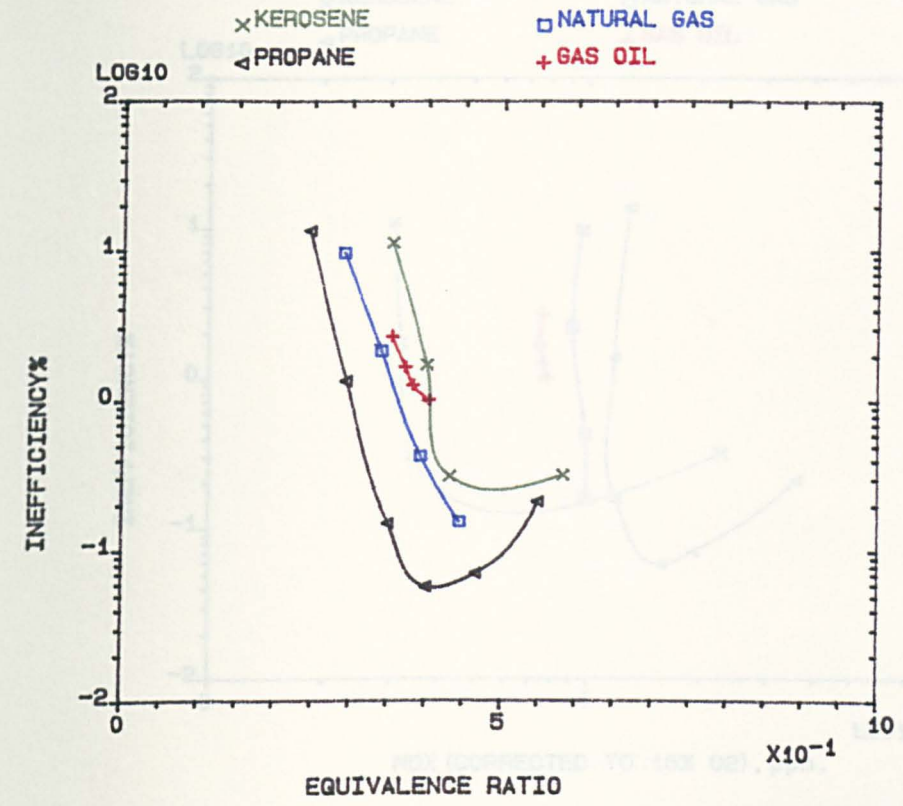

FIG.6.38 FUEL TYPE INFLUENCE ON CO-ROTATING RADIAL SWIRLER (B&C)
MEAN COMBUSTION INEFFICIENCY% FOR CENTRAL RADIAL INJECTION, 600K.

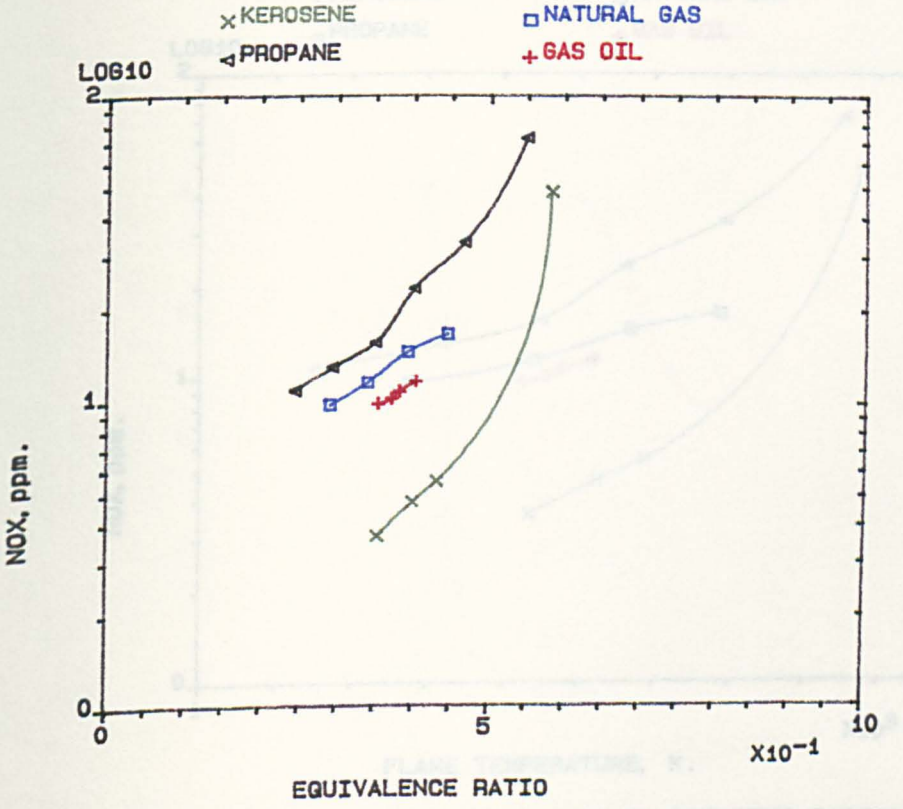

FIG.6.39 FUEL TYPE INFLUENCE ON CO-ROTATING RADIAL SWIRLER (B&C)
MEAN EMISSIONS OF NOX, FOR CENTRAL RADIAL INJECTION, 600K.

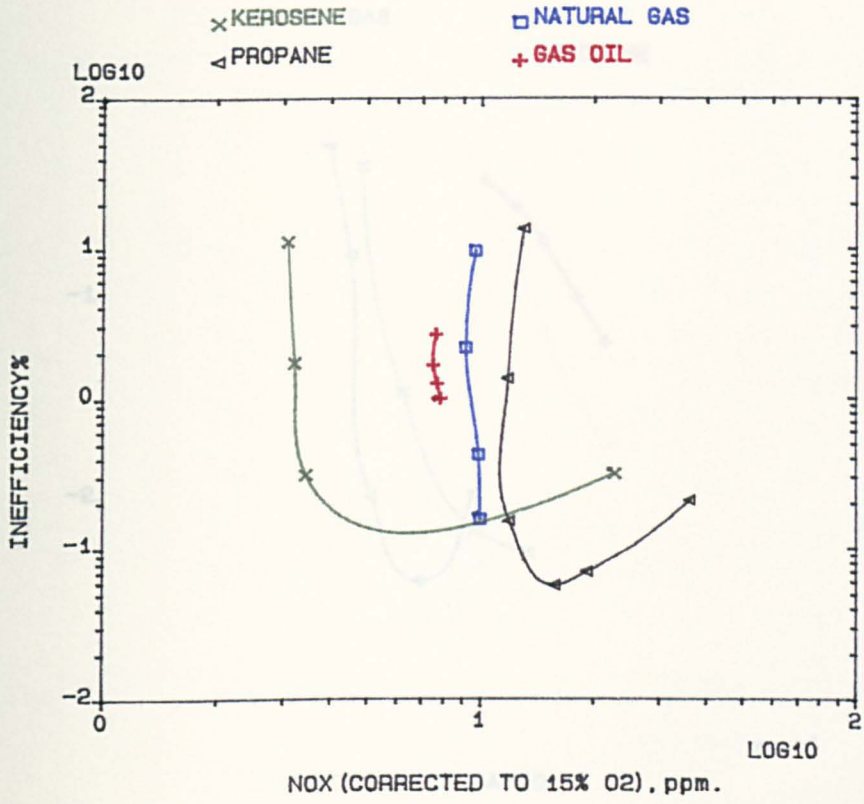

FIG.6.40 FUEL TYPE INFLUENCE ON CO-ROTATING RADIAL SWIRLER (B&C). NOXc VARIATION WITH INEFFICIENCY% FOR CENTRAL RADIAL INJECTION, 600K.

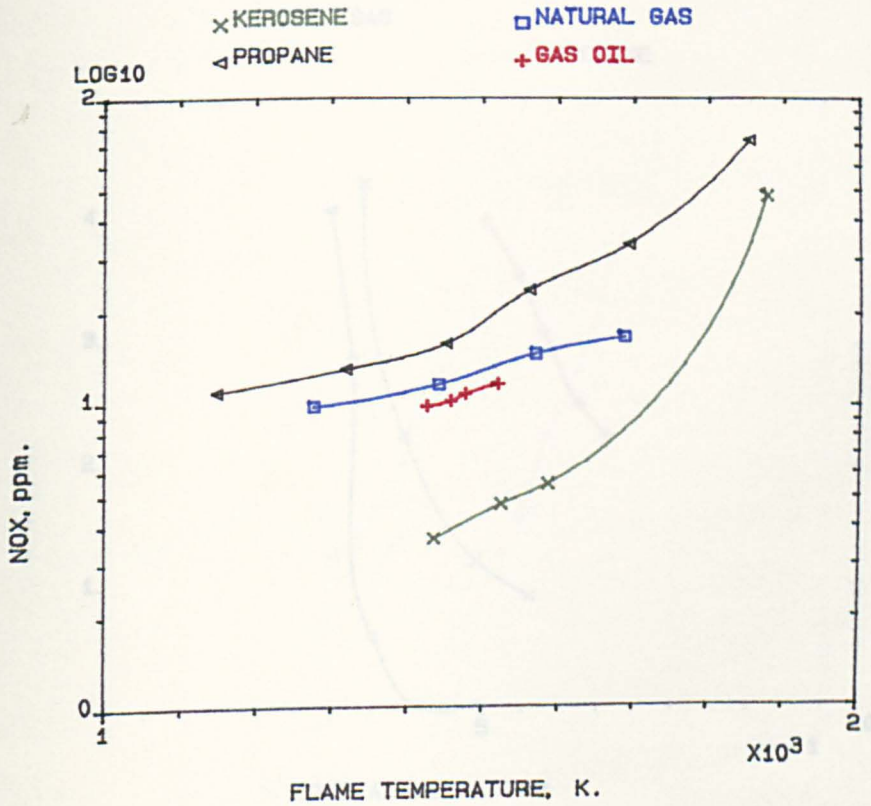

FIG.6.41 FUEL TYPE INFLUENCE ON CO-ROTATING RADIAL SWIRLER (B&C). NOX VARIATION WITH FLAME TEMPERATURE FOR CENTRAL RADIAL INJECTION, 60

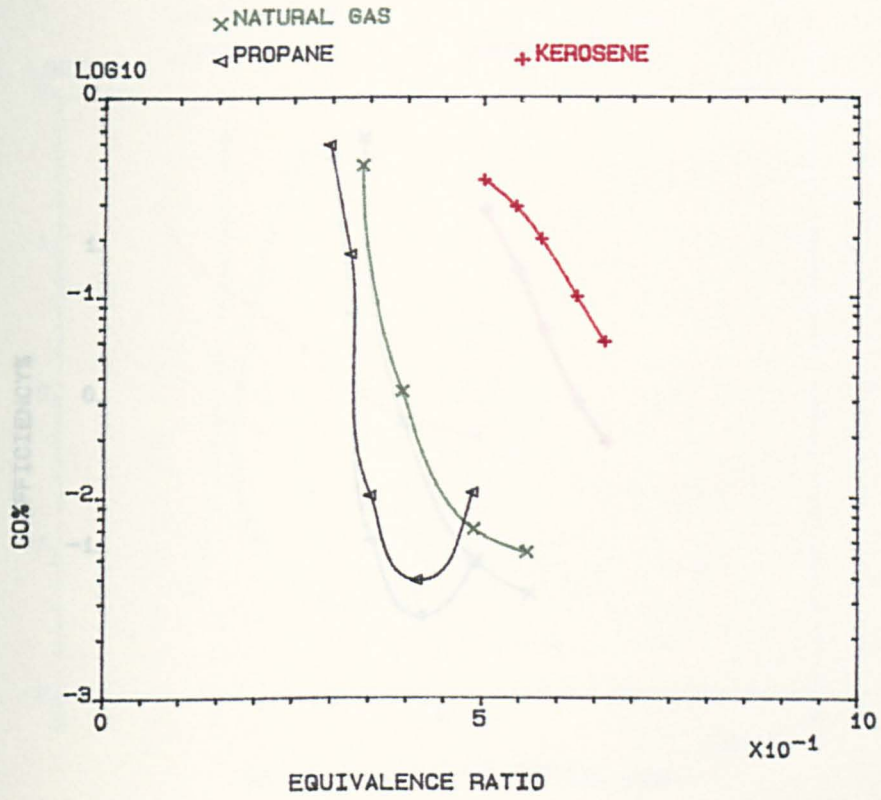

FIG.6.42 FUEL TYPE INFLUENCE ON COUNTER-ROTATING RADIAL SWIRLER (B&C) MEAN EMISSIONS OF CO% FOR CENTRAL RADIAL INJECTION, 600K.

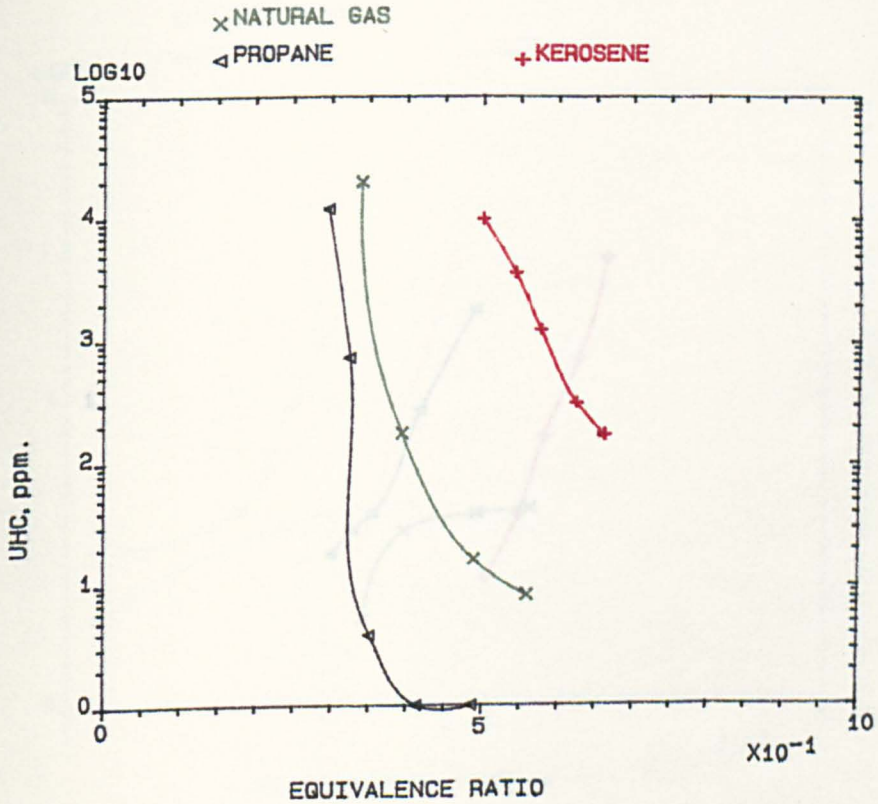

FIG.6.43 FUEL TYPE INFLUENCE ON COUNTER-ROTATING RADIAL SWIRLER (B&C) MEAN EMISSIONS OF UHC, FOR CENTRAL RADIAL INJECTION, 600K.

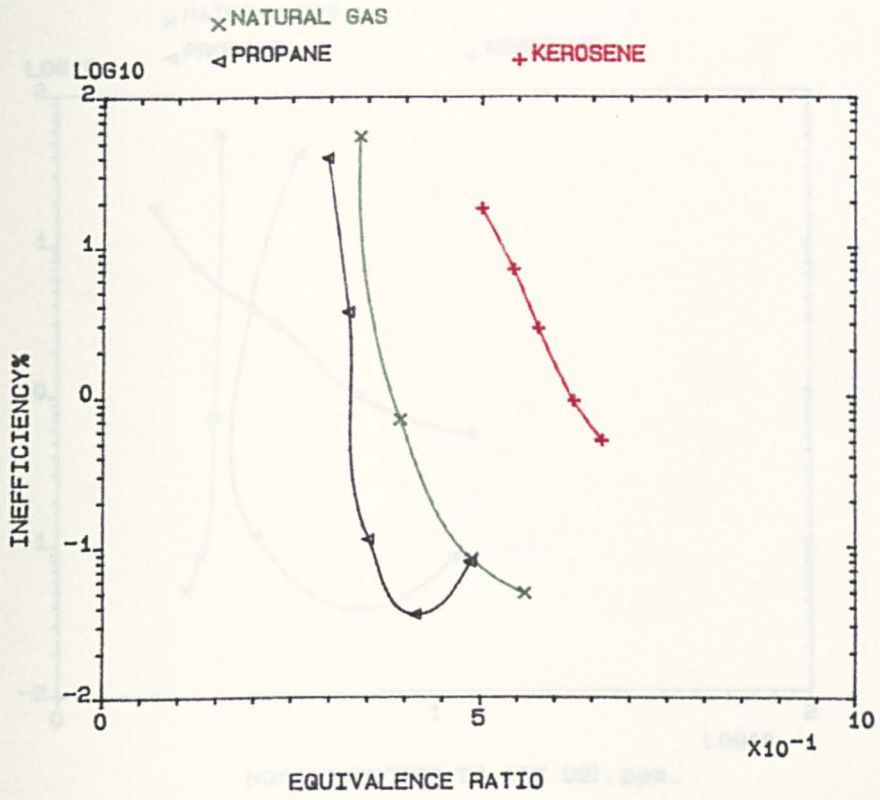

FIG.6.44 FUEL TYPE INFLUENCE ON COUNTER-ROTATING RADIAL SWIRLER (B&C)
MEAN COMBUSTION INEFFICIENCY% FOR CENTRAL RADIAL INJECTION, 600K.

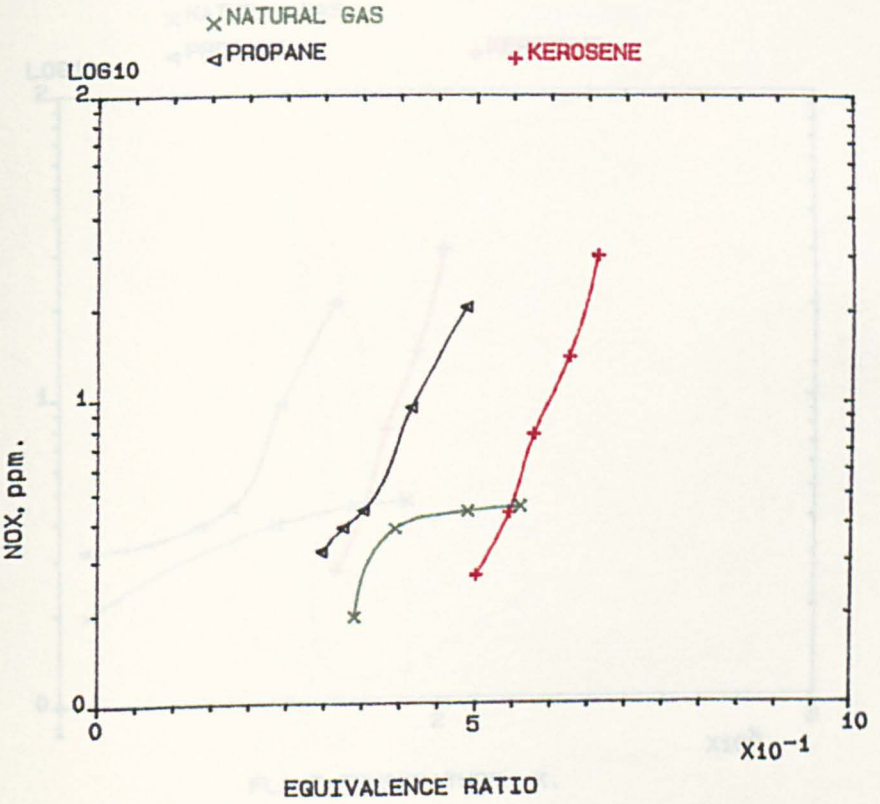

FIG.6.45 FUEL TYPE INFLUENCE ON COUNTER-ROTATING RADIAL SWIRLER (B&C)
MEAN EMISSIONS OF NOX, FOR CENTRAL RADIAL INJECTION, 600K.

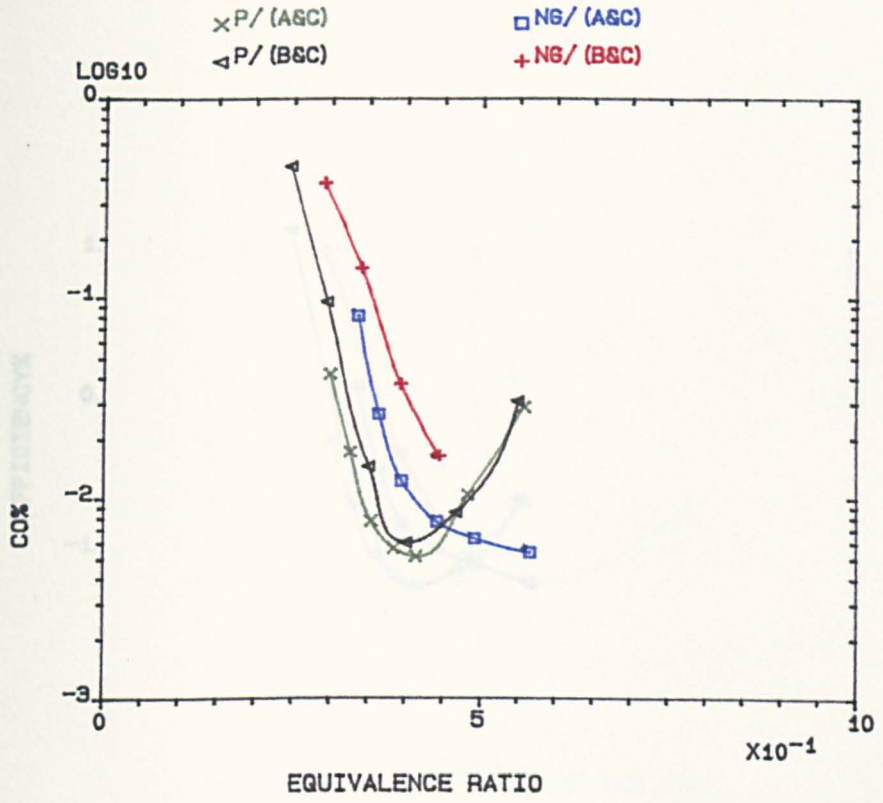

FIG.6.48 COMPARISON BETWEEN CO-ROTATING RADIAL SWIRLERS (B&C) AND (A&C) FOR CENTRAL RADIAL INJECTION, 600K.

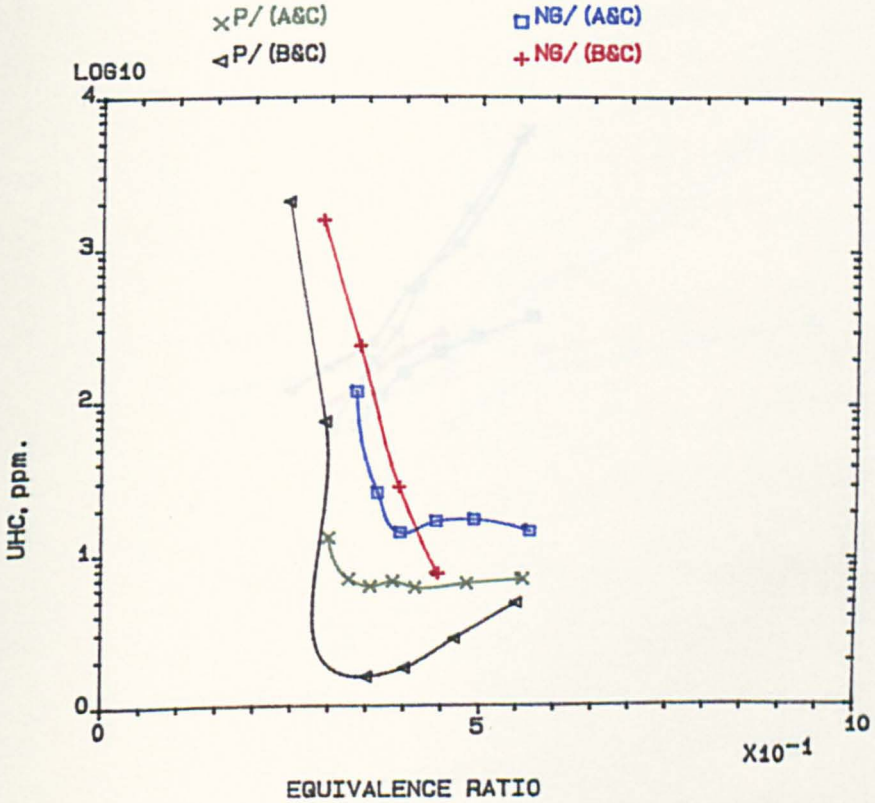

FIG.6.49 COMPARISON BETWEEN CO-ROTATING RADIAL SWIRLER (B&C) AND (A&C) FOR CENTRAL RADIAL INJECTION, 600K.

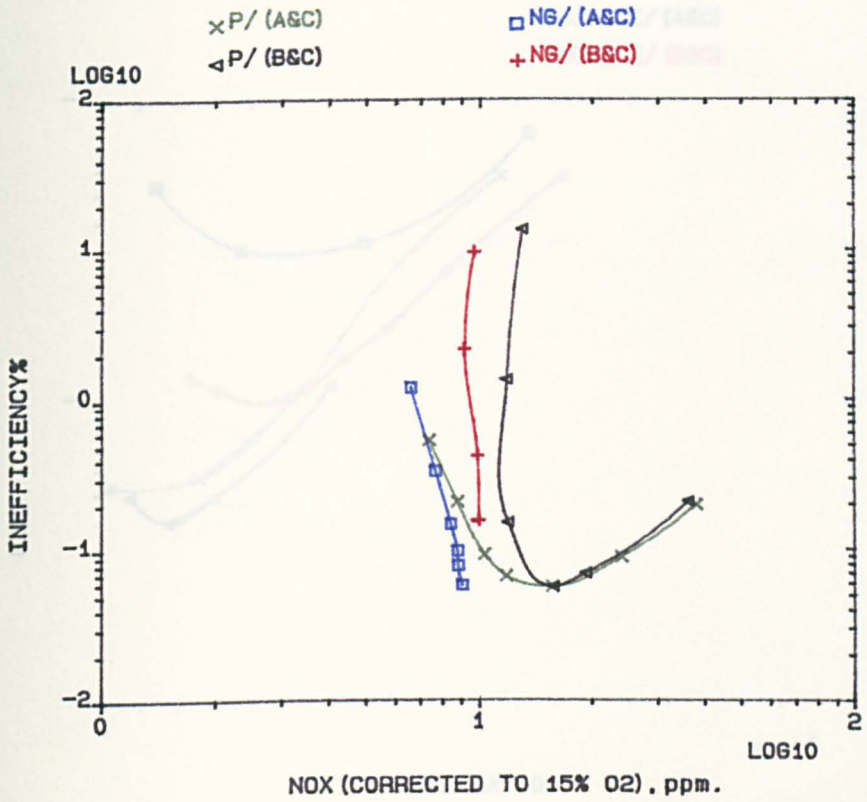

FIG.6.52 COMPARISON BETWEEN CO-ROTATING RADIAL SWIRLERS (B&C) AND (A&C), FOR CENTRAL RADIAL INJECTION, 600K.

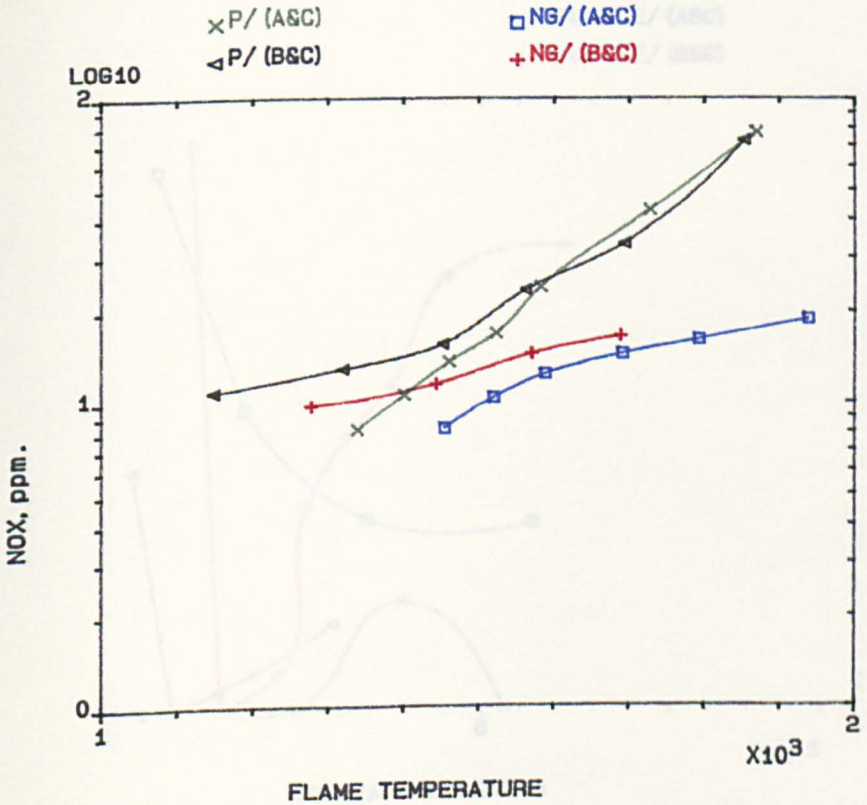

FIG.6.53 COMPARISON BETWEEN CO-ROTATING RADIAL SWIRLERS (B&C) AND (A&C) FOR CENTRAL RADIAL INJECTION, 600K.

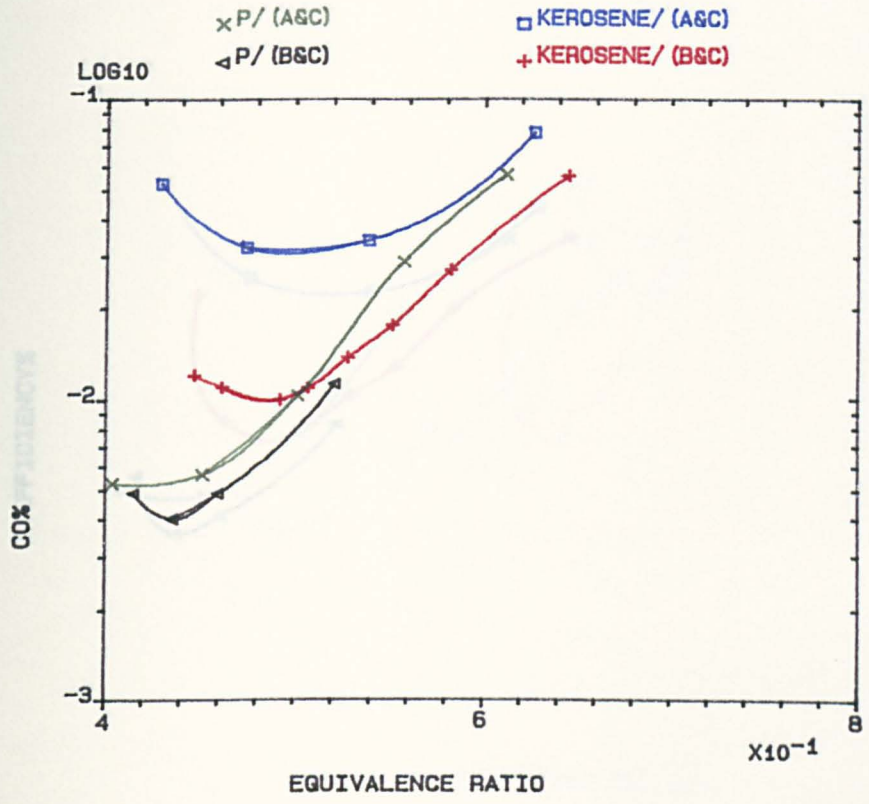

FIG.6.54 COMPARISON BETWEEN CO-ROTATING RADIAL SWIRLERS (B&C) AND (A&C) , USING 76mm WALL INJECTION, 600K.

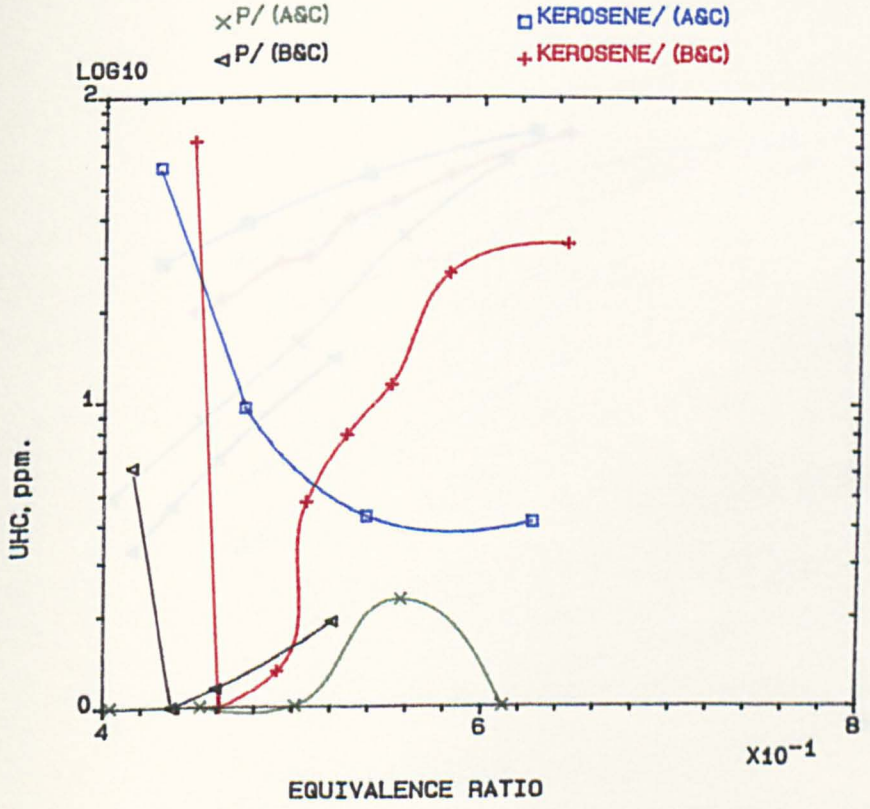

FIG.6.55 COMPARISON BETWEEN CO-ROTATING RADIAL SWIRLERS (B&C) AND (A&C), USING 76mm WALL INJECTION, 600K

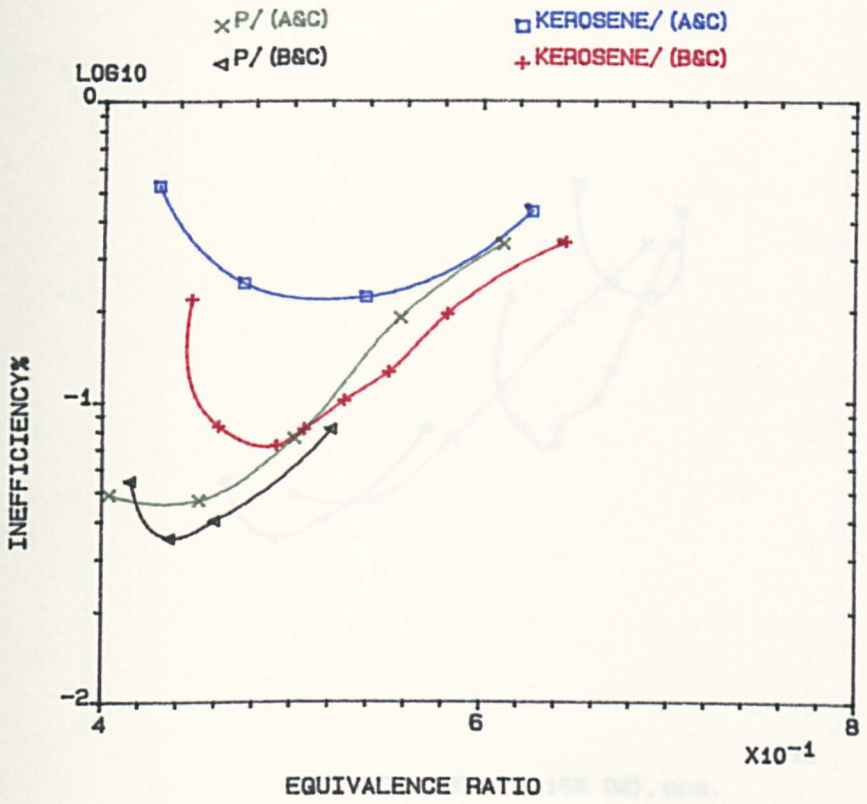

FIG.6.56 COMPARISON BETWEEN CO-ROTATING RADIAL SWIRLERS (B&C) AND (A&C). USING 76mm WALL INJECTION, 600K.

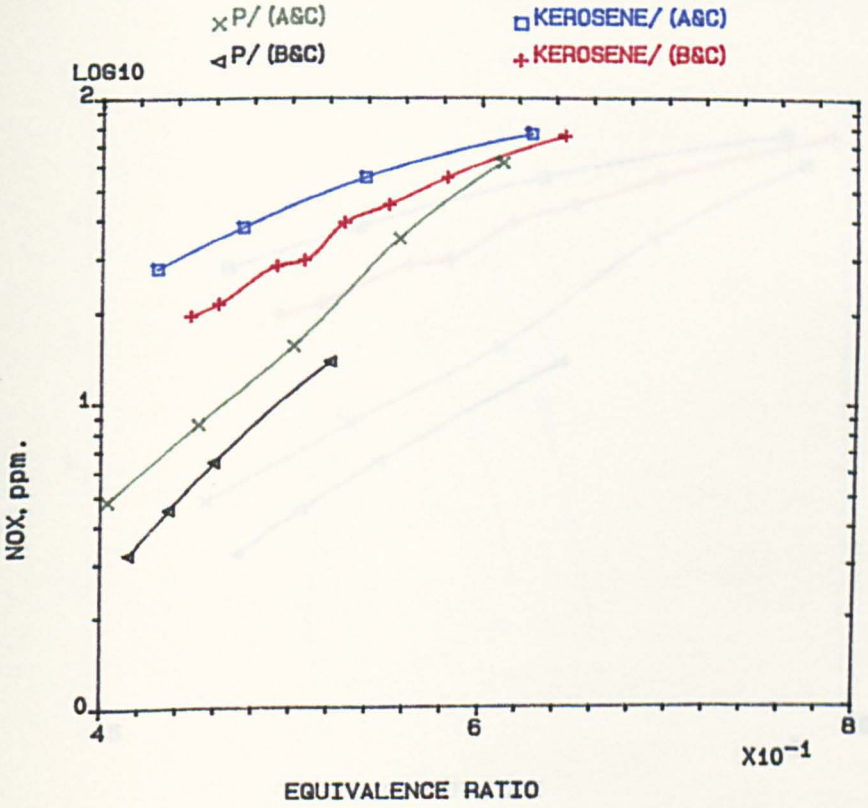

FIG.6.57 COMPARISON BETWEEN CO-ROTATING RADIAL SWIRLERS (B&C) AND (A&C). USING 76mm WALL INJECTION, 600K.

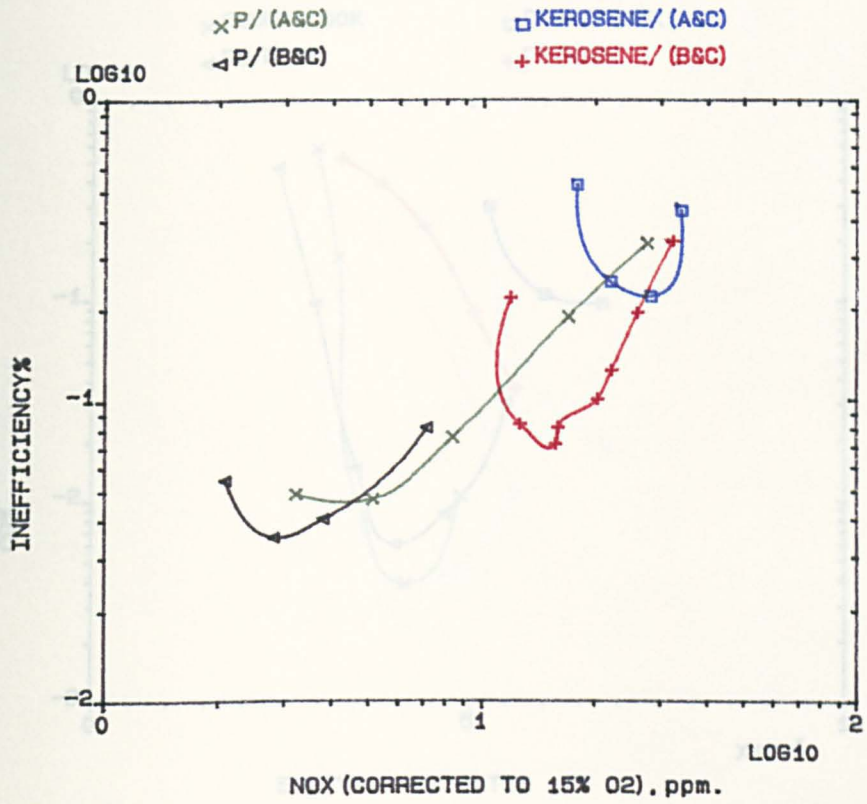

FIG.6.58 COMPARISON BETWEEN CO-ROTATING RADIAL SWIRLERS (B&C) AND (A&C). USING 76mm WALL INJECTION. 600K.

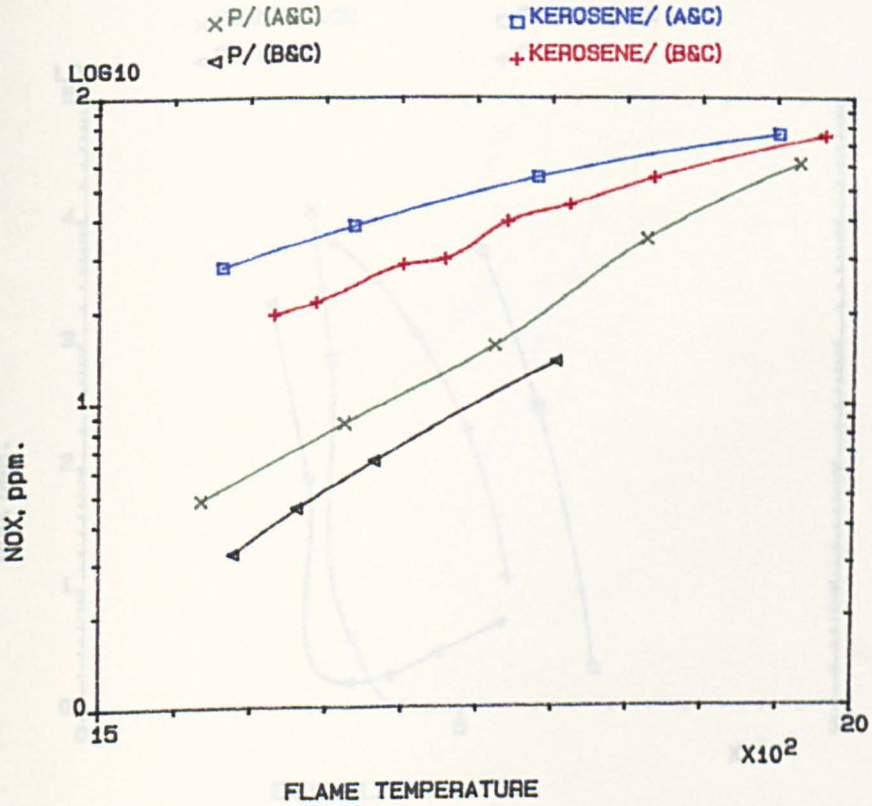

FIG.6.59 COMPARISON BETWEEN CO-ROTATING RADIAL SWIRLERS (B&C) AND (A&C). USING 76mm WALL INJECTION. 600K.

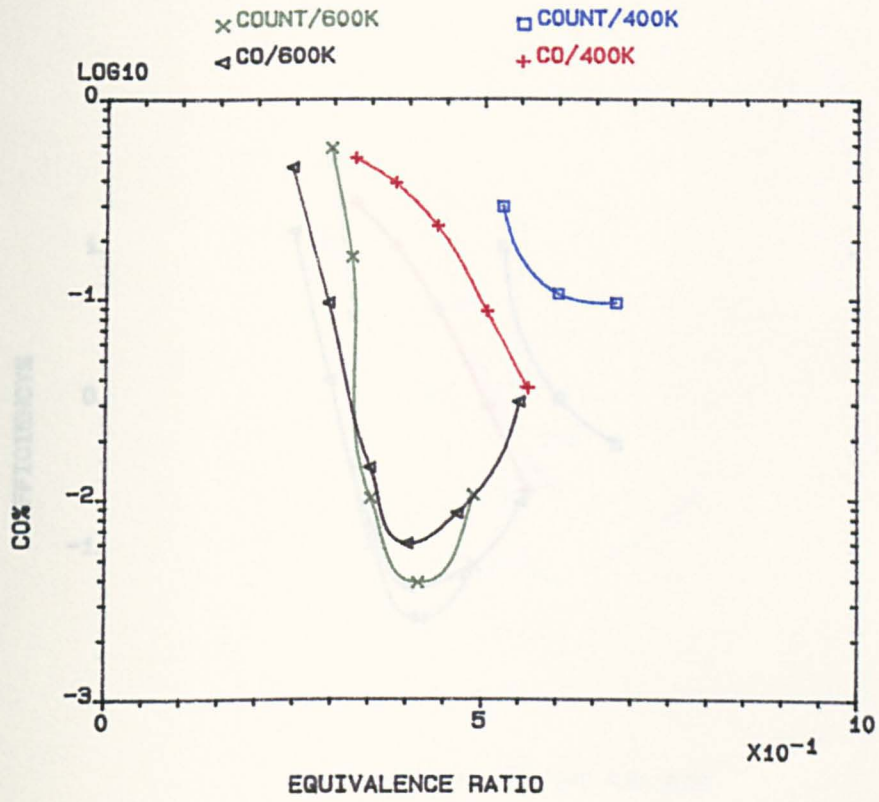

FIG.6.60 COMPARISON BETWEEN CO AND COUNTER-ROTATING RADIAL SWIRLERS (B&C) FOR PROPANE CENTRAL RADIAL INJECTION.

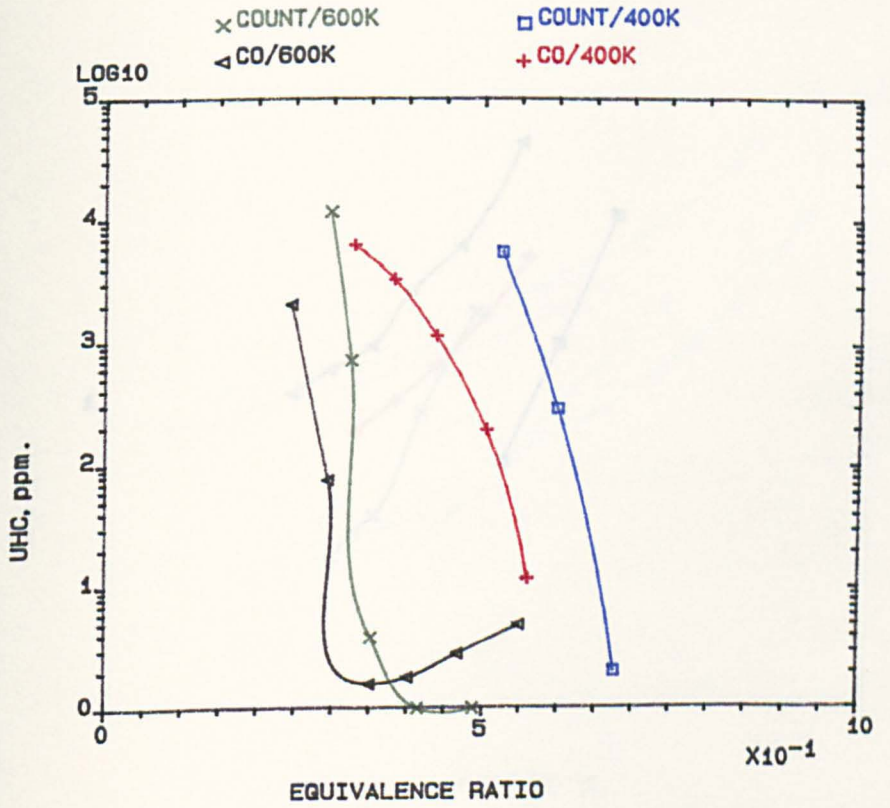

FIG.6.61 COMPARISON BETWEEN CO AND COUNTER-ROTATING RADIAL SWIRLERS (B&C) FOR PROPANE CENTRAL RADIAL INJECTION.

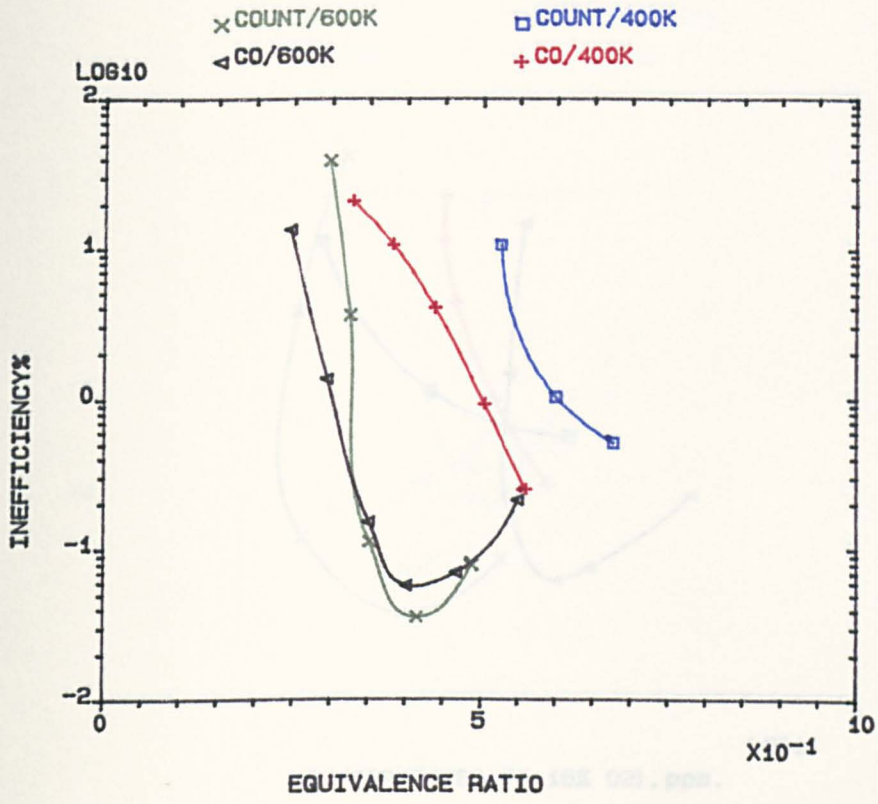

FIG.6.62 COMPARISON BETWEEN CO AND COUNTER-ROTATING RADIAL SWIRLERS (B&C) FOR PROPANE CENTRAL RADIAL INJECTION.

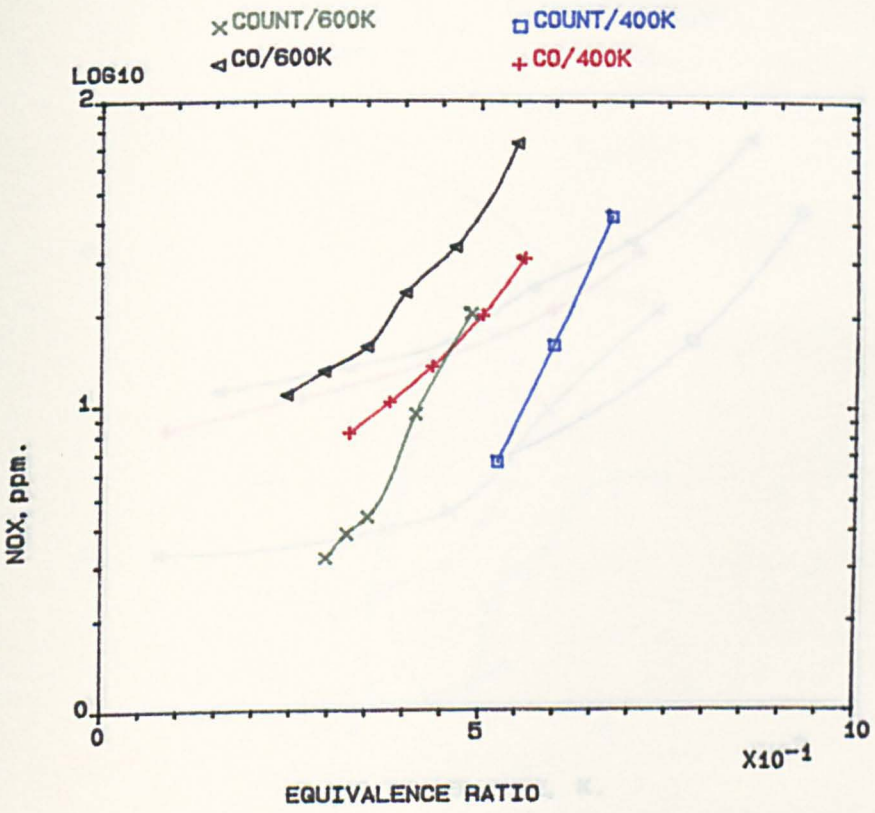

FIG.6.63 COMPARISON BETWEEN CO AND COUNTER-ROTATING RADIAL SWIRLERS (B&C) FOR PROPANE CENTRAL RADIAL INJECTION.

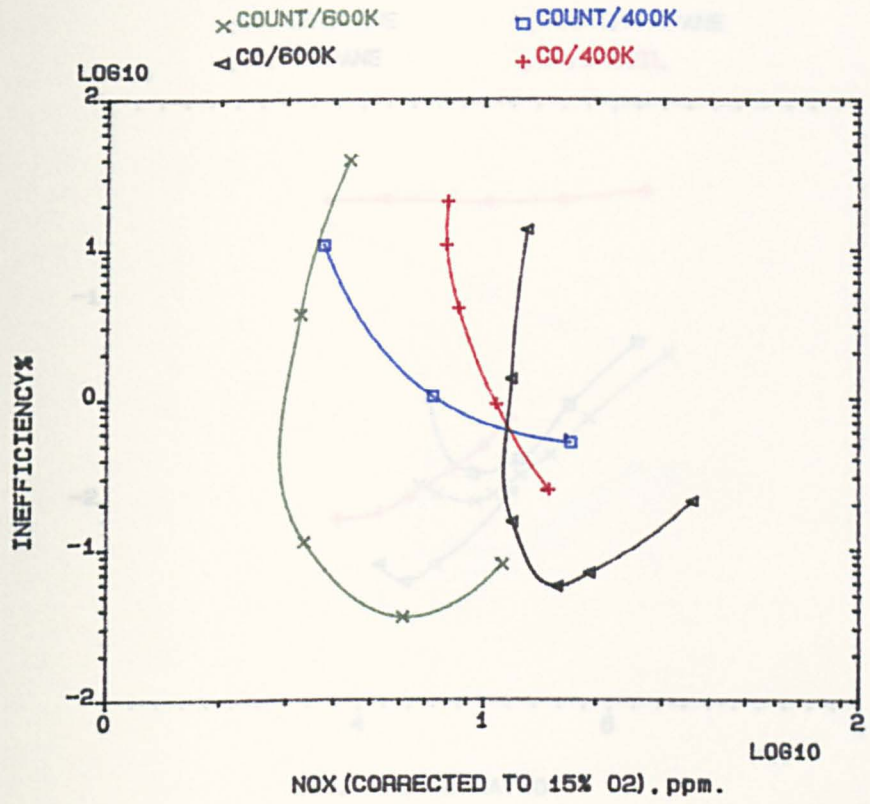

FIG.6.64 COMPARISON BETWEEN CO AND COUNTER-ROTATING RADIAL SWIRLERS (B&C) FOR PROPANE CENTRAL RADIAL INJECTION.

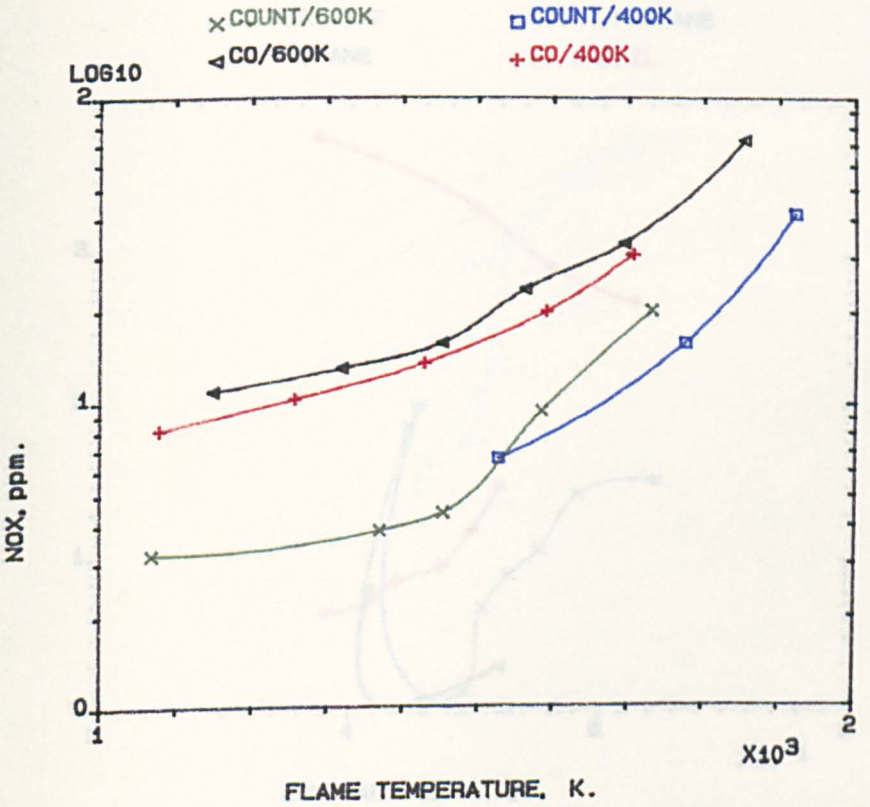

FIG.6.65 COMPARISON BETWEEN CO AND COUNTER-ROTATING RADIAL SWIRLERS (B&C) FOR PROPANE CENTRAL RADIAL INJECTION.

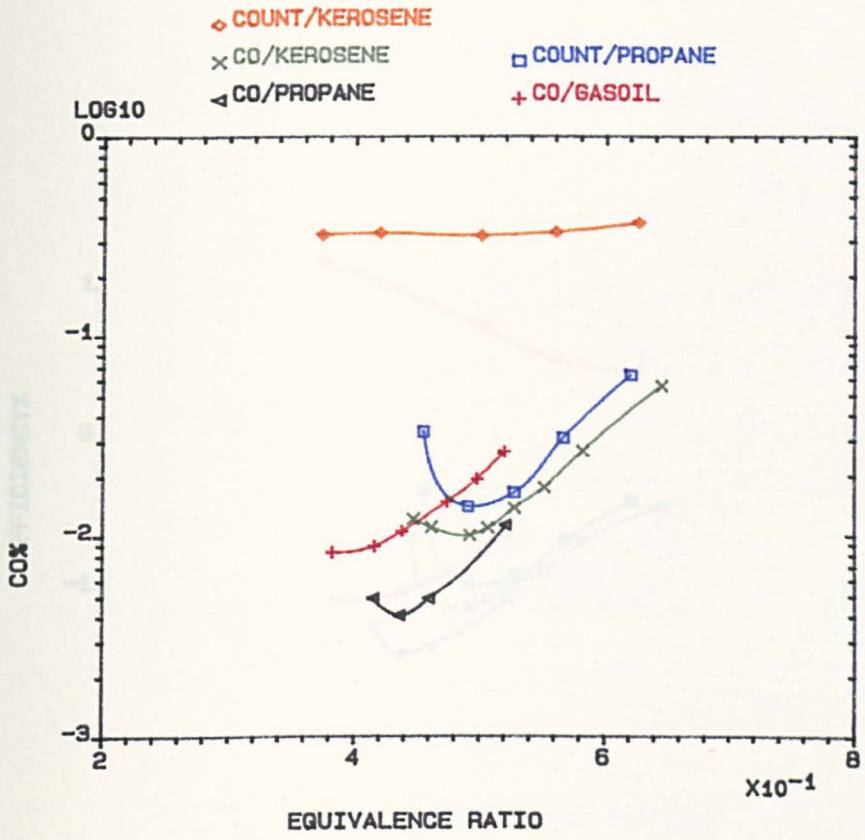

FIG.6.66 COMPARISON BETWEEN CO AND COUNTER-ROTATING RADIAL SWIRLERS (B&C) USING 76mm WALL INJECTION, 600K.

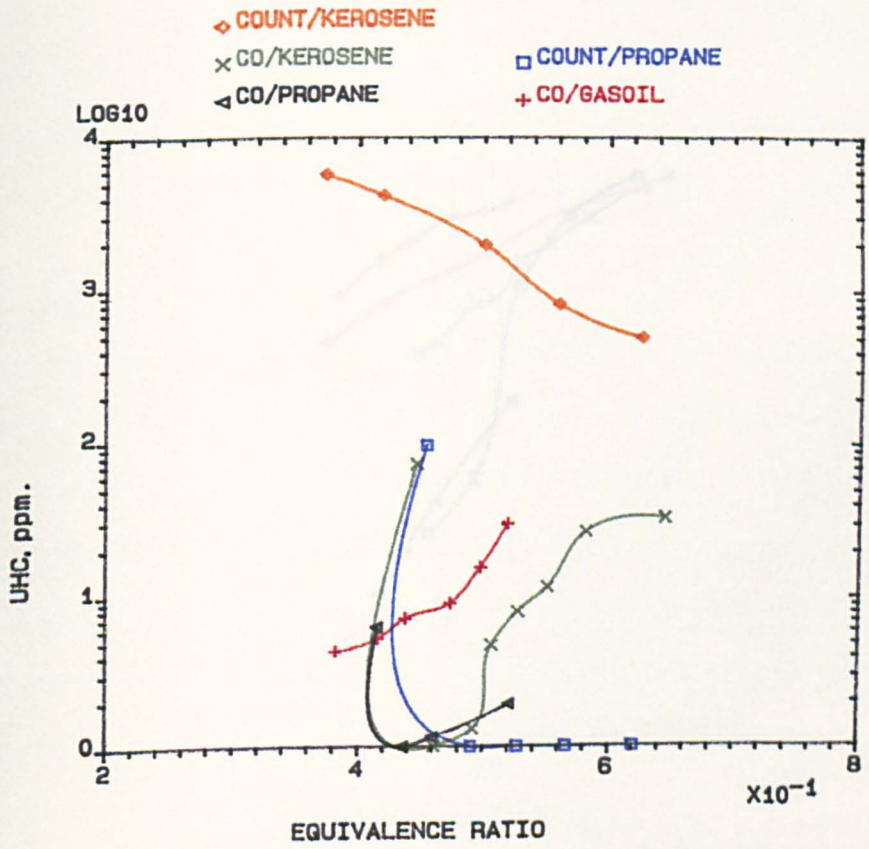

FIG.6.67 COMPARISON BETWEEN CO AND COUNTER-ROTATING RADIAL SWIRLERS (B&C) USING 76mm WALL INJECTION, 600K.

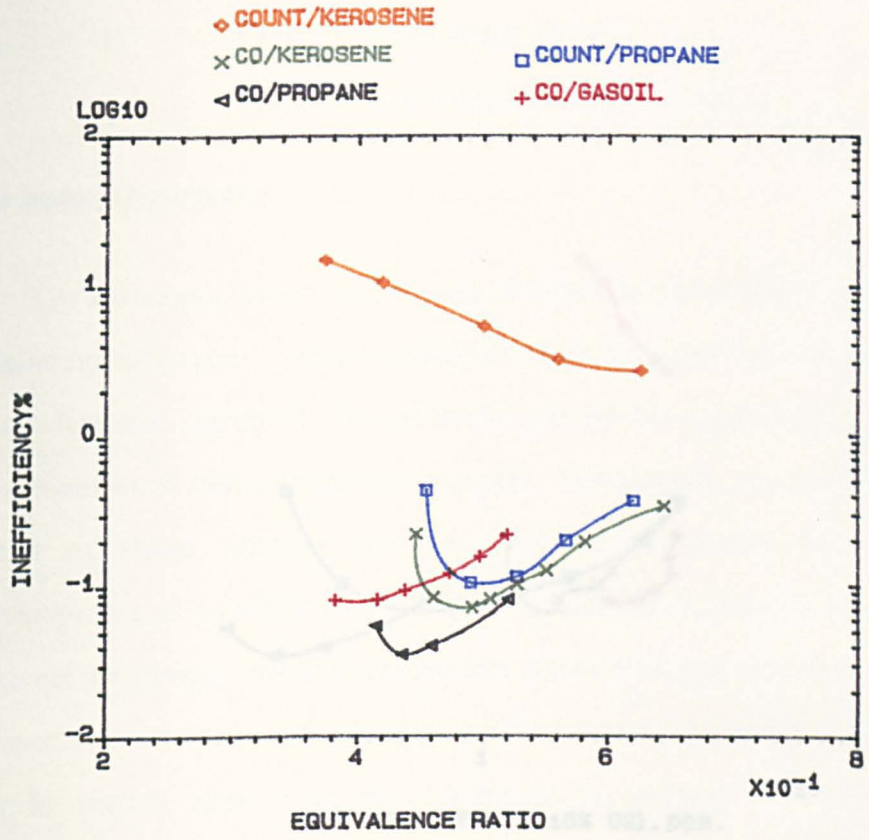

FIG.6.68 COMPARISON BETWEEN CO AND COUNTER-ROTATING RADIAL SWIRLERS (B&C) USING 76mm WALL INJECTION, 600K.

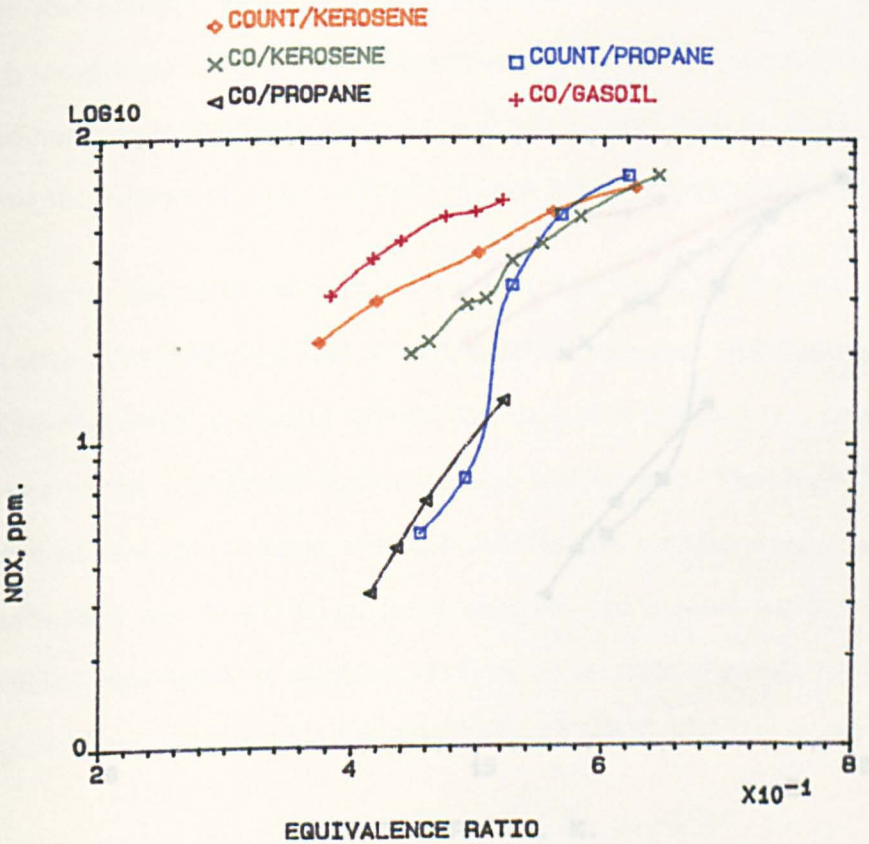

FIG.6.69 COMPARISON BETWEEN CO AND COUNTER-ROTATING RADIAL SWIRLERS (B&C) USING 76mm WALL INJECTION, 600K.

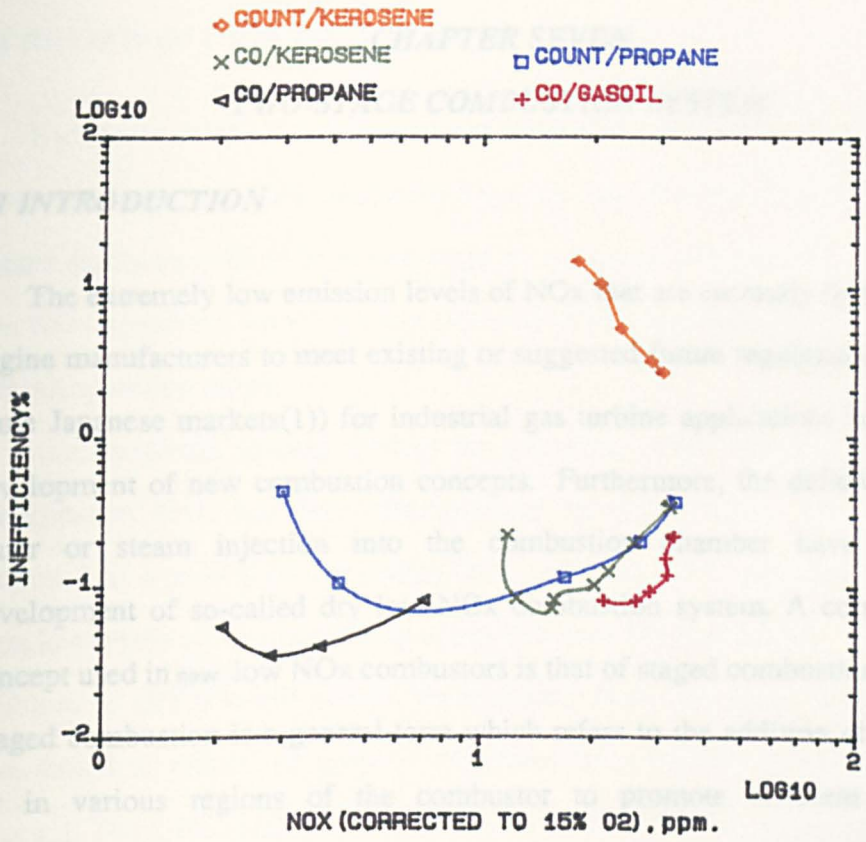

FIG.6.70 COMPARISON BETWEEN CO AND COUNTER-ROTATING RADIAL SWIRLERS (B&C) USING 76mm WALL INJECTION, 600K.

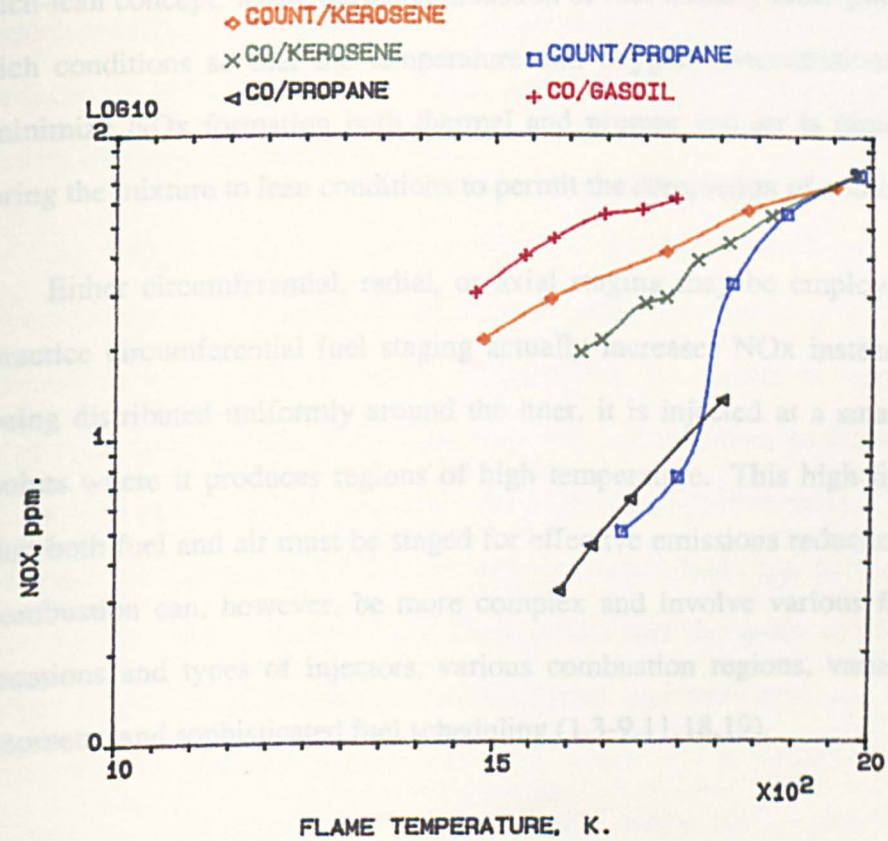

FIG.6.71 COMPARISON BETWEEN CO AND COUNTER-ROTATING RADIAL SWIRLERS (B&C) USING 76mm WALL INJECTION, 600K.

CHAPTER SEVEN

TWO-STAGE COMBUSTION SYSTEM

7.1 INTRODUCTION

The extremely low emission levels of NOx that are currently being sought by engine manufacturers to meet existing or suggested future regulations (15 ppm in some Japanese markets(1)) for industrial gas turbine applications has led to the development of new combustion concepts. Furthermore, the deficiencies in the water or steam injection into the combustion chamber have led to the development of so-called dry low NOx combustion system. A common design concept used in new low NOx combustors is that of staged combustion.

Staged combustion is a general term which refers to the addition of fuel and/ or air in various regions of the combustor to promote different combustion environments in different sections of the combustor. Staged combustion is used to modulate combustion stoichiometry so that NOx and CO emissions are both well controlled. The most common type of staged combustion is probably the rich-lean concept, where partial combustion of fuel initially takes place under fuel rich conditions so that the temperature and oxygen concentrations are low to minimize NOx formation both thermal and prompt and air is rapidly added to bring the mixture to lean conditions to permit the completion of combustion.

Either circumferential, radial, or axial staging may be employed(2), but in practice circumferential fuel staging actually increases NOx instead of the fuel being distributed uniformly around the liner, it is injected at a small number of points where it produces regions of high temperature. This high lights the fact that both fuel and air must be staged for effective emissions reduction(2). Staged combustion can, however, be more complex and involve various fuel injection locations and types of injectors, various combustion regions, variable air flow geometry and sophisticated fuel scheduling (1,3-9,11,18,19).

7.2 REVIEW OF PREVIOUS WORK

Kuroda et al(10) developed a two-stage combustor to meet stringent NOx limitations in Japan. Their combustion system has a fuel-air control mechanism to ensure stable switching from one-stage to two-stage combustion. They reported that NOx emissions were very low not only at full load but also in the entire gas turbine operating range.

A partial oxidation staging concept for gas turbine combustors using broadened specification fuels has been demonstrated by Clayton(12). The concept was proposed as a means of controlling NOx, CO and UHC pollutant emissions to ultra low levels while maintaninig acceptable lean blowout limits.

Sjoblom et al(13) tested double recirculation zone two stage combustor which was aimed to reduce all gaseous emissions by using the rich-lean combustion concept. The UHC goal was met and the CO concentration was close to the goal whereas the NOx level was reduced by 25 - 30%. Furthermore, Sjoblom(14) investigated the effect of primary/secondary fuel flow split on emissions. Flash vaporization was employed to ensure complete vaporisation of the secondary fuel, which was heated to 600K by the combustor inlet air. The best configuration reduced the NOx by 54%, CO by 59% and UHC by 97% as compared to emission levels for some standard combustor.

By using radial flow swirler White et al(16,20) developed a combustor concepts for the dry reduction of thermal NOx, the control of NOx from fuels containing high levels of organic nitrogen, and the control of smoke from low hydrogen content fuels. They used lean-lean and rich-lean combustion concepts for a wide variety of fuels and operation of their combustion system involved lean primary zone operation for the low energy content fuels and rich-lean mode for the medium energy content fuel. Their results met the goals of providing NOx levels below 75 ppm corrected to 15% oxygen, and were generally insensitive to inlet pressure and temperature conditions. Lewis and Holladay(15) developed a burner using an air and fuel staging concept, where the combustion zone was divided into two equal parts, a pilot zone and a secondary zone. The engine light-

off and idle was on the pilot zone fuel only. Secondary zone fuel was added as the engine accelerated and the fuel-air ratios in the two zones became equal at high power levels. The mixing inside the burner was achieved at reasonable pressure loss by swirling the pilot and secondary combustion zones in opposite directions (counter-swirl system).

Smith(17) developed a burner with the concept of fuel staging through primary fuel injection and a pilot fuel injector which was situated downstream of the former. The pilot flame was intended to operate only at simulated part load operation to provide an ignition source for the primary combustion process. Pilot fuel was introduced onto external surface of the injector centerbody where it mixed with air-assisted flow. The pilot was designed to operate at a higher fuel/air ratio than the primary combustion process and, consequently, was considerably more stable than the main flame.

Rosfjord et al(18) employed rich-lean concept on a stationary gas turbine combustion system to evaluate the synthetic fuel character effects on combustor emissions, performance, and durability. Four synthetic fuels and NO.2 petroleum distillate fuel were tested in a subscale combustor over a wide range of conditions. They showed that rich-lean combustor results indicated an increase in smoke and liner heating but NOx emissions were very low and insensitive to combustor pressure and fuel bound nitrogen. Rosfjord et al(19) used gaseous fuels produced from coal with heating values much lower than natural gas. Their objective was to evaluate the performance and emission characteristics of a rich-lean staged combustion and achieve ultra low NOx and CO emissions for coal gas fuel with heating values of 210 kJ/mol or higher. Lean combustion needed to achieve the same with lower heating values. Moreover, they reported that staged combustion had the ability to limit the NH3 to NOx conversion rate to less than 5 percent.

Sotheran et al(21) demonstrated an axially staged premixed low NOx emissions combustor. Particular emphasis was placed on the many mechanical and thermal problems which were encountered and which seem characteristic of the type, of these, the risks of autoignition and flash back in the premixing duct were perhaps,

the most severe.

The General Electric company developed various dry combustor methods to reduce NOx emissions(4). Their low NOx development work had progressed to the point that by 1980, the dry low NOx combustor had evolved to a dual fuel, two-stage combustion system with six primary nozzles arranged in an annulus and one secondary nozzle in the centre body. The modes of operation of this combustor are summarised in Fig.7.2. Ignition, acceleration and low load operation take place with the flame only in the primary zone. Low power operation was possible on the first stage burning where typical diffusion flames existed to provide a good flame stability and low CO emissions. Second stage burning provided to reduce NOx levels compared with the primary combustor but at the cost of an increase in CO and UHC. In the lean-lean mode a trade-off was possible between NOx emissions and CO and UHC at a fixed overall equivalence ratio where NOx emissions were reduced as the second stage fuel flow was increased and CO and UHC increased as the secondary fuel flow was increased. Finally, the premixed mode offered low NOx emissions at high power conditions. During this premixed operation, the fuel split was varied to achieve optimum emissions. However, CO and UHC were found to increase when the operation was switched to the premixed mode.

There are other methods which offer a dry reduction in gaseous pollutants. One of those involved the catalytic combustion technology which have been investigated by some workers(22,23,24). However, more development efforts are needed to make such equipment commercially viable. Catalyst materials must be developed that will have long life and thermal resistance. The catalyst bed should withstand about 1300C for near future gas turbines with a high thermal shock resistance However, no catalyst is currently good enough to meet all these requirements.

7.2.1 OXIDES OF NITROGEN FROM STAGED COMBUSTION

The NO formation rate is strongly dependent on temperature and hence for the adiabatic combustion in gas turbines is strongly dependent on the equivalence ratio(25). In view of difficulties establishing the extent of NO to NO_2 reaction in the gas sample probe(26,29) the results are mainly reported as NOx($NO+NO_2$). The NO to NO_2 conversion in the flame, may occur via the HO_2 radical where the cooler air swirling around the central hot combustion products from the pilot region mixes.

There have been some reports on two stage combustion as a means of controlling prompt NO(40). Martin et al(37) investigated the behavior of fuel NO in two stage combustion. Similar work was conducted by Gerhold et al(38). The control of both thermal NO and fuel NO by two stage combustion was reported by Sadakata et al(27,39). In their investigation(27), they reported the effect of air preheating upon the emissions of NO, HCN and NH3 from two stage combustion. Their results demonstrated that air preheating up to 300C did not significantly increase the thermal NO and fuel NO and that the concentration of the hydrocarbon and HCN which might be an intermediate product, during the conversion process from NH3 to NO was decreased by 50% in the primary stage of the two-stage combustion. In general, rich/lean two stage systems are need to reduce NOx emissions for fuels with significant fuel nitrogen. For other fuels lean/lean two stage combustors are required.

7.3 PRESENT APPROACH

The lean/lean two-stage combustion system used for the present investigation is illustrated in Fig.7.4 and plate.7.1 which consists of two burning zones arranged in series. The aim was to achieve lean combustions at 0.4 equivalence ratio at both low and high power conditions which was produce minimum NOx and CO emissions at all powers.

The objective was to provide a long residence time at the lower power condition, to minimize CO and UHC and to provide rapid combustion followed by

quenching, thereby minimising NOx emissions. The hot products leaving the 76mm combustor(pilot zone) pass through another small 76mm extension section(main zone), which comprises the peripheral injecter at the throat of a 140mm combustor(main stage) the fuel added through the 8 holes via the 76mm wall injecter. The action of the second stage radial swirler serves to quickly mix and distribute the main fuel with air plus the dilution with hot products from the pilot stage to achieve a uniformly lean mixture. The pilot stage fuelled by central radial fuel injection. However, it provides all the temperature rise needed for low power operation. The two-stage combustion system was operated at conditions corresponding to three different air split ratios between the pilot stage and the secondary main stage which they were successively at (50, 30 and 17% pilot combustor air flow) or 1.041/1 , 0.587/1 and 0.333/1 for the inlet temperature of 400K and 600K.

In the previous chapter, the co-swirl system gave a good overall performance using large swirlers in conjunction with peripheral fuel injection. The same principles were adapted in the present work.

The test plan intended for this investigation was to use different combustor lengths for the pilot stage starting with 320mm, 160mm, 80mm and using the same configuration as the double-swirl systems. However, only the 320mm combustor length was investigated for the different air split ratios of pilot/main stage. This was because similar outer plenum chamber casings were not available for different pilot lengths.

Axial staging may take any of several forms, but a typical approach would involve the following features(2):

1- A lightly loaded pilot zone employing well mixed fuel injection which acts as a source of heat for other downstream combustion zones and provides the temperature rise at idle condition.

2- One main stage or more additional combustion zones with its own separate supply of well-mixed fuel and air.

Fig.7.3 illustrates the control of combustion temperature with staged combustion for three staged system(2).
The gas analysis results were recorded for each inlet temperature and for pilot or both pilot/main stages separatly.

For the present work only one main stage was used. The main aim was the regulation of combustion temperature to achieve minimal emissions at all operating conditions.

7.4 TEST PROCEDURES

The main test procedures were the same as for single stage combustion in Appendix(F) except for the light-up of the second stage combustor. The greater the first stage ignition fuel flow rate, the smaller the fuel flow rate necessary for second stage ignition. In other words, the more intensive the flame in the first stage, the more easily the fuel in the second stage ignites. However, there was an igniter to help light-up the fuel in the second stage as shown in Fig.7.3. When the two stages were working at the same time, the pilot stage was then sustained at a specific equivalence ratio and the fuel/air was varied in the main stage combustor. The main stage equivalence ratio was set for the minimum NOx emissions compatible with a high combustion efficiency.

7.5 WEAK EXTINCTION

The weak extinction equivalence ratio was measured for each stage following the general procedures in Appendix-F. Two main steps were carried out in order to record the weak limits, first, was to measure the pilot stage weak extinction alone. Second, was to maintain the pilot stage at a specific equivalence ratio while recording the weak extinction of the second stage. The measured weak extinction data are summarised in Table(7.1), which shows the comparison between the three air split ratios of pilot/main stage for the different conditions stated.
Flame observation indicated that the second stage weak extinction was a very strong function of the first stage equivalence ratio. The 600K tests conducted with

two pilot equivalence ratios for the system fuelled with natural gas at an air split of (0.333/1) showed that the weak extinction of the second stage combustion was nearly 2.5 times lower when the pilot operational equivalence ratio was changed from 0.11 to 0.23. Similar results were found by Oven et al(29) who used a double-swirl combustor. Their results indicated that reaction takes place outside the recirculation zone, in a thick turbulent flame and that the flame stabilised in the low speed flow approaching the forward stagnation point. A stagnation point, but not a large recirculation zone, is the essential flow feature for combustion stabilisation. Their work was supported by the work reported by Panton and Sweat(35) who have studied gaseous diffusion flame stabilised by vortex breakdown generated in the boundary layer of a delta wing at high angle of attack. Their observations indicated that both the axisymmetric and the spiral form of vortex breakdown are capable of stabilising combustion. The spiral form is characterised by stagnation points in the vortex core, but there are no significant zones of organised recirculating flow(36).

In the present work, baffled central radial fuel injection was used in conjunction with radial swirler(A) which previously, has been demonstrated poor lean stability limits compared with others. By placing the baffle in the way of the spiral reverse flow can break the vortex core earlier on before it reaches the vertical plane of radial swirler outlet. Furthermore, the injecter was placed approximately (70mm) downstream of swirler vertical back plate so, the fuel injected in the inner boundary , just before the swirl jet impingement on the pilot combustor wall. The results showed that by using this technique superior weak weak extinction limits were achieved to that achieved by other conditions and for both stages, but with sacrifices in the combustion efficiency as demonstrated previously with single swirler combustor test.

The reason behind the superior weak extinction limits in the second stage combustor was due to the generation of the high levels of highly combustible species such as CO and UHC which generated local rich zones in the second stage inlet section and that extended the weak extinction. The spiral reversed flow seems to be vital to recirculate the unburned species upstream for more burnout.

That led to the abandonment of the baffle with the central injection system.

Introducing a smaller flow area swirler change the air split ratio of pilot/main stage to (0.587/1). This gave good improved stability limits for both stages. Using a thin smaller swirler gave an air split ratio of (0.333/1) and the lean stability for the second stage combustion was more or less the same for Kerosene and Natural gas when combined with pilot at an equivalence ratio of 0.11. Large improvements in stability limits were achieved when changing the latter equivalence ratio to 0.23. This was due to the change in the pilot outlet temperature which gave rise to a higher central core temperature of the second stage which stabilised the main flame.

For the pilot stage, decreasing the swirler depth to reduce the airflow tend to increase the swirl number, thereby increasing the potential rotational ring at the swirler outlet region. This will estabilish stagnant points in that region which gives a wider lean stability. It has been demonstrated using the water model technique with radial swirler(A) that the rotational potential ring was very close to the central injecter. This tended to give narrow stability limits.

7.6 WALL STATIC PRESSURE AND TEMPERATURE PROFILES

In the present work there was no measurement of the pilot stage combustor wall static pressure or axial temperature profiles, and the only the second stage combustor wall static pressure and temperature profiles were measured with the two stages operational and the pilot stage sustain at specific equivalence ratio. Figs.7.5 - 7.24 illustrates those profiles for the second stage combustor wall for the different air split ratios of pilot/main stage.

Fig.7.7 shows that for an air split ratio of (1.041/1) using natural gas, there were two aerodynamic zones. The first one was associated with the impingement of the second stage swirler flow shear layer when it expanded through the 140mm combustor, and the second one was associated with the flow emerging from the central core of the second stage swirler which was promoted by the pilot

combustor. Those two zones followed by the decay of swirl flow. The temperature profiles in Fig.7.8 reflect the above flow experience where the initial high wall temperature was associated with fuel being injected peripherally and combustion initiated there.

For the 0.587/1 pilot/main stage air split ratio at 400K inlet temperature, the static wall pressure showed the same two aerodynamics zones as at the 1.041/1 flow split as shown in Fig.7.9. The wall temperature profiles are also similar with a high emissive temperature at the second swirler shear layer impingement region, indicating good combustion of the second stage fuel. stage combustor uniformly except for equivalence ratio of 0.42 where slow propagation of the flame indicated by low temperature at first, and developed until it reaches its peak beyond 200mm downstream. At 600K inlet temperature, the wall static pressure and temperature profiles are shown in Figs.7.11 and 7.12 respectively and are again similar to those at 400K with two aerodynamics zones and flame development as the first.

Perhaps the most unusual profiles were that associated with the flow split ratio of 0.333/1 as shown in Figs.7.13 - 7.24. Investigating the temperature profiles one can notice the sudden drop in the wall temperature for propane and natural gas. The sudden drop is located at an axial distance of 75mm downstream of the 76mm wall injecter(peripheral). It is considered to be due to the secondary swirler shear layer flow impingement without this region burning, but the corner recirculation and inner recirculation either side of the shear layer burning. At this low pilot air flow the combustion characteristics are clearly worse than for other flow splits. The emission results also show that this flow split was worse than 0.587/1.

7.7 MEAN COMBUSTOR EXIT EMISSIONS

7.7.1 Pilot/Main air split ratio of (1.041/1)

The measured mean exhaust results for this condition were presented in Figs.7.25 - 7.44 for two inlet temperature and fuels types.

A baffled central injecter was used in the pilot stage to inject the fuel at

approximately 70mm away from the swirler vertical back plate. This action gave very wide stability limits but with sacrifice on the combustion efficiency which was due to the poor mixing between the fuel and swirling air. As demonstrated previously using the water model technique that there was a vortex core present with the swirler and by placing the baffled injector 70mm away downstream of the swirler back plate the vortex core could not transfer fuel upstream. This gave a shorter residence time for combustible species such as CO and UHC to burn-out which gave a higher combustion inefficiency as can be seen from Figs.7.25 and 7.26 for 400K inlet temperature and from Figs.7.33 - 7.34 for 600K inlet temperature. So, it seems breaking-up the central vortex core was not in the benefit of good combustion performance. However, at higher inlet temperature (ie.600K) the CO and UHC emissions were substantially reduced.

The combined effect of high CO and UHC emissions at 400K inlet condition gave a higher combustion inefficiency as shown in Fig.7.27. The lowest combustion inefficiency being encountered with propane injection at an equivalence ratio of 0.45 which was just below 1.0%, while for the natural gas it was above 2.0%. The NOx emission profiles followed inversely the same trends as the combustion inefficiency as shown in Fig.7.28. Perhaps, the presence of the combustible agents such as UHC strongly facilitated the oxidation of NO to NO_2 as reported by Bromly et al(25).

The NOx corrected to 15% oxygen and standard day humidity as a function of combustion inefficiency is shown in Fig.7.29. The propane and natural gas promoted approximately 20 and 14ppm compatible with the lowest combustion inefficiency of 0.7% and 1.7% respectively. Fig.7.30 shows the NOx corrected to 15% as a function of equivalence ratio where the natural gas can be seen to exhibit nearly half of the NOx corrected to that of the propane.

For both stages at 600K inlet temperature, with the pilot maintained at an equivalence ratio of 0.241 for propane and 0.269 for natural gas, the system exhibited less CO and a very small contribution of UHC as shown in Figs.7.31 and 7.32 for all equivalence ratios except for those very near the weak limits. The combined effect of low CO and UHC emissions yielded a low combustion

inefficiency as shown in Fig.7.33. A low combustion inefficiency was promoted by both gaseous fuels and the combustion efficiency was better than 99%. However, the NOx levels promoted by the two fuels with this air split ratio were high which were mainly due to the high formation of NOx emissions in the pilot stage, much more than in the main stage as shown in Fig.7.34.

The NOx level were maintained at the same level as the pilot stage for equivalence ratio ranging between 0.241-0.500 and between 0.269-0.500 for propane and natural gas respectively. The contribution of the second stage combustion to NOx was small with natural gas compared with propane fuel as shown in Fig.7.34. Thus, for this air split ratio the lowest NOx corrected to 15% oxygen and day humidity were 24 and 14ppm compatible with the lowest combustion inefficiency of 0.025% and 0.015% for propane and natural gas respectively as shown in Figs.7.35 and 7.36. Although, these are low NOx emissions, they are considerably higher than than the ultra low NOx of the single stage 76mm swirlers.

7.7.1.1 Oxides of Nitrogen

For the present work the moderate flame temperatures and the rapid formation of NO, indicate that NO is formed via the prompt mechanism as can be seen from Figs.7.37 - 7.38 for the pilot only at 400K inlet temperature and Figs.7.39 - 7.44 for both stages at 600K inlet temperature for propane and natural gas. Fig.7.39 shows nitric oxides as a function of the metered equivalence ratio. The NO_2 contribution to the total NOx up to an equivalence ratio of 0.241 is approximately 10ppm. However, beyond that equivalence ratio the NO becomes the major predominant contributer to the total NOx emissions and the NO_2 contribution was nearly half that of NO. When using the system at high power below an equivalence ratio of 0.4 the NO_2 production becomes predominant in the production of the NOx emissions as shown in Fig.7.40 for the system fuelled with propane.

Figs.7.41 and 7.42 show the nitric oxides as a function of equivalence ratio

for the system fuelled with natural gas for the pilot stage and for both stages respectively at the inlet temperature of 600K. Below an equivalence ratio of 0.269 the NO_2 was the main contributer in the NOx production. However, beyond this equivalence ratio NO becomes the major promoter of the NOx formation. This was propably due to the temperature rise with a lower oxygen concentration, NO is sensitive to the flame temperature more than the NO_2 as this formed most rapidly at low temperatures.

With both stages fuelled with natural gas while the pilot stage was sustained at a 0.269 equivalence ratio(A/F=62/1) the NO contributed the major part of the NOx which was kept constant throughout the equivalence ratio range shown in Fig.7.42. The reason for the high NO was due to the initial mixing of fuel/air. Variation of NOx formation as a function of flame temperature are shown in Figs.7.43 and 7.44 for propane and natural gas respectively. The moderate flame temperatures and the formation of NO rapidly, indicate that NO formed via prompt mechanism, perhaps with a little contribution from thermal NO due to local rich region in the pilot.

7.7.2 Pilot/Main air split ratio of (0.587/1)

The combustor exit emissions products as a function of equivalence ratio are shown in Figs.7.45 - 7.50 for a double staged system with an air split ratio of 37% pilot air and 63% for the main stage burner.

The main interest was the condition at 400K inlet temperature which simulate the low power operation and the 600K inlet temperature for both stages which simulated the high power operation. The other tests were carried out for comparison reason and to investigate the influence of each mode on the combustion performance and emissions.

Figs.7.45 and 7.46 shows the CO and UHC emissions as a function of equivalence ratio. The pilot at 400K inlet temperature exhibited higher CO emissions than at higher power conditions at an inlet temperature of 600K. While the pilot stage was sustained at a 0.116 equivalence ratio or (A/F=135/1), the main stage fuel

flow to the air ratios were varied. Fig.7.46 shows that there was only a trace of UHC emissions for all operational equivalence ratio except that near weak extinction where UHC emissions increased. The combined effects of CO and UHC emissions can be deduced from the combustion inefficiency as a function of equivalence ratio which is shown in Fig.7.47. The system exhibited a low combustion inefficiency of less than 0.1%, except for pilot at 400K inlet temperature where the inefficiency was equal to 0.1%. However, the pilot at the 400K inlet condition exhibited 10ppm of uncorrected NOx emission which was compatible with a 99.7% combustion efficiency as shown in Figs.7.47 and 7.48. The 600K inlet condition promoted an ultra low uncorrected NOx emission of 6ppm at an equivalence ratio of 0.116 and stays on until the second stage combustion was initiated at equivalence ratio of 0.4. Thereafter, the NOx emissions increased which was due to the rise in the flame temperature as will be discussed later. The correlation between combustion inefficiency and the level of NOx emited from the system corrected to 15% O2 and standard day humidity is shown in Fig.7.49, where the lowest corrected NOx was exhibited at high power operation(ie.600K inlet temperature) with both stages on. The low Nox emissions can be achieved with very low power operation and with both stages on as shown in Fig.7.50 and without a sacrifice in the combustion efficiency of 99.9%. Thus, staging the combustion process with an air split ratio between the pilot/main stage of 0.587/1 can promote low NOx emissions which easily meet the EPA standard of 75ppm at 15% O2, which convert to 20 - 24ppm at 1bar for most industrial gas turbines.

7.7.2.1 Oxides of Nitrogen

Nitric oxides formation as a function of metred equivalence ratio are presented in Figs.7.51 - 7.54 for the two inlet temperatures of 400K and 600K and for both stages. These plots give the general picture of the dominant species behind the formation of NOx emissions. It is clear that NO was the dominant part of the NOx, with little contribution by NO_2 to the total NOx which it did not exceed 5ppm at all operational equivalence ratios.

Figs.7.55 and 7.56 shows the total NOx formation as a function of gas analysis based flame temperature which proves beyond doubts that the moderate flame temperatures and the rapid formation of NO, indicates that the NO is formed via the prompt mechanism. This is in strong contrast with the 1.041/1 flow split when significant levels of NO_2 were generated.

7.7.3 Pilot/Main split ratio of (0.333/1)

The improvement in the emissions level when reducing the air split led to the consideration of a lower proportion of pilot stage air. This pilot air mass flow rate was designed to be about 25% of the total inlet air, while maintaining the same overall pressure loss as before of around 4.2%. Three fuels were tested in the main stage section, using the 76mm wall injection system(peripheral). These fuels were propane, natural gas and kerosene. However, only two fuel were used in the pilot stage, they were propane and natural gas.

7.7.3.1 Using propane for both stages

Figs(7.57) and (7.58) show the CO and UHC emissions as a function of the metered equivalence ratio for the low and high power operation fuelled with propane in both stages. The results of the pilot at 600K inlet temperature and of both stages burning together at the 400K inlet condition were for comparison reasons and to investigate the influence of simulated power output on the emissions characteristics. It should be noticed that when operating the pilot and main stage together ,the pilot was sustain at an equivalence ratio of 0.1 at 400K inlet temperature and at 0.096 at 600K inlet temperature for which at these two equivalence ratios the lowest NOx were encountered compatible with a combustion efficiency of better than 99.6%. However, for pilot stage at 400K the lowest CO emissions were encountered at an equivalence ratio of 0.1 (A/F=142/1) and below this value the production rate exceeded the oxidation rate, as the temperature was too low. A different picture for the pilot at 600K inlet temperature was found, the oxidation rate was predominant and the lowest CO encountered was at equivalence ratio of 0.096 or (A/F=163/1) fuel air ratio. The

emission of UHC were very low for both inlet temperature. The highest UHC emissions were exhibited near the weak limits. However, the improvement in the emission production were evidently clear from figs(7.57) and (7.58) at the high power condition or the 600K inlet temperature. The combined influence of CO and UHC emissions are presented as combustion inefficiency as a function of equivalence ratio as shown in Fig.7.59.

Fig.7.60 shows the NOx emissions as afunction of equivalence ratio. The high power condition exhibited higher NOx emissions then the lower power which was due to increase NO formation as can be seen from Fig.7.63 and 7.64, since the NO formation rate is strongly dependent on temperature(25) Sadakata et al(27) reported that the effect on NOx of air preheating up to 300C was three times higher than that of nonpreheated case using city gas in a two stage combustion system. Emissions of both thermal NO and fuel NO were not significantly increased. Thus the present low NOx at 600K indicate that the NO was formed via the prompt mechanism. The contribution of NO_2 emissions to the total NOx emissions was constant at just above 5ppm. Figs.7.65 and 7.66 show the rapid formation of NO as a function of the flame temperature, and the much lower NOx emissions of the main stages.

The lowest NOx corrected to 15% oxygen and standard day humidity compatible with the lowest combustion inefficiency are presented in Figs.7.61 and 7.62. Again with this system the EPA NOx standard can be met easily.

7.7.3.2 Comparison Between Propane and Natural-Gas Combustion

The general characteristics of the two-stage sytem for the pilot/main stage air split of (0.333/1) fuelled with propane or natural gas are shown in Figs.7.67 - 7.76. The propane pilot equivalence ratio was 0.1. The pilot fuelled with natural gas was used with two different equivalence ratios of 0.11 and 0.23 at 600K inlet temperature or the high power condition. That was to investigate the influence of varying the pilot equivalence ratio on the performance of the main stage combustion and the combustor exit emissions. Fig.7.67 shows that propane exhibited lower CO emission than natural gas at an equivalence ratio of 0.4 when

both stages were working together at the simulated high power condition.

Natural-gas exhibited higher UHC emissions than propane as shown in Fig.7.68 for all operational equivalence ratios due to the slower reaction rate(30). The highest UHC emissions occured for the two stages fuelled with natural gas while keeping the pilot stage running at 0.11 equivalence ratio and operating the main stage at equivalence ratios higher than 0.4. Due to the high UHC emissions level the test had to be terminated. The resultant very high combustion inefficiency is shown in Fig.7.69, the combustion inefficiency was above 10%. To overcome this problem, the pilot equivalence ratio was raised to new level of 0.23. As expected, this resulted in an improvement in the total emissions of CO and UHC and the combustion inefficiency as shown in Fig.7.69. At 0.52 (A/F=32/1) the natural gas promoted a high combustion efficiency of better than 99.9%. However, propane promoted the same combustion efficiency at a lower equivalence ratio of 0.4 (A/F=40/1).

The total NOx emissions as a function of equivalence ratio is shown in Fig.7.70. The pilot stage fuelled with propane was kept running at an equivalence ratio of 0.096 which exhibited low NOx emissions of 5.5ppm. This shows that there was a good mixing effects between the fuel and air The pilot stage fuelled with natural gas was operated at two equivalence ratios of 0.11 and 0.23, where the NOx emissions exhibited were 5ppm and 20ppm respectively. Propane exhibited a rapid increase in NOx emissions beyond an equivalence ratio of 0.4 when the two stages were operating together. This was due to the high production of NO as shown in Fig.7.73. Which shows that NO was the dominant part in the production of the total NOx formation. The same argument applied to the natural gas case as shown in Fig.7.74 for the pilot at 0.11 equivalence ratio. However, when the pilot was at 0.23 equivalence ratio the system exhibited NO_2 levels nearly half that of NO and that occured at an equivalence ratios below 0.4 as shown in Fig.7.75. That was the same equivalence ratio where the UHC was at high level. The above results contradicted some of the work of previous workers(25,31,32) who found that the presence of highly combustible species such as the hydrocarbons had a greater effect than carbon monoxides and strongly facilitated the oxidation of NO

to NO_2.

The pilot and main NOx emission were constant over the temperature range (1400-1900K) for the natural gas case while in the propane case, it increased rapidly as shown in Fig.7.76.

The lowest NOx corrected to 15% oxygen and standard day humidity were exhibited by propane as shown in Figs.7.71 and 7.72, for equivalence ratios below 0.45. The NOx level was below 10ppm for equivalence ratios below 0.45 for propane and for natural gas the corrected NOx vel was 10ppm and above for the equivalence ratios below 0.45 and that was when the pilot kept on equivalence ratio of 0.23. Low levels of corrected NOx was exhibited by the pilot fuelled with natural gas at an equivalence ratio of 0.11, but was more of a sacrifice in terms of combustion efficiency as shown in Fig.7.71. For both propane and natural gas the NOx levels were higher than for the main radial swirler alone with wall or passage injection.

7.7.3.3 Influence of using combination of two different fuels

Two different fuels were used in this section. The pilot stage was fuelled with propane and the main stage with liquid kerosene. This was done to investigate potential main stage problems with liquid fuel. NO dual fuel system was available for liquid fuels. The use of the propane pilot was merely to simulate the first pilot flow in the main swirler liquid fuel tests. Propane is often used to simulate vaporised kerosene fuel(30). In the present work two inlet temperatures were investigated to study the influence of different power output on the general characteristics of emissions. For the inlet temperature 400K the pilot stage was a working equivalence ratio of 0.115 (A/F=135/1) and at 600K inlet condition the pilot stage was kept running at 0.096 (A/F=163/1). These two equivalence ratios were compatible with the lowest pilot NOx emissions and a combustion inefficiency of more than 99%.

Figs.7.77 and 7.78 shows the CO and UHC emissions as a function of metered equivalence ratio. At 600K inlet temperature the system exhibited much lower CO

and UHC than at 400K inlet which was due to the generation of higher heat release from the pilot stage(inner jet). This was an improvement to the vaporisation level in the second stage combustor inlet region which was reflected in the combustion inefficiency profile as shown in Fig.7.79. The low combustion efficiency at 400K inlet temperature was attributed to the reaction quenching due to the mixture dilution in the shear layer. At both temperature a high efficiency was demonstrated, indicating no major combustion efficiency problem at any power output.

Fig.7.80 shows the total NOx as a function of equivalence ratio Imperfect fuel and air mixing was thought to be the main reason behind the rapid NO formation(33). It is most propably that NO was only formed in the early part of the main stage combustor which contained the radical rich turbulent flame reaction zone. Furthermore, NO is very sensitive to flame temperature which explain the rapid increase in the NOx formation. However, the increase in NOx and the NOx levels were higher than for a single radial swirler with wall injection. The NO_2 formation contributed very little to the total NOx level as shown in Figs.7.83 and 7.84. The NO_2 was at a constant level throughout the indicated equivalence ratios. That was contradictory to what has been reported by other workers (25,31,32). NO formation was the major part of the NOx emissions.
The lowest Nox corrected to 15% oxygen and a standard day humidity was attained at a 0.45 equivalence ratio as shown in Figs.7.81 and 7.82. However, the lowest corrected NOx compatible with the lowest combustion inefficiency at 600K inlet temperature was 17ppm and for the 400K inlet temperature was approximately the same. However, there is reason to believe that this system could be improved to obtain much lower NOx emissions than the present level, and that could be done by using a shorter pilot combustor than the present one so as to minimise pilot NOx. Moreover, a shorter pilot combustor might increase the shear stresses between the two swirling jets(inner and outer) and by increasing the shear acting on the liquid film, produce a finer spray(34), which means more uniform mixing between fuel and air and less NOx formation.

7.7.4 COMPARISON BETWEEN THE DIFFERENT AIR SPLIT RATIOS

Figs.7.87 and 7.88 show the CO and UHC emission of the two stage combustion system fuelled with propane in both stages as a function of equivalence ratio for different pilot/main stage air split ratios but the same pressure loss. The low CO emissions were exhibited for all air split ratios but the lowest CO was achieved with split ratios of 0.587/1 and 0.333/1, the same applied to the UHC emissions. That was due to the higher residence time acquired by the low split air ratios pilot stage. The combined effects of CO and UHC emissions were reflected on the combustion inefficiency of the system as shown in Fig.7.89. The lowest combustion efficiency promoted by the system with air split ratio of (0.587/1) was better than 99.9%. All split ratios exhibited a minimum combustion inefficiency of less than 0.1%.

The total NOx emissions contributed by the two split ratios of 0.587/1 and 0.333/1 were much lower than that of 1.041/1. Moreover, ultra low NOx of approximately 5.0ppm was found for the split ratio of (0.587/1) at an equivalence ratio of 0.4 (A/F=40/1).

The NOx corrected emissions to 15% oxygen and a standard day humidity are presented as a function of combustion inefficiency and equivalence in Figs.7.91 and 7.92 respectively. The split ratios of 0.587/1 and 0.333/1 exhibited similar NOx and were the lowest NOx corrected compatible with the lowest combustion inefficiency which easily met the EPA NOx regulation

So, from the above discussion the split ratios acquired by the two stage combustion system should lie between the ratio of 0.587/1 and 0.333/1 to achieve lower NOx corrected, an order of 5ppm at most compatible with high combustion efficiency of 99.9%. These NOx emissions are close to, but higher than, the ultra low NOx single swirler results with passage or 76mm wall injection in chapter five.

7.8 CONCLUSIONS

1- The preliminary tests conducted in the present work using the dry lean-lean two-stage combustion concept have confirmed that the goal of EPA regulation may be achieved, whilst satisfying operating power range.

2- The combustor is capable of stable swiching from the pilot stage to two stage combustion without difficulties.

3- The total air split ratios for pilot/main stage to achieve good combustion performance with low NOx emission should be lie between 0.587/1 and 0.333/1.

4- Ultra low NOx emissions of approximately 5ppm were achieved with combustion efficiency better than 99.9% using propane as fuel for the existing configuration with air split ratio of 0.587/1.

5- It is evidently from the NO and NO_2 formation profiles as a function of metered equivalence ratio that the NO was the major contributor to the total NOx formation with the present system, and there was only little NO_2 contribution to the total NOx.

6- Ultra low NOx emissions can be achieved with other fuels such as natural gas and kerosene without sacrifices in terms of the combustion efficiency by reducing the pilot stage combustor length thus to increase the shear acting between the swirling jets.

7- The present combustor is considered to be a good basic configuration for further investigation to reduce all emissions.

CHAPTER SEVEN

REFERENCES

7-1 Aoyama K. and Mandai S.: Development of Dry low NOx combustor for a 120-MW Gas Turbine. ASME J. Engineering for Gas Turbines and Power. Vol.106,pp.795-800, 1984.

7-2 Lefebvre A.H. : Gas Turbine Combustion. Hemisphere Publishing corporation, 1983.

7-3 Washam R.M: Dry low NOx combustion system for utility gas turbines. ASME paper no.83-JPGC-GT-13, 1983.

7-4 Hilt M.B and Walso J.: Evolution of NOx Abatement technique through combustor design for heavy-duty gas turbines. ASME J. Eng. for Gas Turbines and Power, vol.106, pp.825-832, 1984.(also see ASME 84-G-48)

7-5 Lefebvre A.H: Pollution control in continuous combustion engines. 15th symposium(Int.) on combustion, The Combustion Institute, pp.1169-1180, 1974.

7-6 Lew H.G., Decorso S.M., Vermes G., Carl D., Havener W.J., Schwab J. and Notardonato J.: Low NOx and fuel flexible gas turbine combustors. ASME J. Eng. for Power, vol.104, pp.303-313, 1982.

7-7 Novick A.S., Troth D.L. and Yaccobucci H.G.: Design and preliminary results of fuel flexible industrial gas turbine combustor. ASME J. Eng. for Power, vol.104, pp.368-376, 1982.

7-8 White D.J., Batakis A., LeGren R.T and Yacobucci H.G.: Low NOx combustion system for burning heavy residual fuels and high fuel-bound nitrogen fuels. ASME J. Eng. for Power, vol.104, pp.377-385, 1982.

7-9 Cutrone M.B, Hilt M.B, Goyal A., Ekstedt E.E. and Notardonato J.: Evaluation of advanced combustors for dry NOx supression with nitrogen bearing fuels in utility and industrial gas turbines. ASME J. Eng. for Power, vol.104, pp.429-438, 1982.

7-10 Kuroda M. et al: Development of dry-two-stage low NOx combustor for a gas turbine, ASME paper no. 87-GT-64, 1987.

7-11 Jones R.E : Gas Turbine Engine Emissions-progress and future. Prog. in Energy and Combustion Sci.,4,pp.73-113, 1978.

7-12 Clayton R.M.: A partial oxidation staging concept for gas turbines using broadened specification fuels. ASME paper no. 79-GT-169, 1979.

7-13 Sjoblom B.G.A and Zelterstrom K.A: A double recirculation zone two-stage combustor. AIAA paper 79-7019, 1979.

7-14 Sjoblom B.G.A: Premixing and flash vaporisation in a twostage combustor. ASME paper no. 81-GT-41, 1981.

7-15 Lewis G.D. and Holladay T.E.: Design of a succeful low emissions burner. ASME paper no. 80-GT-12, 1980.

7-16 White D.J., Batakis A., LeCren R.T and Yacobucci H.G.: Low NOx combustion system for burning heavy residual fuels and high fuel bound nitrogen fuels. ASME paper 81-GT-109, 1981.

7-17 Smith K.O.: Ultra-low NOX combustor concept for methanol firing. ASME paper 83-GT-29, 1983.

7-18 Rosfjord T.J., Sederquist R.A. and Angello L.C.: Fuel tolerance of staged combustors. ASME paper no. 82-GT-195, 1982.

7-19 Rosfjord T.J.,McVey J.B., Sederquist R.A. and Schult.of;.of 3 D.F: Combustion of coal gas in staged combustor. ASME paper no. 83-GT-108, 1983.

7-20 White D.J., Kubasco A.J., LeGen R.T and Notadonato J.J: Combustion characteristics of hydrogen carbon monoxide based gaseous fuels. ASME paper no.83-GT-143, 1983.

7-21 Sotheran A., Pearce D.E and Overton D.L: Some practical aspects of staged premixed, low emissions combustion. ASME paper no. 84-GT-88, 1984.

7-22 Furuya T., Hayata T., Yamanaka S. and Koezuka J.: Hybrid catalytic combustion for stationary gas turbine concept and small scale test results. ASME paper 87-GT-99, 1987.

7-23 Mori K., Kitajima J., Kajita S. and Ichihara S.: Development of a catalytic combustor for small gas turbine. ASME paper 87-GT-62, 1987.

7-24 Hoshino A., Kajita S., Hagiwara Y. and Fujimato K.: Preliminary tests of catalytic combustion in a small gas turbine. ASME paper 87-GT-100, 1987.

7-25 Bromly J.H., Barnes F.J. and Little L.H.: The effect of low levels of CO, H2 and Hydrocarbons on NO_2/NO ratios in heated gases. J. Inst. Energy,pp.89-97, June, 1988.

7-26 Johnson G.M., Smith M.Y and Mulcahy M.F.R: The presence of NO_2 in premixed flame. 17th Symposium (Int.)on Combustion, The combustion Institute,pp.647-660, 1978.

7-27 Sadakata M., Fujioka Y. and Kunii D.: Effect of air preheating on emissions of No,HCN and NH3 from a two-stage combustion 18th Symposium (Int.) on Combustion, The Combustion Inst., pp.65-72, 1981.

7-28 Claypole T.C. and Syred N.: The effect of swirl burner aerodynamics on NOx formation. 18th Symposium(Int.) on Combustion, The Combustion Inst.,pp.81-89, 1981.

7-29 Oven M.J., Gouldin F.C. and McLean W.J.: Temperature and species concentration measurements in a swirl stabilized combustor. 17th Symposium(Int.) on Combustion, The Combustion Inst., pp.363-374, 1979.

7-30 Wear J.D. and Jones R.E.: Comparison of combustion characteristics of ASTM A-1, propane, and natural gas fuels in a annular Turbojet combustor. NASA TN D-7135, Jan. 1973.

7-31 Sano T.: NO_2 formation in the mixing region of hot burned gas with cool air. Comb. Science Tech.,43, pp.259-269,1985.

7-32 Jaasma D. and Borman G.: Peculiarities associated with the measurement of oxides of nitrogen produced by diffusion flames. Comb. Sci. Tech., 23,pp83-88, 1980.

7-33 Appleton J.P. and Heywood J.B.: The effects of imperfect fuel-air mixing in a burner on NO formation from nitrogen in the air and fuel. 14th Symposium (Int.) on Combustion, The Combustion Inst., pp.777-786, 1974.

7-34 Blumcke E., Eickhoff H., Hassa C. and Koopman J.: Analysis of the flow through double swirl airblast atomizers. Combustion and Fuels in Gas Turbine Engines, AGARD-CP-422, 1987.

7-35 Panton P.L. and Sweat R.H.: Comb. and Flame, 30, pp.133-142, 1977.

7-36 Faler J.H. and Leibovich S.: Disrupted states of vortex flow and vortex breakdown. Phys. Fluids,20, pp.1385-1400, 1977.

7-37 Martin F.J. and Dederick P.K.: Nox from fuel nitrogen in Two-Stage combustion. 16th Symposium(Int.) on Combustion, The Combustion Inst.,pp.191-198, 1977.

7-38 Gerhold B.W. Fenimore C.P. and Dederick P.K.: Two-Stage combustion of plain and N doped oil. 17th Symposium(Int.) on Combustion, The Combustion Inst.,pp.703-713, 1979.

7-39 Sadakata M., Nawada M. and Kunii D.: International Chem. Eng.,20,409, 1980.

7-40 Yamagishi K., Nozawa M., Yoshi T., Tokumoto T. and Kakegawa Y.: A study of NOx emission characteristics in Two-Stage combustion. 15th Symposium(Int.) on Combustion, The Combustion Inst.,pp.1157-1166, 1975.

TABLES

Table (7.1)
Measured Weak Extinction for Two-Stage Combustion

Air Split Ratios Pilot/Main	Fuel Type Pilot/Main	Inlet Temp.	Weak Extinction (EQR.) Pilot/Main	Weak Extinction (A/F) Pilot/Main	Overall Pressure Loss %
1.041/1	Propane	400	0.012(Pilot)	1290(Pilot)	4.9
		600	0.011/0.058	1379/269	4.6
	Natural Gas	400	0.049(Pilot)	341(Pilot)	4.9
		600	0.013/0.095	1235/175	4.6
0.587/1	Propane	400	0.112/0.171	140/92	5.0
		600	0.045/0.203	345/77	4.8
00.333/1	Propane	400	0.093/0.228	168/69	4.7
		600	0.057/0.216	275/72	4.2
	Propane/ Kerosene	400	0.093/.290	168/51	4.7
		600	0.057/0.272	275/55	4.2
	Natural Gas	600	0.076/0.296	217/56	4.2
		600	0.076/0.115	217/144	4.2

FIGURES

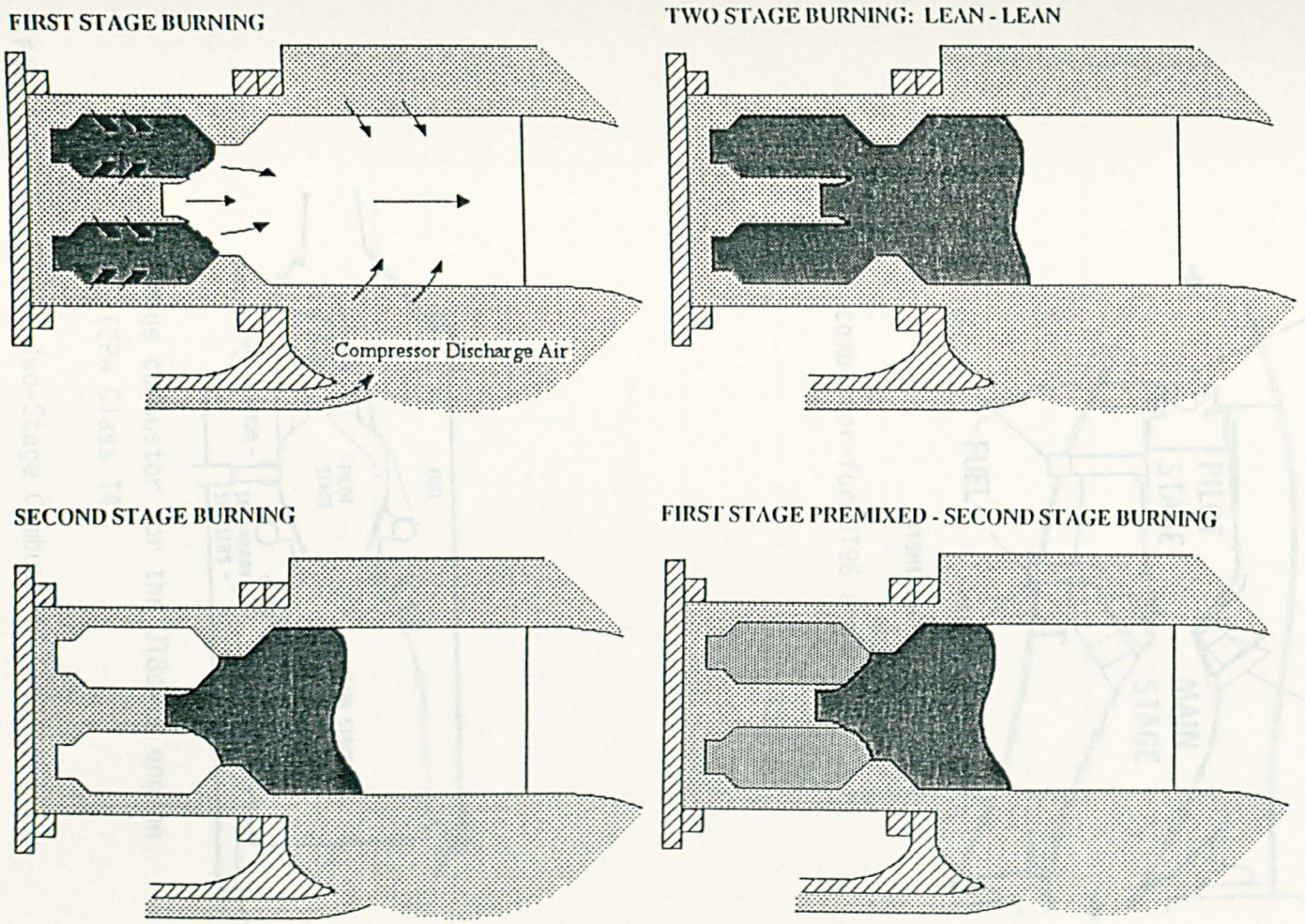

FIG.7.1 Dry Low NOx Combustor Operating Modes(4).

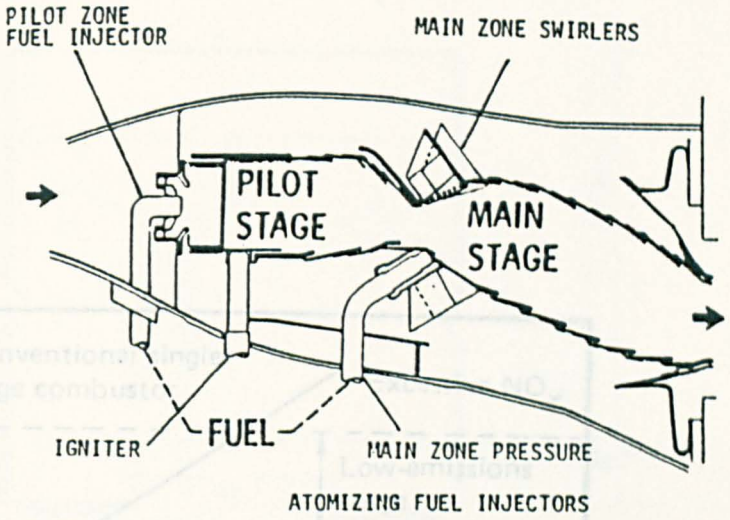

a. Vorbix combustor for JT96 engine.

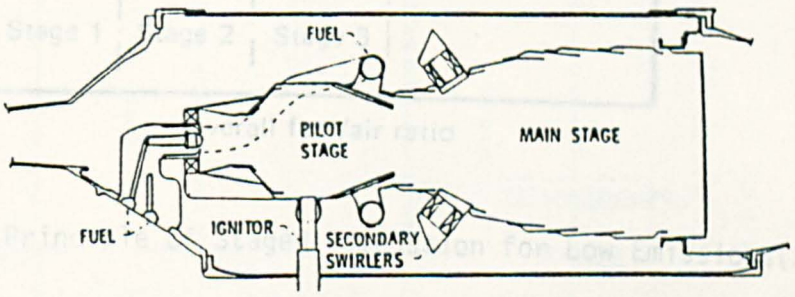

b. Two-stage combustor for the JT8d-17 engine.
(EPA Class T4)

FIG.7.2 Practicale Two-Stage Combustion Systems.(11)

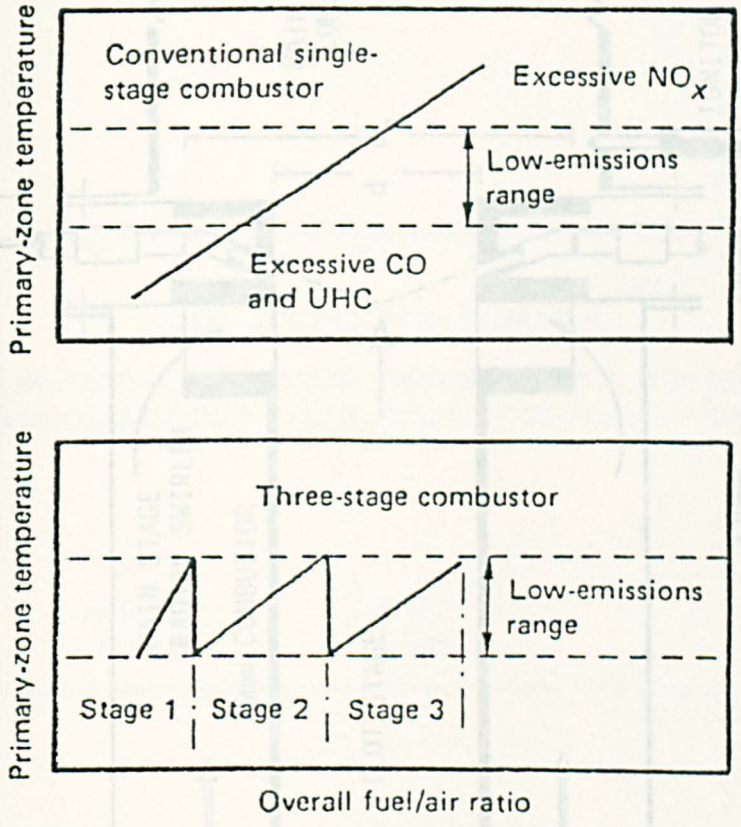

FIG.7.3 Principle of Staged Combustion for Low Emissions(2).

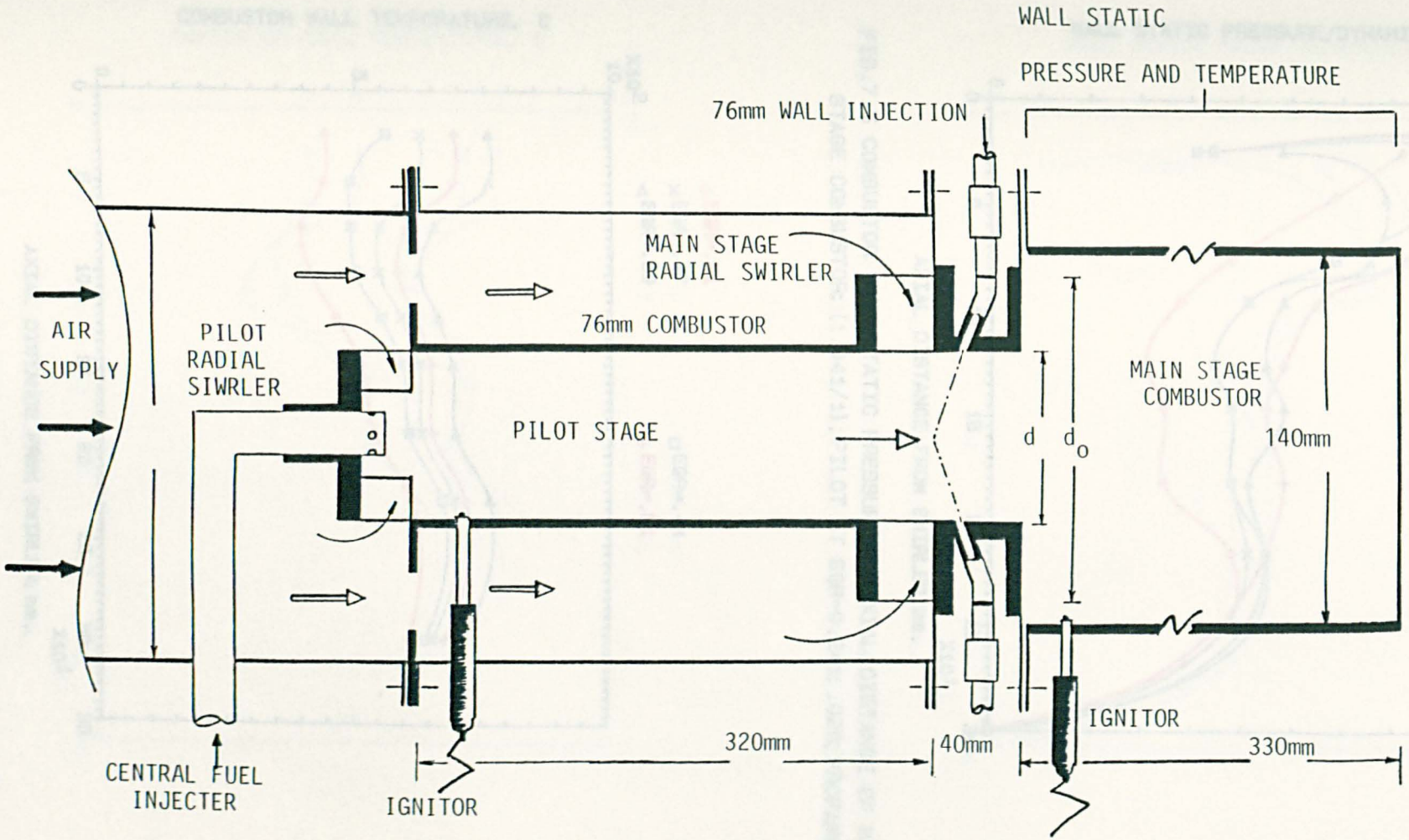

FIG.7.4 Schematic diagram of the Two-Stage Combustor used in the present work.

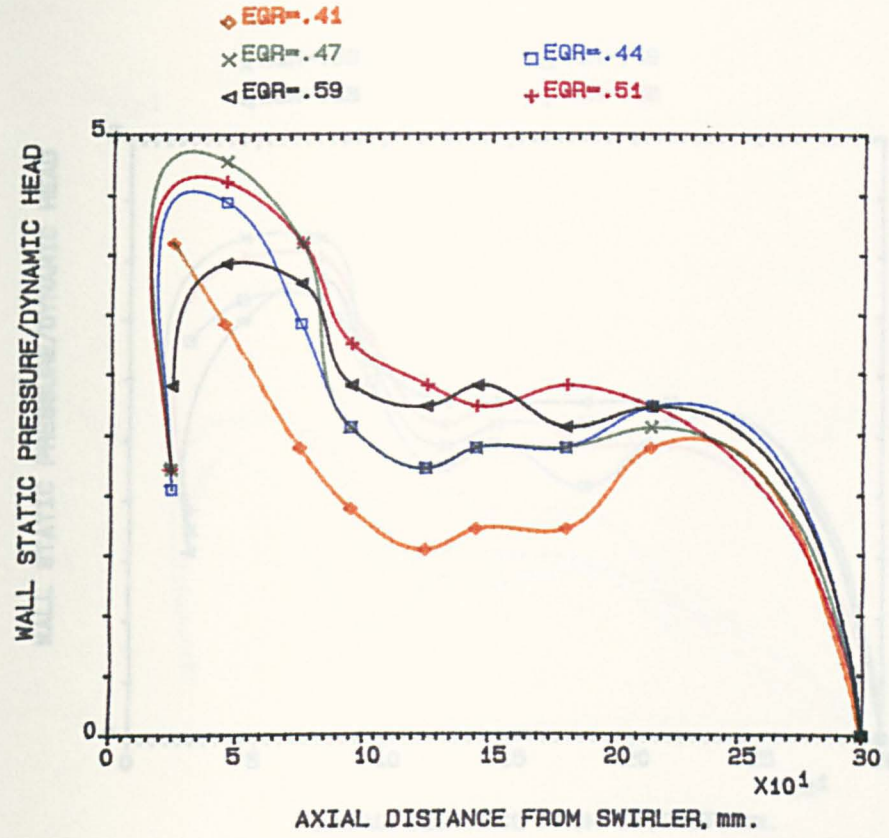

FIG.7.5 COMBUSTOR WALL STATIC PRESSURE V. AXIAL DISTANCE OF MAIN STAGE COMBUSTOR; (1.041/1); PILOT AT EQR=0.241; .028; PROPANE; 600K.

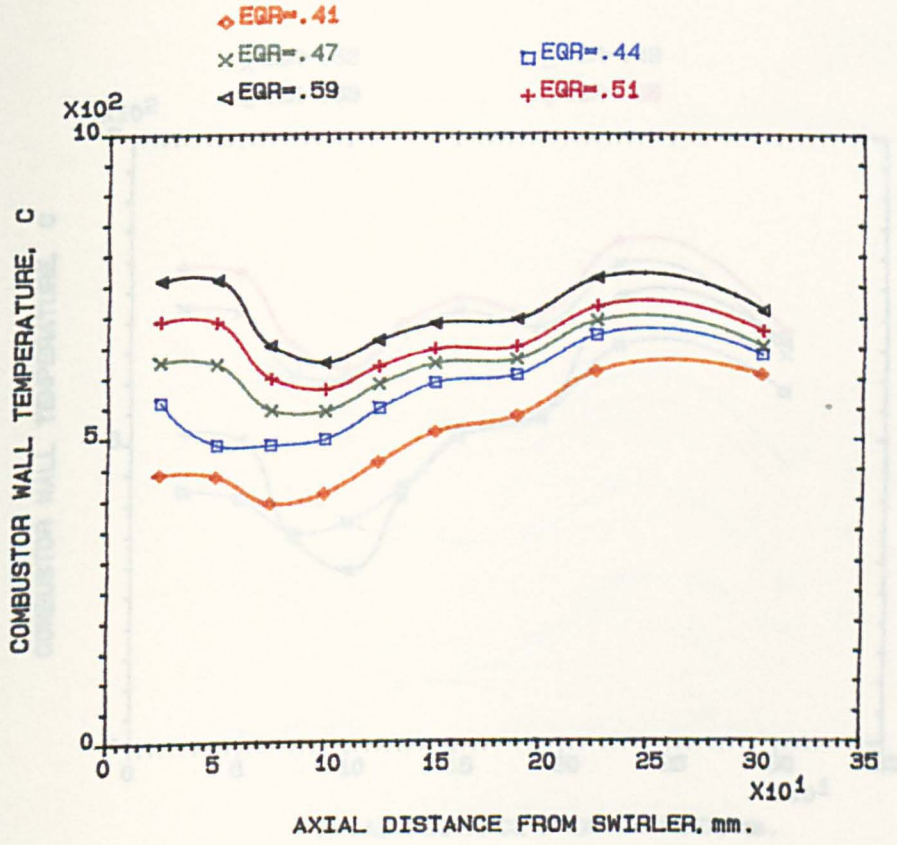

FIG.7.6 COMBUSTOR WALL TEMPERATURE V. AXIAL DISTANCE OF MAIN STAGE COMBUSTOR; (1.041/1); PILOT AT EQR=0.241; .028; PROPANE; 600K.

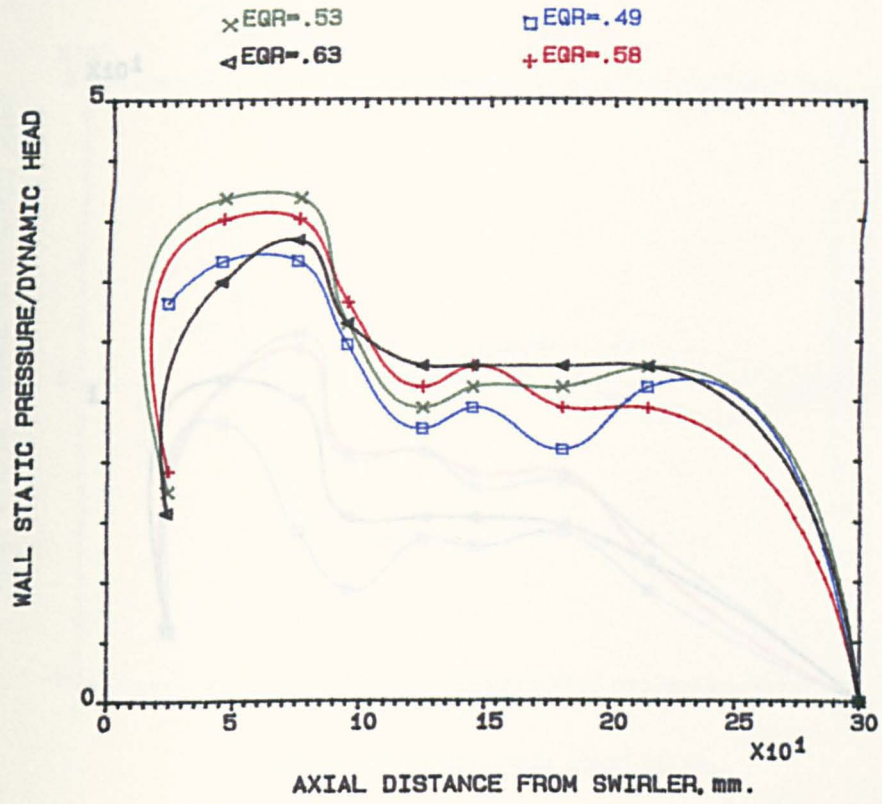

FIG.7.7 COMBUSTOR WALL STATIC PRESSURE V. AXIAL DISTANCE OF MAIN STAGE COMBUSTOR; (1.041/1); PILOT AT EQR=0.269; .028, NATURAL GAS, 600K.

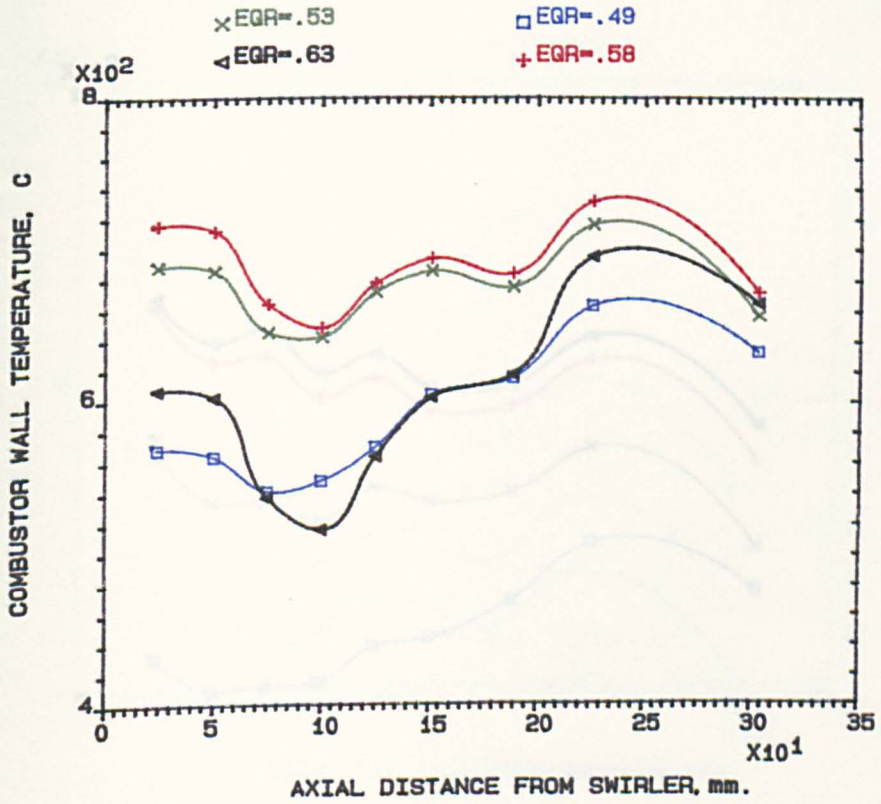

FIG.7.8 COMBUSTOR WALL TEMPERATURE V. AXIAL DISTANCE OF MAIN STAGE COMBUSTOR; (1.041/1); PILOT AT EQR=0.269; .028, NATURAL GAS, 600K.

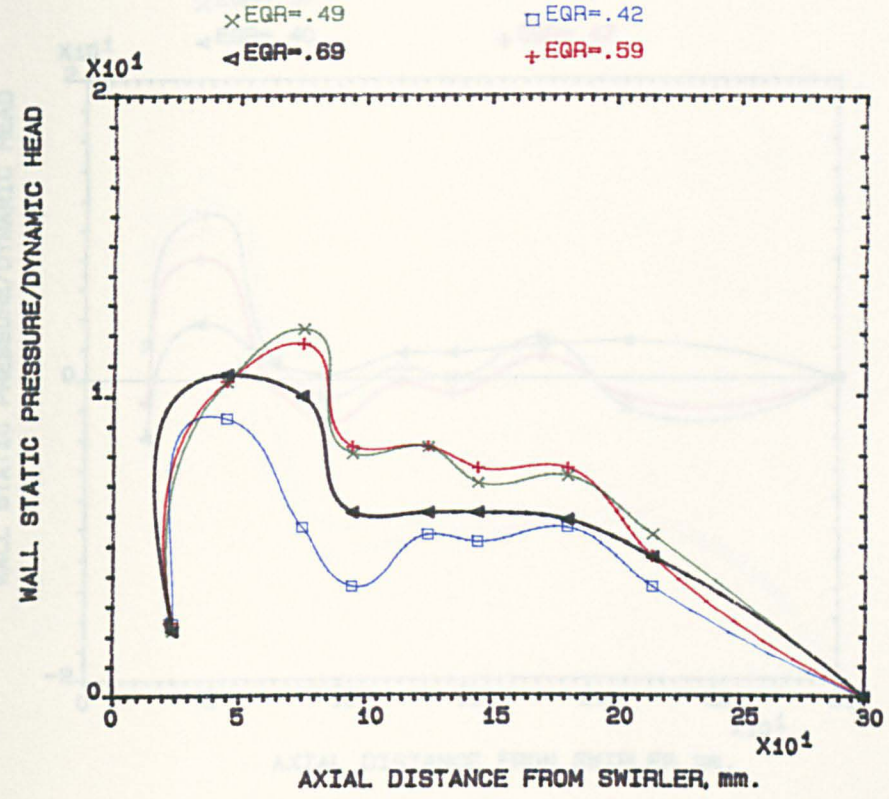

FIG.7.9 COMBUSTOR WALL STATIC PRESSURE V. AXIAL DISTANCE OF MAIN STAGE COMBUSTOR; (0.587/1); PILOT AT EQR=0.175; .023, PROPANE, 400K.

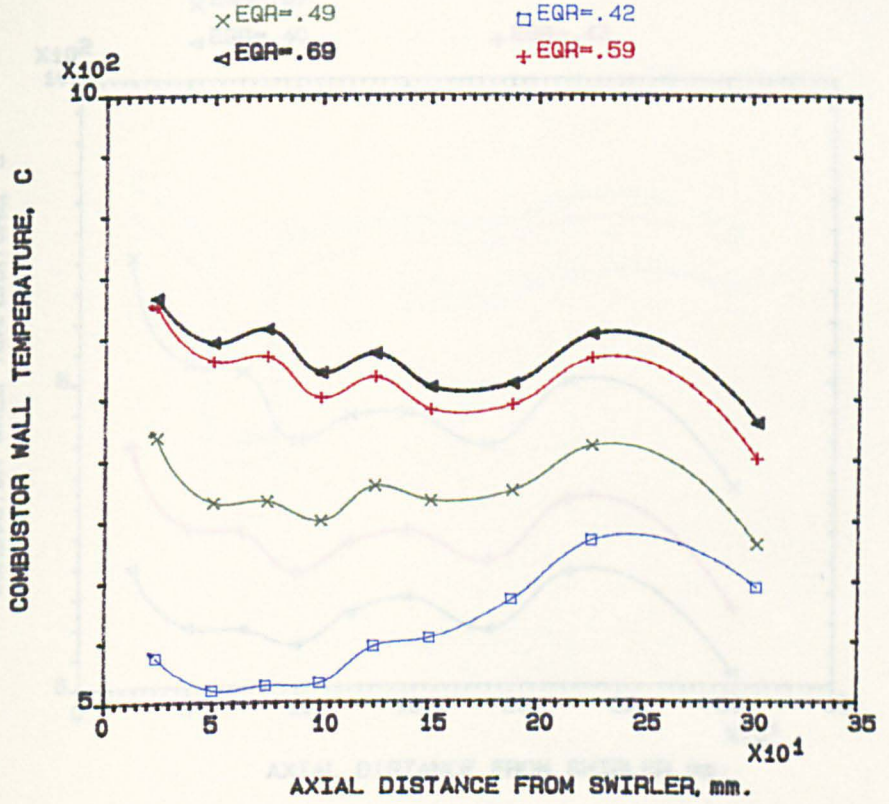

FIG.7.10 COMBUSTOR WALL TEMPERATURE V. AXIAL DISTANCE OF MAIN STAGE COMBUSTOR; (0.587/1); PILOT AT EQR=0.175; .023, PROPANE, 400K.

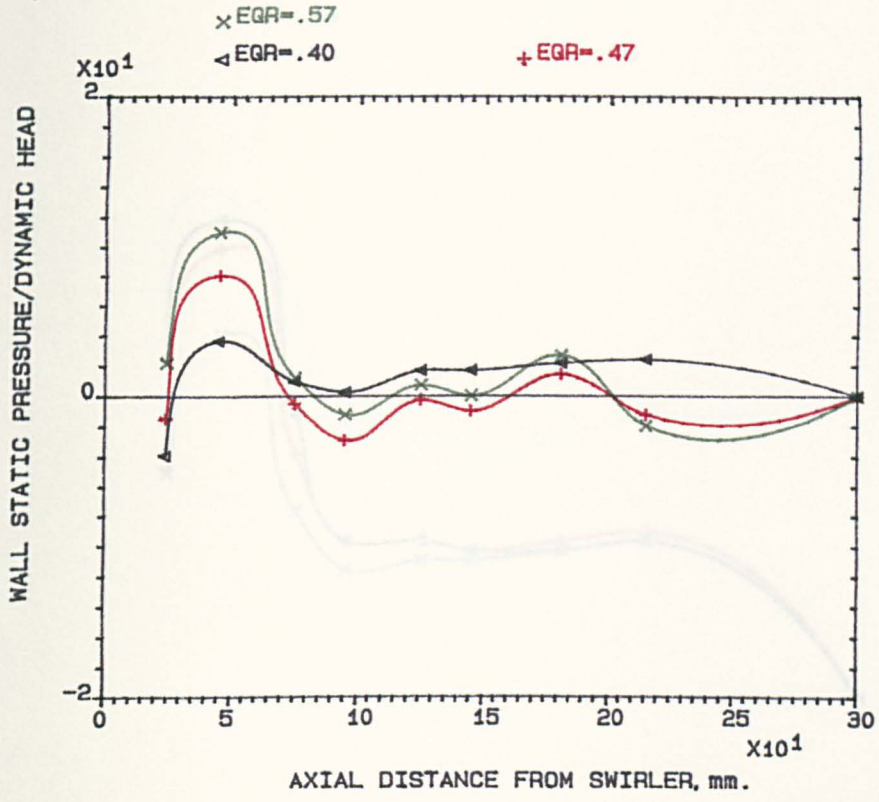

FIG.7.11 COMBUSTOR WALL STATIC PRESSURE V. AXIAL DISTANCE OF MAIN STAGE COMBUSTOR: (0.587/1); PILOT AT EQR=0.116; .023, PROPANE, 600K.

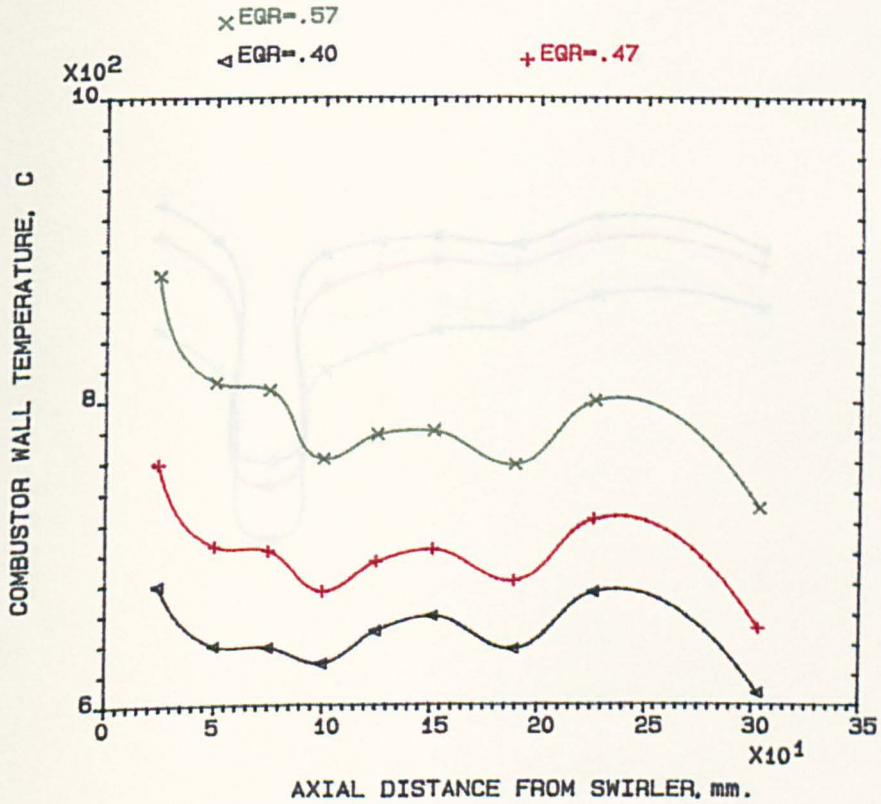

FIG.7.12 COMBUSTOR WALL TEMPERATURE V. AXIAL DISTANCE OF MAIN STAGE COMBUSTOR: (0.587/1); PILOT AT EQR=0.116; .023, PROPANE, 600K.

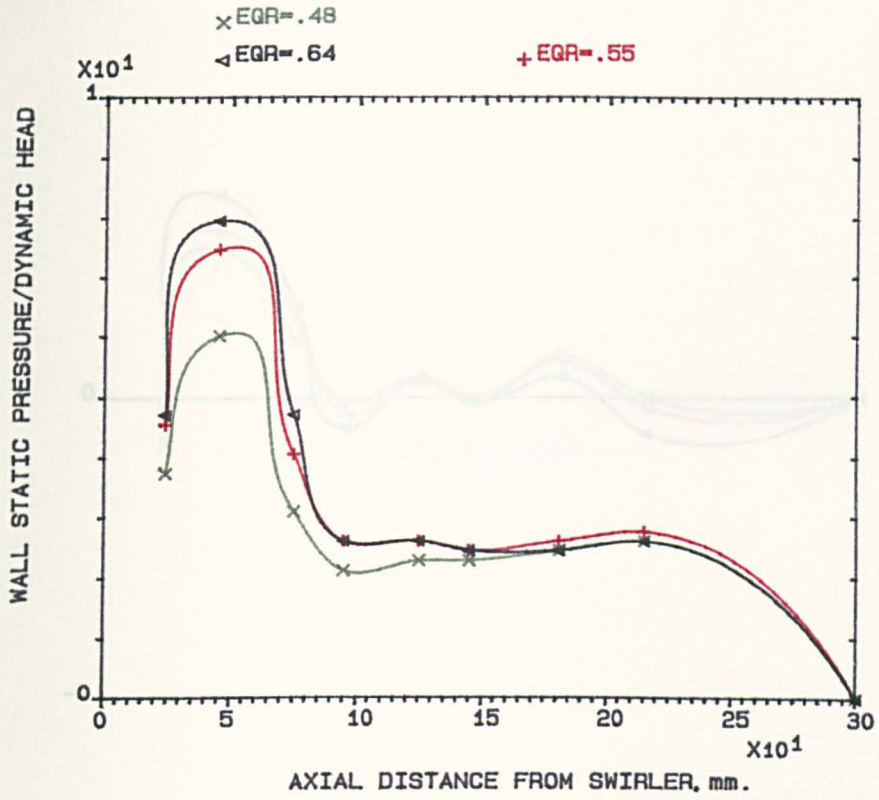

FIG.7.13 COMBUSTOR WALL STATIC PRESSURE V. AXIAL DISTANCE OF MAIN STAGE COMBUSTOR; (0.333/1); PILOT AT EQR=0.110; .028, PROPANE, 400K.

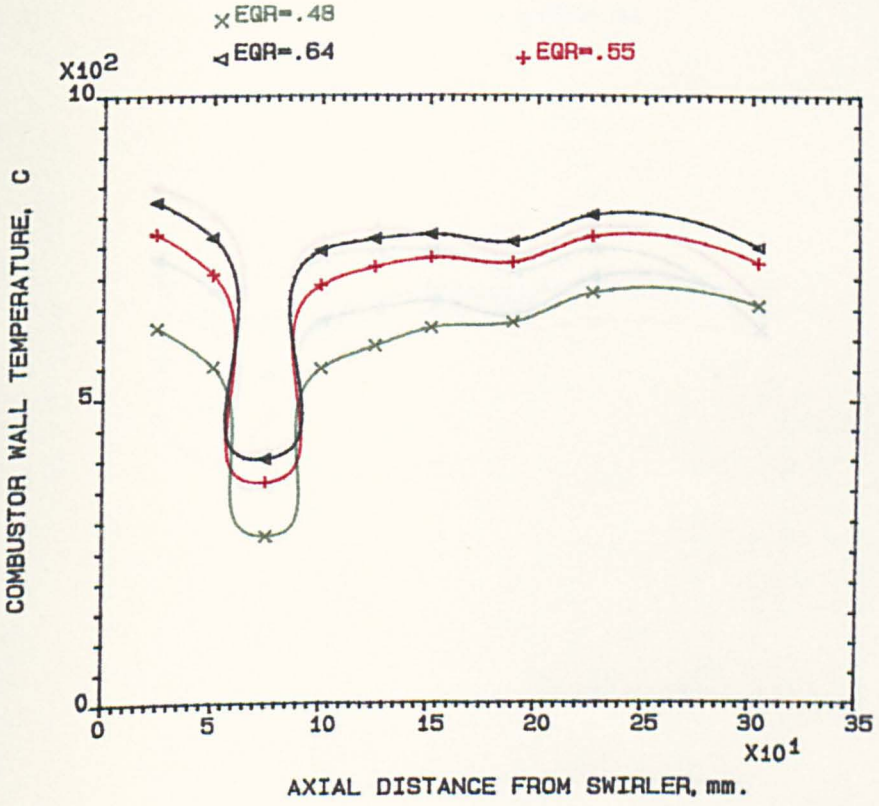

FIG.7.14 COMBUSTOR WALL TEMPERATURE V. AXIAL DISTANCE OF MAIN STAGE COMBUSTOR; (0.333/1); PILOT AT EQR=0.110; .028, PROPANE, 400K.

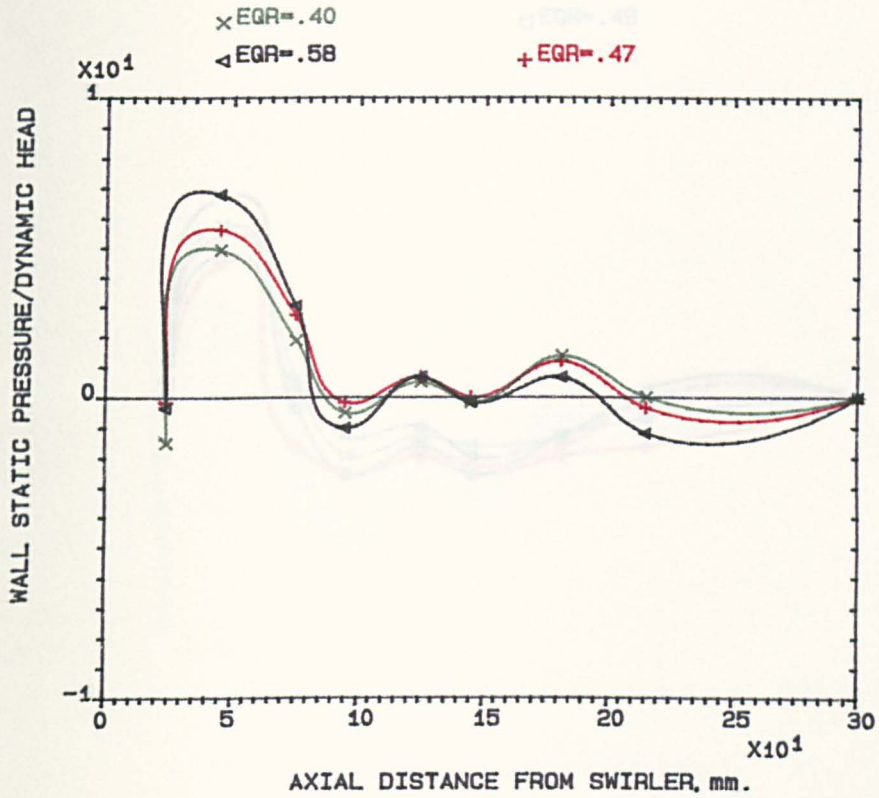

FIG.7.15 COMBUSTOR WALL STATIC PRESSURE V. AXIAL DISTANCE OF MAIN STAGE COMBUSTOR; (0.333/1); PILOT AT EQR=0.096; .028, PROPANE, 600K.

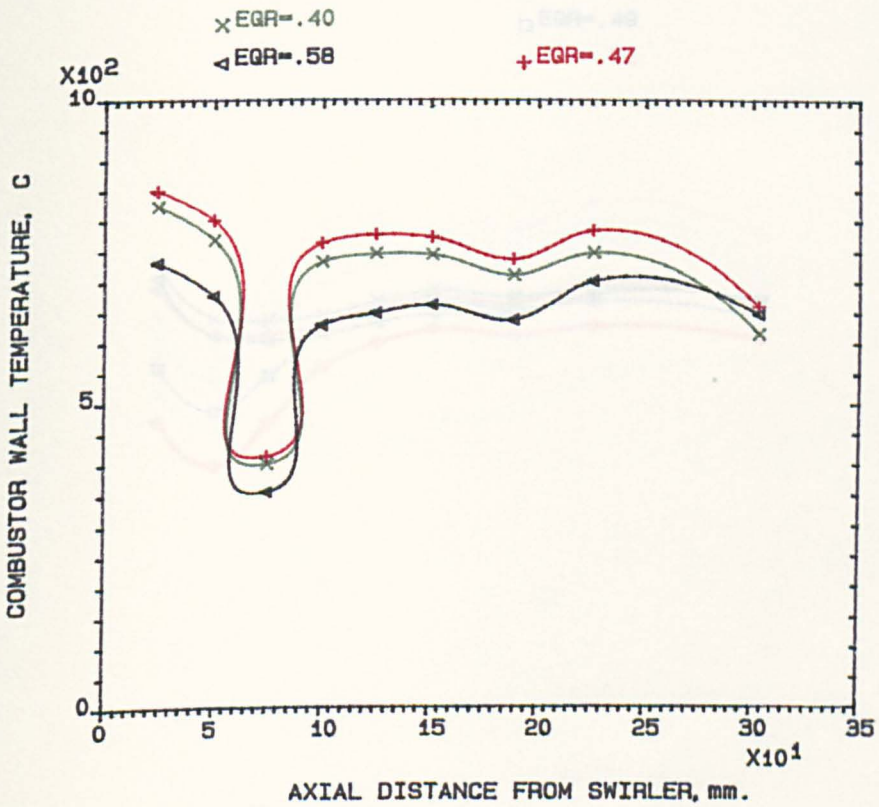

FIG.7.16 COMBUSTOR WALL TEMPERATURE V. AXIAL DISTANCE OF MAIN STAGE COMBUSTOR; (0.333/1); PILOT AT EQR=0.096; .028, PROPANE, 600K.

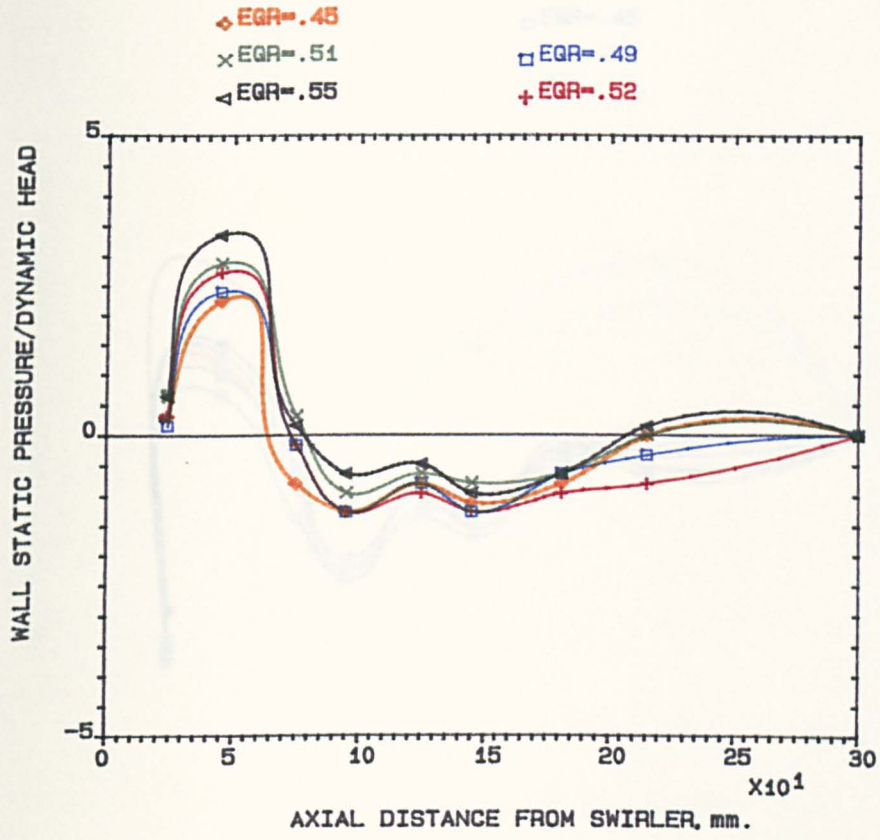

FIG.7.17 COMBUSTOR WALL STATIC PRESSURE V. AXIAL DISTANCE OF MAIN STAGE COMBUSTOR; (0.333/1); P/PILOT AT EQR=0.115; .028; KEROSENE; 400K.

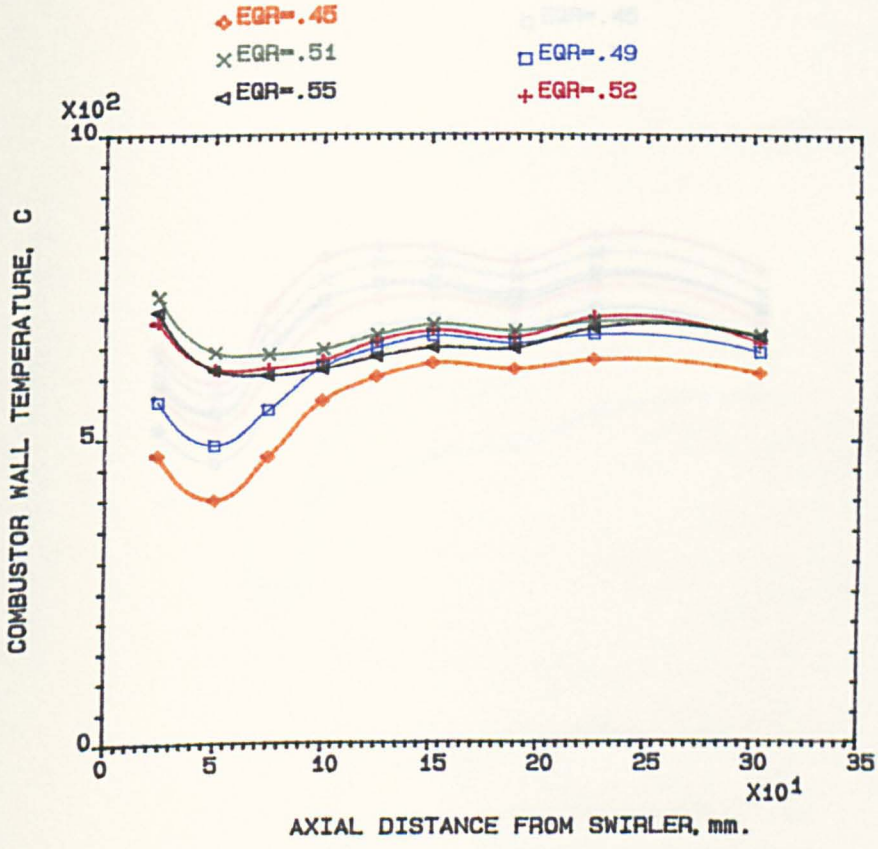

FIG.7.18 COMBUSTOR WALL TEMPERATURE V. AXIAL DISTANCE OF MAIN STAGE COMBUSTOR; (0.333/1); P/PILOT AT EQR=0.115; .028; KEROSENE; 400K.

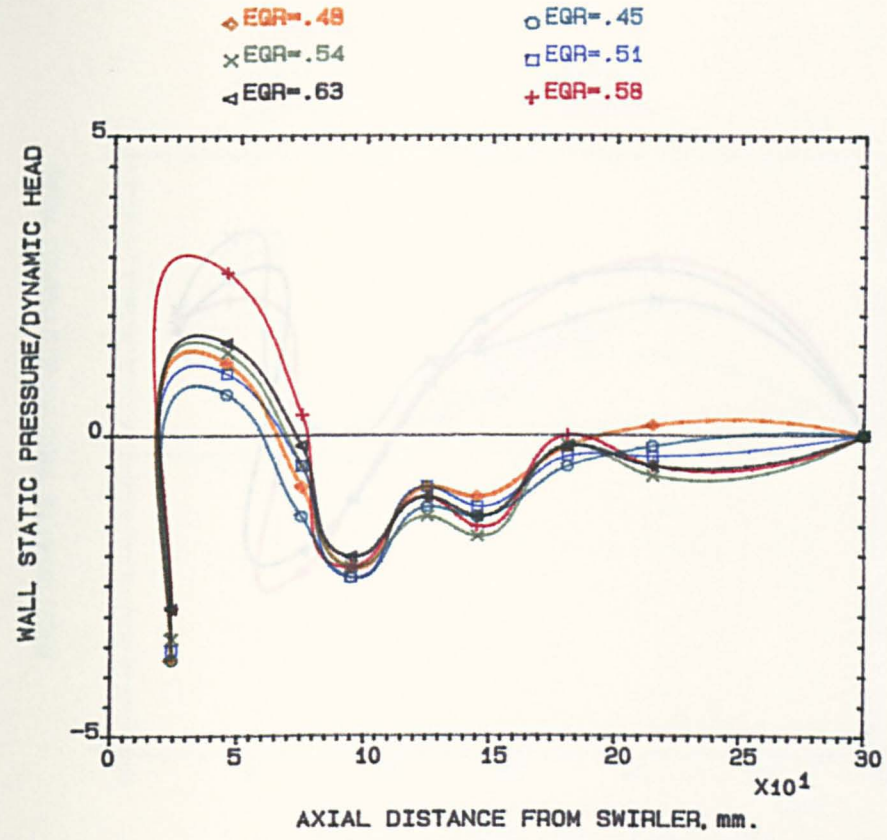

FIG.7.19 COMBUSTOR WALL STATIC PRESSURE V. AXIAL DISTANCE OF MAIN STAGE COMBUSTOR; (0.333/1); P/PILOT AT EQR=0.096; .028; KEROSENE; 600K.

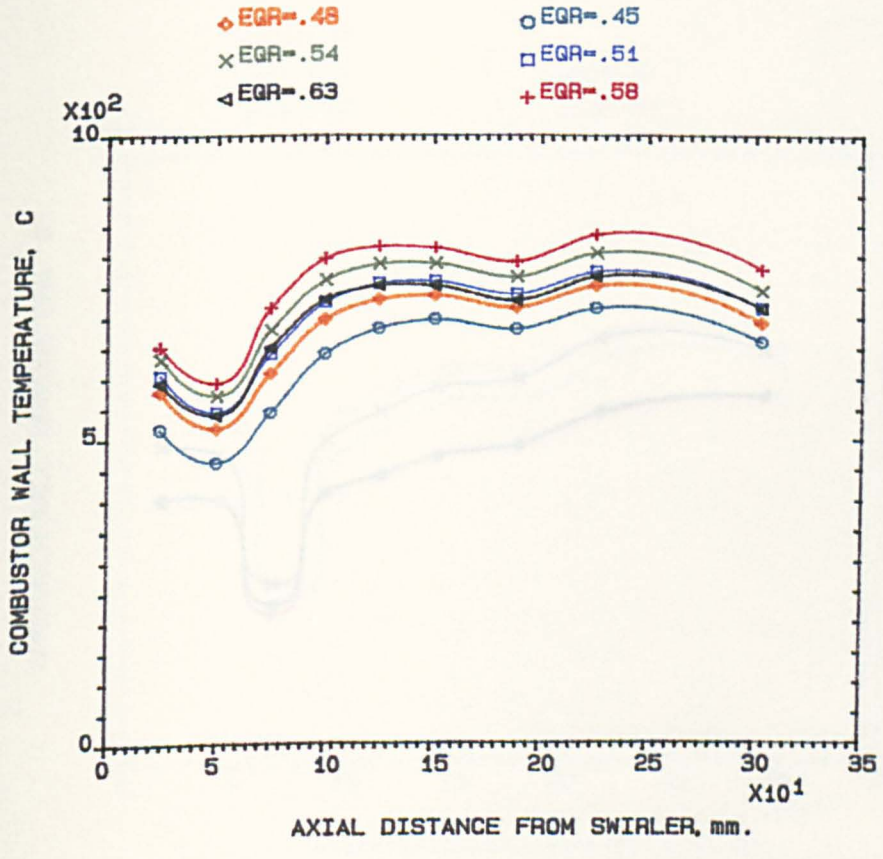

FIG.7.20 COMBUSTOR WALL TEMPERATURE V. AXIAL DISTANCE OF MAIN STAGE COMBUSTOR; (0.333/1); P/PILOT AT EQR=0.096; .028; KEROSENE; 600K.

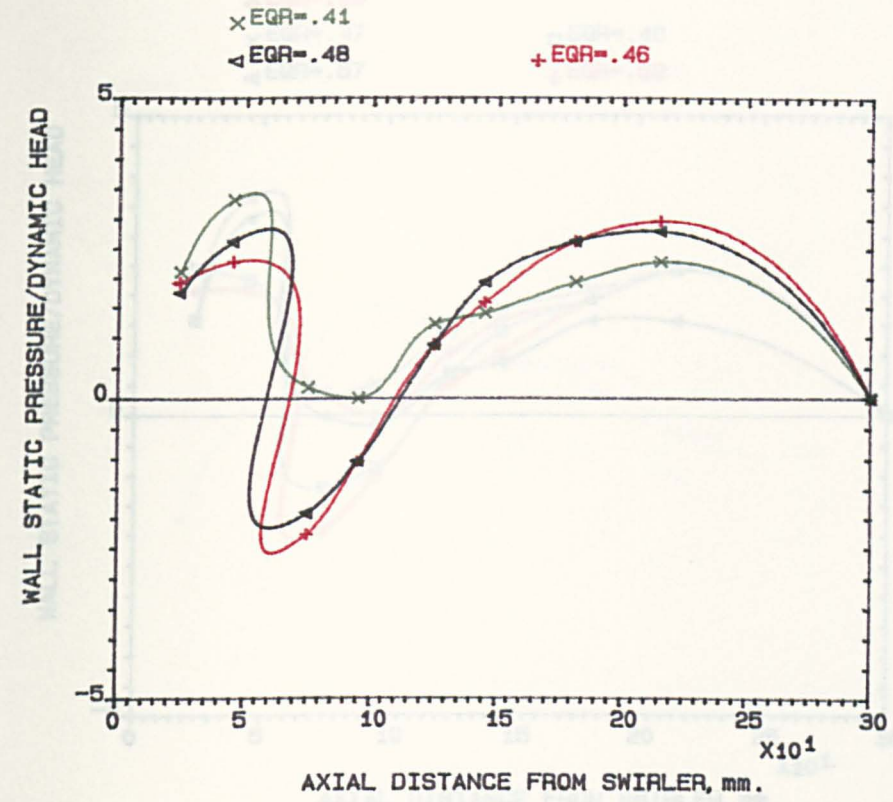

FIG.7.21 COMBUSTOR WALL STATIC PRESSURE V. AXIAL DISTANCE OF MAIN STAGE COMBUSTOR; (0.333/1); PILOT AT EQR=0.111; .028, NATURAL GAS, 600K.

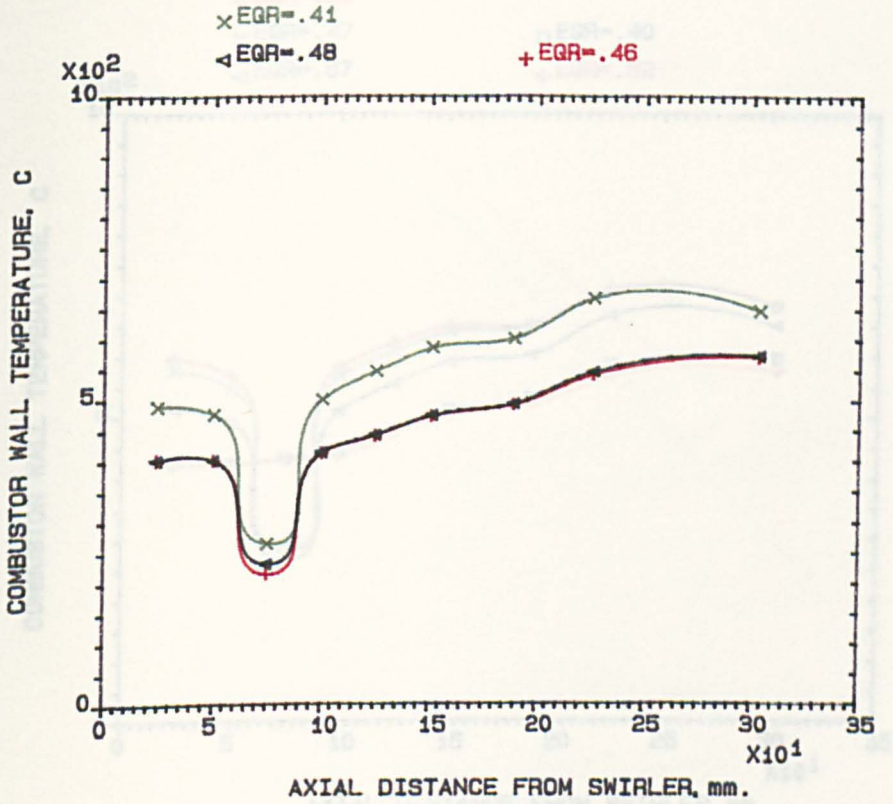

FIG.7.22 COMBUSTOR WALL TEMPERATURE V. AXIAL DISTANCE OF MAIN STAGE COMBUSTOR; (0.333/1); PILOT AT EQR=0.111; .028, NATURAL GAS, 600K.

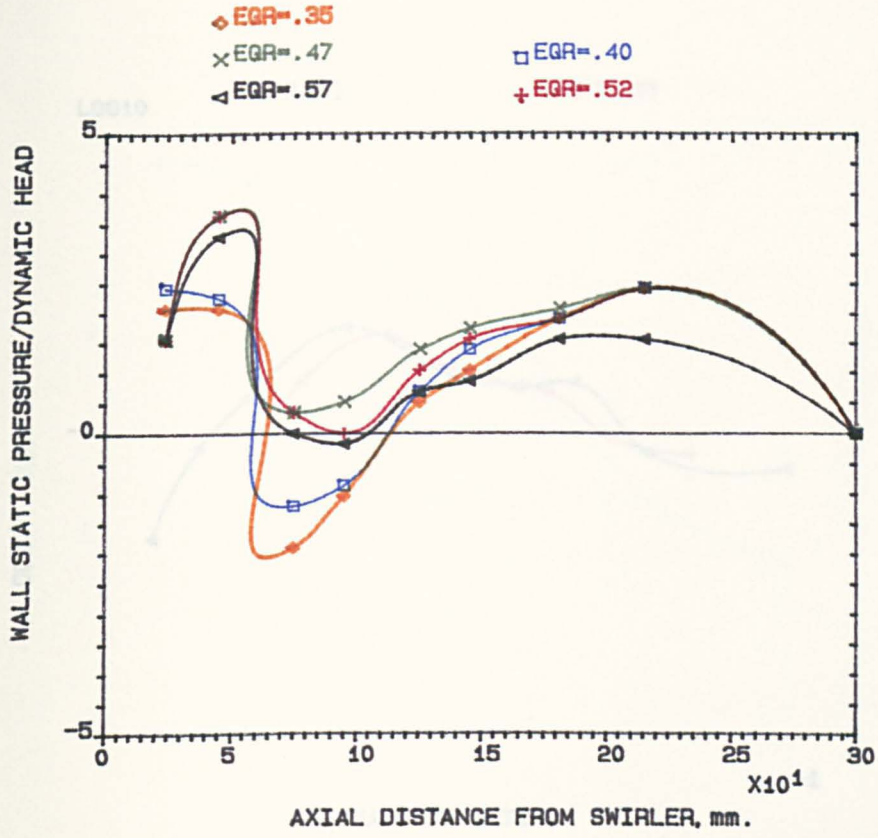

FIG.7.23 COMBUSTOR WALL STATIC PRESSURE V. AXIAL DISTANCE OF MAIN STAGE COMBUSTOR; (0.333/1); PILOT AT EQR=0.230; .028, NATURAL GAS, 600K.

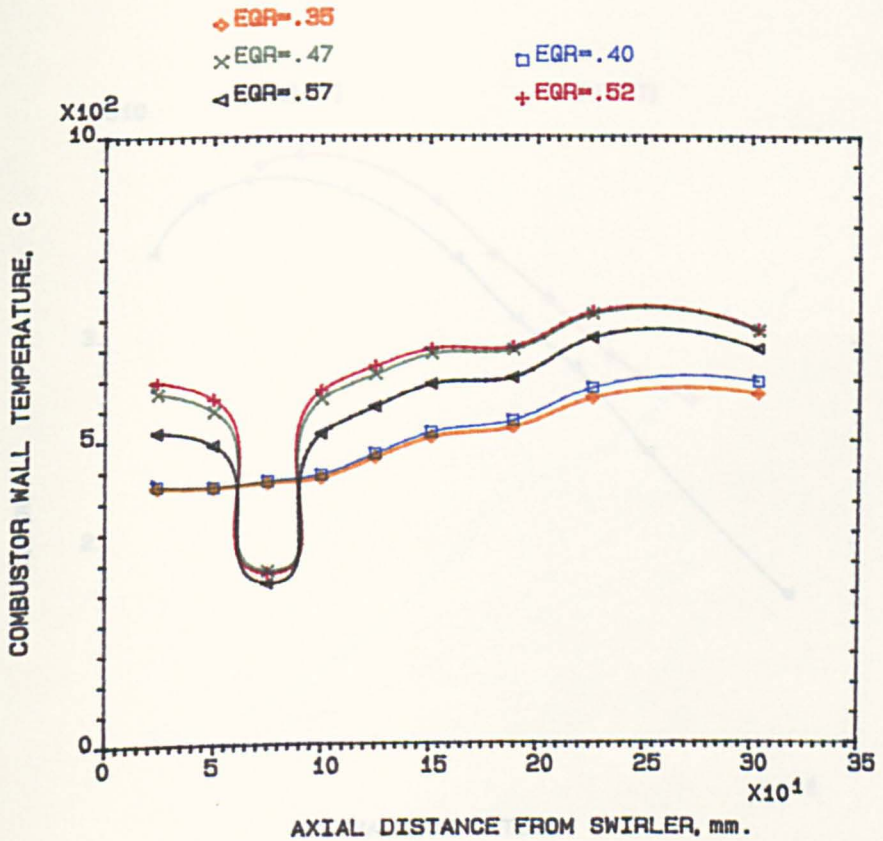

FIG.7.24 COMBUSTOR WALL TEMPERATURE V. AXIAL DISTANCE OF MAIN STAGE COMBUSTOR; (0.333/1); PILOT AT EQR=0.230; .028, NATURAL GAS, 600K.

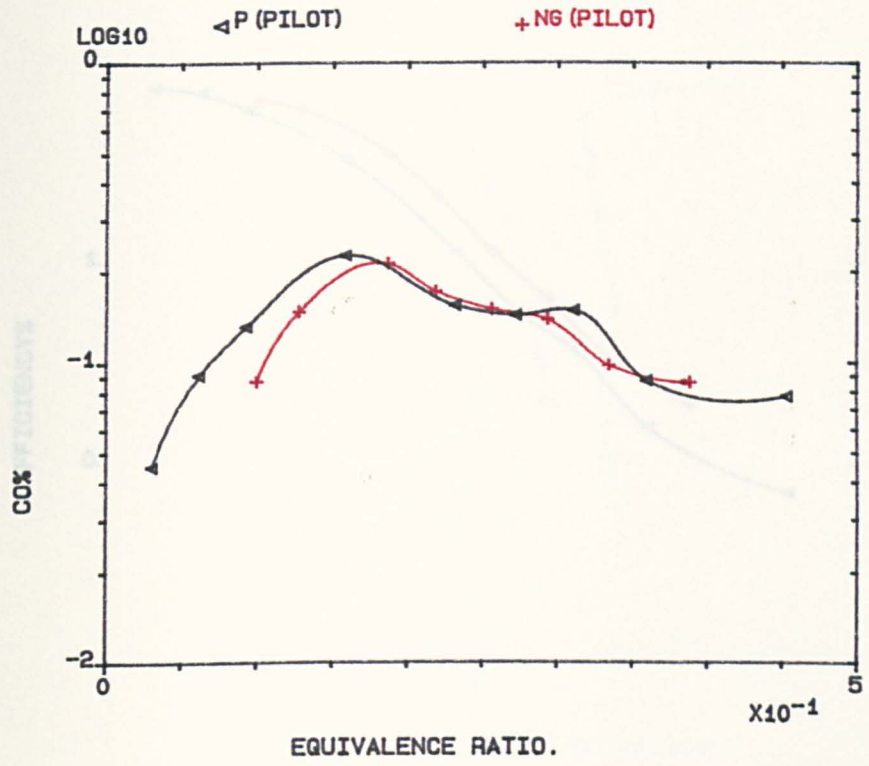

FIG.7.25 CO% V. EQR. FOR PILOT/MAIN AIR SPLIT RATIO OF (1.041/1), USING NATURAL GAS OR PROPANE FOR PILOT ONLY. MN=.028, 400K.

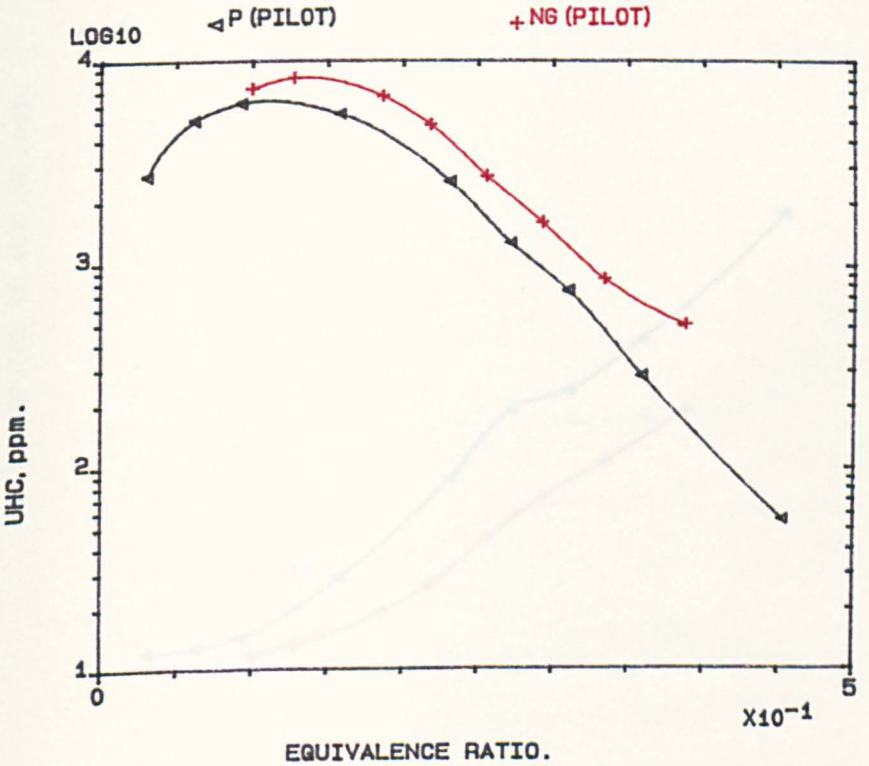

FIG.7.26 UHC V. EQR. FOR PILOT/MAIN AIR SPLIT RATIO OF (1.041/1), USING NATURAL GAS OR PROPANE FOR PILOT ONLY. MN=.028, 400K.

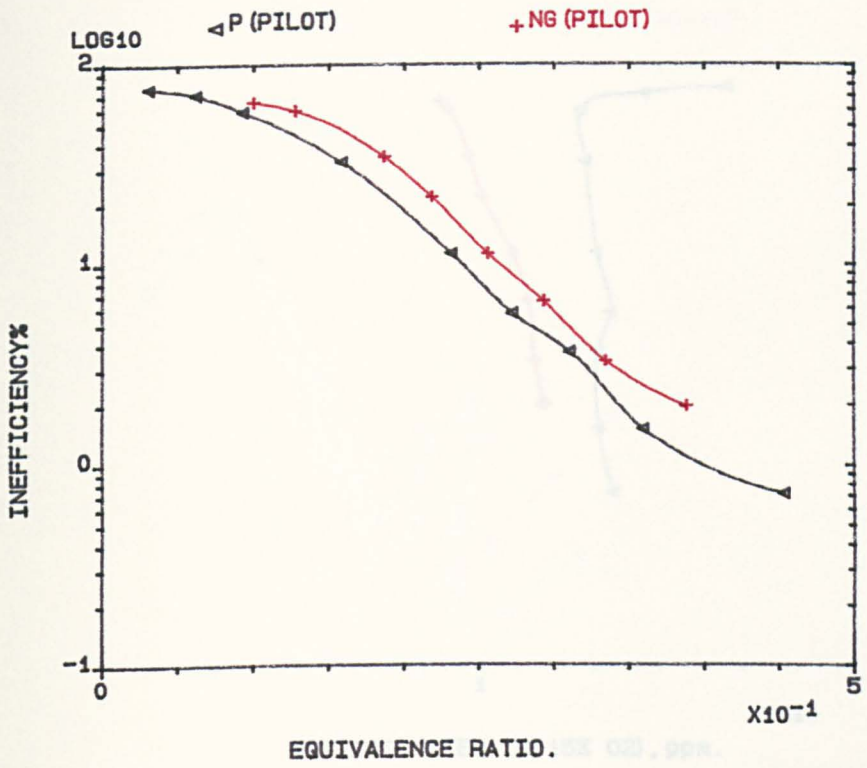

FIG.7.27 INEFF% V. EQR. FOR PILOT/MAIN AIR SPLIT RATIO OF (1.041/1). USING NATURAL GAS OR PROPANE FOR PILOT ONLY. MN=.028, 400K.

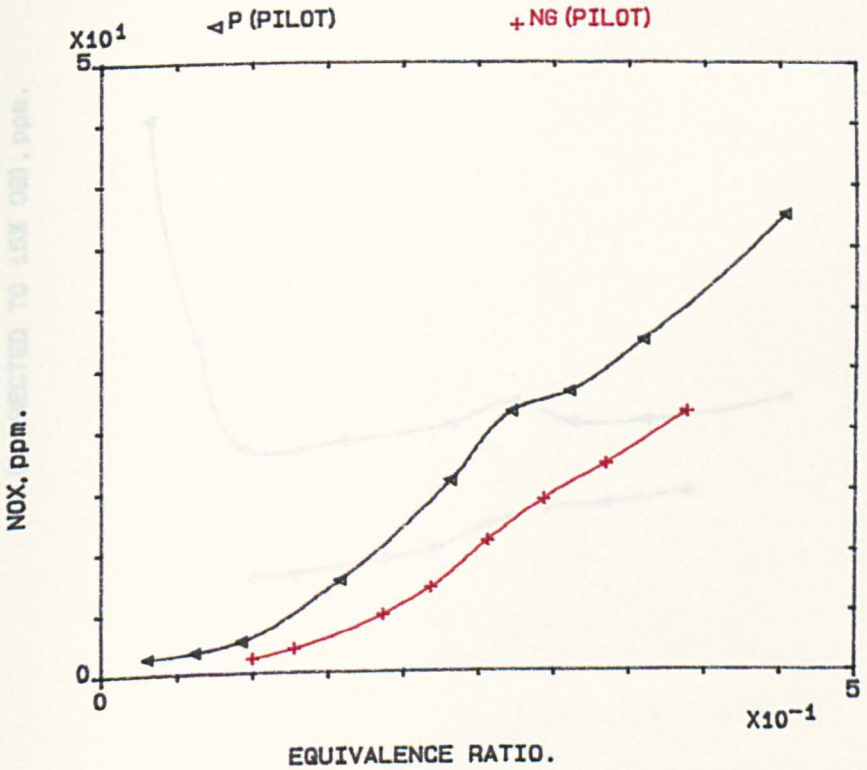

FIG.7.28 NOX V. EQR. FOR PILOT/MAIN AIR SPLIT RATIO OF (1.041/1). USING NATURAL GAS OR PROPANE FOR PILOT ONLY. MN=.028, 400K.

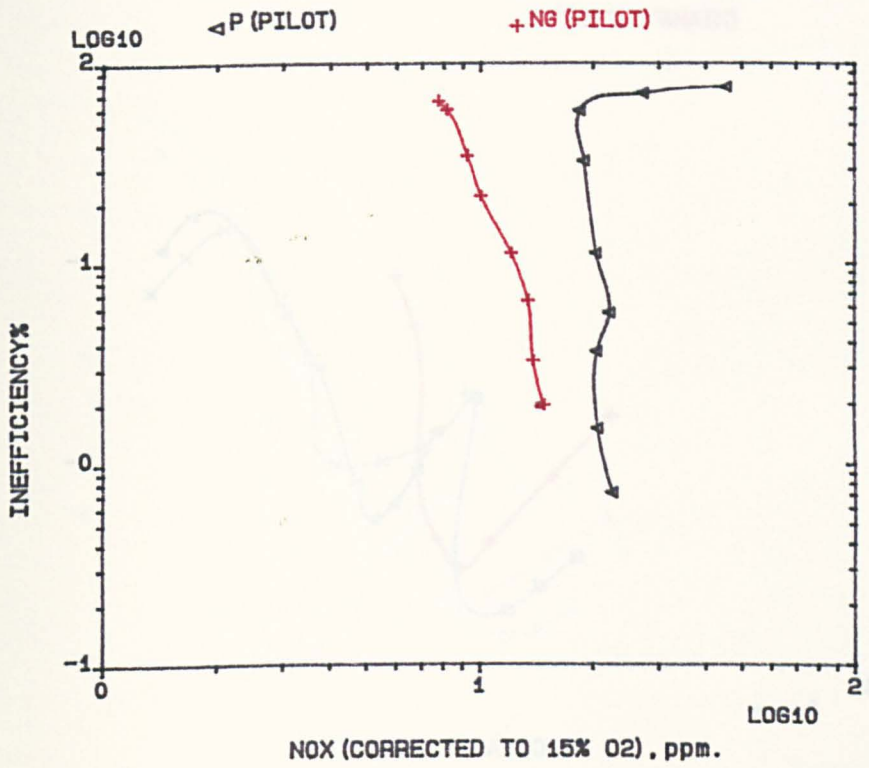

FIG.7.29 INEFF% V. NOXC FOR PILOT/MAIN AIR SPLIT RATIO OF (1.041/1), USING NATURAL GAS OR PROPANE FOR PILOT ONLY, MN=.028, 400K.

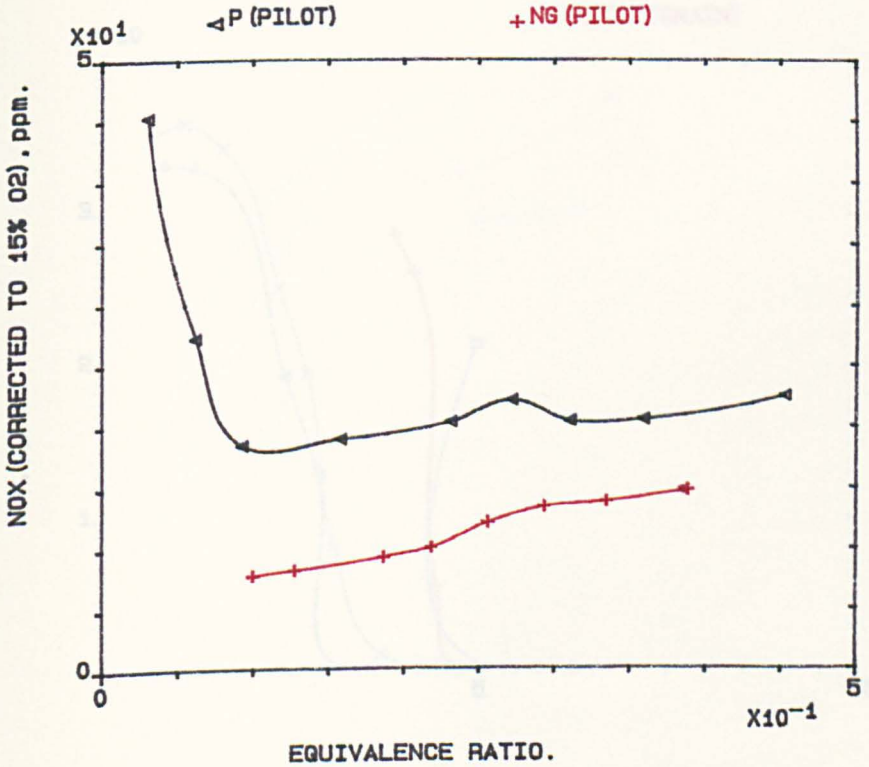

FIG.7.30 NOXC V. EQR. FOR PILOT/MAIN AIR SPLIT RATIO OF (1.041/1), USING NATURAL GAS OR PROPANE FOR PILOT ONLY, MN=.028, 400K.

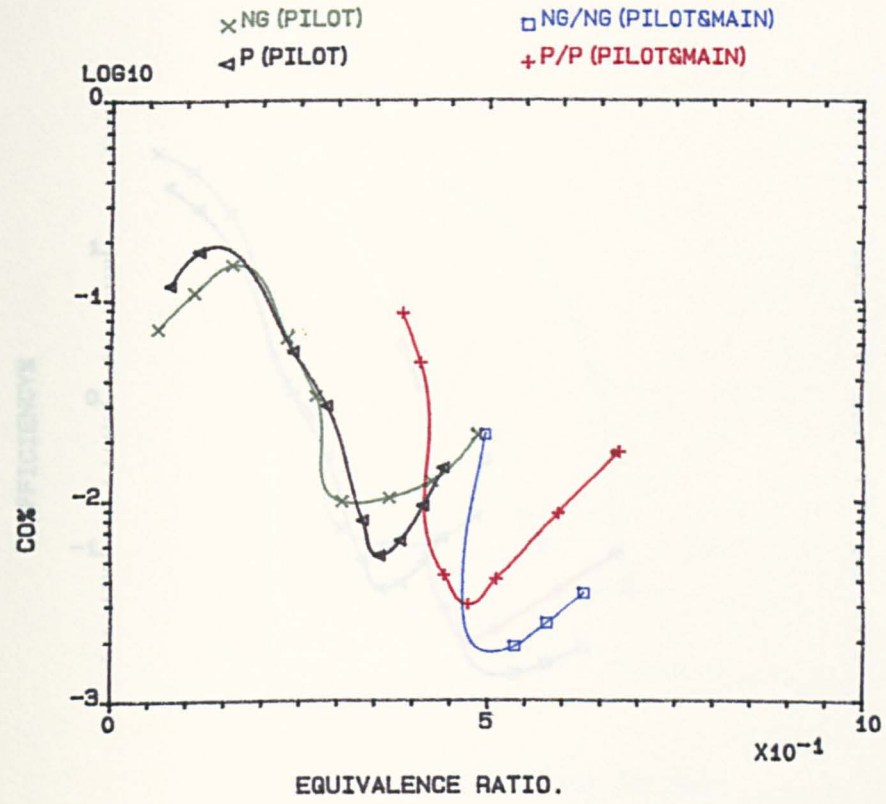

FIG.7.31 CO% V. EQR. FOR PILOT/MAIN AIR SPLIT RATIO OF (1.041/1). USING NATURAL GAS OR PROPANE FOR BOTH STAGES. MN=.028. 600K.

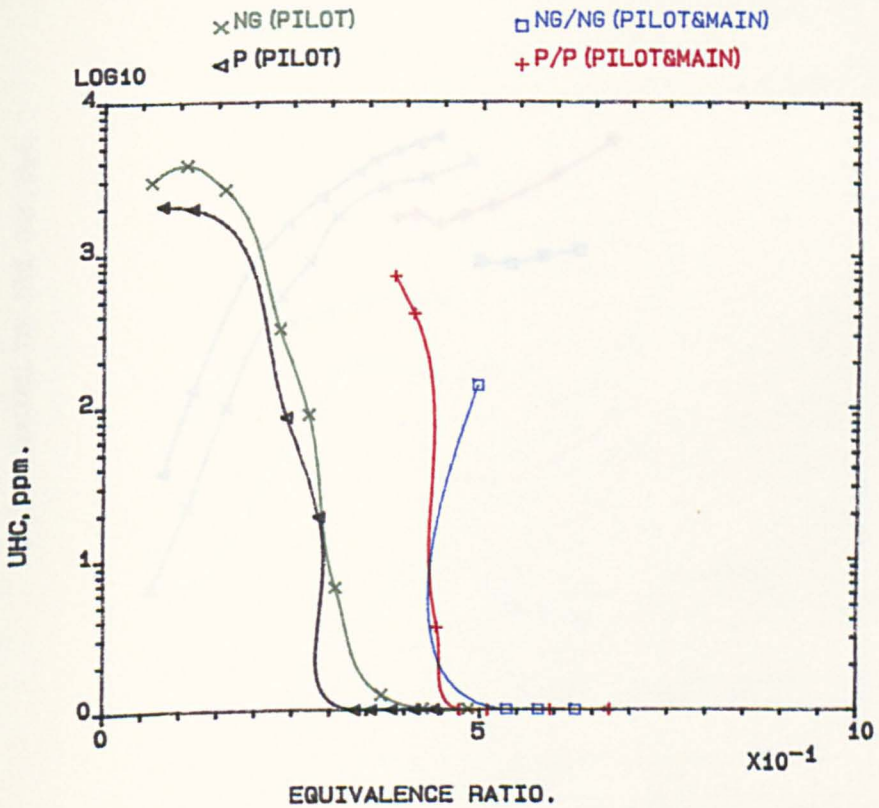

FIG.7.32 UHC V. EQR. FOR PILOT/MAIN AIR SPLIT RATIO OF (1.041/1). USING NATURAL GAS OR PROPANE FOR BOTH STAGES. MN=.028. 600K.

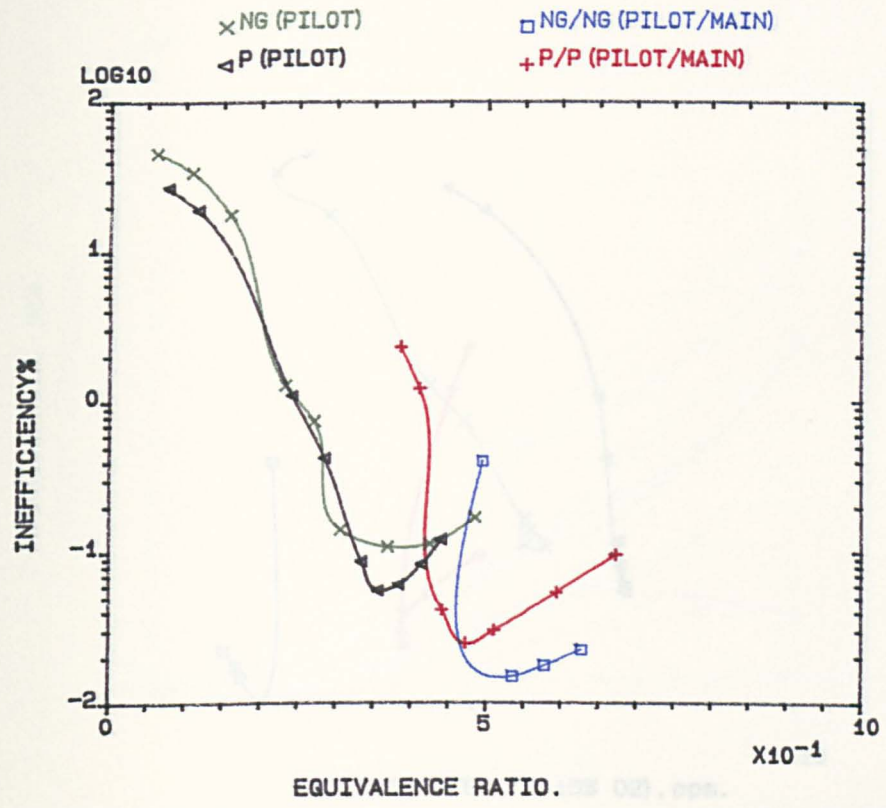

FIG.7.33 INEFF% V. EQR. FOR PILOT/MAIN AIR SPLIT RATIO OF (1.041/1), USING NATURAL GAS OR PROPANE FOR BOTH STAGES, MN=.028, 600K.

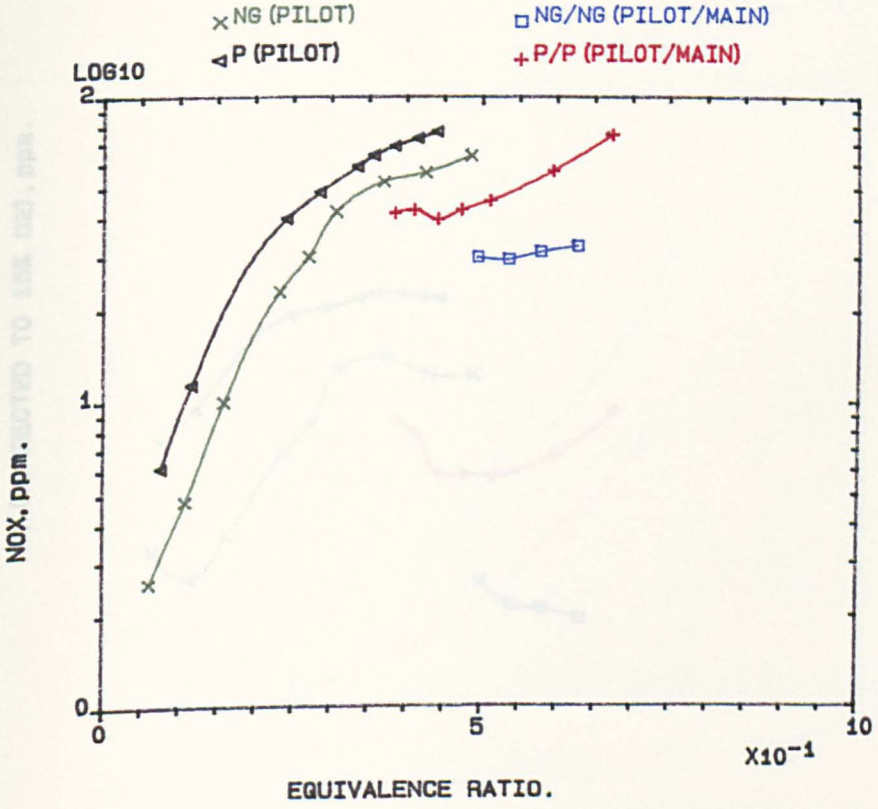

FIG.7.34 NOX V. EQR. FOR PILOT/MAIN AIR SPLIT RATIO OF (1.041/1), USING NATURAL GAS OR PROPANE FOR BOTH STAGES, MN=.028, 600K.

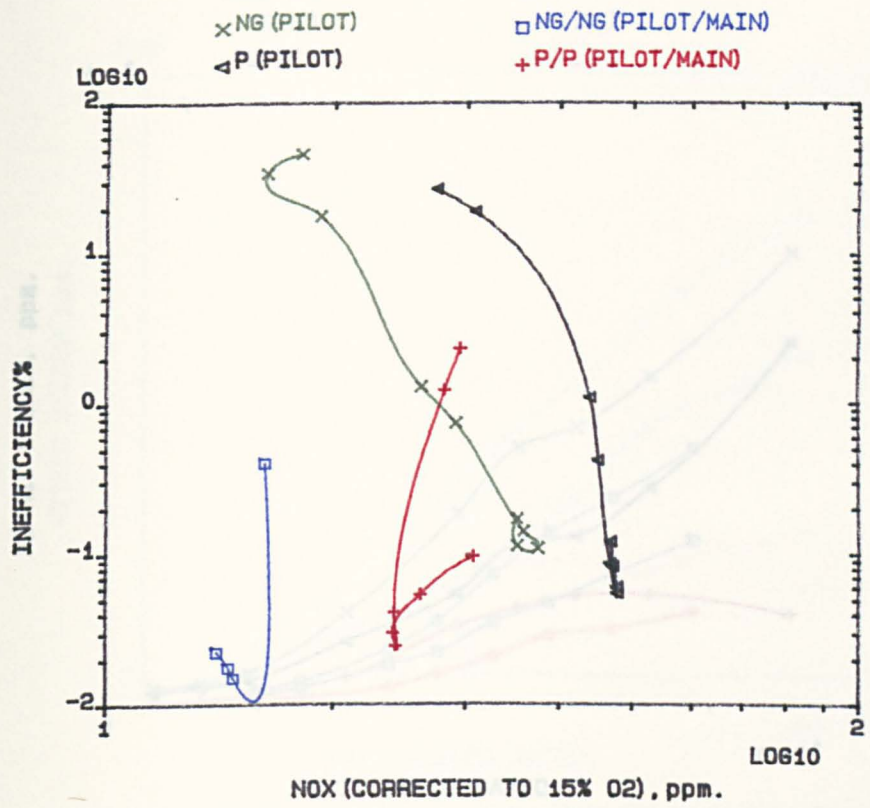

FIG.7.35 INEFF% V. NOXC FOR PILOT/MAIN AIR SPLIT RATIO OF (1.041/1), USING NATURAL GAS OR PROPANE FOR BOTH STAGES, MN=.028, 600K.

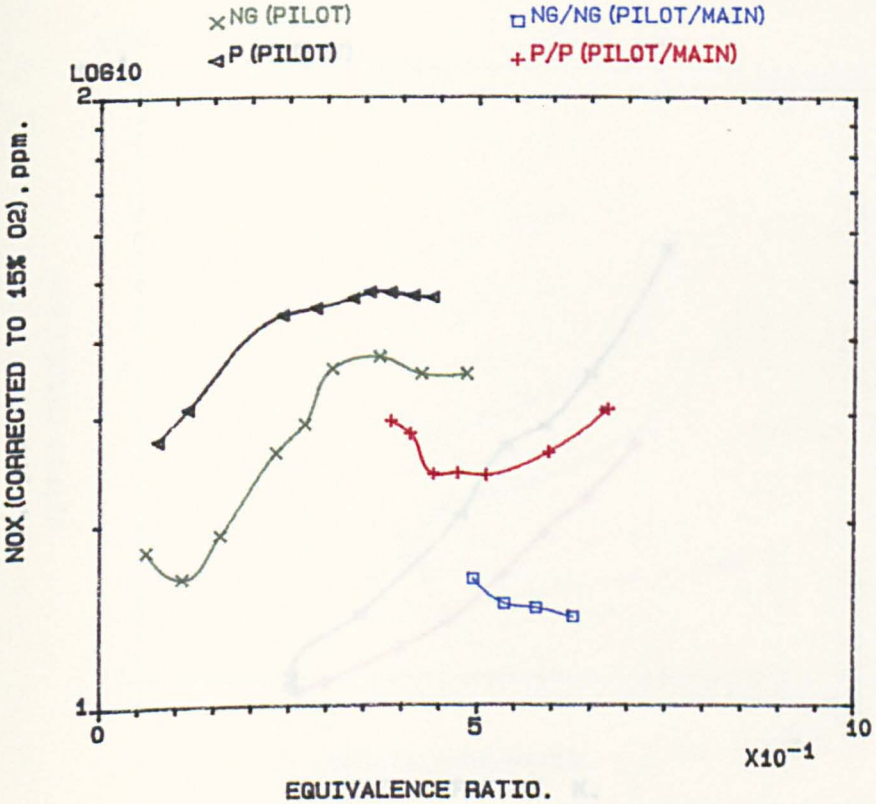

FIG.7.36 NOXC V. EQR. FOR PILOT/MAIN AIR SPLIT RATIO OF (1.041/1), USING NATURAL GAS OR PROPANE FOR BOTH STAGES, MN=.028, 600K.

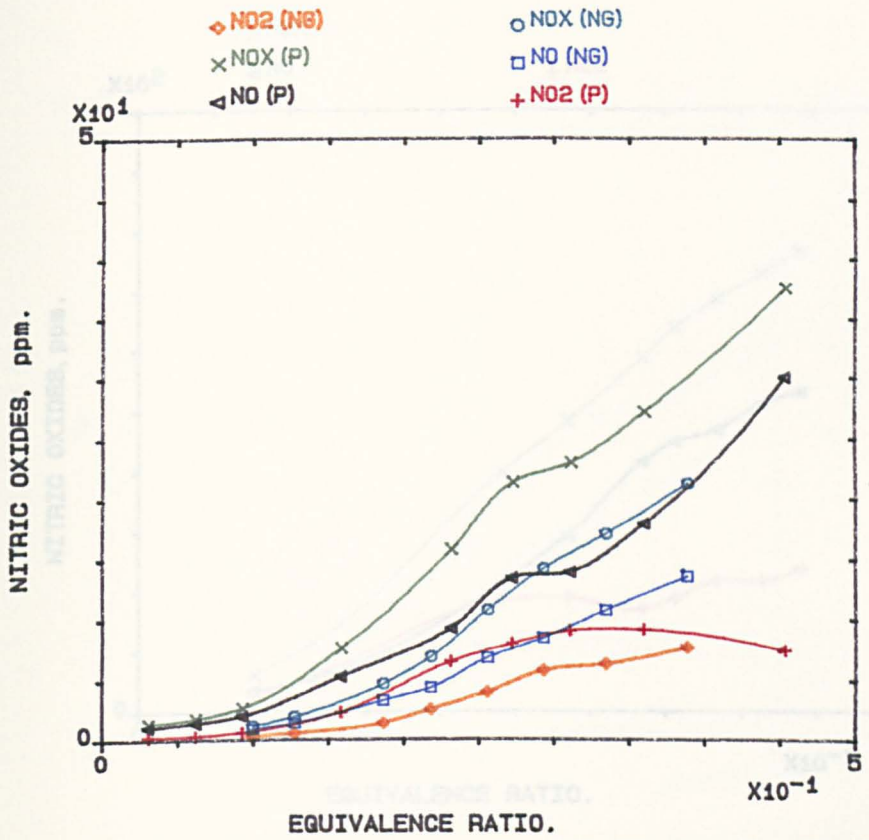

FIG.7.37 NITRIC OXIDES V. EQR. FOR PILOT/MAIN AIR SPLIT RATIO OF (1.041/1); PROPANE OR NATURAL GAS; PILOT ONLY; MN=0.028; 400K.

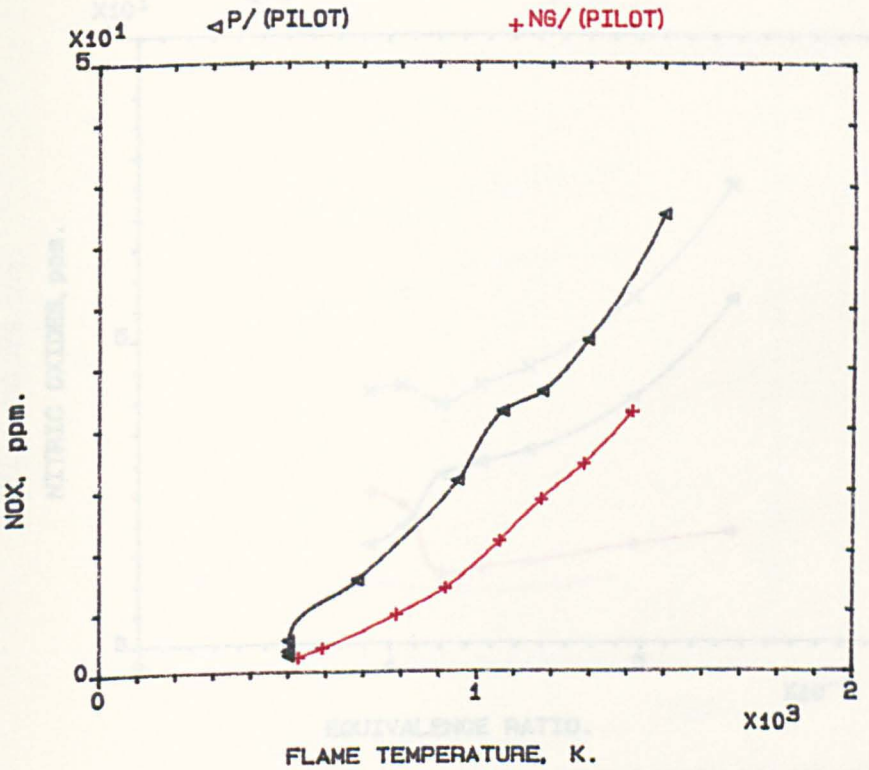

FIG.7.38 NOX V. FLAME TEMP. FOR PILOT/MAIN AIR SPLIT RATIO OF (1.401); PROPANE OR NATURAL GAS; PILOT ONLY; MN=0.028, 400K.

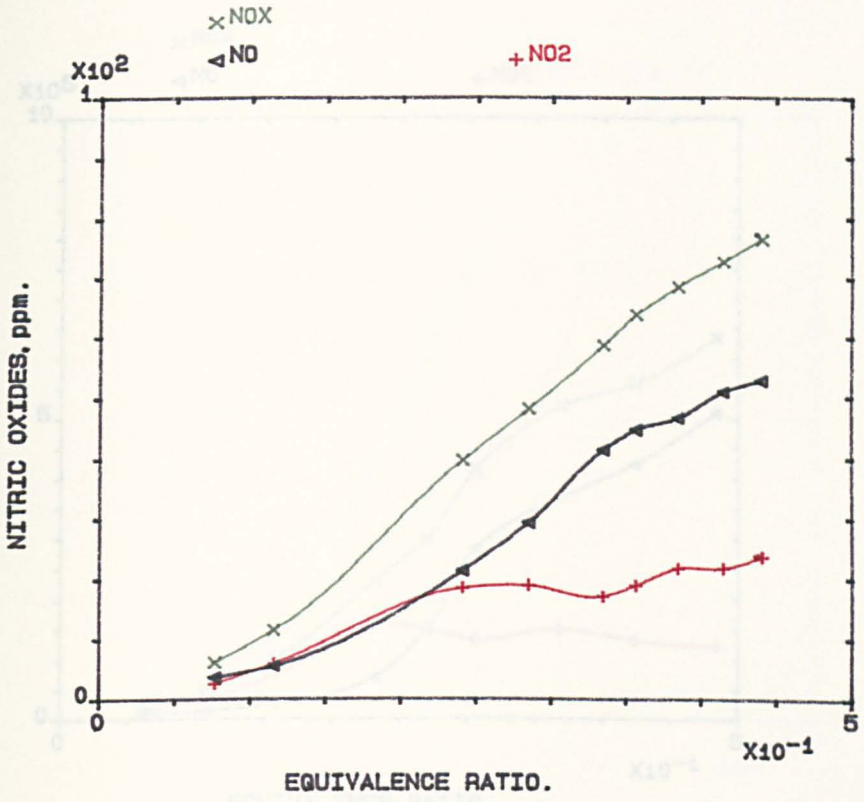

FIG.7.39 NITRIC OXIDES V. EQR. FOR PILOT/MAIN AIR SPLIT RATIO, OF (1.041/1). USING PROPANE FOR PILOT ONLY. MN=.028, 600K.

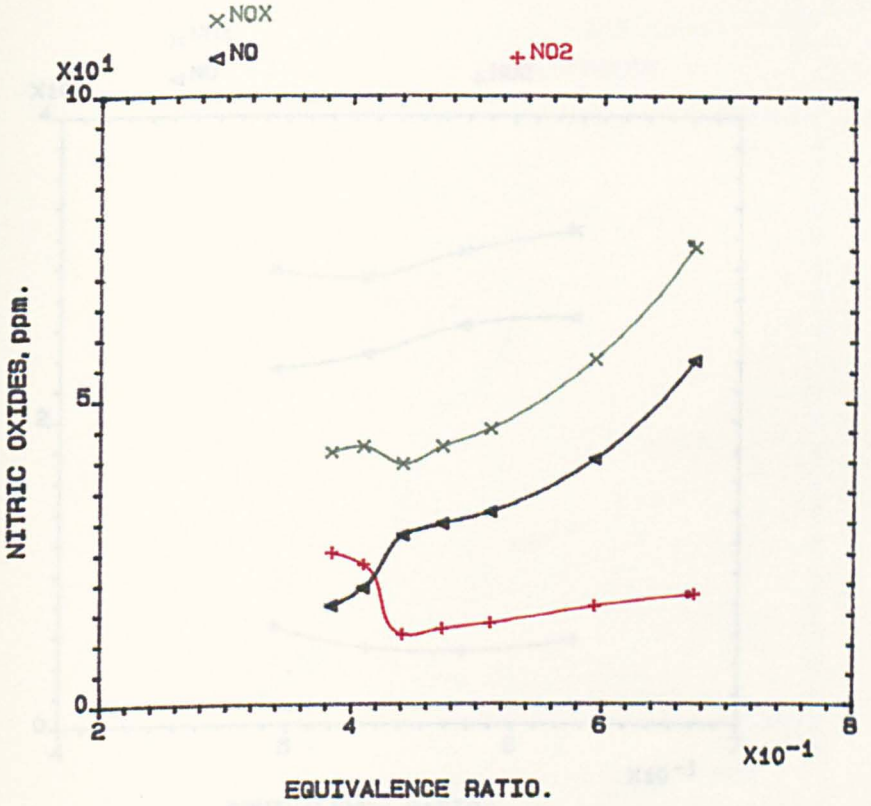

FIG.7.40 NITRIC OXIDES V. EQR. FOR PILOT/MAIN AIR SPLIT RATIO, OF (1.041/1). USING PROPANE FOR BOTH STAGES, MN=.028, 600K.

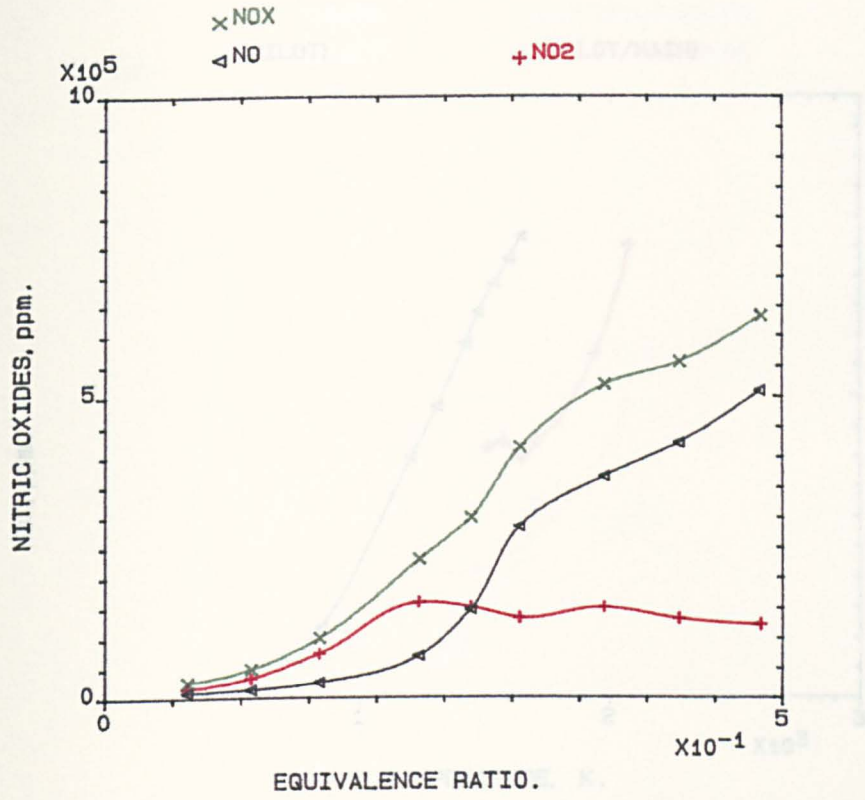

FIG.7.41 NITRIC OXIDES V. EQR. FOR PILOT/MAIN AIR SPLIT RATIO, OF (1.041/1), USING NATURAL GAS FOR PILOT ONLY. MN=.028, 600K.

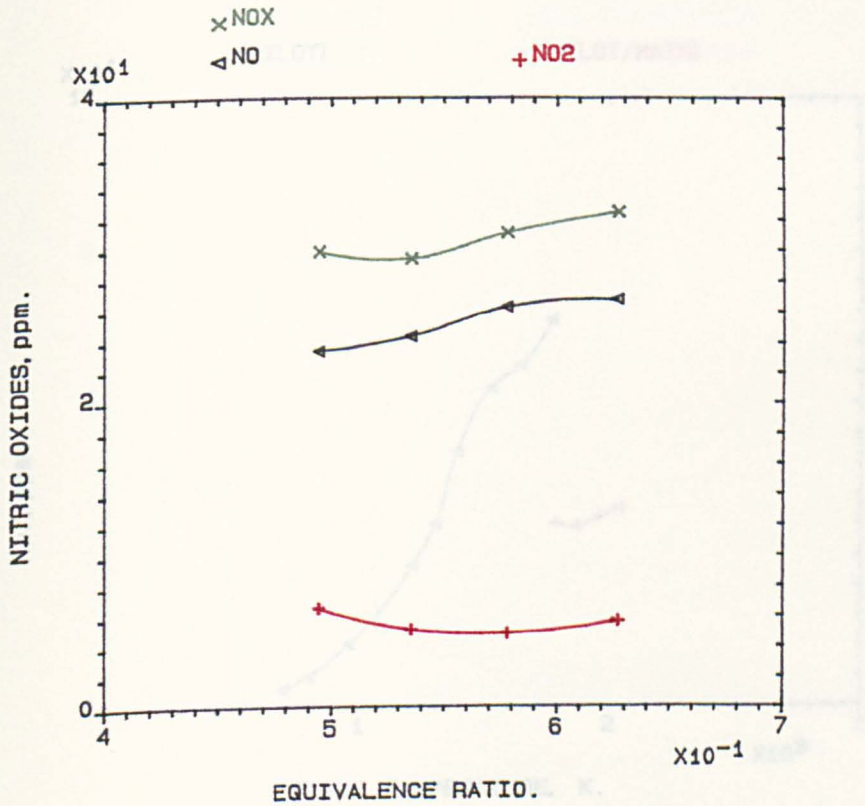

FIG.7.42 NITRIC OXIDES V. EQR. FOR PILOT/MAIN AIR SPLIT RATIO, OF (1.041/1), USING NATURAL GAS FOR BOTH STAGES, MN=.028, 600K.

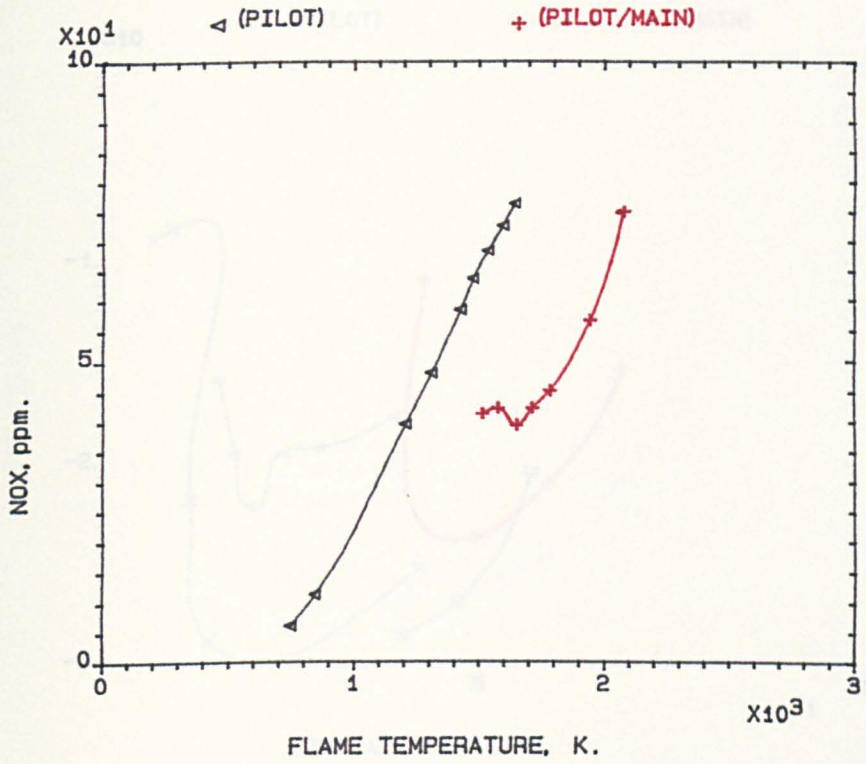

FIG.7.43 NOX V. F.TEMP. FOR PILOT/MAIN AIR SPLIT RATIO OF (1.041/1). USING PROPANE FOR BOTH STAGES. MN=.028, 600K.

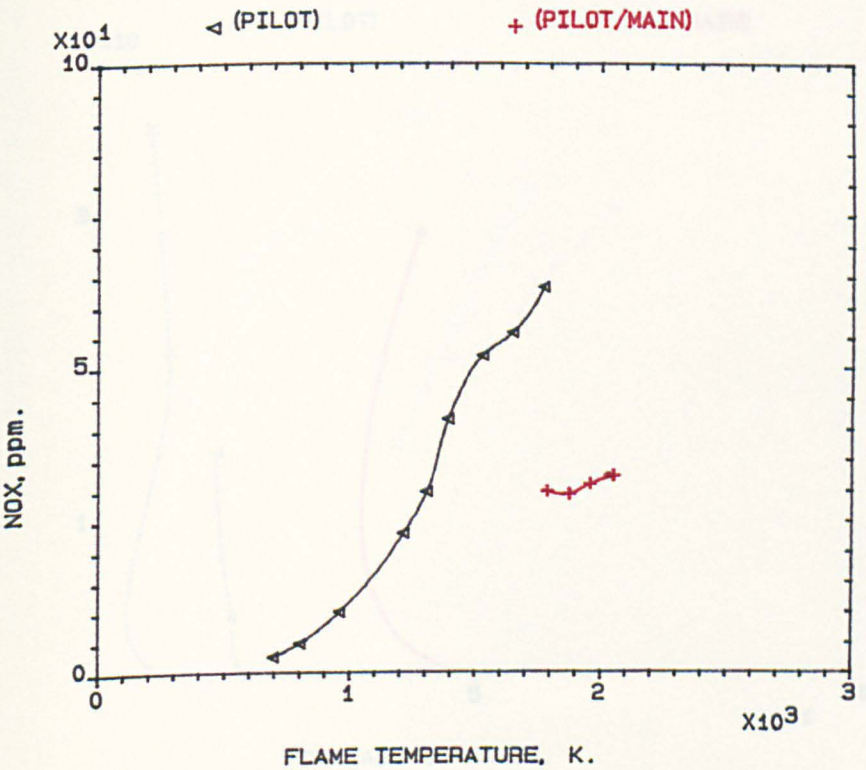

FIG.7.44 NOX V. F.TEMP. FOR PILOT/MAIN AIR SPLIT RATIO OF (1.041/1). USING NATURAL GAS FOR BOTH STAGES. MN=.028, 600K.

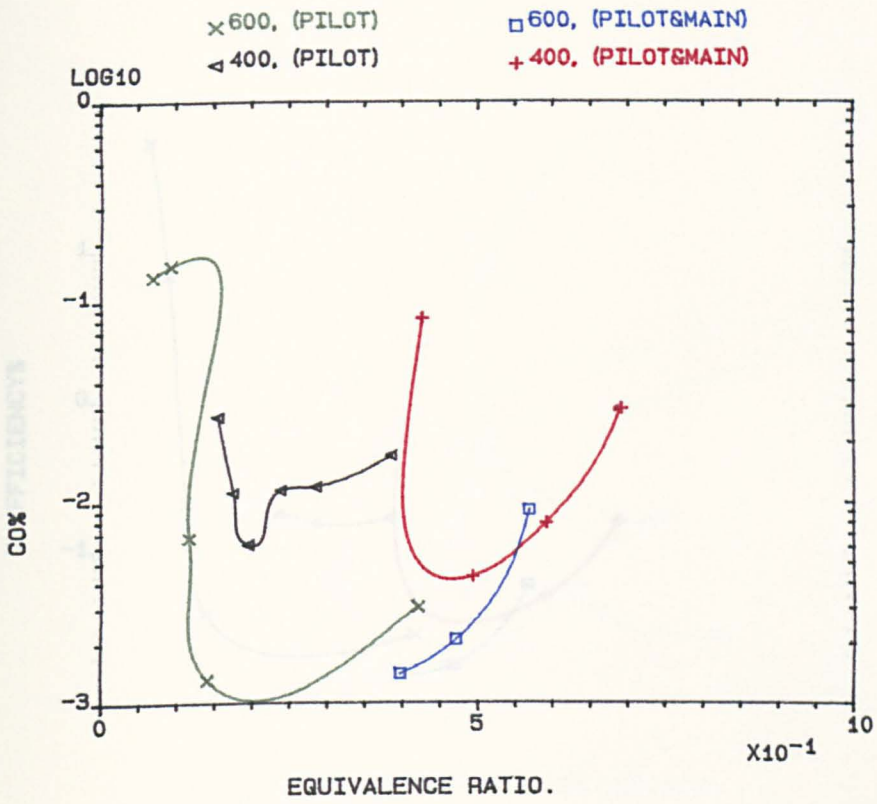

FIG.7.45 CO% V. EQR. FOR PILOT/MAIN AIR SPLIT RATIO OF (0.587/1), USING PROPANE FOR BOTH STAGES, MN=.028, FOR 400K & 600K INLET.

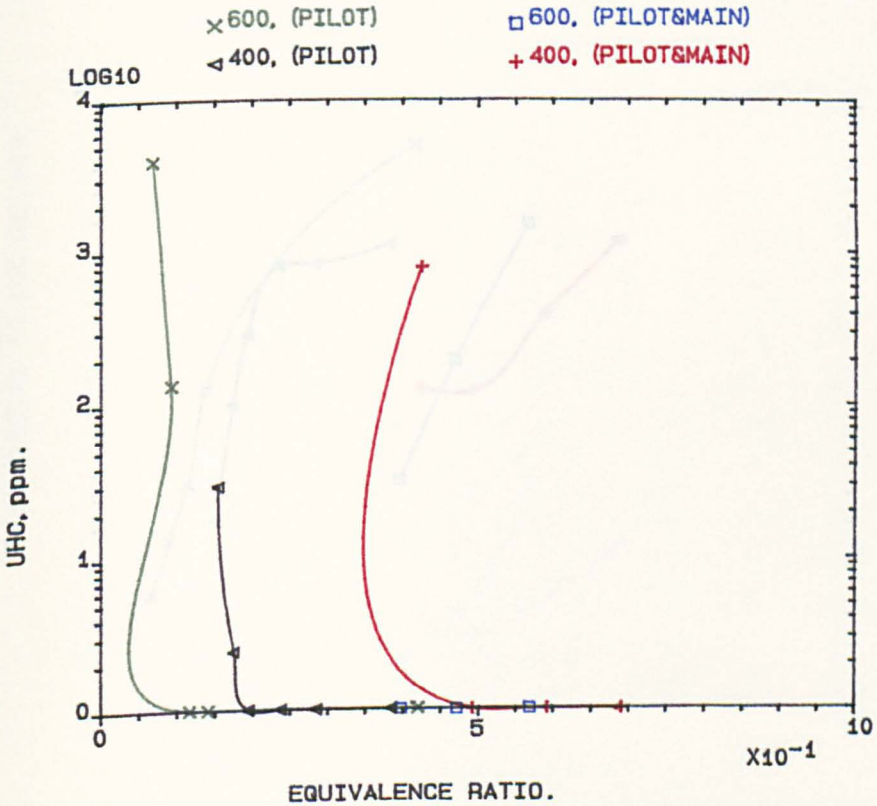

FIG.7.46 UHC V. EQR. FOR PILOT/MAIN AIR SPLIT RATIO OF (0.587/1), USING PROPANE FOR BOTH STAGES, MN=.028, FOR 400K & 600K INLET.

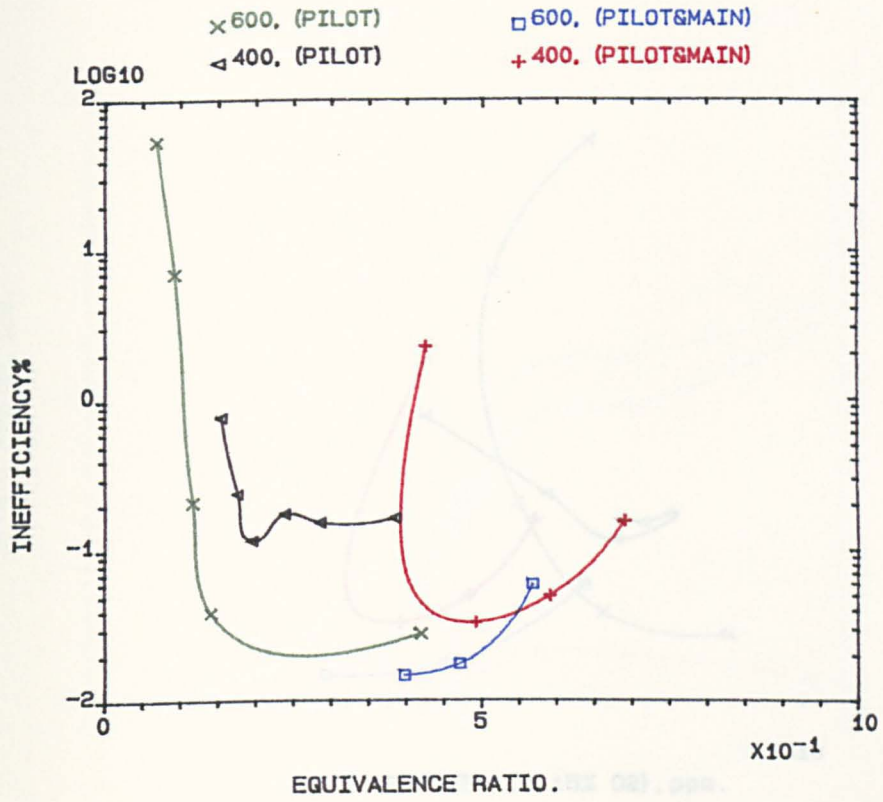

FIG.7.47 INEFF% V. EQR. FOR PILOT/MAIN AIR SPLIT RATIO OF (0.587/1), USING PROPANE FOR BOTH STAGES, MN=.028, FOR 400K & 600K INLET.

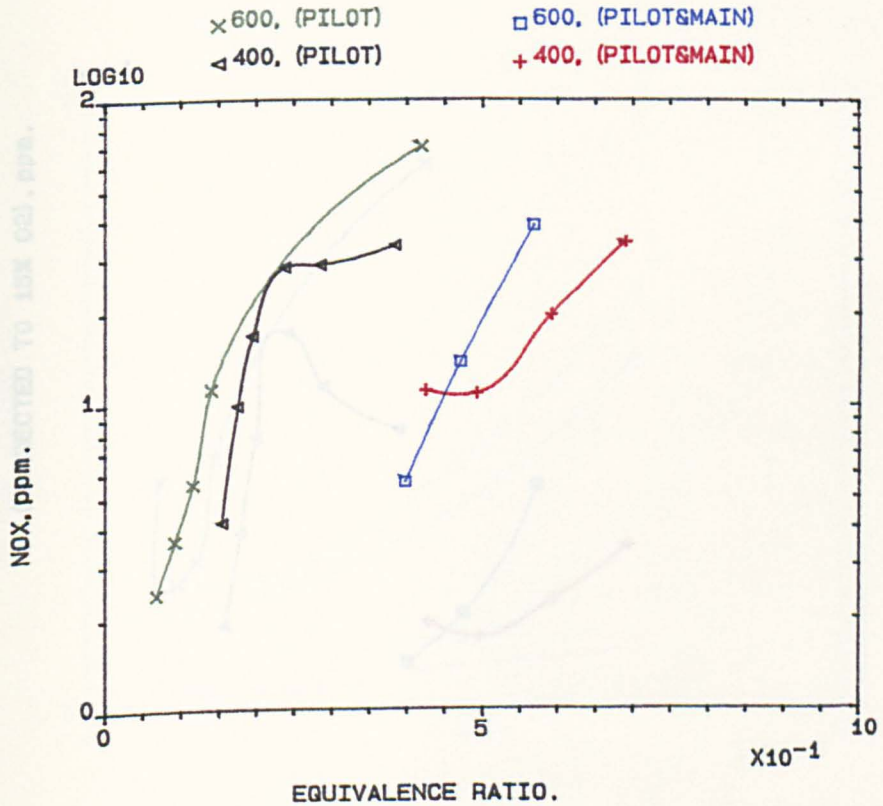

FIG.7.48 NOX V. EQR. FOR PILOT/MAIN AIR SPLIT RATIO OF (0.587/1), USING PROPANE FOR BOTH STAGES, MN=.028, FOR 400K & 600K INLET.

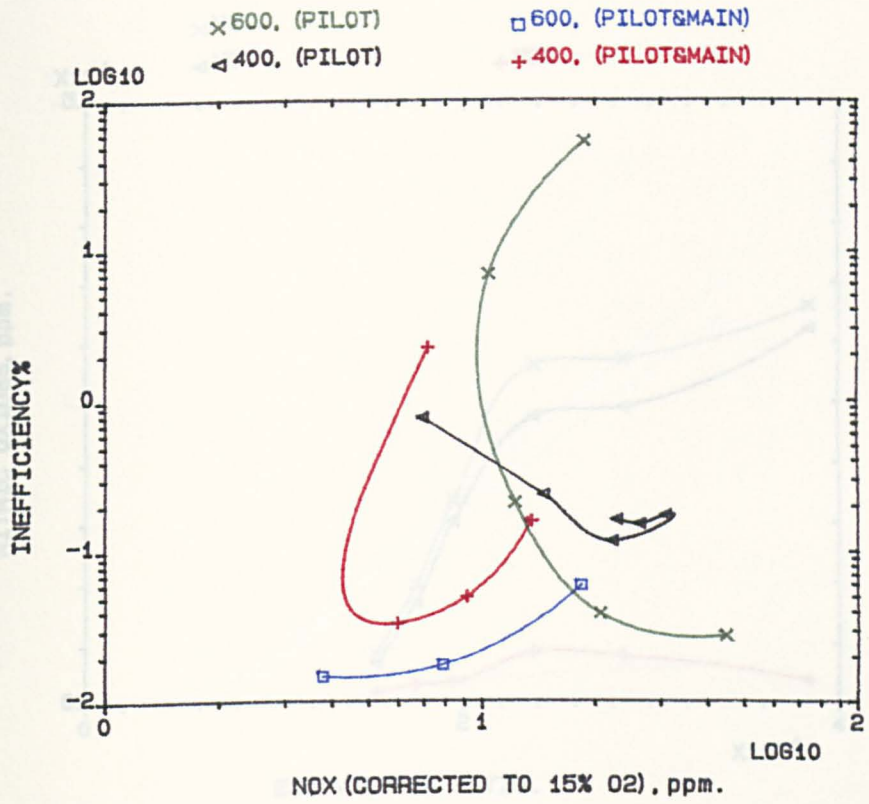

FIG.7.49 INEFF% V. NOXC FOR PILOT/MAIN AIR SPLIT RATIO OF (0.587/1). USING PROPANE FOR BOTH STAGES, MN=.028, FOR 400K & 600K INLET.

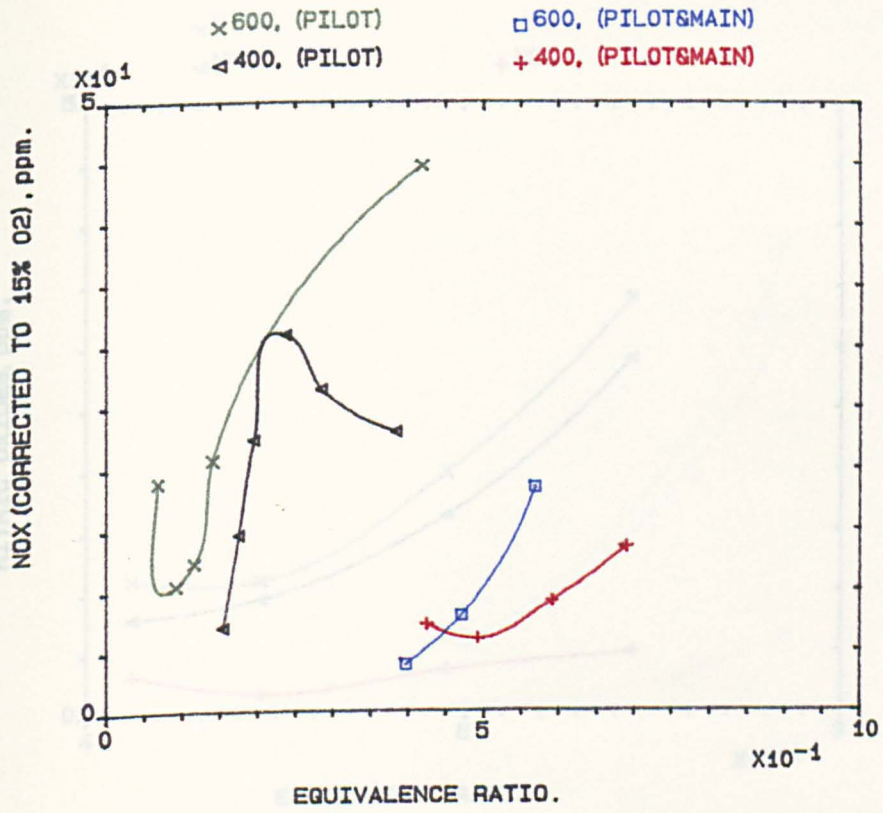

FIG.7.50 NOXC V. EQR. FOR PILOT/MAIN AIR SPLIT RATIO OF (0.587/1). USING PROPANE FOR BOTH STAGES, MN=.028, FOR 400K & 600K INLET.

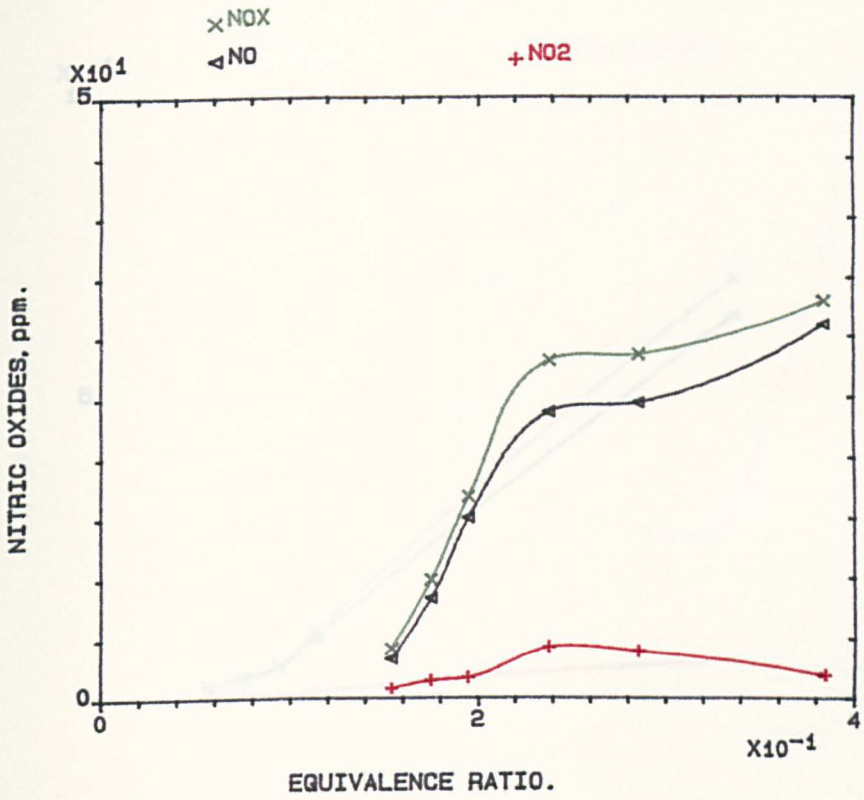

FIG.7.51 NITRIC OXIDES V. EQR. FOR PILOT/MAIN AIR SPLIT RATIO, OF (0.587/1). USING PROPANE FOR PILOT ONLY. MN=.028. 400K.

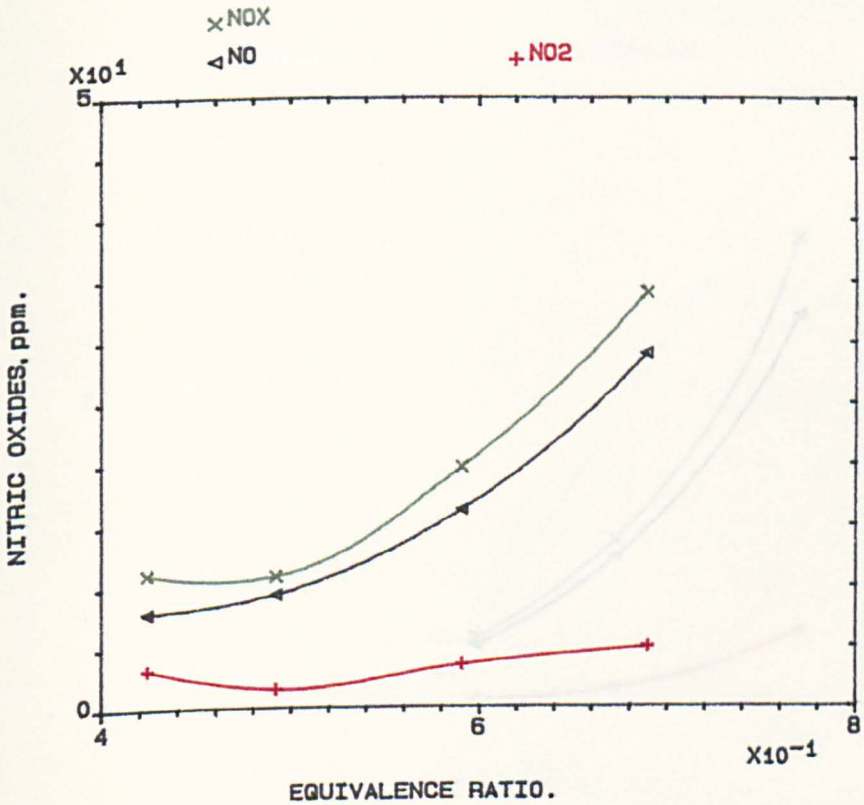

FIG.7.52 NITRIC OXIDES V. EQR. FOR PILOT/MAIN AIR SPLIT RATIO, OF (0.587/1). USING PROPANE FOR BOTH STAGES. MN=.028. 400K.

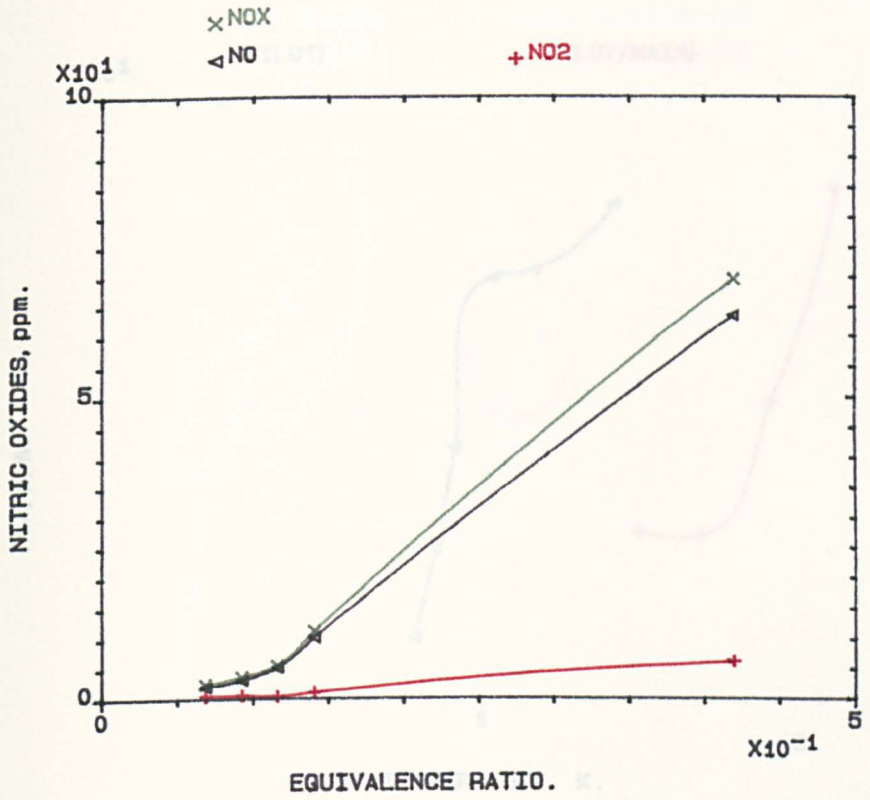

FIG.7.53 NITRIC OXIDES V. EQR. FOR PILOT/MAIN AIR SPLIT RATIO, OF (0.587/1). USING PROPANE FOR PILOT ONLY. MN=.028. 600K.

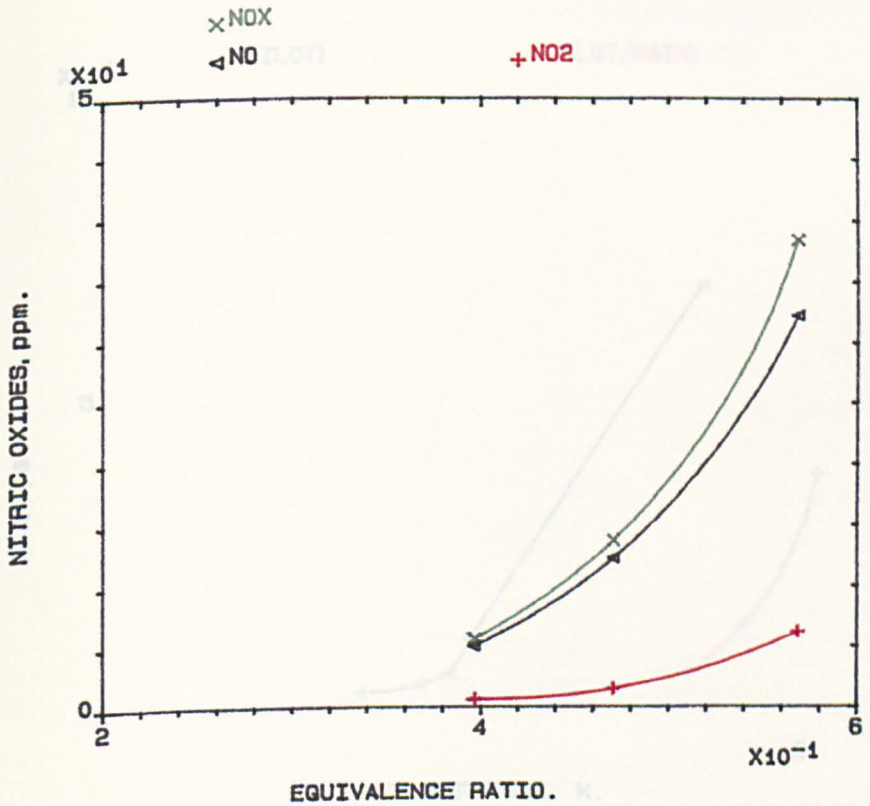

FIG.7.54 NITRIC OXIDES V. EQR. FOR PILOT/MAIN AIR SPLIT RATIO, OF (0.587/1). USING PROPANE FOR BOTH STAGES. MN=.028. 600K.

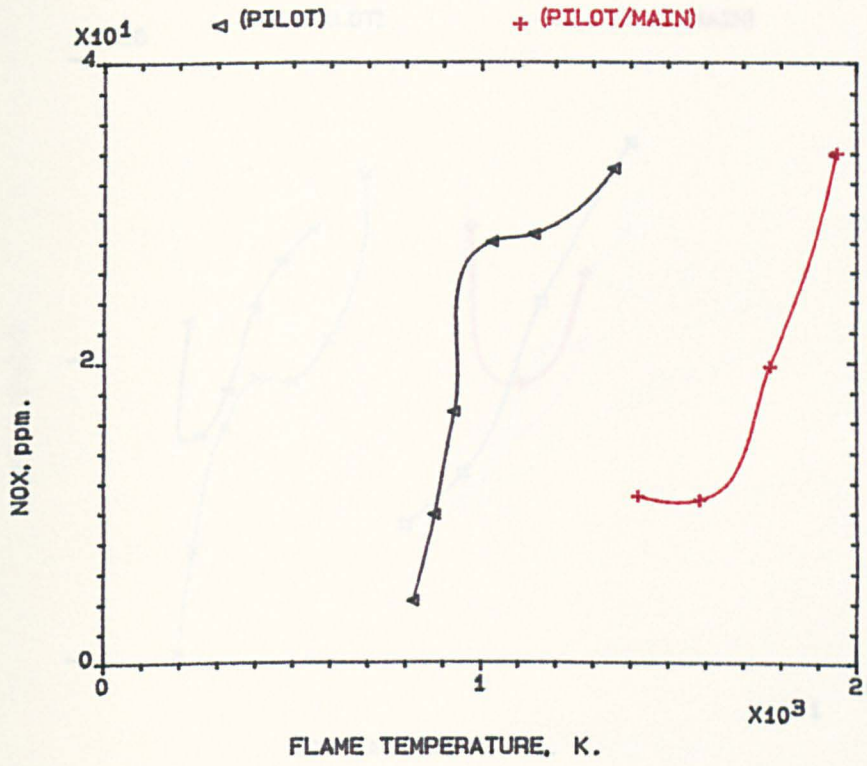

FIG.7.55 NOX V. F.TEMP. FOR PILOT/MAIN AIR SPLIT RATIO OF (0.587/1). USING PROPANE FOR BOTH STAGES. MN=.028. 400K.

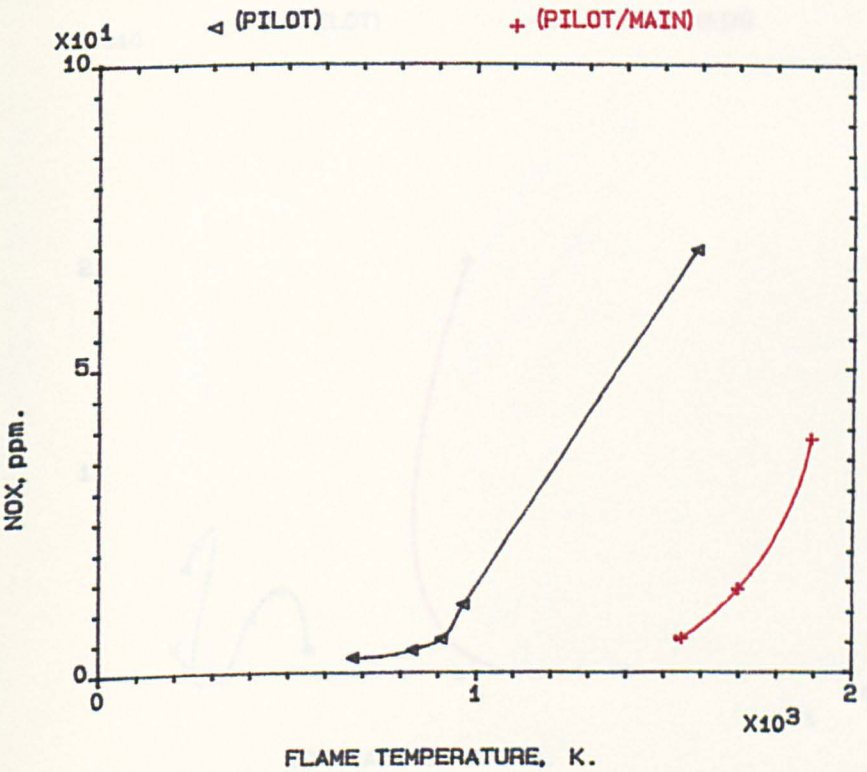

FIG.7.56 NOX V. F.TEMP. FOR PILOT/MAIN AIR SPLIT RATIO OF (0.587/1). USING PROPANE FOR BOTH STAGES. MN=.028. 600K.

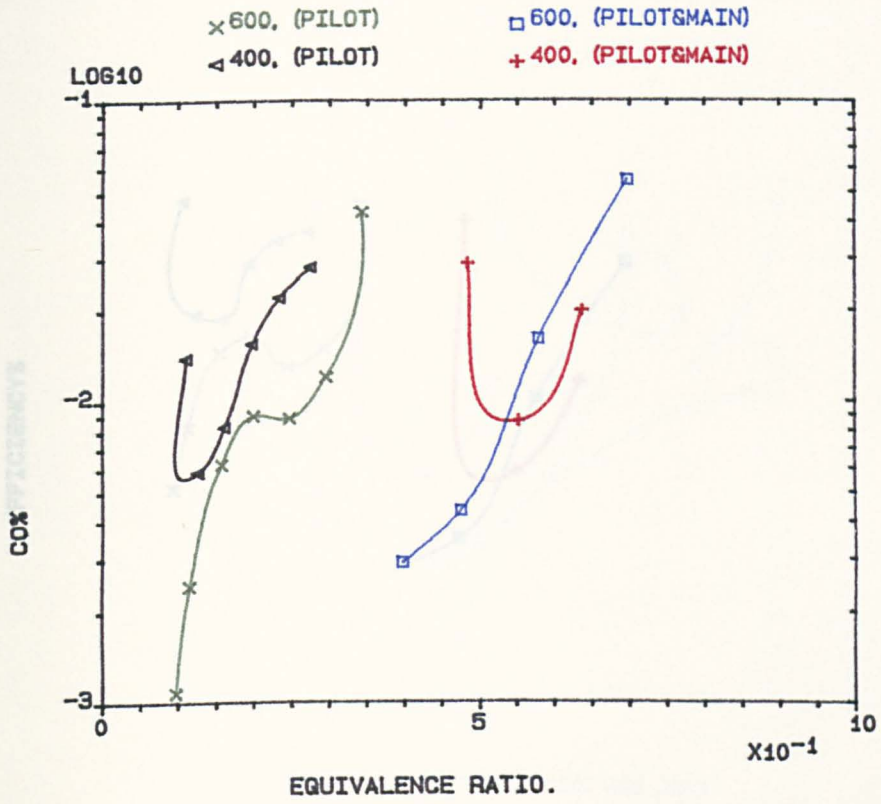

FIG.7.57 CO% V. EQR. FOR PILOT/MAIN AIR SPLIT RATIO OF (0.333/1). USING PROPANE FOR BOTH STAGES, MN=.028, FOR 400K & 600K INLET.

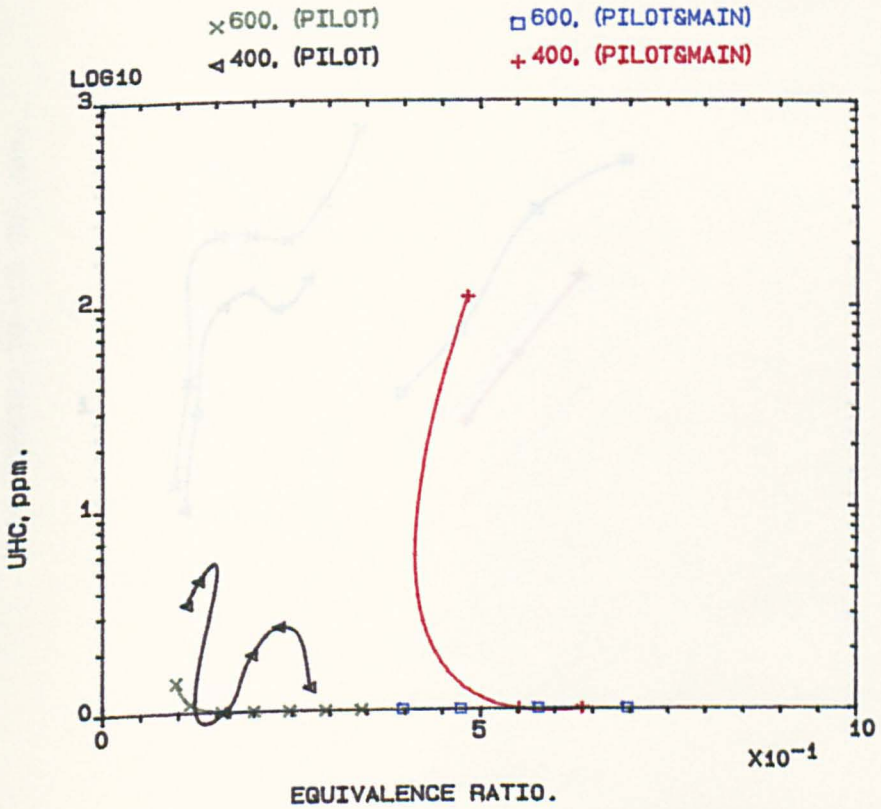

FIG.7.58 UHC V. EQR. FOR PILOT/MAIN AIR SPLIT RATIO OF (0.333/1). USING PROPANE FOR BOTH STAGES, MN=.028, FOR 400K & 600K INLET.

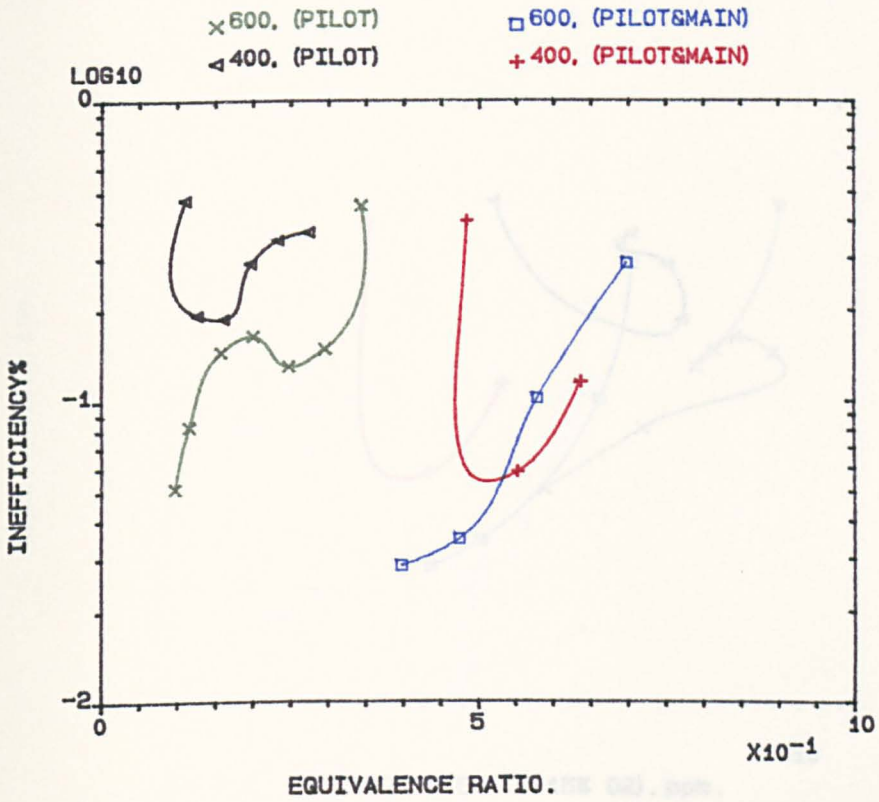

FIG.7.59 INEFF% V. EQR. FOR PILOT/MAIN AIR SPLIT RATIO OF (0.333/1). USING PROPANE FOR BOTH STAGES, MN=.028, FOR 400K & 600K INLET.

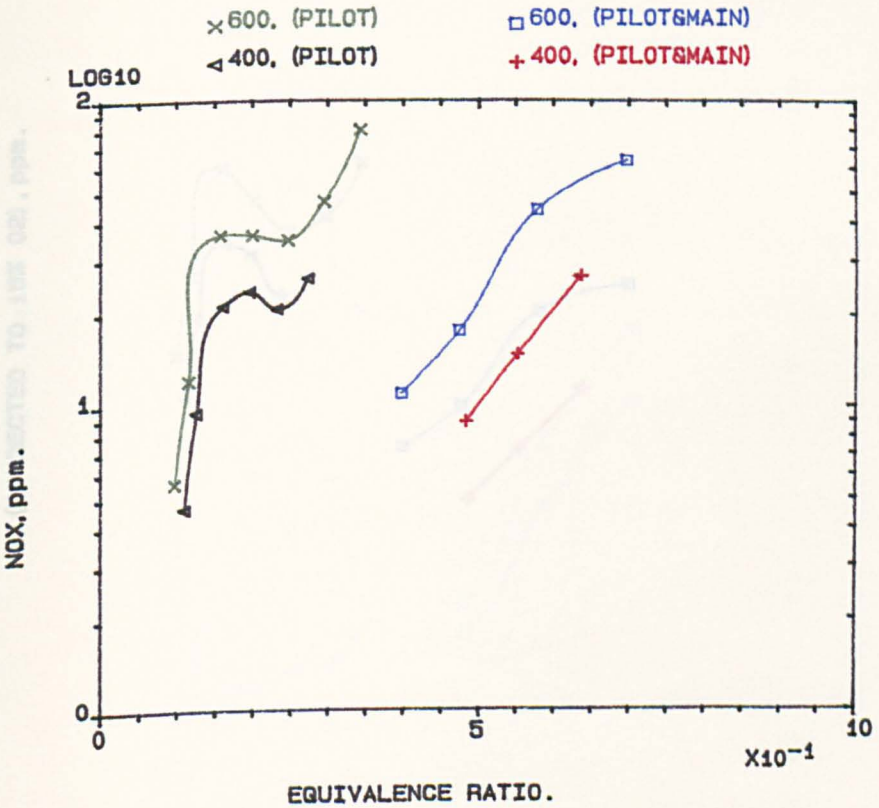

FIG.7.60 NOX V. EQR. FOR PILOT/MAIN AIR SPLIT RATIO OF (0.333/1). USING PROPANE FOR BOTH STAGES, MN=.028, FOR 400K & 600K INLET.

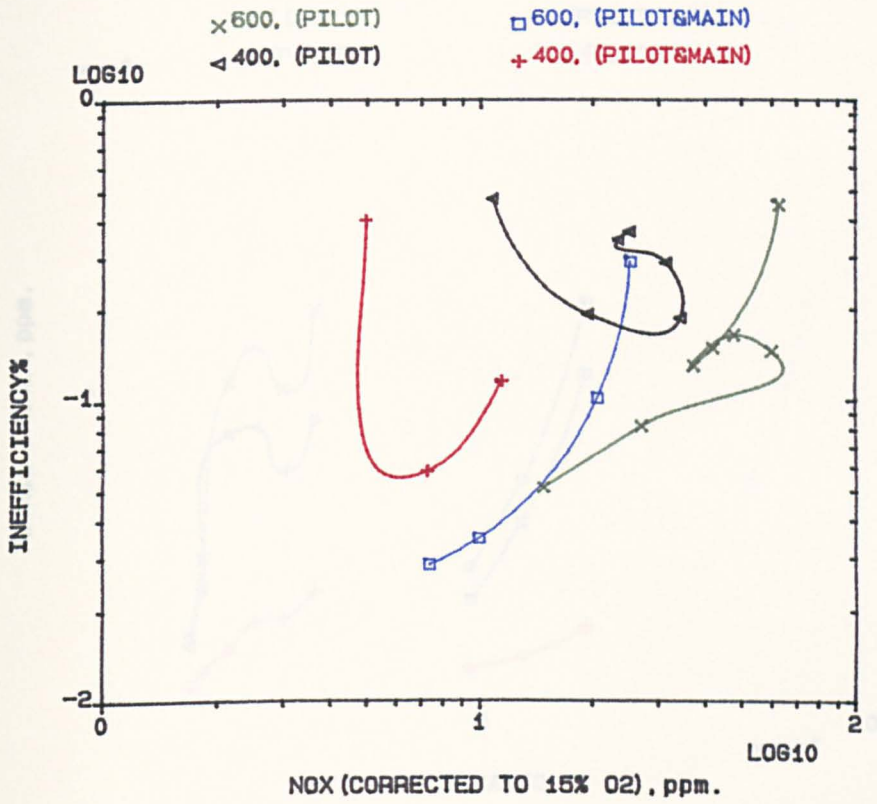

FIG.7.61 INEFF% V. NOXC FOR PILOT/MAIN AIR SPLIT RATIO OF (0.333/1). USING PROPANE FOR BOTH STAGES, MN=.028, FOR 400K & 600K INLET.

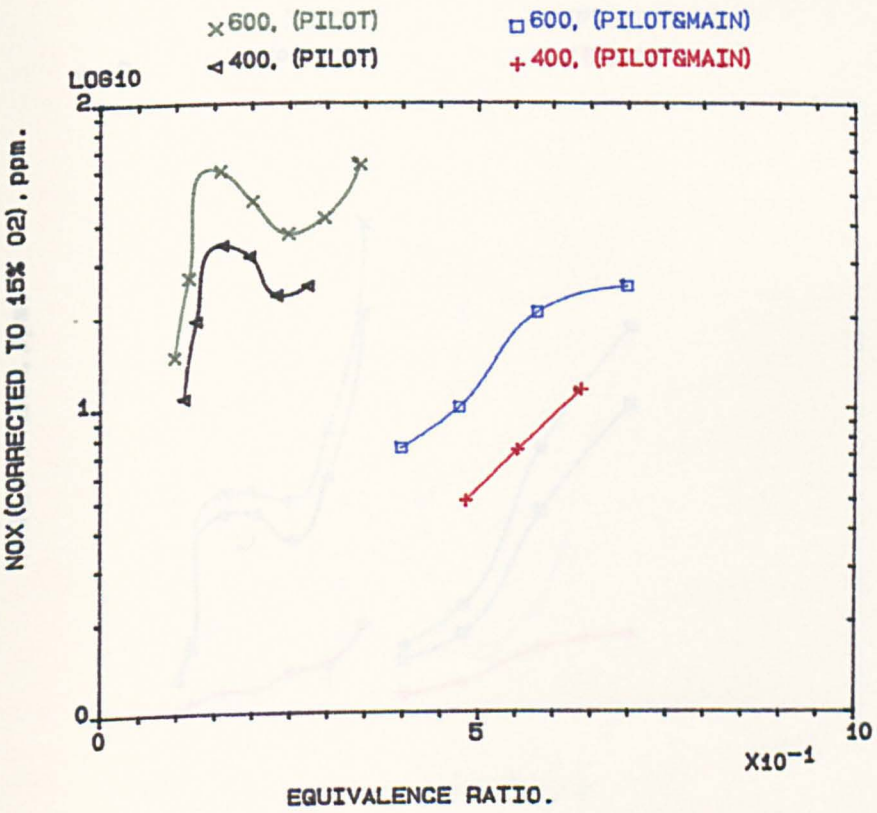

FIG.7.62 NOXC V. EQR. FOR PILOT/MAIN AIR SPLIT RATIO OF (0.333/1). USING PROPANE FOR BOTH STAGES, MN=.028, FOR 400K & 600K INLET.

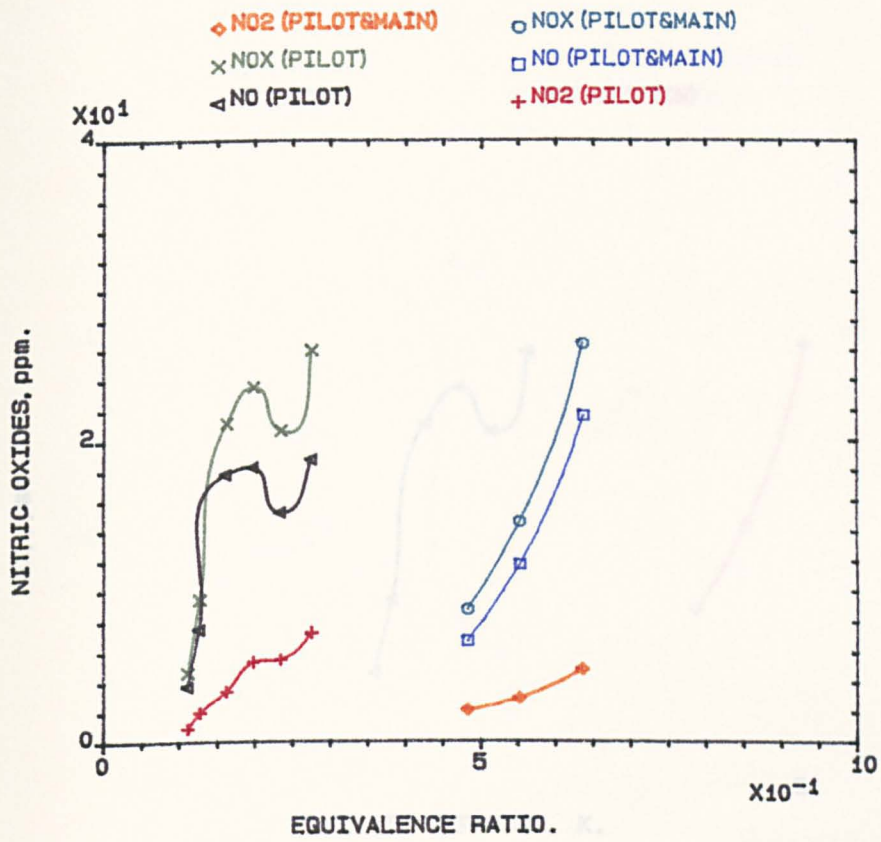

FIG.7.63 NITRIC OXIDES V. EQR. FOR PILOT/MAIN AIR SPLIT RATIO. OF (0.333/1). USING PROPANE FOR BOTH STAGES. MN=.028. 400K.

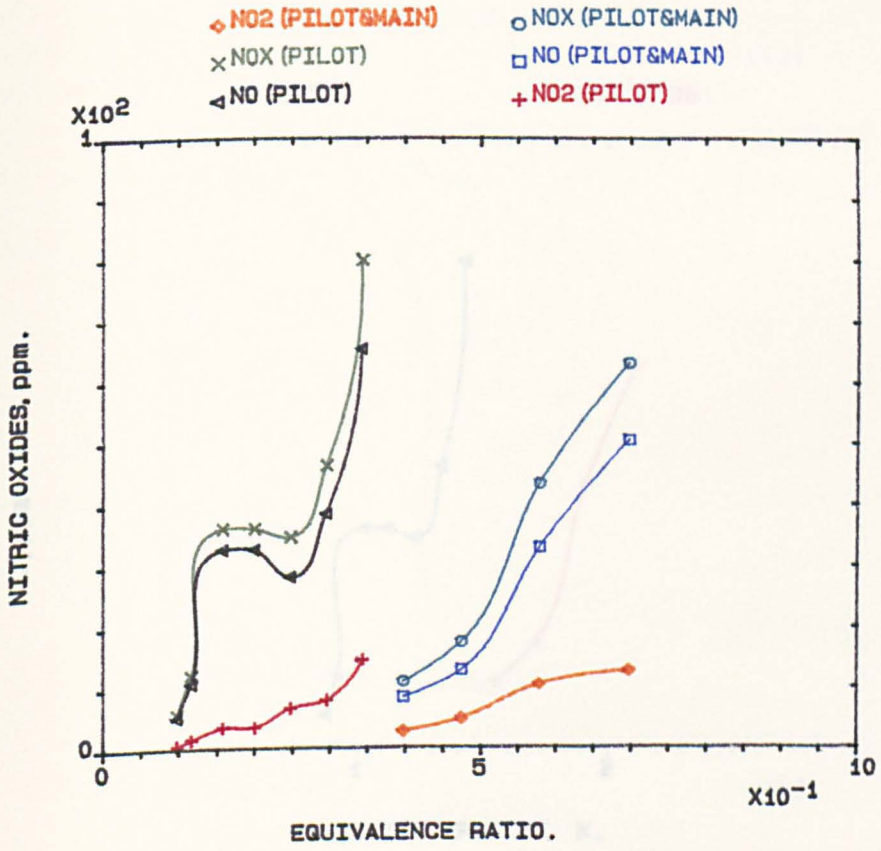

FIG.7.64 NITRIC OXIDES V. EQR. FOR PILOT/MAIN AIR SPLIT RATIO. OF (0.333/1). USING PROPANE FOR BOTH STAGES. MN=.028. 600K.

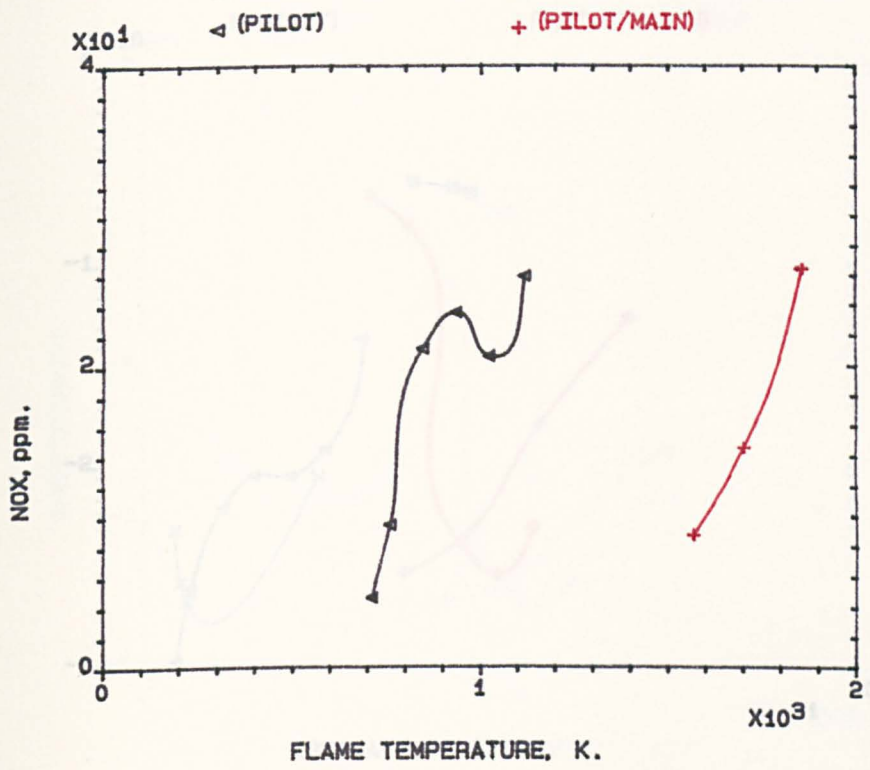

FIG.7.65 NOX V. F.TEMP. FOR PILOT/MAIN AIR SPLIT RATIO OF (0.333/1), USING PROPANE FOR BOTH STAGES, MN=.028, 400K.

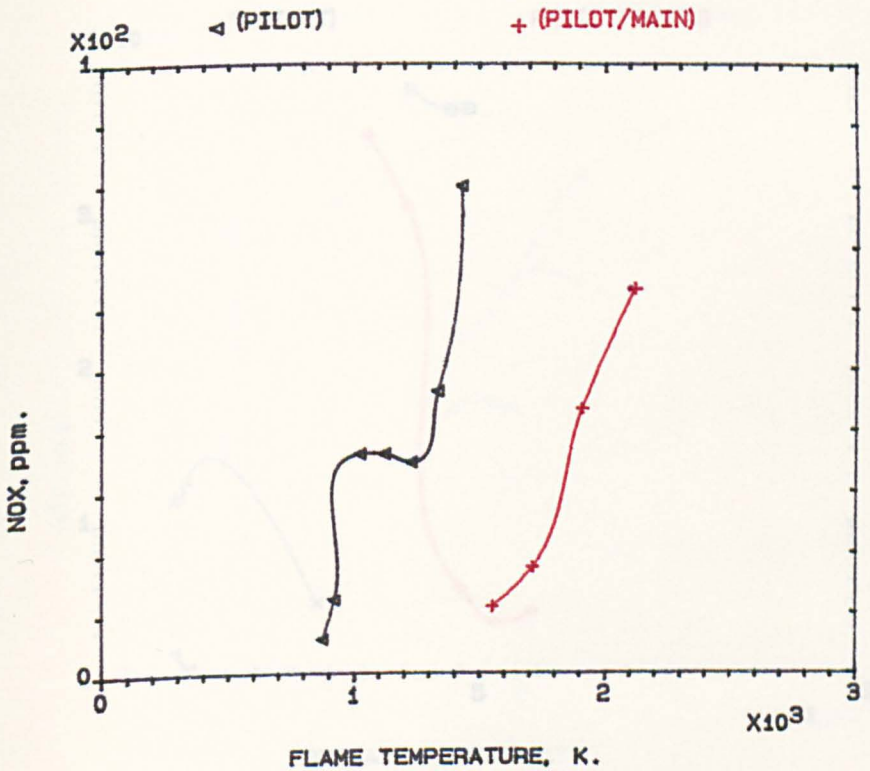

FIG.7.66 NOX V. F.TEMP. FOR PILOT/MAIN AIR SPLIT RATIO OF (0.333/1), USING PROPANE FOR BOTH STAGES, MN=.028, 600K.

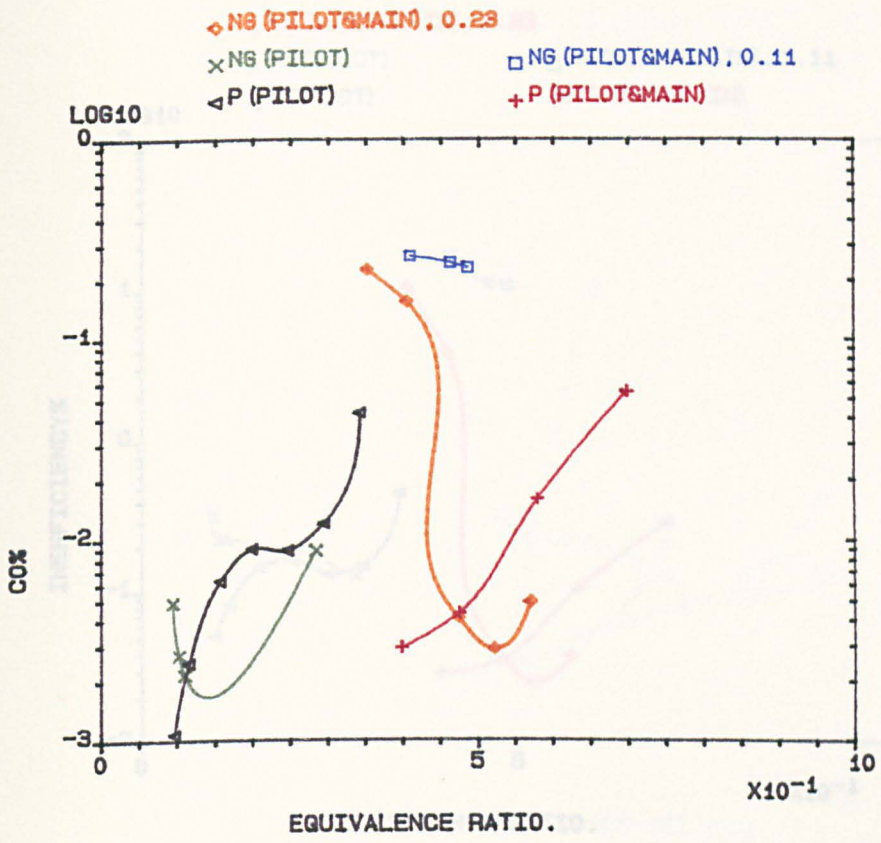

FIG.7.67 CO% V. EQR. FOR PILOT/MAIN AIR SPLIT RATIO OF (0.333/1). USING NATURAL GAS OR PROPANE FOR BOTH STAGES. MN=.028. 600K.

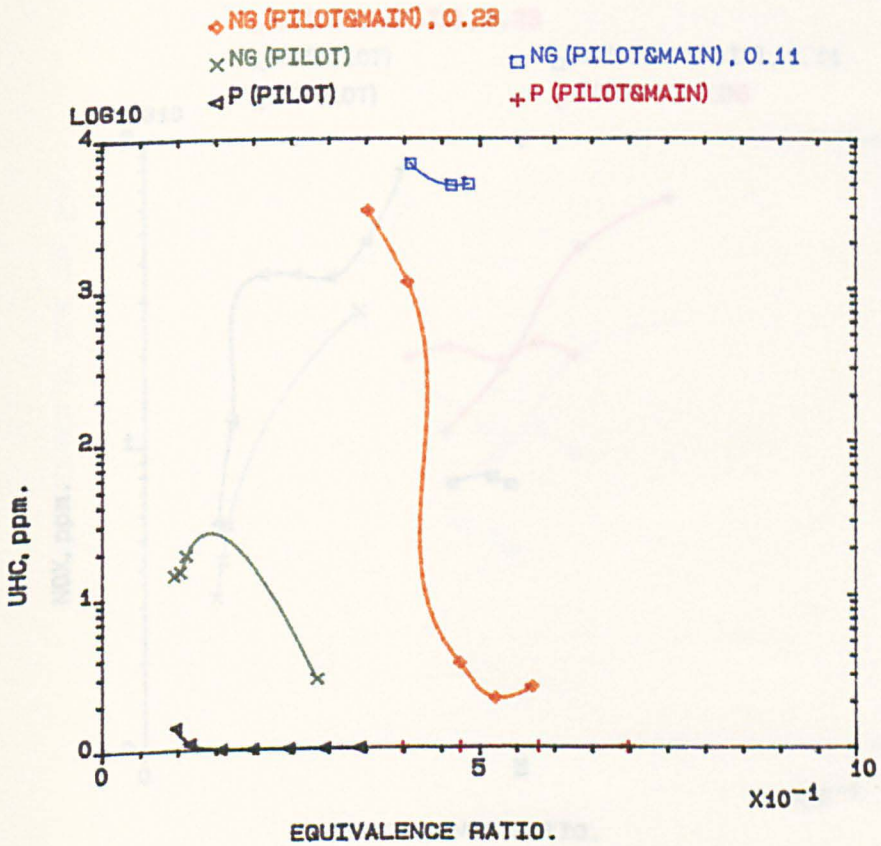

FIG.7.68 UHC V. EQR. FOR PILOT/MAIN AIR SPLIT RATIO OF (0.333/1). USING NATURAL GAS OR PROPANE FOR BOTH STAGES. MN=.028. 600K.

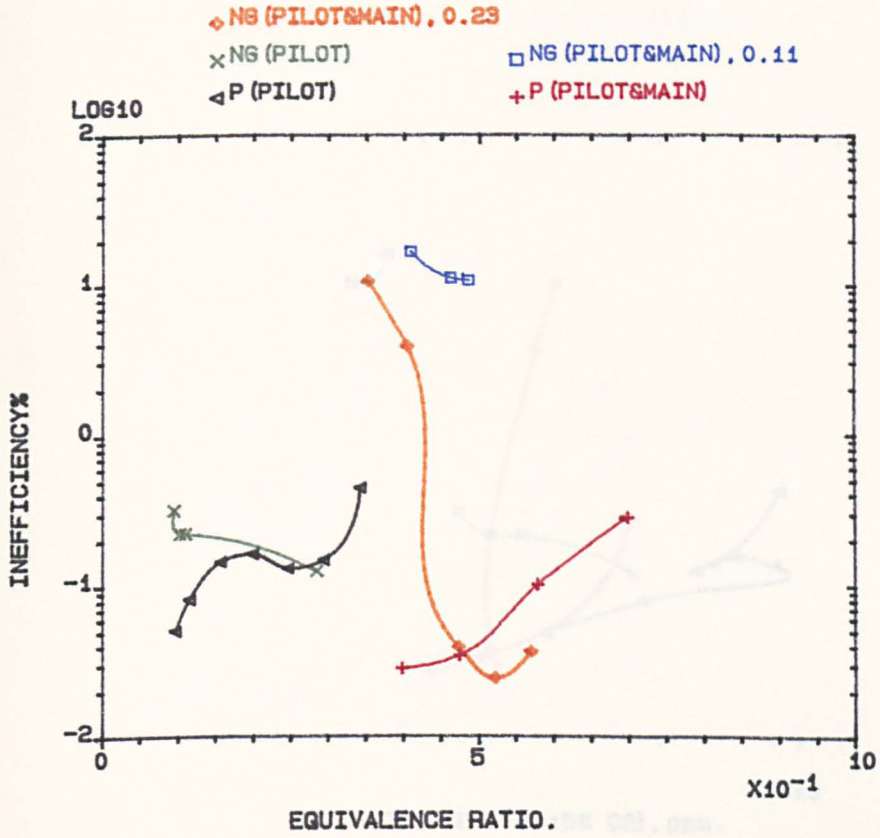

FIG.7.69 INEFF% V. EQR. FOR PILOT/MAIN AIR SPLIT RATIO OF (0.333/1). USING NATURAL GAS OR PROPANE FOR BOTH STAGES. MN=.028. 600K.

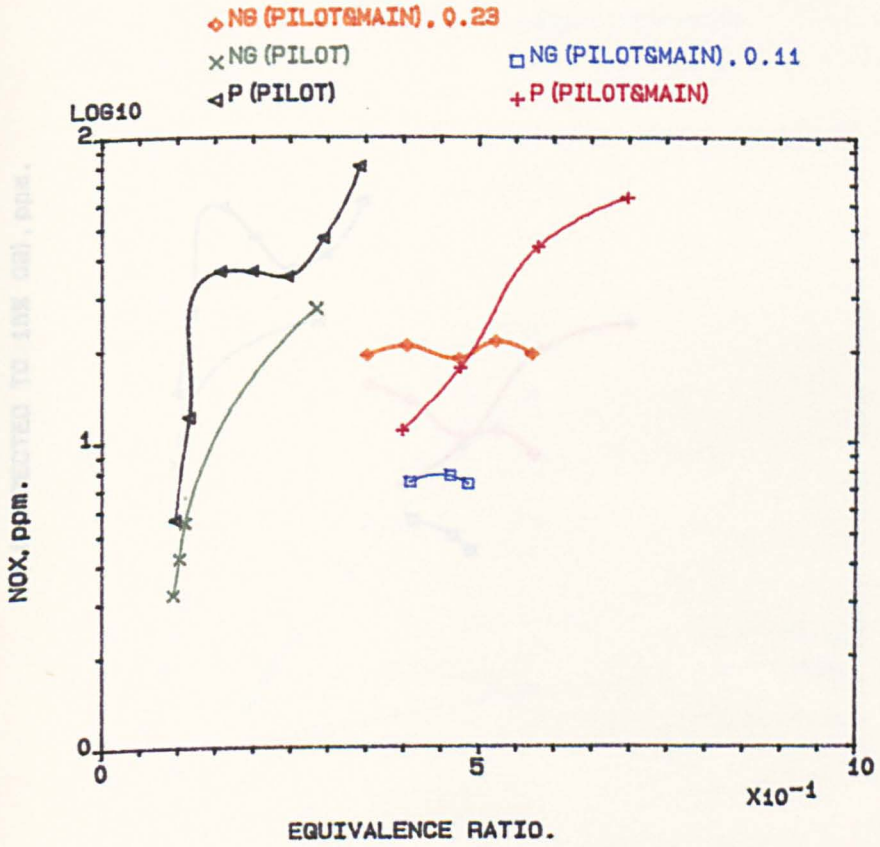

FIG.7.70 NOX V. EQR. FOR PILOT/MAIN AIR SPLIT RATIO OF (0.333/1). USING NATURAL GAS OR PROPANE FOR BOTH STAGES. MN=.028. 600K.

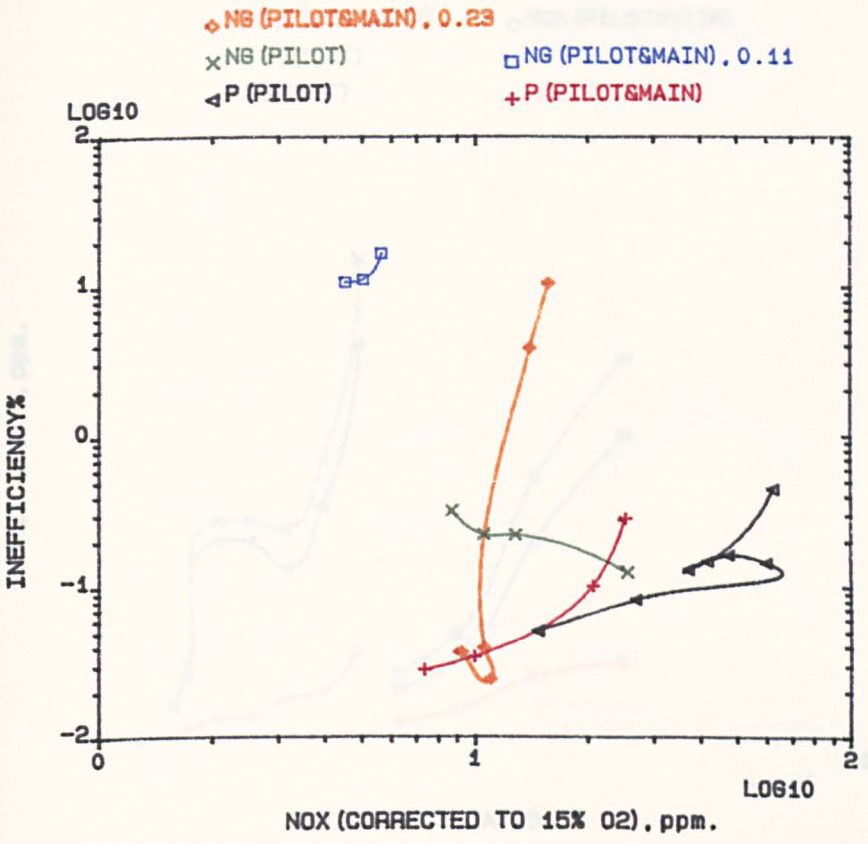

FIG.7.71 INEFF% V. NOXC FOR PILOT/MAIN AIR SPLIT RATIO OF (0.333/1). USING NATURAL GAS OR PROPANE FOR BOTH STAGES, MN=.028, 600K.

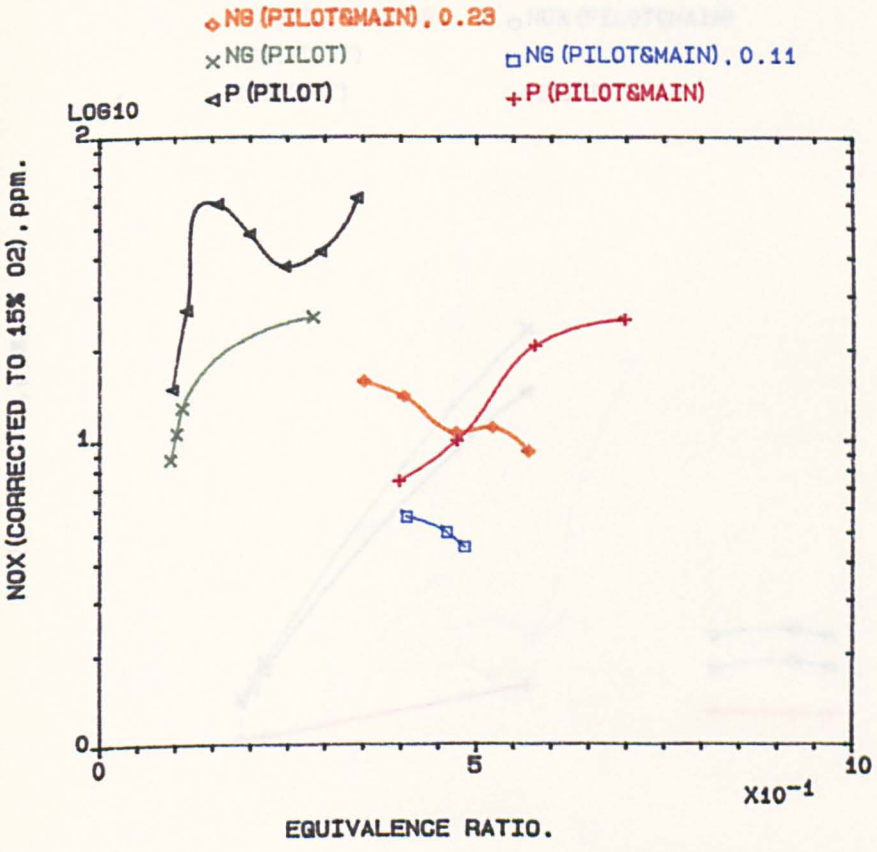

FIG.7.72 NOXC V. EQR. FOR PILOT/MAIN AIR SPLIT RATIO OF (0.333/1). USING NATURAL GAS OR PROPANE FOR BOTH STAGES, MN=.028, 600K.

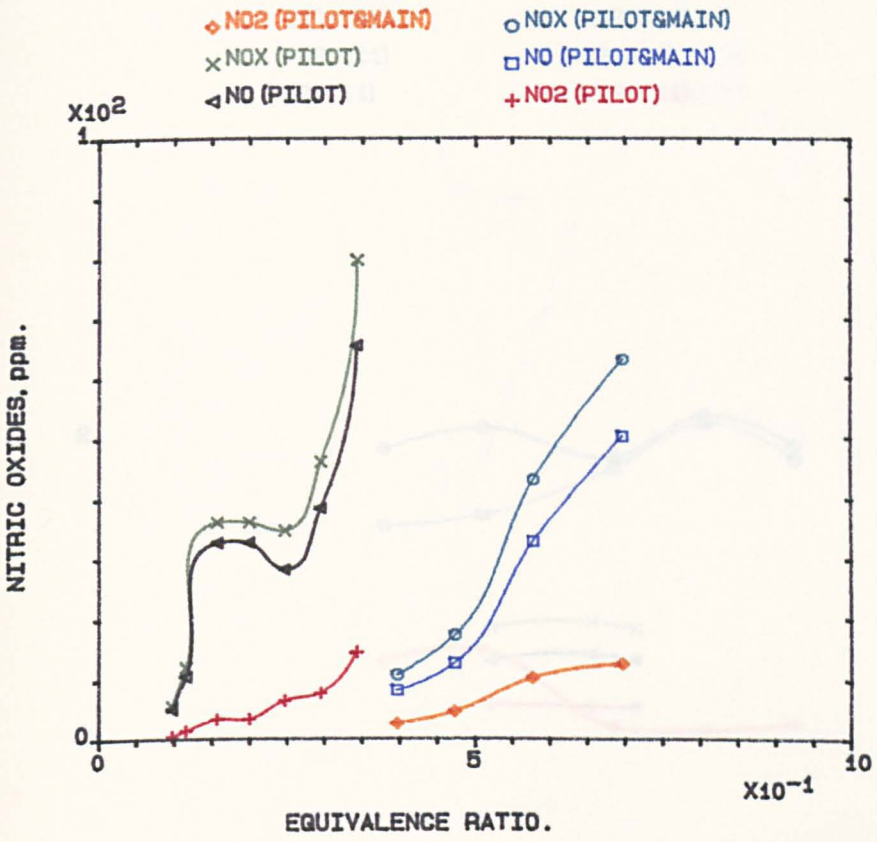

FIG.7.73 NITRIC OXIDES V. EQR. FOR PILOT/MAIN AIR SPLIT RATIO, OF (0.333/1). USING PROPANE FOR BOTH STAGES, MN=.028, 600K.

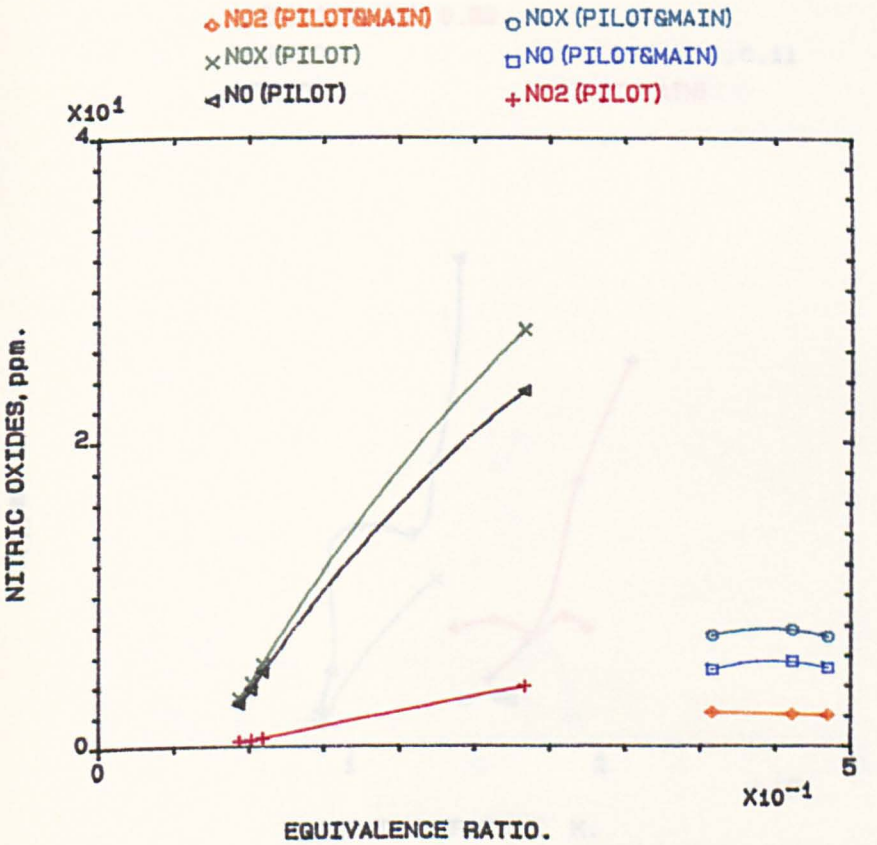

FIG.7.74 NITRIC OXIDES V. EQR. FOR PILOT/MAIN AIR SPLIT RATIO, OF (0.333/1). USING NATURAL GAS FOR BOTH STAGES, MN=.028, 600K.

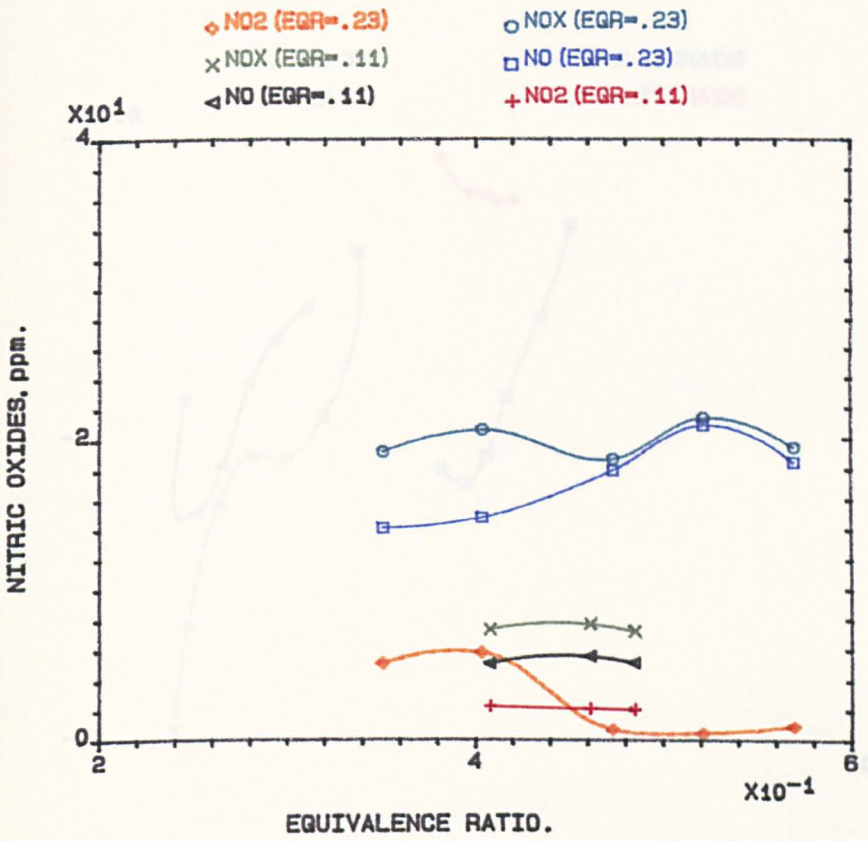

FIG.7.75 INFLUENCE OF CHANGING PILOT EQR. ON NITRIC OXIDES EMISSIONS, FOR (0.333/1), USING NATURAL GAS FOR MAIN STAGE ONLY, MN=.028, 600K.

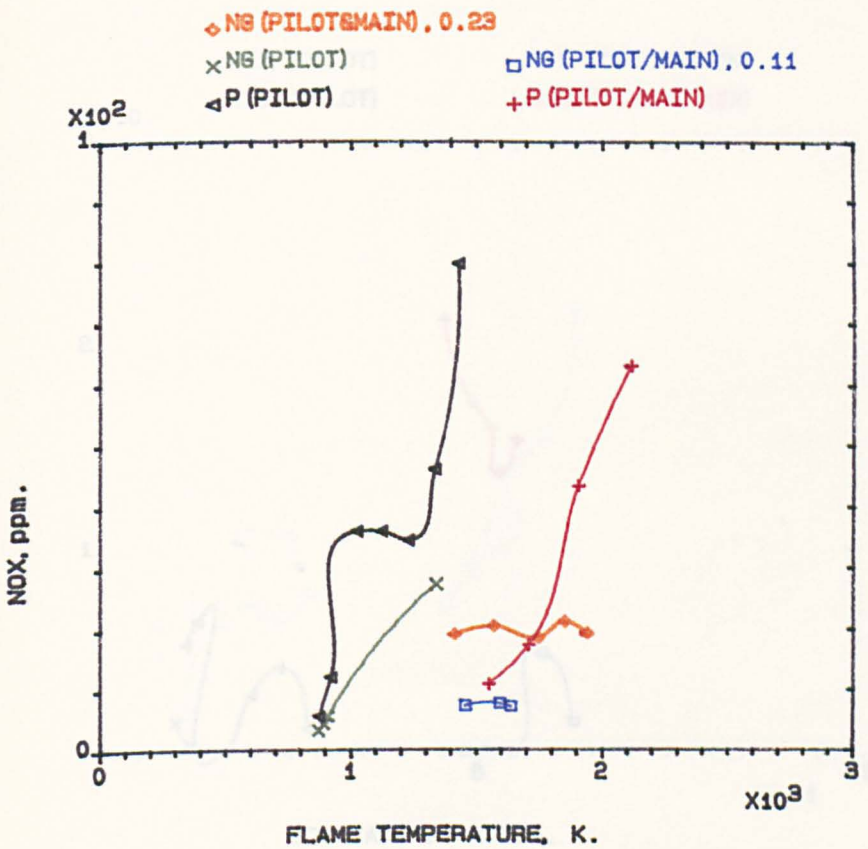

FIG.7.76 NOX V. F.TEMP. FOR PILOT/MAIN AIR SPLIT RATIO OF (0.333/1), PROPANE OR NATURAL GAS, BOTH STAGES, MN=.028, 600K.

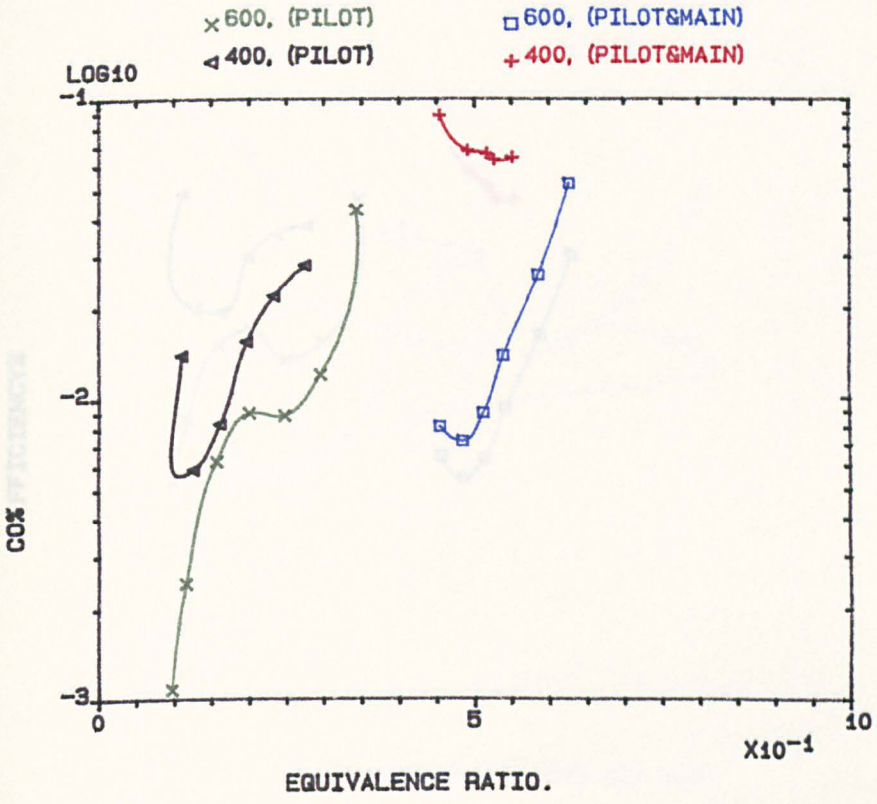

FIG.7.77 CO% V. EQR. FOR PILOT/MAIN AIR SPLIT RATIO OF (0.333/1), PROPANE FOR PILOT & KEROSENE FOR MAIN STAGE, MN=.028, 400K & 600K.

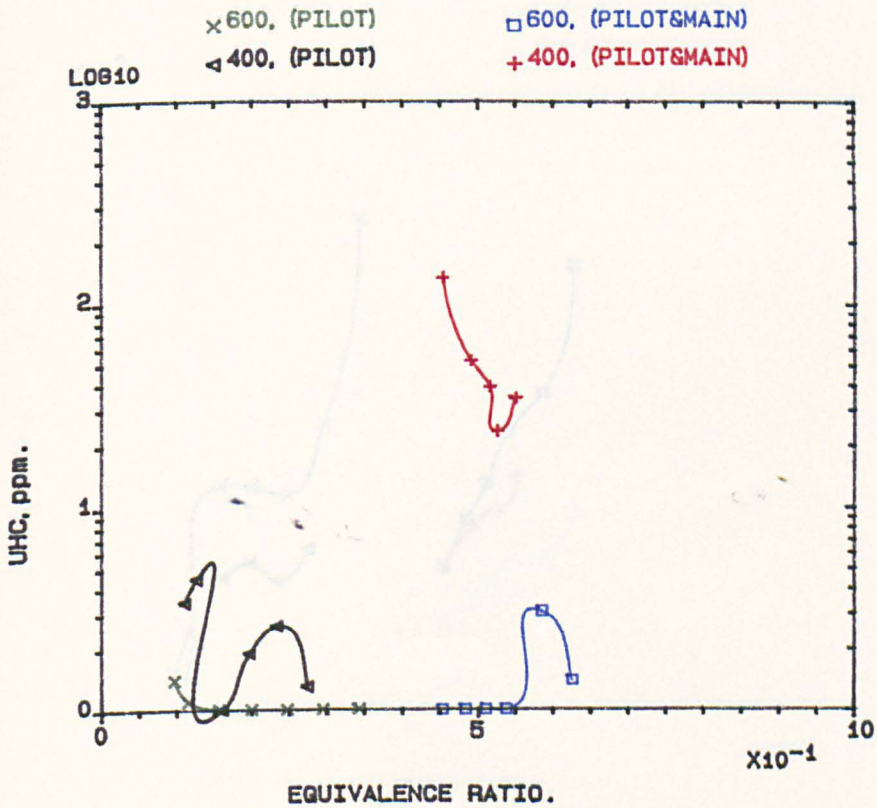

FIG.7.78 UHC V. EQR. FOR PILOT/MAIN AIR SPLIT RATIO OF (0.333/1), PROPANE FOR PILOT & KEROSENE FOR MAIN STAGE, MN=.028, 400K & 600K.

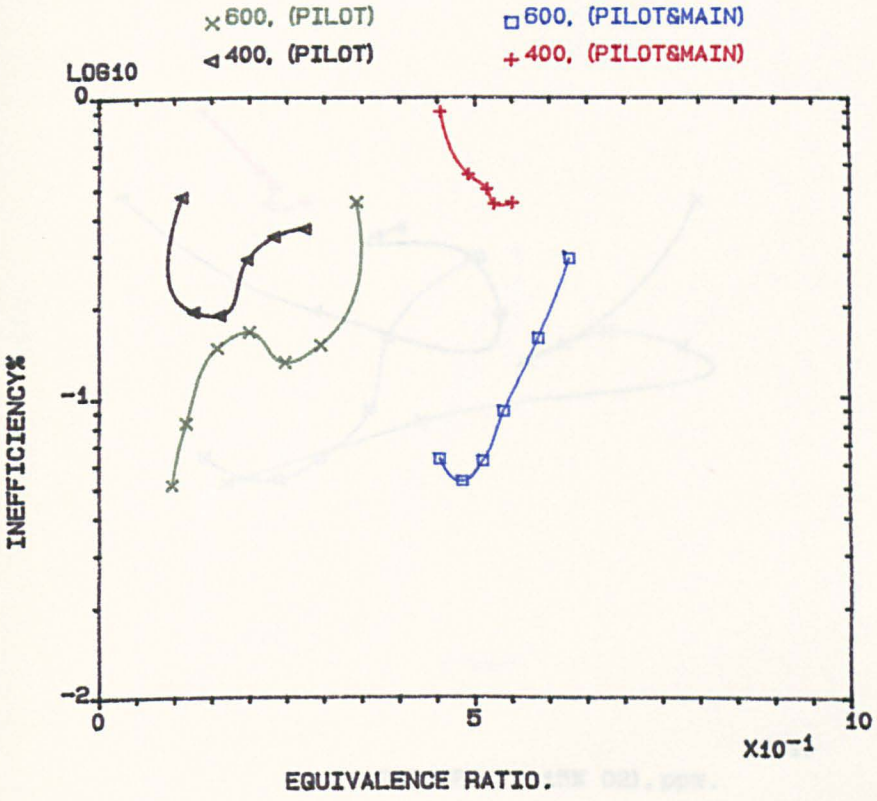

FIG.7.79 INEFF% V. EQR. FOR PILOT/MAIN AIR SPLIT RATIO OF (0.333/1), PROPANE FOR PILOT & KEROSENE FOR MAIN STAGE, MN=.028, 400K & 600K.

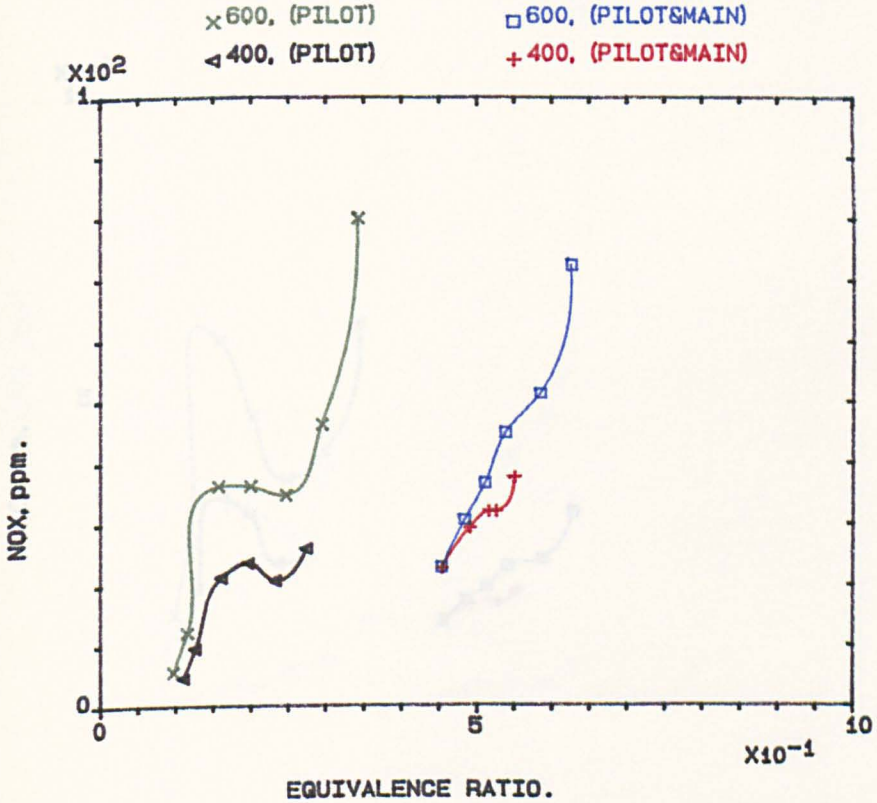

FIG.7.80 NOX V. EQR. FOR PILOT/MAIN AIR SPLIT RATIO OF (0.333/1), PROPANE FOR PILOT & KEROSENE FOR MAIN STAGE, MN=.028, 400K & 600K.

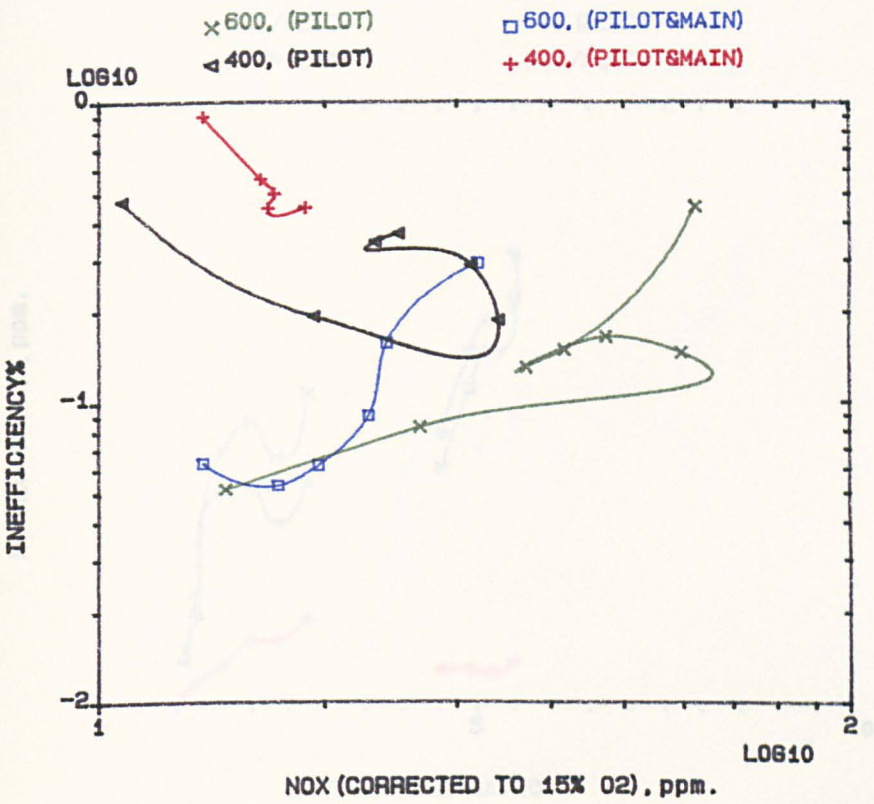

FIG.7.81 INEFF% V. NOXC FOR PILOT/MAIN AIR SPLIT RATIO OF (0.333/1). PROPANE FOR PILOT & KEROSENE FOR MAIN STAGE, MN=.028, 400K & 600K.

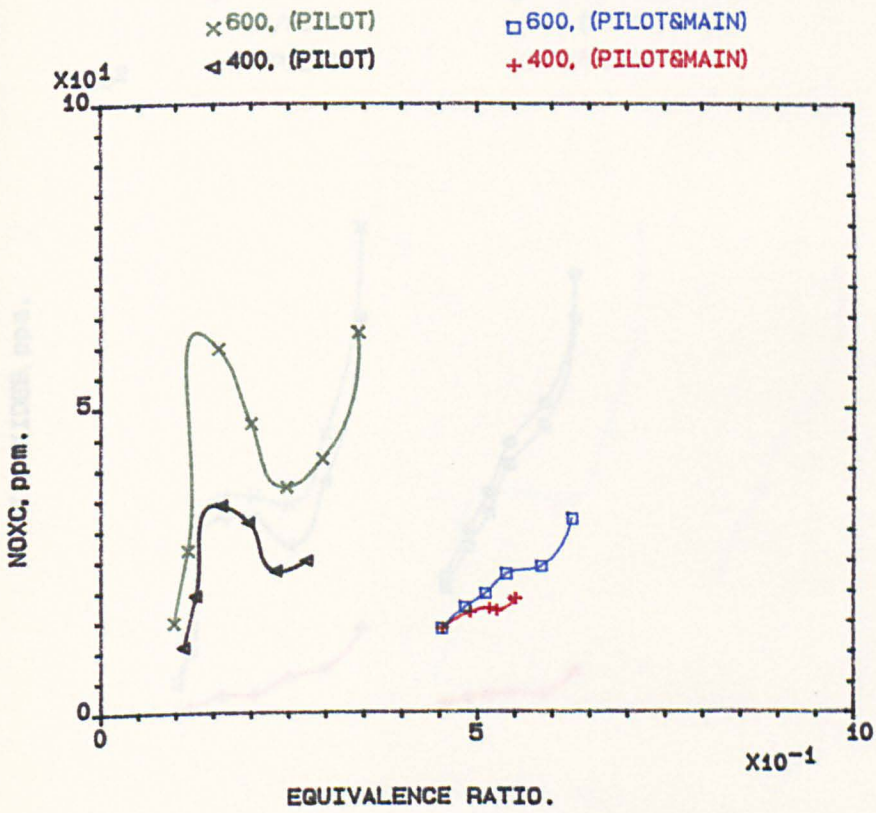

FIG.7.82 NOXC V. EQR. FOR PILOT/MAIN AIR SPLIT RATIO OF (0.333/1). PROPANE FOR PILOT & KEROSENE FOR MAIN STAGE, MN=.028, 400K & 600K.

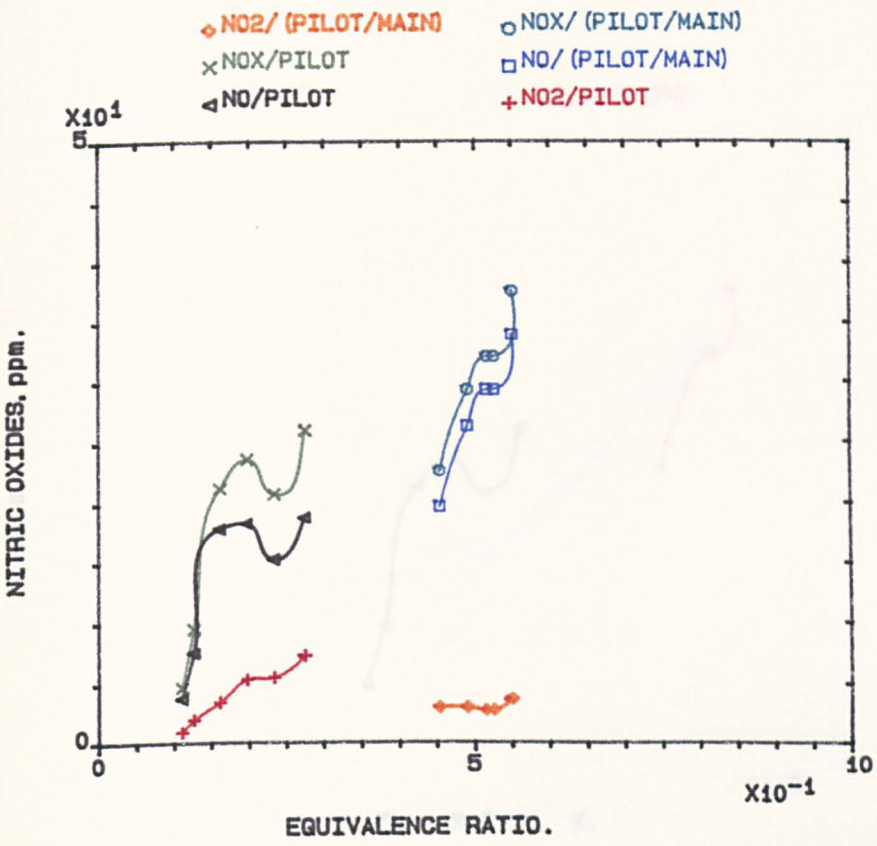

FIG.7.83 NITRIC OXIDES V. EQR. FOR PILOT/MAIN AIR SPLIT RATIO OF (0.333/1). PROPANE FOR PILOT & KEROSENE FOR MAIN STAGE, MN=.028, 400K.

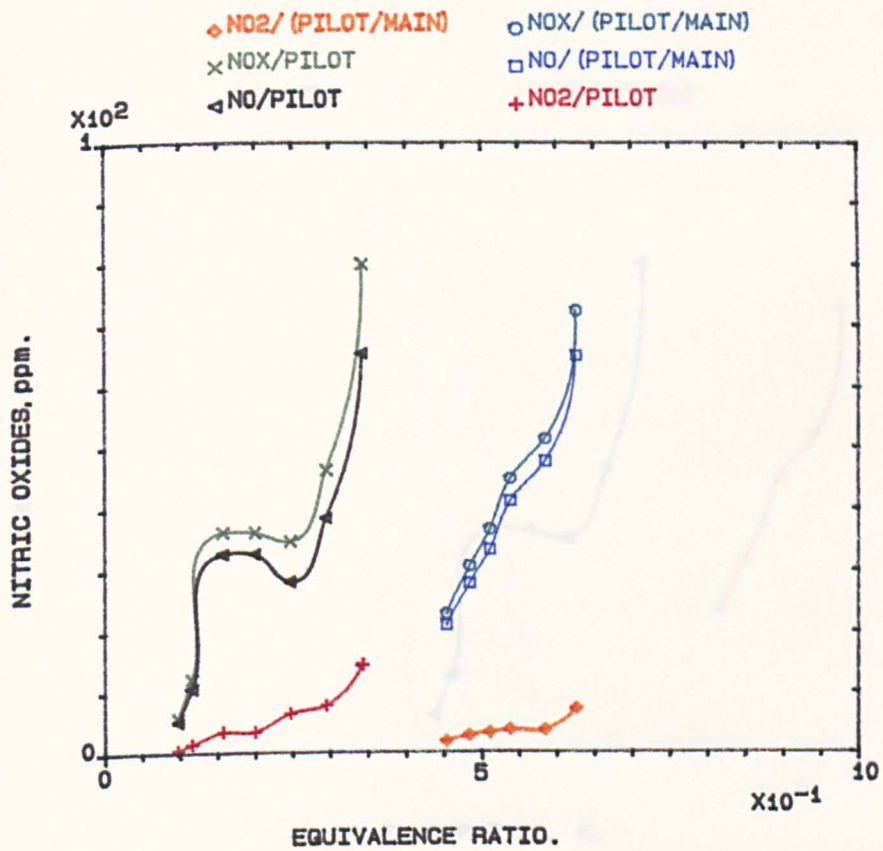

FIG.7.84 NITRIC OXIDES V. EQR. FOR PILOT/MAIN AIR SPLIT RATIO OF (0.333/1). PROPANE FOR PILOT & KEROSENE FOR MAIN STAGE, MN=.028, 600K.

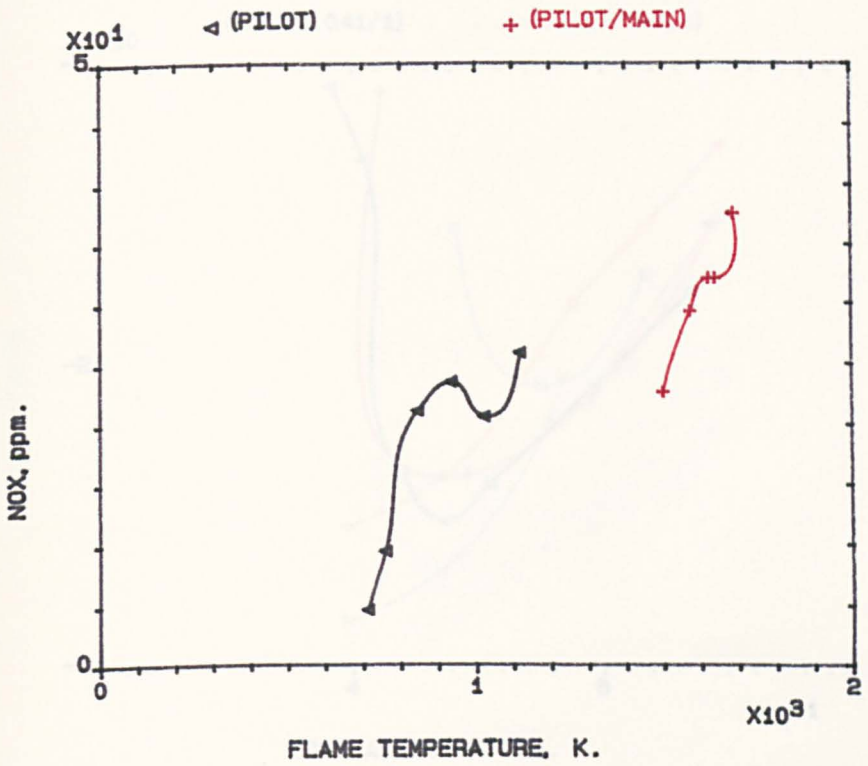

FIG.7.85 NOX V. F.TEMP. FOR PILOT/MAIN AIR SPLIT RATIO OF (0.333/1)
USING PROPANE FOR PILOT & KEROSENE FOR MAIN STAGE, MN=.028, 400K.

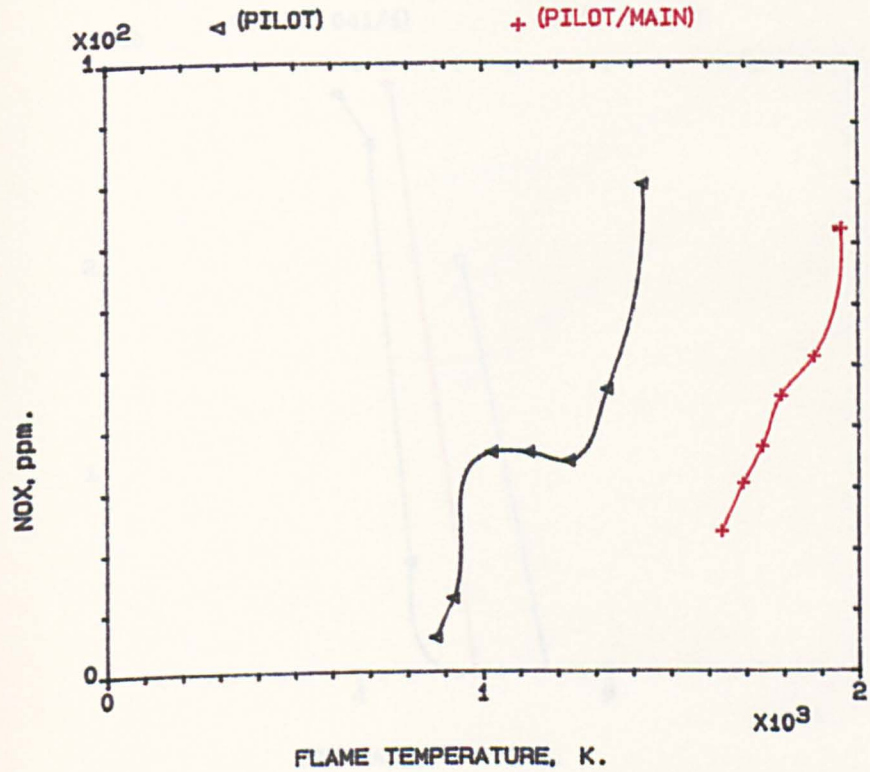

FIG.7.86 NOX V. F.TEMP. FOR PILOT/MAIN AIR SPLIT RATIO OF (0.333/1)
USING PROPANE FOR PILOT & KEROSENE FOR MAIN STAGE, MN=.028, 600K.

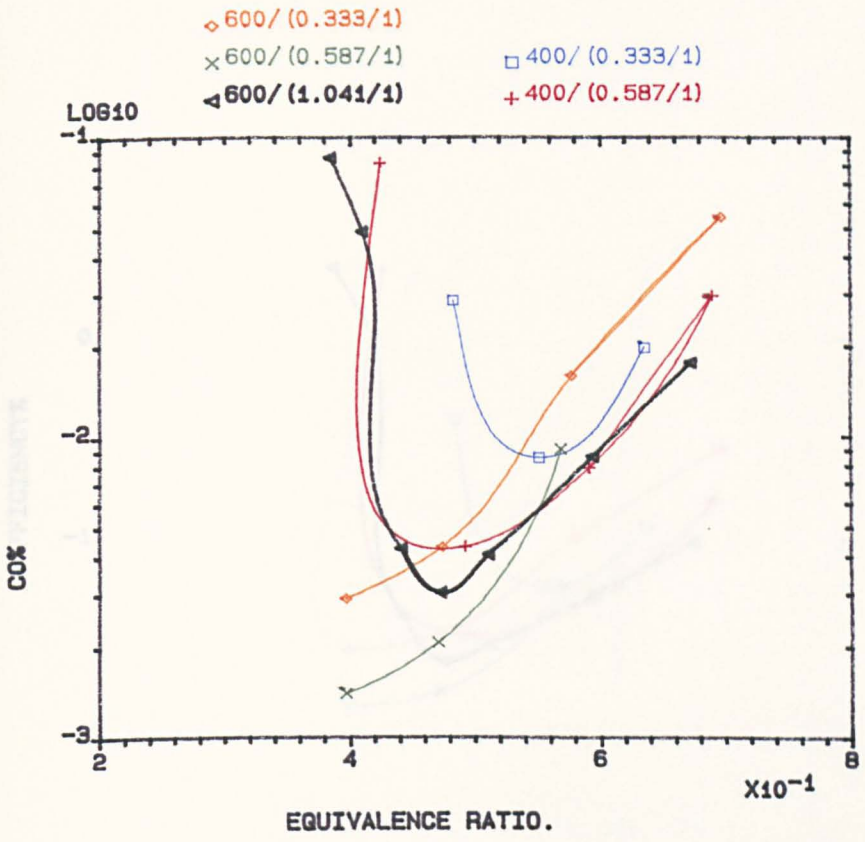

FIG.7.87 INFLUENCE OF AIR SPLIT RATIO OF PILOT/MAIN STAGE ON EMISSIONS OF MAIN STAGE, PROPANE, PL=4.2%, 400K & 600K INLET.

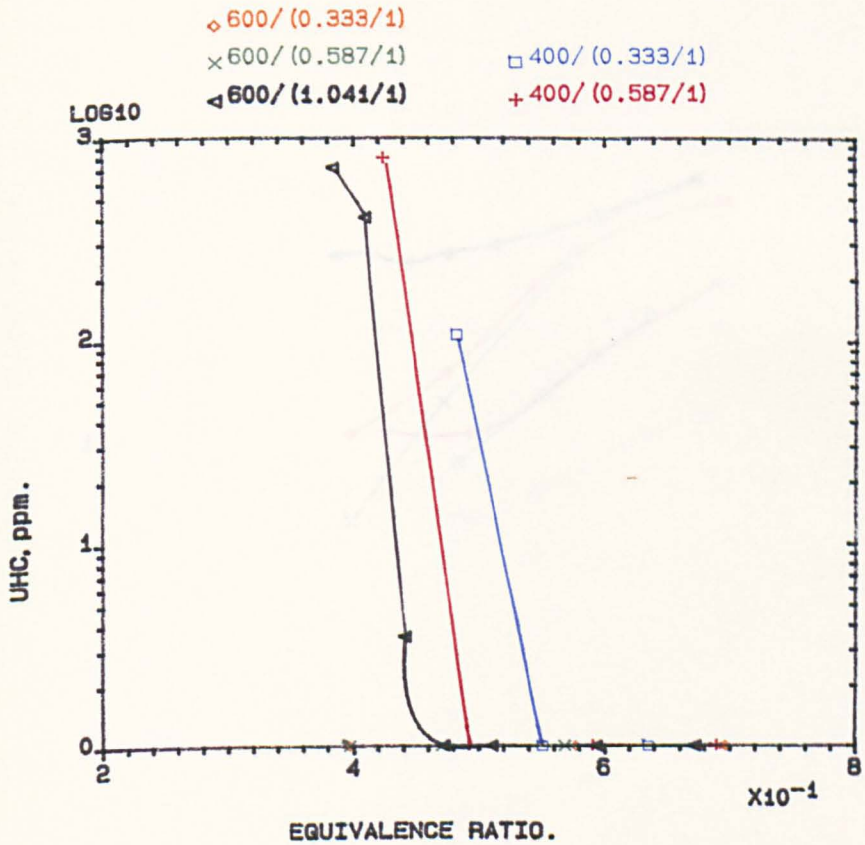

FIG.7.88 INFLUENCE OF AIR SPLIT RATIO OF PILOT/MAIN STAGE ON EMISSIONS OF MAIN STAGE, PROPANE, PL=4.2%, 400K & 600K INLET.

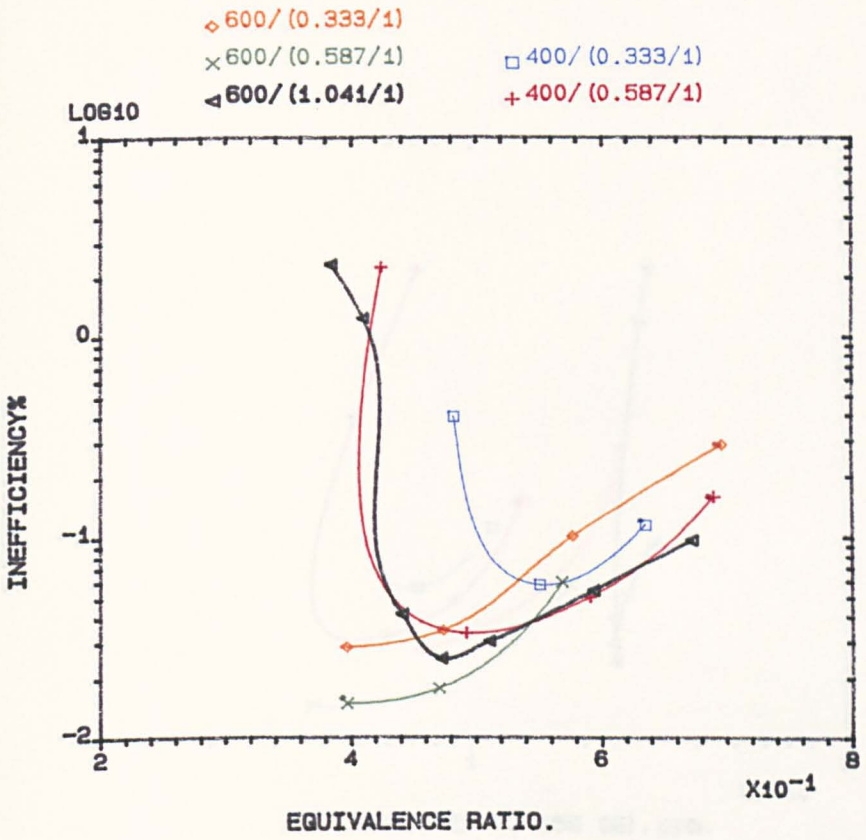

FIG.7.89 INFLUENCE OF AIR SPLIT RATIO OF PILOT/MAIN STAGE ON EMISSIONS OF MAIN STAGE, PROPANE, PL=4.2%, 400K & 600K INLET.

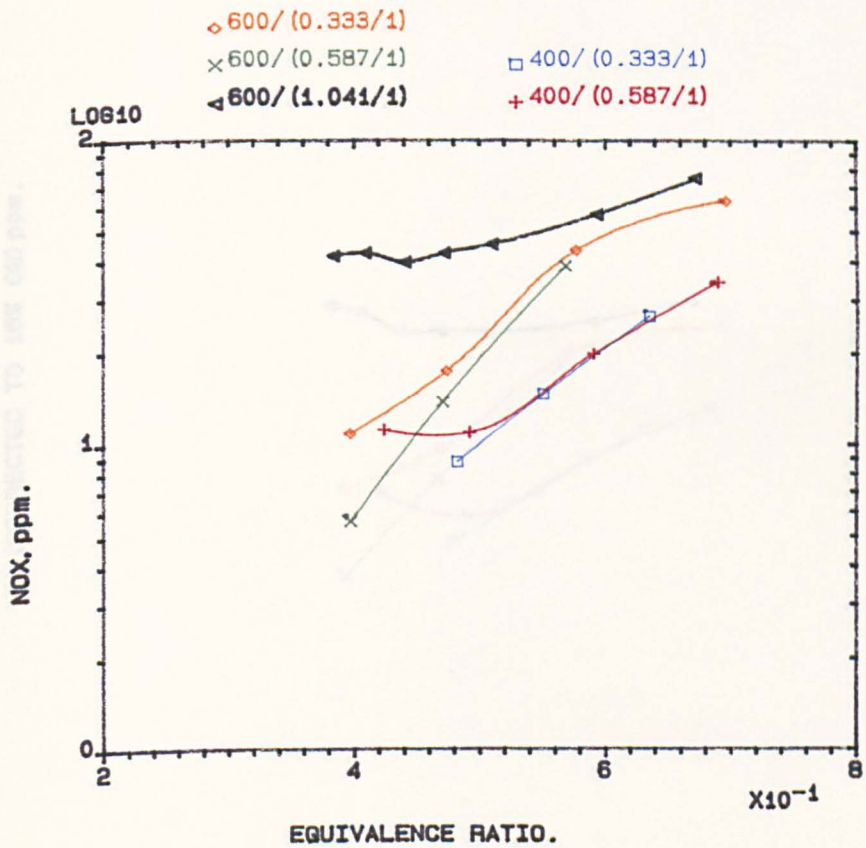

FIG.7.90 INFLUENCE OF AIR SPLIT RATIO OF PILOT/MAIN STAGE ON EMISSIONS OF MAIN STAGE, PROPANE, PL=4.2%, 400K & 600K INLET.

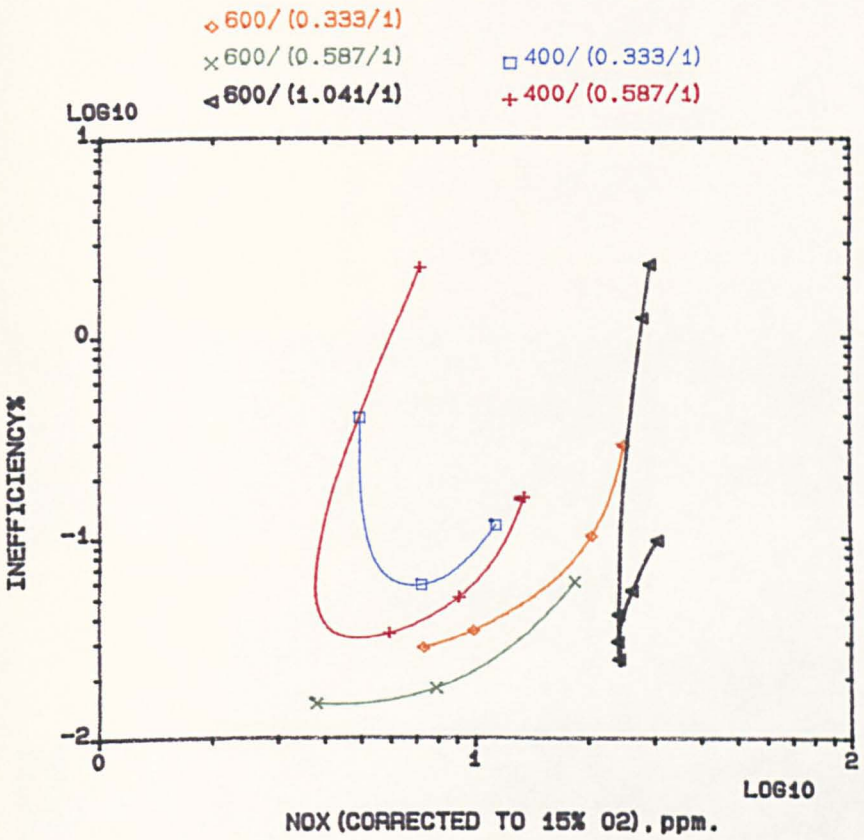

FIG.7.91 INFLUENCE OF AIR SPLIT RATIO OF PILOT/MAIN STAGE ON EMISSIONS OF MAIN STAGE, PROPANE, PL=4.2%, 400K & 600K INLET.

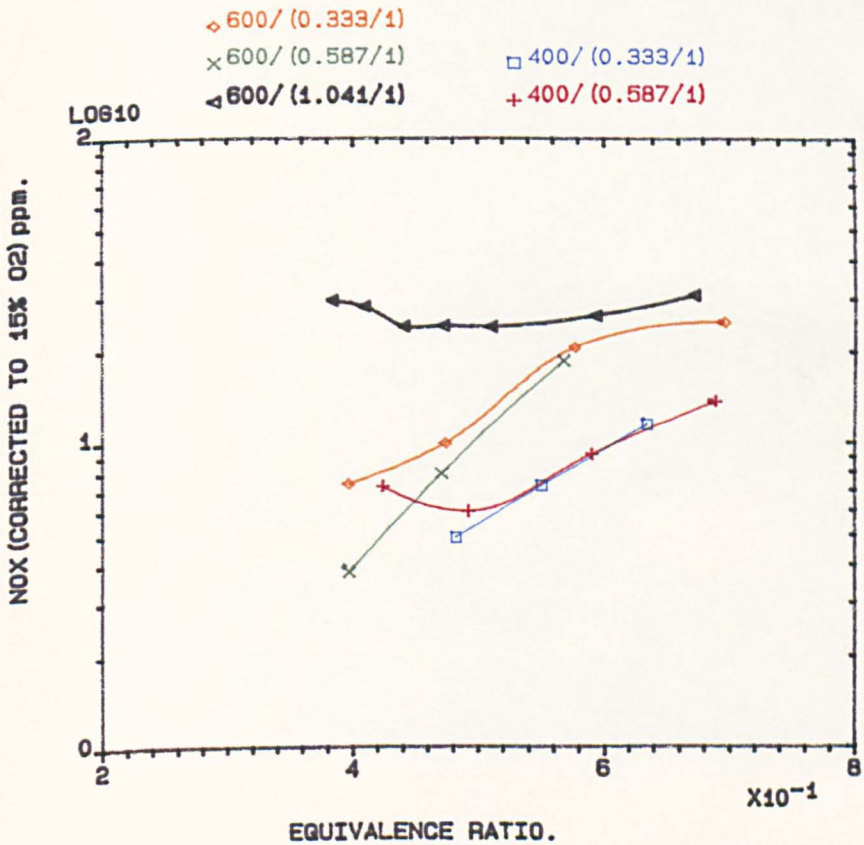

FIG.7.92 INFLUENCE OF AIR SPLIT RATIO OF PILOT/MAIN STAGE ON EMISSIONS OF MAIN STAGE, PROPANE, PL=4.2%, 400K & 600K INLET.

PLATES

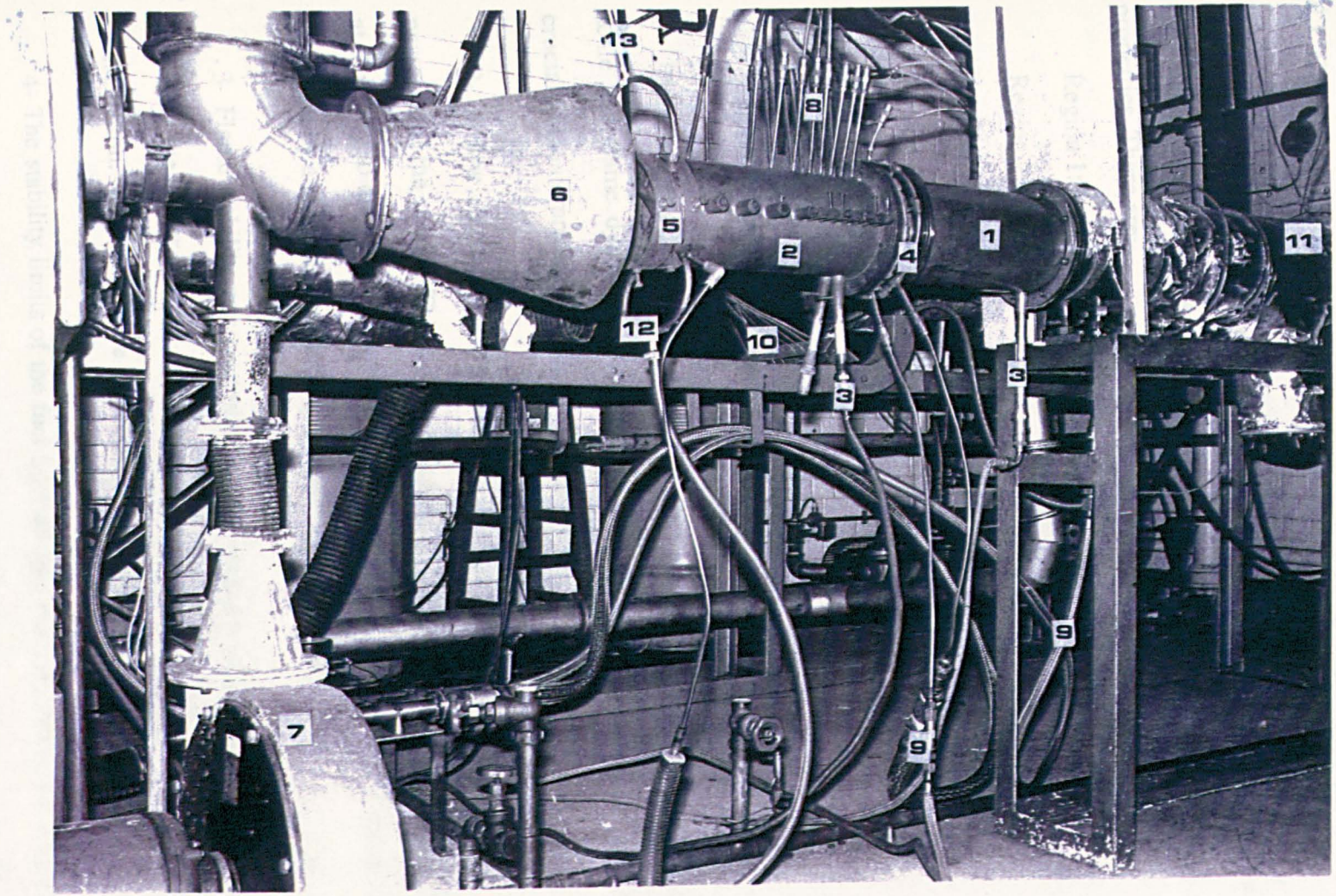

1- Pilot stage combustor.
2- Main stage combustor
3- Igniters.
4- 76mm wall injector.
5- Mean exhaust sampling probe.
6- Ehaust Fan.
7- Exhaust stack.
8- Wall static pressure taps.
9- Fuel pipes.
10- Thermocouples.
11- Electric air preheater.
12- Water inlet pipe.
13- Water outlet pipe.

Plate 7.1 Two-Stage Combustion Rig Assembly.

CHAPTER EIGHT

CONCLUSIONS AND RECOMENDATION FOR FUTURE WORK

At the end of each chapter there are more detailed conclusions. However, the general conclusions drawn from the present work are as follows:

8.1 GENERAL CONCLUSIONS

1- Water-model visualisation shown that the flow imposed by radial swirler have many characteristics and can be divided into 7- regions each with separate properties. These are:-

Region 1: Swirler outlet flow contraction

Region 2: Corner recirculation zone.

Region 3: Outer recirculation downstream the impingement point.

Region 4: Central recirculation zone.

Region 5: Flu ctuating central-spiral reverse zone.

Region 6: Shear layer between 2&3.

Region 7: Shear layer between 4&5.

These regions can be considered as a documentation of the turbulent mixing scale and flame dynamics. Visualisation technique, although simple but very crucial to the iterpretation of a modelling data base.

2- A low discharge coefficient was caused mainly by separation in the passages of the swirler. This was experienced in the back plate vertical plane and at the entry to the passages near the outer curvature of the passages. These can be minimise by a specially profiled radial swirler and approach duct.

3- Flame stability was controlled by fuel and air mixing in the shear layer between the outer corner recirculation and the opposing direction inner recirculation. The vortex core played no part in mixing process.

4- The stability limits of the fuel injected into the base of the swirling shear layer. The centraly radialy outward proved to be superior to those for the fuel

injected anywhere else.

5- Improvement in the fuel/air mixing was demonstrated by radial vane swirlers with fuel injection in the curved passages, though there was some unmixedness in the stabilising swirling shear layer to give a considerable extension of the premixed stability.

6- The radial traverse results demonstrated the strong influence of the fuel injection method on the local shear layer mixing near the swirler outlet. The passage injection peak equivalence ratio was half of that for the central injection. This was the main reason for the lower NOx emissions with passage fuel injection. The NOx originated in the near burner region and concluded to be due to the prompt NOx mechanism with little contribution of thermal NOx generation, as temperature above 1800K had been eleminated.

7- Placing a 76mm wall injector immediately after the swirler outlet, can give more mixing between fuel/air with lower NOx levels than for passage injection. The wall injector increases the high velocity shear layer flow residence time. Also centrifugal burnt/unburnt gas mixing is inhanced.

8- Radial swirler systems for natural gas exhibits ultra low NOx emissions approximated by 30% - 50% or more than that of propane for the same tests conditions.

9- Comparison between axial and radial swirler reveals that even though the mean emissions at the exit plane of the combustor were the same, there were difference in the mixing process especially near the swirlers outlet region which gave a greater chance for the radial swirler turbulent flow to contact the fuel jet as it leaves the injector. In case of axial swirler the fuel travelled some distance before coming into contact with the turbulent air jet. Thus the fuel/air mixing processes effected the details of the flame structure and the axial swirler had slightly higher NOx emissions than radial swirlers.

10- The test program on dry lean-lean two-stage combustion concept proved to be capable of a good stability by switching from pilot to main stage combustion and can achieve low NOx levels at 1 bar pressure condition.

11- The isothermal flow-field calculation using the computer code "FLUENT" proved the importance of an accurate and complete inlet boundary conditions and it is paramont in swirling system. The calculations were sensitive to the shape and distribution of all three mean velocity components. 3D computation through the swirler vanes were carried out for the first time.

8.2 CHARACTERISATION OF THE EXPERIMENTAL DATA

The relation between the combustion performance to the main operating variables such as pressure, temperature, mass of the air flow and combustor dimensions is one of the requirements of the gas turbine designer. Such relationship was established by Lefebvre(1,2) which summerised the past experience data that have been done on several combustors. These data were correlated against all important variables. Fig.8.1 and 8.2 shows such chart in which the combustion efficiency and inefficiency were plotted against θ parameter that it was drived from burning velocity consideration where θ is given by the following:

$$\theta = \frac{P_2^{1.75} \, A_{ref} \, D^{0.75}_{ref} \, \exp\left(\frac{T_2}{300}\right)}{m_a}$$

Where

P_2 = inlet pressure, Pa

T_2 = inlet temperature, K

A_{ref} = maximum cross sectional area of combustor, m2

D_{ref} = maximum diameter or width of the combustor, m

m_a = combustor air mass flow, kg/s

The θ parameter for the present work were calculated from the conditions of the optimum cases of the combustors fuelled with gaseous and liquid fuels. These

results were plotted on the same chart of Lefebvre(1) for comparison. However, the present results achieved much lower combustion inefficiency at low and high load conditions as shown in Figs.8.1 and 8.2 than all the systems considered by Lefebvre(1,2), in spite of the high pressure which is favourable for even less inefficiency used in the conventional combustor data.

Table 8.1 shows the summarised optimum low NOx results of some previous and recent published works. Representation of the results were corrected to 15% oxygen for both NOx and CO emissions and some of the published results were as a function of engine load. Some investigators were operating their test section at high inlet pressures. To prevent any complexities in the present comparison the NOx emissions of the other workers were corrected using the Zeldovich NOx kinetics square root pressure correction relation and tabulated in Table 8.1 together with present atmospheric operated results.
As demonstrated by Table 8.1, the present results can be considered in some tests superior especially using a combustor fuelled with natural gas using the non conventional passage or wall injection fuel systems.

Brown Boveri one of the large industrial gas turbine manufacturers developed a low NOx burner which used steam or water injection that can be used for liquid fuel injection and capable of NOx reduction as low as 38-60 ppm for 150 MW gas turbine(14). Moreover, there is a second generation combustor still under development with a dual fuel conical premix burner to meet the future NOx emissions limits down to 25 ppm. which is well below the present and planned limits for gas or liquid fuels without having to inject steam or SCR.

8.3 COMPARISON BETWEEN THE RADIAL SWIRLER AND JET MIX PERFORMANCE

Some of the present results were compared with the work done by Abdul-Hussain et al(18) on the Jet mix stabilisers which were obtained on the same combustion rig at 1 bar condition. Fig.8.3 shows the comparison between the two results using three fuel injector configurations, passages, central and 76mm wall

injection with swirler B, B&C counter rotating and swirler C respectively. It is evidently clear that the radial swirler system is superior to that of jet mix system and it is capable of achieving Ultra low Nox levels lower than the existing Jet mix combustion system at a combustion efficiency better than 99.9%.

8.4 NOX PRESSURE DEPENDENCY

Fig.8.4 shows that the NOx pressure dependency of the low NOx work done by Furuya et al(15) seems to disapear. This is an unusual result compared to that of conventional combustor data when thermal NOx gives a $P^{1/2}$ pressure dependence. However, it has also been reported by Ekstedt et al(16) that there is no apparent effect of pressure on NOx during catalytic combustor tests at 0.41 MPa and 1.1 MPa. Moreover, Roffe and Venkataramani(17) have found that the NOx emission level were independent of operating pressure for premixed systems. Thus, perhaps for the radial swirlers system which demonstrated highly good mixing ability with minimal thermal NOx especially with the non-conventional fuel injection systems such as passage injection, have a weak dependence of the NOx emissions (mostly dominated by prompt NOx) with pressure

Furuya et al(15) showed that for a 100mm diameter catalyst combustor tested at atmospheric pressure the NOx formation was just below 10 ppm uncorrected to 15% oxygen for fuel methane. The present NOx results are below these catalytic results.

8.5 RECOMENDATION FOR FUTURE WORK

1- Plate 8.1 shows three types of radial swirlers designed by the author. These radial swirlers can be used for different fuel injection modes and two different size of radial central fuel injection system. It will be very crucial to compare their performance and flow regime patterns with the present work to determine the influence of the radial inlet shape on the overall characteristics of swirl generation.

2- Investigation on the passages and 76mm wall injector can be extended to study other means of improving the stability limits on these two systems. Such as, increasing the number of holes or making some improvement on the present injectors design.

3- More work needs to done on the combination of two or more swirlers that have the same passages depth to be compared with that of a single swirler with equivalent passage depth as the combination. Fuel staging between the passage should be investigated.

4- The counter rotating double swirler should be extensively investigated as the central injection system had ultra low NOx emissions with a wide stability.

5- Work can be carriedout on the double staged combustion system to study the influence of the pilot length on the combustion performance of the main stage combustor.

6- Finally, The measurements of local velocity profiles and the turbulent intensities of the combustor flow-field especially that near the swirler outlet will add crucial information to the present experimental and theoretical results.

CHAPTER EIGHT

REFERENCES

8-1 Lefebvre A. H.: Gas Turbine Combustion, Hemisphere publishing corporation, 1986.

8-2 Lefebvre A. H.: Theoretical aspects of gas turbine combustion performance. CoA Note Aero. No. 163. The college of Aeronautics, Granfield Inst. Tech., August 1966.

8-3 Sotheran A., Pearce D. E. and Overton D. L.: Some practical aspects of staged premixed, low emissions combustion. ASME paper No. 84-GT-88 ,1984.

8-4 Aoyama K. and Mandai S.: Development of a dry low NOx combustor for a 120 MW gas turbine. ASME paper 84-GT-44, 1984.

8-5 Becker B. and Schulten W.: Advanced gas turbine for efficient and reliable combined cycle plants. Coal gasification and synthetic fuels for power generation. San Francisco, California, 1985.

8-6 Kuroda M., Iizuka N, Sato I., Wada K.,Tokunaga K. and Hata T.: Development of dry two-stage low NOx combustor for a gas turbine. ASME paper 87-GT-64, 1987.

8-7 Maghon H.: Wirschaftliche loesung des NOx-problems bei gasturbinen. Paper published in Elektrotechnische Zeitschrift, Jan. 2, pp.58-61, 1988.

8-8 Smith K. O., Angello L. C. and Kurzynske F.R.: Design and testing of an ultra-low NOx gas turbine combustor. ASME paper 86-GT-263, 1986.

8-9 Smith K. O., Wade G. W. and Samii M. H.: Performance testing of a low emissions, natural-gas fired, small gas turbine combustor. ASME paper 89-GT-266, 1989.

8-10 Smith K. O. and Cowell L. H.: Experimental evaluation of a liquid-fuelled, lean-premixed gas turbine combustor. ASME paper 89-GT-264, 1989.

8-11 Smith K. O.: Ultra-low NOx combustor concept for methanol firing. ASME paper 83-GT-29, 1983.

8-12 Smith K.O., Kurzyncke F.R. and Angello L.C.: Experimental evaluation of fuel injection configurations for a lean premixed low NOx gas turbine combustor. ASME paper 87-GT-141, 1987.

8-13 Davis L. B. and Washam R. M.: Development of a dry low NOx combustor. ASME paper 89-GT-255, 1989.

8-14 Jeffs E. :Asea Brown Boveri introducing a dual fuel dry low NOx design. Gas Turbine World, Vol.19, No.3, May-June 1989.

8-15 Furuya T., Hayata T., Yamanaka S., Koezuka J., Yoshine T. and Ohkoshi A.: Hybrid catalytic combustion for stationary gas turbine-concept and small scale test results. ASME paper 87-GT-99, 1987.

8-16 Ekstedt E. E. et al: Clean catalytic combustor program, final report. NASA CR-168323, 1982.

8-17 Roffe G. and Venkataramani K. S.: Emission measurements for a lean

premixed propane/air system at pressure up to 30 atmospheres. NASA CR-159421.

8-18 Abdul-Hussain U.S., Andrews G.E. and Shahabadi A.R.: Jet mixing shear layer combustion: An ultra low NOx system for natural gas fired gas turbines. I. Mech. E. combustion in engines conference, May 1988.

TABLES

Table (8.1)

Present work results as compared with some of the previous and recent publications		
References	Emissions at	15% oxygen, ppm.
	NOx	CO
Sotheran et al(3)	12	5900
Aoyama et al(4)	11	*
Becker and Schulten		
(5) 9% pilot	6	5
Kuroda et al(6)	13.6	50
Maghon(7)		
0% premixed	15	90
92% premixed	2	7
Smith et al (8)		
EQR.=0.65	7	45
EQR.=0.72	11	45
Smith et al(9)	6	7
Smith and Cowell(10)		
EQR.=0.32	4	170
EQR.=0.35	8	420
Smith (11)		
Methanol	3	160
Smith et al (12)		
Natural gas		
(configuration(A)	< 3	1000
Injector(configuration(B)	≈3	100-200
(configuration(C)	3	800
Davis and Washam(11)		
Natural Gas	6	15
Liquid Fuel	40	15
PRESENT WORK	AT 600K	
Direct Central Injection(P)	10	21
Direct Central Injection(NG)	7.0	20
Premixed (P)	1.5	8
Passage(P)	2.3	20
Passage(NG)	1.3	22
76mm Wall(P)	1.6	12
76mm Wall(NG)	1.0	12

FIGURES

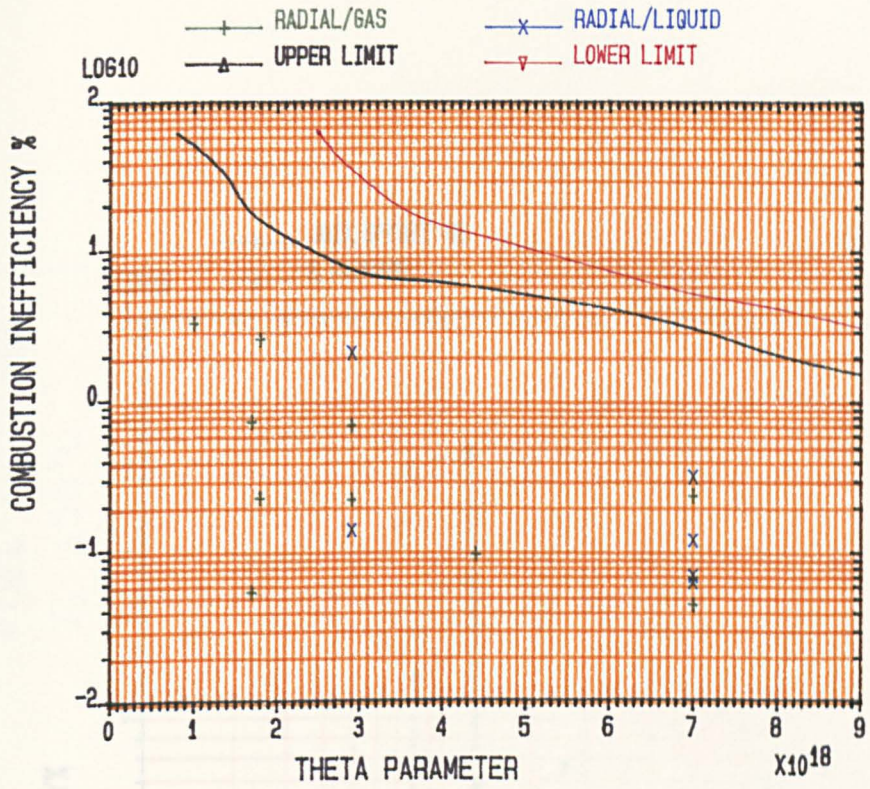

FIG.8.1 RADIAL SWIRLER COMBUSTION SYSTEMS PERFORMANCE ON THE DESIGN CHART OF LEFEBVRE (1).

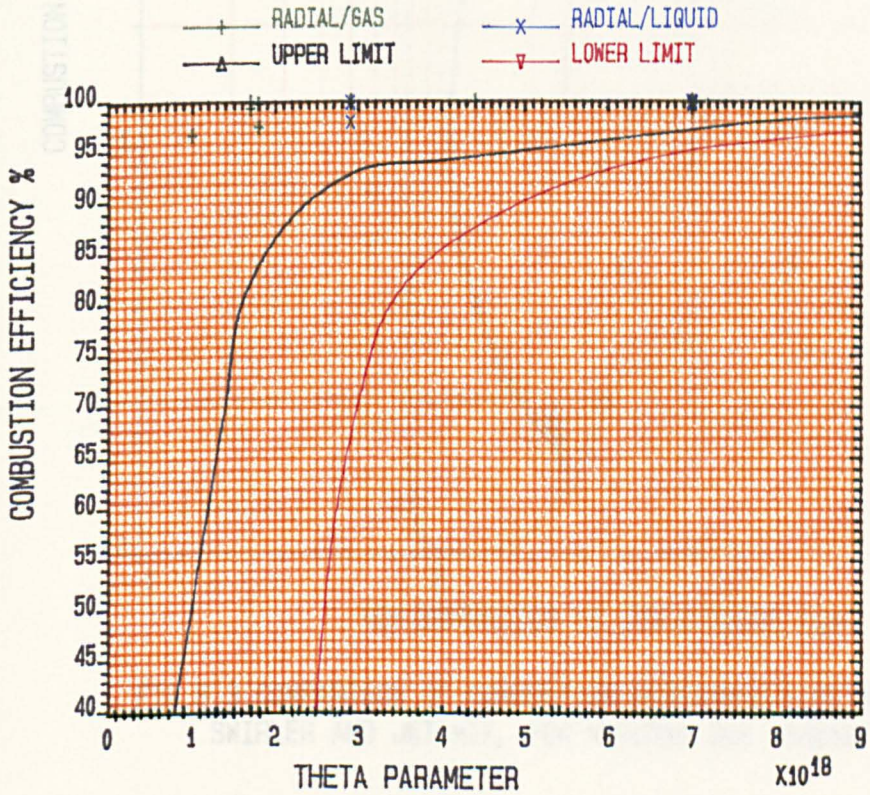

FIG.8.2 RADIAL SWIRLER COMBUSTION SYSTEMS PERFORMANCE ON THE DESIGN CHART OF LEFEBVRE (1).

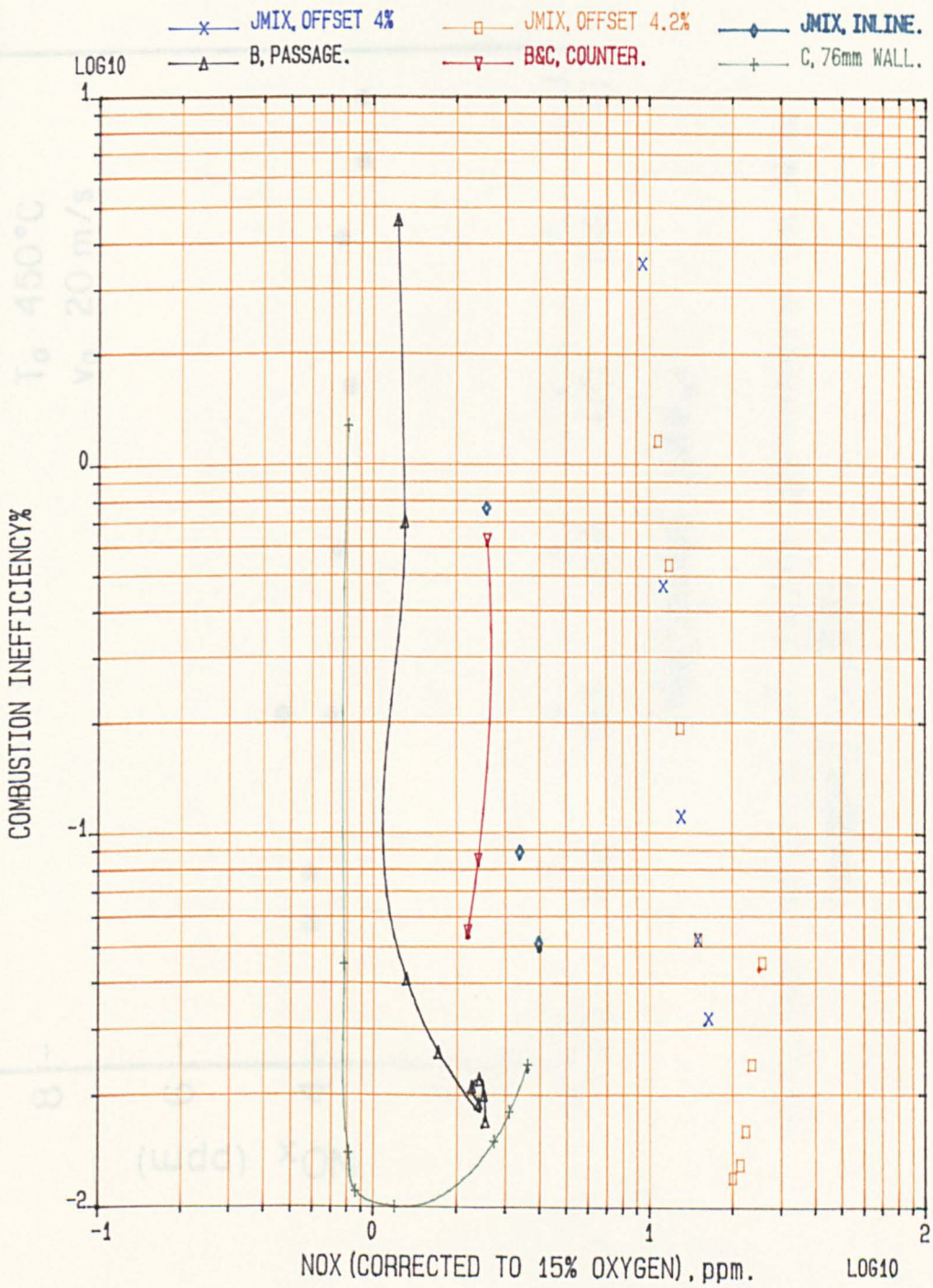

FIG.8.3 COMPARISON OF COMBUSTION PERFORMANCE BETWEEN RADIAL SWIRLER AND JET MIX, FOR NATURAL GAS , 140mm COMBUSTOR, 600K.

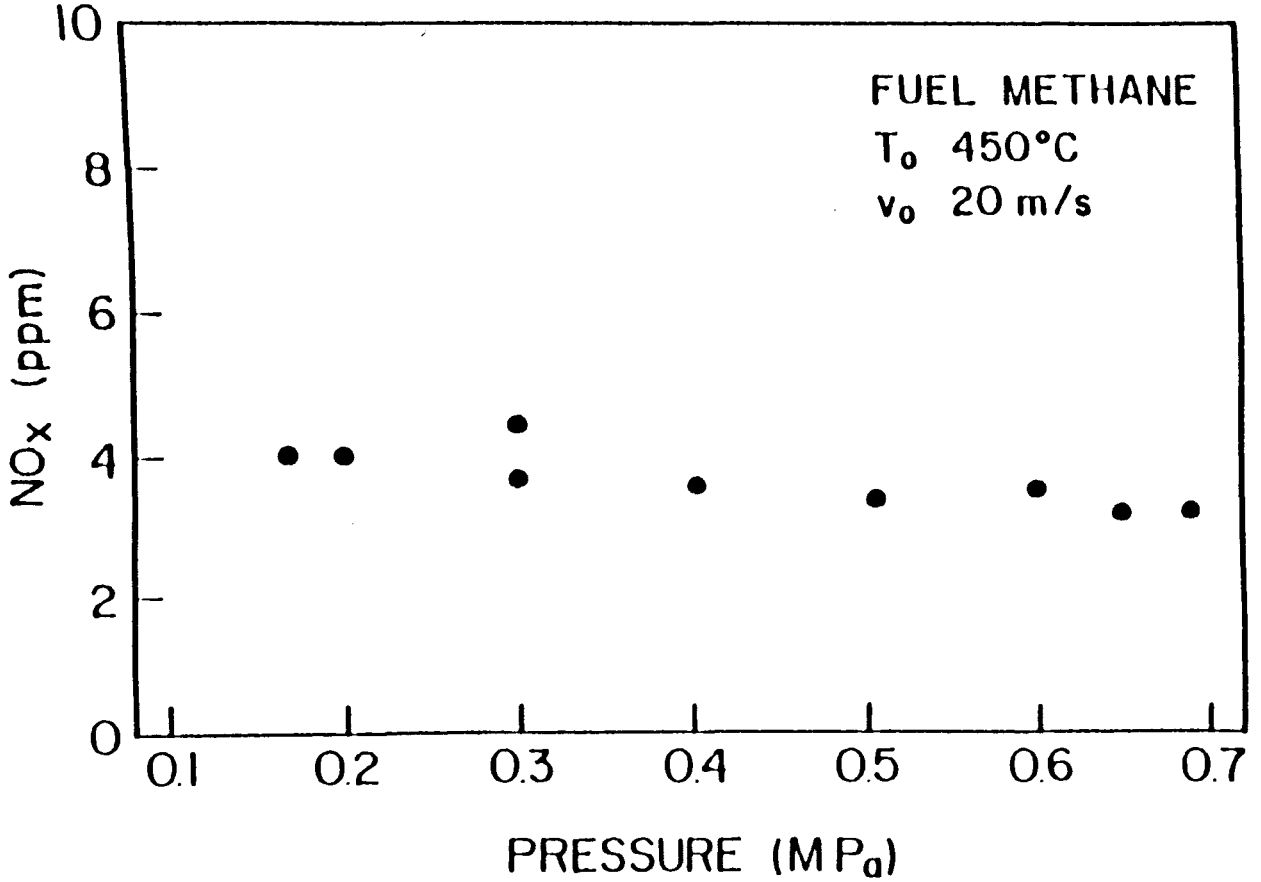

Fig.8.4 Effect of inlet pressure on NOx formation.(15)

PLATES

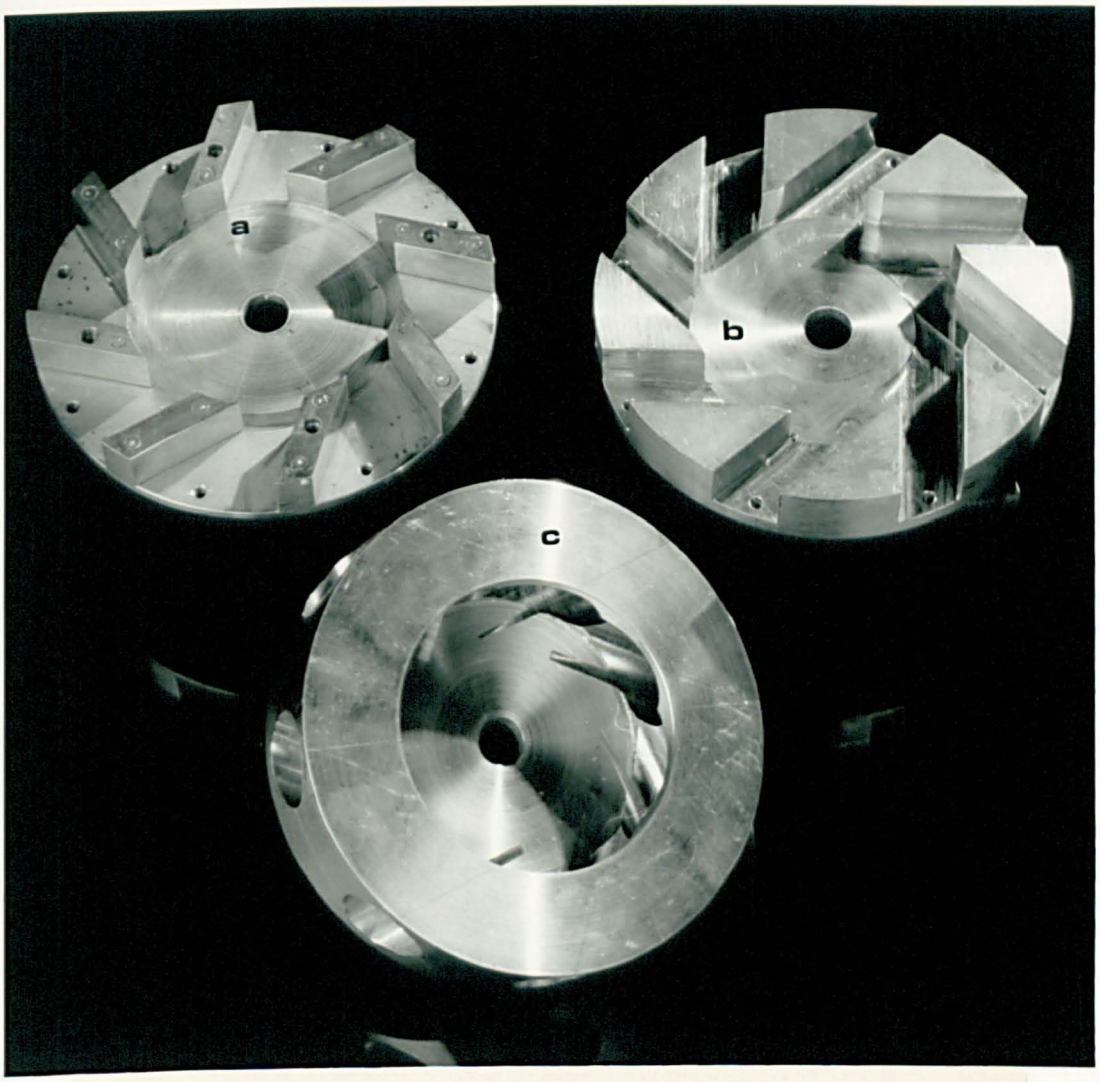

Plate 8.1 New designs of three types of radial flow swirlers, designed by the author.
a- Straight-Vanes.
b- Straight-Passages.
c- Circular-Holes.

GENERAL APPENDIXES

GENERAL APPENDIX

APPENDIX A

A-1 SWIRLER PRESSURE DROP AND DISCHARGE COEFFICIENT

The swirler pressure drop and discharge coefficient were measured downstream a flame tube with different pressure monitoring devices. The total and static pressure difference can be shown to be the same (1).

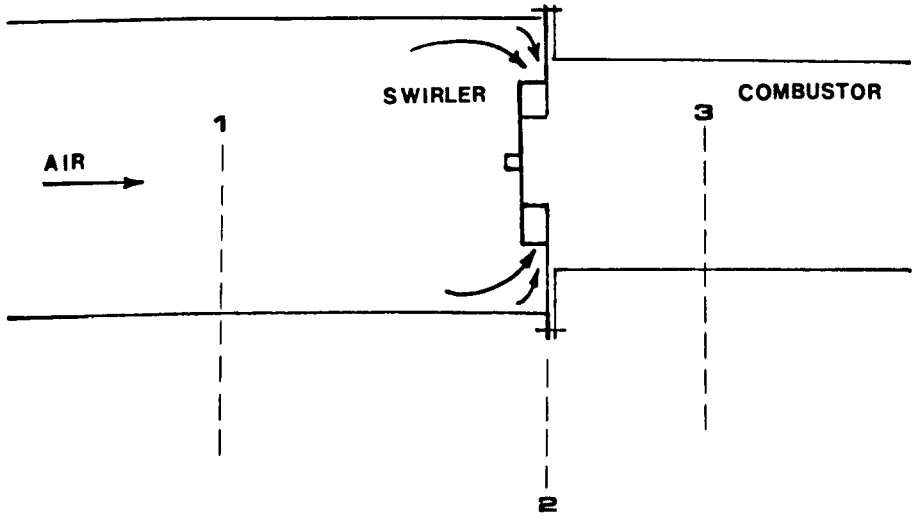

Provided that the velocities at plane 1 and 3 are uniform, then the stabiliser pressure drop is equal to the static pressure at plane 1 with reference to the atmosphere.

$$p = p_{1T} - p_{3T} = (h_{1T} - h_{3T})\rho_w . g \quad \text{..... A 1}$$

Since the velocity is constant then equation A 1 will be

$$p = p_{1S} - p_{3S} = (h_{1S} - h_{3S})\rho_w . g \quad \text{..... A 2}$$

$$p = \Delta h * 9787.03 \quad \text{..... A 3}$$

The pressure drop as percentage of upstream pressure is:

$$\Delta p/p\ \% = \Delta p * 100/(p_a + \Delta p) \quad \text{..... A 4}$$

where

h = pressure in H_2O

Δp = pressure loss N/m^2

ρ_w = water density Kg/m^3

g = gravimetric acceleration

Δh = pressure difference in H_2O

p_a = atmospheric pressure in N/m^2

A-1.1 Discharge Coefficient

It can be shown that the pressure loss can be expressed in terms of discharge coefficient C_D

$$\dot{m} = C_D \cdot A_2 (2\rho\Delta p)^{1/2} \quad \text{..... A 5}$$

where

Δp = measured pressure loss

A_2 = swirler open area

ρ = inlet density

C_D = overall discharge coefficient

$$C_D = \dot{m} / A_2 (2\rho\Delta p)^{1/2} \quad \text{..... A 6}$$

$$p = \rho RT \quad \text{..... A 7}$$

$$M = V/(\gamma RT)^{0.5} = R/\gamma)^{0.5} \cdot \dot{m}\, T^{0.5} / AP = (1/\gamma\rho P)^{0.5} \cdot \dot{m}/A_1 \quad \text{.....A 8}$$

Equations A 6 and A 8 may be combined to get:

$$\Delta P / P = \gamma/2 \left[M/C_D \cdot A_1/A_2\right]^2 \quad \text{..... A 9}$$

A-1.2 Correction of the pressure drop to reference Mach No.

The pressure drop is a function of Mach no., equation A 9. It is useful to correct the measured pressure drop of the stabiliser to the standard Mach no. of 0.0467 (Mref).

$$(\Delta P/P)corr = (\Delta P/P)meas. \left[M\ ref/M\ meas.\right]^2 \quad .... A\ 10$$

A-1.3 Calculation of Reynolds Number

$$R_e = V\rho D/\mu \quad ..... A\ 11$$

from the ideal gas law and Mach no. definition:

$$R_e = (\gamma/RT)^{0.5} P_1 . M . D/\mu \quad ..... A\ 12$$

$$= \sqrt{T_{in}} / (S1 + S2 .S + S3 .S^2 + S4 .S^3 + S5 .S^4) * 10E\text{-}6 \quad .....A\ 13$$

where

Tin = combustor inlet temperature K

S = 100/Tin S3 = 13.5083

S1 = 0.552795 S4 = 39.3531

S2 = 2.81089 S5 = -41.4194

A-1.4 Pressure Loss Due to Change in The Area

The pressure loss due to a flow expansion in the pipe may be given by the Borda-Carnot equation below (1)

$$K_{1t} = (1 - A_1/A_2)^2 \quad ..... A\ 14$$

A-2 CALCULATION OF AIR MASS FLOW AND MACH NUMBER:

Air mass flow rate was calculated according to BS1042 (1). The basic equation of the mass flow rate is given by

$$\dot{m} = C Z E \varepsilon A \sqrt{2\rho P} \quad ..... A1$$

where C = Discharge Coefficient

Z = Correction factor

ε = Expansibility factor expressed as

$$\varepsilon = \left\{ \frac{\gamma}{\gamma - 1} \cdot \frac{1 - s}{1 - s r^{2/\gamma}} \cdot \frac{1 - r^{(\gamma-1)/\gamma}}{1 - r} \right\}^{1/2} \quad \text{..... A2}$$

γ = Ratio of the specific heats at constant pressure to that at constant volume.

and r = Ratio of the absolute pressure at the upstream tapping to that at the venturi throat.

A = Throat area m

ΔP = Pressure difference in (Pa)

E = 1/(1-s) where $s = (d/D)^2$

d = Throat diameter, m

D = Pipe diameter , m

For a venturi type metering device with throat dia.=0.0352806 m and upstream pipe dia. = 0.158344 m

s = 4.96 E-2

E = 1.0012

From Figure 52.A , BS1042

C_D = 0.9865

A = 0.993 and

$\rho = P_1 / RT_1$

R = Gas constant for air = 287.04

Equation A 1 becomes

$$m = 7.969 \text{ E-3} * \varepsilon * (P_1 H_1 / t_1)^{1/2} \quad \text{..... A3}$$

where

H_1 = Pressure difference in M H O

P_1 = Inlet pressure (N/M)

T_1 = Inlet temperature K.

For 76 mm or 140 mm dia. pipe the flow velocity V_3

$$V_3 = \dot{m} / \rho A \qquad \text{..... A4}$$

and the flow Mach no. = flow speed / speed of sound

$$M = V_3/(\gamma RT)^{0.5} = (R/\gamma)^{0.5} * (\dot{m} T^{0.5})/ AP \qquad \text{.... A5}$$

V_3 is sometimes referred to as the reference velocity.

APPENDIX B

B-1 FUEL FLOW CALCULATION

Fuel flow calculations are performed for both gaseous (propane and methane) and liquid fuel (kerosene and gas oil).

B-1.1 GASEOUS FUEL

The composition of propane and methane was regularly analysed using a gas chromatography instrument.

All the rotameters were calibrated by the manufacturer at 15 C^{o} and 760mm Hg. To account for the change in the fuel density the relationship between the volumetric flow and density in the flow metering devices is taken as follows:

The densities of industrial propane and Methane were calculated by the following equations.

$$\rho_{propane} = 0.01(X_{C2H6} \cdot \rho_{C2H6} + X_{C3H6} \cdot \rho_{C3H6} + X_{C3H8} \cdot \rho_{C3H8} + X_{C4H10} \cdot \rho_{C4H10}) \quad \text{..... B1}$$

$$\rho_{methane} = 0.01(X_{CH4} \cdot \rho_{CH4} + X_{C2H6} \cdot \rho_{C2H6} + X_{C3H8} \cdot \rho_{C3H8} + X_{CO2} \cdot \rho_{CO2} + X_{N2} \cdot \rho_{N2} + X_{O2} \cdot \rho_{O2}) \text{ .. B2}$$

Where

$\rho_{propane}$ = density of industrial propane at 0 C^{o} or 273 K

$\rho_{methane}$ = density of methane at 0 C^{o} or 273 K

$\underline{X}$ = The fraction of fuel compositions in percentage.

$\underline{\rho}$ =The density of fuel compositions at 0 C^{o}

ρ_{C2H6} = 1.339 Kg/m^3 ρ_{CH4} = 0.7157 Kg/m^3

ρ_{C3H6} = 1.875 " ρ_{N2} = 1.2498 "

ρ_{C3H8} = 1.965 " ρ_{O2} = 1.4276 "

ρ_{C4H10} = 2.59 " ρ_{CO2} = 1.9635 "

The G.E.C rotameter reading was corrected using the equation B3 to account

for the density changes of the fuel to the rotameter actual temperature and pressure.

$$\rho_{\text{fuel A}} = \rho_{\text{fuel}} * (273/(T + 273)) * ((PAT + .00187h)/ 0.76) \quad \text{..... B3}$$

where

$\rho_{\text{fuel A}}$ = The actual density of the fuel (propane or methane) in the rotameter

ρ_{fuel} = The density of the fuel (propane or methane) at 0 C° and 760mm Hg.

T_f = Fuel temperature in C°

h = Rotameter static pressure inch W.G.

PAT = Atmospheric pressure in m Hg

The fuel mass flow rate was calculated by equation B4

$$\dot{m}_f = V / 60000 * (\rho_{\text{fuel A}} * \rho_{\text{CxHys}}) \quad \text{..... B4}$$

where

ρ_{CxHys} = density of CxHy at 15 C° and 760mm Hg

x=1 , y=4 for CH4 (methane)

x=3 , y=8 for C3H8 (propane)

$\dot{V}$ = Indicated fuel flow l/min

$\dot{m}_f$ = Mass flow rate Kg/sec

B-1.2 LIQUID FUELS

The mass flow rate for kerosene and gas oil were corrected by equation B5 and B6 respectively

$$\dot{m}_f = \frac{\dot{V} * (0.8 - 0.7E\text{-}3 (T_f - 15.0))}{60} \quad \text{..... B5}$$

$$\dot{m}_f = \frac{\dot{V} * (0.828 - 0.67E\text{-}3 (T_f - 15.0))}{60} \quad \text{..... B6}$$

where

$\dot{V}$ = Indicated fuel flow

T_f= Fuel temperature in C°

The liquid fuel rotameter was calibrated for kerosene by the manufacturers. The rotameters had to be re-calibrated in order to get the actual fuel flow rate for gas oil. This was done experimentally by allowing a quantity of gas oil to pass through the rotameters and measuring the indicated fuel flow rate, and also measuring the actual fuel flow rate at the fuel injection point. A 6 degree polynomial was then fitted through the sample points and the coefficients of the polynomial were calculated. In this way every time the indicated flow rate was given, the actual fuel flow rate was calculated using the polynomial equation B7.

$$\dot{V}_A = a_o + a_1 \dot{V} + a_2 \dot{V}^2 + ... + a_6 \dot{V}^6 \qquad ..... \text{B7}$$

$\dot{V}_A$ = Actual fuel flow rate for gas oil

$a_o = 0.2128E\text{-}1$ $\qquad a_4 = 0.2661E+2$

$a_1 = -0.20960$ $\qquad a_5 = -0.252E+2$

$a_2 = 0.4155E+1$ $\qquad a_6 = 0.9284E+1$

$a_3 = -0.1391E+2$

APPENDIX C

C-1 ELEMENTS ATOMIC BALANCE EQUATIONS

The air and fuel reaction equation was considered as follows:

RCxHy+Z(O2+NORN2+A1H2O+A2CO2+A3AR)=

A4CO2+A5CO+A6H2O+A7O2+A8NO+A9NO2+A10AR+A11CsHt+A12N2

from the rig metered air-fuel ratio (AFR).

R = FM/fuel molecular weight (FMWT)

Z = AM/air molecular weight (AMWT)

$$R = Z \frac{AMWT}{FMWT} * FAR \qquad \text{..... C1}$$

where

FAR = 1/AFR

carbon atomic balance

$$RX + Z * A2 = A4 + A5 + S\ A11 \qquad \text{..... C2}$$

Hydrogen Atomic Balance

$$R\ Y + 2\ A1\ Z = 2\ A6 + T\ A11 \qquad \text{..... C3}$$

Oxygen Atomic Balance

$$Z(2 + A1 + 2A2) = 2\ A4 + A5 + A6 + 2A7 + A8 + 2A9 \qquad \text{..... C4}$$

Nitrogen Atomic Balance

$$Z + NOR + 2 = A8 + A9 + 2\ A12 \qquad \text{..... C5}$$

Argon (AR) Balance

$$A3\ Z = A10 \qquad \text{..... C6}$$

For 100 moles of products

$$A4+A5+A6+A7+A8+A9+A10+A11+A12 = 100 \qquad \text{..... C7}$$

Equations C 1 to C 7 are to be solved for

A6, R, Z, A12, A7 and A10

For six unknowns, six equations are necessary for the exact solution; in this case the seventh equation will be used for checking the accuracy of metering air-fuel ratio and gas analysis measurements.

C-2 FOR CO AND CO2 DRY AND UHC, NO AND NOX ANALYSED ON WET BASIS (CO2 BASE)

Solution of equation C1 to C6 while C7 left for accuracy checking. Also the calculated moles of O2 can be checked with the measured moles of O2 for accuracy checking.

$$A4 = DCO2\ (1-0.01\ A6) \qquad \ldots\ldots\ldots\ C8$$

$$A5 = DCO\ (1-0.01\ A6) \qquad \ldots\ldots\ldots\ C9$$

From equations C1, C2, C3 and C9

$$Z = \frac{DCO2-0.01\ DCO2\ A6 + DCO-0.01\ A6\ DCO + SA11}{X\ .\ FAR\ .(AMWT/FMWT) + A2} \qquad \ldots\ldots\ldots\ C10$$

From C1 and C3

$$Z = \frac{2\ A6 + T\ A11}{Y\ .\ FAR\ .(AMWT/FMWT) + A2} \qquad \ldots\ldots\ldots\ C11$$

Assume

$$B1 = X\ .\ FAR\ .(AMWT/FMWT) + A2$$

$$B2 = Y\ .\ FAR\ .(AMWT/FMWT) + 2\ A1$$

solution to equation C10 and C11

$$A6 = \frac{(DCO2+DCO+S\ A11)B2 - B1\ T\ A11}{2\ B1 + B2\ (0.01\ DC02 + 0.01\ DCO)} \qquad \ldots\ldots\ldots\ C12$$

Air and fuel moles can be calculated from equations C11 and C1 respectively. A7, A4, A5, A12 and A10 can be calculated from equations C4, C8, C9, C5 and C6 respectively and C7 is left for final check.

For CO and O2 dry and UHC, NO and NOx analysed on wet basis (O2 Base).

Here the calculated CO2 can be checked with the measured CO2 for accuracy checking.

$$A7 = DO2\ (1 - 0.01A6) \qquad \text{..... C13}$$

From C1, C2, C4, C8 and C13

$$Z = \frac{0.01A6DCO-DCO-2SA11+A6+2DO2-0.02A6DO2+A8+2A9}{2+A1+2A2-2.(AMWT/FMWT).FAR-2A2} \text{..... C14}$$

From C14,C11 and assuming B3 =X. FAR.(AMWT/FMWT)-1-0.5 A1

$$A6 = \frac{B2(DCO-A8+2SA11-2DO2-2A9)-2TA11\ B3}{B2\ (0.01DCO+1-0.02DO2)+4B3} \qquad \text{..... C15}$$

The rest of the unknowns can be calculated as mentioned above in C 2.

APPENDIX D

CALCULATION OF COMBUSTION PERFORMANCE FROM EXHAUST GAS ANALYSIS

D-1 ELEMENTS ATOMIC BALANCE EQUATIONS

The general equation of fuel and air combustion can be written as follows:

$$R\ C_X H_Y + Z\ (O_2 + NOR\ N_2 + A4\ H_2O + A2\ CO_2 + A3\ Ar) =$$

$$A4CO_2 + A5CO + A6H_2O + A7O_2 + A8NO + A9\ NO_2 + A10Ar + A11\ C_S H_T + A12\ N_2$$

The fuel was taken as a mixture of hydrogen and carbon at atomic ratio of

C/H = X/Y and R = No. of moles of fuel.

Air was taken as a mixture of oxygen, nitrogen, argon, CO2 and H2O which can be calculated from the atmospheric humidity. The concentration of N2, Ar, CO2 and H2O is taken as ratio to oxygen.

For 100 moles of products the hydrogen, oxygen, carbon, nitrogen and argon balances are given as follows:

1. Carbon Balance,

$$R * X + Z * A2 = A4 + A5 + A11 * S \qquad \text{..... D1}$$

2. Hydrogen Balance,

$$Y * R + 2 * Z * A1 = 2 * A6 + T * A11 \quad \text{..... D2}$$

3. Oxygen Balance,

$$Z (2 + A1 + 2 A2) = 2A4+A5+A6+2A7+A8+2A9 \quad \text{..... D3}$$

4. Nitrogen Balance,

$$Z + NOR * 2 = 2 * A12+ A8+ A9 \quad \text{..... D4}$$

5. Argon Balance,

$$Z * A3 = A10 \quad \text{..... D5}$$

6. Total Moles,

$$A4+ A5+ A6+ A7+ A8+ A9+ A10+ A11+A12 = 100 \quad \text{.....D6}$$

From the above equations X and Y are known from the type of fuel used. NOR, A2 and A3 are taken from standard atmospheric air tables, and A1 is calculated from the known atmospheric temperature and humidity. A4, A5, A8, A9 and A11 are the measured concentration of the respective gases in the exhaust. The equations are to be solved for R, Z, A6, A7, A10 and A12.

From equations D5, D6 and D3

$$Z(2 + A1+ 2 A2+ 2 A3)= 200- A5- A6- A8- 2 A11- 2 A12 \quad \text{.....D7}$$

from equations D4 and D7

$$Z(2 +A1 +2 A2+2 A3+2 NOR)= 200- A5 -A6 +A9 -2 A11 \quad \text{..... D8}$$

from equation D2

$$R = (2 A6+ T*A11- 2Z*A1) / Y \quad \text{..... D9}$$

Sub D9 in equation D1 to eliminate R

$$X/Y (2A6+ T*A11- 2Z*A1) +ZA2 = A4+ A5+ A11*S \quad \text{..... D10}$$

$$Z= (A4+ A5+ A11*S-X/Y(2*A6+T*A11))/ (A2-2X/Y A1) \quad \text{..... D10a}$$

Equations D8 and D10a solve for A6

$$\frac{200-A5-A6+A9-2A11}{2+A1+2A2+2A3+2NOR} = \frac{A4+A5+A11*S-X/Y(2+A6+T*A11)}{(A2-2X/Y\ A1)} \quad \text{..... D11}$$

Two procedures are shown bellow. One is CO2 base where O2 is calculated

and checked with the measured amount (D 2), and the other (D 3) is O2 base, ie. CO2 is calculated and checked with the measured CO2 for accuracy checked.

D-2 For CO and CO2 dry analysis while NO,NOx and UHC analysed on wet basis (CO2 base).

This sampling technique was used for all the test. ie. a heated sample pump was used for NO and UHC but water was always removed for CO and CO2 gas analysers.

$$A4 = DCO2\ (1-0.01\ A6) \qquad \text{..... D12}$$

$$A5 = DCO\ (1-0.01\ A6) \qquad \text{..... D13}$$

Here equation D11 will be

$$\frac{200-DCO-A9-2A11+A6\ (0.01DCO-1)}{2+A1+2A2+2A3+2NOR} =$$

$$\frac{DCO2+DCO+A11*S-X.T.A11/Y-A6(0.01DCO2+0.01DCO+2X/Y)}{A2-2X\ .\ A1\ /\ Y} \qquad \text{..... D14}$$

Assume,

$$B1 = 200-DCO-A9-2A11$$

$$B2 = 0.01\ DCO-1$$

$$B3 = DCO2+DCO+A11S-X.T.A11/Y$$

$$B4 = 0.01\ DCO2+0.01DCO+2X/Y$$

$$G1 = 2+A1+2A2+2A3+2NOR$$

$$G2 = A2-2X.A1\ /Y$$

Solution of equation D14 will be

$$A6 = \frac{G1 * B3 - B1 * G2}{B2 * G2 + B4 * G1} \qquad \text{..... D15}$$

$$Z = (B1 + A6 * B2) / G1 \qquad \text{..... D16}$$

$$R = (2A6 + TA11 - 2\ Z\ A1) / Y \qquad \text{..... D17}$$

D-3 FOR CO AND O2 DRY ANALYSIS WITH NO,NOX AND UHC ANALYSED on wet basis (O2 base).

$$A7 = DO2\ (1-0.01\ A6) \qquad \text{..... D18}$$

Eliminating A4 from D3 and D1

$$Z = (A6 * B2 + B1)/ G2 \qquad \text{..... D19}$$

From D11 and D8

$$A6 = (G2 * B2 - G1 * B1)/(G1 *B3 - G2* B4) \qquad \text{..... D20}$$

Where

$$B1 = A11\ (X.T/Y-S)-0.5\ DCO +DCO2+ 0.5A8+A9$$

$$B2 = 200-DCO+A9-2A11$$

$$B3 = 2X/Y +0.005DCO+0.5-0.01DO2$$

$$B4 = 0.01\ DCO -1$$

$$G1 = 2 +A1+2A2+2A3+2NOR$$

$$G2 = 1+A1\ (0.5 + 2X/Y)$$

Z, R, A4, A10 and A12 can be found from D19, D9, D1, D5 and D4. D6 is left for final check. Also DCO2 can be checked with the measured value for accuracy.

Based on gas analysis the air/fuel ratio equation

$$AFR = (Z * \text{Air MW}) / (R * \text{Fuel MW}) \qquad \text{..... D21}$$

MW = Molecular Weight

The stoichiometric air/fuel ratio

$$AFRS = \frac{(32.0+NOR*28.0+A1*18.0+A2*44.01+A3*39)*(X+Y/4)}{(12.01 * X + 1.008 * Y)} \qquad \text{..... D22}$$

Equivalence Ratio

$$\emptyset = AFRS / AFR \qquad \text{..... D23}$$

Knowing the pollutant concentration and the fuel moles used to produce this pollutant, the emission index, defined as the ratio of grams of pollutant to kilogramme of fuel , can be calculated as follows,

$$EI_{NOx} = 44.0(A8 +A9)/R(X*12.01+Y*1.008) \qquad \text{..... D24}$$

$$EI_{CO} = 28.01\ A5/ R(X*12.01+Y*1.008) \qquad \text{..... D25}$$

$$EI_{HC} = 16.04*A11/ R(X*12.01+Y*1.008) \qquad \text{..... D26}$$

D-4 CALCULATION OF SPECIFIC HUMIDITY AND ATMOSPHERIC WATER VAPOUR MOLAR RATIO

For a mixture of air and water vapour, at atmospheric condition, the saturated water vapour partial pressure as a function of atmospheric temperature was expressed by the following polynomial equation:

$$P_{sat} = a + bT + cT + dT + eT \quad \text{..... D27}$$

Where T_a = ambient temperature in C^{o} and the constants

a = 592.3
b = 53.3
c = 0.8106
d = 0.03299
e = 4.714E-4

From the relative humidity definition

$$P_{WV} = P_{sat} * RH/100 \quad \text{..... D28}$$

P_{WV} = Water vapour N/m^2

RH = Relative humidity %

The specific humidity (A), or the Mole fraction of water vapour in relation to dry air, is given by the following equation:

$$A = (R_a * MW_a / R_{WV} * MW_{WV}) * P_{WV} / (P - P_{WV}) \quad \text{..... D29}$$

Where R, MW and R, MW are the gas constant(.287 KJ/Kg K), molecular weight of air and the gas constant(.4624 KJ/Kg K) and molecular weight of water vapour respectively. P = atmospheric pressure N/m^2

D-5 CALCULATION OF AIR MIXTURE CONCENTRATION

Air is taken as a mixture of oxygen, nitrogen, carbon dioxide, argon, and water vapour.

The ratio of N2, CO2, Ar and water vapour are used in the general chemical equation and is determined as follows:

For 100 moles of air

Argon is taken as a fixed percentage of 0.93

CO2 = 0.035%, nitrogen-oxygen ratio = 3.72 and water

vapour is calculated as shown in the previous section.

$$O2 = (100.0 - (CO2 + Ar + A))/ (1+ NOR) \quad \text{..... D30}$$

$$A1 = A/O2 = P_{WV} / O2$$

$$A2 = CO2 / O2 = 0.035 / O2$$

$$A3 = Ar / O2 = 0.93 /O2$$

$$NOR = 3.72$$

D-6 COMBUSTION EFFICIENCY

Combustion inefficiency is calculated due to the inefficiency of unburned hydrocarbon and carbon monoxide measured at the combustor exit.

$$\eta = 1 - \eta_{HC\ ineff} - \eta_{CO\ ineff} \quad \text{..... D31}$$

$$\eta = 1 - \frac{m\,HC * CV\,HC}{m_f * CV_f} - \frac{m\,CO * CV\,CO}{m_f * CV_f} \quad \text{.....D31}$$

Where

$\dot{m}$ = mass flow rate

CV= calorific value

For an air and fuel combustion

$$1 + AFR = M * MWT / \dot{m} \quad \text{..... D32}$$

Substituting D32 in D31

$$\eta = 1 - \frac{MHC * MWTHC * CVHC}{M_p * MWT_p * CV_f}(1+AFR) - \frac{MCO * MWTCO * CVCO}{MWT_p * CV_f * M_p}(1+AFR) \quad \text{....D33}$$

CV_{CO} = 67.6 Kcal/Mole

CV_{CH4} = 222.8 Kcal/Mole

CV_{C3H8} = 530.6 Kcal/Mole

The formula recommended by the Enviromental Protection Agency (4) was used to adjust nitrogen oxide levels. The 15% oxygen in the exhaust is typical of full power stationary gas turbines and 3% oxygen for furnances application.

$$NOx_C = NOx_{obs} * (20.9-CORR) /(20.9 - O\ \%\ actual) \quad \text{..... D51}$$

Where

NOx_C = Corrected NOx to 15% PPM

NOx_{obs} = Measured NOx PPM

CORR = 15% or 3% oxygen in the exhaust for the gas turbine or furnace application respectively.

O_2 = Oxygen concentration in the exhaust gases %

Further correction is also recommended to adjust to ISO standard dry condition by the following ambient condition correction factor:

$$NOx = NOx_C * e^{19(H_{obs} - 0.00633)} \quad \text{..... D52}$$

Where

H_{obs} = Specific humidity of ambient air at test and e = 2.718

APPENDIX E

FLAME TEMPERATURE AND COMPOSITION CALCULATIONS

E-1 CALCULATION OF UNDISSOCIATED FLAME TEMPERATURE (TUD)

The undissociated products of hydrocarbon fuel and air combustion are CO2, H2O, N2, Ar, CO and O2. Oxygen exists only at lean mixtures (Ø< 1) and its value is zero at stoichiometric while CO exists only at rich mixtures (Ø> 1).

For lean mixtures the chemical equation including water vapour, carbon dioxide and argon in the atmospheric air is given by:

$$RC_X H_Y + Z/Ø\ (O2 + NORN2 + AH2O + A2CO2 + A3Ar) = CO2 + H2O + O2 + N2 + Ar$$

If the unburned hydrocarbon is measured as methane in % and fuel is used as propane, equation D33 will be:

$$\eta = 1 - 0.065(1+AFR) * UHC\ \% - 0.00197 * (1+AFR) * CO\ \% \quad \text{..... D34}$$

If unburned hydrocarbon is measured as propane as a % and the fuel used is propane, equation D33 will be:

$$\eta = 1 - 0.01544 * (1+AFR) + UHC\ \% - 0.00197 * (1+AFR) * CO\% \quad \text{..... D35}$$

The datum of complete combustion ($1-\eta=0$) when both CO and UHC at the combustor exit is equivalent to zero. This is not the case if equilibrium concentration of CO is taken into account. Combustion inefficiency due to CO equilibrium is calculated using CO equilibrium obtained from the flame temperature calculations and substituted in equation D33. However, for liquid fuel another procedures were adapted to calculate the combustion efficiency(7). The ratio (m_p / m_f) is given as in ref.(7) to be:

$$(m_p / m_f) = 1 + AFR \quad \text{.....D36}$$

Where

m_f = Fuel mass flow rate.

m_p = Wet products mass flow rate.

AFR = Air to fuel ratio.

Due to equation (D36) it can be deduced that the volumetric rate of the exhaust gases (Qe) is:

$$Qe = (m_p / \rho_e) = m\,(1+AFR) / \rho_e \quad \text{.....D37}$$

ρ_e = The density of the exhaust gases.

The volumetric rate of CO = Qe* A5/100 .....D38

The volumetric rate of UHC= Qe* A11/100 .....D39

ρ_{CO} = 1.185 Kg/m at 15 C and atmospheric pressure.

Then the density at the test conditions will be

$$\rho_{CO} = 3.3682*10^{-3} * \frac{P}{Ta} \qquad \text{.....D46}$$

P and Ta are the pressure and temperature at the sample test conditions.

Knowing that the universal gas constant=8.3143 N.m/mol K and assume:

TM= Total moles at exit.

W =Total exit gases weight.

W=A11*16.042+A12*28.0134+A10*39.948+A7*32+A6*18.01534+A4*44.01
+A5*28.01+A8*30.0067+A9*46.0067

Then the ratio (ρ_{CO}/ρ_{e}) can be evaluated as:

$$(\rho_{CO}/\rho_{e}) = 28.004*TM/W \qquad \text{.....D47}$$

Also

$$(\rho_{HC}/\rho_{e}) = 16.03435*TM/W \qquad \text{.....D48}$$

The unburned hydrocarbon was measuerd as methane in %.

The calorific values according to ref.(9) are:

CV_{CO} =10.101265 MJ/kg.

CV =50.03684 MJ/kg.

CH4

CV = 46.5 MJ/kg

Kerosene

CV = 45.6 MJ/kg

Gas Oil

Then the inefficiency can be found as follows:

A-FOR KEROSENE

From equations D44 , D45 , D47 and D48 :

$$(I-\eta)_{CO} = 6.0833509 * \frac{TM}{W} * (1+AFR) * \frac{A5}{100}$$

$$(I-\eta)_{HC} = 17.2539 * \frac{TM}{W} * (1+AFR) * \frac{A11}{100}$$

From eq.(D42)

$$I-\eta = \frac{TM}{W} * (1+AFR) * (6.0833509*A5+17.2539*A11)/100$$

B-FOR GASOIL

Similar steps to that in (A) will give:

$$I-\eta = \frac{TM}{W} * (1+AFR) * (6.203417*A5+17.59448*A11)/100$$

D-7 NITROGEN OXIDES CORRECTION

The source of CO2 in the products is equal to the sum of atmospheric CO2 and CO2 formed from the burning of the fuel carbon, and similarly with H2O.

To calculate the adiabatic temperature (Tud), assuming no work or heat transfer from the system, the energy released by the reactant (r) must be absorbed by the products (P) and the enthalpy balance will be given by:

$$\Sigma X_r (\Delta \overset{o}{H}_r + \Delta H_{T_i})_r = \Sigma X_p (\Delta \overset{o}{H}_f + \Delta H_{Tud})_p \qquad \text{..... E1}$$

Where

ΔH_T = Rise in sensible enthalpy from 298.15 to T

ΔH^o_f = Enthalpy of formation

X_r X_P = No. of moles of reactants and products respectively

Ti, Tud = Initial and undissociated temperatures (K)

In equation E1 the reactant and product concentration are known, H and H obtained from JANAF tables (2). Only Tud was assumed and changed until the right hand side of equation E1 is equal to the left hand side.

The enthalpy change associated with the combustion process must take into account dissociation for near stoichiometric flames. Generally for flame temperatures less than 1800 K dissociation isnot important and an undissociated flame temperature calculation procedure can be used. The thermal balance method between the enthalpy released by the reactants and that absorbed by the products to find the adiabatic flame temperature was allright for gaseous(ie. Propane and Methane) since the sensible enthalpy and the heat of formation were available in JANAF Tables and other well known tables. But for liquid fuels (ie. Kerosene and Gas Oil) the above values were not available in these tables. If a Chromatography analysis for Kerosene and Gas Oil is done it might be possible to get the percentages of the components of the fuel of known enthalpies in the

tables. This was variable from test to another and it will be very complicated to be sure of the percentages which are reacted during the combustion process. Therefore the following way was adopted with Kerosene and Gas Oil to find the adiabatic flame temperature.

The calorific values of Kerosene and Gas Oil (at room conditions) are obtainable from reference (4), also their calorific values can be found by a test in the laboratory on a sample of the fuel with calorimeter under constant pressure or at constant volume and then converted to that of constant pressure. The calorific value is defined as: [The heating provided by the combustion of a specified quantity of a fuel in a standard apparatus (calorimeter) under specified conditions] (4).

From the above definition, and taking into consideration the heat treatments to raise the temperatre of the fuel from the room conditions to the inlet temperature which are subtracted from the calorific value to get the heating value (HI) of the fuel at (Tin) as mensioned in the previous section it can be deduced that:

$$R * HI = (Hp)_{T_2} - (Hp)_{T_1}$$

or

$$(Hp)_{T2} = (Hp)_{T1} + R * HI \qquad \text{.....E2}$$

Where

Hp = Rise in sensible enthalpy of the products from 298.15 K to T.

T1 = Initial temperature of the fuel/air mixture.

T2 = The theoritical flame temperature.

HI = The Fuel heating value at constant pressure.

R = No. of moles of the fuel.

It is assumed in the above equation as shown that the reaction goes to completion in an adiabatic process. In other words all of the heating value of the fuel is used to heat the products of combustion.

The lower calorific value was used since the water vapor in the products is very definitely in the vapor state at the flame temperature.

Since the products of combustion are a mixture of several gases, the determination of the undissociated flame temperature can be found by a trial and error method.

The rise in sensible enthalpy from 298.16 K to the inlet temperature or the equilibrium flame temperature can be taken from JANAF tables 2 .

E-2 ADIABATIC FLAME TEMPERATURE INCLUDING DISSOCIATION:

The total enthalpy of the burned products in equilibrium may be computed in this case depending on the chemical reaction equation shown in Appendix C which includes the dissociated products of combustion. The combustion efficiency was affected mainly by dissociation at temperatures higher than 1800 K. Therefore it was taken into consideration in the calculation of the heating value of the fuel. So eq.(E2) will be written here as:

$$(Hp)_{T2} = (Hp)_{T1} + HI^{*}R^{*} \qquad \text{.....E3}$$

$(Hp)_{T1}$ could be taken as the same as that computed in the previous section at inlet temperature.

While $(Hp)_{T2}$ here is the total enthalpy of the burned mixture (including those of the dissociation products) at the equilibrium temperarure.

η = The combustion efficiency

The combustion efficiency was taken in the calculations to find the experimental flame temperature at the whole range of (A/F) ratios to be compared with the ideal flame temperature.

APPENDIX F

F-1 CALIBRATION

All the instruments were calibrated prior and after completion of each test by calibration gas cylinders from Morgan's and Rank Hilger. These cylinders contained a cocktail of all the gases above and were analysed by B.O.C. All the NOx calibration gases were cross calibrated against a reference B.O.C. Spectroseal calibration gas. Towards the end of the test programme this procedure was adopted for all other gases. This was to check the accuracy of the calibration cylinders to reduce any possible errors that might be caused by calibration as explained before.

The gas analysis were used to compute 'wet' concentrations of CO and CO2, the air to fuel ratio, combustion efficiency, equilibrium CO, NOx emissions corrected to 15% oxygen and the flame temperature. The flame temperature calculation was based on an energy balance, assuming no heat losses and no dissociation. A full equilibrium program was used to check the range of equivalence ratios over which this latter assumption was valid. All the calculations are set out as in the previous Appendices.

F-2 GENERAL TEST PROCEDURE

The experimental procedure for mean exit and radial gas sampling are as follows:

1- Switch on the gas analyser system power about 1 hour before light up to stabilise the analyser's electronics and the NOx and FID analysers oven temperatures. Also switch on the sampling oven, the heated teflon sampling line and the heated lines to the FID and NOx analysers.

2- Switch on the vacuum pump for the NOx analyser and light up the FID He/H2-air detector flame. Pass the zero gas and then the calibration gas through all the analysers to set up their calibration ready for

measurements.

3- For mean sampling, set up the sampling probe at the combustor exit, or for radial sampling, aline the sampling probe with the appropriate port hole at the side of the combustor for traversing. For axial traverse the probe alined with the combustor centreline at the combustor outlet.

4- Start the main air blower, switch on the control panel and set the reference or reduced Mach number at the desired inlet temperature 305K, 400 K or 600 K corresponding to low or high power.

5- The following readings are taken before light up: venturi static pressure, atmospheric pressure, venturi differential pressure, venturi temperature, combustor inlet static pressure and inlet temperature, air humidity and ambient temperature and combustor wall static pressure profiles.

6- The light up procedure is as follows:

A. Supply cooling air to the observation window.

B. Open the sampling probe cooling water

C. Switch on the ignitor and observe the spark through the window.

D. Energies the fuel solenoid valve.

E. Open the nitrogen purge valve

F. Open the fuel valve and supply fuel to the rig for 10 seconds. If light up is not successful, shut the fuel valve and repeat the procedure after the nitrogen purge sequence.

For mean exit sampling

7- Establish a weak stable flame, correct the air mass flow and inlet temperature, find the noise limit by increasing the fuel flow and carry out a weak extinction (WE1).

8- Light up again and establish a condition close to the noise limit. Note all readings in 5 and CO, CO2, UHC, NO, NOx, O2, H2, fuel flow, fuel temperature, fuel pressure, relative humidity, ambient temperature and gas sample probe outlet temperature.

9- Decrease the A/F ratio in small steps of 0.05 equivalence ratio. Repeat all readings in 8 at each fuel setting and determine the maximum efficiency equivalence ratio. Establish weak extinction (WE2).

For radial and axial traversing

10- Establish a weak stable flame. Move the probe into the combustor and position such that the probe sampling point is flush with the wall. Note the gas sample readings. Traverse the probe in radially or axially at small increments taking notes of the gas sample readings at each point.

11- Remove the sampling probe and position at the next port hole along the combustor. Repeat the procedure in 10.

12- Remove gas analysis probe. Light up again for flame photography.

13- Check zero and span on gas analysers.

14- Purge the fuel line with nitrogen.

Table (G.A.1)
Axial Swirler Design Details[9] Used For Comparison
With Radial Swirler (B)

Axial Swirler	Vane Angle	Blade Type	l (mm)	h (mm)	t_b (mm)	dh (mm)	d (mm)	A_2 $(mm)^2$	Swirl number	Pressure loss %
SW5	30	Straight	46.5	7.5	0.98	47.3	70	1697.66	0.49	1.18
SW6	45	"	26.2	5.8	1.57	40.60	70	1663.32	0.81	1.70

where

l = Vane depth

h = Axial distance between hub and swirler outer flange

t_b = Swirler vane thickness

dh = Swirler hub diameter

d = Swirler outer diameter

A_2 = Swirler perpendicular open area

GENERAL APPENDIX

REFERENCES

G.A-1 AlDabagh N.A : Emissions and Stability of Gas Turbine combustors with Rapid Fuel and Air mixing. Ph.D Thesis, Fuel and Energy Dept., University of Leeds., 1984.

G.A-2 BS1042, :Methods for the Measurement of Fluid Flow in Pipes. British Standard 1042, Part 1, 1964.

G.A-3 JANAF Thermochemical Tables, Dow Chemical Company, Midland, Michigan, 1960.

G.A-4 Lister , D.H and Wedlock ,M.I. "Measurements of Emissions Variability of a large Turbofan Aero-Engine" ASME paper No. 78-GT-75,1978.

G.A-5 J.W.Rose and J.R.Cooper "Technical data on fuel",7th edition.1977

G.A-6 Williams, A. "Combustion of sprays of Liquid fuels",1976

G.A-7 E.M. Goodger "Combustion calculations"

G.A-8 Abdul Aziz M.M.: Liquid Fuelled jet shear-layer Gas-Tur bine combustion. Ph.D Thesis, Fuel and Energy Dept., University of Leeds, 1988.

G.A-9 Kowkabi M. : Swirl combustor for low emission gas turbines. Ph.D thesis, Fuel and Energy Dept., Leeds University, 1987.

PUBLISHED PAPERS DURING THE COURSE OF THE PROJECT

1- Alkabie H.S. and Andrews G.E. and Ahmad N.T.: Lean low NOx primary zones using radial swirlers. ASME paper 88-GT-245, 1988.

2- Alkabie H.S and Andrews G.E.: Influence of fuel placement on NOx emissions from flames stabilised by radial swirlers. Joint meeting of the British and French sections of the combustion Institute Rouen, 1988.

3- Andrews G.E., Abdul Aziz M.M., Abdul Hussain U.S., Al Dabbagh N.A., Ahmad N.A, Al shaikly A.F., Alkabie H.S., Kowkabi M. and Shahabadi A.R.: High intensity burners with low NOx emissions. British Flame Days 1988, Furnace Combustion Research and its applications , The Institute of Energy, 1988.

4- Alkabie H.S. and Andrews G.E.: Ultra low NOx emissions for gas and liquid fuels using radial swirlers. ASME paper 89-GT-322, 1989.

5- Alkabie H.S. and Andrews G.E.: The influence of fuel placement on NOx emissions from flames stabilised by radial swirlers. ICDES Int. Coll. on Dynamics of Explosion and Reactive Systems, University of Michigan, July 1989.

6- Alkabie H.S. and Andrews G.E.: The influence of fuel placement on NOx emissions from flames stabilised by radial swirlers at gas turbine primary zone conditions. IMechE HQ seminar on Gas Turbines-Technology and Development, 1989.